PROCEEDINGS OF THE 10th INTERNATIONAL CONGRESS ON CATALYSIS · PART A

New frontiers in catalysis

EDITED by L. GUCZI, F. SOLYMOSI, P. TÉTÉNYI



BUDAPEST '92

AKADÉMIAI KIADÓ, BUDAPEST

NEW FRONTIERS IN CATALYSIS

PART A

9597

NEW FRONTIERS IN CATALYSIS

Proceedings of the 10th International Congress on Catalysis, Budapest, 19–24 July, 1992

PART A

Editors

L. GUCZI
Institute of Isotopes of the Hungarian Academy of Sciences
P. O. Box 77, H-1525 Budapest, Hungary

F. SOLYMOSI
Institute of Solid State and Radiochemistry, József Attila University
P. O. Box 168, H-6701 Szeged, Hungary

P. TÉTÉNYI
Institute of Isotopes of the Hungarian Academy of Sciences
P. O. Box 77, H-1525 Budapest, Hungary

MTAK 0 00000 04300 7

AKADÉMIAI KIADÓ, BUDAPEST 1993

691788

This book is published as Volume 75 in the Elsevier series
Studies in Surface Science and Catalysis

Joint edition by
Elsevier Science Publishers, Amsterdam, The Netherlands
and
Akadémiai Kiadó, Budapest, Hungary

MAGYAR
TUDOMÁNYOS AKADÉMIA
KÖNYVTÁRA

ISBN 963 05 6489 0 (Series)
ISBN 963 05 6490 4 (Part A)

© 1993 Elsevier Science Publishers B. V.

All rights reserved.

Printed in Hungary

M. TUD. AKADÉMIA KÖNYVTÁRA
Könyvleltár 182.6./19 ..93 sz.

PREFACE

The Tenth International Congress on Catalysis was held in Hungary, Budapest, July 19-24, 1992 under the auspices of the Council of the Congress on Catalysis, the Hungarian Academy of Sciences, the Chemical Society of Hungary and the International Union of Pure and Applied Chemistry. Z. G. Szabó was the Honorary Chairman and P. Tétényi and F. Nagy served as the Chairman and Co-Chairman, respectively. The Organizing Committee included L. Guczi (Chair), A. Sárkány (Secretary) M. Bartók, P. Fejes, Gy. Gáti, D. Kalló, J. Margitfalvi, L. Markó, Z. Paál, J. Petró and F. Solymosi.

More than 1000 delegates (including local organizers) attended the Congress which was headquartered in the Budapest Convention Centre located in the pleasant hills of the Buda part of the Hungarian capital. As has been the tradition in previous Congresses, this Congress was divided into two parallel sessions with 105 oral presentations and two further sessions in which 360 posters were displayed. All these presentations and posters were chosen by the Paper Selection Committee from the approximately 800 abstracts that were submitted. The theme of the Congress was "New Frontiers in Catalysis". Judging from the lively discussions (on the average 9 per oral presentation) this theme was of considerable interest to the participants. Both the papers selected for oral presentation (together with discussions) and those in the poster sessions are contained in these Proceedings.

We are grateful to the outstanding scientists who accepted our invitation to present the 6 plenary lectures that introduced the various topics covered in the Congress.

Generous financial contributions from the Council of the European Communities and many institutions and corporations made it possible for about 80 scientists from Central and Eastern Europe, the EC countries, China, USA and India to participate in the Congress. Several students were also able to attend because they were allowed to pay a reduced registration fee.

Social events including receptions, a Congress banquet, a concert, sightseeing tours and excursions were organized to make the stay of our foreign guests more enjoyable.

The Organizers are deeply indebted to the scientists from 42 countries who accepted our invitation to come to Hungary and make the Congress yet another outstanding success in the 40 year tradition of such events. We hope you enjoyed the meeting and will find these Proceedings a valuable addition to your catalysis library. Our best wishes go to the Organizers of the Eleventh International Congress on Catalysis which will be held during July 1996 in Baltimore, Maryland in the United States.

Budapest, December 1992

The Editors

CONTENTS

PART A
Preface V
Catalysis: Past, Present and Future
J. A. Rabo 1
Interfacial Coordination Chemistry: Concepts and Relevance to Catalysis Phenomena
M. Che 31
New Catalytic Aspects of Heteropolyacids and Related Compounds - To the Molecular Design of Practical Catalysts
M. Misono 69
The Catalytic Conversion of Methane to Oxygenates and Higher Hydrocarbons
J.H. Lunsford 103
New Reactions in Various Fields and Production of Specialty Chemicals
W.F. Hölderich 127

Structure-Function Relationships in Heterogeneous Catalysis: The Embedded Surface Molecule Approach and its Applications
P. Johnston and R. W. Joyner 165
Isotopic Tracer Studies of Chain Propagation and Termination during Fischer-Tropsch Synthesis over Ru/TiO_2
K. R. Krishna and A. T. Bell 181
Liquid Phase Oxidation of Glyoxal to Glyoxylic Acid by Air on Platinum Catalysts
P. Gallezot, F. Fache, R. de Mesanstourne, Y. Christidis, G. Mattioda and A. Schouteeten 195
The Effect of Oxygen Binding Energy on the Selective Oxidation of Butane over $V/\gamma\text{-}Al_2O_3$
P. J. Andersen and H. H. Kung 205
Secondary Oxygen Exchange Reactions during the Partial Oxidation of Methane
M. M. Koranne, J. G. Goodwin, Jr. and G. Marcelin 219
Role of Free Radicals in Heterogeneous Complete Oxidation of Organic Compounds over IV Period Transition Metal Oxides
Z. R. Ismagilov, S. N. Pak, L. G. Krishtopa and V. K. Yermolaev 231
^1H Broad-Line NMR at 4 K for Studying the Acidity of Solids: Application to Zeolites
P. Batamack, C. Doremieux-Morin and J. Fraissard 243
Preparation of Bifunctional Catalysts by Solid-State Ion Exchange in Zeolites and Catalytic Tests
H. G. Karge, Y. Zhang and H.K. Beyer 257
Transition Metal/Zeolite Catalysts by Design: Nucleation and Growth of Mono- and Bimetallic Particles in Zeolite Y
W. M. H. Sachtler, Z. Zhang, A. Yu. Stakheev and J. S. Feeley 271
Promotion of H-ZSM-5 by Alumina
J. Völter, H. D. Lanh, B. Parlitz, E. Schreier and K. Ulbricht 283
The Effect of Preparation Method on Metal-Support Interaction in Pd/L-Zeolite Catalysts
G. Larsen and G. L. Haller 297
On the Nature of Superactive Centers in H-FeZSM-5 Zeolites. Quantum-Chemical Calculations
M. J. Filatov, A. G. Pelmenschikov and G. M. Zhidomirov 311

CO Oxidation on Pd(110): A Model System for Chemical Oscillations in Heterogeneous Catalysis
M. Ehsasi, M. Berdau, A. Karpowicz, K. Christmann and J. H. Block 321
Nature of Metal-Metal Bonding in Mixed Metal Catalysts
R. A. Campbell, J. A. Rodriguez and D. W. Goodman 333
The Reduction of Nitric Oxide by Hydrogen over Pt, Rh and Pt-Rh Single Crystal Surfaces
H. Hirano, T. Yamada, K. I. Tanaka, J. Siera and B. E. Nieuwenhuys 345
Spectroscopic Studies on the Reaction Pathways of Methanol Dissociation on Pd Catalyst
A. Berkó, J. Raskó and F. Solymosi 359
Cyclotrimerisation of Acetylene to Benzene over Single Crystal Palladium and Gold/Palladium Surfaces and over Supported Palladium Catalysts
C. J. Baddeley, R. M. Ormerod and R. M. Lambert 371
Surface Chemistry for Automotive Emissions Control: Interactions of Nitric Oxide on a (111) Pt-Rh Alloy Surface
G. B. Fisher, C. L. DiMaggio and D. D. Beck 383
Shape Selective Alkylation of Benzene with Long Chain Alkenes over Zeolites
S. Sivasanker, A. Thangaraj, R. A. Abdulla and P. Ratnasamy 397
Comparison of SAPO-37 with Faujasites in Cracking Reactions
M. Briend, M. Derewinski, A. Lamy and D. Barthomeuf 409
Catalytic Activity of Modified ZSM-5 Zeolites in the Dehydrogenation and Aromatization Reactions of Propane and n-Butane
P. Fejes, J. Halász, I. Kiricsi, Z. Kele, Gy. Tasi, I. Hannus, C. Fernandez, J. B. Nagy, A. Rockenbauer and Gy. Schöbel 421
Mechanism of Coke Formation during the Transformation of Propene, Toluene and Propene-Toluene Mixture on HZSM-5
P. Magnoux, F. Machado and M. Guisnet 435
Hydrocarbon Formation from Methanol/Dimethyl Ether over Protonated Zeolites and Molecular Sieves. New Insights from Recent Experiments
S. Kolboe 449
H-D Exchange between Zeolites and Alkanes. Evidence for Formation and Rearrangement of Pentacoordinated Carbonium Ions
C. J. A. Mota, L. Nogueira, S. C. Menezes, V. Alekstich, R. C. L. Pereira and W. B. Kover 463
New Surface Nb-Dimers Chemically Interacted with SiO_2: Regulation of the Catalysis by Molecular Design of Reaction Sites
N. Ichikuni and Y. Iwasawa 477
Expert Systems Approach to Catalyst Design - Application and Experimental Verification
T. Hattori, H. Niwa, A. Satsuma, S. Kito and Y. Murakami 489
Metal Oxide Vapour Synthesis (MOVS): A New Preparative Method for Heterogeneous Metal Oxide Catalytic Systems
E. C. Alyea, K. F. Brown, K. J. Fisher and K. D. L. Smith 503
Designing of New Catalysts for Olefin Metathesis on the Base of Photoreduced Silica-Molybdena
V. B. Kazansky, B. N. Shelimov and K. A. Vikulov 515
SiO_2-Grafted Dinuclear Molybdenum Catalyst Derived from $Mo_2(OAc)_4$ Highly Active for Olefin Metathesis Reaction
M. Ichikawa, Q. Zhuang, G.-J. Li, K. Tanaka, T. Fujimoto and A. Fukuoka 529
Molecular Design of Supported Metal Oxide Catalysts
I. E. Wachs, G. Deo, D. S. Kim, M. A. Vuurman and H. Hu 543

Structural Characteristics of Alumina-Supported Activated Hydrodesulfurization Catalysts. An XPS, NO Adsorption and Sulphydryl Group Study
L. Portela, P. Grange and B. Delmon 559
Structure-Function Relations in Layered Transition Metal Sulfide Catalysts
M. Daage, R. R. Chianelli and A. F. Ruppert 571
Elementary Steps of Hydrogenative Sulfur-, Nitrogen- and Oxygen-Removal from Organic Compounds on Sulfided Catalysts
H. Schulz and N.M. Rahman 585
Sites Characterization on Model Ruthenium Sulphide
M. Lacroix, C. Mirodatos, M. Breysse, T. Decamp and S. Yuan 597
High Resolution Electron Microscopy Characterization of the Poorly Crystalline Structure of Molybdenum Disulfide-Based Catalysts
S. Fuentes, M. Avalos-Borja, D. Acosta, F. Pedraza and J. Cruz 611
Deuterium Solid State NMR Study of Molecular Mobility and Catalytic Dehydration of tert.-Butyl Alcohol on H-ZSM-5 Zeolite
A. G. Stepanov, A. G. Maryasov, V. N. Romannikov and K. I. Zamaraev 621
Stationary Liquid-Phase Homogeneous Transition Metal Catalysis
I. T. Horváth 635
An in situ Radioactive Tracer Technique for Studying Adsorption-Desorption Dynamics on a Working Catalyst
U. Schröder, L. Cider and N. - H. Schöön 643
Application of Scanning Tunneling Microscopy/Spectroscopy (STM/STS) to Catalyst Research: Pt/SiO_2
M. Komiyama and M. Kirino 659
Characterization and Catalytic Properties of Pt-Ir Small Bimetallic Cluster in NaY
O. B. Yang and S. I. Woo 671
Laser Raman Characterization of Surface Phase Precious Metal Oxides Formed on CeO_2 Micro Domains Generated within an Alumina Host by Sol Synthesis
L. L. Murrell, S. J. Tauster and D. R. Anderson 681
Direct Propane Ammoxidation to Acrylonitrile: Kinetics and Nature of the Active Phase
A. Andersson, S. L. T. Andersson, G. Centi, R. K. Grasselli, M. Sanati and F. Trifiro 691
Catalytic Oxidation of Fluorene to 9-Fluorenone - Development and Characterization of Catalysts
F. Majunke, H. Borchert and M. Baerns 707
Ammoximation of Cyclohexanone on Titanium Silicalite: Investigation of the Reaction Mechanism
A. Zecchina, G. Spoto, S. Bordiga, F. Geobaldo, G. Petrini, G. Leofanti, M. Padovan, M. Mantegazza and P. Roffia 719
On the Catalytic Oxidation of Methanol with Vanadium (IV) in Sulphuric Acid Solution
R. Larsson and B. Folkesson 731
Role of Chromium Introduced into 12-Molybdophosphates as Catalysts for Oxidation of Hydrocarbons
K. Brückman and J. Haber 741
Correlation between Catalytic and Structural Properties of Modified Molybdenum and Vanadium Oxides in the Oxidation of Ethane in Acetic Acid or Ethylene
M. Merzouki, B. Taouk, L. Tessier, E. Bordes and P. Courtine 753
The Promoting Effect of La_2O_3 on the CO Hydrogenation over Rh/SiO_2
A. L. Borer and R. Prins 765
Effect of Chlorine on the Rhenium-Alumina Interaction in Low-Loaded Re/Al_2O_3 and $PtRe/Al_2O_3$ Industrial Catalysts
G. Munuera, P. Malet and A. Caballero 781

A New Approach to Loss of Alkali Promoter from Industrial Catalysts: Importance of Excited States of Alkali
L. Holmlid, K. Engvall, C. Aman and P. G. Menon 795
The Relation between Catalytic and Electronic Properties of Supported Platinum Catalysts: The Local Density of States as Determined by X-Ray Absorption Spectroscopy
M. Vaarkamp, J. T. Miller, F. S. Modica, G. S. Lane and D. C. Koningsberger 809
Direct MAS/MES Evidence for Electronic Metal-Support Interactions in Dilute ^{57}Co and ^{57}Fe Carbon and Alumina-Supported Catalysts
C. H. Bartholomew, L. R. Neubauer and P. A. Smith 821
Formation and Properties of Dispersed Pd Particles over Graphite and Diamond
O. S. Alekseev, L. V. Nosova and Yu. A. Ryndin 837
Kinetics of Alkane Hydrogenolysis on Clean and Coked Platinum and Platinum-Rhenium Catalysts
G. C. Bond, R. H. Cunningham and E. L. Short 849
Toluene Hydrogenation over Supported Platinum Catalysts
S.-D. Lin and M. A. Vannice 861
The Catalytic Activity of MoO_x/ZrO_2 in the Hydrogenation and Metathesis of Propene
V. Indovina, A. Cimino, D. Cordischi, S. Della Bella, S. De Rossi, G. Ferraris, D. Gazzoli, M. Occhiuzzi and M. Valigi 875
Pt-Sn-Alumina Catalysts: Relating Characterization and Alkane Dehydrocyclization Data
B. H. Davis 889
Bimetallic $Pt\text{-}Sn/Al_2O_3$ and $Pt\text{-}Au/SiO_2$ Catalysts: A Comparison of Reactivity, Adsorption behavior and Microstructure
J. Schwank, K. Balakrishnan and A. Sachdev 905
Hydroformylation of 1-Hexene by Soluble and Zeolite-Supported Iridium Species
J.-Z. Zhang, Z. Li and C.-Y. Wang 919

PART B
Bulk Tungsten Carbide as Catalyst in Hydrocarbon Reactions: Association of Selectivity Differences with Surface Composition as Compared to the Selectivity of Pt Series Metals
A. Frennet, G. Leclercq, L. Leclercq, G. Maire, R. Ducros, M. Jardinier-Offergeld, F. Bouillon, J-M. Bastin, A. Löfberg, P. Blehen, M. Dufour, M. Kamal, L. Feigenbaum, J-M. Giraudon, V. Keller, P. Wehrer, M. Cheval, F. Garin, P. Kons, P. Delcambe and L. Binst 927
Surface and Catalytic Properties of Molybdenum Nitrides
L. T. Thompson, C. W. Colling, D. Choi, B. G. Demczyk and J.-G. Choi 941
n-Hexane Isomerization on High Specific Surface Mo_2C Activated by an Oxidative Treatment
M. J. Ledoux, C. Pham-Huu, H. Dunlop and J. Guille 955
Highly Dispersed Metal Colloids: Spectroscopy and Surface Chemistry in Solution
J. S. Bradley, J. M. Millar, E. W. Hill, C. Klein, B. Chaudret and A. Duteuil 969
Preparation of Amorphous Cu-Ti and Cu-Zr Alloys of High Surface Area by Chemical Modification
S. Yoshida, T. Kakehi, S. Matsumoto, T. Tanaka, H. Kanai and T. Funabiki 981
A Mechanistic Proposal for Alkane Dehydrocyclization Rates on Pt/L-Zeolite. Inhibited Deactivation of Pt Sites within Zeolite Channels
E. Iglesia and J. E. Baumgartner 993
Hydroconversion of n-Alkanes and Decalin over Bifunctional Pt/Mazzite Catalysts
F. Fajula, M. Boulet, B. Coq, V. Rajaofanova, F. Figueras and T. Des Courieres . . . 1007

Effect of Sulfur on the Performance of Pt/KL Hexane Aromatization Catalyst
J. L. Kao, G. B. McVicker, M. M. J. Treacy, S. B. Rice, J. L. Robbins, W. E. Gates, J. J. Ziemiak, V. R. Cross and T. H. Vanderspurt 1019
Aromatization of n-Hexane by Aluminium-Stabilized Magnesium Oxide-Supported Noble Metal Catalysts
E. G. Derouane, V. Jullien-Lardot, R. J. Davis, N. Blom and P. E. Hojlund-Nielsen . . 1031
Effect of the Alkali Cation on Heptane Aromatization in L Zeolite
R.F. Hicks, W.-J. Han and A. B. Kooh 1043
Reduction and Aromatization Activity of MoO_3/Al_2O_3 Catalysts: The Identification of the Active Mo Oxidation State on the Basis of Reinterpreted Mo 3d XPS Spectra
W. Grünert, A. Yu. Stakheev, R. Feldhaus, K. Anders, E. S. Shpiro and Kh. M. Minachev 1053
Reaction Routes for Methane Conversion on Transition Metals at Low Temperature
T. Koerts and R. A. Van Santen 1065
The Mechanism of Alkane Oxidative Dehydrogenation on Chloride and Oxychloride Catalysts
R. Burch, S. Chalker and P. Loader 1079
Transient Isotopic Studies of the Role of Lattice Oxygen during Oxidative Coupling of Methane on Sr/La_2O_3 and Ca/ThO_2 Catalysts
Z. Kalenik and E. E. Wolf 1093
The Role of the Proton in Oxidation Processes on Metal-Oxygen Cluster Compounds
S. Kasztelan, G. B. McGarvey and J. B. Moffat 1105
Correlations between p-Type Semiconductivity and C_2 Selectivity for Oxidative Coupling of Methane (OCM) over Acceptor Doped $SrTiO_3$
C. Yu, W. Li, W. Feng, A. Qi and Y. Chen 1119
Mechanistic Aspects of the Selective Oxidation of Methane to C_1-Oxygenates over MoO_3/SiO_2 Catalysts in a Single Catalytic Step
M. A. Banares, I. Rodriguez-Ramos, A. Guerrero-Ruiz and J. L. G. Fierro 1131
On the Mechanism of Xylene Isomerization and its Limitations as Reaction Test for Solid Acid Catalysts
A. Corma, F. Llopis and J. B. Monton 1145
Aluminum Coordination and Lewis Acidity in Aluminas and Steamed Zeolites
H. Yong, D. Coster, F. R. Chen, J. G. Davis and J. J. Fripiat 1159
Characterization of Basic Sites on Fine Particles of Alkali and Alkaline Earth Metal Oxides in Zeolites
H. Tsuji, F. Yagi, H. Hattori and H. Kita 1171
ZrO_2-SO_4^{2-} Catalysts. Nature and Stability of Acid Sites Responsible for n-Butane Isomerization
P. Nascimento, C. Akratopoulou, M. Oszagyan, G. Coudurier, C. Travers, J.F. Joly and J. C. Vedrine 1185
Catalytic Activity for Vapor-Phase Aldol Condensation and Acid-Base Properties of Metal-Oxide Catalysts
M. Ai 1199
Reactions of Multifunctional Organic Compounds - Hydrogenation of Acrolein on Modified Pt-Catalysts
T. B. L. W. Marinelli, J. H. Vleeming and V. Ponec 1211
Acetonitrile Synthesis from CO, H_2 and NH_3 over Fe/C and K,Fe/C
M. V. Badani, L. M. Eshelman and W. N. Delgass 1223
Reductive Amination of Diethylene Glycol to Morpholine on Supported Nickel Catalysts - Its Activity, Selectivity, Stability and Possibility of Reactivation
K. Jiratova, O. Solcova, H. Snajdaufova, L. Moravkova and H. Zahradnikova 1235
An Improved Asymmetric Oxidation of Sulfides to Sulfoxides by Titanium Pillared Montmorillonite - The First Example in Heterogeneous Catalysis
B. M. Choudary, S. Shobha Rani and Y. V. Subba Rao 1247

Hydrogenation of CO_2 over Copper, Silver and Gold/Zirconia Catalysts: Comparative Study of Catalyst Properties and Reaction Pathways
A. Baiker, M. Kilo, M. Maciejewski, S. Menzi and A. Wokaun 1257
Shape-Selective Reactions for Methylamine Synthesis from Methanol and Ammonia
K. Segawa and H. Tachibana 1273
Selective Catalytic Reduction of NO by Hydrocarbon in Oxidizing Atmosphere
M. Iwamoto, N. Mizuno and H. Yahiro 1285
The Making of Catalysts by Controlled Oxidative Degradation of Planar Metal Complexes on Alumosilicate Supports: Exhaust Gas Purification Catalysts for Power Plants, Automobiles and Small Outfits
F. Steinbach, A. Brunner, H. Müller, A. Drechsler, S. Frömming, W. Strehlau and U. Stan 1299
Oxidation of CO on Pd Particles on α-Al_2O_3: Reverse Spillover
L. Kieken and M. Boudart 1313
Microkinetic Analysis of the Selective Catalytic Reduction (SCR) of Nitric Oxide over Vanadia/Titania-Based Catalysts
J. A. Dumesic, N.-Y. Topsoe, T. Slabiak, P. Morsing, B. S. Clausen, E. Törnqvist and H. Topsoe 1325
An Infrared Study of an Active NO Decomposition Catalyst
J. Valyon and W. K. Hall 1339
Acidity of WO_x/TiO_2 Catalysts for Selective Catalytic Reduction (SCR)
F. Hilbrig, H. Schmelz and H. Knözinger 1351
Membrane Catalysis over Palladium and its Alloys
J. N. Armor and T. S. Farris 1363
Fixed Bed Catalytic Reactors Based on Sintered Metals
F. van Looij, A. Mulder, A. Q. M. Boon, J. F. Scheepens and J. W. Geus 1377
Mixed Spinels with Cerium--SO_x Emission Control from Fluid Catalytic Cracking (FCC) Regenerator
J. S. Yoo, A. A. Bhattacharyya, C. A. Radlowski and J. A. Karch 1391
Sintering, Poisoning and Regeneration of Pt/MgO
J. Adamiec, J. A. Szymura and S. E. Wanke 1405
Development of a Micro Hydroprocessing Test for Rapid Evaluation of Catalysts
C. Sudhakar, L. T. Mtshali, P. O. Fritz and M. S. Patel 1419
Alkali Promoter Synergism in Selective Oxidation
M. M. Bhasin and C. D. Hendrix 1431
C-C Bond Formation via β-Addition with Oxygen Retention Reversal in Oxygenate Synthesis
K. Klier, R. G. Herman, P. B. Himelfarb, C.-W. Young, S. Hou and J. A. Marcos . . . 1441
Selective Gasoline Synthesis from CO_2 on a Highly Active Methanol Synthesis Catalyst and an H-Fe-Silicate of MFI Structure
T. Inui, T. Takeguchi, A. Kohama and K. Kitagawa 1453
The Selective Synthesis of C_2+ Oxygenates from Syngas Related Reactions over Ni- and Rh-Based Catalysts
M. W. Balakos, S. S. C. Chuang, R. Krishnamurthy and G. Srinivas 1467
Development of New Catalysts Formulations for Higher Alcohols Synthesis. Characterisation, Reactivity, Mechanistic Studies and Predictive Correlations
A. Kiennemann, S. Boujana, C. Diagne and P. Chaumette 1479
Characterization of MoS_x-K^+/SiO_2 Catalysts for Synthesis of Mixed Alcohols from Syngas
H.-B. Zhang, Y.-Q. Yang, H. P. Huang, G. D. Lin and K. R. Tsai 1493
Catalytic Activity of Reduced $Cu_xZn_{(1-x)}O$ and $CuO/Cu_xZn_{(1-x)}O$ in CO_2/H_2 Reactions
D. Stirling, F. S. Stone and M. S. Spencer 1507

Reactivities of Surface Intermediates on an Sm_2O_3 Catalyst Studied by in situ Infrared Spectroscopy
Y. Sakata, M. Yoshino, T. Fukuda, H. Yamaguchi, H. Imamura and S. Tsuchiya 1519
In situ Investigation of the Water-Gas Shift Reaction over Magnetite by Mössbauer Spectroscopy
A. Andreev, I. Mitov, V. Idakiev, T. Tomov and S. Asenov 1523
In situ FT-IR Study of O_2, CO, CO_2, CH_4 and C_2H_4 Adsorption or Reaction on the La_2O_3/MgO Catalyst
S. Shen, R. Hou, , W. Ji, Z. Yan and X. Ding 1527
Study by in situ Laser Raman Spectroscopy of a VPO Catalyst in the Course of n-Butane Oxidation to Maleic Anhydride
J. C. Volta, R. Olier, M. Roullet, F. B. Abdelouahab and K. Bere 1531
Investigation of Water-Gas Shift Reaction Under Dynamic Conditions
P. Capek and K. Klusacek 1535
Application of the Transient Response Method to the Study of the Catalytic System $NO+O_2+CO/CuO$
D. Panayotov and D. Mehandjiev 1539
Characterization and Activity of Vanadium Oxide Catalysts in Selective Catalytic Reduction of Nitric Oxide
U. S. Ozkan, Y. Cai, M. W. Kumthekar and L. Zhang 1543
Theoretical Study of CO Chemisorption on Rh and Pd Clusters
A. Goursot, I. Pápai and D. R. Salahub 1547
New Dynamic Method Approach to the Roles of Reversible and Irreversible Adsorption in Heterogeneous Catalysis
G. Lu, S. Chen and S. Peng 1551
Discrimination and Regulation of Multi-Reaction Pathways in Heterogeneous Catalysis
M. Kobayashi, T. Kanno and M. Hakozaki 1555
Adsorption Study by Transient Tracing Methods. Theory and Modeling
P. Szedlacsek, A. Efstathiou, C.O. Bennett and S. L. Suib 1559
In situ Determination of Surface Carbon Species Formed on Rh/Al_2O_3 during CO/H_2 Reaction by Using Various Transient and Isotopic Methods
A. M. Efstathiou, T. Chafik, D. Bianchi and C. O. Bennett 1563
The Calculation of Surface Orbital Energies for Specific Types of Active Sites on Dispersed Metal Catalysts
R. L. Augustine, K. M. Lahanas and F. Cole 1567
Oxidation and Removal of Chlorinated Hydrocarbons
J. M. Berty, H. G. Stenger, Jr., G. E. Buzan and K. Hu 1571
Structure and Reactivity of Carbidic Intermediates for the Methanation Reaction on Ni(100), Ni(111) and Ni(110) Surfaces
H. Hirano and K. Tanaka 1575
Cl Adsorption on Ag(111) and its Promoter Action
D. Wang, K. Wu, Y. Cao, X. Wei and X. Guo 1579
The $NO+H_2$ Reaction on Pt(100): Steady State and Oscillatory Kinetics
M. Slinko, T. Fink, T. Löher, H. H. Madden, S. J. Lombardo, R. Imbihl and G. Ertl . . 1583
HREELS/TDS Identification of Intermediates in the Low-Temperature H_2+O_2, $NO+H_2$, NH_3+O_2 Reactions on Pt(111) Surface
V. V. Gorodetskii, M. Yu. Smirnov and A. R. Cholach 1587
Surface Science Studies on the Mechanism for H-D Exchange of Methane over Pt(111) Surfaces Under Vacuum
F. Zaera 1591
Catalysis at Experimentally Designed Surfaces: n-Butane Hydrogenolysis at Sn/Group VIII Surface Alloys
A. D. Logan and M. T. Paffett 1595

Surface Science and Kinetic Studies on Model Cu/Rh(100) Catalysts
J. Szanyi and D. W. Goodman 1599
Angular Distribution of Desorbing Reaction Products and Dynamics of Some Catalytic Processes on the Surfaces of Pt and Ir
M. U. Kisliuk, V. V. Savkin, T. N. Bakuleva, A. G. Vlasenko, V. V. Migulin, I. I. Tretiakov and A. V. Sklyarov 1603
Ship-in-Bottle Synthesis of NaY Zeolite-Included Pt_9 and Pt_{12} Carbonyl Clusters: Structures and Catalysis in CO+NO Reaction
G.-J. Li, T. Fujimoto, A. Fukuoka and M. Ichikawa 1607
The Preparation and Characterization of High-Silica Y Zeolite Prepared by Combined Chemical and Hydrothermal Dealumination
X. Liu, Z. Pei, L. She, X.-W. Li, J. Shao, S. Lin, R. Tang and X. Mao 1611
Active Sites of Novel Iron Supported Y-Type Zeolite
R. Iwamoto, I. Nakamura and A. Iino 1615
A Novel Application of XRD Technique for the Characterization of Secondary Pore Structure in Modified Y-Zeolites
S. D. Phatak, R. P. Mehrotra, S. M. Dhir and T. S. R. Prasada Rao 1619
IR-Spectroscopic Evidence for Acetonitrile Interaction with Carbenium Ions in Zeolites
D. S. Bystrov, A. A. Tsyganenko and H. Forster 1623
Acid-Base Properties of Zeolites: An XPS Approach Using Pyridine and Pyrrole Probe Molecule
R. B. Borade, M. Huang, A. Adnot, A. Sayari and S. Kaliaguine 1625
Sulfate as Promotor of Acidity of High Microporous and Thermostable Titanium Pillared Montmorillonite
F. Admaiai, A. Bernier and P. Grange 1629
Platinum Cluster Supported on Zeolite A by Ion Exchange of $Pt(NH_3)_4^{2+}$
R. Ryoo and S. J. Cho 1633
Preparation of Thermalstable Pillared Clays
S. Mendioroz, F. Gonzalez, C. Pesquera, I. Benito, C. Blanco and G. Poncelet 1637
In situ X-Ray Analysis of CO- and CH_3OH-Induced Growth of Pd Particles Encaged in Zeolite Y
W. Vogel 1641
Metal-Support Interactions on Pd-Containing Zeolite Catalysts
M. F. Savchits, Eh. Ya. Ustilovskaya, V. Z. Veshtort, L. A. Agabekova and Yu. G. Egiazarov 1645
Transfer of Metal Ions between Metal Oxides and Zeolites. Preparation of Highly Active Cu-Zeolite Based Catalysts for Reduction of NO_x at Low Temperature
B. Wichterlova, Z. Sobalik, M. Petras, I. Jirka and V. Bosacek 1649
Microkinetic Analysis of Isobutane Reactions Catalyzed by Y Zeolite
J. E. Rekoske, R. J. Madon, L. M. Aparicio and J. A. Dumesic 1653
Peculiarities of Ethylene Conversion on Zeolites and Phosphoric Acid
A. G. Anshits, S. N. Vereshchagin and N. N. Shishkina 1661
Benzene Alkylation in Vapour-Phase with Ethene on a Zeolite Catalyst
G. Maria, G. Pop, G. Musca and R. Boeru 1665
On the Nature of Zeolite Catalyst Effect on the Selectivity of Toluene Nitration by Acyl Nitrates
S. M. Nagy, K. A. Yarovoy, L. A. Vostrikova, K. G. Ione and V. G. Shubin 1669
Interactions in Monoalkylbenzenes Disproportionation Among Zeolite Characteristics and Reaction Mechanisms
I. Wang, T.-C. Tsai and C.-L. Ay 1673
New Support Materials for Rhodium Catalysts: Characterization of Rh/$AlPO_4$-31 and Rh/MnAPO-31
A. Trunschke, H. Zubowa, B. Parlitz, R. Fricke and H. Miessner 1677

Transformation of Thiols and Organic Sulfides over Zeolites
M. Ziolek and P. Decyk 1681
Para-Selectivity of ZSM-5 Type Metallosilicates for Alkylation of Toluene with Methanol
S. Namba, H. Ohta, J.-H. Kim and T. Yashima 1685
Hydroxylation of Toluene with Hydrogen Peroxide on HY Zeolites with Various Si/Al Ratios
T. Yashima, Y. Kobayashi, T. Komatsu and S. Namba 1689
Toluene Alkylation over Aluminophosphate-Based Molecular Sieves
S. H. Oh and W. Y. Lee 1693
The Cracking Reaction Path in 1-Hexene Isomerization on SAPO-11 and Pd/SAPO-11
S.-Y. Lim and S.-J. Choung 1697
Epoxidation of Alkenes Catalyzed by Decatungstate as Pillars in Layered Double Hydroxides
T. Tatsumi, H. Tajima, K. Yamamoto and H. Tominaga 1703
Conversion of Ethane into Aromatic Compounds on ZSM-5 Zeolites Modified by Zinc
F. Roessner, A. Hagen, U. Mroczek, H. G. Karge and K.-H. Steinberg 1707
In Situ FTIR and GC Kinetic Studies: Complementary Methods in the Mechanistic Study of Butanol Dehydration on Zeolite H-ZSM-5
M. A. Makarova, E. A. Paukshtis, J. M. Thomas, C. Williams and K. I. Zamaraev . . . 1711
Catalytic Properties of Ferrisilicate Analogs of Some Medium Pore Zeolites in C_7 and C_8 Aromatic Hydrocarbon Reations
A. Raj, K. R. Reddy, J. S. Reddy and R. Kumar 1715
The Influence of the Catalyst Preparation on the Catalytic Properties of Zeolite-Supported Catalysts
Y. W. Chen and W. J. Wang 1719
Reactions of Acetone, Methanol and Ammonia on ZSM-5 Zeolites
J. Novakova, L. Bosacek, Z. Dolejsek and L. Kubelkova 1723
Regioselective Hydrogenation Using Platinum-Support Zeolite Modified by CVD-Method
H. Kuno, M. Shibagaki, K. Takahashi, I. Honda and H. Matsushita 1727
Nickel, Cobalt and Zinc Substituted Synthetic Mica-Montmorillonite: Synthesis, Characterization and Propene Oligomerization Activity
J. C. Q. Fletcher, A. P. Vogel and C. T. O'Connor 1731
Isobutane/1-Butene Alkylation on Pentasil-Type Zeolite Catalysts
J. Weitkamp and P. A. Jacobs 1735
Active Sites in HZSM-5 and SAPO Molecular Sieves for Alcohol Conversion
C. Bezouhanova, Yu. Kalvachev and H. Lechert 1739
The Synthesis of Cobalt Supported Catalysts by Electroless Plating Techniques
N. J. Coville, S. E. Colley, J. A. Beetge and S. W. Orchard 1743
A New Precursor for the Preparation of Novel Copper Chromite Catalysts
R. Prasad 1747
Pd_1Fe_{99}: Pd Surface Segregation and Catalytic Activity
J. C. Bertolini, Y. Debauge, P. Delichere, J. Massardier, J.L. Rousset, P. Ruiz and B. Tardy 1751
A Study of Spreading of Vanadia on Titania Polymorphs Using Mechanical Mixtures
M. Sanati, A. Andersson and L. R. Wallenberg 1755
Structure and Activity of Copper Catalysts Prepared from Amorphous Cu-Zr and Cu-Ti Alloy Precursors: A Comparative Study
Á. Molnár, T. Katona, Cs. Kopasz and Z. Hegedüs 1759
Preparation of W/Al_2O_3 by Chemisorption of $WOCl_4$ to Surface Saturation
M. Lindblad and L. P. Lindfors 1763

Highly Active V_2O_5 Thin Films Prepared by Chemical Vapor Deposition on Silica for Oxidative Dehydrogenation of Alcohols
T. Okuhara, K. Inumaru, M. Misono and N. Matsubayashi 1767
Influence of the Chemical Composition on the Preparation of Cu-Co-Zn-Al Mixed Oxide Catalysts with a High Metal Dispersion
A. J. Marchi, J. I. Di Cosimo and C. R. Apesteguia 1771
Sol-Gel Derived Heterogeneous Catalysts
T. Walton and P. A. Sermon 1775
Forming of Pyrogenic SiO_2 and TiO_2 and their Applications as New Types of High Surface Area Catalyst Supports
M. Bankmann, B. Despreyroux, H. Krause, J. Ohmer and R. Brand 1781
New Preparation Method of Small Particles in Ni/SiO_2 Catalysts Involving Chelate Ligands
Z. X. Cheng, C. Louis and M. Che 1785
Stepwise Monitoring of Mixed Oxide Catalyst Preparations by XAS Spectroscopy
O. Clause and M. Che 1789
Improving SO_2 Resistence of Base Metal Perovskite Type Oxidation Catalyst
W. Li, H. Dai and Y. Lieu 1793
Carbide Catalysts: Laser Pyrolysis Synthesis and Catalytic Activity
J. M. Stencel, P. C. Eklund, X.-X. Bi, B. H. Davis, G.T. Hager and F.J. Derbyshire . . 1797
Structural Support Effects in the Systematic Preparation of Pd/SiO_2 Catalyst for Methanol Synthesis by Ion Exchange Techniques
A. L. Bonivardi, M. A. Baltanas and D. L. Chiavassa 1801
The Advantageous Use of Microwave Radiation in the Preparation of Supported Nickel Catalysts
G. Bond, R. B. Moyes, S. D. Pollington and D. A. Whan 1805
New Preparation Methods for Active Superfine Catalysts by Spray Reaction
T. Uematsu, S. Shimazu, T. Kameyama and K. Fukuda 1809
Preparation of Supported Cu-Ni Bimetallic Catalysts by Alkoxide Method with High Activities for Hydrogenation or Dehydrogenation
T. Sodesawa, S. Sato and F. Nozaki 1813
Dy-Cu Alloy Films: Catalytic Activity, Composition, Structure
K. N. Zhavoronkova and O. A. Boeva 1817
Adsorption and Catalytic Properties of Highly Disperse Silver Catalysts
N. E. Bogdanchikova, D. A. Bulushev, Yu. D. Pankratiev and A. V. Khasin 1823
New Insight into the Changing Catalyst/Polymer Morphology during Olefin Polymerization: The Application of Tomography
W. C. Conner, M. Ferrero, S. Webb, R. Sommer, M. Chiovetta, K. Jones and P. Spanne 1827
Catalytical and High Resolution Electron Microscopy Studies of the System $Pt/ZnAl_2O_4$ with Several Platinum Contents
G. Aguilar-Rios, M. A. Valenzuela, D. R. Acosta and I. Schifter 1831
The Application of Dilatometry for Investigation of Heterogeneous Catalysts
L. A. Rudnitsky and A. M. Alekseev 1835
Artificial Control of Catalytic Activity of Pd by a Shear Horizontal Surface Acoustic Wave
Y. Inoue, H. Kawaguchi, M. Matsukawa and K. Sato 1839
Characterization of Silica-Supported Palladium-Cobalt Alloys
W. Juszczyk, Z. Karpinski, Z. Paál, J. Pielaszek 1843
Temperature-Programmed Reduction in Catalysis: A Critical Evaluation of the Method
G. Fierro, M. Lo Jacono, M. Inversi, G. Moretti, P. Porta and R. Lavecchia 1847

Scanning Tunneling Microscopy Study of Pd/Graphite: Microstructure and Reactivity
K. L. Yeung and E. E. Wolf 1851
IR Study of Adsorption and Deuteration of d_6-Acetone on Pt/ZnO Catalysts: Effects of the Sample Pretreatments
F. Boccuzzi, G. Ghiotti and A. Chiorino 1855
Surface Energetic Characterization of Supported Metal Catalysts by Gas/Solid Titration Microcalorimetry
J. M. Guil, A. P. Masia, A. R. Paniego and J. M. T. Menayo 1859
Study of the Effects of Annealing on the Morphology of Platinum Cluster Size on Highly Oriented Pyrolytic Graphite by Scanning Tunneling Microscopy
S. Lee, H. Permana and K. Y. S. Ng 1863
Distribution of Mo Oxidation States in Reduced Mo/Al_2O_3 Catalysts. Correlation with Catalytic Activity
J. Yasumaru, M. Yamada, M. Houalla and D. M. Hercules 1867
Effect of Catalyst Preparation on the Performance of Supported Ru-Cu Bimetallic Systems
R. Maggiore, C. Crisafulli, S. Scire and S. Galvagno 1871
Revisiting Diffuse Reflectance Spectroscopy for the Characterization of Metal and Semiconducting Oxide Catalysts
A. Rakai, A. Bensalem, J. C. Muller, D. Tessier and F. Bozon-Verduraz 1875
The Thermal Stability of the Adsorbed/Lattice Oxygen Species on the Oxide Catalysts Surfaces
M. Caldararu and N. I. Ionescu 1879
Chemical Anchoring of Noble Metal Amine Precursors to Silica: An in situ UV Diffuse Reflectance Study
W. Zou and R. D. Gonzalez 1883
Reaction Sites on the Al_2O_3 Support of Pd/Al_2O_3
J. L. Falconer, B. Chen, S. A. Larson and E. C. Hsiao 1887
The External Magnetic Field Effect on the H_2-O_2 Reaction on the SnO_2 Surface
H. Ohnishi, H. Sasaki and M. Ippommatsu 1891
Characterization of Different Surface Mo Species in Mo/Al_2O_3 Catalysts by Time Differential Perturbed Angular Correlation
S. Guida, Y. Tingyun, Y. Fushan, R. Liguo and N. Xinbo 1895

PART C
New Catalytic Phases for the HDN and MHC Reactions in CoMoP-Alumina Catalysts
A. Morales, R. Prada-Silvy and V. Leon 1899
Multi-Purpose $Ni-Mo/Al_2O_3$ Catalysts for Gas Oil Hydrotreating
A. F. Somogyvári, M. C. Oballa and P. S. Herrera 1903
Characterization of Phosphorus Containing $Ni-W/Al_2O_3$ Catalysts
P. Atanasova and T. Halachev 1907
Concerted Mechanism of Thiophene Hydrogenolysis by Sulfide HDS Catalysts
A. N. Startsev 1911
Highly Active $Ni-W/Al_2O_3$ Catalyst for Upgrading Unconventional Feedstocks
H. Shimada, T. Kameoka, H. Yanase, M. Watanabe, A. Kinoshita, T. Sato, Y. Yoshimura, N. Mastubayashi and A. Nishijima 1915
Adsorption and Activation of Thiophene on MoS_2, Co_9S_8 and RuS_2
C. Rong and X. Qin 1919
Correlation of HDS Activity with Heat of Adsorption over Carbon Supported CoMo Catalysts
S.-K. Ihm, Y.-H. Moon and C.-D. Ihm 1923

Effect of Fluoride on the Surface Structure of WO_3/Al_2O_3 Hydrotreating Catalysts
R. L. Cordero, J. R. Solis, J. V. G. Ramos, A. B. Patricio and A. L. Agudo 1927
Hydrodesulfurization Activity of Zeolite Supported Nickel- and Cobalt Sulfide Catalysts
W. J. J. Welters, T. I.Korányi, V. H. J. de Beer and R. A. van Santen 1931
Enhanced HDS Activity via Multiple Impregnation of Sulfided Mo/Al_2O_3 Catalysts
C.-S. Kim, F. E. Massoth, C. Geantet and M. Breysse 1935
Surface Structure of Molybdenum Nitride and its Activity for Hydrodesulfurization and Hydrodenitrogenation
M. Nagai, T. Miyao, T. Tsuboi and T. Kusagaya 1939
Hydrocracking Gas Oils from Synthetic Crude with Mixed Pillared Clay-Alumina Supported Catalysts
J. Monnier, J.-P. Charland, J. R. Brown and M. F. Wilson 1943
Transformations of Thiophene, Tetrahydrothiophene and Butanethiol over Co-Black, Co/Al_2O_3, Mo/Al_2O_3 and $Co\text{-}Mo/Al_2O_3$ during Temperature-Programmed Reaction
V. V. Rozanov, Y. Tzao and O. V. Krylov 1947
Partial Oxidation Reaction of Methane with Oxygen or Carbon Dioxide by Transition Metal Catalysts Supported on Ultrafine Single-Crystal Magnesium Oxide
O. Takayasu, I. Matsuura, K. Nitta and Y. Yoshida 1951
Surface Oxygen Species and their Reactivities in the Oxidation of CH_4, C_2H_6 and C_2H_4 over Cerium Oxide at Mild Temperatures
C. Li, Q. Xin, X. Guo and T. Onishi 1955
Oxidative Catalytic Conversions of Tetrahydrofuran Derivatives
R. Skolmeistere, L. Leitis, M. Fleisher and M. Shymanska 1959
Role of Mo and Sb in Oxide Catalysts for Selective Oxidation of Propylene
B. Zhou, X. Guo and K. T. Chuang 1963
Partial Oxidation of Methane at Low Pressure over Silica Gel and Silica-Supported Sn, Zr and Ge Oxides
T. Ono, K. Ikuta and Y. Shigemura 1967
The Influence of the Support on the Performance of Heterogeneous Catalysts for the Wacker Oxidation of Alkenes
A. W. Stobbe-Kreemers, J. J. F. Scholten, M. Soede and J. W. Veenman 1971
Optimization of $NiO/MoO_3/TeO_2$ Catalytic System for Direct Oxidation of Propene to Acrylic Acid
C. Mazzocchia, R. Anouchinsky, A. Kaddouri and E. Tempesti 1975
Role of Amorphous Phase and its Modification in V-P-O Catalysts for Maleic Anhydride Synthesis from Butane
N. Yamazoe, H. Morishige, J. Tamaki and N. Miura 1979
Selective Oxidation and Ammoxidation of Propane to form Acrolein and Acrylonitrile
Y. Moro-oka, N. Miura, N. Fujikawa, Y.-C. Kim and W. Ueda 1983
Oxidation of Propene on Alkaline Metal-Doped MoO_3/TiO_2 Catalysts: A FT-IR Study
C. Martin, I. Martin, C. Mendizabal and V. Rives 1987
Oxidation of Methanol to Formaldehyde over Antimony-Molybdenum Oxide Catalyst
R. S. Mann and R. A. Diaz-Real 1991
A Comparison between Epoxidation and Degradation of Ethylene and Propylene over Silver
C. Henriques, M. F. Portela, C. Mazzocchia and E. Guglielminotti 1995
Liquid-Phase Oxidation of Benzene with Molecular Oxygen Catalyzed by Cu-Zeolites
T. Ohtani, S. Nishiyama, S. Tsuruya and M. Masai 1999

Formation of Formaldehyde from Methanol over Supported Titanium Oxide
H. Imai, Y. Murakami and H. Irikawa 2003
A Study on P-Mo-As Heteropoly Compounds as Catalyst for Selective Oxidation of Methacrolein
B. Zhong, W. Zheng, R. He, G. Huang and X. Li 2007
Silica as an Ammoximation Catalyst for the Production of Cyclohexanone Oxime
D. P. Dreoni, D. Pinelli, F. Trifiro, Z. Tvaruzkova, K. Habersberger and P. Jiru . . . 2011
Kinetics of the Redox Reactions of the O_2:Propylene:γ-Bismuth Molybdate System: A TAP Reactor Study
D. R. Coulson, P. L. Mills, K. Kourtakis, P. W. J. G. Wijnen, J. J. Lerou and L. E. Manzer 2015
Partial Oxidation of Propene in the Presence of Steam
Y. A. Saleh-Alhamed, R. R. Hudgins and P. L. Silveston 2019
The Kinetics of Activation of Industrial and Model Iron Catalysts for Ammonia Synthesis in Dried and Wet Atmosphere
A. Baranski, A. Kotarba, J. M. Lagan, A. Pattek-Janczyk, E. Pyrczak and A. Reizer . . 2023
The Modifying Role of Ru, Mo and Rare-Earth Elements (REE) in the Creation of New Generation of Catalysts Based on Iron Hydroxides
R. V. Chesnokova, L. M. Dmytrienko, I. G. Brodskaja, A. M. Alekseev, A. A. Vasilevitch, N. A. Dubyaga and I. I. Bondartsova 2027
The Role of Various Modes of Adsorbed CO in Synthesis Gas Conversion on Lanthanide Ions Promoted by Supported Pd Catalysts
Yu. N. Nogin, N. V. Chesnokov and V. I. Kovalchuk 2031
Influence of the Interaction of Support with Active Species on Sintering and Stability of Alumina Supported Oxide Catalysts
O. A. Kirichenko, M. P. Vorob'eva and V. A. Ushakov 2035
Structural Transformation and Catalytic Behaviors of Rhodium Ternary Oxides during Calcination and Reduction Treatments
K. Kunimori, H. Oyanagi, H. Shindo, T. Ishigaki and T. Uchijima 2039
Marked Support Effect of Dispersed ZrO_2 Catalysts in Propene-Deuterium Addition and Exchange Reaction
S. Naito, M. Tanimoto, M. Soma and Y. Udagawa 2043
Acidity Generation of Binary Metal Oxide Catalysts
A. Gervasini, G. Bellussi, J. Fenyvesi and A. Auroux 2047
Effects of Potassium Addition on the Performance of a Nickel/Magnesia Catalyst for Steam Reforming of Methane
S. Kitabayashi, Y. Ogino, T. Yamazaki and S. Ozawa 2051
Weakening of Hydrogen Poisoning by Sm_2O_3 Promoter in Activation of Dinitrogen on Ru/Al_2O_3 Catalyst
Y. Kadowaki, S. Murata and K.-I. Aika 2055
XANES, EXAFS and Reaction Studies of Some Well-Dispersed Ferric Oxide Catalysts
W. Ji, Y. Kuo, S. Shen, S. Li and H. Wang 2059
CO_2 Derivatives Adsorbed on Promoted Surfaces
J. A. K. Paul, Y. Shao and O. Axelsson 2063
The Effect of Metallic Promoters on Supported Cobalt Catalysts
A. Hoff, E. A. Blekkan, A. Holmen and D. Schanke 2067
The Structure-Activity Relationship of Re_2O_7 Metathesis Catalysts Supported on Phosphated Alumina and Silica-Alumina
R. Spronk and J. C. Mol 2071
Modification of the Site Structure of $MoS_2/\gamma\text{-}Al_2O_3$ Catalysts by Addition of P, F and Alkaline Elements
O. Poulet, R. Hubaut, S. Kasztelan and J. Grimblot 2075

Cerium Oxides Supported on Alumina-Crystallite Structures and Catalytic Activity
M. Haneda, T. Miki, T. Mizushima, N. Kakuta and A. Ueno 2079
The Role of Zirconium Dioxide in the Activation of Water and as the Catalytic Site for Low-Temperature Steam Reforming over Rh/ZrO_2
A. Igarashi, T. Ohtaka, T. Honnma and C. Fukuhara 2083
Surface Structure and Reactivity of Magnesia-Supported Nickel Catalysts: A Model System
A. Parmaliana, F. Arena, F. Frusteri, N. Mondello and N. Giordano 2087
Effect of Tin and Iron Deposition on the Catalytic Properties of Platinum Supported on Graphite
E. Lamy-Pitara, L. El Ouazzani-Benhima and J. Barbier 2091
Properties of a Laterite Iron Mineral: Characterization, Catalytic Behavior and Promoter Effect
M. R. Goldwasser, M. L. Cubeiro, M. J. Perez Zurita and C. Franco 2095
Platinum Catalysts Supported on High Surface Area Molybdenum or Tungsten Trioxides for Hydrogenation Reactions
C. Hoang-Van, O. Zegaoui and Y. Arnaud 2099
Pt-C Interaction in Catalyst Supported on a Carbon Black Subjected to Different Heat Treatments
F. Coloma, C. Prado-Burguete and F. Rodriguez-Reinoso 2103
Mechanism of the Effect of Additives on Catalytic Properties of Palladium
L. N. Edygenova, N. V. Anisimova, A. V. Korolev and D. M. Doroshkevich 2107
Pt-Ge/Al_2O_3 Catalysts: Influence of the Thermal Treatments and the Redox Cycles
J. A. M. Correa, S. R. de Miguel, G. T. Baronetti, A. A. Castro and O. A. Scelza 2111
Effect of the Support on the Copper State in Copper-Titanium Oxidation Catalysts
T. S. Petkevich, L. Ya. Mostovaya, Yu. G. Egiazarov and N. A. Kovalenko 2115
Effect of Addition of Pd, Co and Pd-Co on CeO_2. Syngas Conversion and Acetaldehyde Reaction
H. Idriss, C. Diagne, J. P. Hindermann, A. Kinnemann and M. A. Barteau 2119
The Role of Electric Field Acting on the Characteristic of Adsorption of Solid Surface, the Oxygen Adsorption on Tin Oxide Film in an External Electric Field
R. Zhou 2123
Catalytic Behaviour of $LiFeO_2$ Anode for Solid Oxide Fuel Cells
R. T. Baker, I. S. Metcalfe, P. H. Middleton, P. Petrolekas and B. C. H. Steele 2127
Electrochemical Modification of the Activity and Selectivity of Metal Catalysts
M. Stoukides, D. Eng, P.-H. Chiang and H. Alqahtany 2131
The Selective Hydrogenation of Acetylene by the Electrochemically Pumped Hydrogen over Cu in the Presence of Abundant Ethylene
K. Otsuka, T. Yagi and M. Hatano 2135
Solid Electrolytes for in situ Promotion of Catalyst Surfaces: The NEMCA Effect
C. G. Vayenas, S. Bebelis, I. V. Yentekakis, P. Tsiakaras, H. Karasali and Ch. Karavasilis 2139
Theory and Experiment of Photo-Activation of Catalytic Sites and Active Site-Support Interactions
O. Novaro and J. Garcia-Prieto 2143
Photocatalytic and Physicochemical Studies on Metallised Titania Systems
B. Viswanathan, U. D. Mary and R. P. Viswanath 2147
Heterogeneous Photocatalysis: Mechanistic Considerations of Photocatalytic Reductions and Photocatalytic Oxidations on Semiconductor Oxide Surfaces
R.I. Bickley, L. Palmisano, M. Schiavello and A. Sclafani 2151
De-NO_x-ing Photocatalysis - Excited States of Copper Ions Anchored onto Zeolite and their Role in Photocatalytic Decomposition of NO at 275 K
M. Anpo, T. Nomura, Y. Shioya, M. Che, D. Murphy and E. Giamello 2155

A Novel Series of Photocatalysts with an Ion-Exchangeable Layered Structure of Niobate
K. Domen, J. Yoshimura, T. Sekine, J. Kondo, A. Tanaka, K. Maruya and T. Onishi 2159
Photocatalysis by Coordinatively Unsaturated Rhodium Complex Stabilized on Porous Glass for Alkane Dehydrogenation
Y. Wada, C. Nakano, Y. Yamauchi and A. Morikawa 2163
Heterogeneous Photocatalysis as a Method of Water Decontamination: Degradation of 2-, 3- and 4-Chlorobenzoic Acids over Illuminated TiO_2 at Room Temperature
J.-C. D'Oliveira, W. D. W. Jayatilake, K. Tennakone, J.-M. Herrmann and P. Pichat 2167
Investigation of the Electron Transfer Mechanism between Methyl Viologen Radicals and Protons Via a Noble Metal Catalyst
R. Bauer and H. A. F. Werner 2173
Metal Fibre - A Novel Catalyst Material for Selective Dehydrogenation of Alcohols
B. Zhang, L. Lu, Y. Xiao, D. Jin, J. Ai and Z. Zhou 2177
Use of Electron Spectroscopy Methods in the Study of the Structure of Surface Layers of Hydride Catalysts
R. Kh. Ibrasheva, R. G. Baisheva, Z. Kaizi, T. A. Solomina, G. I. Leonova and K. A. Zhubanov 2181
Shape-Selectivity of Alkali Metals Graphite Intercalation Compounds for Catalytic Isomerization, Hydrogenation and Alkylation of Aliphatic and Aromatic Hydrocarbons
S. Tsuchiya, S. Sakai, M. Kikugawa, T. Mitsuno and Y. Sakata 2185
Activation and Reactivity of Titanium Oxynitrides in Ammonia Decomposition
C. H. Shin, G. Bugli and G. Djega-Mariadassou 2189
A Study on the Preparation and Characterization of a NiP Catalysts
J. Shen, Z. Li, Q. Zhang, Y. Chen, Q. Bao and Z. Li 2193
Investigations of Hydrodenitrogenation of Quinoline over Molybdenum Nitride
K. S. Lee, J. A. Reimer and A. T. Bell 2197
CO Oxidation, NO Decomposition and NO Reduction by CO on Superconducting and Related Cuprates
I. Halász, A. Brenner, M. Shelef and K. Y. S. Ng 2201
The Active Oxygen on the Li/La_2O_3 Catalyst Surface and its Catalytic Behavior in the Oxidative Coupling of Methane
L. Wang, J. Wang, S. Yuan and Y. Wu 2205
Oxidative Coupling of Methane over SrO Promoted La_2O_3/CaO: A Comparative Study of the Kinetics and Mechanism
Y.-D. Xu, L. Yu, J.-S. Huang and Z.-Y. Lin 2209
Oxidative Coupling of Methane over Sol-Gel Magnesium Oxide Catalysts: Effect on Selectivity to Olefin Formation
R. Gomez, T. Lopez, L. Herrera, A. A. Castro, O. Scelza, G. Baronetti, E. Lazzari, A. Cuan, M. Campos, E. Poulain, A. Ramirez-Solis and O. Novaro 2213
Influence of the Ion Charge and Coordination State on Catalytic Properties of Barium Ferroniobate for Methane Oxidation
D. Filkova, I. Mitov, L. Petrov, V. Bychkov, M. Sinev, Yu. Tulenin and P. Shiryaev . . 2217
Reaction Performances of Methane Oxidative Coupling Along Catalyst Bed with Sm-CaO Catalyst
C. Tang, L. Lin, Z. Xu and J. Zang 2221
Effect of Pressure on the Methane Oxidative Dimerization
Yu. P. Tulenin, A. A. Kadushin, V. A. Seleznev and A. F. Shestakov 2225

Methane Oxidative Coupling over Complex Metal Oxides Possessing K_2NiF_4 and Related Structure
Q. Yan, Y. Jin, Y. Wang, Y. Chen and X. Fu 2229
Oxidative Coupling of Methane over $PbO/PbAl_2O_4$ Catalysts
S.-E. Park and J.-S. Chang 2233
Characterization of TiLaNa Catalysts in the Oxidative Coupling of Methane
S. Rossini, S.-T. Brandao, O. Forlani, L. Lietti, A. Santucci, D. Sanfilippo and P. Villa 2237
Catalytic Properties of Ca-Doped La_2O_3 Catalysts for Coupling of Methane
X. Yang, Y. Bi, K. Zhen and Y. Wu 2241
Synergy between High Temperature Stable Carbonates and Irreducible Oxides: Destruction of Non-Selective Surface Oxygen on Oxidative Coupling of Methane Catalysts
J.-L. Dubois and C. J. Cameron 2245
Laser Stimulated Oxidative Coupling of Methane to Ethene on $LiClO_4/Pb_3(PO_4)_2$
S-H. Zhong and H-Q. Ma 2249
Temperature-Programmed Studies of Surface Oxygen Species in the Oxidative Coupling of Methane
G. W. Keulks, N. Liao, W. An and D. Li 2253
Oxidative Dimerization of Methane on Alkali Chloride Promoted Co_3O_4
M. Gratzel, D. Klissurski, J. Kiwi and K. R. Thampi 2257
Oxidative Coupling of CH_4+CD_4 Mixture over Manganese Oxide Catalysts
Y. G. Borodko and L. M. Ioffe 2261
A Comparison of the behavior of Catalysts for Methane Coupling by Transient Analysis
R. Spinicci and A. Tofanari 2265
Oxidative Coupling of Methane to C_2 Hydrocarbons over Doped Titania Catalysts
D. Papageorgiou, D. Vamvouka and X. E. Verykios 2269
The Importance of Carbon Dioxide in Oxidative Coupling of Methane
A. Machocki 2273
Kinetic Effects in Conversion of Propane, Isobutane and Propane-Isobutane Mixtures on K-Pt/γ-Al_2O_3 Catalysts, Modified by Sn and In
L. C. Loc, H. S. Thoang, N. A. Gaidai and S. L. Kiperman 2277
The Reaction of Reduction Catalyzed by Homogeneous and Immobilized Binuclear Rh(II) Complexes with Rh-Rh Bond
V. Z. Sharf and V. I. Isaeva 2281
A Highly Active, Heterogeneous Hydroformylation Catalyst: Rh(CO)(acac)L,L= =poly-TRIM Bound Phosphine
J. Hjortkjaer, B. Heinrich, C. Andersson and A. Nikitidis 2285
Selective Hydrogenation of C_4 - Acetylenes over an Ion-Exchanged Copper on Silica Catalyst
J. T. Wehrli, D. J. Thomas, M. S. Wainwright, D. L. Trimm and N. W. Cant 2289
Chiral Metal Transition Complexes in Zeolites: Enantioselective Hydrogenation of Dehydrophenylalanine Derivatives
A. Corma, M. Iglesias, C. del Pino and F. Sánchez 2293
Selective Vapor Phase Hydroformylation of Olefins over Cluster-Derived Cobalt Catalysts Promoted by Alkaline Earth Oxides
K. Takeuchi, T. Hanaoka, T. Matsuzaki, Y. Sugi, M. Reinikainen and M. Huuska . . . 2297
Design of Platinum Based Metallic Catalysts for Selective Hydrogenation of Crotonaldehyde
A. Jentys, C. G. Raab and J. A. Lercher 2301
1,3-Butadiene Hydrogenation in 1-Butene over Alumina Supported Pd-Ag Catalysts
J. W. Hightower, B. Furlong, A. Sárkány and L. Guczi 2305

Oxidative Dehydrogenation of Propane in Presence of Rare Earth Vanadates
J. Castiglioni, P. Poix and R. Kieffer 2309
Reactions of Cyclopropane and 1-Butene over Reduced Molybdena-Alumina Catalysts
I. Oliveros, C. Bolivar, P. Marcano, C. Scott, M.J. Perez Zurita and J. Goldwasser . . 2313
Effects of Mixtures of Modifiers on Optical Yield in Enantioselective Hydrogenation: a Test of the Template Model
K. E. Simons, P. A. Meheux, A. Ibbotson and P. B. Wells 2317
Ni/M Type Bimetallic Reducing Systems
Zs. Bodnár, T. Mallát and J. Petró 2321
New Aspects on the Mechanism of Olefin Polymerization with Reduced Philipps Catalysts
H. L. Krauss, H. A. Schmidt, B. Siebenhaar, P. Wolff and Q. Xing 2325
The Role of Porosity in Ethylene Polymerization on Cr/SiO_2 Catalysts
I. G. Dalla Lana, J. A. Szymura and P. A. Zielinski 2329
Partial Hydrogenation of Alkynes and Dienes on Highly Selective $Fe\text{-}Cu/SiO_2$ Catalysts
Y. Nitta, Y. Hiramatsu, Y. Okamoto and T. Imanaka 2333
Supported Dehydrogenation Catalysts Based on Iron Oxide
D. E. Stobbe, F. R. van Buren, A. J. van Dillen and J. W. Geuss 2337
Sulfur Resistance of Nickel Catalysts Supported on K-Clinoptilolite Containing Iron in Ethylbenzene Hydrogenation
A. Arcoya, X. L. Seoane and J. Soria 2341
Heterogeneous Ethylene Hydroformylation Catalyzed by Oxide-Supported $[Rh_{12}(CO)_{30}]^{2-}$ Anion: Influence of the Nature of the Support
C. Dossi, A. Fusi, L. Garlaschelli, R. Psaro and R. Ugo 2345
Isolated and Competitive Hydrogenation to Characterize Ni-B Catalysts
G. Jannes, P. Kerckx, B. Lenoble, P. Vanderwegen, C. Verlinden and J.P. Puttemans 2349
The Role of Surface Fugacities and of Hydrogen Desorption Sites in Catalytic Reactions of Alkanes
E. Iglesia, J. E. Baumgartner and G. D. Meitzner 2353
Heterogeneous Catalysis of α-Octene Hydroformylation. the Catalytic Behaviors of Non-Homodisperse EGG-Shell Catalysts
W. Huang, L.-H. Yin and C.-Y. Wang 2359
Hydroformylation of Ethylene over Silica-Supported Pt/Sn Catalysts
P. Ramirez de la Piscina, J. L. G. Fierro, G. Muller, J. Sales and N. Homs 2363
Kinetics of 2,2,3,3-Tetramethylbutane Hydrogenolysis over Rh/Al_2O_3 Catalysts
B. Coq, T. Tazi, R. Dutartre and F. Figueras 2367
Surface Organometallic Chemistry on Metals: Role of a Surface Organometallic Fragment $Sn(n\text{-}C_4H_9)x$ on the Selective Hydrogenation of Citral with a Rh/SiO_2 Catalyst
B. Didillon, A. El Mansour, J. P. Candy, J. M. Basset, F. Le Peletier and J. P. Boitiaux 2371
Hydrogenolysis of Methylcyclobutane on Supported Pt Model Catalysts
C. Zimmermann and K. Hayek 2375
Preparation of Egg-Shell Type Pd-Ag and Pd-Au Catalysts by Selective Deposition and Hydrogenation of 1,3-Butadiene
H. Miura, M. Terasaka, K. Oki and T. Matsuda 2379
Hydrogenation and Deuteration of Butadiene and Cyclohexadiene over Reduced and Sulfided Molibdena-Alumina
A. Rédey, D. Smrz and W. K. Hall 2383
Hydrocracking Boscan Heavy Oil with Unimodal and Bimodal Catalysts
M. Ternan and J. Menashi 2387

A Kinetic Model for Aromatization Processes over ZSM-5 Catalysts. Aromatization of Short Chain Hydrocarbons over HZSM-5
D. B. Luk'yanov, V. I. Shtral, V. I. Timoshenko and S. N. Khadzhiev 2391
On the Role of Reversible and Irreversible Adsorption Hydrogen in the Dehydrogenation and Reforming Reactions
Y. Sun, S. Chen and S. Peng 2395
Catalyst Design for the Upgrading of Australian Coal-Derived Liquids
A. T. Townsend and F. P. Larkins 2399
The Use of Intermetallic Hydrides on Basis Lanthan with Nickel and Cobalt for Hydrogenation of Asphaltenes Concentrate
N. M. Parfenova, I. M. Halperin, S. R. Sergienko, V. A. Pherapontov and E. V. Starodubtzeva 2403
n-Hexane Isomerization and Aromatization on the Catalysts Derived from Alumina-Supported Pt-Sn Clusters
X. Li, Y. Wei, J. Cheng and R. Li 2407
The Effect of Rhodium Particle Size on n-Butane Hydrogenolysis Activity and Selectivity
D. Kalakkad, S. L. Anderson and A. K. Datye 2411
Pretreatment Effects on Active State and Aromatization Activity of Ga/ZSM-5 Catalysts
K. M. Dooley, C. Chang, V. Kanazirev and G. L. Price 2415
New Modification Method of Pt/L Zeolite Catalyst for Hexanes Aromatization
H. Katsuno, T. Fukunaga and M. Sugimoto 2419
High Temperature Sensitivity of Paraffin Hydrocracking
R. T. Hanlon, C. R. Kennedy, R. A. Ware and S. S. Wong 2423
Effect of Modification of the Alumo-Platinum Reforming Catalyst with Dy, Cr, Ba and Nytrogen on its Catalytic and Physico-Chemical Properties
G. M. Sen'kov, E. A. Skrigan, E. A. Paukshtis, M. F. Gorbatsevich, A. M. Nikitina and E. N. Ermolenko 2427
Transformation of Propane over Ga/HZSM-5 Catalyst: On the Nature of the Active Sites for the Dehydrogenation Reaction
P. Meriaudeau and C. Naccache 2431
Study of the Selective Semi-Hydrogenation of Various Carbon-Carbon Triple Bonds over a Pd/Sepiolite Catalyst
M. A. Aramendia, V. Borau, C. Jimenez, J. M. Marinas, M. E. Sempere, F. J. Urbano and L. Villar 2435
n-Arylhydroxylamines Transformation in the Presense of Heterogeneous Catalysts
I. A. Makaryan and V. I. Savchenko 2439
Highly Efficient Enantio-Differentiating Hydrogenation Catalyst Prepared from Ultrasonicated Raney Nickel by Asymmetric Modification
A. Tai, T. Kikukawa, T. Sugimura, Y. Inoue, S. Abe, T. Osawa and T. Harada 2443
New Vapor Phase Process for Synthesis of Ethylenimine by Catalytic Intramolecular Dehydration of Monoethanolamine
M. Ueshima, Y. Shimasaki, K. Ariyoshi, H. Yano and H. Tsuneki 2447
Catalyst for Vinyl Chloride Synthesis
N. A. Prokudina, V. V. Chesnokov, B. P. Zolotolvskii, L. N. Yelesina, V. G. Yenakaeva and V. F. Tarasov 2451
A New Process for Production of 1,3-Dimethyladamantane
K. Takagi and Y. Naruse 2455
Palladium Based Catalysts for Hydrogenation of Nitrobenzene
E. Brazi, G. Cordier and G. N. Sauvion 2459
Modification of Pd and Pt by Thiophene and Carbon Tetrachloride during Hydrogenation and Isomerization of (+)-Apopinene
G. V. Smith, F. Notheisz, A. G. Zsigmond and M. Bartók 2463

Selective Hydrogenation of Carbonyl Groups by Means of Hectorite-Intercalated Rhodium Complexes
S. Shimazu, T. Chiaki and T. Uematsu 2467
Enantioselective Hydrogenation of α-Keto Esters over Pt/Al_2O_3 Catalyst: Kinetic Aspects of the Rate Acceleration Effect Induced by Addition of Cinchonidine
J. L. Margitfalvi, B. Minder, E. Tálas, L. Botz and A. Baiker 2471
Crotonaldehyde Hydrogenation over Pt/TiO_2 Catalysts. Influence of the Catalysts Pretreatments
R. Makouangou, A. Dauscher and R. Touroude 2475
Selective Hydrogenation of α,β-Unsaturated Aldehydes over Supported Ru
A. Waghray, R. Oukaci and D. G. Blackmond 2479
Hydrogenolysis of Tetrahydrofurane on Platinum
K. Kreuzer and R. Kramer 2483
Influence of Polymer Support Morphology on Ion-Exchanger Catalysts Activity in tert.-Alkyl-Methyl Ethers Synthesis
K. Jerabek, T. Hochmann and Z. Prokop 2487
Mechanism of Catalytic Organic Solid-Gas Reactions
R. Lamartine, F. Sabra and A. Selatnia 2491
Infrared Study of Coke Deposition on Alumina
J. Datka and R. P. Eischens 2495
Hydrogen Surface Concentration Effect on the Temperature-Programmed Hydrogenation of Adsorbed Carbonaceous Species on an Iron/Alumina Catalyst
H. Halafi, E. Borgstedt, A. M. Efstathiou, S. L. Suib and D. Bianchi 2499
FTIR and Catalytic Studies of the Effects of Sulphur Poisons on Cu/Al_2O_3 Catalyst Selectivity
M. B. Padley, C. H. Rochester, G. J. Hutchings, P. I. Okoye and F. King 2503
Enhancement of the Stability of PtSn Catalysts in Regeneration Cycles by Al_2O_3 Doping with Rare-Earth Oxides
Y. Fan, L. Lin, J. Zang and Z. Xu 2507
Development of a New Catalyst for the Hydroconversion of Heavy Oils
M. M. Ramirez de Agudelo and C. Galarraga 2511
Molecular Poisoning of Ni/SiO_2 Catalyst. A Magnetic and Catalytic Study of the Effect of Thiophene, Carbonyl Sulfide and Carbon Disulfide Adsorption
J. B. Baumgartner, R. Frety and M. Guenin 2515
Effect of Sintering in O_2 Atmosphere on the Surface Properties of $PtRh/Al_2O_3$ Catalysts
S. Kacimi, C. Kappenstein and D. Duprez 2519
Coke Deposits on Pt/Al_2O_3 Catalysts: FTIR and HRTEM Studies
L. Marchese, E. Borello, S. Coluccia, G. Martra and A. Zecchina 2523
Molecular Orbital Study of the Chemisorption of Small Molecules on MgO Surfaces
H. Kobayashi, A. St. Amant, D. R. Salahub and T. Ito 2527
Applications of a New Isothermal Single Pellet Diffusion Reactor
S. S. Au, J. B. Butt and J. S. Dranoff 2531
Coke Elimination from $Pt\text{-}Re/Al_2O_3$ by Ozone Containing Mixtures
C. L. Pieck, E. L. Jablonski and J. M. Parera 2535
New Model of Deactivation of Iron Catalysts for Ammonia Synthesis
W. Arabczyk and K. Kalucki 2539
Pore Restriction in Resid Hydrotreating Catalysts
P.-S. E. Dai and B. H. Bartley 2543
Effect of the Internal Mass Transfer Resistance on the Ni/Al_2O_3 Deactivation by Thiophene
S. Zrncevic and V. Tomasic 2547
A Study of Coke Formation in Resid Catalytic Cracking
T. C. Ho 2551

Selective Hydrogenation of Adiponitrile (ADN) to Hexamethylenediamine (HMD) in the Liquid Phase on Raney Catalysts: Synergetic Effect between the Base in the Solution and the Iron Dope on the Catalyst
J. F. Spindler, G. Cordier, J. Jenck and P. Fouilloux 2555
Acid Resistant Copper Chromium Oxide Catalysts Used in the Hydrogenolysis of Fatty Acids
K. Kochloefl, G. Maletz, G. Hausinger and M. Schneider 2559
Synthesis of Anthraquinones by Cyclization of Ortho-Benzoylbenzoic Acids in the Presence of Solid Acid Catalysts
S. A. Amitina and V. G. Shubin 2565
Acid-Base Properties of Sulfided Ni-Mo-Y Zeolite Catalysts for Water-Gas Shift Reaction
M. Laniecki and W. Zmierczak 2569
Investigation on Adsorption and Acid-Base Properties of Solid Catalysts by Infrared Thermography
S. Marengo, G. Raimondini and P. Comotti 2573
Nature of the Extra-Framework Aluminum in MFI Type Zeolites Synthesized in Fluoride Medium. Influence on the Catalytic Properties of Zeolites
Q. Chen, J. L. Guth and J. Fraissard 2577
Boron - an Acidity and Texture Modifier for Alumina Supported Catalysts
S. Engels, E. Herold, H. Lausch, H. Mayr, H.-W. Meiners and M. Wilde 2581
Sulfate-Modified Superacid ZrO_2 Catalysts: Study of the Surface Acidity and of the Activity towards Alcohols
C. Morterra, G. Cerrato, C. Emanuel and V. Bolis 2585
Highly-Dispersed Heteropoly Anions on Metal Oxide Carriers Modified with Silane Coupling Agents and their Catalytic Properties
Y. Kera, H. Nishizima and M. Kamada 2589
New Catalytic Systems: Heteropolyanions Doped Conjugated Polymers as the Catalysts for Ethyl Alcohol Conversion
J. Pozniczek, I. Kulszewicz-Bajer, M. Zagorska, M. Hasik, A. Bielanski and A. Pron 2593
Effects of Thermal Treatment on Surface Properties and Catalytic Activities of a Prepared TiO_2-ZrO_2 Catalyst
J. A. Navio, M. Macias, F. J. Marchena, J. M. Campelo and J. M. Marinas 2597
Gas Phase Synthesis of MTBE over Acid Zeolites
A. Nikolopoulos, T. P. Palucka, P. V. Shertukde, R. Oukaci, J. G. Goodwin, Jr. and G. Marcelin 2601
Acidity-Tunable Pillared Mica Catalyst Derived from Talc
K. Urabe, I. Kenmoku, K. Kawabe and Y. Izumi 2605
Beckmann Rearrangement over Solid Acid Catalysts
T. Curtin, J. B. McMonagle and B. K. Hodnett 2609
Synthesis of Solid Superacids of Tungsten Oxide Supported on Tin Oxide, Titanium Oxide and Iron Oxide and their Catalytic Action
K. Arata and M. Hino 2613
Effect of the Method of Platinum Inclusion into Spherical Promoter of Catalytic Cracking Termofor on its Activity in CO Combustion
M. I. Levinbuk, V. B. Melnikov, H. K. Shapieva, V. I. Vershinin, V. A. Kuzmin and V. Je. Varshaver 2617
Cooxidation CO and H_2 on Palladium Catalyst
N. A. Boldyreva and V. K. Yatsimirsky 2621
The Structure of Supported Pd, Kinetics and Mechanism of the Low-Temperature Oxidation of Carbon Monoxide
S. N. Pavlova, V. A. Sadykov, D. I. Kochubei, B. N. Novgorodov, G. N. Kryukova and V. A. Razdobarov 2625

Transition Metal Compound Oxide Catalysts for Lowering the Light Off-Temperature of Particles from Diesel Exhaust
C. Setzer, W. Schütz and F. Schüth 2629
FTIR Study of Reduction Mechanism of NO by C_2H_4 and C_3H_8 on Vanadium Oxides Layered on ZrO_2
T. Ohno, F. Hatayama, T. Maruoka and H. Miyata 2633
The Selective Catalytic Reduction of Nitrogen Oxides with Ammonia in a Catalytically Active Ljungstroem Heat Exchanger
H.-G. Lintz and T. Turek 2637
Evaluation of Nitrous Oxide Formation over Rhone-Poulenc's DN 110 SCR Catalyst
E. Garcin and F. Luck 2641
Catalytically Accelerated Solid-Gas Reaction between NO and Ba-Cu-O for Efficient NO Removal
M. Machida, S. Ogata, K. Yasuoka, K. Eguchi and H. Arai 2645
Catalytic Property of Perovskite-Type Oxides for the Direct Decomposition of Nitric Oxide
Y. Teraoka, T. Harada, H. Furukawa and S. Kagawa 2649
TPD-Analysis of Metallic Three-Way Catalysts. Effect of Zr, Si, La and Ba on Thermal Aging
M. Huuska and T. Maunula 2653
Mechanistic Studies of CO Oxidation on Highly Dispersed Gold Catalysts for Use in Room-Temperature Air Purification
M. Haruta, S. Tsubota, T. Kobayashi, A. Ueda, H. Sakurai and M. Ando 2657
Low-Temperature Oxidation of Light Paraffins and Olefins at Solid Surfaces: FT-IR Studies
G. Busca, V. Lorenzelli, G. Ramis and V. S. Escribano 2661
Catalytic Diesel Engine Emission Control. - Studies on Model Reactions over a EUROPT-1 (Pt/SiO_2) Catalyst
E. Xue, K. Seshan, J. G. van Ommen and J. R. H. Ross 2665
Carbon-Oxygen Reaction on Cu/V/K Catalyst for Soot Oxidation
P. Ciambelli, V. Palma and S. Vaccaro 2669
Kinetics of the Selective Catalytic Reduction of NO by NH_3 over a Commercial Catalyst
W. R. A. M. Robinson, J. G. van Ommen, A. Woldhuis and J. R. H. Ross 2673
Selective Catalytic Reduction of NO on Copper-on-Alumina in the Cleanup of High Sulfur Content Flue Gas: Catalyst Development and Design
G. Centi, N. Passarini, S. Perathoner, A. Riva 2677
The Role of NO_2 in the Selective Catalytic Reduction of NO_x
J. Blanco, P. Avila and J. L. G. Fierro 2681
Catalysts for the Elimination of Sulphur Dioxide from Streams by the Claus Reaction at Low Temperature
E. Alvarez, A. Mendioroz and J. M. Palacios 2685
Promoter Effects on Platinum Catalysts for Automotive Exhaust Control
J. R. Gonzalez-Velasco, J. Entrena, J. A. Gonzalez-Marcos, J. I. Gutierrez-Ortiz and M. A. Gutierrez-Ortiz 2689
Correlation of Bulk and Surface Thermodynamics of some Transition Metal Oxides; Application to Exhaust Gas Catalysts
A. D. van Langeveld, A. C. T. van Duin, J. W. Bijsterbosch, F. Kapteijn and J. A. Moulijn 2693
Coadsorption and Reaction of NO and CO on Cu/Al_2O_3 Catalysts
R. Hierl, H.-P. Urbach and H. Knözinger 2697
Activity and Electronic Properties of Automotive Emission Control Catalysts
B. H. Engler, D. Lindner, E. S. Lox and P. Albers 2701

Alumina Supported Manganese Catalysts for Low Temperature Selective Catalytic Reduction of NO with NH_3
L. Singoredjo and F. Kapteijn 2705
Reduction of Nitric Oxide by Carbon Monoxide on Palladium Based Bimetallic Catalysts
J. Massardier, A. El Hamdaoui, G. Bergeret and A. Renouprez 2709
Activity and Characterization of Palladium Catalysts for Nitric Oxide Decomposition
A. Ogata, A. Obuchi, K. Mizuno, A. Ohi and H. Ohuchi 2713
Effect of Calcination on V-O-Ti-P Catalysts
J. Soria, J. C. Conesa, M. Lopez-Granados, J. L. G. Fierro, J. F. Garcia de la Banda and H. Heinemann 2717
Methanol Synthesis over Copper Based Catalysts: Comparison of Co-Precipitated, Raney-Type and Catalysts Derived from Amorphous Alloy Precursors
A. C. Sofianos, J. Heveling, M. S. Scurrell and A. Armbruster 2721
Activity and Selectivity of Ruthenium-Cobalt Bimetallic Catalysts in Carbon Monoxide Hydrogenation
S. A. Korili and G. P. Sakellaropoulos 2725
Surface Kinetics and Periodic Operation of Higher Alcohol Synthesis
J.-L. Li, Q.-M. Zhu, J.-L. Hu and N.-J. Yuan 2729
Mechanism of Selective CO Hydrogenation to Isobutene over Oxide Catalyst
K. Maruya, A. Takasawa, T. Haraoka, M. Aikawa, T. Arai, K. Domen and T. Onishi 2733
Conversion of C_1-C_4 Alcohols into Aromatics on the Modified ZSM-5 Zeolites. Active Centres and Reaction Pathways
D.-Z. Wang, J.-Y. Wang and X.-D. Lu 2737
Activities and Selectivities of Supported Co-Ru, Co-Pd and Co-Pt Bimetallic Catalysts in Fischer-Tropsch Synthesis
M. P. Kapoor, A. L. Lapidus and A. Yu. Krylova 2741
New Ternary Cu-V-Zn Catalyts for Conversion of CO_2 by H_2 into Methanol
N. Kanoun, M. P. Astier, F. Lecomte, B. Pommier and G. M. Pajonk 2745
Alkali-Promoted MoS_2 Catalysts for Alcohol Synthesis: The Effect of Alkali Promotion and Preparation Condition on Activity and Selectivity
H. C. Woo, T. Y. Park, Y. G. Kim, In-S. Nam, J. S. Lee and J. S. Chung 2749
New Alkene Oligomerization Catalyst $NiSO_4/\gamma$-Al_2O_3 and its Characteristics
T. Cai, D. Cao and L. Li 2753
Catalytic Properties of Partially Reduced Fe/SiO_2 in CO Hydrogenation
S. H. Moon, C. W. Park and H. K. Shin 2757
Hydrogenation of Carbon Monoxide over Rh/ZrO_2 Catalysts Promoted by Molybdenum Oxide
E. Guglielminotti, E. Giamello, F. Pinna, G. Strukul, S. Martinengo and L. Zanderighi 2761
Identifying the Reaction Network of the Higher Alcohol Synthesis over Alkali-Promoted ZnCrO Catalysts
L. Lietti, E. Tronconi and P. Forzatti 2765
Effects of Formic Acid and CO_2 in CO Hydrogenation to Methanol over Copper-Based Catalysts and Nature of Active Sites
J. Cai, Y. Liao, H. Chen and K. R. Tsai 2769
Comparison of ZnO-Supported Cu, Cu-Mn, Cu-Fe, Cu-Co and Cu-Ni Catalysts in CO Hydrogenation
P. A. Sermon, M. A. M. Luengo (Yates) and Y. Wang 2773
Methanol Synthesis from CO_2 and H_2 over Supported Copper-Zinc Oxide Catalyst. Significant Influence of Support on Methanol Formation
H. Arakawa and K. Sayama 2777

CO_2 Hydrogenation over Platinum Group Metals Supported on CeO_2: Evidence for a Transient Metal-Support Interaction
A. Trovarelli, G. Dolcetti, C. de Leitenburg and J. Kaspar 2781
Potassium Promotion of Cu-ZnO-Al_2O_3 Catalysts for Higher Alcohol Synthesis
I. Boz, D. Chadwick, I. S. Metcalfe and K. Zheng 2785
Conversion of Syngas to Aromatic Hydrocarbons on Cobalt-Manganese-Zeolite Catalysts
G. Bäurle, K. Guse, M. Lohrengel and H. Papp 2789
Light Olefins Formation from Syngas over ZrO_2-ZnO Catalysts
W. Zhang, R. Gao, G. Su and Y. Yin 2793
High Selectivity of Diesel Fraction in Fischer-Tropsch Synthesis with Co/Nb_2O_5
A. Frydman, R. R. Soares and M. Schmal 2797
The Catalytic Behavior of Some Zr-Ni-Co-Cu-Ru Intermetallic Compounds in Fischer Tropsch Reactions
I. R. Harris, I. T. Caga, A. Y. Tata and J. M. Winterbottom 2801
X-Ray Powder Diffraction In Situ Characterisation of the (Cu, Zn, Al)-Hydrotalcite Phase in Cu-ZnO-Al_2O_3-Catalysts Highly Active in Methanol Synthesis
K. Richter, W. Kraus, G. Nolze and B. Peplinski 2805
Catalyst Component Interactions in Ag-Cu/ZnO/Al_2O_3 Catalyst for Carbon Oxygenate Synthesis
E. Kis, G. Lomic, G. Boskovic, R. Neducin and P. Putanov 2809
Cobalt Reducibility and Magnesium Promotion in Silica-Supported Fischer-Tropsch Catalysts
I. Puskás, T. H. Fleisch, J. B. Hall, B. L. Meyers and R. T. Roginski 2813
Transient Response Study of the Oxidation and Hydrogenation of Carbon Monoxide Adsorbed on Pd/Al_2O_3
G. Kadinov, S. Todorova and A. Palazov 2817
Higher Alcohol Synthesis over Functionalized Solid-Base Catalysts from Methanol as a Building Block
W. Ueda, T. Ohshida, T. Kuwabara and Y. Morikawa 2821
In Situ ^1H NMR Study of the Adsorption of Hydrogen and Formic Acid on Copper Based Methanol Synthesis Catalysts
A. Bendada, J. B. C. Cobb, B. T. Heaton and J. A. Iggo 2825
Isomerisation of Long-Chain n-Alkanes on Pt/H-ZSM-22 and Pt/H-Y Zeolite Catalysts and on their Intimate Mixtures
J. A. Martens, L. Uytterhoeven, P. A. Jacobs and G. F. Froment 2829
Kinetics of Bimodal Grain Size Distribution of a Ni Catalyst During Hydrogenation of CO
M. Kolb, M. Agnelli and C. Mirodatos 2833
Critical Point Properties of the Surface Structure During CO Oxidation
M. Kolb 2837
Selectivity Effects Related with Reaction Mechanism and Diffusion Limitations over Deactivating Catalysts
K. Kumbilieva, S. L. Kiperman and L. Petrov 2841

Author index 2845

Guczi, L. *et al.* (Editors), *New Frontiers in Catalysis*
Proceedings of the 10th International Congress on Catalysis, 19-24 July, 1992, Budapest, Hungary
© 1993 Elsevier Science Publishers B.V. All rights reserved

CATALYSIS: PAST, PRESENT AND FUTURE

J. A. Rabo

UOP, Tarrytown Technical Center, 777 Old Saw Mill River Road, Tarrytown, New York 10591, USA

1. FOUR DECADES OF CATALYSIS

Has catalysis fulfilled its expectations in the last 40 years? How does progress in catalysis compare with other areas of science and technology? Furthermore, what is the impact of catalysis on human society and environment today? The 10th International Congress on Catalysis (ICC) has assembled to consider these important questions. During these 40 years, electronics has emerged from fundamental science to a consumer industry, whose diverse products touch many aspect of daily life. Biochemistry and related biosciences grew from intractable complexity to a systematic unveiling of life's chemical mechanism, and technologies have revolutionized the pharmaceutical industry.

In these 40 years, catalysis grew to become the critical technological underpinning of our chemicals, fuels, and pharmaceutical industries. Catalysis has also become the principal challenge for future progress in these technologies. Future catalysis will be aimed at reducing the cost of raw materials and creating new, exciting products that use catalysts of higher catalytic specificity.

How important is catalysis to industry and, more broadly, to humanity? A recent report [1] set the value of the worldwide catalyst market at $5 billion, with $1.9 billion alone in the United States. The cost of catalyst is estimated to be about 0.1 percent of the value of the fuels produced and about 0.22 percent of the petrochemicals produced [2]. This cost translates to worldwide product values for fuels and chemicals of $2.4 trillion. This amount is more than the gross national product (GNP) of some major industrial nations and is about half of the U.S. GNP. Clearly, the impact of catalysis must be measured by the impact of its products, not by the cost of the catalyst itself [3]. In the last decade, catalysis has become the critical technology for the protection of our environment in addition to its role in the fuel and petrochemical industries. Part of the challenge is to reduce pollutants emitted in the processing of fuels and chemicals, and another is to help produce new, environmentally friendlier fuels and chemicals. An additional and ever-growing role is to reduce undesirable emissions from automobiles and power plants. In this field alone, the yearly catalyst market in the United States was about $650 million in 1989. In Europe, the total catalyst market was $900 million in the same period, and growth was projected to $1.8 billion by 1993, with autoemission catalysts being the fastest growing component.

The societal impact of these industries, fuels and petrochemicals, in which catalysis is a critical component also needs to be considered. According to a recent study of U.S. industry, the chemicals and allied products industry was the largest of all U.S. industries, with yearly sales of $210 billion compared, for example, with $127 billion for automobiles [4]. Employment in chemicals in the United States was 805,000 compared to 1.04 million in automobiles. Another excellent study reports that of the 63 major product and 34

process innovations between 1930 and 1980 in the chemicals and fuels industries, more than 60% of the products and 90% of the processes were based on catalysis [5]. This information clearly points to the critical role of catalysis not only to the chemical and fuel industries but also to the economic progress of society as a whole [6].

In the four decades since the first ICC, catalysis technology has blossomed in large measure as a result of the enthusiasm of participating scientists. The industrial challenge and competition to rapidly develop new catalytic processes substantially contributed to progress in catalysis. Over these years, the ICC has provided an important forum to report on new discoveries in catalysis science and technology. The major events reported at past ICC's have been reviewed in several articles [7,8].

2. COMPLEXITY OF CATALYSIS

The amazing concept of catalysis, that a foreign material can greatly accelerate chemical reactions without itself changing (ultimately) in the process, has inspired many theoreticians and experimentally inclined chemists and chemical engineers. This field offers opportunities of great scientific and enormous economic significance. As a result, catalysis, which began as a one-time experimental endeavor in chemistry, substantially broadened in the last 40 years to include among its researchers representatives of a wide array of disciplines, such as chemistry, engineering, and materials and surface science. The totality of these disciplines reflects the multidisciplinary character of the field of catalysis. The amazing chemical concept of catalytic phenomena inspired the birth of many early "theories," many of which required modifications or did not survive a careful check of their general applicability. Problems usually involved lack of adequate limitations given for the applicability of the proposed hypotheses.

To conceive the best future strategy for catalysis as a whole, scientists must first to recognize how far they still have to go before they see the "light at the end of the tunnel." The important questions are whether the whole scientific basis of catalytic phenomena has been uncovered and whether catalysis phenomena have been adequately described to render solutions that are tractable using present science. The answers to these questions can be found in the following brief review of progress in two important areas: metal catalysis and acid catalysis with zeolites.

2.1 Metal Catalysis

Science in *metal catalysis* has been greatly aided by two factors. First, studies of single metal crystals provided a model for practical, finely dispersed, supported metal catalysts. Second, the evolution of an amazing array of surface science techniques provided in situ investigative tools, such as surface crystallography using low-energy electron diffraction (LEED), for the study of metal surfaces. In addition, the structure of ligands, such as hydrogen, carbon monoxide, and olefins, has been defined together with the metal atom or cluster with which they are associated. In this field, ^{13}C nuclear magnetic resonance

(NMR) spectroscopy, electron energy loss spectroscopy (EELS), and other spectroscopic techniques have been particularly effective [9].

Because optimized industrial metal catalysts usually contain one or two metals and an oxide in addition to a variety of additives, much attention has been given to alloy chemistry, particularly on the metal surface, on metal-oxide interaction, and on adsorbate-adsorbent interaction. The complexity raised by these phenomena induced attempts to generalize the chemistry by taking into account concepts from both organometallic chemistry and solid-state chemistry. The significance of electronic versus structure effects has been debated at length.

In spite of the enormous growth in information on the surface chemistry of noble metals, some of the most important aspects of metal catalysis remain unexplained, and the apparent complexity of the phenomena seems to have grown. For example, recent surfaces studies [10] show that chemisorbed ligands significantly change the structural position of the adjacent metal atom by stretching their bonds relative to their adjacent metal atoms. This suggests a balancing act between the organometallic complex formed with the reactant molecule and the metal crystal itself, based on the thermodynamic preference of each species. Quantitative evaluation of the energy balance between the short-range effects in the organometallic "molecule" and the long-range effects in the metal crystal is difficult, and this evaluation can be handled only by using approximations, particularly regarding the long-range effect. In hydrocarbon catalysis on noble metals, a carbonaceous overlayer covers a significant amount of the metal, affecting or even templating the surface metal layer, with important involvement in surface chemistry and in catalytic mechanism [11]. The specific role of this carbon overlayer is unknown. Most recently, researchers found that under certain conditions carbon monoxide and oxygen on platinum produce a dynamic cycle, which forms a carbon-monoxide-rich overlayer followed by an oxygen-rich overlayer in a cyclic manner [12]. Furthermore, both the carbon-monoxide-rich overlayer and the oxygen-rich overlayer display a long-range order, which suggests a long-range directing effect of unknown source. Again, the problem of reconciliation between short-range and long-range effects emerges. Clearly, even when using the whole array of surface science techniques available today, the study of noble metal single crystals still reveals new, unexplained phenomena. Recently interest has grown in the modeling of catalytic phenomena on noble metals using both ab initio methods as well as a variety of approximations in the computations for the long-range effects that cannot be handled today by rigorous, ab initio methods even with the use of supercomputers.

By comparison with single crystals, industrial metal catalysts are vastly more complex. Instead of having well-grown crystals, they usually contain a variety of supported metal clusters or alloy particles. Industrial catalysts are usually multifunctional, that is, they serve more than one role in chemistry and technology. The result is a complex catalyst composition and chemistry with chemical interaction between the various ingredients. For these reasons, chemical intuition and experience play as large a role as science, used as predictive tool, in developing new and better industrial catalysts. Thus, in spite of great

enlargement of knowledge, researchers are still searching for the "light at the end of the metal catalysis tunnel."

2.2 Acid Catalysis with Zeolites

In catalysis with metal oxides, the elucidation of catalytic phenomena has been aggravated by a lack of techniques available to define the structure of the surface with the precision required to construct useful theoretical models for reaction intermediates. This troublesome uncertainty about surface structure was to be absent in *acid catalysis with zeolites*. Researchers hoped that X-ray crystallography would provide precise information on all atoms in the zeolite crystal, and thus catalytic sites would be well defined. Now, 35 years after the first experiment with crystalline H-Y zeolite and after three decades of great success in industrial applications, researchers may finally be close to explaining, with some precision, the structure and chemistry of protonic catalytic sites in zeolites.

In this case, the problem of characterizing protonic sites rests on the fact that these sites are usually introduced by a proton attack on an oxide ion via thermolysis of the NH_4^+ cation. The proton, with its large electron affinity and minuscule size, affects not only the lone electron pair of the adjacent oxide ion, but also the bonds surrounding the newly formed acidic hydroxyl group. The result is a dislocation in the Si-OH-Al linkage that evaded precise characterization until recently.

The experiments with H-X and H-Y zeolites 35 years ago showed that with aluminosilicates, crystallinity is critical for strong acid catalytic action [13]. Early hopes to define the protonic catalytic sites were hampered by the chemical instability of the primary protonic sites in zeolite crystals. This instability caused various degrees of framework aluminum hydrolysis. Whether the partially hydrolyzed aluminum, or possibly its combination with the nonhydrolyzed protonic site, is the strong acid catalytic site has been a recurring question all through the years. The hundreds of IR spectroscopic investigations involving protonic zeolites provided little more than fingerprint-type characterization. ^1H MAS NMR spectroscopy also offered hope for fundamental information on protonic acidity [14]; however, the small range of the proton chemical shift limits the observation of differences between acidic hydrogens in solid acids to a small range. Furthermore, the acid catalytic action in catalysis should correspond to the deprotonation energy of the solid, that is, the energy needed to transfer the proton from the catalyst to the reactant, more than to the mere polarity of the O-H linkage, which has been traced by static spectroscopic observations. The actual transfer of the proton involves substantial changes in the bond structure all around the protonic site. These changes depend on many material factors, including the polarity of the O-H linkage and the polarizability of the surrounding bonds, as well as some long-range effects.

Theoretical modeling has been applied to elucidate the case of zeolite acidity by using $R_3Al\text{-}OH\text{-}SiR_3$ type molecules and, more recently, by using larger model segments of the zeolite crystal. The most important result of the theoretical modeling work is the conclusion that the bond structure of the Al-OH-Si group controls the ionic character, or

the acidity, of the O-H linkage. According to this model, the deprotonation energy of zeolites decreases with increasing Si-OH-Al bond angle [15]. Thus, the intrinsic strength of acid sites must also increase with increasing Si-OH-Al bond angles. This conclusion, drawn from theory, finds good corroboration with the relationship between Al-O-Si bond angles of zeolites such as Y, mordenite, and ZSM-5 and their acid catalytic activity.

The precision of theoretical modeling becomes questionable when it has to reconcile the results between short- and long-range effects in zeolite structures. The problem is centered on a recently proposed interpretation regarding the cause of the great difference in acid catalytic activity and acid strength between H-zeolite crystals and amorphous silica-alumina gels [16]. The interpretation rests on the idea that without the influence of outside factors, the protonated Al-OH-Si group prefers to form strongly covalent O-H bonds by forming relatively low (sp^3-type) Al-O-Si bond angles. In zeolites, and particularly in silicon-rich zeolites, the Al-O-Si bond angles range between 135 and 170°; thus, they are higher than sp^3-type bond angles. It was suggested that lowering these high angles for the Al-OH-Si units, without affecting the nonprotonated Si-O-Si linkages, is prevented or at least minimized by the zeolite crystal to maintain long-range order. Thus, if long-range order in the crystal prevails over the short-range bonding preference of the Al-OH-Si group, then the original, large bond angles will be retained. In this case, the zeolite retains its crystallinity and displays strong acidity. In cases where the local bonding preference prevails (adjacent to OH group), then the crystal may collapse, and the OH groups will be of much weaker acidity.

The H-zeolites with high aluminum and consequently high H-content ($Si/Al \leq 2$) indeed lose crystallinity, and crystalline H-zeolites all require the presence of stable Si-O-Si linkages. The observed structural loss is probably the result of the reduction of the bond angle in the Al-OH-Si groups. The maintenance of crystallinity and the consequent strong acidity found in silicon-rich zeolites ($Si/Al > 2$) depend on an energy balance between the favored bond formation in the Al-OH-Si group and the bond formation favored by the crystal. The latter favors retention of long-range order and symmetry. Here again, the issue is the balance and reconciliation between the short- and the long-range effects.

The arguments, outlined previously, attribute the lower acidity of amorphous silica-alumina gel to lower Al-OH-Si bond angles relative to those found in crystalline H-zeolites. However, the following most recent experimental evidence suggests a new and unanticipated chemical step, which is a new addition to the complexity of this catalytic phenomenon. [17] ^1H MAS NMR evidence taken following dehydration of amorphous silica-alumina gel and H-Y zeolite indicates that upon removal of the last H_2O molecule, the amorphous material responds by actually breaking the Si-O linkage in the Al-OH-Si unit while the dehydrated H-Y zeolite maintains its original Al-OH-Si linkages. These distinctly different chemical steps presumably occur because when the stabilizing H_2O ligand is removed, the Al-OH-Si unit prefers to form a strong O-H bond in the silica-alumina gel by cleaving the Si-O bond and forming a strongly covalent Al-OH linkage. This step is prevented in silicon-rich zeolites, probably because of the stabilizing effect of the long-range atomic order and related lattice energy of the crystal.

2.3 Summary

These two short and sketchy excursions into metal and acid catalysis certainly do not portray the depth of science in these fields. They were only intended to exemplify the point that catalysis researchers are still "digging deep in the tunnel." Although some light is filtering through, the basic problem remains the same as before: to search for the definition of the catalytic site and the steps of the catalytic reaction mechanism.

This brief review suggests that the best strategy for future catalysis is to continue fundamental research, with the goal of understanding these phenomena. Until such understanding is achieved, the discovery of major new catalysts may evolve more from chemical intuition and experience in the field than from the use of scientific knowledge applied as a predictive tool of research.

3. NEW OPPORTUNITIES IN CATALYSIS TECHNOLOGY*

3.1 Chemicals

3.1.1 Lower Cost Feedstocks

For typical commodity chemical processes, feedstock constitutes about 60 to 70% of the total manufacturing costs. Thus, a great financial impact can result from moving to a lower cost feedstock. For example, the Monsanto process for making acetic acid by methanol carbonylation involved a feedstock change: a shift from ethylene, which was used in the previously dominant Wacker process, to methanol. Since its launching in 1970, the Monsanto process has captured most of the world's new capacity for making acetic acid. Feedstock price changes in recent years have further magnified the cost advantage of the methanol carbonylation route.

By far the strongest current thrust toward lower cost feedstocks is the effort to substitute alkanes (ethane, propane, and butane) for the corresponding olefins and to convert methane to olefins or aromatics. The difference in price between these alkanes and their olefin counterparts can frequently be as much as 10¢ per pound, which is substantial. An excellent example is the production of maleic anhydride, a monomer for specialty plastics. Over the last 40 years, advances in catalytic technology have enabled the industry to switch from high-priced, toxic benzene to butenes and, more recently, to the lower cost butane. This latter development was possible only as a result of the discovery of the vanadyl phosphate catalyst by Chevron Research and Technology Company. A new process for producing maleic anhydride by using novel catalyst and reactor technologies is currently under development by Du Pont and is scheduled for commercialization in the mid-1990s.

---

* Section 3 has been adapted with minor changes from Reference 18.

An extensive worldwide effort is now under way to develop the catalytic oxidative coupling of methane to petrochemicals as well as liquid fuels. This effort encompasses oxidative coupling of methane to ethylene or aromatics, oxidative methylation of propylene to C_4 olefins, and dehydrogenative coupling of methane to aromatics. This area of methane conversion captured exceptional interest and attention all over the world in the mid-1980s.

The relative abundance of LPG (liquefied petroleum gas, containing mostly propane and butane) and the strong demand for aromatics have prompted British Petroleum (BP) and UOP to develop a process for the catalytic conversion of LPG to aromatics. [19] The new process employs a zeolite-based catalyst developed by BP in conjunction with UOP's continuous catalyst regeneration system. The LPG is converted to a mixture of aromatics, 95% of which are benzene, toluene, and xylenes. The aromatics yield is about 65%. In another alkane utilization project, BP Chemicals is developing a process for the direct one-step ammoxidation of propane to acrylonitrile. The key to the process is a proprietary catalyst. Now at the pilot-plant stage, the process is targeted for commercialization in the mid-1990s.

A new commercial development in catalytic alkane dehydrogenation relates to the production of isobutylene and propylene. The isobutylene requirement is for the production of gasoline octane enhancers (for example, methyl tertiary butyl ether, or MTBE), and the propylene need is driven by changes in the feedstock used to produce ethylene. These changes have resulted in less by-product propylene production. Several companies have recently installed or are currently installing new plants for the production of isobutylene and propylene via new dehydrogenation technology (UOP). [20] This remarkable development may provide opportunities for new catalysts that would be capable of promoting oxidative dehydrogenation of lower alkanes (for example, ethane, propane, and isobutane) to their corresponding olefins. Direct functionalization of hydrocarbons remains a significant approach (for example, ethane to ethanol, propane to acrylonitrile, and butane to maleic anhydride or 1,4,butanediol).

The catalytic dehydrogenation of paraffins is also widely practiced commercially for the production of linear olefins in the C_{10}-C_{17} range. These olefins are used in the manufacture of biodegradable detergent intermediates. Typically, olefins in the C_{10}-C_{14} range are used in the production of linear alkylbenzene (LAB), whereas heavier olefins in the C_{14}-C_{17} range are used in the preparation of detergent alcohols via hydroformylation. The preparation of yet heavier olefins by catalytic dehydrogenation is also possible for specialized applications, including the manufacture of synthetic lubricating oils and oil additives. Worth noting at this point is the recent introduction of solid (heterogeneous) acid catalysts by UOP for the alkylation of benzene with heavy olefins in the production of LAB. [21] These acid catalysts can replace traditional catalysts, such as hydrogen fluoride (HF) or aluminum chloride ($AlCl_3$) that are used for this purpose. With these solid acid catalysts, the operational hazards associated with the handling and processing of corrosive catalysts can be avoided, and the environmental consequences of this alkylation process can be ameliorated.

The C_1 chemistry (that is, chemical processes with carbon monoxide, carbon dioxide, or methanol as the starting material) now provides another interesting arena for feedstock-driven innovations in industrial catalysis. The aftermath of the oil embargo of 1973 was an extensive worldwide effort to pursue C_1 chemistry for the production of chemicals as well as fuels. This effort eventually subsided when the cost of carbon from C_1 sources such as coal and natural gas appeared unable to compete effectively with the cost of C_1 from petroleum-based sources, even at the much inflated prices of the latter. However, some significant changes have occurred in the last decade, and so the opportunities for making chemicals via C_1 chemistry should be revisited. In particular, methanol should be considered as a feedstock because of the substantial downward trend in the cost of methanol relative to the cost of ethylene.

Recent reports indicate that rhodium-based homogeneous catalysts promote the reductive carbonylation of methanol to acetaldehyde at selectivities approaching 90% and at much lower pressure than required for prior-art catalysts. With the addition of ruthenium as cocatalyst, the in situ reduction of acetaldehyde to ethanol may possibly be achieved, thus providing a new catalyst system for the homologation of methanol to ethanol.

One great challenge for catalysis has been the possibility of producing ethylene glycol via the oxidative coupling of methanol rather than the standard process based on ethylene as feedstock. Significant progress has been made recently in the catalytic oxidative dimerization of dimethyl ether to dimethoxyethane. Dimethoxyethane, in turn, should be hydrolyzable to ethylene glycol. Unlike methane coupling, which requires a temperature in excess of 600°C, the oxidative coupling of dimethyl ether proceeds at about 200°C with a mixed magnesium-tin oxide catalyst. By using the ether rather than methanol, protection against side reactions has been achieved. These results are an extremely interesting lead that, coupled with the favorable trends in methanol pricing, could pave the way to another major advance in industrial catalysts: the production of ethylene glycol from dimethyl ether. In addition to acetaldehyde, ethanol, and ethylene glycol, other large-volume chemicals currently made from ethylene or propylene may become attractive candidates for manufacture via C_1 chemistry.

3.1.2 New Catalytic Oxidation Processes

Of the different classes of catalytic reactions, hydrocarbon oxidation (that is, reaction with oxygen) generally has the lowest selectivity. In addition to the desired partial oxidation products, significant quantities of carbon monoxide, carbon dioxide, and water are often obtained. The result is complex and costly separations that, in turn, lead to processes with unusually high capital intensity. The annual capital expenditure for oxidation processes, per annual pound of product, is usually several times that for nonoxidative catalytic processes.

Well-recognized examples of major opportunities include the one-step oxidation of methane to methanol, of higher alkanes to alcohols, of propylene to propylene oxide, and of benzene to phenol. Recent reports of success in these areas are tantalizing and suggest

that catalytic oxidation should be one of the most important and fruitful areas for innovation in industrial catalysis.

3.1.3 New Products

New developments in catalysis can and will be the enabling technology that gives rise to new products in many sectors of the chemical industry. The potential impact of catalysis on new products is described in the following sections on polymers, pharmaceuticals, and biologically derived products.

3.1.3.1 Polymers

The production of raw polymers (for example, pellets) in the United States approached 60 billion pounds per year in 1990, which corresponds to a $30 billion business. In terms of fabrication into end-use articles, such as synthetic fibers, films, containers, and structural parts, the polymer business is significantly larger. Catalysis contributes to both monomer and polymer synthesis for a major part of this industry.

Every polymer scientist involved with synthesis or structure-property studies has a wish list for new monomers or polymers that have not yet been synthesized via clear-cut economic routes for commercial practice. Almost every family of polymeric materials can utilize advances in catalysis in monomer production or in the polymerization process. Changes in material requirements, environmental issues, feedstock availability and economics, and worldwide competitive pressures make future catalytic advances extremely important.

The primary area of intense catalytic activity involves the synthesis of new or improved polyolefins. This industry, which evolved out of the original Ziegler-Natta catalyst discovery in the 1950s, produces tens of billions of pounds per year of polyolefins worldwide. New catalyst breakthroughs can lead to new markets of significant volume, including diversified products such as syndiotactic polypropylene, true thermoplastic elastomers, for example, propylene-elastomeric polypropylene resin (EPR) and propylene block copolymers; and the incorporation of polar monomers into various polyolefin classes. For example, if acrylates, vinyl esters, acrylonitrile, and the like can be incorporated into the present low-pressure polyolefin synthesis, the result would be a new family of olefin-based polymers that are likely to have major commercial significance. Of course, improvements in the present catalytic systems will have a pronounced effect on the polyolefins that are commercially available. Improvements in molecular weight distribution control (for example, narrow molecular weight distribution), the ability to synthesize EPRs in gas-phase reactors, and the control of catalyst decay (for example, improved efficiency) are advances that will surely occur.

Novel metathesis catalysts for the synthesis of cyclic olefins have resulted in a host of new polymeric structures. Several of these, such as *trans*-poly(octenamer), have reached commercial status. The few catalysts that are effective are often expensive and require

unattractive precautions during industrial scaleup. Further advances could make this area a promising one for industrial exploitation.

In the field of functionalized monomers, the trend will likely revolve around new or existing monomers via biomass, coal, or C_1 conversion as the carbon source availability changes together with economics. Improved catalysts for creating monomers from agricultural commodities or waste materials offer increasingly important opportunities. This field can benefit from the genetic engineering of specific enzyme catalysts. Oxidative coupling of methanol to ethylene glycol and ethanol to 1,4-butanediol can open new routes to these important monomers. A new process (noted earlier) involving the one-step ammoxidation of propane to acrylonitrile could change the commercial position. Other possibilities, for example, using shape-selective catalysts such as zeolites, could yield lower cost routes to 4,4-diphenol via phenol coupling. Such a molecule is of interest for liquid crystalline and engineering polymers. Improved nonphosgene routes to diisocyanates are desired. Functionalized oligomers such as hydroxyl (OH)-, amino (NH_2)-, and carboxyl (COOH)-terminated polyolefins can yield important blocks for step-growth polymers, such as urethanes and polyesters. Functionalized fluoroolefin oligomers for inclusion in step-growth polymers can likewise offer a new variety of polymers. A nonchlorine route to siloxane polymer precursors is also desired.

In the field of polymers, a number of prior failures primarily resulting from the unavailability of appropriate catalysts have been well documented in the literature. The reaction of acetaldehyde to yield polyvinyl alcohol is one such example. Because phosgene is highly toxic, a nonphosgene route to polycarbonate is desirable. The polymerization of phenol to a highly linear unsubstituted poly(1,4-phenylene oxide) of high molecular weight would be of interest as would the polymerization of polyphenylene by benzene coupling. Many other novel polymers are waiting to be polymerized from available monomers.

Cationic polymerization continues to be an area of increasing research made possible by improved Lewis or Brønsted acid catalysis. Continued improvement can yield higher molecular weights and industrially acceptable process conditions. Extension to other monomers, such as vinyl acetate, would be of future interest. Anionic polymerization is of interest primarily for unique block copolymers. However, the extension to additional monomers and the resultant block structures deserve more attention.

3.1.3.2 Pharmaceuticals

The 1990s will definitely be labeled the "decade of chirality." Many of the opportunities and challenges in this explosively evolving field stem from the pharmaceutical area and the growing recognition that the "wrong" enantiomer of a racemic drug represents a medical pollutant whose toxic side effects can far outweigh the therapeutic value of the pharmaceutically active enantiomer. The classic example in this area is thalidomide. The R-isomer of thalidomide is an effective sedative; tragically, the drug was sold as the racemate, and it was subsequently discovered that the S-isomer is a powerful teratogen. More recently, Eli Lilly was forced to withdraw its Oraflex anti-inflammatory drug

because of liver damage caused by the "inactive" R-isomer. Although recent regulatory changes by the U.S. Food and Drug Administration stopped short of requiring that all drugs be sold as a single enantiomer, the trend in this direction by drug companies is obvious.

Among the available strategies for the manufacture of optically pure substances is asymmetric catalysis, which has powerful and unique advantages. Perhaps the foremost is the multiplication of chirality, the stereoselective production of a large quantity of chiral product by using a catalytic amount of a chiral source. Unlike fermentation, asymmetric catalysis is characterized by generality; processes are not limited to "biological"-type substrates, and the R- and S-isomers are made with equal ease. Asymmetric catalysis also circumvents the disposal of large amounts of spent nutrient media that are generated during fermentation. By comparison, optical resolution (or diastereomeric crystallization) is extremely labor intensive and necessarily produces 50% of the "wrong" isomer, which must be destroyed or racemized in a separate step.

3.1.3.3 Biologically Derived Products

The rapidly growing field of biotechnology brings with it opportunities in the field of enzyme-catalyzed reactions. The role of genetically engineered microorganisms in synthesizing rare and valuable peptides used in human therapeutics is now well established. The same techniques of molecular biology can also be used to enhance the properties of enzymes as catalysts for industrial processes that are similar to classic catalytic technology.

This approach can potentially revolutionize the applications of biological systems in catalysis. Enzymes and other biological systems work well in dilute aqueous solution at moderate temperature, pressure, and pH. The reactions catalyzed by these systems are typically environmentally friendly in that few by-products or waste products are generated. The catalysts and the materials that they synthesize are, as a rule, biodegradable and therefore do not persist in the environment. The reactions are typically selective with extremely high yields; and enzymes can be used to catalyze a whole sequence of reactions in a single reactor, resulting in vastly improved overall yields with high positional specificity and 100% chiral synthesis in most cases. The improved use of enzyme catalyst technology with whole-cell catalysis, reactions catalyzed by single enzymes, and mixed enzymatic and chemical syntheses are all important for the development of new catalyst technology.

Whole cells of various microorganisms are being used more frequently in the catalytic synthesis of complex molecules from simple starting materials. The use of whole microbial cells as biosynthetic catalysts takes advantage of one of the unique properties of enzymes: they were designed by nature to function together in complex synthetic or degradative pathways. Because of this property, whole cells and microorganisms can be used as catalytic entities that carry out multiple reactions for the complete synthesis of complex chiral molecules. A patent was recently issued for a genetically engineered *Escherichia coli* that synthesizes the molecule D-biotin directly from glucose. Biotin has three chiral

centers, and the current chemical synthesis requires 13 to 14 steps with low yields. Similarly, researchers are constructing a microorganism that directly catalyzes the synthesis of a vitamin C precursor from glucose. Combining genes from various organisms results in a process that uses a microbially synthesized intermediate with a final chemical conversion to vitamin C. Whole cells of microorganisms are also used in the synthesis of antibiotics from carbohydrate starting materials, and whole cells are used in the biocatalysis of certain steroids. A number of specialty chemicals with complex synthetic schemes can be produced most efficiently by intact microorganisms using a series of enzyme-catalyzed reactions designed by nature to work together.

The biotechnology field also has a growing number of examples of reactions of industrial significance catalyzed by isolated enzymes. The conversion of corn starch into corn syrup by the enzymes alpha- and gluco-amylase and glucose isomerase is a large industrial process for generating corn sweetener for soft drinks and other uses. The enzymatic conversion of acrylonitrile to acrylamide has recently been commercialized in Japan. Japanese companies and researchers have been diligent in developing enzymatic processes for the synthesis of fine chemicals. Enzyme-catalyzed reactions are used by the Japanese for the synthesis of monosodium glutamate, L-tryptophan, and phenylalanine.

The stereospecificity of enzyme-catalyzed reactions has been used to advantage in polymer synthesis as well. Workers at ICI have developed a combined enzymatic and chemical process for the synthesis of polyphenylene from benzene. Benzene is oxidized to a *cis*-dihydrodiol by an enzyme-catalyzed oxygenation. The diol is derivatized, polymerized, and rearomatized to give polyphenylene in a reaction that cannot be carried out by classical chemical methods because of solubility problems. This new route to polyphenylene is an excellent example of combined enzyme and classic chemical synthesis to make a product that is otherwise too expensive for practical use. Other biological polymers are also finding their way into the field of catalysis in various applications. Microorganisms are used to synthesize materials such as poly(beta-hydroxybutyrate), a biodegradable plastic, and researchers are exploring a series of synthetic silklike materials that may have uses in applications requiring high tensile strength.

3.2 Production of Fuels

3.2.1 Summary of Challenges for Fuel Processing Catalysis in the 1990s

Some of the challenges for fuel processing catalysis in the 1990s are:

- Changing feedstocks
  - Heavier feeds
  - Higher sulfur and metals content
- Alternative fuels, CH_4, Syngas
- Changing fuel product slate
  - More motor fuel
  - Less fuel oil

- Changing motor fuel specifications and environmental issues
  - Gasoline reformulation
  - Desulfurization of motor fuels including diesel oil
  - Reduction of SO_x and NO_x emissions
  - Use of noncorrosive, inert catalysts
- Provide economic raw materials for petrochemicals

Some of these challenges and opportunities in petroleum catalysis are described in the following sections.

3.2.2 Existing Fuels

Although the current understanding of how the individual components of gasoline affect various environmental issues is limited, several components in gasoline are now considered harmful to the environment if released to the atmosphere in high concentration as either spills, vaporization losses, or the result of incomplete combustion. They include aromatics, notably benzene, which is a carcinogenic reagent; high-vapor-pressure hydrocarbons such as butane; and reactive hydrocarbons such as olefins and sulfur compounds, which could promote the formation of smog and acids. The petroleum industry is responding to these concerns by directing its research toward gasoline reformulation, which will require a number of advances in catalytic technology.

Innovations in catalytic cracking catalysts over the last 30 years have improved the conversion of the heavier components of crude oil to gasoline and diesel oil, allowing a reduction in crude imports to the United States of more than 400 million barrels a year. In the future, new types of cracking catalysts and additional process steps will be required to produce motor fuels that are environmentally more acceptable. To reduce the aromatics content of gasoline and at the same time provide higher octane, paraffinic components will require that fluid catalytic cracking (FCC) catalysts produce more olefins. The highly reactive olefins can be isomerized, oligomerized, or alkylated with paraffins to produce gasoline components. They can also be reacted with methanol to produce a variety of high-octane ethers. For example, the zeolite ZSM-5 has been shown to be active in producing olefins when mixed with conventional faujasite-type cracking catalysts. Molecular sieve catalysts have also been proved active in isomerizing and oligomerizing olefins to a variety of liquid fuels.

Cracking catalysts will also have to become more rugged to endure the higher temperatures required to produce more olefins for subsequent processing into high-octane gasoline components. The catalytic cracking process has been the workhorse of modern refineries for 30 years and, with improved catalysts, will continue to be the main process for converting the heavier end of crude oil into more environmentally acceptable components for gasoline and diesel fuels.

3.2.3 Oxygenates for Octane Boosting

The need to reduce the amount of aromatics in gasoline has created a need for organic oxygenates as replacement octane enhancers. Today the two predominant oxygenates used as octane enhancers are methyl tertiary butyl ether (MTBE) and ethanol (EtOH). However, other oxygenates, such as alcohols, ethers, acetates, and carbonates, are known octane boosters. Some of these compounds have been evaluated only partially for their performance characteristics and may represent major growth opportunities in oxygenated fuels. Currently, approximately 150,000 barrels per day of oxygenated compounds (MTBE and EtOH) are added to gasoline in the United States. By the year 2000, projections indicate that 750,000 barrels per day (the equivalent of roughly 10% of current U.S. production of petroleum) of oxygenates will be required in the United States for the gasoline pool. In the United States, the 1990 MTBE production capacity was 117,200 barrels per day. By 1993, it is targeted at 256,400 barrels per day. Iso-olefins (for example, isobutylene) are now produced as a by-product of fluidized catalytic crackers in petroleum refineries. These quantities will support the production of ether at a rate of only 200,000 to 300,000 barrels per day. The isomerization of nC_4 to C_6 olefins produced in the catalytic cracking process could substantially boost the production potential of gasoline oxygenates without substantial added cost to the refiner. The catalyst challenge here is to achieve high skeletal isomerization selectivity and particularly to attain adequate catalyst life, that is durability, and still carry out the isomerization reaction.

The process technology leading to the majority of oxygenates now in use has been made efficient through catalyst modifications and engineering design. However, new processes leading to the same oxygenates may have cost advantages if different building blocks and feedstock sources (crude oil versus coal versus natural gas) are used.

The precursors of established octane enhancers, alcohols and ethers, rely heavily on natural gas and crude oil as their feedstock supply. Industry estimates suggest that when crude oil prices pass approximately $30 per barrel, coal gasification to syngas and the conversion of syngas to hydrocarbons and oxygenates may become cost competitive. Therefore, indirect liquefaction of coal may be a way to produce oxygenated fuels for the transportation industry.

3.3 Environmental Protection

Public interest in protecting the environment has increased and expanded greatly. The challenge is to preserve the benefits of modern technology without seriously contaminating the natural world.

Three strategies are available for reducing the impact of chemicals on the environment: waste minimization, emission abatement, and remediation. Waste minimization calls for the design and development of products and processes that are inherently low polluting or nonpolluting. The abatement of emissions can often be achieved by trapping harmful effluents or converting them to harmless substances, for example, conversion of nitric

oxide to nitrogen. Where an environmental insult has occurred, effective means of remediation are needed to restore the environment to its "green" state. As shown by the examples in the following sections, catalysis can contribute to these three approaches.

3.3.1 Alkylation Catalysts

The alkylation of paraffins with olefins is one of the major refinery operations. The process reacts isobutane with olefins, generally propylene and butenes, to produce highly branched C_7 and C_8 paraffins, respectively. They constitute a premium high-octane gasoline component (95 to 98 research octane number for C_4 alkylate). The alkylation process is assuming increasing importance with increased olefin production from modern FCC units and with the recent emphasis on clean fuels of lower aromatics content.

Both of the currently used liquid acid catalysts, sulfuric acid and hydrogen fluoride, are corrosive. Acid waste disposal in the process catalyzed by sulfuric acid is of increasing environmental concern because liquid hydrogen fluoride is a potential health hazard. As a result of increasing concerns and possible legislative action addressing environmental and safety issues, current alkylation processes may face critical scrutiny.

Exploratory studies have shown that new catalysts can be developed that are cleaner and safer than those presently used. However, powerful acid catalysts are still required for alkylation. The formidable challenge to the industry is the production of a novel catalyst system that makes a new process economically feasible: a new process must have high yield of alkylate, selectivity to produce high-octane gasoline, long life cycle, regenerability, and greatly reduced environmental and safety risks. This challenge would benefit from broad-based fundamental studies of acid catalysis and from increased exploratory research. At the present time, no satisfactory solid motor fuel alkylation catalyst exists. An alternative, if temporary, solution in this field may be a combination of modifications both in the chemistry of the currently used halide catalyst and the process design that can substantially reduce undesirable emissions, and even the hazard of accidental emissions, in the alkylation process.

3.3.2 Replacements for Chlorofluorocarbons

Chlorofluorocarbons (CFCs) are now believed to contribute to the seasonal ozone depletion over the Antarctic continent. However, because they are crucial to many aspects of modern society and have no available replacements, ceasing their production immediately is not practical. By 1988, the total CFC consumption worldwide had grown to 2.5 billion pounds per year for use as refrigerants, foam-blowing agents for polystyrene and polyurethane, and industrial solvents and cleaning agents.

Ironically, the high stability and inertness of CFCs, which make them so valuable, have led to their downfall. Once released at ground level into the atmosphere, they rise slowly into the stratosphere, where they are degraded by high-energy radiation from the sun and release chlorine-containing free radicals that trigger a catalytic ozone depletion

cycle. Following detailed, though not definitive studies, agreement was reached on a major global environmental treaty, the Montreal Protocol, to phase out CFC production by the turn of the century. A race by all CFC producers then began to find suitable and environmentally acceptable substitutes. The strategy is to reduce its atmospheric lifetime by introducing hydrogen into the molecule so that it is removed from the atmosphere by reaction with hydroxyl radicals in the stratosphere. The commercially viable synthesis of these new compounds is a major challenge for catalysis because catalysts used for the production of CFCs lack the required selectivity and activity to be acceptable for the production of hydrogen-containing substitutes.

The projected costs for these molecules, hydrogenated chlorofluorocarbons (HCFCs), are approximately two to five times those of the CFCs they are replacing because of the complexity of the new manufacturing processes. Although rapid progress is being made toward the production of HCFCs, they are not entirely satisfactory and may have to be phased out in turn. Consequently, major advances in catalytic science and technology will be required to develop more acceptable substitutes before the turn of the century.

3.3.3 Emission Abatement

Catalytic technology is playing an ever-increasing role in environmental protection. In 1989, for the first time in the United States, the market for emission control catalysts (largely for automotive emissions) exceeded the market for petroleum refining catalysts. However, the area of stationary emission control (for example, from power plants) has been flagged as one that will experience large (20% per year) growth in the years ahead. Many chemical production plants also need to reduce emissions. Thus, novel catalysis will in many cases be the critical technology that enables most of the benefits created by the chemical and petroleum industries to be maintained, but with improved preservation of the environment.

Catalysts for automotive emission control are now well developed in the United States and, in general, meet mandated standards for removal of hydrocarbons, CO, and NO_x. Recent Clean Air Act revisions will require significantly greater reductions in 1993 in the emissions of hydrocarbons, CO, and NO_x than those that are now mandated. In addition, stringent local automobile emission standards, as in California and Vermont, will require up to a tenfold reduction in emissions by the late 1990s. These reductions will require more active catalysts, new catalyst supports (for example, metallic supports), and new reactor designs that enhance low-temperature performance. A first step in this direction is the electrically heated converter, which offers a severalfold reduction in emissions over currently available technology. Because of the rapidly escalating price of rhodium, which promotes NO_x reduction, the industry needs to develop lower cost NO_x reduction catalysts or practical catalysts for NO_x decomposition. Cleaner gasolines may provide opportunities to develop lower cost catalysts that contain a smaller amount of the expensive noble metals. Finally, an improved technology needs to be developed for recovering rhodium because of its high cost.

The control of power plant emissions is another major area of opportunity for catalysis. In particular, NO_x emissions need to be removed either via selective catalytic reduction (SCR) or, if achievable, via the preferable NO_x dissociation. The abatement of NO_x from power plants is important in efforts to control acid rain and photochemical smog, the latter being linked with harmful ozone production. Selective catalytic reduction removes NO_x in flue gas by reacting oxides of nitrogen with ammonia to form nitrogen and water. First commercialized in Japan, SCR is now being used extensively there. It has also been commercialized in Germany. The catalyst is the heart of SCR technology, and it must provide both high activity and high selectivity (toward nitrogen formation). Major improvements in SCR catalyst performance can be achieved through the strategic design of the catalyst pore structure.

3.3.4 Biodegradation of Organic Waste

Enzymes, like man-made catalysts, accelerate the rate of reactions. Reactions catalyzed by enzymes include the oxidation and hydrolysis of natural and synthetic organic chemicals regarded as pollutants of soil and groundwater. Enzymes have some natural advantages over other catalysts in the degradation of environmental pollutants. Enzymes are most active against materials at low concentration (micromolar to millimolar range) in the presence of water and can be simple and inexpensive to manufacture because they are grown along with microorganisms. Enzymes themselves are biodegradable.

Enzymes can exhibit either narrow or broad substrate specificity. The latter characteristic is desirable for enzymes that attack and degrade organic contaminants. For example, methane monooxygenase has an amazingly broad substrate specificity and can catalyze the oxidation of alkenes; ethers; and alicyclic, aromatic, or heterocyclic molecules. This enzyme system can also degrade synthetic organics, such as the chlorinated solvents chloroform, dichloroethylene, trichloroethylene, and 1,1,1-trichloroethane. The ability of enzymes to degrade natural organics, such as the components of gasoline, crude oil, and most solvents, as well as synthetic organics, such as trichloroethylene or polychlorinated biphenyls, means that most, if not all, organic contaminants can be degraded in reactions catalyzed by enzymes.

Chlorinated organics, such as dichlorodiphenyl and trichloroethane and its by-product dichlorodiphenyl ethylene, pentachlorophenol, chlorocatechols, and other chlorinated aromatics used as preservatives and pesticides, are degraded in oxidation reactions catalyzed by enzymes from bacteria and other microorganisms. Even the most complex halogenated organics, such as polychlorinated biphenyls (PCBs) and chlorinated solvents, are subject to catalytic attack by certain microorganisms.

The PCBs were developed earlier in the century as oils for use in electrical equipment and as lubricating fluids in industrial applications because they gave good insulating and lubricating properties without being explosive or flammable. However, PCBs were later discovered to bioaccumulate and are now classed as environmental hazards. Recently, enzymes have been found in microbes that will reductively dechlorinate PCBs and oxidize

them in the presence of molecular sieves. Even though these enzymes had not evolved simply to degrade PCBs, they have a broad-enough substrate specificity to catalyze the initial degradation of PCB molecules in the environment. The use of oxygenates with broad substrate specificity in bacteria may be the only practical method of treating PCB-contaminated soil and water because of the low cost and adaptability of oxygenates in the environment.

Similarly, chlorinated solvents have been widely adopted because of their excellent solvent properties and lack of flammability. Trichloroethylene (TCE), perchloroethylene, and trichloroethane have been used widely in the past as dry cleaning solvents and chemical degreasers for metal finishing and electronic applications. Surprising numbers of different oxidative enzyme systems that will attack TCE or other chlorinated aliphatics have been identified.

The technique of enzyme recruitment offers the prospect of producing single organisms that contain a spectrum of genetically engineered enzymes capable of degrading hazardous waste in the environment. Enzyme recruitment permits microorganisms to degrade new molecules and broadens the ability of microorganisms to attack synthetic organic chemicals. The idea of using enzymes that can reproduce themselves, can be made cheaply, and can work under conditions that are often found in the environment may be one of the most effective means modern science can devise for treating and degrading hazardous waste, including organic chemicals synthesized to be stable under harsh conditions. The broad substrate specificity of certain enzymes offers the opportunity to use enzyme catalysis for improving and protecting the environment.

4. NEW TRENDS IN CATALYSIS

4.1 New Catalytic Materials

In the last four decades, the largest impact on heterogeneous catalysis technology was the introduction of new catalytic materials. The catalyst base expanded to include a host of new oxides, zeolites, immobilized enzymes, membranes, and clays. The discovery of *synthetic zeolites* grew out of an interest in providing the industry with adsorbents that had superior separation selectivity, based on polarity and molecular sieve effects. Because the zeolite crystal has uniform pores of the size of small to medium molecules throughout its entire length, diffusion was expected to be a potential problem. The utility of zeolites as catalysts was based on the discovery that large-pore zeolites can be transformed to strong acid catalysts by introducing acidic O-H groups, either by applying cation exchange with multivalent cations or by thermalyzing ammonium cations. Slow diffusion did not become a practical problem, even though the reactant molecules in the first major applications, catalytic cracking and hydrocracking, were close in size to the pores of the Y zeolite. Later, the molecular sieve effect as well as the limiting diffusion rates have been successfully applied to benefit catalytic selectivity in several commercial processes.

The successful use of protonic zeolites, with their strong acidity, in a large number of commercial applications inspired the discovery of a much wider range of microporous crystals with well-defined intracrystalline pores and cavities. Through creative research strategies, such as the use of templates in synthesis, the family of molecular sieve crystals has grown beyond aluminosilicates to include pure silica, aluminophosphates, and a wide variety of additional, diverse compositions with up to six or even more framework elements [22]. Most of these materials are capable of transforming to a protonic form and thus can act as acid catalysts. The pore sizes vary from about 3 Å to about 20 Å. However, the pore size that may be achievable in the future with creative synthesis strategy has no theoretical limit.

The chemical composition originally limited to aluminosilicates and silica has expanded to include more than a dozen elements without any emerging rule that would exclude the incorporation of additional elements as framework ions [23]. At present, the field of new microporous crystals is growing rapidly, is freed by the original limitations in composition, and is fueled by an amazing inflow of creative ideas in material synthesis.

Important catalyst applications of microporous crystals have protonic acidity as the principal catalytic function. So far, materials containing silicon and aluminum display the strongest acidity, which benefits cracking, hydrocracking, and small-paraffin isomerization reactions. With other chemical compositions, the intrinsic acid strength tends to become weaker, and thus, it can be controlled with the choice of framework elements. The underlying cause of changes in protonic acid strength in microporous crystals is complex. Part of the problem is that with several compositions, the site of protonic acidity has not been established with precision. For aluminosilicates and for most other microporous crystals, the underlying cause of strong acidity has been emerging only recently (see Section 2). The intrinsic acid strength of a H-zeolite hydrogen is controlled both by chemical and structural factors. With the wide choice of available chemical compositions, crystal structures, pore shapes and sizes, the design of catalytic sites that meet desired acid strength and steric requirements has come close to reality. Acid strength and a shape-selective reaction environment can be "engineered" into unique combinations by using appropriate synthesis and postsynthesis treatment strategies to achieve improved catalytic selectivity for both old and new catalytic reactions (see Section 3).

Although catalysis with microporous crystals rests mainly on acid catalysis, these materials are also often used as bifunctional catalysts, which usually contain a noble metal that is finely dispersed in the microporous surface in the crystals. The proximity between small noble metal clusters and acid sites within the intracrystalline pores is the reason for effective catalytic action with these materials. The study of these metal dispersions has resulted in a substantial body of scientific literature during the last 30 years.

Among the elements used in the formulation of new microporous crystals are several transition metals and other elements with variable valence. Molecular sieves containing these elements provide the opportunity to introduce transition metal catalysis or redox catalysis by framework ions contained in the crystal structure. These new compositions

offer new opportunities in catalysis because they have transition metal ions in low, tetrahedral coordination. Depending on the crystal structure and chemical composition, these ions are all in one or in a small number of crystallographically well-defined sites. By comparison with traditional, supported transition metal oxides, these new crystals offer unique advantages based on the potential uniformity of the transition metal ion sites and the high concentration of catalytic sites throughout the crystal. Recent NMR experiments indicate that tetrahedral aluminum ions in aluminophosphate molecular sieves readily accept water molecules by assuming octahedral coordination in a reversible process. Such evidence suggests that framework-transition-metal ions may also be capable of interacting directly with reactant molecules. These materials offer new opportunities to catalysis in the future.

Aluminophosphate-based molecular sieves have been reported to show high selectivity and stability in several new or improved industrial applications, including catalytic dewaxing, olefin isomerization, C_8 aromatics processing, and production of the C_2 to C_4 olefins from methanol. The realization of new, successful catalytic applications will also be helpful in providing new incentives for the rapidly expanding synthesis research activities for new microporous crystals.

Clays belong to the original category of catalytic materials used in old-time catalysis. With their ion exchange capacity used to generate acid sites, clays have provided cheap catalysts for nonregenerable catalyst applications in the petroleum industry. The rebirth of interest in clay products rests on the high and uniform surface area obtainable by delamination and by the conceptual adaptability of postsynthesis treatments used successfully with zeolites in the past. Recently, the highest interest has been associated with the ability to vary the gallery space between clay layers by the introduction of uniform inorganic or organic cationic pillars, which provide large, accessible surface area and molecular sieve action that is defined by the size of the pillar. By comparison with zeolites and other three-dimensional microporous crystals, the geometry and the chemistry of the gallery space is less uniform for pillared clays because of the somewhat ill-defined position of the pillars in the gallery space. This limits expectations for shape-selective action similar to those known for zeolites.

Recent advances in pillared clay synthesis resulted in the development of large-surface materials with about 18 Å uniform gallery spacing and with hydrothermal stability matching that of steam-stabilized zeolites. Such properties render clay products as good catalyst candidates in catalytic cracking and hydrocracking for treatment of heavy petroleum fractions. Delaminated clays remain attractive catalyst candidates in applications where low catalyst cost is critical. Clearly, the future of clay-based materials rests on the adaptation of synthesis strategies applied for the modification of the clay layers and on better control of pillar ordering.

Homogeneous catalysis benefits from its close relationship with organometallic chemistry. This branch of chemistry, with many research incentives of its own, provides the basic chemistry as well as most of the synthetic methods needed for the "construction"

of advanced homogeneous catalysts. Recently, one of the prominent aspects of homogeneous catalysis relates to a desire to use paraffins as feedstocks in organic synthesis and the synthesis of chiral compounds. Taking ideas from the catalytic function and structure of enzymes, they also adopt ligands to achieve the specific steric hinderance required for stereospecific synthesis steps. Of course, the predictability of the catalytic function is limited here also by the influence of factors both within and beyond the transition metal complex, such as the solvent, additive functions, and redox phenomena. However, strategic manipulation of relevant parameters can result in success, as may be illustrated by the synthesis of the drug naproxen. Currently, the noncatalytic chemical synthesis produces a mixture of the two optical monomers from which mixture the S-naproxen must be separated because the R-naproxen is a toxin. Recently, the selective synthesis of the desired S-isomer has been achieved with high selectivity by asymmetric hydrogenation of α-(6-methoxy-2-napthyl) acrylic acid with a ruthenium complex containing a chiral ligand. Similar success was achieved in synthesizing L-dopa, which is used in the treatment of Parkinson's disease. The stereospecific synthesis of chiral compounds at a level of selectivity that permits the direct use of the product without the currently required expensive separation and purification is an important future objective in catalysis. Beyond the obviously important applications in the production of pharmaceuticals, chiral compounds also offer new material properties for both monomer and polymer molecules. New properties for chiral compounds produced at moderate cost by highly selective and efficient catalysts would create new applications and new markets well beyond what can be envisioned today.

An interesting marriage between enzymes and microporous crystals is the occlusion of small, enzymelike molecules in the intracrystalline cavities of zeolites [23]. If successful, this approach in catalysis will result in higher catalyst stability, lower cost, and easy use of enzyme action in a traditional, and cheap, continuous flow operation.

4.2 Catalyst Characterization and Theoretical Modeling

The last four decades have seen the evolution of many new catalyst characterization techniques. Many of them were adapted from surface science, a distinct discipline in science that has its own theories and rapidly developing techniques. In addition, techniques previously used in material science have also been widely adapted to catalysis. A critical discussion of the methods would require a long review of its own (see list of prominent techniques in Table 1). This section discusses only the trends that are particularly relevant to future progress in catalysis.

Catalysts and catalytic phenomena are characterized for several reasons. First of all, catalyst characterization is needed to define a catalyst beyond its chemical composition and its crystalline components so that its catalytic properties can be reproduced. Furthermore, in the development of new catalysts, new chemical concepts regarding composition or structure are conceived. Following synthesis, the match between the chemical concept and the actual catalyst product must be confirmed. Catalysts also undergo changes in use. Industrial catalysts are usually used for several months or years before they are replaced,

regenerated, or rejuvenated. In this period, the catalyst degrades in performance to a certain extent, and so developing a characterization that indicates the change in the property most relevant to catalytic performance is important. Successful industrial catalysts are often multifunctional, that is, containing several catalyst components; and their manufacture requires meticulous characterization following each significant catalyst synthesis step. Regeneration, or rejuvenation, of used catalysts also requires a proof of restoration of critical catalyst properties, including both physical and chemical characteristics. Therefore, characterization routinely involves a long list of physical and chemical methods and usually also includes an actual catalysis test.

The practical need to monitor the evolution and the replication of catalysts resulted in the adoption of many of the techniques listed in Table 1. Clearly, catalyst characterization serves many needs from research to manufacture. The characterization may relate to the catalyst support, to the precursor phases of the catalyst, to the catalytic site, or to the catalytic reaction itself.

In most cases, the information gained is used to judge successful reproduction of structural or chemical characteristics of the bulk or the surface of the catalyst but is insufficient to reveal the structure or chemistry of the catalytic site itself. Although these techniques serve a well-justified purpose, additional methods that are capable of unveiling the chemistry of catalytic reaction steps at the catalytic site and revealing the structure and chemistry of the catalytic site itself at an atomic scale are important for future progress. Rapid progress in catalysis depends on the predictive value of these experiments. Therefore, the precision used to define the catalyst and its reaction mechanism will affect the effectiveness of the specific steps chosen in the evolution of new superior catalysts. The most effective approach in characterization requires the use of methods simulating the reaction environment or at least conditions compatible with the reaction conditions. Although experiments of this type require complex manipulation of the catalyst sample and the reaction environment, they have been successfully adopted in many research laboratories. Aiming at direct, in situ observation of catalytic phenomena must be an important future goal in catalysis research. The problem is considerable.

Information on the identity of reaction intermediates is of great value because it gives the clearest focus in the design of further catalyst improvement steps. A description of the structure at the catalytic site can be used as a basis to model catalytic phenomena. Here, an important question is the degree of precision needed to build useful theoretical models for the catalyst. Ultimately, a useful operational linkage should be established between characterization and theoretical modeling, both of which are important research tools in the design of advanced catalysts. Today, for many cases, such conceptualization of catalyst development is not realistic. However, recent progress in computer techniques has been dramatic, bringing improvements in speed and in cost reduction.

Methods of surface chemistry have already been successfully adapted in many cases to catalytic studies. Various analytic methods, such as NMR, LEED, EELS, and FTIR spectroscopy (Table 1), have been used to identify the chemistry and structure of small

chemisorbed molecules, such as CO and ethylene. Nuclear magnetic resonance has become a particularly powerful and diverse tool in the hands of leading NMR scientists to probe catalysis at the molecular level. Some of the sophisticated NMR methods applied to catalytic surfaces suggest great potential for this technique in identifying reaction intermediates for both metal and acid catalysts. For example, ^{13}C NMR evidence recently helped to identify the reaction-intermediate alkoxy complex formed between propylene and H-Y zeolite. This observation showed that in acid catalysis at low reaction temperatures, an alkoxy reaction intermediate prevails; but at higher temperatures, where this complex becomes unstable, a "true" carbocation type mechanism sets in. However, more that just these two options for reaction intermediates need to be considered because a recent mechanistic study has shown convincing evidence for the parallel occurrence of both bimolecular H^- shift type and superacid type monomolecular mechanisms in the cracking of hydrocarbons.

5. CATALYSIS OF THE FUTURE

At its best, progress in science and technology is discontinuous; it is based on creative, unanticipated discoveries. Therefore, any projection of the future in catalysis will surely miss some of the most important elements. Thus, the future can be projected only on the basis of present knowledge, identified needs, and anticipated improvements. The easier part of the projection is based on identified needs for new products, environmental control, and desired economic improvements, such as the use of cheaper feedstocks. These topics with anticipated future directions have been discussed in Section 3.

This section focuses on some of the basic principles and directions that seem worthy of contemplation in the formulation of a research strategy for new catalysts and related processes. This discussion covers catalyst characterization, catalyst synthesis, industrial catalytic process development, and the discipline of future catalysis.

5.1 Characterization of Catalysis Phenomena

Any experimental plan developed for the creation of a better catalyst requires a description of the catalytic site and its chemical and catalytic function that is as accurate as possible. Superior knowledge of the active site obviously translates to a better plan for catalyst improvement. This consideration leads to the most important future objective in catalysis science: the *characterization of catalytic sites at the atomic and molecular level*, with sufficient detail in chemistry and structure to allow the planning of modifications that will lead to desired changes in chemical and catalytic characteristics. This objective requires a depth of knowledge similar to that in available homogenous catalysis.

Beyond the atomic and molecular description of the catalytic site itself, scientists must also seek to understand the relationship between the chemistry of the active site and long-range effects exerted by the crystalline base or other long-range phenomena such as ordered overlayers. As was discussed in Section 2, the long-range effects are important, and in some cases they are the key to catalytic phenomena. The formation of a catalytic

site or the formation of reaction intermediates tends to distort the crystal and cause disorder. The direction of the long-range effect is generally the maintenance or restoration of lattice order to minimize lattice energy and thus to increase thermodynamic stability of the whole crystal. The quantitative assessment of the preferred bond structure at the molecular catalytic site (short-range effect) and the effect of the distortion caused by the active site on the whole crystal (long-range effect) is difficult because of the large size of the computational terms related to the long-range effect. Therefore, scientists need to search for some traceable spectroscopic evidence to monitor long-range stress in catalyst crystals.

Characterization of catalytic active sites at the atomic scale received a great boost from the development of electron tunneling and electron force microscopes. These methods have the potential to describe the surface structure of both metals and oxides and to reveal even small atomic dislocations. They can even map atoms and molecules in the chemisorbed overlayer. More important, these techniques also have some future potential for indicating the bonding characteristics of surface atoms by applying perturbations. Such measurements may ultimately be developed to characterize the chemistry of surface atoms.

Today, the electron tunneling and atomic force microscopes are designed to monitor the surface of single crystals. To render these revolutionary, atomic-level characterization techniques useful to catalysis, scientists have to redesign the delicate mechanical control system to allow monitoring of microcrystalline material. Such redesign would involve the development of improved mechanics and computer software to allow the mapping of small crystal surfaces and the automatic reorientation of the sample to find the next crystal surface. The development of electron tunneling and atomic force spectroscopic techniques for microcrystalline catalysts would be an important step in achieving catalytic site characterization of practical catalysts at the atomic level.

Future progress in catalysis science also needs improved knowledge of the reaction chemistry so that scientists can contemplate modifications for improvement. With this long-range objective in mind, the determination of the catalytic reaction steps and reaction intermediates is essential to future progress. Recent years have seen excellent progress in this field from a variety of sophisticated techniques, including ^{13}C NMR, EELS, and FTIR, for the identification of chemisorbed molecules and catalytic reaction intermediates on noble metals [9]. The next step in this field is to extend the application of these techniques to industrial catalysts, including supported metal catalysts and acidic zeolites, under practical reaction conditions. In this field, methods with adequate response time are needed to identify relatively unstable reaction intermediates as well. The ultimate purpose of gaining detailed knowledge about catalytic sites and catalytic reaction intermediates is to bring catalysis, as a branch of chemistry, to the level where the experimental plan of a catalyst chemist compares in predictive scientific quality to that experienced in inorganic or organic synthesis.

To render the conceptual planning in catalysis manageable, to reduce available choices, and to rank the experimental options based on relevant scientific considerations, the

modeling of the catalytic site and catalytic reaction intermediates is desirable. If scientists are to prepare theoretical models that can be used as predictive tools in the design of better catalysts, they need to be well aware of the chemistry and physics of bulk solids and surfaces as well as molecules. Quantum-mechanical modeling should be applied with a critical attitude in the application of any assumption used to abbreviate the computation for the short-range and, especially, the long-range effects. The development of scientifically reliable theoretical modeling is a challenging and difficult task. Today, ab initio calculations are still limited to small atom clusters, or they require the use of generalized or simplified expressions for long-range effects.

The future direction in theoretical modeling is almost obvious. If current trends in computer and software development are considered, scientists cannot escape the conclusion that in the future, computational modeling will probably grow faster than any other area in catalysis science. For this reason, theoretical modeling will no doubt have an important place in future catalysis.

5.2 Catalyst Synthesis

Catalyst synthesis, a critical subdiscipline of catalysis, has a methodology of its own. Since the great success of zeolite catalysts in industry, catalyst synthesis adopted several synthesis topics and characterization methods from material science. Today the objectives of catalyst synthesis are far-reaching. They include the whole variety of industrial oxide catalysts, supported metals, biocatalysts, and zeolites as well as microporous or layered materials with wide ranges of chemical compositions, pore sizes, and crystal structures. With zeolites, large pore size seems to be of premium value. Large-pore zeolites with pore sizes of about 8 Å are yearly bested by new-generation, microporous crystals, with pore sizes of 12 and most recently with 20 Å. The main incentive for catalysis in this field is that these large pores, acting as molecular sieves, may benefit catalytic selectivity in the treatment of heavy petroleum products. They may also act as receptors for immobilized, enzymelike molecules. At present, this area of synthesis research is achieving a high rate of productivity worldwide.

As scientists look for fundamental principles in the strategy for future catalysts, they must recognize the differences between biocatalysts and man-made catalysts. Biocatalysts have uniform catalytic sites, and consequently they have high catalytic specificity to the product they catalyze. Man-made heterogeneous catalysts, such as oxides, supported metals, and even acidic zeolites, contain a range of active sites. Consequently, catalytic specificity to the desired product is lower. This simplistic comparison between biocatalysts and heterogeneous catalysts points to catalyst-site uniformity as a desirable feature for future heterogeneous catalysts.

Several approaches have recently been used to develop solid catalysts with uniform catalytic sites. The "fixing" of enzymes on supports and, more recently, the immobilization of enzymelike molecules in zeolites are good examples. In the latter case, catalytic molecules, such as porphyrine, phtalocyanine, or salen, that may contain a variety of

transition metals have been immobilized in zeolite crystal cavities using ship-in-bottle synthesis. Recent data indicate synergistic phenomena between the zeolite structure and the occluded complex. These phenomena give rise to substantial stabilization of the complex, and the result is much superior catalytic turnover numbers relative to the solution of the same complex. In addition, catalytic specificity is strongly influenced not only by the active complex itself, but also by the uniform spatial constraint around the active site. This spatial constraint is provided by the intracrystalline environment (regio selectivity) of the zeolite support.

Microporous crystals may also offer several new strategies for providing uniform catalytic sites. Recent developments in the synthesis of microporous crystals, particularly in aluminophosphates, permit the synthesis of compositions containing a variety of transition metal ions, or other elements of variable valence, in the crystal framework. These tetrahedral ions, which occupy well-defined positions on the intracrystalline surface, can occupy identical crystallographic sites by the proper choice of crystal type, transition metal, and its concentration. Some tetrahedral cations have been observed to be capable of reversible change in coordination, from tetrahedral to octahedral, upon hydration-dehydration cycles, vide infra. Therefore, these transition metal cations are probably accessible, in varying degrees, to catalytic reactants as well.

Uniform catalytic sites combined with shape selectivity offer new opportunities in catalysis. The substitution of aluminum or other small framework cations with the much larger transition metal cations must result in a distortion of the substituted crystal site that causes stretching and bending of adjacent bonds. This crystal site distortion must result in a distortion of the local site symmetry and may lead to stereospecificity or even chirality. Such changes may form the basis for stereospecific catalysis.

In other fields of catalyst synthesis, a particularly important breakthrough in catalysis would be the synthesis of thin, continuous layers of microporous crystals that are usable as catalytic membranes. This development would probably revolutionize not only catalyst synthesis but also catalytic reactor design because of its large potential applications in combining molecular sieve separation with catalysis. In spite of its enormous potential impact, no new, inspiring approaches that are comparable in novelty and creativity to those used in the synthesis of new molecular sieves have been reported in this field.

Aiming at the formation of uniform surfaces and uniform catalytic sites, scientists may imagine that the atomic force microscope or a mechanical system of similar design may be used not only to monitor the surface layer of crystals but also to modify them. Ultimately scientists may devise a mechanism to imprint or replicate uniform surface structures on metals or oxides so that they become uniform catalytic sites. In the interest of maintaining high catalytic specificity, several interesting strategies have been already described in Sections 2.1.3.2 and 3.1.3.3. with regard to biologically derived catalytic systems.

5.3 Industrial Catalytic Process Development

The objective of industrial catalysis is to develop economically superior processes based on innovations that lead to the use of cheaper feedstocks, to higher product yield, or to other process efficiencies that translate to superior process economics. Industrial research organizations depend on their experience, which is based on both successful and unsuccessful experiments in catalyst synthesis or on the process side, to develop their favored research strategy.

Recent success in the use of bio-derived catalysts in a variety of pharmaceutical syntheses and specialty chemicals syntheses substantially broadened the spectrum of the knowledge base on which the research strategy for new catalytic processes should be conceived. Because of the differences in applicable catalyst types, such as enzymes, zeolites, superacids, and supported metal systems, both the catalysts and the processes of reasonably conceived competing approaches may be profoundly different. They may even require researchers of different disciplines for efficient, creative pursuit. For this reason, future industrial success for new catalysis technology will probably favor those scientists who can consider all potential options from the point of view of catalyst type and process approaches to develop the best conceptual research strategy toward a new process objective. Of course, ultimate success in all cases depends on one or more creative researchers who make the key discoveries needed for the catalyst or process.

Developing new competitive catalytic process technology is indeed a complex job that requires a broad-minded research organization and people of excellence in a whole spectrum of disciplines, including chemical synthesis, chemical engineering, and material science. Looking toward the needs of future catalysis technology in the 1990s and beyond, the following fundamental guidelines come to mind:

- Learn from biocatalysis and seek catalyst synthesis approaches that develop catalysts with uniform catalytic sites. Look for approaches for uniform catalytic sites not only in the use of enzymelike species but also in seeking novel approaches of "surface synthesis" using both metals and oxides. Industrial catalysts are often multifunctional. Sometimes the functions relate to two interacting catalytic steps (bifunctional catalysts). However, in many cases, one or more catalyst additives are only present to help correct a certain catalyst deficiency, such as rapid metal aggregation, or to aid catalyst burn-off. Based on past experience, if a new catalyst does not have sufficiently high catalytic selectivity or activity, fixing these initial problems requires using additives, dopants, or expensive catalyst regenerative or rejuvenation methods often requires large cost and long time. For these reasons, a strategy aiming at uniform catalytic sites may be a rewarding principle.
- Acid catalysis is the most common and important catalytic function in industrial catalysis. All ranges of acidity, including mild, strong, and "super" acidity, are important for distinct areas of industrial applications.

  Environmental considerations place high priority on the development of chemically inert, solid superacids. This fact focuses on the theory of solid acids.

Theory is needed to elucidate the specific role and contributions of structural and chemical factors affecting strong and super acidity as well as on the interaction between protonic and Lewis acid sites. The goal is to gain maximum acid strength. A basic understanding here would provide a rich basis for new, superior synthesis approaches to solid acid catalysts in the whole range of acidity.

- Catalytic process technology with solid catalysts rests in most cases on the use of the traditional fixed-bed reactor, often with relatively unsophisticated flow control for feed and product. Imaginative catalyst flow control, such as fluid- or moving-bed applications, revolutionized catalytic cracking, gasoline reforming, and ethylene polymerization, can release the processes from reactor-size constraints and provide superior operational control and stability with added benefits in the optimization of operating conditions. In several areas, new creative engineering may benefit future catalysis technology. New imaginative process solutions may be similar to those successfully applied recently in sorption-separation processes with respect to countercurrent reactant-flow control, use of desorbents, and so forth. These ideas may find applicability in cases of multistep catalytic reactions conducted on a single catalyst, particularly in cases using multiple feeds.

5.4 The Discipline of Catalysis

The makeup of the discipline in catalysis is continuously evolving. In the last 40 years, the addition of scientists from surface science, material science, inorganic synthesis and theory has given catalysis enormous scientific strength. The most important aspect of this change is the broadening of scientific topics and the focus toward more quantitative scientific methods. This trend will, no doubt, stay with catalysis in the future as well. The field will broaden to include biocatalysis and new areas of inorganic synthesis for catalytic materials. Surface science will blossom, together with theory, particularly when theory can play a role as a predictive tool in an operational linkage between conceptual planning and catalyst synthesis.

Changes in the future makeup of the discipline of catalysis must be reflected in the institutional training of future scientists. Therefore, efforts should be made to develop broad as well as scientifically sound curriculums at selected universities where catalysis programs are on the teaching agenda.

REFERENCES

1. Creek, B. F.: Chem. Eng. News 1989, 67(22)29.
2. Chem. Week, 1979, 124(14)47.
3. Roth, J. F.: Chemtech, June 1991, 357.
4. Chemtech 1990, 20(4)224.
5. Bennett, M. J.; Boccone, A. A. and Vline, C. H.: Chemtech 18, 162 (1988).
6. Cusumano, J. A.: Chemistry for the 21st Century; Thomas, J. M.; Zamaraev, K. I.; Blackwell Scientific Publication, 1992.
7. Heinemann, H.: Proc 9th Int. Conf. on Catalysis, Vol. 5, pg 1-10, 1988.

8. Heinemann, H.: Catalysis Science and Technology, Vol 1, pg. 1-41, Springer Verlag 1981.
9. Slichter, C. P.: Ann. Rev. Phys. Chem. 1986, 37, 25-51.
10. Somorjai, G. A.: ACS Symposium series, Vol. 428, pg. 218, 1990.
11. Somorjai, G. A.:
12. (a) Somorjai, G. A.: Catalysis Letters, Vol. 12, pg. 17, 1992.
(b) Erte, S.: Oscillatory, Adv. Catalysis, in print.
13. Rabo, J. A.; Pickert, P. E.; Stamires, D. N.; Boyle, J. E.: Proc. 2nd Intern. Congr. Catalysis, Edition Tech., Paris, 1960, 2055.
14. Pfeiffer, H.; Freude, D. and Hunger, M.: Zeolites, 5, (1985) 274-286.
15. (a) Dwyer, J. and O'Malley, P. J.: Stud. Surf. Sci. Cat., 35, (1988) 5.
(b) Carson, R.; Cooke, E. M.; Dwyer, J.; Hinchliffe, A. and O'Malley, P. J.: Zeolites as Catalysts Sorbents and Detergent Builders, Extended Abstract, 1988, 151-152.
16. Rabo, J. A. and Gajda, G.: Catal. Rev. Sci. Eng. 31(4), (1989-90) 385-430.
17. Doremieux-Morin, Batanak, Martin, Brépeaultaud, and Fraissand: Catalysis Letters 9, (1991) 403-410.
18. Bell, T. B.; Boudard, M.; Ensley, B. D.; Estell, D.; Grubbs, R. H.; Hegedus, L. L.; Manzer, L. E.; Rabo, J. A.; Rebek, Jr., J.; Roth, J. F.; Somorjai, G. A.; Weekman, V. W.: Catalysis Look to the Future, National Academy Press, USA, 1992.
19. Gosling, C. D.; Wilcher, F. P.; Sullivan, L.; and Mountford, R. A.: Process LPG to BTX Products, Hydrocarbon Processing, (1991).
20. Gregor, J. H.; Bakas, S. T.; and Olowetz, M. A.: Converting Field Butanes into MTBE, presented at the Gas Processors Association, Anaheim, CA, Mar. 16-18, 1992.
21. Vora, B. V.; Pujado, P. R.; Imai, T.; and Fritsch, T. R.: Recent Advances in the Production of Detergent Olefins and Linear Alkylbenzenes, presented at the Society of Chemical Industry, University of Cambridge, England, Mar. 26-28, 1990.
22. Flanigen, E. M.; Patton, R. L.; Wilson, S. T.: Stud. Surf. Sci. Catal., 37(Innovation Zeolite Mater. Sci.) (1990) 13-27.
23. (a) Schulz-Ekloff, et al.: Zeolites, 4 (1984) 30-34.
(b) Jacobs, P. et al.: Stud. Surf. Sci. Catal, 59 (1991) 395-403.
(c) Zakarova, et al., Vestn. Mosk. Univ., Ser. 2c Khim. 18(G) (1977), 660-663.

Table 1
Prominent Analytical Techniques

Technique	Abbrev.	Type of Information
Low-energy electron diffraction	LEED	Two-dimensional structure and registry with metal surface
Auger electron spectroscopy	AFS	Elemental analysis
X-ray photoelectron spectroscopy	XPS1	Elemental analysis and valence state
Ion scattering spectroscopy	ISS	Elemental analysis
Ultraviolet photoelectron spectroscopy	UPS	Electronic structure
Electron energy loss spectroscopy	EELS	Molecular structure
Infrared spectroscopy	IRS	Molecular structure
Laser Raman spectroscopy	LRS	Molecular structure
X-ray diffraction	XRD	Bulk crystal structure
Extended X-ray absorption fine structure	EXAFS	Bond distance and coordination number
Transmission electron microscopy	TEM	Crystal size, shape, morphology, and structure
Scanning transmission electron microscopy	STEM	Microstructure and composition
Scanning tunneling microscopy	STM	Microstructure
Ultraviolet spectroscopy	—	Electronic state
Mössbauer spectroscopy	—	Ionic state
Nuclear magnetic resonance spectroscopy	NMR	Molecular structure and motion

Guczi, L. *et al.* (Editors), *New Frontiers in Catalysis*
Proceedings of the 10th International Congress on Catalysis, 19-24 July, 1992, Budapest, Hungary
© 1993 Elsevier Science Publishers B.V. All rights reserved

INTERFACIAL COORDINATION CHEMISTRY: CONCEPTS AND RELEVANCE TO CATALYSIS PHENOMENA

M. Che

Laboratoire de Reactivite de Surface et Structure, URA 1106, CNRS, Universite P. et M. Curie, 4, Place Jussieu, 75252 Paris Cedex 05, France

"Seen from the bottom of a well, the sky appears very small" (Han Yu, 768-824)

Abstract

The concepts of the so-called ***interfacial coordination chemistry*** (ICC) are established for complexes interacting with oxide surfaces and involving transition metal ions (TMIs). The latter can function either as probes of their own interaction with the oxide surface, as adsorption and/or catalytic sites or as precursors of oxide-supported metal particles in mono or polymetallic systems. The concepts of ICC are compared with those of solution and solid state coordination chemistries and a general classification of the different coordination chemistry types is proposed. The analogies and differences are stressed and concern the mobility, accessibility and reactivity of the transition metal complexes. Those parameters, which are largely dependent on the bonding strength of the TMI with the oxide support and in turn on the role of the oxide support and choice of the preparation method, determine the catalytic properties. Examples of catalytic reactions will be given which involve the oligomerisation of olefins and the oxidation of methanol and can be described at a molecular level. Finally, the importance of the bonding strength of TMIs with the oxide support will be stressed in determining the preparation and properties of small supported metal particles which exhibit a strong memory effect with respect to their oxidized precursor state. The present molecular approach suggests that both the preparation and catalytic phenomena can be seen in a more predictive manner and that more effort should be devoted in the future to fundamental research in this area.

1. INTRODUCTION

In all their compounds, cations are surrounded by anions or neutral molecules. The groups immediately surrounding a cation are called ligands and the branch of chemistry which is concerned with the combined behaviour of cations and their ligands is called coordination chemistry (CC) [1]. The principles have been established from results obtained essentially by Jørgensen and Werner at the turn of the century on solution complexes containing only one transition metal ion (TMI) surrounded by ligands [1].

The main goals were to understand the properties of such complexes, i.e., their reactivity towards simple reagents such as silver nitrate, their structures, the nature of the different chemical bonds involved, and the presence and number of geometric as well as optical complexes. Later, attention was focused on their optical and magnetic properties along with their chemical behaviour particularly in redox and ligand substitution reactions. Successive theories were proposed (valence bond, crystal field, molecular orbital, angular overlap..) which have greatly helped to improve our understanding of transition metal complexes in solution and inorganic transition metal compounds in the solid state.

Attempts have been made in the past to apply such theories to catalytic systems. It must be recognized that they were by and large more successful for homogeneous than for heterogeneous systems, which involve complex gas-solid or liquid-solid interfaces. The present review is aimed at showing that substantial progress has now been made for heterogeneous systems so that a general picture of a field which we shall call ***interfacial coordination chemistry*** (ICC) can be presented. It concerns the preparation of catalysts composed essentially of TMIs and oxide supports, their catalytic properties in the oxidized state and finally the preparation of supported transition metals.

2. EARLY STUDIES OF INTERFACIAL COORDINATION CHEMISTRY

2.1. Transition metal ions supported on oxides

The preparation of supported catalysts via the deposition of transition metal complexes on metal oxides has been known for a long time and can be considered as an example of coordination chemistry at the liquid-solid interface. For instance, the ability of silica to adsorb Na^+, Ag^+, Cu^{2+} and Fe^{3+} ions had been noted by several authors as early as 1925 [2-4]. In 1932, using chemical analysis, Berton [5] showed that $Cu(NH_3)_4^{2+}$ and $Ni(NH_3)_6^{2+}$ could adsorb on silica with loss of 2 NH_3 molecules. Later, Smith and Jacobson [6] observed the same type of effect with Ag^+, Zn^{2+}, Cu^{2+}, Ni^{2+} and Co^{2+} ions complexed with ammonia, ethylenediamine and diethylenetriamine ligands. In 1961, Kozawa [7] assumed that the adsorption of complexes leads to bonds between the metal cation and the silica surface. The next two papers are important contributions to our understanding of coordination chemistry at interfaces. Burwell et al. [8] presented evidence that the adsorption of trans-$Co(en)_2Cl_2^+$ on silica occurs by substitution of a Cl^- ligand by a surface SiO^-

group and gave some insight into the bonding of labile and inert transition metal complexes with silica. Using UV-vis. spectroscopy also, in addition to magnetic measurements, Hathaway and Lewis showed in 1969 [9] that the surface of silica could act both as a bi- or terdentate ligand towards the Ni(II) ion. In 1972, Anderson [10] showed that the exchange technique, to which we shall return later, leads to an octahedral complex much more effectively bonded to the surface than via the impregnation method.

The first successful attempt to rationalize the adsorption of transition metal complexes on inorganic oxides was made by Brunelle [11] and concerned cationic complexes of Pt [12-16], Pd [16-19], Co, Ni, or Cu [9,16] on silica or alumina or anionic complexes of Pt [16,20-24], Pd [18,19] or other precious metals such as Au, Rh, Ru and Ir [16,24] on alumina. The results were explained in terms of surface polarization of oxides as a function of pH and adsorption of counterions by electrostatic attraction. The previous results show that transition metal complexes can be bonded to the support surface either by electrostatic adsorption or through ligand substitution. There was, however, no ***systematic*** study of the changes occurring to the complex during the successive preparation steps.

2.2. Zeolitic and layered materials

Zeolitic materials have well defined crystalline structures and exhibit, inside cavities of known dimensions, cationic sites where cations can be sited [25,26]. Transition metal complexes may either be synthesized within the zeolitic cavities (ship in a bottle synthesis) or exchanged in as complex cations [27]. This has the advantage that the site symmetry is better defined than on conventional oxides. There are unfortunately complicating factors due to synthesis and/or postsynthesis treatments which lead to locations other than cation exchange sites: lattice framework positions, surface defect sites, oxide agregates inside or outside pores, bulk oxides on the external zeolite surface [28]. However, if care is taken, it is possible to study TMIs essentially in cationic exchange positions.

The coordination of the TMIs in zeolites, mostly investigated after ion exchange and drying and/or calcination, has been reviewed by Kazanskii and coworkers [29,30]. One of the most important aspects which emerged from the latter studies is that TMIs can change cationic sites upon adsorption [31,32]. For example, it was shown by spectroscopic studies that TMIs can reversibly migrate upon water ad(de)sorption between hidden sites where they are bonded to framework oxygen ions (S_I in hexagonal prisms and/or $S_{I'}$ in sodalite cages with octahedral and C_{3v} symmetries respectively) and the large cavities of faujasite-type zeolites where they can freely tumble in the form of hexaaqua complexes [33,34]. This is an interesting case where the TMI-zeolite bonding can reversibly change from iono-covalent to electrostatic.

Similar studies have been conducted in layered materials which indicate that the adsorbed complexes can adopt distorted symmetries [35,36].

2.3. Simple and mixed oxides

One of the first rationalizations of catalysis was the electronic theory of catalysis [37] which attempted to find a relationship between the catalytic properties of solids and their electronic properties estimated in terms of the

band theory. Much experimental work was stimulated by these ideas but the results often did not support the precepts of the theory [38].

A new approach was then taken and catalysis no longer studied from a delocalized and physical standpoint but from a localized and chemical one thanks to Dowden and Wells [39] who, at the 2nd International Congress on Catalysis in Paris, proposed to apply the ***crystal field theory*** to catalytic phenomena. Their paper can be regarded as one of the major contributions to the field together with that of Taylor [40] who was the first to describe active surface sites. If simple concepts of electron transfer are augmented by the application of crystal field theory in the investigation of the coordination changes in distorted surface complexes, then it emerges that any rate-controlling step which involves the adsorption of a species so polarised as to restore near octahedral symmetry about a surface cation (in an ionic solid) contributes to higher energies of activation and lower activities at the cation electron configurations d^0, d^5 and d^{10}. The same authors were also able to suggest that the theory provides a reasonable basis for the exploration of the relationship between homogeneous and heterogeneous catalysis and stressed the importance of lattice defects. Point defects were shown to play an important role not only in adsorption [41] but also in catalysis [42,43] with, in some cases, mechanisms derived from coordination chemistry principles [44]. Dislocations were also shown to be important in catalysis [45].

As pointed out by Burwell et al. [46,47], oxide surfaces will contain coordinatively unsaturated anions as well as cations and chemisorption will frequently involve both. They introduced the ***cus*** (coordinatively unsaturated) notation as a subscript attached to anions or cations to stress the coordination aspect [48]. Haber and Stone [49] considered chemisorption as a process by which the coordination characteristic of the bulk is partially or completely restored (Fig. 1) and calculated the crystal field stabilization (CFS) afforded by the chemisorption of oxygen on the various crystallographic faces of a nickel oxide crystal. They found that for low overall coverage of NiO by oxygen, the adsorption on (110) planes is particularly strong so that those planes are covered at the expenses of the (100) and (111) planes, thus giving a theoretical foundation for expecting crystallographic inequality.

The early sixties period turned out to be very important since the work of Dowden and Wells [39] triggered a number of major contributions. In this context of new interest in localized electronic defects, the concept of using oxide solid solutions was largely investigated by Selwood, Cimino, Stone and coworkers [50-53]. The principle, as applied to oxide catalysis, is to select a diamagnetic oxide of high crystal symmetry as the matrix (solvent) and to dissolve in it a second oxide which contains an ion or ions of particular catalytic interest [54]. In many cases the solute oxide is a transition metal oxide. The potentialities of solid solutions can now begin to be appreciated since one can investigate not only the catalytic activity of a selected TMI as the catalyst changes from insulating and paramagnetic behaviour in very dilute solutions to semiconducting and magnetic behaviour for increasing TMI concentrations, but also how adsorbed molecules are bonded to the TMI, depending on its location (face, edge or corner) and coordination at the surface.

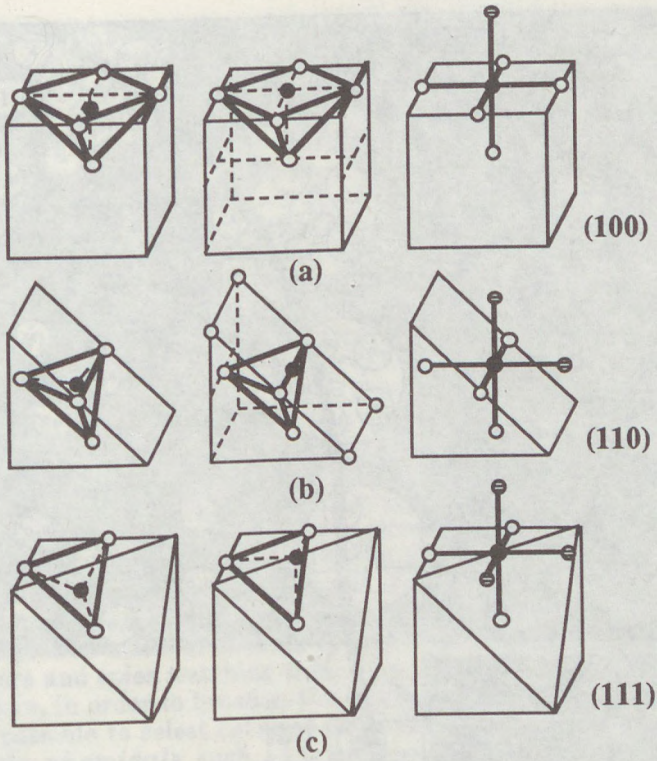

Figure 1. Changes in nickel ion coordination during the chemisorption of oxygen on NiO. (a), (100) plane; (b), (110) plane; (c), (111) plane. Diagrams in the middle column refer to a bare surface at the instant of cleavage. Left column, bare surface, relaxed position; right column, after adsorption of oxygen. black circles : nickel ion; open circles : lattice oxygen ions; shaded circles : adsorbed oxygen ions [49].

3. THE PRESENT TRENDS IN INTERFACIAL COORDINATION CHEMISTRY

As summarized above, early work that often did not distinguish electrostatic adsorption (Fig. 2, model III) [55] from grafting [56] (Fig. 2, model IV) [55] was mainly concerned with the gas-solid interface, since the catalysts were studied ***after*** preparation rather than ***during*** preparation.

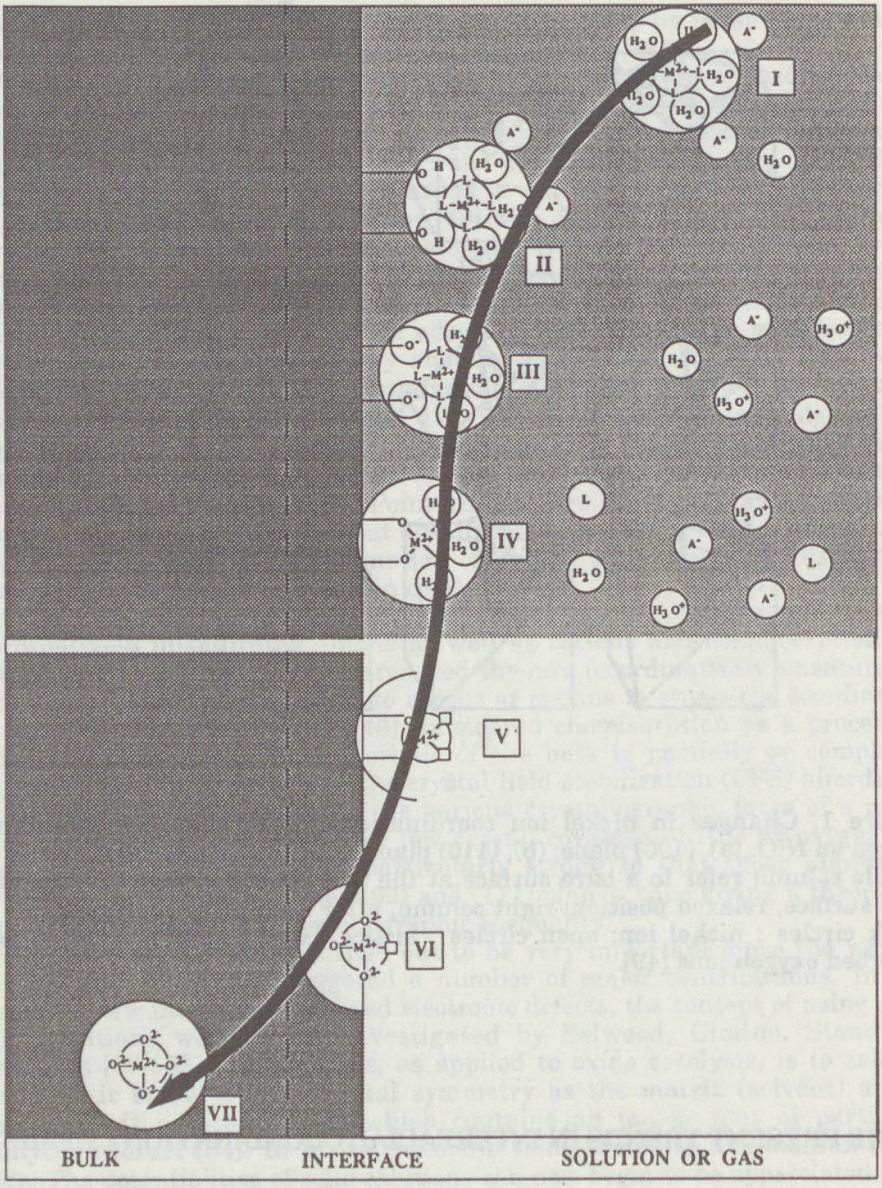

Figure 2. Representation of the outer sphere of solvation and coordination sphere of TMIs at various positions relative to the oxide-fluid (solution or gas) interface. The left-hand side represents the solid oxide. The shaded part on the right-hand side represents the solution while the lower white part on the same side represents the gas [55]. The meaning of the arrow is given in § 4.4.

Now it is known, particularly from zeolite preparation chemistry, that the different types of zeolites which are finally obtained have their origin in the very early stages of the hydrothermal process, i.e., during the aqueous chemistry part of their genesis. The same should be true for the preparation of oxide systems, all the more as often amorphous rather than crystalline materials are obtained. This has been a strong motivation particularly in our laboratory to follow the ***ion-support interactions*** (ISI) which develop through the successive stages of catalyst preparation. This generally implies the study of the ***liquid-solid interface*** before that of the gas-solid interface.

This approach raises a number of questions:
Are there any concepts which can help our understanding of catalyst preparation? What is the role of the support? Which are the parameters which are at hand to control ISI? How many different types of surface species are obtained? What does it mean to select one preparation method rather than another? Finally, having answered those questions, can we then hope to move from catalyst preparation to catalyst design?

In order to answer those questions, we need to have a suitable ***probe***. It is particularly fortunate that TMIs act most often as catalytic sites on an oxide support for they turn out to be also the most appropriate probes to follow their own interaction with the oxide support and ***see*** the evolution of the catalytic system all along its preparation. Because of their partly filled d orbitals, any change in their first coordination sphere immediately affects their optical and magnetic properties and can thus be detected by spectroscopy. In short, TMIs are both actors and spies watching their own acting.

Furthermore, in order to broaden the interest of our approach, we have tried as much as possible to select catalyst preparation methods which only require rather ***simple chemicals*** such as transition metal mononuclear complexes, essentially aqueous solutions and simple oxides, on the one hand, and are similar to those used in the industry, on the other hand. This differs from the supported homogeneous catalysis approach [57] where more involved inorganic or organometallic compounds or clusters are anchored [56] onto oxide supports, often via organic solvents. This aspect, which is well documented elsewhere [58-61], is not dealt with in this review. Neither will we cover the case of polyoxometalates or polyoxoacids which will be discussed by Misono in this Congress [62].

4. ICC CONCEPTS AND TRANSITION METAL IONS AS PROBES

In order to know how the properties of transition metal complexes are modified at fluid-solid interfaces during the different catalyst preparation steps, we need to have a reference state. Because of the wealth of data and theories available on solution CC, the latter appears to be the most convenient one.

4.1. The reference state: solution coordination chemistry

In aqueous solution, TMIs are complexed (Fig. 2, model I) by water and/or other ligands. This defines the inner sphere usually called coordination

sphere. One defines also an outer sphere of solvation formed by a layer of water molecules, with which the complex can move (i.e., rotate and translate) within the liquid medium. The concepts of such complexes, which are well established and described in textbooks [1], need not be repeated here.

4.2. The role of the support and the competitive ion exchange method

In order to understand the role of the support, the strategy adopted is to use a ***transition metal complex*** and investigate how the coordination sphere is modified during the preparation method and further post-synthesis (deposition) treatments.

4.2.1. The fluid-solid interface during competitive ion-exchange

Because of its pedagogical interest, the competitive ion exchange method has been selected to show that, if the adequate parameters of each preparation step are controlled, it becomes possible to obtain the TMI successively (Fig. 2) in solution (model I), then on (models II-V) and in (model VI) the surface, to finally reach the bulk of the oxide (model VII). In the following, we will often refer to the Ni/SiO_2 system, which has been studied in a more systematic way.

4.2.1.1. The physical nature of the oxide surface

The mobility of a TMI is strongly modified in the pore of an oxide. The ***perturbation*** produced by the liquid-solid interface, important for the first two layers of water which are strongly immobilized [63], decreases as one moves away from the surface. This anomalous water which has a thickness of 8 or 10 water layers freezes at temperatures lower than 0°C but does not crystallize. Cations can be trapped within this glassy matrix .

The previous results have been obtained on a set of copper impregnated silicas with a mean pore diameter ranging from 4 to 100 nm [64]. The EPR signal of Cu^{2+} ions ($3d^9$, S = 1/2, I = 1/2) was found to be characteristic of their location. For pores smaller than 6 nm and containing only a few layers of water, the signal, below -40°C, is axially symmetric due to Cu^{2+} in the glassy matrix. In large pores, a second EPR signal, isotropic and typical of Cu^{2+} in bulk water, is superimposed on the first one. At room temperature, the rotation or reorientation rate in the first layers of water was found to be 1.5 times slower than in bulk water. Both signals are assigned to the $[Cu(H_2O)_6]^{2+}$ complex and it appears that there is no specific adsorption at the surface.

The perturbation can be more important in faujasite-type zeolites with smaller pores. During the exchange procedure, copper ions enter into the supercages through the large windows (0.8-0.9nm). With a capacity of 28 water molecules and 1.14nm internal diameter [65], those cages can accomodate the $[Cu(H_2O)_6]^{2+}$ complex with its outer sphere of solvation. An EPR study [66] shows that the rotation rate of the complex is 10 times slower than in bulk water, due to the close vicinity of the cavity walls. In all the examples cited above, the coordination chemistry of the TMIs is basically ***not changed*** and model I (Fig. 2) is convenient. Only the mobility of TMIs is affected by the solid, which can be considered as a ***microcontainer***, all the more as the pores are smaller.

The interface appears to drastically affect the dielectric constant of water. The associated dipoles in the first water layer in contact with the surface are aligned. As a consequence, the dielectric constant ε of water drastically decreases from its bulk value 78.5 to 32 in the second layer and 6 in the first layer [67]. This is discussed further in the next section.

A direct physical interaction is likely to occur between TMIs and the oxide for pHs that do not lead to dissociation of surface OH groups. Through its OH groups, the oxide is able to enter the outer sphere of solvation of the complex in the same way as the solvent molecules (Fig. 2, model I) and thus acts as a ***solid solvent*** (Fig. 2, model II). This aspect, which is little documented, is different from that encountered in zeolites which can act as solid ionic solvents [68] or in oxides where TMIs come to rest after high temperature diffusion to form doped or mixed oxides (§ 2.3) [69].

Copper ions deposited at the surface of alumina or magnesia by impregnation (see § 4.3.1) are characterized by EPR as species immobilized at room temperature [64]. This specific interaction refers now to the ***chemical nature*** of the oxide surface and this is considered in the next paragraphs.

4.2.1.2. The oxide surface as a supramolecular counterion or capacitor plate

Oxides in aqueous suspension are generally electrically charged as shown directly by electrophoresis experiments [11]. This is attributed to the amphoteric dissociation of the surface hydroxyl groups following the reactions:

$$SOH_2^+ \Leftrightarrow SOH + H^+ \qquad K_1 \qquad (1)$$

$$SOH \Leftrightarrow SO^- + H^+ \qquad K_2 \qquad (2)$$

where K_1 and K_2 are the equilibrium constants of processes (1) and (2) respectively. There is a characteristic pH = $(pK_1 + pK_2)/2$ called the isoelectric point (IEP) or zero point charge (ZPC) at which a given immersed oxide surface has a zero net charge [70], i.e., $[SOH_2^+] = [SO^-]$. At a pH above its IEP, the oxide surface is negatively charged so that cations may be adsorbed. By contrast, at a pH below its IEP, the oxide surface is positively charged leading to an adsorption of anions [11]. The IEP can be used to predict molecular structures of surface metal oxide species on oxide supports [11,71]. It is important to stress that the primary role of the pH, on the solid side, is to act as a ***surface charge selection switch*** [72,73].

In practice, the ion exchange method is often used in its competitive form, where two types of ion compete for the same adsorption sites. The equilibria can be represented by the following equations:

$$SOH_2^+ A^- + B^- \Leftrightarrow SOH_2^+ B^- + A^- \qquad \text{competitive anion exchange} \qquad (3)$$

$$SO^- C^+ + D^+ \Leftrightarrow SO^- D^+ + C^+ \qquad \text{competitive cation exchange} \qquad (4)$$

In contrast to impregnation where both the cations and their counter-anions (or vice-versa) are deposited, the ion exchange method leads to the adsorption of ***only*** one type of ions. Another very interesting feature of the ion exchange

method is that the counterion (see equation 5 below) can be easily removed by washing since it is repelled from the surface which possesses charges of the same sign. This is an important advantage over the impregnation method where washing cannot be used owing to the weak interaction between the precursor and the surface.

The secondary role of the pH, now on the solution side, is to act as a ***transition metal complex selection switch*** [73]. In many complexes, the nuclearity and coordination number remain constant and only the nature of the ligands changes (Fig. 3a) [74]. In some others, the nuclearity and coordination number vary, as in polyoxo- molybdates and tungstates [75].

Cation exchange of nickel on silica using nickel nitrate in water-ammonia solution has been studied in detail by UV-vis. spectroscopy [76]. The NO_3^- counterion, monitored by a band at 33000 cm^{-1} assigned to the ($n \rightarrow \pi^*$) transition, is removed upon successive washings (Fig. 4). This indicates that the exchange has occurred with the oxide surface which acts as a ***supramolecular counterion***. Here, the TMI is bonded to the oxide surface by ***ligand-screened electrostatic adsorption*** (Fig. 2, model III). The reaction can be written as follows:

$$(Ni^{2+}, 2NO_3^-) + 2\,\{\equiv SiO^-, NH_4^+\} \Leftrightarrow 2\,(NH_4^+, NO_3^-) + \{2\,\equiv SiO^-, Ni^{2+}\} \qquad (5)$$

where Ni^{2+} stands for the hexaammine $[Ni(NH_3)_6]^{2+}$ complex.

In parallel, a set of 3 bands characteristic of octahedral Ni(II) ($3d^8$) is also observed. At a pH above 9, the $[Ni(NH_3)_6]^{2+}$ complex is adsorbed without modification of its UV-visible spectrum even after the 2nd washing step, indicating a pure electrostatic adsorption with formation of ***surface ion pairs***, $\{2\,\equiv SiO^-, [Ni(NH_3)_6]^{2+}\}$, where the whole surface is considered as an ion. Adsorbed complexes exhibit reactivities, such as ligand exchange, closely similar to those of their solution analogues [8].

The decrease of the dielectric constant ε of water mentioned earlier (§ 4.2.1.1) greatly favors the stability of ion pairs at the surface. The forces maintaining the TMIs on a negatively charged surface can be described in the double layer electrostatic model [77] and are similar to those involved between the plates of a capacitor so that the oxide surface can be envisaged as a ***capacitor plate***.

Ammonium ions also present in the solution can compete with the nickel hexaammine complexes to occupy the exchange sites of silica as follows:

$$2\{\equiv SiO^-, NH_4^+\} + [Ni(NH_3)_6]^{2+} \Leftrightarrow \{2\,\equiv SiO^-, [Ni(NH_3)_6]^{2+}\} + 2\,NH_4^+ \qquad (6)$$

The competition level between NH_4^+ and Ni^{2+} ions, expressed as the ratio of their concentrations, allows to better control the amount and dispersion of nickel adsorbed.

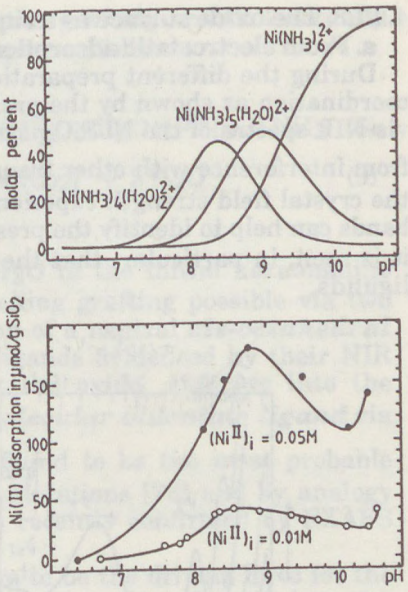

Figure 3. (a) Distribution of the Ni(II) ammine complexes as a function of pH for (NH_4^+) = 1M; (b) Amounts of Ni(II) adsorbed on SiO_2 as a function of pH after exchange with 0.01 and 0.05M initial Ni(II) ammoniacal solutions [74].

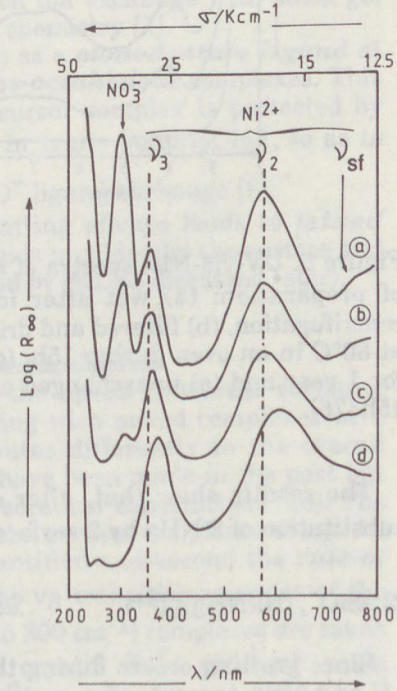

Figure 4. UV-vis. spectra of a 2.7 wt% Ni/SiO_2 sample: (a) after exchange with a 4 M NH_3 solution, (b) after a first washing with a 1.33 M NH_3 solution, (c) after a second washing with a 0.44 M NH_3 solution and (d) after a third washing with a 0.148 M NH_3 solution. All the spectra are recorded after centrifugation [76].

4.2.1.3. The oxide surface as a supramolecular ligand

a. From electrostatic adsorption to grafting

During the different preparation steps, the Ni(II) ions remain in octahedral coordination as shown by the presence of 3 spin-allowed transitions in the UV-vis-NIR spectra of the Ni/SiO_2 system (Fig. 5) [78]. Because it is essentially free from interference with other transitions, the ν_3 band has been used to measure the crystal field strength experienced by the Ni(II) ions [76]. The near IR (NIR) bands can help to identify the presence of NH_3 and H_2O ligands (Fig. 5) [79] and it is seen, in particular, that the Ni(II) complex gradually looses its ammonia ligands.

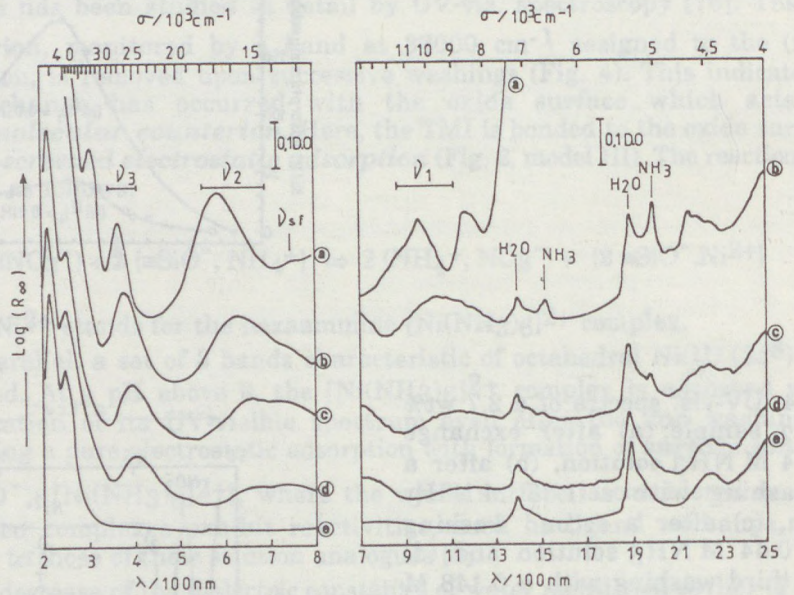

Figure 5. UV-vis-NIR spectra of a 1.7 wt% Ni/SiO_2 sample after different steps of preparation: (a) wet after ion exchange in a 1.5 M NH_3 solution and centrifugation, (b) filtered and dried at 20°C in air for 15 h, (c) filtered and dried at 80°C in an oven during 15h, (d) calcined at 500°C in oxygen and rehydrated for 1 year and (e) unexchanged ammoniated silica dried at 80°C in an oven for 15h [76].

The results show that, after electrostatic adsorption, ***grafting*** occurs via substitution of 2 NH_3 by 2 surface $\equiv SiO^-$ ligands according to the process:

$$\{2 \equiv SiO^-, [Ni(NH_3)_6]^{2+}\} \quad \Leftrightarrow \quad [Ni(NH_3)_4(\equiv SiO)_2] \quad + \quad 2\,NH_3 \qquad (7)$$

Since grafting occurs during the third washing step (Fig. 4) in conditions of pH and NH_3 concentration corresponding to the stability range of the complex

$[Ni(NH_3)_4(H_2O)_2]^{2+}$, it is most likely that the grafting reaction actually proceeds via the intermediate tetraammine complex as follows:

$$\{2 \equiv SiO^-, [Ni(NH_3)_6]^{2+}\} + 2\,H_2O \Leftrightarrow \{2 \equiv SiO^-, [Ni(NH_3)_4(H_2O)_2]^{2+}\} + 2\,NH_3 \quad (8)$$

$$\{2 \equiv SiO^-, [Ni(NH_3)_4(H_2O)_2]^{2+}\} \Leftrightarrow [Ni(NH_3)_4(\equiv SiO)_2] + 2\,H_2O \quad (9)$$

It appears that the ligand exchange NH_3/H_2O in the initial hexaammine complex ***weakens*** the coordination sphere making grafting possible via two surface bonds (Fig. 2, model IV), with formation of a neutral ***cis-octahedral complex***. The latter still contains ammonia ligands evidenced by their NIR bands (Fig. 5). It is important to note that the oxide, entering into the coordination sphere of Ni^{2+}, becomes a ***supramolecular bidentate ligand*** via vicinal $\equiv SiO^-$ groups. The latter have been found to be the most probable grafting sites, on the basis of geometrical considerations [76] and by analogy with the silicate structure [80]. This has been recently confirmed by EXAFS studies [81].

The ***chelating effect of the surface*** appears to be the driving force for the formation of the surface cis-octahedral complex. Equation (7), which is the sum of equations (8) and (9), is accompanied by an entropy increase with the release of water molecules and the disappearance of charged species leading to a subsequent disordering of nearby solvent molecules [82]. This aspect, already mentioned in earlier thermodynamical studies on ion exchange with silica gel [83] is well documented in solution coordination chemistry [1].

In certain cases, the oxide surface can act also as a ***monodentate ligand*** at the fluid-solid interface and lead to surface ***trans-octahedral*** complexes. This occurs, for instance, when the TMI in the precursor complex is protected by strong field ligands, such as ethylenediamine in $trans\text{-}Co(en)_2Cl_2^+$, so as to offer only one possible grafting site by a $Cl^-/\equiv SiO^-$ ligand exchange [8].

The last point worth to mention is that grafting always leads to ***mixed complexes*** with two types of ligands : ***rigid*** ligands provided by the surface and ***mobile*** ligands provided by the fluid phase (liquid or gas, as discussed later).

b. The oxide surface and the ligand spectrochemical series

The inclusion of the oxide surface within the spectrochemical series of ligands is a difficult problem since we are dealing with mixed complexes with different types of ligands, which each contributes differently to the overall crystal field experienced by the TMI. Attempts have been made in the past but failed to give conclusions in agreement with theoretical expectations [36]. The problem can however be solved, providing first the surface complexes along the different preparation steps be prepared and identified and second the ***rule of average environment*** [84] be applied [76]. The ν_3 transition energies of the $[Ni(NH_3)_6]^{2+}$ (28 200 cm^{-1}) and $[Ni(H_2O)_6]^{2+}$ (25 300 cm^{-1}) complexes are taken as references [85-87]. The decrease of the crystal field strength upon substitution of NH_3 by H_2O in the $[Ni(NH_3)_6]^{2+}$ complex is assumed to be a

linear function of the number of NH_3 ligands. A bathochromic $\Delta\nu_3$ shift of -480 cm^{-1} is thus readily obtained for each NH_3 substituted by H_2O.

Since the ν_3 transition of $[Ni(\equiv SiO)_6]^{4-}$ in solution is not available, we have to apply the rule using $[Ni(H_2O)_6]^{2+}$ (25 300 cm^{-1}) and $[Ni(\equiv SiO)_2(H_2O)_4]$ (24 700 cm^{-1}) as references. The composition of the latter complex derives from the fact that ammonia is no longer detected in its spectrum (Fig. 5d) and that more than two bonds between Ni^{2+} and the surface would lead to a very distorted symmetry and hence to more than the three bands observed. The application of the rule of average environment gives a shift of -300 cm^{-1} for each H_2O molecule replaced by a $\equiv SiO^-$ ligand in the $[Ni(\equiv SiO)_2(H_2O)_4]$ complex.

The substitution first of NH_3 by H_2O ($\Delta\nu_3$ = -480 cm^{-1}) and then of H_2O by $\equiv SiO^-$ ($\Delta\nu_3$ = -300 cm^{-1}) gives a total bathochromic shift of -780 cm^{-1} when NH_3 is replaced by $\equiv SiO^-$. The values derived above allow to ***insert the $\equiv SiO^-$ ligand within the spectrochemical series*** as follows:

$$\equiv SiO^- < H_2O < NH_3 \qquad (10)$$

This order is consistent with theoretical expectations. As a matter of fact, the three ligands are all σ–donors. However, it is known from molecular orbital theory that the crystal (ligand) field they can produce is all the more important as their π-donor character decreases [1]. This is in good agreement with the presence of two, one and zero lone pairs on the donor atom for the $\equiv SiO^-$, H_2O and NH_3 ligands respectively. The oxalate $C_2O_4^{2-}$ ligand, with two terminal O^- ions, appears to be a very close analogue of the surface bidentate ligand which is a ***σ donor - π donor weak ligand***. Similar results are obtained with the Cu/SiO_2 system prepared by ion exchange from $[Cu(en)_2]^{2+}$ precursors [88]. The same approach has been taken for other systems such as Pd/SiO_2, Pd/Al_2O_3 and Pd/faujasite-type zeolites using square planar Pd(II) precursor complexes and led to a ***spectrochemical series of supports*** [89].

4.2.1.4. The oxide surface as a reactant

A number of papers have reported the presence of intermediate compounds (silicates in particular) after preparation involving the liquid-solid interface, which suggests that the support can act as a ***reactant***. Although there has been no systematic study on this aspect, the contact time between the solution and the support seems to play an important role. For instance, after an exchange process of 500 hours, nickel is found to be essentially as a nickel silicate deposited on silica [90,91].

There are some favourable conditions for the oxide surface to become a reactant. One of the main parameters to achieve this goal is again the pH which, in its third role (see § 4.2.1.2), controls the ***solubility of the oxide*** depending on its acid-base character [11]. For instance, the solubility of an

acidic oxide such as silica increases rapidly in a basic medium [92]. An amphoteric oxide such as alumina dissolves either in basic or acidic medium, while basic oxides such as NiO dissolve only in acidic medium [11]. The solubility of the oxide can be regarded as a depolymerisation process leading to ***support monomers***, which can then copolymerise with the transition metal complexes regarded as ***solution monomers***. This reaction, particularly for long contact times of the oxide support with the exchange solution, can lead to new phases such as nickel silicates for the Ni/SiO_2 system.

Since the pH conditions required for the oxide dissolution ***coïncide*** with those required for ion exchange, it is important to look for parameters which can put the two latter phenomena out of phase, i.e., inhibit the copolymerisation process. It is first necessary to understand how bond formation occurs between ***molecular*** solution species. Sol-gel processes indicate that there are some preferred pathways such as :

$$\text{M-OH} + \text{M-H}_2\text{O} \Leftrightarrow \text{M-OH-M} + \text{H}_2\text{O} \quad (11)$$

$$\text{M-OH} + \text{M-OH} \Leftrightarrow \text{M-O-M} + \text{H}_2\text{O} \quad (12)$$

where M represents the support ion and/or any TMI.

Olation (reaction 11) and ***oxolation*** (reaction 12) are condensation processes in which a ***hydroxy*** or an ***oxo bridge*** between two metal centres are formed respectively [93]. It becomes clear now that if H_2O, OH or O, which all are bridging ligands, are substituted by non bridging ones such as NH_3 around the transition metal ion, bond formation between the two metal centres will be inhibited.

This is illustrated by recent EXAFS experiments performed with the Ni/SiO_2 system [81]. At pH around 9, in a domain where the silica surface can dissolve, the coordination sphere of Ni^{2+} ions, which is protected by ammonia or ethylenediamine (en), is not modified by electrostatic adsorption on the support. This shows that M-O-M bond formation does not occur in presence of such ***strong non bridging ligands***.

Below pH around 9, ammonia in smaller concentration can be substituted by the weaker water ligand to form penta- and tetraammine complexes (Fig. 3a). Under these conditions, the coordination sphere is ***weakened*** and grafting of the Ni^{2+} ions occurs with formation on silica of a surface silicate, where a large proportion of nickel ions are engaged. This demonstrates that the support, although less soluble than at the pH of the preceding example, can nevertheless become a reactant, because olation (reaction 11) between Si-OH and the Ni-OH_2 end of molecular $[Ni(NH_3)_{6-n}(H_2O)_n]^{2+}$ solution monomers (n=1,2) can now occur. The stability of the species involved and the kinetics of the processes (oxide dissolution and bond formation by copolymerisation), which all are temperature dependent, seem to be important factors. As a matter of fact, drying experiments performed at higher temperatures (353K) always lead to silicate, whatever the pH of the exchange solution. By contrast, the $Ni(en)_3^{2+}$ complex, which is very stable above pH 7 and involves ***non bridging and strong chelating ligands***, does not lead to silicate formation but to isolated Ni^{2+} ions stable up to calcination temperatures of 500°C [81].

We can now better understand [94], at least from a qualitative point of view, the curves of Figure 3b. If the ion exchange were the only process involved, the

amount of Ni deposited onto silica as a function of the pH of the exchange solution would qualitatively follow the exchange capacity derived from the pH dependence of the zeta potential of silica (Fig. 6) [73]. Note here that the fourth role of the pH, on the solid side again, is to control quantitatively the ***exchange site concentration***.

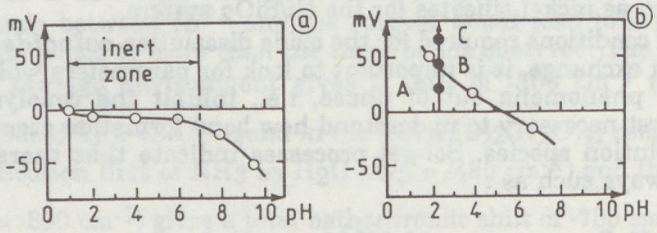

Figure 6. The variation of the exchange capacity expressed by the pH dependence of the zeta potential of a) SiO_2 and b) TiO_2 obtained by electrophoresis [73].

The latter shows that the cationic exchange capacity of silica is negligible in the so-called inert zone and increases significantly only above pH 7 (the negative sign just indicates that the surface charge is negative as expected from equation 2). The experimental results, however, show (Fig. 3b) that the ion exchange is not the only process involved.

Below pH 6, the absence of adsorption is explained by the vicinity of the isoelectric point of silica: the surface charge density is very low and the amount of Ni(II) complexes adsorbed electrostatically is therefore negligible. On the other hand, the dissolution of silica is also negligible, hence nickel silicates cannot form. While the amount of adsorbed nickel is expected to increase after the inert zone above pH 7, the presence of the maximum around 8.6 is against expectation. The latter can be explained by reference to Figure 3a which exhibits also maxima for tetra- and pentaammine Ni(II) concentrations precisely around this pH. The spectroscopy results (§ 4.2.1.3. a) have shown that the tetraammine complex is indeed important in the grafting process. Between pH 8 and 10, it is likely that the ion exchange of Ni(II) ions onto silica gives rise to a mixture of nickel silicates and Ni(II) electrostatically adsorbed whose relative concentrations probably depend on the contact time between the exchange solution and the support. Above pH 9.5, it is clear that the complexation of Ni(II) as hexaammine (Fig. 3a) with no bridging ligand inhibits the silicate formation and favours pure electrostatic adsorption, which is quantitatively limited, the competition with NH_4^+ ions being important. The adsorption decrease between pH 8.6 and 10 is due to the increase of hexaammine Ni(II) concentration. The sharp adsorption increase when pH exceeds 10 can be attributed to the dissolution of silica which becomes significant above pH 8. The mechanism of Iler [92] (Fig. 7) explains how the latter leads to a significant increase of the silanol groups density and hence of the exchange capacity of silica.

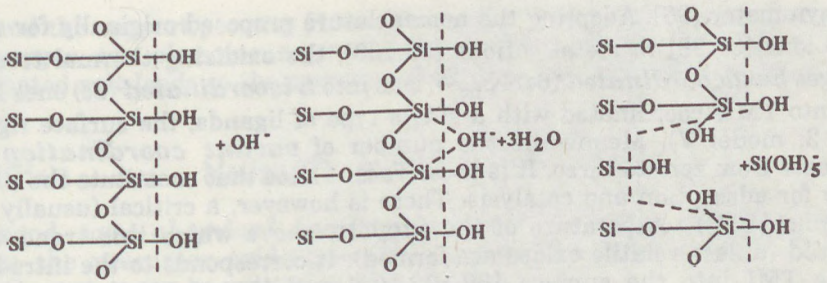

Figure 7. The solubility of SiO_2 and the formation of new surface OH groups [92].

As shown above, the two domains of interfacial coordination chemistry (§2.1.2.3.) and ***surface solid state chemistry*** (this §) have distinct characteristics with the oxide surface acting essentially as supramolecular ligand and reactant respectively. The previous results suggest that parameters in the frontier region between the two domains are not completely known as yet. It is felt, in particular, that the contact time between the support and the exchange solution is an important parameter but this has not been much studied. The passage from one to the other domain may be reversible. For instance, Clause et al. [95] have shown that the nickel silicate phase formed in samples prepared by ion exchange from ammoniacal solutions could decompose and that thermal treatment under reduced pressure favoured the process.

4.2.2. The fluid-solid interface during oxidizing thermal treatment

In § 4.2.1.3., the experimental conditions were such (oxidizing conditions, short contact times between the solid and the liquid and ligand excess) that the TMIs remained in the same oxidation state and coordination number as those of their solution precursors. If we now, say by thermal treatment in oxidizing atmosphere, slowly remove the ligands, we can still keep the oxidation state constant while decreasing the coordination number at the gas-solid interface.

The TMIs grafted on the surface by reversible ion exchange reactions are expected to be highly dispersed on the surface. Under calcination in pure oxygen, the exchanged ions behave as isolated species and never lead to NiO up to 700°C. From the number and intensity of the bands in the UV-vis-NIR spectra, it is possible to conclude that the symmetry of the Ni^{2+} ions decreases when the calcination temperature increases from 25 to 700°C leading to a change of the coordination number from 6 to 3 (Fig. 8). In the latter case, the oxide surface becomes a ***terdentate ligand***. In addition to the 2 first iono-covalent bonds created during grafting (reaction 7), a dative bond is formed with a bridging oxygen of a siloxan surface group (Si_2O) leading basically to a

C_{3v} symmetry [96]. Adopting the nomenclature proposed originally for surface oxide ions [97,98] to metal cations [99,100], the oxidizing thermal treatment changes ***hexacoordinated*** (6c) Ni_{6c}^{2+} ions into ***tricoordinated*** (3c) ones Ni_{3c}^{2+}, i.e., into TMIs coordinated with a single type of ligands, the surface rigid one (Fig. 2, model V). Meanwhile the number of ***vacant coordination sites*** increases from zero to three. It is those vacant sites that constitute the ***driving force*** for adsorption and catalysis. There is however, a critical (usually called Tamman [101]) temperature of the support, above which this trend will be reversed (unless volatile oxides are formed). It corresponds to the introduction of the TMI into the support [69,102,103] and thus to an increase of the coordination number up to the one imposed by the host matrix [102,103]. The temperature appears also as an important parameter to switch from interfacial coordination chemistry to ***bulk solid state coordination chemistry*** (Fig. 2, model VII).

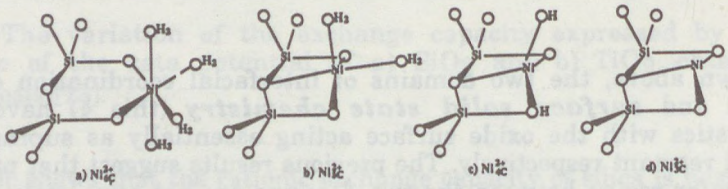

a) Ni_{6c}^{2+} b) Ni_{5c}^{2+} c) Ni_{4c}^{2+} d) Ni_{3c}^{2+}

Figure 8. The changes of coordination experienced by grafted complexes upon oxidizing thermal treatment of the Ni/SiO_2 system.

4.3. The role of the support as a function of the preparation method

As described for the competitive ion exchange method, the support oxide fullfils a different role at each step of the preparation. There exists no systematic study for other catalyst preparation methods. There are however enough results to be able to draw some conclusions for the most common preparation methods [73,104]. Whenever possible, we will insist on the role of the support at each preparation step and also on coordination chemistry aspects.

4.3.1. Impregnation

In this method, a preformed support is impregnated with an aqueous solution of a metal salt. Here ***both*** the TMI and its counter ion are deposited on the support which acts only as a ***mere physical surface***. It should be noted that there is no washing step after impregnation, since the metal salt would be eliminated, owing to the ***weakness*** of interaction with the support. The subsequent drying step, usually performed at around 100°C, is important since the metal salt is reformed from the individual solvated cations and anions and redistributed at the support surface in a way which depends both on the drying

speed and the support porosity [104]. During the calcination step performed in air or oxygen, two phenomena generally occur. First, the decomposition of the impregnated salt leads to the corresponding oxide according to a reaction such as :

$$MoO_4(NH_4)_2 \rightarrow MoO_2(OH)_2 \text{ (or } MoO_3 + H_2O) + 2\,NH_3 \qquad (13)$$

and second, some ***chemical bonding*** is established upon dehydroxylation between the precursor oxide and the support. A typical example for the Mo/Al_2O_3 system can be written as follows [105]:

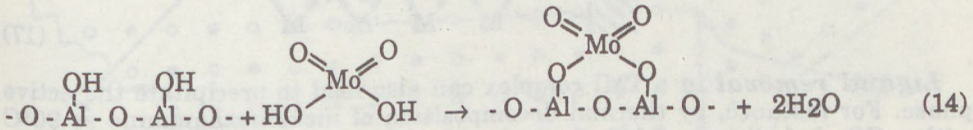

(14)

During the latter step, it can be seen that the support through its hydroxyl groups acts as a ***reactant***.

4.3.2. Deposition-precipitation

Deposition-precipitation [106,107] consists in precipitating a metal salt on an oxide surface by varying the pH of the solution homogeneously. Geus et al [106-108] proposed the thermal decomposition of urea to produce OH^- ions, which becomes significant above 60°C. It is important the pH be raised slowly, so as to involve the OH groups in ***copolymerisation*** processes described by reactions (11) and (12) between solution monomers and the support as a solid and no longer as dissolved monomers. The following scheme illustrates the fact that the surface is a ***nucleation initiator*** because of the favorable ***acid-base*** reaction between the surface hydroxyl groups and the metal hydroxy complex :

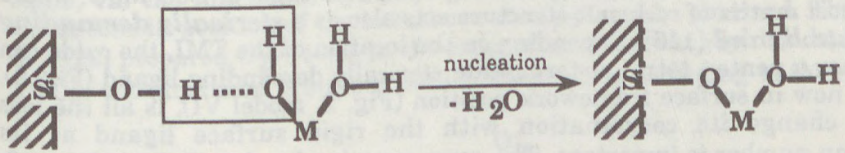

(15)

The hydroxy complex can be formed by L/OH^- ***ligand substitution*** (L = H_2O, NH_3..) or a dissociation reaction [109] such as :

$$M^{n+}(H_2O) \rightarrow M(OH)^{(n-1)+} + H^+ \qquad (16)$$

The subsequent step of ***growth*** can then occur via ***olation*** (see reaction 11), i.e., elimination of water from the μ-(H_3O_2) ligands [110] leading to a μ-(OH) ***bridging ligand***, considered to be the first step of precipitation [111,112]. The surface plays the role of a ***reactant*** with its hydroxyl groups as shown below. The difference with the growth mechanism occurring in solution is that TMI's have to diffuse into the pores of the oxide and reach the support surface.

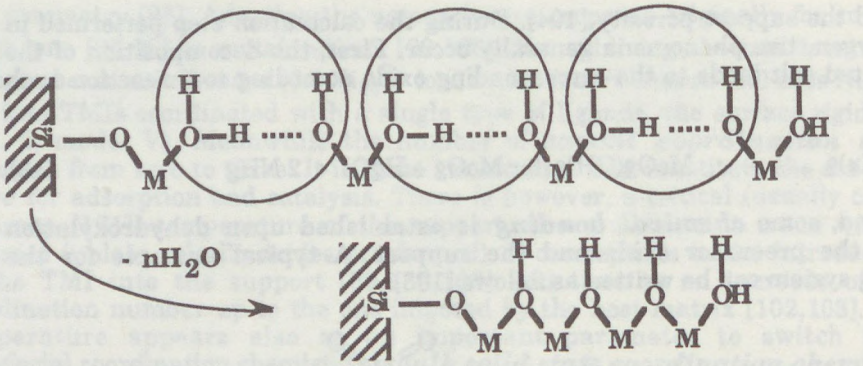

(17)

Ligand removal in a TMI complex can also lead to precipitate the active phase. For instance, by thermal decomposition of nickelhexaammine at 90°C with a CO_2 bubbling a nickel aluminium hydroxycarbonate is precipitated on alumina. This however occurs with γ- or θ-Al_2O_3 but not observed with α-Al_2O_3 [113]. This example shows that the surface is not inert and because of the dissolution of the oxide to form ***molecular*** species, it can act as a ***reactant*** [114], thus changing the nature of the precipitate [113]. Clause et al. [115] reached the same conclusion for the Ni/SiO_2 system and presented evidence by EXAFS that nickel silicates likely of nepouite structure, ($Ni_3Si_2O_5(OH)_2$), were formed.

4.3.3. Coprecipitation

The coprecipitation in a precursor form (hydroxides, carbonates..) of both the support and the active phase from a solution has the advantage to produce an intimate mixing. The coprecipitate leads on calcination to a support with the active component dispersed throughout the bulk as well as at the surface. The support can thus be considered as a ***solid solvent***.

The ideal case is obtained for systems such as NiO-MgO or CoO-MgO, where the MgO host matrix of rock-salt structure acts also as a ***sterically demanding polydentate ligand*** [116]. Depending on the location of the TMI, the oxide can act as either a penta-, tetra- or terdentate sterically demanding ligand (Fig. 9). The TMI, now in surface framework position (Fig. 2, model VI), is all the less likely to change its coordination with the rigid surface ligand as its coordination number is important. The same notation has been adopted for O^{2-} [97,98] and TMIs [99,100] in positions of ***low coordination*** and can be easily extended to other types of ions, providing the coordination number be known. This problem, easy for TMIs, becomes major for s and p group elements, because they lack partly filled d orbitals.

4.3.4. Grafting

This process consists in performing a chemical reaction between a metal chloride (or oxochloride) and the hydroxyl groups of an oxide as follows [117]:

$$MCl_n + m\ S\text{-}OH \rightarrow MCl_{n-m}(OS)_m + m\ HCl \qquad (18)$$

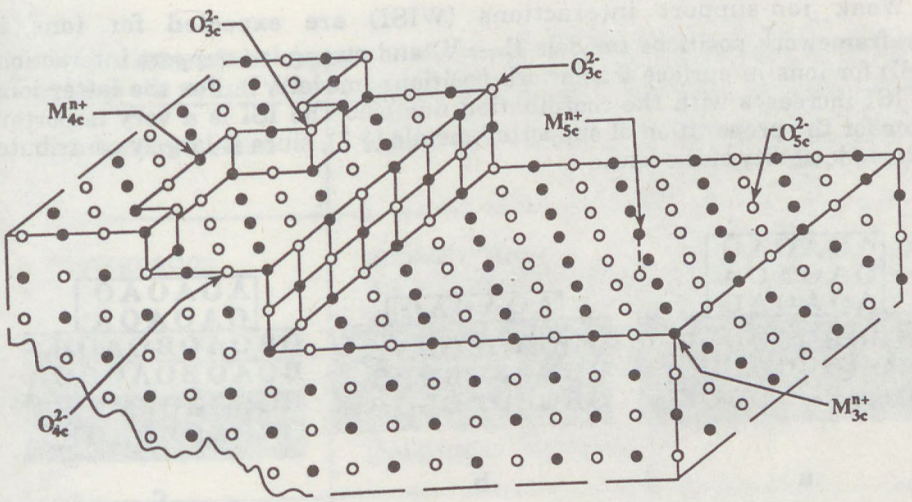

Figure 9. Representation of a surface (100) plane of MgO showing surface imperfections such as steps, kinks, corners, etc.. which provide sites for M_{lc}^{n+} and O_{lc}^{2-} ions of low coordination (lc = 3c, 4c, 5c). M^{n+} ions can be either Mg^{2+} or TMIs such as Co^{2+}, Ni^{2+} etc.

where M stands for the metal and S for the support while m=1-3 depends on the reaction conditions and content of surface hydroxyl groups [118,119]. The metal (oxo)chloride is either gaseous or dissolved in an organic solvent [120,121]. This approach. The advantage with metal (oxo)chloride vapour is to deal with isolated molecules. Grafting leads directly to model IV of Figure 2 with the oxide, via the functional hydroxyl groups, acting as a ***molecular reactant***. Oxide ions in position of the lowest coordination can be obtained. Thus, Anpo et al. [122] prepared O_{1c}^{2-} ions, in the form of terminal vanadyl bonds, by reacting $VOCl_3$ with hydroxyl groups of porous Vycor glass according to the reaction :

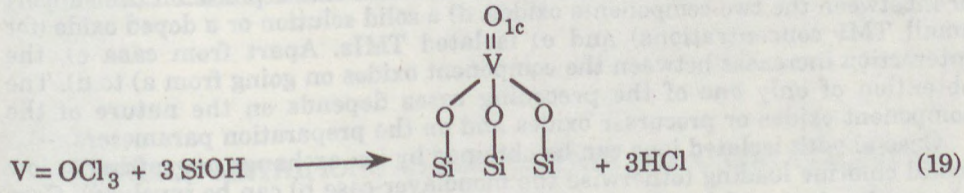

4.4. The nature of ion-support interactions

Table 1 summarizes the main points discussed in the previous sections. It also gives the nature of ion-support interactions (ISI) [73]. The strength of ISI ***increases*** along the sequence of models (I → VII) given by the arrow in Figure

2. Weak ion-support interactions (WISI) are expected for ions in extraframework positions (models II → V) and strong ion-support interactions (SISI) for ions in surface framework positions (model VI). For the latter ions, the ISI increases with the coordination number. The ISI is a very important factor for the preparation of supported metals (§ 7), since it largely contributes to the reducibility of the ions.

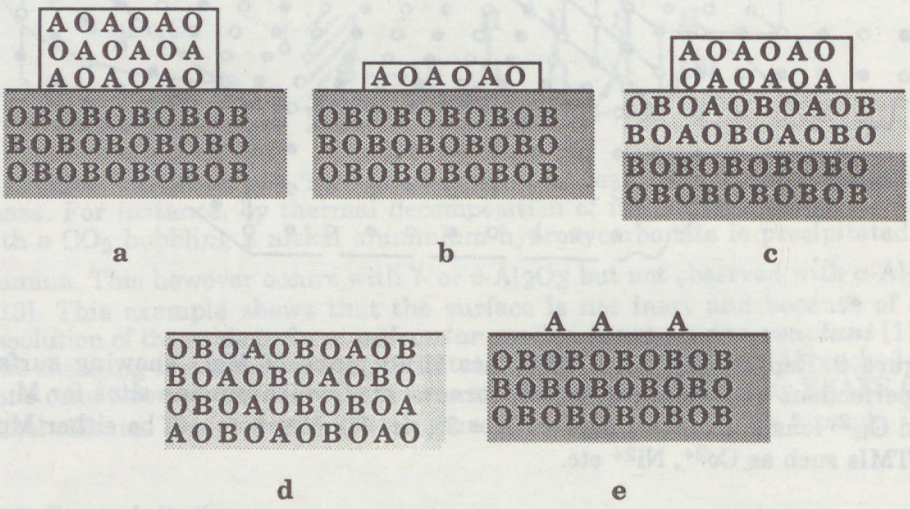

Figure 10. The various possible interactions between TMIs or oxides and a support oxide, where A stands for TMIs, B for support cations and O for O^{2-} oxide ions [73].

Figure 10 extends the different possible interactions [73], first considered by Roozeboom et al. [123], between the support and the active phase with formation of a) a 3-dimensional (3D) metal oxide on the support, b) a 2D metal oxide (monolayer or islands) on the support, c) an intermediate phase on the support or inbetween the two components oxides, d) a solid solution or a doped oxide (for small TMI concentrations) and e) isolated TMIs. Apart from case e), the interaction increases between the component oxides on going from a) to d). The obtention of only one of the preceding cases depends on the nature of the component oxides or precursor oxides and on the preparation parameters.

Case e) with isolated ions can be obtained by ion exchange or grafting at low metal chloride loading (otherwise the monolayer-case b) can be involved). Case b) may be produced by the so-called solid-solid adsorption which consists in heating a mechanical mixture of the active precursor and the support [124]. This leads to a spontaneous dispersion of the active precursor on the support.

Despite the clear-cut distinction between the systems of Figure 10, the real situation is very often a combination of the different cases.

Table 1
The various roles of the support oxide as a function of the catalyst preparation method and the nature of ion-support interaction [73]

Preparation method	Role of the support	Nature of the TMI-support interaction
Impregnation	Microcontainer Mere physical surface Solid solvent	Van der Waals forces Van der Waals forces Hydrogen bonding
Deposition-Precipitation	Acid-base reactant (Nucleation initiator)	Iono-covalent bonding
Coprecipitation	Solid solvent (Sterically demanding polydentate ligand)	Iono-covalent bonding
Ion exchange	Capacitor plate Reactant (mono- or polydentate ligand)	Ion pair (Electrostatic adsorption) Iono-covalent bonding (Grafting)
Grafting	Reactant (mono- or polydentate ligand)	Iono-covalent bonding

5. TRANSITION METAL IONS AS ADSORPTION AND CATALYTIC SITES

Many adsorption and catalysis studies have been performed in the past. We will again restrict our attention to studies related to TMIs either in their oxidized or reduced state and select examples which emphasize the coordination chemistry and molecular aspects.

5.1. Adsorption sites

5.1.1. Surface ions in framework positions

A well known example of adsorption in solution coordination chemistry is the reversible fixation of molecular oxygen by cobalt complexes, referred to as reversible oxygen carriers [125] following the reaction :

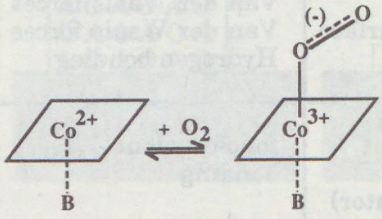

(20)

where cobalt ions are coordinated to a Lewis base B and square planar sterically demanding ligands such as Schiff bases, porphyrins etc..

Recently, the same type of reversible adsorption has been observed on purely inorganic systems [126]. A good example of ***synthetic heterogeneous inorganic oxygen carrier*** is represented by dilute CoO-MgO solid solutions. Even in a high surface area state, the latter are mainly in the form of microcrystals of prevalent cubic shape. On the faces of such cubes (Fig. 9), the Co_{5c}^{2+} ions are penta-coordinated, i.e., in a coordination similar to that of their solution analogues. It can be seen that, in the solid system, the equatorial square planar ligand is constituted by 4 O_{5c}^{2-} ions and the Lewis base by an axial O_{6c}^{2-} ion. The reversibility of oxygen adsorption has been studied by IR and ESR [127] and the end-on structure of the oxygen superoxide adduct confirmed with ^{17}O by ESR [128]. Both were found to be again similar to those of their solution analogues [126,129].

The coordination of oxide anions has been successfully determined in the case of alkaline-earth oxides by diffuse reflectance and photoluminescence techniques, which both led to similar results [97]. In spite of the large variety of possible configurations to be expected in a high surface-area oxide, the reflectance spectra [130,131] show only a few bands for the alkaline-earth oxides investigated. Each band can be considered as representing a particular ***local surface coordination*** of the oxide ions.

The bands in the spectra are changed by the adsorption of gases : those of lowest frequency corresponding to ions in lowest coordination are most affected. The adsorbing gases convert low-coordination surface ions to ions of higher coordination and the higher Madelung potential arising from this increase in coordination displaces the surface absorption toward higher frequency. The absorption bands measured in the reflectance spectra and the corresponding bands in the excitation spectra [132] match well for all the alkaline-earth oxides [97]. These results demonstrate that a real ***surface anion coordination chemistry*** is made possible by such techniques and this can be regarded as a major advance. Recent results indicate that static and dynamic photoluminescence techniques can now be applied to follow catalyst behaviour

during preparation and catalysis [133,134] and photochemistry on solid surfaces [135].

On alkaline-earth oxides, adsorption of CO at 300K involves a very small fraction of surface sites (below 0.5%) and occurs on the most ***basic*** sites, i.e., tricoordinated O_{3c}^{2-} ions (Fig. 9) [136]. The situation is rather complex because the probe molecule on those sites is not only a ligand but also a reactant [137]. At 77K, the CO coverage is very high and adsorption produces bands due to CO adsorbed on ***acidic*** Mg_{5c}^{2+}, Mg_{4c}^{2+} and Mg_{3c}^{2+} sites, whose relative intensities also depend on the morphology of the particles [137]. Similar conclusions are obtained on MgO-CoO and MgO-NiO solid solutions.

The main conclusion to be drawn is that the reactivity of the surface ions in framework positions, which is essentially ***a function of their location*** at the oxide surface, is all the more important as their coordination is low. Similar conclusions were reached earlier by Kibblewhite and Tench [138] in adsorption studies of halogens on MgO.

5.1.2. Ions in extraframework positions

By contrast with the previous systems, it is possible to maximize the concentration of M_{3c}^{n+} ions, i.e., in positions of low coordination, using ion exchange or grafting methods. Thus, it was found (§ 4.2.2.) that the calcination of the Ni/SiO_2 system, prepared by competitive ion exchange, produces Ni_{3c}^{2+} ions. By slight reduction, it is possible to obtain Ni_{3c}^{+} ions, isoelectronic with Cu^{2+} ($3d^9$) and thus observable by ESR. Upon adsorption of ^{13}C (I=1/2) labeled CO, ESR signals with hyperfine structures are observed which reversibly depend upon the pressure. The magnetic parameters can be analyzed to give the following models [139] :

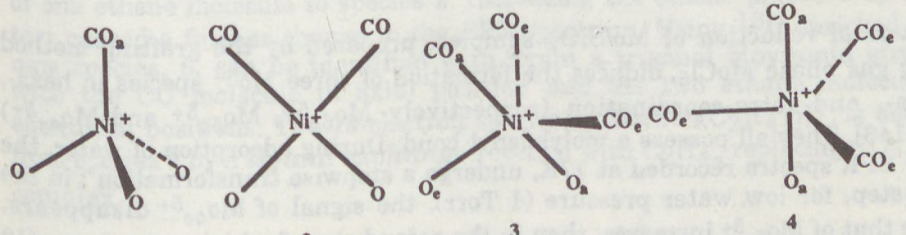

(21)

where a stands for axial and e for equatorial. Some of the models have been confirmed by IR using $^{12}CO/^{13}CO$ isotopic mixtures [140].

The important conclusion is that now the TMI coordination is able to change and reversibly depends on ***the ligand gas phase pressure***. In the sequence 1 to 4 above, the surface ligand changes from ter- to monodentate. The change in coordination is such that the TMI forms bonds with gas phase monodentate ligands so as to restore its preferred coordinations, i.e., those observed in solutions. This can be illustrated by Figure 11 which gives a plot of the $g_\perp$ ESR component as a function of $g_{//}$, so that each point represents a particular complex [141]. The dashed regions have been drawn from ESR data of solution

complexes [142]. It can be seen that, in the sequence 1 to 4, the coordination of Ni^+ ions gradually moves toward that of their solution analogues. In other words, due to its rigidity, the surface ligand imposes a ***distorted coordination*** to Ni^+ ions. As soon as gas phase monodentate (and thus sterically non demanding) ligands become available, Ni^+ ions impose their coordination and therefore take up their preferred geometry. The same trend is observed for the Ni^{2+} state. Upon water adsorption, the low coordinated $Ni_{3c}{}^{2+}$ ions restore their octahedral coordination moving backward from model d) to a) (Fig. 8).

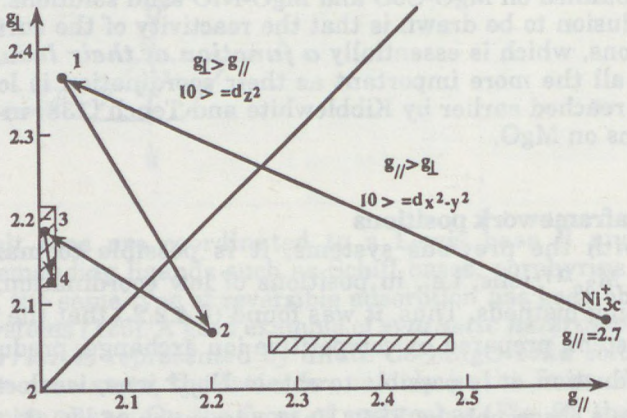

Figure 11. The $g_\perp$ ESR component of grafted and solution Ni^+ complexes plotted as a function of $g_{//}$ (adapted from ref. 141). The structure of the grafted complexes is given by the models 1 to 4 drawn in (21)

Thermal reduction of Mo/SiO_2 samples, prepared by the grafting method using gas phase $MoCl_5$, induces the formation of three Mo^{5+} species in hexa-, penta-, and tetra-coordination (respectively $Mo_{6c}{}^{5+}$, $Mo_{5c}{}^{5+}$ and $Mo_{4c}{}^{5+}$) [120,143]. They all possess a molybdenyl bond. During adsorption of water, the Mo^{5+} EPR spectra recorded at 77K, undergo a stepwise transformation : in the first step, for low water pressure (1 Torr), the signal of $Mo_{4c}{}^{5+}$ disappears, while that of $Mo_{5c}{}^{5+}$ increases, then in the second step, for higher pressures (18 Torr), the signal of $Mo_{5c}{}^{5+}$ disappears while that of $Mo_{6c}{}^{5+}$ increases. The spin concentration remains constant during these changes and water only acts as a ***ligand***. While adsorption can change the number of bonds with the support surface for Ni/SiO_2, this is not observed with the Mo/SiO_2 system, probably because the iono-covalent bonding with the oxide surface involves higher oxidation state for molybdenum than for nickel ions.

5.2. Catalytic sites

The reactivity of a TMI depends on its ability to be coordinatively unsaturated in order to i) bind one or several reactive ligand(s), ii) catalyse their

transformation into (a) given product(s), iii) and finally release the product(s) recovering its original unsaturated state. The generality of the ligand dissociation-association process has led to formulate the 18-electron stability rule and the 16- and 18-electron rule [1,57,144] for reactivity of transition metal complexes, both valid essentially for σ donor - π acceptor strong ligands such as CO, CN^- and organic unsaturated molecules. The latter rule has been very useful in discernment of preferred reaction pathways in homogeneous catalysis [1,57,144]. This rule does not apply to weak σ donor - π donor ligands such as those involved in the preparation of catalysts ($\equiv SiO^-$, H_2O, NH_3, etc..). This rule will not be obeyed strictly by surfaces complexes which concern mixed ligands, i.e., weak and strong ligands. Using the electron counting adopted in coordination chemistry [57], with ***two electrons*** for the surface rigid oxygen ligand [139,141,145], complexes 1 and 2 are both 17-electron species, while 3 and 4 are 19-electron species which are known to be very reactive [146,147]. This is considered next.

5.2.1. Dimerisation of olefins

As Ni^+ ions are the active sites in the homogeneous olefin dimerisation reaction [148], the coordination of ethene onto supported Ni^+ ions has also been investigated [139]. The 17-electron dicarbonyl species 2 progressively reacts with ethene giving rise to a complex EPR spectrum assigned, by employing ^{13}C enriched CO, to the 19-electron $[Ni(CO)_2(C_2H_4)]^+$ species, 5, with two inequivalent CO ligands. The similarity between the EPR g tensors of species 3 and 5 suggests that the structure of the latter is probably a trigonal bipyramid with one axial CO_a ligand and one equatorial CO_e ligand. Thus the ethene molecule is in an equatorial position and species 5 is the result of the ***addition*** of one ethene molecule to species 2. Increasing the ethene pressure up to 600 torr caused a further change in the EPR spectrum. Using ^{13}C enriched CO, a new species, 6, can be identified with again a trigonal bipyramid structure with the CO molecule in axial position and the two ethene molecules in equatorial positions. The 19-electron species 6, $[Ni(CO)(C_2H_4)_2]^+$, is obtained from species 5 by a ***ligand exchange*** reaction with C_2H_{4e} replacing CO_e in the complex.

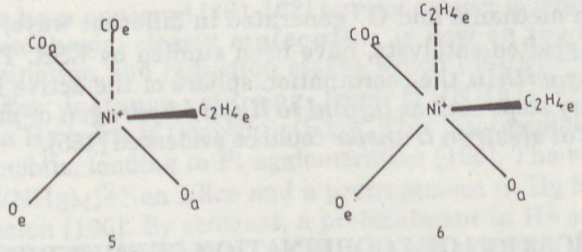

(22)

Catalytic activity tests were performed on systems containing the two species 5 and 6. With species 5, no appreciable dimerisation reaction is observed after 24 hours whereas with species 6, it does occur. The product distribution is very close to that observed in the catalytic tests performed without carbon monoxide. It is therefore necessary that two ethene molecules be bonded to the same Ni^+ ion for dimerisation to take place. It is important to note that there are ***four types of ligands*** around the Ni^+ ion : 1) the reactants which are transformed into the 2)nd type of ligands, i.e., the products, 3) the CO ***spectator ligand***, which all are mobile ligands, and finally 4) the rigid surface ligand.

When alkylphosphines rather than CO are used as spectator ligands, two effects are observed [149]. The first, of ***electronic*** nature, is proportional to the number and basicity of the alkylphosphines introduced and leads to an increase of the electronic density at the metal centre. This can be followed by IR using CO as a probe molecule [96,141]. The consequence is a weakening of the affinity for soft Lewis bases such as the reaction products (for instance, butenes for ethene dimerisation) and an increased stability of the catalyst by a weakening of the Ni^+-products bond. To this electronic effect, is superposed a conjugated ***steric effect*** due to both the surface and the spectator ligand, characterized by a ***Tolman angle*** [57]. For instance, with bulky alkylphosphines the selectivity can be drastically increased in 1-butene [149] or 2-3 dimethyl-1 butene [150] for ethene and propene dimerisation respectively.

5.2.2. Oxidation of methanol

Methanol oxidation via the selectivity of the products obtained appears to be one of the most suitable molecular probe. Known to be structure sensitive [151,152], this reaction can also distinguish acid-base from redox catalysis [153]. In addition, it was found to be very sensitive to molybdenum dispersion, by comparing catalysts prepared by impregnation and grafting, with low and high dispersion respectively [154]. On the former catalysts, formaldehyde is the main product. On grafted Mo/SiO_2 samples, the relative amounts of formaldehyde and methyl formate, which are the main products, depend on molybdenum dispersion, the latter product becoming more important for increasing dispersions. On the basis of kinetic data, the following mechanism was proposed : on Mo sites, methanol leads to formaldehyde which spills over to silica, where it further reacts with methoxy groups to form methyl formate via a hemiacetal intermediate. In order to confirm this mechanism, model reactions between methanol and O^- generated in different ways, both adsorbed on the surface of grafted catalysts, have been studied by ESR. The mechanism was found to occur ***within*** the coordination sphere of the active Mo^{5+} sites and different elementary steps such as ***ligand to ligand hydrogen*** or ***proton transfer*** and ***ligand to metal electron transfer*** could be evidenced [155].

6. THE CLASSIFICATION OF COORDINATION CHEMISTRIES

On the basis of the models given in Figure 2 and of the results given in § 4 and 5, it is possible to propose a simple classification of the different types of CC

related to systems involving TMIs and oxide supports. This classification [55] can be easily extended to other supports (sulfides in particular).

ICC is clearly ***intermediate*** between solution (Fig. 2, model I) and solid state (Fig. 2, model VII) CC. It can be subdivided into two CC referring to ions in extraframework positions (Fig. 2, model II-V), on the one hand and to surface ions in framework positions (Fig. 2, model VI and Fig. 9), on the other hand. Whereas the reactivity of the former ions depend on the gas phase pressure in the former case, it essentially depends for the latter on the location of the ions at the surface. In following the arrow in Figure 2, the reactivity, mobility and accessibility of the TMIs continuously decrease by contrast with ISIs, which continuously increase. Concerning the mobility and as pointed out earlier [72], the zeolites present such a structure that ions can move from hidden sites to large cavities on adsorption of polar molecules. The interface can now be defined, from the standpoint of the probe, as the ***intermediate region*** where there is a ***transition*** from the properties of TMIs in solution to those in the solid state: it extends from 8 to 10 water layers, on the liquid side (see § 4.2.1.1), to a depth, on the solid side, equivalent to the radius of the TMI solvation sphere (see Fig. 2). The importance of the interface has already been pointed out by Haber [156].

7. TRANSITION METAL IONS AS PRECURSORS OF SUPPORTED METALS

7.1. The present knowledge

Although the preparation of supported metal particles in real systems has been the subject of numerous studies [104,157], the concepts which can be used to control ***a priori*** their preparation are still ill-defined. This is in contrast to model systems where the concepts are better established, particularly as regards to the mechanisms of nucleation and growth [158] and the control of the size of supported metal particles [159]. In model systems, the latter are obtained for instance by condensation of metal vapours on flat substrates [160]. The common concern, however, to both types of systems is to identify the processes which lead to metal particles and the ***nature of their bonding*** with the support.

Perhaps, the best understood systems are those involving metal particles in zeolitic matrices, which were extensively studied more than a decade ago. Several reviews have appeared [161-163] but the subject is witnessing a renewed interest. The emphasis, clearly ***molecular***, is now on the elementary steps during the calcination and reduction stages which influence the final metallic state [164]. For instance, starting from $[Pt(NH_3)_4]^{2+}$ in Y zeolite, a pretreatment in H_2 leads to $[Pt(NH_3)_2(H)_2]^{\circ}$. This intermediate bears no charge and is highly mobile, leading to Pt agglomeration [165]. The same is thought to occur with $[Pd(NH_3)_4]^{2+}$ on silica and a pretreatment in H_2 likewise gives rise to a poor dispesion [166]. By contrast, a pretreatment in He or Ar leads to very highly dispersed Pd particles, while a pretreatment in oxygen gives intermediate dispersions. In the case of Pd exchanged Y zeolite, it is possible to regenerate the isolated Pd^{2+} ions by contacting the metal particles with nitric oxide [167].

Returning to metals supported on conventional oxides, a literature survey indicates that small metal particles appear as wetting the support. They are very flat, forming one-dimensional structures and irregular agglomerates of two to threee monolayers thick [168]. They are usually not completely reduced and the unreduced or partly reduced remaining ions are located at the metal-support interface [169,170]. Those ions appear to act as anchoring sites for the metal particles and constitute a ***chemical glue***.

Although this has not been realized, two types of chemical glue can be distinguished. In the first, the anchoring sites are ***exposed framework cations*** due to O^{2-} vacancies and direct metal atom-cation bonding becomes possible, as suggested by EXAFS results on the Rh/TiO_2 system [171]. The second type of chemical glue is likely to be composed of ***extraframework*** cations as in the case of metals in zeolites. In model systems such as Pt/SiO_2 [160] or Ni/SiO_2 [172], prepared by metal vapour condensation on oxides kept at low temperatures, so as to avoid surface atom diffusion, the cations, extraframework by preparation, are most probably generated by reoxidation of the impinging atoms by surface hydroxyl groups giving off molecular hydrogen. However as discussed earlier [173], the concentrations of the order of 3.10^{12} cm^{-2} are too low to detect the cations.

7.2. The challenge

It is generally accepted that the stronger the ISI in supported systems, the smaller the metal particle size generated by thermal reduction of the precursor system. This statement is however ambiguous, since the stronger the ISI, the higher the reduction temperature and the more important the surface diffusion of the atoms obtained. This should lead eventually to larger particles. It is also accepted, other things being equal, that the mean particle size obtained for a given system increases with the metal content. Finally, the presence of several types of ISIs is thought to be detrimental to the obtention of monodisperse metal particles.

With this picture in mind, how then can we ***control a priori*** the size and the physico-chemical properties of metal particles supported on oxides? It is important to answer those questions. The lack of control of those characteristics is the most probable explanation for the discrepancies observed between the results reported by different authors for the same system and reaction when turnover frequencies are plotted against particle size [104].

7.3. A possible new approach

Marcilly gave a very thoughtful account of the preparation of supported metal catalysts and insisted on the importance of the nucleation and growth processes and of the saturation parameter [157]. The approach we have taken is to separate the nucleation and growth processes and this is illustrated for the Ni/SiO_2 system [174]. A ***two-step procedure*** is adopted with: i) creation of Ni nuclei ; the hypothesis is that the latter are nickel ions in ***strong interaction*** with silica and thus difficult to be reduced, ii) formation of a "reservoir" of nickel atoms for the particle growth on the ionic nuclei ; the hypothesis is that the nickel ions, precursors of the atom reservoir, must be in ***weak interaction*** with the support, so as to be reduced at low temperatures. This should lead to atoms, with limited diffusion ability on the silica surface.

From results of previous works performed on the Ni/SiO_2 system, the blank samples were prepared by incipient wetness impregnation from a solution of nickel nitrate on silica. After temperature programmed reduction (TPR), the average diameter of nickel particles measured by transmission electron microscopy (TEM) is about 60Å for samples containing from 1.5 to 3.5 wt% Ni.

The nickel nuclei were prepared using two different methods leading to Ni ions in strong interaction with silica :

- by cation exchange with nickel ethylenediamine, followed by calcination in air in order to decompose the ethylenediamine. After TPR, the average Ni particle diameter for samples containing less than 2.4 wt% Ni is smaller than 20Å .
- by impregnation of high amounts of nickel, followed by a thorough washing in water in order to eliminate nickel interacting weakly with silica. The average particle diameter after TPR is less than 25Å for samples containing from 0.64 to 5.1 wt% Ni.

Nickel was then impregnated on samples containing the "nuclei". After reduction, the average particle diameter is smaller and the size distribution is more homogeneous than for the blank samples, even if the total metal loading largely exceeds that of the latter. The striking result is that the average ***particle size can decrease when the overall amount of metal increases***, providing the number of nickel nuclei be increased for a given amount of impregnated nickel and whatever the preparation method of the nuclei. It can also decrease, when the amount of impregnated nickel decreases for a fixed number of Ni nuclei.

These results suggest the possibility of controlling the mechanisms of nucleation and growth during the formation of nickel metal particles supported on silica. It appears possible to control not only the particle size by the number of nuclei and the amount of metal in the "reservoir" but also the electronic properties (by the atoms to cations ratio), which both are crucial points for the preparation of supported metal catalysts. It is hoped that this approach can be easily extended to bimetallic supported catalysts, and may lead the way to control also the composition and the electronic structure of bimetallic systems, in the same way as for model systems [175].

The implications of ICC in the preparation of supported metal particles are obvious since they can help to produce the adequate ISIs in the oxidized precursors. The examples above show that the final metallic state exhibits a ***strong memory effect*** with respect to its oxidized precursor. As the reduction proceeds, hydroxyls groups are formed which can be used in further cation deposition by ion exchange and this opens up new possibilities for catalyst design [176].

8. CONCLUSIONS AND POSSIBLE DIRECTIONS FOR THE FUTURE

In this review, an attempt has been made to establish the emerging concepts of interfacial coordination chemistry (ICC) and their relevance to catalysis phenomena. This led to raise two important questions : what is the role of the oxide support? and what is the nature of ion-support interaction (ISI)?. The adopted approach has been to take the transition metal ion as its own probe and to study its interaction with the oxide support during the successive steps of

catalyst preparation, involving both the liquid-solid and gas-solid interfaces. In contrast to expectation, the obtention of different types of ISI can be turned into an advantage to control the preparation of supported metal particles. We have mainly concentrated our attention to cationic transition metal complexes but the approach is the same for anionic complexes. It is our hope that, though probably not definitive, the answers to the two previous questions may help to consider both the preparation and catalytic phenomena in a more predictive manner, i.e., to move from catalyst preparation to catalyst design, as mentioned earlier [177-179]. They may also form a reasonable basis to understand catalysis at a molecular level particularly during the reaction.

Future progress will certainly come from a concerted effort to i) adapt the currently available techniques to in-situ studies, ii) investigate kinetic phenomena involving labile and inert complexes in catalyst preparation, iii) model the elementary steps which describe catalyst preparation and catalytic reactions at a molecular level, iv) perform theoretical calculations to provide a more solid foundation to existing models and evidence new directions for future experimental work, and v) transfer and adapt the concepts of relevant fields to that of catalysis and further enlarge and/or improve the existing basic concepts, such as those presented here. This can be achieved particularly with model systems, such as zeolites with well defined structures. Those solids were shown to present a rich coordination chemistry and to possess properties similar to those of cryptands [72]. For the latter reason, they have been recently named zeolates [180]. They are the subject of intensive research and are likely to lead to new approaches and new materials.

It is fair to recognize that the recent advances we have witnessed in the last years in ICC owe much to modern characterization techniques [181].

The present molecular approach suggests that more effort should be devoted in the future to fundamental research in this area.

Acknowlegments

It is a pleasure to thank most warmly my collaborators, whose dedication, skill and enthusiasm led to the work reported in this paper. They all have contributed to the common goal. I also wish to acknowledge the collaboration with a number of foreign laboratories on various aspects of coordination chemistry, photochemistry, spectroscopy and catalysis. I am indebted to Pr M. Anpo and Dr T. Setoyama (Japan), Prs K. Dyrek and J. Haber and Drs K. Brückman and Z. Sojka (Poland), Drs B. Canosa and A.R. Gonzalez-Elipe (Spain), Prs E. Giamello, S. Coluccia and A. Zecchina (Italy), Dr K. Hadjiivanov (Bulgaria), Pr. J.M. Thomas (UK), and Pr. C.O. Bennett (USA), for their valuable collaborations. I am grateful to Université P. et M. Curie, CNRS, Institut Français du Pétrole (Drs E. Freund, C. Marcilly, J.P. Boitiaux and O. Clause), Rhône Poulenc (Drs J.P. Brunelle, G. Blanchard and G.N. Sauvion) and Gaz de France (Dr J. Saint-Just) for providing the intellectual environment and the financial support. Finally, I wish to dedicate this contribution to Pr J. Turkevich, Drs C. Naccache and B. Imelik and the late Dr A.J. Tench. I owe them so much.

9. REFERENCES

[1] For a review see, for instance, F.A. Cotton and G. Wilkinson, Basic Inorganic Chemistry, Wiley, New York, 1976; K.F. Purcell and J.C. Kotz, Inorganic Chemistry, Saunders, Philadelphia, 1977; F.A. Cotton and G. Wilkinson, Advanced Inorganic Chemistry, 4th ed., Wiley, New York, 1980; J.E. Huheey, Inorganic Chemistry, Principles of Structure and Reactivity, Harper, Cambridge, 1983; N.N. Greenwood and A. Earnshaw, Chemistry of the Elements, Pergamon Press, Oxford, 1987; G. Wilkinson, R.D. Gilliard and J.E. McCleverty (eds.), Comprehensive Coordination Chemistry, Pergamon Press, Oxford, 1987. For a complete discussion of the earliest work in coordination chemistry, see G.B. Kauffman, J. Chem. Educ., 36 (1959) 521; Classics in Coordination Chemistry, Part 1: The Selected Papers of A. Werner; Part 2: Selected Papers (1798-1899), Dover, New York, 1968, 1976.

[2] W.A. Patrick and E.H. Barclay, J. Phys. Chem., 29 (1925) 1400.

[3] G. Testoni, Ann. Chim. Applicata, 16 (1926) 45.

[4] G.W. Smith and L.H. Reyerson, J. Am. Chem. Soc., 52 (1930) 2524.

[5] R. Berton, C. R. Acad. Sci., 195 (1932) 384.

[6] G.W. Smith and H.W. Jacobson, J. Phys. Chem., 60 (1956) 1008.

[7] A. Kozawa, J. Inorg. Nucl. Chem., 21 (1961) 315.

[8] R.L. Burwell Jr, R.G. Pearson, G.L. Haller, P.B. Tjok and S.P. Chock, Inorg. Chem., 4 (1965) 1123 .

[9] B.J. Hathaway and C.E. Lewis, J. Chem. Soc., 1969, p. 1176.

[10] J.H. Anderson, J. Catal., 26 (1972) 277.

[11] J.P. Brunelle, Pure Appl. Chem., 50 (1978) 1211.

[12] V.S. Boronin, V.S. Nikulina and O.M. Poltorak, Russ. J. Phys. Chem., 37 (1963) 626.

[13] H.A. Benesi, R.M. Curtis and H.P. Studer, J. Catal., 10 (1968) 328.

[14] T.A. Dorling, B.W.J. Lynch and R.L. Moss, J. Catal., 20 (1971)190.

[15] J.P. Brunelle, A. Sugier and J.F. Lepage, J. Catal., 43 (1976) 273.

[16] J.P. Brunelle and A. Sugier, C. R. Acad. Sci., 276C (1973) 1545.

[17] E. Echigoya, L. Furuoya and K. Morikawa, J. Chem. Soc. Jpn, Ind. Chem., 71 (1968) 1768.

[18] B. Samanos, P. Boutry and R. Montarnal, C. R. Acad. Sci., 274C (1972) 575.

[19] F. Bozon-Verduraz, A. Omar, J. Escard and B. Pontvianne, J. Catal., 53 (1978) 126.

[20] R.W. Maatman and C.D. Prater, Ind. Eng. Chem., 49 (1957) 253.

[21] R.W. Maatman, Ind. Eng. Chem., 51 (1959) 913.

[22] R.W. Maatman, P. Mahaffy, P. Hoekstra and C. Addink, J. Catal., 23 (1971) 105.

[23] E. Santacesaria, S. Carra and I. Adami, Ind. Eng. Chem., 69 (1977) 41.

[24] J.C. Summers and S.A. Ausen, J. Catal., 52 (1978) 445.

[25] D.W. Breck, J. Chem. Educ., 41 (1964) 678.

[26] D.W. Breck, Zeolite Molecular Sieves, Wiley, New York, 1974.

[27] J.H. Lunsford, Molecular Sieves II, J.R. Katzer (ed.), Am. Chem. Soc., Washington, 1977, p. 473.

[28] P. Ratnasamy, 2nd Indo-French Seminar on Catalysis, Paris, 1992.

[29] I.D. Mikheikin, G.M. Zhidomirov and V.B. Kazanskii, Russ. Chem. Rev., 41 (1972) 468.
[30] V.D. Atanasova, V.A. Shvets and V.B. Kazanskii, Russ. Chem. Rev., 50 (1981) 209.
[31] C.M. Naccache and Y. Ben Taarit, J. Catal., 22 (1971) 22.
[32] P. Gallezot, Y. Ben Taarit and B. Imelik, C. R. Acad. Sci., 272C (1971) 261; J. Catal., 26 (1972) 295.
[33] A. Nicula, D. Stamires and J. Turkevich, J. Chem. Phys., 42 (1965) 3634.
[34] C. Naccache and Y. Ben Taarit, Chem. Phys. Letters, 11 (1971) 11.
[35] M. Che, J. Fraissard and J.C. Védrine, Bull. Groupe Franç. Argiles, 26 (1974) 1.
[36] For a review, see M.B. McBride, Advan. Soil Sci., 10 (1989) 1
[37] Th. Wolkenstein, Théorie Electronique de la Catalyse sur les Semi-Conducteurs, Masson, Paris, 1961.
[38] For a review, see F.S. Stone, J. Solid State Chem., 12 (1975) 271.
[39] D.A. Dowden and D. Wells, Actes du Deuxième Congrès International de Catalyse, Ed. Technip, Paris, 2 (1960) 1499; see also the general discussion, ibid, p. 1649.
[40] H.S. Taylor, Proc. Roy. Soc., London, A108 (1925) 105.
[41] R.L. Nelson and A.J. Tench, J. Chem. Phys., 40 (1964) 2736.
[42] J.H. Lunsford and T.W. Leland, Jr, J. Phys. Chem., 66 (1962) 2591.
[43] M. Boudart, A. Delbouille, E.G. Derouane, V. Indovina and A.B. Walters, J. Am. Chem. Soc., 94 (1972) 6622.
[44] E.J. Arlman and P. Cossee, J. Catal., 3 (1964) 99.
[45] J.M. Thomas, Advan. Catal., 19 (1969) 293.
[46] R.L. Burwell Jr, A.B. Littlewood, M. Carder, G. Pass and C.T.H. Stoddart, J. Am. Chem. Soc., 82 (1960) 6272.
[47] R.L. Burwell Jr and C.J. Lower, Proc. Int. Congr. Catal., 3rd, Amsterdam, 2 (1965) 804.
[48] R.L. Burwell Jr, G.L. Haller, K.C. Taylor and J.F. Read, Advan. Catal., 20 (1969) 1.
[49] J. Haber and F.S. Stone, Trans. Faraday Soc., 59 (1963) 192.
[50] E.G. Vrieland and P.W. Selwood, J.Catal., 3 (1964) 359.
[51] A. Cimino, R. Bosco, V. Indovina and M. Schiavello, J. Catal., 5 (1966) 271.
[52] A. Cimino, M. Schiavello and F.S. Stone, Discuss. Faraday Soc., 41 (1966) 350.
[53] A. Cimino, V. Indovina, M. Pepe and M. Schiavello, J. Catal., 14 (1969) 49
[54] For a review see ref. [38] and F.S. Stone, Chemical and Physical Aspects of Catalytic Oxidation, J.L. Portefaix and F. Figueras (eds), CNRS, Paris, 1980, p. 457.
[55] M. Che, O. Clause and L. Bonneviot, Proc. Int. Congr. Catal., 9th, Calgary, 4 (1988) 1750.
[56] I.M. Campbell, Catalysis at Surfaces, Chapman and Hall, London, 1988. p. 64. The author gives the following definitions: an anchored (or immobilized) catalyst is created by the binding of a species, without substantial change in its structure, to a solid surface, while a grafted catalyst is produced when an initial structure bound to a surface is altered considerably by subsequent treatments. For the latter, he gives

the example of a Mo/SiO_2 system prepared by reaction of $MoCl_5$ with a silica surface and used in methanol oxidation (M. Che, C. Louis and J.M. Tatibouët, Polyhedron, 5 (1986) 123).
[57] G.W. Parshall, Homogeneous Catalysis, Wiley, New York, 1980.
[58] Yu.I. Yermakov, B.N. Kuznetsov and V.A. Zakharov, Catalysis by Supported Complexes, Elsevier, Amsterdam, 1980.
[59] B.C. Gates, L. Guzci and H. Knözinger (eds), Metal Clusters in Catalysis, Elsevier, Amsterdam, 1986.
[60] J.M. Basset and A.K. Smith, Fundamental Research in Homogeneous Catalysis, M. Tsutsui (ed.), Plenum, New York, 1 (1977) 69.
[61] N.D.S. Canning and R.J. Madix, J. Phys. Chem., 88 (1984) 2437.
[62] M. Misono, this congress.
[63] A.A. Antoniu, J. Phys. Chem., 68 (1964) 2754.
[64] V. Bassetti, L. Burlamacchi and G. Martini, J. Am. Chem. Soc., 101 (1979) 5471.
[65] J. Turkevich, Catal. Rev., 1 (1968) 1.
[66] G. Martini and L. Burlamacchi, Chem. Phys. Lett., 41 (1976) 129.
[67] J. O'Bockris, M.A.V. Denavathan and K. Muller, Proc. Roy. Soc., London, 274 (1963) 55.
[68] J.A. Rabo and P.H. Kasai, Progr. Sol. State Chem., 9 (1975) 1.
[69] A. Davidson and M. Che, Colloids Surf., 000 (1992) in press.
[70] G.A. Parks, Chem Rev., 65 (1965) 177.
[71] G. Deo and I.E. Wachs, J. Phys. Chem., 95 (1991) 5889.
[72] M. Che and L. Bonneviot, Pure & Appl. Chem., 60 (1988) 1369.
[73] M. Che and L. Bonneviot, Successful Design of Catalysts. Future Requirements and Development, T. Inui (ed.), Elsevier, Amsterdam, 1988, p. 147.
[74] O. Clause, Thèse de Doctorat, Université P. et M. Curie, Paris, 1989, p. 45 (Fig. 3a), p. 50 (Fig. 3b).
[75] C.F. Baes and R.E. Mesmer, The Hydrolysis of Cations, Krieger, Malabar, 1986, p. 253.
[76] L. Bonneviot, O. Legendre, M. Kermarec, D. Olivier and M. Che, J. Colloid Interf. Sci., 134 (1990) 534.
[77] J.A. Davis, R.O. James and J.O. Leckie, J. Colloid Interf. Sci., 63 (1978) 480
[78] Ni(II) is a d^8 system and is octahedral in solution when surrounded by weak ligands such as O^{2-}, OH^-, H_2O and NH_3 [1].
[79] M.L. Hair, Infrared Spectroscopy in Surface Chemistry, Dekker, New York, 1967, p. 79.
[80] G.W. Brindley and G. Brown, Crystal Structures of Clay Minerals and their X-Ray Identification, Mineralogy Society, London, 2nd Edition, 1980, p. 2.
[81] L. Bonneviot, O. Clause, M. Che, A. Manceau and H. Dexpert, Catal. Today, 6 (1989) 39.
[82] J. Palerm, personal communication.
[83] D.L. Dugger, J.H. Stanton, B.N. Irby, B.L. McConnell, W.W. Cummings and R.W. Maatman, J. Phys. Chem., 68 (1964) 757.
[84] C.K. Jørgensen, Acta Chem. Scand., 10 (1956) 887; Struct. Bonding, 1 (1966) 234
[85] C.K. Jørgensen, Acta Chem. Scand., 9 (1955) 116.

[86] C.K. Jørgensen, Acta Chem. Scand., 9 (1955) 1362.
[87] C.K. Jørgensen, Inorganic Complexes, Academic Press, New York, 1963, p. 54.
[88] O. Clause, L. Bonneviot, M. Che, M. Verdaguer, F. Villain, D. Bazin and H. Dexpert, J. Chim. Phys., 86 (1989) 1767.
[89] M. Che, J.F. Lambert and F. Bozon-Verduraz, in the press.
[90] R. Burch and A.R. Flambard,, Preparation of Catalysts III, G. Poncelet, P. Grange and P.A. Jacobs (eds), Elsevier, Amsterdam, 1983, p. 1.
[91] M. Houalla, F. Delannay, I. Matsuura and B. Delmon, J. Chem. Soc., Trans. Faraday I, 76 (1980) 2128.
[92] R.K. Iler, The Chemistry of Silica, Wiley, New York, 1979, pp. 63-65.
[93] C.J. Brinker and G.W. Scherer, Sol-Gel Science, Academic Press, New York, 1990, p. 26.
[94] O. Clause, M. Kermarec, L. Bonneviot, F. Villain and M. Che, J. Am. Chem. Soc., 114 (1992) 4709.
[95] O. Clause, L. Bonneviot and M. Che, J. Catal., 000 (1992) in press.
[96] D. Olivier, L. Bonneviot, F.X. Cai, M. Che, P. Gihr, M. Kermarec, C. Lepetit-Pourcelot and B. Morin, Bull. Soc. Chim., 1985, p. 370.
[97] M. Che and A.J. Tench, Advan. Catal., 31 (1982) 77.
[98] M. Che, Adsorption and Catalysis on Oxide Surfaces, M. Che and G.C. Bond (eds.), Elsevier, Amsterdam, 1985, p. 30.
[99] M. Che, K. Dyrek and C. Louis, J. Phys. Chem., 89 (1985) 4526.
[100] M. Che, B. Conesa and A.R. Gonzalez-Elipe, J. Phys. Chem., 90 (1986) 618.
[101] G. Tamman, Z. Anorg. Chem., 157 (1926) 321.
[102] Ph. de Montgolfier, P. Mériaudeau, Y. Boudeville, and M. Che, Phys. Rev. 14B (1976) 1788.
[103] P. Mériaudeau, Y. Boudeville, Ph. de Montgolfier, and M. Che, Phys. Rev. 16B (1977) 30.
[104] M. Che and C.O. Bennett, Advan. Catal., 36 (1989) 55.
[105] M. Dufaux, M. Che and C. Naccache, J. Chim. Phys., 67 (1970) 527.
[106] J.A. van Dillen, J.W. Geus, L.A.M. Hermans and J. van der Meijden, Proc. Int. Congr. Catal., 6th, London, 2 (1977) 677.
[107] L.A.M. Hermans and J.W. Geus, Preparation of Catalysts II, Elsevier, Amsterdam, 1979, p. 113.
[108] J.W. Geus, Preparation of Catalysts III, Elsevier, Amsterdam, 1983, p. 1.
[109] M. Che and A.J. Tench, Advan. Catal., 32 (1983) 1.
[110] M. Ardon, A. Bino and K. Michelsen, J. Am. Chem. Soc., 109 (1987) 1986.
[111] J.A. Lawick and R.A. Plane, J. Am. Chem. Soc., 81 (1969) 3564.
[112] J.E. Finholt, M.E. Thompson and R.E. Connick, Inorg. Chem., 25 (1986) 489.
[113] H. Schaper, E.B.M. Doesburg, J.M.C. Quartel and L.L. van Reijen, Preparation of Catalysts III, Elsevier, Amsterdam, 1983, p. 301.
[114] A.C. Vermeulen, J.W. Geus, R.J. Stol and P.L. de Bruyn, J. Colloid Interf. Sci., 51 (1975) 449.
[115] O. Clause, L. Bonneviot, M. Che and H. Dexpert, J. Catal., 130 (1991) 21.
[116] M. Che and L. Bonneviot, Zeit. Phys. Chem., NF, 152 (1987) 113.
[117] C. Louis, M. Che and F. Bozon-Verduraz, J. Chim. Phys., 79 (1982) 803.

[118] J.C.W. Chien, J. Am. Chem. Soc., 93 (1971) 4675.
[119] S.I. Kol'tsov, A.A. Malygin, A.N. Volkova and V.B. Aleskovskii, Russ. J. Phys. Chem., 47 (1973) 558.
[120] M. Che, C. Louis and J.M. Tatibouët, Polyhedron, 5 (1986) 123.
[121] C. Louis and M. Che, J. Catal., 135 (1992) 156.
[122] M. Anpo, M. Sunamoto and M. Che, J. Phys. Chem., 93 (1989) 1187.
[123] F. Roozeboom, T. Fransen, P. Mars and P.J. Gellings, Z. Anorg. Allg. Chem., 449 (1979) 25.
[124] For a review, see Y.C. Xie and Y.Q. Tang, Advan. Catal., 37 (1990) 1.
[125] R.D. Jones, D.A. Summerville and F. Basolo, Chem. Rev., 79 (1979) 139.
[126] M. Che, K. Dyrek, E. Giamello and Z. Sojka, Zeit. Phys. Chem., NF, 152 (1987) 139.
[127] E. Giamello, Z. Sojka, M. Che and A. Zecchina, J. Phys. Chem., 90 (1986) 6084.
[128] Z. Sojka, E. Giamello, M. Che, A. Zecchina and K. Dyrek, J. Phys. Chem., 92 (1988) 1541.
[129] D. Getz, E. Melamud, B.L. Silver and Z. Dori, J. Am. Chem. Soc., 97 (1975) 3846.
[130] A. Zecchina, M.G. Lofthouse and F.S. Stone, J. Chem. Soc., Faraday Trans. I, 71 (1975) 1476.
[131] A. Zecchina and F.S. Stone, J. Chem. Soc., Faraday Trans. I, 72 (1976) 2364.
[132] A.J. Tench and G.T. Pott, Chem. Phys. Lett., 26 (1974) 590.
[133] M. Anpo, M. Kondo, S. Coluccia, C. Louis and M. Che, J. Am. Chem. Soc., 111 (1989) 8791.
[134] M. Anpo and M. Che, Advan. Catal., 000 (1993) in press.
[135] M. Anpo and T. Matsuura (eds.), Photochemistry on Solid Surfaces, Elsevier, Amsterdam, 1989.
[136] S. Coluccia, M. Barico, L. Marchese, G. Martra and A. Zecchina, Spectrochim. Acta, submitted.
[137] A. Zecchina, S. Coluccia, G. Spoto, D. Scarano and L. Marchese, J. Chem. Soc., Faraday Trans., 86 (1990), 703.
[138] J.F.J. Kibblewhite and A.J. Tench, J. Chem. Soc., Faraday Trans. I, 70 (1974) 72.
[139] L. Bonneviot, D. Olivier and M. Che, J. Mol. Catal., 21 (1983) 415.
[140] M. Kermarec, D. Delafosse and M. Che, J. Chem. Soc., Chem. Commun., 1983, p. 411.
[141] M. Che, L. Bonneviot, C. Louis and M. Kermarec, Mat. Chem. Phys., 13 (1985) 201.
[142] K. Nag and A. Chakravorty, Coord. Chem. Rev., 33 (1980) 87.
[143] C. Louis and M. Che, J. Phys. Chem., 91 (1987) 2876.
[144] C.A. Tolman, Chem. Soc. Rev., 1 (1972) 337.
[145] J.M. Basset and A. Choplin, J. Mol. Catal., 21 (1983) 95.
[146] Q.Z. Shi, T.G. Richmond, W.C. Trogler and F. Basolo, J. Am. Chem. Soc., 104 (1982) 4032.
[147] G.J. Bezem, P.H. Rieger and S. Visco, J. Chem. Soc., Chem. Commun., 1981, p. 265.
[148] B. Bogdanovic, Advan. Organomet. Chem., 17 (1979) 105.
[149] F.X. Cai, Thèse de Doctorat, Université P. et M. Curie, Paris, 1986.
[150] C. Lepetit, Thèse de Doctorat, Université P. et M. Curie, Paris, 1987.
[151] J.M. Tatibouët and J.E. Germain, J. Catal., 72 (1981) 375.

[152] J.C. Volta and J.L. Portefaix, Appl. Catal., 18 (1985) 1.
[153] C. Rocchiccioli-Deltcheff, M. Amirouche, G. Hervé, M. Fournier, M. Che and J.M. Tatibouët, J. Catal., 126 (1990) 591.
[154] C. Louis, J.M. Tatibouët and M. Che, J. Catal., 109 (1988) 354.
[155] Z. Sojka and M. Che, J. Phys. Chem., in the press.
[156] J. Haber, Proc. Int. Congr. Catal., 8th, Berlin, 1 (1984) 85.
[157] C. Marcilly, Catalyse par les Métaux, B. Imelik, G.A. Martin and A.J. Renouprez, Editions du CNRS, Paris, 1984, p. 121.
[158] A. Masson, Contribution of Clusters Physics to Materials Science and Technology, J. Davenas and P. Rabette (eds), M. Nijhoff, Dordrecht, 1986, p. 295.
[159] H. Schmeisser, Thin Solid Films, 22 (1974) 83.
[160] A. Masson, B. Bellamy, G. Colomer, M. M Bedi, P. Rabette and M. Che, Proc. Int. Congr. Catal., 8th, Berlin, 4 (1984) 333.
[161] D. Delafosse, J. Chim. Phys., 83 (1986) 761.
[162] P.A. Jacobs, Metal Microstructures in Zeolites, P.A. Jacobs (ed.), Elsevier, Amsterdam, 1982, p. 71.
[163] P. Gallezot, Metal Clusters, Wiley, New York, 1986, p. 220.
[164] S. T. Homeyer and W.M.H. Sachtler, Zeolites: Facts, Figures, Future, Elsevier, Amsterdam, 1989, p. 975.
[165] R.A. Dalla Betta and M. Boudart, Proc. Int. Congr. Catal., 5th, Miami Beach, 2 (1973) 1329.
[166] W. Zou and R.D. Gonzalez, Catal. Letters, 12 (1992) 73.
[167] M. Che, J.F. Dutel, P. Gallezot and M. Primet, J. Phys. Chem., 80 (1976) 2371.
[168] S. Fuentes, A. Vazquez, R. Silva, J.G. Perez-Ramirez and M.J. Yacaman, J. Catal., 111 (1988) 353.
[169] T. Huizinga and R. Prins, J. Phys. Chem., 87 (1983) 173.
[170] L. Bonneviot, M. Che, D. Olivier, G.A. Martin and E. Freund, J. Phys. Chem., 90 (1986) 2112.
[171] S. Sakellson, M. McMillan and G.L. Haller, J. Phys. Chem., 90 (1986) 1733.
[172] Y. Hadj Romdhane, B. Bellamy, V. de Gouveia, A. Masson, and M. Che, Appl. Surface Sci., 31 (1988) 383.
[173] A. Masson, B. Bellamy, Y. Hadj Romdhane, H. Roulet, G. Dufour and M. Che, Surface Sci., 173 (1986) 479.
[174] Z.X. Cheng, C. Louis and M. Che, Z. Phys., 20D (1991) 445.
[175] V. de Gouveia, B. Bellamy, A. Masson, and M. Che, Structure and Reactivity of Surfaces, C. Morterra, A. Zecchina and G. Costa (eds), Elsevier, Amsterdam, 1989, p. 347.
[176] K. Hadjiivanov, J.M. Tatibouët, J. Saint Just and M. Che, in the press.
[177] D.L. Trimm, Design of Industrial Catalysts, Elsevier, New York, 1980.
[178] G.J.K. Acres, A.J. Birds, J.W. Jenkins and F. King, Catalysis (London), 4 (1981) 1.
[179] L.L. Hegedus, R. Aris, A.T. Bell, M. Boudart, N.Y. Chen, B.C. Gates, W.O. Haag, G.A. Somorjai and J. Wei, Catalyst Design, Wiley, New York, 1987.
[180] G.A. Ozin and S. Özkar, Chem. Mater., 4 (1992) 511.
[181] B. Imelik and J.C. Védrine (eds.), Les Techniques Physiques d'Etude des Catalyseurs, Technip, Paris, 1988. To appear in english.

Guczi, L. *et al.* (Editors), *New Frontiers in Catalysis*
Proceedings of the 10th International Congress on Catalysis, 19-24 July, 1992, Budapest, Hungary
© 1993 Elsevier Science Publishers B.V. All rights reserved

NEW CATALYTIC ASPECTS OF HETEROPOLYACIDS AND RELATED COMPOUNDS - TO THE MOLECULAR DESIGN OF PRACTICAL CATALYSTS

M. Misono

Department of Synthetic Chemistry, Faculty of Engineering, The University of Tokyo, Bunkyo-ku, Tokyo 113, Japan

Abstract

Recent progress in basic and application studies of heteropoly compound catalysts oriented to "catalyst design" is described, placing stress on the merits of their molecularly well-defined structure. Based on this, future opportunities of heteropoly compound catalysts are discussed, with examples of promising basic researches as well as existing industrial processes.

1. INTRODUCTION

1.1. Catalyst design of practical catalysts based on crystalline mixed oxides

There are many demands in our society for new efficient catalysts in the various fields of energy/resources, synthesis of materials, and environment [1]. But the requirements imposed on the new catalysts are very severe and can not be satisfied by the simple extrapolation of the existing catalytic technology.

Novel concepts for catalyst design are desirable for the development of new catalysts that meet those requirements. Catalyst design at atomic level utilizing advanced surface technology is one of the possibilities. It has been demonstrated in laboratory that atomically controlled surfaces are sometimes very active. However, if one considers the necessary conditions of industrial catalysts; high volume density of active sites (for this, porous materials are needed), stability, economy, etc., the synthesis of industrial catalysts by this method turns out to be unrealistic at least in a mid-term perspective.

As an alternative way, we have attempted molecular design of mixed oxide catalysts by using "crystalline compounds", of which the bulk structure is known and which have potentially high activity and selectivity so as to be applicable to practical uses. Heteropoly compounds, perovskites and zeolites are the examples that we chose as starting materials [2].

We assume that the following relationships, Scheme 1, are essential for the design of catalysts and that the molecular design of catalysts would become possible if the relationships are established at the atomic/molecular level.

1.2. Heteropoly compounds as catalysts

Heteropolyanions and isopolyanions are polymeric oxoanions (polyoxometalates) formed by condensation of oxoanions [3]. The term heteropoly

Scheme 1. Useful relationships for catalyst design

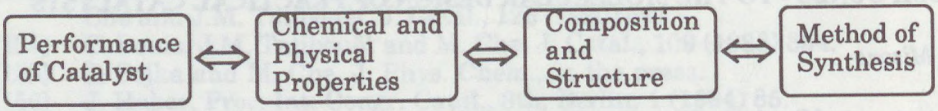

compounds (HPA) is used for the acid forms and the salts. HPA-related compounds are organic and metallo-organic complexes of polyanions.

HPA catalysts are used as acid as well as oxidation catalysts both in solid state and in solution. Various types of catalysis exist for HPA: Three different types for solid HPA catalysts (surface, bulk-type (I) (=pseudoliquid) and bulk-type (II) catalysis, both in gas-solid and in liquid-solid systems) and two types for solution systems (homogeneous and phase-transfer catalysis), as described in the later section. Advantageous characteristics of HPA catalysts are summarized in Table 1.

Attempts to utilize HPA for catalysts have a long history as compiled in the reviews on HPA in 1952 and 1978 [4]. A bench scale test was reported for alkylation of aromatics in 1971. First industrial process with a HPA catalyst was launched in 1972 for the hydration of propene in liquid phase. The essential role of Keggin structure for oxidation of methacrolein was clearly indicated in a patent in 1975. Systematic basic researches of heterogeneous catalysis started in the mid 70's mostly in Japan to elucidate the quantitative correlations between the acid-redox properties and catalytic performances of HPA [2, 4 - 7]. Pseudoliquid phase (bulk-type (I) catalysis) was reported in 1979 and the bulk-type (II) behavior in 1983. Similar efforts for homogeneous systems were carried out in the same period actively in Russia and Japan. In the 80's, several new industrial processes were initiated in Japan by using

Table 1
Advantages of HPA catalysts

1. Catalyst design
- 1-1. By the control of acidic and redox properties.
  HPA having wide range of the two properties can be prepared.
- 1-2. By multi-functionality.
  Acid + redox, multielectron transfer, etc.

2. Molecularity – metal oxide cluster
- 2-1. Molecular design of solid catalysts.
- 2-2. Cluster models of mixed oxide catalysts and of relationships between solid and solution catalysts.
- 2-3. Description of catalytic processes at atomic/molecular level. Spectroscopic study and model compounds of reaction intermediates.

3. Unique reaction field
- 3-1. Bulk-type catalysis. "Pseudoliquid" and bulk-type (II) behavior provide unique reaction fields.
- 3-2. Pseudoliquid makes spectroscopic and stoichiometric studies feasible and realistic.
- 3-3. Phase-transfer catalysis.

4. Unique basicity of polyanion
- 4-1. Selective coordination and stabilization of reaction intermediates.
- 4-2. Ligands for metals and organometallics.

HPA catalysts, as listed in Table 2 [1]. In addition, there are a few small-scale processes. The research activity of HPA catalysis is now very high and seems to still grow, if a huge number of papers published every year and a wide variety of reactions to which HPA catalysts are applied are considered.

We reviewed thoroughly the heterogeneous catalysis of HPA in 1987 [4]. Catalysis in solution has been reviewed in 1982 [6], 1983 [8] and 1992 [9]. The latter [9] also describes catalytic reactions on solid HPA. Two typical industrial processes have been sketched in our recent review [1]. To avoid overlapping with those reviews, I shall not try in this article to cover the whole literature, but describe only the essential characteristics of HPA catalysts with discussion on the future opportunities, according to the items given in Table 1. Stress will be placed on the progress in the last five years mainly of heterogeneous catalysis. So early works will not be referred individually, but only referred to previous reviews, unless the citation is indispensable. Usage of HPA for a precursor of oxide catalysts as well as the cases in which polyanions decompose by some reasons are not included in this article, although sometimes good performances are observed. We believe that, if one wishes to design catalysts taking advantage of the molecular nature of HPA, one must be very careful about the structure and stoichiometry.

Table 2
Large-scale industrial processes using heteropoly compounds

Reaction	Phase	Capacity (10^3 t / year)	Start	Remarks
Hydration of propene	liq (aq)	50	1972	first HPA process (dilute HPA)
Oxidation of methacrolein	gas-solid	220	1982	Mo-V-P
Hydration of isobutene	liq (aq) two phases	56	1984	C4 separation (conc. HPA)
Hydration of n-butene	liq (aq)	40	1985	to MEK
Polymerization of THF	liq (THF-aq)	2-3?	1987	phase-transfer catalysis

2. STRUCTURE, ACIDITY, AND REDOX PROPERTIES, etc.

2.1. Structure of heteropolyanion - primary structure

Several heteropolyanion structures are known; Keggin ($XM_{12}O_{40}$), Silverton ($XM_{12}O_{42}$), Anderson (XM_6O_{24}), Lindqvist (XM_6O_{24}), Waugh (XM_9O_{32}), Dawson ($X_2M_{18}O_{62}$) structures, etc. [3]. We called the polyanions the primary structure differentiating from the secondary structure as described below [7]. They are oxide cluster ions with high molecular weight. As an example, the structure of $PW_{12}O_{40}$ (a Keggin-type heteropolyanion) is shown in Figure 1a. In this polyanion, twelve WO_6 octahedra surround a PO_4 tetrahedron. W is called polyatom or addenda atom and P heteroatom or central atom. There are four different oxygen atoms in this structure (one terminal, two bridging and one inner oxygen). Hereafter, PMo12, etc. will be used for $PMo_{12}O_{40}$, etc.,

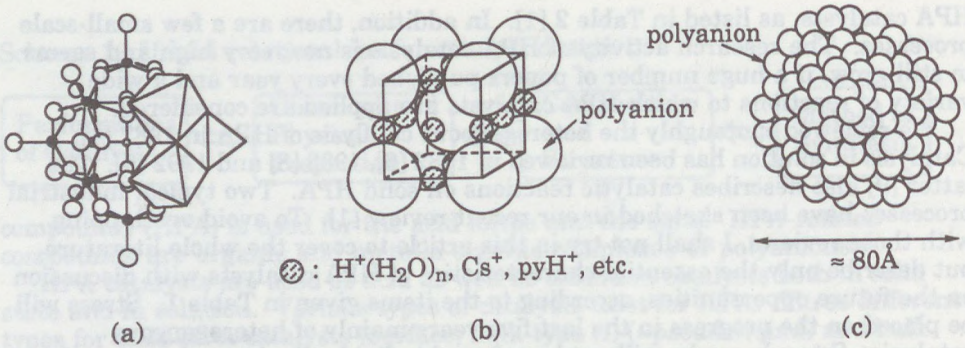

Figure 1. Primary, secondary and tertiary structure of HPA.
(a) Primary structure (Keggin structure, $PW_{12}O_{40}$), (b) Secondary structure ($H_3PW_{12}O_{40}\cdot 6H_2O$), (c) Tertiary structure (Cs2.5 salt, cubic structure as (b)).

unless the use is misleading. Similarly HPMo12, Cs2.5PW12, etc. denote $H_3PMo_{12}O_{40}$, $Cs_{2.5}H_{0.5}PW_{12}O_{40}$, etc.

In aqueous solution, they tend to be hydrolyzed at high pH. The stability and the dynamic equilibrium of dissociation-association of polyanions are dependent on several factors such as the constituent elements, the degree of reduction and the kind of solvents (and coexisting molecules; oxygen-bases like alcohols and ethers usually stabilize Keggin structure so as to be used for purification-extraction). Lacunary polyanions formed by partial hydrolysis are important intermediates for the synthesis of mixed-polyatom polyanions and related complexes [3]. Complexes of polyanions with organic molecules are good model compounds of reaction intermediates.

Acidity and redox properties also vary widely, as reviewed before in relation to catalysis [4, 8, 9]. These are the most important features of HPA catalysts. The Keggin heteropolyanions are very strong acids in general and release all the protons in aqueous solution, while the extent of dissociation much differs in organic solvents. Quantum mechanical studies on the electronic structure of polyanions are being continued [10].

2.2. Structure in the solid state - secondary and tertiary structure

HPA in the solid state is an ionic crystal (sometimes amorphous) consisting of large polyanion, cation, water of crystallization and some additional molecules. As we pointed out previously [7], it is important for the understanding of the catalysis of solid HPA to distinguish between the primary structure and the secondary structure (Figures 1a and b). Recently, it was realized that, in addition to these structures, the tertiary and higher order structures (the structures of HPA as assembly) were very influential on the catalytic function (Figure 1c). The preparation process is very important in this respect.

Behavior of the salts of small cations such as Na and Cu (group A salts) is similar to that of the acid forms, but is very different in several respects from the group B salts (salts of large cations like Cs, K and NH_4) [4]. The secondary

structure of the former is flexible and, due to this nature, polar molecules are readily absorbed in interstitial positions of the solid bulk to cause pseudoliquid behavior. The group A salts are very soluble in water and other polar solvents, while the group B salts are not. Absorption property and solubility are closely related with each other, since both depend on the coordination of absorbed molecule or solvent with polyanion and cation. Thermal stability of group B salts is high. This is presumably due to the absence of proton and water in the lattice of B salts, as the decomposition starts by the water formation from oxygen of polyanion and proton (or water) in the lattice. The thermal stability of HPA catalysts particularly of the mixtures (or solid solutions) is of great concern in heterogeneous catalysis.

The states of proton and water of crystallization in the acid form were studied by high resolution solid-state P-NMR and IR [11]. Higher basicity of bridging oxygen was indicated by preferential bonding of proton. The structure and dynamics of water were examined by H-NMR and it was indicated that water molecules tended to be structured at higher water contents [12]. Baba et al. observed for Ag-HPA reversible changes of line width of H-NMR and catalytic activity by the introduction of hydrogen and suggested a correlation between proton mobility and catalytic activity [13].

Interesting behaviors of HPA in the solid state have been reported by Siedle and coworkers [14]. For example, the following hydrogenation takes place in the solid state (Eq (1)).

$$[(PPh_3)_2Ir(C_8H_{12})]_3PW_{12}O_{40}\ (\text{solid}) + 9H_2 \longrightarrow [(PPh_3)_2IrH_2]_3PW_{12}O_{40}\ (\text{solid}) + 3C_8H_{16} \quad (1)$$

Photo-polymerization found by Kudo and coworkers was developed to synthesize inorganic photoresists, which have high resolution as well as high resistance against oxygen plasma etching [15].

2.3. Acid and redox properties in the solid state

(1) Acidity. As summarized previously [4], the acidity of acid forms generally reflects the acidity in solution. The acidic properties of salts are much more complicated. Five mechanisms have been proposed for the generation of acidity in metal salts [4]; (i) protons in acidic salts, (ii) partial hydrolysis to form weak protons, (iii) acidic dissociation of water coordinated with multivalent metal ion, (iv) Lewis acidity of multivalent metal ion, and (v) protons formed by the reduction of metal ion with H_2. In addition, surface and bulk acidity must be considered in order to understand the acid catalysis of solid HPA. Many efforts are still being devoted for the characterization of acidic properties of HPA, by means of adsorption and thermal desorption of basic molecules [17, 18] as well as by NMR [11, 13, 16].

(2) Reduction-oxidation properties. Two-step reduction of PMo12 by H_2 and corresponding two redox cycles were demonstrated by TPR, IR, and ESR (Eq (2)) [4]. The oxygen involved in the second step is presumed to be the bridging oxygen of Keggin anion. However, studies of the redox chemistry of polyanions

$$xH_2 + PMo_{12}O_{40}^{3-} \longrightarrow 2xH^+ + PMo_{12}O_{40}^{(3+2x)-} \longrightarrow xH_2O + PMo_{12}O_{40-x}^{3-} \quad (2)$$

have been devoted mostly to electron transfer reactions by electrochemical methods and few basic studies exist for the oxygen transfer reactions. Recently, Kawafune and Matsubayashi reported the formation of oxygen-deficient polyanion by an oxygen transfer reaction (Eq (3)) [19]. They assigned this species to a polyanion lacking bridging oxygen on the basis of IR spectral changes during the course of the reduction.

$$PMo_{12}O_{40} + PPh_3 \longrightarrow PMo_{12}O_{39} + Ph_3P{=}O \qquad (3)$$

Structure and reactivity of lacunary polyanions (lacking terminal oxygen) as well as oxygen transfer reactions of mixed-polyatom polyanions and of reduced polyanions have been reported, as well [20]. The progress of those studies would be very useful for the elucidation of oxidation catalysis.

The oxidizing ability of catalyst that changes with the constituent elements of polyanion and countercations is often represented by the rate of reduction of HPA catalysts (reducibility of HPA). Here, the distinction between the surface- and bulk-reducibility is necessary (see later section) [21]. Recently redox potential was measured in the solid state for a single crystal of $H_4SiW_{12}O_{40} \cdot 31H_2O$ [22].

The extent of reversibility of the redox cycle was studied as functions of temperature and the extent of reduction [23]. The redox cycle tends to be reversible if the extent of reduction is low or the reduction is limited to near the surface. The exclusion of V from the polyanion framework upon reduction was indicated for PVMo11 by V-NMR [87].

2.4. Absorption properties and pseudoliquid

The ease of absorption depends on the polarity (or basicity) and the size of molecules to be absorbed and the rigidness of the secondary structure of solid HPA [4]. The rigidness or the reactivity of HPA depends on the countercations (size, charge, etc.) and water content [4, 24]. Alcohols readily move into and out of the bulk of free acids. Pyridine is absorbed easily, but its desorption needs a high temperature. Under controlled conditions uniform pyridinium salts are formed (pyridine:proton = 1:1 and 2:1) and after desorption a cubic secondary structure is maintained [4]. This behavior is utilized to control the tertiary structure, e. g., in the case of the preparation of catalysts for methacrolein oxidation [1].

The quantity of absorbed molecules tends to be integral multiples of the number of protons, forming stable secondary structures. The results of ethanol absorption at 301 K are shown in Figure 2 [25]. At a higher temperature and pressure, the processes are rapid and reversible. Upto the ratio of 2:1, the lattice constant increases only slightly, and above that stoichiometry the lattice starts to expand significantly.

The rate of absorption was measured and analyzed quantitatively, after a controlled pretreatment of HPW12. The rate was higher for more polar (or more basic) and smaller molecules. As reported before such nonpolar molecules as hydrocarbons are adsorbed only on the surface. Group B salts like $Cs_xH_{3-x}PW_{12}O_{40}$ ($x>2$) adsorb even polar molecules only on the surface. Diffusion coefficients in the lattice of HPW12 are ca. 10^3 times lower than those in the micropores of zeolites [25]. Niiyama and his coworkers measured the

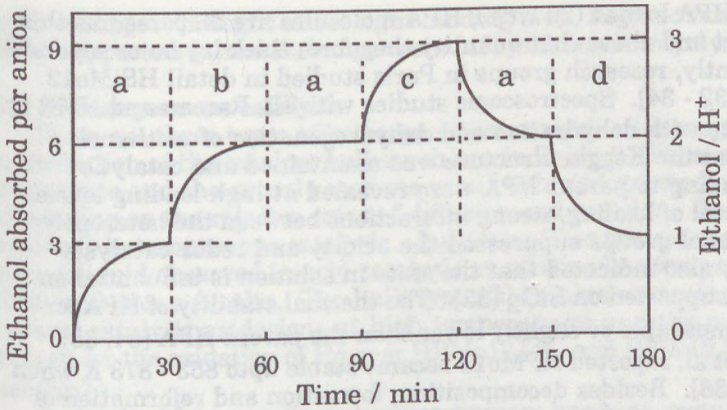

Figure 2. Absorption of ethanol in $H_3PW_{12}O_{40}$ at 301 K [25]. Ethanol pressure/kPa; (a) 0.47, (b) 1.7, (c) 6.0, (d) 0.

effective diffusion constant by means of both transient response method and quartz crystal microbalance. They obtained values of the order of 10^{-11} - 10^{-10} m s^{-1}, which are much lower than those in the gas phase but are close to those in liquid phase [26].

The presence of pseudoliquid phase and its roles in catalysis (bulk-type (I)) have been demonstrated for several heterogeneous acid catalysis [4]. High activity and unique selectivity are often obtained due to this behavior, since nearly all protons in the solid bulk can take part in catalysis and reaction intermediates like carbocations are stabilized by coordination with polyanion in this phase. Spectroscopic and stoichiometric approaches become feasible and realistic owing to the uniform reaction phase and the amplification of surface phenomena into the whole bulk. Phase transition of pseudoliquid phase and characteristic pressure dependencies intrinsic to the phase have already been reported [4, 27].

2.5. Supported HPA

Supported HPA catalysts are important for applications. The structure (primary to tertiary), acid, redox and other properties are very much dependent on the support materials, the level of loading and the method of preparation, as early studies demonstrated [4, 9, 28]. In addition to the ordinary metal oxide supports such as SiO_2, Al_2O_3 and TiO_2, active carbons, ion-exchange resins, and high-surface area salts of HPA have been used. A silane coupling reagent was tested for binding HPA on oxide support [29]. Insolubility in aqueous or organic solvents is also an important property when HPA is applied to liquid-phase reactions.

Basic solids like Al_2O_3 and MgO tend to decompose HPA [4, 30, 91], although significant activities were reported in some cases. On the other hand, SiO_2 is relatively inert. In the cases of HPW12 and HPMo12 on SiO_2, the XRD line widths and intensities as well as the catalytic activities showed that, upto a

certain quantity of HPA loaded (20 wt%), HPA molecules are dispersed as thin layers on the support and above that quantity they form thick layers or separate particles [31]. Recently, research groups in Paris studied in detail HSiMo12 supported on SiO_2 [32 - 34]. Spectroscopic studies with IR, Raman and NMR as well as catalytic tests with dehydration and dehydrogenation of methanol [32, 34] indicated that the Keggin structure was maintained and catalytic properties corresponding to parent HPA were revealed at high loading levels. But, at a very low level of loading, strong interactions between the heteropoly-acid and surface silanol groups suppressed the acidity and redox catalysis predominated. They also indicated that the state in solution is influential on the dispersion after supported on SiO_2 [33]. The thermal stability of HPA on SiO_2 seems to be comparable or slightly lower than the parent HPA [34, 35], whereas Kasztelan et al. reported HPMo12 became stable upto 853 - 873 K when supported on SiO_2 [36]. Besides decomposition, formation and reformation of Keggin structure take place under certain (wet) conditions [4, 37, 38]. The decomposition results in a dramatic change in the catalytic function as shown for example in Figure 3 [34].

K and Cs salts which have high surface areas are useful supports for HPA. Increased stability as well as improved yield in selective oxidation of acrolein was observed when $H_{3+x}PV_xMo_{12-x}O_{40}$'s were supported on K3PMo12 [39, 40]. They claim that free acids covered epitaxially the surface of the support. We suspected, on the other hand, the formation of a solid solution for acidic Cs salts of HPW12 [41] and HPMo12 [42].

A certain kind of active carbon was an excellent support of HPA to make HPA insoluble [43]. It was recently reported that proton transfer from HPA to

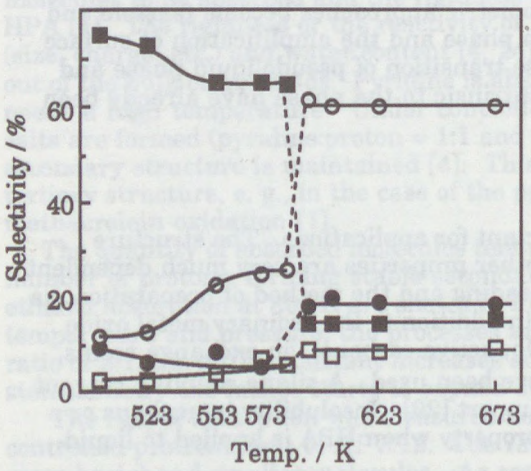

Figure 3. Selectivities of the reaction of methanol over $H_4SiMo_{12}O_{40}\cdot 14H_2O$ (unsupported) as a function of pretreatment temperature [34].
(o); CH_2O, (□); HCOOH, (●); $(CH_3O)_2CH_2$, (■); $(CH_3)_2O$.

carbon support brought about tight binding [44]. High activity was reported for HPA supported on ion-exchange resin [45] and doped in polyacetylene [46].

2.6. Heterogeneous catalysis

There are three types of heterogeneous catalysis with respect to the contribution of the catalyst bulk as shown in Table 3. These three are prototypes and the actual reactions would exhibit intermediate behavior depending on the relative rates of diffusion and reaction. Surface-type is the ordinary heterogeneous catalysis. Bulk-type (I) is the reaction in the pseudoliquid observed in acid catalysis at relative low temperatures for acid form and group A salts. The bulk-type (II) catalysis was demonstrated for several catalytic oxidations at high temperatures and the mechanism was proven for the oxidation of H_2 over HPMo12 [47] and HPW12 [48] (see later section).

Redox (or Mars-van Krevelen) mechanism has been quantitatively shown for the oxidation of H_2 and CO over alkali salts of HPMo12 by the coincidence of the three rates at the stationary oxidation state of catalyst, that is, the rates of catalytic oxidation, reduction and reoxidation of catalyst as summarized in Table 4 [21, 23].

Table 3
Three types of heterogeneous catalysis of HPA

Types	Remarks	Examples
Surface-type	Ordinary type. Reactions take place on the surface. Rate ∝ surface area	Oxidations of aldehydes and CO
Bulk-type (I)	"Pseudoliquid phase". Reactants are absorbed in solid bulk and react. Rate ∝ volume(weight)	Dehydration of alcohols at low temperatures
Bulk-type (II)	Main reactions occur on the surface, but by diffusion of redox carriers, whole bulk takes part. Rate ∝ volume (weight)	Oxidative dehydrogenation, oxidation of H_2

Table 4
Comparison of the rates of reactions at stationary state of HPMo12 at 623 K

Reaction	H_2	CO
Catalytic oxidation	130	2.4
Reduction of catalyst	110	3.1
Reoxidation of catalyst by O_2	110	2.6
Degree of reduction of catalyst	0.30	0.038

Rates are in the unit of 10^{-3} electron anion^{-1} min^{-1}, and degree of reduction in electron anion^{-1}.

3. CONTROL OF ACID AND REDOX PROPERTIES FOR THE DESIGN OF SOLID HPA CATALYSTS

(discussion will be limited to HPA with Keggin anion)

3.1. Control of the acidity of solid HPA

The acidity of acid forms in solid generally follows the acidity in solution that is intrinsic nature of the polyanions. The acidity can be further controlled by salt formation and subsequent heat treatment. Five mechanisms as described above must be taken into account for the control of the acidity of salts. In addition, considerations on the difference between the bulk and surface acidity are necessary for acid forms and group A salts. The bulk protonic acidity of group A salts decreases monotonically with the extent of neutralization. But the hydrolysis during the neutralization produces new weak acid sites (mechanism (ii)). The protonic acidity of group B salts exhibits peculiar changes upon neutralization, due to the significant change in the particle size (hence, the specific surface area) as in the case of Cs salts described below (Figure 5). Variation of the acidity as well as the absorption properties with the extent of neutralization is shown in Figure 4 for typical group A and B salts, that is, Na and Cs salts. It has been reported that the protonic sites created by reduction of counter cations such as Ag (mechanism (v)) show extraordinarily high catalytic activity [9]. Surface protonic acidity of a given bulk composition is sensitive to the method of preparation and pretreatment (due to changes of the surface composition or the tertiary structure).

It must be noted that some discrepancies exist in the acidities reported. For example, Serwicka et al. [17] reported that the acid strength of $H_{3+x}PV_x$-$Mo_{12-x}O_{40}$ strongly depended on the water content, whereas in our experience with HPW12 and HPMo12, water molecules were easily replaced by pyridine to form quantitatively pyridinium salts, and the acid strength did not change with water content [4], water content affecting the rate of absorption but not the equilibrium. They also reported that the acid quantity increased significantly when free acids were supported on K3PMo12 and ascribed the increase to the formation of thin film of the acid on the support. However, as described below, in our experiments, although the surface acidity increased, nearly uniform solid solution was formed by migration of cations. The discrepancies may be in part due to the difference in the HPA used. But, it is evident that cautious and quantitative examination is necessary to elucidate the acidity at molecular level.

3.2. Control of redox properties

The redox properties can be controlled in a similar way as the acidity. Mo-containing polyanions are stronger oxidants and hence better oxidation catalysts in general than W-polyanions, reflecting the redox potential in solution.

The oxidizing abilities measured by the reduction of HPA catalysts were inconsistent in early studies [4], and rational explanations of the differences between group A and B salts, and of the effects of the methods of reduction and preparation were not possible. We were able to solve most of these problems by the concept of surface- and bulk-type catalysis [21, 23]. The reduction by H_2 of free acid and group A salts proceeds both on surface and in bulk, but the

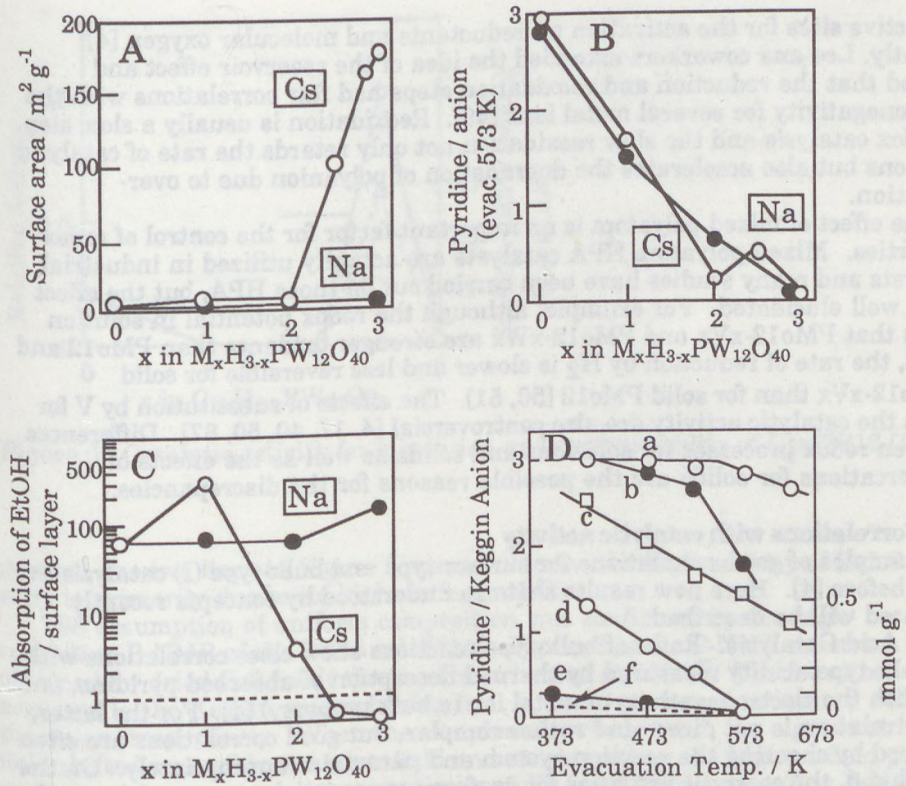

Figure 4. Variations of (A) surface area, (B) acidity (bulk) and (C) absorption property with alkali salt formation, and (D) acid strength distribution measured by thermal desorption of pyridine. (a) $H_3PW_{12}O_{40}$, (b) $H_3PMo_{12}O_{40}$, (c) $NaH_2PW_{12}O_{40}$, (d) $Na_3PW_{12}O_{40}$, (e) $Cs_3PW_{12}O_{40}$, (f) SiO_2-Al_2O_3.

reduction by CO only near the surface. Hence, the rate of reduction by H_2 normalized to catalyst weight can be regarded to represent the oxidizing ability of the catalysts bulk to the first approximation. On the other hand, the rates of reduction by CO divided by the surface area express the oxidizing ability of the surface. In this way, it was shown that the oxidizing ability decreased monotonically for both cases with the increase in the extent of neutralization with alkali, except for the reduction by H_2 of Cs2.5PMo12, for which a higher value than the monotonous change was observed. This high value is due to its very high surface area and rigid secondary structure (this implies that the reaction is not ideal bulk-type).

The reason for the decrease of oxidizing ability with alkali content is not fully understood, although the electronegativity of cation and a role of proton in reduction process are suggested for the reason. Transition metals are believed to play additional roles in the redox processes; that is, a reservoir for electrons

and active sites for the activation of reductants and molecular oxygen [4]. Recently, Lee and coworkers extended the idea of the reservoir effect and showed that the reduction and reoxidation steps had fair correlations with the electronegativity for several metal ions [49]. Reoxidation is usually a slow step in redox catalysis and the slow reoxidation not only retards the rate of catalytic reactions but also accelerates the degradation of polyanion due to over-reduction.

The effect of mixed polyatom is an important factor for the control of redox properties. Mixed-polyatom HPA catalysts are actually utilized in industrial catalysts and many studies have been carried out on those HPA, but the effect is not well elucidated. For example, although the redox potential in solution shows that PMo12-xVx and PMo12-xWx are stronger oxidants than PMo12 and PW12, the rate of reduction by H_2 is slower and less reversible for solid HPMo12-xVx than for solid PMo12 [50, 51]. The effects of substitution by V for Mo on the catalytic activity are also controversial [4, 17, 40, 50, 87]. Differences between redox processes for solutions and solids as well as the effects of countercations for solids are the possible reasons for the discrepancies.

3.3. Correlations with catalytic activity

Examples of good correlations for surface-type and bulk-type (I) catalysis are given before [4]. Here new results that are understood by concepts recently advanced will be described.

(1) Acid Catalysis. Rates of bulk-type reactions show close correlations with the bulk-type acidity measured by thermal desorption of absorbed pyridine, and also with the electronegativity of metal ion (a bulk property) [4]. For the latter, the correlation is not direct and rather complex, but good correlations are often observed by choosing the reaction system and parameter appropriately. On the other hand, the catalytic activities for surface-type reactions are sensitive to the surface composition and change rather irregularly, unless for some reasons the homogenization of the catalyst composition takes place [4]. This is particularly so in the case of group B salts which have more rigid secondary structure.

By taking advantage of this nature of group B salts we synthesized a highly active solid acid catalyst, that is, $Cs_{2.5}H_{0.5}PW_{12}O_{40}$. We prepared carefully several acidic Cs salts, $Cs_xH_{3-x}PW_{12}O_{40}$ (Csx salt) (x = 0, 1, 2, 2.5, 2.75, and 3), and measured their physical, acidic, absorption and catalytic properties. The properties were in several respects in contrast to what we observed for Na salts (see Figure 4). In the gas-solid systems [4], the catalytic activities decreased once to nearly zero, then sharply rose to give a maximum at x=2.5 and fell to zero again at x=3. It was remarkable that the activity at x=2.5 was higher than that of the free acid (x=0). Recently we found that the activity at x=2.5 was even more enhanced for liquid-solid systems [52].

In Figure 5, the rate of alkylation and the surface acidity are shown as functions of x. Here the surface acidity was estimated by multiplying the formal concentration of proton on the surface by the specific surface area. The estimation of the number of surface protons is based on the assumption that the distribution of proton is uniform in the solid and surface. The surface acidity changes as in Figure 5 are understandable, because Cs2.5 and Cs3 salt have very high surface areas (100 - 180 $m^2\ g^{-1}$), due to their very small particle size (6 - 10 nm), and the density of proton decreases monotonically with x. In

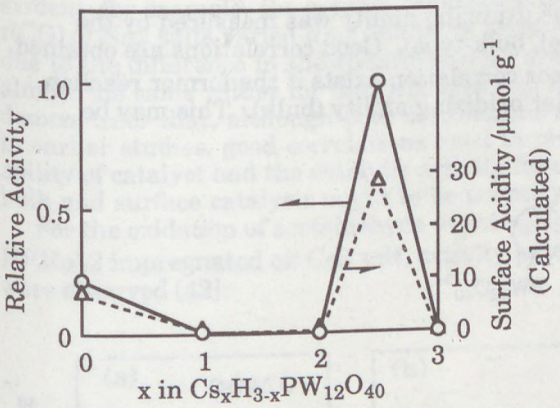

Figure 5. Catalytic activity for alkylation and surface acidity of CsxPW12 [41a].

general, the two lines in Figure 5 agreed. Hence, the high activity of Cs2.5 salts is primarily due to its high surface acidity.

The assumption of uniform composition was confirmed by the high-resolution P-NMR of the Cs2.5 salt [41a]. Figure 6 is the P-NMR spectrum obtained for dried Cs2.5 salt that had been heated at 300 °C. The four lines are assigned to the Keggin anions having 0, 1, 2, and 3 protons coordinated with the anion, respectively. When the samples absorbed water, the signals at lower field shifted reversibly to higher field and overlapped on the highest-field peak, so it was necessary to dry the sample carefully [41a]. The interesting P-NMR spectra reported for acidic salts of potassium are obscured in part by the presence of absorbed water, as the authors indicated [39]. The relative peak intensities in Figure 6 approximately agreed with those expected from the random distribution of protons, indicating uniform acidic salts (i. e., solid solution of Cs salt and free acid). The same P-NMR spectrum was observed after heat treatment of a sample that was prepared by impregnating HPW12 on Cs3 salt to form the same average composition. Hence, it is certain that homogenization proceeded by the migration of Cs ion and proton as suggested before [4].

The results in Figures 5 and 6 demonstrate the importance of the tertiary structure of HPA in heterogeneous catalysis. The activity of Cs2.5 salt was much greater than conventional solid acid catalysts as shown in Figure 7. The much greater activities (per proton) of Csx salts than SiO_2-Al_2O_3 and SO_4^{2-}/ZrO_2 cannot be explained simply by the surface acidity. This might be due to additional effects like acid-base bifunctional acceleration by proton (acid) and polyanion (base) and/or a special state of proton on the surface. High activities of HPA catalysts sensitive to pretreatment have been reported for alkylation and acylation of aromatics in liquid-solid system [53].

(2) Oxidation catalysis. Figure 8a shows the correlation of the rates of oxidation of acetaldehyde (surface-type) with the surface oxidizing ability measured by the reduction of catalyst by CO (r[CO], surface-type). In Figure 8b a similar relationship for oxidative dehydrogenation of cyclohexene (bulk-type)

is presented. In the latter case, the oxidizing ability was measured by the reduction of catalyst with H_2 (r[H_2], bulk-type). Good correlations are obtained for both cases. However, only a poor correlation exists if the former reaction (surface) is plotted against the latter oxidizing ability (bulk). This may be

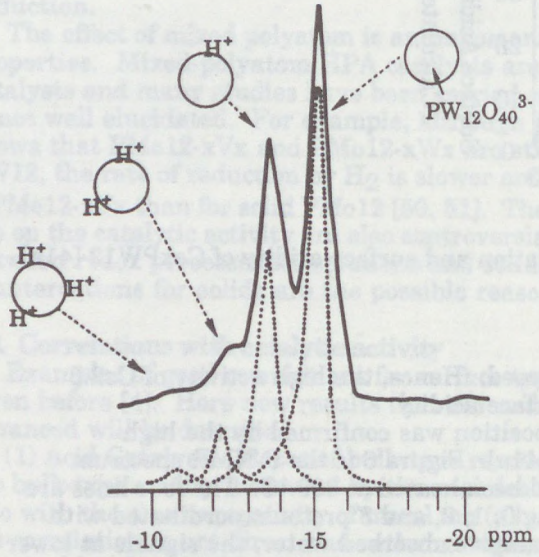

Figure 6. P-NMR of Cs2.5PW12 (calcined at 573 K) [41a].
Dotted line; expected for statistical distribution.

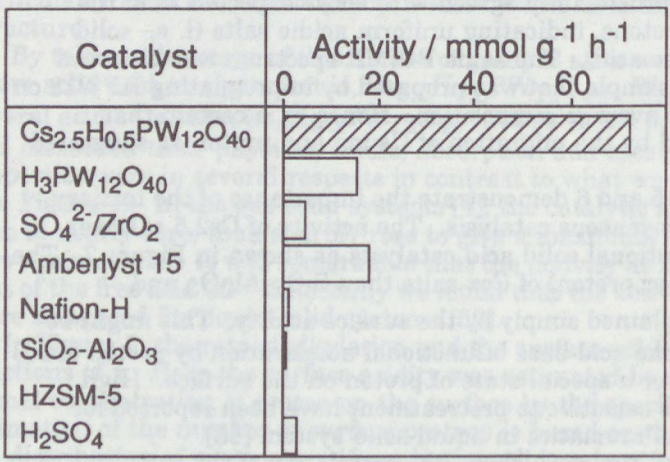

Figure 7. Comparison of the catalytic activities (rates) of several solid acids [52].
1,3,5-Trimethylbenzene + cyclohexene (343 K).

evident; for example, the activity for surface-type reaction (acetaldehyde) and r(CO) of Na2 salts varied from one lot to another (Na2-1 to Na2-4, Figure 8a), due to the difference in the specific surface area, while those Na2 salts had almost the same values for the bulk-type reactions (Figure 8b). These results demonstrate that, although poor correlations and discrepancies were reported in earlier studies, good correlations exist in principle between the oxidizing ability of catalyst and the catalytic activity for oxidation, and that the concept of bulk and surface catalysis ought to be properly considered.

For the oxidation of acetaldehyde over $Cs_xH_{3-x}PMo_{12}O_{40}$ (x = 0 - 3) and HPMo12 impregnated on Cs3 salt, activity patterns similar to that in Figure 5 were observed [42].

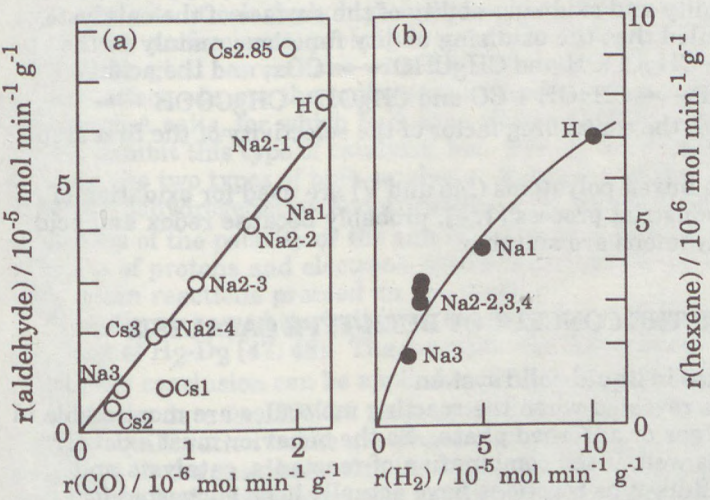

Figure 8. Correlations between catalytic activity and oxidizing ability for (a) oxidation of acetaldehyde (surface-type) and (b) oxidative dehydrogenation of cyclohexene (bulk-type) [31, 42].

(3) Combination of acidity and redox properties in catalysis. The acidity and oxidizing ability work cooperatively for oxidation of methacrolein, while they function competitively for oxidative dehydrogenation of isobutyric acid [4]. These two reactions are contrastive from the standpoint of the bulk vs. surface concept, as well. The former is surface-type and the latter bulk-type. Therefore, the catalyst design of the two reactions should be considerably different, although both reactions form methacrylic acid with HPA catalysts in good yields (Eq (4)). The former is already industrialized (Table 2) and the latter on a development stage [54 - 56].

$$CH_2{=}C(CH_3){-}CHO \longrightarrow CH_2{=}C(CH_3){-}COOH \qquad (4a)$$

$$CH_3{-}CH(CH_3){-}COOH \longrightarrow CH_2{=}C(CH_3){-}COOH \qquad (4b)$$

Scheme 2. Oxidation of acetaldehyde over HPA catalysts

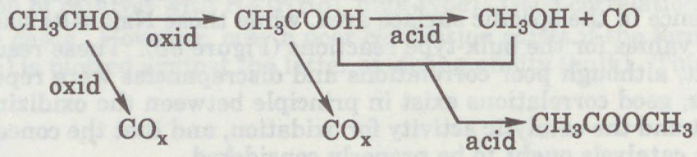

Roles of acidity and oxidizing ability were studied in detail for the oxidation of acetaldehyde [57] using various salts of HPMo12, on the basis of the reaction scheme deduced (Scheme 2). The rate of each reaction step of the scheme was estimated from the oxidations of acetaldehyde and acetic acid, and was compared with the acidity and oxidizing ability of the surface of the catalysts. The comparisons revealed that the oxidizing ability functions mainly in the steps of $CH_3CHO \longrightarrow CH_3COOH$ and $CH_3CHO \longrightarrow COx$, and the acidity accelerates $CH_3COOH \longrightarrow CH_3OH + CO$ and $CH_3OH + CH_3COOH \longrightarrow CH_3COOCH_3$, although the controlling factor of the selectivity of the first step was not made clear.

HPA catalysts with mixed polyatoms (Mo and V) are used for oxidation of methacrolein in the industrial process [1, 4], probably because redox and acid properties of these polyanions are suitable.

4. DEVELOPMENT OF THE CONCEPT OF BULK-TYPE CATALYSIS

4.1. Pseudoliquid phase in liquid-solid system

The pseudoliquid is revealed when the reacting molecules are more stable in this phase than in the gas or adsorbed phase. So the behavior must exist for liquid-solid systems, as well, if the combination of reactants, catalysts and solvents is adequate. Bulk-type reactions have actually been suggested for liquid-solid systems [53, 90]. Figure 9 shows the relative activities of the Cs2.5 salt and the acid form of PW12 for three organic reactions [58]. Both catalysts are much more active than the conventional solid acids, as in Figure 7. In

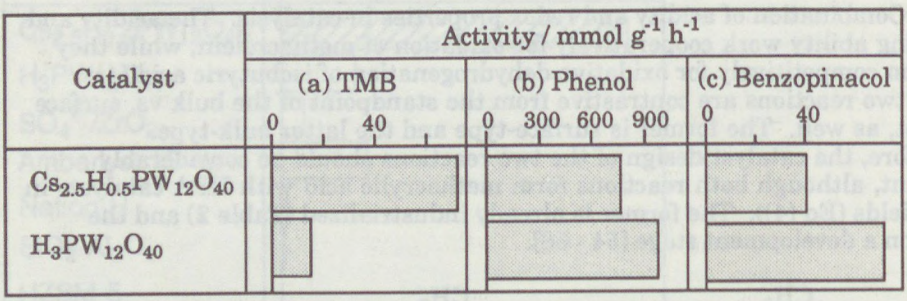

Figure 9. Comparison of the catalytic activities of solid Cs2.5 salt and HPW12 for three reactions in liquid phase [58]. (a) 1,3,5-Trimethylbenzene + cyclohexene (343 K), (b) phenol + 1-dodecene (373 K), (c) rearrangement of benzopinacol (298 K).

addition, it was noted that, as the polarity of reactant increases from the left to the right of the figure, the activity of the free acid increased relatively and became much greater than the Cs2.5 salt for pinacol rearrangement. For the latter reaction, the amount of reacting molecules held by HPW12 was measured during the reaction by analyzing the amount left in solution. As expected, the amount was significant and corresponded to about 20 layers if allotted to surface. This clearly indicates the presence of pseudoliquid behavior, and explains the high activity of HPW12.

4.2. Bulk-type (II) catalysis

In addition to the catalysis in the bulk of the pseudoliquid, there is another class of bulk-type catalysis which was found for oxidation reactions over some HPA catalysts at relatively high temperatures (Table 3). Independence of the rate on the surface area, prolonged reactivity upon repeated pulses of reductants, good correlations with the oxidizing ability of catalyst bulk, smaller support effect, etc. are the indications of the bulk-type behavior. The acid forms and group A salts, for which bulk-type (I) (pseudoliquid) catalysis is observed, tend to exhibit this type of catalysis, too. But the mechanisms are very different between the two types of bulk catalysis. Reactions to form protons such as oxidative dehydrogenation and oxidation of H_2 belong to the bulk-type (II), regardless of the polarity or the size of reactant molecules. Due to the rapid diffusion of protons and electrons, whole bulk participates in the redox cycle, while main reactions proceed on the surface.

Recently we proved the bulk-type catalysis, by analyzing quantitatively the reactions of H_2-D_2 [47, 48]. The reaction was very similar in the presence of O_2, so that the conclusion can be applied to the catalytic oxidation of H_2.

First, the data for HPW12 were analyzed. As shown in Figure 10a, the isotopic equilibration in the gas phase was very rapid, and, to our surprise, the H content in the gas phase also increased rapidly. Hydrogen in the whole system (gas and solid phase) was equilibrated in a short period, while the uptake of H + D by the solid and the formation of water were slow. From

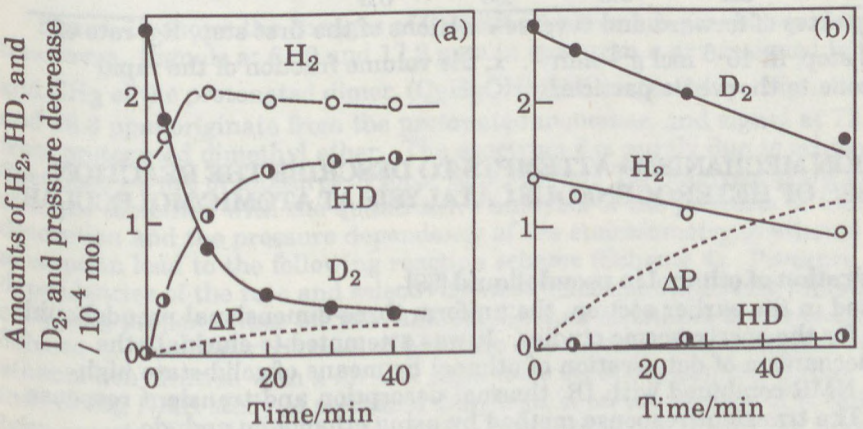

Figure 10. H_2-D_2 reaction over (a) HPW12 and (b) HPMo12 at 573 K [47, 48].

detailed kinetic analysis, Scheme 3 and rate data shown in Table 5 were obtained [48]. First and last steps of the scheme are very rapid and the second step is the slow step, the equilibrium strongly favoring the starting system (left hand side of the first step). Rapid appearance of protons of catalyst into the gas phase is well understood by this scheme.

Thus, the reason why the reduction of catalyst by H_2 becomes bulk-type is that the formation of water from proton and oxygen of polyanion takes place in the whole solid bulk and is rate-determining. It can be shown for HPA catalyst on the basis of a redox mechanism that the rate of catalytic oxidation of H_2 becomes bulk-type, if the rate of catalyst reduction is bulk-type even though the reoxidation is surface-type [21, 47]. In the case of PMo12, R_1 and R_3 were comparable and R_2 was small [47], so that D atoms flow from D_2 in the gas phase into water molecule via solid bulk. Small dependency of the rate on specific surface area was well reproduced also for PMo12 by a simulation using the data in Table 5.

Scheme 3. Isotopic equilibration and exchange of hydrogen isotopes

$$H_2\,(D_2)\,[\text{gas}] \underset{R_1\ (\text{forward})}{\overset{\text{rapid}}{\rightleftharpoons}} H^+\,(D^+)\,[\text{whole bulk}]$$

$$R_2\ (\text{reverse})$$

$$\xrightarrow[R_3]{\text{slow}} H(D)_2O\,[\text{whole bulk}] \xrightarrow{\text{rapid}} H(D)_2O\,[\text{gas}]$$

Table 5
Rate data of H_2-D_2 reaction over HPW12 and HPMo12 at 573 K

	R_1	R_2	R_3	x
HPW12	52	51	0.6	0.8
HPMo12	3.2	0.5	1.8	0.5

R_1 and R_2; rates of forward and reverse reactions of the first step, R_3; rate of the second step, in 10^{-6} mol g^{-1} min^{-1}. x; the volume fraction of the rapid diffusion zone to the whole particle.

5. REACTION MECHANISM - ATTEMPTS TO DESCRIBE THE REACTION PROCESSES OF HETEROGENEOUS CATALYSIS AT ATOMIC/MOLECULAR LEVEL

5.1. Dehydration of ethanol in pseudoliquid [59]

As stated in the earlier section, the uniform three-dimensional pseudoliquid is suitable for the spectroscopic studies. It was attempted to elucidate the reaction mechanism of dehydration of ethanol by means of solid-state high-resolution NMR combined with IR, thermal desorption and transient response methods. The transient response method by using ethanol-d_0 and -d_6 confirmed that a large number of ethanol molecules are absorbed in the

interstitial position of the catalyst bulk under the reaction conditions and the reaction proceeds in this bulk phase. Plausible reaction intermediates such as protonated ethanol dimer, $(C_2H_5OH)_2H^+$, monomer, $C_2H_5OH_2^+$, and ethoxy group coordinated with polyanion were directly detected by NMR. These assignments were supported by IR and fully consistent with stoichiometry of ethanol absorption shown in Figure 2. The chemical shift of proton of the dimer species, 9.5 ppm, suggested that the pseudoliquid is a superacid.

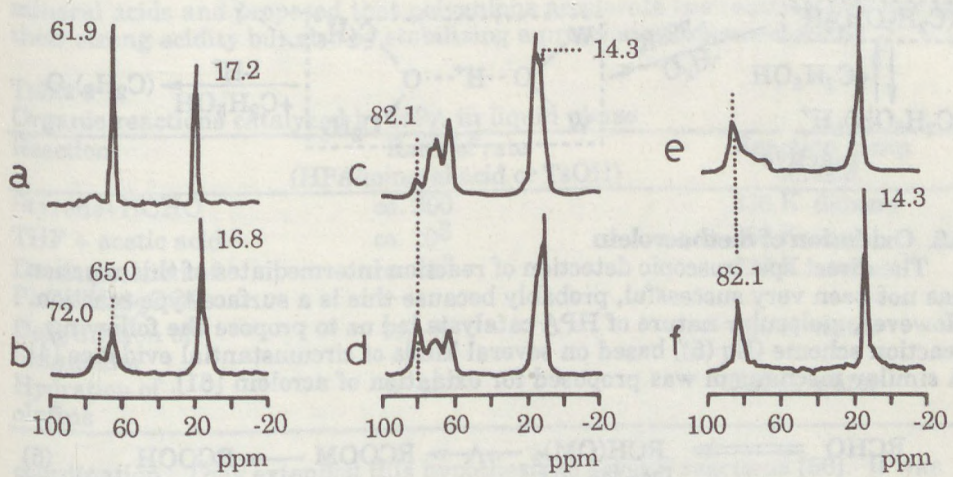

Figure 11. Transformation of protonated ethanol in HPW12 by heat treatment as measured by C-NMR [59]. (a) Dimer, (b) 333 K, (c) 343 K, (d) 363 K, (e) 373 K, (f) 423 K.

Figure 11 shows the changes of C-NMR of ethanol in pseudoliquid upon heat treatment. Signals at 61.9 and 17.2 ppm in spectrum **a** are assigned to CH_2 and CH_3 of the protonated dimer, $(C_2H_5OH)_2H^+$, respectively. Signals at 65.0 and 16.8 ppm originate from the protonated monomer, and signal at 72.0 ppm from protonated dimethyl ether. The spectrum **f** is purely due to ethoxy group. Spectra **b - e** are of mixtures of those four species. The analysis of the spectral changes combined with the quantitative analysis of the products of thermal desorption and the pressure dependency of the stoichiometry of ethanol absorption lead to the following reaction scheme (Scheme 4). Pressure dependencies of the rate and selectivity were semi-quantitatively reproduced by assuming proper values for rate and equilibrium constants of the reactions in Scheme 4. Gradual variations of pressure dependency and selectivity of ethanol dehydration with x for Csx salts were similarly explained [60]. An interesting NMR study of methanol dehydration on the surface of K salt has been reported [82], but it may be obvious that pseudoliquid behavior makes the quantitative study much more feasible.

Scheme 4. Reaction scheme for ethanol dehydration in pseudoliquid phase

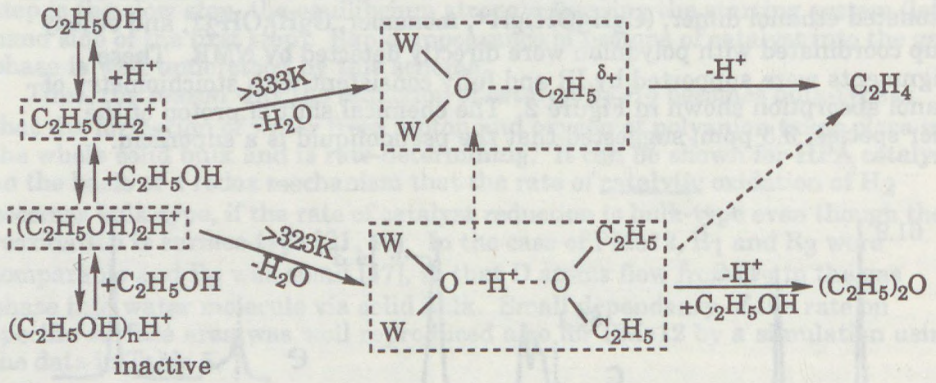

5.2. Oxidation of methacrolein

The direct spectroscopic detection of reaction intermediates of this reaction has not been very successful, probably because this is a surface-type reaction. However, molecular nature of HPA catalysts led us to propose the following reaction scheme (Eq (5)) based on several kinds of circumstantial evidence [4]. A similar mechanism was proposed for oxidation of acrolein [61].

$$RCHO \rightleftharpoons \underset{\{1\}}{RCH(OM)_2} \longrightarrow \underset{\{2\}}{RCOOM} \longrightarrow RCOOH \qquad (5)$$

[M=Mo, H]

The first step is reversible and rapid, being catalyzed by acidity of catalyst as discussed before [4]. Presence of direct exchange of isotopic oxygen between polyanion and methacrolein was recently confirmed by means of an elaborate pulse-mass experiment [62]. This supports the presence of the intermediate, {1}, in Eq (5). The second step is rate-determining and controlled by the oxidizing ability of catalyst, as a fair correlation was observed [7, 63]. Oxygen atoms of polyanion are involved in this step [7]. It is to be pointed out that organic complexes of polyanion that contain essential substructures in common with the intermediates assumed in Eq (5), {1} and {2}, have been reported [4].

6. CATALYSIS IN SOLUTION -- UNIQUE BASICITY OF POLYANION

Many interesting reactions are catalyzed by HPA in solution. Strong protonic acidity as well as unique basicity of polyanions, e. g., coordination with such organic molecules as oxygen-bases (indicating oxophilicity through hydrogen bonding), are the reasons of the efficient catalysis. Solid HPA catalysts in general exhibit good performance for reactions of molecules containing oxygen and nitrogen atoms [4]. This is also related to the oxophilic nature of polyanions and the tendency to form pseudoliquid.

Kozhevnikov and Matveev [8] studied various reactions in aqueous and non-aqueous media catalyzed by HPA, and they correlated the rate of acid catalysis with the acid strength they determined [64]. Izumi's group and Aoshima and coworkers of Asahi Chemical studied further and broadened the possibility of HPA catalysts. High catalytic activities are observed in aqueous solutions as well as in organic media; particularly in the latter case, very high activities are often obtained. Typical examples are listed in Table 6.

Izumi et al. [65] observed for hydration of isobutene in aqueous HPA solution a reaction order higher than one and activation energy lower than that for mineral acids and proposed that polyanions accelerate the reaction not only by their strong acidity but also by stabilizing a protonated intermediate by

Table 6
Organic reactions catalyzed by HPA in liquid phase

Reaction	Ratio of rate (HPA/mineral acid or TsOH)	Reaction temp. solvent
Styrene+HCHO	ca. 300	338 K dioxane
THF + acetic acid	ca. 10^3	368 K neat
Decomposition of $PhC(CH_3)_2OOH$	ca. 10^3	300 K acetone
Dehydration of butanediol	1.5 - 8	430 K water
Hydration of olefins	2 - 10	350 K water

coordination. They extended this hypothesis to several reactions [66]. It was reported recently that the higher activity could be explained solely by stronger acidity, solubility and salt effects, as the rate constant followed Eq (6) including

$$\log k = 1.04H_0 - 3.46 \qquad (6)$$

both HPA and mineral acids [67]. However, other studies indicate that the role of polyanion as soft base is one of the essential feature of HPA catalysis.

Aoshima and coworkers [68] studied hydration of isobutene in aqueous phase (from a mixture of isobutene and n-butenes) and found a very high activity and selectivity in a highly concentrated solution, as shown in Figure 12. Rate was expressed by Eq (7). On the basis of detailed examination, they concluded that the high activity (ca. ten times that of mineral acids) was due to the combination of three factors of similar order (Eq (8));

$$\text{rate} = k\,[H^+][\text{polyanion}][\text{isobutene}] \qquad (7)$$

$$10 \text{ times} \approx 2 \text{ (increase in acid strength)} \times 2 \text{ (solubility increase)} \times 2 \text{ (acceleration by coordination)} \qquad (8)$$

High selectivity (predominance of hydration of isobutene over hydration of n-butenes, and absence of dimerization of isobutene) was assumed to be brought about by the competitive coordination of reactants and water with polyanion and this coordination strongly depends on the concentrations as indicated by

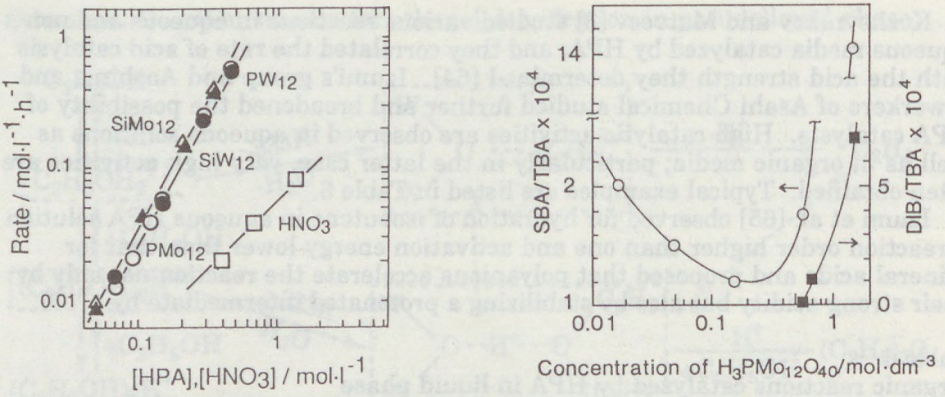

Figure 12. Rates and selectivities of hydration of isobutene catalyzed by HPA in liquid phase at 353 K. SBA; sec-Butyl alcohol, TBA; tert-butyl alcohol, DIB; dimers of isobutene.

the results in Figure 12. The optimization of the concentration and the stabilization of HPA by controlling the oxidation state and adding oxygen-bases were the reasons of the successful commercialization [1].

These remarkable coordination effects were utilized in the industrial process of polymerization of tetrahydrofuran under the conditions of phase-transfer catalysis [69]. Here, the presence of two types of coordination, via proton and water, was indicated by IR and the variation of the former was in parallel with the reaction rate. HPA is efficient for other polymerization reactions like polycondensation of benzyl derivatives [70]. Selective synthesis of glycoside derivatives from saccharides was also possible with HPA [72].

Baba and Ono [71] compared dehydration of 1,4-butanediol catalyzed by HSiW12 in dioxane and in aqueous phase. The rate equation (Eq (9)) in aqueous solution indicated the presence of an additional reaction path (k_2)

$$\text{rate} = (k_1 + k_2 [SiW_{12}O_{40}])[\text{butanediol}][H^+] \qquad (9)$$

which was accelerated in proportion to the concentration of polyanion, thus implying the complex formation between protonated intermediate and polyanion. The rate was 70 times greater in organic media. This was explained by the retardation effect of water coordination in aqueous phase.

Interesting applications of HPA as phase-transfer catalysts for oxidation reactions have been reported by Venturello et al. [73] and Ishii et al. [74]. This is in part related to the unique basicity of polyanion. Peroxopolyanion formed by the reaction with H_2O_2 in aqueous phase becomes slightly soluble into organic phase, where epoxidation of olefin proceeds. Since water is absent in organic phase, secondary reaction to produce diol from epoxide is suppressed, resulting in a very high selectivity of epoxidation. Recently, the structures of probable peroxo intermediates have been reported [75, 76].

HPA catalysts sometimes form a separate liquid phase complexing with solvents. By this phenomena, separation of HPA catalysts from products

becomes easier [77]. Similar two phase formation is utilized in the industrial process of hydration of isobutene [1, 68].

H_2O_2 is used with HPA in uniform solution systems, as well. As listed in Table C (Appendix), variety of reactions have been tested. The effect of mixed-polyatom polyanions is remarkable in the oxidation of cycloolefins to dialdehydes [78 - 80], as shown in Figure 13 for oxidation of cyclopentene in tributyl phosphate. Highest yield was obtained for HPMo6W6 which is a mixture of HPMo12-xWx. The mixing of polyatoms takes place during the preparation in aqueous solution. The mixing does not occur in tributyl phosphate, as shown by the low yield observed for a mixture of HPMo12 and HPW12. The formation of diol, the main by-product, increases with increase in the acidity (or the W content) of HPA. Theoretical explanation of the synergistic effect has been attempted [81], although there is a possibility that the formation of active peroxo species is accompanied by the degradation of Keggin anion.

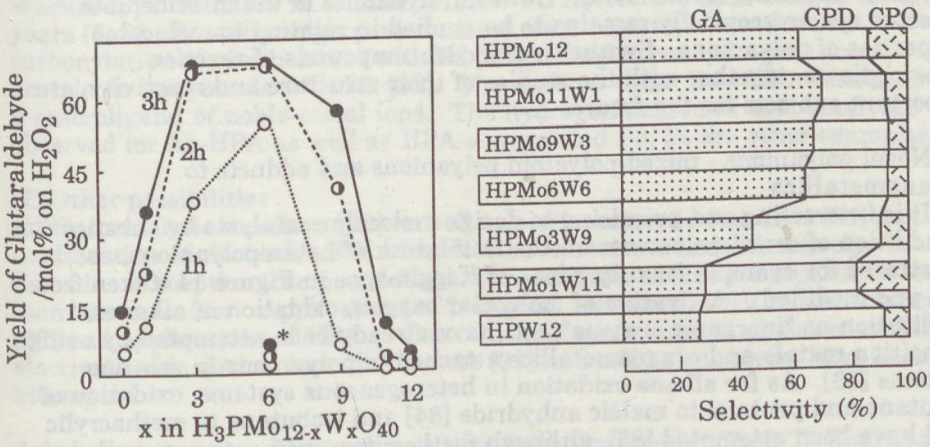

Figure 13. Effects of mixed polyatom on the catalytic oxidation of cyclopentene by H_2O_2 (303 K, solvent: $PO(OBu)_3$) [79]. *; HPMo12 + HPW12, GA; glutaraldehyde, CPD; cyclopentanediol, CPO; cyclopentene oxide.

7. FUTURE OPPORTUNITIES

In Tables A - D of Appendix, various reactions catalyzed by HPA are collected mainly from recent publications (typical examples in early studies are included) [98]. Even though the examples are limited to acid and oxidation catalysis, the high potentiality of HPA catalysts may be obvious.

HPA catalysts are expected to develop in the following directions.

(1) Precise control of acid and redox as well as absorption properties

As described above, the precise control of acidity and redox properties has recently become much more realistic for the molecular design of catalysts. The

concept of bulk- and surface-type properties are important for this purpose. The control of the secondary and tertiary structures are necessary and useful for HPA catalysts in the solid state. Effects of mixed-polyatom polyanions in catalysis are the urgent subjects to be elucidated at molecular level.

(2) Beneficial use of bulk-type catalysis

Although it was shown that, owing to the pseudoliquid behavior, high activity is often obtained and strong dependency of selectivity on the behavior in certain cases, successful applications of the behavior to practically useful reactions have not been reported. Further efforts are desirable to improve existing catalysts, e. g., those for methacrylic acid synthesis, and to create novel catalysts, taking account of the bulk-type (II) catalysis.

(3) Cluster models

Description of elementary processes at atomic/molecular level by using spectroscopy and stoichiometry has been successful to considerable extents, thanks to pseudoliquid behavior. However, dynamics of the intermediate detected spectroscopically remains to be studied in relation to molecular properties of polyanions. Synthesis of model compounds of reaction intermediates, together with the studies of their structure and reactivity, are important subjects for the future.

(4) Novel polyanions - mixed-polyatom polyanions and adducts to organometallics

It is interesting and promising to design molecular catalysts by substitution or addition of certain elements on the framework of heteropolyanions, as illustrated for example for polyanions of Keggin-type in Figure 14 (taken from [3c] and modified). Activation of molecular oxygen, oxidation of alkanes, application as "inorganic enzyme", etc. have already been attempted by using transition metals and organometallics attached to polyanions in solution systems [83]. As for alkane oxidation in heterogeneous systems, oxidation of n-butane and pentane to maleic anhydride [84] and isobutane to methacrylic acid have been attempted [85], although further improvements are needed.

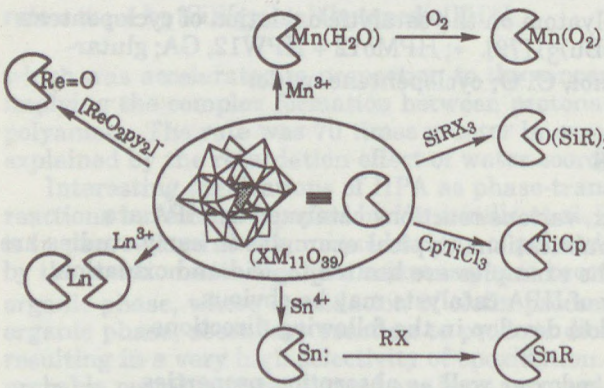

Figure 14. Lacunary polyanions as starting units of molecular design [3c].

Besides Keggin-type polyanions, there are many known polyanions which have been seldom tested of the catalytic function. By choosing the reaction systems properly these polyanions would be stabilized and become promising catalysts. Crystalline molybdophosphates with large cavity [86] and intercalated HPA [88] are potential candidates for catalysts.

(5) Utilization of unique basicity

HPA catalysts exhibit efficient performances when the reaction environment (concentration, solvent, water content, two-phase, etc.) is carefully chosen. This indicates that proper selection of the reaction field for each HPA catalyst leads to invention of novel catalytic systems.

(6) Combination with metals

Complexes of polyanions with organometallics and transition metal-substituted polyanions are described above. In addition, there are HPA catalysts that show high performance in combination with noble metals. Wacker-type oxidation in solution (HPA + Pd salts) have been studied for many years [8, 9]. Recently, high performances were reported for reductive carbonylation of nitrobenzene with Pd [89] and selective hydrogenation of acetylenic compounds with Rh [92]. The authors claim that HPA functions as a macroligand of noble metal ions. The hydrogen-enhanced acid catalyses observed for Ag-HPA as well as HPA + supported Pd, Pt are other examples [9].

(7) Other possibilities

Photocatalytic reactions [93] as well as electrocatalytic reactions [94] and modification of electrodes [95] with HPA have been studied extensively. Selective absorption into pseudoliquid is potentially usable for separation, e. g., membrane reactor. Applications of biological activities of HPA to medicines [96] and applications of HPA to electronic materials such as photoresists [15], electrochromic device, humidity sensor [97] and solid electrolytes have been attempted.

Acknowledgements. The author is very much indebted to Prof. T. Okuhara and other members of our laboratory not only for the collaboration in the research on HPA catalysis but also for the literature search and the preparation of manuscript.

8. REFERENCES

1 M. Misono and N. Nojiri, Appl. Catal., 64 (1990) 1; supplementary tables, submitted to the same journal.
2 M. Misono, in "Future Opportunities in Catalytic and Separation Technology (Eds., M. Misono, Y. Moro-oka and S. Kimura), (Stud. Surf. Sci. Catal., Vol. 54)," Elsevier, Amsterdam, 1990, p 13.
3 (a) G. A. Tsigdinos, Topics Curr. Chem., 76 (1978) 1; (b) M. T. Pope, "Heteropoly and Isopoly Oxometalates," Springer Verlag, Berlin, 1983; (c) M. T. Pope and A. Müller, Angew. Chem. Int. Ed. Engl., 30 (1991) 34; (d) V. W. Day, W. G. Klemperer, C. Schwartz and R.-C. Wang, in "Surface Organometallic Chemistry: The Molecular Approach to Surf. Sci. Catal. (Eds., J. M. Basset and B. C. Gates)," Reidel, Dordrecht, 1988, p 173.
4 M. Misono, Catal. Rev. Sci. Eng., 29 (1987) 269; 30 (1988) 339.
5 M. Misono, Proc. Climax 4th Intern. Conf. Chemistry, Uses Molybdenum (Eds., H. F. Barry and P. C. H. Mitchell) 1982, p 289.
6 There are a few reviews written in Japanese since 1976 (see reference [4]).
7 M. Misono, K. Sakata, Y. Yoneda and W. Y. Lee, Proc. 7th Intern. Congr. Catal., Tokyo, 1980, Kodansha, Tokyo-Elsevier, Amsterdam, 1981, p 1047.
8 I. V. Kozhevnikov and K. I. Matveev, Appl. Catal., 5 (1983) 135.
9 Y. Ono, in "Perspectives in Catalysis, (Eds., J. M. Thomas and K. I. Zamaraev)," Blackwell Sci. Publ., London, 1992, p 431.
10 K. Eguchi, T. Seiyama, N. Yamazoe, S. Katsuki and H. Taketa, J. Catal., 111 (1988) 336; D. Masure, P. Chaquin, C. Louis, M. Che and M. Fournier, J. Catal., 119 (1989) 415.
11 K. Y. Lee, N. Mizuno, T. Okuhara and M. Misono, Bull. Chem. Soc. Jpn., 62 (1989) 1731; Y. Kanda, K. Y. Lee, S. Nakata, S. Asaoka and M. Misono, Chem. Lett., (1988) 139.
12 G. Chidichimo, A. Golemme, D. Imbardelli and E. Santoro, J. Phys. Chem., 94 (1990) 6282.
13 T. Baba, M. Nomura, Y. Ono and Y. Kansaki, J. Chem. Soc. Faraday Trans., 88 (1992) 71.
14 A. R. Siedle and R. A. Newmark, Organometallics, 8 (1989) 1442; A. R. Siedle, T. E. Wood, M. L. Brostrom, D. C. Koskenmaki, B. Montez and E. Oldfield, J. Am. Chem. Soc., 111 (1989) 1665.
15 T. Kudo, A. Ishikawa, H. Okamoto, K. Miyauchi, K. Mochiji and H. Umezaki, J. Electrochem. Soc., 134 (1987) 2607.
16 V. M. Mastikhin, S. M. Kulikov, A. V. Nosov, I. V. Kozhevnikhov, I. L. Mudrakovsky and M. N. Timofeeva, J. Mol. Catal., 60 (1990) 65.
17 E. M. Serwicka, K. Bruckman, J. Haber, E. A. Paukshtis and E. N. Yurchenko, Appl. Catal., 73 (1991) 153.
18 A. Bielanski, A. Cichowlas, D. Kostrzewa and A. Malecka, Z. Phys. Chem. N. F., 167 (1990) 93; A. K. Ghosh and J. B. Moffat, J. Catal., 101 (1986) 238.
19 I. Kawafune and G. Matsubayashi, Inorg. Chim. Acta, 188 (1991) 33.
20 K. Piepgrass and M. T. Pope, J. Am. Chem. Soc., 111 (1989) 753; L. A. Combs-Walker and C. L. Hill, Inorg. Chem., 30 (1991) 4016.
21 N. Mizuno, T. Watanabe and M. Misono, J. Phys. Chem., 89 (1985) 80.
22 P. J. Kulesza, L. R. Faulkner and W. G. Klemperer, J. Am. Chem. Soc., 113 (1991) 379.

23 M. Misono, N. Mizuno and T. Komaya, Proc. 8th Intern. Congr. Catal., Berlin, 1984, Vol. 5, Verlag Chemie-Dechema, 1984, p 487.
24 T. Okuhara, T. Hashimoto, T. Hibi and M. Misono, J. Catal., 93 (1985) 224.
25 T. Okuhara, S. Tatematsu, K. Y. Lee and M. Misono, Bull. Chem. Soc. Jpn., 62, (1989) 717.
26 S. Akaratiwa and H. Niiyama, J. Chem. Eng. Japan, 23 (1990) 143; T. Utada, N. Sugiura, R. Nakamura and H. Niiyama, J. Chem. Eng. Japan, 24 (1991) 417.
27 M. Misono, T. Okuhara, T. Ichiki, T. Arai and Y. Kanda, J. Am. Chem. Soc., 109 (1987) 5535.
28 K. Tanabe, M. Misono, Y. Ono and H. Hattori, "New Solid Acids and Bases," Kodansha, Tokyo-Elsevier, Amsterdam, 1989, p 170.
29 M. Kamada and Y. Kera, Chem. Lett., (1991) 1831.
30 J. A. R. van Veen, P. A. J. M. Hendriks, R. R. Andrea, E. J. M. Romers and A. E. Wilson, J. Phys. Chem., 94 (1990) 5282.
31 N. Mizuno, T. Watanabe, H. Mori and M. Misono, J. Catal., 123 (1990) 157.
32 J.-M. Tatibouet, M. Che, M. Amirouche, M. Fournier and C. Rocchiccioli-Deltcheff, J. Chem. Soc. Chem. Commun., (1988) 1260.
33 M. Fournier, R. Thouvenot and C. Rocchiccioli-Deltcheff, J. Chem. Soc. Faraday Trans., 87 (1991) 349.
34 C. Rocchiccioli-Deltcheff, M. Amirouche, G. Hervé, M. Fournier, M. Che and J.-M. Tatibouet, J. Catal., 126 (1990) 591.
35 M. J. Bartoli, L. Monceaux, E. Bordes, G. Hecquet and P. Courtine, Stud. Surf. Sci. Catal., 72 (1992) 81.
36 S. Kasztelan, E. Payen and J. B. Moffat, J. Catal., 125 (1990) 45.
37 C. R. Rocchiccioli-Deltcheff, M. Amirouche, M. Che, J. M. Tatibouet and M. Fournier, J. Catal., 125 (1990) 292.
38 A. Ogata, A. Kazusaka, A. Yamazaki and M. Enyo, in "Acid-Base Catalysis (Eds., K. Tanabe, H. Hattori, T. Yamaguchi and T. Tanaka)," Kodansha, VCH, 1989, p 249.
39 J. B. Black, N. J. Claydon, P. L. Gai, J. D. Scott, E. M. Serwicka and J. B. Goodenough, J. Catal., 106 (1987) 1.
40 K. Bruckman, J. Haber and E. M. Serwicka, Faraday Disc. Chem. Soc., 87 (1989) 173.
41 (a) T. Nishimura, H. Watanabe, T. Okuhara and M. Misono, Shokubai (Catalyst), 33 (1991) 420; H. Watanabe, T. Nishimura, S. Nakata, T. Okuhara and M. Misono, 63rd National Meetings of Chem. Soc. Japan, March 1992; (b) N. Mizuno and M. Misono, Chem. Lett., (1987) 967.
42 M. Misono, N. Mizuno, H. Mori, K. Y. Lee, J. Jiao and T. Okuhara, in "Structure - Activity and Selectivity Relationships in Heterogeneous Catalysis, (Eds. R. K. Grasselli and A. W. Sleight), (Stud. Surf. Sci. Catal., Vol. 67)," Elsevier, Amsterdam, 1991, p 87.
43 Y. Izumi and K. Urabe, Chem. Lett., (1981) 663.
44 M. A. Schwegler, P. Vinke, M. van der Eijk and H. van Bekkum, Appl. Catal., 80 (1992) 41.
45 T. Baba and Y. Ono, Appl. Catal., 22 (1986) 321.
46 J. Pozniczek, I. Kulszewicz-Bajer, M. Zagorska, K. Kruczala, K. Dyrek, A. Bielanski and A. Pron, J. Catal., 132 (1991) 311.
47 N. Mizuno, T. Watanabe and M. Misono, J. Phys. Chem., 94 (1990) 890.
48 N. Mizuno and M. Misono, J. Phys. Chem., 93 (1989) 3334.

49 H. C. Kim, S. H. Moon and W. Y. Lee, Chem. Lett., (1991) 447.
50 H. Matsumoto, K. Y. Lee and M. Misono, 61st National Meetings of Chem. Soc. Japan, March 1991.
51 S. B. Ziemecki, Proc. 9th Intern. Congr. Catal., Calgary, 1988, 4 (1988) 1798.
52 T. Okuhara, T. Nishimura, K. Ohashi and M. Misono, Chem. Lett., (1990) 1201; T. Nishimura, T. Okuhara and M. Misono, Appl. Catal., 73 (1991) L7.
53 Y. Izumi, N. Natsume, H. Takamine, I. Tamaoki and K. Urabe, Bull. Chem. Soc. Jpn., 62 (1989) 2159.
54 M. Otake and T. Onoda, Proc. 7th Intern. Congr. Catal., 1980, Kodansha, Tokyo-Elsevier, Amsterdam, 1981, p 780.
55 V. Ernst, Y. Barbaux and P. Courtine, Catal. Today, 1 (1987) 167; O. Watzenberger, G. Emig and D. T. Lynch, J. Catal., 124 (1990) 247.
56 G. B. McGarvey and J. B. Moffat, J. Catal., 132 (1991) 100.
57 H. Mori, N. Mizuno and M. Misono, J. Catal., 131 (1991) 133.
58 T. Nishimura, T. Okuhara and M. Misono, Chem. Lett., (1991) 1695.
59 K. Y. Lee, T. Arai, S. Nakata, S. Asaoka, T. Okuhara and M. Misono, J. Am. Chem. Soc., 114 (1992) 2836.
60 T. Okuhara, T. Arai, T. Ichiki, K. Y. Lee and M. Misono, J. Mol. Catal., 55 (1989) 293.
61 E. M. Serwicka, J. B. Black and J. B. Goodenough, J. Catal., 106 (1987) 23.
62 N. Mizuno, T. Watanabe and M. Misono, Bull. Chem. Soc. Jpn., 64 (1991) 243.
63 M. Misono, T. Okuhara and N. Mizuno, in "Successful Design of Catalysts (Ed. T. Inui), (Stud. Surf. Sci. Catal., Vol. 44)," Elsevier, Amsterdam, 1989, p 267.
64 S. M. Kulikov and I. V. Kozhevnikov, Izv. Akad. Nauk SSSR, Ser. Khim., (1982) 492 (Engl. Transl. (1982) 441).
65 K. Urabe, K. Fujita and Y. Izumi, Shokubai (Catalyst), 22 (1980) 223.
66 Y. Izumi, K. Matsuo and K. Urabe, J. Mol. Catal., 18 (1983) 299.
67 I. V. Kozhevnikov, S. Tds. Khankhasaeva and S. M. Kulikov, Kinet. Katal., 30 (1989) 50, (Engl. Transl. (1989), 39).
68 A. Aoshima, S. Yamamatsu and T. Yamaguchi, Nippon Kagaku Kaishi, (1990) 233; (1987) 976, 984.
69 A. Aoshima, S. Tonomura and S. Yamamatsu, Polymers for Advanced Technology, 2 (1990) 127; S. Tonomura, Hyoumen, 30 (1992) 67.
70 K. Nomiya, K. Ishizawa and M. Miwa, J. Mol. Catal., 43 (1987) 221.
71 T. Baba and Y. Ono, J. Mol. Catal., 37 (1986) 317.
72 Eur. Pat. Appl., EP 263,027 (Nippon Fine Chemical Co.) .
73 C. Venturello, E. Alneri and M. Ricci, J. Org. Chem., 48 (1983) 3831; C. Venturello and R. D'Aloisio, J. Org. Chem., 53 (1988) 1553 .
74 Y. Matoba, H. Inoue, J. Akagi, T. Okabayashi, Y. Ishii and M. Ogawa, Synth. Commun., 14 (1984) 865; Y. Ishii, K. Yamawaki, T. Ura, H. Yamada, T. Yoshida, and M. Ogawa, J. Org. Chem., 53 (1988) 3587; S. Sakae, Y. Sakata, Y. Nishiyama and Y. Ishii, Chem. Lett., (1992) 289.
75 C. Venturelllo, R. D'Aloisio, J. C. Bart and M. Ricci, J. Mol. Catal., 32 (1985) 107; L. J. Csanyi and K. Jaky, J. Mol. Catal., 61 (1990) 75.
76 C. Aubry, G. Chottard, N. Platzer, J.-M. Bregeault, R. Thouvenot, F. Chauveau, C. Huet and H. Ledon, Inorg. Chem., 30 (1990) 4409.
77 S. Sato, C. Sakurai, H. Furuta, T. Sodesawa and F. Nozaki, J. Chem. Soc. Chem. Commun., (1991) 1327.

78 H. Furukawa, T. Nakamura, H. Inagaki, E. Nishikawa, C. Imai and M. Misono, Chem. Lett., (1988) 877.
79 M. Misono, K. Y . Lee and N. Mizuno, Report of 116 Committee of JSPS, 42 (1990) 268.
80 N. Mizuno, S. Yokota, I. Miyazaki and M. Misono, Nippon Kagaku Kaishi, (1991) 1066.
81 J . K . Burdett and C. K. Nguyen, J. Am. Chem. Soc., 112 (1990) 5366 .
82 W. E. Farneth, R. H. Staley, P. J. Domaille and R. D. Farlee, J. Am. Chem. Soc., 109 (1987) 4018.
83 D. E. Katsoulis and M. T. Pope, J. Am. Chem. Soc., 106 (1984) 2737; M. Faraj and C. L. Hill, J. Chem. Soc. Chem. Commun., (1987) 1487; N. Mizuno, D. K. Lyon and R. G. Finke, J. Catal., 128 (1991) 84; D. Mansuy, J. -F. Bartoli, P. Battioni, D. K. Lyon and R. G. Finke, J. Am. Chem. Soc., 113 (1991) 7222; J. Lyons, P. E. Ellis, Jr. and V. A. Durante, in "Structure - Activity and Selectivity Relationships in Heterogeneous Catalysis, (Eds. R. K. Grasselli and A. W. Sleight), (Stud. Surf. Sci. Catal., Vol. 67)," Elsevier, Amsterdam, 1991, p 99.
84 G. Centi, V. Lena, F. Trifiro, D. Ghoussoub, C. F. Aissi, M. Guelton and J. P. Bonnelle, J. Chem. Soc. Faraday Trans., 86 (1990) 2775; G. Centi, J. L. Nieto, C. Iapalucci, K. Bruckman and E. M. Serwicka, Appl. Catal., 46 (1989) 197.
85 Japan Kokai, 1988-145,249 (Asahi Chem. Ind.); Japan Kokai, 1991-106,839 (Sumitomo Chem.).
86 R. C. Haushalter, K. G. Strohmaier and F. W. Lai, Science, 246 (1989) 1289.
87 B. Taouk, D. Ghoussoub, A. Bennani, E. Crusson, M. Rigole, A. Aboukais, R. Decressain, M. Fournier and M. Guelton, J. Chim. Phys., 89 (1992) 435.
88 T. Kwon and T. J. Pinnavaia, Chem. Mater., 1 (1989) 381.
89 Y. Izumi, Y. Satoh and K. Urabe, Chem. Lett., (1990) 795.
90 R. Ohtsuka, Y. Morioka and J. Kobayashi, Bull. Chem. Soc. Jpn., 62 (1989) 3195.
91 K. Nowinska, R. Fiedorow and J. Adamiec, J. Chem. Soc. Faraday Trans., 87 (1991) 749.
92 Y. Izumi, Y. Tanaka and K. Urabe, Chem. Lett., (1982) 679; (1985) 1595.
93 E. Papaconstantinou, Chem. Soc. Rev., 18 (1989) 1; R. C. Chambers and C. L. Hill, Inorg. Chem., 30 (1991) 2776.
94 J. E. Toth and F. C. Anson, J. Am. Chem. Soc., 111 (1989) 2444.
95 B. Keita, K. Essardi and L. Nadjo, J. Electroanal. Chem., 259 (1989) 127; 302 (1991) 47; K.-K. Shiu and F. C. Anson, J. Electroanal. Chem., 309 (1991) 115.
96 Japan Kokai, 1990-204,415; 1990-202,823 (Terumo Corp.).
97 N. Mizuno, K. Inumaru and M. Mizuno, Hyoumen Kagaku, 10 (1989) 175.
98 T. Okuhara and M. Misono, J. Synth. Org. Chem. Jpn., in press.

9. APPENDIX

Table A: Homogeneous Acid-Catalyzed Reactions

Reaction	Catalyst	Remarks	Ref.
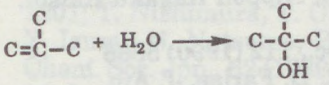	$H_3PW_{12}O_{40}$	T=313~353 K	68
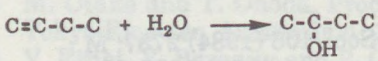	$H_3PW_{12}O_{40}$	T=473 K, 200 atm	a
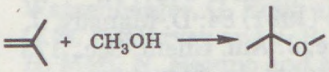	$H_6P_2W_{18}O_{62}$	T=315 K, S≈100% (S: selectivity)	b
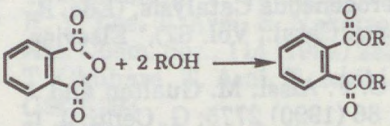	$H_3PW_{12}O_{40}$	T=363~393 K	c
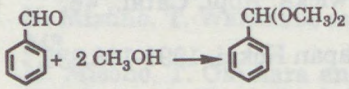	$H_3PMo_{12}O_{40}$	T=298 K, Y=100% (Y: yield)	d
Cyclotrimerization of propionaldehyde	$H_3PW_{12}O_{40}$	T=298 K, Y=85%	77
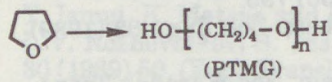 (PTMG)	$H_3PW_{12}O_{40}$· nH_2O (n=0~6)	T=333 K, MW≈3000	69
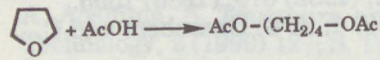	$H_3PW_{12}O_{40}$	T=368 K, $H_3PW_{12}O_{40}$:BF_3•Et_2O = 50 : 1(ratio of activity)	66
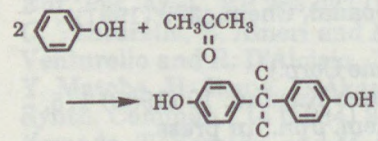	$H_3PW_{12}O_{40}$	T=333 K, S=72% (p, p')	e
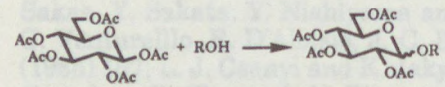	$H_3PW_{12}O_{40}$	T=298 K, Y=60~98% (2 h)	72

a) K. Yamada, Petrotech, 13 (1990) 627, b) G. Maksimov, et al., React. Kinet. Catal. Lett., 39 (1989) 317, c) M. A. Schwegler, Appl. Catal., 74 (1991) 191, d) M. V. Joshi, et al., J. Catal., 120 (1989) 282, e) JP 1990-45,439.

Table B: Heterogeneous Acid-Catalyzed Reactions

Reaction	Catalyst	Remarks	Ref.
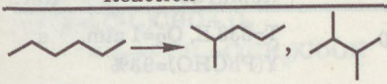	$Pd_{1.5}PW_{12}O_{40}/SiO_2$ $H_3PW_{12}O_{40}/SiO_2$	T=483 K T=348 K	a 91
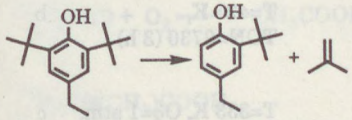	$H_3PW_{12}O_{40}$	T=403 K	b
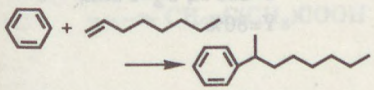	$H_3PW_{12}O_{40}/SiO_2$	T=308 K, sensitive to pretreatment	53
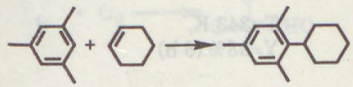	$Cs_{2.5}H_{0.5}PW_{12}O_{40}$	T=343 K, $Cs_{2.5}$:H_2SO_4=3000 : 1 (activity/H^+)	52
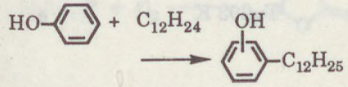	$H_3PW_{12}O_{40}$	T=373 K, $H_3PW_{12}O_{40}$:H_2SO_4 =17 : 1 (activity/H^+)	58
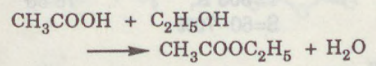	$H_3PW_{12}O_{40}$	T=423 K, S=91% (90%-conv.)	c
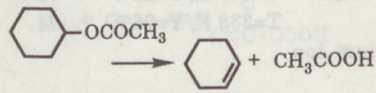	$Cs_{2.5}H_{0.5}PW_{12}O_{40}$	T=373 K, $Cs_{2.5}$:SO_4^{2-}/ZrO_2 =43 : 1 (activity/g)	52
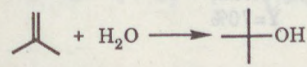	$H_4SiW_{12}O_{40}$ /Amberlyst 15	T=343 K, S=98.6% (11%-conv.)	d
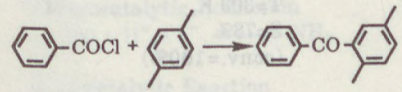	$H_3PW_{12}O_{40}/SiO_2$	T=411 K	53
CH_3OH (CH_3OCH_3) → C_1~C_6 Hydrocarbons	$H_3PW_{12}O_{40}$ $Cs_{2.5}H_{0.5}PW_{12}O_{40}$	T=573 K, T=563 K, S=74% (C_2~C_4 olefins)	e f g
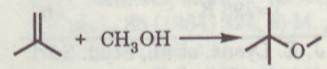	$H_4SiW_{12}O_{40}/SiO_2$	T=263 K, S=94.7% (30%-conv.)	h
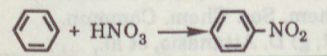	$Cs_{1.5}H_{1.5}PMo_{12}O_{40}$	T=413 K, S=97% (94%-conv.)	i

a) Y. Ono, et al., Stud. Surf. Sci. Catal., 20 (1985) 167, b) S. M. Kulikov, et al., Kinet. Katal., 27 (1985) 750, c) Y. Izumi, et al., J. Catal., 84 (1983) 402, d) T. Baba, et al., Appl. Catal., 22 (1986) 321, e) Y. Ono, et al., 7ICC, Tokyo (1980), p 1414, f) T. Okuhara, et al., J. Chem. Soc. Chem. Commun., (1984) 697, g) H. Hayashi and J. B. Moffat, J. Catal., 77 (1982) 437, h) A. Igarashi, et al., J. Japan Petrol. Inst., 22 (1979) 331, i) JP 1991-300,150.

Table C: Homogeneous Oxidation Reactions

Reaction	Catalyst	Remarks	Ref.
$PhCOCH_2Ph + O_2 \rightarrow PhCOOH + PhCHO$	$H_5PMo_{10}V_2O_{40}$	T=333 K, O_2=1 atm, Y(PhCHO)=93%	a
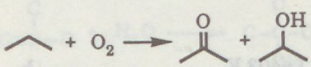	$H_7PW_9Fe_2NiO_{37}$	T=423 K, TON=9730 (3 h)	b
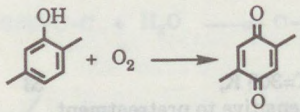	$H_5PMo_{10}V_2O_{40}$	T=333 K, O_2=1 atm, Y=80%	c
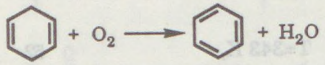	$H_5PMo_{10}V_2O_{40}$	T=343 K, Y=98% (6 h)	d
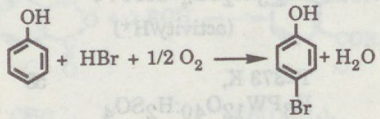	$H_5PMo_{10}V_2O_{40}$	T=293 K	e
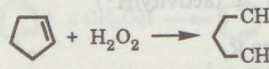	$H_3PMo_6W_6O_{40}$	T=303 K, S=60~70%	78-80
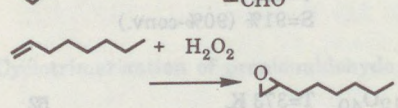	$H^+/WO_4^{2-}/PO_4^{3-}$/QX $(CP)_3PW_{12}O_{40}$ CP=cetylpyridinium ion	T=343 K, Y=82% T=333 K, Y=76%	73 74
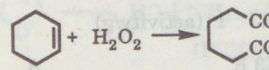	$(CP)_3PW_{12}O_{40}$	*t*-BuOH-reflux, Y=70%	74
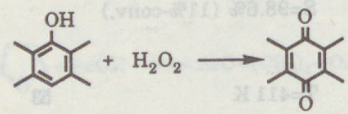	$H_3PMo_{12}O_{40}$	T=303 K, S=78% (conv.=100%)	f
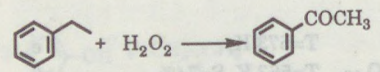	$H_3PMo_{12}O_{40}$	reflux, S=100%	g
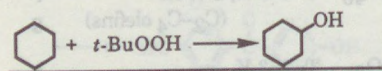	$PW_{11}CoO_{39}^{5-}$	T=298 K	h

a) B. El Ali, et al., J. Chem. Soc. Chem. Commun., (1989) 825, b) J. E. Lyons, et al., Stud. Surf. Sci. Catal., 67 (1991) 99, c) M. Lissel, et al., Tetrahedron Lett., 33 (1992) 1795, d) R. Neumann, et al., J. Org. Chem., 54 (1989) 4607, e) R. Neumann, et al., J. Chem. Soc. Chem. Commun., (1988) 1285, f) M. Shimizu, et al., Tetrahedron Lett., 30 (1989) 471, g) D. Attanasio, et al., J. Mol. Catal., 57 (1989) L1, h) C. L. Hill, J. Am. Chem. Soc., 108 (1986) 536.

MAGYAR
TUDOMÁNYOS AKADÉMIA
KÖNYVTÁRA

Table D: Heterogeneous Redox Reactions

Reaction	Catalyst	Remarks	Ref.
$CH_2=C(CH_3)CHO + O_2 \longrightarrow CH_2=C(CH_3)COOH$	$CsH_3PVMo_{11}O_{40}$	T=553 K, S=80~85%	a
$CH_3CHO + O_2 \longrightarrow CH_3COOH$	$Cs_xH_{3-x}PMo_{12}O_{40}$	T=573 K, S=40~90%	57
$CH_3CH(CH_3)COOH \longrightarrow CH_2=C(CH_3)COOH$	$H_5PV_2Mo_{10}O_{40}$	T=573 K, S=72% (52%-conv.)	b, 56
	$PbFeBiPMo_{12}O_x$	T=673 K, S=80% (97%-conv.)	c
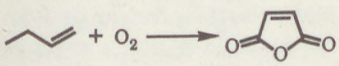	$Cs_{2.5}H_{0.5}PMo_{12}O_{40}+VO^{2+}$	T=563 K, S=31%	d
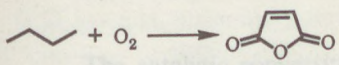	$BiPMo_{12}O_x+VO^{2+}$	T=633 K, S=30~40%	e
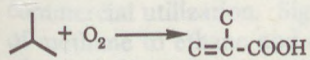	$H_3PMo_{12}O_{40}$	T=623 K, S=45%	85
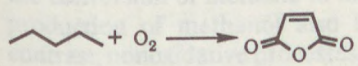	$H_5PV_2Mo_{10}O_{40}$	T=583 K, S=55%	f
Electrocatalytic Reduction $NO + H^+ + e^- \longrightarrow NH_3$	$H_3PW_{12}O_{40}$	T=298 K	94
Photocatalytic Reaction $H_2S + 1/2\ O_2 + h\nu \longrightarrow S + H_2O$	$PV_2Mo_{10}O_{40}^{5-}$	T=298 K	93

a) M. Ueshima, et al., Hyoumen, 24 (1986) 582; S. Nakamura, et al., 7ICC, Tokyo (1980), p 755, b) M. Akimoto, et al., J. Catal., 89 (1984) 196, c) T. Ohara, Shokubai, 19 (1977) 157, d) M. Ai, J. Catal., 85 (1984) 324, e) M. Ai, 8ICC, Berlin (1984), Vol. 5, p 475, f) G. Centi, et al., Appl. Catal., 46 (1989) 197.

Guczi, L. *et al.* (Editors), *New Frontiers in Catalysis*
Proceedings of the 10th International Congress on Catalysis, 19-24 July, 1992, Budapest, Hungary
© 1993 Elsevier Science Publishers B.V. All rights reserved

THE CATALYTIC CONVERSION OF METHANE TO OXYGENATES AND HIGHER HYDROCARBONS

J.H. Lunsford

Department of Chemistry, Texas A&M University, College Station, Texas 77843, USA

ABSTRACT

The catalytic conversion of methane has been achieved both in oxidative and nonoxidative processes, although the yields of useful products are only marginal for commercial utilization. Significant advances have been made in the oxidative coupling of methane to ethane and ethylene. The mechanism generally involves a complex set of coupled heterogeneous and homogeneous reactions. Less progress has been made in the conversion of methane to methanol and formaldehyde; however, it appears that the production of methanol also involves a heterogeneous-homogeneous pathway. By contrast, nonoxidative processes, which occur mainly on metals, are dominated by surface reactions. The conversion of methane alone to higher hydrocarbons has been demonstrated in a cyclic mode, but thermodynamic considerations limit the possibilities for a continuous process. A number of alkylation reactions utilizing methane are thermodynamically feasible, and in a few cases the reactions occur with the aid of a catalyst.

INTRODUCTION

Methane, which is the principal component of most natural gas, is an abundant hydrocarbon resource. In fact, the known reserves of natural gas, in BTU equivalents, are nearly equal to the reserves of liquid petroleum (*i.e.*, crude oil) [1]. Natural gas, however, is often produced in regions of the world that are far removed from major industrial centers, and its transportation is relatively expensive. Therefore, over the past decade considerable effort has been devoted to the development of processes for the conversion of methane to more valuable and easily transportable chemicals and fuels. These processes, which include oxidative coupling and formation of oxygenates, are known as direct processes, in contrast to indirect processes, which involve the formation of synthesis gas (CO and H_2) as the initial step. An economic comparison of several

direct and indirect processes is given in a paper by Renesme *et al.* [2] and references therein.

A number of different processes involving the direct conversion of CH_4 are thermodynamically allowed. These include the oxidative coupling reaction, which in its simplest form may be written as:

$$2CH_4 + \frac{1}{2}O_2 \rightarrow C_2H_6 + H_2O \quad (1)$$

and the conversion of CH_4 to CH_3OH:

$$CH_4 + \frac{1}{2}O_2 \rightarrow CH_3OH \quad (2)$$

These processes, which may occur both homogeneously and over a catalyst, require elevated temperatures. The products generally are more reactive than the methane; therefore, it is difficult to obtain both high conversion and high selectivity for the desired product. This is a classic case of a kinetically controlled reaction, and to date a catalyst has not been discovered that will circumvent these kinetic limitations.

A number of nonoxidative reactions also are thermodynamically allowed [3,4]. For example, the reaction of methane with propylene to form isobutane

$$CH_4 + C_3H_6 \rightarrow i\text{-}C_4H_{10} \quad (3)$$

has a ΔG° of -0.21 kcal/mol at 500K. This reaction is particularly attractive as a source of isobutylene for the production of methyl *t*-butyl ether (MTBE). Limited success has been achieved in promoting these reactions, mainly because of the difficulty in activating methane, which has a C-H bond strength of 104 kcal/mole. As with the oxidative processes, undesirable side reactions often prevail, including the formation of coke.

Several reviews have recently appeared on the catalytic conversion of methane, with emphasis on the oxidative coupling reaction [1,3,5,6]. A recent book edited by Wolf [7] and a collection of papers published in *Catalysis Today* [8] give accounts of recent progress in this area of research. The purpose of this paper is not to provide another comprehensive review, but rather to introduce the reader to this field of research and to identify specific areas where progress has been made in understanding the fundamentals of the catalytic process. Because of the large amount of effort that has been devoted to oxidative coupling and the level of understanding that has been achieved, this subject will be treated more extensively than the formation of oxygenates and nonoxidative reactions.

OXIDATIVE COUPLING

Equation 1 represents an oversimplification of the complex set of reactions that occur during the oxidative coupling process. The mechanistic details will be outlined below; however, the overall reaction can be better described as follows:

$$CH_4 + O_2 \rightarrow C_2H_6,\ C_2H_4,\ CO_2,\ CO,\ H_2O,\ H_2,\ higher\ HC's \qquad (4)$$

The desired product is ethylene, but the technology is already available for converting ethane to ethylene. Therefore, for purposes of describing selectivity or productivity, C_2H_4 and C_2H_6 are often lumped together and defined as C_2 products. If the higher hydrocarbons are included, the group is designated as C_{2+} products. Similarly, the undesirable side products CO and CO_2 are represented by CO_x.

Classes of Catalysts. Catalysts which are both active *and* selective for the oxidative coupling of methane may be described as strongly basic metal oxides, although caution must be exercised in attempting to define or measure basicity. Moreover, the most effective coupling catalysts are not simple basic oxides or even monophasic oxides; therefore, the surface and the bulk compositions may be quite different. Dubois and Cameron [9] have pointed out that most of the active and selective catalysts are composed of basic, irreducible *surface* oxides which form stable carbonate species. They also noted that at high temperatures, the effective catalysts are p-type conductors under a normal oxygen atmosphere.

A representative list of the effective oxidative coupling catalysts is given in Table 1. Comparisons with respect to activity are difficult because the optimum performance is usually achieved under oxygen-limited conditions. All of the results listed in this Table were obtained under co-feed conditions, (*i.e.*, CH_4 and O_2 were simultaneously fed into the reactor). It will be noted that the $LiCl/MnO_2$ and $BaPbO_3$ catalysts contain reducible metal ions, but these probably are covered with a group IA or IIA oxide so that the reagents, and particularly the methyl radical intermediate, do not directly interact with the reducible metal oxide. Previously, it was thought that $BaPbO_3$, an n-type oxide conductor, was an example of a monophasic coupling catalyst; however, more recent work has revealed that the surface rapidly becomes enriched in barium and that a surface BaO/BaO_2 layer is responsible for the coupling reaction [17].

With the exception of the $Ca_4NiK_{0.1}O_x$ catalyst, all of those listed in the Table exhibit favorable selectivities only at $T \geq 650\,^{\circ}C$. The optimum temperature is unique to each catalyst. At these high temperatures, catalyst stability is a serious problem because of sintering or loss of an important component such as Li or Cl. Moreover, gas phase reactions at these elevated temperatures may decrease the selectivity. The $Ca_4NiK_{0.1}O_x$ catalyst of Somorjai, Heinemann, and co-workers [18,19] is of interest because of the high selectivity that has been reported at $600\,^{\circ}C$. However, at this stage of development, the catalyst is relatively inactive, and the high C_{2+} selectivity is maintained only for about 5 h. The hydrocarbon formation reaction may involve a different mechanism from that described in the next section.

TABLE 1. REPRESENTATIVE OXIDATIVE COUPLING CATALYSTS

Catalyst	Temp. °C	Flow-rate mL/(min.g)	Ratio C:O:X[a]	CH_4 Conv. %	Selectivity,% C_{2+}	Selectivity,% CO_x	Ref
7 wt % Li/MgO	720	12	8:4:88	37.8	50.3	49.7	10
La_2O_3	750	10,000	8:2:90	12.2	67.4	32.6	11
4 wt % Na/La_2O_3	775	168	50:9:41	21.8	56.8	43.2	12
1 wt % Sr/La_2O_3	880	3667	91:9:0	15.8	80.8	19.2	13
15 mol % CaO/MgO	750	439	13:1.4:86	16.5	67.1	32.9	14
20 mol % $LiCl/MnO_2$	750	100	5:2.6:92	47.2	64.7	35.3	15
$LiCa_2Bi_3O_4Cl_6$	720	25	20:10:70	41.7	46.5	53.5	16
$BaPbO_3$	800	100	32:8:60	21.3	66.0	34.0	17
$Ca_4NiK_{0.1}O_x$	600	5	29:9:62[b]	10.0	93	7	18

[a]C:O:X refers to mole percentages of CH_4, O_2, and inert gas.

[b]H_2O was used instead of an inert gas.

Mechanism. At the most superficial level, the oxidative coupling reaction may be described by the reaction scheme

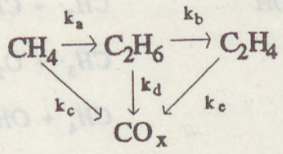

Scheme 1

in which ethane, the initial product, is converted both heterogeneously and homogeneously to ethylene. All three hydrocarbons are potentially a direct source of CO_x. Ideally, one would like to have a system wherein C_2H_4 is the only source of CO_x, and the relative reactivities are $C_2H_6 > CH_4 > C_2H_4$. Normally, the sequence of hydrocarbon reactivity over coupling catalysts is $C_2H_6 > C_2H_4 > CH_4$, although over $LiCl/MnO_x$, Burch and coworkers [20] have reported that CH_4 is more reactive than C_2H_4. Unfortunately, even over this catalyst, the C_2 yield was only 12%.

At a more detailed level, the oxidative coupling reaction involves a network of heterogeneous and homogeneous reactions which may be partially described by Scheme 2 [21]. The heterogeneous portion of this cycle results in the production of $CH_3\cdot$ radicals. These radicals enter the gas phase where they may either couple (the desired reaction) or enter into a chain-branching oxidation process which results in the formation of CO and CO_2. Obviously, CH_4 can be activated in a purely homogeneous manner, and the coupling reaction will occur, but this reaction is strongly quenched by the presence of a surface (even fused-quartz) [22]. At the temperatures and residence times of most catalytic reactions, the purely homogeneous activation of CH_4 is negligible, and the role of the surface is to generate $CH_3\cdot$ radicals.

Evidence to support the significance of surface-generated radicals in the coupling reaction was provided by Campbell *et al.* [23], who employed a matrix-isolation electron spin resonance technique to demonstrate that over Li/MgO, > 40% of the C_2H_6 was derived from gas-phase $CH_3\cdot$ radicals. Recently, Gutman and coworkers [24], using a mass spectrometer, have shown that over Sr/La_2O_3, > 75% of the C_2H_6 resulted from the coupling of $CH_3\cdot$ radicals which emanated from the surface. On these closed-shell metal oxides, the radicals are not strongly bound to the surface; therefore, at the high temperature of the reaction, they rapidly desorb. Their lifetimes on the surface may be so short that their formation could be described as an example of an Eley-Rideal type mechanism. It has been proposed that a reactive form of oxygen (see below) promotes the homolytic cleavage of the C-H bond to produce the gas phase $CH_3\cdot$ radicals and a surface OH^- ion.

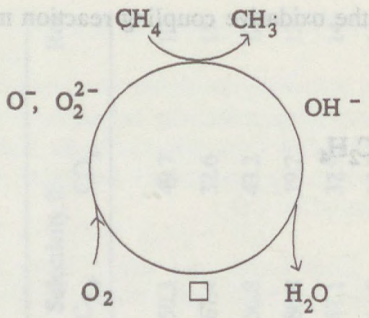

$$CH_3\cdot + CH_3\cdot + M \rightarrow C_2H_6 + M$$

$$CH_3\cdot + O_2 \rightarrow CH_2O + OH\cdot$$

$$CH_4 + OH\cdot \rightarrow CH_3\cdot + H_2O$$

etc.

Scheme 2

Other groups, however, have noted the strong basicity of the oxidative coupling catalysts and have suggested that the cleavage is heterolytic, *i.e.*,

$$\begin{array}{l} CH_3^- \quad H^+ \\ \quad | \qquad | \\ CH_4 + M^{n+}O^{2-} \rightarrow M^{n+} \quad O^{2-} \end{array} \qquad (5)$$

Lapszewicz and Jing [25] have examined four metal oxides of differing basicity for their abilities to promote the oxidative coupling reaction and the isotope exchange reaction between CH_4 and D_2. No direct correlation was observed between the rates of conversion and the isotopic exchange. This observation is evidence against heterolytic cleavage in the coupling reaction. Reaction 5 (forward and reverse) would result in the exchange reaction, which apparently is independent of the coupling reaction.

Experiments utilizing CH_4 and CD_4 have confirmed that ethane is produced by the coupling of methyl radicals and that the coupling probably occurs in the gas phase [26]. The data of Nelson *et al.* [26] and Mims *et al.* [27] showed that the main product of the coupling reaction was CH_3CD_3. Only the coupling of methyl groups could give this result. Moreover, if the methyl groups spent a significant amount of time on the surface, isotopic exchange via reaction 5 would have resulted in a scrambling of H/D in the product molecules.

The kinetic isotope effects (KIE) derived from the coupling reaction with CH_4/CD_4 have also provided valuable information concerning the rate-limiting step in the catalytic cycle. Following the proposal by Ito *et al.* [10], the cycle of Scheme 1 may be written as

$$CH_4 + O_s^- \xrightarrow{k_6} CH_3\cdot + OH_s^- \quad (6)$$

$$2OH_s^- \xrightarrow{k_7} H_2O + O_s^{2-} + \square \quad (7)$$

$$\frac{1}{2}O_2 + \square + O_s^{2-} \underset{k_{-8}}{\overset{k_8}{\rightleftharpoons}} 2O_s^- \quad (8)$$

Here, O_s^- is depicted as the active form of oxygen, but it may, in fact, be a peroxide ion, O_2^{2-}; $\square$ symbolizes an oxygen vacancy. Originally, it was suggested that reaction 6 was not rate limiting, based upon the high reactivity of O^- ions in the gas phase and on surfaces [10]. The results of Cant and co-workers [28,29] and others [30,31], however, have clearly shown that there exists a KIE when CH_4 is replaced by CD_4, or when the two are added simultaneously and the KIE is determined from the isotopic distribution in the product. No isotope effect was detected when D_2O was co-fed with CH_4, indicating that the breaking of an OH bond (reaction 7) was not rate limiting. Based on the observed KIE, it was concluded that reaction 6 was rate limiting [28].

Subsequent results from our laboratory have shown that the KIE is a function of oxygen partial pressure [32]. Over Li/MgO at 700°C, and at a CH_4 pressure of 190 Torr, the KIE varied from 1.30 to 1.45 as the O_2 partial pressure increased from 19 to 190 Torr. These data suggest that there is no single rate-limiting step. Rather, at high partial pressures of O_2, reaction 6 becomes rate-limiting, while at low partial pressures of O_2, reaction 8 occurs at a rate comparable to that of reaction 6. A kinetic model has been developed which adequately accounts for the changes that occur in the KIE as a function of O_2 pressure [32]. The model includes not only reactions 6-8, but also 156 gas phase reactions and the reaction of $CH_3\cdot$ radicals with the surface.

One of the most significant results of the model is its ability to reproduce, in a functional sense, kinetic data obtained by Roos *et al.* [33] over Li/MgO. They found that the CH_4 conversion rate followed a first-order dependence with respect to O_2 and a complex dependence with respect to CH_4, as shown in Fig. 1. The results of the model, which includes comparable rates for reactions 6 and 8, are depicted by the dashed lines which go through the data points in Fig. 1. When k_8 and k_{-8} were made much smaller, the reaction became zero-order with respect to CH_4 pressure over most of the pressure range. The transition from first-order to nearly zero-order at 150 Torr no longer occurred. Roos *et al.* interpreted their results in terms of Langmuir-Hinshelwood kinetics, but it is now evident that the results can be explained equally well by a model in which reactions 6 and 8 occur at comparable rates.

The question of CH_4 adsorption under reaction conditions, as required by Langmuir-Hinshelwood kinetics, has been addressed in several transient studies. Ekstrom and Lapszewicz [34] reported that there is a pool of strongly adsorbed methane onn the surface of Sm_2O_3 and Li/Sm_2O_3 at 700°C. Methane appeared to desorb for

periods in excess of 100 s. The reagent that led to these results was CD_4, which has a molecular weight of 20 amu, the same as that of D_2O. When CH_4 was used instead of CD_4, a much shorter transient was observed [35]. Cameron [36] has pointed out that D_2O, rather than CD_4, could have been the long-lived species, even though a trap was used to remove water vapor.

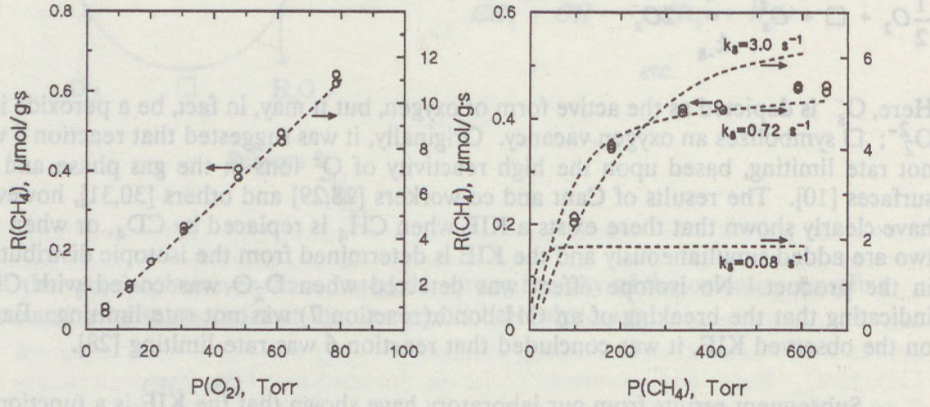

Figure 1. A comparison of the rates of CH_4 conversion with respect to (a) variation O_2 partial pressure and (b) variation in CH_4 partial pressure. The circles represent the experimental data of ref. [33], and the dashed lines were obtained from the model. The experimental data was adjusted for a reaction temperature of 700°C, using an activation energy of 55 kcal/mole. A value of $k_{-8} = 1.02 \times 10^{-13}$ cm^3 $molecule^{-1}s^{-1}$ was used.

Peil *et al.* [37] have found that methane was held up for a short time on Sm_2O_3 at 600°C; however, they did not detect any holdup of CH_4 on Li/MgO at 645°C [38]. Over Sr/La_2O_3, Kalenik and Wolf [39] found that CH_4 was not present as a long-lived species on the surface at 750°C. van der Wiele and co-workers [40] likewise observed that no measurable amount of CH_4 or C_2H_4 was adsorbed on Li/MgO at 800°C. Stratman *et al.* [41] reported that CH_4 is not adsorbed, or is only weakly absorbed, on a $Ba/Sr/Sm_2O_3$ catalyst at temperatures between 300 and 600°C. Thus, it appears that Sm_2O_3 is anomalous in its ability to adsorb CH_4 under reaction conditions.

The Origin and Role of CO_2. Since the utilization of oxidative coupling as a practical process is largely limited by the formation of CO_2, it is important to understand the origin of this undesirable product. The presence of CO_2 not only represents a loss in selectivity, but also a large amount of heat is associated with its formation. The removal of this heat is a major engineering problem associated with the coupling reaction.

As indicated in Scheme 1, CO_2 may be formed from any of the three hydrocarbons, and it may be produced either heterogeneously or homogeneously. Actually, the homogeneous reactions yield mainly CO; however, most of the good coupling catalysts also are effective for the conversion of CO to CO_2. Studies concerning the origin of CO_2 are complicated by the fact that each of the three hydrocarbons competes for the same set of active centers; therefore, results with individual hydrocarbons may not reflect the situation when all three hydrocarbons are present simultaneously. The most definitive experiments have been carried out using ^{13}C-labelled hydrocarbons. Ekstrom and co-workers [42] have carried out a series of experiments in which $^{13}C_2H_4$ or $^{13}C_2H_6$ were added to the feed gas over an Sm_2O_3 catalyst at 700°C and the amount of the ^{13}C in the CO_x was measured. Samarium oxide happens to be one of the oxidative coupling catalysts that gives a relatively large amount of CO. The CO_x products contained a much larger amount of ^{13}C than was present in the feed gas. For example, when the feed gas contained 15% ^{13}C, the CO_x contained *ca.* 50% ^{13}C. These results establish that the CO_x is largely derived from the C_2 products rather than from CH_4 under these conditions.

Nelson and Cant [43] have carried out similar studies over Li/MgO. From data obtained at T > 740°C, they conclude that C_2 oxidation is responsible for the formation of 30-80% of the CO_x, but at T < 700°C, more than 90% of the CO_x is derived from methane. These results suggest that the undesirable secondary oxidation of the C_2 products could be minimized by operating the catalyst at T < 700°C. Nevertheless, one still has to deal with the direct pathways for the total oxidation of CH_4.

The mechanism for the total direct oxidation of CH_4 is not clear, although it is evident that molecular oxygen plays an important role. When N_2O was substituted for O_2 as the oxidant, the selectivity at 3% conversion over Li/MgO at 710°C increased from 50% to 88% [44]. Earlier, we speculated that methylperoxy radicals formed via the equilibrium reaction

$$CH_3\cdot + O_2 \rightleftharpoons CH_3O_2\cdot \qquad (9)$$

were responsible for the total oxidation of CH_4 [45]. Nelson and Cant [43] have argued that this is an unlikely source of CO_2 on the surface. Our model likewise indicates that reaction 9 in the gas phase does not contribute significantly to the formation of CO_2 [32].

Another pathway for the formation of CO_2 involves the reaction of $CH_3\cdot$ radicals with a metal oxide. Methyl radicals will collide with a surface many times (*ca.* 10^5) before they react by coupling with another methyl radical. Each of these collisions with the surface is a potential opportunity for a nonselective reaction. Recently, Tong and Lunsford [46] carried out both qualitative and quantitative studies to determine the extent to which $CH_3\cdot$ radicals react and the oxides which are most reactive. The results

show that the most reactive oxides are those which have multiple cationic oxidation states. The radicals react principally by a reductive addition process, such as

$$CH_3\cdot + M^{(n+1)} + O^{2-} \rightarrow M^{n+}(OCH_3)^- \qquad (10)$$

to form a surface methoxide ion. On transition metal oxides, the methoxide ions are readily oxidized to carboxylates and, ultimately, to CO_2. Quantitative data for the reaction of $CH_3\cdot$ radicals with several metal oxides are given in Table 2, from which it is evident that the reactive sticking coefficient on ZnO is 10^{-5} and on MgO is 10^{-7}. The sticking coefficient on Li/MgO is also 10^{-7}. These values are consistent with the observation that ZnO is a nonselective oxidation catalyst, whereas MgO and Li/MgO are moderately selective. When the rate constants listed in the Table were incorporated into our model, it was found that *ca.* 5% of the CO_2 was derived from these surface reactions at 700 °C over Li/MgO. The contribution of the $CH_3\cdot$ radicals reacting with the surface at 650 °C, for example, may be significantly greater, since the activation energy for the radical reaction is much less than for the overall catalytic reaction.

TABLE 2. RATE CONSTANTS, ACTIVATION ENERGIES, AND STICKING COEFFICIENTS

oxides	k^a,$s^{-1}m^{-2}$	E_a,kcal mol^{-1}	S^a
MgO	3.0×10^2	5.7	1.2×10^{-7}
CeO_2	3.1×10^3		2.1×10^{-6}
NiO	2.1×10^4		
MoO_3	4.3×10^4		
NnO	4.4×10^4	2.6	1.8×10^{-5}

*T = 482 °C

The transient study of Peil *et al.* [38] on Li/MgO revealed that a C_2H_6 precursor remained on the surface for times of *ca.* 3 s at 645 °C. They speculated that the precursor may be adsorbed $CH_3\cdot$ radicals; however, the reversible adsorption of $CH_3\cdot$ radicals on a closed-shell oxide such as Li/MgO seems unlikely, except at a few defect sites. On reducible metal oxides, reaction 10 may be preceded by the reversible reaction which is consistent with the low activation energies reported in Table 2 [46].

$$CH_3\cdot + M^{(n+1)+}O^{2-} \rightleftharpoons H_3C^{\delta+}M^{(n+1-\delta)+}O^{2-} \qquad (11)$$

In almost all transient studies, it has been observed that a significant delay occurs in the desorption of CO_2, but after accounting for the re-adsorption phenomena, the residence time on a selective form of La_2O_3 may be as short as 0.6 s at 620 °C or 0.1 s at 750 °C according to Lacombe *et al.* [47]. van der Wiele and co-workers [40] have

found that CO_2 produced during reaction is hardly adsorbed at all on Li/MgO at 800 °C, although it could poison catalytic sites. Lithium carbonate formation and decomposition is not a part of the catalytic cycle.

Ross and co-workers [33] pointed out that CO_2 strongly poisons active centers on Li/MgO, and the apparent kinetic order with respect to O_2 is affected by the formation of CO_2. Xu *et al.* [48] have recently shown that over Li/MgO the apparent activation energy both for the generation of $CH_3\cdot$ radicals and for the overall consumption of CH_4 is strongly influenced by the presence of CO_2. The intrinsic activation energy for the formation of $CH_3\cdot$ radicals is 26 ± 2 kcal/mole, but upon the addition of only 0.7 Torr of CO_2, the E_a approaches a limiting value of *ca.* 50 kcal/mole. Under conventional catalytic conditions, sufficient CO_2 is produced to attain this limiting E_a. The effect of O_2 may be described as a typical case in which the catalyst is poisoned by a reaction product

$$\frac{dCH_3\cdot}{dt} = \frac{kf([CH_4],[O_2])}{1+K[CO_2]} \tag{12}$$

If $K[CO_2] >> 1$, then

$$k_a = \frac{k}{K}, \quad and \; E_a = E + \lambda \tag{13}$$

where λ is the heat of adsorption for CO_2. Temperature-programmed desorption experiments have shown that CO_2 is strongly held on Li/MgO as surface carbonates [48]; therefore, E_a is dominated by λ.

Nature of the Active Surface. The diversity of the catalysts used in oxidative coupling makes it difficult to generalize about the nature of the active surface, but there is evidence that certain types of oxygen species are involved. These include O^-, O_2^{2-}, O_2^-, and oxide ions in low coordination centers on the surface. In a limited number of cases, spectroscopic evidence is available. Following the earlier studies of Abraham and co-workers [49] on Li-doped MgO single crystals, Lunsford and co-workers [50] suggested that $[Li^+O^-]$ centers were responsible for the activation of CH_4 over Li/MgO catalysts. Although most of the $[Li^+O^-]$ centers observed by ESR are in the bulk of the catalyst, it is proposed that these are in equilibrium with surface O^- centers via hole transport. The $[Li^+O^-]$ centers have also been observed in Li/ZnO catalysts, and the analogous $[Na^+O^-]$ centers have been found in Na/CaO [45,51]. Although the presence of these centers is generally correlated with $CH_3\cdot$ radical formation and coupling activity, their concentrations are small and the reactivity of O^- should be so great that reaction 6 would never be rate-limiting, an observation which is in conflict with the observed KIE. The latter inconsistency has not been reconciled, although it has been suggested that the active centers may be more correctly described as $O^{\delta-}$ ions. Two groups [52,53] have carried out theoretical calculations on the reactivity of Li^+O^- centers with CH_4 (reaction 6), and the most refined calculation indicates a barrier height of only 6 kcal/mole for the hydrogen abstraction reaction, which is considerably less than the experimental value of 25 kcal/mole for $CH_3\cdot$ radical formation [54].

Goodman and coworkers [55] have used high resolution electron energy loss spectroscopy (HREELS) to study centers that are present in a thin film of Li/MgO on a Mo (100) surface. Upon annealing the sample at $T \geq 727\,^{\circ}C$, a loss feature was observed at ~ 1.6 eV, which is attributed to $[Li^{+}O^{-}]$ centers. After annealing at $T \geq 873\,^{\circ}C$, additional loss features were found at 3.6 and 5.3 eV. These two features are assigned to F-aggregates and F-centers (oxygen vacancies containing two electrons) in MgO, respectively. The authors found that the concentration of F-centers correlated well with the formation of ethane, and they concluded that these F-centers were responsible for the generation of $CH_3\cdot$ radicals.

Dubois *et al.* [9] have described the redox mechanism during coupling by the following equilibria:

$$V_O'' \rightleftharpoons V_O' + h^{+} \tag{14}$$

$$O_2(g) + V_O' \rightleftharpoons O_2^{-} \tag{15}$$

$$O_2^{-} + V_O' \rightleftharpoons O_2^{2-} \tag{16}$$

$$O_2^{2-} \rightleftharpoons 2O^{-} \tag{17}$$

where V_O'' represents an oxygen vacancy without an electron; V_O' an oxygen vacancy with one electron, and h^{+} a positive charge carrier. In this nomenclature, a V_O center is equivalent to an F-center. This set of reactions points out that O_2^{-}, O_2^{2-}, and O^{-} may be related through equilibria at the surface, which makes it difficult to establish the role of a particular type of oxygen under reaction conditions. Nevertheless, it is interesting to note that under *ex situ* conditions, O_2^{-} ions have been detected by ESR on La_2O_3 [56,57], and O_2^{2-} ions have been observed by XPS on Ba/La_2O_3 and $BaPbO_3$ catalysts [58,59]. Both Na and Ba are known to form stable peroxides, and Sinev *et al.* [60], as well as Otsuka *et al.* [61] have shown that these peroxides are capable of converting CH_4 to C_2H_6 at relatively low temperatures, although the selectivities were small, and the process was not catalytic.

Peroxide ions have been detected *in situ* at *ca.* 740 °C on Ba/MgO catalysts containing 0.5 and 15 mole % Ba, using laser Raman spectroscopy [62]. As shown in Fig. 2, the O_2^{2-} ions are characterized by a Raman band at 844 cm^{-1}. They are stable in the presence of O_2, but they react over a period of several minutes in CH_4. On the 0.5 mole % Ba/MgO sample, the ions were stable in He for a period of several minutes.

Tong *et al.* [12] observed that CeO_2, upon the addition of Na_2CO_3, was transformed from a total oxidation catalyst into one which was reasonably selective for the conversion of CH_4 to C_2H_4 and C_2H_6. Ion scattering spectroscopy revealed that the surface was essentially covered by sodium oxide/carbonate. Similar results were observed over Na/La_2O_3 and Na/Yb_2O_3, which led the authors to conclude that a sodium oxide phase, probably Na_2O_2, was responsible for the activation of CH_4. A similar model had previously been proposed by Gaffney *et al.* [63] to explain the behavior of a Na/Pr_6O_{11} catalyst, which is effective in the redox mode. In the latter

case, the lanthanide oxide serves not only as a support for the active Na phase, but also as a solid that is capable of storing oxygen.

On a Li/MgO catalyst containing 4.9 wt % Li after reaction at 750 °C, Mirodatos *et al.* [64] observed by XPS that the surface was mainly covered by a lithium oxide/carbonate phase; only 8% of the surface was magnesia. Even at a much lower coverage of 0.023 wt % Li, Martin and Mirodatos [65] point out that there is ample Li_2CO_3 to provide monolayer coverage. They note that pure Li_2CO_3 has a specific activity that is about one-fourth that of a Li/MgO catalyst, and they question whether MgO may be simply a support for the active Li phase. This seems unlikely, however, as both Peng *et al.* [66] and Hutchings *et al.* [67] have recently reported that Li/MgO catalysts containing as little as 0.2 wt % Li give conversions and selectivities comparable to those found in catalysts having much more Li. Moreover, we have observed that a used Li/MgO catalyst containing 0.5 wt % Li had a surface composed mainly of MgO, not a Li phase [68]. Finally, molten Li_2CO_3 is a relatively poor oxidative coupling catalyst [69]. (It should be noted that the melting point of Li_2CO_3 is 723 °C, and a Li/MgO catalyst is active and selective well below this temperature. In general, this catalyst should not be described as a liquid film of Li_2CO_3 on MgO.) As will be discussed below, the Li phase inhibits the catalytic reaction, much as Na_2CO_3 inhibits the activity of La_2O_3 [12], except that in this case, Na_2O_2 appears to become the new active phase. Lithium does not form stable peroxides; hence, it probably does not contribute to the activity of Li/MgO, except through the formation of specific centers.

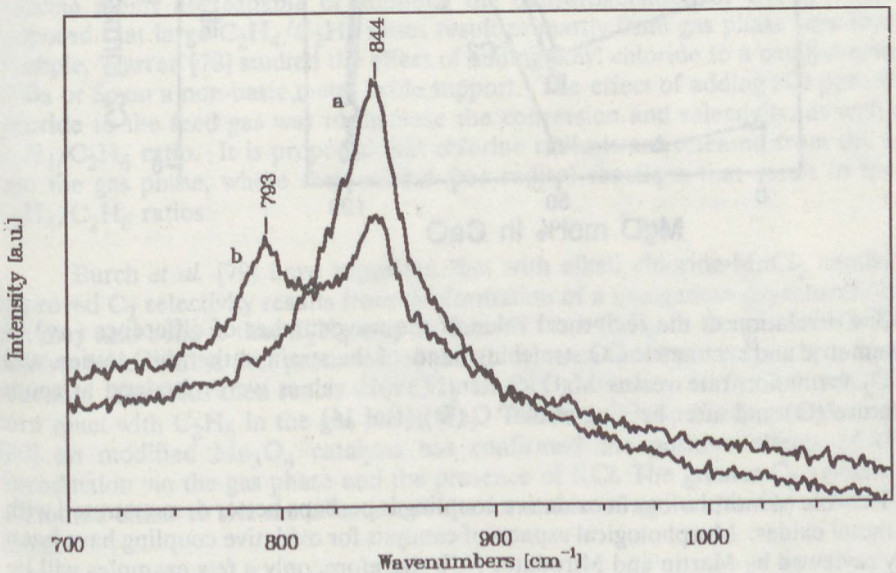

Figure 2. Raman spectra of peroxide ions on 0.5 mole % Ba/MgO at 745°C: (a) spectrum obtained in O_2, (b) spectrum obtained after brief exposure to CH_4.

It has been observed by two groups that the incorporation of CaO into MgO greatly improves the activity and C_2 selectivity of the catalyst [14,70]. As shown in Fig. 3, the C_2 formation rate correlates well with the lattice strain and with the basicity, as determined from the infrared spectrum of a surface carbonate. Phillip *et al.* [14] take this as evidence that segregation and surface reconstruction are incomplete on the high-index planes that form the surface. Cunningham and co-workers [70] had previously concluded that Ca^{2+} causes a "rumpling" of the surface which results in a more active catalyst. The enhanced basicity is associated with the morphological changes in the surface layer.

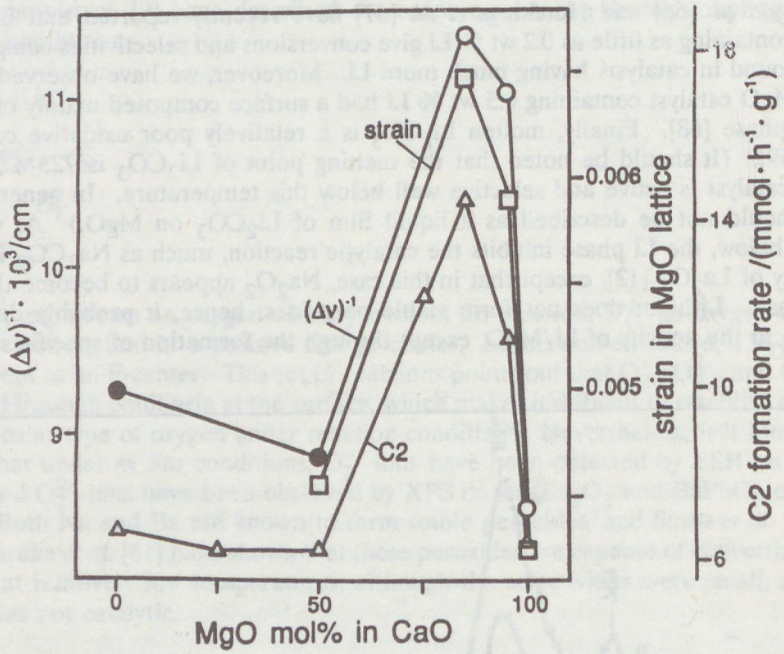

Figure 3. Correlation of the reciprocal value of the wavenumber of difference ($\Delta\nu$) of the asymmetric and symmetric CO stretching band, of the strain in the MgO lattice, and of the C_2 formation rate versus MgO content. $(\Delta\nu)^{-1}$ values were obtained at room temperature (O) and after heating at 600°C (●) (Ref 14).

The role of morphology in oxidative coupling is perhaps better demonstrated with simple metal oxides. Morphological aspects of catalysts for oxidative coupling have been recently reviewed by Martin and Mirodatos [65]; therefore, only a few examples will be given here. The effect of bulk structure is found in the work of Lo *et al.* [71], who studied the catalytic properties of Sm_2O_3 in both the cubic and the monoclinic form. The cubic phase was more active and more selective toward C_2 hydrocarbons than was

the monoclinic phase. A catalyst containing both phases was even more selective for the formation of C_2 hydrocarbons.

The relationship between crystalline morphology and catalytic behavior has recently been demonstrated by LeVan *et al.* [11,72], who studied La_2O_3. The decomposition of lanthanum nitrate in air at either 650 °C (LT) or 800 °C (HT) results in a pure hexagonal structure, but the morphologies of the two materials, as determined by electron microscopy, are very different. The low-temperature treatment results in thin plates, whereas the high-temperature treatment results in smaller, tri-dimensional particles. Both the CH_4 conversion and the C_2 selectivity were greater over the La_2O_3-LT catalyst than over the La_2O_3-HT catalyst. The surface area of the former was greater than that of the latter, which makes it difficult to establish the specific activities. The authors suggest that the greater selectivity over the La_2O_3-LT platelets is related to the more stable oxycarbonates in this material. These oxycarbonates are assumed to be intermediates in the formation of CO_2; therefore, they argue that the more selective catalyst would have the most stable carbonate. In a subsequent publication, LeVan *et al.* [73] note that a strontium-doped La_2O_3 retains a platelet structure at temperatures > 800 °C, and they attribute the high C_{2+} selectivity of the Sr/La_2O_3 catalyst at 850-900 °C to the stabilization of this platelet structure.

The addition of chlorine, either via the gas phase or the catalyst, has a remarkable effect on the product selectivity in oxidative coupling [16,74-78]. The most notable result is the exceptionally large C_2H_4/C_2H_6 ratios that have been achieved. As chlorine atoms are capable of initiating the dehydrogenation of C_2H_6, it has been proposed that large C_2H_4/C_2H_6 ratios result primarily from gas phase reactions. For example, Warren [78] studied the effect of adding ethyl chloride to a catalyst composed of Ba or Sr on a non-basic metal oxide support. The effect of adding 500 ppm of ethyl chloride to the feed gas was to increase the conversion and selectivity, as well as the C_2H_4/C_2H_6 ratio. It is proposed that chlorine radicals are released from the surface into the gas phase, where they initiate free radical reactions that result in the large C_2H_4/C_2H_6 ratios.

Burch *et al.* [79] have suggested that with alkali chloride-$MnCl_2$ catalysts, the improved C_2 selectivity results from the formation of a manganese oxychloride surface, but they also believe that C_2H_4 may be formed from C_2H_6 in the gas voids within the catalyst bed. HCl is first produced on the chlorine-containing catalysts by a hydrolysis reaction. The HCl then reacts with $CH_3\cdot$ or $OH\cdot$ radicals to form Cl atoms, which in turn react with C_2H_6 in the gas phase [75]. Recent work by Lambert and co-workers [80] on modified Mn_3O_4 catalysts has confirmed the positive effects of chlorine introduction via the gas phase and the presence of KCl. The greater C_2 selectivity was attributed either to site modification or the formation of active chlorine radicals on the surface.

We have found that the incorporation of chloride ions into Li-modified MgO results in a stable and active catalyst that is capable of converting CH_4 to C_2H_4 [81].

Ethylene-to-ethane ratios of > 5 have been achieved for periods of 180 h at 640 °C, with C_2 yields of *ca.* 19%. Consistent with the large C_2H_4/C_2H_6 ratios, the catalysts are also effective in the oxidative dehydrogenation of ethane [82]. At 620 °C, C_2H_6 conversions of 75% have been attained, at 78% C_2H_4 selectivity. As shown in Fig. 4, the Cl/Li ratio is a critical factor in obtaining high C_2H_4 productivity; the ratio must be ≥ 0.9 in order to have a good catalyst [68]. The absolute amount of Li^+ (or Cl^-) in the catalyst is of secondary importance. Characterization of the catalyst by TPD, XRD, and XPS methods indicates that a principal role of the chlorine is to bind lithium as LiCl, and thus prevent the formation of Li_2CO_3. The carbonate spreads over the surface and prevents the conversion of C_2H_6 to C_2H_4. Since the activation energy is no longer determined by carbonate formation, E_a decreases from 50 kcal/mole on a Li/MgO catalyst to 35 kcal/mole on a Li-MgO-Cl catalyst. For this system, the role of chlorine-containing molecules in the gas phase is believed to be relatively unimportant.

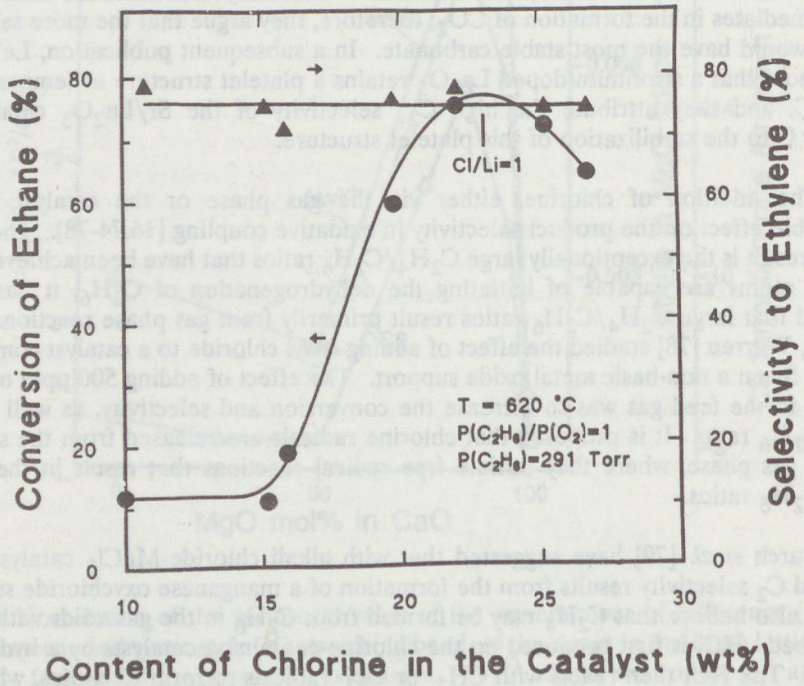

Figure 4. The effect of chloride ions on the oxidative dehydrogenation of ethane over Li-MgO-Cl catalysts.

Thomas *et al.* [16] have shown that a number of monophasic bismuth oxychloride catalysts exhibit exceptionally large C_2H_4/C_2H_6 ratios during the coupling reaction, but their lifetimes were rather brief. Recently, Khan and Ruckenstein [83] have demonstrated that BiOCl-Li_2CO_3-MgO catalysts can be operated for times greater than

5 h at 750°C. Their best catalyst gave 83% C_2 selectivity at 18% CH_4 conversion, with a C_2H_4/C_2H_6 ratio of 2.9. From XPS measurements, it was evident that the Li stabilized the chlorine on the surface. The role of Bi may be to stabilize Li on the catalyst. As noted previously by Ross and co-workers [84], the addition of a third metal to a Li/MgO catalyst greatly improves the lifetime at elevated temperatures by increasing the retention of lithium.

Cross Coupling Reactions. Although most of the research on oxidative coupling has been carried out using only methane as the hydrocarbon, at least two groups have studied the cross coupling between methane and toluene [85,86]. A lithium-promoted Y_2O_3-CaO catalyst was shown to be particularly effective for this reaction [85]. When operating at a $CH_4 : C_6H_5CH_3$ ratio of 20 and a hydrocarbon: O_2 ratio of 10, the conversion of toluene was *ca.* 32% at 700°C. The ethylbenzene and styrene selectivities were 41% and 23%, respectively, based on the moles of toluene converted. At the same conditions, the C_{2+} selectivity was less than the C_{8+} selectivity. No evidence was found for the production of bibenzyl or stilbene; thus, the cross coupling of benzyl radicals was favored over the homo-coupling. Experiments carried out with $C_6D_5CD_3$ and CH_4 confirm the cross coupling reaction. For example, the ethylbenzene fraction was composed of mainly C_6D_5-CD_2-CH_3, with some C_6D_5-CDH-CH_3. The authors believe that the cross coupling reaction occurs on the surface, while the C_2 formation probably occurs in the gas phase.

FORMATION OF OXYGENATES

The direct production of methanol and formaldehyde from methane, both heterogeneously and homogeneously, has recently been reviewed by Brown and Parkyns [87]. They point out that yields of oxygenate are only a few percent, at most, for catalyzed reactions, and they are considerably greater for homogeneous or heterogeneously-initiated reactions. To put matters in perspective, however, it should be pointed out that the conversions and selectivities required for the commercially feasible direct conversion of methane to oxygenates are considerably less than those required for the oxidative coupling reaction.

Two recent developments are noteworthy in the catalytic formation of oxygenates. Lyons *et al.* [88] have reported that iron sodalites, [Fe]SOD, having iron both in the framework and in ion exchange sites are capable of catalyzing the oxidation of CH_4 to CH_3OH with a conversion of 6% and a CH_3OH selectivity of 64%. The reaction was carried out at 442°C, with a 3:1 methane-to-air ratio and a total pressure of 800 psig. The reactor provided an "open reaction zone" for reaction intermediates, which suggests that both heterogeneous and homogeneous reactions are involved.

The second study involves the conversion of CH_4 and O_2 to HCHO over silica catalysts. Although the activity of silica was known for this reaction, Parmaliana *et al.* [89] have shown that quite good formaldehyde selectivities can be achieved over a W.R. Grace Grade 250 MP silica which had been prepared by a sol-gel method. For example,

a selectivity of 77% HCHO was observed at a space time yield of 3.5 $g_{HCHO}/kg_{cat}h$. These results were obtained at 1.7 bar and 520°C in a "specifically designed" batch reactor provided with an external recycle. Both the activities and selectivities of the several silicas that were examined varied greatly. The highest purity silica, Cab-O-Sil M5, had a comparable selectivity of 64%, but the activity was about a factor of 10 less.

NONOXIDATIVE AND RELATED REACTIONS

The catalytic methylation of olefinic and aromatic hydrocarbons, within thermodynamic limitations, offers an interesting opportunity for the utilization of methane. Solid super acids catalyze the addition of CH_4 to C_2H_4, but at high CH_4/C_2H_4 ratios so as to minimize oligomerization [90]. Earlier work by Rieche *et al.* [91] and Löffler *et al.* [4] indicated that such methylation reactions were possible on metals, and more recent studies demonstrate the surface chemistry that is involved. Using ^{13}C-labeled methane, Koerts and van Santen [92] have conclusively shown that ethylene and propylene may be methylated to the corresponding alkanes over Ru/SiO_2 and Co/SiO_2 catalysts. For example, during the methylation of C_2H_4 over Ru/SiO_2, 60% of the propane product contained one ^{13}C atom. These reactions involve a series of steps in which methane is first dissociatively adsorbed on the reduced metal surface at 450°C, which is quickly cooled so as to stabilize CH_x species. Then the alkene is adsorbed on this surface at 50°C. Finally, the catalyst is exposed to flowing H_2 at 50°C, and hydrocarbons are desorbed. A model depicting the reaction cycle is shown in Fig. 5. The principal hydrocarbon product following the reaction of methane and propylene is propane and butane, with smaller amounts of pentane.

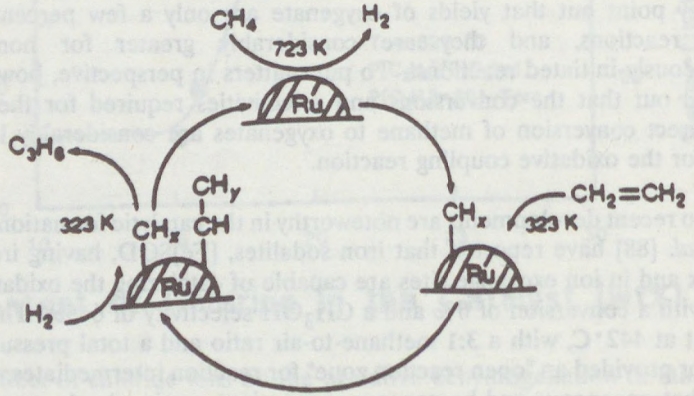

Figure 5. Reaction cycle for the conversion of methane with an alkene to a homologue on ruthenium (Ref 92).

Prior to the work of Koerts and van Santen, Belgued *et al.* [93] had studied the production of higher hydrocarbons when CH_4 was reacted with a supported Pt, Ru and Co catalyst in a similar manner. In this case, CH_4 was added to the reduced metal under a high flow rate so as to remove H_2, and C_2H_6 appeared in the gas phase in a transient manner. Upon substituting flowing H_2 for CH_4, the surface CH_x species were converted into saturated hydrocarbons. The highest yields of C_{2+} products were observed over Ru at 160°C. In this case, 37% of the CH_4 was converted and recovered as higher hydrocarbons. This yield, however, is based on the amount of CH_4 reacted on the metal, not on the total amount of CH_4 that was passed over the catalyst.

In an earlier section it was pointed out that the CaNiK material of Somorjai and Heinemann [18,19] may catalyze the formation of higher hydrocarbons by a mechanism other than through $CH_3\cdot$ radicals. The authors speculate that CH_4 forms CH_x intermediates and H atoms on the surface. The former may react to produce C_yH_x intermediates and then final products by a mechanism similar to that in the Fischer-Tropsch reaction. If such is the case, this catalyst has more in common with the supported metals described above than with the usual oxidative coupling catalysts, but with the distinction that it is able to convert methane to higher hydrocarbons in a catalytic manner.

Similarly, Abasov *et al.* [94] have demonstrated that a preoxidized Ni/Al_2O_3 catalyst at 650°C is capable of converting methane to benzene with up to 51% selectivity, at an initial conversion level of 18%. The reactant gas contained CH_4 and O_2 in a 9:1 ratio. The catalyst deactivated over a period of 20 min, but it could be briefly reactivated by heating in air. Clearly, CH_x groups must be formed on the surface and these combine to produce C_6H_6. The selectivity with which this process occurs is remarkable.

SUMMARY AND PROSPECTS

Since the early work of Keller and Bhasin [95] and Hinsen *et al.* [96] considerable progress has been made in our understanding of the oxidative coupling reaction. Many of the materials that are effective are unique among oxidation catalysts in that they do not contain metal ions that are capable of going through a redox cycle. Instead, the surface oxygen ions appear to change oxidation state. the mechanism of the reaction is also unusual because of the importance of a homogeneous component which may, in fact, limit the C_{2+} yields that can be achieved. The empirical evidence suggests that the maximum yield is about 30% in a conventional reactor. If this is indeed the case, the utilization of oxidative coupling as a commercial process will require either improved separation methods (*e.g.*, in the removal of ethylene from diluted gas streams) or special applications (*e.g.*, the use of oxidative coupling in combination with a gas-fired electrical power plant.

The direct catalytic conversion of methane to oxygenates is at an even more rudimentary stage with respect to fundamental understanding; however, as noted above, the requirements in terms of yield are less demanding. Methanol is a relatively stable molecule in the gas phase, but it reacts rapidly at elevated temperatures on many catalysts. Initial results indicate that the catalytic conversion of methane to methanol also involves both heterogeneous and homogeneous components, with higher pressures favoring the latter.

Although relatively little research has been devoted to the nonoxidative conversion of methane, one can imagine a catalytic cycle in which CH_x fragments are formed from methane on a surface, and these then react, perhaps with another molecule, to yield more useful products. There are analogies between these surface reactions and Fischer-Tropsch chemistry, but to date it has not been possible to maintain activity. With methane reacting alone, graphite is the only thermodynamically stable product at moderate temperatures. One might hope to remove the surface hydrogen selectively, without attacking the CH_x fragment, and there is evidence that this has been achieved to a limited extent.

Clearly, the conversion of methane by direct processes remains a challenging but elusive goal for those working in the field of catalysis. In a sense, the selective activation of methane is one of the "last frontiers" of catalytic science and technology. One can identify with those in the last century who faced the seemingly impossible task of transforming dinitrogen and dihydrogen into ammonia. Hopefully, our success will be equally as remarkable as theirs.

ACKNOWLEDGMENT

The author is indebted to a large group of graduate students and research associates who contributed significantly to the field of methane oxidation during their time at Texas A&M University. These individuals include K.D. Campbell, S.J. Conway, D.Dissanayake, D.J. Driscoll, M. Hatano, P.G. Hinson, T. Ito, K.C.C. Kharas, C.-H. Lin, W. Martir, E. Morales, C. Shi, Y. Tong, D. Wang, J.-X Wang, M. Xu, X. Wang and H.-S. Zhang. In addition, M.P. Rosynek was involved with many aspects of the research and was most helpful in the preparation of this manuscript. The laser Raman studies were carried out with G. Mestl and H. Knözinger at the University of Munich. Financial support was provided by the National Science Foundation and the Gas Research Institute.

REFERENCES

1. J.H. Lunsford, Catal. Today 6, 235 (1990).
2. G. Renesme, J. Saint-Just and Y. Muller, Catal. Today 13, 371 (1992).
3. R. Pitchai and K. Klier, Catal. Rev.-Sci. Eng. 28, 13 (1986).
4. I.D. Löffler, W.F. Maier, J.G. Andrade, I. Thies and P. von R. Schleyer, J. Chem. Soc., Chem. Commun. 1177 (1984).

5. Y. Amenomiya, V.I. Briss, M. Goledzinowski, J. Galuszka and A.R. Sanger, Catal. Rev.-Sci. Eng. 32, 163 (1990).
6. G.J. Hutchings, Chem. Brit. 23, 762 (1987).
7. E.E. Wolf, ed., *Methane Conversion by Oxidative Processes,* Van Nostrand Reinhold, New York, 1992.
8. C. Mirodatos, J.M. Basset, G.A. Martin and J. Saint-Just, eds., Catal. Today, vol. 13, nos. 2,3, 1992.
9. J.-L. Dubois and C.J. Cameron, Appl. Catal. 67, 49 (1990).
10. T. Ito, J.-X Wang, C.-H. Lin and J.H. Lunsford, J. Am. Chem. Soc. 107, 5069 (1985).
11. T. LeVan, M. Chen, M. Kermarec, C. Louis and J.M. Tatibouët, Catal. Lett., 6, 395 (1990).
12. Y. Tong, M.P. Rosynek and J.H. Lunsford, J. Catal. 126, 291 (1990).
13. H. Mimoun, A. Robine, S. Bonnaudet and C.J. Cameron, Appl. Catal. 58, 269 (1990); Chem. Lett. 12, 2185 (1989).
14. R. Phillip, K. Omata, A. Aoki and K. Fujimoto, J. Catal. 134, 422 (1992).
15. K. Otsuka, Q. Liu, M. Hatano and A. Morikawa, Chem. Lett. 903 (1986).
16. J.M. Thomas, W. Ueda, J. Williams and K.D.M. Harris, Faraday Discuss. Chem. Soc., 87 (1989) paper 212.
17. D. Dissanayake, K.C.C. Kharas, M.P. Rosynek and J.H. Lunsford, unpublished results.
18. J. Rasko, G.A. Somorjai and H. Heinemann, Applied Catal., in press.
19. P. Pereira, S.H. Lee, G.A. Somorjai and H. Heinemann, Catal. Lett. 6, 255 (1990); J. Rasko, P. Pereira, G.A. Somorjai and H. Heinemann, Catal. Lett. 9, 395 (1991).
20. R. Burch amd S.C. Tsang, Appl. Catal., 65, 259 (1990).
21. C. Shi, M. Hatano and J.H. Lunsford, Catal. Today, 13, 191 (1992).
22. M. Hatano, P.G. Hinson, K.S. Vines and J.H. Lunsford, J. Catal. 124, 557 (1990).
23. K.D. Campbell, E. Morales and J.H. Lunsford, J. Am. Chem. Soc. 109, 7900 (1987).
24. Y. Feng and D. Gutman, J. Phys. Chem. 95, 6558 (1991); Y. Feng, J. Niiranen and D. Gutman, J. Phys. Chem. 95, 6564 (1991).
25. J. A. Lapszewicz and X.-Z Jiang, Catal. Lett. 13, 103 (1992).
26. P.F. Nelson, C.A. Lukey and N.W. Cant, J. Phys. Chem. 92, 6176 (1988).
27. C.A. Mims, R.B. Hall, K.D. Rose and G.R. Martin, Catal. Lett. 2, 361 (1989).
28. N.W. Cant, C.A. Lukey, P.F. Nelson and R.J. Tyler, J. Chem. Soc., Chem. Commun., 766 (1985);
29. P.F. Nelson, C.A. Lukey and N.W. Cant, J. Catal. 120, 216 (1989).
30. K. Otsuka, M. Inaida, Y. Wada, T. Komatsu and A. Morikawa, Chem. Lett. 1531 (1989).
31. R. Burch, S.C. Tsang, C. Mirodatos and J.G. Sanchez, Catal. Lett. 7, 423 (1990).

32. C. Shi, M. Xu, M.P. Rosynek and J.H. Lunsford, unpublished results.
33. J.A. Roos, S.J. Korf, R.H.J. Veehof, J.G. Van Ommen and J.R.H. Ross, Appl. Catal. 52, 131 (1989).
34. A. Ekstrom and J.A. Lapszewicz, J. Chem. Soc., Chem. Commun., 797 (1988).
35. A. Ekstrom and J.A. Lapszewicz, J. Phys. Chem. 93, 5230 (1989).
36. C.J. Cameron, private communication.
37. K.P. Peil, J.G. Goodwin and G. Marcelin, J. Catal. 132, 556 (1991).
38. K.P. Peil, J.G. Goodwin and G. Marcelin, J. Catal. 131, 143 (1991).
39. Z. Kalenik and E.E. Wolf, Catal. Today 13, 255 (1992).
40. K. van der Wiele, W.M.H. Geerts and J.M.N. van Kasteren in *Methane Conversion by Oxidative Processes* (E.E. Wolf, ed.) Van Nostrand Reinhold, New York, 1992, pp. 259-319.
41. D.J. Statman, J.T. Gleaves, D. McNamara, P.L. Mills, G. Fornasari and J.R.H. Ross, Appl. Catal. 77, 45 (1991).
42. A. Ekstrom, I. Campbell and J.A. Lapszewicz, Appl. Catal. 56, 29 (1989).
43. P.F. Nelson and N.W. Cant, J. Phys. Chem. 94, 3756 (1990).
44. G.J. Hutchings and M.S. Scurrell in *Methane Conversion by Oxidative Processes*, (E.E. Wolf, ed.) Van Nostrand Reinhold, New York, 1992, pp. 200-258.
45. C.H. Lin, J.-X. Wang and J.H. Lunsford, J. Catal. 111, 302 (1988).
46. Y. Tong and J.H. Lunsford, J. Am. Chem. Soc. 113, 4741 (1991).
47. S. Lacombe, J.G. Sanchez M., P. Delichere, H. Mozzanega, J.M. Tatibouet and C. Mirodatos, Catal. Today 13, 273 (1992).
48. M. Xu, C. Shi, M.P. Rosynek and J.H. Lunsford, J. Phys. Chem., in press.
49. Y. Chen, H.T. Tohver, J. Narayan and M.M. Abraham, Phys. Rev. B: Solid State 16, 5535 (1977).
50. D.J. Driscoll, W. Martir, J.-X. Wang and J.H. Lunsford, J.Am. Chem. Soc. 107, 58 (1985); J.-X. Wang and J.H. Lunsford, J. Phys. Chem. 90, 5883 (1986).
51. H.-S. Zhang, J.-X Wang, D.J. Driscoll and J.H. Lunsford, J. Catal. 112, 366 (1988).
52. J. Rodriquez, Y. Aray and R. Ruette, J. Molec. Struct. (Theochem) 210, 323 (1990).
53. K.J. Børve and L.G.M. Pettersson, J. Phys. Chem. 95, 3214 (1991).
54. K.D. Campbell and J.H. Lunsford, J. Phys. Chem. 92, 5792 (1988).
55. M.-C. Wu, C.M. Truong, K. Coulter and D.W. Goodman, unpublished results.
56. J.-X. Wang and J.H. Lunsford, J. Phys. Chem. 90, 3890 (1986).
57. C. Louis, T.L. Chang, M. Kermarec, T. LeVan, J.M. Tatibouët and M. Che, Catal. Today 13, 283 (1992).
58. H. Yamashita, Y. Machida and A. Tomita, Appl. Catal. A: General 79, 203 (1991).
59. K.C.C. Kharas and J.H. Lunsford, J. Am. Chem. Soc. 111, 2336 (1989).
60. M. Yu. Sinev, V.N. Korchak and O.V. Krylov, Kinet. Katal. 27, 1274 (1986).

61. K. Otsuka, Y. Murakami, Y. Wada, A.A. Said and A. Morikawa, J. Catal. 121, 122 (1990).
62. G. Mestel, J.H. Lunsford and H. Knözinger, unpublished results.
63. A.M. Gaffney, C.A. Jones, J.J. Leonard and J.A. Sofranko, J. Catal. 114, 422 (1988).
64. C. Mirodatos, G.A. Martin, J.C. Bertolini and J. Saint-Just, Catal. Today 4, 301 (1989).
65. G.A. Martin and C. Mirodatos in *Methane Conversion by Oxidative Processes* (E.E. Wolf, ed.) Van Nostrand Reinhold, New York, 1992, pp. 259-319.
66. X.D. Peng, D.A. Richards and P. Stair, J. Catal. 121, 99 (1990).
67. G.J. Hutchings, M.S. Scurrell and J. Woodhouse, Catal. Lett. 5, 301 (1990).
68. D. Wang, X. Yang, M.P. Rosynek and J.H. Lunsford, unpublished results.
69. S.J. Conway, J. Szanyi and J.H. Lunsford, Appl. Catal. 56, 149 (1989).
70. J. Cunningham, S. O'Brien, D. McNamara, M. Bourke and R. Egdell in "Proceedings, 9th International Congress on Catalysis" (M.J. Phillips and M. Ternan, eds.) Vol. 4, p. 1719, Chem. Institute of Canada, Ottawa, 1988.
71. M.Y. Lo, S.N. Kamat and G.L. Schrader, Preprints, 196th ACS National Meeting, 33, 378 (1988).
72. T. LeVan, C. Louis, M. Kermarec, M. Che and J.M. Tatibouët, Catal. Today 13, 321 (1992).
73. T. LeVan, M. Che and J.-M. Tatibouët, Cat. Lett., in press.
74. T.R. Baldwin, R. Burch, E.M. Crabb, G.D. Squire and S.C. Tsang, Appl. Catal. 56, 219 (1989).
75. R. Burch, S. Chalker, P. Loader, R. Mariscal, D.A. Rice and G. Webb, Catal. Today 13, 301 (1992); R. Burch, S. Chalker, P. Loader, D.A. Rice and G. Webb, Appl. Catal. A: General, 79, 265 (1991).
76. K. Otsuka, Q. Liu, M. Hatano and A. Morikawa, Chem. Lett. 249 (1986).
77. S. Ahmed and J.B. Moffat, Appl. Catal. 58, 83 (1990).
78. B.K. Warren, Catal. Today 13, 311 (1992).
79. R. Burch, G.D. Squire and S.C. Tsang, Appl. Catal. 46, 69 (1989).
80. G.D. Moggridge, T. Rayment and R.M. Lambert, J. Catal. 134, 242 (1992).
81. P.G. Hinson, A. Clearfield and J.H. Lunsford, J. Chem. Soc., Chem. Commun., 20, 1430 (1991).
82. S.J. Conway and J.H. Lunsford, J. Catal. 131, 513 (1991).
83. A. Khan and E. Ruckenstein, Catal. Lett. 13, 95 (1992).
84. S.J. Korf, J.A. Roos, L.J. Veltman, J.G. van Ommen and J.R.H. Ross, Appl. Catal. 56, 119 (1989).
85. Y. Osada, S. Ogasawara, T. Fukushima, T. Shikada and T. Ikariya, J. Chem. Soc., Chem. Commun., 1434 (1990).
86. K. Wada and Y. Watanabe, Ind. Eng. Chem. Res. 30, 1719 (1991).
87. M.J. Brown and N.D. Parkyns, Catal. Today 8, 305 (1991).
88. J.E. Lyons, P.E. Ellis and V.A. Durante in *Structure Activity and Selectivity Relationship in Heterogeneous Catalysis* (R.K. Grasselli and A.W. Sleight, eds.), Elsevier, Amsterdam, 1991, p. 99.

89. A. Parmaliana, F. Frusteri, D. Miceli, A. Mezzapica and M.S. Scurrell, Appl. Catal. 78, L7 (1991).
90. G.A. Olah, J.D. Felberg and K. Lammertsma, J. Am. Chem. Soc. 105, 6529 (1983).
91. V.A. Rieche, H. Seeboth and H. Wolf, Brennstoff-Chemie 46, 397 (1965).
92. T. Koerts and R.A. van Santen, J. Chem. Soc., Chem. Commun. 345 (1992).
93. M. Belgued, P. Pareja, A. Amariglio and H. Amariglio, Nature 352, 789 (1991); M. Belgued, H. Amariglio, P. Pareja, A. Amariglio and J. Saint-Just, Catal. Today 13, 437 (1992).
94. S.I. Abasov, F.A. Babaeva and B.A. Dadasher, Kinet. Katal. 32, 202 (1991).
95. G.E. Keller and M.M. Bhasin, J. Catal. 73, 9 (1982).
96. W. Hinsen, W. Bytyn and M. Baerns in Proceedings of the 8th International Congress on Catalysis, Berlin, Vol. 3, p. 581, Verlag-Chemie.

Guczi, L. *et al.* (Editors), *New Frontiers in Catalysis*
Proceedings of the 10th International Congress on Catalysis, 19-24 July, 1992, Budapest, Hungary
© 1993 Elsevier Science Publishers B.V. All rights reserved

NEW REACTIONS IN VARIOUS FIELDS AND PRODUCTION OF SPECIALTY CHEMICALS

W.F. Hölderich

Institute for Chemical Engineering and Heterogeneous Catalysis, RWTH Aachen, D-W 5100 Aachen, Germany

1. INTRODUCTION

Considering the broad scope of interesting developments in the synthesis of fine and intermediate chemicals, questions arise how to approach such a topic in order to cover most of the aspects in that field. There are many different viewpoints to be considered: the standpoint of the reaction type such as nucleophilic or electrophilic substitution, oxidation, hydrogenation etc. as well as of the chemical and structural properties of the catalysts. Should heterogeneous as well as homogeneous catalysis be regarded? Are the aspects of the starting materials of more important common interest or only the desired reaction products? Should the environmentally friendly and less energy consuming procedures be the major topic? Or should only the commercial applications and the economic features play the important role?

Finally it was decided to emphasize only heterogeneous catalysis and thereby to have the various types of catalyst systems as guideline. Additionally the viewpoint of commercialization, the question of starting material and particularly the environmental impact are taken into consideration.

The following must be pointed out concerning the economical and environmental aspects. There is a worldwide merchant catalysts market of about 6 billion US-dollars which supports chemical processing and manufacturing industries. They produce goods worth more than fivehundred times that amount. 49 % of these catalysts are used in the production of polymers, 18 % in oxidation reactions, 8 % in hydrogenation and dehydrogenation reactions, 10 % in syngas production and last but not least 16 % for organic synthesis. James F. Roth [1] pointed out that the U.S. market for catalysts in 1989 was about US $ 1.9 billion, including some US $ 630 million for petroleum refining and US $ 750 million for chemical production. These US $ 1.48 billion create a total volume of value for the fuels and chemicals requiring catalysts with about US $ 890 billion, that means about 600 times as much and that represents 18 % of the U.S. gross national producer. Such figures should be roughly similar for the European as well as for the Japanese market. In the lecture entitled "Requirements of catalysis in the fine chemical industry" R. Bader [2], Ciba-Geigy AG, pointed out that 97 % of all industrial heterogeneous catalysts are used in the production of heavy chemicals and only 3 % for the synthesis of fine chemicals. On the other hand, with respect to wealth creation these 3 % account for approximately 20 % of the profit. That is the connection between catalysis and wealth creation. That means in respect to manufacture fine and intermediate chemicals the multiplication factor should be even much higher and that underlines the economic importance and the need of catalysis thereby.

The environmental concerns and regulations increase very much that importance; in the area of environmental protection, catalysis will be essential and without any doubt necessary in particular in fine and intermediate chemical industry, because the kg of by-products (largely inorganic salts) per kg of product are much higher in fine chemicals and specialities than in the case of bulk chemicals as it is assessed by R. Sheldon [216] (Table 1). The increase on going downstream is partly due to the fact that fine chemicals and specialities are often produced in multi-step synthesis. Catalysis will help to avoid such by-product-formation.

Table 1
By-products in chemical industry

INDUSTRY SEGMENT	PRODUCT TONNAGE	KG BY-PRODUCTS/ KG PRODUCT
OIL REFINING	10^6-10^8	ca. 0.1
BULK CHEMICALS	10^4-10^6	< 1 - 5
FINE CHEMICALS	10^2-10^4	5 - 50
PHARMACEUTICALS	10 - 10^3	25 - > 100

2. SOLID AND ACID CATALYSTS

In many manufacturing processes of fine chemicals and organic intermediates, classical acid catalysts such as mineral acids (H_2SO_4, H_3PO_4, HF) or Lewis acids ($AlCl_3$, $FeCl_3$, BF_3, $SnCl_2$) are still applied in homogeneous liquid phase. Such catalysts can not be regenerated and their application causes unavoidable problems with corrosion of the reactors, tubes etc., separation and recycling of the catalyst, high costs for waste disposal and waste water treatment. Various solid acid catalysts have been tried either in gas phase or in liquid phase reactions in order to replace such conventional homogeneous acid catalysts and to avoid those problems. In academic as well as in industrial research laboratories an enormous number of solid acid catalysts have been proposed and tried for a wide variety of reactions.

Such catalysts are:

- metal oxide: Al_2O_3, SiO_2, TiO_2, Nb_2O_5, B_2O_3 etc.
- mixed metal oxides: AL_2O_3/SiO_2, Al_2O_3/B_2O_3, ZrO_2/SiO_2, MgO/SiO_2 etc.
- zeolitic molecular sieves: Al-, B-, Fe-, Ga-zeolites etc.
- clays and pillard clays: betonite, hydrotalcite, montmorillonite etc.
- non-zeolitic molecular sieves: AlPO's, SAPO's, ELAPO's, MeAPO's etc.
- metal phosphates: $AlPO_4$, BPO_4, Li_3PO_4, $SrHPO_4$, $FePO_4$ etc.
- supported heteropolyacids: $H_3PW_{12}O_{40}$, $H_4SiW_{12}O_{40}$, $H_{0.5}PW_{12}O_{2.5}$ etc.
- solid superacids: SbF_5/SiO_2-ZrO_2, ZrO_2-SO_4^{2-}, WO_3-ZrO_2 etc.
- impregnated carriers: H_3PO_4/Al_2O_3, BF_3/Al_2O_3, HF/Al_2O_3 etc.
- metal sulfates: $FeSO_4$, $Al_2(SO_4)_3$, $CuSO_4$, $Cr_2(SO_4)_3$ etc.
- ion-exchange resins: polystyrene-SO_3H, Nafion-H etc.

Till now, unfortunately, only a few of them found commercial application in the production of fine chemicals and intermediates. Some recent examples of academic and industrial interest, from commercial plants or laboratories, will be presented.

2.1 Hydrated niobium pentoxide as acid catalyst

In recent years, K. Tanabe et al. found [3-7] that hydrated niobium pentoxide exhibits a high acid strength ($H_0 < -5,6$) when it is carefully calcinated at temperatures between 100 and 300°C. A noteworthy feature of such a niobic acid catalyst is that it does not deactivate in vapor-phase reactions and furthermore, in contrast to other acid metal oxides, its activity is increased by contacting with steam. K. Tanabe's group applied those materials as catalysts for double bond isomerization of butene, ethylene hydration, esterification of acetic acid with ethanol and dehydration of 1.4-butandiol to form THF.

Regarding these results Sumitomo Chem. [8] is manufacturing 2,5-dimethyl-2,4-hexadiene in the liquid-phase Prins reaction of isobutene with isobutyraldehyde using niobic acid catalyst according to equation 1.

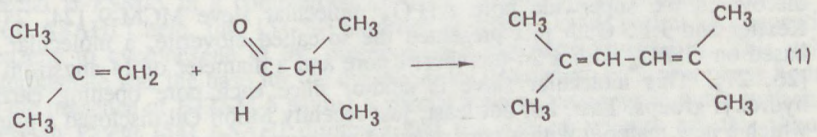

(1)

2,5-dimethyl-2,4-hexadiene which is a valuable intermediate for agricultural chemicals, insecticides, pharmaceuticals and other organic syntheses was formerly produced under pressure in liquid phase using mineral acids, sulfonic acids or heteropolyacids as catalysts. However, this method is not satisfactory because of the low yield (below 40 %), the large amount of by-products and the corrosion problems. Using the niobic acid catalyst these drawbacks could be avoided and yields of about 60 % could be achieved at 250°C. Furthermore this catalyst is superior to other solid acid catalyst as shown in table 2.

Table 2
Production of 2,5-dimethyl-2,4-hexadiene from isobutene and isobutyraldehyde in 2:1 molar ratio at 250°C in a tubular reactor.

Catalyst	Nb_2O_5	HY	SiO_2/Al_2O_3	acid clay
Conversion*	89,3 %	83,5 %	83,4 %	79,4 %
Selectivity*	65,3 %	62,6 %	58,4 %	52,3 %

(* based on isobutyraldehyde)

By increasing the excess of isobutene and the pressure as well as by doping the niobic acid catalyst with phosphoric acid the yield could be increased up to 82 % according to the disclosed patent [8].

2.2 Zeolitic molecular sieves as acid catalysts

In the shift away from homogeneous catalysis towards heterogeneous catalysis, zeolitic materials can play a major role. Because of the chemical and structural properties, zeolite catalysts offer a broad range of possibilities for carrying out reactions with high selectivity in the synthesis of organic intermediates and fine chemicals [9-20, 48]. Over the past ten years, remarkable and rapid progress has been made in this new area. It represents a second promising development in zeolite catalysis in addition to refinery technology and petrochemistry which continue to be still of greatest technical and economic importance.

The reasons for the increasing expansion and for the vast variety of utilization in this second field of zeolite catalysis are:

- The readily reproducible production of clearly defined catalyst surfaces of molecular sieves. This is certainly not something which can be taken for granted.
- The synthesis of novel zeolitic and non-zeolitic molecular sieves. There are constantly new surprises in this field. In 1987-88 the discovery of the $AlPO_4$ molecular sieve VPI-5 by Mark Davis caused a sensation [21-23]. The superwide pores of this molecular sieve are formed by 18 tetrahedra. The pore diameter is about 12 angstrom units. Before that, R. von Ballmoos and E.G. Derouane discovered the superwide pore $A1PO_4$ molecular sieve MCM-9 [24, 25]. H. Kessler and J.L. Guth just presented the so-called cloverite, a molecular sieve based on $GaPO_4$ with a 24-membered pore and a diameter of 14 angstrom units [26, 27]. This molecular sieve is acidic, since each pore opening carries 4 hydroxyl groups. Last, but not least, just recently Mobil Oil disclosed a patent in which a new material with a pore opening of around 1,8 nm is claimed [28].
- The synthesis of isomorphously substituted materials [29-31]
- Various forms of shape selectivity [32-40]: reactant selectivity, product selectivity and restricted transition state shape selectivity. Shape selectivity reflects the relationship between the structure and the mode of action of a zeolite. This shape selectivity is an unique advantageous feature of zeolites compared with other heterogeneous catalysts.
- The scope for modifying the properties of zeolite catalysts [18, 41-45]. This includes:
    - o the broad spectrum ranging from highly acidic via neutral to highly basic zeolites
    - o bi- and polyfunctional catalysts through use of zeolites as support material for active components such as transition or noble metals while preserving the intrinsic zeolite properties such as shape selectivity and acidity or else basicity.
    - o Redox properties as in the case of titanium silicalites
    - o the pore diameter of a zeolite is not predetermined by the structure alone; there are various methods of altering, for example reducing the pore mouth, by CVD-method after the synthesis.
- Zeolites are thermally stable and can be regenerated after deactivation by coking.
- More knowledge about the nature of active centers.

Altogether, with regard to these reasons and to the knowledge and experience gained from petrochemistry and refinery technology which offer a valuable guidance, rich opportunities are provided of designing and employing zeolites as heterogeneous catalysts which are tailored to suit the desired reactions. They can be used as highly selective and active catalysts in almost all kinds of reactions.

In spite of that this new field of zeolite catalysis is still in a relatively early state of development, there are already very exciting commercial applications in zeolite catalyzed production of organic intermediates and fine chemicals:

- The NITTO-process for the production of di- and monomethylamine from of ammonia and methanol in a gas phase reaction in the presence of modified mordenite preventing the formation of trimethylamine. Since 1985 a commercial plant with a capacity of around 40.000 t/a is on stream [46]. Furthermore the production capacity should be expanded up to 50.000 t/a. At 320°C the selectivity for DMA is about 65 % and for TMA less than 5 %. Therefore, in contrast to the conventional production here is no excess of TMA which has to be recycled.

  SRI-International evaluates, that the NITTO-methylamines process can increase the capacity by about 30 - 50 % and reduce the energy consumption by about 40 - 50 % in existing installations (less distillation, no recycling) and can require about 30 - 40 % less capital investment in new plants [47].
  Thus, the product shape selectivity of the mordenite and the possibility of adjusting its acidity and pore opening and of poisoning the outer surface enables to get a much better composition of the product mixture according to commercial requirements than in the case of the classical production over Al_2O_3 [19, 48-50].

- The ASAHI-process for the production of cyclohexanol out of cyclohexene over special H-ZSM-5 in a commercial unit with a capacity of 60.000 t/a since 1990 [46]. ASAHI Chem. Ind. [51-54] has been successful in the partial hydrogenation of benzene to cyclohexene in the presence of a poisoned Ru-catalyst. This valuable intermediate was the base for the cyclohexanol production by liquid phase hydration in the presence of H-ZSM-5 having a special ratio of the inner to outer surface. In a German Patent [54] ASAHI discloses that the size of primary crystals should be smaller than 0,5 μm, in particular less than 0,1 μm or even 0,05 μm. The ratio of the acid sites on the outer surface to the total acid sites of the outer and inner surface should be 0,07/1 or even more i.e. the so called R-value should be higher than 0,07. Using such H-ZSM-5 powder between 100°C and 120°C a conversion of cyclohexene between 10 and 15 % is achieved and the selectivity for cyclohexanol is higher than 98 %.

This new route for manufacturing cyclohexanol which is a very valuable intermediate for the production of adipic acid and caprolactam provides advantages compared with the conventional method: 1 mol H_2 less, one reaction step less and avoidance of the dangerous oxidation with oxygen. That means an energetically and economically favourable and environmentally friendly alternative route. Other companies are also very much involved in this exciting new development [55-57].

Further commercial plants are on stream:

- The TORAY-process for the production of m-chlorotoluene, m-dichlorobenzene and 2,6-dichlorotoluene in a fixed-bed liquid phase isomerization over H-ZSM-5 [58, 59]
- NEPERA-process for the production of pyridine out of acetaldehyde, formaldehyde and ammonia in a fluidized-bed reactor over H-ZSM-5 [60]
- SNAMPROGETTI-process for the production of highly pure isobutene by cleavage of methyl-tert.-butylether (MTBE) in a fixed-bed reactor over a boron-pentasilzeolite [18, 61]
- IDEMITSU-KOSAN-process for the production of adamantane by skeletal rearrangement of tetrahydrodicyclopentadiene in a fixed-bed reactor over a multifunctional Pt-doped Y-zeolite [13, 46, 62]

Maybe in the near future the alkylation of biphenyl by Dow or Catalytica [63-65] or diphenylether by Du Pont [66] to the corresponding para, para-isomers for the production of liquid crystals will go on stream. Also the alkylation of naphthalene e.g. by Ruetgerswerke [67] to form methylnaphthalene which is a very valuable intermediate for vitamine K production has a good chance to be realized. Furthermore the Synfina-process for the cleavage and hydrogenation of polysaccharides to polyhydric alcohols [see Cap. 5.2] is close to technical realization. Assumably, there are several other commercialized processes using acidic shape selective zeolite catalysts. However, the companies do not wish to announce them in the public. Maybe some significant additional applications are explored in a recent industry multiclient report entitled "Speciality Zeolites in Catalysis 1992 to 2000" [68].

A remarkably interesting example taken from the vast variety of reactions for the organic synthesis in the presence of zeolites is the direct amination of olefines with ammonia. Extensive laboratory work is done by BASF and Air Products [14, 19, 69-73]. Various zeolites have been studied as catalysts: HY and rare earth Y, H-offretite, H-clinophtilolite, H-chabazite-erionite and H-erionite, H-mordenite as well as pentasil zeolites. The amination is favoured by low temperature, high pressure and high ammonia-to-olefin ratio. However, a minimum of reaction temperatures is required to activate the olefins and this threshold temperature depends on the olefin structure.

Even though ethylene is effectively aminated by all zeolite catalysts and especially by small pore zeolites such as H-erionite or H-clinoptilolite, propene shows only low conversion and isobutene doesn't react at all over these small pore zeolites. These results reflect shape selective restrictions. Concerning the reaction mechanism it is found [69-71] that acidic sites are necessary and the amination occurs via protonated intermediates as evidenced by the relative ease: isobutene > propene > ethene. On amorphous silica-alumina low conversions and on non-acidic zeolites such as NaY no aminations are observed.

As an example, isobutene reacts with NH_3 over HY to t-butylamine already at 220°C according to equation 2. At 300°C the equilibrium conversion of about 9% is reached. Over this temperature range > 99 % selectivities are obtained using a 2:1 ammonia/isobutene molar feed ratio. Oligomerization of isobutene is not significant below 300°C because ammonia is present in excess. Excellent results can also be obtained if the reaction of isobutene with NH_3 is carried out at 300°C and 300 bar in the presence of Al-, B-, Fe- or Ga-pentasilzeolites; the selectivity amounts to around 99 % at 12-15 % conversion [72, 73]. Furthermore the dialkylation does not occur because of the transition state shape selectivity.

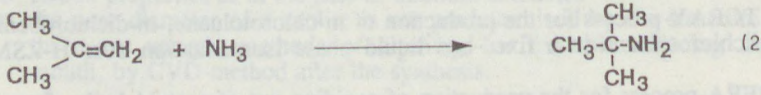

(2)

The X- and Y-zeolites suffer from the disadvantage of rapid deactivation. On the other hand, Re-Y-zeolite and the pentasilzeolites afford commercially acceptable service time.

Although equilibrium conversions are low, the simplicity and high selectivity (more than 99 % as in the Asahi-process) and the absence of inorganic coproducts, as well as extremely toxic starting materials and intermediates of this procedure, provide evidently advantages over the traditional HCN-based Ritter route to t-butylamine starting from isobutene and hydrogen cyanide and the resulting formamide being saponified. Thus, this synthesis-method is worth to be called environmentally safe and friendly.

2.3 Non-zeolitic molecular sieves as acid catalysts

As it is demonstrated in the latter chapter, zeolitic catalysts play an important role in the synthesis of fine and intermediate chemicals. There is hope that non-zeolitic molecular sieves (NZMS) including the whole variety of modifications and isomorphous substitution [21, 24-27, 74-77] give also a great opportunity in highly selective synthesis of organic compounds containing functional groups. Till now, only little literature about this topic appeared and most of it in the patent-literature. A remarkable example is the Beckmann-rearrangement of cyclohexanone oxime to form ϵ-caprolactame in the presence of SAPO-11 or SAPO-41 [17, 19, 78]. The reaction at 350°C over SAPO-11 yields ϵ-caprolactam with 95 % selectivity at 98 % conversion. The disadvantage so far is the necessity of the highly diluted feedstock. Other reactions are:

- vinylmethylether from acetaldehyde-dimethylacetal [18, 79]
- 1.2-dimethoxyethylene from 1.1.2-trimethoxyethane [18, 80]
- neoalkanals from acetals of neopentylglycol [81]
- 8.10-dodecadienol from 9-hydroxy-dode-10-enyl-1-tert-butylether [18, 82]
- vinyl-methyl-ketone from 5-methylen-1.3-dioxolanone [18, 83]
- p-methyl-benzaldehyde by oxidation of p-cresol [84]
- acrylonitrile by ammoxidation of propane [85]
- alkylamine from ammonia and alcohol [86]
- triethylene diamine from cyclic or acyclic amines [87]
- aziridines form alkanolamines [88]
- iron-phthalocyanin-complexes in VPI-5 for the oxidation of alkanes [89]
- alkylation of aromatics [90]

Up to date, there is no indication that one of these reactions catalyzed by a non-zeolitic molecular sieve is commercialized.

A noteworthy reaction is the formation of enol ethers by selectively cleaving C-O bond of acetals according to equation 3 [18, 79].

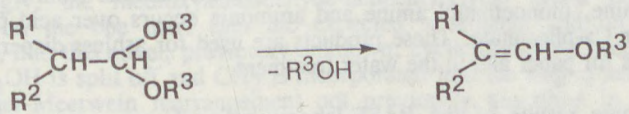

(3)

$R^1 = R^2$ = H, alkyl, aryl; R^3 = alkyl

It is possible to achieve yields of 80 % and higher, when the reaction is carried out in the temperature range 270 - 340 °C and the acidity of the zeolite is reduced or eliminated by alkali-doping. For instance, using a Na-mordenite or a Na-ZSM-5 with a Na_2O/Al_2O_3 ratio of 1 to 1.1 at 300 °C, acetaldehyde-dimethylacetal (DMA) is converted into vinylmethylether with 98 % selectivity at 91 % conversion.

The weakly acidic boron - or iron-pentasil zeolite or non-zeolitic molecular sieves can also be applied for the synthesis of enol ethers from acetals. For example at 300 °C 96 % selectivity of vinyl-methylether at 100 % conversion of DMA is achieved in the presence of a boron-pentasil zeolite. Using SAPO-5 under the same conditions a selectivity of 97 % is obtained at 100 % conversion. The zeolitic and non zeolitic molecular sieve catalysts are superior to the conventional catalysts (supported phosphates, sulphates or carbonates) in terms of both selectivity and effective lifetime. In general, they are also superior to precipitated phosphates and metaloxides such as silica, titania and alumina. Only precipitated BPO_4 is an exception; in this case under comparable conditions 93 % selectivity at 100 % conversion is obtained.

Vinyl ethers, which are of great technical importance for polymerisation, Diels-Alder-reactions etc., are produced by the Reppe synthesis from acetylene and alcohols under pressure and in the presence of strong bases such as KOH. The alternative route, which is based upon readily available acetals and which is carried out at atmospheric pressure in the gas phase, offers advantages both in regard to environmental impact and also at production sites where acetylene is not available.

2.4. Precipitated metal phosphates as acid catalysts

Other noteworthy solid acids are metal phosphates mostly precipitated materials which have been extensivley studied e.g. $AlPO_4$, BPO_4, Ti_3PO_4, $SiHPO_4$ Ge-, Ti-, Zr- and Sn-phosphates [91-96]. In contrast to the metal phosphates with molecular sieve features (NZMS), the metal phosphates without zeolite structure, find already application on a large industrial scale. In the nice reviews published by M. Misono and N. Nojiri [46] as well as J.N. Armor [97] one can find:

- UBE-process for the production of gualacol and geraethol via monoalkyl etherification of dihydroxy benzene in the presence of a aluminium-boron-phosphates.

- ARCO-process for the production of allyl alcohol via isomerization of propylene oxide over Li-phosphate. This is the first of three steps in the first commercial process of butandiol based on propylene oxide. A unit with a capacity of about 30.000 t/a is on stream since 1990.

- AIR-PRODUCTS-process for manufacturing triethylene-diamine (TEDA) from hydroxyethyl piperazine on $SrHPO_4$. TEDA is a large volume catalyst for the production of polyurethane.

- AIR-PRODUCTS-process for manufacturing polyethylene amines in units of approximately 5.000 t/a capacity. This vapor phase synthesis of the mixed alkylamines such as diethylenetriamine or triethylenetetraamine from a mixture of ethylene diamine, monoethanol amine and ammonia occurs over acid phosphates such as Sr- or Ca-phosphate. These products are used for ashless dispersants, wet strength resins for paper and in the water treatment.

In this paper some results of the BASF-laboratory work are presentend in more details. In connection with the aldehyde - ketone rearrangement [15, 98] the reaction behaviour of cyclic acetals was studied in the presence of zeolite catalysts [10, 99], of non-zeolitic molecular sieves and precipitated metalphosphates, respectively [81] as well as of metal oxides [100]. A reaction, similar to the aldehyde-ketone rearrangement, with migration of a carbenium ion and formation of the ketal was expected. However, such an acetal-ketal rearrangement does not take place; instead the formation of the linear neoalkanals according to equation 4 was found. This reaction is also extremely interesting from a mechanistic viewpoint; it amounts to a 1,3-hydride shift, a kind of intramolecular redox reaction.

Acetals of neopentylglycol with different moieties on the aldehyde stem - alkyl, aryl, aralkyl, heteroaryl, etc. - are isomerized in particular over pentasil zeolites at 250-400°C. The selectivities for these neoalkanals are above 90 % for a 50-80 % conversion. Probably, the restricted transition state shape selectivity of the zeolites is responsible for an increasing yield of the linear neoalkanals which fit in the zeolite framework. It must be pointed out that once again zeolites as acidic and shape selective catalysts are superior to conventional catalysts such as silicagel and alumina.

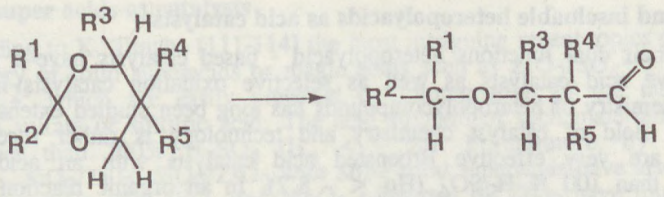

(4)

$R^1 = R^2 = R^4 = R^5$ = H, alkyl, alkenyl, aryl, arylalkyl, alkylaryl, arylalkenyl, alkenylarly, heterocyclic residue; R^3 = H, alkyl

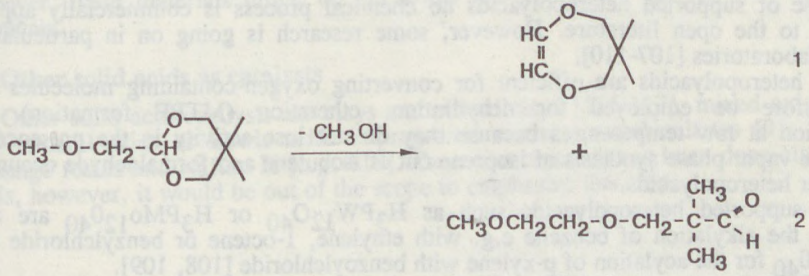

(5)

Surprisingly, the methoxyacetaldehyde-neopentylglycol acetal converts into two compounds, on the one hand into the expected neoalkanal and on the other hand, unexpectedly, into this novel, previously unknown, cyclic dioxolane according to equation 5 [101]. CH_3OH is split off and CH_2 is incorporated into the ring system. This is a form of the Wagner-Meerwein rearrangement not previously described in the literature. A comparison of zeolitic and other solid acid catalysts shows that non-zeolitic, precipitated phosphates such as BPO_4 and $CePO_4$ give rise almost exclusively to this sterically bulky dioxolane. In the presence of BPO_4 at 350°C and WHSV = $3h^{-1}$ 95 % selectivity of the cyclic dioxolane (1) and 3,5 % selectivity of the linear neokanal (2) are achieved at 36 % conversion. On the other hand in case of Ce-doped boron pentasilzeolite under the same reaction conditions (1) is obtained with 62 % selectivity and (2) with 22 % selectivity at 95 % conversion. There is not enough room in a zeolite pore for (1) to be formed. In zeolites, the slender linear neoalkanals are presumably formed on the inside, while sterically bulkier dioxolanes are presumably formed on the outer surface. Furthermore, as can be seen from the product distribution the reaction to form (1) is faster than the formation of (2).

These examples demonstrate once more, how it is possible to direct a reaction of the same feedstock to completely different products just by the choice of a shape selective catalyst such as boron-pentasil zeolite or a non shape selective catalyst such as BPO_4. These novel interesting dioxolanes might be applied for the synthesis of valuable, pharmacologically effective compounds and active compounds for pestizides and polymers.

2.5 Supported and insoluable heteropolyacids as acid catalysts

Because of their dual functions heteropolyacid - based catalysts have a promising future as selective acid catalysts as well as selective oxidation catalysts in organic synthesis. The chemistry of heteropolycompounds has long been studied extensively, but its debut in the field of catalyst chemistry and technology is rather recent [102]. Heteropolyacids are very effective Broensted acid catalysts with an acid strength somewhat lower than 100 % H_2SO_4 (Ho < - 8,2). In an organic reaction by these catalysts created cationic intermediates such as carbenium or oxonium ions are highly stabilized by heteropoly anion to cause a lower activation energy.

As far as utilization of its strong protonic acid function is concerned, heteropolyacid - based catalysts have been applied in form of aqueous solution for commercial plants such as the hydration processes of propene (Tokumyama Soda 36.000 t/a) [103], of n-butene (Idemitsu Petrochemical) [104], of i-butene (Asahi Chem. Ind., 56.000 t/a) [46, 105] to the corresponding alcohols and the polymerization process of THF to polyoxytetramethylene glycol (Poly-THF; Asahi Chem. Ind., 2.000 t/a) [106]. Until now, for the use of supported heteropolyacids no chemical process is commercially applied according to the open literature. However, some research is going on in particular in Japanese laboratories [107-110].

Solid heteropolyacids are efficient for converting oxygen-containing molecules and can therefore be employed for dehydration, etheration (MTBE formation) and esterification at low temperatures because they do not lose activity in the presence of water. The vapor phase synthesis of isoprene out of isobutene and formaldehyde occurs in 1 step over heteropolyacids.

Silica-supported heteropolyacids such as $H_3PW_{12}O_{40}$ or $H_3PMo_{12}0_{40}$ are also active for the alkylation of benzene e.g. with ethylene, 1-octene or benzylchloride and $H_4SiW_{12}0_{40}$ for the acylation of p-xylene with benzoylchloride [108, 109].

M. Misomo et al. [107] recently found insoluable acid cesium salts $H_{3-x}Cs_xPW_{12}0_{40}$ which have a large surface area up to 140 m^2/g and used them for acylation reactions of aromatics. These insoluable Cs salts of heteropolyacids are believed to be effective solid acids for various types of liquid-phase Friedel-Crafts reactions.

Examples which are more related to fine chemicals are the phenol alkylation with dodecene-1, the pinacol rearrangement and the synthesis of glycosides from sugars in liquid phase e.g. the latter according to equation 6 [110].

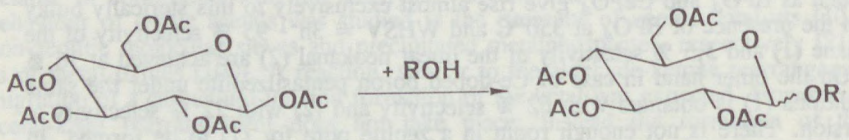

(6)

In this nucleophilic substitution of acylated aldohexose with higher alcohols heteropolyacids are much more active than the conventionally used p-toluene sulfonic acid. At 70 - 130°C yields between 70 and 90 % can be achieved. The high enomer selectivity up to 98 % can be adjusted by changing the strength of the heteropolyacid. Such glycosides might be used as effective and biodegradabel surfactants.

2.6 Solid super acids as catalysts

According to K. Tanabe [111-114] the most intriguing recent topics of solid acids are the discovery of solid superacids or magic acids such as ZrO_2/SO_4^{2-}, TiO_2/SO_4^{2-} and Fe_2O_3/SO_4^{2-} which are easily prepared by impregnation of the metal oxides with ammonium sulfate or sulfuric acid. The acid strength of such materials is about 10000 times higher than 100% H_2SO_4 (H_o < - 16). Furthermore, by impregnation of SiO_2/Al_2O_3, SiO_2/TiO_2, SiO_2/ZrO_2 with SbF_5 solid superacids have also been prepared. Beside these magic acids WO_3 and MoO_3 supported by ZrO_2 have found to have solid super acid features (WO_3/ZrO_2: Ho < - 12,7 and MoO_3/ZrO_2 : Ho <- 14,5).

Such solid acids were used for several reaction types such as isomerization, alkylation, acylation, dehydration, hydration, esterification etc. K. Tanabe et al. [113] reported that Pt doped superacids like Pt-ZrO_2/SO_4^{2-} show a high activity, selectivity and long service time for the Beckmann rearrangement. At 98 % conversion 98 % selectivity was obtained, after 1000 hr time on stream at 250°C the figures are 97 % and 95 %, respectively. For particular reactions it appears that superacids show high efficiency. However, these materials might be too acidic and too active for the synthesis of fine chemicals.

2.7 Other solid acids as catalysts

Other solid acid catalysts are clays and pillard clays [115-117], mixed oxides [118], with mineral acids or Lewis acids impregnated carriers, metal sulfates [91, 118], ion exchange resins and Nafion-H [e.g. 119]. Extensive research has been done also in these fields, however, it would be out of the scope to emphasize that, too.

3. SOLID BASE CATALYSTS

As in the case of conventional acid catalyzed processes in homogeneous liquid-phase, similar problems exist more or less for the use of typical basic catalysts such as NaOH and KOH in liquid-phase reactions. Therefore, there is an ambitious interest for finding and developing new and various solid base catalysts for the organic synthesis of fine and intermediate chemicals. Furthermore by using solid bases as catalysts it is also possible to run the reaction in vapor phase and on a continuous flow either in a fixed or fluidized bed. Quite a reasonable number of solid base catalysts have been developed in academic and industrial research laboratories:

- alkalimetal oxides: Na_2O, K_2O, Cs_2O
- alkali earth metal oxides: MgO, CaO, BaO
- rare earth metal oxides: La_2O_3, Sm_2O_3 etc.
- transition metal oxides: ZnO, ZrO_2, ThO_2 etc.
- solid super bases: γ -Al_2O_3/MOH/M (M = alkali)
- zeolites modified with alkali
- anionic ion-exchange resins

A long time ago, H. Pines already found that solid base catalysts are more effective for double bond isomerization than acid catalysts [120, 121]. Since that day a lot of investigations have been done to study in particular such isomerization reactions in the presence of solid bases. In general, it must be stated that in the case of solid base catalyst

for the synthesis of fine and intermediate chemicals less experiments have been carried out compared to the research of acid catalysis. A few remarkable recently developed reactions will be considered in this paper.

3.1 Alkali earth metal oxide as base catalyst

Alkaline earth metal oxides such as MgO, CaO, SrO, BaO have been known in base catalysis for the reaction of compounds having higher acid strength in comparison to CO_2 and are inactive for compounds with less acidic strength [122]. One of the most remarkable reactions in the presence of those base catalysts is the highly selective alkylation of phenol with methanol over MgO to form 2,6-xylenol. This process was found by General Electric already in 1965 and today it is on commercial scale in several units in various countries [123]. Based on the experience of the butene-isomerization, in fine chemistry base catalysts are mostly used for double bond isomerization [122] as in the following cases:

- α - pinene to ß - pinene over SrO or CaO [124]
- 3-carene to 2-carene over MgO or CaO [125, 126]
- $\Delta^{7(13)}$-protoilludene to $\Delta^{7(8)}$-protoilludene over MgO [127]
- $\Delta^{2(3),7(13)}$-illudadiene to $\Delta^{2(3),7(8)}$ -illudadiene over MgO [127]
- 1-N-pyrrolidino-2-propene to 1-N-pyrrolidino-1-propene over MgO or CaO [128]
- 2-propenyl-ether to 1-propenyl-ether over CaO [122, 129, 130]
- 2,5-dihydrofurane to 1,3-dihydrofurane over CaO
- 3-methoxycyclohexene to 2-methoxycyclohexene over CaO
- 1-allylamine to 2-allylamine over CaO or MgO [122, 128]

The yields of such reactions are always very high. Particularly the isomerization reactions of compounds containing basic N or O take place very nicely in the presence of base catalysts, but can not be carried out over acid catalysts, since the basic sites of the catalyst do not interact with basic groups of the reactants in contrast to acid catalysts where poisoning occurs.

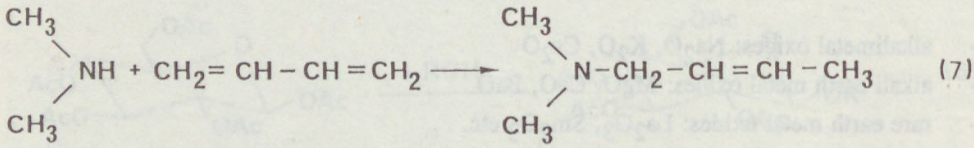

(7)

A noteworthy reaction is also the addition of primary and secondary amines to conjugated diolefins as butadiene in particular catalyzed by CaO to yield secondary and tertiary amines [131-133] according to equation 7. This reaction is in contrast to the direct amination of olefines with ammonia which is performed very well in the presence of acid zeolite catalysts (see chap. 2.2).

3.2 Solid super bases as catalysts

While alkaline metal oxides as catalysts have not found so much interest in industrial research laboratories, there is an intriguing recent topic of solid base as catalysts; researches of Sumitomo Chemicals have developed solid super base catalysts [134-136]. These catalysts consist of alkali metal hydroxide/alkali metal on γ-alumina according to the general formula $(MOH)_x/M_y/\gamma\text{-}Al_2O_3$, wherein M, x, y are described as

M = Li, Na, K, Rb, Cs, x = 5-15 wt. - % on γ - Al_2O_3 and
Y = 3-8 wt. -% on γ - Al_2O_3

They have an extremely high basicity, sometimes higher than $H_0 > 37$. Such super bases, which are sensitive to moisture and CO_2 have to be handled carefully. Nevertheless they are already applied as highly active and effective catalysts for double bond isomerization and side-chain alkylation of alkylbenzenes.

For example 5-vinylbicyclo [2.2.1] hepta-2-ene (1), is almost completely isomerized even at -30°C over γ-Al_2O_3/NaOH/Na (equation 8) to form 5-ethylidene-bicyclo [2.2.1] hepta-2-ene (2), a compound for vulcanization purposes.

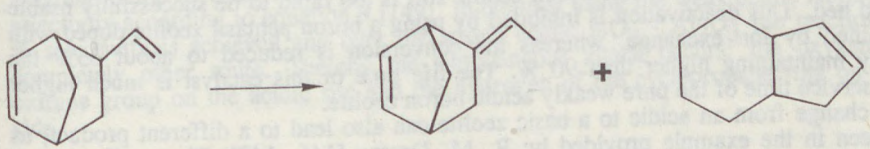

(8)

1 2 3

Compound (1) is thermally unstable and tends to react to tetrahydroindene (3) which can be separated from the desired product (2) only under extreme and very costly conditions. However, at - 30°C in the presence of the superbase, the isomer (2) is obtained with high purity i.e. 99,9 % selectivity at 99,7 % conversion. Thus, after separation of the catalyst, no additional purification step is necessary [135, 136]. This reaction is carried out by Sumitomo Chemicals in a commerical unit having a capacity of 2000 t/a being on stream since 1986.

This superbase catalyst NaOH/Na/γ-Al_2O_3 can also successfully be employed for the isomerization of safrol (1-allyl-3,4-(methylene-dioxy)-benzene) to iso-safrol (3,4-(methylenedioxy-1-propenyl)-benzene) as well as for the isomerization of 2,3-dimethylbutene-1 to 2,3-dimethyl-butene-2, a valuable intermediate for the production of pyrethroids [135, 136].

The side chain alkylation of cumene with ethylene occurs at 40°C over such a superbase to form t-amylbenzene in 99 % selectivity. The conversion of cumene is 99 %. Also this reaction has found its industrial application in Sumitomo Chemical company [135, 136]. In the development and commercial use of solid super bases Sumitomo seems to be far ahead.

3.3 Zeolites as base catalysts

Base zeolites can be prepared by

- ion-exchange of the zeolite with alkali ions such as K, Rb, Cs [137]
- impregnation of neutral zeolite with alkali-compounds
- formation of sodium clusters in zeolites [138-142]
- treatment of zeolites by alkali metal vapor [143]

Using basic zeolites may direct a given reaction to other products in comparison to the use of acidic zeolites and may increase the selectivity of a reaction as well as the service time of a catalyst for the same reaction.

In the work on the aldehyde-keton rearrangement mentioned before (chap. 2.4) [14, 15] aldehydes were used which have not only alpha- and beta-hydrogen atoms but also gamma-hydrogen atoms, as in the case of 2-methylbutanal. These aldehydes do not rearrange to form ketones but dehydration takes place to form dienes, such as isoprene [144, 145]. In fact isoprene is obtained at 400°C over a weakly acidic boron pentasil zeolite with 95 % selectivity at approximately 50 % conversion of 2-methylbutanal. The more acidic aluminium pentasilzeolite is less suitable, since not only dienes but in particular aromatics are formed via aldolcondensation etc. and rapid deactivation occurs. The deactivation of the less acidic boron zeolite still is too rapid to be successfully usable in a fixed bed. This deactivation is inhibited by using a boron pentasil zeolite doped with Cs, obtained by ion exchange, whereas the conversion is reduced to about 35% the selectivity maintaining higher than 90 %. The life time of this catalyst is much higher than the service time of the pure weakly acidic boron zeolite.

The change from an acidic to a basic zeolite can also lead to a different product, as can be seen in the example provided by R. M. Dessau [146, 147]. The cyclization of diketones such as acetylacetones leads - preferably at temperatures of 250 - 350°C - to dimethyltetrahydrofuran if it is carried out over acidic zeolites but to methylcyclopentenones if carried out over basic zeolites. For example, using an acidic H-ZSM-5 with Si/Al = 300 at 350°C 2,5-dimethylfuran (DMF) is produced with 96.1 % yield at 99.8 % conversion of acetylacetone. On the other hand, if this zeolite is doped with alkali ions in excess of their framework Al-content (Si/Al = 300, Na/Al = 7.6) then 89.1 % yield of methylcyclopentenone (MCP) is obtained at quantitative conversion. Only a 4.4 % yield of DMF is observed using that basic zeolite catalyst. The number of alkali ions which are in excess of the corresponding Al content of the zeolite framework are associated with the internal silyloxy groups in the as-synthesized form of high silica zeolites. The behaviour of such a Na-ZSM-5 is very much like sodium silicalite. Because each of the reaction products, either MCP or DMF, is obtained in very high selectivity, and because that is characteristic for the presence of basic or acidic sites in the zeolite catalyst, this reaction maybe, can be used as an easy test for determing the degree of basicity and acidity of such materials.

3.4 Other solid base catalysts

Other solid base catalysts such as rare earth metal oxides and the anionic-ion-exchange resins have been investigated, however, up to date there are no significant developments in the area of fine or intermediate chemicals.

4 ACID-BASE BIFUNCTIONAL CATALYSIS

Speaking about acid catalyzed reactions, one has to be aware that basic sites are also involved more or less in the reaction mechanism. The cooperation of acid sites with basic sites can be extremely effective for specific reactions. Sometimes, such a bifunctional catalyst shows pronounced activity, even if the strength of the acid-base pair sites is much weaker than the acid or basic strength of the isolated solid acid or base.

4.1 Zirkon oxide as acid-base bifunctional catalyst

For example, recently, K. Tanabe et al. [148] studied the decomposition of alkylamines in the presence of ZrO_2 with the dual weak acidic and basic function in comparison to the typical solid acid silica-alumina with high acidity and to the typical solid base MgO with strong base strength. The bifunctional ZrO_2 shows the highest activity and selectivity for the selective dehydrogenation particularly of trialkylamines to form nitriles, where as silica-alumina and MgO are not suitable for this reaction. In the case of silica-alumina, dealkylation and deamination occur to yield olefins and ammonia.

On the other hand, a TiO_2-ZrO_2 catalyst possesses high acidic strength as well as appreciable base strength. This catalyst could be successfully used for the isomerization of 2-carene oxide to form the allylic alcohol cis-2.8-p-mentadiene-1-ol with almost 100 % selectivity according to equation 9 [149]. In contrast using the weak acidic Al_2O_3 only 40 % selectivity is achieved and over the strong acidic SiO_2 - Al_2O_3 the reaction takes a completely other route. Thereby the simultaneous attack occurs: the oxygene of the oxirane group on the acidic site and the hydrogen of the cyclopropane ring on the basic side.

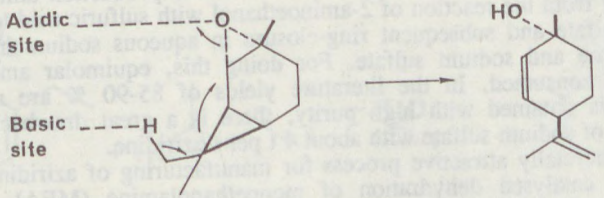

(9)

Several other reactions can be achieved by using this typical solid acid-base bifunctional catalyst ZrO_2 e.g.

- hydrogenation of dienes e.g. 1.3-butadiene [150]
- dehydration of secondary alcohols [151]
  e.g. 4-methyl-2-pentanol or cyclohexyl-ethanol
- vapor-phase esterification of carbonic acids [152]
- vapor-phase ester-interchange reaction [152]

These research investigations of solid acid-base bifunctional catalyst - mostly ZrO_2 - have found already commercial application in the Japanese chemical industry.

4.2 Hydrogenation of aromatic carboxylic acids to aldehydes

In the presence of modified zirconia catalyst e.g. Cr, Zn or Pb doped ZrO_2 aromatic carboxylic acids can be hydrogenated to pure aromatic aldehydes in high selectivity [153]. The reaction is carried out in a fixed bed reactor in the vapor phase at 300 - 400°C. For example, at 350°C and GHSV = 625 h^{-1} the hydrogenation of benzoic acid (acid/H_2-ratio = 2/98 molar) to benzaldehyde over Cr-doped ZrO_2 is achieved with about 96 % selectivity at 98 % conversion.

Since 1988 Mitsubishi Kasei has on stream a multi-purpose plant having 2000 t/a capacity for the production of various aromatic aldehydes, e.g. m-phenoxybenzaldehyde which is used as intermediate for the synthesis of pyrethroids or p-tert.-butyl-benzaldehyde as starting material for pharmaceuticals, fragrances and agrochemicals. The advantages of the Mitsubishi Kasei-process are high yield in one step hydrogenation, high product purity and a cost saving of about 20 to 30% compared with the conventional route.

4.3 Ethylenimine from monoethanolamine

Aziridine (ethylenimine) is a potential chemical intermediate for the production of linear amine-type functional polymers for paper and textile treatment and for the production of pharmaceutical intermediates and various other amines. However, because of the toxicity and carcinogenicity of ethylenimine, this material possesses severe handling difficulties, which make it highly undesirable to store or transport the ethylenimine, so that desirably a process for the production of ethylenimine should begin from inexpensive starting materials, and should provide the ethylenimine in a form which permits its direct feed without intervening isolation or storage of the ethylenimine.

Various processes for the production of aziridine are known [154]. Up to 1990, the liquid-phase Wenker-process has been the basis for all industrial production units. It is a two-step process starting from the reaction of 2-aminoethanol with sulfuric acid to give 2-aminoethyl hydrogen sulfate and subsequent ring-closure in aqueous sodium hydroxide solution to form aziridine and sodium sulfate. For doing this, equimolar amounts of H_2SO_4 and NaOH are consumed. In the literature yields of 85-90 % are reported. Although the aziridine is obtained with high purity, there is a great drawback in the inevitable co-production of sodium sulfate with about 4 t per t aziridine.

Therefore one commercially attractive process for manufacturing of aziridine would be the heterogeneously catalysed dehydration of monoethanolamine (MEA). Several attempts over various heterogeneous catalysts have been made. In the presence of acid catalysts, intermolecular dehydration is mainly promoted to form piperazine, pyrazine, aminoethylpiperazine, diazabicyclooctane, N-hydroxyethyldiaminoethane, acetonitrile, ethylamine and polymers. In contrast, over solid base catalysts ammonia-elimination takes place to produce a large amount of acetaldehyde which can react further to form acetaldehyde, imine, pyrroles and pyridines. Therefore, ethylenimine is usually prepared in low yield by the catalytic dehydration of MEA.

Recently, however, researchers of Nippon Shokubai [155-160] have been very successful in developing a heterogenously catalysed process of MEA-dehydration over weak acid-base bifunctional catalyst. This solid catalyst contains silica as weak acidic component, alkaline earth metal oxides as weak basic component and furthermore promotors of oxides of III, IV, V or VIII group elements to control well-balanced catalyst surface properties. By using such a weak acid-base bifunctional catalyst at temperatures between 350 and 450°C and short contact time, ethylenimine can be produced from MEA in around 70 % of yield with 80-85 % of selectivity. This is a great breakthrough by applying such new bifunctional catalysts. UCC has disclosed [161] that SAPO's are also efficient catalysts for this reaction.

Nippon Shokubai has recently commercialized such a new process for manufacturing aziridine. A unit of 2000 t/a capacity is on stream since 1990. That is about one third of the worldwide demand. This new route is emphasized to have a lot of advantages compared with the conventional method. e.g. continous flow, only one reaction step, high production efficiency with high selectivity, no waste product disposal of the inevitable salt formation and all the other benefits of heterogenously catalysed processes.

5 MULTIFUNCTIONAL NOBEL METAL CATALYSTS

The connection between catalysis and wealth creation is to be seen in terms of selectivity, a smaller number of synthetic steps, simplified waste product disposal and safety considerations. Multifunctional catalysis provides us with some successful results in that development. There are quite a lot of examples in the academic and patent literature [e.g. 10, 13, 48]. However, only two impressive examples will be given.

5.1 N-alkylation of aniline derivatives

The synthesis of N-alkylated anilines is a nice example in which R. Bader and M. Rusek demonstrated a systematic catalyst engineering to build up a suitable catalyst [2, 13, 162, 163]. Usually, N,N-dialkylated aniline derivatives are synthesized by the reaction of anilines with alcohols over acidic catalysts both in liquid phase and gas phase.

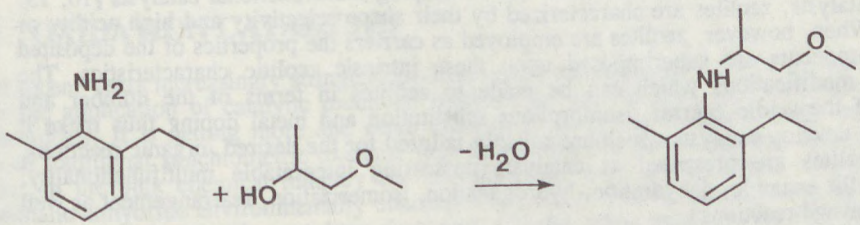

(10)

In contrary the alkylation of a sterically hindered aniline derivative with alkoxy alcohols according to equation 10 in the presence of an acid catalyst was not possible because of side reactions e.g. the cleavage of the alcohol ether. Therefore acid catalysts are not suitable for desired reactions.

Keeping in mind the reductive amination of ketones and aldehydes, respectively, a platinum/tin/calcium doped silica catalyst is developed to solve this problem. At 200°C and 1 bar H_2 98% selectivity at 60% conversion is obtained using a catalyst with the composition of Pt/Sn/Ca-SiO_2 (5 wt.-% Pt, 0.1 wt.-% Ca, Pt:Sn = 5:1). The service life is more than 1000 hours. This multifunctional catalyst combines together three catalytic steps namely dehydrogenation of the alcohol to the carbonyl compound, condensation with the aniline to form the imine and hydrogenation of the imine. It is found that the hydrogenation of the imine was the reaction rate determining step. The engineering of that multifunctional catalyst is shown in table 3.

Table 3
Catalyst engineering for N-alkylation of aniline derivative

catalyst	conversion MEA	selectivity MEA(%)	based on MIOP(%)
$Pt\text{-}SiO_2$	2	29	29
$Pt\text{-}SiO_2(Ca^{2+})$	3	65	65
$Pt,Sn\text{-}SiO_2$	14	93	89
$Pt,Sn\text{-}SiO_2(Ca^{2+})$	66	97	97

200° C, 1 bar H2, 5 wt.-%Pt, 0.1 wt.-% Ca, Pt:Sn = 5:1
MEA = 2-methyl-6-ethyl-aniline, MIOP= 1-methoxy-propanole-2

The addition of Ca improves the selectivity. Doping with Sn increases the activity and selectivity. The best result is obtained by combining both treatments. It is believed that the acid-base properties i.e. dehydration on acidic sites and dehydrogenation on basic sites in addition to the hydrogenation features are very important.

5.2 Cleavage and hydrogenation of polysaccharides

Zeolites offer also an excellent basis for developing multifunctional catalysts [10, 13, 48]. As catalysts, zeolites are characterized by their shape selectivity and high acidity or basicity. When, however, zeolites are employed as carriers the properties of the deposited active components are superimposed upon these intrinsic zeolitic characteristics. The numerous modifications which can be made to zeolites in terms of the number and strength of the acidic centres, isomorphous substitution and metal doping thus make it possible to develop catalysts which are suitably tailored for the desired organic reactions. Today, zeolites are presented as catalysts possessing integratable multifunctionality, involving, for example, dehydration, hydrogenation, isomerization, rearrangement as well as C-O cleavage reactions.

As in hydrocracking reactions [164], P.A. Jacobs et al. used the bifunctional properties of highly dispersed metal modified zeolites in the conversion of polysaccharides to polyhydric alcohols in aqueous medium under high H_2-pressure and temperature [165]. In this process, which is going to be commercialized (equation 11) the cleavage of polysaccharides by hydrolysis on the acidic sites of the zeolites and the following hydrogenation of the aldehydes and ketones, formed as intermediates on the metal component, occur simultaneously.

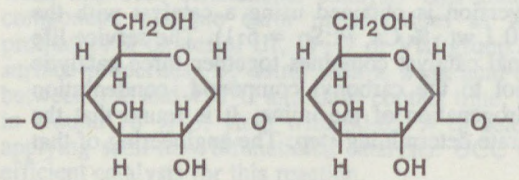

(11)

corn starch

hexitols (1) pentitols (2)

The dual function of the zeolites as carrier as well as acidic catalysts, makes this single-step process possible. Thereby, water-soluble and insoluble polysaccharides such as starch, preferably corn starch, and cellulose or disaccharides such as sucrose, maltose and lactose can be used as starting material. The supported metal is selected from Ru, Cu, Ni, Co and has to be highly dispersed on the zeolite. For example, a 25 wt.-% aqueous suspension of corn starch is converted in an autoclave at 453 K and 5.52 Mpa H_2-pressure in the presence of a Ru ion exchanged H-USTY. The product mixture obtained within 0.58 h contains 96% D-glycitol, 1% D-mannitol and 2% xylitol, i.e. 99% alditols in total. In order to achieve such excellent results, it is necessary that the dispersed Ru is capable of adsorbing 0.73 molecules of CO per Ru atom. If the dispersion CO/Ru, however, is only 0.49, then less than 20% alditols are obtained. At least, there is a dispersion of more than 0.58 requested, and furthermore acidic functions should be so, that the rate constant of hydrolysis of sucrose on the catalyst is greater than 70% of the rate constant of hydrogenation of glucose on the catalyst.

A second very noteworthy result is, that dual component catalysts can be used with great success, too. The mixture of 5% Ru/C component and H-USTY-zeolitic component in a 1:1 weight ratio gives 100% alditols including 95% hexitols and 5 % pentitols in the conversion of 30 wt.-% aqueous suspension of corn starch at 453 K and 1.79 MPa H_2-pressure within 1.5 h, that means a similar result as in the case of the doped catalyst.

This example also demonstrates, how to use natural growing renewable feedstocks as a starting material for intermediates and fine chemicals with similar carbon molecular frames. The nature is the architect of the desired C-frame. That might be one branch of future development in heterogeneous catalysis.

6 OXIDATION CATALYSTS

In recent years increasingly stringend environmental contrains have led to a great interest in the application of catalytic oxidation methods for synthesizing fine and intermediate chemicals. It is getting more and more difficult to carry out industrial scale oxidations with traditional stoichiometric oxidants such as dichromate, permanganate, osmium oxide etc. In the bulk chemical industry for manufacturing e.g. formaldehyde, ethylenoxide, phthalic anhydride environmentally unacceptable processes have been already replaced by cleaner catalytic procedures a long time ago. On the other hand, in the fine chemicals industry has been less pressure in the past to replace the traditional stoichiometric oxidants. There is currently a general trend to develop clean catalytic processes which do not generate large quantities of salts, sometimes up to 50 kg per kg desired product. Although in manufacturing bulk and fine chemicals many principles are in common, there are several basic differences which can have an important influence on process selection. Mostly, fine chemicals must be produced in the liquid phase at moderate temperatures because they are generally complex and multifunctional as well as chemo-, regio- and stereoselectivity play an important role. Therefore, in contrast to the continuous production of bulk chemicals multipurpose installations are batchwise employed for manufacturing fine chemicals. Furthermore, bulk chemicals are often produced by heterogeneously catalysed reactions in the gasphase using molecular oxygen. In contrast fine chemicals are prepared in the liquid phase in the presence of relatively expensive oxidants such as hydroperoxides, alkylperoxides and peroxycarbonic acids over homogeneous catalysts. Examples are the homogeneously catalysed ARCO-process (Mo, W, V) or the heterogeneously catalysed Shell-process (Ti/SiO_2), both for the epoxidation of olefines. Even though, among these oxidants hydrogenperoxide is so far the oxidant of choice because the by-product inevitably produced is only water.

There is currently much interest in the use of solid catalysts for oxidations in the liquid phase. Such active oxidation catalysts can be oxometal or peroxometal species

formed out of a metal such as V, Bi, Mo, W and an oxygen donor [166-170], nobel metal ions such as Pt^{2+}, Pd^{2+}, Ru^{3+} on supports reacting via a redox-mechanism, heteropolyacids, pyrochlore oxides, metal substituted zeolites with redox properties and enzyme mimics (ship in the bottle complexes). There is still the challenge to increase the number of effective oxidation catalysts, to find new process techniques and in particular to use molecular oxygen instead of the more expensive peroxides for the synthesis of fine and intermediate chemicals. A few examples are chosen in this paper.

6.1 Nobel metal on supports at oxidation catalysts

In the field of oxidation catalysts, graphite, various types of activated carbon, alumina, silica, zeolites as well as polymer resins serve as supports for active components such as Pt, Pd, Cu, Ag, Ni, Co and W [e.g. 10, 166, 167]

6.1.1 Production of 2-methyl-1,4-naphthoquinone

Various reactions for the production of hydroxybenzene are illustrative for demonstrating, how in oxidation reactions according to traditional routes the environmentally unfriendly salt production can be diminished or completely avoided. A reaction of commercial interest is the oxidation of 2-methylnaphthalene to 2-methyl-1.4-naphthoquinone (menadione) according to equation 12 [171].

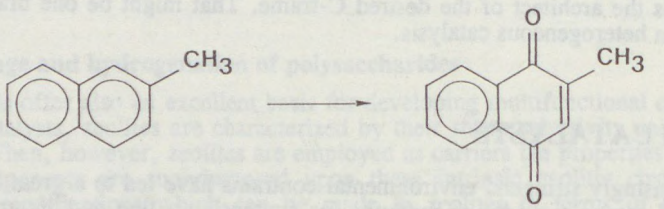

(12)

This menadione is a valuable intermediate for vitamine K. According to the conventional route this reaction was carried out with stoichiometric quantities of chromium trioxide in sulfuric acid, a quite nasty and hazardous oxidation medium. 18 kg of inorganic salt are produced as inevitable by-product per kg naphthoquinone. The new route in which the oxidation occurs in 60% aqueous H_2O_2 over palladium(II) exchanged polystyrene sulfonic acid resin as catalyst leads to around 60% yield of the desired product. Thereby the formation of inorganic salts is avoided and certainly this alternative procedure is environmentally cleaner than the classical way.

6.1.2 Production of citral

The BASF-process for manufacturing citral starting from isobutene and formaldehyde is noteworthy and an outstanding example of using molecular oxygen in the synthesis of fine and intermediate chemicals [172, 173]. Citral is a very valuable intermediate for the production of α- and ß-ionone which have importance as fragrances possessing violet smell used in perfumes and household cleaners or as building units for carotins and vitamine A. It can be isolated from fruits, however, this is not commercial because the demand is several thousand tons a year. The traditional route uses ß-pinene as starting material which is isolated from pine trees. In a five step synthesis ß-pinene is converted to citral in low yields. The drawbacks thereby are the long synthesis route with 5 reaction steps, the provision of the raw material, the problem of having chlorinated compounds and the poor overall yield.

The BASF-route starts from comparatively cheap isobutene and formaldehyde. In this condensation reaction 3-methoxy-butanol (isoprenol) is formed. A central step in this new process is the oxidation of this alcohol to the corresponding aldehyde. In general, as mentioned before, catalytic oxidations with molecular oxygen for the production of fine chemicals are not applicable. A notable exception is the gas phase, regioselective oxidation of isoprenol over a special silver supported catalyst to yield the corresponding aldehyde which is the key precursor for citral manufacture developed by BASF researchers. In a continuous flow reactor at 500°C and a residence time of about 0.001 sec, isoprenol is transformed via aldehyde and Cope-rearrangement over the silver catalyst in the presence of excess of oxygen to citral with 95% yield. In order to keep the residence time short and to avoid hot spot the reaction has to be carried out in a short fixed bed reactor [173]. This example demonstrates nicely that even fine chemicals such as citral can be produced in a commercial unit operating in the gas phase with molecular oxygen as oxidant.

6.2 Heteropolyacids as oxidation catalysts

Another promising approach to develop stable active oxidation catalysts is to incorporate high valent metal species in a stable inorganic matrix such as the anions of heterpolyacids (HPA) or the frameworks of zeolitic and non-zeolitic molecular sieves. It is believed that heteropoly anions as a large-size polyoxometalate ligand may have certain electronic and steric modifying effects on transition metal catalysis. Many heteropoly compounds which incorporate different kinds of transition metals possess several rather unique properties and have been applied recently as catalysts for various types of oxidation and reduction reactions. They are both strong Brönstedt acids and multi-electron oxidants i.e. they are potential bifunctional catalysts. The advantage of such transition metal substituted polyoxometalates can be considered as temperature- and oxygen-resistent in comparison with the metalloporphyrin complexes. The heteropolyanion constitutes a multi-electron ligand that is able to stabilize the reactive high valent oxometal species. Heteropolyacids are mostly water soluble and therefore they find use in hetergeneously as well as homogeneously catalysed oxidation processes, such as the epoxidation of olefins and the synthesis of methacrylic acid from methacroleine [46, 107].

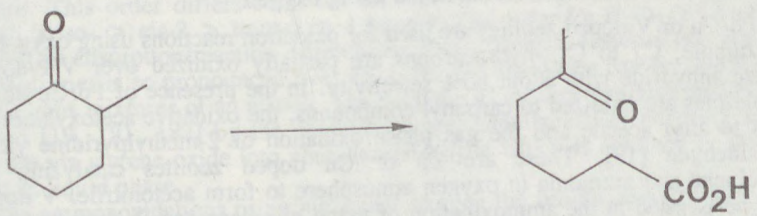

(13)

Just, two examples are given to demonstrate the oxidative properties of transition metal substituted polyoxometalates such as $H_5PMo_{10}V_2O_{40}$. This catalyst has been extensively investigated by Bregeault et al., for the oxidative cleavage of cyclic ketones [174] and of vicinal diols [175] in the presence of oxygen under mild conditions. For example, 2-methylcyclohexanone is oxidatively cleaved at room temperature in the presence of oxygen to form 5-formylpentanoic acid with 90% selectivity at 96% conversion according to equation 13. The oxidative cleavage of 1,2-cyclohexane-diol occurs at 75°C in ethanol and oxygen atmosphere and adipic acid ethylester is obtained with 90% selectivity at 62% conversion. These reactions are of practical interest and are traditionally achieved using stoichiometric oxidants such as periodates or lead tetra acetates causing the already mentioned problems which can be avoided by those HPA

catalysts. The catalytic behaviour of such oxidation catalysts might be promising for the oxidative cleavage. Because of their high reactivity and structural flexibility, catalysts based on heteropolycompounds are of considerable interest and are potentially quite promising for the synthesis of intermediate and fine chemicals.

6.3 Nobel metal pyrochlore as oxidative catalysts

Just recently, Monsanto Comp. disclosed [176] new nobel metal pyrochlore compounds having the formula $A_{2+x}B_{2-x}O_{7-y}$ wherein A is a pyrochlore structure metal cation such as Pb, Bi, Tl, Sn and B is one or more of Ru, Rh, Ir, Os and Pt and x and y are greater than or equal to 0 and less than or equal to 1.0. Such heterogeneous catalysts are used for oxidizing organic compounds with molecular oxygen at a temperature up to about 200°C. In particular, also the oxidative cleavage of vicinal diols is achieved under mild conditions. For example, at 26°C in the presence of $Pb_{2.63}Ru_{1.37}O_{6.5}$ and in basic medium (NaOH) trans-1.2-cyclohexan-diol is converted to the sodium salt of adipic acid with 90.7% yield after 17 hrs.

As in the case of the HPA's these nobel metal pyrochlore heterogeneous catalysts are very promising materials for liquid phase oxidation reactions in the presence of molecular oxygen under mild conditions.

6.4 Zeolites as oxidative catalysts

In the field of oxidation catalysis, zeolites also serve as supports for active components such as Pd, Cu, V, Fe, Zn for performing oxidation and ammoxidation reactions in the presence of elementary oxygen, and influence the product spectrum by virtue of their shape selectivity [10, 19].

As in the case of the large size polyoxometalates as heteropolyanions, high valent redox metal ions can be fixed in the stable lattice of zeolites. The direct application of such zeolites, especially Ti-containing materials, as catalysts for oxidation reactions using H_2O_2 and organic peroxides as the oxygen source has been investigated intensively during the last seven years [10, 19]

6.4.1 Oxidation and ammoxidation reactions using oxygen

Especially Pd/Cu or V doped zeolites are used for oxidation reactions using oxygen as oxidant. For example, C_4 to C_{10}-hydrocarbons are partially oxidized over V/P-doped zeolites to maleic anhydride with about 80% selectivity. In the presence of Pd/Cu doped zeolites lower olefines are oxidized to carbonyl compounds, the oxidative acetoxylation of propylene leads to allyl acetate and the gas phase oxidation of 2-methylpyridine yields pyridine-2-carbaldehyde [19]. There are Zn or Cu doped zeolites catalyzing the conversion of toluene and ammonia in oxygen atmosphere to form acetonitrile. V doped pentasilzeolites were tested in the ammoxidation of p-and m-xylene and Pt doped pentasil zeolites as well as VAPO-5 were used for the preparation of acrylnitrile via ammonolysis of propane or butane [19]. No technical application of such reactions are known so far.

6.4.2 Oxidation and ammoxidation reactions using peroxides

Already about 8 years ago C.D. Chang et al. [177] recognized the use of the pentasil zeolites ZSM-5 and ZSM-11 for the oxygen-transfer from hydrogen peroxide onto hydrocarbons. The shape selective oxidation of phenol with 40% H_2O_2 at 80°C over H-ZSM-5 (Si/Al = 128) yields hydroquinone and catechol in a ratio 99:1. The product shape selectivity is responsible for the high yield of the p-isomer. Current liquid phase, homogeneous, e.g. perchloric acid, catalysed technology for hydroquinone by the hydroxylation of phenol (as practiced by Rhone Poulenc) makes substantial quantities of coproduct, the o-isomer catechol (minimum catechol/hydroquinone ratio is about 1.5:1).

However, in recent years, the discovery of the titanium - containing MFI-type zeolite TS-1 by Enichem scientists has caused a sensation and has led to remarkable progress in the field of oxidation reactions in the presence of aqueous hydrogenperoxide as oxidant. A reasonable number of noteworthy useful oxidation reactions, can be catalysed by TS-1 [19, 178]. At least three of these reactions have found commercial interest either already in a large scale unit or in pilot plant scale.

First, the direct hydroxylation of benzene derivatives with H_2O_2 in the presence of TS-1 is possible [10, 16, 19, 179]. The oxidation of phenol to catechol and hydrochinone is already employed industrially on a large scale, 10.000 t/a in Ravenna, Italy since 1986. The ratio of the p/o-isomers is about 1, the selectivity based on phenol is 92%, based on H_2O_2 80%. A comparison of the different catalysts for this reaction shows that the homogeneous catalysts are less efficient than TS-1. The zeolite-catalysed route also appears to be more attractive than the approach via the p-di-isopropylbenzene. The precise mechanism of action of the Ti-sites in TS-1 in the aromatic hydroxylation with H_2O_2 is as yet unsolved. Isolated lattice Ti, capable of adopting a coordination number in excess of four has been mentioned [178,180] as an important feature.

Two other very promising reactions are the epoxidation of olefins and the ammoxidation of ketones to oximes. Liquid phase epoxidations of olefins and diolefins at temperatures between 0-80°C proceed with selectivities of 75-96% (based on olefin), with H_2O_2-conversion being usually quantitative [10, 19, 20, 48]. TS-1 is a highly effective catalyst for the oxidation of propylene to the industrially very important compound propylene oxide (PO) using H_2O_2 as the oxidant. In methanol at 40°C, propylene oxide is obtained with 93% selectivity at 94% H_2O_2-conversion. If the catalyst is silylated, it is possible to raise the selectivity to 98% while maintaining a comparable conversion. This synthetic route is environmentally friendly and offers a genuine alternative to the technical epoxidation process presently in operation such as the chlorohydrin (about 2 tons $CaCl_2$ per ton PO and chlorinated hydrocarbons are inevitable by-products) and hydroperoxide methods via oxygen. The principle by-product of this reaction in methanol is monomethylether which can be made as main product if the reaction is carried out above 100°C. Enichem is developing right now this process in a pilot plant.

From competition experiments the following order of conversion rate in epoxidation over TS-1 is obtained for the butenes: cis-2-butene > 1-butene > isobutene > trans-2-butene. This order differs from the sequence in homogeneous electrophilic epoxidation which is iso- > cis-2 > trans-2 > 1-butene. The order for H_2O_2/TS-1 reflects diffusion as well as adsorption/reaction differences. The difference between cis- and corresponding trans-alkenes is so pronounced over TS-1 that the cis-alkene can be selectively epoxidized in cis/trans mixtures of an alkene. The versatile Ti catalyst can also combine functions, as shown [19, 181, 182] by the epoxidation and simultaneously occuring isomerization of styrene via styrene oxide into phenylacetaldehyde which is obtained in yields higher than 90% in liquid phase.

In ammonoxidations using molecular oxygen the zeolite also acts as a support for the active components such as V, Mn, Ag, and Pt. Conversely, in the co-oxidation with H_2O_2 on TS-1 it is the zeolite alone which is active. The other noteworthy reaction which can be carried out on titanium zeolites is the liquid phase conversion of cyclohexanone with ammonia and hydrogen peroxide to cyclohexanone oxime [19, 48, 183].

The ammoxidation reaction is carried out by dispersing the Ti-catalyst in an ammonia-cyclohexanone-water-organic liquid phase and by feeding the H_2O_2 to the well-stirred slurry. Tert.-butanol/water is a very efficient solvent, even if other solvents such as benzene and toluene give similar results. Preferred reaction temperature is 80°C. Table 4 compares TS-1 as a catalyst with some other materials. Although amorphous silica supported Ti is catalytically active, TS-1 is the superior catalyst.

Table 4
Ammoxidation[a] of cyclohexanone over various catalysts

Catalyst	Ti %	$H_2O_2/C_6H_{10}C_6H_{10}$ molar		Oxime conv.	select. on H_2O_2	Yield
none	-	1.07		53.7	0.6	0.3
SiO_2 amorphous	0	1.03		55.7	1.3	0.7
Silicalite	0	1.09		59.4	0.5	0.3
H-ZSM-5	0	1.08		53.9	0.9	0.4
TiO_2/SiO_2[b]	1.5	1.04		49.3	9.3	4.4
TiO_2/SiO_2	9.8	1.06		66.8	85.9	54.0
Ti-silicalite (TS-1)	1.5	1.05		99.9	98.2	93.2

[a] In water/t-BuOH; catalyst 2 wt.-%, 80°C; $NH_3:H_2O_2$ molar 2.0; reaction time 1.5 h except for b) (5h)

It could be also demonstrated [184] that the synthesis of ketoximes in the liquid phase on titanium-silicalite is also possible starting from a secondary alcohol in the presence of O_2, H_2O_2 and NH_3. The intermediate ketone doesn't have to be isolated, i.e. several reaction steps can be combined in one. For example, cyclohexanol at about 100°C is converted to cyclohexanone oxime with up to 90% yield. The mechanism of the ketone ammoxidation is not clarified so far. The sequence might contain an NH hydroxylation step. Ti-silicalite proves also to be a useful catalyst for the synthesis of N,N-dialkylhydroxylamines by reaction of dialkylamines with H_2O_2 [185].

Nevertheless, this route avoids co-production of ammonium sulphate associated with the classical reaction cyclohexanone and the toxic hydroxylamine sulphate, and is, therefore, of industrial interest for environmental reasons. Montedipe installed a pilot plant in Bollate, Italy, to develop that environmentally clean process. In conclusion, it can be stated, that titanium-silicalite catalysts are very useful and promising tools for oxidation reactions with unfortunately still expensive H_2O_2. However, these catalysts will presumably be applied in connection with molecular oxygen in the future. Then such novel routes become industrially really competitive to the conventional methods.

6.4.3 Oxidation reactions over enzyme mimics

The discovery of the titanium zeolite TS-1 and its successful employment as a selective oxidation catalyst were a milestone in the area of zeolite catalysis in the 1980's. Recent developments in the selective partial oxidation of nonactivated alkanes on metal phthalocyanine (MPc) complexes trapped in faujasite supercages or VPI-5 and on a FePd system in zeolite A are also very promising [19, 186]. The results point to potential applications of these inorganic mimics of, for instance, the natural Fe-containing monoxygenase enzyme cytochrome P 450 which hydroxylates organic substrates with high regioselectivity. These "ship in the bottle" complexes can not leave the zeolite without destroying the framework. Zeolite catalysts of this type, in which the supercages function quasi as "reaction vessels" with molecular dimensions while imposing steric constraints. That means, in addition to the catalytically active function of the anchored homogeneous catalyst the zeolitic features are superimposed. The inorganic enzyme mimics, i.e. heterogenized homogeneous catalysts thus possess substrate-, regio- and stereoselectivity.

Accordingly they open up the possibility of steering organic reactions, such as partial oxidations, in a particular direction which is less favoured when a homogeneous catalyst is employed. With the development of this type of zeolite catalyst a further step has been taken towards "enzyme modelling". For an excellent review on this subject, the reader is referred to P. Jacobs [186].

This is another approach to heterogenize homogeneous catalysts; in contrast to the other methods no chemical linkage between the homogeneous catalyst and the carrier is involved. The fixation is the result of steric hindrance. Certainly the future will open up wide perspectives in that field of zeolitic and non-zeolitic molecular sieve catalysis.

7. HYDROGENATION CATALYSTS

Heterogeneous hydrogenation catalysts find wide spread application in chemical companies for the manufacture of fine and intermediate chemicals. Metal catalysts such as Ag, Pt, Pd, Cu, Co, Ni, Rh and supported hydrogenation catalysts such as nobel and transition metals, respectively on various carriers such as SiO_2, γ-Al_2O_3, α-Al_2O_3, zeolites, activated carbon, graphite cordierite are industrially used and there is plenty of literature about this topic. Therefore in this paper only new developments will be mentioned. For example it is also reported that Fe-phthalocyanine complexes anchored in zeolites can be used in hydrogenation reactions [187].

Another approach of "ship in the bottle"-complexes is the entrapping of transition [e.g. 188] or nobel metal clusters [e.g. 189-192]. P. Gallezot et al. [191, 192] used such catalysts for regioselective hydrogenation. In this case Pt, Ru or Rh cluster particles are encapsulated in Y-type zeolites (NaY and KY) in order to fill up the supercages. According to the authors such catalysts are much more selective for the hydrogenation of cinnamaldehyde (CAL) to cinnamyl alcohol (COL) than corresponding charcoal supported catalysts. In liquid phase CAL is converted in an autoclave under 40 bar H_2 at 333 K to form COL with 97% selectivity at 25% conversion of CAL using PtY in which the particle size is about 0.5 nm. In contrast only 33% COL are obtained over a conventional Pt/C catalyst at the same conversion of CAL. The reason is, that CAL molecules can adsorb only end-on, i.e. via the C=O group on metal clusters entrapped in the zeolite supercage (see figure 1). However, if the clusters are too small and CAL can enter the supercage then also C=C bond hydrogenation takes place.

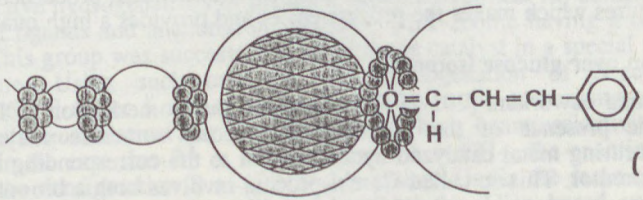

(14)

Also the conversion of 3-methylcrotonaldehyde to the corresponding unsaturated alcohol was investigated. The zeolitic chemical behaviour shows an interaction with the cluster in addition to shape selectivity or geometric considerations. Thus, the selectivity to the unsaturated alcohols could be influenced by both geometry and electronic effects. Whereas in the case of cinnamaldehyde zeolite pore size leads to higher selectivity toward the unsaturated alcohol because of the steric constraints, the mobility and orientation of 3-methylcrotonaldehyde are not hindered by the zeolite structure. However, the selectivity in this case can be increased by narrowing the pore size just by changing Na-ion with the bulkier K-ion. These investigations open up definitely a wide field of future perspectives.

8. HETEROGENIZATION OF HOMOGENEOUS CATALYSTS OR ENZYMES

The heterogeneous catalysts are usually nonuniform and difficult to characterize; the relationship between structure and performance as well as the catalytic active sites are often hard to identify. An exception in this respect might be the application of zeolitic and non-zeolitic molecular sieves with their well defined structural and chemical properties. In contrast, the homogeneous catalysts such as organometallic complexes used in solution are well-characterized and intermediates in the catalytic cycles have been identified and provide valuable insight to the reaction mechanism. These advantages of the highly selective homogeneous catalysts have been extended to solid surfaces and are combined with the processing benefits of solid catalysts including ease of separation from fluid-phase products, no corrosion and applicability at higher temperatures. The efforts already made in this respect offer great prospects for the design of new catalysts [193-195]. In this paper examples will be presented in respect to the fixation of enzymes on carriers and their benefit to the improvement of chemical processes [e.g. 196-200].

8.1 Bioprocess based acrylamide

Acrylamide is a valuable vinyl monomer which is used in polymers, paper reinforcing additives, coagulants and textile processing agents. It has been produced by hydration of acrylonitrile in the presence of copper impregnated on carriers. Nitto's researchers found and developed a new production technology which is based on a microbial enzyme catalyst immobilized by polyacrylamide gel as carrier [6, 196]. The comparison of the classical with the new technology demonstrates that the enzyme process is much simpler and needs less operation steps; the addition of any polymerization inhibitor is not necessary because the reaction can be carried out even in the presence of oxygen i.e. the O_2-removing unit can be saved. Under more than 1000 different types of microorganisms, Rhodococcus sp. N-774 was found to be the best hydratase enzyme. This is highly active and prevents the side-reactions, because only traces of nitrilase and amidase are present. At 0-5°C and pH=7.5-8.5 in a fixed bed bioreactor acrylonitrile was converted over the immobilized enzyme to acrylamide with a selectivity higher than 99.9%. The conversion yields to more than 99.9%, too. The concentration of the aqueous acrylamide at the reactor outlet is more than 20%, up to 50%. Furthermore, Fe^{2+} ions are very effective to increase the activity of the hydratase enzyme in the microorganism. Nitto is using its process in Japan since 1985 and has a capacity of 20.000 tons/a. This is the first enzymatic process applied to a large intermediate chemical proceeded specifically at lower temperatures which makes the process easier and provides a high quality product.

8.2 Isomerization over glucose isomerase

H. van Bekkum and coworkers [201-203] investigated the isomerization of D-glucose to D-fructose in the presence of the immobilized glucose isomerase enzyme and the simultaneously occuring metal catalyzed hydrogenation to the corresponding alcohols, D-glucitol and D-mannitol. This so called Combi-process involves both a bio- and a chemo-catalyst. D-glucose isomerase is immobilized on silica in combination with Cu doped silica catalyst, as most favoured one. For high yields of D-mannitol which is used in sugar-free chewing gums and for pharmaceutical purposes the requirements to the catalyst systems are fast isomerization in order to achieve high D-fructose level, selective hydrogenation of D-fructose and minimum mutual interference as well as maximum activity of the two catalysts. The immobilization of the enzyme prevents assumedly serious interaction of the two catalysts. In water, at pH ~ 7 and 70°C over the chosen catalyst combination yields of 62-66 % are obtained for D-mannitol.

Also this example show the benefit of the enzyme immobilization and of tailored catalyst combination.

9. ENANTIOSELECTIVE CATALYSTS

Enantiomers show different physiological effects. Because of that impact, a wide spread development in the area of asymmetric reactions is going on since the last twenty years [204-208]. The cleavage of racemic mixtures to pure enantiomers was in the beginning. In addition to that chemists are looking for methods and guidelines to obtain enantioselective reactions. The attractive application of solid chiral catalysts for the enantio-selective synthesis is disclosed in the excellent review article of H.U. Blaser, carrying all the various aspects of heterogeneous enantioselective catalysis [205, 208 and the cited references there]. Such solid catalysts are interesting tools to prepare very valuable optically active products from prochiral reactants.

In this paper only the aspect of chirally modified clays and zeolites is considered. B.M. Choudary et al. [209] were successful in using a titanium pillared montmorillonite as heterogeneous catalyst for the Sharpless-epoxidation of allylic alcohols.

Zeolites became involved in the discussion because of the fact that this Sharpless-epoxidation can be improved by the addition of molecular sieves such as 3 Å or 4 Å [210] which might function as water scavanger and when the material scientists realized that zeolite beta should have chiral centers at the interconnections of the channels. The chirality of the zeolite beta includes both sites - right hand and left hand sites - likewise. Up to date, it was not possible to synthesize a zeolite beta with an excess of one site to enable us to carry out enantioselective acid catalysed reactions.

Therefore another approach might be ingenious and helpful. Keeping in mind the idea of "ships in the bottle", first attempts have been made to use optically active amines in Pt- or Rh loaded ZSM-5 [211] as well as Rh-complexes with N-based chiral ligand [212] entrapped in USY-zeolite for asymmetric reactions such as enantioselective hydrogenation or hydroformylation.

R.M. Dessau [211] prepared Pt-loaded H-ZSM-5 with reduced acidity and neutralized these acidic sites by contacting with optically active S-(-)-alpha-methylbenzylamine. This catalyst was used for enantioselective hydrogenation of 2-phenylbutene to the optically active 2-phenylbutane as well as for the conversion of acetylphenone under hydrogenation conditions to form optically active 1-phenyl ethanol. Furthermore, a Rh-loaded H-ZSM-5 was treated with the same amine and the hydroformylation of alpha-methylstyrene was carried out at 100°C in an autoclave over this catalyst to yield the corresponding optically active aldehyde. Unfortunately, no exact yields and characteristic datas were disclosed in that patent.

More recently, A. Corma and his coworkers [212] published very stimulating results of enantioselective hydrogenations of prochiral alkenes over new Rh-complexes containing N-based chiral ligands and anchored on modified USY-zeolite having a certain pore size distribution. This group was successful to prepare the catalyst in a special manner starting from L-proline. Using such catalysts, the hydrogenation of N-acylphenylalanine derivatives at 65°C under 5 atm of hydrogen results in the corresponding hydrogenated compounds with quantitative conversion and with high enantioselectivity according to equation 14. In the case that $R^1 = R^2 = H$ and $R^3 = CH_3$, the enantiomeric excess is 97,9 % with the configuration R at 100 % conversion. Under the same conditions in the presence of homogeneous catalyst 84.1 % and of the silica based catalyst 88.0 %, respectively, are obtained. The results obtained are very promising and are giving rise for future developments in this interesting field of enantioselective reactions in the presence of zeolitic catalysts.

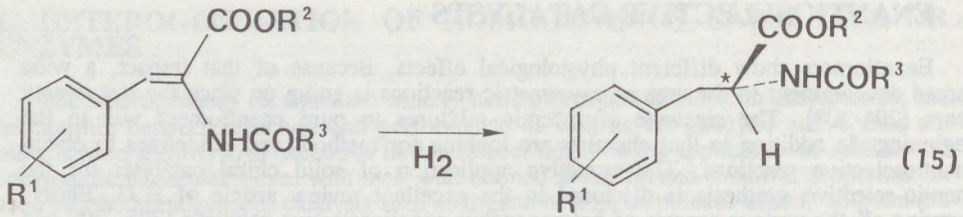

(15)

10 CONCLUSION

In summarizing and analysing the presented facts, and based on the open literature, it is possible to make the following conclusions:

1. There are quite a numerous number of heterogeneous catalysts with their various properties which can be successfully used in the synthesis of fine and intermediate chemicals. A broad and very impressive range of acidic and basic catalysts is already available having all levels of properties between super acid and super base. Furthermore, these materials may have shape selective behaviour or not. In the field of acid and base catalysis there is not such a great need for new materials; rather there is an encouragement to use present catalyst systems and to improve them by thorough and intelligent modifications for the required reactions. The exception is that there is still a necessity to find superlarge pore sized molecular sieves with high thermostability and to develop shape selective catalysts based on such powders. The principles of shape selective behaviour should be kept in mind to control the reaction paths more selective and more efficient.

   Also, the possibility to prepare bifunctional catalysts with combined acidic and basic sites maybe also in addition to that with shape selective properties should be explored because these are gaining in importance and there are already intriguing examples.

   Concerning oxidation catalysts, there is also a great number of materials which can be employed. However, concerning oxidation reactions for manufacturing fine chemicals and intermediates, the use of cheap and environmentally friendly molecular oxygen instead of peroxides will be one of the major targets. Furthermore, whereas in commodity chemistry the oxidative activation of alkanes is of great interest, there is a trend in fine chemical synthesis to use renewable feedstocks such as polysaccharides, e.g. the production of new biodegradating surfactants. For doing these two kinds of investigations, the development of new catalysts have to have a high position in the priority list. In particular heteropolyacid-based catalyst have a promising future as unique selective oxidation catalysts in organic synthesis.

   With respect to hydrogenation and dehydrogenation catalysts one has to constitute that this is the oldest field in heterogeneous catalysis and the knowledge therein is tremendous. Nevertheless, for certain reactions new highly selective catalysts need to be developed.

   There is no doubt about a great need and an extremely ambitious and exciting challenge to find guidelines in the development of chiral heterogeneous catalysts to carry out enantioselective reactions.

That is also true for developing multifunctional catalysts in order to shorten the reaction paths. The development of materials having combined properties as in the case of heteropolyacids with their acidic and oxidative features, seems to have a promising future. In this respect also molecular sieve based catalysts having multifunctional properties should be prepared; molecular sieves can be used as carriers for catalytically active components such as transition and nobel metals. Then in addition to the catalytic behaviour of those components the intrinsic acidic or basic or redox properties of zeolites combined with shape selective features are still present. Such multifunctional catalysts can help to combine several catalytic steps and tailor them optimally to one another. And this will certainly make chemical processes more cost-efficient and will help to minimize the formation of by-products which are produced in the conventional multi-steps synthesis of the dowstream chemicals.

Another noteworthy, economically attractive, very exciting and more selective approach in the synthesis of fine and intermediate chemicals is the immobilization of enzymes. The first reported examples, in which enzymes are firmly anchored to its solid supports such as ceramic materials coated with a special polymer as well as resins and polymers itself, are very promising. Thereby, an advantage is that the ceramic-supported enzymes last longer than the natural enzyme.

The heterogenization of homogeneous highly selective catalysts is another great and challenging topic as it is since a long time. However, "the ship in the bottle" - concept is bringing new ideas in that discussion.

New heterogeneous catalyst systems for the synthesis of fine and intermediate chemicals have been disclosed in recent years. For example, metallic glasses may be useful for oxidation and hydrogenation reactions [213-215] and the pyrochlores for oxidation reaction [176].

2. In respect to the starting materials for the synthesis of fine and intermediate chemicals the C_2-C_4-olefines, butadien and acetylene as well as the aromatics benzene and toluene are still the original base. However, the catalyst scientist should take a look at the renewable raw materials more than they have done before. In the German chemical industry about 10 % of the overall used raw materials are naturally growing compounds. That percentage might be boosted in the long range. The catalytical reactions on the olefinic bonds of fatty acids might be promising aspects for new inexpensive chemical products. One of these is based on natural fats and oils. Biodegradating tensides can be readily produced out of easily available fatty alcohols as well as biodegradating surfactants out of corresponding fatty amines. Furthermore carbohydrates are renewable and readily biodegraded raw materials for the synthesis of highly valuable compounds. The chemical industry should use more intensively the growing natural feedstock, whose compounds have already preformed the desired C-framework. The nature should be the architect of necessary chemical building units.

3. What are the future needed products of fine and intermediate chemical industry? That is a hard and more philosophic question. Certainly the potential impact of heterogeneous catalysis on new products will be in the synthesis of pharmaceuticals and biologically derived products. People say that the 1990's will be the "decade of chirality", that means enantioselective reactions are the most exciting and challenging prospect in near future catalysis.

Introduction of new feedstock and the demand for new products, both stress the influence of the environment on catalysis of the 1990's.

4. Also there is a necessity for a change in the equipment for the production of fine chemicals. The chemical industry is used to carry out such reactions batchwise in a vessel, mostly in a homogeneously catalyzed way. However, with the new perspectives in utilizing heterogeneous catalysts for such kind of processes there is a need for flexible fixed-bed multi-purpose plants in which also small amounts of fine chemicals can be produced. That means design of a new generation of cost-competitive small multi-purpose production units and a new production concept. The redesign of chemical processes to minimize the generation of pollutants is a topic which has to be worked on, too.

   In particular the production of intermediate chemicals and sometimes of fine chemicals, too, occurs in the gas phase at higher temperature, however, for the synthesis of really fine chemicals generally milder operating conditions in chemical plants are requested. In this respect, enzymes and heterogenized enzymes are particularly attractive.

   Furthermore, catalyst development should not be considered without the simultaneous new reactor design as shown in the citral process of BASF; catalyst and process design are a single unit. It is a common and easily arranged practice to improve an existing process by simply replacing the catalyst which is being used with a more efficient catalyst. However, in the case where the employment of a new catalyst system requires also a new process concept, possibly including also a new reactor design and its development to produce the same desired endproduct then there arise some innovatively unfriendly constraints. In addition to the chemical engineering problems and the necessary administrative approvals, the economic assessment of the new process is in western chemical industry based on the fact, that all of the new investment is put on the price structure of the product which has to be compared with the price of the product produced in the paid off amortized process plant. For example that is the case in transfering a homogeneously to a heterogeneously catalyzed reaction. This commonly practiced "standard" investment calculation should be changed to allow more innovation. And this should be practically possible for fine and intermediate chemicals' manufacturing, where the capital investment costs are substantially lower than these of commodity chemicals where the initial capital investments are enormous. In the field of reactor design new aspects such as catalytic distillation, membrane reactor and membrane technology are in discussion.

5. Although catalysis research is still dominated by experimental and empirical studies, theoretical efforts and the use of computers are becoming increasingly important. Computer aided catalyst design opens new vistas in not too distant future. Some of the appropriate techniques are already being applied to "zeolite"-related catalysis. The computer images allow us to model complicated processes and to visualize them in graphic form to extend our range of ideas in the synthesis of fine and intermediate chemicals.

6. Concerning social political aspects heterogeneous catalysis has to play an increasing role in environmental protection because the public is more and more concerned with chemicals effecting pollution and the governmental regulations become more and more stringent. Therefore, in catalytic technology the targets are replacing the homogeneous Lewis acids and bases as well as Brönstedt acids and bases by heterogeneous systems in order to avoid salt-formation in the working up steps, separation and corrosion problems etc. Furthermore, the desire to raise product yield and to lower process costs which was always the driving force for catalyst development has to be reconsidered in our days. This attitude of chemical

industry should be changed. The development of highly selective catalysts and the achievement to carry out reactions with no or only a little formation of undesirable and sometimes toxic by-products should have the highest priority, even in spite of eventually very low conversion of around 10 % and the thereby resulting requirement of energy intensive recyclization. That will benefit to environmental protection in respect to get rid of the by-products and to energy-saving in the separation. Also, in this respect it should be not a good idea to build a plant at a place in countries, just because they have less severe regulations for environmental protection. We have only one world. The emphasis on economic and environmental necessity to minimize intermediate products and species should be the goal whereever it is possible.

In respect to environmental impact also the replacement of hazardous transition metals e.g. Ni, Co, Cr, in particular in oxidation or hydrogenation catalysts by environmentally friendlier novel metals should be a challenging topic, too.

The economic impact of environmental considerations plays also a very important role in defining the development of new technology. Government enforcement of ever severer environmental regulations will in the future make the operation of older, although paid off and amortized plants, less attractive because they will not be able to meet the newer environmental constraints. On the contrary, new plants engineered for higher efficiency and the use of newer and environmentally friendlier catalysts and process feeds, will become more and more attractive to be built and to be operated because they will be raw material and energy more efficient and will at the same time meet more the stringent environmental requirements. Unfortunately, the outdated cost calculation practices still stand in the way of progress but is only a matter of time that this short-sightness will be understood.

7. As a result of the foregoing, the assessment that catalysis in chemical industry is mature and therefore research and development is not necessary or less demanding than in other industries is superficial. Even more, if one realizes that each reaction needs its own efficient catalyst to meet all the technical and environmental requirements. Each problem needs its own solution; there is no general recipe. Maybe the maturity of catalyst development is correct for bulk chemicals, however, certainly not for fine chemicals. Even in the field of bulk chemicals there is some doubt about such a statement.

8. Based on the open literature and analyzing the presented facts, in the commercial application of new acid, new base as well as of new acid-base bifunctional catalysts and of oxidation catalysts based on heteropolyacids in the field of fine and intermediate chemicals the Japanese companies seem to be ahead.

In this respect, it appears that the Japanese industry is beginning to adopt the newer and more innovative accounting principles and thus stimulating new process innovation particularly in the fine chemicals' industry. In Europe and the US the companies seem to be somewhat behind in adopting the newer approaches which stimulate not only research but also modern and profitable technology. Also, it seems that the Japanese industry is able to pick up very fast new innovative developments and results offered by universities and other public research institutions and to apply them immediately.

Furthermore, long range and not only bottom-line thinking seems to be required for an innovative chemistry in the field of fine and intermediate chemicals. Apparently, the Japanese research might be done on a longer range basis and not at the bottom-line. It appears, that they are not be quite as much concerned with the immediate pay back of research investment as the industrialized western countries.

Also, it appears that the Japanese commercialize the processes at a much earlier stage than in western companies. This gives them the advantages of being the first in an area, although they are aware of the higher risk according to the well known

risk/reward ratio. The Japanese seem to act faster, maybe also because of less administrative inconveniences.

In general, chemical industry should pay more attention to long term research and to develop more substantive relations with academic people.

9. Economic reports about commodity catalysts for producing bulk chemicals for petroleum processing and refining are very much concerned with MTBE, alkylated gasoline, hydrogen-demand, sulfur reduction etc.. However, there is a great lack of information in the field of fine and intermediate chemicals. Certainly the chemical companies do have such information which they do not wish to announce them in public. Therefore, for academic researchers who are going to work in this area it will be hard to find guidelines for their research.

In spite of all what is said, the task of the industrial chemist is to develop an environmentally clean industrial synthesis in which the endproducts are so much more valuable than the starting materials that they not only justify the production costs, but also provide an acceptable profit. It is eagerly awaited what will happen in the near, not too distant future as well as in the long term future in respect to heterogeneous catalysis for fine and intermediate chemicals in order to maintain or to improve the quality of our life and to keep clean our environment.

REFERENCES

1 J.F. Roth in S. Yoshida, N. Takezawa and T. Ono (eds.) Catalytic Science and Technology, Vol. 1, Kodansha, Tokyo, 1990, p. 3
2 R. Bader, 8th Basel-Meeting for Chemical Technique, Oct. 21, 1987
3 S. Fujie, T. Jizuka and K. Tanabe, Proceedings of 56th Catalyst Symposium, 1985, Kanazuwa, p. 94
4 Z. Chen, T. Jizuka and K. Tanabe, Chem. Lett. (1984) 1085
5 T. Jizuka, K. Ogasawara and K. Tanabe, Bull. Chem. Soc. Jpn. 56 (1983) 2927
6 T. Jizuka, S. Fujie. T. Ushikubo, Z. Chen and K. Tanabe, App. Catal.28 (1986) 1
7 K. Tanabe, Material Chem. Phys. 17 (1987) 217
8 Y. Higashio and K. Takahashi, EP 0215567 (July 4, 1990) Sumitomo Chem. Co.
9 P.B. Venuto and P.S. Landis, Adv. Catal. 18 (1968) 259
10 W.F. Hoelderich, Stud. Surf. Sci. Catal. 49A (1989) 69
11 W.F. Hoelderich in K. Tanabe et al. (Eds.); "Acid-Base Catalysis", Proceedings of the Symposium Acid-Base Catalysis, Sapporo, Japan, 1988, Kodansha Ltd., 1989, p.1
12 H. van Bekkum and H.W. Kouwenhoven, Stud. Surf. Sci. Catal. 41 (1988) 45
13 W.F. Hoelderich, Stud. Surf. Sci. Catal. 41 (1988) 83
14 W.F. Hoelderich, M. Hesse and F. Näumann, Angew. Chem. 27 (1988) 226
15 W.F. Hoelderich, Pure and Appl. Chem. 58 (1986) 1383
16 R.F. Parton, J.M. Jacobs, D.R. Huybrechts and P.A. Jacobs, Stud. Surf. Sci. Catal. 46 (1989) 163
17 W.F. Hoelderich, Stud. Surf. Sci. Catal. 46 (1989) 193
18 W.F. Hoelderich, see in [1], p. 31
19 W.F. Hoelderich and H. van Bekkum, Stud. Surf. Sci. Catal, 58 (1991) 631
20 W.F. Hoelderich, Stud. Surf. Sci. Catal. 67 (1991) 257
21 M.E. Davis, C. Montes and J.M Garces, in M. Occelli and H. Robson (Eds.), Zeolite Synthesis, Vol. 398, ACS Symp. Ser., 1989, ACS, Washington, DC, USA, p. 291

22 M.E. Davis, C. Saldarriaga, C. Montes, J.M. Garces and C. Crowder, Zeolites 8 (1988) 362
23 M.E. Davis, C. Montes, P.E. Hathaway and J.M. Garces, Stud. Surf. Sci. Catal. 49A (1989) 199
24 E.G. Derouane, L. Maistriau, Z. Gabelica, A. Tuel, J.B. Nagy and R. von Ballmoos, Appl. Catal. 51 (1989) L 13.
25 E.G. Derouane and R. von Ballmoos EP 0146 389 (1983) Mobil Oil Corp.
26 H. Kessler et al., Mat. Res. Soc. Symp. Proc. Vol. 233, 1991
27 J.L. Guth, NATO-Workshop, "Zeolite Microporous Solids: Synthesis, Structure and Reactivity", Lisboa, Portugal, 1991, NATO ASI Series C, Vol. 352. p. 49
28 J.S. Beck, C.T. Chu, I.D. Johnson, C.T. Kresge, M.E. Leonowicz, W.J. Roth and J.C. Vartuli WO 91/11390 (Aug. 8, 1991) Mobil Oil Corp.
29 M. Thielen, M. Geelen and P.A. Jacobs in Proceedings of the International Symposium on Zeolite Catalysis, Siofok, Hungary, 1985, p.1
30 J. Weitkamp, H. Beyer, G. Borbely, V. Cortes-Corberan and S. Ernst, Chem.-Ing.-Tech. 58 (1986) 969
31 J.C. Janson, E. Biron and H. van Bekkum, Stud. Surf. Sci. Catal. 37 (1988) 133
32 S.M. Csiscery, ACS Monograph 171 (1976) 680
33 S.M. Csiscery, Zeolites 4 (1984) 202
34 S.M. Csiscery, 4th Symp. on Zeolite Science and Technology of Japan, Tokyo, Nov. 1988
35 W.O. Haag, R.M. Lago and P.B. Weisz, Faraday Disc. 72 (1982) 317
36 N.Y. Chen, ACS Symposium Series Vol. 368, 29 (1988) 468
37 S.M. Csiscery, J. Catal. 108 (1987) 433
38 P.A. Jacobs and J.A. Martens, Stud. Surf. Sci. Catal. 28 (1986) 23
39 E.G. Derouane, J. Catal. 100 (1986) 541
40 P. Ratnasamy, Indian. J. Technol. 25 (1987) 653
41 R. Szostak, Stud. Surf. Sci. Catal. 58 (1991) 153
42 R.P. Townsend, Stud. Surf. Sci. Catal. 58 (1991) 359
43 D. Barthomeuf, Mat. Chem. Phys. 17 (1987) 49
44 D. Barthomeuf, G. Coudurier and J.C. Vedrine, Mat. Chem. Phys. 18 (1988) 553
45 A. Auroux and A. Gervasini, J. Phys. Chem. 94 (1990) 6371
46 M. Misono and N. Nojiri, Appl. Catal. 64 (1990) 1
47 W.S. Fong, SRI-International, PEP Review No. 89-3-4, 1991
48 W.F. Hoelderich see in [27], p. 579-599
49 G. Schmitz, J. Chim. Phys-Chim. Biol. 77 (1980) 393
50 I. Mochida, A. Yasutake and H. Fujitsu, J. Catal. 82 (1983) 313
51 M. Kohono, Chemistry and Industry (Jp) 41 (1988) 936
52 M. Chono and H. Ishida, EP 0113 116 (July 11, 1984) Asahi Kasei Comp.
53 M. Tojo and Y. Fukuoka, EP 0162 475 (Nov. 27, 1985) Asahi Kasei Comp.
54 O. Mitsui and K. Yohei, DE 34 41 072 (May 23, 1985) Asahi Kasei Comp.
55 T. Shirafuji, K. Sakai and K. Hirose, EP 0224 116 (June 3, 1987) Sumitomo
56 T. Shirafuji and I. Kawata EP 0227 931 (July 8, 1987) Sumitomo Chem. Co.
57 G. Blanchard, M. Costantini and J. P. Lecomte, EP 0341 163 (Nov. 11, 1989) Rhone-Poulenc
58 K. Iwayama, Y. Magatani and K. Tada EP 0278 729 (Feb. 09, 1987); JO 1254633; JP 62-15049; JP 63-93738; Toray Ind. Inc.
59 S. Okazaki and H. Jouhouji, Bull. Chem. Soc. Jpn. 59 (1986) 1931
60 D. Feitler, W. Schimming and H. Wetsbein, EP 0131 887 (Jan. 23, 1985) Nepera
61 M. Taramasso, G. Manara, V. Fattore and B. Notari, US 4.656.016 (Apr.7, 1987), Snamprogetti, S.p.A.
62 K. Honna, M. Sugimoto, N. Shimizu and K. Kurisaki, Chem. Lett. (1986) 315
63 G.S. Lee, J.J. May, S.C. Rocke and J.M. Garces, Catal. Lett. 2(1989) 243

64 G.S. Lee, K.A. Burdett and J.J. Maj US 4.996.353 (May 16, 1989) Dow Chem. Co.
65 J.D. Fellmann, R.J. Saxton, P.R. Wentrcek, E.G. Derouane, P. Massiani and CNRS, WO91/03443 (March 21, 1991) Catalytica
66 D.R. Corbin, E. Kumpinsky and A. Vidal, EP 0316 133 (May 17, 1989) Du Pont
67 J. Weitkamp, M. Neuber, W. Höltmann, G. Collin and H. Spengler EP 0280 055 (Aug. 31, 1988) Rütgerswerke
68 C.F. Payn, Speciality Zeolites in Catalysis 1992-2000, Catalyst Consultants Inc. 1992
69 M. Deeba, M.E. Ford and T.A. Johnson, Stud. Surf. Sci. Catal. 38 (1987) 221
70 M. Deeba and M.E. Ford, J. Org. Chem. 53 (1988) 4594
71 M. Deeba, M.E. Ford and T.A. Johnson, J. Chem. Soc. Chem. Commun. 8 (1987) 562
72 V. Taglieber, W.F. Hoelderich, R. Kummer, W.D. Mross and E. Saladin EP 0133 938 and EP 0132 736 (July 27, 1983) BASF AG
73 W.F. Hoelderich, V. Taglieber, H. Pohl, R. Kummer and K.G. Baur, DE 36342747 (July 23, 1987) BASF AG
74 E.M. Flanigan, R.L. Patton and S.T. Wilson, Stud. Surf. Sci. Catal. 37 (1987) 13
75 E.M. Flanigan, B.M. Lok, R.L. Patton and S.T. Wilson, in Y. Murakami et al. (Eds), New Developments in Zeolite Science and Technology, Elsevier, New York, 1986, pp. 103
76 R. Szostak, T.L. Thomas and D.C. Sieh, Catal. Lett. 2 (1989) 63
77 B.M. Lok, B.K. Marcus, L.D. Vail, E.M. Flanigan, R.L. Patton and S.T. Wilson EP 0159 624 (Oct. 30, 1985) UOP
78 K.D. Olson, EP 0251 168 (Jan. 07, 1988), UCC
79 W.F. Hoelderich, N. Goetz and L. Hupfer, DE 3 804 162 (Feb. 11, 1988) BASF AG
80 W.F. Hoelderich, D. Koeffer and W. Bertleff, DE 3 720 850 (July 24, 1987) BASF AG
81 W.F. Hoelderich, F. Merger and H. Lermer, EP 0291 807 (Nov. 23, 1988) BASF AG
82 W. Mackenroth, W.F. Hoelderich, R. Becker and W. Seufert, EP 0305 913 (March 08, 1989) BASF AG
83 W.F. Hoelderich, L. Hupfer and K. Schneider, DE 3 726 126 (Aug. 06, 1987) BASF AG
84 H. van Bekkum et al., see in [27] Poster
85 A. Miyamoto, Y. Iwamoto, H. Matsuda and T. Inui, Stud. Surf. Sci. Catal. 49 (1989) 1233
86 K.D. Olson and S.W. Kaiser, EP 0324 267 (Dec. 23, 1987) UOP
87 K.D. Olson, S.W. Kaiser, W.T. Reichle, A.R. Doumouy and D.J. Schreck, WO 89/05810 (Dec. 18, 1987) UCC
88 K.D. Olson and S.W. Kaiser, WO 89/06229 (Dec. 18, 1987) UCC
89 R.F. Parton, L. Uytterhowen and P.A. Jacobs, Stud. Surf. Sci. Catal. 59 (1991) 395
90 R.J. Pellet, G.N. Long and J.A. Rabo, EP 0249 913 (Dec. 23, 1987) UCC
91 K. Tanabe, "Solid Acids and Bases", Academic Press, New York, 1970
92 J.B. Moffat, Catal. Rev.-Sci. Eng. 18 (1978) 199
93 A. Tada, see in [11] p. 439
94 A. Tada, Mat. Chem. Phys. 17 (1987) 145
95 A. Ginestra and P. Patrono, ibid 17 (1987) 161
96 K. Segawa, S. Nakata and S. Asaoka, ibid. 17 (1987) 181
97 J.N. Armor, Appl. Catal. in press
98 W.F. Hoelderich, Stud. Surf. Sci. Catal. 67 (1991) 257

99 W.F. Hoelderich, F. Merger and R. Fischer, EP 0199 210 (Oct. 29, 1986) BASF AG
100 W.F. Hoelderich and F. Merger, DE 3715 755 (May 12, 1987) BASF AG
101 F. Merger, W.F. Hoelderich, J. Frank, T. Dockner and M. Sauerwald DE 3826 303 (Aug. 03, 1988) BASF AG
102 M.T. Pope, Heteropoly and Isopoly Oxometalates, Springer-Verlag 1983
103 Y. Onoe, Kagaku Kokyo 26 (1975) 355
104 T. Yamada, Jpn. Chem. Ind. Assoc. Monthly 40 (1987) 12
105 A. Aoshima, Catalyst (Jp.) 29 (1987) 378
106 A. Aoshima and S. Tonomaru, Kagaku Kokyo 40 (1987), 763
107 M. Misono, Catal. Rev.-Sci. Eng. 29 (1987) 269
108 Y. Izumi, N. Natsume, H. Takamine, I. Tamaoki and U. Urabe, Bull. Chem. Soc. Jap. 62 (1989) 2159
109 T. Yamaguchi, A. Mitoh and K. Tanabe, Chem. Lett. (1982) 1229
110 K. Kinomura and T. Sakakibara, 56th Nat'l Meeting of the Chemical Society of Japan 1988, personal information by Y. Izumi
111 T. Yamaguchi, T. Jim and K. Tanabe, J. Phy. Chem. 90 (1986) 3148 and 4794
112 T. Yamaguchi, T. Jin, T. Ishida and K. Tanabe, Mat. Chem. Phys. 17 (1987) 3
113 K. Tanabe and T. Yamaguchi, Stud. Surf. Sci. Catal. 44 (1989) 99
114 K. Arata, Advances in Catal. 37 (1990) 165
115 R. Burch, Pillared clays, Catalysis Today Vol. 2, Nos 2/3 (1988)
116 S. Yamanak, T. Nishihara, M. Hattori and Y. Suzuk, Mat. Chem. Phys. 17 (1987) 87
117 D.E.W. Vaughan, ACS Symp. Series 368, Cap. 19 (1988) 308
118 K. Tanabe "Advances in Acidic and Basic Materials Part 1", Mat. Chem. Phys., Elsevier, Lausanne, 1987, Vol. 17
119 A. Mitschker, R. Wagner and P.M. Lange, Stud. Surf. Sci. Catal. 41 (1988) 61
120 H. Pines and W.M. Stalick "Base-Catalyzed Reaction of Hydrocarbons and Related Compounds "Academic Press, New York, 1977
121 H. Pines "The Chemistry of Catalytic Hydrocarbon Conversions" Academic Press, New York, 1981, p. 123
122 H. Hattori, Mater. Chem. Phys. 18 (1988) 533
123 General Electric, US 3.446.856 (1964)
124 R. Ohnishi and K. Tanabe, Chem. Lett. (1974) 207
125 K. Shimazu, H. Hattori and K. Tanabe, J. Catal. 48 (1977) 302
126 K. Arata, J.O. Bledsoe and K. Tanabe, J. Org. Chem. 43 (1978) 1660
127 H. Hattori, K. Tanabe, K. Hayano, H. Shirahama and T. Matsumoto, Chem. Lett. (1979) 133
128 A. Hattori, H. Hattori and K. Tanabe, J. Catal. 65 (1980) 245
129 H. Matsuhashi and H. Hattori, J. Catal. 85 (1984) 457
130 H. Matsuhashi, H. Hattori and K. Tanabe, Chem. Lett. (1981) 341
131 Y. Kakumo, H. Hattori and K. Tanabe, Chem. Lett. (1984) 649
132 Y. Kakuno, H. Hattori and K. Tanabe, Chem. Lett. (1982) 2015
133 Y. Kakuno and H. Hattori, J. Catal. 85 (1984) 509
134 G. Suzukamo, M. Tukao, T. Hibi, K. Tanaka and K. Chikaishi' see in [11]
135 G. Suzukamo, M. Fukao and M. Minobe, Chem. Lett. (1987) 585
136 G. Suzukamo, Catalyst (Shokubai) 32 (1990) 230
137 R.P. Townsend, Stud. Surf. Sci. Catal. 58 (1991) 359
138 L.R. Martens, P.J. Grobet, W.J. Vermeiren and P.A. Jacobs, Stud. Surf. Sci. Catal. 28 (1986) 935
139 L.R. Martens, W.J. Vermeiren, D.R. Huybrechts, P.J. Grobet and P.A. Jacobs, in W.J. Phillips et al. (Eds.), Proc. 9th Int. Congr. Catal. Calgary, Canada (1988), Chem. Inst. Canada, Ottawa (1988) Vol. 1, 420
140 L.R. Martens, P.J. Grobet and P.A. Jacobs, Nature 315 (1985) 568

141 L.R. Martens, P.J. Grobet, W.J. Vermeiren and P.A. Jacobs, Stud. Surf. Sci. Catal. 31 (1987) 531
142 P.A. Jacobs, Stud. Surf. Sci. Catal. 29 (1986) 357
143 J.A. Rabo, C.L. Angell, P.H. Kasai and V. Schomacker, Disc. Faraday Soc. 41 (1966) 328
144 W.F. Hoelderich, F. Merger, W.D. Mross and G. Fouquet, EP 0162 385 (Nov. 27, 1985) BASF AG
145 W.F. Hoelderich, P. Hettinger and F. Merger, EP 0219 042 (Apr. 22, 1987) BASF AG
146 R.M. Dessau, US 4.658.045 (Apr. 14, 1987) Mobil Oil Corp.
147 R.M. Dessau, Poster 214 in J.C. Jansen et al. (Eds.): "Zeolites for the Nineties", 8th IZC, Amsterdam, The Netherlands, July 1989
148 B. Xu, T. Yamaguchi and K. Tanabe, Chem. Lett. (1988) 281
149 K. Arata, J.O. Bledsoe and K. Tanabe, J. Org. Chem. 43 (1978) 1660
150 K. Tanabe, Materials Chem. Phys. 13 (1985) 347
151 T. Yamaguchi, H. Sasaki and K. Tanabe, Chem. Lett. (1973) 101
152 K. Takahashi, M. Shibazaki and M. Matsushita, Bull. Chem. Soc. Japan 62 (1989) 2353
153 T. Maki and T. Yokoyama, Chemistry & Industry (Japan) 42 (1989) 1042
154 Ullmann's Encyclopedia of Industrial Chemistry VCH, Weinheim, Germany 1985, Vol. A3, p. 239
155 M. Ueshima and Y. Shimasaki, Chemistry & Industry (Japan) 43 (1990) 349
156 Y.H. Hino, Y. Shimasaki and M. Ueshima EP 0227 461 (July 01, 1987) Nippon Shokubai
157 Y.H. Hino, Y. Shimasaki, M. Keshima, H. Tunoki and H. Yano, EP 0228 898 (July 15, 1987) Nippon Shokubai
158 Y. Shimasaki, M. Keshima, H. Tunoki and K. Ariyoshi, EP 0230 776 (Ang. 05, 1987) Nippon Shokubai
159 M. Ueshima and H. Tsuneki, see in [1] p. 357
160 M. Ueshima, Y. Shimasaki, Y. Hino and H. Tsumeki, see in [11], p. 41
161 K. Olson and S. Kaiser, WO 89/05797 (June 29, 1989) and WO 89/06229 (July 13, 1989) UCC
162 M. Rusek, EP 0190 101 (Aug. 6, 1986), Ciba-Geigy AG
163 M. Rusek, Proceedings 9th Int. Congr. Catal., Calgary, Canada, 1988, Vol. 3, p. 1138
164 A.P. Bolton, ACS Monograph 171 (1976) 714
165 P.A. Jacobs and H. Hinnekers, EP 0329 923 (Ang. 30, 1988) Synfina-Oleofina S.A.
166 A. Bielanski and J. Haber, "Oxygen in Catalysis", Marcel Dekker, Inc., New York, 1991
167 G. Centi and F. Trifiro, Stud. Surf. Sci. Catal. Vol. 55
168 R.A. Sheldon, Bull. Soc. Chem. Belg. 94 (1985) 65
169 H. Mimoun in G. Wilkinson et al. (Eds.) Comprehensive Coordination Chemistry, Pergamon, New York, 1987, Vol. 6, p. 317
170 K.A. Jorgensen, Chem. Rev. 89 (1989) 431
171 S. Yamaguchi, M. Inoue and S. Enomoto, Chem. Lett. (1985) 827
172 M. Eggersdorfer, Florida Catalysis Conference, Florida, USA, April 1990
173 A. Aquila, K. Brenner, W. Ruppel, H. Schultheiß and O. Wörz, Symposium "Heterogene Katalyse", "Technische Reaktionen", Lahnstein, Germany, March 1991
174 J.M. Bregeault, B. El Ali, J. Mercier, J. Martin and C. Martin, C.R. Acad. Sci. Paris 309 (1989) 459
175 B. El Ali, J.M. Bregeault, J. Mercier, J. Martin, C. Martin and O. Convert, J. Chem. Soc. Chem. Commun. (1989) 825
176 T.R. Felthouse, US 4.959.494 (Sep. 25, 1990) Monsanto Comp.

177 C.D. Chang and S.D. Hellring, US 4.578.521 (1986) Mobil Oil Corp.
178 B. Notari, Stud. Surf. Sci. Catal. 37 (1987) 413
179 A. Esposito, M. Taramasso, C. Neri, and F. Buonomo, BR 2116974 (1985) Anic
180 R.A. Sheldon, Stud. Surf. Sci. Catal. 55 (1990) 1
181 C. Neri and F. Buonomo, EP 0102 097 (1984) Anic SpA.
182 W.F. Hoelderich and N. Goetz, Proceedings 9th Int. Zeol. Congr., Montreal, 1992, in press
183 P. Roffia, G. Leofanti, A. Cesana, M. Mantegassa, M. Padovan, G.Petrini, S. Tonti and P. Gervasutti, Stud. Surf. Sci. Catal. 55 (1990) 43
184 P. Roffia, G. Paparatto, A. Cesana and G. Tauszik, EP 0301 486 (1989) Montedipe SpA
185 S. Tonti, P. Roffia, A. Cesana, M.A. Mantegazza, and M. Padovan, EP 0314147 (1989) Montedipe SpA
186 P. Jacobs, see in [48], p. 555
187 A.N. Zakharov, Mendeleev Commun. (1991) 80
188 D.J. Koh, J.S. Chung and Y.G. Kim, J. Chem. Soc. Chem. Commun. (1991) 849
189 C.L. Scheu, H. Knoezinger and W.M.H. Sachtler, Catal. Lett. (1989) 129
190 S.T. Homeyer and W.M.H. Sachtler, J. Catal. 118 (1989) 266
191 P. Gallezot, A. Giroire-Fendler and D. Richard, Catal. Lett. (1990) 5
192 D.G. Blackmond, RE. Oukaci, B. Blanc and P. Gallezot, J. Catal. 131 (1991) 401
193 F.R. Hartley, "Supported Metal Complexes", D. Reidel Publ. Comp., Boston, 1984
194 G.A. Ozin and C. Gild, Chem. Rev. 89 (1989) 1749
195 D.C. Bailey and S.H. Langer, Chem. Rev. 81 (1981) 110
196 J. Watanabe, J. Soc. Org. Syn. Chem. (1988) 46
197 Y. Nishimara, M. Ishida and R. Haga, EP 271289 (June, 15. 1988) Hitachi Ltd.
198 H. Tilscher, K. Dialer and W. Jäger, DE 3421049 (Dec. 12, 1985) TU München
199 S. Pedersen and T. Hansen WO 90/05778 (May 31, 1990) Novo-Nordisk
200 M. Capka, Collect. Czech. Chem. Commun. 55 (1990) 2803
201 M. Makkee, A.P.G. Kieboom and H. van Bekkum, Starch/Stärke 37 (1985) 232
202 M. Makkee, A.P.G. Kieboom and H. van Bekkum, Carbohydrate Res. 138 (1985) 225 and 237
203 M. Makkee, A.P.G. Kieboom and H. van Bekkum, Recl. Trav. Chim. Pays - Bas 103 (1984) 361
204 R. Noyori, Chem. Soc. Rev. 18 (1989) 187
205 H.U. Blaser, Tetrahedron: Asymmetry, 2 (1991) 843
206 J.S.M. Wai, J. Marko, J.S. Svendsen, M.G. Finn, E.N. Jacobsen and K.B. Sharpless
207 W. Keim and T. Röthel, Chem. Ind. 10 (1990) 48
208 H.U. Blaser and M. Müller, Stud. Surf. Sci. Catal. 59 (1991) 73
209 B.M. Choudary, V.L.K. Valli and A. Durga Prasad, J. Chem. Soc., Chem. Commun. (1990) 1186
210 R.M. Hanson and K.B. Sharpless, J. Org. Chem. 51 (1986) 1922
211 R.M. Dessau US 4554262 (Nov. 19, 1985) and US 4666874 (May 19, 1987) Mobil Oil Corp.
212 A. Corma, M. Iglesias, C. del Pino and F. Sanchez, J. Chem. Soc. Chem. Commun., (1991) 1253
213 C. Schild, A. Wokaun and A. Baiker, J. Molec. Catal. 63 (1990) 223 and 243
214 K.S. Suslic, S.B. Choe, A. Cichowlas and M.W. Grinstaff, Nature 353 (1991) 414
215 A. Baiker, Faraday Discuss. Chem. Soc. 87 (1989) 239
216 R. Sheldon personal communication

Guczi, L. *et al.* (Editors), *New Frontiers in Catalysis*
Proceedings of the 10th International Congress on Catalysis, 19-24 July, 1992, Budapest, Hungary
© 1993 Elsevier Science Publishers B.V. All rights reserved

STRUCTURE-FUNCTION RELATIONSHIPS IN HETEROGENEOUS CATALYSIS: THE EMBEDDED SURFACE MOLECULE APPROACH AND ITS APPLICATIONS

P. Johnston and R. W. Joyner

Leverhulme Centre for Innovative Catalysis, Department of Chemistry, University of Liverpool, P.O.Box 147, Grove St., Liverpool L69 3BX, United Kingdom

Abstract

A new systematic approach to describing the active site in heterogeneous catalysis is defined. Called the **embedded surface molecule** method, this considers the active site as a 'surface molecule', consisting of those atoms of reagent, catalyst and product that participate directly in the catalytic reaction. The surface molecule is embedded in a matrix which modifies the electronic environment of the site and also supplies reagent species to the site by surface diffusion. The ESM concept emphasises the need to consider bond forming reactions in heterogeneous catalysis and to take advantage of the knowledge of bond formation that has been developed in other branches of chemistry, particularly homogeneous catalysis.

The application of the ESM approach is illustrated by considering the mechanism of formation of C_2 and higher oxygenates and hydrocarbons from synthesis gas, by supported rhodium catalysts. A series of cofeeding experiments is reported that show for the first time the importance of nucleophilic attack by adsorbed hydroxyl groups in oxygenates synthesis, and indicate the existence of an intermediate common to oxygenate and hydrocarbon synthesis, possibly an adsorbed ethylidyne species. The results suggest the existence of parallel mechanisms for oxygenate formation: CO insertion for pi-bonded olefins, and OH attack on sigma bonded species.

1. INTRODUCTION

Since it was introduced by H. S. Taylor [1], the active site has become a concept of central importance in heterogeneous catalysis. There is still, however, no general agreement on how an active site should be described or on procedures that best allow it to be pictured. In the belief that this represents a significant conceptual barrier to the progress of catalysis, a new approach has been devised, called the **embedded surface molecule**, or ESM method. The ESM analysis is a systematic procedure within which available knowledge can be combined to generate the most accurate description of the reaction mechanism or the active site.

Surface science continues to provide the most detailed information on surface reactivity of relevance to heterogeneous catalysis [2], but it has a single inherent drawback that is rarely recognised. Surface science techniques are much better at following process in which bonds are broken than those in which bonds are made. Bond making is usually a bimolecular process, in which two surface entities come together, and it is therefore

difficult to study with methods that are still slow and insensitive compared to the relevant timescales and surface coverages. By contrast, other areas of chemistry have been conspicuously more successful in understanding the ways in which chemical bonds are formed. A relevant example is the homogeneous catalytic hydrogenation of alkenes by Wilkinson's catalyst, where the mechanism is well understood and it has been possible to define the structure and energetics of both intermediates and transition states using optimised Hartree - Fock calculations [3].

The ESM approach therefore has two main aims:

1) to provide a systematic framework within which to consider catalytic reactivity, and:

2) to use more effectively information on the mechanism of bond forming reactions from other areas of chemistry

2. THE EMBEDDED SURFACE MOLECULE APPROACH

2.1 Definition of the Surface Molecule

Progress in understanding bond making reactions in chemistry has depended on recognising that the reactivity of large molecules can often be described by considering only small fragments, the functional group chemistry of organic molecules being a salient example. Even though a typical heterogeneous catalyst is an extended system, there will be considerable advantages if it can be described as a small molecule, the surface molecule.

The surface molecule is defined as:
those atoms that participate directly in the catalytic act, and any ligands that exert important local influence: the participating atoms are those of relevant fragments of the reagent and product molecules, and those atoms in the catalyst surface which bind the reagent, product and any intermediate complexes.

In this definition the surface molecule may look rather like a working homogeneous catalyst. This is not accidental, since it is intended to take advantage of information from homogeneous catalysis wherever possible. In its emphasises on parallels to homogeneous catalysis, the ESM approach acknowledges a debt especially to the work of Muetterties [4], Rooney [5] and Basset [6].

It is important to recognise that the chemistry of an atom in a metal or a metal oxide will be significantly different from that of an isolated atom or cluster. The interaction of the surface molecule with its matrix is referred to as **embedding** and it is important to recognise the major consequences that the embedding may have.

2.2 The Role of Embedding

The embedding matrix influences the surface molecule in three significant ways, by constraining the physical structure of the ESM, by influencing the electronic environment of the ESM, and by acting as a source of reacting species, through surface diffusion.

The structural role of the matrix will be most important for reactions that are structure sensitive and these will be discussed in more detail elsewhere [7]. The electronic consequences of embedding are often profound, as for example when a single metal atom forms part of a larger

particle, but they are also relatively well understood. By contrast, the role of the catalyst surface in acting as a supplier of reacting species seems largely to have been ignored. We are accustomed to consider two main types of catalyst reactivity, the Langmuir - Hinshelwood mechanism and the Eley - Rideal mechanism, yet we have not fully absorbed the lesson of a significant number of surface science studies, that the Eley - Rideal mechanism probably does not occur. Where reactions with Eley - Rideal kinetics have been studied, such as CO oxidation, it has been found that both of the reacting species are adsorbed and that the reaction mechanism is really Langmuir - Hinshelwood [8].

Since Eley - Rideal reactions are very rare, we must accept that reacting species normally come together by processes of surface diffusion. Mediating this is a crucial role of the matrix in any catalytic reaction.

3. CONSTRUCTING THE EMBEDDED SURFACE MOLECULE

The ESM analysis is performed in three step, designated:

1) **the proposal stage,**
2) **the synthesis stage, and**
3) **the evaluation stage.**

The main role of the proposal stage is to suggest important possible bond making intermediates for the reaction. In the synthesis stage all of the information that is available on the catalyst and the reaction is considered and candidate embedded surface molecules proposed. An intermediate may give rise to more than one surface molecule proposal. In the evaluation stage experimental tests of each of the ESM's are derived, all of the evidence is assessed and the ESM's are ranked. The whole of the ESM procedure has been cast in the form of a flowsheet for systematic implementation, and this will be described elsewhere [7].

3.1 The Proposal Stage

The main purpose of the proposal stage is identify the most important or difficult bond making steps in the reaction of interest. The outcome of this stage is the proposal of intermediates that may be involved in bond formation. For reactions involving only C, H and O, the scale of increasing difficulty of bond formation is:

$$H - H < C - H = O - H \ll C - C = C - O$$

In suggesting intermediates, evidence from surface science or other heterogeneous studies should be exploited to the full, but it will normally be necessary to seek guidance from molecular organic chemistry or homogeneous catalysis. It is of the essence of the ESM philosophy to assume that surface reactivity parallels that observed elsewhere in chemistry, unless there is evidence to the contrary. Bond breaking may be significant for some reactions, particularly those that are structure sensitive and involve difficult dissociations, (eg C - C, N - N, C - O), and this should be considered first [7].

3.2 The Synthesis Stage

In the synthesis stage the consequences of embedding are considered, and surface molecules are proposed for each of the suggested intermediates. There is insufficient space to consider electronic consequences here, (see Ref 7), but it is important at this stage to identify fixed and diffusing species and to consider how many catalyst atoms are involved in the surface

molecule. Normally one of the reacting entities will diffuse sufficiently slowly that it may be considered immobile. In combination with the catalyst atoms and any suggested ligands, this fixed species will form the surface molecule **before reaction.** The more rapidly diffusing species then arrives at the ESM, forming the ESM **at reaction.** It will be common to propose several ESMs for each intermediate of interest, for example containing different numbers of catalyst atoms or different ligands.

3.3 The Evaluation Stage

This last part of the ESM procedure has two stages, the proposal of experimental tests and the ranking of the ESMs once experiments have been completed. This procedure might be adopted in any mechanistic study; the advantages claimed for the ESM approach are its systematic nature and its emphasis on parallels between surface reactivity and chemical reactivity more generally.

4. AN EXAMPLE: APPLICATION OF THE ESM ANALYSIS TO THE MECHANISM OF SYNTHESIS GAS CONVERSION OVER RHODIUM

Rhodium catalysts are of interest because of the unique range of products that they can generate from synthesis gas, (CO / H_2). As shown in Table 1, these include hydrocarbons typical of those found in the Fischer Tropsch synthesis, methanol, and a wide variety of C_2 and higher oxygenates. We have used this set of reactions as a proving ground for the ESM analysis and now present a condensed description of our results and conclusions. Catalyst preparation and test procedures have been described previously [9], and all experiments were carried out with a 1% Rh/Al_2O_3 catalyst, at 250 C and 5 bar pressure, with a 1/1 CO / H_2 ratio and GHSV $\equiv$ 3000 h^{-1}. Conversion of carbon monoxide was typically 5%.

The general view of the mechanism by which oxygenates other than methanol are formed is that carbon monoxide insertion occurs into a metal -

Table 1
Product distribution, (mass %), from synthesis gas conversion over a 1% Rh/Al_2O_3 catalyst, (for conditions see text).

Hydrocarbons	%	Oxygenates	%
Methane	42.9	Methanol	10.0
Ethane	3.3	Ethanol	14.9
Ethylene	1.0	Acetaldehyde	5.5
Propane/Propylene	4.5	Acetic acid	4.9
C_4	4.9	Methyl acetate	0.3
C_5	1.2	Ethyl acetate	0.2
C_6 and higher	0.8	Dimethyl ether	3.6
		Other ethers	0.6
Carbon dioxide/ vol %	0.2	Propionaldehyde	1.4

carbon bond [10], and that this insertion is chain terminating, in agreement with a mechanistic proposal that we made fifteen years ago [11].

In the first step of applying ESM, the important **bond forming reactions** are identified. For the synthesis of a C_2 oxygenate or hydrocarbon the way that the C - C bond is formed is clearly important. For the oxygenate it may also be necessary to consider C - O bond formation. If reaction occurs by CO insertion this becomes is redundant, but the ESM approach requires examination of all possibilities. Possible support for a mechanism in which the integrity of the C - O bond is not retained is provided by the isotopic studies of Katzer [14]. An interesting sequence is where the C - C bond is formed first, followed by the C - O bond, opening the possibility of a common parent intermediate for C_2 oxygenates, and C_3 and higher hydrocarbons have. Possible species containing the C - C bond are adsorbed ethylid**yne**, or ethylid**ene** that we have previously suggested might be the crucial species in initiating Fischer Tropsch chain growth [12], in a proposal that closely followed that of McCandlish [13].

The ESM approach next requires that we search for evidence as to the detailed mechanism by which the bonds of interest are formed. CO insertion has already been mentioned, and a possible surface molecule is shown in Fig. 1 A. The diffusing species is probably CO, which is well known to be mobile on metal surfaces, and the parallel with homogeneous carbonylation chemistry is very clear.

Of clear relevance to the way in which the C - O bond might be formed is the Wacker synthesis of aldehydes. This is thought to occur by the nucleophilic attack of a hydroxyl ligand, or a water ligand, on an olefin pi-bonded to the metal atom that forms the homogeneous catalyst [15]. Three possible ESMs are considered, as shown in Fig. 1 B - D. Each involves nucleophilic attack by an adsorbed OH, (the diffusing species), respectively on pi-bonded ethylene, ethylidene and ethylidyne. The ESMs thus contain one, two and three surface rhodium atoms.

The next stage of ESM analysis involves experimental tests of the proposed surface molecules. To search for the involvement of Wacker chemistry, used here as a shorthand for nucleophilic attack by OH, a number of cofeeding experiments designed to influence the surface concentration of key species have been performed.

4.1 Cofeeding experiments: Results and discussion

The reactivity of the cofed molecules can be divided into three groups; water and carbon dioxide were inactive, and caused no changes in the selectivities shown in Table 1. Oxygen and ethylene predominantly influenced the yield of a small sub-set of products, as shown in Tables 2 and 3. Oxygen cofeeding increased the yield of acetaldehyde, while suppressing the production of ethanol and acetic acid; oxygen also suppressed methanol formation, apparently by oxidising the relevant intermediate to carbon dioxide. Reactions observed for ethylene were reduction to ethane, and hydroformylation to propionaldehyde and propyl alcohol, although there was a limited degree of incorporation into C_3 and higher hydrocarbons. Acetaldehyde increased the yields of most of the products observed, with the exceptions of methane and methanol, as shown in Table 4. The influence of all of the cofed molecules was reversible, selectivities reverting to those given in Table 1 when the added molecule was removed from the feed.

A

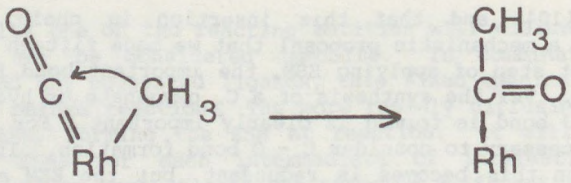

CO insertion (methyl migration) to give a rhodium acyl.

B

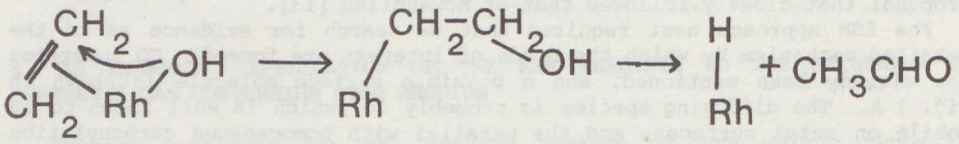

Nucleophilic attack by OH on pi-bonded ethylene, followed by ß hydrogen elimination.

C

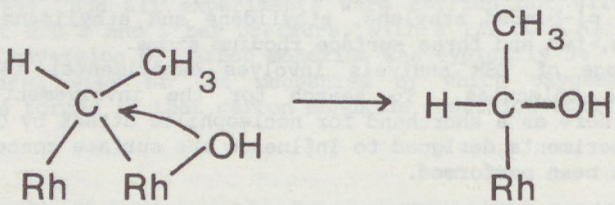

Nucleophilic attack by OH on adsorbed ethylidene.

D

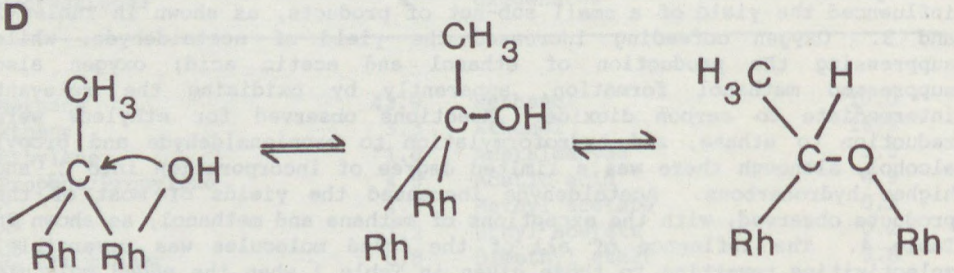

Nucleophilic attack by OH on adsorbed ethylidyne.

Fig. 1. Four proposed surface molecules.

Table 2
Results of cofeeding 1% ethylene: As noted in the text, ethylene appears to react independently of the synthesis gas, with a conversion of ca 86 %: the table shows the selectivity of that reaction

Product	Selectivity / %
Ethane	76.6
Propyl alcohol	10.8
Propionaldehyde	5.7
Propane/Propylene	0.6
C_4 and higher hydrocarbons	3.0
Diethers	2.6
Other oxygenates	0.7

Table 3
Results of cofeeding 2.0% oxygen: oxygen causes significant changes only in the selectivity to those products shown below

Product	Selectivity change compared to synthesis gas only / %
Methanol	-24
Ethanol	-35
Acetaldehyde	+54
Acetic acid	-54
Methyl acetate	-74
1.1 Dimethoxy ethane	*
Carbon dioxide	+280

* Dimethoxy ethane was not detected before cofeeding oxygen; during cofeeding it represents 2.7% of total product yield.

Table 4
Changes caused by cofeeding 1% acetaldehyde: note that some changes are %, while for others are orders of magnitude

Hydrocarbons	Change	Oxygenates	Change
Methane	-3%	Methanol	-18%
Ethane	+14%	Ethanol	x10
Ethylene	+23%	Acetaldehyde	-
Propane/Propylene	+60%	Acetic acid	x9
C_4	x5		
C_5 and higher	x19	Propyl alcohol	*
		Propionaldehyde	x3
		Ethers	x3

* Trace concentration only, not changed by cofeeding

The significance of these results is as follows:

* Water is not activated by the rhodium surface: this is not surprising since noble metal surfaces are rather inert with respect to water activation [16]. The water cofeeding experiments therefore have little mechanistic importance.

* Carbon dioxide is not activated by the catalyst, again this is unsurprising [17].

* The reactivity of ethylene is largely that expected from a pi-bonded species. Application of ESM concepts suggests that, as in homogeneous catalysis, hydrogenation of ethylene initially involves the alkene pi-bonded to a single rhodium atom [3,7]. By analogy with homogeneous chemistry, it is probable that the hydroformylation reaction also involves the pi-bonded olefin. The cofed ethylene appears to react independently of the other synthesis gas reactions that are occurring on the rhodium catalyst, since the degree of incorporation into the hydrocarbons is minimal and the yield of oxygenates other than propyl alcohol and propionaldehyde is largely unaffected. It is tempting to suggest that ethylene is activated at sites that are different from those involved in the synthesis gas chemistry, perhaps isolated rhodium atoms. The ethylene results do, however indicate that the extent of any nucleophilic attack by OH at such sites is very minor, compared to hydrogenation and hydroformylation.

* The results of oxygen cofeeding are more relevant to the mechanism of the various synthesis gas reactions, since an oxygen adatom is likely to behave indistinguishably from a similar adatom derived from the dissociation of carbon monoxide. The level cofed in our experiments is equivalent to < 40% of the surface oxygen produced at steady state reactivity and we believe that oxygen adatoms are rapidly hydrogenated to

yield adsorbed hydroxyl groups. The most significant result of oxygen cofeeding is the increase in the yield of acetaldehyde, largely unaccompanied by changes in the other C_2 oxygenates. This represents clear evidence that nucleophilic attack by adsorbed hydroxyl groups is an important mechanism in the synthesis of C_2 and higher oxygenates on our rhodium catalysts.

The results also indicate an interesting possible route to the carbon dioxide observed in the reaction. Oxygen cofeeding reduces the methanol yield substantially, while at the same time doubling CO_2 production. A clear inference is that one of the intermediates en route to methanol is oxidisable. While it is unclear what this might be, a possibility must be adsorbed formyl. The results make it unlikely that formate, a fully oxidised species that is argued to be the key intermediate in methanol synthesis on copper catalysts [17], is the intermediate here.

* The changes observed on cofeeding acetaldehyde are the most striking and wide ranging, since the yield of most products increases, the only exceptions being methane and methanol. The small decrease in the yield of the C_1 products indicates that the integrity of the C - C bond in the aldehyde molecule is retained throughout, which is very important mechanistically. The increase in yield of the other products strongly suggests that they are formed from a common intermediate that can easily be derived from acetaldehyde. There have been no single crystal spectroscopic studies to define the mode of adsorption of acetaldehyde on rhodium or other transition metal surfaces. However it seems certain that adsorption will involve a lone pair of electrons on the oxygen, and possibly also the carbon atom. By comparison with ethylene, which appears to undergo preferentially pi-bonded interactions with the surface, the presence of the oxygen atom in acetaldehyde allows the surface to differentiate between the two carbon atoms in the molecule, with the formation of an asymmetrically adsorbed species. We suggest that during catalytic reaction there is a dynamic equilibrium between adsorbed acetaldehyde and adsorbed ethylidyne and OH, as proposed in surface molecule D, (Fig. 1). The ethylidyne species can be a common intermediate en route to C_2 oxygenates, and also to C_3 species through interaction with a surface methylene [12].

These results and those noted from cofeeding oxygen establish the mechanistic importance of surface hydroxyl groups, but in addition show that the mechanism is formally different to Wacker chemistry. Here OH attack is on a hydrocarbon species sigma bonded to the catalyst, rather than pi-bonded as would be typical for Wacker chemistry [12]. The observation that the yield of ethane does not rise when acetaldehyde is added is a reflection of the well known stability of the surface ethylidyne species with respect to hydrogenation [19].

The results suggest that there are parallel paths to C_2 and higher oxygenates. The importance of the CO insertion reaction, leading to a surface acyl species, (surface molecule A) is established by the ethene cofeeding experiments. The oxygen and acetaldehyde results show the importance of nucleophilic attack by OH(ads), probably through surface molecule D. They also open up an intriguing possibility that will require further experimental study, namely that insertion chemistry to yield oxygenates occurs mainly with pi-bonded hydrocarbon entities, and that nucleophilic attack by OH(ads) predominates at sigma bonded hydrocarbon species like ethylidyne.

5. ACKNOWLEDGEMENTS

A number of people made helpful comments during the development of the ESM concept. RWJ is especially grateful for useful discussions with Drs. J.C. Frost and Marina Slinko, Prof. J.L. Gland, and Prof. Gabor Somorjai, who also provided generous hospitality for a period during which the ideas were undergoing development. We are grateful to SERC and the Leverhulme Trust for financial support.

6. REFERENCES

1 H.S. Taylor, Proc. R. Soc. A, 108 (1925) 105.
2 R.W. Joyner, JCS Faraday Trans, 86 (1990) 2675; G.A. Somorjai, J. Phys. Chem., 94 (1990) 1013.
3 N. Koga, C. Daniel, J. Han, X.Y. Fu and K. Morokuma J. Amer. Chem. Soc., 109 (1987) 3455.
4 E.L. Muetterties and J. Stein, Chem. Rev., 79 (1979) 479.
5 J.J. Rooney, J. Mol. Cat., 31 (1985) 147.
6 J.M. Basset, J.P. Candy, A. Choplin, P. Defour, P. Loussard and C. Santini, Heterogeneous Catalysis and Fine Chemicals, Ed. M. Guissnet, Elsevier, Amsterdam, 1988.
7 R.W. Joyner, submitted to J. Catalysis.
8 G. Ertl, CRC Crit. Rev. Solid State Mater. Sci., 10 (1982) 349.
9 P. Johnston, R.W. Joyner, P.D.A. Pudney, E.S. Shpiro and B.P. Williams, Faraday Disc. Chem. Soc., 89 (1990) 91.
10 M. Ichikawa and T. Fukushima, JCS Chem. Commun. (1985) 321.
11 R.W. Joyner, J. Catal., 50 (1977) 176.
12 R.W. Joyner, Catal. Lett., 1 (1988) 307.
13 L.E. McCandlish, J. Catal., 83 (1983) 362.
14 A. Takeuchi and J.R. Katzer, J. Phys. Chem., 86 (1982) 2438.
15 R.H. Crabtree, Organic Chemistry of Transition Metals, Wiley, New York, 1988.
16 P.R. Norton in D.A. King and D.P. Woodruff (eds.), Chemical Physics of Solid Surfaces, Vol. 4, pp 32, Elsevier, Amsterdam, 1982.
17 J. Nakamura, J.A. Rodriguez and C.T. Campbell, J. Phys.: Condensed Matter, 1 (1989) SB149.
18 G.C. Chinchen, P.J. Denny, J.R. Jennings, M.S. Spencer and K.C. Waugh, Appl. Catal., 36 (1988) 1.
19 D. Godbey, F. Zaera, R. Yeates and G.A. Somorjai, Surface Sci., 167 (1986) 150.

DISCUSSION

Q: P. Tétényi (Hungary)

By estimating reactivity within this embedded method we possibly should take into account the strength of metal-carbon, metal-hydrogen and metal-oxygen interaction. This can help to explain the ratio of the different reaction routes. For example by rough estimation process A should be an exothermic, while process B an endothermic one.

This approach can help in estimation of the differences between different metals with respect to their selectivity, for example between Rh and Ru, as Ru interacts especially strongly with oxygen.

Here, of course, we should be cautious because of the collective character of metal-substrate interaction. If we assume, however, the embedded surface molecule approach, then we can speak of the single M-C, M-O and M-H interaction. Would you be kind to comment on this ?

A: R. W. Joyner

You raise a number of valuable points and indicate how the embedded surface molecule approach might be developed numerically. Your comments regarding exothermic reactions draw attention to an interesting difference between the surface molecules depicted in Figure 1. The surface acyl species in A is likely to be a relatively stable intermediate product of the insertion reaction, and its formation may be exothermic, as you point out you suggest that formation of Rh-(CH_2-CH_2-OH) by nucleophilic attack of the OH group would be endothermic, so that the insertion reaction will be favoured. Unlike the surface acyl, it seems probable that Rh-(CH_2-CH_2-OH) represents a transition state in this reaction, so that its formation would be expected to be exothermic. If this is so the thermochemical argument is not appropriate, as it is comparing an intermediate at the bottom of a potential well, with a transition state at a saddle point.

Regarding your second point, in applying embedded surface molecule concepts it is not necessary to consider only single metal-carbon or other single bonds. The ESM analysis can be applied using the most sophisticated data available.

Q: F. Solymosi (Hungary)

I would like to ask you about the active sites of Rh catalyst. As you know the adsorption of CO on supported Rh induces the oxidative disruption of Rh_x cluster and leads to the formation of isolated Rh(0) and Rh(I). Did you observed the occurrence of this process under the conditions applied by you? If you did, do not you think that Rh(I) plays a role in the formation of oxygenated compound?

A: R. W. Joyner

Thank you very much for your interesting questions. Our EXAFS studies suggest that only Rh(0) is stable at reaction temperatures in synthesis gas. I feel that we must undertake more experiments before I want to commit myself to a picture of the active site or sites.

Q: F. Solymosi (Hungary)

Yes, the EXAFS is a very good method to establish the structural change of Rh_x crystallite. But this process can be also followed by IR spectroscopy [1], which is much more sensitive to detect the presence of Rh(I) species. It is true that the high-temperature adsorption of CO is not favorable for the oxidative disruption process, but the addition of O_2 to reacting gas mixture can promote the formation of Rh(I).

[1] F. Solymosi and M. Pásztor, *J. Phys. Chem.*, **89**, 4789 (1985)

A: R. W. Joyner

I agree that infrared spectroscopy is more sensitive to Rh(I) species than EXAFS. The

advantage of EXAFS is that it gives a true average of the species present in the sample, in comparison to infrared spectroscopy, where quantification is rarely attempted.

I am glad you accept that Rh(I) species are unstable at high temperature. I would point out that (with the exception of those experiments where oxygen was cofed), our work has been conducted in highly reducing atmospheres with no CO_2 or oxygen in the feed. Even in the oxygen cofeeding experiments the atmosphere is overall highly reducing as the concentration of [CO + H_2] is markedly in excess of that of oxygen. There is therefore no clear reason to invoke Rh(I) entities.

Q: M. M. Bhasin (USA)

1) How does your surface embedded approach differ from the CO-insertion mechanism proposed by us and other researchers in this area ? Looking at your proposal, it does not appear to be different. Also, is such-surface involved in your ESM approach?

2) As is well known rhodium on γ-alumina forms stable oxidized Rh species. Assuming you used γ-alumina, did you find evidence for oxidized Rh by spectroscopic or other techniques ?

I would also like to ask another question that I was not able to ask. Have you used or can you use this ESM approach to predict product distribution and/or rate enhancements observed with several binary Rh catalysts such as Rh-Fe, Rh-Mn, etc. and alkali modified catalyst systems?

A: R. W. Joyner

1) The CO insertion mechanism which we include in Figure 1, Scheme A is indeed the same as has been proposed many times for the formation of C_2 and higher oxygenates. This is recognized in our text, where we refer explicitly to the studies of Ichikawa et al.

The use of the term "embedded" is not meant to imply sub-surface species and would only do so where specifically indicated. There is no suggestion of sub-surface species in the CO hydrogenation studies presented here.

2) The possible role of oxidized rhodium species has received much attention. We have so far looked for such species only by in situ X-ray absorption spectroscopy, particularly EXAFS [2-4]. We observe the Rh(I) entities in the presence of CO at room temperature that have been reported by others, notably Prins et al. [5]. However in synthesis gas even at quite low temperatures, (<373 K), these readily convert to metallic rhodium. The sensitivity of EXAFS to Rh(I) is difficult to estimate, but we conclude that at least 95% of rhodium in the working catalyst is in the zerovalent state.

3) The ESM approach can indeed be used to consider the role of additives such as iron, manganese or alkali metals to rhodium catalysts. A detailed reply would be lengthy but the following example of the thinking that might result may be of interest.

Suppose that the proposal in our paper is correct, and Wacker chemistry indeed provides a route to oxygenates on rhodium catalysts. One would then consider a different range of additives to enhance catalyst performance, compared to those that would be of use if one wished to enhance CO insertion. The ESM approach is not a short cut to mechanistic analysis, rather it is a systematic means of revealing interesting possibilities which might not otherwise be considered.

[2] P. Johnston, R. W. Joyner, P. D. A. Pudney, *J. Phys. Condensed Matter*, **1**, SB171 (1989)

[3] P. Johnston, R. W. Joyner, P. D. A. Pudney, E. S. Shpiro, B. P. Williams, *Faraday Disc. Chem. Soc.*, **89**, 91 (1990)

[4] P. Johnston, R. W. Joyner, Submitted to *JCS Faraday Trans.*

[5] H. F. T. Van't Blik, D. C. Koningsberger, R. Prins, *J. Phys. Chem.*, **87**, 2264 (1983)

Q: V. Ponec (The Netherlands)

1) Pure Rh(0), on a support free of contaminations produces only hydrocarbons and some aldehydes but no alcohols. The latter reaction requires a promoter. In your case (I believe

your alumina was contamination free) this could have been Rh-Al mixed oxides, traces of it are sufficient - possibly - to produce alcohol. Did you consider this possibility?

2) In several papers (Ponec, Catal. Today 1992, Ponec and Nonnemann, in Studies in Surface Sciences and Catalysts, Natural Gas Conversion, 1992) model has been suggested (supported by many pieces of experimental information) of an active site. This model comprised Rh^{n+} for methanol synthesis and transition metal oxide for ethanol production. Would this model be applicable to your results ?

A: R. W. Joyner

1) As I said in my response to Dr. Solymosi and Dr. Bhasin, the best characterization we have of the oxidation state of rhodium under in situ conditions comes from our EXAFS studies. These provide no evidence for any oxidation state other than Rh(0). As I have noted previously we cannot exclude the possibility of small quantities of other species such as rhodium alminates. Also, as I have said in another reply, selectivity variations between supports may be explained by the role of the support as a supplier of OH groups, without having to invoke compound formation.

2) I believe that we can be certain that no rhodium oxide remains under our synthesis conditions. As noted elsewhere [4] the selectivity of these catalysts to oxygenates increases with time on stream, which is certainly not consistent with oxide formation, as the environment is highly reducing.

Q: K. Tamaru (Japan)

In your "embedded surface molecule method" surface molecule is defined as "those atoms that participate directly in the catalytic act". The surface species which we can observe by spectroscopic techniques are not always real reaction intermediates. The most important point in your method is, accordingly, how to identify the real surface molecules which "participate directly in the catalytic act", rather than how to speculate about those molecules.

A: R. W. Joyner

As you suggest, the problem of differentiating between active sites and spectator species in catalysis can only be solved by the development of spectroscopic and other techniques of sufficient sensitivity. In proposing active species in catalysis we must nevertheless consider all presently available evidence. I believe that we must also:

1) Take account of relevant knowledge from the rest of chemistry,

2) Approach our analysis in as systematic a manner as possible.

The embedded surface molecule approach is intended as a framework within which all these points can be considered together.

Q: L. Zanderighi (Italy)

1) The selectivity of the CO/H_2 reaction strongly depends on the support and the morphology of Rh particles. Why have you not taken into account these factors in the proposed surface molecules (Figure 1) ? Indeed if the embedded surface molecules approach cannot take into account this factor, it is only a formal model, not a physical one.

2) You have assumed that carbon dioxide does not influence product distribution. Experimental evidences indicated that. The product distribution is influenced through the WGSR, and its intermediates (surface carbonates and formate) [6].

[6] Marengo et al., *Chem. Eng. Sci.*, **47**, 2783 (1992)

A: R. W. Joyner

1) I agree that both support and catalyst morphology may be important. Specifically the support may serve as a source of OH groups and this may be one reason why the selectivity of rhodium catalysts is strongly support dependent. At this stage I do not have sufficiently detailed evidence to include these factors in the proposed embedded surface molecule although I will try to do this in the future.

I do not accept that features such as these cannot be included within the embedded surface molecule framework. The proposed means by which the ESM should be constructed is indeed formal, although I suggest that systematic is a more appropriate description. However, the ESM, once constructed is very much a physical model of the active site and the mechanism of the reaction.

2) The evidence is indeed that the water gas shift reaction is very slow for Rh/Al_2O_3 catalysts. The selectivity to CO_2 is very low, typically <<0.5% (see Table 1, in our paper). Also, when we added 1% water to the feed there was no observable change in conversion or selectivity. We are therefore fully justified in ignoring the water gas shift reaction for these materials.

Q: D. Duprez (France)

You mentioned that in your ESM model the matrix supplies reagent species to the metal site by surface diffusion. What is the impact of this surface diffusion on the kinetics of reaction ?

A: R. W. Joyner

Your raise an important and interesting question about the role of surface diffusion. The limited amount of data available on rates of surface diffusion has recently been summarized by Baetzold [7]. It is clear that some species, notably chemisorbed hydrogen and carbon monoxide, diffuse very readily. For others, and in particular atomic adsorbates like oxygen and nitrogen, the rates may be much slower. My intuition is that there will not be many reactions where surface diffusion will be the rate limiting step, but they are likely to be those that are carried out at high temperatures and low pressures. Under those conditions surface coverages will be low and surface diffusion may thus be important.

Surface diffusion however plays another important role that needs to be considered in any fundamental study of catalytic reaction, it mediates the geometry of interaction between adsorbed species. It is well recognized that the relative orientation of colliding species in the gas phase can influence reaction probability [8] and the same may be expected to be true on the surface [9].

[7] R. C. Baetzold, in "Metal-Surface Reaction Energetics", Ed. E. Shustorovitch, pub. VCH Inc. Weinheim, 1991, pp. 109
[8] D. H. Parker, K. K. Chakravorty, R. B. Bernstein, *J. Phys. Chem.*, **85**, 466 (1981)
[9] R. W. Joyner, *Catal. Today*, **12**, 355 (1992)

Q: J. Ruczkowski (Poland)

It seems that the concept of the embedded surface molecule method (ESM) is more closely related to the knowledge of bond formation taken from inorganic chemistry and more precisely coordination chemistry, then homogeneous catalysis.

The word "ligand" is a typical one existing in coordination chemistry and when theoretical aspects of catalysis started to develop, this term comes into the catalytic glossary. In the last two decades we can find in the literature some fine articles [10, 11] where authors tried to describe catalytic processes in heterogeneous catalysis from the standpoint of coordination chemistry utilizing the same concepts which applied in solutions. My opinion is that the influence between those mentioned scientific areas in solving problems can be presented as follows:

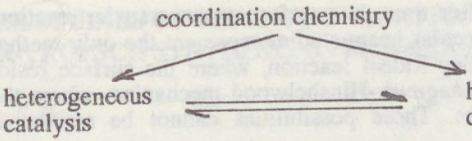

[10] H. Noller and W. Klading, *Catal. Rev. Sci. Eng.*, 13, 149 (1976)
[11] M. Anpo, T. Suzuki, Y. Yamada and M. Che, Proc. 9th Int. Congr. on Catalysis, (Eds: M. Ternan and J. Phillips), The Chemical Institute, Ottawa, Vol. 4, 1513 (1988)

A: R. W. Joyner

Thank you for your interesting remarks, which are more in the nature of a comment than a question. The ESM approach is a conscious attempt to allow us to take advantage of knowledge from the whole of chemistry, including coordination chemistry and homogeneous catalysis. However I believe that it is important to recognize that unique features in heterogeneous catalysis are provided by the medium in which the "active molecule" is located. These are at the most extreme for a metal particle, where the electron distribution is dramatically altered from that of a metal ion in solution. That is why I believe it is necessary to introduce the concept of embedding. If the embedding in the matrix is ignored then we will not be able to account for the profound difference that exist between homogeneous and heterogeneous catalysis.

Q: D. Wang (China)

Rh, in the "right" form - supported on Al_2O_3 (e.g. your work), promoted with La_2O_3 (Ponec, Bell) or as Rh complexes in zeolites (Ichikawa) - shows superior selectivity for oxygenates. Your work suggests that this could be due to the existence of a pathway of nucleophilic attack by hydroxyl groups. Is there direct characterization of hydroxyl groups under oxygenate forming conditions on those forms of Rh showing selectivity for oxygenates?

A: R. W. Joyner

I am not aware of any systematic study or characterization of the role of hydroxyl groups, as anticipated in our "Wacker type" mechanism. Such an investigation, perhaps using infrared spectroscopy, could be very worthwhile.

Q: E. W. Kuipers (The Netherlands)

I would like to remark on your statement, that from molecular beam work one can conclude, that "real" Eley-Rideal reactions are extremely unlikely. In my opinion, drawing this conclusion from MB studies is not right, since only a few reactions have been studied in this way. One of these studies actually even did show on ER reaction (proton transfer from Pt to DABCO). Above this, these MB studies only scanned a very small part of the total partition function of gas-phase reactants. We should also keep in mind, that the "pressure" in MB's is very small whereas the surface can be already completely covered. I do agree however, that ER mechanisms are highly improbable, since at the surface scrambling of states occurs at ~10^{13} Hz. For such a collision rate from the gas phase one would need pressures of around 10000 bar. So due to a transfer from three to two dimensions. The surface of a heterogeneous catalyst is a perfect supplier of reactants.

A: R. W. Joyner

Thank you for your helpful contribution. I accept your remarks about the relatively restricted range of reactions that have been studied by molecular beam methods. I also admire your very recently published studies which conclusively show the occurrence of the Eley-

Rideal mechanism for the first time, in a surface proton transfer reaction [12]. It is important to note, however, that molecular beam studies represent the only method that we can use to differentiate between an Eley-Rideal reaction, where the surface residence time is as you point out ~10^{-13} s, and a Langmuir-Hinshelwood mechanism where the residence time can still be very short, <1 ms. These possibilities cannot be separated by normal kinetic measurements.

My main concern is to point out that Eley-Rideal reactions appear to be very rare, and that in heterogeneously catalyzed reactions the surface will normally have the important role of bringing reacting species together by surface diffusion. The numbers mentioned in your second paragraph make my point very eloquently.

[12] E. W. Kuipers, A. Vardi, A. Damon, A. Amirav, *Surface Sci.*, **261**, 299 (1992)

Guczi, L. *et al.* (Editors), *New Frontiers in Catalysis*
Proceedings of the 10th International Congress on Catalysis, 19-24 July, 1992, Budapest, Hungary
© 1993 Elsevier Science Publishers B.V. All rights reserved

ISOTOPIC TRACER STUDIES OF CHAIN PROPAGATION AND TERMINATION DURING FISCHER-TROPSCH SYNTHESIS OVER Ru/TiO_2

K. R. Krishna and A. T. Bell

Center for Advanced Materials, Lawrence Berkeley Laboratory and Department of Chemical Engineering, University of California, Berkeley, CA 94720, USA

Abstract

Transient response isotopic tracer experiments have been used to study chain growth during Fischer-Tropsch synthesis over a Ru/TiO_2 catalyst. This involves observation of the incorporation of ^{13}C into reaction products after an abrupt switch from $^{12}CO/D_2$ to $^{13}CO/D_2$ in the feed. Values for the rate constants for initiation, propagation and termination are determined by fitting theoretically generated curves to the observed transient response. The rate coefficient for chain initiation is found to be independent of temperature, whereas the rate coefficients for propagation and termination increase with temperature. The activation energy for chain termination is significantly higher than that for chain propagation, explaining the observed decrease in chain growth probability, α, with increasing temperature. Coverages by reaction intermediates are also estimated. The dominant species are monomeric building units which occupy 0.2-0.6 ML. Alkyl species that are the direct hydrocarbon product precursors occupy < 0.2 ML and adsorbed CO covers 0.7 ML. Total coverage by CO and the reaction intermediates equals CO uptake of a fresh catalyst.

1. INTRODUCTION

Mechanistic studies of hydrocarbon production by FTS over Fe, Co and Ru have led to the consensus that FTS occurs by the following reaction sequence [1-3]:

1. $CO_g \rightleftarrows CO_s$
2. $H_{2,g} \rightleftarrows 2H_s$
3. $CO_s \rightarrow C_s + O_s$
4. $O_s + H_s \rightarrow OH_s$
5. $H_s + OH_s \rightarrow H_2O_s$
6. $C_s + H_s \rightleftarrows CH_s$
7. $CH_s + H_s \rightleftarrows CH_{2,s}$
8. $CH_{2,s} + H_s \rightleftarrows CH_{3,s}$
9. $CH_{3,s} + H_s \rightarrow CH_{4,g}$
10. $CH_{3,s} + CH_{2,s} \rightarrow CH_3CH_{2,s}$
11. $CH_3CH_{2,s} + H_s \rightarrow CH_3CH_{3,g}$
12. $CH_3CH_{2,s} \rightarrow CH_2CH_{2,g} + H_s$
13. $CH_3CH_{2,s} + CH_{2,s} \rightarrow CH_3CH_2CH_{2,s}$

14. $C_nH_{(2n+1),s} + CH_{2,s} \rightarrow C_{(n+1)}H_{[2(n+1)+1],s}$

15. $C_nH_{(2n+1),s} + H_s \rightarrow C_nH_{(2n+2),g}$

16. $C_nH_{(2n+1),s} \rightarrow C_nH_{2n,g} + H_s$

A number of investigators have used transient-response isotopic tracer experiments to study FTS for the purpose of estimating the rate coefficients for chain propagation and termination [4-6]. In such experiments, a sudden switch in the isotopic composition is made from $^{12}CO/H_2$ to $^{13}CO/H_2$ [7, 8], while maintaining a constant feed composition. The contents of ^{13}C and ^{12}C in the hydrocarbon products is then monitored as a function of time. The dynamics of the appearance and disappearance of ^{13}C and ^{12}C in the products reflects the rates of chain propagation and termination. By appropriate simulation of the experimental results, the rate coefficients for chain propagation and termination, k_p and k_t, can be determined. Information concerning the surface coverages by various intermediates can also be determined from these simulations.

Zhang and Biloen [4] have looked at the successive incorporation of ^{13}C into the C_{1-3} hydrocarbon products over Co and Ru catalysts. For Co, it was estimated that at 483 K, the apparent value of the rate constant for propagation decreased from 0.045-0.025 s^{-1}, and the corresponding value of the rate coefficient for chain termination increased from 0.02-0.04 s^{-1} as the D_2/CO ratio increased from 1 to 6.55. Coverage by alkyl chains varied from 0.19-0.25 ML. The total coverage by monomeric species was much smaller. These authors estimated that the rate coefficient for propagation for Ru was $\geq 1s^{-1}$. Based on similar experiments, Mims *et al.* [5] have estimated the apparent rate coefficient for chain propagation to be 2-4 s^{-1} for a promoted Fe catalyst at 510 K and a H_2/CO ratio of 1 (15), and 2 s^{-1} for Co at 475 K and a H_2/CO ratio of 2 [6]. For both Fe and Co, the coverage by the monomeric species exceeded the coverage by hydrocarbon chains.

Yokomizo and Bell [9] have used isotopic tracer techniques, in combination with temperature-programmed reduction and infrared spectrsocopy, to look at carbon species on the surface of a titania-supported Ru catalyst. A carbidic carbon species was observed on the surface, 80 % of which served as a monomeric building block and 20 % of which acted as the precursor to methane. A value of k_t of 0.044 s^{-1} was obtained at T = 463 K, p_{CO} = 50 torr and a D_2/CO ratio of 3. The total coverage by C_1 species was reported to be 0.25 ML and the coverage by C_{2+} species leading to hydrocarbon product was estimated to be 0.1 ML.

The objective of the present investigation is to estimate the rate coefficients for chain initiation, propagation and termination, and to study their dependence on temperature and D_2/CO ratio. A further aim of this effort is to determine the surface coverages by the various reactive carbonaceous species present on the catalyst. A Ru/TiO_2 catalyst was used for these investigations because of the high specific activity of Ru for FTS and its characteristically high value of α, the probability of chain growth [10]. The absence of alcohols from the products of FTS over Ru was a further reason for choosing this metal. Titania was used to support and disperse the ruthenium since titania-supported Group VIII metals are known to be more active than silica- or alumina-supported Group VIII metals [11-14].

2.0 EXPERIMENTAL

A 3.3% Ru/TiO_2 catalyst was prepared by incipient wetness impregnation of Degussa P-25 titania with an aqueous solution of $RuCl_3.H_2O$ (Strem). Details of the preparation are given in ref. [15]. The dried catalyst was reduced at 503 K to minimize encapsulation of the Ru crystallites by titania. The metal content of the catalyst was determined by X-ray fluorescence.

The chloride level after reduction was below the detection limit (0.02%). The dispersion of Ru was determined by H_2 chemisorption to be 15.5%, while the CO uptake on the freshly reduced catalyst was 1.3 ML (ML based on H_2 chemisorption). The BET surface area, determined from a N_2 isotherm at 77 K was 47.5 m^2/gm.

D_2, ^{12}CO, ^{13}CO and He were supplied from a gas manifold to a low dead-volume quartz microreactor. UHP H_2 (Matheson Gas) or D_2 (Union Carbide) were further purified by passage through a Deoxo unit (Engelhard Industries) and water was removed by a molecular sieve 13X trap. UHP CO (99.999% pure, Matheson Gas) was passed through a glass bead trap maintained at 573 K to remove iron carbonyls, an Ascarite trap to remove CO_2 and a molecular sieve trap to remove water. UHP He was passed through a molecular sieve trap to remove water. ^{13}CO (Isotec Inc, 99% ^{13}C) was used as supplied.

The steady-state distribution of reaction products was determined by gas chromatography (GC) and the temporal variation in the distribution of ^{12}C and ^{13}C in each product was determined by isotope-ratio gas chromatography-mass spectroscopy [16-18]. For the latter technique, each product sample is first sent to a Perkin-Elmer Sigma 3B gas chromatograph containing a fused silica capillary column (0.25mm i.d. x 50 m) coated with a 1 μm film of SE-54 for separation of C_1-C_{14} hydrocarbons. The column effluent is split into two streams; one line (0.11 mm i.d.) is sent to an FID detector for quantification, while the other transfer line (0.20 mm I.D.) is routed to a capillary combuster. This latter stream is mixed with O_2 and combusted to CO_2 in a 2 m long capillary (0.2 mm i.d.) containing Pt wire (0.13 mm o.d.) maintained at 873 K. Details of the capillary combuster are given in ref. [18]. The effluent from the combuster is leaked into the vacuum chamber containing the probe of an UTI 100C quadrupole mass spectrometer. The leak is accomplished by coupling the exit of the combuster directly to the inlet capillary restrictor of the mass spectrometer. By continuously monitoring masses 44 and 45, the fraction of ^{12}C and ^{13}C in each of the products can be determined.

3. THEORETICAL MODELLING

Simulation of the experimentally observed transients was carried out on the basis of the scheme shown in Figure 1. This scheme is identical to that used by Zhang and Biloen [4] and by Mims and McCandlish [6]. In Fig. 1, CO_g and CO_s refer to gas-phase and adsorbed CO, $C_{m,s}$ refers to adsorbed monomeric building units and $C_{n,s}$ and $C_{n,g}$ refer to adsorbed alkyl chains and gaseous products containing n carbon atoms. Reference to reactions 1-16 in the Introduction show that the scheme in Fig. 1 represents a simplification of the more detailed reaction sequence. First, the species C_s, CH_s and $CH_{2,s}$ are treated as a common species, C_m, on the assumption that the individual species are in equilibrium with each other. Second, no distinction is made between chain termination to olefins and paraffins. The rate coefficient for conversion of $C_{m,s}$ to $C_{1,s}$ is the apparent first-order rate constant for chain initiation, k_i. The rate coefficients k_p and k_t, are first-order rate coefficients for chain propagation, and termination. The parameter $\alpha = k_p\theta_m/(k_p\theta_m + k_t)$ and the apparent rate coefficient for propagation $k_p^{app} = k_p\theta_m$. Dependence of any process on adsorbed hydrogen is not shown explicitly.

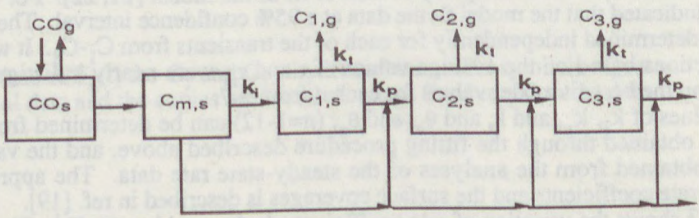

Figure 1. Schematic of chain initiation, growth, and termination mechanism

The scheme presented in Fig. 3 can be used to derive expressions for F_m and F_n, the fraction of labelled carbon in the monomer pool and in the pool of chains of length n, respectively [19]. The final expressions for these functions are given by eqns. 1 and 2.

$$F_m(t) = 1 - \exp(t/\tau_m) \tag{1}$$

$$F_n(t) = 1.0 + \left(\frac{\exp(-\frac{t}{\tau_m})}{n}\right)\sum_{i=1}^{n}(-1)^{i-1}\left(\frac{\tau_m}{\tau - \tau_m}\right)^i + \left(\frac{\exp(-\frac{t}{\tau})}{n}\right)\sum_{i=1}^{n}\frac{1}{\tau^i}\sum_{r=0}^{i-1}\frac{t^{i-r-1}}{(i-r-1)!}\tau^{r+1}\left(\left(-\frac{\tau_m}{\tau - \tau_m}\right)^{r+1} - 1\right) \tag{2}$$

4. RESULTS AND DISCUSSION

The incorporation of ^{13}C and the concurrent decline in ^{12}C in the C_1 and C_{3-8} products was monitored by isotope-ratio GC-MS, following a switch in the feed from $^{12}CO/D_2$ to $^{13}CO/D_2$. The concentration of the C_2 product was too low for mass spectrometric detection. Figure 2 shows representative plots of $F_1(t)$ and $F_n(t)$ for n = 3-8, respectively. The data points in Fig. 2 are based on the measured isotopic fractions in all olefins and paraffins of a given carbon number, since it was observed that the dynamics for products with a given number of carbon atoms could not be differentiated on the basis of structure (i.e., olefin vs paraffin, α-olefin vs β-olefin, n-paraffin vs branched paraffin). While there is considerable scatter in the data, it is observed that the appearance of ^{13}C-labelled carbon in the products is progressively slower as the value of n increases from 3-8. This trend is particularly evident for the C_{6-8} products.

It should be noted that during the transient-response experiment, active surface species that are involved in the main reaction network between the feed CO and gas-phase hydrocarbon products will change in isotopic concentration. Unreactive species such as $C_{\beta''}$, which have reaction time constants significantly longer than those associated with the active reaction intermediates, do not contribute to the transients seen in Fig. 2 to any significant extent [15].

Values of the two parameters τ and τ_m were obtained by fitting the analytical expressions for F_n given by eqn. 11 to the experimental data. This was done using a quasi-Newton method [20] to minimize the objective function $S_n(\tau, \tau_m)$ defined as

$$S_n(\tau, \tau_m) = \sum_{j=1}^{M}\left[F_n^{expt}(t_j) - F_n(t_j)\right]^2 \tag{3}$$

where $F_n^{expt}(t_j)$ and $F_n(t_j)$ are the experimental and theoretical values at time t_j and M is the number of experimental points.

Figure 2 show data and model fits at a temperature of 463K and a ratio of 3. The F-test was used to test the statistical adequacy or lack of fit of the model [21, 22]. For each value of n, the F-test indicated that the model fit the data at a 95% confidence interval. The parameters τ and τ_m were determined independently for each of the transients from C_1-C_8. It was found that the F_n predictions based on the average values of τ and τ_m were nearly indistiguishable from those based on the best-fit model values for each n from 3-7.

The values of k_i, k_p, and k_t and θ_m and θ_n, (n=1-12) can be determined from the values of τ and τ_m, obtained through the fitting procedure described above, and the values of N_{CO}, N_{Cn} and α, obtained from the analyses of the steady-state rate data. The approach used to calculate the rate coefficients and the surface coverages is described in ref. [19].

Figure 3 shows the variation of rate coefficients k_i, k_p, and k_t with T^{-1}. The value of the initiation rate coefficients k_i appears to be independent of temperature. This trend can be

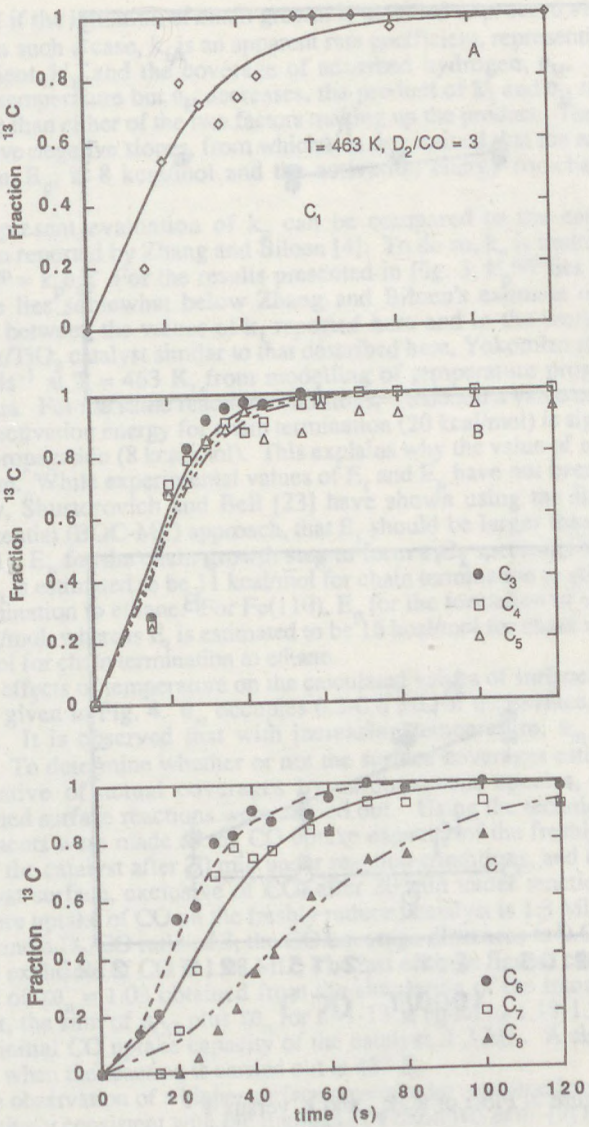

Figure 2. Plots of $F_n(t)$ for C_1 and C_{3-8} hydrocarbons. The symbols represent experimental data and the curves are based on a best fit of eqn. 3 to the data

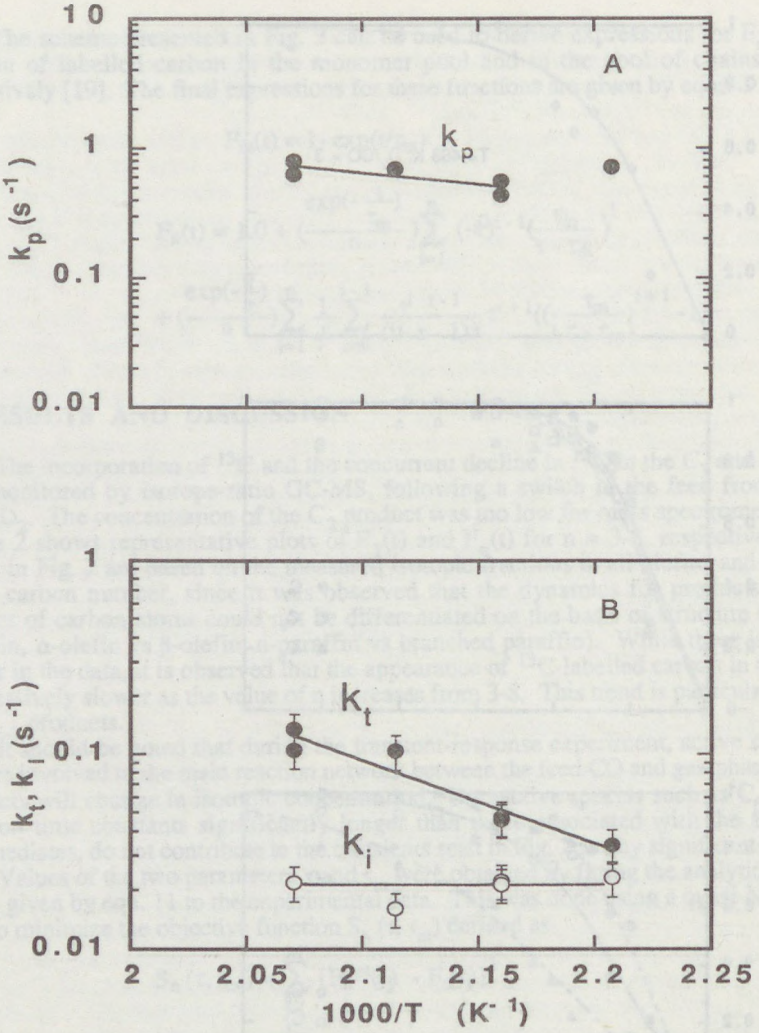

Figure 3. Plots of k_i, k_p, and k_t versus T^{-1}

rationalized if the initiation of chain growth is assumed to proceed via the process $CH_{2,s} + H_s = CH_{3,s}$. In such a case, k_i is an apparent rate coefficient, representing the product of the true rate coeffcient, k'_i, and the coverage of adsorbed hydrogen, θ_H. Since k'_i increases with increasing temperature but θ_H decreases, the product of k'_i and θ_H should be less sensitive to temperature than either of the two factors making up the product. The plots of k_p and k_t versus T^{-1} both have negative slopes, from which it is determined that the activation energy for chain propagation, E_p, is 8 kcal/mol and the activation energy for chain termination, E_t, is 20 kcal/mol.

The present evaluation of k_p can be compared to the estimated apparent rate of propagation reported by Zhang and Biloen [4]. To do so, k_p is multipled by θ_m (see below) to obtain $k_p^{app} = k_p\theta_m$. For the results presented in Fig. 3, k_p^{app} lies between 0.25 and $0.5s^{-1}$. This range lies somewhat below Zhang and Biloen's estimate of $>1\ s^{-1}$. There is close agreement between the values of k_t reported here and in the work of Yokomizo *et al.* [9]. Using a Ru/TiO_2 catalyst similar to that described here, Yokomizo *et al.* determined a value of $k_t = 0.044s^{-1}$ at T = 463 K, from modelling of temperature programmed surface reaction (TPSR) data. For the same reaction conditions, we obtain a value of $k_t = 0.047\ s^{-1}$.

The activation energy for chain termination (20 kcal/mol) is significantly higher than that for chain propagation (8 kcal/mol). This explains why the value of α decreases with increasing temperature. While experimental values of E_t and E_p have not been reported in the literature previously, Shustorovich and Bell [23] have shown using the Bond-Order-Conservation-Morse-Potential (BOC-MP) approach, that E_t should be larger than E_p for Ni and Fe. Thus, for Ni(111), E_p for the chain growth step to form a C_2 species is estimated to be 6 kcal/mol, whereas E_t is estimated to be 11 kcal/mol for chain termination to ethylene and 19 kcal/mol for chain termination to ethane. For Fe(110), E_p for the formation of a C_2 species is estimated to be 20 kcal/mol, whereas E_t is estimated to be 16 kcal/mol for chain termination to ethylene and 32 kcal/mol for chain termination to ethane.

The effects of temperature on the calculated values of surface coverage by carbonaceous species is given in Fig. 4. θ_m occupies 0.3-0.6 ML of the surface, while $\Sigma\theta_n$ occupies 0.12-0.05 ML. It is observed that with increasing temperature, θ_m increases but θ_1 and $\Sigma\theta_n$ decrease. To determine whether or not the surface coverages estimated from the model are representative of actual coverages by carbonaceous species, a series of temperature-programmed surface reactions were carried out. Using the techniques described in ref. [15], measurements were made of the CO uptake capacity of the freshly reduced catalyst, the CO uptake of the catalyst after 20 min under reaction conditions, and the total carbon resident on the catalyst surface, exclusive of CO, after 20 min under reaction conditions. The room-temperature uptake of CO on the freshly reduced catalyst is 1.3 ML. After 20 min of reaction at 463 K and a D_2/CO ratio of 3, the CO coverage decreases to 0.67 ML and the total amount of carbon exclusive of CO is 1.08 ML. The last of these figures compares very favorably with the value of $\Sigma\theta_n = 1.03$ obtained from the simulation of the transient response experiments. Moreover, the sum of θ_{CO} plus $\Sigma\theta_n$ for n=1-13 is equal to 1.19-1.31 ML, in good agreement with the initial CO uptake capacity of the catalyst, 1.3 ML. A similar level of agreement is observed when the reaction is carried out at 483 K.

The observation of a higher surface coverage by monomeric units than by growing chains is qualitatively consistent with the findings of Yokomizo *et al.* [9] for Ru/TiO_2 and Mims *et al.* [6] for Co/Al_2O_3. Yokomizo *et al.* [9] estimate the surface coverage by all C_1 species to be 0.25 ML, and the coverage by C_{2+} chains to be about 0.10 ML. This compares favorably with the present results which indicate a surface coverage of 0.12 ML by C_{2+} species and a coverage of 0.4 by all C_1 species. Since the estimates of surface coverages reported here and by Yokomizo *et al.* [9] are based on completely different methods, the degree of agreement is all the more remarkable.

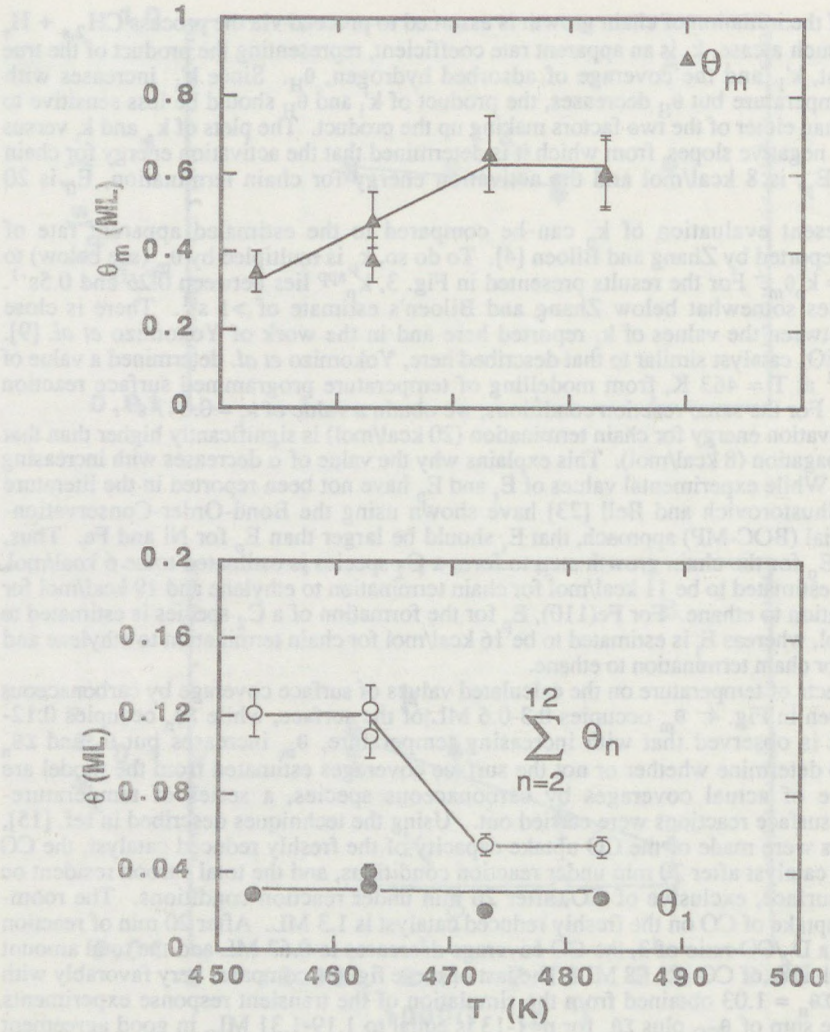

Figure 4. Plots of θ_1, θ_m, and $\Sigma\theta_n$ versus T^{-1}.

5. CONCLUSIONS

Isotopic tracer methods have been used to determine the dynamics of chain initiation, propagation and termination for Fischer-Tropsch synthesis over Ru/TiO_2. Values for the rate coefficients k_i, k_p and k_t were determined by fitting theoretically generated transient response curves to those obtained experimentally. The rate coefficient for chain initiation, k_i, is independent of both temperature. The rate coefficient for chain propagation, k_p has an activation energy of 8 kcal/mol, the rate coefficient for chain termination, k_t, has an activation energy of 20 kcal/mol. The higher activation energy for chain termination than that for chain propagation explains the observed decrease in probability of chain growth, a, with increasing temperature. The surface coverages by various carbonaceous species have also been determined from an analysis of the fitted transient response curves. It is concluded that the dominant species are monomeric building units. These species occupy 0.2- 0.6 ML. Growing alkyl chains, the direct precursors to hydrocarbon products occupy $\leq$ 0.2 ML. Adsorbed CO occupies an additional $\approx$ 0.7 ML. These estimates are found in good agreement with independent measurements made by temperature-programmed reaction spectroscopy.

6. ACKNOWLEDGMENT

This work was supported by the Division of Chemical Sciences, Office of Basic Energy Sciences of the U.S. Department of Energy under Contract DE-AC03-76SF00098.

7. REFERENCES

1. R. B. Anderson,The Fischer-Tropsch Synthesis, Academic Press, New York, 1984.
2. P. Biloen and W. M. H. Sachtler, Adv. Catal., 30 (1981) 165.
3. A. T. Bell, Catal. Rev.-Sci. Eng., 23 (1981) 203.
4. X. Zhang and P. Biloen, J. Catal., 98 (1986) 468.
5. C. A. Mims and L. E. McCandlish, J. Am. Chem. Soc., 107 (1985) 696.
6. C. A. Mims and L. E. McCandlish, J. Phys. Chem., 91 (1987) 929.
7. P. Biloen, J. Molec. Catal., 21 (1983) 17.
8. C. O. Bennett, in Catalysis under Transient Conditions, A. T. Bell and L. L. Hegedus, (eds.), ACS Symposium Series, 178 (1982) 1.
9. G. H. Yokomizo and A. T. Bell, J. Catal., 119 (1989) 467.
10. M. A. Vannice, J. Catal., 37 (1975) 449.
11. M. A. Vannice and R. L. Garten, J. Catal., 56 (1979) 236.
12. M. A. Vannice and C. Sudhakar, J. Phys. Chem., 88 (1984) 2429.
13. R. C. Reuel and C. H. Bartholomew, J. Catal., 85 (1984) 78.
14. J. S. Rieck and A. T. Bell, J. Catal., 99 (1986) 262.
15. K. R. Krishna and A. T. Bell, J. Catal., 130 (1991) 597.
16. M. Sano, Y. Yotsui, H. Abe, and S. Sasaki, J. Biomed. Mass Spec., 3 (1976) 1.
17. D. E. Matthews and J. M. Hayes, Analyt. Chem. 50, (1978) 1465.
18. D. S. Jordan and A. T. Bell, J. Phys. Chem. 90, (1986) 4797.
19. K. R. Krishna, PhD Thesis,, Department of Chemical Engineering, University of California, Berekeley, CA, 1992.
20. V. G. Jenson and G. V. Jeffreys, Mathematical Methods in Chemical Engineering, Second Edition, Academic Press, 1977.
21. G. F. Froment and L. H. Hosten, Catal.-Sci. and Tech. 2, (1981) 97.
22. G. E. P. Box, W. G. Hunter, and J. S. Hunter, Statistics for Experimenters, John Wiley and Sons, New York, 1978.
23. E. Shustorovich and A. T. Bell, Surf. Sci., 248 (1991) 359.

DISCUSSION

Q: L. Zanderighi (Italy)

1) In your paper you have written "if the initiation of chain growth is assumed to proceed via the process $CH_2(s) + H(s) \rightarrow CH_3,(s)$", while in the scheme reported in the introduction this step is at equilibrium. Could you then clear up which is the initiation stage ?

2) How much is the variance of the estimated value of the apparent activation energies for initiation, propagation, and termination? What is the correlation coefficient ?

3) The relative values of the apparent activation energies are surprising. Can you make a comment?

A: A. T. Bell

1) To use as simple a model as possible for the simulation of chain growth and termination, we assumed that $CH_2(s) + H(s) \rightarrow CH_3(s)$ is the rate-determining step. Chain initiation is assumed to begin by the process $CH_3(s) + CH_2(s) \rightarrow C_2H_5(s)$. In so doing, we were able to isolate the monomeric units required for chain growth, $CH_2(s)$ from the centers that initiate chain growth, $CH_3(s)$ and, thus, keep to a minimum the number of rate coefficients required for the simulation. The selection of a different rate determining step, such as $C(s) + H(s) \rightarrow CH(s)$, would have introduced additional rate coefficients into the model. It was our judgement that the scatter in the data did not warrant the use of an overly elaborate model, and, hence, we chose to use the simpler model described in our paper.

2) The variance in the estimated activation energies was not determined. As stated in the text of our paper, the correlation coefficients for the fit of the simulation to the data were in the range of 90-95%.

3) As discussed in the paper, the magnitudes of the apparent activation energies for chain propagation and termination are consistent with the observation that the probability of chain growth decreases with increasing temperature and with previous estimates of these parameters by the bond-order-conservation-Morse-potential approach. The apparent activation energy for chain initiation is smaller than might be expected. We have attempted to rationalize this by recognizing that k_1 is really the product of the true initiation rate coefficient and the equilibrium constant for the adsorption of hydrogen. It is, therefore, conceivable that the true activation energy for chain initiation is comparable in magnitude to the heat of adsorption of hydrogen, which, if so, would give rise to a nearly zero apparent activation energy for initiation.

Q: D. Wang (China)

Are there any estimates of how different (simplifying) assumptions on the reaction kinetics affect deduced rate constants ? In your simplification, you assume equilibrium for the step $C(s) + H(s) \rightarrow CH(s)$ or, equivalently, that this is not a rate determining step. If you, instead, assume that his is a (not necessarily the unique) rate determining step, can you find a fit for your experimental data and are the rate parameters different ?

A: A. T. Bell

Our approach was to choose a reaction mechanism that had been previously established as being consistent with as many independent experimental observations as possible. We then assumed that the rate determining step was the conversion of $CH_2(s)$ to $CH_3(s)$. No other simplifying assumptions were examined. Consequently, I cannot say what effect a change in the assumption of the rate determining step might have on the exact values of the rate coefficients deduced from the fit of the model to the data. I suspect, though, that the orders of magnitude of k_p and k_t will not change, since the time constant of the theoretically determined transients must still agree with those observed experimentally.

Q: R. W. Joyner (United Kingdom)

You suggest that a consensus exists that the first step in Fischer-Tropsch synthesis is a

migratory insertion of surface methylene into a metal-methyl bond, as originally proposed by Brady and Petit. Yet, these experiments conducted in the absence of hydrogen have been criticized, and credible alternative proposals involving methylene species put forward. Can you, therefore, be certain of the first step in your model, and what are the consequences of a different first step from that you assume?

A: A. T. Bell

It is a true that some of Brady and Petit's first experiments with diazomethane were conducted in the absence of hydrogen. In that case, ethylene was observed as the principal product, formed presumably by the coupling of two methylene groups. However, when hydrogen was present in the feed, a homologous series of alkanes and alkenes was observed. Brady and Petit hypothesized at hydrogen was necessary to convert some of the methylene groups to methyl groups, so that the latter species could serve as a chain initiator. With regard to our own modeling efforts, I have to say that one can never be certain that the postulated steps proceed as written. All I can say is that the proposed mechanism for chain growth and termination if fully consistent with precedents in the published literature, which are supported by experimental observation.

Q: D. Bianchi (France)

1) Do you have some data on hydrogen chemisorption to support your argument on the effect of the hydrogen coverage on the evaluation of k_i with the temperature ? Since you do not consider the effect of this parameter on k_t, does this mean that the termination step is the desorption of hydrocarbon ?

2) What is your opinion on the relation between the k values found in your work and the limiting step of the reaction ?

A: A. T. Bell

1) The coverage of the catalyst by hydrogen under reaction conditions was not measured. Attempts to do so in the past by using H_2/D_2 isotopic switches have not been successful because of the inverse isotope effect on the rate of CO hydrogenation and the spillover of hydrogen onto the support. As a consequence, our interpretation of the observed effects of temperature on k_1 is plausible but not certain. While we did not show the results, we have observed that k_t increases with increasing hydrogen concentration in the feed. This is attributable to the fact that k_t in reality represents the sum of the effective rate coefficients for termination to olefins and paraffins. The latter contribution to k_t is the product of a true rate coefficient and the hydrogen coverage. As the hydrogen partial pressure rises, so does the hydrogen coverage and, correspondingly, the value of k_t.

2) As noted in response to the question posed by Dr. Wang, we did not explore alternative assumptions for the rate determining step. Therefore, we cannot say definitively what effect such changes would have. However, as indicated earlier, I doubt that changes in the assumptions about the rate determining step will affect the order of magnitude of k_p and k_t.

Q: K. Klier (USA)

It is remarkable that k_i is associated with a zero activation energy. Since the initiation step appears to be a difficult one, the net frequency factor of k_i must be low. I recognize that k_i is a combined constant of several steps involved in the initiation process. is there a mechanistic explanation for why k_i should have a zero activation energy and a low net frequency factor.

A: A. T. Bell

I agree that it is surprising that k_i has an apparent activation energy of zero. The only way in which I can rationalize this is to remind you that the parameter is the product of a true rate coefficient and the equilibrium constant for hydrogen adsorption. Since the first of these

factors contributes a positive number to the apparent activation energy, and the second factor contributes a negative number, it is conceivable that the two terms just offset each other.

Q: S.-K. Ihm (Korea)
Is it possible to extend your model system by considering the selectivity between olefin and paraffin, particularly in the termination constants? It would be more general to predict the olefin selectivity, which depends strongly upon the nature of different catalysts. Also, do you have experimental data, which could be analyzed in the line of the proposed model extension?

A: A. T. Bell
The experimental data show that the transients for olefins and paraffins of a given carbon number are virtually identical. It is for this reason that we chose not to differentiate between these two products.

Q: J. Goodwin (USA)
Four years ago, Chuck Mims and coworkers presented research on CO hydrogenation using steady-state isotopic tracing and NMR, which led to the conclusion that all carbons in a C_nH_{2n+2} product molecule had similar residence times on the surface. Could you comment on what impact this conclusion has on you assumptions/model and the resulting determination of rate constants.

A: A. T. Bell
What Mims reported was that NMR analyses of butene showed a random distribution of ^{12}C and ^{13}C atoms in the chain. From this observation he concluded that the time constant for chain growth is short relative to the time constant for the displacement of one carbon isotope by another from the monomer pool during an experiment in which a step function change has been made from ^{12}CO to ^{13}CO. Our results are consistent with this conclusion. The time constant for the exchange of carbon isotopes in the monomer pool is 12 s, whereas the time constant for the growth of a C_4 chain is 4 s.

Q: H. Schulz (Germany)
Methane formation is commonly significantly high during CO/H_2 conversion on ruthenium at 1 bar. Excessive methane formation is often regarded as a non-FT reaction, presumably occurring on different sites. Is this complexity taken into account as related to the number and nature of active sites, the fractional surface coverages and the respective rate constants ? How has the number of relevant sites been determined under reaction conditions ?

A: A. T. Bell
While it is true that the mole fraction of methane produced over ruthenium often exceeds that anticipated by the extension of the Schulz-Flory line to C_1, this fact was not taken into account in the present model. We have assumed that all catalyst sites are equivalent, and that processes such as alkane hydrogenolysis do not play a significant role in the production of additional methane.

Q: V. Ragaini (Italy)
Have you considered in your mechanism and in the kinetic scheme, the reduction of catalytic ruthenium centers due to not reactive coke formation ? In fact, coke formation is easy on ruthenium catalysts.

A: A. T. Bell
No, we did not account for coke formation in our model. Since all of the experiments were finished in about 10 min, there was insufficient time for coke formation to occur.

Q: A. Machocki (Poland)

I think that the distribution of species on the catalyst surface is, after a longer time, more complex. A part of the surface is covered small reactive carbonaceous deposits, which are formed probably on sites occupied by chain-hydrocarbon intermediates. So, in fact, the part of the surface useful for hydrocarbon formation should be even smaller than 0.2 ML.

A: A. T. Bell

I do not agree. Under the conditions used in our experiments, most of the surface is available for catalysis, since there is no time to accumulate significant amounts of coke or other species which deactivate the surface. The reported inventories of various species deduced from our model and from independent experiments are consistent, giving further indication that the model captures the essentials of the chemistry.

Guczi, L. *et al.* (Editors), *New Frontiers in Catalysis*
Proceedings of the 10th International Congress on Catalysis, 19-24 July, 1992, Budapest, Hungary
© 1993 Elsevier Science Publishers B.V. All rights reserved

LIQUID PHASE OXIDATION OF GLYOXAL TO GLYOXYLIC ACID BY AIR ON PLATINUM CATALYSTS

P. Gallezot[a], *F. Fache*[a], *R. de Mesanstourne*[a], *Y. Christidis*[b], *G. Mattioda*[b] *and A. Schouteeten*[b]

[a]Institut de Recherches sur la Catalyse-CNRS et Laboratoire de Catalyse et Synthese Organique-UCBL, 2 avenue Albert Einstein, 69626 Villeurbanne Cedex, France
[b]Societe Francaise Hoechst, Centre de Recherches et d`Applications, 64 avenue Gaston Monmousseau, 93240 Stains, France

Abstract
Platinum catalysts were prepared with a high and homogeneous metal dispersion on various carbon supports and used in the oxidation of aqueous solutions of glyoxal with air to obtain selectively glyoxylic acid. The selectivity depends upon the operating conditions and upon the structure and texture of the catalysts. Microporosity and hydrophily of the support tend to decrease the selectivity because they favour multiple readsorption of the molecules leading to overoxidation.

1. INTRODUCTION

A large number of carboxylic acids are prepared industrially by oxidation of aldehydes or alcohols with nitric acid or with other mineral acids. Thus, glyoxylic acid (CHOCOOH), a useful synthon entering into the preparation of a growing number of fine chemicals, is obtained by nitric oxidation of glyoxal (CHOCHO) [1]. This work is part of a continuous research effort to explore alternative routes for glyoxylic acid synthesis, more specifically we have studied the oxidation of aqueous glyoxal solutions with air in presence of supported metal catalysts. Except for the recent development of carbohydrate oxidations [2] metal-catalysed oxidations of oxygenated organic substrates with air is still a largely undeveloped field of catalysis. The selective oxidation of glyoxal to glyoxylic acid is a tough challenge not only because of side reactions (e.g. dismutation) but mainly because of the overoxidation into oxalic acid.

In a previous work [3], we compared the activities and selectivities of platinum metals supported on an active charcoal. In the current study our efforts have centered on the modification of selectivity of platinum catalysts due to the operating conditions and to the structure and texture of the supports. To address this questions catalysts were prepared with similar metal dispersions to avoid any particle size effect.

2. EXPERIMENTAL

2.1. Catalysts

Four types of carbons were used as starting materials to prepare supported platinum catalysts. (i) an active charcoal powder 50S from CECA (BET area 1400m^2g^{-1}); (ii) a furnace carbon black (Vulcan3) from Cabot (non porous, graphitized carbon, 74m^2g^{-1}); (iii) a high surface area graphite from Lonza (HSAG12, 470 m^2g^{-1}); (iv) Cecalite an active charcoal (340 m^2g^{-1}) from CECA with very small (< 1nm) micropores.

To load the metal by ion-exchange these carbon materials were submitted to an oxidizing treatment involving a partial combustion in air followed by a chemical oxidation with sodium hypochlorite as described previously [4]. The platinum catalysts were prepared either by ion-exchange of the acidic groups on the surface of the oxidized carbon supports with $Pt(NH_3)_4^{2+}$ cations followed by H_2 reduction at 300°C or by liquid impregnation of the support with solutions of $PtCl_6^{2-}$ anions followed by reduction with formaldehyde. Experimental details on the ion-exchange procedure have been published previously [4]. Catalysts 2.4 Pt/Cecal, 3.2 Pt/Gr, 4.6 Pt/Gr, 1.3 Pt/Vul and 4 Pt/C have been prepared by ion exchange (Table 1). Metal loading of a non-oxidized active charcoal (CECA 50S) was carried out by liquid impregnation (adsorption) of $PtCl_6^{2-}$ solution and formaldehyde reduction following a procedure described previously [3] which was adapted from a method reported earlier [5]. This procedure was used to prepare catalysts 4.2 Pt/C, 1.8 Pt/C and 2.1 Pt/C. Catalyst 5Pt/C was obtained from a commercial source. Oxide-supported catalysts 6.3 Pt/SiO_2 and $2Pt/TiO_2$ were prepared by impregnation. Catalyst 14 Pt/NaY supported on Y-type zeolite was obtained by ion-exchange.

The composition of the catalysts was determined by chemical analysis. The size of the metal particles and their distribution in the catalyst grains were determined by transmission electron microscopy (TEM) with a JEOL 100CX microscope. Thin sections were cut with an ultramicrotome to check by TEM whether the metal particles were distributed throughout the grain. The characteristics of the samples are given in Table 1.

2.2. Reaction procedure

Glyoxal solutions were oxidized batchwise with air at atmospheric pressure in a 500 ml thermostated glass reactor equipped with a stirrer, a thermometer, a pH electrode, an oxygen electrode and ports for gas inlet, gas outlet and liquid sampling. The pH was regulated automatically with a pH meter (Tacussel) by injection of KOH solutions to neutralize the acids formed. Glyoxal solutions and catalysts were loaded in the reactor and stirred for a few minutes under nitrogen. As air was admitted (0.1 to 1 liter min^{-1}) through the well-stirred solution the oxidation reaction started immediately. Product distribution was measured by HPLC analysis of aldehydes and acids in samples of the reaction medium taken from the reactor at various time intervals [3]. The main products were glyoxylic and oxalic acids and a few percent of glycolic and formic acids. Carbonates were not analysed, they were estimated from mass balance.

3. RESULTS AND DISCUSSION

3.1. Characterization of catalysts

High resolution TEM studies on ultramicrotome thin sections of the microporous catalysts (active charcoal and zeolite) showed that in all the catalysts currently investigated the platinum particles are very homogeneously

distributed throughout the catalyst grain. Furthermore the size distribution is very homogeneous, most particles are within the 1-2 nm size range. It is noteworthy that the two techniques used for the preparation of active charcoal-supported catalysts namely the ion-exchange of $Pt(NH_3)_4^{2+}$ ions followed by H_2-reduction and the liquid impregnation (adsorption) of $PtCl_6^{2-}$ ions followed by formaldehyde reduction give the same very homogeneous dispersion and distribution of platinum particles in the micropores. The commercial catalyst 5Pt/C also exhibits a similar dispersion. The particles sizes in the 14 Pt/NaY zeolite catalyst are smaller than 1.5 nm indicating that the particles are encaged in the micropores.

Direct TEM examination of powders of the nonporous catalysts prepared by ion exchange (3.2 Pt/Gr, 4.6 Pt/Gr, 1.3 Pt/Vul) show that the particle sizes are within 1-2 nm. As reported previously [4], the particles decorate the graphite steps. Particle sizes are given in Table 1.

Table 1
Characteristics of catalysts and reaction data

Catalysts	Preparation[a] mode	Particle[b] size(nm)	Reaction conditions[c] [glyoxal]	glyoxal/Pt	Glyoxal[d] conversion%	Selectivity[e] %	Remarks
5Pt/C		1-2.5	0.35	342	96	73	
6.3Pt/SiO_2	1	1.5-2.5	0.35	342	19	0	
2Pt/TiO_2	1	2-3	0.35	342	0	0	
14Pt/NaY	2	<1.5	0.1	173	90	39	f
4.2Pt/C	1	1-2	0.1	173	85.5 94.5	70 36.5	f g
2.4Pt/Cecal	2	<1	0.1	327	92	30	f
3.2Pt/Gr	2	1-2	0.1	237	99.5	53	f
1.8Pt/C	1	1-2	0.9	919	93	31	
4.6Pt/Gr	2	1-2	0.9	377	94	57	g
1.3Pt/Vul	2	1-2	0.1	178	95	61	f
2.1Pt/C	1	1-2	0.35	763	88	74	
4Pt/C	2	1-2	0.35	415	88	53	

(a) preparation: 1 by liquid impregnation, 2 by ion-exhange. (b) range of particle size measured by TEM. (c) oxidation at pH = 7.5, T = 313 K, 1100 rpm, flowing air (1 liter min^{-1}), concentration in $mol.liter^{-1}$. (d) conversion at maximum of Gly yield (except remark g). (e) selectivity to Gly at maximum Gly yield. (f) stirring speed 500 rpm. (g) selectivity after the maximum of Gly yield.

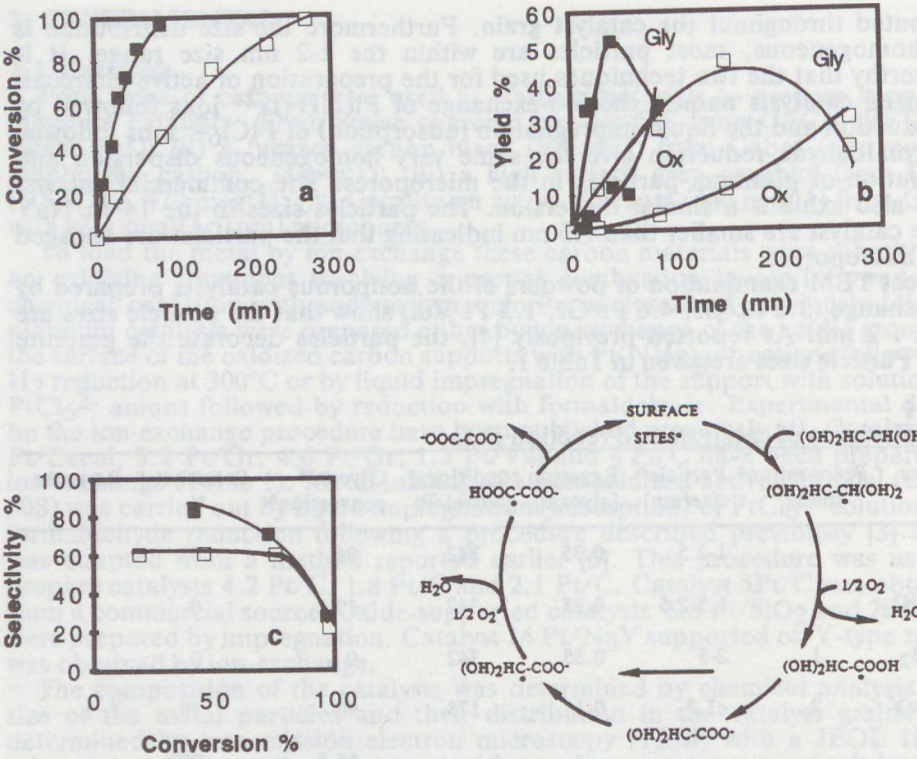

Figure 1. a- glyoxal conversion vs. time at 400 (open symbol) and 1100 rpm (full symbol) stirring speed (catalyst 5Pt/C, [glyoxal] = 0.17 mol liter^{-1}, glyoxal/Pt = 170). b- Yields of Gly and Ox acids vs. time at 400 and 1100 rpm. c- Selectivity to Gly vs. conversion at 400 and 1100 rpm. d- Tentative scheme for the mechanism of glyoxal oxidation.

3.2. Preliminary experiments

Earlier studies [3] have shown that it is necessary to maintain the pH at ca. 7.5 and the temperature at ca. 40°C to minimize secondary reactions (overoxidation to oxalic acid, and dismutation to glycolic acid).

Figure 1a give the glyoxal conversion as a function of time on catalyst 5 Pt/C stirred in a glyoxal solution (0.17 mol liter^{-1}) at 400 and 1100 rpm in presence of bubbling air. The conversion is faster at 1100 rpm but higher stirring speeds did not significantly improve the reaction rate, therefore subsequent experiments were conducted at 1100 rpm unless otherwise specified.

Figure 1b gives the yields in glyoxylic (Gly) and oxalic (Ox) acid as a function of time. Gly is initially the main reaction product, then Ox is formed at the expense of Gly. This suggests that glyoxal oxidation proceeds in two consecutive

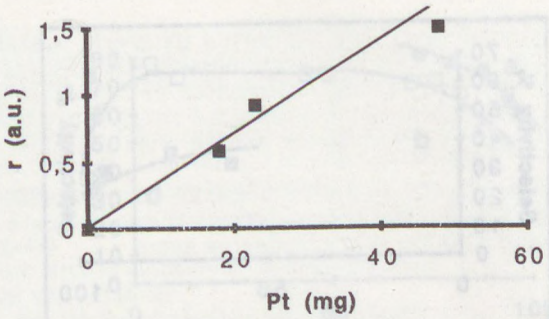

Figure 2. Initial rate of glyoxylic acid formation (arbitrary unit) vs mass of platinum.

steps as proposed in the scheme given in Figure 1d. Gly is probably formed via oxydehydrogenation on the metal surface of one of the hydrated aldehyde functions. Then the adsorbed Gly molecule can either desorb from the metal to the liquid phase or roll over and readsorb on the second group to be oxidized into Ox. Ultimately, as the contact time increases, the solvated Gly molecules readsorb and are oxidized.

Figure 1c gives the selectivity to Gly as a function of glyoxal conversion. The selectivity is lower at low stirring speed. This is probably due to liquid-solid mass transfer limitation: at low stirring speeds the Gly molecules once formed have a higher probability of remaining in a stagnant liquid layer in the vicinity of the metal surface and to readsorb. The importance of the stirring speed on the selectivity is further exemplified by the comparison of two oxidations, one conducted in the glass reactor, the other in a stainless-steel autoclave equipped with a more efficient stirring system. Under the same reaction conditions (1100 rpm, [Glyoxal] = 0.86 mol liter^{-1}, Glyoxal/Pt = 998) and on the same catalyst (1.8 Pt/C) the selectivity was 70 % at 76 % conversion in the glass reactor compared to 94 % at 82 % conversion in the autoclave.

To complete these preliminary experiments the influence of the catalyst mass on the initial rate of glyoxal conversions has been studied. Three oxidations were run on 1.8 Pt/C with glyoxal/Pt ratios of 371, 727 and 958 respectively. Figure 2 shows that the rate of Gly formation is proportional to the mass of metal and thus to the total metallic surface area. This indicates that gas-liquid mass transfer are not rate limiting in this domain; however, this does not rule out mass transfer limitation in the catalyst micropores where the metal is located. The presence during all the reaction of a partial pressure of oxygen in the liquid phase confirm that gas-liquid mass transfer is not rate limiting.

3.3. Oxide-supported catalysts

Catalysts 6.3 Pt/SiO_2 and 2Pt/TiO_2 (Table 1) have been activated at 300°C in flowing H_2 and cooled under Ar. The former catalyst exhibited a very low activity and a poor selectivity, the latter was inactive. This could be due to the formation of a layer of glyoxal in monomeric or oligomeric forms associated via hydrogen bonding with the OH groups covering the surface of the oxide supports.

An immobile layer around the catalyst grains would indeed restrict liquid-solid mass transfer preventing the adsorption-desorption processes on the metal particles located on the support. Under similar reaction conditions, carbon-

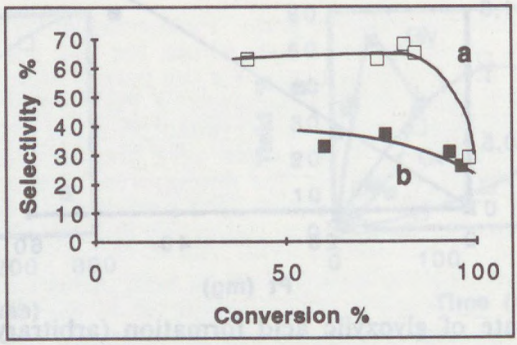

Figure 3. Selectivity to glyoxylic acid vs glyoxal conversion ([glyoxal] = 0.9 mol.liter^{-1}) a-catalyst 4.6 Pt/Gr. b- catalyst 1.8 Pt/C.

supported catalysts are active (*vide infra*) because there are much fewer hydroxyl groups on these hydrophobic supports.

The rate of Gly formation is ten times smaller on the zeolite-supported catalyst 14 Pt/NaY than on the 4.2 Pt/C catalyst, the maximum of Gly yield is 35.5 % instead of 60 % (Table 1); mass balance indicates the formation of 34.5 % of carbonate. The overoxidation is due to the very long residence time experienced by the oxygenated substrates in the zeolite micropores where the metal particles are located; this decreases the reaction rate and favours multiple readsorptions leading to overoxidation. Still, the activity is better than on oxide-supported catalysts possibly because oligomeric forms of glyoxal cannot be formed in zeolite micropores.

3.4. Carbon-supported catalysts

The 2.4 Pt/Cecal catalyst behaves almost like 14.4 Pt/NaY, the selectivity is even lower (Table 1), most of the glyoxal is converted into carbonate. This is not unexpected since Cecalite have micropores smaller than those of Y-type zeolite leading to a larger overoxidation.

The graphite-supported catalyst 3.2 Pt/Gr is less selective at the maximum of Gly yield than the charcoal-supported catalyst 4.2 Pt/C (53 and 70 % respectively, Table 1). However this selectivity is obtained at 99.5 % conversion whereas an 4.2 Pt/C the selectivity is only 36.5 % at 94.5 % conversion (Table 1), thus the graphite supported catalyst is more selective at high conversion. This is probably due to the fact that the metal particles are exposed on the surface of graphite which ease the passage of Gly in the "open" liquid phase whereas Gly molecules formed in the charcoal micropores have a higher probility of readsorbing and oxidizing into Ox. Graphite supported catalysts keep a good selectivity at high conversion especially for more concentrated glyoxal solutions. This is illustrated by the data obtained in the oxidation of a 0.9 mol liter^{-1} glyoxal solution on catalyst 4.6 Pt/Gr compared to catalysts 1.8 Pt/C (Table 1 and Figure 3).

The selectivity of carbon black supported catalyst 1.3 Pt/Vul is quite similar to that of graphite (Table 1) because carbon black is a non-porous, graphitized carbon. As with graphite, the Gly molecules can desorb from the metal surface to the liquid phase without diffusion in the pores.

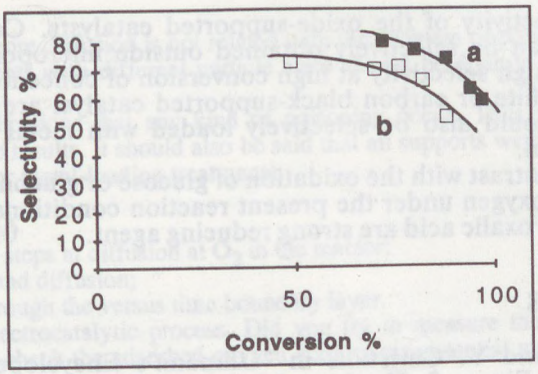

Figure 4. Selectivity to glyoxylic acid vs glyoxal conversion ([glyoxal] = 0.35 mol.liter^{-1}). a- catalyst 2.1 Pt/C. b- catalyst 4 Pt/C.

3.5. Oxidized active charcoal

Two charcoal-supported platinum catalysts 2.1 Pt/C and 4 Pt/C (Table 1) have been compared. The former was obtained by liquid impregnation of a non-oxidized support the latter by ion-exchange of an oxidized support. Although both catalysts have the same dispersion and distribution of metal particles, the data given in Table 1 and in Figure 4 show that 2.1 Pt/C has a higher selectivity than 4 Pt/C. This could be attributed to the larger number of hydroxyl groups on the oxidized support. Indeed, we have shown [6] that the number of acidic groups increases from 0.50 to 1.76 mmol g^{-1} after NaClO oxidation. This could result in a higher affinity of the oxygenated molecules with the support favouring slow diffusion and multiple readsorption.

4. CONCLUSION

The results reported in this study point consistently to the same conclusion, namely that to obtain the highest selectivity to glyoxylic acid the operating conditions and the morphology of the catalyst should be tailored to ease the desorption of the monoacid from the surface and to minimize multiple readsorption leading to overoxidation.

Thus reactions should be conducted with pH regulated by alkali addition to ease the desorption of strongly adsorbed acid molecules from the metal surface to the solution to form solvated glyoxylate [3]. The stirring of the suspension should be efficient in order to minimize the formation of a stagnant layer of oxygenated molecules (glyoxal in monomeric and oligomeric forms, glyoxylic acid) around the catalyst grain; for the same reason the concentration of glyoxal solutions should not be too high.

Although active charcoal supported platinum catalysts can give interesting selectivities (e.g. 74 % Gly yield at 88 % conversion on 2.1 Pt/C) the support should preferably not be oxidized to avoid hydrogen bonding between the oxygenated molecules and OH groups of the support. This is probably the main

cause for the inactivity of the oxide-supported catalysts. Catalysts where the metal particles can be selectively obtained outside micropores seem the best suited to obtain high selectivity at high conversion of concentrated solutions, in that respect graphite or carbon black-supported catalyst are good candidates; active charcoal could also be selectively loaded with metal near the external surface of the grain.

Note that in contrast with the oxidation of glucose or gluconate [2] platinum is not poisoned by oxygen under the present reaction conditions because glyoxal, glyoxylic acid and oxalic acid are strong reducing agent.

5. REFERENCES

1 G. Mattioda and Y. Christidis in "Ullmann's Encyclopedia of Industrial Chemistry" (B. Elvers, S. Hawkins, M. Ravenseroft, J.F. Rounsaville and G. Schulz, Eds.), Vol. A12, p 495, VCH Verlag, Weinhein, 1989.

2 H. van Bekkum in "Carbohydrates as Organic Raw Materials" (F.W. Lichtenthaler, Ed.), p.289, VCH Verlag, Weinheim, 1991.

3 P. Gallezot, R. de Mésanstourne, Y. Christidis, G. Mattioda and A. Schouteeten, J. Catal. (1992), in press.

4 D. Richard and P. Gallezot in "Preparation of Catalysts IV" (B. Delmon, D. Grange, P.A. Jacobs and G. Poncelet, Eds.), p.71, Elsevier, Amsterdam, 1987.

5 J.M.H. Dirkx and H.S. van der Baan, J. Catal., 67 (1981)1.

6 D. Richard, R. de Mésanstourne and P. Gallezot in "19th Conference on Carbon, Extended Abstracts", p. 50, Penn State, 1989.

DISCUSSION

Q: M. Abramovici (USA)

1) Different activity performances could be expected due to particle size differences between activated carbon powders (1-100 μ) and carbon blacks (graphites) which usually consist of particles smaller than 1 μ.

2) Were there any differences in activity performances observed between ion-exchanged and H_2PtCl_6 impregnated catalysts?

A: P. Gallezot

1) The activity (and the selectivity which is our main concern) depends upon the support porosity and for a given porosity it should depend upon the particle size.

2) Impregnated active charcoals obtained by adsorption of $PtCl_6^{2-}$ ions on acid sites have the same metal dispersion (1-2 nm Pt particles uniformly distributed in charcoal grain) as in ion-exchanged samples; however they gave different selectivities as discussed in section 3.5.

Q: M. M. Bhasin (USA)

In the presentation you ascribe the differences in selectivity between Pt on charcoal and graphite entirely to the presence of micropores. It is well known that there are many differences between charcoals and graphites. Purity and hence impurities acting as poisons or promoters can alter the selectivity immensely. To be certain that the pore diffusion is important, did you try to change particles size in a given sample and hence diffusion path length to estimate and quantify the diffusion effects.

A: P. Gallezot

The problem of pore diffusion is not related with the problem of poisoning by impurities. I agree that experiments with different particle sizes should be done to be certain that pore diffusion is important.

We have no indications that any kind of poisoning occur. Thus samples of different origins gave the same results. It should also be said that all supports were thoroughly purified before the oxidizing or metal-loading treatments.

Q: S. Szabó (Hungary)

1) There are two steps at diffusion at O_2 in the reactor:
   a) dissolution and diffusion;
   b) diffusion through the versus time boundary layer.
2) This is an electrocatalytic process. Did you try to measure the material at catalyst particles? Could you check the adsorbed oxygen activity via potential measurement, as in the case at cyclic voltammetry ?

A: P. Gallezot

1) Yes, obviously.
2) We did not do such measurements, this is a good suggestion.

Q: F. Rodriguez-Reinoso (Espana)

You showed that the catalyst supported on the oxidized activated carbon had lower selectivity. Did you study such effect on graphite or carbon black? If not, do you expect the effect to be of the same extent on these support?

Following up a previous question about modifying the functionality of silica, a nice way to analyze simultaneously the effect of porosity and functional groups is to deposit a layer of carbon on the surface of silica and then to prepare the catalyst to be compared with the silica- and activated carbon - supported catalysts.

A: P. Gallezot

We have studied graphite and carbon-black in the oxidized form only. However, since the number of functional groups created on these supports is much lower than on active-charcoal, the hydrophillicity is lower so that we can expect less difference between oxidized and non-oxidized samples.

Q: J.A. Moulijn (The Netherlands)

In your reactor there is an interplay between mass transfer and kinetics.
Which step determines the selectivity ? Is this the desorption of glyoxalic acid ?
If so, I were expect that the following factors are favorable:
- high stirring speed;
- alkene of micropores;
- low oxygen pressure.

Did you study kinetics and what is your conclusion ?

A: P. Gallezot

Indeed, the desorption of glyoxylic acid is the step determining the selectivity. According to the results described in the paper and in agreement with your expectation, the stirring speed and the absence of micropores are favorable factors. The effect of oxygen pressure (not described in this paper) is more complicated because there is a gradient of oxygen concentration from the "open" liquid phase to the liquid phase in the micropores at various depths inside the charcoal grain. Depending on various factors (distribution of metal in the grain, reaction rate, etc.) the oxygen pressure may or may not be favorable.

Q: F. van den Brink (The Netherlands)
Did you consider the possibility that the influence of stirring speed observed in your experiments is caused by mass transfer limitation of oxygen from the gas to the liquid phase rather than from diffusion in the stagnant layer around the catalyst particles ?

A: P. Gallezot
We have checked that the presence of oxygen in the liquid phase, monitored with an oxygen electrode, is only slightly lower during reaction which means that there is no or little gas to liquid mass transfer limitation.

Q: F. Trifiro (Italy)
In your work you took care of consecutive degradation of glyoxilic acids. However from your paper it is possible to see a strong contribution of parallel oxidation of glyoxal to by-products. What are the sites for parallel oxidation of glyoxal ?

A: P. Gallezot
In addition to glyoxylic and oxalic acids, three other products (glycolic acid, formic acid and carbon dioxide) are formed. On platinum catalysts there is less than 10% of these by-products. Clycolic acid is probably formed directly by dismutation of glyoxal, however, formic acid and carbon dioxide are issued by consecutive oxidation from oxalic acid rather than by parallel oxidation of glyoxal.

Q: G. V. Smith (USA)
I am impressed with your high conversions and selectivities over selected carbon supported catalysts, and I believe your interpretations are good. However, I am wondering about your low conversion over Pt/SiO_2 and your zero conversion over Pt/TiO_2. Could pore diffusion be playing an important role for these supports in addition to the "immobile layer" explanation you propose? A pore diffusion problem may be detected and eliminated by grinding the catalyst particles to smaller and smaller sizes and, thereby, shortening the lengths of the pores. Have you performed such experiments?

A: P. Gallezot
Pore diffusion plays undoubtedly a major role to decrease the selectivity to glyoxal. Your suggestion of grinding the catalyst grains can be extended to any support. We have not conducted this kind of experiments.

Q: D. Duprez (France)
You have related the intrinsic metal activity to redox properties of the metal. These redox properties are very sensitive to the nature of the ligand, particularly chlorine. Have you evidence that residual chlorine can modify the activity of catalysts ?

A: P. Gallezot
The main objective of this work was to find the catalysts and the reaction conditions giving the best selectivities. The activities are controlled by various diffusion effects and by oxygen poisoning of the metal surface. The influence of chlorine was not studied.

Q: A. K. Datye (USA)
You have suggested that the low reactivity of oxide-supported catalysts is due to interaction with hydroxyl groups. It is possible to reduce the number of hydroxyls on silica, and make it hydrophobic, by derivatizing with methyl chlorosilanes. Such modified silicas are quite resistant to hydroxylation due to capping methyl groups. Have you considered modifying your silica in this manner and if so what is the effect on activity ?

A: P. Gallezot
We have not tried to perform silica modification; this is a good suggestion.

Guczi, L. *et al.* (Editors), *New Frontiers in Catalysis*
Proceedings of the 10th International Congress on Catalysis, 19-24 July, 1992, Budapest, Hungary
© 1993 Elsevier Science Publishers B.V. All rights reserved

THE EFFECT OF OXYGEN BINDING ENERGY ON THE SELECTIVE OXIDATION OF BUTANE OVER $V/\gamma\text{-}AL_2O_3$

P. J. Andersen and H. H. Kung

Department of Chemical Engineering and Ipatieff Laboratory, Northwestern University, Evanston, IL 60208, USA

ABSTRACT

The oxidation of butane was studied over two $V/\gamma\text{-}Al_2O_3$ catalysts with loadings of 2.9 and 8.2 V/nm^2 using both pulse reaction and steady state measurements. The activity per V ion was about ten times higher on the higher loading sample. In the pulse reaction, the selectivity for oxidative dehydrogenation increased with increasing extent of reduction of the vanadia phase, ϕ, on both catalysts. Small amounts of oxygenates were observed on the lower loading sample. The change in selectivity with ϕ correlated well with changes in the heat of reoxidation of the reduced catalysts, which were determined calorimetrically and were indicative of the binding strength of lattice oxygen in the sample. The difference in dehydrogenation selectivity was also observed in the steady state experiments. These data indicated that the rate limiting and selectivity determining steps were different on these catalysts, and the selectivity for dehydrogenation was strongly affected by the binding energy of lattice oxygen.

INTRODUCTION

Vanadium oxide dispersed on metal oxide supports are effective catalysts for the partial oxidation of alkyl aromatics and olefins. The catalytic behavior depends on both the type of metal oxide support as well as the vanadium loading. Vanadia supported on TiO_2 (anatase) and $\gamma\text{-}Al_2O_3$ form highly dispersed, amorphous phases the structure of which change from isolated vanadia tetrahedra at low loadings to an octahedrally coordinated networked vanadia phase at higher loadings. At high loadings, crystalline V_2O_5 formed in addition to the amorphous vanadia phases [1]. Reaction studies show that the oxidation activity (per supported vanadium ion) of the isolated vanadia species is lower than the activity of the networked vanadia phase [2]. Also, catalysts containing the networked vanadia phase show a higher selectivity to partial oxidation products than both the low loading samples and unsupported, crystalline V_2O_5.

It has been shown for several hydrocarbon oxidation reactions that the lattice oxygen of the metal oxide catalyst is the proximate source of oxygen in the products [3,4]. Thus, the metal-oxygen bond strength of the catalyst may be directly related to the selectivity and

possibly the activity of the catalyst. Temperature programmed reduction experiments on a series of $V/\gamma\text{-}Al_2O_3$ catalysts indicate that the reduction rate of the supported vanadia phase increases as the vanadia loading increases [5]. This change in reactivity could be due to changes in the vanadium-oxygen bond strengths as well as changes in the supported vanadia structure.

We have previously reported calorimetric results demonstrating that the oxygen binding strength is a function of both the vanadia loading and the extent of reduction of a series of $V/\gamma\text{-}Al_2O_3$ catalysts [6]. In this paper, the relationship between the lattice oxygen binding energy and the catalytic behavior of two $V/\gamma\text{-}Al_2O_3$ catalysts in steady state and pulse reactions of butane oxidation are presented. One catalyst sample had a submonolayer coverage and the second had slightly more than a monolayer coverage. They have been shown to have significantly different oxygen binding energies [6].

EXPERIMENTAL

The catalyst preparation procedure was described in detail in Ref 6. The $\gamma\text{-}Al_2O_3$ (surface area = 181 m^2/g) was synthesized from the hydrolysis of aluminum isopropoxide, and vanadium was added as vanadium triisopropoxide to the $\gamma\text{-}Al_2O_3$ in methanol under N_2. After evaporating the methanol, the solid was dried in air at 120°C and then calcined at 520°C. The final vanadium loadings were 8.2 and 23.4 wt% V_2O_5, or 2.9 and 8.2 V atoms/nm^2, respectively. Raman spectra published previously showed, for the 2.9 V/nm^2 sample, a sharp peak at about 1029 cm^{-1} and a broad peak at about 895 cm^{-1} with a small shoulder at about 800 cm^{-1}. The 8.2 V/nm^2 sample also showed these features. However, the 800 cm^{-1} broad peak was the dominant peak [5]. In addition, small peaks at 998 and 530 cm^{-1} were also observed that indicated the presence of a small quantities of crystalline V_2O_5.

Steady state reactions were run in a quartz reactor at atmospheric pressure. The feed was 20/10/70 by volume C_4H_{10}/O_2/He. The catalyst was diluted with quartz powder and supported with quartz wool. The remaining reactor volume was filled with quartz chips. The products were analyzed with on-line gas chromatography using molecular sieve (O_2 and CO), VZ-7 (CO_2, butane, butenes, and butadiene), and Graphpac (crotonaldehyde, acetic acid, and maleic anhydride) columns. In the absence of a catalyst, there was no detectable reaction.

The pulse reactions were performed by passing pulses of butane (0.05 ml at 1 atm) in He over 0.05 g of 8.2 V/nm^2 catalyst and 0.75 g of 2.9 V/nm^2 catalyst. The products were collected in a trap at 77 K and later flashed into a gas chromatograph for analysis. The reduced catalyst was then reoxidized with oxygen pulses.

RESULTS

Differential Reoxidation Heats

The differential heats of reoxidation at 300°C and 500°C reported previously for the two $V/\gamma\text{-}Al_2O_3$ samples examined in this study are shown in Figs. 1a and 2a. For these measurements, the samples were reduced with H_2 and then incrementally reoxidized with O_2 doses in a static adsorption calorimetry apparatus to obtain the reoxidation heats as a function of the degree of reduction of sample, ϕ, which was defined as the number of oxygen atoms

Figure 1 8.2 V/nm^2 Catalyst

a. Reoxidation Heats 300 & 500 °C

b. Butane Pulse Selectivities & Conversions (400 °C)

c. Catalyst Reduction & Reoxidation Rates (400 °C)

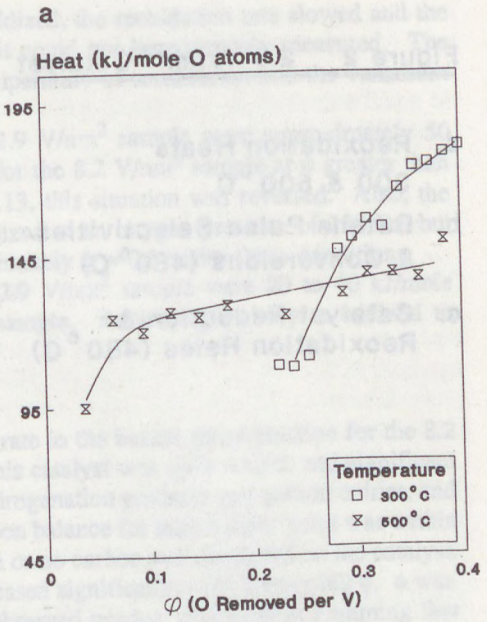

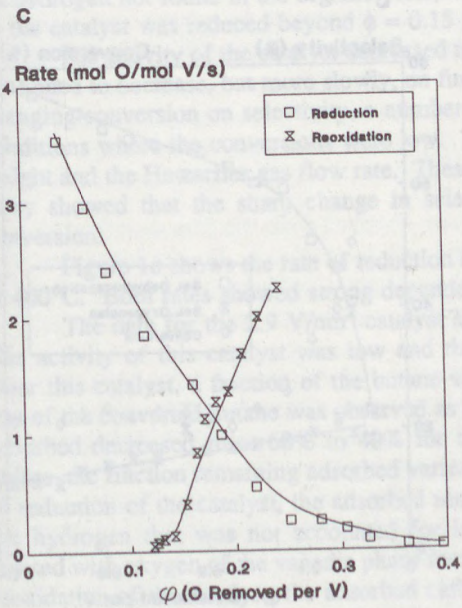

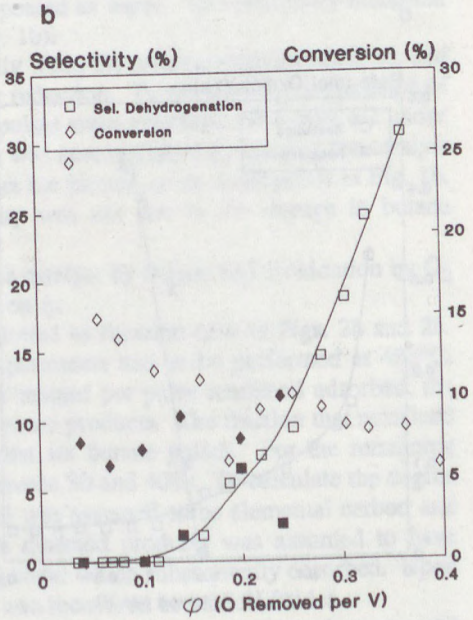

Figure 2 2.9 V/nm^2 Catalyst

a. Reoxidation Heats 300 & 500 °C

b. Butane Pulse Selectivities & Conversions (480° C)

c. Catalyst Reduction & Reoxidation Rates (480 °C)

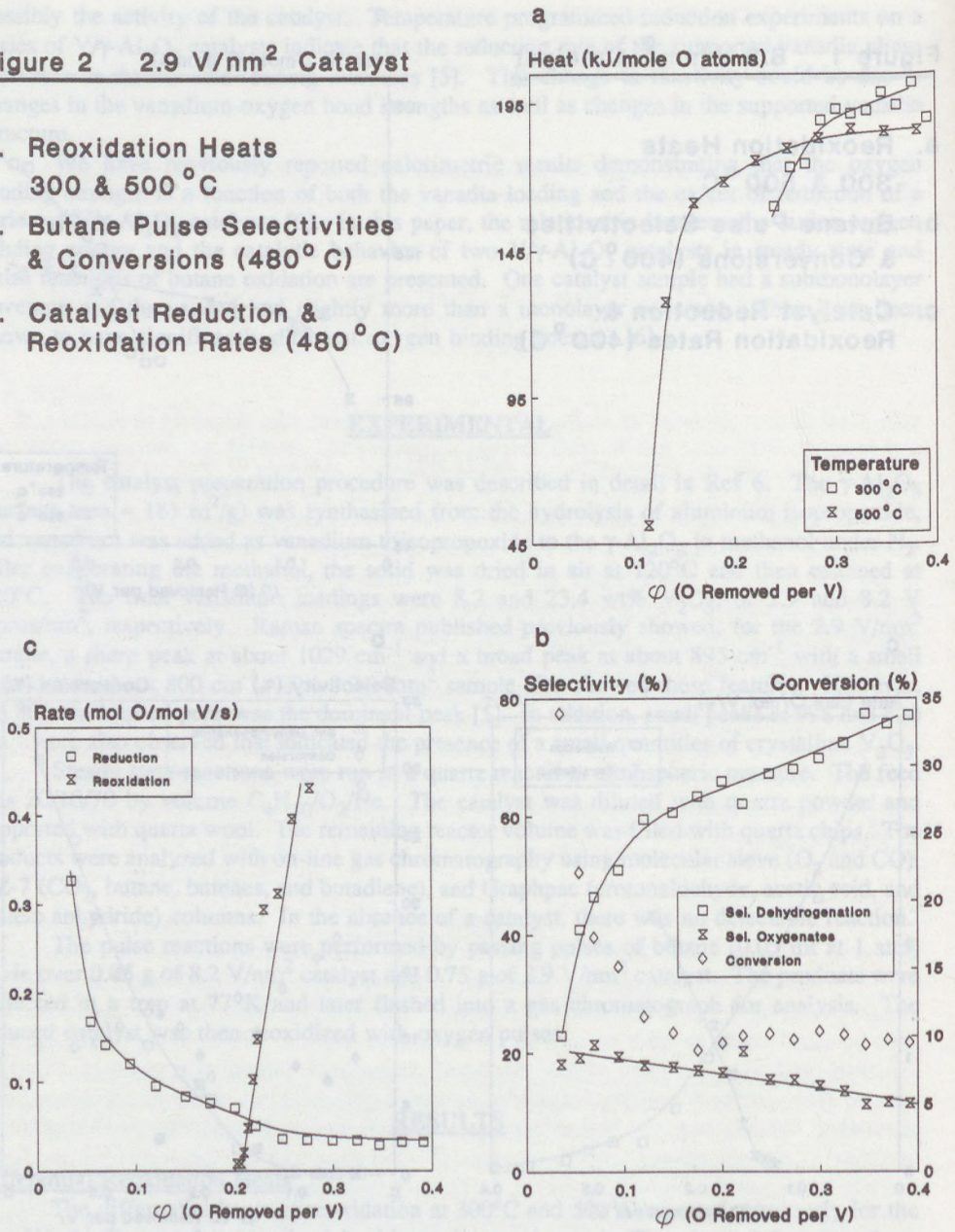

removed per vanadium ion. As the samples reoxidized, the reoxidation rate slowed and the heat generated per oxygen dose decreased until it could not be accurately measured. The point at which this occurred depended on the temperature of reoxidation and the vanadium loading, as shown in the figures.

At 500°C, the reoxidation heats for the 2.9 V/nm^2 sample were approximately 50 kJ/mole O atoms higher than the heat measured for the 8.2 V/nm^2 sample at ϕ greater than approximately 0.13. For ϕ smaller than about 0.13, this situation was reversed. Also, the 8.2 V/nm^2 sample was almost completely reoxidized at an oxygen pressure of 133 Pa, but the 2.9 V/nm^2 sample only reoxidized to approximately $\phi = 0.1$ under these conditions.

At 300°C, the reoxidation heats for the 2.9 V/nm^2 sample were 20 to 40 kJ/mole larger than those measured for the 8.2 V/nm^2 sample. Both samples only reoxidized to approximately $\phi = 0.2$ in 133 Pa of O_2.

Pulse Reduction/Reoxidation Experiments

The product distribution and the reaction rate in the butane pulse reaction for the 8.2 V/nm^2 catalyst are shown in Figs. 1b and 1c. This catalyst was quite active, and significant conversions were observed at 400°C. Only dehydrogenation products and carbon oxides, and no oxygenated products were observed. The carbon balance for each butane pulse was within experimental uncertainties (± 3%) indicating little or no carbon was deposited on the catalyst. The selectivity to dehydrogenation products increased significantly with increasing ϕ. ϕ was calculated from the butane conversion and the observed product distribution, assuming that all hydrogen not found in the organic products appeared as water. The selectivity increased as the catalyst was reduced beyond $\phi = 0.15$ (Fig. 1b).

The activity of the catalyst decreased rapidly when the catalyst was first reduced, and continued to decrease, but more slowly, on further reduction. To establish the importance of changing conversion on selectivity, a number of pulses were administered at low ϕ's under conditions where the conversions were low. This was accomplished by varying the catalyst weight and the He carrier gas flow rate. These data are plotted as the solid points in Fig. 1b. They showed that the sharp change in selectivity was not due to the change in butane conversion.

Figure 1c shows the rate of reduction of the catalyst by butane and reoxidation by O_2 at 400°C. Both rates showed strong dependence on ϕ.

The data for the 2.9 V/nm^2 catalyst are plotted as function of ϕ in Figs. 2b and 2c. The activity of this catalyst was low and the experiments had to be performed at 480°C. Over this catalyst, a fraction of the butane which reacted per pulse remained adsorbed, the rest of the converted butane was observed as gas phase products. The fraction that remained adsorbed decreased from 60% to 40% for the first six butane pulses. For the remaining pulses, the fraction remaining adsorbed varied between 30 and 40%. To calculate the degree of reduction of the catalyst, the adsorbed material was assumed to be elemental carbon and the hydrogen that was not accounted for in the detected products was assumed to have reacted with oxygen of the vanadia phase forming water which subsequently desorbed. Upon reoxidation of the catalyst, the adsorbed carbon was recovered as carbon oxides.

The primary selective oxidation products over this catalyst were butenes and butadiene. The selectivities in Fig. 2b were calculated based on the detected products. They increased as the catalyst was reduced. At low ϕ's, over 10% of the products were crotonaldehyde and maleic anhydride, but the amounts decreased as the catalyst was reduced.

At large values of ϕ, small quantities of ethene, propene, propionic acid, and acrylic acid were formed. Fig. 2c shows the rates of reduction by butane and reoxidation of the catalyst. These rates were about one order of magnitude smaller than those for the 8.2 V/nm^2 sample. At small values of ϕ, the rate of reduction decreased rapidly with increasing ϕ. At large values of ϕ, the rate of reduction decreased slowly with ϕ. The opposite behavior was observed for the rate of oxidation by O_2.

Steady State Butane Oxidation

The data for the steady state butane oxidation at 400°C are summarized in Table 1. The γ-Al_2O_3 support had minimal catalytic activity for butane oxidation. The butane conversion over 1 g of the support was < 1% at 400°C and with a feed flow rate of 100 cm^3/min. The product composition was 29% CO and 71% CO_2. Over the 2.9 V/nm^2 catalyst, 45% of the products were the three butene isomers and butadiene. No oxygenates were detected. Over the 8.2 V/nm^2 catalyst, there were slightly more oxygenate products than dehydrogenation products, but the overall selectivity for selective oxidation was low.

Butane oxidation over a physical mixture of the 8.2 V/nm^2 catalyst and the γ-Al_2O_3 support at 400°C produced no oxygenated products. The selectivities to dehydrogenation products were similar to those found when only the pure 8.2 V/nm^2 catalyst was used. Thus the oxygenated products were converted to carbon oxides over the γ-Al_2O_3.

Table 1 also shows the reaction rates over the catalyst. The rate per V ion was approximately an order of magnitude larger over the 8.2 V/nm^2 catalyst than over the 2.9 V/nm^2 catalyst. The rates over the 8.2 V/nm^2 - γ-Al_2O_3 physical mixture and the 8.2 V/nm^2 catalyst were comparable indicating that the catalytic behavior of the mixture was a sum of the two pure components and that the activation of the butane was predominantly by the vanadia.

DISCUSSION

The following interesting observations were obtained from the data described above:

1. The selectivity for dehydrogenation increased with increasing ϕ. For the higher loading catalyst (8.2 V/nm^2), the increase was very rapid for ϕ between 0.2 and 0.3. For the lower loading catalyst (2.9 V/nm^2), the increase was rapid up to ϕ = 0.1, thereafter the increase was slower.
2. The rate of reaction of butane decreased rapidly with increasing ϕ for both catalysts when the catalysts were nearly fully oxidized and then slowly at higher values of ϕ.
3. Comparing the two catalysts in the steady state experiments, the higher loading catalyst was less selective for dehydrogenation, but some oxygenates were observed. This catalyst was also less selective for dehydrogenation in the pulse experiments. On the lower loading sample, small amounts of oxygenated products were detected in the pulse experiment but not in the steady state experiment.

On the 8.2 V/nm^2 sample, where the pulse data were not complicated by carbon deposition, it is interesting to note that the rapid change in conversion and in selectivity occur at different degrees of reduction and that the change in conversion is not the primary reason for change in selectivity (Figs. 1b and 1c). This suggests that the rate limiting step is different from the selectivity determining step. Using deuterium isotope labeling experiments,

Table 1. Product Distribution in Butane Oxidation at 400°C for $C_4H_{10}/O_2/He = 20/10/70$

Cat.[a]	Flow ml/min	C_4 Conv.[b]	R[c]	Product Selectivities[d] CO	CO_2	$1C_4$	tC_4	cC_4	B	A	M
γ-Al_2O_3	100	0.8	-	29	71	0	0	0	0	0	0
2.9 V/nm^2	50	7.0	.4	20	37	10	15	13	5	0	0
8.2 V/nm^2	75	8.2	3.3	39	34	4	4	4	0	2	13
γ-Al_2O_3 - 8.2 V/nm^2 Mixture	100	5.9	3.2	38	46	4	4	8	0	0	0

Footnotes

a. Weight of catalyst used: 1.058 g γ-Al_2O_3, 0.784 g 2.9 V/nm^2, 0.057 g 8.2 V/nm^2, and 0.795 g γ-Al_2O_3 mixed with 0.046 g 8.2 V/nm^2.
b. The carbon balance was 100 ± 3%.
c. Rate expressed as (moles butane reacted/mole vanadium/sec)*10^3
d. The carbon containing products are CO, CO_2, 1-butene ($1C_4$), t-2-butene (tC_4), cis-2-butene (cC_4), butadiene (B), acetic acid (A), and maleic anhydride (M).

previous workers have shown that the rate limiting step in butane oxidation over a V-P-O catalyst is the breaking of a methylene C-H bond to form an adsorbed alkyl and a surface OH group [3]. It is reasonable to assume that the breaking of the first C-H bond is also the rate limiting step in this reaction.

The selectivity for dehydrogenation, oxygenate formation, or combustion should be determined by the rates of subsequent C-H bond breaking, C-C bond breaking, and C-O bond formation. These steps involve very different chemical transformations from that in the first C-H bond breaking.

A simplified version of the reaction scheme is represented in Fig. 3. In this scheme, the steps in which lattice oxygen are involved in a pulse experiment are labelled with [O]. In these steps, lattice oxygens are removed from the catalyst to form C-O bonds with the surface intermediates. Thus, one could expect that the rates of these steps are strongly influenced by the ease of removal of oxygen from the lattice.

Figure 1a shows the relative ease of removal of lattice oxygen from the 8.2 V/nm^2 sample measured as the differential heat of reoxidation. The data were obtained at 300 and 500°C.

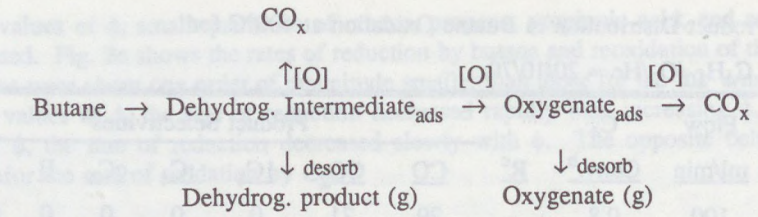

Figure 3. Simplified Butane Oxidation Mechanism

By interpolation, the curve at 400°C would show the differential heat to be low but increasing rapidly for $\phi \leq 0.15$. For larger values of ϕ, the heat attains a high value but increases relatively slowly. This behavior of the differential heat parallels the change in selectivity for dehydrogenation (Fig. 1b). Thus, there is a strong correlation that the selectivity toward C-O bond formation decreases rapidly with increasing binding strength of the lattice oxygen when the binding is stronger than about 110 kJ/mole O. It is also interesting to point out that the rapid change in selectivity with increasing ϕ strongly suggests that it is not due to a change in the oxidation state of V in the active sites.

The gross behavior of the lower loading (2.9 V/nm^2) sample in the pulse reaction can be similarly explained, although the substantial carbon deposition complicates interpretation. For this sample, the lower activity necessitates the use of a higher temperature of 480°C. At this temperature, the dependence of the heat of reoxidation on ϕ should be close to that measured at 500°C (Fig. 2a). Thus, the heat increases rapidly up to $\phi = 0.1$ beyond which it increases slowly.

The change in selectivity for dehydrogenation with ϕ on this catalyst follows this behavior. The selectivity increases slowly for ϕ larger than about 0.1. It increases rapidly at lower ϕ, but in this region a high fraction of butane which reacted in each pulse was undetected due to deposition as carbonaceous deposits on the catalyst, most likely on the alumina surface. Thus the distribution of the detected products does not accurately reflect the intrinsic selectivity of the vanadia.

Deposition of carbonaceous residues also introduces uncertainties in the estimation of ϕ. The assumption that these deposits only contain carbon is unrealistic because most likely they also contain hydrogen and oxygen. Neglecting the presence of hydrogen overestimates ϕ but neglecting oxygen underestimates it such that the errors partially cancel. That this is indeed the case can be seen from the dependence of the rate of reoxidation on ϕ. Figure 2c shows that the rate of reoxidation of the catalyst after the butane pulse reaction changes sharply between $\phi = 0.2$ and 0.25. Previously we have shown that if the sample is reduced by H_2 (and thus there are no carbonaceous deposits), the rate of reoxidation drops sharply at about $\phi = 0.18$ [6]. The similar behavior of these two types of measurements strongly suggests that the assumption introduces only minor errors.

The discussion thus far assumes that the rate limiting step is the activation of butane. The ten-fold difference in the activity of the two samples in both the pulse and the steady state reaction is then due to different densities of active sites which can activate butane. Raman spectroscopic characterization of these samples suggests that a larger fraction of vanadia is in a two-dimensional network in the higher loading sample, whereas there are more isolated

VO_x species in the lower loading sample [6]. The differences in their activities could be explained assuming that the isolated vanadia species are much less active than the two-dimensional network.

Infra-red and calorimetric evidence show that as the vanadia species is reduced, its dispersion also reduces such that three dimensional clusters are formed [6,7]. In this process, the exposed surface area of the vanadia will be lowered. It is possible that the decrease in activity for butane oxidation with increasing ϕ (Fig. 1c and 2c) is due to this clustering process and the reduction in the surface area of the vanadia.

In addition to differences in pulse reactions, the steady state behavior of the two samples are also different. The lower loading catalyst is less active but more selective for dehydrogenation. Unlike the pulse reaction data, this sample produces no oxygenates at steady state. This is probably due to the activity of the exposed alumina in oxidizing the oxygenated products to CO_x. Indeed, the oxygenates produced over the 8.2 V/nm^2 catalyst are absent when this catalyst is physically mixed with γ-Al_2O_3.

Since the selectivity over these catalysts depends on ϕ, it is necessary to know the degree of reduction of the samples at steady state to understand their different selectivities. Comparison of the catalyst reduction and reoxidation rates measured in the pulse reaction experiments give an indication of the magnitude of ϕ at steady state. Since these two rates are equal at steady state, ϕ can be estimated as the point at which the reduction and reoxidation rate curves intersect. Fig. 2c shows that for the 2.9 V/nm^2 catalyst at 480°C, ϕ = 0.2 and for the 8.2 V/nm^2 catalyst at 400°C, ϕ is less than 0.2 (Fig 1c) indicating that this catalyst is less reduced under steady state conditions.

These results agree well with similar experiments in which the rates of catalyst reduction with H_2 and reoxidation with O_2 were measured under static conditions [6]. These experiments also indicated that the lower loading catalyst would be more reduced than the higher loading catalyst under steady state conditions for the H_2-O_2 reaction. Other supported catalysts have been observed to be substantially reduced after steady state catalytic reactions. Gasior et al. analyzed V/TiO_2 (anatase) catalysts for V^{4+} content after steady state o-xylene oxidation [8]. They found that the vanadia phase was composed of 15% to 20% V^{4+} (ϕ = 0.3 to 0.4). They also found the lower vanadia coverage to be more reduced than the higher loading catalyst.

The selectivity in steady state butane oxidation for the two V/γ-Al_2O_3 catalysts may be interpreted in terms of the binding strength of the lattice oxygen to the catalyst. At steady state, ϕ is slightly larger than 0.2 for the 2.9 V/nm^2 sample and slightly smaller than 0.2 for the 8.2 V/nm^2 sample. At these values of ϕ, the differential heats of reoxidation are about 170 and 130 kJ/mole O respectively for the two samples. As has been discussed above, a larger heat represents more strongly bound lattice oxygen which has been correlated to a higher selectivity for dehydrogenation. Thus, the lower loading sample, in which the oxygen is more strongly bound, is more selective.

It should be emphasized that throughout the discussion, the lattice oxygen is assumed to be the oxygen species that participates in the selectivity-determining step. Thus, its binding strength is important in determining selectivity. Subsequent steps may involve adsorbed oxygen, particularly in the steady state reactions. However, these adsorbed oxygens are assumed not to be involved in the selectivity-determining step. Finally, significant amounts of CO_x are formed even at low conversions. This suggests that the combustion reaction also occurs by degradation of surface intermediates before any desorption.

The data do not provide information on the atomic composition of the active sites. In particular, they do not distinguish whether the change in selectivity with ϕ is due to a change in the nature of such sites, or due to preferential removal of one type of site (combustion sites) as ϕ increases, as long as the average oxygen binding energy of the active sites increases with ϕ. In either case, one can conclude that active sites of lower binding energy of lattice oxygen are more active for combustion.

CONCLUSIONS

Both the rates of butane oxidation and the selectivities to partial oxidation products over $V/\gamma\text{-}Al_2O_3$ catalysts depend on the degree of reduction of the catalyst and the vanadium loading. Pulse butane oxidation experiments indicate that the selectivities to dehydrogenation products increase as the catalyst is reduced and the oxygen is more strongly bound to the catalyst. At steady state, the catalyst of a lower vanadia loading is more selective for dehydrogenation and is slightly more reduced. Its higher selectivity can be explained by the higher binding strength of lattice oxygen at steady state.

ACKNOWLEDGEMENT

Support by the National Science Foundation, Division of Chemical and Thermal Systems is gratefully acknowledged.

References

1 (a) Wachs, I. E.; Saleh, R. Y.; Chan, S. S.; Chersich, C. C., Appl. Catal., 1985, 15, 339. (b) Eckert, H.; Wachs, I. E., J. Phys. Chem., 1989, 93, 6796. (c) Went, G. T.; Oyama, S. T.; Bell, A. T., J. Phys. Chem., 1990, 94, 4240.

2. (a) Bond, G. C.; Brükman, K., Faraday Discussions, 1981, 72, 235. (b) Jonson, B.; Rebenstorf, B.; Larsson, R.; Anderson, S. L. T.; Lundin, S. T., J. Chem Soc., Faraday Trans. I, 86, 767. (c) Mori, K.; Miyamoto, A.; Murakami, Y.; J. Chem. Soc., Faraday Trans. I, 1986, 82, 13.

3. Pepera, M. A.; Callahan, J. L.; Desmond, M. J.; Milberger, E. C.; Blum, P. R.; Bremer, N. J., J. Am. Chem. Soc., 1985, 107, 4883.

4. Peacock, J. M.; Parker, A. J.; Ashmore, P. G.; Hockey, J. A., J. Catal., 1969, 15, 398.

5. Kijenski, J.; Baiker, A.; Glinski, M.; Dollenmeier, P.; Wokaun, A., J. Catal., 1986, 101, 1.

6. Andersen, P. J.; Kung, H. H., J. Phys. Chem., in press.

7. (a) Sobalik, Z.; Kozłowski, R.; Haber, J., J. Catal., 1991, 127, 665. (b) Topsøe, N., J. Catal., 1991, 128, 499. (c) Odriozola, J. A.; Soria, J.; Somorjai, G. A.; Heinemann, H.; Garcia de la Banda, J. F. Lopez Granados, M.; Conesa, J. C., J. Phys. Chem., 1991, 95, 240.

8. Gaşior, M.; Gaşior, I.; Grzybowski, B., Appl. Catal., 1984, 10, 87.

DISCUSSION

Q: M. Sinev (Russia)

The extensive studies of different oxide systems showed that there is an alternative mechanism of redox reactions including reoxidation without dehydroxilation of the surface. In other words, the evolution of water may be a result of reduction of the surface and also the result of reoxidation. Generally, we have mixed situation and the heat evolution in reoxidation is dependent on the fraction of water evolved in "red" and "ox" parts of the cycle. Have you measured the concentration of water in outlet gas and what is the exact mechanism of reoxidation in the case of $V/\gamma\text{-}Al_2O_3$ system ?

If you are sure that you have complete dehydroxylation of the surface before reoxidation, what is the origin of the dependence of heat evolution on experimental conditions (mostly temperature) ?

A: H. H. Kung

Incomplete dehydroxylation would affect the measured heats of reduction or reoxidation. To test that our heat measurements were not affected by this effect, we reduced the samples with CO also. In that case, no water was produced. The results [1] showed that the reoxidation heats do not depend on the whether the samples were reduced with hydrogen or CO.

The dependence of the heat on the reoxidation temperature is due to two effects: 1) heat capacity differences between the oxidized and reduced states of vanadia, and 2) the mechanism of reoxidation, which is detailed in ref. 6. Briefly, reoxidation is accompanied by diffusion of lattice oxygen and redispersion of the vanadia particle, both of which are rate processes that depend on the temperature.

[1] P. J. Andersen and H. H. Kung, *J. Phys. Chem.*, **96**, 3114 (1992)

Q: F. Trifiro (Italy)

In the case of oxidation of n-butane to maleic anhydride with a V-P mixed oxide, we have found with the degree of reduction of the catalyst the same mechanism: butane → butenes → oxygenates. Our interpretation was that dehydrogenation requires the V(IV) → V(III) couple, whereas oxygen insertion requires V(V) → V(IV) couple. Is it possible to explain your data with the same hypothesis ?

A: H. H. Kung

We believe that our idea and yours are similar, only that our data are a different representation. The heat of reoxidation directly measures the ΔH of the redox couples. That is, at low ϕ, we were measuring the V(V) → V(IV) couple, and at high ϕ the V(IV) → V(III) couple, plus the heats associated with lattice diffusion and redispersion. Our measurement provides a quantitative explanation on the difference between the two couples.

Q: J. C. Volta (France)

Correlation between selectivity for ODH of alkanes and reducibility appears to be a good approach to study the reactivity of the catalysts. We found also a good correlation on VMgO catalysts for ODH of propane into propene. I think, however, that the alkane/O_2 ratio is an important parameter which has to be studied. What is your opinion on its influence on the selectivity/reducibility correlation ?

A: H. H. Kung

If the reaction proceeds via a redox mechanism, then the steady state degree of oxidation of the catalyst depends on the relative rates of reduction of the catalyst by the hydrocarbon and reoxidation by oxygen. One or both steps could depend on the partial pressures of the reactants. Therefore, the alkane/O_2 ratio should affect the selectivity if it significantly affects the degree of reduction of the catalyst at steady state.

Q: J. Haber (Poland)

In your reaction model, the selectivity is determined by the fate of the first surface intermediate - it can either lose the second hydrogen and desorb as butene or be attacked by oxygen and undergo combustion. The ratio of the rates of these two reaction pathways should strongly depend on the population of the surface with oxygen. This can be easily checked by following the changes of selectivity on addition of oxygen. Have you considered the possibility of experiments in which the surface would be partially reoxidized and the selectivity measured? This could confirm the model.

A: H. H. Kung

Yes, we have first reduced a catalyst and then partially reoxidized it to a certain extent, and then pulse butane over it. The selectivity was found to be comparable to the case where the catalyst was simply reduced to the same extent. However, as was shown in [1], if this experiment were to be carried at a lower temperature such that the lattice diffusion is not fast the degree of reduction in the bulk is not a good measure of the degree of reduction of the surface, and we would expect to observe different selectivities.

We should emphasize that the degree of reduction in the bulk is not a fundamental parameter determining selectivity. The metal-oxygen bond strength is.

Q: M. Bhasin (USA)

The model you proposed for oxidative dehydrogenation selectivity with reducibility of metal oxide (heat of reoxidation) is an interesting one. Have you tried to extend this model to other oxides or to predict a much higher (approaching 100%) selectivity catalyst composition?

A: H. H. Kung

We have not tried to do so yet. Although we believe that reducibility is an important factor, we should not claim that it is the only factor. We need to understand better the relative importance of the various factors before we can predict selectivity quantitatively.

Q: Y. Arnaud (France)

Recently I have sent you some papers so that you know that I am proposing a new theory in view to explain activity and selectivity of oxides.

I consider that your work is very interesting because it deals with an important problem of catalysis. I would emphasize that we have to confirm bond strengths or bonding energies with adsorption-desorption energies or formation enthalpy. The latter only relate to catalytic phenomenon. On oxide surfaces there exist several kinds of oxygen which can be characterized by their coordination number n; c being the bulk one, we have $n = \text{or} < c$.

You measured reoxidation heats of samples in different degrees of reduction and the curves are difficult to interpret. How do you measure ϕ, the degree of reduction ?

A: H. H. Kung

The degree of reduction was measured volumetrically by monitoring the volume of gaseous reductant consumed and knowing the stoichiometry of the reduction reaction. In [1] we compared the degree of reduction so calculated with that determined by chemical titration. The two values compared well.

Q: M. Misono (Japan)

In the case of oxidation of alkanes, the role of adsorbed oxygen could be very important. In this respect, I would like to ask one question.

You showed in Figs. 1c and 2c the rates of reduction and reoxidation as a function of ϕ. If the simple redox model is a good approximation, the rates at the crosspoints in the figures must agree with the rate at the steady state of catalytic oxidation (b). Could you compare the

A: H. H. Kung

If the two rates are measured under the same conditions, then they should agree if the redox mechanism operates. In our case, the rates calculated in the pulse reaction is the average rate when the pulse passes over the catalyst. The partial pressures of the reactants were not the same as those in the steady state reaction. Nonetheless, the rates in the two types of experiments were within a factor of five of each other. In view of the different reaction conditions, this seems to be a satisfactory agreement.

Q: S. L. Kiperman (Russia)

It follows from your communication that the rate-determining step and the selectivity-determining step are different. But it is known that if the reaction proceeds via a rate-determining step, this step is slower and single. Therefore, the question arrives: do you think the selectivity-determining step proceeds quickly or slowly ?

A: H. H. Kung

The selectivity-determining step is the further reaction of the alkyl species (or the reaction of the adsorbed alkene). This step consists of at least two competing reactions: insertion of oxygen into the surface intermediate, and abstraction of the second hydrogen (or desorption of the alkene). It proceeds faster than the rate-determining step. We should add that selectivity is determined by the ratios of the rate constants of the competing steps.

Q: C.-g. Huang (Taiwan)

As shown in your data, the oxidation heat varies not only with the extent of oxygen removed. It also depends upon the pretreatment, i.e. the reduction being carried out at 300 or 500 ^{0}C. I would suspect that different oxygen ions, terminal or bridged, might be removed, depending on the reduction temperature employed. This is reflected in selectivity if it is plotted versus ϕ, in which the pretreatment temperature may appear as a parameter. Could you comment if different oxygen ions are removed ?

A: H. H. Kung

We have not reduced our samples at different temperatures. The temperatures that you refer to are the reoxidation temperatures. As in my reply to M. Sinev, the heat of reoxidation is a function of the temperature.

At this point, we have no information as to whether different oxygen ions are removed under different reaction conditions. In our interpretation of the data, we emphasize that we are only concerned with the single oxygen ion involved in the selectivity-determining step. We believe at this point that this oxygen ion is a bridging oxygen ion.

Q: D. Wang (China)

You interpret your results on changes in catalyst selectivity with the binding energies of lattice oxygen. Can one use here, also, Dr. Rabo's idea of short-range and long-range interactions (see p. 1) and offer an interpretation based on structural changes occurring with the extent of reduction.

A: H. H. Kung

As described in [1], we believe that there is significant structural reorganization during oxidation and reduction of the vanadia species. Therefore, the heat measured involved the energy of breaking or formation of oxygen-cation bonds as well as lattice diffusion and structural reorganization. These effects cannot be deconvoluted in our experiments.

Guczi, L. *et al.* (Editors), *New Frontiers in Catalysis*
Proceedings of the 10th International Congress on Catalysis, 19-24 July, 1992, Budapest, Hungary
© 1993 Elsevier Science Publishers B.V. All rights reserved

SECONDARY OXYGEN EXCHANGE REACTIONS DURING THE PARTIAL OXIDATION OF METHANE

M. M. Koranne, J. G. Goodwin, Jr. and G. Marcelin

Chemical and Petroleum Engineering Department, University of Pittsburgh, Pittsburgh PA 15261, USA

Abstract

In order to better understand the reaction pathway during the partial oxidation of methane, O-exchange with O_2 and CO_2 over V_2O_5/SiO_2 was examined using isotopic transient techniques. It was found that, during the partial oxidation reaction, the O-exchange capability of the V_2O_5/SiO_2 catalyst increased significantly. Secondary exchange reactions of CO_2 with the V_2O_5/SiO_2 were demonstrated. It was also shown that the CO_2 species exchanging with the catalyst were in equilibrium and that the rate of O-exchange with O_2 was much lower than with CO_2. This resulted in an apparently higher contribution of lattice oxygen for O-exchange with CO_2 during the partial oxidation reaction. Thus, the identification of the origin of the O-species involved in the formation of a particular product is greatly complicated by the presence of secondary exchange reactions.

1. INTRODUCTION

The catalytic conversion of methane to ethane or oxygenates over oxide catalysts has acquired increased importance in recent years due to a world-wide surplus of methane. Although the mechanism for the conversion of methane to ethane via an oxidative coupling reaction is well established, there have been few studies to date which examine the reaction mechanism for the partial oxidation of methane to oxygenates (1, 2). One of the major issues in a partial oxidation reaction over oxide catalysts is the role of the lattice oxygen. While it is widely accepted that lattice oxygen participates in the partial oxidation reactions (3-5), the relative contributions of lattice and adsorbed oxygen species still remain unclear (6-8).

In an attempt to identify the role of various oxygen species, isotopic studies have been widely used (3-9). Keulks and coworkers (3, 4) have used isotopic tracers to establish the participation of the lattice oxygen in the partial oxidation of propylene to acrolein. Similar studies have been reported by various researchers to establish the contribution of the adsorbed oxygen vs. that of the lattice oxygen, particularly in the formation of non-selective species like CO and CO_2 (8, 9). However, in such studies the exchange reactions after the formation of the product from a primary species, i.e., secondary oxygen exchange, were often ignored.

The feasibility of using transient isotopic techniques for studying the role of catalyst oxygen has been recently shown (10, 11). In this technique the mechanistic information can be obtained without perturbing the steady-state of the system (12). This paper reports a study of the role of secondary exchange reactions in the partial oxidation reaction using isotopic transient techniques.

2. EXPERIMENTAL

A silica-supported 2% vanadia catalyst was prepared by the wet impregnation technique. The partial oxidation of methane was studied by reacting a mixture of CH_4 and O_2 over the V_2O_5/SiO_2 catalyst in a quartz microreactor system. A detailed description of the preparation and the characterization of the catalysts, and the experimental set-up is given elsewhere (13, 14). The reaction conditions used were: $CH_4 : O_2 : He = 10 : 1 : 20$, T= 600°C, P= 1 atm. Oxygen transients were obtained by switching abruptly from $^{16}O_2$ to $^{18}O_2$ at steady-state and monitoring the products continuously using mass spectrometry.

The CO_2 exchange experiments were carried out by modifying the transient isotopic system as shown in Figure 1. The required amount of CO_2 was obtained by the reaction of CH_4 and O_2 in He over a 3% Pd/SiO_2 catalyst. The resulting products were passed over the V_2O_5/SiO_2 catalyst before analysis. Thus, during a CO_2 transient isotopic run, $C^{18}O_2$ was produced by abruptly switching from $^{16}O_2$ to $^{18}O_2$ at steady-state. The reaction conditions were carefully chosen in order obtain CO_2 transients both in the presence and in the absence of methane (see Table 1).

All transients are reported as normalized rates versus time. Thus, F(t) for $C^{16}O_2$ is the ratio of the exiting flow rate of $C^{16}O_2$ to the total flow rate of CO_2 ($C^{16}O_2 + C^{16}O^{18}O + C^{18}O_2$). All other normalized rates were calculated accordingly. Argon was usually present in one of the isotopes and used as an inert tracer which represented the gas-phase hold-up in the system.

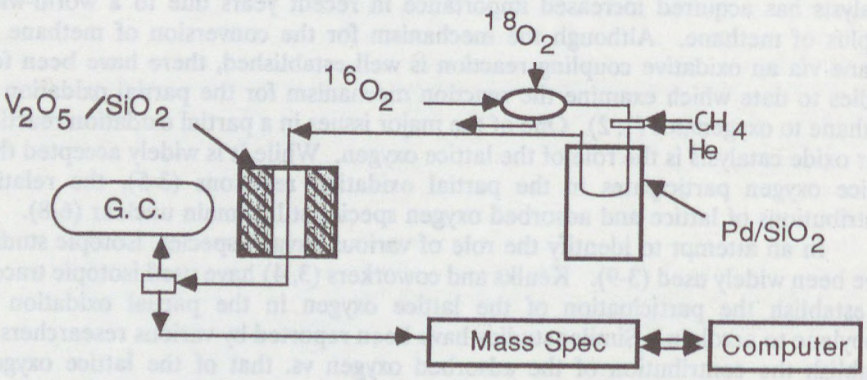

Figure 1. Experimental set-up for CO_2 exchange studies.

Table 1
Summary of the Reaction Conditions for O-Exchange with CO_2.

Run type	Temp °C	Catalyst	Flow rates cc/min
A	550	None	CO_2 = 1, He = 30
B	550	V_2O_5/SiO_2	CO_2 = 1, He = 30
C	600	None	CO_2 = 1, He = 30
D	600	V_2O_5/SiO_2	CO_2 = 1, He = 30
E	550	None	CH_4 = 0.75, CO_2 = 0.75, He = 30
F	550	V_2O_5/SiO_2	CH_4 = 0.75, CO_2 = 0.75, He = 30
G	600	None	CH_4 = 0.75, CO_2 = 0.75, He = 30
H	600	V_2O_5/SiO_2	CH_4 = 0.75, CO_2 = 0.75, He = 30

3. RESULTS

3.1 O-exchange with O_2

The reaction of CH_4 with O_2 at 600°C over the 2% V_2O_5/SiO_2 catalyst yielded HCHO, CO, CO_2 and C_2H_6 as major products with selectivities of 6%, 80%, 10% and 4%, respectively, and a methane conversion of 5%. CH_3OH was detected only in trace amounts. A typical transient obtained by switching from $^{16}O_2$ to $^{18}O_2$ in the absence of methane at steady-state is shown in Figure 2a. It can be seen that some scrambled product signal, $^{16}O^{18}O$, was observed in the absence of methane. Since the only source of $^{16}O_2$ after the isotopic switch was the catalyst itself, the $^{16}O^{18}O$ signal was indicative of the oxygen exchange capability of the catalyst. A similar transient obtained by switching from $^{16}O_2$ to $^{18}O_2$ at steady-state in the presence of methane is shown in Figure 2b. It can be seen that in the presence of methane the scrambled product signal increased significantly indicating a corresponding increase in the oxygen exchange capability of the catalyst. Figure 3 shows the transient for the product CO_2 obtained at 600°C over the catalyst. The large amount of scrambled product, $C^{16}O^{18}O$, suggests at first that catalyst oxygen can readily participate in the formation of non-selective products like CO_2.

3.2 O-exchange with CO_2

In order to verify whether or not the labelled CO_2 results were solely due to a primary reaction of CH_4 with catalyst oxygen, experiments were carried out involving

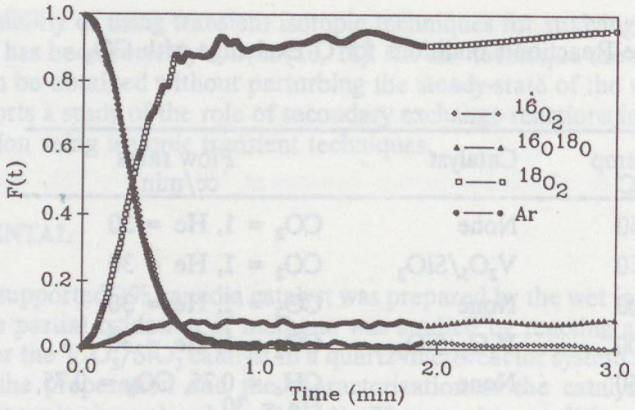

Figure 2a. O_2 transients at 600°C in the absence of CH_4 over V_2O_5/SiO_2 catalyst.

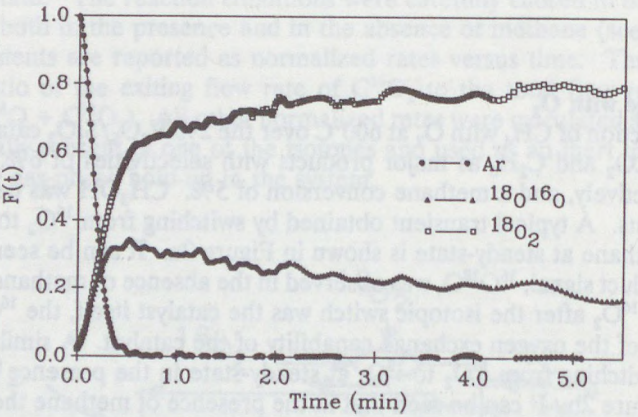

Figure 2b. O_2 transients during the partial oxidation of methane at 600°C over V_2O_5/SiO_2 catalyst.

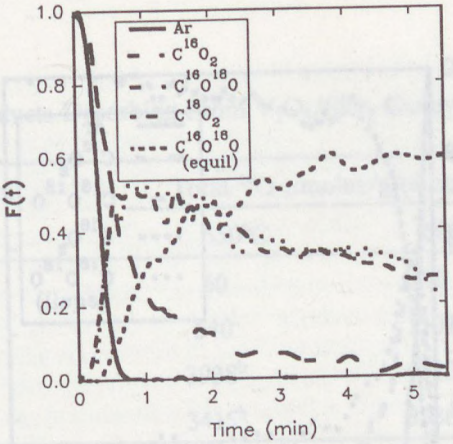

Figure 3. CO_2 transients at 600°C during the partial oxidation of methane over V_2O_5/SiO_2 catalyst.

CO_2 exchange with the catalyst (see Table 1). A methane-oxygen mixture when reacted over a Pd/SiO_2 catalyst yielded CO_2 and H_2O as the only products. For run types A, B, C, and D, stoichiometric amounts of methane and oxygen were reacted totally to CO_2. For run types E, F, G, and H, methane was fed in excess of the stoichiometric amount and a 50% conversion of methane to CO_2 was obtained.

Figure 4 shows a typical CO_2 transient for a blank run, i.e., without the V_2O_5/SiO_2 catalyst (run types A and C). It can be seen that $C^{16}O^{18}O$ initially exhibited a sharp peak which rapidly decreased to zero. This feature was due to the formation of $C^{18}O_2$ by the reaction of CH_4 with $^{18}O_2$ over the Pd/SiO_2 catalyst and indicates the surface oxygen as a source of ^{16}O. In contrast, in the presence of the V_2O_5/SiO_2 catalyst (run types B and D), the scrambled product signal did not relax to zero (see Figure 5) indicating the presence of a source of ^{16}O, in this case the catalyst. This demonstrates that exchange reactions occurred between $C^{18}O_2$ and the catalyst oxygen yielding $C^{16}O^{18}O$ even after 5.5 minutes of reaction.

In order to observe the effect of the presence of methane on the O-exchange with CO_2, transients were obtained using run types E, F, G, and H. In absence of the V_2O_5/SiO_2 catalyst, a similar sharp peak for the scrambled product was observed with the signal relaxing rapidly to zero (run types E and G). However, in the presence of the V_2O_5/SiO_2 catalyst, CO_2 transients were obtained which were similar to those in the absence of methane. Table 2 summarizes the total O-exchanged with all the O-containing species (O_2 CO_2, CO, HCHO, H_2O) up to 5.5 minutes of reaction for O_2 and CO_2 transients. The rates of O-exchange for O_2 and CO_2 at 5.5 minutes and 600°C were also obtained and are summarized in Table 3. These rates were calculated based on the rates of formation of the corresponding scrambled products. It can be seen that the rate of O-exchange for CO_2 is higher than that for O_2.

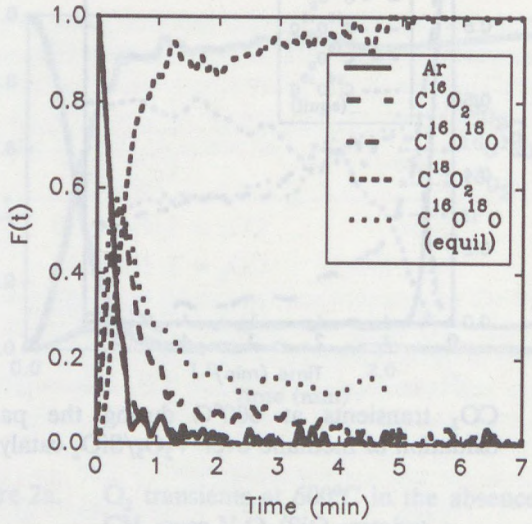

Figure 4. CO_2 transients at 550°C without V_2O_5/SiO_2 catalyst (run type A).

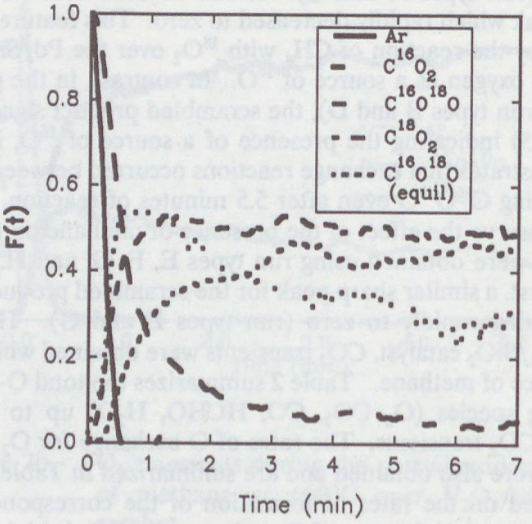

Figure 5. CO_2 transients at 550°C over V_2O_5/SiO_2 catalyst (run type B).

Table 2
Total ^{16}O in All Products Desorbing From V_2O_5/SiO_2 Catalyst

Feedstream	Total ^{16}O μmoles/g of catalyst[a]	
	550°C	600°C
$^{18}O_2$, He	60	90
$^{18}O_2$, CH_4, He	540	1500
$C^{18}O_2$, He	3938[b]	4040[b]
$C^{18}O_2$, CH_4, He	3415[b]	3536[b]

(a) Includes all oxygen containing species for the first 5.5 minutes of reaction.
(b) Differences observed in results with and without CH_4 can be attributed to differences in partial pressure of CO_2.

For the reaction $C^{16}O_2 + C^{18}O_2 \rightleftharpoons C^{18}O^{16}O$ the equilibrium constant equals 4. The equilibrium amounts of $C^{16}O^{18}O$ were obtained from the experimental values of $C^{16}O_2$ and $C^{18}O_2$ and are shown in Figures 3, 4, and 5. Near-equilibrium conditions were achieved in all cases. The relatively large deviations seen after about 5.5 minutes were probably due to the noise in the $C^{16}O_2$ signal which was close to zero.

4. DISCUSSION

Table 2 the lists the amounts of ^{16}O exchanged with O_2 and CO_2 for the first 5.5 minutes of reaction. It can be seen from Figures 2 and 3 and Table 2 that the V_2O_5/SiO_2 catalyst readily participated in the exchange process at 550°C and 600°C. Similar behavior has been reported by various researchers using static systems (15-18). Table 2 shows that, for O-exchange with O_2, the catalyst oxygen participation increased in the presence of methane. Oxygen exchange with O_2 on the catalyst is probably activated by a redox reaction involving reduction of the catalyst by the methane followed by its reoxidation by the feed O_2. Such a behavior is well known in partial oxidation catalysis (19-21).

For O-exchange with CO_2, it is evident from the large scrambled product signal that CO_2 exchanges with catalyst oxygen. Thus, the O-exchange with CO_2 clearly indicates that during methane oxidation on the V_2O_5/SiO_2 catalyst, secondary O-exchange reactions of CO_2 with the catalyst oxygen are possible. As seen from

Table 3
Rate of O-exchange at 600°C over V_2O_5/SiO_2 Catalyst

Exchanging Species	Feedstream	Rate of ^{16}O exchange[a] $x10^{-12}$ atoms/cm^2-s
O_2	$^{18}O_2$, He[b]	0.5
O_2	$^{18}O_2$, CH_4, He[b]	1.4
CO_2	$C^{18}O_2$, He[c]	3.8
CO_2	$C^{18}O_2$, CH_4, He[c]	3.1

(a) Based on surface area of 150 m^2/g.
(b) P = 1 atm, flow rate of O_2 = 1 cc/min, total flow rate = 31 cc/min.
(c) Conditions described in table 1 (run types D and H).

Table 3, the rate O-exchange for CO_2 was about 2-3 times higher than the rate of O-exchange for O_2. Similar trends were observed by Minachev et al. (22) for O-exchange with O_2 and CO_2 over bulk V_2O_5. Hirota et al. (23, 24) have suggested that the dissociative chemisorption of oxygen is more difficult over a non-reduced catalyst than a reduced one and that the dissociation of CO_2 is easier than that of O_2. This can result in higher CO_2 exchange rates.

In contrast to O-exchange with O_2, O-exchange with CO_2 seems to be largely unaffected by the presence or absence of methane (see Table 3). The surface reduction of oxides is known to produce enhanced O-exchange rates (25). Since O-exchange with O_2 is more difficult, it is likely to be more affected by the surface reduction than O-exchange with CO_2. It should be noted that although the oxidation state of the vanadia catalyst during reaction is not known, the surface may contain reduced sites on which rapid exchange can occur.

The mechanism of O-exchange with O_2 involving homomolecular and heteromolecular exchange reactions has been well established (15-18, 26). Several exchange reactions possible for O-exchange with CO_2 are listed below:

$$C^{18}O^{18}O + {}^{16}O_s \rightleftharpoons C^{16}O^{18}O + {}^{18}O_s \quad (1)$$
$$C^{16}O^{18}O + {}^{16}O_s \rightleftharpoons C^{16}O_2 + {}^{18}O_s \quad (2)$$
$$C^{18}O_2 + 2{}^{16}O_s \rightleftharpoons C^{16}O_2 + 2{}^{18}O_s \quad (3)$$
$$C^{16}\underline{O}{}^{18}O + 2{}^{16}O_s \rightleftharpoons C^{16}O_2 + {}^{18}O_s + {}^{16}\underline{O}_s \quad (4)$$
$$C^{16}O_2 + C^{18}O_2 \rightleftharpoons 2\,C^{16}O^{18}O \quad (5)$$

Exchange reactions 1-2 are heteromolecular one-event type (R'); exchange reaction 3-4 are heteromolecular two-event type (R"); and exchange reaction 5 is homomolecular exchange (R) (26). The formation of $C^{16}O^{18}O$ and $C^{16}O_2$ in $C^{18}O_2$ flow indicates the presence of R' and R" type of exchange. However, it is likely that

all the exchange reactions listed above occur simultaneously. The occurrence of these exchange reactions is believed to be due to the presence of surface vacancies (5, 19). Thus, the rate of R' type of exchange, for example, would depend on the concentration of surface vacancies adjacent to the chemisorption site. In fact, the homomolecular exchange can also be surface activated. If $C^{16}O_2$ and $C^{18}O_2$ are chemisorbed on adjacent sites, then an isotopic redistribution is possible to yield the scrambled product. This is probably the case for the large peak seen in the initial part of the transient for a blank run (see Figure 4). In such a case, due to the absence of a source of ^{16}O the scrambled product decreases rapidly to zero. It should be noted that the occurrence of the homomolecular reaction cannot be ruled out for O-exchange with CO_2 over the V_2O_5/SiO_2 catalyst. Patterson and Parker (7) have suggested that the homomolecular reaction is enhanced by surface reduction of the oxide catalyst. The near-equilibrium conditions attained for all the cases examined were probably due to such a process.

The presence of secondary exchange reactions, such as the CO_2 exchange with the catalyst, complicates any interpretation of the role of the lattice oxygen participation in the oxidation reaction. Due to such secondary reactions, it is not possible to ascertain whether the oxygen species in the products are from a primary reaction with the lattice oxygen or from a secondary exchange. A similar suggestion was made by Patterson and Parker (7) for the oxidation of methane over Sb/SnO_2 catalysts. Thus, it is difficult to determine the extent of lattice oxygen contribution in the formation CO_2 during the partial oxidation of methane.

5. CONCLUSIONS

Oxygen exchange with O_2 over V_2O_5/SiO_2 catalyst was studied during the partial oxidation of methane. It was found that the amount of O-exchange increased significantly only in the presence of methane. This can be attributed to a redox reaction making the surface more active for O-exchange in the presence of the methane. Oxygen exchange of CO_2 was shown to be significant with the V_2O_5/SiO_2 catalyst both in the presence and absence of methane, thus providing evidence for secondary exchange reactions. The rate of O-exchange with CO_2 was found to be much higher than with O_2. This is probably because of the ease of dissociation of CO_2 compared to that of O_2. Oxygen exchange with CO_2 involved both homomolecular and heteromolecular exchange reactions. It is speculated that the former is responsible for the rapid equilibration of CO_2. The secondary O-exchange with CO_2 during the partial oxidation of methane is probably responsible for the apparent higher contribution of lattice oxygen seen in the CO_2 transients. It is suggested that the presence of secondary O-exchange makes it difficult to trace the origin of the O-species responsible for oxidation, i.e., absorbed oxygen, lattice oxygen, or gas-phase oxygen.

6. ACKNOWLEDGEMENT

The partial support of the Ben Franklin Technology Center of Western Pennsylvania is gratefully acknowledged.

7. REFERENCES

1. Spencer, N.D., and Pereira, C.J., *J. Catal.*, **116**, 399 (1989).
2. Liu, H.F., Kiu, R.S., Liew, K.Y., Johnson, R.E., and Lunsford, J.H., *J. Am. Chem. Soc.*, **106**, 4117 (1984).
3. Krenzke, L.D., and Keulks, G.W., *J. Catal.*, **61**, 316 (1980).
4. Monnier, J.R., and Keulks, G.W., *J. Catal.*, **61**, 51 (1981).
5. Cant, N.W., Luckey, C.A., and Nelson, P., *J. Catal.*, **124**, 336 (1990).
6. Patterson, W.R., and Parker, I.B., *J. Chem. Soc. Faraday Trans. I*, **79**, 1421 (1983).
7. Patterson, W.R., and Parker, I.B., *J. Chem. Soc. Faraday Trans. I*, **79**, 1431 (1983).
8. Haber, J., *Kinet. Katal.*, **21**, 123 (1980).
9. Sancier, K.M., Wentcrek, P.R., and Wise, H., *J. Catal.*, **39**, 141 (1975).
10. Peil, K.P., Goodwin, J.G., Jr., and Marcelin, G., *J. Am. Chem. Soc.*, **112**, 6129 (1990).
11. Ekstrom, A., and Lapszewicz, J.A., *J. Phys. Chem.*, **110**, 5226 (1989).
12. Biloen, P., *J. of Mol. Catal.*, **21**, 17 (1985).
13. Koranne, M.M., Goodwin, J.G., Jr., and Marcelin, G., to be submitted.
14. Peil, K.P., Goodwin, J.G., Jr., and Marcelin, G., *J. Catal.*, **131**, 143 (1990).
15. Klier, K., Novakova, J., and Jiru, P., *J. Catal.*, **2**, 479 (1963).
16. Novakova, J., Klier, K., and Jiru, P., *in* " Reactivity of Solids" (Schwab, G. M., Eds.) Elsevier, Amsterdam, p. 270 (1964).
17. Novakova, J., and Jiru, P., *Collection Czechoslov. Chem. Commun.*, **1**, 28 (1963).
18. Klisurski, D.G., and Kuncheva, M.M., *Int. Chem. Eng.*, **17**, 488 (1977).
19. Snyder, T.P., and Hill, C.G., Jr., *Catal. Rev.-Sci. Eng.*, **31**, 43 (1989).
20. Grasselli, R.K., *Appl. Catal.*, **15**, 127 (1985).
21. Haber, J., and Serwicka, E.M., *React. Kinet. Catal. Lett.*, **35**, 369 (1987).
22. Minachev, K.M., Antoshin, G.V., Klissurski, D.G., Guin, N.K., and Abadzhijeva, N.Ts., *J. Chem. Soc. Faraday Trans.*, **1**, 691 (1979).
23. Hirota, K., Kera, Y., and Teratani, S., *J. Phys. Chem.*, **72**, 3133 (1968).
24. Hirota, K., and Kera, Y., *J. Phys. Chem.*, **73**, 3973 (1969).
25. Muzuykantov, V.S., Cheskova, K.Ts., and Boreskov, G.K., *Kinet. Katal.*, **14**, 664 (1973).
26. Winter, E.R.S., *J. Chem. Soc.*, 1170 (1950).

DISCUSSION

Q: A. A. Tsyganenko (Russia)

From your quantitative measurements or from your spectroscopic data is it possible to find out which, in particular, surface oxygen participates in the exchange ? Is it oxygen of OH groups, terminal oxygen bound to vanadium, bridged oxygen atoms linking silica and vanadium, etc. ?

A: J. G. Goodwin

In our work we were not able to distinguish between surface oxygen and oxygen from the bulk. As I mentioned in the presentation, it appears that there is an oxygen participation that

exceeds the total amount of oxygen in the vanadia, suggesting that some oxygen from the silica or oxygen at the vanadia-silica participates in the exchange process. However, we were not able to distinguish the particular types of oxygen, especially particular types of surface oxygen, in this study.

Q: S. L. Kiperman (Russia)

You have observed that the isotopic exchange degree was changed after the introduction of methane. Your interpretation was connected with the formation of species adsorbed and their influence on the isotopic exchange of oxygen. But another interpretation is possible. In our study of ethylbenzene oxidative dehydrogenation over vanadia-magnesia catalysts it was shown that the quantity of reactive surface species as well as the ratio of V(V)/V(IV) ions on the surface and in the bulk depends on the compound to be oxidized and the gas-phase oxygen. It is the case of adsorption chemical equilibrium. In this case a part of oxygen species participating in the isotopic exchange depends on the relation of methane and oxygen concentrations in gas-phase. That concept can also explain the interesting results in this investigation.

A: J. G. Goodwin

As we concluded the increase in the exchangeability of vanadia appeared to be related to the presence of methane, probably due to a redox type of mechanism involved in the partial oxidation. The reducing agent, in this case methane, facilitated the exchange of oxygen from the gas-phase with catalyst oxygen.

Q: R. B. Moyes (United Kingdom)

The authors will be aware of the involvement of silica, were used as support, in the formation of oxygenates from methane-oxygen mixtures and also of the suggested role of sodium ions in the silica. It has been suggested that complete removal of sodium ions from silica yields a more active silica. Can the authors comment on the role of silica, especially in relation to Table 2 ?

A: J. G. Goodwin

In our studies at 500 - 600 ^{0}C the silica that we used (Cab-O-Sil, M5) did not show any appreciable oxygen exchange capability in presence or absence of methane. We agree that silica at much higher temperatures or even at these temperatures but at a very low rate can exchange with gas-phase oxygen. However, under the conditions we used, it seems that the presence of vanadia is necessary to achieve a significant rate of oxygen exchange at these temperatures.

Q: F. Solymosi (Hungary)

You have found that the rate of O-exchange with CO_2 is much higher than with O_2. In the conclusion of your paper you explained this by the ease of dissociation of CO_2 compared to that of O_2. I am a little doubtful on the occurrence of the dissociation of CO_2 on vanadia. I would suggest that the formation of carbonate species facilitates the O-exchange with CO_2. This could be easily checked by IR spectroscopy.

A: J. G. Goodwin

You are absolutely right; this probably involves the formation and dissociation of "carbonate-type" species. We did not mean to imply the formation and dissociation of CO_2 directly but rather the formation and dissociation of the CO_2 as carbonate species that facilitates the higher rate of O-exchange with CO_2. It is interesting to note that carbon residence time for CO_2 on the surface is minimal. Thus, it seems that the formation and dissociation of carbonate species is very rapid. However, the existence of CO_2 in a dissociated form cannot be completely ruled out since the carbonate-type species on vanadia is in equilibrium with CO_2 in a dissociated form as suggested in ref. 23 in our paper, based on IR evidence.

Q: X. X. Guo (China)

Your results showed that CO_2 has high a exchange reactivity with lattice oxygen compared to O_2. My comment is that the surface oxygen species under a CO_2 partial pressure may be very different from that under a oxygen partial pressure. The diffusion process of lattice oxygen could be dependent on the chemical form of the surface oxygen species.

A: J. G. Goodwin

We agree with you in that the surface oxygen species in CO_2 exchange may be different from that of O_2 exchange. As was suggested in the answer to the previous question it is likely that the CO_2 exchange may involve a "carbonate-type" species which may facilitate the CO_2 exchange with vanadia. The exchange of lattice oxygen with the surface could be affected by the mixture of the surface species.

Q: K. Klier (USA)

Can you estimate in terms of monolayer exchanged, the extent of oxygen exchange with V_2O_5 ? Based on the our earlier work, I would expect greater than monolayer extent of oxygen exchange if your V_2O_5/SiO_2 catalyst behaves as bulk unsupported V_2O_5.

A: J. G. Goodwin

The amount of oxygen exchanged indicated that all of the oxygen in the V_2O_5 and more was involved in the exchange process as you rightly suspected.

Q: K. Klier (USA)

Do you have data on O_2 transients in terms of $^{16}O^{16}O$, $^{16}O^{18}O$, and $^{18}O_2$ isotopic compositions? The reasons for my asking is to suggest that if O_2/V_2O_5 exchange occurs via a divacancy mechanism (ref. 16), the equilibrium isotopic composition in the gas-phase should not occur in the beginning stages of exchange, and one should observe

$$\{[^{16}O^{18}O]^2\}/\{[^{16}O^{16}O][^{18}O^{18}O]\} < 4$$

Would you accept the suggestion that methane reduces V_2O_5 to increase the oxygen vacancy concentration which then enhances O_2/V_2O_5 exchange ? If so then the divacancy mechanism will be supported by the above equation.

A: J. G. Goodwin

We do have various oxygen transient results. However, we have done most of our experiments in a flow mode rather than a static mode which then masks the initial part of the equilibrium calculations, since the transients are extremely rapid and attain equilibrium rapidly. Hence, we are not able to detect the validity of the relationship that you suggested. However, your suggestion that methane increases the vacancies in the vanadia which then facilitate the oxygen exchange is probably very correct. We do think that an increase in the vacancies in the presence of methane is the cause for an increase in the oxygen exchange capability over vanadia.

Q: D. Duprez (France)

You focussed your attention on the effect of CO_2 produced in the reaction. What about the possibility of secondary exchange by water which is also produced in the reaction?

A: J. G. Goodwin

This is a question that we have asked ourselves. The water transient indicates that the labelled water decays much more rapidly than the labelled CO_2. From this we conclude that while water may influence the CO_2 transients, water is not the sole means by which CO_2 is able to exchange its O_2 with the catalyst. We believe that the catalyst oxygen is directly involved in the exchange process with CO_2 as well.

Guczi, L. *et al.* (Editors), *New Frontiers in Catalysis*
Proceedings of the 10th International Congress on Catalysis, 19-24 July, 1992, Budapest, Hungary
© 1993 Elsevier Science Publishers B.V. All rights reserved

ROLE OF FREE RADICALS IN HETEROGENEOUS COMPLETE OXIDATION OF ORGANIC COMPOUNDS OVER IV PERIOD TRANSITION METAL OXIDES

Z. R. Ismagilov, S. N. Pak, L. G. Krishtopa and V. K. Yermolaev

Institute of Catalysis, Russian Academy of Sciences, Siberian Division, Prospekt Akademika Lavrentieva 5, 630090 Novosibirsk, Russia

Abstract

Using the matrix isolation ESR technique the kinetic dependences of generation of $RO_2^{\bullet}$ radicals formed during n-alcohol and oxygen interaction over IV period transition metal oxides (TiO_2, V_2O_5, Cr_2O_3, MnO_2, Fe_2O_3, Co_3O_4, NiO, CuO, ZnO) were studied at low reagent pressures (P_{total}<14 Pa) over the temperature range of 653 to 823 K. On the example of the oxidation reaction over $CuCr_2O_4/\gamma\text{-}Al_2O_3$ at atmospheric pressure the dependences of radical formation under conditions when secondary radical reactions may develop were investigated. Radical formation on the surfaces is believed to proceed via the common mechanism for all catalysts of the examined series, the chemisorbed surface oxygen species being involved in radical formation.

1. INTRODUCTION

As it has been thouroughly investigated oxidation reactions of organic compounds at high temperatures may proceed via heterogeneous-homogeneous mechanism when surface-generated free radicals before their surface transformations may desorb to the gas phase and take part in gas phase reactions [1, 2]. A large body of literature represents information about an integral heterogeneous-homogeneous process. However, the mechanism of radical formation on the surfaces is still not studied in detail. Therefore, we think that the investigation of radical formation conditions versus temperature, the ratio of components in the reaction mixture, the state of a catalyst and the structure of organic compounds has a special interest.

Series of IV period transition metal oxides (TiO_2, V_2O_5, Cr_2O_3, MnO_2, Fe_2O_3, Co_3O_4, NiO, CuO, ZnO) known to be constituents of mixed oxide systems employed as oxidation catalysts was considered. The correlation between the catalytic

activity of this series and the oxygen binding energy for some oxidation reactions has been previously well established [3,4].

In line with many other researchers we observed the radical desorption from the catalyst surface during the interaction of aldehydes, acids, alcohols, amines and hydrocarbons with molecular oxygen [e.g., 5-9]. Alcohols were found to produce about 10 times more amount of gas-phase radicals as compared to aldehydes or acids having the same carbon skeleton.

2. EXPERIMENTAL

Characteristics of the catalysts are given in the Table 1. The catalyst samples (40-100 mg) of 0.5-1.0 mm fraction were used.

Table 1
Characteristics of the catalysts.

	Fe_2O_3	MnO_2	Co_3O_4	V_2O_5	Cr_2O_3	ZnO	NiO	CuO	TiO_2
S_{BET} (m^2/g)	0.04	41	4	2.6	0.8	5	16	16	1.6

The study of the kinetics of the surface generated gas-phase radical formation was carried out in the low pressure flow reactor using a modification of Matrix Isolation ESR technique [5, 6].

In the present study absolute values of rates, expressed in terms of the total number of spins per unit of time were compared to each other on the basis of catalyst specific surface area. All the absolute values of rates are given below for P_{ROH}=133.3 Pa. The value of the radical accumulation rate in the freezing unit was taken as a measure of the rate of the process taking place on a catalyst surface.

The oxidation reaction of n-propanol over 34% $CuCr_2O_4/\gamma$-Al_2O_3 at atmospheric pressure was studied in a flow set-up with the residence time of appr. 0.06 s. The stable reaction products were analyzed using gas chromatographic method. To determine the concentration of radicals in the gas phase a part of reaction mixture was fed through a quartz capillary placed at the distance of ≅0.5 mm above a catalyst bed into the region with low pressure (≅15 Pa) and further to the Dewar finger cooled to 77 K situated in the cavity of the ESR spectrometer.

3. RESULTS AND DISCUSSION

Our previous studies [7, 8] on radical formation in the course of C_1-C_6 normal alcohols conversion over γ-Al_2O_3 and the typical complete oxidation catalysts $CuCr_2O_4/\gamma$-Al_2O_3, Pt/γ-Al_2O_3 have shown the formation of gas-phase peroxy radicals. In the present study all the oxides examined were capable of promoting gas-phase peroxy radical formation from n-propanol. Moreover, we have reported [ib.] that the process of $RO_2^{\cdot}$ desorption is characterized by linear dependence of the ESR signal intensity versus the $RO_2^{\cdot}$ accumulation time. In our case the same is valid for Cr_2O_3 only. In contrast, the $RO_2^{\cdot}$ accumulation behavior for all other oxides of the IV period

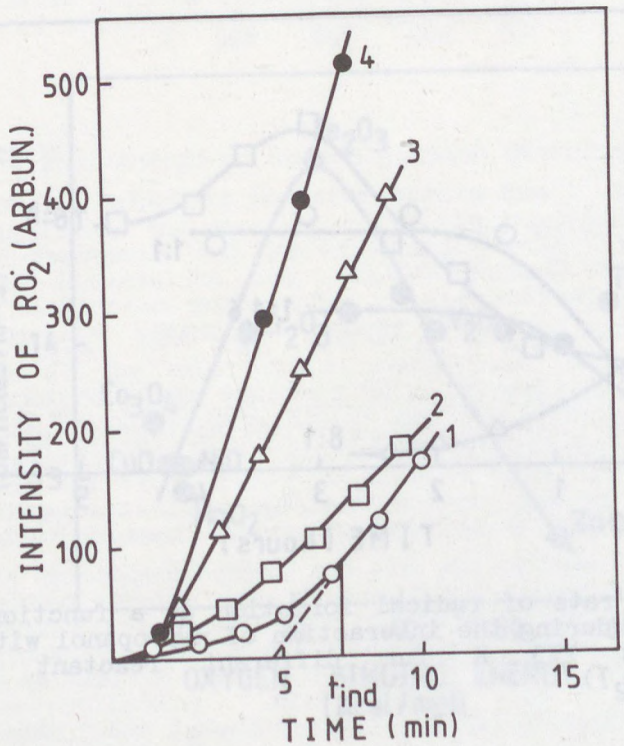

Figure 1. Intensities of $RO_2^{\cdot}$ radical production as a function of the time on stream during the interaction of n-propanol with oxygen ($[C_3H_7OH]/[O_2]=1.3$, $P(O_2)=7.3$ Pa) over CuO:
(1) 797 K, (2) 807 K, (3) 845 K, (4) 891 K.

transition metals is dramatically different from that observed over Cr_2O_3, i.e. accumulation curves with the induction period turned out to be typical, Fig.1.

The variations of the r_{RO2} versus time on stream were studied. Figure 2 shows effects of reaction temperature and ratio of the reactant concentrations ($[ROH]/[O_2]$) on the shape of the dependences $r_{RO2}=f(t)$. We note that the full set of these dependences is the same for all oxides tested. As shown in the Fig. 2 for CuO the following cases can be distinguished:

(a) r_{RO2} passes through a maximum;

(b) r_{RO2} reaches a certain steady-state value;

(c) r_{RO2} drops from a certain initial value to zero.

The latter can be considered as a particular case of (a) and is valid when one of the reactants predominates substantially.

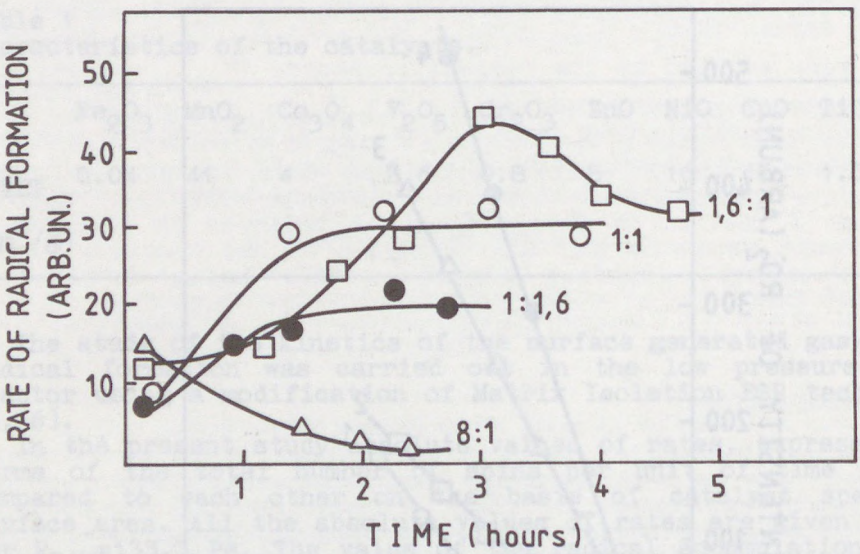

Figure 2. The rate of radical formation as a function of the time on stream during the interaction of n-propanol with oxygen over CuO at 773 K for different reactant mixtures ($[n\text{-}C_3H_7OH]/[O_2]$).

In order to understand the role of the presence of molecular oxygen in the reactant feed in the radical formation activity, the effect of altering oxygen partial pressure has been examined. For Cr_2O_3, V_2O_5 and Fe_2O_3 the rate of radical production (under different $P(O_2)$ conditions maximum r_{RO2}

observed was taken) is described according to zero-order kinetics when $[n\text{-}C_3H_7OH]/[O_2]<1$, and rapidly declines as soon as the ratio increases; for Fe_2O_3, a slight excess of this ratio above 1 leads to a drastic decrease of activity.

For the rest of oxides, $r^{max}_{RO2} = f(P(O_2))$ dependence is described by a "bell"-shape curve; a maximum is attained when the ratio of [ROH] to $[O_2]$ in a reactant mixture is ~ 1.

The above facts, namely, the character of diminution of radical production in the absence of molecular oxygen, Fig. 2, obviously suggests that the reaction proceeds via the surface oxygen species.

When compared on the basis of $RO_2^{\cdot}$-formation rate at 773 K Fe_2O_3 was the most active of the oxides used ($r_{RO2}=2\times10^{15}$ spins/$m^2\times s$), while the minimum r_{RO2} (3×10^{12} spins/$m^2\times s$) was observed for ZnO. These values correspond to the radical

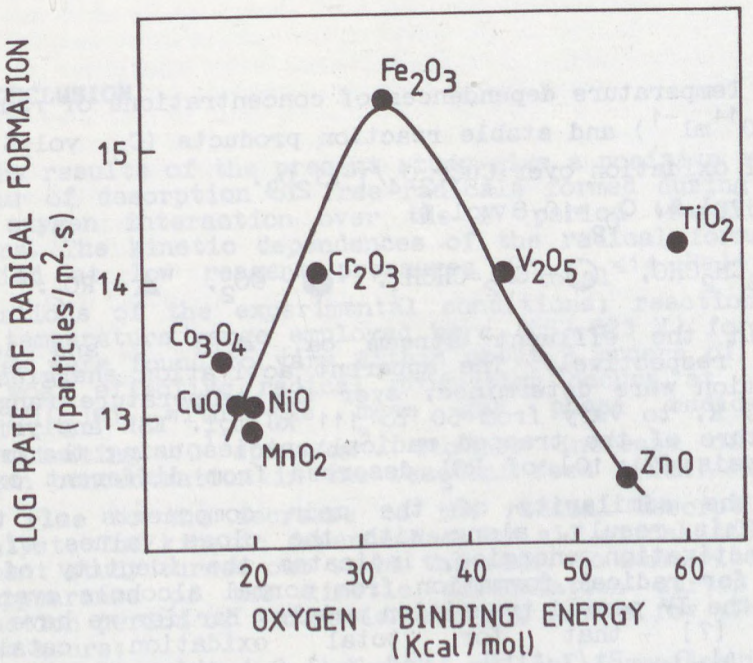

Figure 3. The rate of radical formation as a function of the oxygen binding energy of oxides during the interaction of n-propanol with oxygen. All reactions were carried out under the same experimental conditions, i.e.: T=773 K, $[n\text{-}C_3H_7OH]/[O_2]=1$. The rates are given as their decimal logarithms.

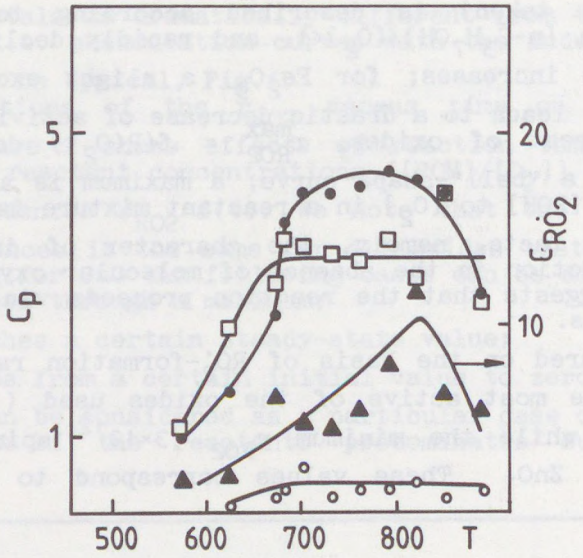

Fifure 4. Temperature dependences of concentrations of radicals ($C_{RO_2^\cdot}$, $*10^{11} ml^{-1}$) and stable reaction products (C_p, vol.%) upon n-propanol oxidation over $CuCr_2O_4/\gamma\text{-}Al_2O_3$.
C_{ROH}=20.5 vol.%, C_{O_2}=10.8 vol.%.

□ - CH_3CH_2CHO, ○ - $CH_2{=}CHCH_3$, ● - CO_2, ▲ - $RO_2^\cdot$.

amounts in the effluent stream ca. 4×10^{11} and 3×10^{10} spins/sm^3, respectively. The apparent activation energies for this reaction were determined, over the temperature range of 653 to 823 K, to vary from 50 to 111 kJ/mol. ESR analysis of the structure of the trapped radical species using the method of photolysis [7, 10] of $RO_2^\cdot$ desorbed from different oxides revealed the similarity of the main components of their spectra. This result, along with the close values of the apparent activation energies, indicates the identity of the mechanism for radical formation from normal alcohols over all oxides of the IV period transition metals. Earlier we have also reported [7] that for total oxidation catalysts ($CuCr_2O_4/\gamma\text{-}Al_2O_3$, $Pt/\gamma\text{-}Al_2O_3$, and $\gamma\text{-}Al_2O_3$) this rate-limiting step apparently includes the splitting of chemisorbed oxygen bond.

Consideration of the correlation shown in Figure 3 revealed that r^{max}_{RO2} changed as a curve with a maximum versus oxygen binding energy (q_s). Here the initial heats of oxygen

removal (i.e. oxygen removal heats at maximum degree of oxidation of the oxide surface) [4] are employed as q_s. The highest activity for radical production turned out to correspond to the oxygen binding energy ~34 kcal/mol (143 kJ/mol) for Fe_2O_3.

The data on n-propanol oxidation at atmospheric pressure have shown that radicals desorbed may initiate a branched chain oxidation reaction in gas phase. Fig.4 represents the results on n-propanol oxidation over $CuCr_2O_4/\gamma\text{-}Al_2O_3$ versus temperature. It is worth mentioning that alcohol transformation with peroxy radicals formation occurs from appr. 573 K. The main stable products are propionic aldehyde and CO_2. Radicals are detected in gas phase. The dependence of radical concentration versus temperature has a "bell" shape and correlates with the temperature dependence of total oxidation product - CO_2 formation. This type of dependence is characteristic for the degenerate - branched chain reactions of oxidation of organic compounds in gas phase [11].

4. CONCLUSION

The results of the present study give a positive evidence in favour of desorption of free radicals formed during n-alcohol and oxygen interaction over the IV period transition metal oxides. The kinetic dependences of the radical formation were studied at low reagent pressures (P_{total}<14 Pa) with wide variations of the experimental conditions; reaction rates in the temperature range employed here (653-823 K) for different oxides were found to vary within about 3 orders of magnitude. The most effective radical production occurs at the ratio $[ROH]/[O_2] \cong 1$ with the mean gas phase radical amount approximating 10^{11} spins/cm^3. Further increase of molecular oxygen concentration in the reactant feed ($[ROH]/[O_2]>1$) will give rise to the decrease of the radical desorption from a catalyst. The kinetic dependences for all oxides tested in the present study turned out to be the same. To summarize they are:
- appearance of the kinetic accumulation curves with the induction period of a duration ranging from a few minutes up to a few hours;
- existence of the dependences of radical formation rate (r_{RO2}) upon reaction time with a maximum, or r_{RO2} increase up to the steady-state value, according to the reagent concentration ratio;
- the observed dependences $r_{RO2}^{max} = f(P(O_2))$ are represented by the "bell"-shaped curves which reached a maximum at $[ROH]/[O_2]$

ratio of ca. 1:1 for TiO_2, MnO_2, Co_3O_4, NiO, CuO, ZnO, or were zero order transforming to a negative one when $[ROH]/[O_2]>1$ for V_2O_5, Cr_2O_3, Fe_2O_3.

From our results described here we conclude the existence of the common mechanism of radical formation for all catalysts of the series studied, the chemisorbed surface oxygen species being involved in radical formation. Furthermore, the most favorable catalyst was found to be Fe_2O_3 showing the highest activity for radical production. A more detailed analysis of this mechanism in terms of surface-redox factor, as has been recently proposed [12], will be published elsewhere.

The heterogeneous-homogeneous oxidation of n-propanol over $CuCr_2O_4/\gamma\text{-}Al_2O_3$ at atmospheric pressure indicates that the rates of radical desorption observed over catalysts studied are sufficient to initiate branched chain reaction in gas phase.

5. REFERENCES

1 Ya.B. Gorokhovatskii, T.E. Kornienko, V.V. Shalya, Heterogeneous-homogeneous reactions, Technique, Kiev, 1972- - in Russian.
2 L.Ya. Margolis, Catal. Rev. 8 (1973) 241.
3 G.K. Boreskov, Catalysis: Science and Technology 3 (1982) 40.
4 G.K. Boreskov, V.V. Popovskii and V.A. Sazonov, Proc. IVth Int. Congress on Catalysis, Vol.1, Akademiai Kiado, Budapest (1971) 439.
5 A.B. Nalbandyan, I.A. Vardanyan, Current status of the Problem of Organic Compounds Oxidation, Armenian Academy of Science, Yerevan, 1986 - in Russian.
6 A.B. Nalbandyan, A.A. Mantashyan, Elementary Processes in Slow Gas-Phase Reactions, Armenian Academy of Science, Yerevan, 1975 - in Russian.
7 V.K. Yermolayev, S.N. Pak, L.G. Krishtopa, Z.R. Ismagilov, K.I. Zamaraev, Khim. Fiz. (in Russian) 7 (1988) 1141.
8 Z.R. Ismagilov, S.N. Pak, V.K. Yermolaev, Proc. of the 9-th Soviet-Japanese Seminar on Catalysis, Novosibirsk, 1990, 193.
9 D.J. Driscoll, K.D. Campbell, J.H. Lunsford, Adv. Catal. 35 (1987) 139.
10 S.N. Pak, V.K. Yermolayev, Z.R. Ismagilov, React. Kinet. Catal. Lett. 32 (1986) 429.
11 N.S. Enikolopyan, Dokl. AN SSSR. 119 (1958) 520.
12 L.G. Krishtopa, V.K. Yermolayev, Z.R. Ismagilov, K.I. Zamaraev, Proc. 8th Soviet-French Seminar, Novosibirsk, 1990, 96.

DISCUSSION

Q: M. M. Bhasin (USA)

How do you explain that Fe_2O_3 has the highest rate of radical formation activity? In your paper I noted that iron oxides has the lowest surface area of 0.04 m^2/g compared to other oxides in the 0.8 to 40 m^2/g. Secondary, is it possible that physical effects, diffusion in pores, etc. are playing a role in the observed activity. Also, would you clarify which structural form of Fe_2O_3 you used and whether the surface areas were measured on fresh, unused or used catalysts?

A: Z. R. Ismagilov

In our paper the rate data are reported per unit of BET surface area, as it is traditionally done in heterogeneous catalysis. I share your interest on the role of surface area: either internal BET surface or outer surface of granules is effective in heterogeneous radical formation and desorption into the gas phase. Our results accepted for the publication in Catalysis Letters, suggest that radicals mostly release from the outer surface of granules, probably because of the short pores diffusion path [1]. Here, the metal oxides examined differ in both the surface area and the porosity. For example, in accordance with our estimations for the Fe_2O_3 sample (α-form) with the surface area of 0.04 m^2/g and its pore radius of ~$6x10^4$ nm, the diffusion path of radicals in pores was approximately 0.3 mm at 773 K [$P_{O2} = P_{ROH}$ = 3.7 Pa, RO_2 amount = $4x10^{11}$ spins sm^{-3}]. This value of the diffusion path is comparable with a size of the catalyst granule (0.5-1 mm). The diffusion path for the V_2O_5 sample, having bidisperse porous structure with pore radius over the range of 50 to 160 nm and of 400 to 10.4 nm, was found to be 0.03 mm (773 K, $P_{O2} = P_{ROH}$ <9.3 Pa, RO_2 amount = $6x10^{11}$ spins sm^{-3}). On the basis of these data the surface generation of gas phase radicals should be probably viewed with the partial participation of the interior catalyst surface. In view of the above observations it is therefore concluded that the role of porosity in gas phase radical production is logical to consider for each particular case.

For α-Fe_2O_3 used in our experiments the BET surface area did not differ for fresh and used samples.

[1] Z. R. Ismagilov, S. N. Pak, *Catal. Lett.*, 1992 (to be published)

Q: O. V. Krylov (Russia)

I can continue a remark of M. Bhasin about surface area. In some radical works it was observed that the yield of radicals or the products is more sensitive to surface area than even to chemical composition. It is very probable that radicals decay occurs in pores of the catalyst. Do you have some data about dependence of radical yield on the surface area or porosity ?

A: Z. R. Ismagilov

As I answered to the previous question we have made theoretical calculations and modelling studies on the role of surface area and the catalyst porosity in the radical production. The details will soon be published [1].

Q: Can Li (China)

I think that the oxygen binding energy according to your definition is contributed by both adsorbed oxygen and lattice (surface and bulk) oxygen, especially for most of reducible oxides. My questions are that:

1) What are the chemisorbed oxygen species which are involving in the radical formation and did you get any direct evidence of the presence of these oxygen species under reaction conditions ?

2) What is the correlation between the oxygen binding energy and formation of chemisorbed oxygen species and is it possible for lattice oxygen participation in the radical formation, especially at high temperatures ?

A: Z. R. Ismagilov

The enhanced interest on the problem of partial oxidation of alkanes result to a considerable progress in the understanding the surface mode which would lead to the production of gas phase radicals. It should be noted that the necessity of the presence of molecular oxygen for radical generation suggested the existence of some surface oxygen species, thoroughly studied by Professor Lunsford et al. In our study we did not examine any definite forms of surface oxygen, and, therefore, we do not have intention to propose a correlation between the oxygen binding energy and the formation of the chemisorbed oxygen species. It is the kinetic data which lead us to propose that the reaction proceeds via the surface oxygen species and, moreover, we suggest, that the rate-limiting step includes the splitting of chemisorbed oxygen bond.

As for the possibility for lattice oxygen participation, the following data seem to give the positive evidence in favour of this. A short time (~5 min) for reaching a maximum r_{RO2} for V_2O_5 is probably due to highly mobile oxygen in the bulk of oxide sample, whereas, for example, for MnO_2, having low oxygen mobility, this process takes a few hours.

Q: M. Sinev (Russia)

Your photolysis method of the identification of the primary radicals is based on the proposal that irradiation leads to break of R-O bond in RO_2 and only this bond. What kind of evidence do you have to prove this proposition ?

A: Z. R. Ismagilov

The ESR spectra of the products of photolysis of RO_2 are rather complex but we propose that irradiation leads mostly to break of R-O bond. I would like to emphasize experimental results proving our proposal:

1) Main components of spectra usually belong to alkyl radical.

2) These alkyl radical spectra in all experiments can be characterized as the spectra of R-radical forming by cleavage of R-O bond in alkylperoxide radical precursor.

Q: J. Novakova (Czechoslovakia)

What matrix do you use to condense the radicals onto the cooled finger ? We have got very good experience with co-feeding adamantane vapors, in which the resolution is high and thermal stability as well as mobility of trapped radicals can be studied.

A: Z. R. Ismagilov

We used mainly matrix of reaction products (to condense radicals from gas phase). In our preliminary experiments with special CO_2 matrix and without it we have seen similar results; both matrixes ensures stability of frozen radicals and showed satisfactory resolution.

Using the method of freezing of radicals one should to take into account that obtained results may be influenced by peculiarities of applied method. We have conducted a series of special experiments to avoid any possible influence of methodical errors on results of accumulation and detection of radicals:

- Varying the duration of radical accumulation we have chosen initial interval of time during which temperature regime of matrix does not change.
- Using a special heating device we have studied the distribution of frozen radicals by the length of cooled finger. It was shown that at mean durations of accumulation the main portion of frozen radicals occur on the edge of freezing unit within =~2 mm length and it give us opportunity to provide quantitive ESR measurements.

Q: P. G. Menon (Sweden)

In your interesting studies, did you notice any threshold temperature above which only the radical formation becomes appreciable ?

A: Z. R. Ismagilov

We have studied the reaction of radical formation on the surface in a wide temperature region (650-800 K). Typical Arrhenius dependences of radical formation were observed and we did not notice any temperature threshold in radical formation in experiments at low pressure.

Nevertheless, when we are discussing oxidation process which proceeds on the surface and in gas phase via radical intermediates at atmospheric pressure appearance of critical phenomena might be expected. It is well known that radical chain reactions may proceed in a stationary regime and auto-accelerated one. The ratio of radicals decay reaction rate to the rate of branching reaction determines the general character of the process.

In our experiments at atmospheric pressure the results on radical formation and products distribution showed that in gas phase reaction proceeds via branched chain mechanism. We observed some threshold in radical formation and ignition of reaction mixture by variation of the ratio ROH:O_2 and we did not notice this phenomenon at variation of the temperature.

Critical phenomena where not in focus of our attention in this study but our experience showed that a detailed investigation demands a special experimental approaches.

Q: M. Shymanska (Latvia)

You have observed the free radical formation on contacting the n-alcohol molecules with some transition metal oxides. Considering that the oxides under study in their catalytic activity and specificity strongly differ, are you sure (or have you any evidence) that in all cases the mechanism of free radical formation is the same ?

Some time ago we have observed that on vanadia catalysts the oxygen molecules at interaction with the surface also form radical like particles (signals in ESR spectra).

A: Z. R. Ismagilov

The proposed mechanism of radical formation described in our paper allows to give a satisfactorily explanation of the experimental results obtained in reactions of alcohol oxidation over oxide catalysts. In general we have enough data on radical formation on solid catalysts showing that mechanism of radical generation depends on chemical structures of organic molecule and the nature of used catalyst. I would like to give a reference to well known publications of Professor Lunsford who have done significant study of radical formation dependence on chemical nature of hydrocarbons.

In addition to my presentation, in our laboratory we have done the study of radical formation during oxidation of series of amines over the same set of catalysts as I reported here. We have established that mechanism of radical formation for alcohols and amines are different.

Q: F. Trifiro (Italy)

Do you exclude the possibility of a direct activation of hydrocarbons by the solid and formation of a radical and a further reaction of organic radical with molecular oxygen to form RO_2 species ?

A: Z. R. Ismagilov

In general we do not exclude direct formation of alkyl radicals on the surface with further transformation to RO_2 in presence of oxygen. In our opinion the specific mechanism depends on chemical structure of organic molecules and surface characteristics of a catalyst. We have provided similar experiments with amines and proposed a mechanism of radical formation which includes the step of alkyl radical formation on the surface [2].

[2] Z. R. Ismagilov, S. N. Pak, V. K. Yermolaev, K. I. Zamaraev, *Doklady AN SSSR*, **V. 298**, No. 3, p. 637-640, 1988, in Russ.

Q: K. P. de Jong (The Netherlands)

1) In your work the contact time is short (typically 0.06 sec). What do you expect for the contribution of radicals to the oxidation process at more conventional contact times, say 1 sec?

2) You have studied the role of radicals for the oxidation of functionalized hydrocarbons (alcohols, amines). What do you expect for pure hydrocarbons ? Will the role of radical be more or less prominent with hydrocarbons ?

A: Z. R. Ismagilov

1) The oxidation reaction observed has a branched chain mechanism in gas phase. It is known that the rate of these reactions depends on a number of parameters including also contact time. Because of peculiarity of a homogeneous constituent in reaction we propose that term "contact time" should be discussed in detail.

For example: if one increase the contact time adding some catalyst into reactor and increasing the height of a catalyst bed significant decreasing of homogeneous component due to decay of radicals in catalyst bed might be observed. From the other hand the homogeneous component might be of high value if catalyst performed in some special space dimensions or placed in reactor with large free volumes between granules.

In case of heterogeneous-homogeneous reactions we have the mutual influence of five to six reaction pathways and the "contact time" in a very specific way depends on such parameters as total pressure of reaction mixture, on concentration or partial pressure of chosen reaction component.

2) We have selected alcohols and amines for our study in accordance with following considerations:

- A priori we proposed that functionalized hydrocarbons with high probability would perform formation of radicals by rupture of bond between carbon atom and functional group. This bond is usually weaker than C-H or C-C bond.
- The selection of the both alcohols and amines are presented in the series of homologous molecules and it is a good opportunity to study reaction dependences by the change of the length of hydrocarbon part of these substances.
- Usage of alcohols and amines also gave us basis for comparison of their reactivity in radical formation, the reaction mechanism and performance in general. There are some similarities and differences.

In the case of hydrocarbons one might expect simultaneous formation of a number of radicals with the same probability depending on the molecular structure. We propose that for oxidation reactions the temperature region of stable radical formation and accumulation would be at least 50-100 K higher than for alcohols.

Q: K. Aika (Japan)

How much percentage of the intermediate on the surface complex are going out to gas phase as a free radical ?

A: Z. R. Ismagilov

In our study we did have not have experiments that could allow us directly follow surface complexes and their dynamic during radical generation. In dependence of reaction conditions rate of radical formation consists of less than one percent of total reaction. But our estimations show that in some cases the rates of radical formation on the surface may gain the same order as the rate of pure heterogeneous total oxidation known for these organic molecules on used catalysts.

Guczi, L. *et al.* (Editors), *New Frontiers in Catalysis*
Proceedings of the 10th International Congress on Catalysis, 19-24 July, 1992, Budapest, Hungary
© 1993 Elsevier Science Publishers B.V. All rights reserved

^{1}H BROAD-LINE NMR AT 4 K FOR STUDYING THE ACIDITY OF SOLIDS: APPLICATION TO ZEOLITES

P. Batamack, C. Doremieux-Morin and J. Fraissard

Laboratoire de Chimie des Surfaces, associe au CNRS - URA 1428, Universite P. et M. Curie; Tour 55, 3^e etage, 4, Place Jussieu, 75252 Paris Cedex 05, France

Abstract

Simulation of 4K broad-line ^{1}H NMR spectra of solids with Brönsted acid properties and loaded with known amounts of water allows the determination of the concentrations of the species: H_3O^+, $H_2O\cdots HO$ and of the remaining initial species: OH and H_2O. This original method, conjugated with ^{1}H HR-NMR (MAS) at ambient temperature, is applied to the comparison of Y and MFI zeolites without and with framework defects.

1. INTRODUCTION

The ^{1}H HR-NMR (MAS) of solid samples in sealed tubes has been developed particularly in the last 8 years (1-6). It was hoped that the acidity of solids would be reflected by the ionicity of the Brönsted sites of the "anhydrous" samples (without any adsorbed gas but still hydroxylated) and could then be measured directly by the chemical shift. On the contrary, the low value of the isotropic chemical shift proved the low ionicity of acid OH bonds (1,2). Thus, the presence of a base is necessary to reveal the acidity. Several methods are based on the adsorption-desorption properties of the acidic solids. Among them multinuclear NMR has been extensively used, but here we shall confine ourselves to ^{1}H NMR (1,2,7). Later, we wished to compare the results with those obtained in the homogeneous phase and especially in aqueous solutions. For this reason we chose to adsorb controlled amounts of water on "anhydrous" H-zeolites in order to study the equilibrium: $OH + H_2O = H_3O^+ + O^-$ (Equ. 1). Another advantage of

this choice is that water molecules are small enough to gain access to all acid sites.

In the presence of adsorbed molecules (water, ammonia), at ambient temperature, hydrogen atoms chemically exchange between the adsorbed molecules and the Brönsted acid SiO(H)T (T for Al or Ga), denoted ZOH in what follows, leading to signal coalescence and, consequently to average values of the chemical shifts of the various species present. For this reason, the Brönsted acidity of zeolites, defined by Equ. 1, cannot be measured by ^1H MAS NMR unless it is performed at sufficiently low temperature. We obtain the concentrations of these oxygen-protonated species from their weighted contributions to the broad-line ^1H NMR spectra by studying the direct dipolar interaction between the nuclear spins of the protons, in the absence of diffusion or rotation of the atom groups, at 4 K. Previous results on HZSM-5 (8) obtained by this method and by high resolution ^1H MAS NMR spectroscopy show, using our experimental conditions, that the measured concentrations correspond to the equilibrium at ambient temperature. We assume that it is the same for all the samples studied. As some water molecules become hydrogen-bonded to ZOH, the concentration of the (H_2O...HOZ) species as a whole must also be considered and determined (9,10).

2. EXPERIMENTAL SECTION AND DESCRIPTION OF THE METHOD

The samples belong to two main families: Y and MFI zeolites. Their characteristics have been already described except for the Ga-MFI sample, which was home-prepared with n-butylamine as template and then calcined in air to 815 K to eliminate the template; the framework Si/Al ratio, determinated by ^{29}Si MAS NMR is 18±3 before calcination and 32±3 after. Sample characteristics are collected in Table 1.

A HY zeolite is denoted ND (for non-dealuminated) to remind us that it contains no extraframework aluminium. There are 47.7 ZOH groups per unit cell and no silanol groups (11,12). The HY zeolite denoted D has been dealuminated by means of an aqueous solution of $(NH_4)_2SiF_6$. It contains 35.8 ZOH and 1.5 silanol groups per unit cell (13). The DED HY sample has been doubly-steamed with exchange of the remaining sodium by ammonium between the steamings. It contains no framework Al but amorphous silico-aluminate debris in the cavities (14).

Three HZSM-5 samples were studied (8). De was synthetised without a template and mildly steamed. TPA and Bu were synthetised with TPA^+ and n-butylamine as templates, respectively. They contain 4 framework aluminium and about 4 bridging hydroxyl groups per unit cell.

In order to prevent dealumination, the samples of the initial hydrated

zeolites either in the ammonium (Y zeolite) or in the hydrogen form (ZSM-5 and Ga-MFI) were first kept under vacuum at room temperature for 24 hours, then heated at 12 Kh^{-1} to 675 K at less than 10^{-2} Pa, kept under these conditions for 16 hours and finally cooled to 300 K. Water vapour is adsorbed step by step, in situ, at 300 K at a pressure below 40% of the saturation pressure; the amount of water in each sample is known by volumetry and gravimetry. After treatment at 375 K for 3 hours to ensure that the water molecules are homogeneously distributed, the samples are sealed.

Table 1
Sample characteristics
The symbols are the following: nBA for n-butylamine, TPA for tetrapropylammonium, HFS for ammonium hexafluorosilicate, St for steaming and Ex for sodium-ammonium exchange.

	HY			HZSM-5			GaMFI
	ND	D	DED	De	Bu	TPA	
Template	no	no	no	no	nBA	TPA	TPA
Si/Al	2.4	4.4	very high	23	23	23	32
Na_2O% (w/w)	1.6	<1	<0.2				
Dealumination treatment	no	HFS	St-Ex-St	St	no	no	no

The spectra are recorded as the derivatives of the absorption signal. They are theoretically symmetrical with respect to the centre and, in practice, the two parts of the experimental spectrum are averaged; for this reason we give only one half of each spectrum. Although it is small, the probe signal is subtracted from each spectrum, both for the MAS and the broad-line experiments.

The broad-line spectra were recorded and simulated as described (8,12,13). The simulated spectra correspond to the weighted sum of the contributions of the various species (H_2O, H_3O^+, $H_2O\cdots HOZ$ and OH) which

were calculated from the corresponding magnetic configurations (15-18, 9,10,19). For H_2O, H_3O^+ and OH only one internal length parameter corresponding to the H H distance is necessary; for $H_2O\cdots HOZ$ or deformed H_3O^+, a magnetic configuration with three spins at the vertices of an isosceles triangle needs two distance parameters. Each of the corresponding functions is then convoluted by a Gaussian, which makes it possible to take into account interactions between the protons of the configuration considered and those belonging to neighbouring configurations, as well as to other nuclei with non-zero spin in the environment (mainly ^{27}Al or ^{69}Ga and ^{71}Ga in the present case). When the effects of these nuclei are small the parameter of each Gaussian is related to a distance X close to the shortest distance between a proton of the configuration considered and a proton outside it. The calculations are normalized to a crystallographic unit cell by means of a numerical base which allows for the total number of protons in the sample, equal to the number of OH groups plus twice the number of water molecules introduced. Moreover, because there is a large number of independent parameters for each simulation, we impose that the concentrations obtained are in agreement with the number of initial ZOH groups and the number of water molecules adsorbed. Finally, the intra-proton distances found must be in the known range corresponding to the various protonated-oxygen groups identified.

The MAS NMR experiments were performed on a Bruker MSL-400 spectrometer at ambient temperature, the rotation frequency being 3 kHz. The pulse delay for recording the spectra of "anhydrous" samples is 1 mn; the other conditions have already been described (1,2,8). Chemical shifts are expressed with the usual conventions without bulk magnetic susceptibility correction. For broad-line NMR we employed a 60 MHz continuous wave spectrometer with phase detection and signal accumulation, using a laboratory-made probe (20).

3. RESULTS

3.1. Broad-line NMR

The broad-line rigid lattice spectra always show three maxima or shoulders (Fig.1): the first, at 1 gauss, is due to ZOH either free, hydrogen-bonded to water or having formed H_3O^+ ions. The "free" water molecules or those hydrogen-bonded to the ZOH contribute greatly to a second maximum at about 6 gauss. Finally, the third at about 10 gauss results mainly from hydroxonium ions. In samples containing very small amounts of water the first maximum is the most important, the two others being weak (Fig.1A). Increasing the water content significantly modifies the appearance of the spectra (Fig.1B): the first maximum

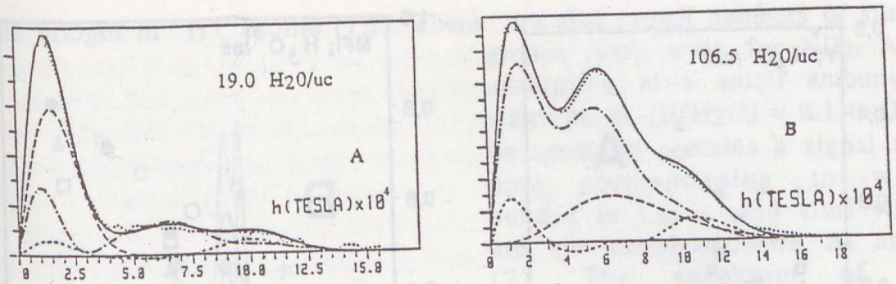

Figure 1. ···· : half-derivative of the experimental absorption spectrum of sample HY ND after adsorption of water; —— : simulated spectrum; weighted contributions of: ---- : hydroxonium ions; ---- : $H_2O\cdots HOZ$; - - - :A: OH; B: H_2O.

decreases in favour of the other two; the second maximum becomes the most important for high hydration levels.

The number of hydroxonium ions formed per initial Brönsted acid site, denoted $N(H_3O^+)$, versus the number of adsorbed water molecules per initial Brönsted acid site, $N(H_2O)$, is shown in Fig. 2, A and B for zeolites of the Y and MFI families, respectively .

For the ND HY zeolite, $N(H_3O^+)$ increases to about 0.2 for $N(H_2O) = 1$; it then remains about constant, in agreement with the previously proposed equations (12) (Fig. 2A):

$$x\ ZOH + y\ H_2O \longrightarrow inf(x,y)\ H_2O\cdots HOZ + /\ x - y\ /\ ZOH \text{ or } H_2O \quad \text{(Equ. 2)}$$

$$H_2O\cdots HOZ = H_3O^+ + ZO^- \quad \text{(Equ. 3)}$$

For the D HY zeolite, $N(H_3O^+)$ is the same as for ND when $N(H_2O) = 1$; when the water content is increased, it remains constant to $N(H_2O) = 2$ and then increases to 0.4 for 4.4 H_2O per site (Fig. 2A).

For the DED HY sample, containing Al atoms only as extra-framework amorphous silica-aluminas, we showed that there is no ZOH bridge in the "anhydrous" zeolite but that adsorption of water can (re)create such bridges (14). There is no detectable hydroxonium up to $N(H_2O) = 1.6$, but for 2.2 H_2O per site, which is the maximum value able to enter this hydrophillic compound, $N(H_3O^+)$ is about 0.2, the number of Brönsted acid sites being known from the total balance of the hydrogen atoms (21).

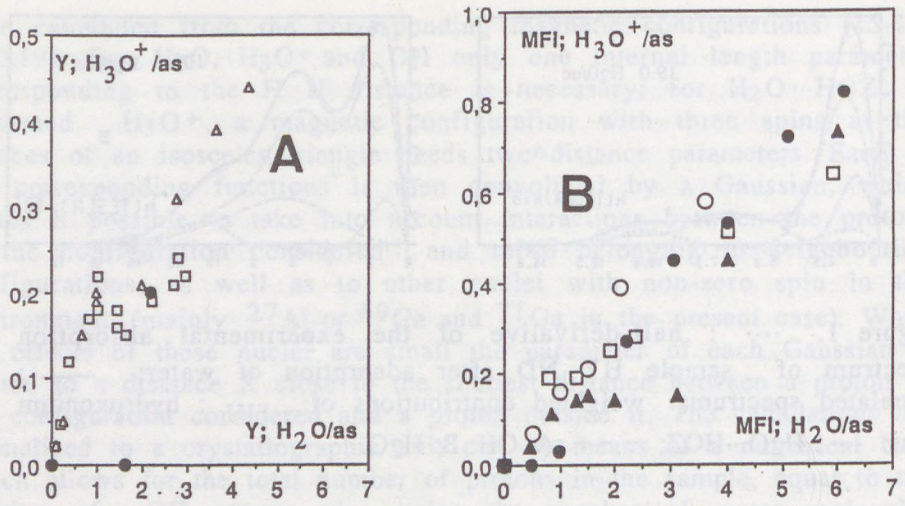

Figure 2. Number of hydroxonium ions formed per initial Brönsted acidic site ($N(H_3O^+)$), versus the number of adsorbed water molecules per initial Brönsted acidic site ($N(H_2O)$) for samples: A: HY family: □: ND; △: D; • :DED. B: HMFI family: □: De; ▲: TPA; O: Bu; • • : Ga-MFI.

For the HZSM-5 samples (8,21) the situation is as follows (Fig. 2B): when $N(H_2O)$ increases from 0 to 1, $N(H_3O^+)$ reaches 0.2 only for the De sample. It remains constant up to $N(H_2O)$ equals 1.5 and 3 for the De and TPA samples, respectively; then it increases strongly to about 0.6 for $N(H_2O) = 6$. The plateau about $N(H_2O) = 1$ is replaced by a small increase for the Bu sample, followed by a stronger one from $N(H_2O) = 1.5$; $N(H_3O^+)$ reaches 0.6 for $N(H_2O) = 3.7$.

For the Ga-MFI sample, there is no hydroxonium ion for $N(H_2O)$ less than 0.7. Then $N(H_3O^+)$ increases continuously, reaching 0.7 for $N(H_2O)$ equal to 5.5.

3.2. MAS NMR

Some of the MAS spectra of the "anhydrous" species have been already published (8,12,14). Those of the D HY, Bu HZSM-5 and Ga-MFI samples are shown in Fig. 3 with the simulated spectra and the signals which make them up.

The spectra of "anhydrous" ND and D HY samples (12) (Fig. 3A) contain the Gaussian signals at 4.3 and 5.4 ppm, characteristic of the protons of

ZOH bridges in HY zeolite (1,2). There are also small numbers of silanol groups (very weak for ND). After adsorption of a small amount of water on D, ($N(H_2O)$ = 0.1 to 0.25) its spectrum contains a signal at 7 ppm corresponding to water bonded to Lewis acid sites which are not extraframework Al atoms (7). The spectrum of the "anhydrous" DED (14) contains a signal due to AlOH groups (1,2). This signal is wide, probably because of a lowering of the real symmetry of the Al atom sites (22,23).

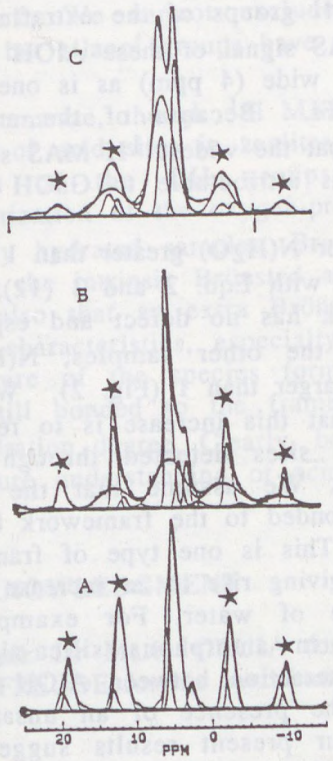

Figure 3. ^1H MAS-NMR spectra (experimental, simulated and components) obtained on "anhydrous" samples (✶: spinning side-bands): A: D HY; B: Bu HZSM-5; C: Ga-HMFI.

The spectra of the "anhydrous" samples of HZSM-5 all show silanol and ZOH groups (2.3 and 4.3 ppm, respectively) (8) (Fig.3 B and C). However, in some spectra, especially that of Bu (Fig 3B), the ZOH signal is partly broadened, leading us to assume that part of the Al atom sites have a low symmetry (22,23). The De sample spectrum (8) contains a normal width (1 ppm) signal of AlOH at 3 ppm. For "anhydrous" Ga-MFI, in addition to normal width expected signals for silanol and ZOH, the spectrum (Fig. 3C) includes a wide Gaussian signal with strong side-bands, located at the same position (4.5 ppm) as ZOH. This signal may also be attributed to GaOH groups as the chemical shift is not known for these species.

4. DISCUSSION

For abscissa values less than unity, $N(H_3O^+)$ increases continuously with $N(H_2O)$ for all samples (Fig. 2A and 2B) with the exception of DED

HY and Ga-MFI (Fig. 2). In these cases, hydroxonium ions are only detectable for large values of $N(H_2O)$ (>1.6 for DED and > 0.7 for Ga-MFI) (Fig. 2 A and B). As already mentionned, there are no initial ZOH in the "anhydrous" DED sample (14), but AlOH groups of the extraframework amorphous debris. The Gaussian ^1H MAS signal of these AlOH groups,, with strong spinning side bands, is then wide (4 ppm) as is one of the 4.5 ppm signal of "anhydrous" Ga-MFI. Because of the analogies between DED and Ga-MFI, we assume that the widest ^1H MAS signal at 4.5 ppm in the spectrum of Ga-MFI is attributable to GaOH species rather than to SiO(H)Ga groups

$N(H_3O^+)$ is approximately constant for $N(H_2O)$ greater than 1 for the ND HY (Fig. 2A). This is in agreement with Equ. 2 and 3 (12), which describe the results when the framework has no defect and especially no dealumination whatsoever. For all the other samples, $N(H_3O^+)$ increases markedly when $N(H_2O)$ is larger than 1 (Fig. 2). We have already shown in the case of D HY that this increase is to relate to defects of the framework (Lewis acid sites detected through water molecules interacting with them) (13). We assume that the Lewis centres are then aluminium atoms still bonded to the framework by less than the initial four Al-O- bonds (25). This is one type of framework defects ; many other types may happen giving rise to an increase in the hydroxonium concentration in presence of water. For example, as already mentionned, we showed that, in amorphous silica-alumina, Brönsted sites can be formed by the interaction between AlOH groups and water molecules (14); of course the presence of an unsaturated neighbour Si atom is then needed. Our present results suggest the possibility of a lowering of the symmetry of some ZOH groups for the Bu HZSM-5 sample (wide 4.3 ppm signal); this has to be confirmed. Moreover, Staudte et al. proved that extraframework aluminium atoms are able to dissociate water molecules and create Brönsted acid sites (26).

5. CONCLUSION

Comparison of some acid zeolites using broad-line NMR at 4 K shows that the number of hydroxonium ions per initial SiO(H)T bridge of the samples, i.e. the dissociation coefficient, increases with the number of adsorbed water molecules. When the number of water molecules is greater than that of initial bridges, the hydroxonium concentration remains constant for the only sample which has no initial defect, ND HY. It increases again strongly for the other samples, whose defects have been characterized by MAS NMR. The defects that we assume to be responsible for the increase in the number of Brönsted acid sites in the

presence of water are the following: extraframework silico-aluminate debris, AlOH (and perhaps GaOH) species still bonded to the framework and Lewis acid sites which can be Al atoms still bonded to the framework. We cannot exclude the presence of some other active centres, but silanol groups have never shown any activity.

To summarize, though ^1H MAS NMR does not allow to determine the strength of acid sites in zeolites directly, it is very helpful through the analysis of the OH groups in "anhydrous" samples and the characterization of the oxygen-protonated species bonded to the T atoms in partly hydrated samples. Broad-line ^1H NMR at 4 K can be used to measure the intrinsic Brönsted acidity of the initial SiO(H)T bridges. It shows also that an extra Brönsted acidity is developed depending on zeolite characteristics, especially on the dealumination (its degree and the nature of the species formed during the dealumination -some of them still bonded to the framework-). This development is related to the hydration degree. Clearly, both ^1H NMR methods will be useful for the future understanding of acidity and dealumination processes.

6. ACKNOWLEDGMENT

We thank Dr Marie GRUIA for preparing the Ga-MFI zeolite and Prof. Dieter FREUDE for his contribution to HZSM-5 study (8).

7. REFERENCES

1 H. Pfeifer, J. Chem. Soc., Faraday Trans. I, 84 (1988) 3777.

2 D. Freude, Stud. Surf. Sci. Catal., 52 (1989) 169.

3 H. Pfeifer, D. Freude and M. Hunger, Zeolites, 5 (1985) 274.

4 G. Engelhardt, H.-G. Jerschkewitz, U. Lohse, P. Sarv, A. Samoson and E. Lippmaa, Zeolites, 7 (1987) 289.

5 D. Freude, J. Klinowski and H. Hamdan, Chem. Phys. Letters, 149 (1988) 355.

6 E. Brunner, H. Ernst, D. Freude, M. Hunger, C.B. Krause, D. Prager, W. Reschetilowski, W. Schwieger and K.-H. Bergk, Zeolites, 9 (1989) 282.

7 M. Hunger, D. Freude and H. Pfeifer, J. Chem. Soc., Faraday Trans., 87 (1991) 657.

8 P. Batamack, C. Dorémieux-Morin, J. Fraissard and D. Freude, J. Phys. Chem., 95 (1991) 3790.
9 C. Dorémieux-Morin, J. Magn. Res., 21 (1976) 419.
10 C. Dorémieux-Morin, J. Magn. Res., 33 (1979) 505.
11 P. Batamack, C. Dorémieux-Morin, R. Vincent and J. Fraissard, Chem. Phys. Letters, 180 (1991) 545.
12 P. Batamack, C. Dorémieux-Morin and J. Fraissard, J. Chim. Phys. 89 (1992) 423.
13 P. Batamack, C. Dorémieux-Morin and J. Fraissard, Cat. Letters, 11 (1991) 119.
14 P. Batamack, C. Dorémieux-Morin and J. Fraissard, Cat. Letters, 9 (1991) 403.
15 G.E. Pake, J. Chem. Phys., 16 (1948) 327.
16 E.R. Andrew and R.J. Bersohn, J. Chem. Phys., 18 (1950) 159.
17 R.E. Richards and J.A.S. Smith, Trans. Faraday Soc., 48 (1952) 675.
18 E.R. Andrew and N.D. Finch, Proc. Phys. Soc., 70B (1957) 980.
19 A.L. Porte, H.S. Gutowsky and J.E. Boggs, J. Chem. Phys., 36 (1962) 1695.
20 R. Vincent, unpublished results.
21 P. Batamack, Doctorat Thesis, P. and M. Curie University, Paris (1991).
22 J. Böhm, D. Fenzke and H. Pfeifer, J. Magn. Res., 55 (1983) 197.
23 E. Brunner, J. Chem. Soc., Faraday Trans., 86 (1990) 3957.
24 W. Schwieger, K.-H. Bergk, D. Freude, M. Hunger and H. Pfeifer, ACS Symposium Series, 398 (1989) 274.
25 P. Batamack, C. Dorémieux-Morin and J. Fraissard, to be published.
26 B. Staudte, M. Hunger and M. Nimz, Zeolites, 11 (1991) 837. Symposium Series, 398 (1989) 274.

DISCUSSIONS

Q: H. G. Karge (Germany)

1) The ^1H broad-line NMR spectra exhibit three strongly overlapping sections with three maxima to which the various protonated species (ZOH, ZOH···OH_2, ZO···H_3O^+, "free" H_2O) contribute to a varying extent. How accurate is the determination of the number of H_3O^+ ions [$N(H_3O^+)$] derived from these spectra by simulation taking into account the "weighted contributions of these oxygen-protonated species", i.e. what are the limits of error ?

2) In this study single water molecules hydrogen-bonded to bridging Si···OH···Al, i.e. ZOH···OH_2, were observed whereas these species were not detected by IR [1]. Could you please comment on this ?

3) It seems to be desirable to prepare one series of homologous acidic zeolite samples, e.g. H-ZSM-5 with decreasing Al/Al+Si and minimum defects, in order to check whether or not the novel 1H NMR technique provides the expected systematic change in the strength of the acidic sites. It would then be of great interest to compare the results with those of other experimental methods which are believed to be suitable for measuring and ranking the acidity strength of solid acids such as zeolites. Could you, please, comment ?

[1] A. Jentys, G. Warecka, M. Derewinski and J. A. Lercher, *J. Phys. Chem.*, **93**, 4837 (1989)

A: J. Fraissard

1) From the weighted contribution of the characteristic protonated species we estimate the limits of error on the determination of the number of H_3O^+ ions to ±12%. The number of adsorbed water molecules on the "anhydrous" zeolite samples is determined with an error of ±5% at present. These limits are given for HY zeolite in the Figures 2A and 2B [2]. The accuracy on the number of adsorbed water molecules will be improved if we can use the same thin glass ampoule for the pretreatment and the various experiments.

2) It is not possible for us to comment on the results of J. Lercher et al. Concerning our study, (i) the differences between the theoretical spectra of the various protonated species are characteristic as long as the distances between hydrogen atoms belonging to distinct species are sufficiently greater than internal H-H distances; that this criterion is satisfied can be checked by examining the distance parameters displayed for the simulation (the displayed values for the inter-species H-H distances are lower than the true ones because of spectral enlargement due to other nuclei with non zero spin); (ii) the assumption that there is no hydrogen-bond between SiO(H)Al and H_2O, i.e. no ZOH···OH_2, leads to no acceptable quantitative simulation of the experimental spectra.

3) We agree that new experiments on series of homologous acid zeolite samples are needed. We are looking forward to doing some on a series of H-ZSM-5 zeolites with various Si/Al ratios; one very important point is that the samples must contain few defects. It would be very interesting to study other sample series: some with only one type of defect. As pointed out in the remark, we must compare the results obtained on the acid strength with those from other methods.

[2] P. Batamack, C. Doremieux-Morin, J. Fraissard, *Catal. Lett.*, **11**, 119 (1991)

Q: J. J. Fripiat (USA)

Are you not afraid that adding water to a zeolite prepared at elevated temperature will hydrolyze some M-O-M bridges (M = Al, Si,etc,) and reconstruct a surface that will be different from that on which acid catalysis will create ?

A: J. Fraissard

We know that hydrolysis of the zeolitic framework of acidic zeolites may happen after water adsorption. We have to find a compromise to ensure that the samples have been homogenized before the NMR experiment and to minimize hydrolysis. Usually, we maintain the samples at 375 K for 2 or 3 hours. Under such conditions, for the ND HY zeolite which

has no initial defect, we see no sign of hydrolysis except when the number of adsorbed water molecules is larger than the number of acid hydroxyl groups. Then the ^1H MAS NMR spectra of the samples show a visible but very small signal corresponding to water molecules of the $(H_2O)_6Al^{3+}$ species.

Q: J. Lercher (Austria)

Our IR spectra of water adsorbed on HZSM-5 (1:1 stoichiometry between water and SiOHAl groups) suggest that the hydroxonium ion is formed and that it is hydrogen bonded to the surface. The difference between these results measured at 300 K and your results might be raised by the shift in the equilibrium caused by a slightly positive enthalpy of the reaction (ΔH 0.5 kJ/mol)

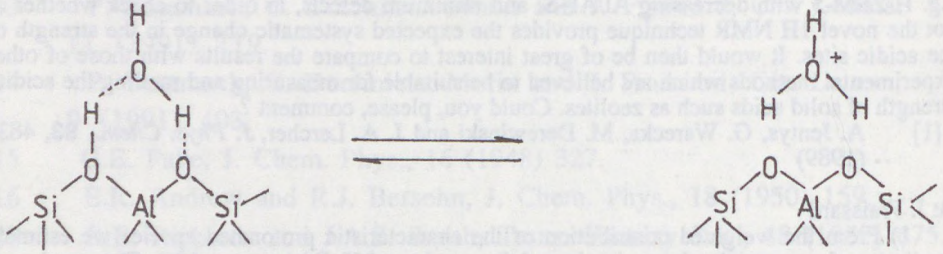

The explanation agrees also very well with recent calculations of Sauer et al.

A: J. Fraissard

The aim of our study is primarily to measure the hydroxonium concentration in the samples. We did not plane to determine the actual symmetry of these ions. nevertheless, we do not claim that the hydroxonium ions do not form hydrogen-bonds to the framework. The optimum geometry proposed by Sauer for these groups (with two hydrogen-bonds to framework oxygens, as you noted) corresponds to a theoretical model with the three H atoms at the apices of any triangle. We have not such a theoretical model programmed now. However, after simulations using an equilateral triangle, we were able to enhance the quality of the simulations for most of the samples by using a theoretical configuration where the H_3O^+ H atoms are assumed to be at the apices of an isosceles triangle. The two equal sides of this triangle are in agreement with the length corresponding to an average dipolar interaction for the two longest sides of Suer's model. The base of the configuration is also in agreement with Sauer's model.

Q: R. Kumar (India)

1) Does your Ga-MFI contain Al ? Table 1 of your paper shows that Si/Al ratio in Ga-MFI is 32. Is it Si/Ga; otherwise what is Si/Ga ?

2) Fig. 2 of your paper shows no difference between MFI and Ga-MFI while in Fig. 3 Ga-MFI exhibits two peaks or splitting in ^1H-NMR at 2.3 and 4.3 ppm. However pure MFI exhibits comparatively a much less intense shoulder at 2.3 ppm apart from the peak at 4.3 ppm. Please comment.

A: J. Fraissard

1) We apologize for the error in Table 1 and in the text: in the case of Ga-MFI the given value (32) is the Si/Ga ratio and not Si/Al. Nevertheless, there is a small amount of Al in the sample due to seeding with MFI crystals during the synthesis.

2) There is indeed a difference between the curves obtained for Ga-MFI and Al-MFI in Figure 2B, especially for values of H_2O/as <1. The MAS NMR signal at 2.3 ppm given by

these samples is attributable to silanol groups, which, in our studies, show no interaction with water, i.e. no appearance of acidity.

Q: J. B. Nagy (Belgium)

Are you going to extend your nice method by using partially deuterated bases, like CD_3OH, ND_2H, etc. ? This could help you to measure the acidity with respect to bases of different strengths.

A: J. Fraissard

We are currently trying some experiments which do not go so far as those you propose but which are moving in the same direction.

Guczi, L. *et al.* (Editors), *New Frontiers in Catalysis*
Proceedings of the 10th International Congress on Catalysis, 19-24 July, 1992, Budapest, Hungary
© 1993 Elsevier Science Publishers B.V. All rights reserved

PREPARATION OF BIFUNCTIONAL CATALYSTS BY SOLID-STATE ION EXCHANGE IN ZEOLITES AND CATALYTIC TESTS

H. G. Karge, Y. Zhang and H.K. Beyer

Fritz-Haber-Institut der Max-Planck-Gesellschaft, Berlin, Germany

Abstract
Bifunctional Pd°-containing zeolite catalysts are prepared by solid-state ion exchange, characterized by acidity measurements and particle size distribution via TEM and tested for hydroconversion of ethylbenzene, dehydrogenation and hydroisomerization of cyclohexane and octene hydrogenation.

1. INTRODUCTION

Solid-state ion exchange in zeolites has been observed and reported in some early studies by *Rabo et al.* [1-2] and *Clearfield et al.* [3]. More recently, systematic work on this phenomenon was carried out by several research groups. *Kucherov* and *Slinkin* (see, e.g., Refs. [4-5]) resumed the ESR approach used by *Clearfield et al.* to follow solid-state ion exchange of transition metal cations into zeolites. Solid-state ion exchange between H-ZSM-5 and nickel and manganese compounds was also studied by *Wichterlová et al.* [6] and *Beran et al.* [7]. *Karge et al.* [8-11] investigated systematically the ion exchange of alkaline, alkaline earth and rare earth cations into zeolites via solid-state reaction. In particular, it was shown that incorporation of La cations into faujasite-type zeolites by solid-state reaction yielded, in a very simple and convenient manner, highly exchanged materials which exhibited excellent performance in acid-catalysed hydrocarbon reactions. Recently, the field of solid-state ion exchange has been reviewed [12].

This paper reports results of experiments aimed at the preparation, via solid-state ion exchange, and the testing of bifunctional zeolite catalysts.

2. EXPERIMENT

The experimental work was focussed on the preparation of Pd-containing H-ZSM-5 catalysts. The following mixtures were employed: PdO/H-ZSM-5, $Pd(NO_3)_2$/H-ZSM-5 and, in particular, $PdCl_2$/H-ZSM-5 or $PdCl_2$, $CaCl_2$/H-ZSM-5. The solid-state reactions were carried out by heating (10 K · min^{-1}) the finely dispersed mixtures in ultra-high vacuum (10^{-5} Pa) to the desired reaction temperatures. The reactions were monitored by in-situ IR or temperature-programmed evolution (TPE) of HCl. Details of the procedures have been described elsewhere [8-12].

As catalytic test reactions, the disproportionation of ethylbenzene, its hydrogenation to ethylcyclohexane and hydroisomerisation to methylcyclohexanes, the dehydrogenation of ethylcyclohexane to ethylbenzene and, finally, the hydrogenation of linear and branched octenes were used. Apparatus and procedure for the catalytic tests were presented in earlier publications (see, e.g., Ref. [13]). H-ZSM-5 was provided by DEGUSSA (Wolfgang, FRG) and had the idealized formula $H_{2.43}Na_{0.12}Fe_{0.31}Al_{2.77}Si_{93.23}O_{192}$. The chemicals (ethylbenzene, ethylcyclohexane, n-octene-(1) and 2.4.4 trimethylpentene-(1) were purchased from MERCK, Darmstadt. They were analytical grade, further purified by three freeze-pump-thaw cycles and finally stored over highly activated 3A molecular sieve.

3. RESULTS AND DISCUSSION

3.1 Introduction of Pd into H-ZSM-5 and preliminary test of the reduced Pd,H-ZSM-5 catalyst.

The experiments showed that Pd cations can be introduced into zeolites by solid-state ion exchange. Solid-state ion exchange was successfully carried out with PdO, $Pd(NO_3)_2$ and $PdCl_2$. In all cases, noble metal contents as usually employed in bifunctional catalysts could be reached. Table 1 shows the decrease in the OH band intensity, as a measure of the degree of exchange, after solid-state reaction of H-ZSM-5 with $CaCl_2$, $PdCl_2$, $Pd(NO_3)_2$ or PdO. The absorbance of the OH band at 3605 cm^{-1} of the starting material was set 100% and a ratio of M/Al = 0.5 employed ($M = Ca^{2+}, Pd^{2+}$). The mixtures were heat-treated at 675 K in high vacuum (HV, 10^{-5} Pa) for 2 h. To check as to whether the integrity of the crystalline zeolite material was maintained the samples were re-exchanged with NH_4^+. It turned out that, within the limits of error, the exchange capacity of the samples, which had been subjected to solid-state reaction, remained unaltered (see Table 1, line 3) in comparison with the starting zeolite. The XRD patterns also showed that no loss of crystallinity occurred upon solid-state reaction.

Table 1 NH_4^+ exchange capacity and IR absorbance of the OH band of H-ZSM-5 and mixtures of H-ZSM-5 with metal compounds

Sample	H-ZSM-5	Mixtures * of H-ZSM-5 with			
		$CaCl_2$	$PdCl_2$	$Pd(NO_3)_2$	PdO
Relative absorbance at 3605 cm^{-1} after (1)	100	66	58	60	45
NH_4^+ content after (1) - (3)	0.37	0.36	0.36	0.34	0.39

* M/Al = 0.5; (1) activation at 675 K, 2 h, in HV; (2) exhange with 1N NH_4Cl solution at 353 K, 12 h; twice repeated for 2 h; (3) NH_4^+ determination [$mmol \cdot g^{-1}$] (Kjeldahl)

The temperature-programmed evolution of HCl and its subsequent titration during solid-state reaction between $PdCl_2$ and H-ZSM-5 is illustrated by Fig. 1. One recognizes that also in this experiment not a complete exchange of Pd^{2+} for H^+ but only an exchange degree of about 64 % was reached. This is at variance with earlier experiments where solid-state reactions with compounds of monovalent cations and H-ZSM-5 or NH_4-ZSM-5 were carried out and a 100 % exchange was obtained [8]. The lower degree of exchange with MCl_2 (and MCl_3, see Ref. [10]) in the case of solid-state reaction with H-ZSM-5 is most probably due to the long distance between framework AlF in this zeolite with a high Si/Al ratio.

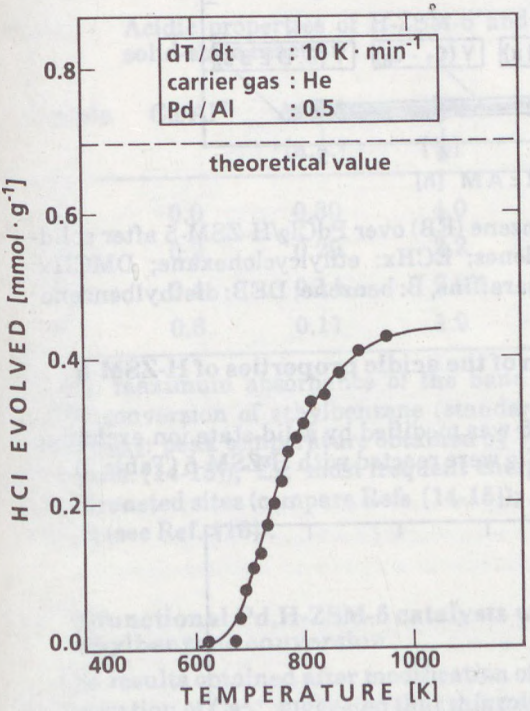

Figure 1. Titration of HCl evolved upon temperature-programmed heating of $PdCl_2$/H-ZSM-5

After reduction of a Pd,H-ZSM-5 sample prepared via solid-state ion exchange corresponding to a Pd loading of 1 wt.-%, a catalytic test for hydrogenation and hydroisomerisation of ethylbenzene was carried out. As can be seen from Fig. 2, the performance of the thus obtained bifunctional catalyst was not satisfactory. Products of hydrogenation and hydroisomerisation (ECHx, DMCHx) were formed with yields comparable to that of the undesired xylenes as well as disproportionation (B, DEB's) and cracking (C1-C8) products.

It was supposed that the acidic and the hydrogenation/dehydrogenation functions of the obtained Pd-loaded H-ZSM-5 catalysts were improperly balanced, i.e. the acidity (density and/or strengths of the acidic Brønsted sites) was too high. Therefore, systematic experiments were carried out to modify and characterize the acidic properties of the catalysts used.

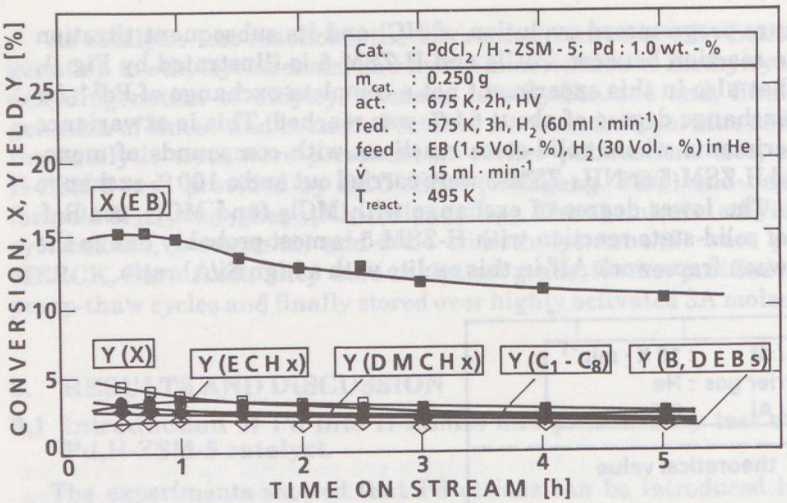

Figure 2. Hydroconversion of ethylbenzene (EB) over $PdCl_2$/H-ZSM-5 after solid-state reaction and reduction; X: xylenes; ECHx: ethylcyclohexane; DMCHx: Dimethylcyclohexanes; C1-C8: C_1-C_8 paraffins, B: benzene; DEB: diethylbenzene

3.2 Modification and determination of the acidic properties of H-ZSM-5 and Pd,H-ZSM-5 catalysts

The acidity of the starting H-ZSM-5 was modified by solid-state ion exchange with $CaCl_2$. Increasing amounts of $CaCl_2$ were reacted with H-ZSM-5 (Table 2).

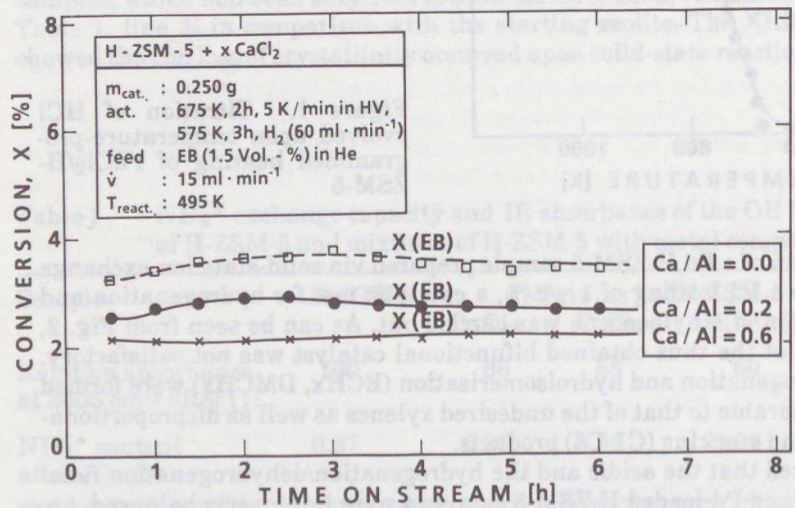

Figure 3. Disproportionation of ethylbenzene over H-ZSM-5 and $CaCl_2$/H-ZSM-5 after solid-state reaction

This resulted in a continuous decrease in the number of acidic OH groups as monitored by standard IR investigation. Correspondingly, the activity of the modified catalysts in disproportionation of ethylbenzene, which is a suitable test reaction for acidic catalysts [13], was reduced (Fig. 3).

However, in contrast to the number of the acidic active Brønsted centres their strength remained essentially unchanged with increasing Ca^{2+} content. This was evidenced by TPD of NH_3 as well as by microcalorimetric measurements of the differential heat of adsorption of NH_3 on the modified zeolites (see Table 2).

Table 2 Acidic properties of H-ZSM-5 and Ca,H-ZSM-5 samples obtained by solid-state reaction

Sample	Ca/Al^F	A(OH) [a.u.]	X(EB) [%]	T_{max} [K]	$\bar{E}_d$ [kJ · mol^{-1}]	ΔH_{ad} [kJ · mol^{-1}]
1	0.0	0.30	4.0	585	99	146
2	0.2	0.20	2.2	610	102	146
3	0.4	0.14	2.0	605	101	138
4	0.6	0.11	1.9	600	102	138

A(OH): maximum absorbance of the band of acidic OH groups at 3605 cm^{-1}; X(EB): conversion of ethylbenzene (standard conditions, see experimental section); T_{max}: peak temperature obtained by TPD of NH_3 from Brønsted sites (compare Refs. [14-15]); $\bar{E}_d$: most frequent energy of activation of desorption of NH_3 from Brønsted sites (compare Refs [14-15]); ΔH_{ad}: differential heat of adsorption of NH_3 (see Ref. [16]).

3.3 Bifunctional Pd,H-ZSM-5 catalysts with modified acidity - ethylbenzene conversion

The results obtained after modification of the acidity of H-ZSM-5 by solid-state incorporation of Ca^{2+} suggested that this might open a promising route for preparing bifunctional Pd,Ca,H-ZSM-5 catalysts. Hence, a series of samples was prepared where $PdCl_2$ and increasing amounts of $CaCl_2$ were simultaneously reacted with the starting zeolite. The Ca/Al^F ratio was varied in the sequence of 0.2, 0.4 and 0.6, (Al^F: framework Al) whereas $PdCl_2$ loadings were employed corresponding to 0.5, 1.0 and 1.5 wt-%.

The materials obtained by simultaneous solid-state ion exchange of H-ZSM-5 with $CaCl_2$ and $PdCl_2$ were reduced (in the micro-flow reactor) and employed for hydrogenation of ethylbenzene. An example of such a catalytic experiment is demonstrated in Fig. 4. The catalytic performance of the reduced Pd,Ca,H-ZSM-5 catalyst is obviously superior to that without $CaCl_2$ addition (compare Fig. 2). The overall activity is much higher, the selectivity toward ECHx significantly improved, and the formation of xylenes, C1-C8, B and DEB's, relative to the total conversion, reduced.

However, the favourable effect of simultaneous introduction of Ca^{2+} decreases with increasing Ca/Al^F (see Table 3). Both activity and selectivity with respect to ECHx became less pronounced. Therefore, an alternative procedure was tried in that $CaCl_2$ and $PdCl_2$ were no longer simultaneously but successively reacted with H-ZSM-5. This, indeed, resulted even in a slight increase in catalytic activity and more importantly, a significant enhancement of the ECHx selectivity (see Fig. 5 and Table 3).

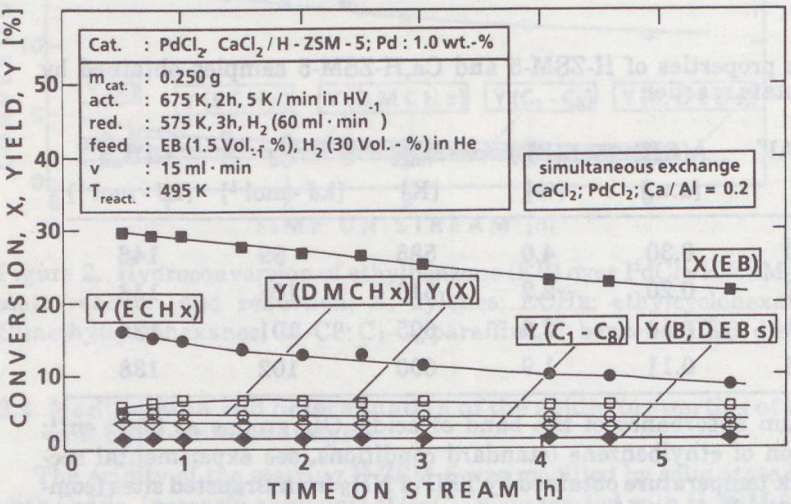

Figure 4. Hydroconversion of ethylbenzene over $PdCl_2$,$CaCl_2$/H-ZSM-5 after simultaneous solid-state ion exchange and reduction (see legend of Fig. 2)

Table 3. Reaction of ethylbenzene over reduced $PdCl_2$,$CaCl_2$/H-ZSM-5; conversion, X, and selectivity, S

		simultaneous exchange				successive exchange		
Ca/AlF		0.0	0.2	0.4	0.6	0.2	0.4	0.6
X (EB)	[%]	11.2	23.5	20.0	7.4	26.0	26.2	27.5
S (ECHx)	[%]	21.0	41.5	43.6	42.7	40.1	54.8	64.7
S (DMCHx)	[%]	19.4	17.0	16.1	22.0	15.4	13.5	9.9
S (B, DEB)	[%]	16.0	5.7	6.4	15.8	4.5	4.7	3.9
S (X)	[%]	24.2	23.2	22.0		27.9	19.3	15.5
S (C1-C8)	[%]	19.4	12.6	11.9	19.5	12.1	7.7	6.0

cat.: $PdCl_2$, x $CaCl_2$/H-ZSM-5; Pd: 1 wt.-%; m_{cat} : 0.250 g; act.: 675 K, 2 h, HV; red.: 575 K, 3 h, H_2 (60 ml · min^{-1}); feed: EB (1.5 vol %), H_2 (30 vol %) in He; $\dot{v}$: 15 ml · min^{-1}; T_{react}: 495 K; TOS: 4 h

Kinetics measurements of hydroconversion of ethylbenzene over reduced Pd,Ca,H-ZSM-5 catalysts (Pd: 1.0 wt.-%; Ca/AlF=0.6) at 388 and 405 K showed that, in the range of ethylbenzene partial pressure, p [EB] = 1.3 kPa to 3.1 kPa (with the other conditions as indicated in Fig. 5), the reaction rates were independent on p [EB]. At p [EB] = 1.33 Pa, and T = 375 to 415 K the rates were, in the range of hydrogen partial pressures, p [H_2], from 10 to 100 kPa, proportional to p [H_2]. The activation energy for ethylbenzene hydroconversion under p [EB] = 1.3 to 3.1 kPa was, in the range from 375 K to 415 K, E_A [EB] = 78.0 kJ · mol^{-1}.

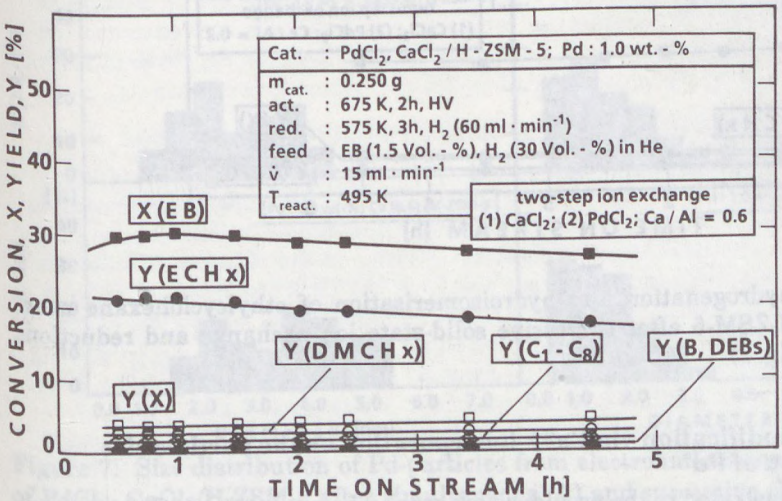

Figure 5. Hydroconversion of ethylbenzene over $PdCl_2$, $CaCl_2$/H-ZSM-5 after successive solid-state ion exchange and reduction (see legend of Fig. 2)

3.4 Bifunctional Pd,H-ZSM-5 catalysts with modified acidity - ethylcyclohexane conversion

After reduction, H-ZSM-5 catalysts loaded with Pd via solid-state reaction were also active in dehydrogenation and dehydroisomerisation of ethylcyclohexane. Similar to the findings with ethylbenzene conversion as a test reaction, the catalytic performance of the reduced Pd,H-ZSM-5 samples improved after modification of the acidic properties by solid-state incorporation of Ca^{2+}. Again, this effect was much more pronounced when the solid-state ion exchange with both metals was conducted successively, i.e., first with $CaCl_2$ and subsequently with $PdCl_2$. An example of the performance of a reduced Pd,Ca,H-ZSM-5 catalyst (Ca/AlF=0.2, Pd: 1.0 wt.-%) in ethylcyclohexane conversion is demonstrated in Fig. 6. The ECHx conversion was three times higher than in the case of non-modified reduced Pd,H-ZSM-5, and the yield of the main dehydrogenation product (EB) was higher by a factor of about 20. Again, the conversion of the feed (ECHx) was almost constant with increasing Ca content but the selectivity toward the main product (EB) increased, provided the solid-state ion exchange was carried out in a two-step procedure.

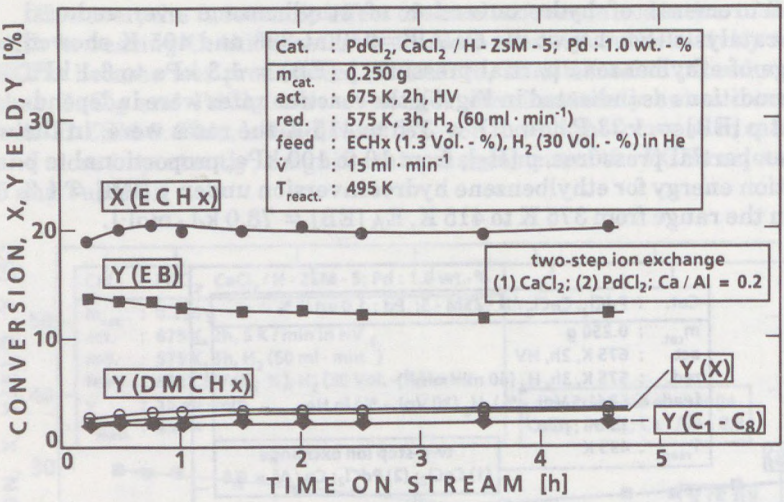

Figure 6. Dehydrogenation and hydroisomerisation of ethylcyclohexane over $PdCl_2$, $CaCl_2$/H-ZSM-5 after successive solid-state ion exchange and reduction (see legend of Fig. 2)

3.5 Effect of modification via Ca^{2+} incorporation on the particle size distribution of Pd°

As was demonstrated in the previous paragraphs, incorporation of Ca^{2+} lowered the acidity (number of acidic Brønsted sites) of the Pd-loaded H-ZSM-5 samples and improved their catalytic properties. However, the effect on the acidity was independent on the procedure of Ca^{2+} exchange into the zeolite. For example, the conversion of ethylbenzene over Pd,Ca,H-ZSM-5 ($Ca/Al^F = 0.2$, Pd = 1.0 wt.-%) upon selective disproportionation into benzene and diethylbenzenes (i.e. in the absence of hydrogen) was essentially the same irrespective as to whether Ca^{2+} and Pd^{2+} were introduced simultaneously or successively. This result suggested that, besides the influence on acidity, the incorporation of Ca^{2+} must have at least one additional effect on the properties of the Pd-loaded H-ZSM-5 samples prepared by solid-state reaction. As a possible explanation it was assumed that the procedure of solid-state ion exchange of Ca^{2+} and Pd^{2+} affects the distribution of Pd^{2+} over the cation sites in Pd,Ca,H-ZSM-5. It appeared likely that this distribution, in turn, influences the particle sizes and dispersion of the Pd° aggregates formed upon subsequent reduction of Pd,Ca,H-ZSM-5. In order to check this assumption, two series of reduced Pd,Ca,H-ZSM-5 samples obtained via (A) simultaneous and (B) successive introduction of Ca^{2+} and Pd^{2+} were investigated by transmission electron microscopy.

The results of evaluation of the electron micrographs are shown in Fig. 7. It is obvious from the representation of case A that simultaneous exchange of Ca^{2+}

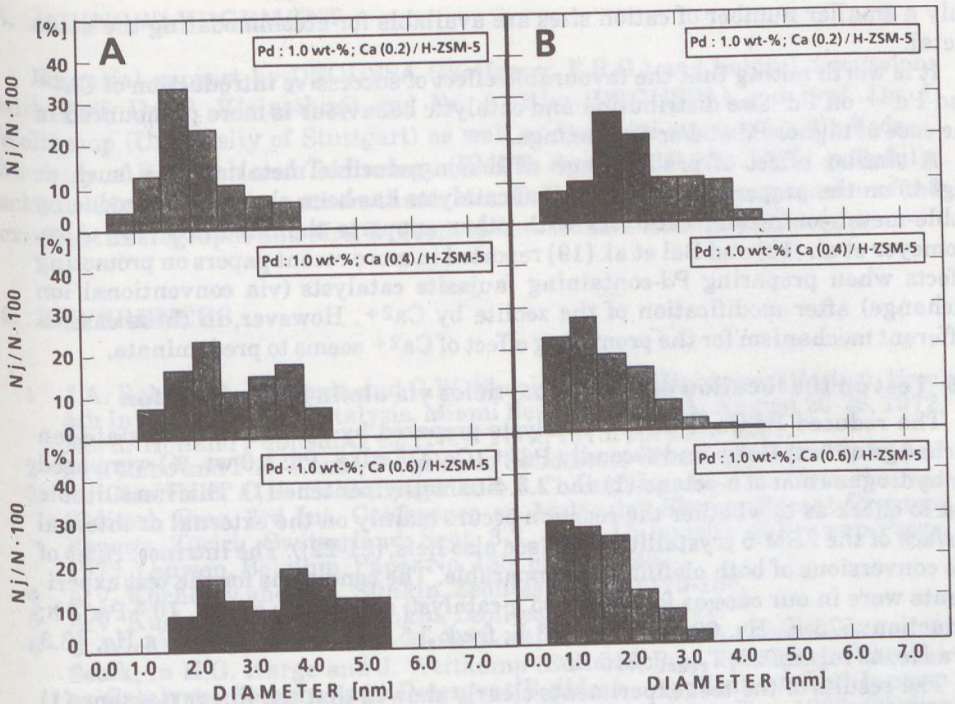

Figure 7. Size distribution of Pd-particles from electronmicroscopic micrographs of $PdCl_2$, $CaCl_2$/H-ZSM-5 after simultaneous (A) and successive (B) introduction of Ca^{2+} and Pd^{2+} via solid-state ion exchange followed by reduction

and Pd^{2+} into H-ZSM-5 results in Pd° particle size distributions which become broader and shift to bigger particles with increasing Ca^{2+} content. As was pointed out previously (vide supra, see Table 3), the catalytic behaviour of these reduced Pd,Ca,H-ZSM-5 deteriorated in the same sequence, i.e. from $Ca/Al^F = 0.2$ through $Ca/Al^F = 0.6$. In contrast, successive exchange of Ca^{2+} brings about particle size distributions which significantly narrow and shift to smaller Pd° aggregates when the Ca^{2+} content is increased. This is in parallel with the continuous improvement of the catalytic performance of these samples with Ca^{2+} contents increasing from $Ca/Al^F = 0.2$ to $Ca/Al^F = 0.6$ (vide supra, see Table 3). A tentative explanation of this finding is as follows. In the case of successive ion exchange, the first step leads to a relative uniform population of the cation sites by Ca^{2+} and to a correspondingly homogeneous distribution of the remaining protons. This in turn gives rise to a uniform distribution of the subsequently introduced Pd^{2+} cations. Reduction of these homogeneously distributed noble metal cations generates a high number of small-sized Pd° particles.

Simultaneous introduction of Ca^{2+} and Pd^{2+} into the H-ZSM-5 structure by solid-state reaction might form more frequently "islands" with either adjacent Ca^{2+} or Pd^{2+} populations. The reduction of such samples is likely to give a smaller number of bigger particles in particular when, by high loadings with Ca^{2+},

only a smaller number of cation sites are available for accommodating the noble metal.

It is worth noting that the favourable effect of successive introduction of Ca^{2+} and Pd^{2+} on Pd° size distribution and catalytic behaviour is more pronounced in the case of higher Pd and/or Ca loadings.

A similar effect of pre-coverage with non-reducible metal cations (such as Mg^{2+}) on the properties of bifunctional catalysts has been observed in producing noble-metal-containing catalysts with other supports than zeolites [17]. Also, Homeyer et al. [18] and Bai et al. [19] reported in more recent papers on promoting effects when preparing Pd-containing faujasite catalysts (via conventional ion exchange) after modification of the zeolite by Ca^{2+}. However, in these cases a different mechanism for the promoting effect of Ca^{2+} seems to predominate.

3.6 Test on the location of the Pd° particles via olefin hydrogenation

The reduced Pd,Ca,H-ZSM-5 catalysts prepared by successive solid-state ion exchange of first Ca^{2+} and secondly Pd^{2+} ($Ca/Al^F = 0.6$, Pd: 1.0 wt.-%) were used for hydrogenation of n-octene-(1) and 2.4.4-trimethylpentene-(1). This is a suitable test to check as to whether the reaction occurs mainly on the external or internal surface of the ZSM-5 crystallites [20] (see also Refs. [21-22]). The intrinsic rates of the conversions of both olefins are comparable. The conditions for the test experiments were in our case as follows: 0.05 g catalyst; activation: 675 K, 10^{-5} Pa, 3 h; reduction: 575 K, H_2, 60 ml · min^{-1}, 3 h; feed: 3.5 kPa octene, 48.3 kPa H_2, 48.3 kPa He, 40 ml · min^{-1}, $T_{react.}$: 315 K.

The results of the test experiments clearly showed that the linear n-octene-(1) was hydrogenated to about 93% whereas the conversion of the branched 2.4.4-trimethylpentene-(1), which had essentially no access to the interior of the reduced Pd,Ca,H-ZSM-5 catalysts, amounted to only about 3%. The straightforward conclusion from this finding is that the finely dispersed Pd° particles produced through the above described procedure are indeed localized inside the porous ZSM-5 structure where they to a very high degree could catalyse the hydrogenation of the slim n-octene-(1) molecules.

4. CONCLUSIONS

Solid-state ion exchange of Pd into H-ZSM-5 is an advantageous method to prepare bifunctional catalysts, possessing both acidic and hydrogenation functions, being capable, for instance, to hydrogenate ethylbenzene and to dehydrogenate and dehydroisomerise ethylcyclohexane. The catalytic performance with respect to activity and selectivity (e.g. for the desired main products ethylcyclohexane or ethylbenzene) can be much improved by modification of the acidity through solid-state incorporation of Ca^{2+}. Successive introduction of first Ca^{2+} and subsequently Pd^{2+} is more effective than simultaneous exchange. This is due to the fact that successive solid-state ion exchange provides, after reduction, more homogeneously and finely dispersed Pd° aggregates than simultaneous solid-state reaction of $CaCl_2$ and $PdCl_2$ with H-ZSM-5. This effect is probably due to a more uniform distribution of Pd^{2+} over the cation sites achieved by successive solid-state ion exchange prior to reduction.

5. ACKNOWLEDGEMENT

Financial support by DEGUSSA (Wolfgang, F.R.G.) and helpful discussions with Prof. Dr. P. Kleinschmit and Dr. A. Kiss (DEGUSSA) and Prof. Dr. J. Weitkamp (University of Stuttgart) as well as financial support by the Federal Ministry of Research and Technology (BMFT, Project 03C 252 A7) is gratefully acknowledged. Also, the authors thank Mrs. U. Klengler for the preparation of the excellent micrographs and Mrs. E. Popović for valuable technical assistance.

6. REFERENCES

1 J.A. Rabo, M.L. Poutsma and G.W. Skeels, in J.W. Hightower (Editor), Proc. 5th Int. Congress on Catalysis, Miami Beach, Flo., USA, August 20-26, 1972, North-Holland Publishing Co., New York, 1973, pp. 1353-1361.
2 J.A. Rabo and P.H. Kasai, Progress in Solid State Chemistry 9 (1975) 1-19.
3 A. Clearfield, C.H. Saldarriaga and R.C. Buckley, in J.B. Uytterhoeven (Editor), Proc. 3rd Int. Conference on Molecular Sieves; Recent Progress Reports, Zürich, Switzerland, Sept. 3-7, 1973; University of Leuwen Press, 1973, Leuwen, Belgium, Paper No. 130, pp. 241-245.
4 A.V. Kucherov and A.A. Slinkin, Zeolites 6 (1986) 175-180.
5 A.V. Kucherov and A.A. Slinkin, Zeolites 7 (1987) 38- 42.
6 B. Wichterlová, S. Beran, L. Kubelková, J. Nováková, A. Smiešková and R. Šebík, in H.G. Karge and J. Weitkamp (Editors), Proc. Int. Symp. "Zeolites as Catalysts, Sorbents and Detergent Builders - Applications and Innovations", Würzburg, FRG, Sept. 4-8, 1988, Elsevier, Amsterdam, 1989; Studies Surf. Sci. Catalysis 46 (1989) 347-353.
7 S. Beran, B. Wichterlová and H.G. Karge, J. Chem. Soc. Faraday Trans. I 86 (1990) 3033-3037.
8 H.K. Beyer, H.G. Karge and G. Borbély, Zeolites 8 (1988) 79-82.
9 H.G. Karge, H.K. Beyer and G. Borbély, Catalysis Today 3 (1988) 41-52.
10 H.G. Karge, G. Borbély, H.K. Beyer and G. Onyestyák, in M.J. Philips and M. Ternan (Editors), Proc. 9th Int. Congress on Catalysis,Calgary, Ottawa, Canada, June 26-July 1, 1988, Chemical Institute of Canada, Ottawa, 1988, pp. 396-403.
11 H.G. Karge, V. Mavrodinova, Z. Zheng and H.K. Beyer, Appl. Catal. 75 (1991) 343-358.
12 H.G. Karge and H.K. Beyer, in P.A. Jacobs, N.I. Jaeger, L. Kubelková and B. Wichterlová (Editors), Proc. Int. Symp. "Zeolite Chemistry and Catalysis", Prague, Czechoslovakia, Sept. 8-13, 1991, Elsevier, Amsterdam, 1991; Studies Surf. Sci. Catalysis 69 (1991) 43-64.
13 H.G. Karge, J. Ladebeck, Z. Sarbak and K. Hatada, Zeolites 2 (1982) 94-102.
14 H.G. Karge and V. Dondur, J. Phys. Chem. 94 (1990) 765-772.
15 H.G. Karge, V. Dondur and J. Weitkamp, J. Phys. Chem. 95 (1991) 283-288.
16 H.G. Karge and L. Jozefowicz, publication in preparation
17 A. Kiss, private communication.
18 S.T. Homeyer, Z. Karpinski and W.M.H. Sachtler, J. Catal. 123 (1990) 60-73.
19 X. Bai, Z. Zhang and W.M.H. Sachtler, Appl. Catal. 72 (1991) 165-178.
20 J. Weitkamp and S. Ernst, private communication.
21 R.M. Dessau, J. Catal. 77 (1982) 304-306.
22 R.M. Dessau, J. Catal. 89 (1984) 520-526.

DISCUSSION

Q: A. O. I. Krause (Finland)

You indicated that the acidity plays an important role in your system. You used chlorides in the catalyst preparation. What are the amounts of chlorides left on the catalysts and do they have any influence ? What would the situation be if some other salts - like nitrates - were used instead of chlorides ?

A: H. G. Karge

The amount of chlorides left after solid-state reaction in the zeolite structure depends, inter alias, on the composition of the chloride/zeolite mixture (under-stoichiometric, stoichiometric or excess amount of chloride), reaction conditions, type of cation (mono-, bi-, tri-valent), type of zeolite structure) etc. This was systematically studied in some cases, for instance with $LaCl_3/NH_4Y$ and $LaCl_3/NaY$. We did not observe any negative effect of the residual chloride. Most of the remaining chlorides could be removed by short contact of solid-state ion-exchanged material with water [1, 2].

We also employed other salts such as nitrates, carbonates, sulfates and acetates. In general, performance of chlorides was better, the reaction of sulfates, acetates and carbonates was negatively affected by decomposition. Only in the case of $Pd(NO_3)_2$, which decomposed in a complicated manner under formation of N_2, N_2O, NO a relatively high and easy exchange with HY was achieved.

[1] H. G. Karge, G. Borbély, H. K. Beyer, G. Onyestyák, *Proc. 9th Int. Congress on Catalysis*, (Eds: M. J. Philips, M. Ternan), Chemical Institute of Canada, Ottawa, **Vol. 1**, 396 (1988)

[2] DGMK-Bereichte-Tagungsbericht 9101, DGMK-Fachbereichtstagung "C_1-Chemie-Angewandte Heterogene Katalyse-C_4-Chemie", Leipzig, ISBN No. 3-928164-07-4, ISSN No. 0938-068X, pp. 191, (1991)

Q: J. Weitkamp (Germany)

1) I am wondering whether the particle size distribution in the final catalyst cannot be influenced by the reduction conditions of Pd(II) introduced via solid-state ion exchange.

2) Your IR data seem to indicate that the weakly acidic sites represented by the 3647 cm^{-1} line are taking part in the solid-state ion exchange in addition to the strongly acidic sites. Can you comment on this ?

A: H. G. Karge

1) We did not find a significant effect of reduction conditions (e.g. pre-oxidation, reduction temperature) on the catalyst performance. However, systematic studies on the influence of those conditions on the particle size distribution were not carried out.

2) Indeed, the weakly acidic so-called silanol groups (indicated by an IR stretch band around 3740 cm^{-1}) do react via solid-state exchange with salts as well, but to a lesser extent than the more strongly acidic bridging OH groups (Brönsted acid sites). However, the cations are only loosely held at the sites of those silanol groups [3].

[3] H. K. Beyer, H. G. Karge and G. Borbély, *Zeolites*, **8**, 79 (1988)

Q: J. Fraissard (France)

When there is a solid-state reaction between zeolites and oxides, there is generally diffusion of the oxide into the channels, lost of crystallinity etc.

With chlorines we may have residual chlorine in the zeolite.

Do you have some comments on these problems ?

A: H. G. Karge

In almost all cases of solid-state reaction between salts or oxides and zeolites studied so far, we did not observe any loss of crystallinity of the zeolite. This was checked by XRD and

measurements of the conventional ion exchange capacity (i.e. in aqueous suspension) of the materials before and after solid-state reaction. Only in the case of $CuCl_2$/HZSM-5 we found, by ^{27}Al MAS NMR, a slight dealumination even though the XRD pattern did not indicate any structural change [4]. If chlorides are used as reactants residual chlorine may indeed be left in the zeolite structure after solid-state reaction. This chloride usually remains in the structure in the form of occluded metal chloride molecules. We did not observe a negative effect of those occluded species, for instance in catalysis of acid catalyzed hydrocarbon reaction [1]. By contrast, according to the pioneering studies by J. Rabo on salt occlusion one would expect an improved thermal stability of the structure which contains some additional salt [5].

[4] H. G. Karge, B. Wichterlova, H. K. Beyer, *J. Chem. Soc. Faraday Trans.*, **88**, 1345 (1992)

[5] J. A. Rabo, Salt Occlusion in Zeolite Crystals, in: *Zeolite Chemistry and Catalysis* (Ed.: J. A. Rabo) ACS monograph 171, American Chemical Society, Washington D. C., p. 332 (1976)

Q: R. Kumar (India)

First of all let me appreciate the work you presented. My question is related to simultaneous vs successive solid state ion exchange of Ca and Pd. Successive method is more effective than simultaneous one. Does competition between Ca(II) and Pd(II) ions, during simultaneous ion-exchange play any role, in addition to the explanation you have given in your paper ? Please comment.

A: H. G. Karge

We feel that in successive ion-exchange the cations introduced first (e.g. Ca(II)) are more homogeneously distributed through the zeolite structure than in the case of competitive simultaneous incorporation with other cations (Pd(II)). The more homogeneous distribution of the Ca(II) cations will, in turn, provide via the "anchoring" effect a more homogeneous distribution and higher dispersion of the noble metal aggregates formed upon subsequent reduction.

Q: W. M. H. Sachtler (USA)

We have applied solid state ion exchange to $PdCl_2$+HY and $PdCl_2$+NaCl, also to $GaCl_3$+HZSM-5. We have also used a related technique to rejuvenate aged Pd/HNaY catalysts and obtained high dispersion of Pd after reduction. My question is: what are your ideas on the mechanism of these processes: are the chlorides sublimed and then physisorbed in the zeolite, or is surface diffusion the prevailing transport mechanism ?

A: H. G. Karge

The mechanism of the solid-state reaction between compounds (salts, oxides) of the cations to be introduced and the zeolite (hydrogen forms, alkaline metal forms, etc.) is still not clarified. Currently we are conducting in situ experiments to solve this problem. It might well be that either of the mechanisms you mentioned will be operative depending on the system. In the case of relatively volatile chlorides such as $PdCl_2$, sorption of $PdCl_2$ molecules into the porous zeolite structure followed by reaction at the OH groups could be predominant whereas surface diffusion prevails in the case of less volatile salts (NaCl) or oxides (Mn_3O_4). Comparison between the reaction in the systems CsCl/HZSM-5 and $Cs_4[PW_{12}O_{40}]$/HZSM-5 showed a significantly less degree of exchange in the case with the big Keggin ions which are unable to penetrate into the zeolite channels. This seems to indicate that for exchange with alkaline metal salts the diffusion of the salt molecules into the pores is a prerequisite for the solid-state ion exchange to occur.

Q: J. M. Thomas (United Kingdom)

My question is prompted by your electron micrograph which shows that there is quite a

a few (2 to 5) atoms they are invisible in the electron microscope (unless special techniques using Rutherford Backscattering for example). What one would like to know is whether, by careful preparation, you can achieve so high a dispersion of Pd that the individual particles are individual particles are invisible in the electron microscope ?

A: H. G. Karge

We are quite aware of the fact that part of the Pd might have smaller sizes than indicated in our histograms derived from electron micrographs. The only thing we claim and could experimentally demonstrate is the increase of Pd(0) dispersion in the case of successive solid-state reaction of, e.g., $CaCl_2$ and $PdCl_2$ with HZSM-5. We did not yet attempt to achieve such a high dispersion that the individual Pd(0) particles become invisible in the electron microscope.

Q: W. O. Haag (USA)

1) The solid state exchange method that you have pioneered presents an important method for preparing dual-functional catalysts. In your catalytic testing, you showed that Ca incorporation can be used to reduce the acidity. I would like to ask if you have examined your bifunctional catalysts in reaction requiring a high acidity such as paraffin isomerization?

2) In your abstract you mention a value of about 100 kJ/mol for the desorption activation energy of the most frequent type of ammonia sorption. This implies a non-homogeneous set of acid sites in your sample we have found that a carefully prepared sample of HZSM-5 shows an NH_3 TPD peak which represents a homo energetic site. The E_a for desorption is 148 kJ/mol, in excellent agreement with your value of 146 kJ/mol obtained by microcalorimetry. This agreement can be taken as evidence that the rate of adsorption of NH_3 on HZSM-5 occurs with essentially no activation energy.

A: H. G. Karge

1) We did not yet employ the bifunctional catalysts prepared via solid-state ion-exchange for isomerization of n-paraffins. However, we reacted ethyl-cyclohexane in the presence of H_2 over reduced (Pd(0)-containing) Ca,HZSM-5 and obtained, besides the main product ethylbenzene, dimethylcyclohexanes.

2) Indeed, the HZSM-5 sample used for preparation of our bifunctional catalysts was a commercial product with a relatively high content of extra-framework aluminium as shown by IR (pyridine adsorption), EPR (NO adsorption) and MAS NMR. The acidity strength was not homogeneous as was also substantiated by deconvolution of the TPD peaks employing a kinetics model described [6].

[6] H. G. Karge and V. Dondur, *J. Phys. Chem.*, **94**, 765 (1990)

Guczi, L. *et al.* (Editors), *New Frontiers in Catalysis*
Proceedings of the 10th International Congress on Catalysis, 19-24 July, 1992, Budapest, Hungary
© 1993 Elsevier Science Publishers B.V. All rights reserved

TRANSITION METAL/ZEOLITE CATALYSTS BY DESIGN: NUCLEATION AND GROWTH OF MONO- AND BIMETALLIC PARTICLES IN ZEOLITE Y

W. M. H. Sachtler[a], *Z. Zhang*[a], *A. Yu. Stakheev*[b] *and J. S. Feeley*[c]

[a]V.N. Ipatieff Laboratory, Center for Catalysis and Surface Science, Northwestern University, Evanston, IL 60208, USA
[b]On leave from the N.D. Zelinskii Institute, Russian Academy of Sciences, Moscow, Russia
[c]Engelhard Corporation, Menlo Park, Edison, NJ 08818, USA

Abstract

A highly dynamic model emerges for mono- and bimetallic particles inside a Y zeolite under conditions of catalytic CO hydrogenation. Nickel tetracarbonyl and Pd carbonyl clusters are the most probable vehicles in a rather dramatic relocation of Ni and Pd atoms between cages, but also between the outer mantle and the inner core of the zeolite. Zeolite protons interfere by acting as anchors and as nucleation sites. Growing metal particles appear able to destroy their zeolite cages.

1. INTRODUCTION

Our research in recent years has identified a number of mechanisms by which mono- or bimetallic particles are formed in zeolite cages, following ion exchange. Of particular importance are: (1) pH of the washing liquid prior to calcination, (2) gas flow and heating program during calcination, (3) reduction temperature, (4) exposure of reduced clusters to CO, and (5) their interaction with zeolite protons. For Ni a high pH during washing promotes hydrolysis, which prevents the escape of Ni^{2+} ions to hidden sites during subsequent calcination, as hydroxide particles in supercages are transformed to easily reducible oxide particles. For Pd very small primary clusters react with CO to form Pd carbonyl clusters which swiftly coalesce to larger clusters; at low temperature this process is controlled by the aperture of the cage windows: in Y sieves it stops at the stage of $Pd_{13}(CO)_x$, in the sieve 5A it stops at $Pd_6(CO)_y$.

Mono- and bimetallic Pd/Y, Ni/Y and (PdNi)/Y catalysts have been tested for the hydrogenation of CO at 10 bar; this work revealed activity and selectivity changes with time on stream that are, in part, ascribed to changes in the size of the metal and alloy particles during the catalytic reaction. In the present work these changes under catalytic conditions will be studied using X-

ray Photoelectron Spectroscopy (XPS) and Extended X-ray Absorption Fine Structure (EXAFS). The former technique permits the analysis of changes in metal concentration in the zone near the external surface of the catalyst which is probed by escaping photoelectrons; the latter technique detects the average coordination number of metal atoms with other heavy atoms, from which the nuclearity of metal particles can be derived. In isolation XPS data can still be ambiguous; for instance an observed decrease in the Ni/Si ratio could mean either that Ni has left the surface zone or that the Ni particles have coalesced to very big clusters. To decide between these alternatives X-ray Diffraction (XRD) has been combined with XPS. In the present work XPS and XRD have been applied to catalysts before and after certain times on stream of CO hydrogenation; EXAFS has been used to monitor effects on Pd nuclearity of CO exposure at various temperatures.

2. EXPERIMENTAL

Preparation and pretreatment conditions and results of catalytic tests of CO hydrogenation over zeolite Y supported Ni, Pd and Pd+Ni were described elsewhere (1). The following nomenclature will be used to refer to samples: Me(A or B) where Me = Ni, Pd, or PdNi; A or B refers to wash at pH = 6 or 10.5, respectively, subsequent to ion exchange with NaY. Equipment and procedure to obtain XPS data were previously published (2).

For EXAFS analysis an ion-exchanged Pd/NaY sample was calcined at 500°C and pelletized in air. After mounting it in the sample holder it was dried in He at 250°C in a cell described previously (3). Following reduction at 200°C and cooling to -195°C the sample was warmed to a specified temperature under 1 atm of CO for 20 min. After cooling to -195°C it was sealed for EXAFS data collection. The temperatures are precise within ± 5°C. Data were collected at station A3 of CHESS. Typical beam energies and currents were 5.0 GeV and 70 mA, respectively.

X-ray diffraction (XRD) data were measured using nickel filtered Cu-K α radiation with a Rigaku Geigerflex Diffractometer. The average metal particle sizes were calculated with the Scherrer equation. The Ni(111) peak at 2Θ = 44.627° and the Pd(111) peak at 2Θ = 40.228° were used for Ni and Pd particles.

3. RESULTS

The EXAFS data show that exposure to CO at or below 0°C does not induce observable changes of the Pd cluster size. The Pd clusters do increase

at 20°C and a major increase occurs at 50°C. In this paper attention is focused on changes of Pd nuclearity; no mention will be made on changes of coordination by CO. Quantitative curve fitting with a Pd foil as the reference gives a nearest Pd-Pd bond length of 2.72±0.02 Å. The first Pd-Pd shell coordination numbers (CN) and Debye-Waller factors (σ) of the samples are given in Table 1. Absorption of CO was large at -40°C and even larger at -80°C, presumably due to capillary condensation.

Table 1 EXAFS Parameters

Sample	pretreatment	CN	$\Delta\sigma^2$ x 100
EXAFS-A	reduced	3.9	0.98
EXAFS-B	CO, T ≤ 0°C	4.0	0.98
EXAFS-C	CO, 20°C	4.9	0.98
EXAFS-D	CO, 50°C	6.9	0.69

Metal/silicon atomic ratios, binding energies, BE, and the Auger parameter, α', all derived from XPS analysis of the monometallic samples, are compiled in Table 2. The Ni samples of the A and B series differ significantly. The Ni/Si atomic ratio of Ni(A) after calcination is close to the bulk value (0.065), and the Ni $2p_{3/2}$ binding energy (857.0 eV) corresponds to Ni^{2+} ions in zeolite (4). The Ni/Si ratio of Ni(B) exceeds the bulk value by more than an order of magnitude. After reduction at 760°C the $Ni2p_{3/2}$ signal completely disappears from the Ni(B) spectrum, but about 10% of the Ni remains unreduced in Ni(A).

After reduction the Ni/Si ratio decreases by approximately 50% for both catalysts. Carbon monoxide hydrogenation does not cause changes in the $Ni2p_{3/2}$ BE. No Ni carbide formation is observed in these samples which had been re-reduced at 500°C before the XPS measurements. During CO hydrogenation the Ni/Si ratio decreases by almost 50% for Ni(A), but by more than an order of magnitude for Ni(B) to a value significantly below the bulk ratio.

Table 2
Atomic ratios, Binding Energies, and α'_{Pd} (eV) from XPS for Monometallic Samples

Sample	Ni/Si	Pd/Si	Ni $2p_{3/2}$	Pd $3d_{5/2}$	α'_{Pd}
Ni(A),calc.	0.044	--	857.0	--	--
Ni(A), red.	0.025	--	851.4	--	--
Ni(A),react	0.014	--	851.4	--	--
Ni(B),calc.	1.00	--	856.2	--	--
Ni(B), red.	0.47	--	851.4	--	--
Ni(B),react	0.034	--	851.3	--	--
Pd(A),calc.	--	0.033	--	337.4	662.2
Pd(A), red.	--	0.025	--	335.5	662.9
Pd(A),react	--	0.019	--	335.4	--
Pd(B),calc.	--	0.041	--	337.6	662.1
Pd(B), red.	--	0.030	--	335.7	662.7
Pd(B),react	--	0.032	--	335.0	663.8

No significant differences are detected between the calcined Pd(A) and Pd(B). The BE of Pd $3d_{5/2}$ is 337.5 eV [i.e. the value of the Pd^{2+} ion (5)] for both samples. The Pd/Si ratios indicate a slight surface Pd depletion with respect to the bulk (0.075). Reduction in flowing H_2 is complete at 500°C. Both samples have higher BE values of Pd $3d_{5/2}$ than bulk Pd (335.0 eV); α'_{Pd} is significantly lower than for bulk Pd (663.7 eV). After reaction both the Pd $3d_{5/2}$ BE and α'_{Pd} are shifted towards the values of bulk Pd. The change in Pd $3d_{5/2}$ BE is smaller for Pd(A) than for Pd(B).

For bimetallic (PdNi)/NaY samples after calcination the values of the Pd $3d_{5/2}$ and Ni $2p_{3/2}$ BE and metal/silicon ratios are quite similar to those found for monometallic samples. However, these values change significantly after reduction. With PdNi(A) the BE's for Ni$2p_{3/2}$ (851.2eV) and Pd $3d_{5/2}$ (334.7eV) are markedly higher and α'_{Pd} (663.6eV) is lower than the values for the bulk metals. The Ni/Si and Pd/Si ratios decrease slightly after reduction (Fig.1). Reaction conditions cause shifts of the Binding Energy of Ni and Pd and of α'_{Pd} towards the values for the bulk metal. For PdNi(B) the BE's of Ni $2p_{3/2}$ and Pd

$3d_{5/2}$ after reduction are equal to those of the bulk metal or even lower. Reduction also results in a twofold decrease in Ni/Si ratio, but a three-fold increase in Pd/Si ratio. After reaction an approximately five-fold decrease in both the Pd/Si and the Ni/Si ratio is observed. The same trend is observed for the PdNi(B) sample treated in CO at 60°C.

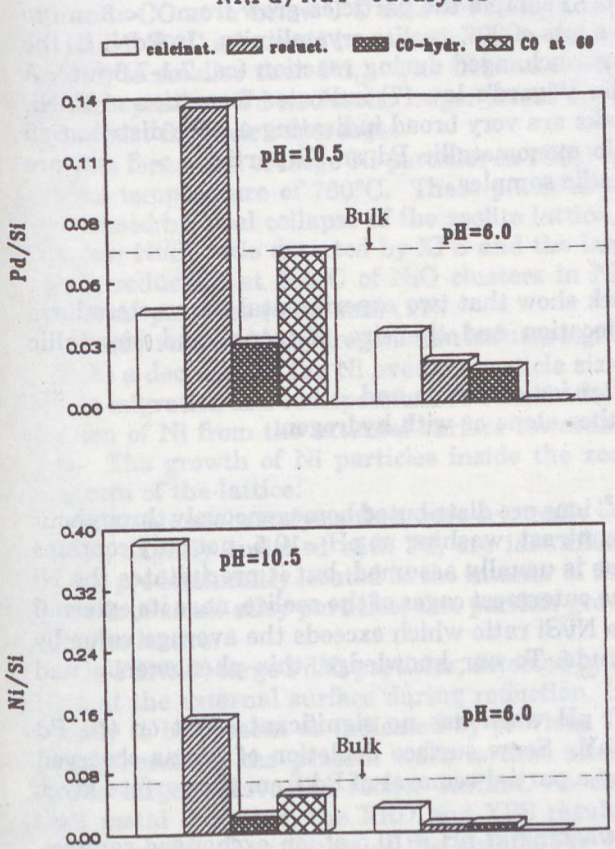

Fig. 1 Metal/Si ratios for PdNi/NaY samples different histories including different pH of wash after ion exchange. --- overall Metal/Si ratio

No loss in zeolite crystallinity upon ion exchange, washing or calcination is detected by XRD (6). However, after reduction at 760°C Ni(A) shows a 30% loss in crystallinity. In the course of the catalytic reaction the average Ni particle size decreases, remarkably, from 23.3 nm to 12.6 nm. No loss of crystallinity is observed. For Ni(B) reduction produces <3 nm Ni particles, but

no loss of zeolite crystallinity. After reaction the Ni particles have increased to 23.9nm; a loss of 30% crystallinity is found. No significant loss in crystallinity was found for NaY exposed to 0.5 atm H_2O at 300°C for 24 h.

After reaction the majority of the metal particles in Pd(A) are still quite small, at the limit of detection of XRD, but in Pd(B) a substantial particle growth occurs: from < 3 nm to 6.5 nm, accompanied by a loss of zeolite crystallinity of 20%.

In the bimetallic PdNi(A) sample the particles grow from < 3 nm to 6.6 nm during reaction with a loss of 30% zeolite crystallinity. In PdNi(B) the average particle size remains unchanged during reaction (ca. 7.1-7.6 nm). A qualitative estimate based on Végard's law (7) indicates formation of $PdNi_x$ alloy particles. However, peaks are very broad indicating a wide distribution of particle compositions. No monometallic Pd or Ni particles > 3 nm are detected in any of the bimetallic samples.

4. DISCUSSION

The results of this work show that two experimental parameters have substantial effects on the location and the size of mono- and bimetallic particles inside zeolite Y:

(a) pH during wash after ion exchange and

(b) exposure to CO, either alone or with hydrogen.

4.1. Effect of pH

After wash at pH=6 Ni^{2+} ions are distributed homogeneously throughout the zeolite microcrystals. In contrast, washing at pH =10.5 not only confines the Ni^{2+} ions to supercages, as is usually assumed, but it precipitates the Ni hydroxide preferentially in the outermost cages of the zeolite, near its external surface. This is manifest by a Ni/Si ratio which exceeds the average value by almost two orders of magnitude. To our knowledge, this phenomenon had never been reported before.

In contrast to Ni/NaY, pH wash has no significant effect on the Pd distribution of calcined Pd/NaY. Some surface depletion of Pd, as observed with XPS, can be explained by a partial removal of Pd from the surface layer during washing.

As shown in Figure 1 washing at pH = 10.5 of ion exchanged samples containing both metals leads to substantial concentration of Ni in the external mantle of the zeolite, which is depleted of Pd. After reduction the mantle contains more metal than the interior, the concentration of either metal is roughly two times higher in the mantle. Reduced samples that had been washed at pH =6, appear to contain small PdNi alloy particles in the interior of the zeolite crystals.

4.2. Effect of Exposure to CO or CO+H_2

As found earlier, primary Pd carbonyl clusters in zeolites migrate and coalesce at room temperature (2,8). The size of the supercage aperture is decisive for the Pd nuclearity of the final carbonyl cluster: $Pd_{13}(CO)_x$ in NaY and $Pd_6(CO)_y$ in 5A (9,10). After reduction the Pd atoms or particles are anchored to the cage wall by protons. The present EXAFS results show that Pd particles with an average CN=3.9 are formed after reduction (Table 1); exposure to CO at or below 0°C does not change their nuclearity appreciably. However, at 20°C a marked increase in CN is detected, although the average nuclearity is smaller than Pd_{13}. The CN=6.9 observed after CO exposure at 50°C corresponds to Pd nuclearity larger than Pd_{13}. It is conceivable that such particles just fill their supercages.

The formation of large Ni particles in Ni(A) is probably due to the high reduction temperature of 760°C. These particles are presumably located in voids, caused by local collapse of the zeolite lattice. This conclusion is based on the low Ni/Si ratio detected by XPS and the large loss of crystallinity. In contrast, reduction at 500°C of NiO clusters in Ni(B) leads to formation of small metal particles (< 3.0 nm) (11).

Carbon monoxide hydrogenation induces significant redistribution of Ni. For Ni(A) a decrease in the Ni average particle size and in Ni/Si atomic ratio suggests migration and redispersion of Ni inside the zeolite. Similarly in Ni(B), migration of Ni from the external surface towards the interior of the zeolite occurs. The growth of Ni particles inside the zeolite induces further local breakdown of the lattice.

With bimetal catalysts that were originally washed at pH=6, large alloy particles, slightly enriched with Pd, are identified after CO hydrogenation. They are predominantly located in the interior of the zeolite. They are formed by growth of small alloy particles; this particle growth causes local collapse of the zeolite lattice.

In PdNi(B) large PdNi particles, detected by XPS and XRD, are initially formed at the external surface during reduction. In addition, small particles are likely to be present as indicated by previous TPD results (12). The most startling result of the present work is that after CO hydrogenation these particles largely leave the zeolite surface. As chemical analysis shows no overall metal depletion, the XRD and XPS results suggest that the metals migrate towards the interior of the zeolite. For PdNi(A) formation of large particles in the interior is accompanied by loss of zeolite crystallinity. For PdNi(B) that originally contained much metal in the mantle, metal migration into the interior of the zeolite leads to a rather dramatic decrease of the Pd/Si ratio.

What emerges from this work is a highly dynamic model of the processes in the catalyst during CO hydrogenation. Presence of CO apparently not only

induces metal migration and coalescence between adjacent cages, but it can also lead to a pronounced metal redistribution on a macroscopic level, viz. between outer surface of zeolite microcrystal and its interior. The most likely migrating species are primary Pd carbonyl clusters and $Ni(CO)_4$. These complexes are stabilized in the zeolite framework, especially in the presence of protons. A strong interaction between carbonyl complexes and zeolite framework, particularly with protons, had been observed previously for $Re_2(CO)_{10}$ on NaHY zeolite (13).

It, therefore, appears logical to attribute the differences between our **A** and **B** series samples to different concentrations of protons due to wash at pH=6 or 10.5. Protons act as chemical anchors; they thus inhibit migration of metal carbonyls. Consequently, metal particle growth is pronounced with **B** samples due to the lower concentration of protons; loss of zeolite crystallinity is a secondary consequence of this growth. The high proton concentration in **A** samples provides a large number of nucleation sites onto which carbonyl complexes or metal particles are anchored.

Formation of the thermodynamically most stable alloy is likely to provide an additional driving force for metal redistribution. This effect will be more pronounced for bimetallic systems with exothermic alloys than for the present system.

5. ACKNOWLEDGEMENT

Support by the US Department of Energy, Grant DE-FG02-87ERA3654, is gratefully acknowledged

6. REFERENCES

1 J.S. Feeley, A.Yu. Stakheev, F.A.P. Cavalcanti, and W.M.H. Sachtler, J. Catal., submitted
2 A.Yu. Stakheev, and W.M.H. Sachtler, J. Chem. Soc. Faraday Trans. 87 (1991) 3703
3 Z. Zhang, H. Chen, and W.M.H. Sachtler, J. Chem. Soc. Faraday Trans. 87 (1991) 1413
4 S. Contarini, J. Michalik, M. Narayana, L. Kevan, J. Phys. Chem., 90 (1986) 4586.
5 M. Narayana, J. Michalik, S. Contarini and L. Kevan, J. Phys. Chem., 89 (1985) 3895.
6 J.S. Feeley, and W.M.H. Sachtler, Zeolites 10, 738 (1990)
7 R. Hultgren, C.A. Zapffe, Am. Inst. Mining Met. Engrs., 58 (1939) 1047.
8 Z. Zhang, H. Chen, L.-L. Sheu, and W.M.H. Sachtler, J. Catal. 127 (1991) 213

9 Z. Zhang, and W.M.H. Sachtler, J. Mol. Catal., 67 (1991) 349
10 Z. Zhang, F.A.P. Cavalcanti, and W.M.H. Sachtler, Catal. Lett., in press
11 M. Suzuki, K. Tsutsumi, H. Takahashi, Y. Saito, Zeolites, 8 (1988) 284.
12 J.S. Feeley, W.M.H. Sachtler, J. Catal., 131 (1991) 573
13 C. Dossi, J. Schaefer, W.M.H. Sachtler, J. Molec. Catal., 52 (1989) 193.

DISCUSSION

Q: Wm. C. Conner (USA)

1) Would you comment on the rate of the hydrogen gas on the movement of metal particles under reaction conditions ? Is there not a difference between H_2 gas and the protons present in aqueous media, specifically the formation of metal hydroxides and the mobility of hydrogen atom on the surface ?

2) As you have shown, the gas phase can have a profound influence on the distribution of metals in zeolites. When the gases are then removed by evacuation, can they then also move or relax to another position ? This would question the use of XPS in vacuum to detect position under reactions condition. Would you comment on the approach you used to transfer the sample to the XPS?

A: W. M. H. Sachtler

At high H_2 pressure and low temperature formation of Pd hydrides is significant. Of greater importance for metal migration in zeolites are, however the forward and backward processes of:

$$M + 2H^+ \rightleftharpoons M^{2+} + H_2$$

In particular for zeolite supported bimetal systems PtM and PdM with M = Cu, Ni or Co, we have evidence for selective oxidation of the M atoms by protons; the M(II) ions tend to migrate to smaller zeolite cages, but if appropriate ligands are offered, they can return to supercages. The reverse process, reduction of ions by H_2 and formation of zeolite protons, is favored at high values of P_{H2}.

2) Our XPS apparatus is equipped with a sample isolation chamber where samples are re-reduced at high P_{H2} and temperature. Pd carbide is destroyed during this reduction and CH_4 is formed. After cooling the samples are transported to the UHV chamber without intermediate exposure to uncontrolled atmospheres. XRD data were taken after decomposing the Pd hydrides, so that Pd carbide could be identified by the change in Pd lattice parameter.

Q: E. G. Derouane (Belgium)

We have shown on past work that ferromagnetic resonance (FMR) in an extremely powerful tool to characterize the state of reduction, the size, the morphology, the surface layer compositions and relaxation of small metallic particles of Ni, Cu-Ni, and Ru-Ni layer compositions and relaxation of small metallic particles of Ni, Cu-Ni, and Ru-Ni dispersed in zeolites. Now that you demonstrated that it is possible to induce and control the migration of (ferromagnetic-containing) species in zeolite Y, which may alter several or all of the above parameters for the ferromagnetic component (Ni or Co), FMR is obviously a method of choice for the investigation of the dynamic character of such catalysts. Can you comment on your intentions in this respect?

A: W. M. H. Sachtler

We have recently published our results on the characterization of Co particles in zeolite NaY using ferromagnetic nuclear resonance. This novel technique is demonstrated to be powerful for determining the size and morphology of superparamagnetic metal particles [1,2]. For example, Co particles of 6_ in the supercages of zeolite Y were identified by the sharp transition from superparamagnetism to ferromagnetism between 4.2 K and 1.3 K, indicating an extremely narrow particle size distribution. Characterization of zeolite

supported PdCo catalysts by the same technique is in progress. In addition, ferromagnetic resonance and magnetic susceptibility measurements are being done for these samples.

[1] Z. Zhang, Y. D. Zhang, W. A. Hines, J. I. Budnick and W. M. H. Sachtler, *J. Am. Chem. Soc.*, **114**, 4843 (1992)

[2] Z. Zhang, S. L. Suib, Y. D. Zhang, W. A. Hines, J. I. Budnick, *J. Am. Chem. Soc.*, **110**, 5569 (1988)

Q: M. Ichikawa (Japan)

1) I would like to touch on the local distribution of alloy particles in may for your systems. A broad distribution of the metal particles having the different composition could be expected for Pd + Ni, Pd + Co being controlled by metal migration, reduction with H_2 and proton-exchange. The specific question is what is the major driving force to form an alloy particle having the inform distribution of metal composition in your catalyst system ?

2) Do you have any positive evidence (EXAFS, XPS or any other spectroscopic technique) to indicate the location of earlier transition metal such as Ni and Co in the bimetallic particles of Pd inside NaY ? Are they residing in the lattice sites anchored by Pd particles or on surface layer of Pd particle, which would be reflected in the selectivity of CO hydrogenation ?

A: W. M. H. Sachtler

1) In general, the driving force for the formation of alloy particles at given overall composition is given by the shape of the $\Delta G = f(x)$ graph, where ΔG is the Gibbs Free Energy of forming an alloy from the elements, x is the composition. If this curve has only one minimum and no inflection points, a continuous series of solid solutions is stable; the individual particles will have compositions near the overall composition. If, however, the $\Delta G = f(x)$ graph has two minima, separated by a local maximum, a miscibility gap exists. For overall compositions in this range, two alloy phases coexist, i.e. the individual particles will have compositions near one of the two minima of ΔG.

2) Our FTIR data of CO adsorbed on PtCu/NaY show that the PtCu particles expose a surface richer in Cu than the particle interior. For PdCu/NaHY our TPR/TPD data suggest that partial oxidation of Cu by protons to Cu(I) is possible with these ions still in contact with the Pd particles. Likewise, oxidation of Ni in PdNi/NaHY by protons appears to produce Ni(II) ions, some of which remaining in contact with Pd particles. It is possible that such ions serve as chemical anchors. In previous work we had identified chemical anchoring of Pt particles by Fe(II) and Cr(III) or Cr(II) ions in zeolite Y.

Q: H. G. Karge (Germany)

Upon H_2-reduction of Ni(II) and Pd(II) supported by NaY OH groups are formed which are attached to the framework of the zeolite. Do the protons of those newly formed Brönsted acid sites affect the properties of the reduced material, for instance its catalytic performance ? Is it possible to eliminate these protons, e.g. by subsequent solid-state reaction with alkaline halides ? If the answer is "yes", how does that change the properties of the catalysts ?

A: W. M. H. Sachtler

The answer is: yes. Zeolite protons form stable adducts with palladium clusters; the catalytic performance of these adducts differs significantly from that of proton-free Pd clusters. protons also act as chemical anchors; i.e. help to maintain a high metal dispersion.

Protons can be removed by secondary ion exchange with alkali ions, by reaction with sodium azide or by adsorption of NH_3 or of hydrocarbon molecules with high propensity of form carbenium ions. Such processes cause remarkable changes of the catalytic activity, moreover agglomeration of the metal clusters to larger aggregates is observed.

Q: A. O. I. Krause (Finland)

You showed two cobalt catalysts with very different selectivities. Are these differences in conversion or reaction rates or were the selectivities compound on the same level of conversion?

A: W. M. H. Sachtler

The selectivities of the PdCo/NaY catalysts, reported during the oral presentation, were obtained at the same conversion level (< 1 %). The catalyst which is exposed to H_2O vapor after calcination, but before reduction, produces mainly hydrocarbons; its activity is roughly 60 % of that of the catalyst which had not been exposed to H_2O vapor and is highly selective to oxygenates. The former catalyst contains mainly PdCo alloy particles of intermediate size; the latter catalyst has highly dispersed Pd particles which are apparently anchored to the zeolite by Co^{2+} ions.

Guczi, L. *et al.* (Editors), *New Frontiers in Catalysis*
Proceedings of the 10th International Congress on Catalysis, 19-24 July, 1992, Budapest, Hungary
© 1993 Elsevier Science Publishers B.V. All rights reserved

PROMOTION OF H-ZSM-5 BY ALUMINA

J. Völter, H. D. Lanh, B. Parlitz, E. Schreier and K. Ulbricht

Center for Heterogeneous Catalysis, Rudower Chaussee 5, D-O 1199 Berlin, Germany

Abstract

H-ZSM-5 • Al_2O_3 catalysts were prepared by mixing and calcining H-ZSM-5 and AlO(OH). Catalytic, TPD and IR studies indicate the following influences of Al_2O_3 on the zeolite. The activities in the conversion of n-hexane and mesitylene are enhanced, the selectivity for the isomerization of mesitylene is increased, the Brönsted acidity is decreased, the Lewis acidity is increased. The increased conversion could be due to a cooperation of B and L sites. The amount of produced coke was determined and studied by EPR spectroscopy. The EPR spin density increases nearly proportional with the amount of coke formed from n-hexane but not with coke from mesitylene. The EPR linewidth decreases with increasing amount of coke, indicating a transition from olefinic to aromatic coke. This transition occurs extremely rapidly when mesitylene is converted on pure H-ZSM-5. It is suggested that this formation of aromatic coke controls the selectivity for the isomerization of mesitylene.

1. INTRODUCTION

The pentasile type zeolite H-ZSM-5 is a well known catalyst for conversions of hydrocarbons and alcohols. Its activity and selectivity can considerably be improved by the addition of oxides as ZnO or Ga_2O_3 [1]. Little is known about the catalytic effect of added Al_2O_3, although Al_2O_3 is often used as a binder in the production of technical H-ZSM-5 catalysts. Only Bragin et al. reported that the activity in the aromatization of ethene can be enhanced by the addition of Al_2O_3 [2] and that there is a distinct influence on the coke production [3]. The oligomerization of propene can be enhanced by the admixing of Al_2O_3, too [4].

In the present paper the influence of added Al_2O_3 on the conversion of a paraffin and an aromatic was studied. In detail n-hexane was selected for a cracking reaction, which proceeds within the channels and mesitylene for an isomerization which proceeds outside the channels due to the bigger diameter of this molecule. Besides catalytic properties the formed coke was studied in dependence on added Al_2O_3 in H-ZSM-5·Al_2O_3 mixtures, using EPR technique.

2. EXPERIMENTAL

The H-ZSM-5·Al_2O_3 catalysts were prepared according to a known technical procedure for the preparation of spheres by dropping the mixtures of peptisized AlO(OH) with H-ZSM-5 (Si/Al=16) into an aqueous solution of NH_3, drying the formed spheres (3-6 mm) and calcining them for 3 h at 500°C. The catalytic tests were performed in a conventional flow reactor in a stream of nitrogen of 9 l h^{-1} containing mesitylene or n-hexane at partial pressures of 6 and 100 torr, respectively, and with amounts of catalysts of 1.0 and 0.1g, respectively. The products were analyzed by on-line gas-chromatography. At the end of the catalytic test the samples were cooled in the stream of N_2 to room temperature within 1 h and maintained in N_2 for further 2 h. The coke content of the samples was determined by combustion in oxygen. The IR spectra were recorded with selfsupported discs (~7 mg cm^{-2}), fixed in an IR cell, preheated in vacuum at 400°C for 2 h and then cooled to -196°C before and after adsorption of CO at this temperature. The TPD profiles were recorded in streaming He (3.6 l h^{-1}) with a heating rate of 10° min^{-1} after pretreating the samples 1 h at 500°C in He and adsorption of NH_3 until saturation at 120°C.
EPR experiments were made at -196°C and 20°C with a ZWG ESR 220 spectrometer operating at x-band wavelength. Diphenylpicrylhydracyl (g=2.0036) and NMR marks were used for calibration and calculation of g values.

3. RESULTS AND DISCUSSION

3.1. Catalysis

The conversion of n-hexane at 500°C was used to study the influence of added Al_2O_3 on the activity of H-ZSM-5. The samples were prepared by mixing H-ZSM-5 with peptisized AlO(OH) and subsequent calcination at 500°C. Physical mixtures were

prepared by mixing H-ZSM-5 with γ-Al_2O_3 or with SiO_2, respectively, and a subsequent calcination at 500°C. The physical mixtures with γ-Al_2O_3 were used only in the catalytic experiments with n-hexane. In the further experiments only alumina was used which was prepared by calcination of AlO(OH) and the expression Al_2O_3 is used for the description of an oxide which was prepared in this way. The catalytic results after 4 h on stream are shown in Figure 1. The physical mixtures of H-ZSM-5 and γ-Al_2O_3 display activities which are very close to the additive activities of the components, represented by the dotted straight line. The data indicate that physically admixed γ-Al_2O_3 exerts nearly no promoting effect. The same is true for physically admixed SiO_2, the conversions are even lower than those obtained with -Al_2O_3. Remarkably Al_2O_3 originally added as AlO(OH) displays a decisive promoting effect. Dilution of the active H-ZSM-5 with 30% of the inactive Al_2O_3 has nearly no negative effect on the conversion. The mixture with 50% Al_2O_3 displays a conversion of 39% instead of 27% calculated for additive activities.

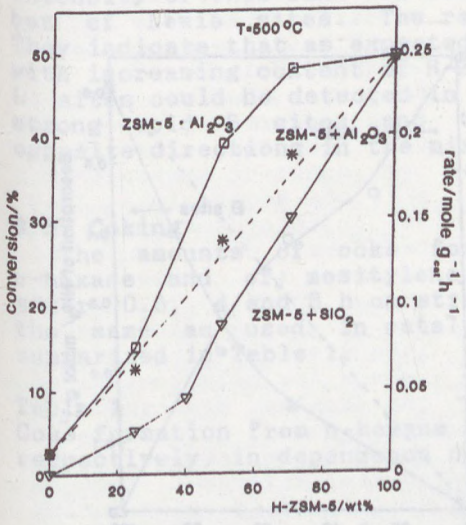

Figure 1. Conversion of n-hexane vs. H-ZSM-5 content of mixtures.

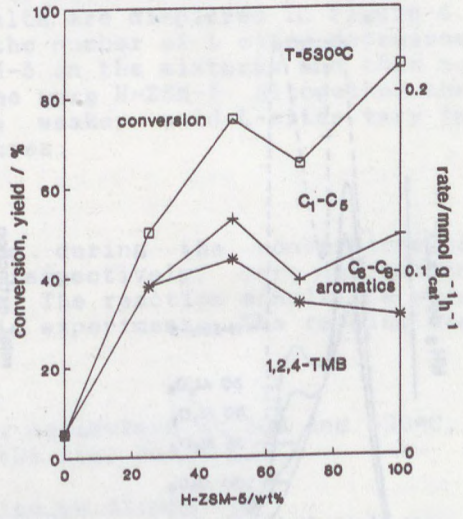

Figure 2. Conversion of mesitylene and yields of products vs. H-ZSM-5 in H-ZSM-5·Al_2O_3 mixtures.

The influence of added Al_2O_3 on the selectivities is less pronounced. The selectivity of Al_2O_3 is characterized by high portions of C_1 and C_2 products. With increasing content of H-ZSM-5 these selectivities decrease whereas those for propane and aromatics increase.

The efficiency of added Al_2O_3 was also studied in the conversion of 1,3,5 trimethylbenzene (TMB, mesitylene) performed during 4 h at 530° C. The catalytic results, in dependence on the content of H-ZSM-5 in the mixture with Al_2O_3 are shown in Figure 2. Here, too, a promoting effect of added Al_2O_3 on the conversion is to be seen. More significant is the shift of selectivities. Pure H-ZSM-5 transforms 65% of the 1,3,5 TMB into C_1-C_5 crack products and demethylated aromatics and only 35% is isomerized to 1,2,4 TMB. However the introduction of Al_2O_3 increases the selectivity for the isomerization up to 72% at the expense of cracking. The selectivity is shifted from predominant cracking to predominant isomerization and the total amount of isomerized 1,3,5 TMB is even higher on the sample containing 75% Al_2O_3 than on pure H-ZSM-5.

3.2. Acidity

The temperature-programmed desorption of adsorbed ammonia was used to determine the acidity of the H-ZSM-5·Al_2O_3 mixtures. The corresponding TPR profiles are presented in Figure 3.

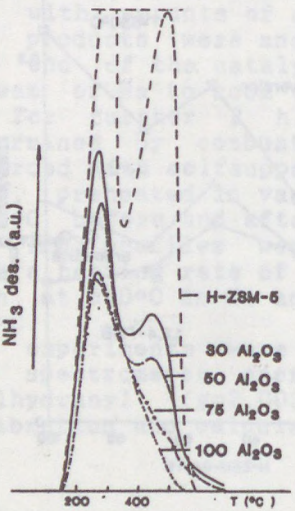

Figure 3. TPD profiles of ammonia from H-ZSM-5 and mixtures with Al_2O_3.

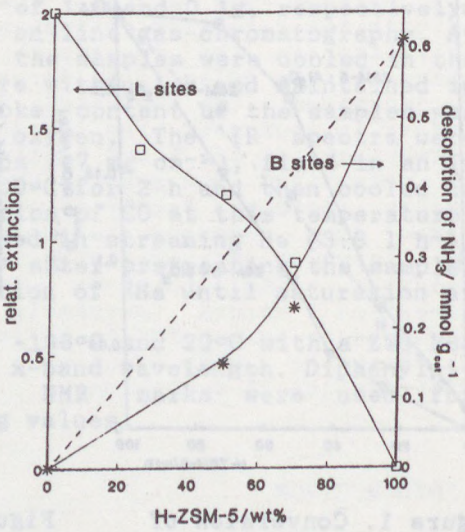

Figure 4. Lewis sites (L) and Brönsted sites (B) vs. H-ZSM-5 in H-ZSM-5·Al_2O_3 mixtures.

The known two-peak profile was obtained from the pure H-ZSM-5. The strong adsorption sites, assigned to the Brönsted sites, are represented by the high temperature peak [5]. This peak is

diminished very sharply by the admixing of only 25% Al_2O_3 and this peak is absent in the sample with 75% Al_2O_3. The area of the high temperature peak was used to calculate the amount of desorbed ammonia thus indicating the number of Brönsted sites. The data are shown in Figure 4 as function of the composition of the mixtures. The curve representing the acidity of the mixtures is well below the straight line representing acidities of mixtures with no interaction of the components. This indicates that a certain portion of the Brönsted sites of the H-ZSM-5 is neutralized by the added alumina.
The reason probably is to be seen in the method of preparation. Basic AlO(OH) peptisized by HNO_3 is mixed with acidic H-ZSM-5 and is subsequently calcinated. It is suggested that during these procedures protons of the zeolite are partially exchanged or neutralized by cationic Al species originating from the AlO(OH).
The relative number of the Lewis sites was determined by IR spectroscopy of adsorbed CO. CO forms a surface complex with threefold coordinated aluminum in Al_2O_3. The formation of this complex can be observed by an IR band at 2192 cm^{-2} [6]. The intensity of this band was used to determine the relative number of Lewis sites. The results are displayed in Figure 4. They indicate that as expected the number of L sites decreases with increasing content of H-ZSM-5 in the mixtures and that no L sites could be detected in the pure H-ZSM-5. Altogether the strong acid B sites and the weaker acid L-sites vary in opposite directions in the mixtures.

3.3. Coking

The amounts of coke formed during the conversions of n-hexane and of mesitylene, respectively, were determined after 0.5, 4 and 8 h on stream. The reaction conditions were the same as used in catalytic experiments. The results are summarized in Table 1.

Table 1
Coke formation from n-hexane and mesitylene at 500 and 530°C, respectively, in dependence on the time on stream

	time on stream (h)					
	0.5	4	8	0.5	4	8
	coke (mg/g_{cat})					
catalyst (wt%)	from n-hexane			from mesitylene		
100 Al_2O_3	0.4	1.5	1.4	-	2.5	4.4
75 Al_2O_3, 25 ZSM-5	1.7	3.8	7.6	1.4	4.4	8.6
50 Al_2O_3, 50 ZSM-5	3.5	10.4	25.0	-	4.4	6.9
30 Al_2O_3, 70 ZSM-5	4.5	13.0	27.5	-	4.3	6.0
100 ZSM-5	7.5	24.8	41.2	1.7	3.9	4.6

The observed coking rates for n-hexane, 5-15 x 10^{-3} $g/g_{zeolite}$, are slightly higher than the rate of 1x10^{-3} $g/g_{zeolite}$, reported by Gielen and Palekar [7]. The data, which are directly obtained after the catalytic experiments, shown in Figure 1 and 2, are displayed separately in Figure 5. The coke, produced from n-hexane within 4 h, increases nearly linearly with increasing content of H-ZSM-5 in the mixture. However the amount of coke from mesitylene is nearly constant for all the mixtures and for H-ZSM-5 and the difference between Al_2O_3 and H-ZSM-5 is relatively small. This means the coke production from n-hexane is very different on Al_2O_3 and on H-ZSM-5 while the coking of mesitylene reveals only small differences between the two catalysts.

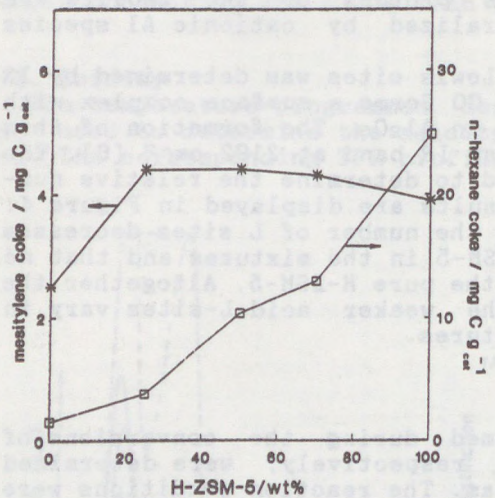

Figure 5. Coke from n-hexane and mesitylene in the dependence on H-ZSM-5 in H-ZSM-5·Al_2O_3.

The low values of mesitylene coke in comparison to those of n-hexane coke are mainly due to the space velocity lower by a factor of 10^{-3} in the experiments with mesitylene.

Further studies of the coke were made using the EPR technique. The observed spectrum consisted of only one single line. This is in accordance with literature data for coke formed at temperatures above 300°C [8,9]. Figure 6 displays the spin intensities of this signal versus the coke content of the samples, described in Table 1.

Each of the samples containing different amounts of zeolite,is coked during 2 or 3 different times on stream. In the case of coked n-hexane the spin concentrations of all the samples can be approximated by a nearly straight line in dependence on the amount of coke. This indicates that at least in this case the radical density is proportional to the coke content. Similar relationships are known for ethene coking [8] and for methanol coking [9]. The spin density, calculated from the slope of the curve, is about 3 x 10^{-4} N/C_{atom}. Literature data are ranging from 10^{-4} to 10^{-3} N/C_{atom} [8,9].

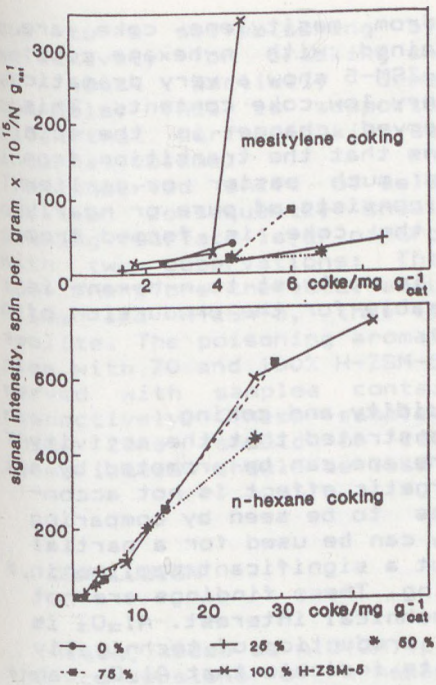

Figure 6. EPR spin density vs. amount of coke on various mixtures of H-ZSM-5·Al_2O_3.

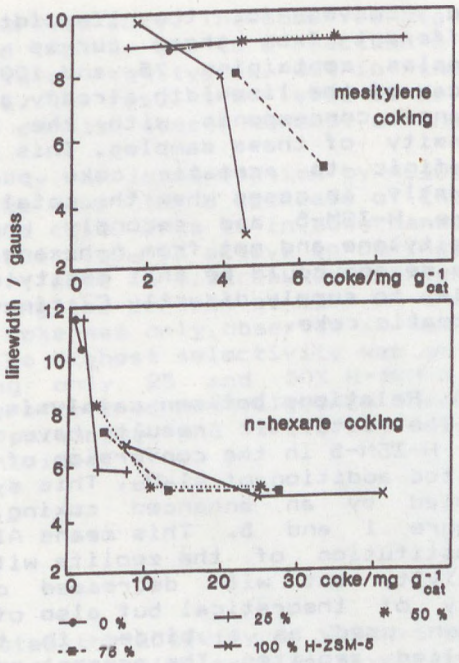

Figure 7. EPR linewidth vs. amount of coke on varios mixtures of H-ZSM-5·Al_2O_3.

However this relation is more complicated with coke from mesitylene. The coke on samples containing up to 50% H-ZSM-5 display an expected linear relationship with the spin intensity. But the samples with 70 and 100% H-ZSM-5 exhibit already at very low coke contents a much higher radical density of about 6×10^{-3} N/C_{atom}. This is a direct hint that coke from mesitylene on H-ZSM-5 has different chemical properties.
Moreover in Figure 7 the linewidth of the EPR signals is plotted in dependence on the coke content. The linewidth has been proposed to indicate the H/C ratio of the coke [10]. Therefore a decreasing linewidth should indicate a transition of olefinic to aromatic coke. Using this explanation, the data shown in Figure 7 reveal the following. In the case of coke from n-hexane the data from all samples can be approximated in dependence on the coke content by one decreasing curve. This means the initial, the small amounts of coke are olefinic, the final, the large amounts are aromatic. This is in accordance with the proposed general mode of coking proceeding via the steps paraffins, olefins, oligomers to mono- and polyaromatics [11].

The curves for the linewidth from mesitylene coke are different from those curves obtained with n-hexane coke. Samples containing 75 and 100% H-ZSM-5 show a very dramatic decay of the linewidth already at very low coke contents. This change corresponds with the observed change in the spin density of these samples. This means that the transition from olefinic to aromatic coke occurs much easier or earlier firstly in cases when the catalyst consists of pure or nearly pure H-ZSM-5 and secondly when the coke is formed from mesitylene and not from n-hexane.
The reason could be that mesitylene in contrast to n-hexane is able to supply directly C_6 rings usable for the production of aromatic coke.

3.4. Relations between catalysis, acidity and coking

The catalytic results have demonstrated that the activity of H-ZSM-5 in the conversion of n-hexane can be promoted by a suited addition of Al_2O_3. This synergetic effect is not accompanied by an enhanced coking, as to be seen by comparing Figure 1 and 5. This means Al_2O_3 can be used for a partial substitution of the zeolite without a significant decline in activity but with decreased coking. These findings are not only of theoretical but also of technical interest. Al_2O_3 is often used as a binder in the production of technically applied zeolites. The present results indicate that Al_2O_3 can be used in a double function as a promotor and as a binder. The reason of the promotion could be the varied acidity. The observed decline of Brönsted sites by Al_2O_3 would not explain an increased activity. But Al_2O_3 introduces Lewis sites into the mixture. A cracking of n-hexane according to dual function mechanism including Brönsted as well as Lewis sites would explain the present results. There are hints in the literature that Lewis sites can play an active role in the abstraction and adsorption of hydrogen [12].
The promotion of the mesitylene conversion by Al_2O_3 should have the same reason as in the case of n-hexane. The dramatic shift of the selectivity towards an isomerization is suggested to be a consequence of the size of the molecule and its specific coking behaviour. The diameter of the mesitylene molecule is larger than the pore width of the H-ZSM-5. Hence the isomerization should be restricted to the outer surface. In previous experiments it could be shown that coke from mesitylene is deposited on the outer surface of the crystals whereas coke from n-hexane fills the pores [13].
The present results indicate that mesitylene easily forms aromatic coke. Behrsing et al. [14] observed that sheets of aromatic coke are poisoning whereas even thick layers of amorphous coke are not. Altogether these results provide direct hints that mesitylene forms poisoning aromatic coke on the outher surface. This supports the conclusion that the observed low selectivity for isomerization on pure H-ZSM-5 is

due to a selfpoisoning by surface coke. The observed high selectivity for cracking should then be due to a reaction of at least partially demethylated mesitylene within the channels. This is supported by the results of Tsiao et al. [15] that surface coking still permits access to most of the internal volume.
The observed shift of selectivty for isomerization by Al_2O_3 addition consequently should be due to a decrease of the poising surface layer of aromatic coke. This is in accordance with two observations: The added Al_2O_3 is active in coking, too. Therefore the total amount of coke is distributed between Al_2O_3 and H-ZSM-5, thus lowering the portion of coke on the zeolite. The poisoning aromatic coke was only observed in samples with 70 and 100% H-ZSM-5. The highest selectivity was observed with samples containing only 25 and 50% H-ZSM-5, respectively. These samples were covered with olefinic coke. This coke should be less poisoning and therefore the isomerization should be less inhibited.

4. CONCLUSION

Al_2O_3, added as AlO(OH) promotes the activity of H-ZSM-5 in the conversions of n-hexane and of mesitylene. Moreover the selectivity in the conversion of mesitylene is strongly shifted towards isomerization at the expense of cracking. In addition the Brönsted acidity is decreased, the Lewis acidity is increased. A cooperation of B and L sites is suggested to be responsible for the observed enhanced conversion. The amount of coke, produced from n-hexane increases with the portion of H-ZSM-5 in the mixtures. The observed EPR spin density of the coke increases nearly proportionally with the amount of coke. In the same sequence the linewidth of the EPR signal decreases, indicating a transition from olefinic to aromatic coke. The formation of aromatic coke from mesitylene occurs much easier on pure H-ZSM-5 than on the mixed catalysts. It is suggested that a surface layer of aromatic coke inhibits the isomerization of mesitylene and that added Al_2O_3 diminishes this layer, thus enhancing the selectivity for isomerization. Altogether the results demonstrate that Al_2O_3, well known as a binder, can be effectively used as a promotor of H-ZSM-5 catalysts, too.

5. REFERENCES

1 D. Seddon, Catal. Today, 6(1990) 351.

2 O.W. Bragin, W.I. Jakerson, T.B. Vasina, S.H. Isajew, L.I. Lafer, W.D. Nissenbaum, Izv. Acad. Nauk, SSSR, Ser. Khim., 1989, 254.

3 W.I. Jakerson, W.D. Nissenbaum, T.B. Vasina, L.I. Lafer, S.A. Isajew, E.E. Denisowa, J.L. Duch, O.W. Bragin, ibid. 1990, 1244.

4 P.B. Weisz, Ind. Eng. Chem. Fundam., 25 (1986) 53.

5 U. Kürschner, B. Parlitz, E. Schreier, G. Öhlmann, J. Völter, Appl. Catal., 30 (1987) 159.

6 L.M. Kustov, V.B. Kazansky, S. Beran, L. Kubelkova, P. Jiru, J. Phys. Chem., 91 (1987) 5247.

7 B. Gielen, M.G. Palekar, Zeolites, 9 (1989) 208.

8 H.G. Karge, J.-P. Lange, A. Gutsze, M. Laniecki, J. Catal., 114 (1988) 144.

9 R.H. Meinhold, D.M. Bibby, Zeolites, 10 (1990) 121.

10 H.L. Retcofsky, G.P. Thompson, R. Raymound, R.A. Friedel, Fuel, 54 (1975) 126.

11 M. Guisnet, P. Magnoux, Appl. Catal., 54 (1989) 1.

12 L.M. Kustov, V.B. Kazansky, J. chem. Soc. Faraday Trans., 87 (1991) 2675.

13 J. Kärger, H. Pfeifer, J. Caro, H. Bülow, H. Schlodder, R. Mostowicz, J. Völter, Appl. Catal., 29 (1987) 21.

14 T.H. Berhsing, H. Jaeger, J.V. Sanders, Appl. Catal. 54 (1989) 289.

15 C. Tsiao, C. Dybowski, A.M. Gaffney, J.A. Sofranko, J. Catal., 128 (1991) 520.

DISCUSSION

Q: J. J. Fripiat (USA)
Have you tried other aluminas than boehmite?

A: J. Völter
Yes, we have also tried mixtures with γ-Al_2O_3. The same thermal treatment at 500 ^0C was used with these mixtures. But no catalytic effect was observed, as to be seen in Figure 1.

Q: J. Datka (Poland)
How do you explain the effect of SiO_2 addition the HZSM-5? Is it the modification of activity or pore blocking ?

A: J. Völter
Up to now we have not characterized the mixtures with SiO_2. We assume a transport inhibition by diffusion through the pores of the SiO_2, which envelopes the zeolite crystals.

Q: T. S. R. Prasada Rao (India)
Will addition of Al_2O_3 to HZSM-5 change the shape selective properties of HZSM-5 ?

A: J. Völter
A shape selectivity in the isomerization of mesitylene could not be observed because the equilibrium concentration of 1.2.3-trimethylbenzene is extremely low. However in the

isomerization of m-xylene an enrichment of p-xylene has been found in additional experiments. This indicates para-selectivity due to added alumina.

Q: D. Kalló (Hungary)

1) What was the crystal size of ZSM-5 ?

2) What was the temperature of contacting or embedding ZSM-5 into alumina; was there an intimate contact between these two constituents ?

3) Did you observe any steric hindrance within the reactive pores during reaction of pseudocumene ?

A: J. Völter

The crystal size was about 5-7 μ. HZSM-5 powder was mixed at room temperature with peptsized pseudo boehmite. Formed spheres were calcined at 500 ^{0}C. No steric hindrance was observed. The equilibrium concentration of 1.2.3-trimethylbenzene is extremely low.

Q: V. Haensel (USA)

The term promotion of HZSM-5 by dilution with alumina requires clarification. The retardation of the formation of aromatic coke is more indicative of a dilution of the very active HZSM-5 rather than a promotion. The best way of comparing catalyst activities is at equal and preferably low conversions (by design different contact times). Under such conditions the ratio of olefinic coke and aromatic coke from mesitylene can be compared.

A: J. Völter

We agree that the term promotion of HZSM-5 by alumina requires further clarifying experiments. Nevertheless, in the case of coking of mesitylene there are several distinct hints on an exceptional behavior:

(i) coking of mesitylene on Al_2O_3 is only slightly slower than coking on HZSM-5 whereas coking of n-hexane occurs much more rapidly on HZSM-5 than on Al_2O_3 (see Figure 5);

(ii) previous experiments (ref. 13 in the paper) indicated that coke from mesitylene mainly is deposited on the outer surface of the HZSM-5 crystals whereas coke from n-hexane is deposited within the channels;

(iii) the concentration of free radicals, the spin density/g of coke is represented by the slope of the curves in Figure 6. In the case of n-hexane coking this density is independent of the composition of the mixtures and of the coke content. However in the case of coke from mesitylene the spin density is low with samples containing 50 or more % Al_2O_3 but is considerably higher with samples containing 70 or 100% ZSM-5. We conclude that this difference in the density of free radicals indicates that the binding state of the C atoms in the coke differs between ZSM-5 rich samples and Al_2O_3 rich samples;

(iv) a shift in the binding state in the coke can directly be deduced from the linewidth of the EPR signal (ref. 10 in our paper). As to be seen in Figure 7, the coke from n-hexane displays the expected smooth transition from olefinic to aromatic coke with increasing coke content. However coke from mesitylene displays an exception. Comparing the same small coke contents, the coke on the Al_2O_3 rich samples exhibits a broad signal samples the linewidth is distinctly narrower. This indicates a rapid transition to aromatic coke on the zeolite sample, only.

To sum up all these findings are consistent with the following model. Coking of n-hexane starts in the channels of HZSM-5 with olefinic coke which is then transformed to aromatic coke. Coke from mesitylene also displays a relatively slow transition from olefinic to aromatic coke on Al_2O_3 rich samples. However on HZSM-5 coke is formed on the outer surface and this enables the very rapid transformation to spacious aromatic coke.

Q: S. Csicsery (USA)

1) Were conversions shown for unit HZSM-5 ?

2) Selectivities in your study were measured at different conversion levels. In consecutive reactions the product mixture could contain a larger absolute amount of the primary product at low conversion than at higher conversion levels. Is it possible that the selectivity effects shown for mesithylene are really effects of the conversion level ?

A: J. Völter

The conversions were shown per weight unit of the mixtures. The dependence of the selectivity for isomerization on the conversion was checked in additional experiments. Different conversion levels were obtained by applying different amounts of catalysts. Typical results are shown in Table 1:

Table 1. Conversion of mesitylene on HZSM-5 and on a HZSM + Al_2O_3 mixture

Amount of catalyst	%	Content of HZSM-5	
		50%	100%
1.0 g	Conversion	76.0	87.0
	Selectivity	58.0	35.0
0.5 g	Conversion	45.9	72.5
	Selectivity	73.2	38.2

The sample containing 50% Al_2O_3 displays a selectivity for isomerization of 58% at a conversion of 76%. The selectivity of the pure HZSM-5 at an even lower conversion of 72.5% was only 38.2%. This indicates that the added Al_2O_3 causes a strong increase of selectivity whereas the lowered conversion has a comparatively small effect.

Q: R. van Nordstrand (USA)

1) Was your boehmite really crystalline boehmite or pseudo boehmite ?
2) Was any acid used with the boehmite for peptization ?
3) What was the source of the boehmite ?

A: J. Völter

We used amorphous pseudo boehmite. It was peptisized with diluted HNO_3. The source of the boehmite was a technical product from the Leuna-Werke AG, Leuna, Germany.

Q: J. Fraissard (France)

During the solid-state reaction there is a migrations of Al_2O_3 into the pores; which causes the formation of Lewis acid sites which are analogous to the non-framework species due to dealuminations.

Since you detect a synergy effect, Brönsted and Lewis acid site should be adjacent. What is the influence of then non-framework species in comparisons with the alumina around the zeolite crystallites?

A: J. Völter

^{27}Al-NMR spectra indicated that the content of framework Al remained unchanged. Up to now we have made no detailed studies concerning the non-framework Al species. An effect of the alumina around the zeolite crystals is to be seen in the coking behavior (Figures 5). Mesitylene is coked on pure HZSM-5 as well as on pure Al_2O_3. n-Hexane is coked almost exclusively on HZSM-5, not on Al_2O_3.

Q: T. Inui (Japan)

It is thought that through mixing or some solid acidity is produced by tight mechanochemical contact. Therefore, a more effective promotion would be expected when

you use an alumina source which has a larger surface area, such as hydrogels of aluminium hydroxide, or more complete mixing of ZSM-5 with some alumina. What do you think about these points of view ?

A: J. Völter
Many thanks for your kind suggestions. We completely agree and will include your proposals in our further program.

Q: W. O. Haag (USA)
Your data on NH_3 TPD show a strong reduction of the Brönsted acid peak occurring at 450-500 ^0C upon addition of alumina. I am surprised that you do not see a new peak at 550-600 ^0C resulting from ammonia desorption from the added alumina. Can you tell us how the samples were prepared and pretreated with NH_3 prior to the TPD experiment ?

A: J. Völter
Dr. H. Berndt from our Center for Heterogeneous Catalysis has reinvestigated the desorption of NH_3 using a method of stepped thermal desorption. He could identify a small high temperature peak from alumina between 360 and 500 ^0C, which is the same region where the high temperature peaks from HZSM-5 and from the mixtures were observed. Therefore the added boehmite should increase the acidity, but the opposite was observed. This is a further support for our conclusion that boehmite interacts with HZSM-5 and decreases the acidity of the mixtures. The relatively low temperature of the high temperature peak could be due to specific experimental arrangements. The conditions of preparation and pretreatment were the same as described.

Q: H. G. Karge (Germany)
Did you observe a hyperfine splitting of the ESR signal in the case of formation of "non-aromatic (olefinic) coke" which would distinguish it from so-called aromatic coke? I think the density of spins gives information about the number of radicals associated with coke species but does not provide any knowledge about their chemical nature. Did you complement your investigations of the nature of the coke by, e.g., ^{13}C MAS NMR, H/C measurements, chemical analysis?

A: J. Völter
We have only studied the coking at 530 ^0C and this "high temperature coke" gives only a single line spectrum which is in accordance with your findings (ref. 8 in our paper). We agree that the spin density gives no information about the chemical nature of the coke. We only conclude that a distinct shift in the spin density is indicative of a shift in the chemical nature. A more detailed discussion is given in on answer to professor Haensel. Up to now we have no further results concerning the nature of the coke.

Guczi, L. *et al.* (Editors), *New Frontiers in Catalysis*
Proceedings of the 10th International Congress on Catalysis, 19-24 July, 1992, Budapest, Hungary
© 1993 Elsevier Science Publishers B.V. All rights reserved

THE EFFECT OF PREPARATION METHOD ON METAL-SUPPORT INTERACTION IN Pd/L-ZEOLITE CATALYSTS

G. Larsen and G. L. Haller

Department of Chemical Engineering, Yale University, New Haven, CT 06520, USA

Abstract

The method of preparation, ion exchange (IE) versus impregnation (IP), effects the final dispersion, acidity and sintering stability of L-zeolite supported catalysts. The origin of the dispersion effect appears to be in the shape and size of the PdO precursor formed upon calcination which is more elongated with respect to the zeolite channel and has a lower nearest neighbor oxide coordination number when IP is used. While acidity introduced into the L-zeolite before preparation does not appear to effect the initial dispersion, acidity introduced after reduction of the IE preparation stabilizes the Pd particles toward sintering in H_2.

1. INTRODUCTION

The discovery that Pt/L-zeolite is a non-acidic reforming catalyst that has high selectivity for the conversion of n-hexane to benzene has stimulated much interest in this catalyst [1]. There is evidence of both geometric (channelling of reactant) [2] and electronic effects [3] on reactions in Pt/L-zeolite. The latter is most evident in the relative adsorption equilibrium constants extracted from competitive hydrogenation of benzene and toluene, a sensitive chemical probe of the electronic structure of the metal [4]. These results suggest that L-zeolite acts as a base toward Pt particles. The degree of interaction also appears to be a function of the preparation method such that impregnation to incipient wetness results in a higher dispersion than ion exchange [5].

The density of states at the Fermi level is about four times greater for Pd than for Pt [6] and correlates with the adsorption equilibrium constants extracted from competitive hydrogenation of benzene and toluene [4]. This suggested that Pd will interact less strongly with L-zeolite channel walls than does Pt but might be stabilized by acid sites. The objective of this study was both to confirm this hypothesis and to investigate the effect of preparation method on the dispersion/interaction to ascertain whether the higher dispersion of the impregnation preparation is a property of the L-zeolite more-or-less independent of the metal.

2. EXPERIMENTAL

2.1. CATALYST PREPARATION

The catalysts were prepared by impregnation to incipient wetness (IP) or ion exchange (IE) using $Pd(NH_3)_4(NO_3)_2$ precursor and KL-zeolite (Tosoh Corp.) to produce approximately 1 wt % Pd. Under an O_2 flow of 36 l/h/g cat, the temperature was ramped from ambient to 623K in 5 h and held this temperature another hour. The temperature was ramped down to 493K in 0.5 h while purging with He. The catalysts were then reduced at 493K for 1 h under pure H_2. A Pd/SiO_2 catalyst was produced by ion exchange using Davison 923 silica following the method of Baltanas et al. [7] except for the Pd precursor, which in our case was once again $Pd(NH_3)_4(NO_3)_2$. This reference catalyst was calcined and reduced exactly in the same fashion as the Pd/L preparations. In an attempt to remove acidity introduced by the reduction of the Pd/KL ion exchange preparation [5], the product was back exchanged by K^+ (or Mg^{2+}, Ca^{2+} or Ba^{2+}). For the impregnation preparation, catalysts were also back exchanged with Mg^{2+}, Ca^{2+} or Ba^{2+} following reduction.

2.2. TITRATION OF ADSORBED H_2 BY O_2

The relative stability of the resulting catalyst dispersion was determined by sintering in one atm of H_2 at different temperatures and measurement of the change in dispersion by O_2 titration of adsorbed H_2. This experiment is carried out in a conventional Pyrex vacuum system. After reduction the glass cell is sealed off and subsequently outgassed at room temperature for 10 min in order to remove the beta-hydride phase [8]. A 3:4 O_2:Pd_s global stoichiometry is derived by assuming that all hydrogen is titrated to H_2O and that the a final Pd_s:O stoichiometry is one. The most significant advantage of this method over the hydrogen chemisorption technique is that it does not require the use of fairly high temperatures necessary for the desorption of surface hydrogen that results after the reduction step. We found this particularly advantageous since our Pd/L catalysts exhibited low sintering resistance.

2.3. EXAFS MEASUREMENTS

The EXAFS coordination number of Pd was determined in a manner similar to that described for Pt [9]. Details of the EXAFS analysis package may also be found in Ref. [10]. The calcined and reduced precursors were characterized by in-situ EXAFS studies performed at the C2 station of the Cornell High Energy Synchrotron Source (CHESS). The experimental setup and data analysis is described elsewhere [9].

2.4. COMPETITIVE HYDROGENATION OF BENZENE AND TOLUENE

The ratio of adsorption constants (toluene/benzene) at 323K were measured by competitive toluene/benzene hydrogenation. Pyrex 0.8 mm ID U-tubes were used as flow reactors for the kinetic measurements at atmospheric pressure. Ultra high purity (uhp) H_2 and He gases were further purified using H_2O and O_2 traps from Analabs. Pre-blended

mixtures of uhp 2.0% benzene/He and 0.6% toluene/He were purchased from Matheson. Typically, a 0.5 g catalytic bed was reactivated under H_2 flow at the reduction temperature for 1 h. The ratio of toluene to benzene adsorption coefficients was kinetically determined at 353K on four selected samples using the method of Tri et al. [11]. The reactor effluent was analyzed by an on-line 5880 Hewlett-Packard gas chromatograph equipped with a 100 m capillary column coated with methylsilicone.

3. RESULTS

The two preparations, ion exchange (IE) and impregnation (IP), and the reference Pd/SiO_2, were characterized by chemisorption (O_2 titration of chemisorbed H_2), catalysis (benzene hydrogenation) and physical analysis of particle size (extended X-ray absorption fine structure, EXAFS). Because we were particularly interested in the anchoring of Pd as it is affected by method of preparation and acidity of the support, the degree of sintering in H_2 was also investigated.

3.1. EXAFS AND DISPERSION

The percent dispersion measured by O_2 titration of chemisorbed H_2 and coordination number from EXAFS analysis of the catalysts reduced at 493K (in situ in the EXAFS cell) are exhibited in Table 1.

Table 1
Percent dispersion by O_2 titration of chemisorbed H_2 and coordination number (CN) from EXAFS analysis of the reduced catalsyts

Catalysts	Percent Dispersion	EXAFS CN
0.77 wt% Pd/K(H)L-IE[a]	26	7.3[d]
Pd/KL-IE,BE[b]	28	
Pd/MgKL-IE,BE	27	
Pd/CaKL-IE,BE	27	
Pd/BaKL-IE,BE	27	
1.08 wt% Pd/KL-IP[c]	26	5.6[e]
Pd/MgKL-IP,BE	25	
Pd/CaKL-IP,BE	24	
Pd/BaKL-IP,BE	24	
2.36 wt% Pd/SiO_2	44	4.2

[a] IE = ion exchange. [b]BE = back exchanged following reduction. [c]IP = impregnation. [d]The dispersion after calcination at 623K and reduction at 493K in situ in the EXAFS cell was 20 percent. [e]The dispersion after calcination at 623K and reduction at 493K in situ was 32 percent.

The EXAFS magnitude functions of the calcined precursors are shown in Figures 1 - 3 for Pd/SiO_2, Pd/K(H)L-IE and Pd/KL-IP, respectively. In each case, these are compared to the magnitude function for bulk PdO.

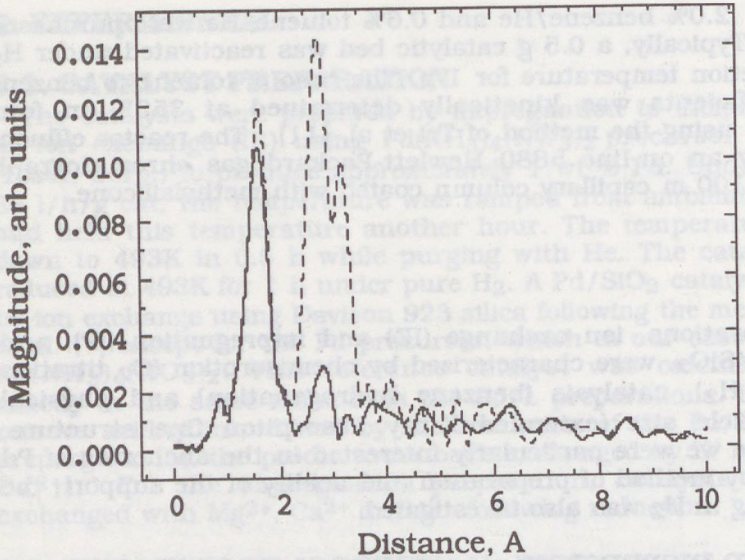

Figure 1. The EXAFS of PdO (dashed line) and of the precursor to Pd/SiO_2 calcined at 623K in situ in the EXAFS cell (solid line).

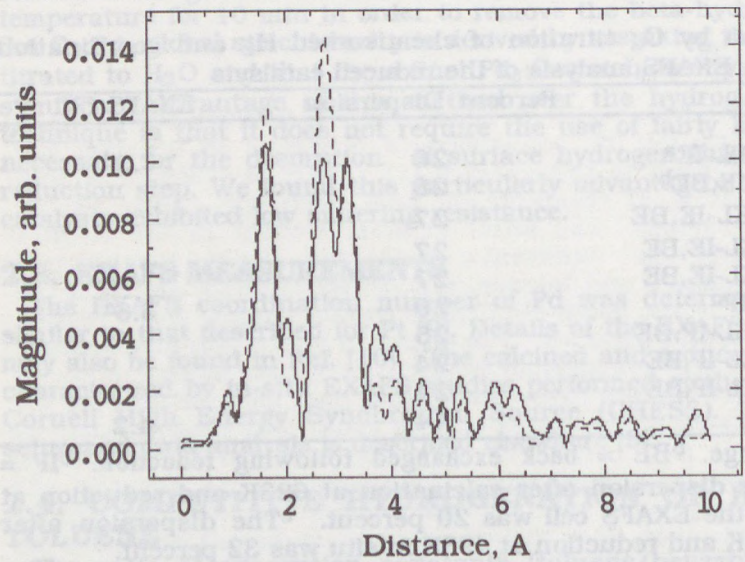

Figure 2. The EXAFS of PdO (dashed line) and of the precursor to Pd/K(H)L-IE calcined at 623K in situ in the EXAFS cell (solid line).

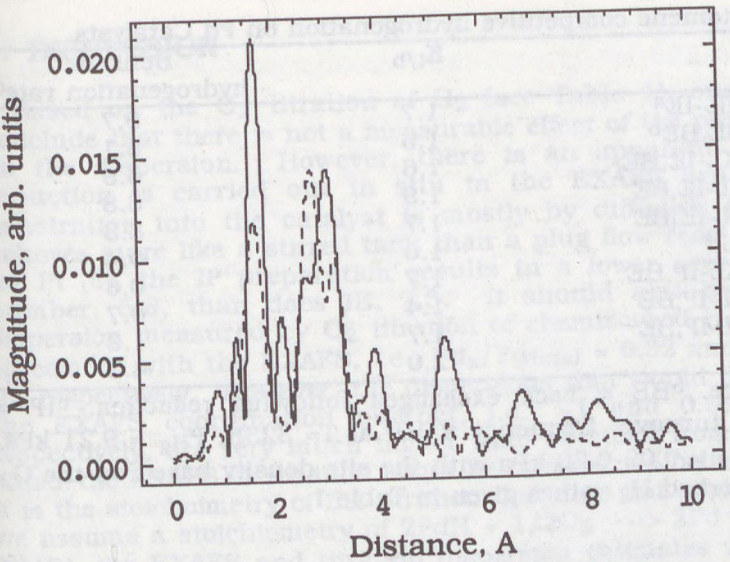

Figure 3. The EXAFS of PdO (dashed line) and of the precursor to Pd/KL-IP calcined at 623K in situ in the EXAFS cell (solid line).

3.2. CATALYTIC STUDIES

The rate of benzene hydrogenation at 323K is given in Table 2. Also, tabulated in Table 2 are the ratios $K_{toluene}/K_{benzene} = K_{t/b}$ measured kinetically by the competitive hydrogenation of benzene in the presence of toluene.

3.3. SINTERING STUDIES

In Figure 4, the relative dispersion (see Table 1 for initial dispersion) is plotted against the temperature at which the catalysts were sintered for one h in 1 atm of H_2. Four catalysts, two from each preparation method with acidity of each varied by K^+ exchange by Mg^{+2}, were investigated by following the dispersion by H_2 titration by O_2. In the critical temperature range between 450K and 600K, the absolute particle size determined by EXAFS was followed under the same conditions in situ in the EXAFS cell. Unfortunately, the different H_2 flow conditions in the cell resulted in somewhat different dispersions (see footnotes to Table 1).

Table 2 Benzene/toluene competitive hydrogenation on Pd Catalysts

Catalysts	$K_{t/b}$	Benzene hydrogenation rate[d]
0.77 wt% Pd/K(H)L-IE[a]	1.7	9.7
Pd/KL-IE,BE[b]	1.6	6.1
Pd/MgKL-IE,BE	1.6	6.9
Pd/CaKL-IE,BE	1.9	6.8
Pd/BaKL-IE,BE	1.7	8.3
1.08 wt% Pd/KL-IP[c]	1.0	0.4
Pd/MgKL-IP,BE	1.7	0.6
Pd/CaKL-IP,BE	1.4	0.7
Pd/BaKL-IP,BE	1.7	1.3
2.36 wt% Pd/SiO_2	2.0	4.2

[a]IE = ion exchange. [b]BE = back exchanged following reduction. [c]IP = impregnation. [d]The turnover frequency x 10^4,at T= 323K, P_{H_2} = 9.21 kPa, P_{bz} = 0.18 kPa, P_{tol} = 0.02-0.20 kPa with the site density based on the O_2 titration of chemisorbed H_2 values given in Table 1.

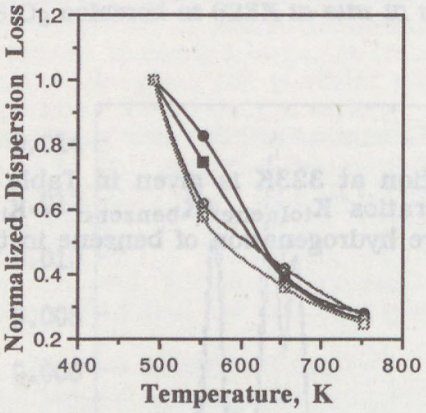

Figure 4. Relative dispersion as a function of sintering temperature for Pd/K(H)L-IE (●), Pd/MgL-IE,BE (■), and Pd/KL-IP (○), and Pd/MgL-IP (□).

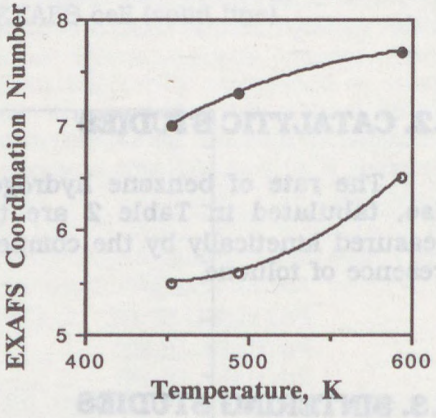

Figure 5. EXAFS C. N. as a function of sintering temperature for Pd/K(H)L-IE (●) and Pd/KL-IP (○).

4. DISCUSSION

Based on the O_2 titration of H_2 (see Table 1), one would have to conclude that there is not a measurable effect of the preparation method on the dispersion. However, there is an apparent effect when the reduction is carried out in situ in the EXAFS cell (where the H_2 penetration into the catalyst is mostly by diffusion because the cell behaves more like a stirred tank than a plug flow reactor). As observed for Pt [5], the IP preparation results in a lower average coordination number, 5.6, than does IE, 7.3. It should also be noted that the dispersion measured by O_2 titration of chemisorbed H_2 is in qualitative agreement with the EXAFS, i.e., Pd_s/Pd_{total} = 0.32 and 0.20, for IP and IE, respectively. However, the dispersions that would be estimated from the EXAFS coordination number, i.e., ~1 and 0.9, for IP and IE, respectively, are very much higher than obtained from titration. While either the EXAFS or titration might be in error, we believe it is likely that it is the stoichoimetry of the titration that does not apply and note that if we assume a stoichiometry of $2PdH + 1/2O_2 \rightarrow 2Pd + H_2O$ (instead of 2PdO), the EXAFS and titration dispersion estimates would be brought into agreement. One could even argue that the basicity of the L-zeolite would decrease the the O_2 chemisorption in this direction, but such an argument cannot be sustained for the case of Pd/SiO_2 where the difference in the EXAFS and titration dispersion estimates is comparable.

The effect of preparation method and varied acidity (cation exchange of K^+ with Mg^{2+}, Ca^{2+} and Ba^{2+}) was examined by the effect on competitive adsorption of toluene and benzene ($K_{t/b}$) and benzene hydrogenation rate, see Table 2. The dominant effect is clearly preparation method and is seen in the benzene hydrogenation rate. Because hydrogenations are generally agreed not to be particle size dependent and because the apparent dispersion is similar (see Table 1), the order of magnitude greater rates on the IE prepared Pd/L catalysts relative to the IP preparation must be attributed to the method of preparation. We will return to a possible interpretation of this observation below after discussion of the observed differences in the precursors observed by EXAFS. The fact that $K_{t/b}$ is neither affected greatly by method of preparation or acidity of the support is perhaps easier to understand. Both theoretical [13] and experimental values for Pd/SiO_2 indicate the there is little selectivity between toluene and benzene ($K_{t/b}$ ~ 1) such that only large perturbations of the electronic structure could effect this.

One of the motivations for this work was to see if the acidity of the support affected the dispersion of Pd. That it does not in the preparations shown in Table 1 is perhaps not surprising since the acidity was varied by ion exchange of K^+ after the Pd particles had already formed. However, in a parallel set of experiments, K^+ was exchanged with NH^{4+} and the zeolite calcined at 773K to form $\bar{K}$(H)L-zeolite (the degree of exchange was 3, 6 and 15% of the 9 K^+ per unit cell) before impregnation with $Pd(NH_3)_4(NO_3)_2$. Measurement of the surface area

after decationation indicated little loss in crystallinity (surface area constant at about 300 m^2/g), but the resulting dispersion was nearly constant also.

Examination by EXAFS of the PdO precursor to Pd particles formed by calcination at 623K, see Figures 1-3 and Table 3, show clear differences based on both the kind of support (SiO_2 vs L-zeolite) and method of preparation (IE vs IP on L-zeolite). The bulk phase that might be expected if the $Pd(NH_3)_4(NO_3)_2$ were completely decomposed would be PdO. On SiO_2, there is no evidence for PdO particles, but an isolated surface species with about 3.6 oxide anions in the coordination shell of Pd would be consistent with the EXAFS magnitude function shown in Figure 1 where no second shell scattering is observed. The second shell Pd-Pd scattering (through Pd-O-Pd bonding) of both the L-zeolite preparations are qualitatively similar to bulk PdO, but there are distinct differences between the IE and IP preparations. In the case of the IE, the EXAFS magnitude function shown in Figure 2 is consistent with small PdO particles with a nearest neighbor oxide coordination number of 3.5 (relative to 4 in the bulk) and 2.9 at 3.08Å and 3.8 at 3.37Å (6.7 total) Pd cations in the next-nearest neighbor shell (relative 8 at 3.05Å and 4 at 3.43Å, 12 total in the bulk). The IP preparation has significantly smaller nearest neighbor CN, 3.0. In the next nearest shell, the distances and total CN, 6.5, is almost the same as for the IE preparation but distribution is quite different. In the IP preparation, the CN of the shorter distance is lower, 1.7, and the CN of the longer distance is greater, 4.8, than in the IE preparation. Qualitatively, it can be said that the PdO like particles are more spherical in the IE preparation and those in the IP preparation are oblong.

Table 3. EXAFS analysis of first three coordination shells (subscripted 1, 2 and 3) of precursors calcined at 623K; N is the CN, DWf the Debye Waller term relative to the PdO reference and R the interatomic distance

Catalysts	N_1	DWf_1 x10^5	R_1 Å	N_2	DWf_2 x 10^5	R_2 Å	N_3	DWf_3 x 10^5	R_3 Å
Pd/SiO_2	3.6	5	2.00	-	-	-	-	-	-
Pd/K(H)L-IE	3.5	9	2.03	2.9	15	3.08	3.8	12	3.37
Pd/KL-IP	3.0	1	2.02	1.7	11	3.07	4.8	10	3.39
PdO(model)	4.0	-	2.02	4.0	-	3.05	8.0	-	3.43

There are two other important (and somewhat strange) observations concerning this PdO like structure of the precursor in the IP preparation. Firstly, there is apparent structure out to distances of 10Å, structure which is not observed in bulk PdO, see Figure 3. Secondly, there is apparently a second scatterer in the nearest shell that is not an oxide ion. This is seen in the magnitude function as peak almost double the size of

the Pd-O peak of bulk PdO. This must be a heavy Z element since the isolated and back transformed EXAFS function can be truncated at 12Å^{-1} and very well fitted by only oxide back scattering to obtain the coordination number of 3.0 given in Table 3, i.e., the other scatterer has intensity only at wavevectors greater than 12Å^{-1}. It is difficult to imagine what this species might be, but aside from the oxide ions needed to balance the Pd^{2+} charge, only the oxide ions of the zeolite lattice and K^+ ions should reside in the zeolite channel after calcination. Thus, one may postulate a Pd-K interaction, but it is not very satisfying since both the Pd and K should be cations at this stage. The long range structure may be more plausibly suggested to be a one dimensional PdO stretched along the zeolite channel. This picture is also consistent with the shapes of the PdO like particles deduced above from the CN. The oblong or stretched PdO particle shape would be likely since the channels would constrain growth in three dimensions and more probable for the IP preparation than the IE preparation since the Pd^{2+} cations would be anchored to the zeolite framework before calcination in the latter case.

While the $K_{t/b}$ is not a very useful parameter to sense the acidity of the support in the case of Pd, the rate of benzene hydrogenation probably is. We have previously observed that there is a correlation between the increase in the acidity of L-zeolite and an increase in the rate of benzene hydrogenation on Pt/L catalysts [3]. Perhaps more to the point, Chou and Vannice have reported a similar correlation for Pd using C, SiO_2, Al_2O_3, SiO_2-Al_2O_3 and TiO_2 supports [14]. Chou and Vannice proposed that the benzene adsorbed on acidic sites on the oxide surface near Pd particles in the adlineation region and that this adsorbed benzene then reacts with H_2 activated by Pd, i.e., that there is an effective increase in site density. This would not involve any change in electronic properties of the metal particles (as implied in our interpretation [3]) and this is reasonable since the particles on normal supports are both much larger and not surrounded by the support as in the case of L-zeolite. Whatever might be the correct mechanistic interpretation of the rate-acidity correlation, the empirical observation from Table 2 is that the IE preparation results in greater acidity than IP. This is to be expected [5], but the fact that the back exchanged (BE) catalysts are not substantially less acidic (see Table 2) implies that the exchange is not very effective in removing the acidity developed during reduction of the IE preparation. Divalent cations were effective for removing acidty of Pt/L-zeolite but K^+ was not [15]. Because both K^+ and divalent alkane earth cations are ineffective with regard to the exchange of H^+ from Pd/L-zeolite, the protons must be more thermodynamically stable in this case and may be directly associated with the Pd as has been suggested for Pd/Y-zeolite [16].

While introduction of acidity into L-zeolite did not provide anchoring sites to increase dispersion (see above), increased acidity does appear to inhibit sintering to a degree. This is most obvious in Figure 4 when a sintering temperature around 550K is used. The IE preparations sinter less rapidly than the IP preparations. It is interesting also that the BE catalysts (K^+ exchanged by Mg^{2+}) sinter slightly less rapidly than the initial Pd/KL catalysts in dependent of preparation method. In the case of the IP catalysts, the BE presumably does not involve any removal of

protons, but is the result of the replacement of K^+ by Mg^{2+} in the L-zeolite channels. The effect on sintering may be greater than on the benzene hydrogenation rate (compare Pd/KL-IP to Pd/MgKL-IP,BE in Table 2 and Figure 4).

5. SUMMARY AND CONCLUSIONS

The property of higher dispersion resulting from an IP preparation than from an IE preparation is apparently a property of the L-zeolite and occurs for both Pt [5] and Pd. While the interaction between L-zeolite and either Pt or Pd is qualitatively similar, the high density of states of Pd appears to cause the interaction to be weaker in the Pd case. This is reflected in the stability with respect to sintering in H_2. Between 493 and 753K, the temperature of reduction has a small effect on dispersion in Pt/L-zeolite [12] while Pd/L-zeolite is very unstable to even modest thermal treatments in H_2. The dispersion decreases to about one fourth of that after the initial 493K reduction following reduction at 753K. Further evidence that this is the result of the high density of states on Pd is indicated by the fact that the relative loss of dispersion by Pd/K(H)L-zeolite (the protons resulting from the reduction of the ion exchange preparation) is slower than Pd/KL-zeolite (impregnation preparation) at 553K.

6. ACKNOWLEDGMENTS

This research was supported by the DoE Office of Basic Energy Sciences. Partial support from Sun Company is also acknowledged. We wish to thank the Cornell High Energy Synchrotron Source for beam time. We also wish to thank Daniel Resasco for measurement of some surface areas.

7. REFERENCES

1 J. R. Bernard, Proc. 5th Int. Conf. Zeolites, p. 686 Heyden, London, 1980.
2 W. E. Alvarez and D. E. Resasco, Catal. Lett, 8 (1991) 53.
3 G. Larsen and G. L. Haller, Catal. Lett., 3 (1989) 103.
4 T. T. Phuong, J. Massardier and P. Gallezot, J. Catal. 102 (1986) 456.
5 L. M. Kustov, D. Ostgard and W. M. H. Sachtler, Catal. Lett., 9 (1991) 121.
6 C. Kittel, Elementary Solid State Physics, p. 162, New York. J. Wiley & Sons, 1962.
7 M. A. Baltanas and A. L. Bonivardi, J. Catal. 125 (1990) 243.
8 J. E. Benson, H. G. Wang and M. Boudart, J. Catal., 30 (1973) 146.
9 B. J. McHugh, G. Larsen, and G. L. Haller, J. Phys. Chem., 94 (1990) 8621.

10 B. J. McHugh, Ph. D. Thesis, Yale University (1991).
11 T. M. Tri, J. Massardier, P. Gallezot, and B. Imelik, Metal-Support and Metal-Additive Effects in Catalysis (B. Imelik et al., eds.), p. 141. Elsevier, Amsterdam, 1982.
12 T. R. Hughes, W. C. Buss, P. W. Tamm and R. L. Jacobson, Proc. 7th Int. Congr. Zeolites, p. 725 Tokyo,1986.
13 C. Minot and P. Gallezot, 123 (1990) 341.
14 P. Chou and M. A. Vannice, J. Catal., 107 (1987) 129.
15 G. Larsen and G. L. Haller, Cataysis Today, in press.
16 S. T. Homeyer, Z. Karpinski and W. M. H. Sachtler, J. Catal. 123 (1990) 60.

DISCUSSION

Q: H. Topsoe (Denmark)

In your work you find that the dispersion measured by EXAFS coordination number analysis is higher than that measured by chemisorption. You favor the dispersion measured by EXAFS for your system, this method may give you the best value of the dispersion but I would like to point out that your true dispersion is most likely lover than that measured by your EXAFS analysis. As we have recently shown [1, 2], this is due to the fact that the EXAFS analysis does not take properly into account the anachronic motion of atoms on small particles and resulting contributions to the low k part of the spectrum. To what extent do you think that the lower dispersions may have an effect on your assignment of the location of your metal particles.

[1] Hansen et al., *Phys. Rev. Letters*, **64**, 3155 (1990)
[2] Clausen et al., *J. Catal.*, submitted

A: G. L. Haller

I have, of course, read the submission to the J. Catal. and am aware of this analysis. I suspect that it is generally true that the EXAFS coordination analysis may under estimated the true particle size. Unfortunately, we do not have an independent particle size analysis by, for example, electron microscopy in the case of Pd in L-zeolite. However, in the case of Pt/L-zeolite which we have investigated more extensively, there is both a good linear correlation between EXAFS coordination number determined size and H/Pt estimation of average particle size and this particle size is in reasonable agreement with what we see by electron microscopy [3] for the EXAFS-H/Pt correlation. In the case of Pd/L-zeolite we estimate dispersions of <0.3 by O_2 titration of chemisorbed H_2 and dispersion ~1 from EXAFS. The former would imply that most of the particles were outside the L-zeolite pores; the latter that most of the particles are inside. It is probable that the true dispersion is somewhere in between these extremes and that we have only a portion of the Pd particles in the L-zeolite pores.

[3] G. Larsen, G. L. Haller, *Catalysis Today*, in press

Q: E. Derouane (Belgium)

The low Pd dispersions that you measure by the titration technique can indicate either that the Pd particles are too big to be in the zeolite L cages, in which case it would explain the low Pd/L-zeolite interaction, or that the stoichiometry you use for the titration is not correct, as just suggested by Sachtler. Should we 100 % agree that the second possibility is the correct one ?

A: G. L. Haller

We are of the opinion that the assumed stoichiometry is in error based on our EXAFS results. However, the EXAFS coordination numbers also are somewhat uncertain (see remark

and reply to the question of H. Topsoe for the reason). Thus, we must agree that the wrong assumed stoichiometry may not be the only reason for the apparent low dispersion measured by titration.

Q: W. P. Hettinger, Jr. (USA)
There are many ionic forms of palladium. The question is: Did you try other ionic species for ion exchange to determine the variation in results which could occur ?

A: G. L. Haller
This was not a variable that we investigated. The exchange precursor was always $Pd(NH_3)_4(NO_3)_2$.

Q: W. M. H. Sachtler (USA)
We have studied the Pd/L system by various methods including TPR. We found that the H_2 consumption for Pd atom was H/Pd = 2 for reduced and reoxidized samples, but for freshly calcined samples it was significantly different from 2. EPR showed a resonance of Pd(III) ions. We assume that Pd(III) in the main channels consume 3 H atoms per Pd, but Pd(III) in cancrinite cages consumes only one H atom per Pd, if the reduction is limited to Pd(III) → Pd(II). How does the existence of Pd(III) ions in L-zeolites affect the interpretation of your EXAFS results ?

A: G. L. Haller
We have not performed TPR and have no direct evidence for Pd(III). With respect to our EXAFS results of the precursors to the Pd metal particles, we would have to observe that the 623 K calcined ion exchanged preparation results in a very good fit to the PdO model both in Pd-O coordination numbers and distances and in both nearest neighbor and second nearest neighbor spheres. However, the impregnated sample (after 623 K calcination) exhibits a Fourier magnitude at the Pd-O distance that exceeds that of bulk PdO, see Figure 3. It is clear that this is mostly coming from intensity in the high k portion of the EXAFS magnitude function. It is possible that this is the result of Pd(III) in the cancrinite cages. This would predict that the TPR results would be distinctly different for ion exchange and impregnation preparations and that there should be more Pd(III) in impregnation preparations.

Q: M. Ichikawa (Japan)
1) How do you eliminate the diffusion control of reactant molecules inside your Pd/L-zeolite ?
2) How do you envision the location of Pd particles attached to oxygen atoms inside L-zeolite in terms of the metal-support interaction? How may O atoms be involved in the anchoring of Pd particles as deduced from the EXAFS data ?

A: G. L. Haller
1) The TOFs are very low so one would not expect diffusion control for this reason. On the other hand, the low reaction temperature almost assured that the pores are filled with liquid reactant so that some effect of transport is a reasonable expectation for all particles not near the surface of the zeolite particles. All we can say is, assuming that most of the Pd is in the zeolite pores for both preparations, the order of magnitude change in rate suggests that the effect is mostly chemical.
2) We have not attempted to analyze our EXAFS at low k where Pd-O contribution would occur after the reduction to metal. There is reason to believe that there may a small component of unreduced Pd (see comment of Sachtler) so it would then be necessary to sort out the contributions from anchoring of Pt metal particles and the interaction of Pd^{3+} in the cancrinite cages. In short, we cannot answer your question.

Q: D. Ostgard (USA)

1) Since the Pd/KL-IP catalyst forms oblong PdO like particles and the Pd/KL-IE forms spherical PdO like particles, is it possible that after reduction the Pd/KL-IP catalyst has more encapsulated Pd in comparison to the Pd/KL-IE analog ? Could this higher lever of "benzene inaccessible" Pd contribute to the lower turnover frequency observed for the Pd/KL-IP catalyst?

2) Why does the back exchange of protons for the Pd/KL-IP catalyst increase the benzene turnover frequency, while the opposite trend is observed for the Pd/KL-IE catalysts?

3) What is the pH of your back exchange solution? Have your ever considered using a basic solution?

A: G. L. Haller

1) The different shapes we have deduced are for the oxide precursors of the ion exchange and impregnation preparations. We have no evidence that the Pd metal shapes are different and, based on the O_2 titration of chemisorbed H_2, the average particle sizes are not different for the two kinds of preparations (although the EXAFS dispersion are, but they were reduced under different conditions from those used in benzene hydrogenation). Note that the Pd/SiO_2 reference catalysts should be expected to have a remarkably larger benzene TOF if transport or steric hindrance were the only cause of variation in TOFs but its value lies in between the two kinds of preparations.

2) In the case of the ion exchange preparation, the back exchange is mostly partly between protons and the cation used for back exchange and this reduces acidity. In the case of the impregnation preparation, the back exchange is between K(I) and doubly charged alkaline earth cations. The latter can cause some hydrolysis of H_2O. Thus, is both cases the rate is being increased when the acidity is increased.

3) The pH was that of distilled water. Although it may appear reasonable to expect that some protons would be incorporated by the zeolite in this situation, the observed $K_{t/b}$ are consistent with net removal of Brönsted acidity. It is likely that a basic solution would have been more effective as you suggest.

Q: C. Apesteguia (Argentina)

Benzene hydrogenation is a structure insensitive reaction on most transition metals, the activity per surface atom being independent of the metal particle size or of support influence. Thus, benzene/toluene competitive hydrogenation reaction is preferentially employed for detecting possible electronic changes of the metal surface. Your results show the contrary effect, benzene hydrogenation rate relating better than benzene/toluene hydrogenation to electronic modification of Pd. What is your interpretation of these results ?

A: G. L. Haller

It has been demonstrated (see our ref. 4) that the $K_{t/b}$ is a very sensitive function of the metal density of states at the Fermi level to the $K_{t/b}$ decreases Ru > Rh > Pd in the second row of group VIII and Os > Ir > Pt and that $K_{t/b}$ is ~1 for Pd on silica support. The exceptionally high density of states of Pd makes $K_{t/b}$ very insensitive to support electronic effects. However, as is true in all of these systems (see ref. 3) the benzene hydrogenation rate is more affected by support effects than $K_{t/b}$. One normally does not try to use this information because 1) there is no internal reference like we have in $K_{t/b}$, it is a kinetic rather than a thermodynamic property so can be compromised by transport as well as chemical effects (see reply to Ostgard) and it is not possible to give the correlation between support (electronic) effect and benzene hydrogenation rate a physical interpretation as we believe we can for $K_{t/b}$. However, in the case of Pd, we have little choice but to fall back the empirical observation that systems where $K_{t/b}$ is discriminating, e.g., Pt/L, the rate of benzene hydrogenation decreases as the metal becomes more electron rich. Thus, the results in Table 2 suggest that Pd in L-zeolite prepared by ion exchange is more electron deficient that Pd/SiO_2 while the impregnation preparation appears to be more electron rich.

Guczi, L. *et al.* (Editors), *New Frontiers in Catalysis*
Proceedings of the 10th International Congress on Catalysis, 19-24 July, 1992, Budapest, Hungary
© 1993 Elsevier Science Publishers B.V. All rights reserved

ON THE NATURE OF SUPERACTIVE CENTERS IN H-FeZSM-5 ZEOLITES. QUANTUM-CHEMICAL CALCULATIONS

M. J. Filatov, A. G. Pelmenschikov and G. M. Zhidomirov

Institute of Catalysis, Russian Academy of Sciences, Siberian Division, Lavrentieva Str. 5, 630090 Novosibirsk, Russia

Abstract

A model of the super active Fe-containing catalytic centers detected in the thermally activated H-FeZSM-5 zeolites [1] is proposed. With the help of the NDDO/MC quantum chemical calculations the extraordinary catalytic properties of these centers in the reactions of oxidation by the N_2O molecules [1,3] are explained. The calculations for some intermediates of the N_2O decomposition reaction have been performed and results are compared with the experimental data [1,2].

1. INTRODUCTION

The results of the experiments [1-3] point to existence of the unusual Fe-containing catalytic centers in the H-FeZSM-5 zeolites (the iron being introduced at the stage of zeolite synthesis in concentration ≈ 1 wt. % of Fe_2O_3). In the reaction (1)

$$N_2O + Z \longrightarrow N_2 + OZ \qquad (1)$$

these centers, following refereed as Z centers, are 2-3 orders of magnitude more active than the iron atoms of Fe_2O_3 surface. A form of oxygen appearing in the reaction (1) exhibit an anomalously high activity in the reactions of O_2 isotopic exchange and oxidation of CO and CH_4 molecules [1].

In the present paper a model of such super active centers is proposed. This model is based on the following reasons. According to the data of e.s.r., i.r. and Mossbauer

spectroscopy [5-10] the Fe atoms in the H-FeZSM-5 specimens exist in two main chemical forms:
a) the lattice atoms in tetrahedral coordination - $Fe^{f*)}$ (signal at g=4.3 in the e.s.r. spectra);
b) the atoms in the super fine nuclei of the ferric hydroxide of the type $nFe_2O_3 \cdot mH_2O$ - Fe^{nf} (signals at g=2.0, 2.3, 5.3 and 7.9 depending on the method of preparation).
The Fe^f atoms are inert towards the adsorption of CO and H_2 molecules at T=77 K and don't react with these molecules up to the temperature T=1073 K [5]. In the same conditions, the Fe^{nf} atoms exhibit chemical activity towards CO and H_2 molecules [5]. This activity is accepted to be due to the low coordinated Fe^{nf} atoms which are formed by dehydroxilation of the nFe_2O_3 mH_2O nuclei during thermal activation [5,10]. A state of such Fe^{nf} atoms in the sufficiently small clusters could differ appreciably from that in a bulk Fe_2O_3.

The ferric hydroxide nuclei could be divided into two types depending on their genesis. Firstly, these are the impurities which are formed during synthesis and appeared in the e.s.r. spectra of as-synthesized specimens as a signal at g=2.0 [6,9,10]. Secondly, these are the nuclei which are formed by the Fe atoms leaving a lattice during thermal activation [6,9,10]. In the e.s.r. spectra this process results in decreasing of the intensity of the signal at g=4.3 and simultaneous increasing of the intensities of the signals at g=2.0 and g=5.3 [9,10]. According to the data of [6] and [3] the dependencies of the relative intensity of Fe^f e.s.r. signals for the as-synthesized specimens and conversion degree of benzene selective oxidation on the Fe content behave similarly. When the iron content being greater than ≈ 2 wt. % of Fe_2O_3, these dependences run into plateau. It is quite naturally to assume that the Z centers are formed by the Fe^f atoms leaving a lattice during thermal activation of a zeolite.

The chemical behavior of Al and Fe atoms in oxides submits to the rule of structural similarity. It is displayed for example in isodimorphism of the next compounds (T = Fe and Al): $K_2O \cdot 11T_2O_3$, $SrO \cdot 6T_2O_3$, MgT_2O_3, $K_2T_2O_3$, α-TO·OH, γ-TO·OH, $T(OH)_3$ etc. [11]. Recently a validity of this rule was confirmed also for zeolite lattices of the type TPO_4 and TZSM-5 [8]. This structural similarity is a consequence of the proximity of chemical properties - ion radii and

---

*) f and nf - abbreviation of the words framework and non-framework respectively.

electronegativity - of Fe and Al atoms and of the same valences of Fe and Al atoms in this compounds. In accordance with that, the mechanism of extraction of Al atoms from zeolite lattices suggested in [12,13] will be used for the case of T=Fe in the present work. According to this mechanism [14] extraction of the Fe atoms from zeolite lattice occurs through the formation of super fine hydroxide clusters of the type 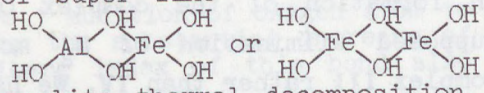 during the initial stages of zeolite thermal decomposition. Comparison of the catalytic properties of Fe-Al-Si and Fe-Si zeolites [1] shows that active sites in both cases are identical [1]. Hence, we set up the hypothesis that the Z centers are formed from the binary ferric hydroxide complex of the type 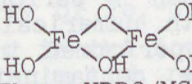 during the thermal activation of zeolite. The NDDO/MC [4] calculations show that the dehydroxilation of these clusters results in the formation of 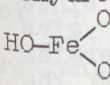 complexes which might exhibit extraordinary catalytic properties in the reactions of N_2O decomposition [1] and benzene oxidation [3]. In the present work the quantum chemical calculations of these hypothetical Z centers and some intermediate structures of the reaction (1) were performed by the NDDO/MC semiempirical method [4]. The calculated heat of the reaction (1) and activation energy are in a reasonable agreement with the experimental data.

2. DETAILS OF CALCULATIONS

As was mentioned in the Introduction our hypothesis is based on the two-by-two mechanism [14] of an emerging of the Fe atoms from zeolite lattice. On this mechanism pairs of the neighboring Fe atoms predominantly leave a lattice at moderate temperatures of zeolite activation. They leave zeolite in the form of super fine ferric hydroxide clusters $Fe_2O_3 \cdot 3H_2O$ (I). Chemisorption activity of such complex is achieved by its dehydroxilation resulting in formation of $Fe_2O_3 \cdot 2H_2O$ (II) cluster. To our hypothesis it is complex II that exhibits extraordinary catalytic properties in the reactions of selective oxidation by N_2O molecules. The decomposition of N_2O on complex II occurs in two steps. Firstly, it is the

adsorption of N_2O molecule. In general case N_2O can be adsorbed in two ways: adsorption by O-end and by N-end of the molecule. Resulting complexes are $N_2O{\cdot}Fe_2O_3{\cdot}2H_2O$ (**III**) and $ON_2{\cdot}Fe_2O_3{\cdot}2H_2O$ (**IV**) respectively. Then disruption of N=O bond with simultaneous elimination of N_2 molecule occurs resulting in formation of the complex $O{\cdot}Fe_2O_3{\cdot}2H_2O$ (**V**). As we have supposed elimination of N_2 molecule can occur only from complex **III** rather than **IV**. We have performed calculations for the corresponding transition state (complex **VI**).

Quantum chemical calculations for these six complexes (see Figure 1) have been carried out by the NDDO/MC semiempirical method [4] with full geometry optimization. The optimization of molecular geometry has been performed by Davidon-Fletcher-Powell method [16] with numerically formed gradients. The calculations have been performed in the UHF approximation with elimination of the contaminating spin components by half-projection operator [17,18]. Multiplicity of all complexes was set equal to one (singlet state) since calculations of high spin states of these complexes give higher energies. For these complexes the zero point energies haven't been calculated, so further we will dealt with the binding energies of complexes rather than heats of formation.

3. RESULTS AND DISCUSSION

The optimized geometries and relative energies for the aforementioned six complexes are shown on Figure 1. The energy of dehydroxilation of complex **I** is 26 kcal/mol. This value consists with the supposition that dehydroxilation can occur during zeolite treating under vacuum at moderate temperature (550°C). Calculated energy of the nitrous oxide decomposition

$$N_2O + \mathbf{II} \longrightarrow N_2 + \mathbf{V}$$

is 22.3 kcal/mol that is in reasonable agreement with the experimental value of (23-19)±3.5 kcal/mol for the heat of the reaction (1) [1]. Binding energy of the terminal oxygen atom in complex **V** is 60.4 kcal/mol. Using this value and calculated binding energy in dioxygen (128.3 kcal/mol) one can evaluate the energy of dissociative adsorption of O_2

$$O_2 + 2(Z) \longrightarrow 2(OZ).$$

The value of 7.5 kcal/mol consists with the experimental estimate of the heat of dioxygen adsorption which varies from 6.0±3.5 to 1.0±3.5 kcal/mol due to the change in surface coverage [2]. Such a low heat of dioxygen adsorption implies that surface oxygen couldn't be generated from molecular O_2 [2].

Activation energy of reaction (1) evaluated from the experimental data is 10±2 kcal/mol [1].According to our calculations activation barrier for the reaction

$$\mathbf{III} \longrightarrow N_2 + \mathbf{V}$$

is 6.2 kcal/mol. To our opinion some difference of this value from experimental one could be explained by the influence of zeolite lattice.

As it can be seen from Figure 1 addition of oxygen atom to the complex **II** is accompanied by the substantial increase of the Fe_1-O_2 bond length. The Wiberg index of this bond also decreases from 0.161 to 0.039. These variations in bond length and bond order give evidence of the substantial weakening of the Fe_1-O_2 bond. Thus, relatively small energy of oxygen binding by complex **II** could be attributed to the compensation of the energy of Fe_1-O^* bond by the increase of Fe_1-O_2 bond strength. It is the low value of oxygen binding energy that might explain a high reactivity of oxygen atoms generated by N_2O decomposition (*i.e.*, in a bulk Fe_2O_3 binding energy of oxygen is 77 kcal/mol [15]).

Thus, according to the above discussion oxidation of the reagents R by the N_2O molecules proceeds through a formation of the highly active oxygen atoms O^* by the scheme

$$N_2O + Fe_2O_3 \cdot 2H_2O \longrightarrow N_2 + O \cdot Fe_2O_3 \cdot 2H_2O$$

$$R + O \cdot Fe_2O_3 \cdot 2H_2O \longrightarrow RO + Fe_2O_3 \cdot 2H_2O$$

A high activity of the O^* atom is explained by a relatively small energy of its addition to the Z-center. A unique feature of the Z-centers is a possibility of compensation of the Fe-O^* bond dissociation energy by the increase of Fe_1-O_2 bond strength. Perhaps such behavior of Z-centers could be attributed to the fact that Fe atoms in such centers are in low spin states and tetrahedral coordinations which are not characteristic for the bulk Fe_2O_3.

Certainly, the scheme of the active site formation discussed above is to a some extent an idealization. In the real zeolite system our hypothetical Z center (binary Fe hydroxide cluster) will be embedded into the lattice or anchored on the surface of zeolite. So, the question about influence of zeolite lattice on the catalytic properties of the Z centers is being open for discussion.

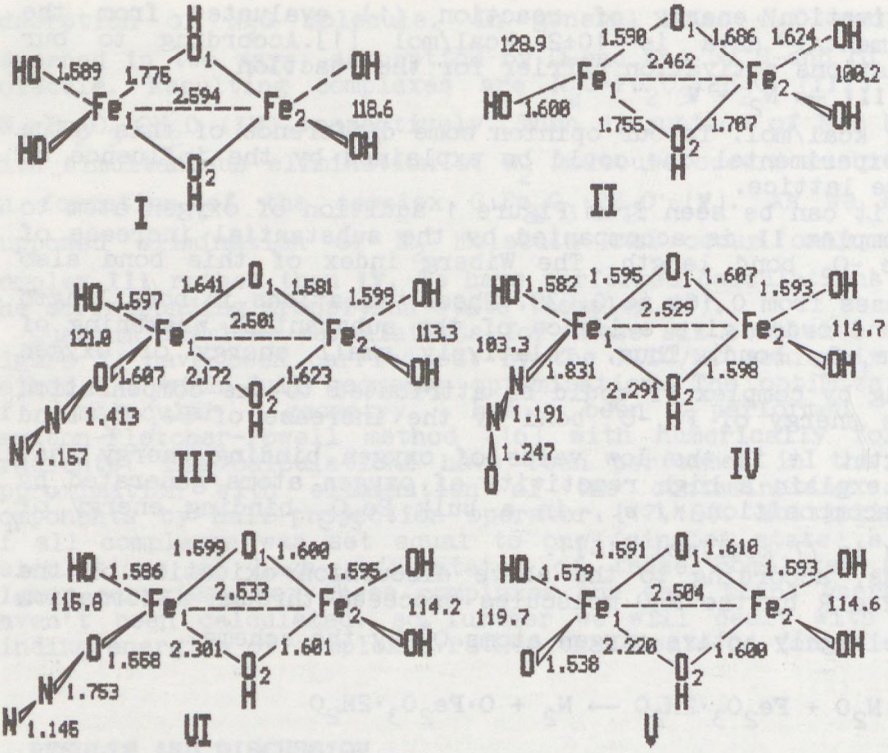

Figure 1. The optimized geometries and relative energies for $Fe_2(OH)_6$ complex, hypothetical Z center and intermediates of the N_2O decompozition reaction

4. ACKNOWLEDGEMENT

We are grateful to Prof. G.I.Panov and Dr. V.I.Sobolev for helpful discussion of our paper.

5. REFERENCES

1 G.I.Panov, V.I.Sobolev and A.I.Kharitonov, J.Mol.Catal., 61(1990)85.
2 V.I.Sobolev, O.N.Kovalenko, A.S.Kharitonov, Y.D.Pankrat'ev, G.I.Panov, Mendeleev Commun.,1991,29,
3 G.I.Panov, G.A.Sheveleva, A.S.Kharitonov, V.N.Romannikov, L.A.Vostrikova, Appl. Catalysis, submitted for publication.
4 M.J.Filatov, I.L.Zilberberg and G.M.Zhidomirov, J.Comput. Chem.,to be published.
5 L.M.Kustov, V.B.Kazansky and P.Ratnasamy, ZEOLITES, 7 (1987)79.
6 K.G.Ione, L.A.Vostrikova and V.M.Mastikhin, J.Mol.Catal. 31(1985)355.
7 R.B.Borad, ZEOLITES, 7(1987)398.
8 A.N.Kotasthane, V.P.Shiralkar, S.G.Negde and S.B.Kulkarni ZEOLITES, 6(1986)253.
9 S.Kaliguine, J.B.Nagy and Z.Gabelica, in S.Kaliaguine (Ed.), Keynotes in Energy Related Catalysis, Elsevier, Amsterdam, 1988, p. 381.
10 W.J.Ball, J.Dwyer, A.A.Garforth and J.Smith, in Y.Murakami et. al. (Eds.), Proc. 7th Int. Zeolite Conf., New Developments in Zeolite Science and Technology, Kodansha, Tokio and Elsevier, Amsterdam, 1986.
11 A.F.Wells, Structural Inorganic Chemistry, Oxford, 1945.
12 A.G.Pelmenshikov, E.A.Paukshtis, V.G.Stepanov, K.G.Ione, G.M.Zhidomirov and K.I.Zamaraev, Proc. 9th Int. Congr. on Catal., Calgary, 1988.
13 A.G.Pelmenshikov, G.M.Zhidomirov and K.I.Zamaraev, in P.A.Jacobs and R.A. van Santen (Eds.), Zeolites: Facts, Figures, Future, 8th Int. Zeol. Conf., Elsevier, Amsterdam, 1989.
14 P.Bodart, J.B.Nagy, G.Debras and P.A.Jacobs, J.Phys.Chem. 90(1986)5183.
15 G.K.Boreskov, Geterogennii kataliz, Nauka, Moskow, 1986.
16 R.Fletcher, M.J.D.Powell, Computer J., 6(1963)163.
17 P.A.Cox, M.H.Wood, Theor. Chim. Acta, 41(1976)269.
18 Y.G.Smeyers, A.M.Brucena, Int. J. Quant. Chem., 14(1978)641.

DISCUSSION

Q: W. K. Hall (USA)

Our extensive studies of N_2O decomposition over Fe-zeolites have shown the Fe(II)/Fe(III) couple formed when Fe(II) is base-exchanged into the zeolite is very effective for this reaction. Would you please furnish some further details concerning the preparation and characterization of these materials. Further information is needed to define the catalytically active component.

A: M. J. Filatov

Zeolites with iron content varied from 0.003 to 4.8% wt. Fe_2O_3 were synthesized by hydrothermal method. The samples were converted to H-form by the treatment with ammonia buffer solution followed by calcination in air at 873 K. After calcination samples were loaded into the reactor and treated under vacuum at 823 K for 2 hours. In these conditions reduction of Fe(III) cations appears to be somewhat problematic.

Q: T. Inui (Japan)

I appreciate your result involving heterogeneity of active sites. Recently, we obtained results of the precise distribution of the NH_3 adsorbed in the vicinity of metal incorporated into the framework of various metallosilicates having MFI structure by computer simulation. The Monte Carlo method in the case of zeolite, which has strong acidity, surprisingly much NH_3 adsorbs in large concentration only on very limited number of sites. It seems to be similar to the results you obtained at the super active center. Did you compare the nature of the superactive center in other MFI-metallosilicates which have different acid strengths, such as H-Al-silicate and H-Zn-silicate which have stronger and weaker acidity, respectively, or do you think that your calculation result fits specifically for only HFeZSM-5 ?

A: M. J. Filatov

In our hypothesis and calculations we did not use explicitly the properties of HFeZSM-5 zeolite lattice. So, the results of calculations could be discussed as valid for the metallosilicates other than HFeZSM-5 zeolite. Perhaps, during thermal activation HFeZSM-5 lattice serves as a specific generator of super fine ferric hydroxide clusters. However, investigation of this problem could not be performed only by quantum chemical methods. It is necessary to use other instrumental methods.

Q: V. Kazansky (Russia)

Do the clusters which you used in your calculations, represent the extra lattice iron or that in the zeolite crystal lattice ?

A: M. J. Filatov

These clusters represent extra lattice iron atoms. According to our hypothesis these clusters are formed by framework Fe(III) cations leaving zeolite lattice during thermal activation.

Q: O. Novaro (Mexico)

My question is on the theoretical aspects, but it relates to the previous questions concerning the choice of the structures that you propose. Empirical calculations such as yours are not able to predict in absolute terms, only in relative terms. Therefore one would expect systematic comparison between different possible structures in order to determine the most stable ones, as well as to study the most catalytically active sites, a comment already advanced by people who preceded me in the questions.

A really definitive theoretical study with absolute predictions would require full ab initio calculations as done by few groups including ours. This could be done for the systems that you are interested in, but would necessarily imply the use of extensive CI calculations to

include correlation effects. More importantly the transition metal atoms excited states would have to be included because in our recent work they have shown to be intimately related to the catalytic phenomenon.

A: M. J. Filatov

Your concept about relationship between excited states of atoms and catalytic phenomena is very interesting, but it requires further investigation. As for our model, it is not necessary to use the spectroscopic excited states in order to explain extraordinary catalytic properties of ferric hydroxide clusters. The NDDO/MC semiempirical method used in our calculations has been tailored for quantitative calculations of transition metal compounds molecular geometry and binding energy. This method has been tested in the calculations of a wide number of organic molecules and transition metal complexes and it shows the same accuracy as well-known semiempirical methods MINDO/3, MNDO, AM1. Detailed description of the NDDO/MC method you can find in the International Journal of Quantum Chemistry, Vol. 43, Special issue devoted to M. J. S. Dewar.

Q: B. Wichterlova (Czechoslovakia)

You have determined the location of Fe(III) ions in the framework sites and in the cation sites according to the ESR signals at g = 4.3 and 2.0 respectively. However, in some cases both signals can originate from the framework Fe(III) as presented in the Zeolite Conference Proceedings, Amsterdam, 1989 and Prague 1991. I would like to recommend you to use for the Fe(III) location, together with ESR spectra, the reducibility and ion exchange ability of Fe(III) ions, as those located in the framework are not reduced in hydrogen up to 670 K and are not exchanged.

A: M. J. Filatov

In our hypothesis we have used the results of the work (ref. 6 in our paper) where assignment of ESR signals has been performed. There is a correlation between intensity of ESR signal of framework iron atoms and reaction rate. One can suppose that catalytic sites could be formed by the framework Fe(III) ions themselves. During thermal activation some defects of crystal structure could be formed in the vicinity of these atoms and resulting defects could serve as catalytic centers. However, if we remove extra lattice iron atoms, e.g. by washing, zeolite completely looses catalytic activity in the N_2O decomposition reaction. This fact shows that catalytic centers are situated on the zeolite outer surface rather than in zeolite lattice. Taking in mind the aforementioned correlation between ESR signal of Fe atoms and a number of catalytic centers one can suppose that catalytic sites are formed by framework iron atoms leaving zeolite lattice during thermal activation.

Guczi, L. *et al.* (Editors), *New Frontiers in Catalysis*
Proceedings of the 10th International Congress on Catalysis, 19-24 July, 1992, Budapest, Hungary
© 1993 Elsevier Science Publishers B.V. All rights reserved

CO OXIDATION ON Pd(110): A MODEL SYSTEM FOR CHEMICAL OSCILLATIONS IN HETEROGENEOUS CATALYSIS

M. Ehsasi[a], *M. Berdau*[a], *A. Karpowicz*[a], *K. Christmann*[b] *and J. H. Block*[a]

[a]Fritz-Haber-Institut der Max-Planck-Gesellschaft, Faradayweg 4-6, D-W 1000 Berlin 33, Germany
[b]Institut für Physikalische Chemie, Freie Universität Berlin, Takustrasse 3, D-W 1000 Berlin 33, Germany

Abstract

The oxidation of CO on a Pd(110) surface has been studied over a wide pressure range (10^{-6} to 10^{-1} Torr) using work function change measurements ($\Delta\Phi$), mass spectrometry and photoemission electron microscopy (PEEM). The reaction shows bistability and hysteresis for lower pressures ($p < 10^{-3}$ Torr). At pressures above 10^{-3} Torr regular oscillations were observed near the transition region. The phase diagram of $CO_{ad} + O_{ad}$ reaction on Pd(110) shows a characteristic cross-shaped feature indicating a relationship between the hysteresis and oscillations. Experiments on two separated Pd(110) crystals mounted in the same reactor showed clearly that the reaction of various oscillatory areas is mainly synchronized through the gas phase. The influence of flow rate and coupling intensity on oscillatory behaviour on one (single) and one (divided) sample were investigated. Entrainment, rate enhancement and aperiodic oscillations were observed. Formation of adsorption islands and spatio-temporal pattern were imaged by employing a photoelectron emission microscope. Travelling waves as well as oval shaped rings and the formation of spirals could be detected as a result of reaction diffusion coupling.

Introduction

One of the most fascinating aspects of a chemical reaction taking place under conditions far from equilibrium is that instead of exhibiting a steady state rate it is likely to exhibit instabilities and oscillations. Oscillations have been observed in a number of reactions in heterogeneous catalysis. A well known example is the oscillating reaction of CO oxidation on platinum group metals. This reaction has been studied extensively over the past two decades [1, 2].

However, despite the large number of studies in this field (and although the CO oxidation reaction represents one of the better understood reactions), no common consensus on the origin(s) of instabilities has yet emerged.

Experiments thus far have been performed on surfaces ranging from supported catalysts at high pressures (atmospheric pressure) to single crystal surfaces at lower pressures ($p < 10^{-2}$ Torr). The mechanism of oscillations at higher pressures consists in the formation and slow removal of surface oxides or surface carbon [3, 4], whereas at lower pressures (mostly on platinum surfaces) the origin of oscillations can be explained by the reconstruction of the surface [5, 6], and by the formation of a strongly bonded oxygen state [7].

Bridging the pressure gap in the study of oscillatory phenomena in heterogeneous catalysis is the observation of oscillations on a Pd(110) surface. The experiments on this surface [8] were performed over a wide pressure range (10^{-4} to several Torr). The characteristic behaviour of oscillations seems to be unchanged over this extended pressure region, indicating that one oscillatory mechanism is continously at work.

In contrast to platinum surfaces, palladium surfaces represent a class of catalysts which are similar in their catalytic activities to platinum, but are less likely to undergo structural changes under reaction conditions. The stability of the Pd(110) surface under reaction conditions has made it possible to study a number of phenomena which are crucial to the understanding of oscillatory rates. These studies and a number of key experiments are discussed below.

1. THE LANGMUIR-HINSHELWOOD PROCESS

The reaction for CO oxidation on platinum group metals follows a Langmuir-Hinshelwood (LH) type process by which the reactants react from an adsorbed state. The steps of LH process are as follows:

$CO + * \rightarrow CO_{ad}$	CO adsorption
$O_2 + * \rightarrow 2\,O_{ad}$	Oxygen dissociation and adsorption
$CO_{ad} + O_{ad} \rightarrow CO_2 + 2*$	reaction of oxygen and CO and CO_2 desorption

where * refers to an empty surface site.

Under the steady flow of reactants the reaction rate exhibits three different reactive regions. These are *high reactivity*, *low reactivity* and a *transition region* connecting the two. Figure 1 shows the rate of reaction as a function of CO pressure while the sample temperature and O_2 pressure were kept constant. In the high reactive region, the surface concentration of CO was low, but increased near the transition point. Beyond this point, large islands of CO began to form and finally poisoned the surface by occupying the active sites.

The top part of figure 1 shows the variation of work function ($\Delta\phi$) measured simultaneously with the reaction rate. In this case, the work function measurement shows the change from an oxygen-covered surface to a CO-covered surface. The work function change measurements were performed using a Kelvin probe which proved to be a useful technique for following the surface reactivity to pressures up to several Torr. In the transition region the work function varies according to the reaction rate.

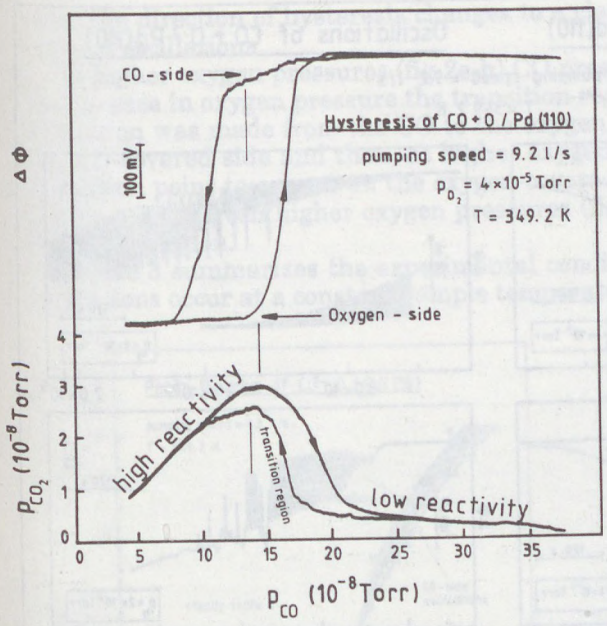

Figure 1. CO_2 production rate as a function of CO pressure. Sample temperature and oxygen pressure were kept constant.

The figure 2e shows the occurrence of oscillations near the transition point at higher pressures. The CO pressure was used as a variable parameter and was reduced linearly by a pressure controller. In this figure the work function change measurement shows the commencement of oscillations near the CO-covered surface. A transition from regular behaviour to aperiodic behaviour follows (fig 2h). The oscillations continue on the oxygen-covered side where a further decrease in CO pressure causes an increase in oscillation frequency.

The rate equations of LH steps do not give oscillatory solutions. However, they predict bistability and hysteresis. An additional process, namely *feedback* is required for rate oscillations to start. As will be shown in the next section, the formation and the slow removal of subsurface oxygen can provide the required feedback.

2. HYSTERESIS AND OSCILLATIONS

In studying a new oscillatory system such as the Pd(110) surface, it is important to see the conditions which give rise to oscillations. In particular, it is important to see how the system evolves from a steady-state condition into an oscillatory state. The first step, therefore, is to characterize the temperature and pressure conditions that give rise to oscillations.

This reaction, similar to many other oscillating systems, shows bistability and hysteresis. Figure 2 shows experiments performed under a constant sample temperature. At lower oxygen pressures (fig 2a-d), the reaction rate exhibits a counterclockwise hysteresis with respect to the increase and decrease of CO pressure, as measured by work function change (fig. 2c,d). Under the influence of an additional process--- feedback---, the hysteresis region narrows

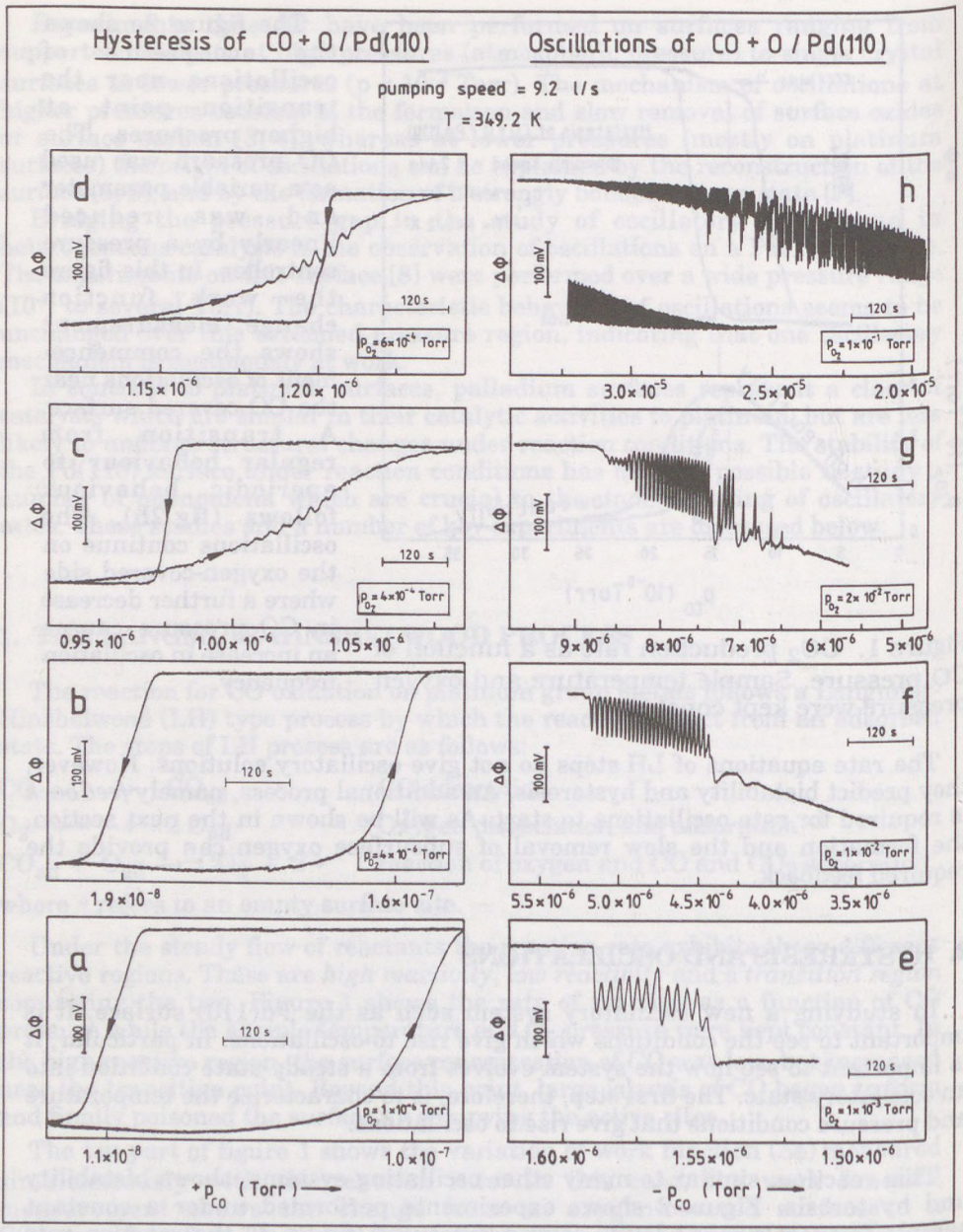

Figure 2. Reaction of CO oxidation on Pd(110) showing hysteresis at lower oxygen pressures (a-d), and oscillations at higher pressures (e-h).

until the direction of hysteresis changes to a clockwise rotation, signifying the onset of oscillations.

At higher oxygen pressures (fig 2e-h) CO pressure was reduced slowly. With an increase in oxygen pressure the transition region broadens. In this case, the transition was made from the CO to the oxygen side. Oscillations appear near the CO-covered side and then, at higher oxygen pressures, extend beyond the transition point to appear on the oxygen-covered side. Mixed mode oscillations can be seen at even higher oxygen pressures (fig 2h). They appear close to the transition region.

Figure 3 summarizes the experimental conditions for which bistability and oscillations occur at a constant sample temperature. This diagram exhibits a characteristic cross-shaped feature.The boundaries that contain the limits of the hysteresis cross at higher oxygen pressures, forming the boundaries for the oscillating regions. The high reactive steady state is shown on the left side and the low reactive steady state is shown on the right. One of the most significant aspects of this diagram is that it shows the relationship between bistability and oscillations.

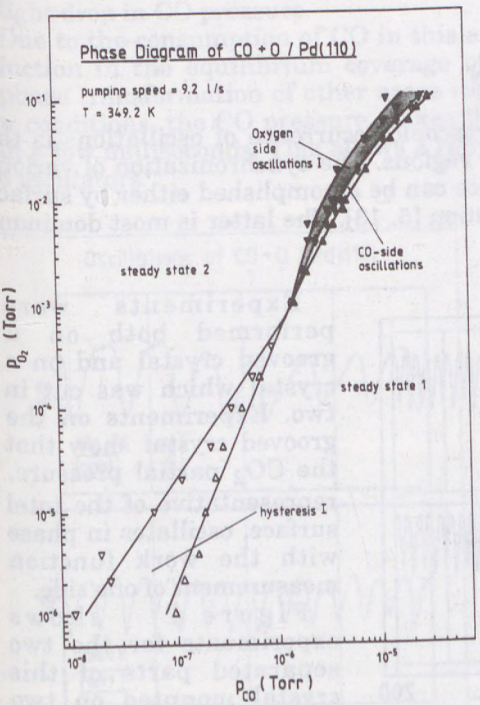

Figure 3. Phase diagram of CO oxidation reaction on Pd(110) under an isothermal condition.

Under the influence of a "slow" feedback, which in this case is the formation and slow removal of subsurface oxygen [9], the characteristic times for which the transition occurs from one branch to another change. At the crossing point these characteristic times are comparable (fig 2d), whereas beyond the crossing point in the oscillatory region, the slow process determines the time behaviour of the system.

Under the influence of a "slow" feedback, which in this case is the formation and slow removal of subsurface oxygen [9], the characteristic times for which the transition occurs from one branch to another change. At the crossing point these characteristic times are comparable (fig 2d), whereas beyond the crossing point in the oscillatory region, the slow process determines the time behaviour of the system.

The unusual shape of hysteresis in the oscillatory region is due to the formation of subsurface oxygen, as has been shown in previous studies [8, 9].

The phase diagram of the type shown here can provide the building blocks for mechanistic studies and, most important, can provide a basis for theoretical consideration of the feedback process.

A computer simulation based on slow formation and removal of subsurface oxygen by Basset and Imbihl has shown that oscillations do indeed occur [10]. However, for further clarification of the role of the feedback a more detailed analysis of the models based on cross-shaped phase diagrams is required [11]. Experiments in well-known homogeneous phase reaction systems such as the Belousov-Zhabotinsky reaction have also shown similar types of cross-shaped phase diagrams. These diagrams are crucial for the understanding of oscillatory mechanisms and for finding new oscillatory systems [12].

3. GAS PHASE COMMUNICATION

An important condition for the macroscopic occurrence of oscillations is the synchronization of various oscillatory regions. The synchronization of various regions on a large single-crystal surface can be accomplished either by surface diffusion and/or gas phase communication [5, 13]. The latter is most dominant on a Pd(110) surface.

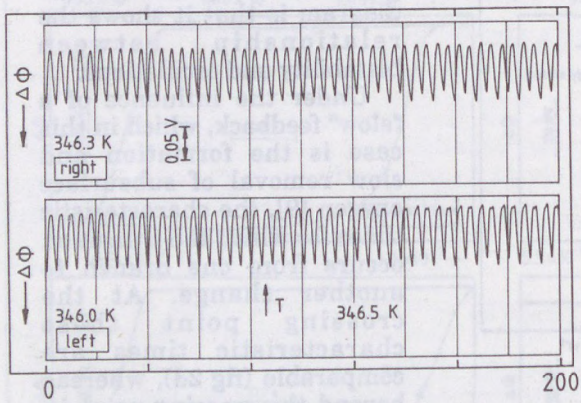

Figure 4. Oscillations under strong coupling and occurrence of period doubling. The arrow indicates the point where the temperature of the left sample was increased. ($p_{O_2} = 5 \cdot 10^{-2}$ Torr, $p_{CO} = 2 \cdot 10^{-5}$)

Experiments were performed both on a grooved crystal and on a crystal which was cut in two. Experiments on the grooved crystal show that the CO_2 partial pressure, representative of the total surface, oscillates in phase with the work function measurement of one side.

Figure 4 shows experiments for the two separated parts of this crystal mounted on two holders. The distance between the two crystals was 1.5 cm. The temperature of each crystal could be varied independently.

This figure shows that both samples oscillate in phase. Almost every detail of their shape is similar. By changing the temperature of one sample, the oscillations on the other sample follow in phase. In this case, they are exhibiting period doubling and other aperiodic behaviour. This experiment

clearly demonstrates that the two samples synchronize immediately, i.e., within milliseconds, through the gas phase.

The mechanism for this gas phase communication can be explained simply by considering the steps of the Langmuir-Hinshelwood process under flow conditions. Under a limited flow rate, the pressure of the reactants can drop due to their consumption by the surface and conversion to CO_2. Under the experimental conditions which were chosen for these experiments, the CO pressure could change by as much as 10-20%. The oxygen pressure was 3 orders of magnitude higher.

Therefore, any fluctuations of p_{O_2} were negligible. If we consider a surface which is mostly covered by CO, the formation of a reactive region is followed by a slight drop in CO pressure.

Due to the consumption of CO in this area, a drop in CO pressure causes a reduction in the equilibrium coverage of CO in other islands. This allows in-phase transformation of other areas into reactive regions. Under molecular flow conditions, the CO pressure makes this adjustment in the system in less than a few milliseconds. This allows a rapid synchronization of various regions and oscillators.

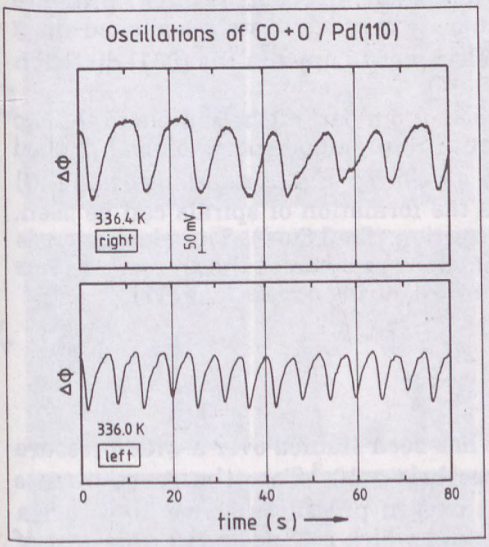

Figure 5. Oscillations under reduced coupling conditions. The right sample is driven by the left sample at one half of the driving frequency. ($p_{O_2} = 4 \cdot 10^{-2}$ Torr, $p_{CO} = 6.6 \cdot 10^{-5}$ Torr)

The gas phase communication can influence the oscillations mainly in two ways. First, a change in the flow rate can affect the amplitude and shape of oscillations. Second, a change in the coupling intensity between the two surfaces can give rise to a number of new phenomena which have been predicted for the homogeneous phase reactions. These phenomena are: *entrainment*, *enhancement*, *oscillator death* and *rhythmogenisis* [13-16].

Figure 4 shows that under strong coupling conditions, the two crystals behave as almost one sample. With a reduction in the coupling intensity the two oscillators oscillate with different frequencies. In this case, the slower oscillator is driven by the fast one (fig 5).

4. SPATIAL PATTERN FORMATIONS

Gas phase communication is not the only way to synchronize oscillations. Coupling of reaction and diffusion can give rise to travelling waves and spatial pattern formation, as has been recently shown for homogeneous and heterogeneous reaction systems [17, 18].

A photoemission electron microscope (PEEM) [19] was used to image the spatial structure resulting from differences in local work function. A UV source (deuterium lamp) with an energy of 6.9 eV was used to emit photoelectrons from the surface.

CO adsorption on Pd(110) causes a work function increase of approximately 1 eV. On the other hand, adsorption of oxygen increases the work function only by 500 to 700 meV. Therefore, regions covered with CO appear darker than oxygen-covered or "reactive" regions.

Figure 6.1a shows CO- and oxygen-covered regions existing for reaction conditions within the transition region. A reduction of CO pressure causes the disappearance of CO islands and the formation of oxygen islands. In figure 6.2a-d a time sequence is shown for which the rapid formation of oxygen islands can be seen especially well along the [1$\bar{1}$0] direction. For reaction conditions on the CO side close to the oscillatory region, a small reduction in CO pressure triggers reaction waves. These waves can be seen as white stripes aligned along the [1$\bar{1}$0] direction. They move with a velocity of 10 μm/s in the [001] direction (fig 6.2a-d).

Formation of waves travelling from the bottom part of the sample to the top can be seen in figure 6.3a-d. These waves are the upper parts of oval shaped rings (figures 6.4a-d)which travel with a velocity of 4 μm/s along the [1$\bar{1}$0] direction. For even lower CO pressures the formation of spirals can be seen, which are elongated along the [1$\bar{1}$0] direction (fig 6.5a-d). The elongation is caused by two different rates of diffusion along and across the troughs, as has been observed similarly on the Pt(110) surface during oscillations [17].

Conclusions

Oxidation of CO on a Pd(110) surface has been studied over a wide pressure range (10^{-6} to 10^{-1} Torr). For pressures below 10^{-3} Torr the reaction rate exhibits bistability and hysteresis. At oxygen pressures above 10^{-3} Torr,a reversal in the direction of hysteresis occurs which coincides with the start of oscillations. The nature of oscillations remains unchanged for pressure conditions approaching several Torr. The phase diagram for isothermal reaction conditions exhibits a characteristic cross-shaped feature and clearly shows that a relationship exists between the bistability phenomenon and oscillations on the Pd(110) surface. Furthermore, the phase diagram shows that the transformation of the steady state into the oscillatory region is caused under the influence of the formation and slow removal of subsurface oxygen (the feedback process).

The experiments with a grooved crystal and with two separated crystals show clearly that the synchronization process between various oscillatory

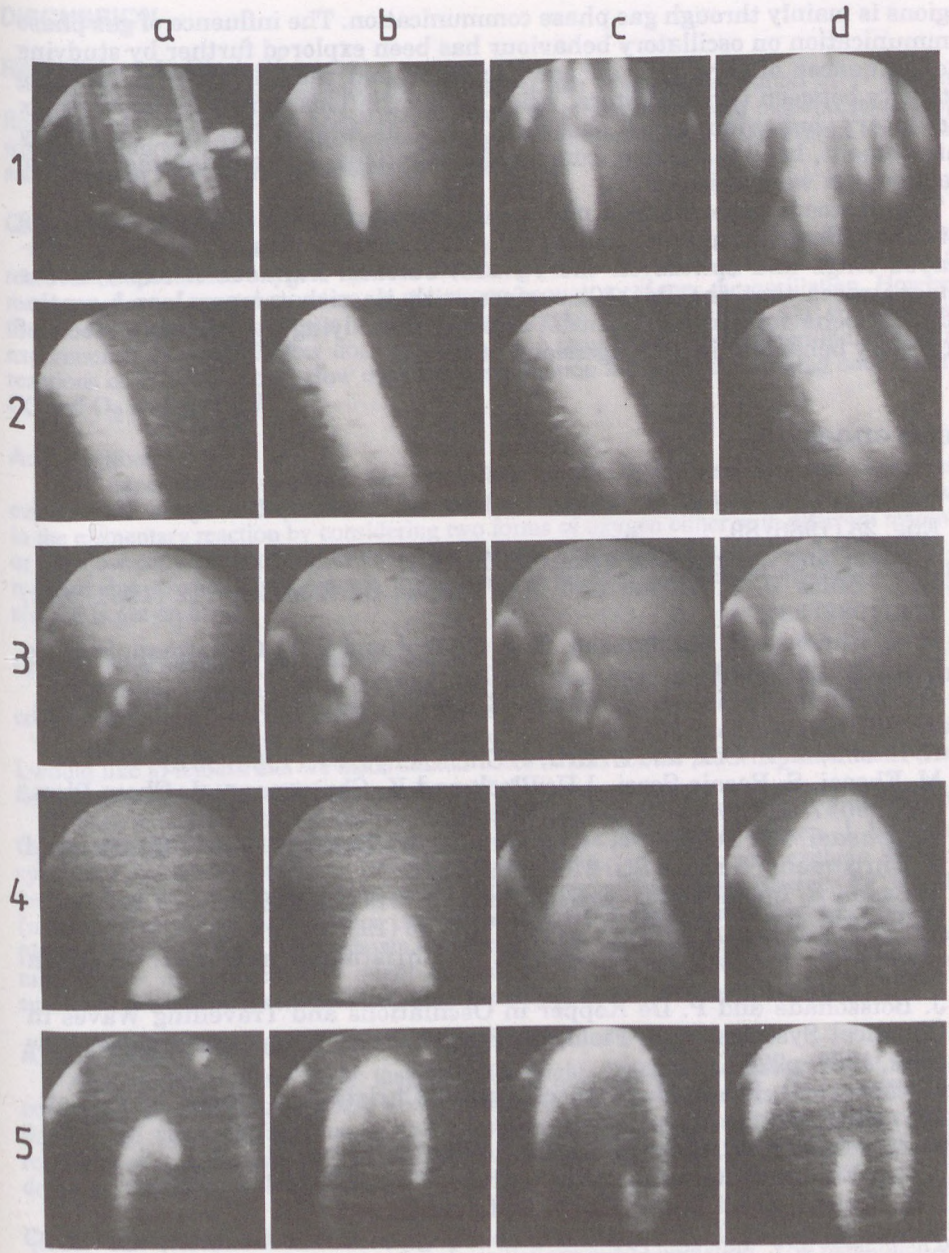

Figure 6. PEEM images of the Pd(110) surface during CO oxidation reaction. The diameter of the imaged area is 380 μm.
(pumping speed = 51 l/s, $p_{O_2} = 4 \cdot 10^{-3}$ Torr, $8 \cdot 10^{-7} < p_{CO} < 2 \cdot 10^{-6}$ Torr, T = 352.9 K)

regions is mainly through gas phase communication. The influence of gas phase communication on oscillatory behaviour has been explored further by studying the influences of flow rate on one oscillator and the variation of coupling intensity between two oscillators. When such variations were induced, complex oscillatory behaviour was observed such as phase locking, frequency entrainment, bead formation, composed oscillations, and enhancement of the reaction rate were observed.

The photoemission electron microscopy measurements show that coupling between diffusion and reaction leads to the formation of reaction waves, oval-shaped rings and spirals on the Pd(110) surface. This set of experiments demonstrates that the Pd(110) surface with its rich temporal and spatio-temporal behavior provides a model system for studying the various aspects of oscillatory behaviour in heterogeneous catalysis.

References

1 For a review see L. F. Razon and R. A. Schmitz, Catalysis Rev. Sci. Eng. 28 (1986) 89.
2 T. Engel and G. Ertl, Adv. Catal. 28 (1979) 1.
3 B. C. Sales, J. E. Turner and M.B. Maple, Surface Sci. 112 (1981) 272; 114 (1982) 381.
4 V. A. Burrows, S. Sundaresan, Y. J. Chabal and S. B. Christman, Surface Sci. 180 (1987) 110.
5 M. Eiswirth, P. Möller, K. Wetzel, R. Imbihl. and G. Ertl, J. Chem. Phys. 90 (1989) 510.
6 R. Imbihl, M. P. Cox, and G. Ertl, J. Chem. Phys. 84, (1986) 3519 .
7 M. Ehsasi, S. Rezaie-Serej, J.H. Block and K. Christmann, J. Chem Phys. 92 (1990) 7596.
8 M. Ehsasi, C. Seidel, H. Ruppender, W. Drachsel, J.H. Block and K. Christmann, Surface Sci. 210 (1989) L198.
9 S. Ladas, R. Imbihl and G. Ertl, Surface Sci. 219 (1989) 88.
10 M. Bassett and R. Imbihl., J. Chem. Phys. 93 (1990) 811.
11 M. Ehsasi. T. Rebitzki, M. Berdau, K. Christmann and J. H. Block, in preparation.
12 J. Boissonade and P. De Kepper in Oscillations and Travelling Waves in Chemical Systems, R. J. Field, M. Burger, Eds.; Wiley-Interscience: New York, 1985; p223.
13 M. Ehsasi, O. Frank, J. H. Block and K. Christmann, Chem. Phys. Lett. 165 (1990) 115.
14 M. Marek, I. Stuhl, Biophys. Chem. 3 (1975) 241.
15 K. Bar-Eli and S. Reuveni, J. Phys. Chem. 89 (1985) 1329.
16 I. R. Epstein, React. Kinet. Catal. Lett., 42 (1990) 241.
17 S. Jakubith, H. H. Rotermund, W. Engel, A. von Oertzen, G. Ertl, Phys. Rev. Lett. 65 (1990) 3013.
18 Y. Kuramoto, Chemical Oscillations, Waves and Turbulence, (Springer-Verlag, Berlin, 1984)

19 We are grateful to Dr. W. Engel for his assistance in the construction of the photoemission electron microscope.

DISCUSSION

Remark by J. H. Block (Germany)

The PEEM pictures presented by Dr. Ehsasi had a spatial resolution of ~~ 0.2 μm. Recently, oscillations of the CO-oxidation could be observed by field electron microscopy with a resolution of ~~ 2.0 nm. This new work by V. Gorodetskii, J. H. Block, M. Dradsil and M. Ehsasi is illustrated in a 300 s Video film.

Q: S. I. Woo (Korea)

One of your conclusions is that oscillatory behavior is caused by the formation and slow removal of subsurface oxygen, because the change of the O_2 sticking coefficient due to the reconstruction of crystal structure, is not strong enough to trigger the oscillation. However, the evidence for the existence of subsurface oxygen was not given. Do you have any experimental evidence ? How does this subsurface oxygen incorporate into the elementary reactions of CO oxidation ? How does the concentration influence the sticking coefficient of CO and O_2 on Pd(110) ?

A: J. H. Block

The experimental evidence for subsurface oxygen is indirect, deduced from static experiments. The slow formation of subsurface oxygen and its removal can be incorporated in the elementary reaction by considering two forms of oxygen either with different reactivity or the slow conversion of one to the other. The sticking probability of both, CO and O_2, are reduced due to subsurface oxygen formation, but direct experimental information for this surface is not on hand.

Q: B. E. Nieuwenhuys (The Netherlands)

The results shown are fascinating. For the first time the importance of gas phase communication for synchronization was demonstrated.

Concerning the oscillatory behavior found for the CO + O_2 reaction on a Pt field emitter I would like to remark that we made similar observations for the NO + H_2 reaction over a Rh field emitter. (M F H van Tol et al., to be published).

I have a question concerning the proposed mechanism of the oscillations found for CO + O_2 on Pd(110) involving formation and removal of subsurface oxygen. I have much sympathy for this mechanism. However, I am wondering if you can exclude the model proposed by Ertl et al. for CO + O_2 over Pt(100): a periodic transition between Pt(100) (1x1) (with relatively high activity) (or oxygen) and Pt(100) (5x1) (with low activity). In the plenary lecture of King it was shown that the Pd(110) surface is reconstructed by CO to the missing-row reconstruction. It might be that the non-reconstructed and the reconstructed surfaces have different activities for oxygen resulting in an oscillatory behavior.

A: J. H. Block

Although it is very likely that Pd(110) might undergo reconstruction at high CO coverages, the change or increase of the sticking probability for oxygen adsorption which is 0.9 for the clean surface due to reconstruction cannot significantly change the surface reactivity as it is the case with Pt(100) surface. Therefore, the reconstruction is not likely to dominate the oscillation mechanism.

Q: M. M. Bhasin (USA)

This is an excellent demonstration of oscillations in CO oxidation. You mentioned that it is done under isothermal conditions. The question is that it may be isothermal as you measured but is the temperature truly isothermal particularly in regions where oscillations are going on. As I recall R. Schmitz and his group had found large temperature differences on catalysts (otherwise isothermal) at substantially higher pressure than those employed in your work. Have you measured temperatures by some infrared imaging device to determine actual temperatures.

A: J. H. Block

No, we have not used infrared imaging of the surface temperature. Low pressure oscillations on single crystal surfaces are extremely sensitive to small temperature adjustment. Slight temperature change can cause the sample to leave the oscillatory region, on the other hand the amount of heat produced by the reaction is far less than the amount of heat which sample looses due to radiation. Also experiment performed at 260 K on Pt(210) where the heat production is 3 orders of magnitude less than 420 K oscillations are still observed.

Guczi, L. *et al.* (Editors), *New Frontiers in Catalysis*
Proceedings of the 10th International Congress on Catalysis, 19-24 July, 1992, Budapest, Hungary
© 1993 Elsevier Science Publishers B.V. All rights reserved

NATURE OF METAL-METAL BONDING IN MIXED METAL CATALYSTS

R. A. Campbell[a], *J. A. Rodriguez*[b] *and D. W. Goodman*[a]

[a]Department of Chemistry, Texas A&M University, College Station, TX 77843-3255, USA
[b]Chemistry Department, Brookhaven National Laboratory, Upton, NY 11973, USA

Abstract

The nature of the electronic and physical properties of ultrathin Cu and Pd films on Ta(110) have been studied using X-ray photoelectron spectroscopy (XPS) and temperature programmed desorption (TPD). The results indicate that monolayers of Cu and Pd on Ta(110) have lower electron densities than that measured for the surface atoms of Cu(100) and Pd(100), respectively. By comparison of the present results with those for other Cu, Ni and Pd films, correlations are found among the electronic perturbations of the monolayer films, the metal-substrate cohesive bond strength and the chemisorption properties of the monolayer films toward CO. A simple model is described to explain the direction and magnitude of the electronic perturbations. Surface electronegativity is defined and is found to be quite different from electronegativities in bulk alloys. The electronic state of the metal overlayer is determined to be an excellent indicator of the ability to chemisorb CO.

1. INTRODUCTION

The catalytic stability, selectivity and/or activity of a bimetallic catalyst are known in many cases to be superior to the anaolgous properties of a monometallic catalyst [1]. There has been much emphasis on understanding the changes that occur in the structural, electronic and chemical properties of catalysts upon the addition of the second metal through studies employing model catalysts [2-4]. The model catalysts are prepared in an ultrahigh vacuum (UHV) environment by vapor depositing a second metal onto a transition metal single-crystal substrate. These bimetallic systems then can be probed by a variety of surface science techniques or the UHV system can be coupled to an elevated pressure reactor for studying reaction kinetics [3].

As part of an effort to understand the physical and electronic properties responsible for the catalytic advantages of bimetallic systems, our laboratory has been involved in a systematic study of the properties of Pd, Ni and Cu films supported on transition metal substrates. In this paper we report the results for Pd and Cu ultrathin films on Ta(110). The physical and electronic properties of the metal films were studied

by X-ray photoelectron spectroscopy (XPS) and temperature programmed desorption (TPD).

By comparing the present results with those previously reported for Pd, Ni and Cu ultrathin films, we provide correlations for the chemical and electronic properties of bimetallic systems. The studies show correlations exist among the metal-substrate bond strengths, charge transfer between the overlayer and substrate, and the chemisorption properties of these systems. The results indicate that the cohesive metal-substrate bond strength is directly affected by charge transfer where there is a gain of electron density by the element initially having the greater fraction of empty states in its valence band. We present a qualitative determination of electronegativity at the surface which is found to differ greatly from that found for bulk electronegativities. It will also be shown that the electronic state of the bimetallic system is a very good indicator of its ability to chemisorb CO.

2. EXPERIMENTAL

A conventional UHV chamber with a base pressure of $\leq 4 \times 10^{-10}$ Torr was used for this work and is described in detail elsewhere [5]. The system was equipped with Auger electron spectroscopy (AES), XPS, low energy electron diffraction (LEED) and TPD capabilities.

Manipulator capabilities allowed for resistive heating to 1600K and liquid nitrogen cooling to 115K. An electron beam assembly allowed for flashing the sample to 2300K. The Ta(110) crystal was mounted by spotwelding to Ta support leads and the surface temperature was monitored by a W/5%Re-W/26%Re thermocouple spotwelded to the sample edge. The surface was cleaned by successive annealing cycles to 2500K. The cleanliness and long-range order were verified with AES, XPS and LEED.

Pd and Cu were evaporated onto the crystal surface at a substrate temperature of ~350K (unless stated otherwise) by resistively heating a W wire wrapped with high purity Pd or Cu wire. Following evaporation the surfaces were annealed to 500K to remove any contaminants, with no impurities detectable by AES or XPS. All adsorbate coverages are reported with respect to the number of Ta(110) surface atoms, 1.30×10^{15} atoms/cm^2, with one Cu (Pd) atom corresponding to $\theta_{Cu(Pd)} = 1.0$ ML. A linear heating rate of 10K/s was used in all the desorption experiments.

The Pd(3d), Cu(2p) and Ta(4f) XPS spectra in section 3 were obtained with an Al Kα X-ray source. The Pd($3d_{5/2}$) and Cu($2p_{3/2}$) binding energies were referenced against the Ta(4f) peak with an experimental error of ± 0.03 eV. Detection was normal to the surface in XPS and AES.

3. RESULTS

The desorption spectra of Cu (m/e=63) from the Ta(110) surface are shown in Fig. 1. The spectra are similar to other desorption spectra of Cu from single crystal substrates [6-10]. The feature at 1225-1325K is attributed to desorption of the first Cu monolayer. The low temperature feature at 1050-1225K, which displays a common leading edge and continues growing with increasing Cu coverage, is due to multilayer Cu

The results for the desorption of Pd monolayers from the Ta(110) surface have been previously reported [15]. These results indicate that the first monolayer of Pd on Ta(110) has an activation energy for desorption of 97 kcal/mol and a desorption temperature of 1540K. Pd films of greater than one monolayer exhibit TPD spectra with Pd desorption features both above and below the temperature observed for the Pd monolayer. These results are indicative of Pd dissolution into the Ta(110) substrate and alloy formation during TPD analysis. It was concluded that Pd multilayers, with the exception of the first layer, when heated to temperatures above 600K, form an alloy with the substrate.

In Fig. 2b the Pd($3d_{5/2}$) binding energy is plotted as a function of Pd coverage (monolayers). The binding energies of the Pd($3d_{5/2}$) peaks are measured after the Pd was deposited at a substrate temperature of ~350K with a subsequent anneal to 500K. The results are similar to those observed for the Cu/Ta(110) system. A constant Pd($3d_{5/2}$) binding energy of 336.25 eV is observed up to ~1 ML. Between 1 and 1.3 ML a slight increase in the binding energy is observed which is attributed to the relaxation of the first Pd monolayer [16]. At Pd coverages >1.3 ML, the binding energy decreases until a value of 335.60 eV is reached at ~20 ML. Pd coverages of <2.5 ML were calibrated using TPD area analysis and Pd(3d)/Ta(4f) XPS intensity ratios. The 20 ML Pd coverage was approximated by the attenuation of the Ta(4f) peak. Using the results described for the Pd monolayers [16,17] we find that a supported monolayer of Pd atoms on Ta(110) is perturbed +0.90 eV with respect to the surface atoms of Pd(100). These results are consistent with charge transfer from the Pd overlayer to the Ta(110) substrate.

4. DISCUSSION

The present XPS results as well as those previously reported [7,14,16-19] have shown that monolayers of Cu and Pd are electronically perturbed with respect to the surface atoms in the Cu and Pd (100) surfaces. In Fig. 3a the Cu($2p_{3/2}$) binding energy shift is shown, with respect to the Cu(100) surface atoms, for the $Cu_{1.0}$/Ta(110) system and for the $Cu_{1.0}$/Mo(110) [18], $Cu_{1.0}$/Re(0001) [7], $Cu_{1.0}$/Ru(0001) [14] and $Cu_{1.0}$/Rh(100) [14] systems. The results indicate that charge is transferred from the Cu overlayer to the substrate when the substrate has a valence d-band that is less than half occupied (Ta, Mo) with the perturbation increasing the less occupied the valence band. For substrates with a valence d-band more than half occupied (Ru, Rh) charge transfer from the substrate to the Cu overlayer is implied, with the perturbation increasing the more occupied the valence band. Little perturbation is observed for a valence band that is half occupied (Re).

A simple model has evolved to explain the direction and magnitude of the charge transfer in Cu overlayers. This model is explained taking into consideration orbital mixing: hybridization of the occupied states of metal A (electron rich) with the unoccupied levels of metal B (electron poor), leading to a loss of "A" character in the occupied states and thus a reduction in the electron density of metal A. In this model it is considered that Cu has a 4s valence band that is half occupied. Thus, when Cu is placed on a substrate that has a less than half occupied valence band (electron poor with respect the Cu 4s valence level) there is charge transfer from Cu overlayer to the substrate. Similarly, when the Cu monolayer is adsorbed onto a substrate with a valence

desorption. The Cu coverages in this section are calculated using TPD area analysis with saturation of the high temperature feature being defined as $\theta_{Cu} = 1.0$ ML.

The $Cu(2p_{3/2})$ peak position is plotted as a function of Cu coverage in monolayers in Fig. 2a. The Cu films were prepared by vapor depositing Cu onto the Ta(110) substrate at ~350K and then annealing to 500K. The $Cu(2p_{3/2})$ XPS spectra were then acquired with the resulting peak positions plotted in Fig. 2a. For submonolayer Cu coverages the $Cu(2p_{3/2})$ peak position remains at a constant binding energy of 933.03 ± 0.03 eV. The binding energy decreases to 932.90 eV at ~2 ML and remains constant with increasing Cu coverage.

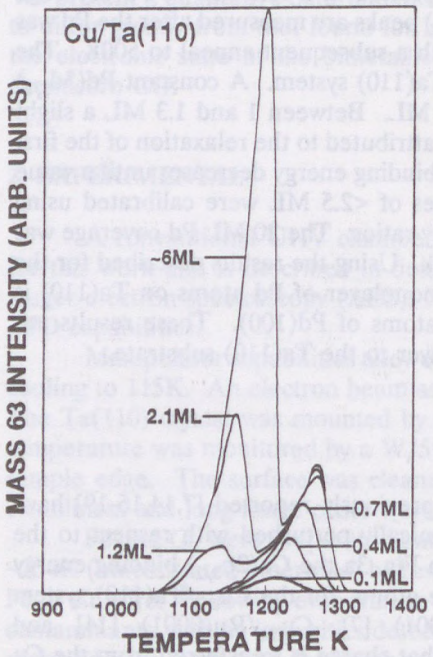

Figure 1. Temperature programmed desorption of Cu from Ta(110).

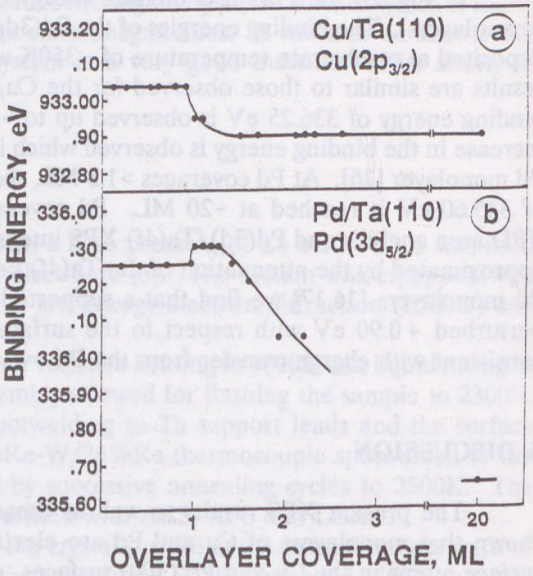

Figure 2. a) $Cu(2p_{3/2})$ binding energy as a function of Cu coverage on Ta(110). b) $Pd(3d_{5/2})$ binding energy as a function of Pd coverage on Ta(110).

The results from Fig. 2a indicate that atoms in a Cu monolayer supported on Ta(110) have a higher binding energy than bulk Cu atoms. This is quite different from the relative value of surface atoms compared to bulk atoms in a Cu(100) single crystal. Measurements indicate that the surface atoms have a $Cu(2p_{3/2})$ binding energy that is 0.22 eV below that found for bulk Cu atoms [11]. The difference in binding energy between bulk and surface atoms is a consequence of the surface atoms having a lower coordination number [12-13]. Using the method described in reference [14] the $Cu(2p_{3/2})$ peak position is shifted +0.30 eV with respect to the surface atoms of Cu(100). This result is consistent with charge transfer from the Cu overlayer to the Ta(110) substrate.

band that is more than half occupied (electron rich), Cu accepts charge from substrate. The magnitude of the perturbation increases (decreases) as the valence level of the substrate becomes less (more) occupied. When the substrate has a half occupied valence band there is no core-level perturbation predicted. This theory correctly explains the results in Fig. 3a.

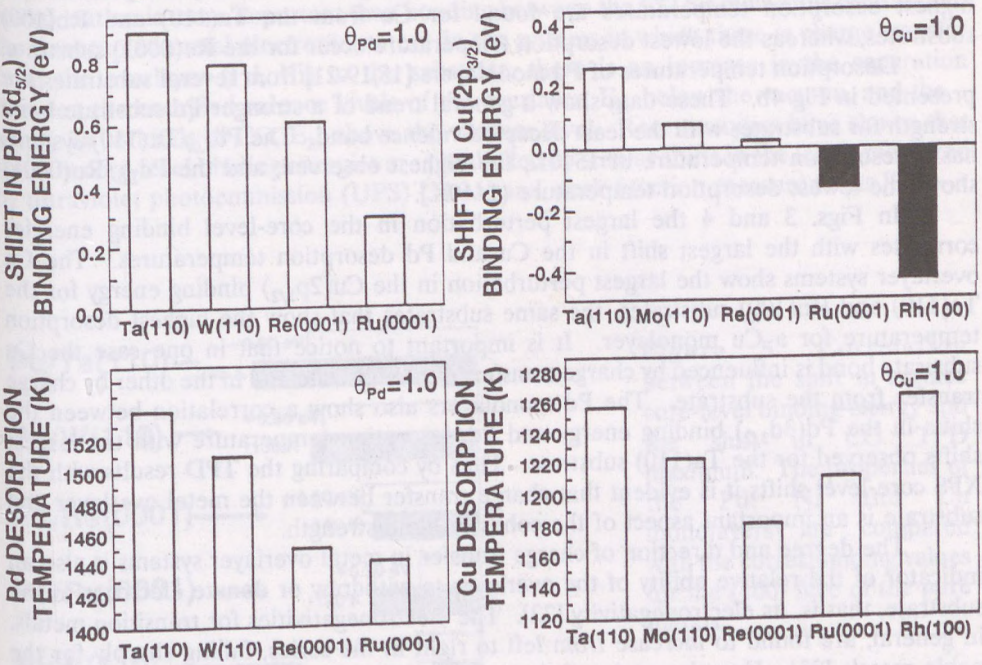

Figure 3. a) The $Cu(2p_{3/2})$ binding energy $Pd(3d_{3/2})$ shift relative to Cu(100) surface atoms for a Cu monolayer on several single crystal surfaces. b) Thermal desorption temperatures of a Cu monolayer from transition metal surfaces.

Figure 4. Shifts in the binding energy for monolayers of Pd on several substrates relative to the surface atoms of Pd(100). b) Thermal desorption temperature of Pd monolayers from several single crystal surfaces.

The results in Fig. 4a for the perturbation in the $Pd(3d_{5/2})$ binding energy, with respect to the surface atoms of Pd(100), for Pd monolayers [17,19] on several substrates indicate that in all cases there is charge transfer from the Pd overlayer to the substrate. The data also indicates that the magnitude of the perturbation decreases as the substrate "moves" to the right in the transition series. This result can be explained using our electron rich/electron poor model employed for the Cu overlayer systems. In this case Pd is always considered the electron rich metal since its valence d-band is more occupied than any of the substrates. Thus, as the electron density of the valence band increases (left to right in the transition series) the magnitude of the perturbation, from a loss of Pd electron density, decreases due to a reduced fraction of empty valence level in the substrate.

The desorption temperature of a Cu monolayer is a good qualitative indicator of its cohesive bond strength with the substrate. In Fig 3b. the desorption temperature for a monolayer of Cu from the Ta(110), Mo(110) [6], Re(0001) [7], Ru(0001) [8,9] and Rh(100) [10] substrates is presented. The strongest Cu-substrate bond strengths occur when the substrate is found at the extreme left or right in the transition series. The highest desorption temperatures are found for Cu from the Ta(110) and Rh(100) substrates, whereas the lowest desorption temperature occur for the Re(0001) substrate.

Desorption temperatures of Pd monolayers [15,19-21] from several substrates are presented in Fig 4b. These data show a general trend of a stronger Pd-substrate bond strength for substrates with the least occupied valence band. The $Pd_{1.0}$/Ta(110) systems has a desorption temperature of 1540K, the highest observed, and the $Pd_{1.0}$/Ru(0001) shows the lowest desorption temperature (1440K).

In Figs. 3 and 4 the largest perturbation in the core-level binding energies correlates with the largest shift in the Cu and Pd desorption temperatures. The Cu overlayer systems show the largest perturbation in the Cu($2p_{3/2}$) binding energy for the Ta(110) and Rh(100) substrates, the same substrates that show the highest desorption temperature for a Cu monolayer. It is important to notice that in one case the Cu substrate bond is influenced by charge transfer to the substrate and in the other by charge transfer from the substrate. The Pd monolayers also show a correlation between the shifts in the Pd($3d_{3/2}$) binding energy and Pd desorption temperature with the largest shifts observed for the Ta(110) substrate. Thus by comparing the TPD results with the XPS core-level shifts it is evident that charge transfer between the metal overlayer and substrate is an important aspect of the cohesive bond strength.

The degree and direction of charge transfer in metal overlayer systems is also an indicator of the relative ability of the overlayer to withdraw or donate electrons to the substrate, that is, its electronegativity [22]. The electronegativities for transition metals, in general, are found to increase from left to right in the series, falling sharply for the noble metals [23]. Experimental and theoretical results [24-27] indicate that for three dimensional alloys, involving Ta, W, Au and Pt, charge is expected to flow from the element on the left to the element on the right of the Periodic table. The charge transfer measured with XPS allows for the determination of the electronegativities of Cu, Pd and Ni monolayers with respect to the substrate. Qualitatively the electronegativities at the surface have been determined to be as follows: Ta(110) > W(110) > Mo(110) > Re(0001) ≈ Cu > Ru(0001) > Rh(100) > Ni > Pd, decreasing from left to right in the transition series. This general trend is exactly the opposite from that observed for bulk alloys.

The origin of these modified electronegativities is not clear; however, these results indicate that charge transfer at the surface cannot be accurately predicted using bulk electronegativities.

In addition to the perturbations observed for the electronic properties of model bimetallic systems, the chemical properties of the overlayer have also been found to be perturbed. For example, the desorption temperature of CO from the $Pd_{1.0}$/Ta(110) system [15] is found to be 235K below that observed for Pd(100). In Fig. 5 the shift in the CO desorption temperature for Cu, Ni and Pd monolayers is shown relative to the temperature measured for CO desorption from the corresponding (100) metal surfaces along with the shift in the core-level binding energies of the clean overlayers. It is noticed that for these systems there is a good qualitative correlation between the two sets

of data. This correlation is explained through the use of the Blyholder bonding model for CO to transition metals [28,29]. In this model we assume that the CO-metal bond is dominated by the donation of electron density from the occupied electronic states of the metal into the unoccupied CO $2\pi^*$ molecular orbitals (π backdonation). Recent theoretical [30-32] and inverse photoemmission [33] studies have shown that π backdonation is more important than bonding between the CO 5σ molecular orbitals and the unoccupied metal electronic states. In the systems in which there is charge transfer from the overlayer (Pd, Ni) to the substrate, there is an increase in the separation between the occupied valence levels of the overlayer, E_{vb} below the vacuum, and the empty $2\pi^*$ orbitals of CO, $E_{2\pi}$ above the vacuum level. Recent studies have shown that shifts in core-level binding energies are parallelled by similar shifts in the levels measured by ultraviolet photoemmission (UPS) [34,35] and work function measurements [36].

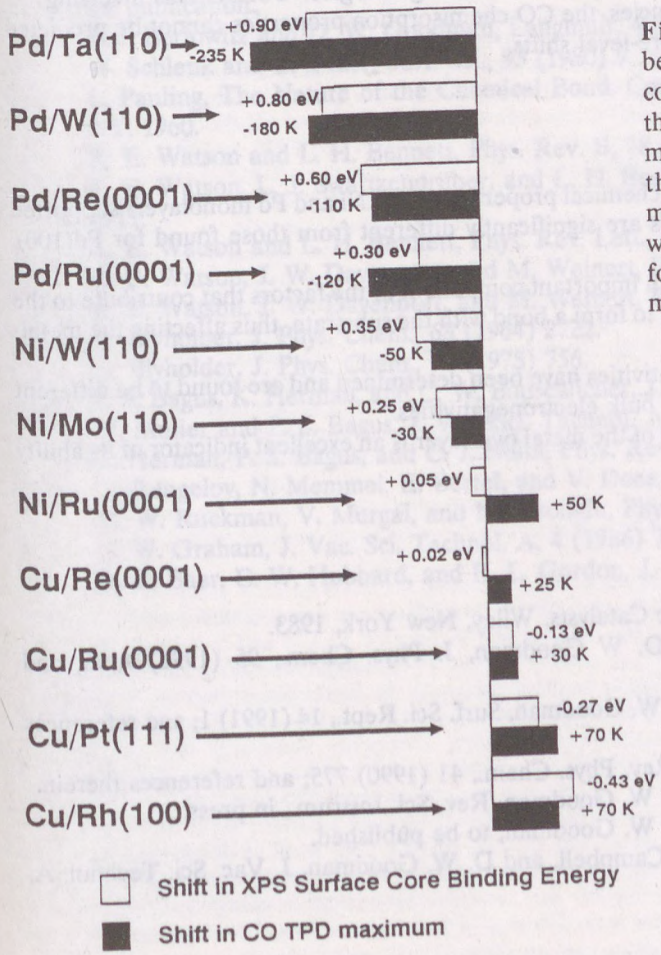

Figure 5. Correlation between the shift in surface core-level binding energy and the shift in CO TPD maximum. The properties of the Pd, Ni and Cu monolayers are compared with the corresponding values for the (100) face of the pure metals.

According to first order perturbation theory an increase in the $E_{2\pi}$-E_{vb} separation should lead to a decrease in the CO-metal bond strength. The data for Ni and Pd overlayers indicate that the largest perturbations in the core-level binding energies also show the largest decrease in the CO desorption temperatures. For the Cu overlayer cases in which the substrate donates charge to the Cu, the $E_{2\pi}$-E_{vb} separation is decreased, resulting in a stronger CO-Cu bond strength. These results indicate that the density of states near the Fermi level of the metal overlayer is, in general an excellent indicator of the ability to chemisorb CO.

In Fig. 5 the $Ni_{1.0}$/Ru(0001) and $Cu_{1.0}$/Re(0001) systems do not conform to the general trends. A reduction in the core-level binding energy is not accompanied by a reduction in the CO desorption temperature. Instead an increase in the CO desorption temperature is observed. These systems have approximately the same occupation levels in the valence band and thus the admetal-substrate interaction can affect the relative position and symmetry of the admetal valence levels in the absence of charge transfer and without significantly altering the core-level binding energies. For systems involving similar valence band occupancies, the CO chemisorption properties cannot be predicted simply from the observed core-level shifts.

5. CONCLUSIONS

1) The electronic and chemical properties of Cu, Ni and Pd monolayers supported on transition metal substrates are significantly different from those found for Pd(100), Ni(100) and Cu(100).

2) Charge transfer is an important component of the factors that contribute to the ability of the metal overlayers to form a bond with the substrate, thus affecting the metal-substrate bond strength.

3) Surface electronegativities have been determined and are found to be different from the results observed for bulk electronegativities.

4) The electronic state of the metal overlayer is an excellent indicator of its ability to chemisorb CO.

6. REFERENCES

1 J. H. Sinfelt, Bimetallic Catalysts, Wiley, New York, 1983.

2 J. A. Rodriguez and D. W Goodman, J. Phys. Chem., 95 (1991) 4196; and references therein.

3 J. A. Rodriguez and D. W. Goodman, Surf. Sci. Rept., 14 (1991) 1; and references therein.

4 C. T. Campbell, Ann. Rev. Phys. Chem., 41 (1990) 775; and references therein.

5 R. A. Campbell and D. W. Goodman, Rev. Sci. Instrum., in press.

6 R. A. Campbell and D. W. Goodman, to be published.

7 J. A. Rodriguez, R. A. Campbell, and D. W. Goodman, J. Vac. Sci. Technol. A, in press.

8 K. Christman, G. Ertl, and H. Shimuzu, J. Catal., 61 (1980) 397.
9 J. T. Yates, C. H. F. Peden, and D. W. Goodman, J. Catal., 94 (1985) 576.
10 X. Jiang and D. W. Goodman, Surf. Sci., 255 (1991) 1.
11 W. F. Egelhoff, Phys. Rev. B, 29 (1984) 4769.
12 D. E. Eastman, F. J. Himpsel, and J. F. van der Veen., J. Vac. Sci. Technol., 20 (1982) 609.
13 W. F. Egelhoff, Surf. Sci. Rept., 6 (1987) 253.
14 J. A. Rodriguez, R. A. Campbell, and D. W. Goodman, J. Phys. Chem., 95 (1991) 2477.
15 B. E. Koel, R. J. Smith and P. J. Berlowitz, Surf. Sci., 231 (1990) 325.
16 R. A. Campbell, W. K. Kuhn, and D. W. Goodman, to be published.
17 R. A. Campbell, J. A. Rodriguez, and D. W. Goodman, Surf. Sci., 240 (1990) 71.
18 J. A. Rodriguez, R. A. Campbell, and D. W. Goodman, J. Phys. Chem., 95 (1991) 5716.
19 R. A. Campbell, J. A. Rodriguez, and D. W. Goodman, J. Chem. Phys., submitted for publication.
20 P. J. Berlowitz and D. W. Goodman, Langmuir, 4 (1988) 1091.
21 W. Schlenk and E. Bauer, Surf. Sci., 93 (1980) 9.
22 L. Pauling, The Nature of the Chemical Bond, Cornell University Press, Ithica, NY, 1960.
23 R. E. Watson and L. H. Bennett, Phys. Rev. B, 18 (1978) 6439.
24 R. E. Watson, L. J. Swartzendruber, and L. H. Bennett, Phys. Rev. B, 24 (1981) 6211.
25 R. E. Watson and L. H. Bennett, Phys. Rev. Lett., 43 (1979) 1130.
26 R. E. Watson, J. W. Davenport, and M. Weinert, Phys. Rev. B, 35 (1987) 508.
27 R. E. Watson, J. W. Davenport, and M. Weinert, Phys. Rev. B, 36 (1987) 6396.
28 G. Blyholder, J. Phys. Chem., 68 (1964) 2722.
29 G. Blyholder, J. Phys. Chem., 79 (1975) 756.
30 P. S. Bagus, K. Herman, and C. W. Bauschlicher, J. Chem. Phys., 81 (1984) 1966.
31 W. Muller and P. S. Bagus, J. Vac. Sci. Technol. A, 3 (1985) 1623.
32 K. Herman, P. S. Bagus, and C. J. Nelin, Phys. Rev. B, 35 (1987) 9467.
33 G. Rangelov, N. Memmel, E. Bertel, and V. Dose, Surf. Sci., 251 (1991) 965.
34 M. W. Ruckman, V. Murgai, and M. Strongin, Phys. Rev. B, 34 (1986) 6759.
35 G. W. Graham, J. Vac. Sci. Technol. A, 4 (1986) 760.
36 D. R. Baer, C. W. Hubbard, and R. L. Gordon, J. Vac. Sci. Technol. A, in press.

DISCUSSION

Q: V. Ponec (The Netherlands)

Several very good theoretical papers calculated electron density contours for several monolayers, like Fe on W (or other similar combination). These maps do not indicate any charge transfer of importance. Even monolayers of alkali metals (and that is an extreme case) do not show an extended charge transfer. Why do you insist that you B.E. shifts (XPS data) prove an electron transfer? The shifts can be explained alternatively, for example, by other initial state effects, than charge transfer.

A: D. W. Goodman

Our theory is based on general trends observed for Cu, Ni and Pd films supported on several metal substrates. It explains in a simple and clear way all the existing experimental data. Reliable quantum-mechanical calculations that deal in a systematic way with the bimetallic surfaces in Figures 3, 4 and 5 have not been published. A detailed explanation for the correlations in Figures 3 and 4 will require the use of a theoretical method that is able to predict cohesive energies and charge distributions at a quantitative level.

It is well known that shifts in core-level binding energies can depend not only on charge-transfer processes but also on other phenomena. However, for the bimetallic systems investigated in this study, the magnitude and direction of the core-level shift are dominated by charge transfer effects. For example, in the case of Pd/Ta(110) the direction of charge transfer predicted by XPS agrees with the results of work function measurements, UPS, CO-FTIR, CO-HREELS and CO-TPD. In a similar way, XPS and all the other techniques indicate that the bond of Ni on W(110) is less ionic than that of Pd [1], and that Pd transfers more charge to W(110) than to Ru(0001) [2].

[1] J. A. Rodriguez and D. W. Goodman, *Surf. Sci.*, **257**, 897 (1992)
[2] R. A. Campbell et al., *Phys. Rev. B*, in press (1992)

Q: D. A. King (United Kingdom)

I am going to attempt to come between Vladimir and Wayne. To Vladimir, I would point out that recent interpretations of theoretical calculations for Cs on W surfaces at low coverages, suggesting that there is no charge transfer, are incorrect. The charge is transferred to the image plane between the ion and its image, according to the classical model: this happen to lie between Cs and W atoms, but this does not indicate covalency, as pointed out recently [3]. And to Wayne, I would point out that in the same paper we showed that you cannot interpret core level shift data in terms of charge transfer alone: final state (relaxation) and environmental contributions can be at least as big, and in some cases these various efforts are additive, but in others they can cancel each other out.

[3] Benesh and King, *Chem. Phys. Lett.* (1992)

A: D. W. Goodman

We cannot rule out that final-state effects contribute to the core-level shifts of the bimetallic surfaces. Nevertheless, the correlations in Figures 1, 3, 4 and 5 indicate that the core-level shifts are dominated by initial-state effects. Particularly interesting are the data for Cu/Rh(100) and Cu/Ta(110) in Figure 3a. The change in the direction of the core-level shift cannot be explained on the basis of final-state effects.

Q: H. Niemantsverdriet and R. van Santen (The Netherlands)

1) Binding energy shifts caused by alloying are relatively small, therefore we wonder if strain effects in the overlayer have an effect as well. If we take a surface layer of Pd on bulk Pd, as referenced, and attribute, for simplicity, the surface core level shift to the narrowed d-band and the resulting negative charge on the surface atoms, then stretching of the Pd surface layer narrows the d-band further and increases the negative charge on the surface atoms. Compression goes the other way. Do you have an idea about the magnitude of this "horizontal" contribution to the binding energy shifts of your metal layers.

2) Although we do not disagree that charge transfer is involved, to some extent, we are not sure that it is the only reason for the altered chemisorption of CO. It is well documented that interaction energies of adsorbed molecules with surfaces change with the geometry and the coordination of metal atoms in the surface. Strain effects alter the local geometry of the overlayer atoms from substrate to substrate. It seems to us that your interpretation in terms of changes in electron donation properties is too simple, as structural and electronic effects are inseparable.

A: D. W. Goodman

1) According to your hypothesis stretching of the Pd surface layer should increase the negative charge on the surface atoms, moving their core-levels to lower binding energy. The experimental results show a different trend. A pseudomorphic monolayer of Pd on Ta(110) has a lower atomic density and a higher Pd $3d_{5/2}$ binding energy than the surface layer of Pd(111) or Pd(100). The "strain effect" also cannot explain the data in Figure 3a. for Cu/Rh(100) and Cu/Ta(110). The surface atomic densities of Cu/Rh(100) and Cu/Ta(110) are both much smaller than that of Cu(100), but the direction of the core-level shift is different in each case. The "strain effect" plays a role in the properties of a metal overlayer, but in many bimetallic systems, the importance of this effect is secondary when compared to that of charge transfer [1].

2) The "strain effect" cannot explain the CO chemisorption properties of Pd and Ni overlayers [4]. For monometallic surfaces, it is well established that the strength of the metal-CO bond increases when the atomic density of the surface decreases. Thus, strained overlayers should show an increase in the strength of the metal-CO bond. However, a monolayer of Pd on Ta(110) or W(110) has a smaller surface-atomic density and CO desorption temperature than those of Pd(111). The effects of stretching the Pd atoms are overcome by those of charge transfer from Pd to the Ta or W substrate. The Pd-Pd separation in Pd/Re(0001) is almost identical to that of Pd(111), nevertheless, the supported Pd monolayer shows a decrease of ~100 K in the CO desorption temperature. This change in the chemical properties cannot be attributed to structural differences.

[2] R. A. Campbell et al., *Surf. Sci.*, **240**, 71 (1992)

Q: W. Grünert (Germany)

1) The electron transfer reported by you should be also reflected in the structure of the conductive bands of your systems. Have you performed UPS with your systems ?

2) What is the reason for the intermediate increase of the Pd FWHM when you build up a system with many monolayers of Pd on you system ?

A: D. W. Goodman

1) UPS results indicate that the shifts in the core-levels track the shifts in the valence levels [1]

2) For systems with medium Pd coverages, the convolution of electron emissions from the metal-metal interface and top layers is responsible for the increase in the FWMH.

Q: D. Chadwick (United Kingdom)

Many of the metals used in your study have loss features associated with their photoelectron peaks in a metal-metal system with significant metal-metal bonding, one might expect the loss processes associated with on component to be weakly excited in the photoelectron spectrum of the other component. Have you attempted to study the loss features in the photoelectron spectra ?

A: D. W. Goodman

This is an interesting point and indeed may well be the case; however, we have not carried out these kinds of experiments.

Q: J. C. Bertolini (France)

You show a nice correlation between the upward shift of Pd core levels (for Pd deposited on metals) and the CO bond strength. But, with respect to particle size effect it is exactly the contrary (i.e. for very small sizes the Pd 3d levels shift upwards while the CO bond strength is increased). Can you comment on that ?

A: D. W. Goodman

We are not familiar with the details of the experiments to which you refer for very small Pd particles. The comparison of photoemission results for a solid and a small particle is not a trivial task due to changes in the screening of the core-hole. In a solid metal, the electron screening of the core-hole is much more effective than in a small metal particle, and as a consequence the core levels of a solid should appear at a lower binding energy than those of a particle. Thus, it is not surprising that uncoordinated atoms of very small Pd particles have a higher Pd 3d binding energy and a stronger metal-CO bond than the atoms of solid Pd.

Q: D. Wang (China)

What is the "degree of applicability" of your developed model of metal-metal interaction to the case of supported bimetallics of very small particle size? In particular, please comment with reference to the difference between your models of mixed metals where the individual components are in separate phases and bimetallics in the form of small particles where the individual components are well-mixed [5].

[5] J. H. Sinfelt, *Bimetallic Catalysts*, Wiley, New York, (1983)

A: D. W. Goodman

After comparing our results for bimetallic surfaces with those reported in the literature for bulk three-dimensional alloys, we have found important differences in the direction of the charge transfer between metals [1]. The nature of a heteronuclear metal-metal bond depends strongly on the geometry of the system. Bimetallic systems involve species with similar electron donor-electron acceptor properties, and the subtle balance that determines the flow of charge transfer between elements can be easily affected by changes in the coordination number or in the geometrical arrangement of the atoms. In principle, data for bimetallic surfaces or bulk alloys should be extrapolated with caution when predicting the behavior of small particles.

Guczi, L. *et al.* (Editors), *New Frontiers in Catalysis*
Proceedings of the 10th International Congress on Catalysis, 19-24 July, 1992, Budapest, Hungary
© 1993 Elsevier Science Publishers B.V. All rights reserved

THE REDUCTION OF NITRIC OXIDE BY HYDROGEN OVER Pt, Rh AND Pt-Rh SINGLE CRYSTAL SURFACES

H. Hirano[a], *T. Yamada*[a], *K. I. Tanaka*[a], *J. Siera*[b] *and B. E. Nieuwenhuys*[b]

[a]The Institute for Solid State Physics, University of Tokyo, 7-22-1 Roppongi, Minato-ku, Tokyo 106, Japan
[b]Gorlaeus Laboratories, Leiden University, P.O.Box 9502, 2300 RA Leiden, The Netherlands

ABSTRACT

The reduction of NO by hydrogen has been studied over $Pt_{0.25}$ - $Rh_{0.75}$ (100), (111), (410), Rh(100) and Pt(100) single crystal surfaces in the 10 mbar range. The surfaces were analysed using AES and LEED. Both the activity expressed as conversion after a constant reaction time and selectivity depend strongly on the surface structure and composition. The activity for the (100) surfaces decreases in the order Pt(100) ≥ Pt-Rh(100) > Rh(100). The activity of pure Rh is drastically enhanced by alloying with 25% Pt. The selectivity towards N_2 for the (100) surfaces decreases in the order Rh(100) > Pt-Rh(100) > Pt(100) at a temperature of 575K and Rh(100) > Pt(100) > Pt-Rh(100) at 520K . The activity for the alloy surfaces decreases in the order Pt-Rh(100) > Pt-Rh(410) > Pt-Rh(111), and the selectivity towards N_2 formation decreases in the order Pt-Rh(410) > Pt-Rh(100) > Pt-Rh(111), at 520K and 575K. The differences in selectivity and activity can be understood on the basis of the relative concentrations of N, NO and H on the various surfaces.

INTRODUCTION

The catalytic reduction of NO by hydrogen is of great importance for the emission control of automotive exhaust gases [1]. Reduction of NO with H_2 may produce several N-containing products such as N_2, NH_3 and N_2O. The formation of NH_3 and N_2O is undesired and catalysts favouring N_2 as a major reaction product are required. The noble metals Rh and Ru are very efficient for this purpose [1]. Metals like Pt and Pd, on the other hand, favour under certain conditions the reaction pathway which leads to the formation of NH_3 in large quantities [1]. More information is needed on the factors determining the large differences in the selectivity of the NO-H_2 reaction over different metals and surfaces structures. Previously, it was

found that the selectivity may be determined by the relative concentrations of NO, N and H distributed over the catalyst surface [2,3]. Nitrogen adatoms formed on a Pt-Rh(100) [3,4] or a Rh(100) [5] surface are easily hydrogenated at 400-450K, resulting in the formation of NH_{ads}. Dinitrogen can be formed in a large temperature range provided that sufficient N atoms are available. Below 600K, the main contribution to the formation of N_2 over the Pt-Rh(100) surface occurs via the reaction $NO_{ads} + N_{ads} \rightarrow N_2 + O_{ads}$. In this work, the reduction of NO by hydrogen was studied over the (111), (100) and (410) surfaces of a $Pt_{0.25}$-$Rh_{0.75}$ single crystal and the pure Pt(100) and Rh(100) single crystal surfaces. The purpose of this paper is to establish the effects of the surface structure and alloying on the kinetics and selectivity of the NO-H_2 reaction. A comparison between pure Pt(100) and Rh(100) on the one hand, and Pt-Rh(100) on the other, provides the information needed to understand the effect of alloying.

Kinetic results

In fig.1 the formation rates of NH_3, N_2 and N_2O over the Pt(100) surface are shown versus reaction time at two selected temperatures, 520K and 575K.

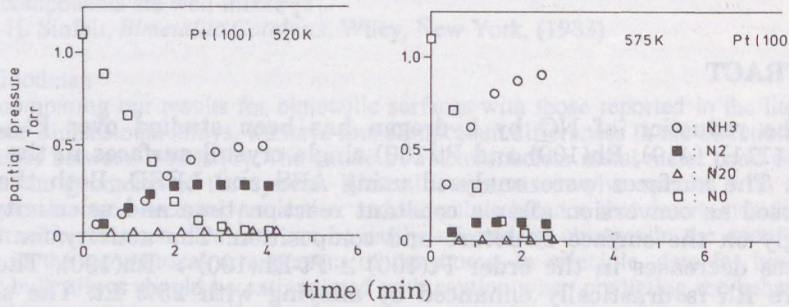

Figure 1 Formation of N_2, NH_3 and N_2O over Pt(100) (1x1).

The reaction was performed in a batch reactor at a total pressure of 6 mbar with a NO/H_2 ratio of 1 to 5. For details, concerning the experimental equipment we refer to previous papers [2-4]. The NO consumption indicates that the reaction of NO with H_2 proceeds relatively easy at both temperatures. Nitric oxide is converted into N_2 and NH_3 in comparable amounts at 520K. On the other hand, more NH_3 is formed at 575K. The formation of N_2O was below the limit of detection at both temperatures. The formation rates of N_2, NH_3 and N_2O over Rh(100), under identical conditions as described for Pt(100), are shown in fig.2. The conversion of nitric oxide over the Rh(100) surface proceeds much slower than over the Pt(100) surface. The reaction is very slow at 520K and the detection of products is difficult. Although formed in minor concentrations N_2 was the only reaction product detected. At 575K, the conversion of nitric oxide has increased drastically and detection of products is easily accomplished. The main product is still N_2, although the contribution of N_2O is significant. The formation of NH_3 was below the limit of detection, even at high conversions of nitric oxide. At 575K, total NO conversion is reached after 20 min. of reaction time.

The results obtained on Pt-Rh(100) are shown in fig.3. The reduction of nitric oxide by hydrogen proceeds relatively easy at 520K and 575K. The activity of this surface is only slightly smaller than that of the Pt(100)

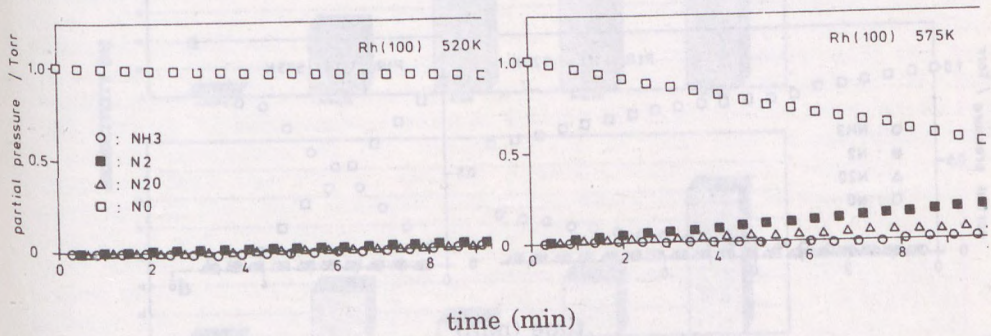

Figure 2
Formation of N_2, NH_3 and N_2O over Rh(100).

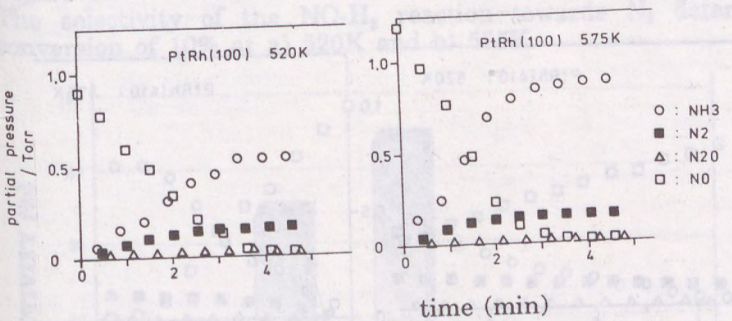

Figure 3
Formation of N_2, NH_3 and N_2O over Pt-Rh(100).

surface. N_2 and NH_3 are the products which are formed in detectable concentrations. A remarkable observation is that that the selectivity towards N_2 at 520K is higher over the Pt(100) surface than over the Pt-Rh(100) surface. Although Rh(100) has the higher selectivity towards N_2, alloying Pt(100) with Rh, lowers the selectivity towards N_2. These differences in selectivity towards N_2 are small but reversed at 575K.

The results obtained on Pt-Rh(111) are shown in fig.4. The only reaction product formed over this surface is NH_3, and the formation rates of N_2 and N_2O are below the limit of detection at 520K and 575K, even after long periods of reaction time. The conversion of NO is relatively slow compared with the Pt(100) and Pt-Rh(100) surfaces. The reaction rate increases rapidly when the temperature is raised to 575K. Total NO conversion at this temperature is reached after 5 min. Fig.5 shows the results obtained over the Pt-Rh(410) surface. The reaction products formed are N_2 and NH_3. The NO conversion is slower than over the Pt(100) and Pt-Rh(100) surfaces but

higher than over the Pt-Rh(111) surface. The selectivity towards N_2 is relatively high, a higher selectivity towards N_2 is only observed over the Rh(100) surface.

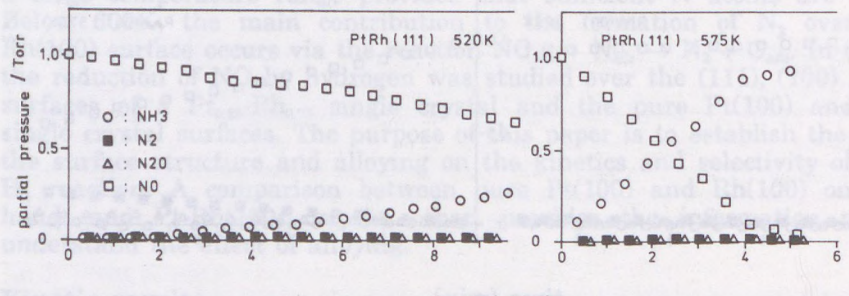

Figure 4
Formation of N_2, NH_3 and N_2O over Pt-Rh(111).

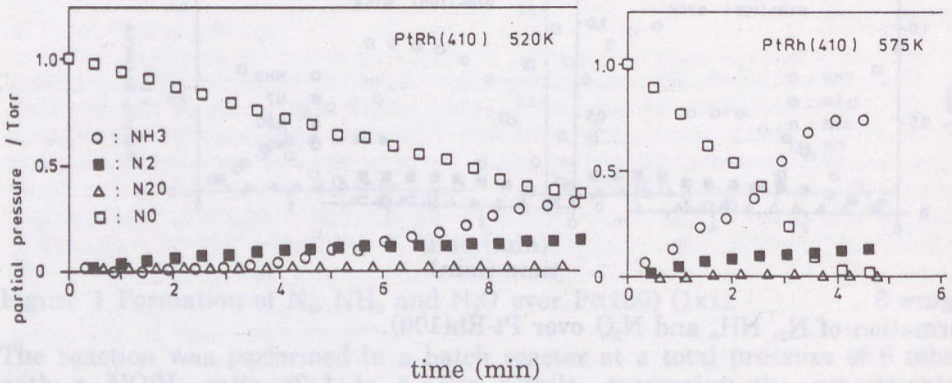

Figure 5
Formation of N_2, NH_3 and N_2O over Pt-Rh(410).

The results for the selectivity and activity expressed as conversion after a constant reaction time of the NO-H_2 reaction for the various surfaces are summarised in fig's 6 and 7, respectively. The selectivities towards N_2 determined at a total NO conversion of 10% are shown in fig.'s 6a and 6b for 520 and 575K, respectively. Large differences exist in the selectivities towards N_2 for the various surfaces. It ranges from 0% over the Pt-Rh(111) surface to 100% over Rh(100) at 520K. The conversion after 3 minutes of reaction time varies from 5% over the Rh(100) surface to 90% over the Pt(100) surface at 520K. It should be noted that the activity for all the surfaces shown in fig. 7 are expressed as conversion measured after 3 minutes of reaction time.

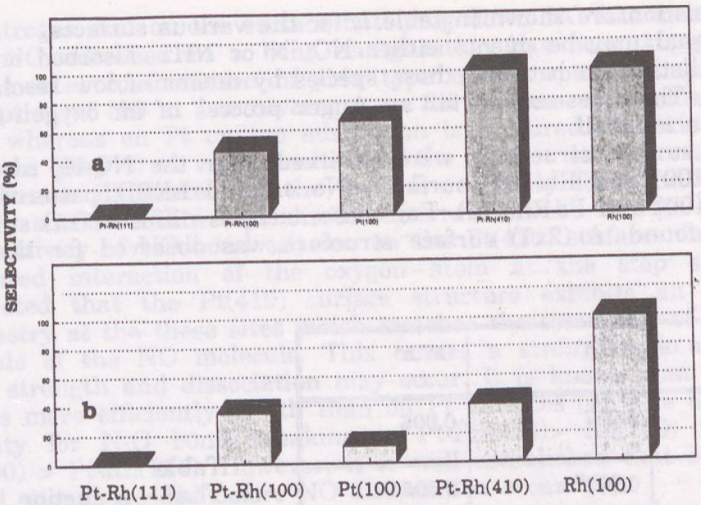

Figure 6
The selectivity of the NO-H_2 reaction towards N_2 determined at a total conversion of 10% at a) 520K and b) 575K.

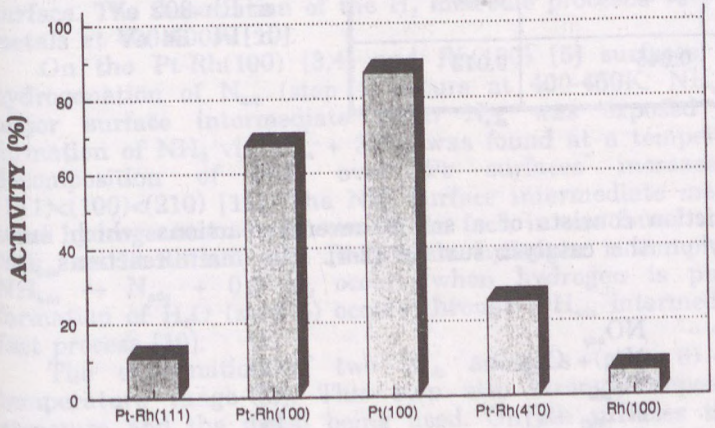

Figure 7
The NO conversion after 3 minutes of reaction time at 520K.

Spectroscopic results - After the reaction was stopped, the reactor was evacuated and the sample was transferred to the UHV chamber for spectroscopic analysis by AES and LEED. It should be noted that the information concerning the physical and chemical state of the surfaces is obtained after the reaction was stopped and the surface composition and structure may not be the same as under the reaction conditions. However, as will be shown further on, the AES and LEED results provide useful additional information which may lead to a better understanding of the processes taking place on the various surfaces.

AES - The N_{380eV} and O_{510eV} AES signal intensities normalised by the proper

metal AES transistion are shown in table I, for the various surfaces. The nitrogen signal may be due to either NO, N or NHx adsorbed on the surface and no distinction between these species by means of low resolution AES is possible. The cross-section for an Auger process of an oxygen atom bound to nitrogen is small.

LEED - C(2x2) surface structures were observed after the NO-H_2 reaction over the Pt-Rh(100) and Rh(100) surfaces. No ordered LEED patterns are observed for Pt(100) and Pt-Rh(111). For these surfaces diffuse (1x1) surface structures were found. A (2x1) surface structure was observed for the Pt-Rh(410) surface.

Surface	N/Rh[a]	O/Rh[a]
Pt-Rh(111)	0.057	0.006
Pt(100)	0.013[b]	0.0055[b]
Pt-Rh(100)	0.038	0.055
Pt-Rh(410)	0.065	0.035
Rh(410)	0.045	0.012

Table I
The reduction of nitric oxide by hydrogen over Pt, Rh and Pt-Rh single crystal surfaces.
a: Rh 302 eV
b: Pt 64 eV

DISCUSSION

The NO-H_2 reduction consists of a set of several reactions which may occur simultaneously on the catalyst surface [2-4]. The main reactions are displayed below.

$$NO_{(g)} + [] \rightarrow NO_{ads} \quad (1)$$
$$NO_{ads} + [] \rightarrow N_{ads} + O_{ads} \quad (2)$$
$$H_{2(g)} + [] \rightarrow 2H_{ads} \quad (3)$$
$$N_{ads} + 3H_{ads} \rightarrow NH_{3(g)} + [] \quad (4)$$
$$O_{ads} + 2H_{ads} \rightarrow H_2O_{(g)} + [] \quad (5)$$
$$N_{ads} + N_{ads} \rightarrow N_{2(g)} + [] \quad (6)$$
$$NO_{ads} + N_{ads} \rightarrow N_{2(g)} + O_{ads} + [] \quad (7)$$
$$NO_{ads} + N_{ads} \rightarrow N_2O_{(g)} + [] \quad (8)$$

(where [] stands for surface vacancy or vacancies)

Each of these steps may have a different rate of reaction over the various surfaces. In the next section a brief description is given of the various steps according to the literature.

The adsorption of NO at room temperature (step 1) occurs with a high sticking probability on Pt and Rh surfaces. Several adsorbed complexes have been reported, including on top and bridged [6]. Usually, NO adsorbs with

the nitrogen end on the surface but lying down NO has also been reported. Also, NO adsorbed in a bent configuration has been suggested, although experimental confirmation of this type of adsorption complex is difficult. Adsorption of NO at low coverages on Rh surfaces occurs mainly on bridged sites, whereas on Pt on top adsorption is favoured. Dissociation of the NO molecule (step 2) is very sensitive to the surface structure and composition [7]. This is illustrated by the very low activity for bond scission on the Pt(111) surface and a high dissociation rate on the Pt(410) surface [8]. The high activity of NO bond scission on the Pt(410) surface may be due to an enhanced interaction of the oxygen atom at the step sites. Masel [8] suggested that the Pt(410) surface structure exhibits an electron orbital symmetry at the these sites which matches the symmetry of the antibonding orbitals of the NO molecule. This causes a strong weakening of the N-O bond strength and dissociation may occur. It is known that NO dissociation occurs more efficiently on Rh than on Pt surfaces [7]. The order in intrinsic activity for N-O bond breaking is Pt-Rh(410)> Rh(100) > Pt-Rh(100) > Pt(100) > Pt-Rh(111). However, it is well established that a number of free metal sites is needed before NO dissociation occurs [9].

The adsorption of the H_2 molecule (step 3) proceeds with a relatively low sticking probablity on Pt and Rh surfaces at 400-500K. The sticking probability of hydrogen depends on the surface structure. On the Pt(100) surface a higher sticking probability is measured than on the Pt(111) surface. The dissociation of the H_2 molecule proceeds very fast on group VIII metals at 400-500K [10].

On the Pt-Rh(100) [3,4] and Rh(100) [5] surfaces it was found that hydrogenation of N_{ads} (step 4) occurs at 400-450K. NH_{ads} was found as a major surface intermediate when N_{ads} was exposed to hydrogen. The formation of NH_3 via $N_{ads} + 3H_{ads}$ was found at a temperature of 450K. The decomposition of NH_3 over Pt surfaces increases in the order (111)<(100)<(210) [11]. The NH_x surface intermediate may decompose before total hydrogenation has occurred. In fact, it was found that the formation of NH_{ads} on Pt-Rh(100) and Rh(100) in hydrogen is completely reversible and $NH_{ads} \rightarrow N_{ads} + 0.5\ H_2$ occurs when hydrogen is pumped off [4]. The formation of H_2O (step 5) occurs through OH_{ads} intermediates and is a very fast process [10].

The combination of two N_{ads} adatoms (step 6) occurs in a wide temperature range [3]. This step also strongly depends on the surface structure and the metal being used. On Rh surfaces the metal-N bond is stronger than on the corresponding Pt surfaces. The metal-N bond strength increases in the order (111) < (100). In contrast to the Pt(100) surface where this step occurs almost instantaneously at the reaction temperatures considered, build-up of N_{ads} takes place on the Rh(100), Pt-Rh(100) and Pt-Rh(410) surfaces.

The $NO_{ads} + N_{ads}$ reaction can give $N_{2(g)} + O_{ads}$ or $N_2O_{(g)}$ via steps 7 and 8, respectively. On Pt-Rh(100) it was found that step 7 is a main route through which $N_{2(g)}$ is formed in the temperature range below 600K [3]. At higher temperatures step 6 is the dominant mechanism for N_2 formation. Little is known about the specific contributions of steps 7 or 8 over Pt and Rh surfaces.

Based on the kinetic and spectroscopic results described in this paper a

model is proposed for the plane to plane variation of the selectivity and activity of the NO-H_2 reaction over the Pt,Rh and Pt-Rh alloy surfaces.

As shown in fig.6 the selectivity of the NO-H_2 reaction for N_2 varies between 0 and 100% after 10% NO conversion. The NO conversion after 3 min. of reaction time as displayed in fig 7 varies between 5 and 90%. A low conversion over Pt-Rh(111) is observed in combination with a high selectivity towards NH_3 (≈100%). It is known that dissociation of NO is slow over the Pt-(111) surface, and that the behaviour of Pt-Rh alloy surfaces towards NO dissociation displays a Pt-like behaviour at high NO coverages. The high normalised N_{380eV} AES signal intensity on Pt-Rh(111) observed by AES is ,therefore, assigned to molecularly adsorbed NO. The Pt-Rh(111) surface will be covered mainly by NO under reaction conditions and the coverages of N_{ads} and O_{ads}, are small. This is also supported by the low normalised O_{510eV} signal intensity. Only NH_3 is formed as a product. The NH_3 molecule may be formed through process 4 as over Pt-Rh(100) or via an [NOH] intermediate. Gorodetskii [12], reported the formation of [NOH] on Pt. However, the [NOH] intermediate was found to be unstable at temperatures higher than 400K. The formation of NH_3 is favoured over the formation of N_2O or N_2. No ordered LEED structures were observed on Pt-Rh(111), indicating that the NO molecules do not form large ordered islands. Thus, for the Pt-Rh(111) surface it is assumed that step (2) occurs relatively slow, and the O_{ads} and N_{ads} react to H_2O and NH_3 through steps (5) and (4), respectively. N-N combination is unlikely due to the low concentration of N_{ads}. The formation of N_2 and N_2O is below the limit of detection, indicating that steps (7) and (8) do not take place at a detectable rate.

The conversion of NO over the Pt-Rh(100) surface after 3 min. reaction time at 520K is almost 70% and the selectivity towards N_2 is 32%. The normalised N_{380eV} AES signal intensity is 0.038 and for the O_{510eV} normalised signal intensity a value of 0.055 has been found. By EELS it was found that the N_{380eV} signal intensity is caused by nitrogen atoms [4]. This surface may be covered by a small amount of NO_{ads}, and a larger amount of O_{ads} and N_{ads}. Also H_{ads} which is not detectable by means of AES may be present on the surface. A c(2x2) surface structure is observed by means of LEED. Both O_{ads} and N_{ads} form a c(2x2) surface structure on the Pt-Rh(100) surface. However, the LEED pattern as observed after the NO-H_2 reaction resembles the pattern observed for the Pt-Rh c(2x2)-N surface structure. Islands of N adatoms may facilitate the formation of N_2 via step 6. The large O_{510eV} signal could be partly due to the formation of subsurface oxygen. Thus, for this surface NO dissociation occurs easily and the formation of N_2 through step 6 has increased. The high activity indicates that free sites remain available during the reaction. These sites probably consists of Pt atoms since the Rh atoms may be covered by N_{ads}.

Over Pt(100) the highest conversion was observed and the selectivity towards N_2 is 60% at 520K. The dissociation of NO over Pt(100) proceeds easily provided that vacancies are available. Since steps 4,5,6, and most likely also step 7 are fast these free sites remain available during the course of the reaction. This is supported by the low N_{380eV} and O_{510eV} signal intensities. The N_{380eV} signal intensity is partly due to the Pt_{382eV} peak. The Pt(100) surface exhibits a higher selectivity towards N_2, than the Pt-Rh(100) alloy surface at 520K. Pure Rh, however, has a higher selectivity towards N_2

than pure Pt. This may be explained by an effect of strongly bound nitrogen atoms on the rhodium atoms surrounding the platinum atoms. At 520K, the nitrogen atoms adsorbed on Rh sites are strongly bound to the surface and the formation of N_2 is slow. If an NO molecule dissociates on Pt sites, the nitrogen atoms may be surrounded by a matrix of strongly bound nitrogen atoms on Rh sites. The formation of N_2 will be slow at this temperature and the subsequent hydrogenation of this N-atom on the Pt-site can occur. On Pt(100), the nitrogen atom may recombine with NO, or N on other neighbouring Pt-sites forming N_2 or N_2O and N_2 respectively. The formation of NH_3 through $N_{ads} + H_{ads}$, over "isolated" Pt-sites is reduced. This explains the enhanced NH_3 production over the Pt-Rh(100) alloy surface at 520K in comparison with pure Pt(100). The high conversion of NO over the Pt-Rh(100) and Pt(100) surfaces is explained by the intrinsic high NO dissociation activity combined with the relatively low M-N bond strength on platinum which prevents that the reaction is inhibited by blocking of active sites by N_{ads}. At 575K, the selectivity towards N_2 over the Pt-Rh(100) surface is higher than over the Pt(100) surface. At this temperature the enhancement of the N_2 production over Pt-Rh(100) may be ascribed to N-N combination from sites containing few or more Rh atoms. The N_2 production over the Rh(100) surface is observed at 575K.

The selectivity towards N_2 and the activity over Pt-Rh(410) at 520K are 100% and 20%, respectively. The value for the selectivity towards N_2 is 40% at 575K. It is known that the dissociation of NO proceeds relatively easy on this surface and a high concentration of nitrogen is found by means of N_2 TDS. The nitrogen atoms adsorbed at the steps of the single crystal surface have an enhanced adsorption energy. The activity will decrease due to the higher number of metal sites which are occupied by strongly bound nitrogen. This is illustrated by the relatively low conversion of NO over the Pt-Rh(410) surface. The value for the normalised N_{380eV} signal intensity is 0.065, the largest found in this study. These nitrogen atoms are strongly bound to the step sites of the surface. At these sites an enhanced NH_x decomposition may also take place before total hydrogenation to NH_3 has occurred. The oxygen concentration on or near the surface layer is quite large as indicated by the normalised O_{510eV} signal intensity of 0.035. The LEED pattern after the reaction points to a (2x1) surface structure. The single crystal surface may facet under the reaction conditions. However, if this would be the case desorption of the adsorbates restores the structure characteristic of the f.c.c. (410) surface.

The selectivity towards N_2 has the highest value for the Rh(100) surface. However, the conversion of NO is low at temperatures below 600K, due to the high number of strongly bound nitrogen atoms. This is also reflected by the high value of the N_{380eV} AES signal intensity, 0.045. By EELS it was found that this signal is mainly caused by adsorbed nitrogen atoms. The accumulation of N adatoms during the NO-H_2 reaction at a total pressure of 2 x 10-7 mbar over a polycrystalline Rh surface was reported by Obuchi et al [13]. The high selectivity towards N_2 may be explained by the high number of nitrogen atoms on the surface. A c(2x2) surface structure was found by means of LEED. The relatively low O_{510eV} AES signal indicates that this structure consists mainly of N_{ads}. Therefore, it is believed that large islands of N_{ads} are formed during the reaction. This facilitates the

formation of N_2 via step 6. By EELS it was found that NH_{ads} can actually be formed on the Rh(100) surface [5]. However, NH_3 is not formed under the described reaction conditions. The low rate of NH_3 formation may be caused by a low H_{ads} concentration in the N_{ads} islands and the formation of NH_x species at the boundaries of these islands only. Also, an enhanced decomposition of NH_x could take place on Rh. The low activity of the NO/H_2 reaction at 520K is ascribed to the low number of free active sites available for reaction. Most of the metal atoms are blocked by nitrogen atoms, or NO molecules. At 575K, N_2O formation is observed, this indicates that even at this temperature the number of free sites must be relatively small. The N_2O intermediate will decompose into N_2 and O_{ads} if a sufficient number of vacancies is available. If these vacancies are absent, N_2O will desorb from the surface.

CONCLUSIONS

The activity and selectivity of the $NO-H_2$ reaction over Pt, Rh and Pt-Rh surfaces depends strongly on the metal and surfaces structure. The activity at 520K decreases in the order Pt(100) ≥ Pt-Rh(100) > Pt-Rh(410) > Pt-Rh(111) > Rh(100). The selectivity towards N_2 on the other hand decreases in the order Rh(100) > Pt-Rh(410) > Pt(100) > Pt-Rh(111). The selectivity towards N_2 ranges from 100% to 0%. The selectivity is determined by the relative concentrations of NO, N and N adsorbed on the various surfaces. A high selectivity towards N_2 is observed with relatively strong adsorbed nitrogen atoms on Rh(100) and Pt-Rh(410). However, the high selectivity towards N_2 is at the expense of the activity for the reaction.

REFERENCES

1 K.C.Taylor in "Automotive Catalytic Converters (Springer, Berlin, 1984)
2 J.Siera, B.E.Nieuwenhuys, H.Hirano, T.Yamada and K.I.Tanaka, Catal.Lett. 3 (1989) 179
3 H.Hirano, T.Yamada, K.I.Tanaka, J.Siera, P.Cobden and B.E.Nieuwenhuys, Surf.Sci. 262 (1992) 97
4 T.Yamada, H.Hirano, K.I.Tanaka, J.Siera and B.E.Nieuwenhuys, Surf.Sci. 226 (1990) 1
5 to be published
6 R.F.van Slooten and B.E.Nieuwenhuys, J.Catal. 122 (1990) 429 and refs. therein
7 R.M.Wolf, J.Siera, F.C.M.J.M.van Delft and B.E.Nieuwenhuys, Faraday Disc. Chem.Soc. 87 (1989) 275
8 R.I.Masel, Catal.Rev.Sci.Eng. 28 (1986) 335
9 R.M.Wolf, J.W.Bakker and B.E.Nieuwenhuys, Surf.Sci. 246 (1991) 135
10 B.E.Nieuwenhuys, Surf.Sci. 126 (1983) 307
11 D.G.Löffler and L.D.Schmidt, Surf.Sci. 59 (1976) 195
12 V.V.Gorodetskii, private communication
13 A.Obuchi, S.Naitom, T.Onishi and K.Tamaru, Surf.Sci. 130 (1983) 29

DISCUSSION

Q: Z. Schay (Hungary)

1) Have you considered the dissociation of NO assisted by adsorbed hydrogen ?

2) If H_a removes only oxygen, at low coverage NO adsorption and dissociation should occur and on hydrogen adsorption (following the NO adsorption) only water and no N_2 should be formed. Is this true ?

A: B. Nieuwenhuys and K. Tanaka

1) From a thermodynamic point of view hydrogen could facilitate the dissociation of NO. However, we have not found any direct evidence for such an effect. All our experiments including TDS, XPS and FEM studies show that dissociation of NO starts at temperatures at which some of the adsorbed NO desorbs, creating vacant metal sites required for NO dissociation. In this stage hydrogen can also be adsorbed on the surface and it reacts with oxygen resulting in more vacancies and, hence, in faster dissociation and reaction. The observed reaction temperatures of hydrogen with NO adsorbed at low coverages do not differ significantly from the NO dissociation temperatures [1,2]. Therefore, hydrogen assisted NO dissociation does not seem to play an important role. However, at relatively high hydrogen pressures hydrogen seems to be able to displace some of the more weakly bound adsorbed NO and reaction starts at lower temperature [1]. This effect may also called "hydrogen assisted NO dissociation".

2) Starting with a low NO precoverage, dissociation starts at a much lower temperature than on surfaces initially covered with a monolayer NO. On some Rh surfaces dissociation can already start below room temperature [1]. NO dissociation and interaction of NO with hydrogen have been studied in detail on a PtRh(100) surface using LEED, AES and EELS [2]. In the presence of NO at $T > 350$ K the (1x1) surface structure is slowly converted to an oxygen (3x1) surface structure due to NO dissociation and Rh surface segregation. In the presence of a NO + H_2 mixture the surface structure formed is the nitrogen c(2x2) showing again that hydrogen reacts more easily with oxygen than with nitrogen.

[1] R. M. Wolf, J. W. Bakker, B. E. Nieuwenhuys, *Surf. Sci.* **246**, 135 (1991)

[2] H. Hirano, T. Yamada, K. I. Tanaka, J. Siera, B. E. Nieuwenhuys, *Surf. Sci.*, **222**, L804 (1989); *ibid* **262**, 97 (1992)

Q: R. W. Joyner (United Kingdom)

Your conclusion that the selectivities are proportional to surface coverage are at first sight not surprising, since presumably you are dealing with Langmuir-Hinshelwood kinetics. But it suggests that the activations energies observed an those for desorption and not reaction. Do you agree and do you make different observations at higher temperatures ?

A: B. Nieuwenhuys and K. Tanaka

Yes. The activities and the selectivities shown in the figure have been measured at relatively low temperatures (500-600 K), where for some of the surfaces the reaction rate may be controlled by desorption. An example is the Rh(100) surface. The intrinsic activity of the Rh(100) surface for NO dissociation and reaction is high. However in this low temperature range the activity found for this surface is very low due to nitrogen inhibition. As a result the order in activity and selectivity of the various surfaces examined are dependent on the temperature. An example can be found in Figure 6 showing that at 520 K the Pt-Rh(410) surface is more selective to N_2 formation than the Pt-Rh(100) whereas at 575 K the Pt-Rh(100) surface shows a better selectivity.

Q: J. H. Block (Germany)

My question concerns the surface composition of the Pt-Rh alloy. Frequently chemisorption processes are combined with surface segregation of one of the alloy compounds. Is such a phenomenon observed ?

A: B. Nieuwenhuys and K. Tanaka

Yes. Pt-Rh alloy surfaces show a very dynamic behavior in adsorption and reaction. Under reducing conditions Pt surface segregation is observed. Under oxidizing conditions, Rh segregates to the surface. The O induced (O from O_2, or NO) Rh surface segregation can eventually lead to the separation of Rh-oxides. Under reducing conditions alloy formation takes again place.

Q: R. A. van Santen (The Netherlands)

The presentation focuses an the role of nitrogen. However it is well known that O_2 has a large negative effect on the rate of NO reduction. What information do you have on the role of oxygen in the reaction ?

A: B. Nieuwenhuys and K. Tanaka

It is right that Rh, Pt and Pt-Rh alloy catalysts are not selective towards the reduction of NO in the presence of oxygen. On the other hand our paper (see Table I and the text) suggests that there is no direct relation between the amount of oxygen (from NO) as found by AES and the activity/selectivity, while we did find a correlation between activity/selectivity and the N concentration. In our opinion this result is caused by the fact that the oxygen measured by AES is situated beneath the surface (subsurface O) and is not adsorbed on the surface. It should also be kept in mind that hydrogen-rich conditions were used in our experiments (H_2/NO ratio of 5/1), because it was the purpose of the study to examine the selectivity to NH_3, N_2 and NO formation.

Q: D. Chadwick (United Kingdom)

Your activities and selectivities are quoted after 3 minutes reaction time. For those cases with high N coverage, can you comment on the products observed from zero to 3 minutes reaction time ?

A: B. Nieuwenhuys and K. Tanaka

Due to space limitation we could not show the variation of the rates of formation of the various products with increasing reaction time. For the Pt-Rh(100) surface we have published these data in an earlier paper [3]. For Rh(100), the surface with a high N coverage, the only reaction product observed at 500-600 K from zero to 3 minutes is N_2. The order in conversion/selectivity for the various surfaces studied does not change going from zero to three minutes.

[3] H. Hirano, T. Yamada, K. I. Tanaka, J. Siera, P. Cobden and B. E. Nieuwenhuys, *Surf. Sci.*, **262**, 97 (1992)

Q: G. B. Fisher (USA)

1) In actual automotive exhaust, among the gases present on the rich side of stoichiometry are NO, CO and H_2. Do you have any experiments which indicate how the NO-H_2 reaction completes with the NO-CO reaction on the Pt-Rh alloys ?

2) You have shown the trade-off between selectivity to N_2 formation and activity for the NO-H_2 reaction on several surfaces. Does it seem reasonable that this is most directly related to an inhibition of the H_2 dissociation step in the reaction in the presence of high N atom surface coverage which lead to good N_2 selectivity? I would seem reasonable from one point of view, since in 1988 [4] we found that high N atom coverage on Rh(111) dramatically inhibited dissociative O_2 adsorption. It would be very interesting to know the rate constant of H_2 dissociative chemisorption (and NO dissociation) as a function of N atom coverage on these alloys.

[4] G. B. Fisher, et al., *Proc. of the 9th Int. Cong. on Catalysis* (Eds.: M. J. Phillips and M. Ternan), The Chemical Institute, Ottawa, p. 1355, (1988)

A: B. Nieuwenhuys and K. Tanaka

1) No. We have measured the NO + H_2 and NO + CO reactions over Pt-Rh alloys. However, we did not study the NO reduction in the presence of both CO and H_2. NO reduction with hydrogen is a much faster reaction than NO reduction with CO. In an atmosphere of CO, NO and H_2 the CO adsorption will compete with NO and hydrogen adsorption. Hence, we may expect CO inhibition of the reduction of NO by hydrogen at lower temperatures ($T < 500$ K).

2) The model that you propose: inhibition of hydrogen adsorption/dissociation by a high concentration of N adatoms seems reasonable to us. It is well documented in the literature that for dissociation of CO, NO and O_2 several adjacent free metal atoms are required. For hydrogen the available information is not that clear. In many papers it has been reported that H_2 dissociation requires an ensemble of free metal atoms. However, other papers suggest that hydrogen can also dissociate an isolated Pd or Pt atoms in the surface. We found that hydrogen can adsorb on Pt-Rh(100) or Rh(100) covered with an overlayer of N_{ads} to form NH_a [5]. Hence, we do not have a direct answer on the question to which extent H_2 dissociation is inhibited by a high concentration of N_{ads}. We agree that it would be interesting to know the rate constants of H_2 dissociative adsorption and NO dissociation as a function of N atom coverage.

[5] K. I. Tanaka, T. Yamada, B. E. Nieuwenhuys, *Surf. Sci.*, **242**, 503 (1991)

Q: G. A. Sormorjai (USA)

Would it be advantageous to study alloy effects by depositing one monolayer of both alloy components on a third, neutral metal instead of one monolayer of one component on the single crystal of the other metal ?

A: B. Nieuwenhuys and K. Tanaka

In the studies described in our papers bulk Pt-Rh alloys have been used. In general, three different types of alloy surfaces can be prepared:

1) two dimensional alloys prepared by depositing component A on a substrate of component B:

2) by depositing of both components A and B on an inert substrate:

3) by using a bulk alloy A-B.

Each approach has its specific advantages and limitations. In 3) the bulk composition is well-defined and it is easy to study the large effect of the surface structure on adsorption and catalysis. For Pt-Rh alloys most of the work has been done with 3). Some limited information is available for surfaces prepared by 1) and 2) [6]. These results are in line with those reported for bulk single crystal surfaces of Pt-Rh.

[6] L. D. Schmidt et al. and K. I. Tanaka et al., to be published

Guczi, L. *et al.* (Editors), *New Frontiers in Catalysis*
Proceedings of the 10th International Congress on Catalysis, 19-24 July, 1992, Budapest, Hungary
© 1993 Elsevier Science Publishers B.V. All rights reserved

SPECTROSCOPIC STUDIES ON THE REACTION PATHWAYS OF METHANOL DISSOCIATION ON Pd CATALYST

A. Berkó, J. Raskó and F. Solymosi

Institute of Solid State and Radiochemistry of József Attila University, P.O.Box 168, 6701 Szeged, Hungary

Abstract

The adsorption and dissociation of methanol on Pd(100) and supported Pd catalysts were investigated in the temperature range 90-300 K. By means of photoelectron, infrared and thermal desorption spectroscopies, condensed layer, chemisorbed and dissociated methanol were distinguished. Methanol decomposes through the formation of a methoxy species. No adsorbed CH_3 was detected either on Pd(100) or on supported Pd. In the latter case the transient formation of acetaldehyde was identified at 200 K. Potassium additives significantly increased the extent of dissociation, markedly stabilized the methoxy species formed, and induced a small extent of cleavage of the methanolic C-O bond.

1. INTRODUCTION

Study of the adsorption and dissociation of methanol on metal surfaces is considered to provide an important insight into the mechanism of methanol synthesis. Spectroscopic studies on single-crystal surfaces of Pt metals unequivocally showed that the primary step in the dissociation of chemisorbed methanol is cleavage of the O-H bond, and formation of the methoxy species [1,2]. However, Winograd et al. [3], recently reported that below a monolayer of adsorbed methanol on Pd(111) surface the rupture of both O-H and C-O bonds occurs: the primary decomposition products were adsorbed methyl, methoxy and water. An interesting finding of this study was that the methyl group formed on Pd(111) exhibited an unusually high thermal stability: it was detected even above 400 K.

The work of Winograd et al. initiated several studies on this subject and led to a controversy [4-7]. The O-H bond breaking of methanol dissociation has been questioned by Yates et al. [4]. They found no isotopic exchange in the desorbing CO and methanol products from coadsorbed $^{13}CH_3{}^{16}OH$ and $^{12}CH_3{}^{18}OH$. They pointed out that, if > 1% of adsorbed methanol dissociated by C-O bond fission, this would have been detected via the production of $^{13}C^{18}O$ or an isotopically mixed methanol species. The low thermal stability of CH_3 group produced by the dissociation of CH_3I on Pd(100) surface was also not in accord with the results of Winograd et al. [3]. In this case, however, coadsorbed iodine was also present, which could influence the stability of CH_3 groups [7].

In the present comparative study we examine the reaction pathways of methanol dissociation both on a Pd(100) single-crystal at low pressure and on supported Pd at high pressure. Attention is also paid to the effect of an alkali additive on this process.

2. EXPERIMENTAL

The experiments with the Pd single-crystal were performed in an ultrahigh vacuum system with a background pressure of 5×10^{-10} mbar, produced with an ion-getter and titanium sublimation pumps. The system was equipped with a quadrupole mass analyzer, an electrostatic hemispherical analyzer (Leybold-Hereaus LHS-10), a differentially pumped UV photon (He I, II) source for UPS, an Al Kα X-ray anode for XPS and an electron gun for AES measurements. All binding energies, Eb, are reported relative to the Pd Fermi level which places the Pd $3d_{5/2}$ level at 335.3 eV. The cleaning procedure, deposition of potassium and other experimental details are described in our previous paper [7,8].

Infrared spectra were recorded with a Biorad (Digilab Div.) Fourier transform infrared spectrometer with a wavenumber accuracy of ± 2 cm^{-1}. Pd/SiO_2 samples were prepared by incipient wetting of silica (Cabosil) with an aqueous solution of palladium chloride with or without potassium nitrite. The self supporting wafers were oxidized and reduced at 573 K for 60 min.

3. RESULTS

3.1. Clean Pd(100)

XPS studies. The featureless baseline in the C(1s) region for clean Pd reveals that no carbon impurity is present. The low exposure of the clean Pd(100) surface to methanol at 90 K produced a feature at 286.4 eV in the C(1s) spectrum. This binding energy corresponds well to the previously values reported for methanolic C(1s) [3, and references therein]. The C(1s) peak shape and position remained constant up to ~ 2.0 L exposure. With further increase of the methanol exposure, the peak shifted to higher binding energy and became broader, which is regarded as an indication that two closely related carbon atoms are present. It is very likely that this change in the C(1s) region of the XPS spectrum results from the formation of a multilayer. This is supported by the TPD measurements; the first monolayer of adsorbed methanol is completed at about 1.8-2.0 L; above this exposure, formation of a multilayer begins.

Figure 1A depicts C(1s) spectra at low methanol exposure as a function of temperature. The C(1s) intensity decays between 170 and 200 K as a result of the desorption of methanol. It is an important feature that no splitting of the C(1s) peak is observed at 90-170 K, although the fwhm value (~ 2.1 eV) of the peaks for 150 and 170 K suggests the contribution of two C-containing compounds. Upon heating to 200 K, a new weak feature developed at 285.7 eV. This could be either adsorbed methoxy or CO, or both, as XPS can not differentiate between them. It is an important observation that this peak underwent very little change up to 400 K before the desorption of CO.

In subsequent experiments, methanol was adsorbed at 300 K. In this case we obtained one intense signal at 285.9 eV in the C(1s) region which intensified with gradual increase of the methanol exposure. This peak disappeared completely by 500 K. No remaining carbon was detected by sensitive XPS measurements above this temperature.

UPS measurements. The adsorption of methanol on Pd(100) markedly suppressed the intensity of the Pd d-band and produced photoemission peaks at 5.2,

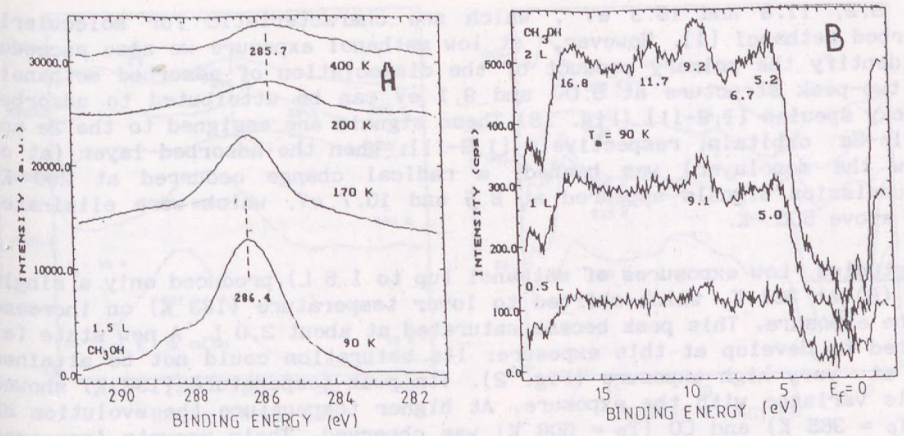

Figure 1. XPS of the C(1s) level (A) and He II UPS (B) of adsorbed methanol on clean Pd(100) at different temperatures.

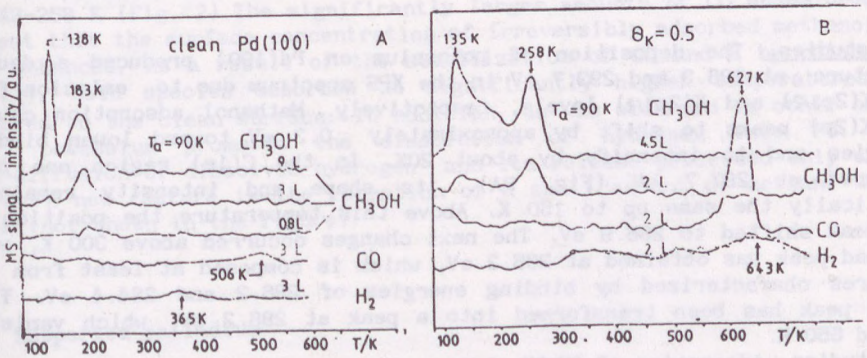

Figure 2. TPD spectra following methanol adsorption on clean (A) and K-dosed Pd(100) (B).

6.7, 9.2, 11.8 and 16.3 eV , which are characteristic for molecularly adsorbed methanol [1]. However, at low methanol exposure we also succeded to identify the primary product of the dissociation of adsorbed methanol: the two-peak structure at 5.0 and 9.1 eV can be attributed to adsorbed methoxy species [1,9-11] (Fig. 1B).These signals are assigned to the 2e and the 1e-5a orbitals, respectively [1,9-11]. When the adsorbed layer (at or below the monolayer) was heated, a radical change occurred at 200 K: photoemission signals appeared at 8.5 and 10.7 eV, which were eliminated only above 500 K.

TPD studies. Low exposures of methanol (up to 1.5 L) produced only a single peak (β) at 201 K, which shifted to lower temperature (183 K) on increase of the exposure. This peak became saturated at about 2.0 L. A new state (α) started to develop at this exposure: its saturation could not be attained even at very high exposure (Fig. 2). Its peak temperature (138 K) showed little variance with the exposure. At higher temperature the evolution of H_2 (T_p = 365 K) and CO (T_p = 506 K) was observed. Their amounts increased only up to the formation of a methanol monolayer (2.0 L), but even at this stage only a fraction of the values corresponding to saturation for adsorbed CO and H was attained. Neither methane nor water evolution was observed.

3.2. Potassium-dosed Pd(100)

The adsorption and reaction of CH_3OH on K-dosed Pd was studied at different K coverages, but only results obtained at monolayer K are reported here.

XPS studies. The deposition of potassium on Pd(100) produced a double structure at 296.3 and 293.7 eV in the XPS spectrum due to emission from the K($2p_{3/2}$) and K($2p_{1/2}$) levels, respectively. Methanol adsorption caused the K(2p) peaks to shift by approximately 0.3 eV toward lower binding energies and to intensify by about 20%. In the C(1s) region one peak appeared at 287.7 eV (Fig. 3A), its shape and intensity remaining practically the same up to 150 K. Above this temperature the position of the peak shifted to 286.9 eV. The next changes occurred above 300 K, when a broad peak was obtained at 285.3 eV, which is composed at least from two features characterized by binding energies of 286.2 and 284.4 eV. This broad peak has been transformed into a peak at 286.2 eV, which vanished around 650 K.

UPS studies. Adsorption of CH_3OH at low exposure produced two weak peaks in the HeII UPS spectrum, at somewhat different energies than for the clean surface, at 4.6 and at 8.5 eV. On increase of the exposure, all the emissions due to adsorbed methanol appeared (Fig. 3B). When the adsorbed layer was heated, however, the two-peak structure at 4.6 and 8.5 eV again became the dominant spectral feature. Both peaks were seen up to about 450 K. Above this temperature, another pair of peaks developed at 8.6 and 11.9 eV and were eliminated above 600 K.

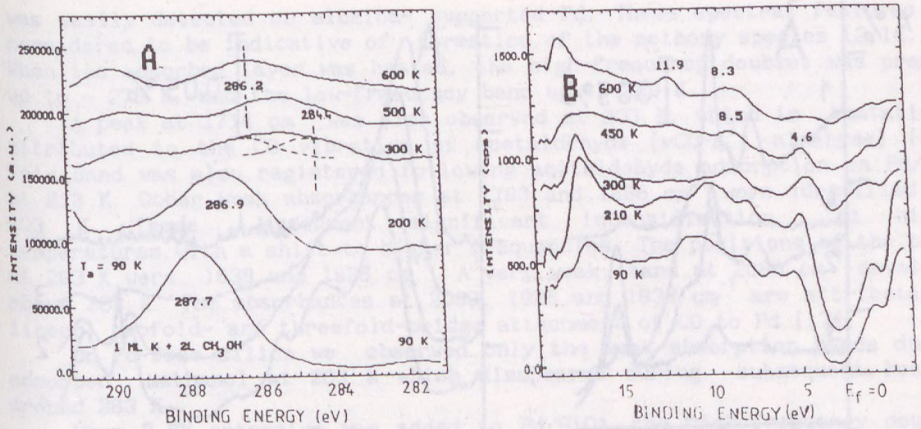

Figure 3. Effects of potassium on XPS (A) and UPS (B) spectra of adsorbed methanol on Pd(100) surface

TPD studies. In the presence of preadsorbed potassium, the amount of reversibly adsorbed methanol increased by a factor of 2-3, and T_p shifted to 242-258 K (Fig. 2). The significantly larger amounts of CO and H_2 formed suggest that the surface concentration of irreversibly adsorbed methanol is also enhanced. As a result of the stabilization of CO and H by potassium [12,13], both species desorbed at significantly higher temperatures as compared to the clean surface. In addition, as was observed in other cases [13], potassium promoted the dissolution of hydrogen into Pd. The back-diffusion of dissolved hydrogen and its release proceeded only above 600 K. A new feature is the formation of a small amount of methane above 300 K (not shown in the figure).

3.3. Supported palladium

In this case the adsorption and dissociation of methanol were studied by means of infrared spectroscopy. Spectra following methanol adsorption and evacuation at 203 K are presented in Fig. 4. The absorption bands at 2954 and 2848 cm^{-1} can be assigned to the asymmetric and symmetric stretching vibrations of the methyl group [2]. The symmetric deformational motion σ(methyl) is observed at1450 cm^{-1}. The rocking vibration, γ(methyl), which should give a band at 1170-1120 cm^{-1}, was not detected due to the low transmittance of the Pd/SiO_2 sample in this frequency range. However, it

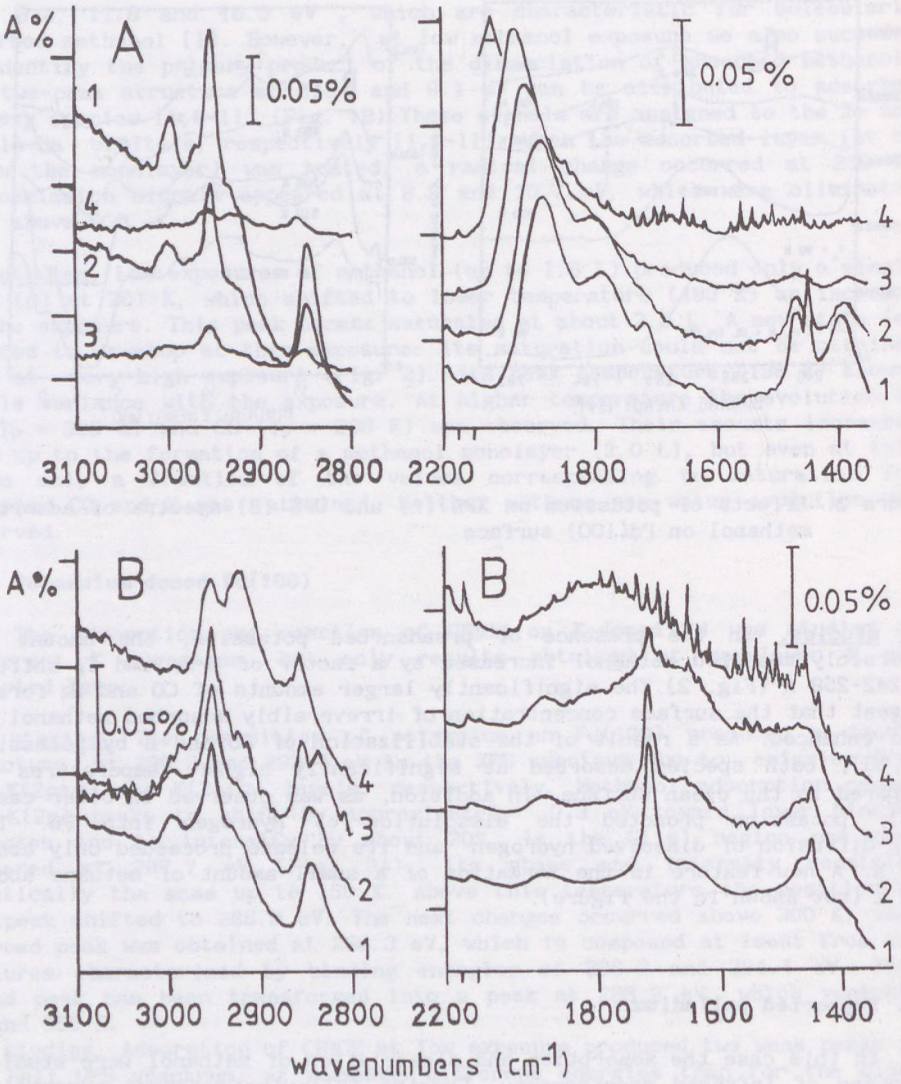

Figure 4. IR spectra of adsorbed CH_3OH on 10% Pd/SiO_2 (A) and 2,5% K + 10% Pd/SiO_2 (B): (1) 1 Torr CH_3OH at 213 K and evacuation at (2) 213 K, (3) 253 K, (4) 293 K.

was easily detected on alumina- supported Pd. These spectral features are considered to be indicative of formation of the methoxy species [2,14,15]. When the adsorbed layer was heated, the high-frequency doublet was present up to ~ 273 K, and the low-frequency band up to 263 K.

A peak at 1714 cm^{-1} was also observed at 203 K, which is tentatively attributed to the CO vibration of acetaldehyde [νCO-ξ^2 aldehyde] [16]. This band was also registered following acetaldehyde adsorption on Pd/SiO_2 at 213 K. Other weak absorbances at 1786 and 1886 cm^{-1} were identified at 203 K. These underwent significant intensification at higher temperatures, with a shift to higher frequencies. The positions of the peaks at 293 K were 1838 and 1926 cm^{-1}. A very weak band at 2080 cm^{-1} developed above 203 K. The absorbances at 2080, 1926 and 1838 cm^{-1} are attributed to linear, twofold- and threefold-bridge attachment of CO to Pd [17].

On Pd-free silica we observed only the weak absorption bands due to adsorbed methanol at 203 K which disapeared during subsequent heating around 263 K.

When 2.5% potassium was added to Pd/SiO_2, the high-frequency doublet appeared at 2954 and 2845 cm^{-1}, and the low-frequency band at 1450 cm^{-1}. In this case the band characteristic for the CO vibration of acetaldehyde has been detected at 1717 cm^{-1}. In contrast with the K-free sample, all these bands exhibited relatively high stability; they vanished only at and above room temperature. Another interesting feature is the appearance of absorption band at 2925 cm^{-1} which became quite intense above 253 K. It is worth mentioning that only very weak bands were identified in the CO stretching region of 1800-2100 cm^{-1} at 200-300 K (Fig. 4B).

4. DISCUSSION

4.1. Clean Pd(100)

Methanol readily adsorbs on a clean Pd(100) surface, with a high sticking probability, which is almost constant up to monolayer. By means of TPD measurements, we can distinguish a chemisorbed (β) and a condensed layer (α), with desorption energies of 46.0 and 35.0 kJ/mol respectively. It may be assumed that the methanol initially adsorbed on Pd(100) dissociates, the O-H bond undergoing cleavage to give methoxy and H. However, XPS measurements at 90 K did not reveal the formation of any dissociation products of methanol. The C(1s) signal at 286.4 eV in the XPS spectrum clearly belongs to chemisorbed methanol. This is supported by the more molecular sensitive UPS spectra, which showed the characteristic photoemission signals of the adsorbed methanol molecule at and above monolayer [1,11].

However, in harmony with the results of Christmann and Demuth [1], the analysis of the magnified difference (UPS) spectra revealed that the

dissociation of adsorbed methanol also occurs to a small extent and methoxy species is formed (Fig. 1B). A larger fraction of it is hydrogenated to methanol and desorbs with Tp = 183 K. A smaller fraction of adsorbed methoxy further dissociates to CO(a) and H(a).This latter process is characterized by a shift of the C(1s) binding energy to 285.7 eV, and by the appearance of new signals in the UPS spectrum at 8.5 and 10.7 eV. This is supported by the OKLL Auger spectra of the adsorbed species, which are practically the same as those observed following CO adsorption. (The kinetic energy of the CO feature is almost 2 eV lower than that of the CH3OH feature and its intensity is considerably higher.) Further evidence for CO was provided by the elimination temperature of all these peaks in XPS and UPS (~ 450-500 K), which corresponds to the desorption of CO from Pd(100).

It is important that there is no spectroscopic evidence of rupture of the methanolic C-O bond or formation of the methyl(a) species on a clean Pd(100) surface. The C(1s) binding energy of methyl(a) produced by the thermal dissociation of methyl iodide on clean Pd(100) appeared at 284.2 eV, and a single photoemission signal in the UPS at 8.5 eV [7,18]. The adsorbed methyl group produced in this way was not stable, as its characteristic signals vanished at or below 250 K, leaving behind a small amount of carbon. The above feature suggests that the behavior of the Pd(100) surface, as regards reactivity towards methanol, differs basically from that of the Pd(111) surface [3].

4.2. K-promoted Pd100)

Preadsorbed potassium dramatically altered the adsorption and reactions of methanol on the Pd(100) surface, as evidenced by the changes in the TDS, XPS and UPS spectra. The most important features were as follows: (i) preadsorbed potassium only slightly altered the sticking coefficient of methanol, (ii) it increased the binding energy of chemisorbed methanol, and (iii) it resulted in an increase in the surface concentration of irreversibly bonded methoxy species and caused its significant stabilization.

The basic question is the effect of potassium on the pathway of methanol dissociation. In this case it was more easy to detect the two-peak structure at 4.6 and 8.5 eV in the UPS associated with methoxy species. As potassium at monolayer on Pd(100) exhibits mainly a metallic character [19], we may assume the occurrence of a direct chemical interaction between methanol and metallic potassium even at 90 K, in which the surface species $KOCH_3$ is formed:

$$K + CH_3OH = CH_3OK + H(a)$$

The photoemission signals attributed to the methoxy species were present in the spectra even after the coadsorbed layer had been heated to 450 K, indicating the high thermal stability of KOCH3 on Pd(100).

Although, O-H bond cleavage is the major pathway of methanol dissociation on K-dosed Pd(100), the appearance of a new C(1s) feature at 284.4 eV at 300 K and the desorption of methane suggests, that the formation of CH3 species may also occur in the presence of potassium. Following the dissociation of CH3I on K-promoted Pd(100), the C(1s) binding

energy due to the adsorbed CH_3 group was identified at the same kinetic energy [18].

Other spectral changes occurred above 450-500 K. A new C(1s) signal appeared in the XPS spectrum at 286.2 eV, and new photoemissions at 8.3 and 11.9 in the UPS, which can be attributed to CO(a) formed in dissociation of the methoxy species. This assignment is in harmony with the high stability of this new peak and the high-temperature release of adsorbed CO (Fig. 2B). There is no doubt that potassium also interacted with the CO formed, and increased its binding energy to Pd. The peak temperature for desorption of CO agrees well with the value obtained following CO adsorption on potassium-dosed Pd(100) [12].

4.3. Supported Pd

The features observed on supported Pd are in harmony with those found for the Pd(100) surface.

In order to establish whether methanol dissociation involves cleavage of methanolic C-O bond and formation of the CH_3 species, the adsorption of CH_3I was examined on the same Pd samples. Methyl group formed in the dissociation on Pd/SiO_2 is characterized by absorption bands at 2930 (C-H stretching) and 1390 cm^{-1} (C-H asymmetric bending). Nearly identical features were observed on single-crystal surfaces by means of HREELS [20]. Analysis of the spectra of methanol adsorbed at different temperatures led to the conclusion that the methyl group was not formed to a detectable extent on clean Pd/SiO_2. In the presence of potassium, however, there was a clear absorption band at 2925 cm^{-1} above 253 K, which may indicate the formation of CH_3 or CH_x species. This should be confirmed by more detailed measurements.

In conclusion, it may be stated that the primary route of dissociation of methanol on both Pd(100) and Pd/SiO_2 surfaces is O-H cleavage. Potassium promotes the dissociation and greatly stabilizes the methoxy species in the form of $K\text{-}OCH_3$. It appears that cleavage of the O-C bond also occurs to a small extent in the presence of a potassium additive.

References

1 K. Christmann and J.E. Demuth, J. Chem. Phys., 76 (1982) 6308, 6318.
2 J.L. Davis and M.A. Barteau, Surf. Sci., 187 (1987) 387.
3 R.J. Levis, J. Zhicheng and N. Winograd, J. Am. Chem. Soc., 111(1989) 4605.
4 X. Guo, L. Hanley and J.T. Yates, Jr., J. Am. Chem. Soc., 111 (1989) 3155.
5 N. Kruse, M. Rebholz, V. Matalin, G.K. Chuah and J.H. Block, Surf. Sci., 238 (1990) L457.
6 M. Rebholz, V. Matalin, R. Prins and N. Kruse, Surf. Sci., 251/252 (1991) 1117.
7 F. Solymosi and K. Révész, J. Am. Chem. Soc., 113 (1991) 9145.
8 F. Solymosi and K. Révész, Surf. Sci., 259 (1991) 95.
9 J. Paul, L. Wallden and A. Rosén, Surf. Sci., 146 (1984) 43.
10 B.A. Sexton, A.E. Hughes and N.R. Avery, Surf. Sci., 155 (1985) 366.
11 F. Solymosi, A. Berkó and T.I. Tarnóczy, J. Chem. Phys., 87 (1987) 6745.

12 A. Berkó and F. Solymosi, J. Chem. Phys., 90 (1989) 2492.
13 F. Solymosi and I. Kovács, Surf. Sci. 259 (1991) 95., F. Solymosi and I. Kovács, Surf. Sci. 260 (1992) 139.
14 C. Schild, A. Wokaun and A. Baiker, J. Mol. Catal. 63 (1990) 223.
15 J.C. Lavalley, J. Saussey, J. Lamotte, R. Breault, J.P. Hindermann and A. Kiennemann, J. Phys. Chem. 94 (1990) 5941.
16 M.A. Henderson, Y. Zhou and J.M. White, J. Am. Chem. Soc., 111 (1989) 1185. J.L. Davis and M.A. Barteau, J. Am. Chem. Soc., 111 (1989) 1782.
17 A.M. Bradshaw and F. Hoffmann, Surf. Sci. 72 (1978) 513.
18 K. Révész and F. Solymosi, Surf. Sci. in press
19 A. Berkó and F. Solymosi, Surf. Sci., 187 (1987) 359.
20 Y. Zhou, M.A. Henderson, W.M. Feng and J.M. White, Surf. Sci., 224 (1989) 376.

DISCUSSION

Q: G. A. Somorjai (USA)

1) It is interesting that you detect methyl adsorbed on Pd(111) and methoxy on Pd(100). What is your experimental evidence for this?

2) CO/H_2 produce methanol over Pd on La_2O_3 perhaps because of the presence of different oxidation states of Pd. Have you considered the study of oxygen coadsorption with CH_3OH?

A: A. Berkó

1) Both UPS and XPS measurements show that the energy positions of the peaks following CH_3OH adsorption on Pd(100) are characteristic for methoxy species. The positions of C 1s signals for CH_3O and CH_3 are separated by 1.5-2 eV and well distinguishable. CH_3 on Pd(111) was detected in ref. 3 in the paper.

2) We performed some experiments for coadsorption of oxygen and methanol, too. We concluded that in the presence of oxygen the amount of the irreversible adsorbed methanol increases and the C 1s signal characteristic for $(CH_3O)_a$ is more intensive.

Q: J. H. Block (Germany)

Considering the influence of a potassium overlayer it would be interesting to know the properties of the layer with lowest work function ($\Theta = 0.1$). In a paper by G. K. Chuak et al. [1] it was shown that the CH_3OH decomposition on Rh could be retarded by a positive electrostatic field. This field effect should be highest at lowest work function.

[1] G. K. Chuak et al., *Journal de Physique*, **47**, 59 (1986) and *J. Catal.*, **119**, 342 (1989)

A: A. Berkó

We found both on Pd(100) (present study) and on Rh(111) [2] that the stabilizing effect of potassium at $\Theta_K \sim 0.10$, when potassium is almost completely ionized, is much less than at or above monolayer, when potassium is mainly in metallic form.

[2] F. Solymosi, A. Berkó and T. I. Tarnóczi, *J. Chem. Phys*, **87**, 6745 (1987)

Q: D. Chadwick (United Kingdom)

In the case of the potassium promoted palladium surfaces, the photoelectron peaks of carbon and potassium are close together. Carbon has a low cross section compared to potassium and the satellite lines of potassium occur in the C 1s range. In these circumstances it can be difficult to unambiguously identify minority carbon species.

A: A. Berkó

The XPS spectra of Pd(100) covered by monolayer potassium really show some features in the C 1s range which can be certainly ordered to potassium caused satellites. We believe, however, that the photoelectron peaks in the difference spectra entirely due to adsorbed species formed during CH_3OH adsorption.

Guczi, L. *et al.* (Editors), *New Frontiers in Catalysis*
Proceedings of the 10th International Congress on Catalysis, 19-24 July, 1992, Budapest, Hungary
© 1993 Elsevier Science Publishers B.V. All rights reserved

CYCLOTRIMERISATION OF ACETYLENE TO BENZENE OVER SINGLE CRYSTAL PALLADIUM AND GOLD/PALLADIUM SURFACES AND OVER SUPPORTED PALLADIUM CATALYSTS

C. J. Baddeley, R. M. Ormerod and R. M. Lambert

Department of Chemistry, Unviesity of Cambridge, Lensfield Road, Cambridge, CB2 1EW, United Kingdom

Abstract

Kinetic and spectroscopic studies of ethyne cyclisation to benzene over Pd and Pd/Au yield detailed information about the reaction mechanism. The existence of a critical ethyne coverage threshold for reaction is dramatically demonstrated by experiments using coadsorbed NO which compresses the reactant surface phase without itself participating in the reaction. Results obtained from both single crystal model systems and supported Pd catalysts clearly show that C_4H_4 is the crucial surface intermediate in the cyclisation reaction. Data obtained with well characterised Pd/Au single crystal systems reveal the sensitivity of this reaction to the electronic structure, atomic composition and morphology of the metal surface.

1. INTRODUCTION

In favourable cases [1,2], electron spectroscopic measurements combined with kinetic studies, carried out on model single crystal surfaces can yield fundamental and unambiguous information about catalytic reaction mechanisms and the role of promoters and poisons in catalysis. One such example is the low temperature cyclotrimerisation of acetylene to benzene on Pd(111), an efficient and unusual reaction, reported almost simultaneously by Tysoe *et al* [3] and by Sesselmann *et al* [4].

A remarkable feature of the reaction is the evolution of benzene at very low temperatures (~200 K). Another striking observation is that the benzene is evolved in two very different temperature regimes; clearly resolved desorption maxima occur at ~230 K and ~530 K. The mechanism of this interesting reaction has been studied by a variety of methods [5-8]. Deuterium isotope labelling was used to establish that the molecular pathway from acetylene to benzene proceeds via an associative mechanism, involving no cleavage of C-C or C-H bonds [6]. An earlier molecular beam study suggested that the reaction proceeds via a C_4 intermediate [5]. It was also demonstrated that dissociative chemisorption of cis-3,4-dichlorocyclobutene ($C_4H_4Cl_2$: DCB) could be used to seed the surface with a C_4H_4 species [7]. This C_4H_4 species reacted with coadsorbed C_2D_2 to form benzene ($C_6H_4D_2$) with identical kinetics to those exhibited by the overall acetylene trimerisation reaction (C_6D_6). $C_6H_4D_2$ (from C_4H_4 and C_2D_2) and C_6D_6 (from $3C_2D_2$), thus strongly suggesting that the molecular formula of the C_4 intermediate in acetylene cyclisation is indeed

C_4H_4. Further experiments confirmed that benzene desorption is the rate determining step for the evolution of benzene into the gas phase [6]. The chemical identity and chemisorption geometry of the C_4H_4 species has been investigated using HREELS, NEXAFS and ARUPS [8-10,], which together indicate that the C_4 species is a tilted metallocycle.

In this paper we present recent work aimed at further elucidating the mechanistic chemistry of acetylene cyclotrimerisation, addressing in particular the mode of low temperature benzene formation. Both single crystal model systems and practical catalysts have been used. We have investigated the reactive properties of thin Pd overlayers on an Au(111) substrate and those of Au/Pd surface alloy phases derived from such overlayer systems, with respect to their activity towards benzene formation, in an attempt to establish the role of "geometric" and "electronic" effects on the catalytic chemistry. As this is a *synthesis* reaction which occurs both under UHV conditions and at atmospheric pressure, it represents an excellent system for the study of promoter activity and catalyst poisoning and the role of electronic and structural effects in catalysis.

2. EXPERIMENTAL

The single crystal work was carried out in two different UHV chambers, described previously [NO, ADES]. The Pd(111) and Au(111) specimens were cleaned by standard methods desribed previously [11,12]. Palladium was deposited using a resistively heated collimated source which was outgassed for prolonged periods before use. Research grade acetylene purified by bulb-to-bulb distillation was admitted to the sample using calibrated quartz capillary arrays.

Catalysts containing between 2 and 10 % w/w Pd dispersed on silica, alumina, titania and charcoal supports were used in a single-pass quartz tube microreactor with mass spectroscopic detection. Following pretreatment in flowing oxygen at 473 K, samples were reduced in hydrogen at 470 K or 770 K, before purging in helium at 770 K and cooling in helium to the reaction temperature. Palladium surface areas were determined by CO chemisorption followed by temperature programmed desorption.

3. RESULTS AND DISCUSSION

A characteristic feature of acetylene cyclotrimerisation on Pd(111) is that there is a distinct acetylene coverage threshold below which benzene formation does not occur; instead only self-hydrogenation, fragmentation and decomposition of the reactant occur. This coverage threshold coincides with the point at which the $(\sqrt{3}x\sqrt{3})R30°$ LEED structure of the acetylene overlayer reaches its maximum degree of perfection [5]. Deuterium labelling shows that although benzene formation does not occur until the $\sqrt{3}$ structure is complete the reactively formed benzene molecules do contain acetylene molecules that were initially chemisorbed into the $\sqrt{3}$ sites [6], i.e. it is *not* a second more weakly bound acetylene species that is responsible for benzene formation.

These results can be explained by the requirement of sufficiently close approach of three chemisorbed acetylene molecules for reaction to occur: a

high molecular packing density in the reacting adsorbed layer then leads to the formation of weakly bound tilted benzene molecules, which undergo facile desorption at ~200 K giving rise to the low temperature desorption peak. As the surface becomes depleted, the remaining benzene molecules can adopt a flat-lying strongly bound adsorption geometry, and do not desorb from the surface until the temperature exceeds 500 K.

This hypothesis is very strongly supported by the results of experiments involving two-dimensional compression of the acetylene overlayer on Pd(111) caused by the addition of a chemically inert 'spectator' molecule, nitric oxide. Using LEED and TDS we have shown that the coadsorption of nitric oxide and acetylene on Pd(111) leads to islanding behaviour; acetylene adsorption leads to compression of the coadsorbed NO into separate domains. We have exploited this to test the compression/tilting hypothesis referred to above.

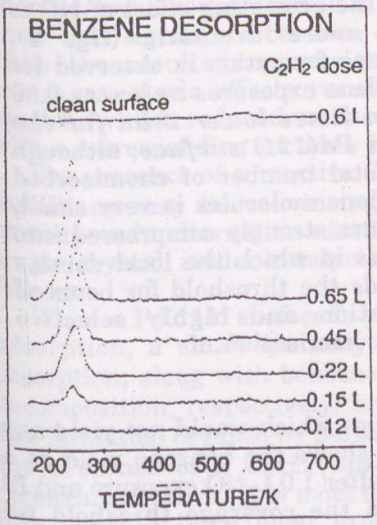

Figure 1. Benzene formation induced by coadsorbed NO. Surface predosed with 0.7 L NO at 300 K followed by varying doses of C_2H_2 at 170 K. Top spectrum shows 0.6 L C_2H_2 on clean Pd(111) at 170 K.

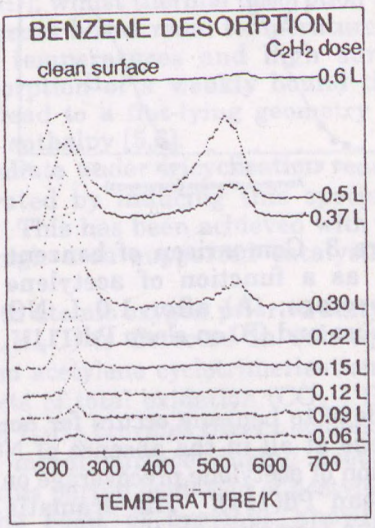

Figure 2. Benzene formation induced by coadsorbed NO. Varying precoverages of C_2H_2 dosed at 140 K followed by 1.0 L NO.

In the case of the acetylene component the effects of compression are most dramatically illustrated by the very large change observed in the threshold for benzene formation. When the NO pretreated surface is cooled to 170 K and exposed to acetylene, the onset of benzene formation occurs at much lower acetylene doses than on the clean Pd(111) surface (fig. 1). It can be seen that very substantial benzene production occurs in the acetylene exposure range

0.15-0.60 L, whereas on the clean Pd(111) surface benzene is only detected for acetylene exposures ≥ 0.6 L. The known coverage dependence of the acetylene sticking probability [5] can be used to express these exposures as actual acetylene coverages: for the clean surface the threshold for benzene formation occurs at $\theta = 0.33$, whereas in the presence of preadsorbed NO it occurs at an apparent coverage of $\theta \leq 0.08$. Thus, the presence of preadsorbed NO results in phase separation and compression leading to local densities of acetylene which are at least a factor of four greater than they would be on the clean Pd(111) surface.

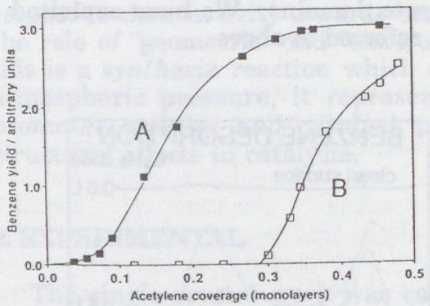

Figure 3. Comparison of benzene yield as a function of acetylene precoverage; (A) after 1.0 L NO exposure and (B) on clean Pd(111).

If the order of adsorption is reversed, the same phenomenon is observed, as one might expect if separate adsorbate islands are being formed. However, in this case the promoting effect of NO is even more dramatic (fig. 2), benzene formation is observed for acetylene exposures as low as 0.06 L, ***ten times lower than for the clean Pd(111) surface***; although the total number of chemisorbed acetylene molecules is very small, they are strongly compressed into islands in which the local density exceeds the threshold for benzene formation and highly selective cyclotrimerisation of acetylene to benzene occurs for acetylene loadings which would not yield any benzene at all in the absence of NO. Figure 3 shows the benzene yield as a function of acetylene precoverage on Pd(111), A) after 1.0 L NO exposure and B) on clean Pd(111). The dramatic reduction in the coverage threshold for benzene formation in the presence of coadsorbed NO is clearly observed. At sufficiently high NO exposures and moderate acetylene coverages, e.g. $\theta(C_2H_2) = 0.16$, there is effectively 100% conversion of acetylene to benzene. In the absence of nitric oxide the highest efficiency observed is ~30% [13].

From Figure 1, it is also evident that the presence of coadsorbed NO leads to a dramatic change in the kinetics of benzene desorption; all the benzene is evolved in a single low temperature desorption peak at ~240 K, in contrast to the clean surface where reactively formed benzene desorbs in two peaks [5,6]. The present results strongly support the proposed mechanism for this process whereby conditions of surface crowding lead to formation of a tilted, weakly bound benzene species. On the unpromoted surface, benzene desorption and the transformation of unreacted acetylene to vinylidene reduces the surface coverage to such an extent that the benzene molecules can adopt a more strongly bound flat-lying geometry, giving rise to the high temperature benzene desorption peak. However, in the presence of NO, strong compression of the acetylene domains is maintained throughout the reaction. This results

in all the benzene being evolved from a high density system and hence only the low temperature peak is observed.

The tilted adsorption geometry of benzene at high surface coverages on Pd(111) has been confirmed by NEXAFS, XPS and UPS [14]. In these experiments a dense benzene overlayer was chemisorbed on Pd(111) at low temperature. The variation in intensity of the C (1s)→π* resonance as a function of polarisation vector angle corresponds to a tilt angle of about 33° between the molecular plane and the metal surface, i.e. at high coverages benzene is indeed significantly tilted with respect to the Pd(111) surface - in this case the necessary surface pressure is provided by the benzene molecules themselves. ARUPS measurements for benzene adsorbed at room temperature indicate a parallel adsorption geometry [15] in apparent disagreement with the above result. However, our XPS measurements show that there is a ~35% reduction in adsorbate coverage when a low temperature chemisorbed layer is warmed to 300 K [10,14D], whilst thermal desorption data show that significant benzene desorption occurs below room temperature [6]. Thus the results are consistent: at low temperatures and high surface coverages, steric effects result in the adsorption of a weakly bound tilted species, whilst reduced surface coverages lead to a flat-lying geometry [15] with a corresponding increase in adsorption enthalpy [5,6].

The presence of a reactive C_4H_4 intermediate under tricyclisation reaction conditions may be convincingly demonstrated by inducing this species to participate in alternative reaction channels. This has been achieved with both single crystal model catalysts and with high area supported catalysts, as follows.

When a Pd(111) surface is precovered with atomic oxygen prior to acetylene adsorption, a small quantity of furan (C_4H_4O) is detected in subsequent desorption, along with benzene and H_2 (from acetylene cyclotrimerisation and decomposition, respectively) and the products of total oxidation (CO_2 + H_2O). The formation of furan by partial oxidation of C_4H_4 provides **direct** evidence for the presence of a C_4H_4 species on the metal surface during acetylene cyclotrimerisation. It is most unlikely that this partial oxidation of acetylene to furan would have been predicted on the basis of previous knowledge; coadsorbed oxygen and hydrocarbon generally react to form H_2O and CO_2, and acetylene would be expected to be the most susceptible of all hydrocarbons to combustion. However, given the apparently unique ability of Pd(111) to generate substantial surface concentrations of the C_4H_4 metallocycle from C_2H_2, the scavenging of the C_4H_4 by coadsorbed oxygen to yield C_4H_4O is not unexpected.

When the C_4H_4 species is generated on the surface by the dissociative chemisorption of $C_4H_4Cl_2$, furan is also formed but in much larger yield, confirming that the $C_4H_4Cl_2$ can indeed be used as a reagent for dosing the surface with the relevant C_4 intermediate. Furan formation is found to be favoured at lower oxygen coverages (as can be seen from figure 4); at higher oxygen coverages, total oxidation to CO_2, CO and H_2O is favoured, and a lower coverage of C_4H_4 is attained due to the decreased availability of chemisorption sites. At low oxygen precoverages the overall selectivity towards furan formation is as high as 80%.

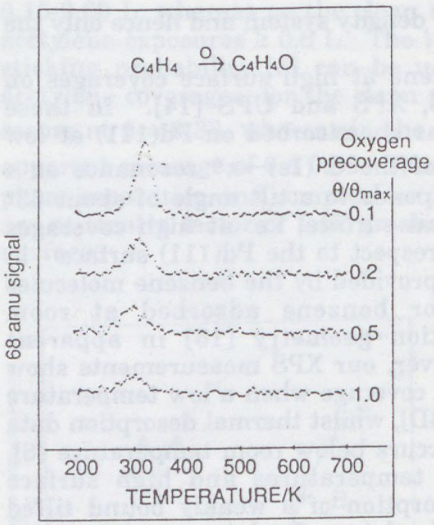

Figure 4. Partial oxidation of C_4H_4 intermediate to furan showing effect of oxygen precoverage.

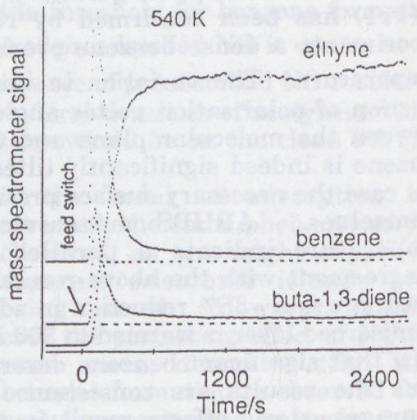

Figure 5. Time variation in benzene, buta-1,3-diene and acetylene production on switching gas feed from He to acetylene at 540 K; Pd/Al_2O_3 catalyst.

In order to establish whether the studies performed on well characterised single crystal surfaces under UHV conditions yield information which is relevant to an understanding of the properties of practical high area supported catalysts, we investigated the behaviour of practical supported Pd catalysts under high pressure conditions. For temperatures above 480 K, switching the gas feed from helium to acetylene immediately resulted in a high level of benzene synthesis which fell off with time to a substantially lower steady state value. This behaviour occurred for all the samples employed, including those supported on charcoal and TiO_2, and a typical benzene reaction profile for a Pd/Al_2O_3 sample is shown in figure 5. In addition to benzene, ***butadiene and butene*** are detected as products; both exhibiting the same time profile as benzene. No C_3 or C_5 products were detected. The fall from the initial high level of benzene production to its steady state level correlates with the increase in the amount of unreacted acetylene to its maximum level.

The synthesis of the C_4 species, butadiene and butene, and the complete absence of any C_3 or C_5 products, provides direct evidencefor the presence of a C_4 species on the surface under steady state reaction conditions. We propose that this C_4 species is precisely the C_4H_4 metallocycle identified by single crystal work [7-9,11]; butadiene and butene are exactly what one would predict

as primary and secondary hydrogenation products, respectively, of this key C_4H_4 intermediate. These observations demonstrate that in this case there is a direct correspondence between structure and reactivity data obtained with model systems under idealised conditions of low pressure and the behaviour of a practical catalyst under working conditions (>10^{12} times higher pressure).

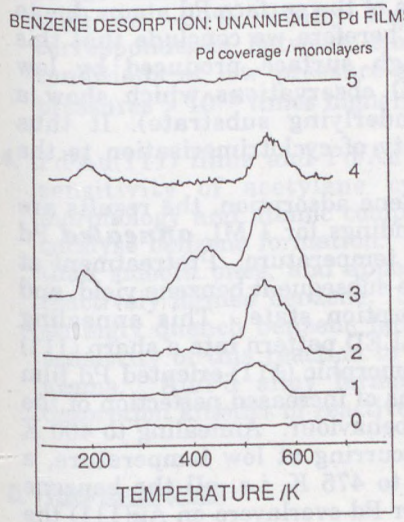

Figure 6. Benzene desorption from unannealed Pd films of increasing thickness deposited on Au(111) at < 170 K, following a saturation exposure of acetylene (6 L/170 K).

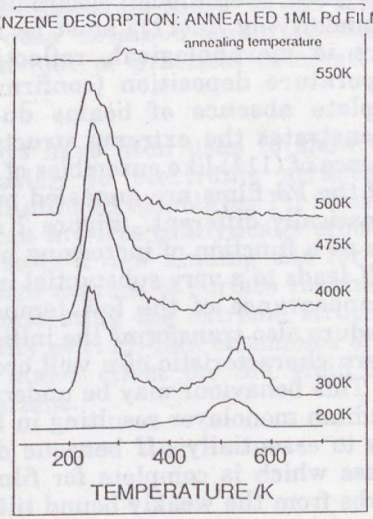

Figure 7. Benzene desorption following saturation acetylene exposure (6 L/170 K).

The available evidence indicates that acetylene cyclotrimerisation is sensitive to both the atomic geometry and the electronic structure of the surface. This may be investigated further by the application of alloy systems. We have demonstrated that gold is totally inert towards acetylene trimerisation and have therefore used Pd/Au(111) thin films of varying thickness and morphology and Au/Pd surface alloys of different compositions in order to examine "geometric" and "electronic" effects in the cyclisation of acetylene to benzene. Figure 6 shows the desorption of reactively formed benzene from ***unannealed*** Pd films deposited on Au(111) at < 170 K, as a function of Pd overlayer film thickness. The bottom spectrum confirms the inertness of the Au(111) surface towards cyclotrimerisation, while the second spectrum demonstrates that a 1 monolayer (ML) unannealed film of Pd is active towards benzene formation, though the yield is quite small and all desorption occurs from the high temperature desorption state, with no low temperature desorption occurring, indicating an appreciable effect due to the underlying

gold. 2 ML and 3 ML Pd films give rise to increased benzene formation and a new desorption state appears at ~410 K, intermediate in temperature between the two desorption maxima associated with the clean Pd(111) surface [5,6]. We attribute this feature to the effects of surface roughness of the Pd film arising from the low deposition temperature; this is in line with LEED data which shows the Pd overlayer to be highly disordered at this thickness. It can be seen that for 5 ML ***unannealed*** Pd films benzene formation is almost entirely suppressed, even though electronic perturbation of the surface Pd atoms due to the underlying Au(111) must be negligible. Therefore we conclude that this effect is morphological, reflecting the rough surface produced by low temperature deposition (confirmed by LEED observations which show a complete absence of beams due to the underlying substrate). It thus demonstrates the extreme structure sensitivity of cyclotrimerisation to the presence of (111)-like ensembles of Pd atoms.

If the Pd films are annealed prior to acetylene adsorption, the results are dramatically different. Figure 7 shows our findings for 1 ML ***annealed*** Pd films as a function of increasing pre-annealing temperature. Pretreatment at 300 K leads to a very substantial increase in the subsequent benzene yield, and the appearance of the low temperature desorption state. This annealing procedure also transforms the initially diffuse LEED pattern into a sharp (111) pattern characteristic of a well ordered pseudomorphic (111)-oriented Pd film [12]. This behaviour may be understood in terms of increased perfection of the palladium monolayer resulting in Pd(111)-like behaviour. Annealing to 400 K leads to essentially ***all*** benzene desorption occurring at low temperature, a process which is complete for films annealed to 475 K, i.e. all the benzene desorbs from the weakly bound tilted state. For Pd overlayers on Au(111) the onset of Au and Pd intermixing is detectable between 200 K and 300 K, with significant intermixing occurring by 475 K. These effects may be attributed to the progressive breaking up of Pd ensembles at the surface resulting from increased interdiffusion of Au and Pd with increasing preannealing temperature. In some respects this is analogous to the NO-induced behaviour described earlier. For temperatures above 525 K metal interdiffusion is rapid such that for films preannealed to 550 K, benzene formation is almost completely suppressed.

4. CONCLUSIONS

1. Coadsorbed nitric oxide exerts a very large promoting effect on the conversion of acetylene to benzene on Pd(111). This effect is attributable to the formation of separate adsorbate domains of high local coverage as a result of strong mutual compression. Under appropriate conditions benzene synthesis occurs at an apparent acetylene coverage which is ten times less than the critical coverage threshold observed on clean Pd(111); ~100% conversion to benzene occurs.

2. Steric crowding leads to reactively formed benzene being generated in a tilted geometry followed by subsequent low temperature evolution into the gas phase. As the surface becomes depleted of reactant and product species, the remaining benzene molecules adopt a more strongly bound, flat-lying geometry, which desorbs in the high temperature peak.

3. The presence of a reactive C_4H_4 intermediate under tricyclisation reaction conditions has been demonstrated with both single crystal model catalysts and high area supported catalysts, using coadsorbed oxygen and hydrogen, respectively. These reagents provide competing reaction channels, leading to the synthesis of furan from preoxygenated Pd(111) and butadiene and butene under steady state turnover conditions over supported Pd catalysts. In the former case the overall selectivity towards partial oxidation can be as high as ~80%, whilst the latter demonstrates there is a direct correspondence between single crystal data obtained under idealised conditions of low pressure and the behaviour of practical catalysts at pressures > 10^{12} times higher.

4. Pd/Au(111) films and Pd/Au surface alloys have been used to show the sensitivity of acetylene cyclotrimerisation to electronic structure, morphology and atomic composition. Well ordered monolayer Pd films do catalyse benzene formation. Rough Pd films are less catalytically efficient than smooth ones, and appear to give rise to a new binding site for the reactively formed benzene. Sufficiently high degrees of surface roughness strongly quench benzene formation demonstrating the extreme structure sensitvity of this reaction to the availability of (111)-like ensembles of Pd atoms. Au/Pd alloy formation has a major effect on the yield and desorption kinetics of reactively formed benzene.

5. REFERENCES

1. R.B. Grant and R.M. Lambert, *J. Catalysis*, 1985, **92**, 364
2. R.B. Grant and R.M. Lambert, *Langmuir*, 1985, **1**, 29.
3. W.T. Tysoe, G.L. Nyberg and R.M. Lambert, *J. Chem. Soc., Chem. Commun.*, 1983, 623.
4. W. Sesselman, B. Woratschek, G. Ertl, J. Küppers, H. Haberland, *Surface Science*, 1983, **130**, 245.
5. W.T. Tysoe, G.L. Nyberg and R.M. Lambert, *Surface Science*, 1983, **135**, 128.
6. C.H. Patterson and R.M. Lambert, *J. Phys. Chem.*, 1988, **92**, 1266.
7. C.H. Patterson and R.M. Lambert, *J. Am. Chem. Soc.*, 1988, **110**, 6871.
8. C.H. Patterson, J.M. Mundenar, P.Y. Timbrell, A.J. Gellman and R.M. Lambert, *Surface Science*, 1989, **208**, 93.
9. H. Hofmann, F. Zaera, R.M. Ormerod, R.M. Lambert, D.K. Saldin, J.M. Yao, L.P. Wang, D.W. Bennet and W.T. Tysoe, in preparation.
10. R.M. Ormerod, Ph.D. Thesis, Cambridge, 1989.
11. R.M. Ormerod and R.M. Lambert, *Catalysis Letters*, 1990, **6**, 121.
12. R.M. Ormerod, C.J. Baddeley and R.M. Lambert, *Surface Science*, 1991, **259**, L709.
13. H. Hofmann, F. Zaera, R.M. Ormerod, R.M. Lambert, D.K. Saldin, J.M. Yao, L.P. Wang, D.W. Bennet and W.T. Tysoe, *Surface Science*, in press.
14. H. Hoffmann, F. Zaera, R.M. Ormerod, R.M. Lambert, L.P. Wang and W.T. Tysoe, *Surface Science*, 1990, **232**, 259.
15. F.P. Netzer and J.U. Mack, *J. Chem. Phys.*, 1983, **79**, 1017.

DISCUSSION

Q: M. M. Bhasin (USA)

It is a very nice piece of work. I am quite intrigued by the role of NO in acetylene trimerisation to benzene. You mentioned that NO does not react but merely plays a "compression" role to bring acetylene molecules together for benzene formation. If this is so, NO should not be unique and other oxygenated compounds including O_2 should also work. Have you studied such molecules for assisting in acetylene trimerisation?

A: R. M. Ormerod

This is a good question. We have in fact studied the coadsorption of O_2 and acetylene on Pd(111) ion in considerable detail [1] and find that the activity of benzene formation and kinetics of benzene desorption are very different from those observed for the NO/acetylene system. Coadsorbed atomic oxygen generally suppresses benzene formation, with desorption being relatively favoured from the high temperature desorption state. These observations, which contrast strongly with those for the NO/C_2H_2 system, can however be rationalized in terms of our understanding of the reaction pathway.

In the case of nitric oxide, C_2H_2 coadsorption results in the formation of separate domains of high local coverage [2], which is facilitated by the essentially continuous compressibility of the unit cell of NO on Pd(111). In the case of preadsorbed oxygen, a rigid lattice is adopted, i.e. the unit cell cannot be compressed, and acetylene molecules can adsorb within the p(2x2) structure formed by O atoms [1]. However, at very low oxygen precoverages an effect similar to the "NO effect" is observed, as O atoms form islands and the acetylene molecules preferentially chemisorb outside these islands. This means that acetylene preferentially adsorbs into a restricted region of the surface, which results in a lowering of the threshold coverage for benzene formation [1].

In summary, we agree that NO should not be unique in this respect and this supported by our observation of a similar effect in the O_2/C_2H_2 system at low oxygen coverages; the requirements being that the coadsorbate has a unit cell which can be compressed, and a mutual repulsion exists between it and acetylene such that separate domains of the two species are formed. Thus we predict that such an effect, though not as dramatic, would be observed following coadsorption of CO and acetylene on Pd(111).

[1] R. M. Ormerod, R. M. Lambert, *J. Phys. Chem.* (1992) in press
[2] R. M. Ormerod, R. M. Lambert, *Surface Sci.*, **225**, L20 (1990)

Q: F. S. Stone (United Kingdom)

You explain the very interesting result of the effect of NO in facilitating benzene formation from adsorbed acetylene as a two-dimensional compression, NO being described as a chemically inert spectator molecule. However, NO may in fact be exerting a chemical effect, its electron donor adsorption on Pd serving to weaken the π-bonding between the co-adsorbed acetylene and the metal, i.e. to decrease the heat of adsorption of acetylene. Acetylene molecules thereby become more mobile and able to react more readily. The heat of adsorption of the product benzene may be similarly reduced by co-adsorbed NO, rendering its desorption more facile.

A: R. M. Ormerod

We explain the effect of NO in facilitating acetylene cyclotrimerisaion to benzene as a two-dimensional compression, on the basis of a combined LEED/thermal desorption investigation which we have reported in more detail elsewhere [2]. Briefly, LEED and TDS indicate that nitric oxide exists in islands of high local coverage, despite having been initially adsorbed to only a low coverage on the Pd(111) surface, as a result of the strong mutual compression between the NO and C_2H_2 molecules. This leads to the formation of separate domains of adsorbed NO and C_2H_2 of high local coverage (above the $\sqrt[3]{3}$ coverage threshold for benzene formation) despite the actual exposure being considerably less than that required to form benzene on the clean Pd(111) surface. This effect occurs as a consequence of the

continuous compressibility of the unit cell of NO on Pd(111) and the mutual repulsion which exists between the NO and C_2H_2 molecules.

In the above we have considered NO as a chemically inert spectator molecule, though we acknowledge that there may also be an additional effect associated with NO. However, such an effect is likely to be small since LEED and TDS clearly demonstrate that adsorption occurs into separate domains and therefore a chemical effects only likely to occur at the domain boundaries. Thus, in summary, all our observations can be rationalized in terms of our understanding of this reaction and a two-dimensional compression, without the need to invoke a chemical effect, though the latter cannot be completely excluded as an additional effect.

Q: S. Siegel (USA)

Recently, Professor Taube (Stanford University, USA) described η^2-benzene complexes of certain transition metals. These complexes may serve as useful models for the structure and properties of your weakly adsorbed benzene. Alkyl substitution lowers the stability of these complexes, a characteristic of mono-alkene complexes in which electron transfer from metal to the π^* (anti-bonding) alkene orbital can be important. In contrast, η^6-benzene complexes are stabilized by alkyl substitution. Is it reasonable to suppose, therefore, that the co-adsorbed NO changes the relative stability of the two forms of adsorbed benzene through an electronic effect?

A: R. M. Ormerod

The work of Professor Taube on η^2- and η^6-benzene complexes is very interesting and certainly may be of some relevance to the cyclotrimerisation of acetylene to benzene on extended Pd surfaces. However, as in our answer to professor Stone`s question/comment, the crucial factor is the strong mutual compression of the nitric oxide and acetylene into separate domains of high local coverage, and thus any electronic interaction between the NO and acetylene is only likely to occur at the domain boundaries. In our proposed reaction pathway all the benzene is synthesized at low temperature in a weakly bound tilted conformation. On the clean Pd(111) surface, desorption of some of the benzene and the transformation of unreacted acetylene to vinylidene increases the amount of free surface to such an extent that the remaining benzene molecules can adopt a more strongly bound flat-lying geometry, which gives rise to the high temperature benzene desorption peak. However, in the presence of nitric oxide, strong compression of the acetylene/benzene domains is maintained throughout the temperature range of the low temperature benzene desorption state. Thus, all the benzene is evolved from a high density system and hence only the low temperature peak is observed.

Q: C. J. Cameron (France)

What was the reasoning behind the addition of Au to Pd ? Was a combustion carried out after benzene desorption in order to determine whether other higher hydrocarbons such as polyacetylene are on the catalyst surface?

A: R. M. Ormerod

Previous work by ourselves and other research groups indicated that the efficiency of acetylene cyclotrimerisation is sensitive to both the atomic geometry and the electronic structure of the metal surface. Bimetallic alloys have been used for a variety of catalytic reactions in an attempt to elucidate effects of electronic structure and surface geometry (ligand and ensemble effects). Having predicted and then demonstrated that gold is totally inert towards acetylene cyclisation, the Au(111)/Pd system was chosen since it enables one to readily investigate the effect of variations in both the thickness and roughness of evaporated Pd films upon the trimerisation reaction, whilst thermal treatment can lead to surface alloy formation providing another way of altering the surface properties in a systematic and controlled manner. We have found that the trimerisation reaction is indeed strongly influenced by such factors and this has increased our understanding of this interesting and unusual reaction. Classical electronic dopants (e.g. K and Cl) were avoided as these

immediately introduce effects associated with site-blocking because the trimerisation reaction is very sensitive to geometric effects since it relies on the formation of an ensemble of three acetylene molecules [1] and thus it is difficult to separate electronic and structural effects using such additives.

In previous work we have demonstrated that the surface is free of carbon after a desorption sweep to 900 K, [3] and thus no higher hydrocarbon such as polyacetylene remain on the catalyst surface. The reaction can in fact be cycled many times in this manner without a decrease in benzene yield [4]. However, this is not a result of complete conversion to benzene; on the clean Pd(111) surface the maximum conversion to benzene is about 30 % [3], the remaining ~70% acetylene undergoing dehydrogenation, decomposition and subsequent dissolution into the Pd bulk, an effect which is relatively unique to Pd. Subsequent oxygen chemisorption and temperature programmed desorption leads to high temperature CO desorption indicating that this carbon can be segregated back to the surface by thermal oxygen treatment. In the case of NO/C_2H_2 coadsorption almost complete conversion to benzene occurs such that none of the acetylene undergoes thermal decomposition, and so both the surface and bulk remain free of carbon.

[3] H. Hoffmann, F. Zacra, R. M. Ormerod, R. M. Lambert, M. Yao, D. K. Saldin, L. P. Wang, D. W. Bennett, W. T. Tysoe, *Surface Sci.*, **268**, 1 (1992)

[4] W. T. Tyso, G. L. Nyberg, R. M. Lambert, *Surface Sci.*, **135**, 128 (1983)

Q: V. Ponec (The Netherlands)

Do you think that in your Pd on Au systems absolutely no Au atoms penetrated through and into the Pd layer? Is it really excluded ? Bearing in mind the surface sensitivity of Auger and XPS methods, I have some doubts.

A: R. M. Ormerod

In referring to a monolayer of Pd we do not necessarily imply that there is no Au in the top layer. However, a combination of angle-resolved Auger and XPS, and ion-scattering measurements suggest that the extent of intermixing is only very small at 170 K and only slightly greater at 300 K, significant intermixing not occurring until the temperature exceeds 450 K. This accounts for the benzene desorption behavior observed in Figure 7 of the paper. One of the reasons why gold was chosen for this study (aside from it being inert for the trimerisation reaction) was the knowledge that intermixing was likely to readily occur to give a range of surface compositions electronically modified with respect to clean Pd(111), without suffering from the problems associated with site-blocking electron donating and accepting additives such as potassium and chlorine.

Q: M. Ichikawa (Japan)

It seems to me, that the reaction of acetylene trimerised to benzene require the same size of metal ensemble. Basically you suggest that the benzene formation proceed by a single Pd atom isolated on the Pd Au alloy system or how do you appreciate the role of Au in alloying with Pd in terms of electronic effects or ensemble-breaking effects to explain the effect in acetylene trimerisation reaction ?

A: R. M. Ormerod

We are not proposing that a single Pd atom is capable of catalyzing the cyclotrimerisation of acetylene, though we are suggesting that an Au atom can substitute for a given Pd atom, and the ensemble that Pd atom was associated with remains active for benzene formation, as neither the structural nor electronic properties are strongly perturbed. In another paper we have used coadsorbed oxygen to identify the critical ensemble necessary for trimerisation to occur [1]; this being the availability of three three-fold hollow sites around a single Pd atom, one acetylene molecule adsorbing into each of these. In the Pd/Au system, if a single Pd atom is surrounded by 6 Au atoms we would consider this to be too electronically modified for benzene formation to occur. However, if it is surrounded by say 3 Au atoms and 3 Pd atoms then acetylene adsorption may be able to adsorb sufficiently strongly in the three three-fold hollow sites to enable cyclotrimerisation to occur.

Guczi, L. *et al.* (Editors), *New Frontiers in Catalysis*
Proceedings of the 10th International Congress on Catalysis, 19-24 July, 1992, Budapest, Hungary
© 1993 Elsevier Science Publishers B.V. All rights reserved

SURFACE CHEMISTRY FOR AUTOMOTIVE EMISSIONS CONTROL: INTERACTIONS OF NITRIC OXIDE ON A (111) Pt-Rh ALLOY SURFACE

G. B. Fisher, C. L. DiMaggio and D. D. Beck

Physical Chemistry Department, General Motors Research and Environmental Staff, Warren, MI 48090-9055, USA

ABSTRACT

As part of a study of catalytic materials important for automotive emissions control, the adsorption and dissociation of nitric oxide on a $Pt_{10}Rh_{90}(111)$ crystal has been studied using high resolution electron energy loss spectroscopy (EELS), temperature programmed desorption (TPD), Auger electron spectroscopy (AES), ion scattering spectroscopy (ISS), and low energy electron diffraction (LEED). The composition of the surface region according to AES and ISS was enriched in Pt to be about 30% Pt-70% Rh. Low coverages of NO (<0.05 sat.) adsorbed at 100 K are molecular, but dissociate completely upon annealing. By measuring the isothermal disappearance of the NO stretching mode in EELS, the activation energy for dissociation for NO on this surface was determined to be (27 $\pm$ 2) kcal/mole with a pre-exponential of (9 $\pm$ 1) x 10^{12} sec^{-1}. This activation energy is intermediate between the 19 kcal/mole and 45 kcal/mole values of the same quantity on the Rh(111) and Pt(111) surfaces, respectively. These results indicate that even the presence of 10 atomic percent Pt in the bulk significantly reduces this Pt-Rh alloy's ability to dissociate NO relative to a pure Rh surface.

1. INTRODUCTION

Reactions involving nitric oxide represent an important area of research in automotive exhaust catalysis, since NO_x emissions from automobiles are known to contribute to urban smog. In order to remove NO, as well as CO and hydrocarbons, from automotive exhaust, noble metals such as Rh and Pt have been used in catalytic converters to promote the NO reduction reaction ($2NO + 2CO \rightarrow N_2 + 2CO_2$) and other reactions, such as the CO oxidation reaction ($2CO + O_2 \rightarrow 2CO_2$). Previous studies have shown that Rh is chiefly responsible for the removal of NO, especially in rich exhaust, while both Rh and Pt catalyze the CO oxidation reaction [1-5]. More recent studies of noble metal particles present in in-use catalysts indicate that the particles are clearly bimetallic and not separate clusters of Rh and Pt [6]. These recent findings together with a report of beneficial synergistic reactivity of Pt-Rh alloys toward catalyzing automotive exhaust reactions [7] has motivated further research involving Pt-Rh alloys.

In order to gain a clearer picture of the fundamental role of alloy particles in the catalysis of NO and CO reactions, several groups have carried out high pressure and UHV studies probing the interaction of CO, O_2, H_2, and NO

with Pt-Rh alloy surfaces [8-14]. The justification for these studies, in part, is based upon the previously demonstrated ability of UHV derived rate constants to be successfully applied to rate expressions which quantitatively predict the CO oxidation and NO-CO reduction reactions which occur under real world conditions [15-17]. In the present study, our attention is focused on how NO interacts with a Pt-Rh alloy containing 10% Pt by atomic percent. Again, since it is known that Rh is the active metal for NO dissociation, the effects induced by the presence of Pt atoms in the Rh lattice on the NO dissociation energy has been explored. These results will help determine if, for example, Pt aids or inhibits Rh in the dissociation of NO in the absence of other species present to influence reaction parameters. Such results may then in turn be used in developing accurate reaction models involving NO at the higher pressures present in automotive exhaust.

Although the bulk composition of the Pt-Rh(111) crystal used in this study is 10% Pt, surface segregation has been previously reported in Pt-Rh alloy studies [8,10,11], so it was certainly necessary to measure our sample's surface composition. Auger electron spectroscopy (AES) is the standard method for surface composition measurement, but it provides a result which averages over roughly three atomic layers near the surface. Noble gas ion scattering spectroscopy (ISS) as we have done it has the inherent advantage that it probes only the atoms in the first layer at the surface. We have found our sample to be enriched in Pt in the surface region [18-20]. Under the conditions employed in this study and from previous work, we have also concluded that the alloy surface is stable and laterally well mixed [19,20]. Therefore, the effects we observe on this (111) surface appear to be largely the result of compositional changes in the surface and not heterogeneity of this surface. Hence, we have been able, for the first time, to obtain a reaction rate constant on an alloy surface of known surface composition.

2. EXPERIMENTAL ASPECTS

The surface chemistry experiments undertaken in this study were performed in a UHV chamber equipped with spectrometers for electron energy loss spectroscopy (EELS), Auger electron spectroscopy (AES), low energy electron diffraction (LEED), and thermal desorption spectroscopy (TPD). The EELS spectrometer used here employs two 127° sectors with an angle of incidence of 60° with respect to the surface normal. The beam energy was 3.5 eV with a FWHM of the elastic peak of 6-8 meV. All EELS spectra presented in the figures were taken in the specular direction. TPD spectra were taken line of sight to a mass spectrometer fitted with a conical collimator positioned approximately 2 mm from the crystal surface during desorption runs. All desorptions were performed at a constant ramp rate of 5 K/s. The crystal temperature was monitored with a chromel/alumel thermocouple which also completed a feedback loop that controlled the crystal temperature.

The $Pt_{10}Rh_{90}(111)$ boule used in this study was obtained from the Materials Research Corporation. The crystal subsequently cut and polished from this boule was found to be within 1/2° of the 111 plane. Details of the initial cleaning procedure were presented elsewhere [21]. However, once bulk impurities were removed, annealing in oxygen was sufficient to remove surface contaminants adsorbing out of background. Throughout the duration of this study, the equilibrated surface composition of the Pt-Rh crystal determined by the Auger line shapes and intensities of the Pt and Rh losses did not vary.

The gases used for the following experiments were of research purity. In order to minimize background adsorption of contaminant gases as well as residual dosing gases, all adsorptions were done line of sight from collimated array dosers at low chamber pressures ($<1.5 \times 10^{-10}$ torr). At the sample-to-doser distance used in this study, an amplification factor of 100 was determined for NO over background adsorption.

The surface composition was most concretely determined in a second ultrahigh vacuum chamber equipped with a differentially-pumped ion gun, electron gun, x-ray line source, and a charged particle energy analyzer for ion scattering spectroscopy (ISS) and AES. For the ion scattering experiments, the ion source was filled with a backpressure of 99.995% Ne which was 99.9% enriched with Ne^{20} to improve the resolution of the ISS experiments. In order to minimize the removal of surface atoms during the analysis, a beam current of 10.0 ± 0.2 nA was used and the beam was rastered over a 3 mm x 3 mm square region. Using a measurement time of 15 min, we have determined that the maximum amount that could be removed during the analysis is 10% of a monolayer [18].

3. RESULTS

3.1 Surface Composition from ISS and AES

In order to obtain reference intensities for our ISS and AES experiments, data was first taken on Pt(111) and Rh(111) over the same temperature range as in these experiments. Further details are discussed in Ref. 18. After correcting for the sensitivity difference between Pt and Rh in ISS, the ISS scattered ion peak areas were used to obtain the surface composition as a function of sample temperature. The result of this determination showing the Pt surface concentration is shown (solid circles) in Fig. 1. As the sample temperature is increased from 30°C to 600°C (303 K to 873 K), the composition of the surface remains constant. Above 600°C, however, the surface becomes "enriched" in Pt. The Pt content on the surface increases up to a value of 30% ± 2% at 1000°C (1273 K), but does not increase further as the temperature is increased from 1000°C to 1150°C (1423 K). Upon cooling, the Pt-enriched surface is maintained. During one of the subsequent heating and cooling experiments in vacuum, the sample temperature was maintained at 900°C and at 800°C for a period of 6 h prior to the ISS measurement. These tests were performed to determine whether the equilibrium composition at these temperatures was diffusion-limited. In these two treatments we did not observe a departure from the 30% Pt composition on the surface.

Auger measurements were also obtained for a similar series of experiments, with the results (solid squares) also shown in Fig. 1 . The Auger data also suggests that the surface composition remains constant as the sample temperature is increased from 30°C to above 600°C, and the Pt enrichment of the surface occurs as the temperature is increased from 600°C to 1150°C. At the latter temperature, the surface composition is 35% Pt. Upon cooling, the Pt concentration on the surface appears to decrease slightly, reaching 33% around 700°C. At the higher temperatures, the Auger lineshape broadened noticeably. Due to this phenomenon, the use of Auger to obtain surface composition information at high temperatures is not dependable. The ISS determination of the surface concentration is taken by the authors to be a generally more accurate analysis. It is important to note, however, that the qualitative trend observed in the AES data agrees with that in the ISS data. We will consider some of the quantitative differences in the Discussion.

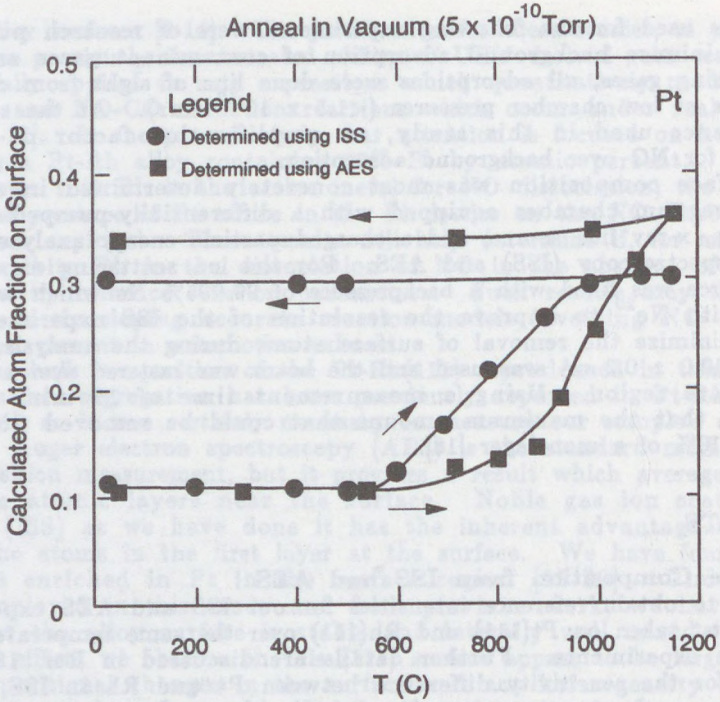

Figure 1. Surface composition of $Pt_{10}Rh_{90}(111)$ at various temperatures in vacuum calculated from the peak areas in the ion scattering spectra, or the Auger signal ratios, after correcting for the sensitivity difference between Pt and Rh. Spectra were obtained after annealing 1 h for $T < 900°C$ or after annealing 10 min for $T \geq 900°C$.

It is well to note that all of these surface compositions hold in vacuum. In a separate study, we have determined the variation in surface composition of this crystal as a function of temperature in the presence of an oxygen or hydrogen atmosphere ranging in pressure from 10^{-6} to more than 10 Torr [18]. The high pressure end of this range approximates partial pressures that exist in automotive exhaust.

3.2 NO Adsorption at 100 K - TPD

The desorption spectra of molecularly adsorbed NO at 100 K [20] show that annealing the initial adsorption of molecular NO results in complete dissociation. Complete NO dissociation continues up to an exposure of 0.07 L (~0.1 monolayer) at which point molecular NO begins to desorb as well as dissociate. The peak desorption rate of NO is at 430 K.

Although TPD indicates that low coverage exposures of NO dissociate upon heating, EELS clearly shows that the low temperature adsorption of NO is predominantly molecular (Fig. 2). NO initially adsorbs with characteristic frequencies of 1510 cm^{-1} and 1620 cm^{-1} with the 1510 cm^{-1} mode being the

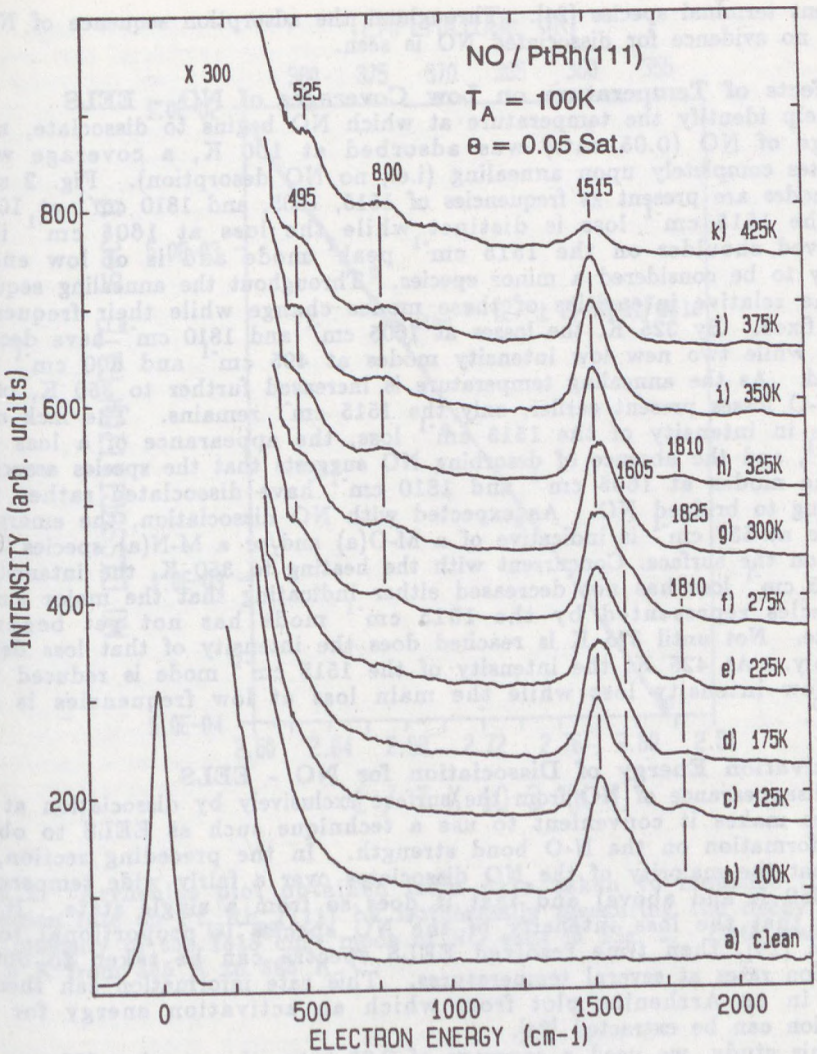

Figure 2. EELS spectra of a low NO coverage (0.05 of saturation) adsorbed on $Pt_{10}Rh_{90}(111)$ at 100 K, (b), and subsequently heated to the successively higher temperatures {curves (c) - (k)} indicated on the figure.

major species. The behavior of the 1510-1570 cm^{-1} loss is similar to that observed on Pt(111) [22,23] and Rh(111) [24]. By comparison to these single constituent surfaces, this mode clearly falls in the range for bridged NO species. The other NO loss that appears at 1620 cm^{-1} and shifts to 1644 cm^{-1} is above the range generally associated with bridged NO and below the frequencies observed for terminally bonded NO. It could indicate the presence

of a bent terminal species [24]. Throughout the adsorption sequence of NO at 100 K, no evidence for dissociated NO is seen.

3.3 Effects of Temperature on Low Coverages of NO - EELS

To help identify the temperature at which NO begins to dissociate, a low coverage of NO (0.05 sat.) was adsorbed at 100 K, a coverage which dissociates completely upon annealing (i.e., no NO desorption). Fig. 2 shows three modes are present at frequencies of 1515, 1605, and 1810 cm^{-1} at 100 K. Only the 1515 cm^{-1} loss is distinct while the loss at 1605 cm^{-1} is an unresolved shoulder on the 1515 cm^{-1} peak mode and is of low enough intensity to be considered a minor species. Throughout the annealing sequence only the relative intensities of these modes change while their frequencies remain fixed. By 325 K, the losses at 1605 cm^{-1} and 1810 cm^{-1} have declined slightly while two new low intensity modes at 495 cm^{-1} and 800 cm^{-1} have appeared. As the annealing temperature is increased further to 350 K, of the three N-O losses present earlier, only the 1515 cm^{-1} remains. The lack of an increase in intensity of the 1515 cm^{-1} loss, the appearance of a loss near 500 cm^{-1}, and the absence of desorbing NO suggests that the species associated with the modes at 1605 cm^{-1} and 1810 cm^{-1} have dissociated rather than converting to bridged NO. As expected with NO dissociation, the emergence of a loss at 537 cm^{-1} is indicative of a M-O(a) and/or a M-N(a) species being formed on the surface. Concurrent with the heating to 350 K, the intensity of the 1515 cm^{-1} loss has not decreased either indicating that the major surface NO species represented by the 1515 cm^{-1} mode has not yet begun to dissociate. Not until 375 K is reached does the intensity of that loss decline noticeably. At 425 K, the intensity of the 1515 cm^{-1} mode is reduced to a broad low intensity loss while the main loss at low frequencies is now 525 cm^{-1}.

3.4 Activation Energy of Dissociation for NO - EELS

The disappearance of NO from the surface exclusively by dissociation at low coverages makes it convenient to use a technique such as EELS to obtain more information on the N-O bond strength. In the preceding section, we found that the majority of the NO dissociates over a fairly wide temperature range (350 K and above) and that it does so from a single state. If one assumes that the loss intensity of the NO species is proportional to its coverage [24], then time resolved EELS spectra can be taken to obtain dissociation rates at several temperatures. This rate information can then be plotted in an Arrhenius plot from which an activation energy for NO dissociation can be extracted [24].

For this study, we used a coverage of 0.03 saturation so that NO present on the surface would be characterized by a single loss at 1510 cm^{-1}. To monitor the progress of dissociation, a series of time resolved EELS spectra were obtained by intermittently taking EELS spectra after annealing the NO coverage over intervals of time to a fixed temperature. Plotting, I_{NO}/I_0, the ratio of the NO mode's intensity relative to the elastic peak intensity, versus the annealing time yields a plot of the decay of the NO mode's intensity as a function of time under isothermal conditions. The dissociation rate is obtained simply by determining the slope of this plot. This process was carried out at seven annealing temperatures between 355 K and 385 K and enough data was obtained to construct the Arrhenius plot in Fig. 3. From this plot, the heat of dissociation for NO on this surface was found to be (27 $\pm$ 2) kcal/mole with a pre-exponential of (9 $\pm$ 1) x 10^{12} sec^{-1}. The determination of this rate constant for this surface has been been the main goal of this study.

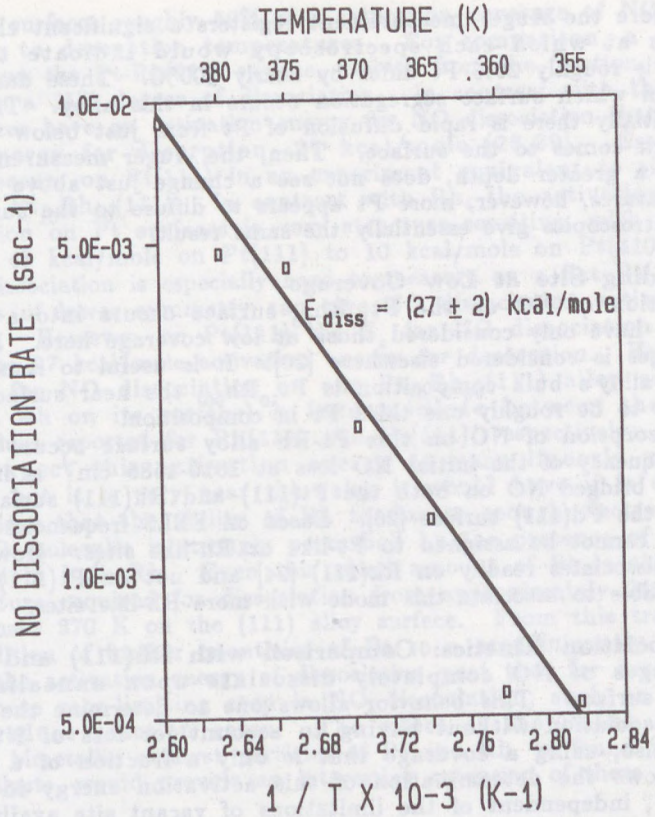

Figure 3. Arrhenius plot obtained from data taken to measure the NO dissociation rate on $Pt_{10}Rh_{90}(111)$ by isothermally measuring the decay of the EELS intensity of the 1515 cm^{-1} mode of NO seen in Fig. 2. Data was taken every 5 K from 355 K to 385 K.

4. DISCUSSION

4.1 Surface Composition

Our ISS observations of a Pt-enriched surface composition for this sample are in general agreement with earlier Auger measurements of this same Pt-Rh(111) sample [19,20] and with other studies of similar Pt-Rh alloy samples [8]. Other researchers have also observed Pt enrichment of high Rh content and high Pt content Pt-Rh alloys [e.g., 10,11]. This is the first detailed study comparing Auger and ISS measurements as a function of temperature. The equilibrated surface composition of the surface measured by each method gives essentially the same value, which is heartening to those who only have Auger spectrometers available to them.

It is interesting to note in Fig. 1, however, that as the temperature is raised the ISS measurement shows the first layer surface concentration

increasing before the Auger measurement registers a significant change. The temperatures at which each spectroscopy would indicate the surface concentration is roughly 20% Pt differ by nearly 200°C. These data may bear on the way in which surface segregation occurs in this alloy. These results imply that initially there is rapid diffusion of Pt from just below the surface, much of which comes to the surface. Then, the Auger measurement, which averages over a greater depth, does not see a change just above 600°C. At higher temperatures, however, more Pt appears to diffuse to the surface region and both spectroscopies give essentially the same result.

4.2 NO Bonding Site at Low Coverage

The adsorption of NO on the $Pt_{10}Rh_{90}$ surface occurs into a number of states, but we have only considered those at low coverage here. Behavior at higher coverages is considered elsewhere [20]. It is useful to remember that although this alloy's bulk composition is $Pt_{10}Rh_{90}$, the near surface region is enriched in Pt to be roughly one third Pt in composition.

Initially, adsorption of NO on this Pt-Rh alloy surface occurs in bridged sites. The frequency of the initial NO loss at 1510-1585 cm^{-1} is in the same range seen for bridged NO on both the Pt(111) and Rh(111) surfaces [22-25], as well as on the Pd(111) surface [26]. Based on EELS frequencies alone, this bridging mode cannot be assigned to Pt-like or Rh-like sites. However, since bridging NO dissociates readily on Rh(111) [24] and not on Pt(111) [22,23], it is more reasonable to associate this mode with more Rh-like sites.

4.3 NO Dissociation Kinetics: Comparison with Rh(111) and Pt(111)

Low coverages of NO completely dissociate upon annealing on the $Pt_{10}Rh_{90}(111)$ surface. This behavior allows one to determine the activation energy for dissociation without having to account for loss of NO through desorption. Also, using a coverage that is only a fraction of a monolayer (0.03 sat.) allows the determination of this activation energy in the "zero coverage limit", independent of the limitations of vacant site availability and coadsorbed reaction products present at higher coverages. Since the variation of the EELS loss intensity of the 1520 cm^{-1} bridging mode was used in this study, this also removed the influence and monitoring of the probable bent species which could effect the value for E_a. The log of the decrease in the loss intensity is linear with time [20] indicating that the dissociation process is first order. As reported in the results section, plotting several of these rates yielded an $E_a = (27 \pm 2)$ kcal/mole with a pre-exponential of $(9 \pm 1) \times 10^{12}$ sec^{-1}. This E_a value for NO dissociation is very similar to the estimated Ea for NO desorption from the Pt-Rh surface of 26 $\pm$ 2 kcal/mole [20]. This is consistent with our observation that desorption and dissociation are seen to occur over the same temperature range. The balance between these competing processes shifts from favoring dissociation at low to intermediate coverages to favoring desorption at higher coverages, because of site blocking by NO and its dissociation products and possibly electronic effects induced by additional NO.

The NO heat of dissociation obtained from this work for $Pt_{10}Rh_{90}(111)$ can be compared to values obtained for Rh(111) and Pt(111). Root et al. [24] used the same approach as in this work and found that the activation energy for NO dissociation on Rh(111) is 19.2 ± 0.3 kcal/mole with a pre-exponential near 10^{14} s^{-1} kcal/mole. These values on Rh surfaces may be relatively structure-insensitive, since E_a for NO dissociation on Rh(100) has been found to be 18 ± 1 kcal/mole with a normal first order pre-exponential [16,27] On

both of these surfaces roughly 50% of a saturation coverage of NO dissociated upon heating to desorption temperatures. For comparison, a dissociation measurement on the Pt-Rh(111) surface, derived from the fraction of N_2 which desorbs, yields a 25% degree of dissociation. In contrast with these surfaces, Pt(111) surfaces have an activation energy for NO dissociation that exceeds the activation energy for desorption, 27 kcal/mole [28,29]. Essentially no dissociation occurs on Pt(111) in an experiment equivalent to that done on Rh(111) and $Pt_{10}Rh_{90}$(111). In contrast with Rh, the activation energy for NO dissociation on Pt surfaces is very structure sensitive, with cited values varying from 45 kcal/mole on Pt(111) to 10 kcal/mole on Pt(410) [30]. The E_a for NO dissociation is especially hard to measure on a flat Pt(111) surface, because steps of lower symmetry can give NO dissociation activity at lower temperatures. However, on Pt(111) the E_a for NO dissociation is certainly well above the 27 kcal/mole activation energy for desorption. Hence, we find that the E_a for NO dissociation on our $Pt_{10}Rh_{90}$(111) alloy surface (with 30% Pt-70% Rh on its surface) is intermediate between the 19 and 45 kcal/mole values reported for Rh(111) and Pt(111), respectively. There is no reason to expect this activation energy to vary linearly with surface composition, but it is very near the value it would have if it did. In any case, it is clear that the ability of Rh to donate enough electron density to dissociate NO molecules is strongly perturbed by the presence of just 10% Pt concentration in bulk Rh. Even this small amount of Pt in the bulk raises the temperature required for dissociation from approximately 240 K on pure Rh(111) to near 370 K on the (111) alloy surface. From this trend, it seems that the addition of further quantities of Pt to a predominantly Rh substrate could push the activation energy of dissociation past that for desorption. For reactions whose rate-limiting step is NO dissociation, such an effect would appear to reduce reaction rates. The effect of the Pt/Rh ratio on the reactivity of bimetallic catalyst particles of Pt and Rh, as found in automotive exhaust catalysts, would provide an interesting extension of these results.

5. CONCLUSIONS

NO adsorption at low coverages on the PtRh(111) surface is characterized by the presence of a dominant bridging species at 1510 cm^{-1}. As on Rh(111), it appears that NO adsorbed in bridging Rh-like sites displays the greatest tendency to dissociate. We conclude that $Pt_{10}Rh_{90}$(111) behaves like a stable, well-mixed alloy surface; its interaction with nitric oxide, especially its heat of dissociation, is clearly distinguishable from that of Pt or Rh alone.

The influence of Pt in the Pt-Rh(111) surface is reflected in the high E_a obtained for NO dissociation relative to a purely Rh surface. It appears that even these small bulk concentrations of Pt are enough to raise the E_a for dissociation high enough to allow desorption to become a competitive process at all but the lowest coverages. This effect suggests that any addition of Pt to a Rh substrate may be detrimental to the reactivity of the surface toward NO dissociation. Based on this study, if NO dissociation is the rate limiting step in the process of catalyzing the NO reduction reaction with CO or H_2 under high pressure conditions, a Pt-Rh catalyst would not appear to offer improved reactivity over Rh. However, because of the complexity of the gas mixtures present in automotive exhaust and the presence of other species, such as ceria, on the actual supported catalyst, the selectivity of the surface toward specific reaction steps is impossible to predict without further model studies.

REFERENCES

1 K. C. Taylor, in Vol. 5 of "Catalysis: Science and Technology," (eds., J. R. Anderson and M. Boudart), Springer-Verlag, Berlin, 1984, p. 119.
2 K. C. Taylor, CHEMTECH, 20 (1990) 551.
3 J. T. Kummer, Prog. Energy Combust. Sci., 6 (1980) 177.
4 L. L. Hegedus and J. J. Gumbleton, CHEMTECH, 10 (1980) 630.
5 J. Wei, Adv. Catal., 24 (1977) 57.
6 S. Kim and M. J. D'Aniello, Jr., Appl. Catal., 56 (1989) 23; 45.
7 S. H. Oh and J. E. Carpenter, J. Catal., 98 (1986) 178.
8 F. L. Williams and G. C. Nelson, Appl. Surf. Sci., 3 (1979) 409.
9 J. Wang and L. D. Schmidt, J. Catal., 70 (1981) 187; 71 (1981) 411.
10 M. Ahmad and T. T. Tsong, Surf. Sci., 149 (1985) L7.
11 F.C.M.J.M. van Delft, A. D. van Langeveld, and B. E. Nieuwenhuys, Surf. Sci., 189/190 (1987) 1129.
12 F.C.M.J.M. van Delft, G. H. Vurens, M. C. Angevaare-Gruter, and B. E. Nieuwenhuys, in "Catalysis and Automotive Pollution Control," (eds. A. Crucq and A. Frennet), Vol. 30, Studies in Surface Science and Catalysis, Elsevier, Amsterdam, 1987, p. 229.
13 F.C.M.J.M. van Delft, J. Siera, R. J. Vreeburg, M. J. Koster van Groos, A. D. van Langeveld, and B. E. Nieuwenhuys, in "Catalysis: Theory to Practice," (eds. M. J. Phillips and M. Ternan), Proceedings of the 9th International Congress on Catalysis, Chemical Institute of Canada, Ottawa, 1988, p. 1355.
14 T. Yamada, H. Hirano, K. Tanaka, J. Siera, and B. E. Nieuwenhuys, Surf. Sci., 226 (1990) 1.
15 S. H. Oh, G. B. Fisher, J. E. Carpenter, and D. W. Goodman, J. Catalysis, 100 (1986) 360.
16 G. B. Fisher, S. H. Oh, J. E. Carpenter, C. L. DiMaggio, S. J. Schmieg, D. W. Goodman, T. W. Root, S. B. Schwartz, and L. D. Schmidt, in "Catalysis and Automotive Pollution Control," (eds. A. Crucq and A. Frennet), Vol. 30, Studies in Surface Science and Catalysis, Elsevier, Amsterdam, 1987, p. 215.
17 G. B. Fisher, S. H. Oh, C. L. DiMaggio, S. J. Schmieg, D. W. Goodman, and C. H. F. Peden, in Catalysis: Theory to Practice, (eds., M. J. Phillips and M. Terna, (Chemical Institute of Canada, Ottawa, 1988), p. 1355.
18 D. D. Beck, C. L. DiMaggio, and G. B. Fisher, submitted to Surface Science.
19 G. B. Fisher and C. L. DiMaggio, submitted to Surface Science.
20 C. L. DiMaggio and G. B. Fisher, submitted to Surface Science.
21 G. B. Fisher and S. J. Schmieg, J. Vac. Sci. Tech. A, 1 (1983) 1064.
22 H. Ibach an S. Lehwald, Surf. Sci., 76 (1978) 1.
23 J. L. Gland and B. A. Sexton, Surf. Sci., 94 (1980) 355.
24 T. W. Root, G. B. Fisher, and L. D. Schmidt, J. Chem. Phys., 85 (1986) 4679.
25 C.-T. Kao, G. S. Blackman, M. A. Van Hove, G. A. Somorjai, and C.-M. Chan, Surf. Sci., 224 (1989) 77.
26 M. Bertolo and K. Jacobi, Surf. Sci., 226 (1990) 207.
27 J. S. Villarubia and W. Ho, J. Chem. Phys., 87 (1987) 750.
28 J. A. Serri, J. C. Tully, and M. J. Cardillo, J. Chem. Phys., 79 (1983) 1530.
29 C. T. Campbell, G. Ertl, and J. Segner, Surf. Sci., 115 (1982) 309.
30 R. I. Masel, Catalysis Rev., 28 (1986) 335.

DISCUSSION

Q: D. A. King (United Kingdom)

I am also interested in understanding exactly what is being reported as the activation energy for NO dissociation, for Pt, Rh and Pt-Rh surfaces. This is presumably the barrier between the chemisorbed NO molecule and the dissociative products on the surface, N and O adatoms. The puzzle is that, at least in the case of Pt, your figure would appear to be larger than the heat of adsorption for the molecular chemisorbed state. On heating the surface, desorption should therefore be preferable to dissociation. Does your measurement of the activation energy for the process take this into account, and if so, how? If the crossover point is below the potential energy zero, reported to the gas phase molecule, why does not dissociation occur directly on collision from the gas phase? Is this due to efficient energy exchange with the surface during the collision ?

A: G. B. Fisher

NO behaves quite understandably on these surfaces, not much differently than a number of systems examined by the questioner. For Pt(111), with an activation energy of desorption for NO, E_{des}, of 27 kcal/mole and an E_a of 45 kcal/mole (see Ref. 30 in the paper), NO, indeed, does desorb before dissociating on Pt(111). Careful studies (see Refs. 28, 29 in the paper), in fact, have shown that any dissociation on Pt(111) occurs at steps. Of course, for Rh(111) the crossover point in a one-dimensional representation of the NO_{ads} and the N_{ads} and O_{ads} potential wells is below the potential energy zero, referenced at the gas phase molecule. The E_{des} is about 26 kcal/mole, while E_a is 19 kcal/mole (see Ref. 24 in the paper). Hence, after being adsorbed at low temperatures into the molecular state, low coverages of NO dissociate completely and there is no NO desorption. However, the situation is more complicated in that the activation energy for dissociation is determined at low coverage, while its value clearly increases with increasing coverage. Also, E_{des} has only been measured at higher coverages in TPD. Collisions from the gas phase on 100 K surfaces are so well accommodated that no dissociation occurs, but at higher surface temperatures, still below the desorption temperature, dissociation can occur. There is evidence that dissociation does occur for the initial coverages that arrive at the surface at 300 K, but E_a is increasing so rapidly with increasing coverage that the dominant species in a saturation coverage adsorbed at that temperature is molecular NO. Hence, even though all of a low coverage of NO adsorbed at 100 K will be dissociated at 250 K on Rh(111), a saturation coverage at 100 K can be heated above 400 K before any dissociation occurs. With no vacant sites available, no dissociation can occur, until NO desorption begins around 400 K [1, 2]

[1] T. W. Root, L. D. Schmidt, G. B. Fisher, *Surface Sci.*, **134**, 30 (1983)
[2] S. B. Schwartz, G. B. Fisher, L. D. Schmidt, *J. Phys. Chem.*, **92**, 389 (1988)

Q: C.-G. Huang (Taiwan)

NO dissociation energy should be a thermodynamic property. It depends upon the difference between the initial NO molecular state and the states of dissociated N and O atoms. As seen in your data, it varies in the range of 19 to 65 kcal/mole, depending upon the metal used. Could you hypothesize what factors cause this large difference in dissociation energy?

A: G. B. Fisher

The activation energy for NO dissociation is the energy required to surmount the barrier between the adsorbed NO molecular state on a particular surface and the state where atomic N and O are bound to the same surface. It is not a thermodynamic property, since it depends on the pathway or transition state the molecule use to become dissociated. The electronic character of the metal and the binding site are both important factors in determining what transition states are available to the molecule. In our Ref. 30, R. I. Masel discusses the variation in activation energy for dissociation of NO E_a on a number of single crystal Pt

surfaces. E_a NO varies from 45 kcal/mole on Pt(111) to about 10 kcal/mole on Pt(410). Clearly the symmetry of the NO binding site is important on these surfaces in determining whether sufficient charge donation occurs to dissociate the molecule. In contrast, the E_a NO on (100) and (111) Rh surfaces are nearly identical, so the electronic character of the surface controls dissociation in that case.

Q: D. Wang (China)

Your work shows that NO dissociation is an activated process. This can raise a "pressure gap" question about the UHV estimate(s) of rate parameters. That is, if the adsorbates were first heated (energized) in the gas phase prior to adsorption, would determined rate parameters be different ?

A: G. B. Fisher

The variations in energy due to heating in the gas are quite small compared with other energies in these reactions. Rate parameters should not vary under normally achievable circumstances. Reaction models using our UHV-determined rate parameters for the CO-O_2 and NO-CO reactions have quantitatively predicted the high pressure rates of these reactions (see refs. 15 and 16 in our paper) over a wide range of temperatures and pressures. In particular, the same kinetics hold over eight orders of magnitude in pressure for the CO-O_2 reaction on Rh(111) [3]. For reactions with strongly-bound reactants like these, the "pressure gap" is bridged very easily, because the coverage of reactants, which controls the reaction rate, can be similar over a wide range of pressures and temperatures. What is important in successfully mimicking reactions in UHV is bridging the "coverage gap" to coverages that occur under the conditions of interest.

[3] S. B. Schwartz, L. D. Schmidt, G. B. Fisher, *J. Phys. Chem.*, **90**, 6194 (1986)

Q: C. H. Bartholomew (USA)

What are the effects of O_2 and H_2O on the coverages and heats of adsorption of NO and CO on Pt, Rh, and Pt-Rh?

A: G. B. Fisher

This sounds like it would make a great thesis topic for one of the questioner's students. Much more is known about the effect of oxygen on NO and CO adsorption than for water. For instance, on Rh(111) preadsorbed oxygen prevents NO dissociation and reduces the peak NO desorption rate by 40 K [4]. Presumably because atomic oxygen occupies the same sites as the N_a and O_a from dissociated NO would take, dissociation is inhibited and would be also on Pt(111) and the alloy. In the case, of heating CO coadsorbed with oxygen on these surfaces, CO_2 is usually formed before CO would desorb. For CO and water coadsorbed on Pt(111) and Rh(111) there is a very interesting study [5], which shows there are repulsive interactions between CO and H_2O on Rh(111) and attractive interactions between them on Pt(111). I am not immediately aware of any coadsorption studies of NO and H_2O on these metals, but a literature search on the subjects raised in this question might reveal considerably more.

[4] F. T. Wagner, T. E. Moylan, S. J. Schmieg, *Surface Sci.*, **195**, 403 (1988)
[5] T. W. Root, L. D. Schmidt, G. B. Fisher, *Surface Sci.*, **134**, 30 (1983)

Q: R. W. Joyner (United Kingdom)

Some related questions designed to guide those of interested in academic studies of these systems

1) is it certain that alloying is beneficial in practical catalysts?

2) if so, when are the effects most noticeable, what are the conditions and what are the metal ratios in the alloy?

A: G. B. Fisher

1) For catalysts in general, there are several examples of beneficial effects of alloying [6]. For most automotive catalyst formulations, bimetallic particles are clearly formed. The studies done in Ref. 6 show, with microanalytical techniques, that most of the metal particles in an automotive catalyst are multi-metallic, so alloying is clearly a possibility for metals that are miscible throughout their phase diagram like Pt and Rh. No benefit has been found in vehicle tests from separating Pt and Rh, and there are laboratory studies that show beneficial effects of alloying (Ref. 7 in our paper). However, this is not a heavily explored area.

2) The Pt:Rh ratios in automotive catalysts are generally between 10:1 and 5:1. With that information, a research project could be begun to answer your question.

[6] J. H. Sinfelt, "Bimetallic Catalysts: Discoveries, Concepts, and Applications", (John Wiley, New York, 1983)

Q: X. X. Guo (China)

What do you think of one co-adsorption effect of CO and NO. Is it an important factor in the design a bimetallic alloy catalyst?

A: G. B. Fisher

The "coadsorption effect of NO and CO" may refer to the difference in results when NO and CO are adsorbed competitively on Rh(111) and Pt(111). NO will displace CO on Rh(111) and CO will displace NO on Pt(111) [7, 8]. This is one of many factors to consider in designing a catalyst, bimetallic or not.

[7] T. W. Root, L. D. Schmidt, G. B. Fisher, *Surface Sci.*, **150**, 173 (1985)
[8] T. W. Root, G. B. Fisher, L. D. Schmidt, *J. Chem. Phys.*, **85**, 4687 (1986)

Q: J. Kaspar (Italy)

Why did you use such high rhodium content in your Rh-Pt alloy ? Secondly, what happens to the surface composition when you use a lower Rh content ?

A: G. B. Fisher

1) When we started these studies we wanted to be sure we would see effects large enough to measure. Since we knew from previous work (e.g. ref. 8 in our paper) that the surface would probably enrich in Pt, we decided to begin our work at the Pt deficient end of the alloy composition range to see if we could vary the surface composition over a wide range. We were able to move to a 30% Pt-rich surface from a 10% Pt bulk composition, but we also found the equilibrated surface composition was very stable and difficult to vary in UHV.

To be nominally relevant a Pt-rich alloy would be a better choice since automotive catalyst Pt:Rh ratios vary mainly between 10:1 to 5:1. However, there are so many other differences between these studies and those of really relevant systems, that the choice of the precise model system is probably not so important.

2) Generally speaking, the surface composition for lower Rh content bulk alloys enrich in Pt when heated in vacuum. To see specific examples, one may look at our Refs. 8 and 10, in our paper and several appears by B. E. Nieuwenhuys and his collaborators, (e.g. refs. 11-14 in our paper) and [9]

[9] F. C. M. J. M. van Delft, B. E. Nieuwenhuys, Siera, R. M. Wolf, *I.S.I.J. Int.*, **29**, 550 (1989)

Q: K.-I. Tanaka (Japan)

We studied precisely the $(NO+H_2)$ reaction on the (100), (111) and (410) surfaces of $Pt_{0.75}Rh_{0.25}$ alloy, and the following two remarkable differences were found on the (100) and (111) surfaces as presented in "O-S".

1) The selectivity towards N_2 was 100% on the (100) surface but 0% on the (111) surface for the reaction of $NO+H_2$.

Did you compare the activity for the reaction of NO+CO on (100) with that on (111) surface of your Rh rich alloy?

2) We can accumulate N_a on the (100) + (111) surfaces by reacting O_a with H_2 or CO. We found the N_a on the (100) surface gives a C(2x2)-N ordered structure, but the N_a on the (111) surface gives only a diffuse LEED pattern. Did you observe some structures for the N(a) on your (111) surface?

3) We want to know the minimum required amount of Rh on the surface. From this view point, what is the reason you used a Rh-rich alloy ?

A: G. B. Fisher

1) No, we have not yet done any NO+CO reaction studies on the (100) or (111) surfaces of Pt-Rh alloys. We have been collaborators in studies of the NO+CO reaction over Rh(100) and Rh(111) surfaces at high (~10 Torr) pressures [10] and refs. 15-17 in our paper (Rh(111) only) and at low (~10^{-6} Torr) pressures [11].

2) We have always seen sharper adsorbate spots in LEED patterns for adsorbates on Rh(100) than on Rh(111). I can find no definite record of a LEED pattern for N atoms on Rh(111).

3) See my answer to the same question from Dr. Kaspar.

[10] C. H. F. Peden, D. W. Goodman, D. S. Blair, P. J. Berlowitz, G. B. Fisher, S. H. Oh, *J. Phys. Chem.*, **92**, 1563 (1988)

[11] S. B. Schwartz, G. B. Fisher, L. D. Schmidt, *J. Phys. Chem.*, **92**, 389 (1988)

Q: B. E. Nieuwenhuys (The Netherlands)

It was proposed that the Pt and Rh atom of PtRh(111) are well-mixed in the surface layer. We have also found that the Pt and Rh atoms are randomly distributed over a clean PtRh(111) surface. However, in the presence of adsorbates the distribution of Pt and Rh over the surface may change. The effect of oxygen on the surface composition is well documented. Professor Chesters and coworkers (Norwich, UK) in collaboration with my group made some interesting observations for CO on PtRh(111) using RAIRS. The results indicate that Pt-islands are formed when CO is adsorbed on the surface at 300 K. It is our experience that the surface composition, the surface structure and the distribution of Pt and Rh atoms over the surface may vary with changing experimental conditions.

A: G. B. Fisher

This comment emphasizes the complexities that one can potentially find when working with bimetallic systems.

Q: J. C. Bertolini (France)

It is a priori surprising that the surface composition of $Pt_{10}Rh_{90}$ alloys, say $Pt_{30}Rh_{70}$ in the surface, does not change with temperature (in the range 1173 - 1473 K where no diffusion problems do occur). Do you think, and have you evidence, that this signifies that the Pt surface enrichment extends to some layers below the surface ?

A: G. B. Fisher

Data taken with ISS in ref. 18 as we sputter through the equilibrated surface region shows that the vacuum-annealed surface enrichment has dropped within a few per cent of the bulk value in the first 1.0 nm of the surface or within 3 to 4 layers. Hence, the enrichment drops off very rapidly into the bulk, but clearly involves more than the first layer for this alloy.

Guczi, L. *et al.* (Editors), *New Frontiers in Catalysis*
Proceedings of the 10th International Congress on Catalysis, 19-24 July, 1992, Budapest, Hungary
© 1993 Elsevier Science Publishers B.V. All rights reserved

SHAPE SELECTIVE ALKYLATION OF BENZENE WITH LONG CHAIN ALKENES OVER ZEOLITES

S. Sivasanker, A. Thangaraj, R. A. Abdulla and P. Ratnasamy

National Chemical Laboratory, Pune 411 008, India

Abstract

The alkylation of benzene with 1-hexene, 1-octene, 1-dodecene and a mixture of C_{10}-C_{13} olefins (alkylation feed used in LAB manufacture) was carried out over a number of zeolites. While zeolite Y does not exhibit shape-selectivity effects, the other wide pore zeolites, β, mordenite and ZSM-12, exhibit shape-selectivities favouring the formation of the less bulky 2-ϕ isomers during the alkylation. The studies suggest that both product and transition state type shape-selectivities influence product distribution. An examination of the composition of the phenyl isomers obtained over zeolites can lead to conclusions regarding their pore characteristics.

1. INTRODUCTION

Linear alkylbenzenes (LAB) are valuable industrial chemicals used in the manufacture of detergents. These are manufactured by the alkylation of benzene with linear olefins using anhydrous HF [1]. Due to the hazardous nature of anhydrous HF, efforts are on to find environmentally safer catalysts like solid acids [2-5]. UOP has recently announced a new process which uses a proprietary solid acid catalyst [6].

During the alkylation of benzene with long chain alkenes (C_{10}-C_{13}), a mixture of alkyl benzenes with the phenyl-group attached to different carbon atoms is obtained. Of the different isomers, the most preferred component in detergent manufacture is the 2-phenyl (2-ϕ) isomer which possess better emulsibility characteristics than the others. When alkylating benzene with long chain olefins over zeolites, there is a possibility of producing more of the less bulky 2-ϕ isomer than the others due to their narrow pore dimensions. Unlike the alkylation of benzene with lighter (C_2-C_4) olefins [7-9] over zeolites not much information on alkylation with longer alkenes, especially C_{10}-C_{13} is available. This paper reports the alkylation of benzene with 1-hexene, 1-octene, 1-dodecene and a mixture of C_{10}-C_{13} olefins over a number of medium and wide pore zeolites.

2. EXPERIMENTAL

2.1 Materials

1-hexene (99 + % pure), 1-octene (98 % pure) and 1-dodecene (95 % pure) were obtained from Aldrich Chemical Company, USA and used as such. The major impurities in the above compounds were the corresponding alkanes and double-bond isomers. The mixture of C_{10}-C_{13} olefins (alkylation feed) was obtained from a commercial LAB manufacturer. The alkylation feed contained about 10 wt.% olefins and 90 % paraffins.

Table 1
Composition and characteristics of the zeolites used

Zeolite	SiO_2/Al_2O_3 (mole)	Surface area (m^2/g) Zeolite	Non-zeolite*	Pore-system	Source
H-Y[1]	6.2	530	120	3-D; 0.74 nm openings; 1.3 nm cages	Linde, USA
RE-Y[2]	5.1	775	37	-do-	PQ-zeolites, Holland
DAl-Y	10.4	644	5	-do	Linde, USA Dealuminated [10]
H-M (1)[3]	17.7	598	1	1-D; 0.67 x 0.7 nm	Norton, USA
H-M (2)	43.9	568	66	-do-	Dealuminated [11]
H-M (3)	99.2	538	85	-do-	-do-
H-β	35.0	500	191	3-D; 0.75nm and 0.55 nm	PQ-zeolites, Holland
H-β(Ga)[4]	48.1	351	109	-do-	Synthesized [12]
H-EU-1	40.0	432	64	1-D; 0.58 x 0.41 nm (side pockets : 0.68 x 0.58 x 0.81 nm)	Synthesized [13]
H-K-L[5]	6.1	350	3	1-D; 0.71 nm	Linde, USA
H-ZSM-12	111.5	342	55	1-D; 0.57 x 0.6 nm	Synthesized [14]
H-ZSM-5	39.4	413	7	2-D; 0.54 x 0.56 nm and 0.51 x 0.55 nm	United Catalysts India Ltd., India
Si-Al[6]	11.4	-	437	Av. dia. = 2.7 nm	Prepared

*: Includes contribution from external surface of zeolite crystallites.
1: US-Y sample.
2: 70 % RE-exchanged from NH_4^+-form; calcined to obtain H-form.
3: H-mordenite.
4: Gallium isomorph of β.
5: Exchanged with NH_4NO_3 to convert to H-form (50 % exchange).
6: Amorphous SiO_2-Al_2O_3.

The pure olefins and the olefin mixture were dried over silica-gel, while benzene (> 99.9 % pure) was dried over molecular sieves (4A) prior to use.

A number of zeolites and molecular sieves were used in these studies. Their source and properties are presented in Table 1.

2.2 Methods

The alkylation reaction was carried out either at atmospheric pressure using a glass (10 mm i.d) reactor or in a stainless steel (SS 316; 19 mm i.d) reactor (Catatest, Model BL-2, Géomecanique, France) at high pressures. Both the glass and SS reactors were fixed bed down-flow types.

The catalyst was always dried at 480° C for 6 h in flowing dry air, prior to the start of the run. The dry catalyst was then cooled to the reaction temperature in a flow of dry N_2. Benzene was injected first for a one hour period at the reaction temperature prior to injection of the actual alkylation mixture (Olefins + Benzene). The exact reaction parameters used in different experiments will be presented along with the data in the later sections.

The analysis of the reactants and products was carried out using a capillary column (HP 1, 50 m X 0.5 mm) in a gas chromatograph (FID; HP model 5880 A).

3. RESULTS AND DISCUSSION

3.1 Alkylation with 1-hexene

Table 2 presents the results of the alkylation of benzene over a number of zeolites. Two different types of zeolites have been used in these studies, *viz.*, Zeolites possessing pores with 12 membered ring (12 MR) openings (wide pore zeolites) and those with 10 membered ring (10 MR) openings (medium pore zeolites). The wide pore zeolites used are H-Y H-β, H-M, H-L and H-ZSM-12. The medium pore zeolites are EU-1 and ZSM-5. For comparison purposes an amorphous SiO_2-Al_2O_3 was also used.

Zeolite Y possess a three dimensional pore system (0.74 nm dia.) with cages (1.3 nm dia.). This has the most open pore system among the large-pore (12 MR) zeolites. Zeolite β has a three dimensional pore system consisting of two types of pores (0.73 and 0.55 nm dia.). Mordenite, L and ZSM-12 possess non-connecting unidimensional pores with cross sections of 0.67 x 0.7 nm, 0.71 nm and 0.57 x 0.60 nm, respectively.

The medium pore zeolite ZSM-5 has a two dimensional pore system with two types of pores along two perpendicular axes. The pore dimensions for the two sets of pores are 0.54 x 0.56 nm and 0.51 x 0.55 nm. EU-1 has a unidimensional pore system (0.58 x 0.41 nm) with side pockets of dimensions (0.68 x 0.58 x 0.81 nm).

When alkylation was carried out with 1-hexene, the 2-ϕ and 3-ϕ isomers were found to be produced (Table 2). Similar results have also been obtained Venuto *et al.* [15] during their limited study on benzene alkylation with 1-hexene over RE-X. The 1-ϕ isomer (wherein the phenyl group is attached to the terminal carbon of hexene) was not detected due to the lower stability of the primary carbenium ion compared to the secondary carbenium ions [16]. The 3-ϕ isomer is produced by the isomerization of the C2-carbenium ion to the C3-carbenium ion which occurs rapidly even at relatively low temperatures over even weak acid sites.

As the stability of $(C2)^+$ and $(C3)^+$ ions are nearly the same, one should obtain 2-ϕ and 3-ϕ isomers in near equal amounts, i.e., the ratio of the 2-ϕ-hexane to 3-ϕ-hexane (2-ϕ/3-ϕ) should be ≤ 1. However, Table 2 shows that the 2-ϕ/3-ϕ ratio is always > 1 for all the zeolites and even silica-alumina. The reason for this is the competitive nature of the alkylation and olefin-isomerization reactions and the lack of any skeletal isomerization at the conditions of the reaction. Even before the equilibration of the hexene isomers (or carbenium ions) is achieved, alkylation of the reactant 1-hexene to the 2-ϕ isomer takes place.

The values of the 2-ϕ/3-ϕ ratios on the large pore zeolites are mostly close to 1. The one exception is ZSM-12 which has a value of 2.66. This could be due to its highly puckered ring system leading to a smaller pore-opening (0.57 x 0.60 nm). It is surprising to note that even in the case of silica-alumina which possesses an average pore-diameter much larger (~ 2.7 nm) than those of the zeolites, the 2-ϕ content is large (2-ϕ/3-ϕ = 1.91). The reason is probably related to its lower acidity (acid strength) when compared to the zeolites and the consequent slower isomerization of the C2 carbenium ion.

Table 2
Alkylation of benzene with 1-hexene over different catalysts

Zeolite	TOS (h)	Conversion, (wt.%) 1-hexene	C_6-olefins[a]	$C_6^=$ utilization (wt. %) < C_6 fraction	C_6-satu-rates[b]	Others[c]	C_6-ϕ[d]	2-ϕ/3-ϕ	Δ[e]
Col. No.:	1	2	3	4	5	6	7	8	9
DAl-Y	4	93.55	88.21	17.76	13.91	5.10	63.23	1.26	
	15	65.01	27.18	8.01	26.36	2.72	62.91	1.36	0.9
RE-Y	4	92.20	84.37	0.31	15.54	3.11	81.04	1.20	
	17	54.33	20.71	-	39.74	1.21	59.05	1.26	0.5
H-β	3	100.00	100.00	12.56	50.53	2.10	34.81	1.50	
	9	100.00	94.68	0.60	8.72	1.27	89.41	2.08	9.7
H-β(Ga)	2	94.51	55.06	0.30	24.07	2.32	73.31	2.11	
	10	95.68	32.55	-	50.85	-	49.15	2.85	9.3
H-M (1)	4	100.00	88.35	10.06	62.80	5.90	21.24	1.30	
	18	96.94	35.58	0.48	57.93	1.80	39.79	3.10	12.9
H-M (1)*	3	100.00	99.52	17.06	43.23	18.24	21.47	2.14	
	18	97.99	82.32	0.60	6.04	8.20	85.16	4.27	14.2
H-M (2)	4	66.36	65.13	0.61	1.15	8.95	89.29	3.37	
	19	61.51	58.01	0.54	5.69	3.50	90.27	4.27	6.0
H-K-L	3	83.44	19.14	0.16	72.99	1.83	25.02	1.84	
	19	70.78	15.19	-	86.11	0.33	13.56	2.16	2.0
ZSM-12	4	98.39	75.07	0.13	11.17	4.76	83.94	2.66	
	19	92.90	67.66	0.12	12.28	2.80	84.82	2.84	1.2
H-EU-1	2	95.75	32.18	2.46	46.68	4.01	46.85	5.70	
	14	96.19	31.81	0.94	48.55	3.63	46.68	7.65	18.3
ZSM-5	4	94.39	27.35	12.29	48.56	18.20	20.95	12.00	
	13	94.58	23.34	3.77	58.05	16.28	21.89	8.13	- 41.1
Si-Al	4	94.66	26.58	20.13	62.27	5.68	11.81	1.91	
	8	81.29	10.84	1.11	61.62	12.27	24.35	2.39	11.3

Conditions : Temp. (K) = 413; Press. (MPa) = 0.1; WHSV (h^{-1}) = 4.0; Benzene : 1-hexene (mole) ratio = 10; * : 433 K also in the case of H-M (1).

a: Excluding double bond isomerization to i-$C_6^=$.
b: 2-Me and 3-Me pentanes and n-hexane.
c: Mostly < C_6-alkyl benzenes and heavier material.
d: n- and i-products; n-ϕ > > i-ϕ; mostly monoalkyl benzenes.
e: Δ = Change in 2-ϕ/3-ϕ ratio per hour x 100.

In the case of the two medium pore zeolites, EU-1 and ZSM-5, the 2-ϕ/3-ϕ ratios are much larger (5.7 and 12.0, respectively) indicative of the shape-selectivity of these zeolites. It is, however, interesting to note that EU-1 which has a much smaller pore opening than ZSM-5 leads to a lower 2-ϕ/3-ϕ ratio. Apparently, product shape-selectivity (which is determined by the size of the pore opening) is not the only important factor in determining the 2-ϕ/3-ϕ ratios. The presence of large side pockets in EU-1 (Table 1) provides enough space for the bimolecular alkylation reaction, which leads to the formation of the bulkier 3-ϕ isomer. In ZSM-5, apparently bimolecular reactions are sterically more hindered [17]. Thus, the above results indicate that both product and transition state selectivities may be playing a role in determining the 2-ϕ/3-ϕ ratios in the case of zeolites.

The change of the 2-ϕ/3-ϕ ratio during run is presented in column 9, Table 2. In the case of DAl-Y, the change is negligible (0.9 units). The rate of change is highest (12.9) for mordenite, while β possesses an intermediate value of 9.7. The magnitude of the above changes are related to the size and type of the pore systems. The 3-dimensional pore systems (Y and β) produce smaller changes. Mordenite with a unidimensional pore system leads to a larger change in the 2-ϕ/3-ϕ ratio with increasing duration of run. However, the change of the ratio in both L, possessing a larger pore diameter (0.71 nm) and ZSM-12, possessing smaller pore openings (0.57 x 0.6 nm) is similar (2.0 and 1.2, respectively).

The selectivity for the 2-ϕ isomer increases in the case of EU-1, while it decreases rapidly in the case of ZSM-5. The decrease in the formation of the bulkier 3-ϕ isomer over EU-1 is due to probably the blockage (or non-accessibility) of the side-pockets wherein such isomers may be formed preferentially. The decrease in the 2-ϕ isomer formation over ZSM-5 is probably due to the progressive blockage of the pore-openings and the increased contribution of the external surface to the reaction as the reaction progresses.

The initial activity and deactivation rate (decrease in conversion with time) of the different zeolites is found to be again different (column 3, Table 2). The large pore zeolites, Y and Mordenite have higher initial activities and also deactivate rapidly. While the rapid deactivation of Y is attributed to its larger acid site density, deactivation of mordenite is due to its unidimensional pore system. The medium pore zeolites, EU-1 and ZSM-5, both possess low initial activities and deactivation rates. Similarly, they also possess low selectivities for hexyl-benzenes (column 7, Table 2). Again, the selectivities for hexyl-benzene production do not change significantly in the case of the above two zeolites.

Zeolite Y and ZSM-12 exhibit good selectivities for hexyl-benzene formation both initially and after a TOS of 15-19 h, while β and H-M (1) exhibit high selectivities only after many hours on stream. The dealuminated mordenite H-M (2), on the other hand, has good selectivities both when TOS = 4 and 19 h.

The shape-selectivity of zeolites is accentuated by the presence of extraneous materials inside the pores or at the pore-openings. The presence of extraneous materials inside the pores is often detected by the adsorption of hydrocarbons and NMR-methods [18]. The amorphous content of zeolite samples was quantitatively estimated by the adsorption of Argon using the t-plot method [19]. However, how much of this amorphous material affects the pore openings or the pore-dimensions is not easy to determine. Zeolite-β and its Ga-isomorph β (Ga) contain substantial amounts of amorphous materials (Table 1). We also find that their 2-ϕ/3-ϕ ratios are higher than even that of mordenite. Similarly, the dealuminated mordenite, H-M (2), also contains

amorphous materials and has a larger 2-ϕ/3-ϕ ratio than H-M (1). However, eventhough RE-Y is more amorphous than DAl-Y, the 2-ϕ/3-ϕ ratios are similar in the two zeolites due to the larger and more open pores in the FAU-system.

Increasing the temperature of the reaction in the case of H-M (1) increases olefin conversion without increasing the selectivity for alkyl benzenes formation (Table 2). Similar results were also observed in the case of Y and β.

3.2 Alkylation with 1-octene

The alkylation of 1-octene was carried out over the two wide pore zeolites Y and mordenite which possess significantly different pore structures. The results are presented in Table 3.

Table 3
Alkylation of benzene with 1-octene

Zeolite	TOS (h)	C_8-olefin conv. (wt.%)	Product distribution, (wt. %)								
			Alkyl-benzenes							Others*	2-ϕ/4-ϕ+
			< C_8	C_8							
				i-2-ϕ	2-ϕ	i-3-ϕ	3-ϕ	i-4-ϕ	4-ϕ		
H-Y	6	~ 100	20.85	0.23	6.12	0.14	4.77	0.16	4.28	63.45	1.43
	12	~ 100	16.49	0.39	11.17	0.31	8.70	0.28	7.77	54.89	1.44
H-M (1)	3	95.8	17.30	0.46	27.01	2.75	16.16	3.13	2.66	30.53	4.74
	5	95.9	3.13	1.32	24.33	1.29	11.59	1.26	1.39	55.69	9.68

Conditions : Temp. (K) = 413; Press (MPa) = 0.1; WHSV (h^{-1}) = 1.0; Benzene : Olefin (mole) ratio = 20.

* : Includes cracked and isomerization products.
\+ : Includes iso-phenyl compounds also.

As expected, Y does not appear to possess any shape-selectivive effect, while mordenite possesses very large shape-selective characteristics. The 2-ϕ/3-ϕ ratio (measure of shape-selectivity) increases rapidly with increasing time on stream in the case of mordenite, but does not increase in the case of Y (last column, Table 3). Large amounts of iso-compounds are found to be produced over both zeolites the i-ϕ-formation being more in the case of mordenite. As the mordenite pores are narrower than Y, this observation is surprising. This suggests that the contribution of the external surface of the crystallites to the reaction is probably significant in the case of mordenite.

3.3 Alkylation with 1-dodecene

The results of the alkylation studies carried out with 1-dodecene are presented in Table 4. The studies were carried out at a pressure of 0.6 MPa and a temperature of 408 K at which conditions benzene remains in the liquid phase. Also a low space velocity (WHSV = 0.8 h^{-1}) was used. Under the above conditions, catalyst deactivation was much smaller, 100 % conversion being observed for upto about 20 h for most of the catalysts. The lower deactivation noted at 0.6 MPa is probably due to the solvent action

of liquid benzene dissolving away the deactivating components from the catalyst surface. Under the above conditions, the yields of the C_{12}-alkylated products (ϕ-dodecanes) were also high, the selectivities being > 80 % in the case of RE-Y, SiO_2-Al_2O_3 and β.

Table 4
Alkylation of benzene with 1-dodecene

Catalyst	C_{12}-alkyl benzene distribution, (wt. %)+						
	2-ϕ	3-ϕ	4-ϕ	5-ϕ	6-ϕ	2-ϕ/6-ϕ ratio	2-ϕ/3-ϕ ratio
Si-Al	33.4	21.9	14.8	15.6	14.2	2.4	1.5
RE-Y	17.6	19.1	19.8	22.0	21.5	0.8	0.9
H-β	39.1	26.4	18.9	10.8	4.8	8.2	1.5
H-M (2)++	563.7	35.4	0.9	tr	-	70.7**	1.8
H-M (3)++	65.8	34.2	tr	-	-	-	1.9
HF*	16.7	16.4	17.5	24.1	25.3	0.7	1.0

Conditions : Temp. (K) = 408; Press. (MPa) = 0.6; WHSV (h^{-1}) = 0.8 ; Benzene : Olefin (mole) ratio = 10; Conversion of olefin ~ 100 %; Data obtained at 10 h on stream)

\+ : Includes iso-phenyl compounds.
++: Conversion incomplete.
* : C_{12}-alkyl benzene fraction from commercial LAB: liquid phase reaction; WHSV indeterminate.
** : 2-ϕ/4-ϕ ratio.

As discussed in an earlier section, based on the relative stabilities of the different secondary carbenium ions, one would expect the isomer content to increase with the C-number. This is found to be so in the case of both HF and RE-Y. Apparently, RE-Y is non-shape selective even during alkylation with a large molecule like dodecene. β and mordenite, which were both non-shape selective or weakly shape-selective during alkylation with 1-hexene, now exhibit marked shape-selectivities with dodecene. Olson has also observed differences in isomer distribution of dodecyl benzenes during studies using HF, H_2SO_4 and $AlCl_3$ [20].

The shape-selectivity effect, as expected, is much larger for the unidimensional mordenite system than for β; in fact, mordenite is so shape-selective that the 6-ϕ isomer is not detected at all. Further, both H-M (2) and H-M (3) deactivated more rapidly than the other zeolites, the selectivity for the C_{12} alkyl benzenes being less than 10 % at the above conditions. Interestingly, silica-alumina is found to produce relatively more of the 2-ϕ and 3-ϕ isomers when compared to HF or RE-Y. Apparently, as discussed earlier, acidity differences are probably responsible for this behaviour.

3.4 Alkylation with mixture of olefins (C_{10}-C_{13})

The results of alkylation with a commercial mixed olefin feed (C_{10}-C_{13}) are presented in Table 5. The composition of the feed according to the C-fractions is also presented in the table. Due to the large number of isomeric olefins in each carbon fraction, and the difficulty in separating and identifying them, estimation of the individual components has not been carried out.

Table 5
Alkylation of benzene with a mixture of (C_{10}-C_{13}) olefins+

Product		Product distribution, (wt. %)					
		Catalyst					
C_n	n-ϕ	H-M (1)*	H-β	H-Y	RE-Y	Si-Al	HF**
C_{10}	2	22.5	8.0	4.7	2.9	4.9	5.0
	3	7.2	3.5	2.8	2.8	3.4	3.5
	4	6.3	2.9	2.6	3.5	2.5	3.0
	5	13.1	2.5	2.6	5.0	3.0	3.1
C_{11}	2	38.5	16.1	11.4	7.9	12.0	5.9
	3	8.8	10.1	7.3	7.4	8.0	5.8
	4	tr	7.8	6.4	7.9	5.7	6.4
	5	-	2.1	6.2	8.8	5.9	8.4
	6	-	3.1	3.1	3.9	2.7	4.3
C_{12}	2	3.6	10.5	10.9	6.1	11.8	5.7
	3	tr	7.1	7.3	6.6	8.0	5.7
	4	-	5.2	6.2	7.0	5.4	6.1
	5	-	2.9	6.4	8.4	5.7	8.4
	6	-	1.3	6.4	7.0	5.2	8.8
C_{13}	2	-	6.7	4.0	2.3	4.5	2.9
	3	-	4.3	2.8	2.3	4.5	2.9
	4	-	2.2	2.4	2.8	2.0	3.2
	5	-	1.9	2.6	3.2	2.0	4.3
	6	-	0.8	2.6	3.0	2.0	4.7
	7	-	1.0	1.3	1.2	0.8	2.0
2-ϕ (%)		64.6	41.3	31.0	19.2	33.2	19.6

Conditions : Temp. (K) 408; Press. (MPa) = 0.6; WHSV (h^{-1}) = 0.8; Benzene : Olefin (mole) ratio = 10.

\+ : Composition of feed (wt. %) : Olefins (total) = 9.7; C_{10} = 1.9; C_{11} = 3.1; C_{12} = 2.9; C_{13} = 1.8. Paraffins (C_{10}, C_{11}, C_{12} and C_{13}) constitute the rest.

* : Conversion incomplete.

** : Composition of parent olefin mixture not known; Commercial LAB product; liquid phase reaction; WHSV indeterminate.

The results are found to be similar to those reported earlier. SiO_2-Al_2O_3, H-β, H-Y and H-M produce more 2-ϕ isomers than RE-Y and HF. As expected, shape-selectivity in the case of H-M and H-β increases with increase in the C-number of the fraction. It is to be noted that the end-phenyl isomers of the C_{11} and C_{13}-alkyl benzenes are present in smaller quantities due to the lower alkylation probability (half) at the central carbon atoms.

At the conditions of the study, the conversions of the olefins over the samples (except H-M (1)) were 100 %. The selectivity for alkyl benzenes were also very high, being > 90 % for all the catalysts (except H-M (1)).

The influence of process parameters on the life of H-Y in the alkylation with mixed olefins is presented in Table 6. Increasing the temperature beyond 403 K does not increase the life (defined as time at which > 0.1 % olefin is found in the product) of the catalyst. Similarly, operating at low benzene to olefin ratios lowers the life of the catalyst. Increasing the pressure increases the life of the catalyst, though beyond 0.6 MPa the effect is not significant. The reason for increased life at higher pressures has already been explained as being due to the solvent action of liquid benzene present in the system.

Table 6
Alkylation of benzene with a mixture of olefins: Influence of process parameters on life of catalyst*

Benzene : Olefin (mole) ratio	Temp. (K)	Press.** (MPa)	Life of catalyst+ (h)
10	413	0.1	24
10	413	0.6	76
10	413	3.0	80
10	373	0.6	Incomplete conversion
10	403	0.6	70
10	423	0.6	72++
5	413	3.0	55
10	413	3.0	80
15	413	3.0	76

Conditions : Vertical flow SS reactor; WHSV (h^{-1}) = 0.8.

* : Catalyst, H-Y.
** : Pressurized with N_2
\+ : Life for < 0.1 % olefin content in product; ± 4 h.
++ : Product was pale yellow.

4. CONCLUSIONS

Zeolite-Y does not exhibit shape-selectivity effects in the alkylation of benzene with long-chain alkanes with C-number as large as 13. Mordenite and β exhibit shape-selectivities, their shape-selectivities being more pronounced with increasing C-number of the alkane. The shape-selectivities observed are attributed to both product and transition-state types.

5. ACKNOWLEDGEMENTS

We thank Dr. H.S. Soni, Anuj Raj and J.S.Reddy for their help during the above study. This work was partly funded by UNDP.

6. REFERENCES

1. P.R. Pujado, in " Handbook of Petroleum refining process" (R.A. Meyers, ed.), Mc Graw-Hill, 1986.
2. R.T. Sebulsky and A.M. Henke, Ind. Eng. Chem., Process Dev., 10 (1971) 272.
3. He Ming-Yuan, L. Zhonghui and and M. Enze, Catal. Today, 2 (1988) 321.
4. L.B. Young, US Pat. 4, 301, 317 (1981).
5. T. Berna, L. Jose, D. Moreno and Alfonso, EP Appl. 0 353, 813 (1991).
6. B.V. Vora, P.R. Pujado, T. Imai and T.R. Fritsch, Paper presented in "Recent advances in the detergent industry", Society of Chemical Industry, Univ. of Cambridge, England, 26-28 March 1990.
7. J.J. Wise, US Pat. 3, 251, 897 (1966).
8. K.A. Becker, H.G. Karge and W.D. Streubel, J.Catal., 28 (1973) 403.
9. W.W. Kaeding and R.F Holland, J.Catal., 109 (1988) 212.
10. D.W. Breck and G.W. Skeels, in "Proc. 6th Intern. Zeol. Conf." (D.H. Olson and A. Bisio, eds.), Butterworths, 1984, p.87.
11. J. Bandiera, C. Hamon and C. Naccache, Proc. 6th Intern. Zeol. Conf. (D.H. Olson and A. Bisio, eds.), Butterworths, 1984, p.337.
12. R.N. Bhat and R. Kumar, J.Chem.Biotechnol., 48 (1990) 453.
13. J.L. Casci, B.M. Lowe and T.V. Whittam, EP Appl. 42 226 (1981).
14. A.R. Pradhan, Thesis, Univ. Poona (1991); S. Ernst, P.A. Jacobs, J.A. Martens and J. Weitkamp, Zeolites, 7 (1986) 25.
15. P.B. Venuto, L.A. Hamilton, P.S. Landis and J.J. Wise, J.Catal., 5 (1966) 81.
16. A. Corma, A. Lopez Agudo, I. Nebot and F. Tomas, J.Catal., 77 (1982) 159.
17. D.H. Olson and W.O. Haag, Am. Chem. Soc. Symp. Ser. 248 (1984) 275.
18. A.Corma and J.Nieman, Proc. Akzo Catal. Symp. 1991, Fluid Catalytic Cracking, Scheveningen, The Netherlands, p.217.
19. M.F.L. Johnson, J.Catal., 52 (1978) 425.
20. A.C. Olson, Ind.Eng.Chem., 52 (1960) 833.

DISCUSSION

Q: H. G. Karge (Germany)
You mentioned the rapid deactivation of mordenite catalysts used for benzene alkylation by long chain alkenes. During our early work on benzene alkylation by ethene or propene, we observed the same phenomenon. However, the life time of the mordenite catalysts was much improved via dealumination. Possibly, dealuminated mordenites may also exhibit a better performance in the case of alkylation of benzene by long alkenes.

A: P. Ratnasamy
Our experiments on alkylation with long chain olefins over mordenites dealuminated to different levels upto a SiO_2/Al_2O_3 ratio of about 100 have suggested the existence of an optimum SiO_2/Al_2O_3 ratio of about 45.

Q: W. O. Haag (USA)
As you pointed out in your paper, there are two possibilities to account for high selectivity for 2-phenylalkane: (1) a rapid alkylation relative to isomerisation or (2) shape selective preference via transition state or product diffusion control. We have also examined benzene alkylation with linear olefins. We used, for example, mordenite catalyst and either 1-octene or 4-octene. If alkylations were fast relative to isomerisation, the predominant product in the latter case would be 3-phenyloctane. However, both olefins give the same product distribution which was predominantly 2-phenyloctane. Thus, shape selective control is the operating mechanism.

A: P. Ratnasamy
We agree that shape selective control is probably the primary operating mechanism in mordenite catalysts.

Q: D. Kalló (Hungary)
Did you determine the primary products of alkylation at low conversions ?

A: P. Ratnasamy
No, we did not.

Q: D. Barthomeuf (France)
With regard to fast deactivation, do you think that it arises from the acidity of the zeolite, from the microporosity or from other parameters. Do all the zeolites you study give the same deactivation rate ?

A: P. Ratnasamy
Different zeolites deactivate at different rates. Both acidity (especially acid site density) and microporosity probably influence the rate of deactivation.

Q: H. Schulz (Germany)
As a procedure for reactivation of the catalyst, a simple thermal treatment could be successful (as we have observed in the regime of reamination) during methanol conversion on HZSM-5 (International Zeolite Conference in Montreal, July, 1992). Have you tried this procedure in your experiments for the various zeolites ? Could you also give some numbers in deposit selectivity, because these would characterize the task of reactivation further ?

A: P. Ratnasamy
We have also observed that a limited reactivation takes place (especially in the case of some high silica zeolites) with thermal treatments under certain conditions.
The shape selectivity change (Column 9 in Table 2) is a measure of "DEPOSIT" effects. Real numbers in % deposits are not available.

Q: K. P. de Jong (The Netherlands)

1) How do you characterize the heavy deposits present on the spent catalyst in order to discriminate between what you called "heavy alkylate" and "oligomeric species"?

2) You mentioned that solvent extraction suffices to rejuvenate the catalysts. Which solvents are appropriate? Which procedures (e.g. temperature, time) for extraction did you apply?

A: P. Ratnasamy

1) Heavy alkylates are poly-alkylation products of benzene, while oligomeric species are dimers, trimers etc. of the long chain olefin.

2) Passing benzene at reaction conditions for 10 hours was found to remove a significant fraction of the heavy deposits.

Guczi, L. *et al.* (Editors), *New Frontiers in Catalysis*
Proceedings of the 10th International Congress on Catalysis, 19-24 July, 1992, Budapest, Hungary
© 1993 Elsevier Science Publishers B.V. All rights reserved

COMPARISON OF SAPO-37 WITH FAUJASITES IN CRACKING REACTIONS

M. Briend, M. Derewinski, A. Lamy and D. Barthomeuf

Laboratoire de Reactivite de Surface et Structure, URA 1106 CNRS, Universite P. et M. Curie, 4 place Jussieu, 75252 Paris Cedex 05, France

Abstract

The n-octane cracking has been studied with a series of H-SAPO-37 of increasing Si content and for HY, dealuminated HY and LZY-82. The influence of framework Si content in SAPO-37 strongly depends on the pretreatment temperature which very likely modifies the distribution of atoms in the structure. Silica impurities are not involved in this process. The catalytic activity of H-SAPO-37 increases up to a pretreatment of 1173 K while that of the Si-Al faujasites decreases. In this high pretreatment temperature range SAPO-37 is more active than the faujasites. The selectivity indicates a higher olefin/paraffin ratio for the Si rich SAPO-37 samples i.e. a lower hydrogen transfer activity. The ratio iso-olefin/iso-paraffin is higher in SAPO-37 than in LZY-82 while it is the opposite for the ratio branched/non branched products.

1. INTRODUCTION

SAPO-37 molecular sieve which has the faujasite structure (1) exhibits acidic (2-5) and catalytic properties (3,5-13). It was shown that in the n-decane hydrocracking (8) or in the o-xylene isomerization (10) H-SAPO-37 is as active as HY. It can also be compared to USY in the cracking of gas oil (6,9). By contrast it is 10 to 15 times less active than USY in the cracking of n-heptane (9) and n-octane (12). The question arises as to which parameters may affect the catalytic properties upon modifications due to pretreatment conditions (temperature, atmosphere) or due to the presence of additional reactants or phases in the solid.

2. EXPERIMENTAL

A series of SAPO-37 materials with increasing Si contents are prepared with tetramethyl-(TMA) and tetrapropyl (TPA) ammonium hydroxides as templates (1,2,4,12). HNaY (referred to as HY) containing 10 Na^+/u.c. and LZY-82 (framework Si/Al= 4.5) from Union Carbide are used. A Y zeolite dealuminated with $(NH_4)_2$ Si F_6 (14) gives HYD sample (framework Si/Al= 7). The table 1

* On leave from the Institute of Catalysis and Surface Chemistry , Krakow, Poland.

Table 1
Characterization of SAPO-37 materials

	Si-0.12	Si-0.13	Si-0.14	Si-0.16	Si-0.20	Si-0.22
Si x[a]	0.12	0.13	0.14	0.16	0.20	0.22
Al y	0.50	0.49	0.48	0.48	0.50	0.46
P z	0.38	0.38	0.38	0.36	0.30	0.32
Z^+/u.c.[b]	22.3	20.7	21.7	21.9	19.7	18.5
a_0[c]	24.76	24.76	24.75	24.74	24.70	24.71
Thermal stability						
O_2 (K)	nd[d]	1270 ± 30	nd	nd	nd	1320 ± 30
O_2+H_2O(K)	nd	1275 ± 30	nd	nd	nd	1240 ± 30

[a] x, y, z : atomic fraction
[b] number of charges per unit cell (from template content)
[c] unit cell parameter for as synthetized samples
[d] not determined

summarizes the chemical composition of the SAPO's. They are referred to by the atomic fraction of silicon. The crystallinity of the zeolites was checked to be very good in the as synthetized form or after the catalytic test. The n-octane cracking was carried out at 723 K in a flow of hydrogen (flow rate 13.2 ml/min.) with $P_{n\text{-}oct}/P_{H_2}$= 0.06. SAPO-37 materials were activated from 873 K to 1223 K under flowing oxygen for 6 h in the standard pretreatment. It was checked that TPA and TMA were decomposed after heating at 873 K (4,15). The temperature was then decreased under oxygen to 723 K. A He flow was passed for a few minutes through the catalyst to purge the system and hydrogen was introduced. Specific pretreatments will be described further. The accuracy on per cent conversion is 10 %. Each catalytic test was performed on a fresh sample.

3. RESULTS

The highly crystalline samples described in the paper consist of only SAPO-37 as a pure phase. Attempts to introduce Si contents higher than an atomic fraction of 0.22 lead to silica as an extraphase which could be removed by ultrasonic treatment finally giving a pure SAPO-37 phase with a framework Si content of 0.19. For an ideal SAPO-37 structure where all the atoms Si, Al, P have the same environment, the Si content is x = 0.125 (2). Table 1 shows higher values of x which are interpreted as due to the presence of islands rich in Si (7,12,16). For the present case, these islands consist of only silica as seen by NMR (12) in the as synthetized materials. No Si-Al faujasite phase comparable to that described in (7,16) is observed. The existence of these islands decreases, for a given number of Si atoms, the number of Si-O-Al negatively charged species, i.e. of the protonic centers. This is confirmed by the decrease in the

number of charges Z per unit cell as the Si content increases (table 1). The catalytic activity should reflects these changes. In addition it is well known that the catalytic properties of zeolites also depend on the pretreatment and on test conditions. The various parameters are considered in what follows.

In the experimental conditions used, the SAPO-37 materials loose 20 to 40 % of their activity between 5 and 35 minutes after the beginning of a run. The n-octane % conversion and the selectivities remain then constant. After up to 15 h on stream the catalyst is white showing the absence of coke. In the same experimental conditions HY zeolite becomes black.

3.1. Standard pretreatment at 873 K

For the same pretreatment as SAPO-37, HY or LZY-82 give conversions between 20 to 25 % compared to 1 to 3 % for SAPO-37. Experiments conducted with HY at a higher flow rate (56.2 ml/min) decrease the conversion to a value close to that of SAPO's. This flow is used for comparison of the samples in table 2. The higher activity for the Si-Al faujasites is explained by Corma et al. (9) by the need for stronger acid sites in the cracking of n-paraffins compared to that of gas oil. The n-octane cracking results are reported in table 2 for five SAPO-37 samples typical of low (x = 0.12-0.13) or high (x = 0.16 to 0.22) Si contents. The two first materials give very similar results different from the ones of Si-0.16, -0.20 and -0.22. They are characterized by a higher conversion. The products range up to C_5 hydrocarbons. For the C_4-C_5 domain for which the accuracy is good, the table 2 gives the molar fraction in the products (alkanes, alkenes, branched or not). Samples Si-0.12 and Si-0.13 are again similar and different from the ones with high Si content. They give a lower formation of n-alkanes

Table 2
n-Octane cracking at 723 K after activation at 873 K (flow rate 13.2 ml/min for SAPO's materials)

	Si-0.12	Si-0.13	Si-0.16	Si-0.20	Si-0.22	HY[a]
Conversion %	1.9	2.0	1.3	1.3	1.6	2.7
n-alkanes[b]	22	22	25	26	24	24
iso-alkanes	21	21	9	14	15	18
n-alkenes	42	42	39	40	35	33
iso-alkenes	15	15	27	20	26	25
iso/n	0.6	0.6	0.6	0.5	0.7	0.75
o/p	1.3	1.3	1.9	1.5	1.6	1.4
C_2[c]	3	3	9	6	7	5
C_3	21	21	25	23	25	25
C_4	47	48	38	43	41	43
C_5	23	23	21	22	22	22
C_3/C_4	0.45	0.44	0.66	0.54	0.61	0.58

(a) flow rate (56.2 ml/min)
(b) mole per cent for C_4 and C_5 only
(c) For C_2 to C_5 the difference to 100 % is due to thermal cracking

and iso-alkenes with a higher production of iso-alkanes and n-alkenes. The situation for the two classes of materials (low or high Si) is then reverse for iso-alkanes and iso-alkenes. The selectivity expressed as the ratios of iso to non branched hydrocarbons (iso/n) and of olefin/paraffin (o/p) shows for the first ratio no major change with the Si content due to a compensation effect in the changes in linear and branched products. The values are close to 0.75 obtained for HY at a similar % conversion. The o/p ratio higher for the Si rich materials reflects the important production of iso-alkenes for Si-0.16 to Si-0.22 catalysts. It is higher than for HY. This suggests that the hydrogen transfer decreases in the order : HY > Si-0.20 > Si-0.22 > Si-0.16.

The three last materials pretreated at 873 K appear the most interesting with a low hydrogen transfer activity and a high iso-alkenes production. The distribution of the products with the C number shows also in table 2 very similar behavior of Si-0.12 and Si-0.13 compared to Si-0.16 to Si-0.22. The two Si-poor catalysts give less light hydrocarbons C_2 and C_3 which is in line with higher hydrogen transfer (17) as seen above. The ratios C_3/C_4 which may express the influence on catalysis of the field gradient in the cages (18) is lower in Si-0.12 and Si-0.13 suggesting an homogeneous field in the cages. This is in line with a regular distribution of isolated Si atoms as seen by NMR in these two samples (12) which generates mainly isolated Si-OH-Al acidic sites homogeneously distributed in the framework. The higher values obtained for the other samples including HY are in agreement with an heterogeneous field related to an irregular distribution of charges in the framework i.e. to the existence of Si islands in SAPO's.

3.2. Influence of pretreatment temperature

The per cent conversion as a function of pretreatment temperature is reported in figure 1A for four SAPO-37 typical of the two classes (low or high silica contents) described above. It shows that the order of catalytic activity observed after the 873 K pretreatment (table 2) is no longer valid. For 923 K and higher heating temperatures the two silicon poor materials are the less active due to a sharp decrease in conversion between pretreatments at 873 and 923 K. A second feature of figure 1A is the increase in n-octane cracking up to 1173 K for all the samples. This is usually not observed in catalysis with Si-Al zeolites, the catalytic properties decreasing in the 1000-1200 K range. This is described in figure 1B which compares a SAPO-37 sample (Si-0.22) with HY, HYD, LZY-82 pretreated at increasing temperatures and tested in the same experimental conditions (i.e. a flow rate of 13.2 ml/min). For the three faujasite-type catalysts the % conversion decreased regularly for temperatures of pretreatment ranging from 873 K to 1223 K. The SAPO-37 catalysts behaviour is then unique. It will be considered further with regards to simultaneous results of selectivity. Between 1173 and 1223 K the SAPO-37 materials loose their catalytic properties. This is related to the beginning of the structure collapse (15). At around 1173 K, the SAPO's particularly the Si rich become more active than HYD or LZY-82.

The selectivity changes for all the reaction products have been checked for all the samples and all the pretreatment temperatures. The main results for $C_4$and C_5 hydrocarbons are summarized in the figure 2 for the products classified like in table 2 as n- or iso-alkanes and n- or iso-alkenes. The fig. 2A

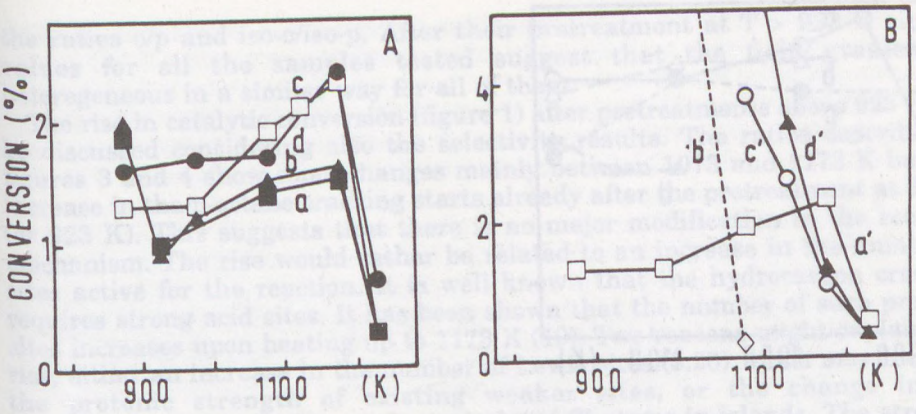

Figure 1. Changes in % conversion in n-octane cracking at 723 K as a function of pretreatment temperature for (A), Si-0.12 (a), Si-0.13 (b), Si-0-16 (c), Si-0.22 (d) and (B), Si-0.16 (a'), HY (b'), HYD (c'), LZY-82 (d') (flow rate 13.2 ml/min).

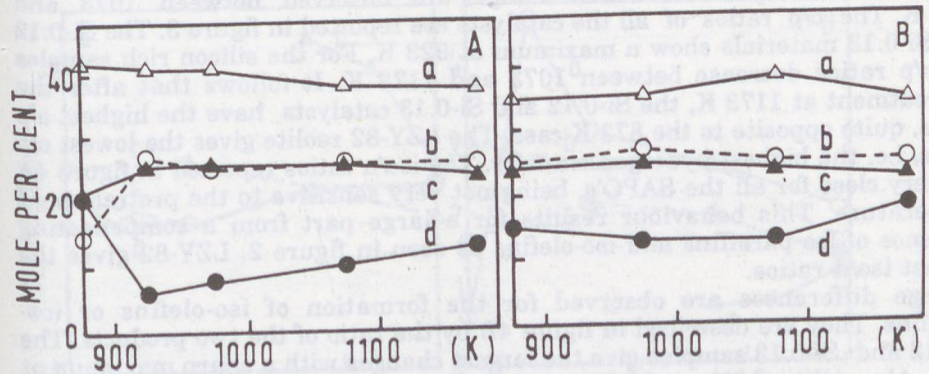

Figure 2. Changes in the products distribution as a function of pretreatment temperature for Si-0.12 (A) and Si-0.22 (B). (a) : n-alkenes, b : iso-alkenes, c : n-alkanes, d : iso-alkanes.

represents the results for Si-0.12 which are identical to those of Si-0.13. The silicon rich samples are exemplified in figure 2B by the sample Si-0.22. The behaviour of the two classes of SAPO's are somewhat different. For the silicon poor catalysts big changes occur between pretreatment temperatures of 873 and 923 K for the iso-paraffins and iso-olefins. The iso-paraffins decrease by around 75 % due to the drop of the formation of isopentane and isobutane. Simultaneously a rise in iso-olefins production by almost 50 % is due to an increase in the formation of isobutene. For pretreatment temperatures higher than 923 K a slow increase in iso-paraffins and a small decrease in

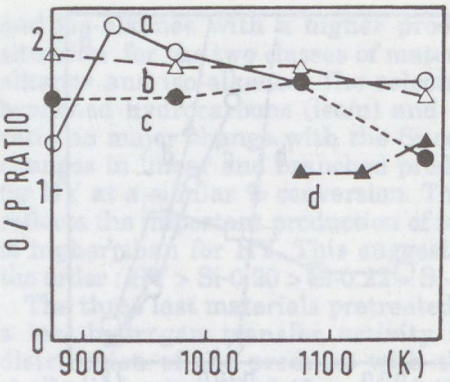

Figure 3. Changes in the ratio olefin/paraffin as a function of pretreatment temperature for Si-0.12 and Si-0.13 (a), Si-0.16 (b), Si-0.22 (c), LZY-82 (d).

n-olefins are observed. The Si-0.22 catalyst is not very sensitive to the pretreatment temperature. Small changes are observed between 1073 and 1173 K. The o/p ratios of all the catalysts are reported in figure 3. The Si-0.12 and Si-0.13 materials show a maximum at 923 K. For the silicon rich samples the o/p ratios decrease between 1073 and 1173 K. It follows that after the pretreatment at 1173 K, the Si-0.12 and Si-0.13 catalysts have the highest o/p ratios, quite opposite to the 873 K case. The LZY-82 zeolite gives the lowest o/p ratios, i.e. the highest hydrogen transfer. The iso/n ratios reported in figure 4A are very close for all the SAPO's, being not very sensitive to the pretreatment temperature. This behaviour results for a large part from a compensating influence of iso-paraffins and iso-olefins as seen in figure 2. LZY-82 gives the highest iso/n ratios.

Large differences are observed for the formation of iso-olefins or iso-paraffins. They are described in figure 4B by the ratio of the two products. The Si-0.12 and Si-0.13 samples give the largest changes with a sharp maximum at 923K. Above this temperature all the SAPO's show a decrease in the ratio isol-efin/iso-paraffin. All of them give higher ratios than LZY-82.

Table 2 showed that the C_3/C_4 ratio of the catalysts Si-0.12 and Si-0.13 pretreated at 873 K is lower than for the other materials. For higher pretreatment temperatures of all the SAPO's this ratio is 0.66 ± 0.02, value very similar to that of LZY-82 (0.66) pretreated between 1073 and 1173 K. The increase of this ratio for the two silicon poor materials strongly suggests that the field distribution in their cages (14,18) is changed between 873 and 923 K and becomes similar to the one in the other catalysts. This may be explained by a change in the distribution of charges, some isolated Si atoms forming islands. In the same temperature range a minimum in the oxidizing and reducing properties is observed for the samples Si-0.13 reflecting similarly strong modifications of the properties as the dehydroxylation proceeds (5). This may also explain the minimum observed in percent conversion for the two silicon poor samples in figure 1A and the maxima seen in figures 3 and 4B for

the ratios o/p and iso-o/iso-p. After their pretreatment at T > 923 K similar values for all the samples tested suggest that the field gradient is heteregeneous in a similar way for all of them.

The rise in catalytic conversion (figure 1) after pretreatments above 923 K can be discussed considering also the selectivity results. The ratios described in figures 3 and 4 show some changes mainly between 1073 and 1173 K but the increase in the n-octane cracking starts already after the pretreatment at 973 K (or 923 K). This suggests that there is no major modification in the reaction mechanism. The rise would rather be related to an increase in the number of sites active for the reaction. It is well known that the hydrocarbon cracking requires strong acid sites. It has been shown that the number of such protonic sites increases upon heating up to 1173 K (19). Two reasons might explain this rise, either an increase in the number of Lewis sites (5,20) which may increase the protonic strength of existing weaker sites, or the change in the environment of Si which transforms isolated Si atoms in islands. The strength of sites at the border of the islands is higher than for isolated Si atoms (7). This second hypothesis would explain the increase in oxidizing and reducing power of sites in the same temperature range. This point is still under study.

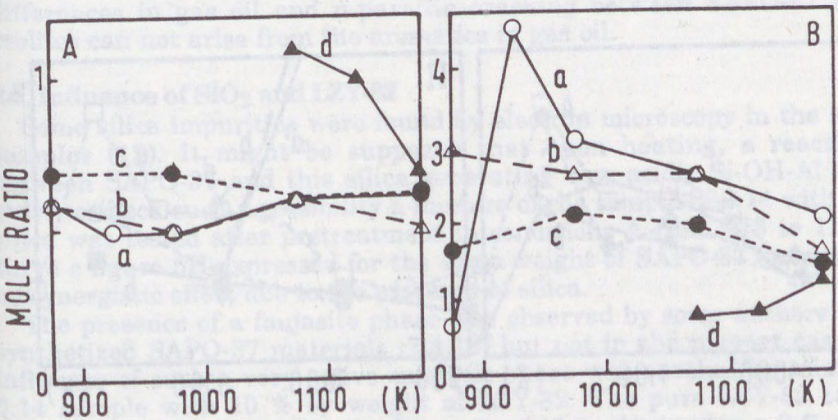

Figure 4. Changes in the ratios total iso/total n (A) and iso-alkene/iso-alkane (B) as a function of pretreatment temperature for Si-0.12 and Si-0.13 (a), Si-0.16 (b), Si-0.22 (c), LZY-82 (d).

3.3. Influence of pretreatment amosphere

In order to better understand the changes occuring in the SAPO-37 materials upon heating, different procedures have been followed involving O_2 (necessary to burn the template), He, H_2 or N_2. In the standard pretreatment (A) after the oxygen treatment at each temperature T, the temperature is decreased from T to 723 K in an oxygen flow. After a few minutes under He in order to purge the

system the hydrogen flow is established and the reaction starts immediately. Three other ways have been checked after the pretreatment at T (K) under oxygen for 8 hours. They are :
B) At the temperature T change of the gas from O_2 to H_2 (after a He purge) standing two hours at T(K) and decrease of the temperature to 723 K at which the reaction is started. C) At the temperature T change of the gas from O_2 to He and keeping the temperature at T(K) for 2h more. Decrease of the temperature to 723 K. Introduction of H_2 and starting of the reaction. D) At the temperature T keeping of the O_2 flow and decrease of the temperature to 723 K. After a purge with He, keeping of a H_2 flow for 2h before starting the reaction. E) An influence of nitrogen has been observed on the properties of SAPO-37 (9,21). A pretreatment has been conducted under a N_2 flow (50 ml/min) at 823 K for 4 h. It is followed by a treatment under oxygen at 1073 K. The procedure is then carried out as in A.

The figure 5I reports for sample Si-0.14 and for the various cases the n-octane conversion as a function of pretreatment temperature T. Some remarks can be drawn. The trend for an increase in conversion already seen in figure 1A for all the samples pretreated according to A is observed for the procedures B, C and D up to around 1100 K. In this temperature range no major influence of the atmosphere is seen after the template decomposition

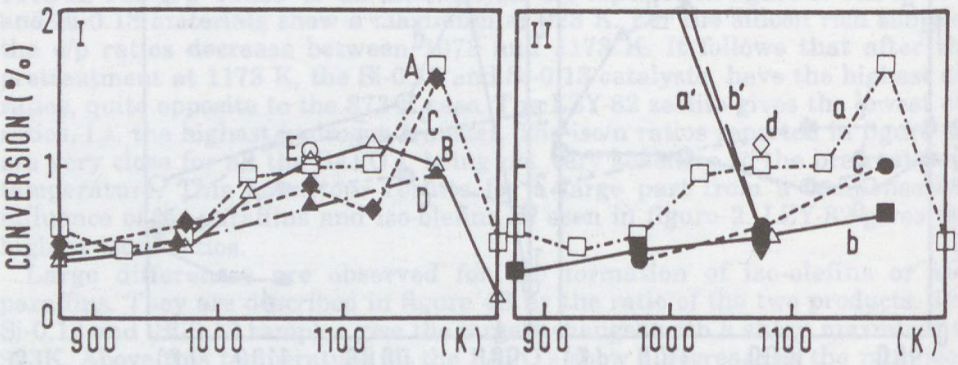

Figure 5. Changes for sample Si-0.14 in the % conversion as a function of pretreatment temperature (I) for various pretreatments noted A, B, C, D, E (see text) and (II) for various test modifications after the standard pretreatment A, Si-0.14 (a), Si-0.14 with feed n-octane + toluene (b), Si-0.14 + SiO_2 (c), LZY-82 (a') LZY-82 with feed n-octane + toluene (b') (For LZY-82 the flow rate is 56.2 ml/min instead of 13.2).

in oxygen. The template decomposition in nitrogen (E) followed by the burning of coke in oxygen does not modify significantly the results either. The main differences occur for the pretreatment at 1173 K where the procedures A and C give high conversions while B and D lead to 30 to 40 % lower conversions. For

the two last treatments hydrogen is contacted with the samples for 2 h either at T or at 723 K before the test. In the cases of A and C no reducing atmosphere is involved before starting the catalytic test. This fact seems to be the directing feature which improves the performances. This occurs at a temperature where a large increase in Lewis acidity (4,5) and reducing properties (5) are observed. This might correspond to some reorganization of the materials.

3.4. Influence of toluene

The gas oil cracking was reported to give similar activities for SAPO-37 and USY while SAPO-37 was ten times less active than USY in n-hexane cracking (9). The lower activity of SAPO-37 in the present study compared to HY, LZY-82 and HYD (figure 1) at temperatures of activation less than around 1150 K suggested to look at the influence of non-paraffinic hydrocarbons present in gas oil. A mixture of toluene and n-octane ($P_{tol}/P_{n\text{-}oct}$= 0.1) was used as the feed. The ratio $P_{hydrocarbons}/P_{H_2}$ was as previously. The curve b figure 5II shows a lower activity in the presence of toluene compared to the measurements in the absence of the aromatic (curve a) for the same pretreatment A. The influence of toluene was checked on LZY-82 tested at a flow rate of 56.2 ml/min (instead of 13.2 ml/min) in order to have conversion rates close to those of SAPO-37. The tests performed after pretreatments at 973 and 1073 K (figure 5II) give similar results in the presence (b') or not (a') of toluene. It can be concluded that the differences in gas oil and n-paraffin cracking between SAPO-37 and the Y zeolites can not arise from the aromatics in gas oil.

3.5. Influence of SiO_2 and LZY-82

Some silica impurities were found by electron microscopy in the silicon rich samples (12). It might be supposed that upon heating, a reaction occurs between SAPO-37 and this silica generating new acidic Si-OH-Al species. In order to check such a possibility a mixture of the sample Si-0.14 with 15 % pure silica was tested after pretreatment in conditions A from 973 to 1173 K. The curve c figure 5II expressed for the same weight of SAPO-37 as curve a shows no synergistic effect due to the presence of silica.

The presence of a faujasite phase was observed by some authors in their as synthetized SAPO-37 materials (7,8,16) but not in the present case (12). The influence of such a very active catalytic phase was checked by mixing the Si-0.14 sample with 10 % by weight of LZY-82. The pure LZY-82 tested after pretreatment A at 1073 K at a flow rate of 13.2 ml/min give a 9 % conversion. After mixing with SAPO-37 the point d shows only a slight increase in conversion of the pure SAPO phase (curve a). This indicates, no synergistic effect due to LZY-82.

In conclusion SAPO-37 materials exhibit properties which change upon heating in a way not observed previously for Si-Al zeolites. The presence of phosphorous very likely induce modifications of the Si location which then involves changes in acidic and catalytic behaviour.

Acknowledgments
We thank D. Delafosse and M.J. Peltre for very interesting discussions.

4. REFERENCES

1 B.M. Lok, C.A. Messina, R.L. Patton, R.T. Gajek, T.R. Cannan, E.M. Flanigen, US Patent N° 4 440 871 (1984).
2 L. Sierra de Saldarriaga, C. Saldarriaga, M.E. Davis, J. Am. Chem. Soc., 109 (1987) 2686.
3 E.M. Flanigen, R.L. Patton, S.T. Wilson, in "Innovation in Zeolite Materials Science" (Eds P.J. Grobet et al.), Stud. Surf. Sci. Catal., 37 (1988) 13.
4 S. Dzwigaj, M. Briend, A. Shikholeslami, M.J. Peltre, D. Barthomeuf, Zeolites, 10 (1990) 157.
5 B.L. Su, A. Lamy, S. Dzwigaj, M. Briend, D. Barthomeuf, App. Catal., 75 (1991) 311.
6 G.C. Edwards, J.P. Gilson, V. Mc Daniel, US Patent n° 4 681 864 (1987).
7 J.A. Martens, C. Janssens, P.J. Grobet, H.K. Beyer, P.A. Jacobs in "Zeolites, Facts, Figures, Future", (P.A. Jacobs and R.A. Van Santen, eds), Stud. Surf. Sci. Catal., 49A (1989) 215.
8 J.A. Martens, P.J. Grobet, P.A. Jacobs, J. Catal., 126 (1990) 299.
9 A. Corma, V. Fornes, M.J. Franco, F.A. Mocholi, J. Perez-Pariente, in "Fluid Catalytic cracking II" (M.L. Occelli, ed) Am. Chem. Soc. Washington D.C. 452 (1991) 79.
10 J. Dwyer, K. Karim, A.F. Ojo, J. Chem. Soc. Far. Trans., 87 (1991) 783.
11 A.F. Ojo, J. Dwyer, J. Dewing, K. Karim, J. Chem. Soc. Far. Trans., 87 (1991) 2679.
12 P.P. Man, . M. Briend, M.J. Peltre, A. Lamy, P. Beaunier, D. Barthomeuf, Zeolites, 11 (1991) 563.
13 J.M. Lopes, F. Lemos, F. Ramoa Ribeiro, E.G. Derouane in "Zeolite Chemistry and Catalysis" (P.A. Jacobs et al., eds), Stud. Surf. Sci. Catal., 69 (1991) 365.
14 C. Mirodatos, D. Barthomeuf, J. Catal., 114 (1988) 121.
15 M. Briend, A. Shikholeslami, M.J. Peltre, D. Delafosse, D. Barthomeuf, J. Chem. Soc. Dalton Trans., (1989) 1361.
16 L. Maistriau, N. Dumont, J.B. Nagy, Z. Gabelica, E.G. Derouane, Zeolites, 10 (1990) 243.
17 P.B. Venuto, E.T. Habib, Fluid Catalytic Cracking with Zeolites Catalysts, Marcel Dekker, New York, (1979) 98-117.
18 C. Mirodatos, D. Barthomeuf, J. Catal., 93 (1985) 246.
19 Bao Lian Su, D. Barthomeuf, submitted.
20 M. Briend, M.J. Peltre, A. Lamy, P. Man, D. Barthomeuf, J. Catal., submitted.
21 J. Pires, M. Brotas de Carvalho, F.R. Ribeiro, E.G. Derouane, React. Kin. Catal. Lett., 43 (1991) 313.

DISCUSSION

Q: W. P. Hettinger, Jr. (USA)

Catalytic cracking activity and selectivity of a catalyst are quite sensitive to contact time and temperature. Further, in commercial use the catalyst temperature drops from regeneration temperature to exit temperature of the reactor, due to endothermic reaction. All of this short period of time, of 1-4 seconds, the catalyst is deactivating also due to coke formation. Have you studied conversion performance as a function of time and temperature so as to better characterize the performance of a SAPO-31 crystal versus a faujasite crystal ?

A: D. Barthomeuf

With regard to deactivation it was checked that with time on stream, SAPO-37 deactivates less than faujasites and after 15 h it keeps a light color while faujasites become black. The effect of pretreatment temperature described in this paper suggests in SAPO-37 a redistribution of atoms in the solid upon heating. Such a change is expected to occur in the regeneration step at the first regeneration. Other studies on the effect of temperature or contact time are in progress.

By comparison with the large amount of work published on faujasites, the small number of studies carried out on SAPO-37 do not allow yet to answer all questions.

Q: B. W. Wojciechowski (USA)

We have recently become aware of the fact that various hydrocarbon cracking processes proceed in various measure via two processes. Initiation involving the protolysis reaction and chain propagation involving hydrogen transfer and isomerization. In all cases where the propagation reaction is significant dilution of the reactant by an "inert" leads to a change in the olefin/parafin ratio and in isomerization selectivity. In view of this, using different flow rates (of carrier I presume) for HY and SAPO catalysts distorts any interpretations based on the measurement of these quantities.

A: D. Barthomeuf

Only in the part 3.1 of the paper which compares samples after pretreatment at 873 K, different flow rates were used for, on the one side SAPO-37 and on the other side HY. In this part it is shown that conversion and selectivities of SAPO-37 (i.e. measured at the same flow rate) depends on the Si content. In the part 3.2 where all the samples, pretreated at high temperature, are compared at a same flow rate (13.2 ml/min) LZY-82 give selectivities different from SAPO's.

The study of the catalytic activity of SAPO's is at its beginning compared to all what has been done on Si-Al faujasites and it is difficult to speculate in detail on what mechanism is occurring on these new materials.

Q: T. S. R. Prasada Rao (India)

It is a very interesting piece of work and results are encouraging when we discuss about FCC catalysts, the question of hydrothermal stability is very important. How far SAPO's are hydrothermally stable ? Do they compare with Y zeolite in this aspect ?

A: D. Barthomeuf

We studied the thermal and hydrothermal stability of SAPO-37 [1]. SAPO-37 is very stable at high temperature even in the presence of water. By contrast it is not stable below 373 K - 353 K in atmospheric conditions. In this temperature range it is very stable in dry conditions.

[1] *J. Chem. Soc., Dalton Trans.*, **1989**, 1361

Q: J. B. Nagy (Belgium)

Did you also determine the number and strength of the acid sites in both SAPO-37 and

faujasite ? Did you find a relationship between the acidity and the catalytic activity ? In SAPO-37 there are acid sites of different nature, indeed.

A: D. Barthomeuf

We compared the acidity of SAPO-37 and faujasites in previous papers [2-4]. The main conclusions are as follows: i) above a Si content of 0.12 the number of acid sites in SAPO-37 decreases due to the formation of Si islands at higher Si levels; ii) the acid strength of "isolated" Si atoms is of medium strength; iii) the protons linked to SiO_4 tetrahedra at the border of Si islands are very strong, even stronger than in ultrastable Y.

[2] S. Dzwigaj, M. Briend, A. Shikoleslami, M. J. Peltre and D. Barthomew, *Zeolites*, **10**, 157 (1990); *ibid.*, **11**, 563 (1991)

[3] Bao Lian Su, A. Lamy, S. Dzwidgaj, M. Briend and D. Barthomeuf, *Appl. Catalysis*, **75**, 311 (1991)

[4] *Stud. Surf. Sci. Catal.*, **69**, 313 (1991)

Guczi, L. *et al.* (Editors), *New Frontiers in Catalysis*
Proceedings of the 10th International Congress on Catalysis, 19-24 July, 1992, Budapest, Hungary
© 1993 Elsevier Science Publishers B.V. All rights reserved

CATALYTIC ACTIVITY OF MODIFIED ZSM-5 ZEOLITES IN THE DEHYDROGENATION AND AROMATIZATION REACTIONS OF PROPANE AND n-BUTANE

P. Fejes[a], *J. Halász*[a], *I. Kiricsi*[a], *Z. Kele*[a], *Gy. Tasi*[a], *I. Hannus*[a], *C. Fernandez*[b], *J. B. Nagy*[c], *A. Rockenbauer*[d] *and Gy. Schöbel*[a]

[a]Applied Chemistry Department, József Attila University, Rerrich tér 1, 6720 Szeged, Hungary
[b]Laboratoire de Dynamique et Structure des Materiaux Moleculaires, 59655 Villeneuve d`Ascq Cedex, France
[c]Laboratoire de Catalyse, Facultes Universitaires Notre-Dame de la Paix, 5000 Namur, Belgium
[d]Central Research Institute of Chemistry, Hungarian Academy of Sciences, Pusztaszeri út 59, 1025 Budapest, Hungary

Abstract

In order to enhance catalytic activity in the dehydrogenation and aromatization of light paraffins, a set of potential catalysts: (i) *V(f)-ZSM-5* (originating from *direct synthesis*), (ii) *V(ex)-ZSM-5* ("ex": partial exchange of H^+ in *H-ZSM-5* by VO^{2+} ions), and (iii) *solid* exchange of *H* in *H-ZSM-5* for *Ga, In*, and *V* by baking the mixtures of *ZSM-5* with the respective oxides were investigated by physical (XRD, IR, ESR, MAS-NMR spectroscopy, and adsorption) and chemical methods. In the "as synthesized" *V(f)-ZSM-5* sample V^{4+} ions reside in framework positions according ESR and ^{51}V-MAS-NMR spectra. Coincidence between experimental and theoretical spectra could be attained only by supposing the existence of *two* different framework surroundings. The structure of *V(f)-ZSM-5* is strained: heating (especially in the presence of water vapour) causes release of *V* from the framework. Severe conditions cause clustering of V^{4+} in the voids with the annihilation of hyperfine splitting in the ESR spectra. Catalytic results demonstrate that in the presence of modifyers propane and n-butane conversion turns from cracking to dehydrogenation and aromatization pathways.

1. INTRODUCTION

Increasing attention has been directed recently toward zeolitic materials, especially metallo-silicalites which show enhanced activity in the dehydrogenation and aromatiza-

tion of light paraffins [1-4], conversion of methanol to hydrocarbons [5], propane ammoxidation to acrylonitrile [6] and even in liquid phase oxidation of phenol to a mixture of hydroquinone and catechol [7].

Trivalent ions (like Fe^{3+}, Ga^{3+} and B^{3+}) used for the substitution of Al^{3+} in the structures are suitable for tuning the Brönsted acidity of the zeolite. *Tetravalent* ions like Ti^{4+}, Ge^{4+} do not endow the framework with net electric charge or acidic property, therefore, the catalytic behaviour, if any, is due to the properties of the heteroatoms.

Most promising are those substitutions where the extraneous ions are transition metals *possessing several* (but at least two) *oxidation states*. In accordance with Pauling's minimum radius ratio these ions can be introduced into the zeolitic lattice with the greatest probability if their ionic radii are close to that of Si^{4+}, while the framework itself remains uncharged in the substitution process. It means in other words that from this class of metals those in the fourth oxidation state are the most favoured substituents for Al^{3+}. The more or less stable "as synthesized" form can then be brought into an "out of balance" condition by artificially changing the oxidation state of the (mostly transition-) metallic component. Lower oxidation states than four generate net negative electric charge in the framework with cation exchange (and acidic) properties, higher oxidation state of the substituent ion leads, at least in principle, to net positive charge of the framework and anion exchange.

As concerns the experimental methods, either direct hydrothermal synthesis and solid phase ion exchange may result in isomorphous substitution, nevertheless, their extent can be very different.

This paper deals with the modification of *ZSM-5* zeolites with Ga_2O_3, In_2O_3, V_2O_5 and VCl_3 applying solid exchange, and by introducing V^{4+} in hydrothermal synthesis. The catalysts were characterized by XRD, IR-spectroscopy, physical adsorption and for the V^{4+} and V^{5+} containing samples by ESR- and ^{51}V-MAS-NMR spectroscopy, respectively. Catalytic activity was tested in the (oxidative/non-oxidative) dehydrogenation of propane and n-butane.

2. EXPERIMENTAL

Catalyst preparation

V^{4+}*(f)-ZSM-5* (f = "framework") sample was synthesized with a SiO_2 to VO_2 ratio equal to 42 by X-ray fluorescence analysis. This value was very close to that (Si/V = 40) reported by *Miyamoto et al.* [6].

The synthesis was carried out (cf. [8]) at pH = 9.1, outgoing from the batch composition: 1.0 SiO_2, 0.2 VO_2, 39.2 H_2O, 0.3 *TPA-Br*. It is worth to note here that *ZSM-5 seeds* (Si/Al = 40.0) *were added to the slurry* to facilitate crystallization.

The product was fully crystalline by X-ray diffraction and had *ZSM-5* structure in both "as synthesized" (A.S.) and "burned off" (B.O.) forms.

The catalyst samples containing Ga^{3+}, In^{3+}, V^{5+} (V_2O_5) and V^{3+} (VCl_3) as modifying additives were prepared by baking the physical mixtures of Ga_2O_3/*H-ZSM-5*, or In_2O_3/*H-ZSM-5*, V_2O_5/*H-ZSM-5* and VCl_3/*H-ZSM-5* at 873 K. The *H-ZSM-5* was a standard sample with Si/Al = 40.0.

The same *ZSM-5* sample was used in order to obtain V^{4+}*(ex)-ZSM-5* (ex = "exchanged") by ion exchange in 0.1 molar vanadyl oxalate solution.

Catalyst characterization

The catalysts were characterized by XRD, IR-spectroscopy and for the vanadium containing samples by ESR- and MAS-NMR-spectroscopy. ESR spectra were recorded on a JEOL-FE-3X type spectrometer in the X-band using Mn^{2+} in *MgO* matrix for field calibration. ^{51}V- and ^{29}Si-NMR spectra were taken on a Bruker MSL 400 spectrometer using MAS conditions. The frequency, the pulse width and waiting time were for ^{51}V: 105.2 MHz, 1.0 μs and 0.2 s and for ^{29}Si: 79 MHz, 4.0 μs (90°), 10.0 s, respectively.

Change in acidity of the samples as the result of the modification was followed by IR-spectroscopy; N_2 adsorption at 77 K, oxygen and hydrogen uptake of catalysts were measured in a volumetric equipment.

Catalytic reactions

Conversion of propane and n-butane was studied in a fixed-bed flow reactor in the presence and in the absence of O_2 under atmospheric pressure. 0.5 g solid sample was filled in a quartz tubular reactor, and a pretreatment in nitrogen flow at 500 °C was utilized for 3 hours to standardize the catalyst surface. For catalytic test the inlet gas composition of 20% alkane + 80% nitrogen or 10% alkane + 10% oxygen + 80% nitrogen was used. Product analysis was performed by GC using an on-line Porapack-Q column for the analysis of gaseous compounds, and a 30 m long SPB-1 capillary column for the analysis of the collected liquid phase.

3. RESULTS AND DISCUSSION

3.1. Characterization of catalysts

3.1.1. *V*-containing samples

Characterization by ESR-spectroscopy

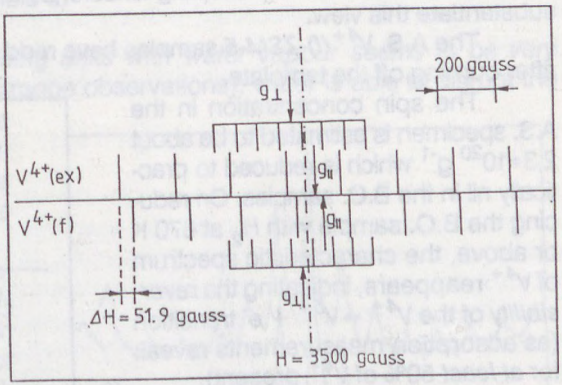

Fig. 1: Line diagram of ESR spectra

The $V^{4+}(ex)$ and $V^{4+}(f)$ ESR spectra (which were registered at ambient temperature) consist of sixteen slightly unevenly spaced lines arising from the flipping of the $3d^1$ unpaired electron of V^{4+}-ion and its interaction with the nuclear spin of the 100% abundant ^{51}V nucleus (I=7/2) which gives rise to an eightfold hyperfine splitting of all anisotropic components.

The structure of the spectra is depicted in Fig. 1. The difference between the spectra of $V^{4+}(ex)$ and $V^{4+}(f)$ is slight; at first sight the spectrum of $V^{4+}(f)$ is shifted to higher fields which means 52 gauss for the first parallel lines diminishing to 16 for the last ones due to the greater spectral width of the $V^{4+}(ex)$ spectrum.

Table 1 summarizes the main diagonal elements of the g-and the hyperfine coupling tensors (A). Notable differences show up only in the *parallel* components ($g_\parallel$) of

Table 1
ESR parameters of *V*-containing materials

Compound	$g_{\parallel}$	$g_{\perp}$	$A_{\parallel}$ (gauss)	$A_{\perp}$ (gauss)	<g>	<A>
VO^{2+}(ex)-ZSM-5	1.963	2.007	190.8	75.4	1.992	113.9
V^{4+}(f)-ZSM-5 (A.S.)	1.949	1.990	185.8	72.5	1.976	110.3
VO^{2+}(ex)-NaY	1.963	2.007	190.8	75.4	1.992	113.9

the (g) and in the *perpendicular* components ($A_{\perp}$) of the hyperfine coupling tensors (A).

The reduced values of the g and A tensors main diagonal elements for the V^{4+}*(f)* specimen can be interpreted by a lesser separation of the vanadium d-orbitals or by the weakening of the covalent character of *V-O* bonds. Though the reduced covalency of planar σ-bond should increase the anisotropic angular contribution to the hyperfine interaction, the observed hyperfine constants for the V^{4+}*(f)* specimen are actually reduced which indicates the overcompensating role of the Fermi interaction if the symmetry is distorted. The values of the coupling tensors (by the reduction of the Fermi contact term) substantiate this view.

The A.S. V^{4+}*(f)-ZSM-5* samples have reddish-yellow colour which turns to white after burning off the template.

The spin concentration in the A.S. specimen is estimated to be about $2.3*10^{20}$ g^{-1} which is reduced to practically nil in the B.O. samples. On reducing the B.O. sample with H_2 at 670 K or above, the characteristic spectrum of V^{4+} reappears, indicating the *reversibility* of the $V^{4+} \rightleftharpoons V^{5+} + e^-$ transition (as adsorption measurements reveal: for *at least* 50% of V^{4+} present).

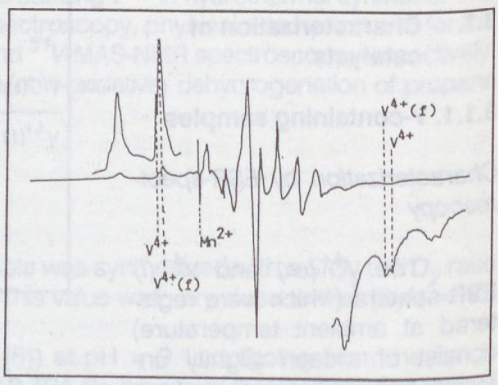

Fig. 2: ESR spectrum of sample exhibiting grey colour

Upon dehydration of hydrated B.O. V^{4+}*(f)-ZSM-5* zeolites (colour: yellow) at 570 K or above in vacuum the colour of the samples turns to grey, a clear indication for formation of a mixed (V^{4+} and V^{5+}) oxidation state of vanadium ions. As ESR spectra reveal, a complex set of events takes place during the heating in the presence of water vapour, the colour change being only one *visible consequence* out of many.

Fig. 2 shows an ESR spectrum of a sample exhibiting grey colour. The magnified parts (at low and high fields) *disclose the presence of two* V^{4+}*-species*. The very complex spectrum (consisting of 32 lines + 6 Mn^{2+} calibration lines; here shown only

one) looks like the superposition of *two* spectra, one for V^{4+}*(ex)* (weaker lines) and one for V^{4+}*(f)*, the only difference being that at high fields the sequence of lines [caused by the greater spectral width of V^{4+}*(ex)*] is reversed here.

Prolonged steaming at 570 K makes the V^{4+}*(ex)* lines more intense, eventually the whole spectrum coalesces into a broad signal lacking hyperfine structure on which only the Mn^{2+} calibration lines can be recognized (Fig. 3). The spectrum is caused in all probability by hydrated clusters of *V*-oxides in the zeolitic voids.

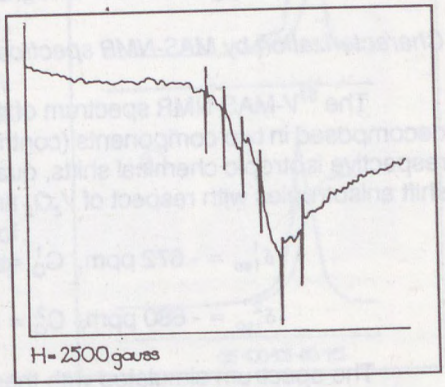

Fig. 3: ESR spectra of steamed sample

All these observations clearly indicate the presence of V^{4+} *in special framework positions* in the A.S. samples the number of which might be limited, setting an upper limit for the VO_2/SiO_2 ratio at about 0.025. *At least 50% of* V^{4+} *ions are situated on channel walls* capable to participate in fast redox reaction steps. Another part is more or less hidden, nevertheless, it is still accessible to O_2 (or H_2).

The interaction of V^{4+}*(f) building units with water vapour seems to be very specific* (colour changes and other strange observations): water is able to disrupt the strained *V-O-Si* linkages and causes release of *V* which is not a very attractive feature when these materials are applied under arduous conditions as heterogeneous catalysts.

The V^{4+}*-ZSM-5* specimens obtained by solid exchange with VCl_3 exhibit similar ESR spectra as shown in Fig. 2, however, *the intensities for* V^{4+}*(f) are smaller than for* V^{4+}*(ex)*. Whether the nests of the zeolitic structure are filled up with VO_2 units, or real "framework exchange" occurs is open for further investigations.

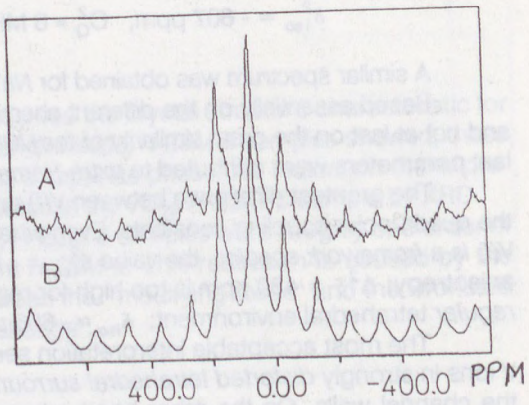

Fig. 4: Experimental (A) and theoretical (B) ^{51}V-MAS-NMR spectra of V(f)-ZSM-5

As concerns location of V^{4+}*(f)* ions in the zeolitic framework, models can be imagined and depicted, nevertheless, they are and remain speculative for a while without solid substantiation.

As a closing remark of these ESR studies it's worthwhile to mention that incompletely oxidized V^{4+}*(f)* specimens still in contact with O_2 at ambient temperature

show the characteristic ESR spectrum of O_2^- radical ion ($<g> = 2.0027$; g_{zz} set partly resolved, the g_{xx} and g_{yy} lines unresolved). It is believed that this radical ion is quite unstable, therefore, only its degradation products (eventually O^{2-} ions) can be made responsible for oxygen transfer at high temperatures.

Characterization by MAS-NMR spectroscopy

The ^{51}V-MAS-NMR spectrum of the A.S. *V(f)-ZSM-5* specimen can tentatively be decomposed in two components (contributions about 10% and 90%, respectively). The respective isotropic chemical shifts, quadrupolar coupling constants and the chemical shift anisotropies with respect of V_2O_5 are:

$$\delta^1_{iso} = -672 \text{ ppm}, \quad C^1_Q = 3.9 \text{ MHz} \quad \text{and} \quad \Delta^1\delta = 510 \text{ ppm}$$

$$\delta^2_{iso} = -680 \text{ ppm}, \quad C^2_Q = 3.7 \text{ MHz} \quad \text{and} \quad \Delta^2\delta = 430 \text{ ppm}$$

The spectrum simulated with these constants resulted in a good fit (see Fig. 4) with that observed experimentally. Work is in progress to arrive to a better refinement using spectra from different frequencies.

The *VCl_3/H-ZSM-5* specimen obtained with solid exchange resulted in a spectrum (with respect of *$VOCl_3$*) which could be decomposed also in two components (contributions 88% and 12%, respectively) with the following parameters:

$$\delta^1_{iso} = -612 \text{ ppm}, \quad C^1_Q \cong 6 \text{ MHz} \quad \text{and} \quad \Delta^1\delta = 480 \text{ ppm}$$

$$\delta^2_{iso} = -607 \text{ ppm}, \quad C^2_Q \cong 6 \text{ MHz} \quad \text{and} \quad \Delta^2\delta = 800 \text{ ppm}$$

A similar spectrum was obtained for *NaY* (*Si/Al* = 2.2) exchanged with *$VO(COO)_2$*.

Based essentially on the different chemical shifts, quadrupolar coupling constants and not at last on the great similarity of the *VCl_3/H-ZSM-5* and *V^{4+}(ex) NaY* spectra these last parameters were attributed to *extra-framework V species*.

The greatest difference between *V(f)* and *V(ex)* ^{51}V-NMR spectra is manifested in the quadrupolar coupling constants. Even when it is believed that irrespective of notation *V(f) is a framework species*, the value $\delta^2_{iso} = -680$ ppm and especially the chemical shift anisotropy: $\Delta^2\delta = 430$ ppm is too high for regular tetrahedrally coordinated *V* ions (for *regular* tetrahedral environment: $\delta_{iso} \approx -605$ ppm, $\Delta\delta < 100$ ppm [9]).

The most acceptable interpretation seems to suppose the presence of isolated *V* ions in strongly *distorted tetrahedral surroundings* as part of the framework near to the channel walls. On the other hand adsorption studies with H_2 and O_2 do not substantiate such a high (90%) contribution to the NMR spectrum by this species (see later).

The MAS ^{29}Si-NMR spectrum of the *V(f)* sample (Fig. 5.b) is shifted to lower fields by about 2 ppm as compared with the reference *ZSM-5* (Fig. 5.a). The origin of this shift is not clear yet; probably due to the presence of paramagnetic *V* species modifying the magnetic interaction of *Si* nuclei. Work is in progress to decompose the ^{29}Si-NMR spectrum quantitatively in order to determine the contribution from the *Si(1V)* configuration.

Characterization by I.R. spectroscopy

The absorption of silanol groups at 3740 cm^{-1} could clearly be observed on *V(f)-ZSM-5* samples which were activated in vacuum or in O_2 at 673 K. After hydrating the samples thus pretreated and evacuated at 723 K the I.R. spectrum shows a broad *OH* band centered at 3600 cm^{-1} in addition to the *Si-OH* band.

Acidity tests with pyridine as a probe molecule showed only Lewis acidity, therefore, it can be concluded that the concentration of Brönsted acidic sites is negligible independently of the pretreatment conditions.

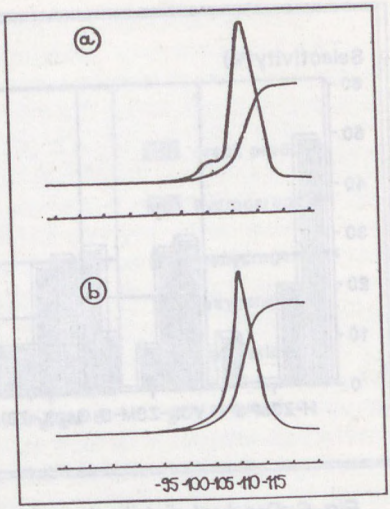

Fig. 5: MAS ^{29}Si-NMR spectra of the a: reference ZSM-5 sample b: V-ZSM-5 sample

Adsorption studies

No H_2 or O_2 uptake could be observed below 570 K. At 670 K the hydrogen adsorption of the (at the same temperature) preoxidized *V(f)-ZSM-5* sample in repeated cycles was nearly twice (2.21 cm^3/g, S.T.P.) that of oxygen (1.10 cm^3/g, S.T.P.) indicating a *real redox behaviour*. As the spin concentration: $2.3*10^{20}$ spin/g might be overestimated, the previous values reveal that *at least 50%* of the *V* ions are involved in this redox reaction.

3.1.2. Other samples

Each modified catalyst sample preserved the crystal structure characteristic for zeolite *ZSM-5*. As the XRD patterns taken on the *oxide/H-ZSM-5* samples showed, these specimens contained part of the oxides as a separate phase. No indication of the presence of any foreign phase could be detected in the *VCl_3/H-ZSM-5* sample by XRD.

The Brönsted acidities of the *oxide/H-ZSM-5* samples were roughly one order of magnitude lower than those of the parent *H-ZSM-5*. This reduction is caused by the "neutralization" reaction taking place between the "modifying oxide" and the Brönsted acidic sites of the zeolite during "solid exchange".

3.2. Catalytic investigations

The results of the catalytic measurements in the reactions of propane (+ O_2), and *n*-butane (+ O_2) are shown in Figures 6-9 (the reaction temperature: 723 K, space velocity: 1500 h^{-1}, time on stream: 3 h).

In the absence of dioxygen the conversions of the paraffins were low in comparison to those where O_2 was present.

The differences in the conversions over the different catalysts are not considerable (except for *H-ZSM-5*), the lesser activity of the modified *ZSM-5* samples can be

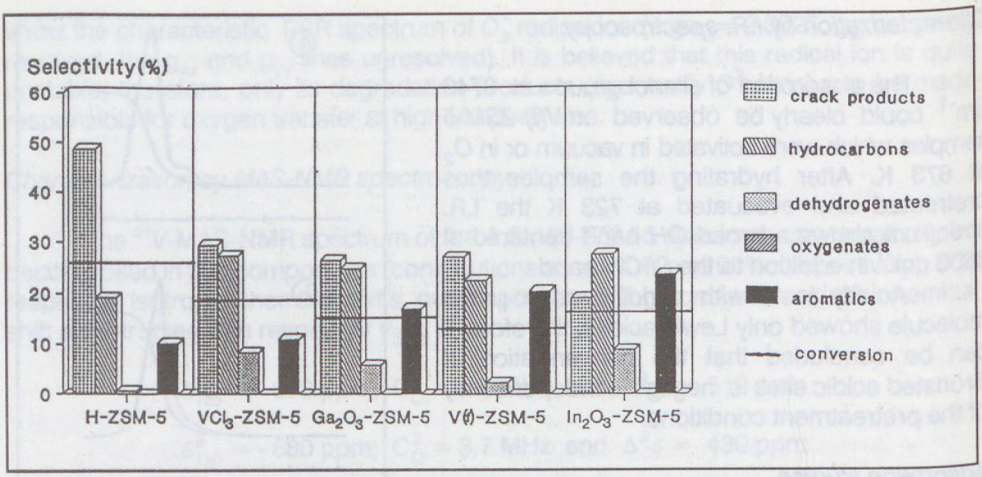

Fig. 6: Product distribution of propane transformation in the absence of O_2 over different catalysts

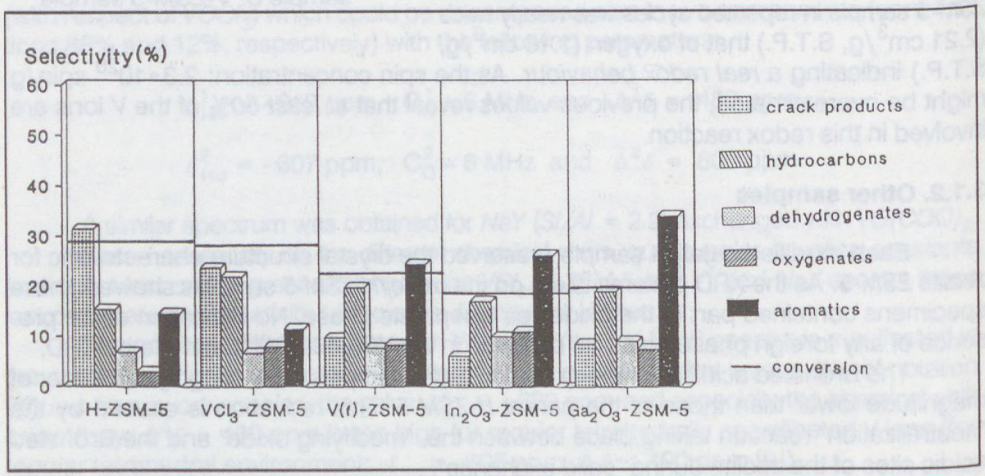

Fig. 7: Product distribution of propane transformation in the presence of O_2 over different catalysts

accounted for by the decreasing Brönsted acidity.

For the product distribution (the selectivities are computed on common *C* basis) over *H-ZSM-5* the high cracking activity is characteristic, the amounts of dehydrogenates (propene or *n*-butenes) and aromatics are below 10%. The *VCl_3/H-ZSM-5* behaves similarly as *H-ZSM-5* in the absence of O_2. A significant increase in aromatics production

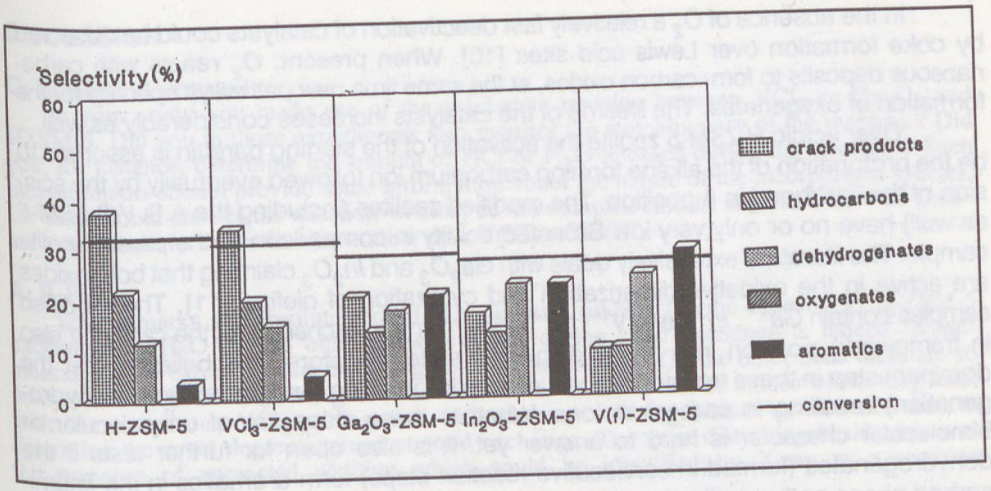

Fig. 8: Product distribution of *n*-butane transformation in the absence of O_2 over different catalysts

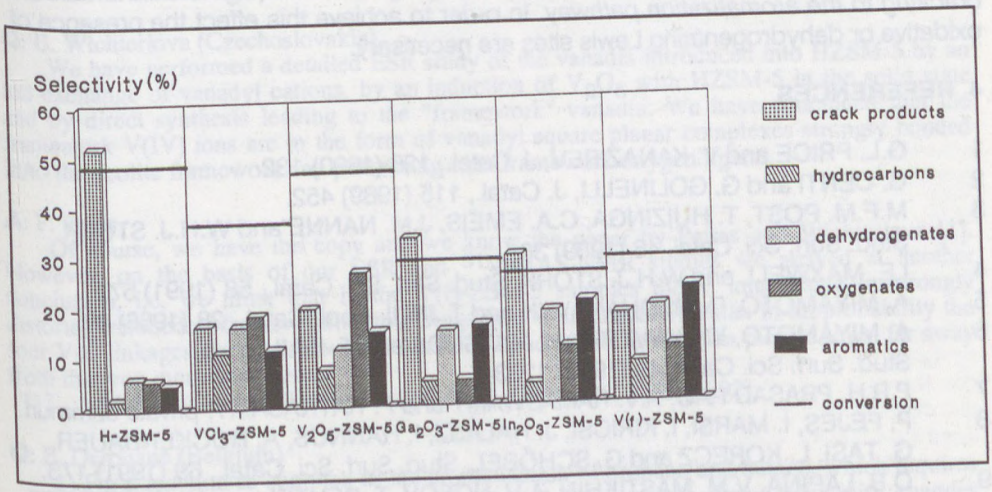

Fig. 9: Product distribution of *n*-butane transformation in the presence of O_2 over different catalysts

with concurrent decrease of crack products can be observed when Ga_2O_3 and In_2O_3 are added to zeolite *H-ZSM-5*. The catalytic effect of *V(f)-ZSM-5* is similar; in the reactions of *n*-butane the highest aromatic selectivity was found over this catalyst both in the absence and in the presence of dioxygen. The formation of oxygenates is characteristic for catalysts containing vanadium in extra-framework positions.

In the absence of O_2 a relatively fast deactivation of catalysts could be observed by coke formation over Lewis acid sites [10]. When present, O_2 reacts with carbenaceous deposits to form carbon oxides, at the same time new pathways open up for the formation of oxygenates. The lifetime of the catalysts increases considerably as well.

Over acidic *H-ZSM-5* zeolite the activation of the starting paraffin is assumed to be the protonation of the alkane forming carbonium ion followed eventually by the scission of the *C-C* bond in β position. The modified zeolites (including the A.S. *V(f)-ZSM-5* as well) have no or only very low Brönsted acidity in comparison to the parent zeolite sample. The literature extensively deals with Ga_2O_3 and In_2O_3 claiming that both oxides are active in the oxidative dimerization and cyclization of olefins [11]. The modified samples contain Ga^{3+}, In^{3+} and V^{4+} (V^{5+}) ions mainly in exchange (in the case of *V* also in framework) position in a highly dispersed state, therefore, it is believed that the dominant step in these transformations is dehydrogenation (and/or oxidative dehydrogenation) resulting in carbenium ions. Whether these steps are of unimolecular or bimolecular character is hard to answer yet. It is also open for further tests if the dehydrogenates (formed in consecutive reaction steps) form aromatics in the chemisorbed phase or the cyclization takes place as a homogeneous gas phase reaction.

These results demonstrate that by suppressing the Brönsted acidity via addition of Ga_2O_3 and In_2O_3 to zeolite *H-ZSM-5* or introducing *tetravalent* ions, like V^{4+}, capable to participate in reversible redox steps, *propane and n-butane conversion turns from cracking to the aromatization pathway*. In order to achieve this effect the presence of oxidative or dehydrogenating Lewis sites are necessary.

4. REFERENCES

1 G.L. PRICE and V. KANAZIREV, J. Catal., 126 (1990) 132.
2 G. CENTI and G. GOLINELLI, J. Catal., 115 (1989) 452.
3 M.F.M. POST, T. HUIZINGA, C.A. EMEIS, J.M. NANNE and W.H.J. STORK, Stud. Surf. Sci. Catal. 46 (1989) 365.
4 I.E. MAXWELL and W.H.J. STORK, Stud. Surf. Sci. Catal., 58 (1991) 571.
5 A. MIYAMOTO, D. MEDHANAVYN and T. INUI, Appl. Catal., 28 (1986) 89.
6 A. MIYAMOTO, Y. IWAMOTO, H. MATSUDA and T. INUI, Stud. Surf. Sci. Catal. 49 (1989) 1233
7 P.R.H. PRASAD RAO, A.V. RAMASWAMY and P. RATNASAMY, private commun.
8 P. FEJES, I. MARSI, I. KIRICSI, J. HALÁSZ, I. HANNUS, A. ROCKENBAUER, G. TASI, L. KORECZ and G. SCHŐBEL, Stud. Surf. Sci. Catal., 69 (1991) 173.
9 O.B. LAPINA, V.M. MASTIKHIN, A.V. NOSOV, T. BEUTEL and H. KNÖZINGER, Catal. Lett., 13 (1992) 203.
10 C.R. BAYENSE, A.J.H.P. VAN DER POL and J.H.C. VAN HOOFF, Appl. Catal., 72 (1991) 81.
11 J. HALÁSZ, K. VARGA and P. FEJES, J. Mol. Catal., 51 (1989) 303.

Acknowledgement

The grants (OTKA No. 693/86, 1182/90 and 1614/90) of the Hungarian Academy of Sciences is gratefully acknowledged.

DISCUSSION

Q: H. Karge (Germany)

In your study you made use of the solid-state reaction between VCl_3 or Ga_2O_3 and HZSM-5. Did you in those experiments also monitor the stoichiometry of the reaction ? Did you, for instance, determine the amount of HCl or H_2O released during the reaction ? Such measurements should provide some information about the nature of the incorporated species, i.e. they should answer the question whether or not complex cations such as VCl^{2+} or GaO^{+} are accommodated on cation sites rather than V(III) or Ga(III).

A: P. Fejes

Your remarks are absolutely right. The amount of HCl (in the case of VCl_3-ZSM-5 exchange) or H_2O (in the other cases) evolved during solid exchange is indeed "some" measure of the extent of reaction taking place during heating. On the other hand there are so many disturbing effects (see e. g. the structural water of the zeolite or oxides which may react with the anhydrous VCl_3 setting free HCl without exchange) that we did not aim to determine the exact degree attained at solid exchange. The most disturbing beside this was the presence of unreacted additive which could be identified by X-ray as a separate crystalline phase.

I am afraid the same difficulties are general in solid exchange which we tried to circumvent about 8 years ago by separate volatilization of the active ingredient. This approach is feasible when you deal e.g. with VCl_3. However, what to do if you want to introduce V in exchange position using V_2O_5 ?

Q: B. Wichterlova (Czechoslovakia)

We have performed a detailed ESR study of the vanadia introduced into HZSM-5 by an ion exchange of vanadyl cations, by an induction of V_2O_5 with HZSM-5 in the solid state and by direct synthesis leading to the "framework" vanadia. We have concluded that the framework V(IV) ions are in the form of vanadyl square planar complexes strongly bonded in/to the zeolite framework and possessing extraframework oxygen ligand.

A: P. Fejes

Of course, we have the copy and we know the paper by Petras and Wichterlova [1]. However, on the basis of our ESR and ^{51}V-MAS-NMR studies we arrived at another conclusion, i.e. we think that in the V(f)-ZSM-5 samples the V ions reside in strongly distorted tetrahedral framework surroundings near to the channel walls. In all probability the four V-O linkages are not equivalent: one V-O bond is shorter and this picture is not far away from that you mentioned here.

[1] M. Petras and B. Wichterlova, *J. Phys. Chem.*, **96**, 1805 (1992)

Q: E. Derouane (Belgium)

1) For a reaction as complex as the aromatization of propane and butane, which requires both acidic and dehydrogenation sites, one should not conclude about selectivity changes without information about the absolute or relative amounts of these sites. Even more, when comparisons are made at different conversion levels. Finally, it is difficult to conclude about differences between impregnated and synthesized V-ZSM-5 materials without information on the V-content in the different phases.

2) Early work from Mobil, in the early seventies, demonstrated clearly that addition of O_2 to an alkane/alkene feed increases dehydrogenation and aromatization over zeolites containing redox species. That is indeed what you report for propane and you also observe a reduction in cracking. For butane, however, using V(f)-ZSM-5 you report an increased catalytic activity and no change in dehydrogenation and aromatization. How do you explain the difference between propane and butane ?

A: P. Fejes

1) First of all, for aromatization to be effective dehydrogenation sites are absolutely sufficient. Ring closure (e.g. in the case of hexatrienes having appropriate conformation) may take place as a homogeneous gas phase reaction.

Selectivity is an experimental information which you obtained from analytical data. It is another question how to explain it ? Regarding the extreme complexity of catalytic steps involved (even when we are working on the elementary steps of cracking since 30 years) we were aiming to separate groups of similar reactions (cracking, formation of oxygenates, aromatics, etc.) and to see how they change in dependence of catalyst compositions in a narrow range of conversion (exception Figure 9). Flow reactor is unsatisfactory to arrive to exactly the same conversion.

The V-content in the A. S. samples was exactly measured by X-ray fluorescence. The other samples obtained with solid exchange necessarily contained unreacted oxide prohibiting exact analysis for the zeolitic phase.

2) We do not report about increased catalytic activity for V(f)-ZSM-5 in general. We just state that for aromatization V(f)-ZSM-5 is the second and third best catalyst with propane feed and the best if the feed is butane. The explanation is to be found in the complex set of elementary transformations the unrevealing of which might be the task of heterogeneous catalysis for the next decade.

Q: K. Dooley (USA)

Your paper states "Reversible oxygen and hydrogen uptake was observed for V-containing samples only", you also report a very low ratio or cracking products to aromatics for Ga_2O_3-ZSM-5 in propane aromatization. However, the patent literature indicates that your Ga-ZSM-5 should be the best of the materials which you tested. I suspect that your Ga_2O_3-ZSM-5 sample was insufficiently reduced. We have shown [2, 3] that Ga_2O_3 reduction, ultimately to Ga^+Z^- (Z^- is an anionic lattice site of the zeolite) is absolutely necessary in preparing active GaZSM-5 catalysts from mechanical mixtures, and in some cases impregnates. We have also seen that, subsequent to this initial reduction, redox behavior for GaZSM-5 can be observed. Did you determine the dispersion or Ga in your samples ?

[2] G. L. Price, V. Kanazirev, *J. Catal.*, **176**, 767 (1990)
[3] K. M. Dooley, C. Chang, G. L. Price, *Appl. Catal. A.*, **84**, 17 (1992)

A: P. Fejes

You are right. Oxygen and hydrogen uptake was measured for the A.S. V(f)-ZSM-5 samples only. The Ga and In containing ZSM-5 specimens which were prepared by solid exchange have not been reduced at all. In the light of your remarks this might be the reason that the observed selectivity for aromatics (between about 20-30%) was markedly less than that characteristic for the best of this sort of catalysts. Nevertheless, I would like to stress that these experiments were not aiming to arrive to the best catalyst formulations.

As far as dispersion of Ga in the samples prepared by solid exchange is concerned, may I mention that the ultimate catalyst was a very complex mechanical mixture consisting of exchanged ZSM-5 zeolite and unreacted oxide prohibiting any attempt to determine dispersion of Ga in the zeolitic phase.

Q: J. N. Armor (USA)

1) What is the level of exchange of vanadium into ZSM-5 and Y type zeolites and what is the wt% of vanadium in these materials for the ion-exhanged preparations ?

2) For the solid state exchange - did you see a difference in performance for vanadium oxide and catalysts derived from VCl_3 derived products ?

It is very important to determine the level of vanadium exchange and distinguish between precipitated or exchanged forms of vanadium for ion exchanged preparations.

A: P. Fejes

1) It is impossible to obtain complete exchange of (Na)-ZSM-5 (after B.O. acidic sites were neutralized in 0.01 molar NaOH) or NaY in 0.1 molar vanadyl oxalate solution. In the case of (Na)-ZSM-5 the degree of exchange was about 52%, for NaY it was about 64%. These samples were utilized only in the ESR and ^{51}V-MAS-NMR studies. Though we omitted to mention it in the paper the ^{23}Na-MAS-NMR spectra were also registered the analysis of which we have to skip here.

2) For VCl_3-ZSM-5 and V_2O_5-ZSM-5 we have comparative data only for the conditions of Figure 9. The two specimens behave similarly in spite of the differences in the degree of exchange and even in the quality of active sites (VCl_3-ZSM-5 contains V mainly in the V(III) oxidation state which is dominantly V(V)in the case of V_2O_5-ZSM-5).

Guczi, L. *et al.* (Editors), *New Frontiers in Catalysis*
Proceedings of the 10th International Congress on Catalysis, 19-24 July, 1992, Budapest, Hungary
© 1993 Elsevier Science Publishers B.V. All rights reserved

MECHANISM OF COKE FORMATION DURING THE TRANSFORMATION OF PROPENE, TOLUENE AND PROPENE-TOLUENE MIXTURE ON HZSM-5

P. Magnoux[a], *F. Machado*[b] *and M. Guisnet*[a]

[a]URA CNRS 350, Laboratoire de Catalyse en Chimie Organique, UFR Sciences, 40, avenue du Recteur Pineau, 86022 Poitiers, France
[b]Universidad Central de Venezuela, Escuela de Quimica, Facultad de Ciencias, Apartado 47102, Caracas, Venezuela

Abstract

The formation of coke was investigated during the transformation of propene, of toluene and of a mixture propene-toluene on a HZSM5 zeolite. At 120°C while no products are desorbed from the zeolite, coking occurs very rapidly from propene and from the mixture, slowly from toluene. The coke molecules result mainly from condensation reactions : from propene the main "coke" components are C_{12}-C_{35} aliphatic hydrocarbons, from toluene, methyldiphenyl and triphenylmethane compounds, from the mixture, diisopropyltoluenes. These coke molecules are located inside the pores, their retention being due to their low volatility and also, for diisopropyltoluenes, to a steric blockage at channel intersections. At 450°C very little toluene is transformed. Propene and the mixture are rapidly converted into C_2-C_7 olefins and C_6-C_8 aromatics. The rate of coking is not very dependent on the reactant. Whatever the reactant, methylpyrenes are the main coke components. However these coke molecules are probably formed through different reaction paths from toluene or from propene and propene-toluene mixture. They are sterically blocked at channel intersections. Mechanisms are proposed to explain the formation of the various coke molecules.

INTRODUCTION

The main cause of deactivation of zeolites is the formation and the retention of secondary products heavier than the reactants and the desired products inside the pores or on the outer surface of the crystallites. Although these compounds are not always polyaromatic most of the authors call them coke. The major difficulty in the determination of the modes of coking and of deactivation is to establish the composition of coke [1]. *In situ* spectroscopic methods (IR, ^{13}C NMR, UV-VIS, EPR) can give information concerning the coke content, the chemical identity of coke components during the reaction, the nature of the active sites and the mode of deactivation [2]. Unfortunately none of these methods is able to give the coke composition [3].

To determine the complete distribution of the coke components, the totality of the coke must be recovered from the coked zeolite (e.g. by dissolving the zeolite in

acid or basic solutions) then analyzed through adequate techniques (GC, HPLC, HNMR, MS, electron microscopy...). Thanks to this method, often associated with the characterization of the coked zeolites by adsorption, the effect of the pore structure on the modes of coking and deactivation of zeolites during hydrocarbon transformations is now well-understood [1]. Coking and deactivation however depend also on the characteristics of the active sites and on the operating conditions : temperature, reactants... While the effect of the reaction temperature was extensively investigated [4-11] the influence of the nature of the reactant [12-15] has been little studied. The reactant is often olefinic or paraffinic, more rarely aromatic and only three papers [13,14,16] concern hydrocarbon mixtures which, however, are frequently used as reactant or are formed as products in industrial processes.

The aim of this work is to specify at low (120°C) and at high (450°C) temperatures the rate of coking the composition, the location and the mode of formation of coke during the transformation of propene, of toluene and of a mixture propene-toluene on a HZSM5 zeolite.

EXPERIMENTAL

HZSM5 ($Na_{0.001}H_{2.1}Al_{2.1}Si_{93.9}O_{192}$, spherulite) was synthesized by a method proposed by Guth and Caullet [17]. The transformation of propene (a), toluene (b) and of the mixture propene-toluene (c) was carried out in a flow reactor at 120°C and 450°C, under the following conditions : a) $P_{propene}$ = 0.1 bar, $P_{nitrogen}$ = 0.9 bar ; b) $P_{toluene}$ = 0.15 bar, $P_{nitrogen}$ = 0.85 bar ; c) $P_{propene}$ = 0.1 bar, $P_{toluene}$ = 0.15 bar, $P_{nitrogen}$ = 0.75 bar. Reaction products were analyzed on line by GC with a 50 m fused silica capillary column Plot Al_2O_3/KOH for the transformation of propene, a 30 m fused silica capillary column DB Wax for that of toluene and a 50 m fused silica capillary column CP Sil 5 for that of the mixture. For the kinetic study of coking the WWH (grams of reactant injected per gram of zeolite and per hour) was equal to 9.7 (propene), 32.2 (toluene) and to 9.7+ 32.2 (propene + toluene mixture). The coked samples used for coke analysis were obtained by operating with a WWH value of about 1.0 (propene), 3.2 (toluene) and to 1.0 + 3.2 (propene + toluene mixture). The experimental methods used to recover and to analyze the coke components have already been described [18].

RESULTS

1. Reaction products

The reaction products were analyzed on line during the kinetic study of coking.

- At 120°C, there were no products observed during the transformation of propene and of toluene ; traces of isopropyltoluene (0.1 % conversion) were found in the transformation of the mixture propene-toluene. Moreover a small amount of oligomers (C_{12}-C_{22}) was found by condensing the effluents of transformation of propene during the preparation of the coked samples for coke analysis.
- At 450°C very little toluene was converted (0.3 %), benzene being the main product with traces of xylenes and light alkenes and alkanes. Propene was converted at 65 % into a mixture of aliphatic compounds (10 % C_2, 5 % C_3, 25 %

C_4, 10 % C_5, 10 % C_6-C_7) mainly olefinic and of C_6-C_8 aromatics (6 %). The same products with practically the same distribution were observed from the mixture propene-toluene. Most of them resulted therefore from transformation of propene. The conversion calculated on propene (55 %) was smaller than that obtained with pure propene (65 %). Whatever the reactant the deactivation of the zeolite was slow.

2. Rate of coke formation

At 120°C, the formation of coke was much faster from propene than from toluene (Table 1). At short time-on-stream the percentage of coke formed from the mixture propene-toluene was practically the same as from propene while at long time-on-stream it was slightly greater. At 450°C, the coking rate was not very dependent on the reactant. The formation of coke from propene and from the mixture was much slower than at 120°C while slightly slower from toluene.

Table 1
Percentages of coke (wt %) formed on HZSM5 for various time-on-stream t (mn). P : propene ; T : toluene

Reactant \ t	120°C				450°C		
	2	5	60	360	15	60	360
P	7.5	7.3	8.0	8.9	0.7	0.9	1.3
T		0.5	1.1	1.9	0.6	0.9	1.2
P+T	7.0	8.0	8.4	9.4	0.7	1.0	2.4

3. Coke composition

Table 2 gives the color and the percentage of coke of the samples prepared for coke analysis. Whatever the operating conditions all the coke components were soluble in methylene chloride. Most of them were located inside the pores for they were not dissolved by soxhlet extraction (maximal yield 5 % for 24 hrs).

Table 2
Characteristics of the coked samples t : time-on-stream ; wt % C : percentage of coke. P : propene ; T : toluene

T(°C)	Reactant	t(h)	Color	wt % C
120	P	6, 20	beige	9.0, 9.5
	T	6, 20	yellow clear	0.5, 1.0
	P+T	6, 20	yellow clear	9.0, 9.7
450	P	6	grey	3.0
	T	6	grey	1.6
	P+T	6	grey	2.6

3.1. At 120°C, the composition of coke depended very much on the reactant but very little on time-on-stream. This is clearly shown by GC, MS and HNMR analysis.

The main families of the coke components determined by GC-MS analysis are given in table 3. From toluene three families were found, the components resulting from the association of 2 or 3 toluene molecules. The coke formed from propene contains C_{12} to C_{35} aliphatic hydrocarbons with a number of unsaturations + cycles equal to O (alkanes), to 1 (olefins or cyclanes) or to 2 (diolefins or cyclenes). The main components of the coke formed from the propene-toluene mixture have the same general formula (C_nH_{2n-6}). They are mono, bi or triisopropyltoluenes resulting from the alkylation of toluene by propene. n-Propyltoluenes and diphenylmethane compounds were also found but in small amounts. On the other hand the aliphatic hydrocarbons formed from pure propene were not observed.

Table 3
Coke formed on HZSM5 from various reactants (P : propene ; T : toluene) at 120°C. Main families of components and main components in each family.

Reactant (% coke)	General formula	In + Cy	Developed formula	Formula	bp 760 (°C)	Size (Å)
P	C_nH_{2n+2}	0	alkanes	$C_{12}H_{26}$	175	4.3
						x
(9 wt %)	C_nH_{2n}	1	alkenes and/or	to	to	10-35
	C_nH_{2n-2}	2	naphtenes	$C_{35}H_{72}$	488	
T	C_nH_{2n-14}*	8	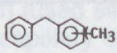	$C_{15}H_{16}$	265	(6x9.5)
			x=0-4	x=2		
(0.5 wt %)	C_nH_{2n-16}	9	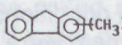	$C_{13}H_{10}$	290	(6x9.5)
			x=0-2	x=0		
	C_nH_{2n-22}	12	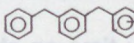	$C_{23}H_{24}$	≈380	
			x=0-3	x=3		(6x15.5)
P+T	C_nH_{2n-6}	4		$C_{13}H_{20}$*	210	(6x9.5)
				x=2		
(9 wt %)			x=1-3			

In+Cy : Number of unsaturations + cycles ; * : Main families

3.2. At 450°C, GC, MS and HNMR analysis show that the composition of coke depends little on the reactant. The main components belonged to two families

whose general formulae were C_nH_{2n-16} and C_nH_{2n-22}, which corresponds to methylpyrenes and methylfluorenes. In the case of toluene, traces of C_nH_{2n-18} compounds (methylphenanthrene or anthracene) were also observed (Table 4).

Table 4
Coke formed on HZSM5 from various reactants (P : propene ; T : toluene) at 450°C. Main families of components and main components in each family

Reactant (% coke)	General formula	In + Cy	Developed formula	Formula	bp760 (°C)	Size (Å)
P	C_nH_{2n-16}	9	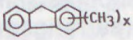 x=0-4	$C_{16}H_{16}$ x=3	295	(6x9.5)
(3 wt %)	C_nH_{2n-22}*	12	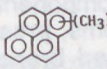 x=0-5	$C_{19}H_{16}$ x=3	400	(8.5x8.5)
T	C_nH_{2n-16}	9	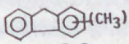 x=0-3	$C_{15}H_{14}$ x=2	290	(6x9.5)
	C_nH_{2n-18}	10	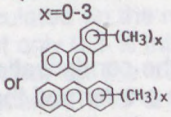 x=0-2	$C_{15}H_{12}$ x=1	340	(6x9.5) (6x8.5)
(1.6 wt %)	C_nH_{2n-22}*	12	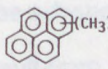 x=0-4	$C_{19}H_{16}$ x=3	400	(8.5x8.5)
P+T	C_nH_{2n-16}	9	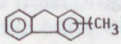 x=2-4	$C_{16}H_{16}$ x=3	295	(6x9.5)
(2.6 wt %)	C_nH_{2n-22}*	12	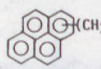 x=0-5	$C_{19}H_{16}$ x=3	400	(8.5x8.5)

In+Cy : Number of unsaturations + cycles ; * Main families.

DISCUSSION

Whatever the temperature and the reactant, heavy secondary reaction products are formed and remain blocked in or on the ZSM5 zeolite. For simplification these products will be called coke, even if their components are not always polyaromatic. The mode of formation of the coke components, the cause of their retention and their location will be examined.

1. Mode of coke formation

1.1. At 120°C

At this temperature and whatever the reactant there are practically no desorbed products. However from propene and from the mixture propene-toluene the initial rate of coke formation is relatively high. Thus in the first two minutes the conversion of propene into coke is above 20 % and that of the mixture above 5 % while that of toluene is only 0.2 %. This difference in reactivity can be explained from the differences in the difficulty of the reactions involved in the formation of the different cokes.

1.1.1. From propene

Coke is constituted of alkanes, alkenes and cyclanes having 12 to 35 carbon atoms. Obviously, these compounds cannot result from a simple oligomerization of propene but involve other reactions i.e. rearrangement and cracking of oligomers, condensation of olefinic cracking products with propene, cyclization, hydrogen transfer between oligomers. The coke components are different from those found on a USHY zeolite (28 to 34 carbon atoms, presence of compounds with 3 or 4 insaturations + cycles, more pronounced branching [18]). However the same reactions are probably involved in the formation of coke with both zeolites, the lower density of the acid sites of HZSM5 and the steric constraints at their vicinity limiting hydrogen transfer reactions and oligomerization of branched olefins.

1.1.2. From toluene

The coke components result from the condensation of 2 or 3 toluene molecules. Methyldiphenyl and triphenylmethane are formed through the following reactions.

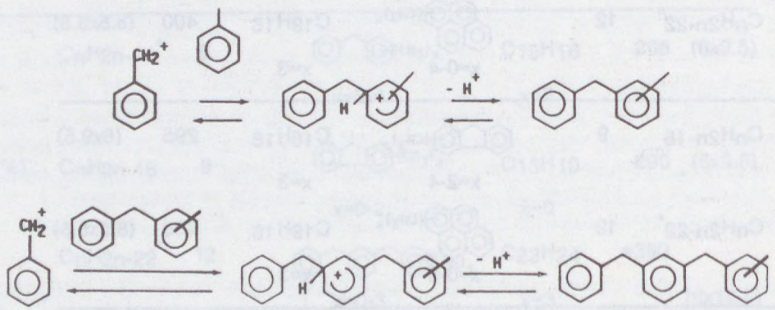

Methyldiphenylmethane compounds were proposed as intermediates in toluene disproportionation [19]. Their formation and that of triphenylmethane compounds is slow for i) they require strong acid sites and ii) these bimolecular reactions are very limited in the narrow space available near the acid sites of HZSM5 (channel intersections). With USHY, diphenyl and triphenylmethane compounds were also observed but they led rapidly through cyclization and hydrogen transfer to anthracenic and phenanthrenic hydrocarbons [20]. Here again the lower density of the acid sites of HZSM5 and steric constraints explain the differences in coke composition.

1.1.3. From the mixture propene-toluene

The main coke components result from the alkylation of toluene by propene :

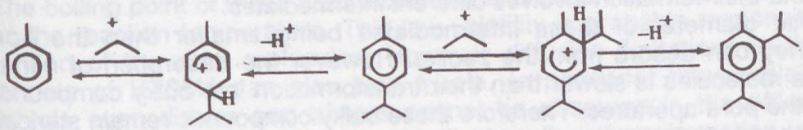

Toluene inhibits the reactions of propene condensation. This could be due to the greater basicity of toluene with consequently a stronger adsorption on the acid sites (in the form of benzenium ions) and above all a preferential attack of isopropyl carbocations by toluene. The formation of diphenylmethane compounds is very limited, which seems to show that propene affects either the adsorption of toluene in the form of benzylic cations or the attack of these cations by toluene molecules.

1.2. At 450°C

Whatever the reactant the formation of coke is very slow. From propene and from the mixture propene-toluene it is much slower than the conversion into desorbed products : thus, in the first 15 minutes, propene is converted at 0.3 % into coke against 65 % into desorbed products, the mixture propene-toluene at 0.07 % against 15.7 % (conversions calculated on the mixture). On the other hand 0.08 % toluene is converted into coke but only 0.3 % into desorbed products.

The reactant has very little effect on the coke composition. The main coke components are always alkylpyrenes and among alkylpyrenes, the trimethylpyrenes are always predominant. The other coke components are fluorenic compounds. Two hypotheses can be advanced to explain the similarity of the coke components :

1. Alkylpyrenes and fluorenes result from the same reactions probably between aromatic and olefinic compounds (see reactions 1 in figure 1). This is quite possible from the mixture but also from propene for propene is rapidly transformed into C_2-C_7 alkenes and benzenic compounds. This is more improbable from toluene for only traces of alkenes are observed in the reaction products.

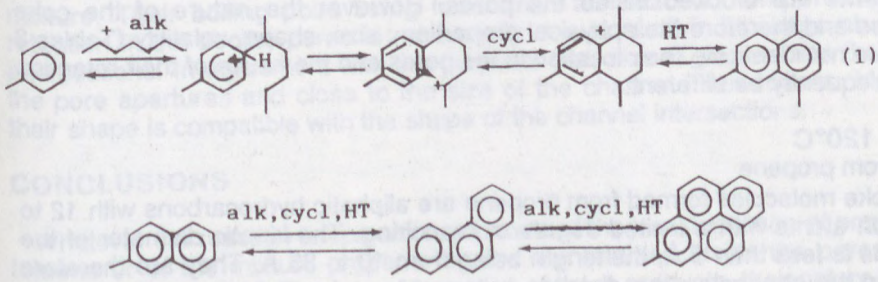

alk : alkylation, cycl : cyclisation, HT : Hydrogen Transfer

Figure 1. Formation of pyrene from alkenes + benzenic compounds

2. Coke components result from different reaction paths : e.g. path 1 from the mixture propene-toluene and from propene (Figure 1) and path 2 from toluene (Figure 2) and their formation involves different intermediates.

The kinetic diameter of these intermediates being smaller than the pore apertures they can desorb from the zeolite. However the desorption of certain intermediate molecules is slower than their transformation into bulky compounds, larger than the pore apertures. Therefore these bulky compounds remain sterically blocked at channel intersections and constitute the coke components. Obviously their size and their shape are determined by the size and the shape of the channel intersections.

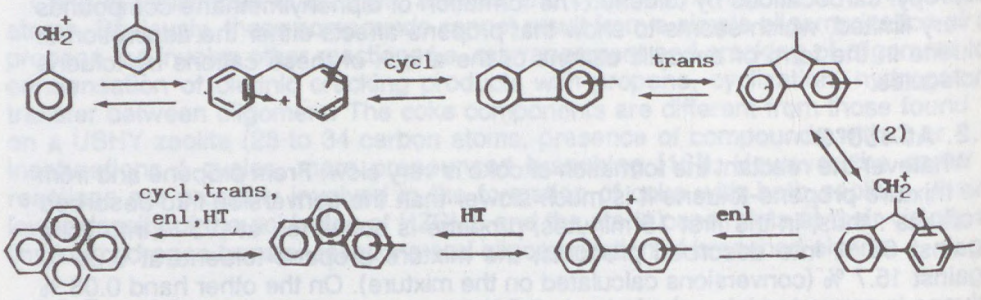

cycl: cyclisation,trans: transalkylation,enl: enlargment of cycle
HT: Hydrogen Transfer

Figure 2. Formation of pyrene from toluene.

2. Location of the coke molecules and cause of their retention

Whatever the temperature and the reactant all the coke components are soluble in methylene chloride after dissolution of the zeolite in a hydrofluoric solution. However more than 95 % of coke cannot be recovered by a 24 hour soxhlet treatment of the coked zeolite by methylene chloride. This shows that the coke components are blocked inside the pores. However the nature of the coke molecules and therefore their physical properties : size, shape, volatility (Tables 3 and 4) are not identical. Their location in the pores and the cause of their retention can consequently be different.

2.1. At 120°C

2.1.1. From propene

The coke molecules formed from propene are aliphatic hydrocarbons with 12 to 35 carbon atoms with a limited degree of branching. The kinetic diameter of the molecules is less than 5 Å, the length being from 10 to 35 Å. They are therefore located in the channels ; the distance between two channel intersections being equal to 10 Å, the coke molecules occupy a volume comprising 2 to 4 channel intersections. The maximum number of coke molecules is equal to about 2.10^{20} per gram of zeolite, i.e. about half of the channel intersections and 1.5 times less than the theoretical number of acid sites. The volume occupied by the coke

molecules estimated from the density of C_{12}-C_{35} alkanes is equal to 0.115 cm^3/g which corresponds to 70 % of the pore volume of the zeolite.

The boiling point of these coke molecules is between 175 and 490°C i.e. higher than the reaction temperature. This low volatility is probably responsible for the retention of the coke molecules. However diffusion limitations in the narrow channels of HZSM5 can also play a role. In particular they explain why no products even dimers and trimers cannot be observed in the effluents, their desorption from the zeolite being slower than their transformation into bulkier compounds.

2.1.2. From toluene

The kinetic diameter of the coke molecules is close to that the channels and their boiling point much higher than the reaction temperature. Given their shape and size these molecules are located at channel intersections for their migration in the narrow channels of HZSM5 is certainly slow. Another cause of their retention in the zeolite pores is their low volatility.

2.1.3. From the mixture propene-toluene

Diisopropyltoluenes are the main coke components. Their kinetic diameter is greater than the apertures of the channels and their size and shape compatible with the size and shape of the channel intersections. Therefore these molecules are sterically blocked at channel intersections. This steric blockage does not occur in the case of para-isopropyltoluene which was also observed in the coke components. This coke molecule which is smaller than the aperture of the channels is then retained in the zeolite pores only because of its low volatility.

The maximum number of coke molecules (about $3.8.10^{20}$ per gram of zeolite) is close to the number of channel intersections and slightly greater than the number of acid sites. It can therefore be concluded that each coke molecule occupies one channel intersection. The volume occupied by the coke molecules estimated from the density of isopropyltoluenes, is of about 0.10 cm^3 per gram of zeolite i.e. close to the volume of the channel intersections (0.13 cm^3g^{-1}).

2.2. At 450°C

The same coke components are formed from propene, from toluene or from the mixture. Their boiling point being lower than the reaction temperature, their retention in the zeolite pores is necessarily due to a steric blockage at channel intersections. In agreement with this proposal their size is greater than the size of the pore apertures and close to the size of the channel intersections. Moreover their shape is compatible with the shape of the channel intersections.

CONCLUSIONS

Whatever the reaction temperature, products of the transformation of propene, of toluene or of the mixture propene-toluene are retained inside the pores of the HZSM5 zeolite (coke). The rate of formation of these products, their nature and the cause of their retention inside the pores depend mainly on the temperature. At low temperature coke molecules result principally from condensation reactions while at high temperature, alkylation, cyclization and hydrogen transfer reactions are also involved. At low temperature the retention in the pores of the coke molecules

is mainly due to their low volatility, at high temperature to their steric blockage at channel intersections. Because of the easier retention of the coke molecules in the zeolite pores, the rate of coke formation is greater at low than at high temperature.

ACKNOWLEDGMENTS

F.M. acknowledges a fellowship within the frame of the postgraduated programme of cooperation CEFI-CONICIT.

REFERENCES

1 M. Guisnet and P. Magnoux, Appl. Catal., 54 (1989) 1.
2 H.G. Karge, in "Introduction to zeolite science and practice", (H. van Bekkum, E.M. Flanigen, J.C. Jansen, eds.), Studies in Surface Science and Catalysis, Vol. 58, 531, Elsevier, Amsterdam 1991.
3 M. Guisnet and P. Magnoux, in "Zeolite Microporous Solids : Synthesis, Structure and Reactivity" (E.G. Derouane, ed.), NATO ASI Series, to be published.
4 D. Eisenbach and G Gallei, J. Catal., 56 (1979) 377.
5 B.E. Langner, Ind. Eng. Chem. Processs. Des. Dev., 20 (1981) 326.
6 D.G. Blackmond, J.G. Goodwin and J.E. Lester, J. Catal., 78 (1982) 247.
7 A.K. Ghosh and R.A. Kydd, J. Catal., 100 (1986) 185.
8 J.P. Lange, A. Gutsze and H.G. Karge, J. Catal., 114 (1988) 136.
9 H.G. Karge, J.P. Lange, A. Gutsze and M. Laniecki, J. Catal., 114 (1988) 144.
10 P. Magnoux, V. Fouché and M. Guisnet, Bull. Soc. Chim., (1987) 696.
11 J.R. Anderson, Y.F. Chang and R.J. Western, J. Catal., 118 (1989) 466.
12 S. Maixner, C.Y. Chen, P.J. Grobet, P.A. Jacobs and J. Weitkamp, in "New Developments in Zeolite Science and Technology", Proc. 7th Int. Zeolite Conference (Y. Murakami et al, eds.), Elsevier, Amsterdam (1986) 693.
13 D.E. Walsh and L.D. Rollmann, J. Catal., 49 (1977) 369.
14 D.E. Walsh and L.D. Rollmann, J. Catal., 56 (1979) 195.
15 J. Kärger, H. Pfeifer, J. Caro, M. Bülow, H. Schlodder, R. Mostowicz and J. Völter, Appl. Catal., 29 (1987) 21.
16 L.D. Rollmann and D.E. Walsh, in "Progress in Catalyst Deactivation" (J.L. Figuereido, ed.), NATO ASI Series, Vol. 54, 81, Martinus Nijhoff Publishers, The Hague, 1982.
17 J.L. Guth and Ph. Caullet, J. Chim. Phys., 83 (1986) 155.
18 P. Magnoux, P. Roger, C. Canaff, V. Fouché, N.S. Gnep and M. Guisnet, in "Catalyst Deactivation" (B. Delmon and G.F. Froment, eds.), Studies in Surface Science and Catalysis, 34, 317, Elsevier 1987.
19 M. Guisnet and N.S. Gnep, in "Zeolites : Science and Technology" (F.R.Ribeiro et al, eds.), NATO ASI Series E80, 571, Martinus Nijhoff Publishers, The Hague (1984).
20 P. Magnoux, C. Canaff, F. Machado and M. Guisnet, J. Catal., to be published.

DISCUSSION

Q: Wm. C. Conner (USA)

Do you have any information as to the decrease in total pore volume measured by adsorption (N_2 or other) with the formation of coke in your samples ? Is the decrease in adsorption volume greater or equal to the volume of coke being formed? In a similar manner does the effective diffusivity decrease linearly or more rapidly with "coke" retention by the ZSM-5 ?

A: M. Guisnet

In this study the coked samples were not characterized by adsorption. However adsorption experiments with nitrogen and n-hexane were previously carried out on ZSM5 samples coked during n-heptane cracking at 450 ^{0}C [1]. For these samples the composition of coke was similar to that found during propene transformation at the same temperature. At low coke content (<3 wt%) the decrease in the adsorption volume was practically equal to the volume of coke being formed. Due to pore blockage by bulkier coke molecules it becomes greater at high coke content. These bulkier molecules, non soluble in organic solvents result from the overflowing on the outer surface of the zeolite crystallites of the coke molecules located at the channel intersections close to the surface.

[1] P. Magnoux, P. Cartraud, S. Mignard and M. Guisnet, *J. Catal.*, **106**, 242 (1987)

Q: H. Schulz (Germany)

I feel it contributes significantly to the confusion in zeolite catalysis if any deposit, adsorbate or encapsulate, be it a paraffin, olefin or aromatic - together with real coke - irrespective of the molecular weight, is now termed "coke".

I have missed in the presentation quantitative values of individual "coke" compounds. These could be tried to be correlated to the zeolite pore architecture (diameter of cages and windows, kind of interlinking). Have you tried to evaluate this question ?

A: M. Guisnet

The difficulty is due to the fact that, with zeolites, the formation of real coke (highly polyaromatic compounds) begins by the steric blockage of relatively small molecules in the cavities or at the channel intersections. These small molecules contribute to the deactivation of zeolites, which has not been taken into account by most of the researchers who have used the rigorous definition of coke. obviously it is only for reason of commodity that we use the term "coke" for all the compounds blocked in (and on) the zeolite and responsible for deactivation. However as you have probably noted, the definition we employed for the term "coke" was given in the second slide.

Concerning your question, the size of the "coke" molecules and of the channel intersections of the ZSM-5 zeolite were compared in the presentation (see also the size of the "coke" molecules in tables 3 and 4 of the paper).

Q: N. A. Prokudina (Russia)

What sites of the zeolite are active at high and at low temperature ?

A: M. Guisnet

It is well demonstrated that all the steps involved in the formation of coke both at low and at high temperatures can be catalyzed by protonic acid sites.

Q: S. Csicsery (USA)

Did you see any evidence of coke made from fulvene type intermediates ? Such intermediates were believed to constitute a large part of coke formed from olefins via conjunct polymerization and hydrogen transfer.

A: M. Guisnet

As shown in the paper all the components of the coke formed at 450 ^{0}C from propene and from the toluene-propene mixture can result from successive reactions implying aromatics and olefins (alkylation, cyclization, hydrogen transfer, etc,). Furthermore, neither cyclopentadiene compounds nor adamantanes were found, contrarily to what was observed with SAPO 34 [2]. Therefore, the participation of cyclopentadiene (and fulvene) compounds in coke formation, if it exists, is probably very limited.

[2] J. R. Anderson et al., *J. Catal.*, **124**, 259 (1990)

Q: P. G. Menon (Sweden)

Will not the rate of coking determine to some extent the exact location of the coke lay-down in ZSM-5 ? If the coking rate is high, the coke could be deposited at the pore mouths, leading to rapid pore plugging. If the coking rate is slow, a gradual and more uniform coverage of the total pore volume is possible. Such effects have been reported by Panchenkov and coworkers in the 1970's for cracking even on amorphous silica-alumina catalysts. Should they not be still more pronounced with ZSM-5 ?

A: M. Guisnet

As you quite rightly emphasize with coke-maker molecules (olefins, polyaromatics, etc,) as reactants the formation of coke can be faster than the diffusion of the reactants (or of the coke precursors) inside the zeolite crystallites with consequently a coke deposit on the outer part of the crystallites and a blockage of the access to the inner pores. This was shown during the very rapid coking of a USHY zeolite in 1-methylnaphtalene transformation [3]. However, the coking of HZSM-5, even with the toluene-propene mixture (or propene) at 120 ^{0}C, is slower and there is no significant shell coking as shown by the equality between the maximum number of "coke" molecules and the number of channel intersections.

[3] M. Guisnet and P. Magnoux, *"Zeolite Microporous Solids: Synthesis, Structure and Reactivity"*, (Eds.: E. G. Derouane et al.), Kluwer Academic Publishers, p. 457 (1992)

Q: J. P. Fraissard (France)

1) Why do you remove the coke from zeolite instead of studying it directly by ^{13}C-MAS-NMR ?

2) Do the ZSM-5 samples containg some non-framework Al species? If yes, there should be a relationship between the location of these species and the location of coke, at least at the beginning of the coking.

A: M. Guisnet

1) Spectroscopic techniques such as ^{13}C-MAS-NMR, FTIR, etc, have the advantage of not modifying the coked samples and of allowing an in-situ characterization of coke. However, while these methods give information on the chemical identity of the coke components, unfortunately none of them is able to give the coke composition i.e. the complete distribution of the coke components. Thus, through ^{13}C-MAS-NMR the coke formed on HZSM-5 during toluene transformation at 450 ^{0}C will be defined as a mixture of aromatic and polyaromatic compounds while with our method (removal of coke by dissolving the zeolite in hydrofluoric acid then analysis through GC-MS) the coke will be defined as a mixture of various methylfluorenes, methylanthracenes and methylpyrenes (Table 4) in a known percentage. This composition is essential to specify the mode of coke formation. On the other hand from the size of the coke molecules and from their volatility, their location (in the channel intersections, in the channels, on the outer surface of the crystallites) and the cause of their retention (steric blockage) can be deduced. Moreover the mode of zeolite deactivation can be determined from the deactivating effect of the individual coke molecules [4].

2) The total and the framework Si/Al ratios of the HZSM-5 sample are practically

Actually, a preferential formation of coke in the supercages of dealuminated Y zeolites containing non framework Al species has been found during n-heptane cracking at 450 ^{0}C [5].

[4] M. Guisnet and P. Magnoux, *Appl. Catal.*, **54**, 1 (1989)
[5] Q. L. Wang, G. Giannetto and M. Guisnet, *J. Catal.*, **130**, 471 (1991)

Guczi, L. *et al.* (Editors), *New Frontiers in Catalysis*
Proceedings of the 10th International Congress on Catalysis, 19-24 July, 1992, Budapest, Hungary
© 1993 Elsevier Science Publishers B.V. All rights reserved

HYDROCARBON FORMATION FROM METHANOL/DIMETHYL ETHER OVER PROTONATED ZEOLITES AND MOLECULAR SIEVES. NEW INSIGHTS FROM RECENT EXPERIMENTS

S. Kolboe

Department of Chemistry, University of Oslo, P.O.Box 1033 Blindern, 0315 Oslo, Norway

Abstract

The transition from being in a C-C non-active state to a C-C active state, at temperatures well below 300 °C, of two H-ZSM-5 zeolites has been studied. The development of activity was followed, A: by combining reactor effluent analysis and IR spectroscopy of the adsorbate, B: by carrying out the reaction in a thermal analysis instrument which allowed GC analysis of products formed, and the simultaneous monitoring of weight and heat effects due to adsorbate formation and reactions taking place in the catalyst bed.

Introduction

The possibility of converting methanol to hydrocarbons (and water) over protonated zeolites and zeolite analogues like the SAPO's is now well known. The reaction mechanism and other details of the reaction have been discussed in a large number of papers since the reaction itself was first published by Mobil workers in 1976/77 [1]. A survey of part of the literature is given in refs. [2-4]. Apart from the need for a protonated zeolite there is no consensus on the reaction mechanism.

It has recently become clear that the protonated zeolite (e.g. H-ZSM-5) in a fully calcined state (heating above 500°C in air or oxygen for several hours) is initially inactive for hydrocarbon formation from the C_1 oxygenates methanol (MeOH) or dimethyl ether (DME) at temperatures not much in excess of 300 °C. Such a system only gradually turns into a C-C active system [5-10]. Below 300 °C the initiation period may be several hours. A reaction mechanism invoking the presence of carbocations within the zeolite framework as a necessary ingredient for catalytic activity has been proposed to account for this and other observations [8,9].

The main objective of the work to be reported here is to throw some light on the processes which take place in the initial stage when the catalyst turns into a C-C active state. The emphasis will be on two sets of results. One set was obtained using a combination of IR spectroscopy and flow reaction cell, the other by using

a thermal analysis instrument allowing simultaneous measurement of sample weight and heat evolution in the catalyst/reactant system while also allowing analysis of the gas phase surrounding the catalyst.

A considerable number of papers have been published where the authors have invoked IR spectroscopy in order to obtain additional information on the methanol/DME to hydrocarbons reaction (MTG, MTO, MTH). The majority of the studies have concentrated on H-ZSM-5 as catalyst. References to most of the earlier literature may be found in recent papers by Mirth et al. and Kubelkova et al., or in the papers referenced therein [11-13].

Experimental.

While experiments similar to the ones to be described here have been carried out on various zeolites and molecular sieves the attention will here be turned towards results on H-ZSM-5. There are no indications of fundamentally different behaviour between the various zeolites towards the methanol to hydrocarbons reactions.

The ZSM-5 used for the IR studies reported here has been provided by Mobil Research and Development Corp. in the NH_4-exchanged form. It has previously been thoroughly characterized [14]. Si/Al=26. The sample was calcined in the cell by heating to slightly above 500 °C in flowing air. The calcination was monitored by the IR spectra.

The sample used for thermogravimetric studies was synthesized by procedures closely similar to the original Mobil patent [15]. It was characterized by XRD, nitrogen adsorption (BET), catalytic activity and chemical analysis.

The IR (FTIR) spectra were measured on a BIORAD FTS-7 equipped with DTGS detector at resolution 2 cm^{-1}. It was typically worked with 128 scans. The spectral range was restricted to 4000-1300 cm^{-1}. The IR absorption of both the sample and the CaF_2 windows determined the lower limit. The samples were pressed into fairly thin wafers (30 mg) and put into the IR cell where the calcination took place. The cell itself was a further evolution of the one used by Forester and Howe [14]. The measurements were performed using nitrogen carrier gas (40 mL/min) which might pass, or bypass, an evaporator allowing MeOH concentration to be varied within wide limits, through the cell. It was found that the quality of the spectra - especially in the water vapour regions - depended upon the cell being kept in exactly the same position during a whole series of measurements. Care was therefore taken to avoid any displacement of the cell from the moment the calcination of NH_4-zeolite started until the experiment was finished and the wafer taken out.

Reactions were studied in a thermal analysis apparatus (Stanton Redcroft STA 785) which allows the simultaneous measurement of weight and heat evolution in a sample. It was worked with 30 mg sample weight. The instrument's weighing sensitivity is < 1 μg. Heat effects are measurable down to < 10 μW. The instrument was operated under flowing conditions (N_2) and by a slight modification any desired compound can be added to the carrier gas, continually or in pulses. It can be operated isothermally or temperature programmed between - 100 and + 625 °C. Products were analyzed by GC using Porapak T or N columns.

Results and discussion.

MeOH is converted into hydrocarbons at an easily measurable rate at temperatures above ≈200 °C over an activated H-ZSM-5 catalyst. But unless it has been activated an H-ZSM-5 which has been fully calcined by heating to 500 °C in air for 10-20 h does not convert MeOH into hydrocarbons. The activation may be obtained by adding a small quantity of an alkene to the system [6-9], or by desorbing previously adsorbed MeOH/DME. At some critical coverage a sudden transformation into a C-C active state, whereupon hydrocarbons are formed, takes place [16].

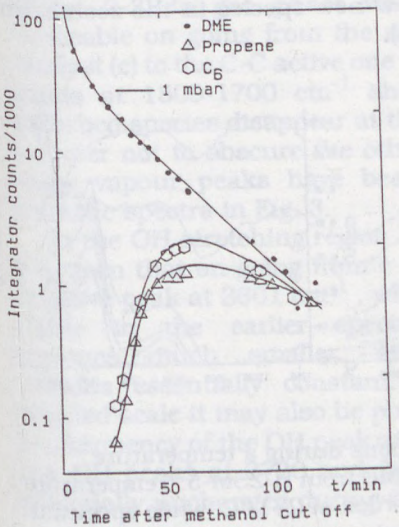

Figure 1. Evolution of C-C activity over H-ZSM-5 at constant temperature (220 °C) and gas flow when reactant feeding is stopped. Only C_3 and C_6 products are displayed.

Two examples where C-C bond formation is obtained by desorbing preadsorbed MeOH/DME at slightly above 200 °C are shown in Figs. 1 and 2. In both cases there would have been no C-C activity if the system had been left under the same conditions except for a constant MeOH/DME pressure ≈100 mbar. These examples were both obtained on H-ZSM-5, but analogous behaviour has been observed over HY and other zeolites [22].

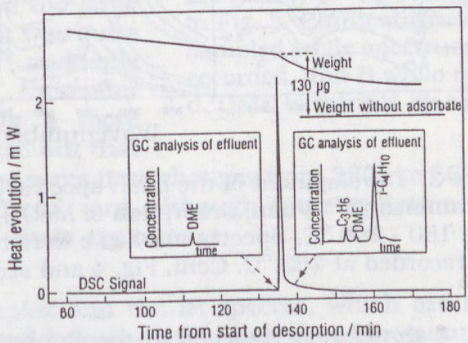

Figure 2. Sudden appearance of C-C forming activity during desorption of DME from H-ZSM-5 at 210 °C [16].

Catalyst activation followed by IR spectroscopy.

Very similar experiments were carried out in this work with the reaction system within an IR spectrometer with the objective to monitor changes taking place at the moment the system turned into a C-C active state from a C-C nonactive state.

The following experiment was performed using a sample of NH_4-ZSM-5 provided by Mobil. About 30 mg of the zeolite was pressed into a wafer, put into the IR cell and calcined by slowly heating to 520 °C in an air stream. The catalyst was exposed to a flow of MeOH (≈ 5 mbar) in Nitrogen carrier gas (37 mL/min) at 150 °C for 15 min. The effluent, which was analyzed (by GC) at intervals, showed that ≈10 % of the methanol was converted to DME. After flushing the cell for 150

minutes there were bands in the 2700-3100 cm^{-1} region showing that the major components of the adsorbate was methanol (2853 and 2956 cm^{-1} with a shoulder at 2979 cm^{-1}), but they also showed the presence of lesser amounts of DME (shoulders at 2842 and 3010 cm^{-1}, see below). The temperature was now raised to 177 °C and methanol was again admitted (same flow and concentration as before) for 40 min, before again cutting off methanol. After 25 minutes the MeOH/DME content of the effluent gas had fallen to 2 % of the value while feeding, and no gas phase was seen in the spectra. The temperature was slowly raised (2 °C/min to a final value of 290°C). Fig. 3 shows the development of the CH stretching region during this phase of the experiment, while the gas chromatograms recorded at 253 °C and 263 °C are shown in Fig. 4. The spectra are difference spectra of (zeolite+adsorbate) and zeolite with no adsorbate recorded at the same temperature. Positive bands show new species in the zeolite, and negative bands show diminishing species (OH).

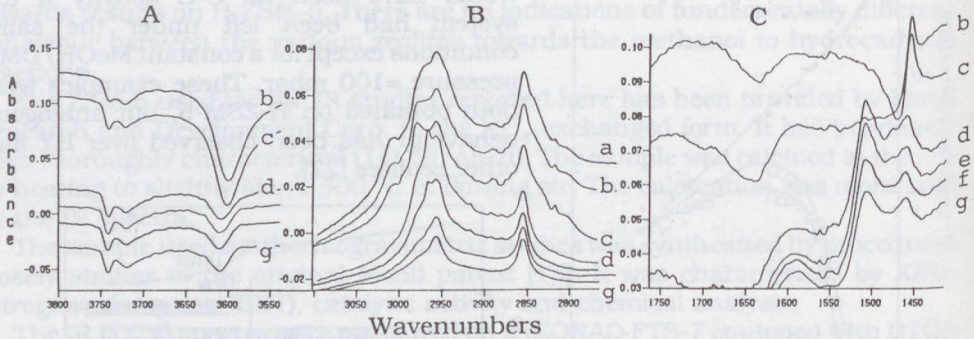

Figure 3. Development of the main spectral regions during a temperature programmed (2 °C/min) desorption of MeOH/DME from H-ZSM-5. Temperature range 180 - 290 °C. Spectra marked c were recorded at 251 °C, while spectra d were recorded at 263 °C. Conf. Fig. 4 and see text.

Fig. 4 shows very clearly that the catalytic activity is very different in the two cases, the temperature difference being far too small to account for the change. It is furthermore know that a similar effect may be observed also under isothermal conditions (Fig.s 1 and 2).

The spectra in Fig. 3 (parts A, B and C) show a similar drastic change on going from spectrum c to spectrum d (recorded at 251 and 263 °C). The shoulder (in part B) at 3010 cm^{-1} (DME?) disappears and the dominant peak at 2979 cm^{-1} is strongly reduced. The new peak at 2966 cm^{-1} may possibly be due to gas phase isobutane, and a slight broadening visible on the low frequency side of the 2956 cm^{-1} peak may be propene. Isobutane and propene are the dominant gas phase products (besides water which was not analyzed, but which, before water vapour bands were subtracted, was clearly seen in spectra d and e.) The peak at 2855 cm^{-1} does not seem to undergo any dramatic changes. It decreases fairly regularly during the whole experiment, as it also appears that the main component of the 2956 cm^{-1} peak does.

Simultaneously with the spectral changes around 2900 cm^{-1} marked changes

were also observed in the CH bending region (1450 -1550 cm^{-1}) and the OH stretching region (3500-3750 cm^{-1}). The bending spectra are displayed in Fig. 3 part C. Again the spectrum changes markedly on going from c to d. In d there is a new peak at 1510 cm^{-1} which does not decrease appreciably with time. Simultaneously it appears that the peak at 1456 cm^{-1} disappears (or decreases strongly) and is replaced by another peak at 1460 cm^{-1}. Also this peak appears rather stable at 290 °C. A considerable increase (factor 2-3) in gas phase water was also noticeable on going from the not C-C active catalyst (c) to the C-C active one (d). The broad bands at 1500-1700 cm^{-1} showing OH in adsorbed species disappear at the same time. In order not to obscure the other details the water vapour peaks have been subtracted from the spectra in Fig. 3.

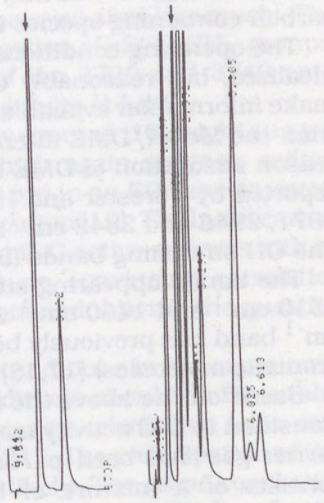

Figure 4. IR cell effluent analysis while recording spectra in Fig. 3. Chromatogram A was sampled while spectrum c was recorded, and B while recording d. DME is marked by an arrow.

In the OH stretching region (Fig. 3 part A) it is seen that on going from c to d the large negative peak at 3601 cm^{-1} , which was quite stable in the earlier spectra, suddenly becomes much smaller, and thereafter remains essentially constant. On a more detailed scale it may also be pointed out that the frequency of the OH peak at the same time changes from 3601 to 3611 cm^{-1}. The OH peaks at 3720 and 3740 cm^{-1} are, although some evolution is seen, essentially unchanged during the whole experiment.

Interpretation of the spectra.

The adsorption system is complex and the IR spectra, which are not very sharp, do not allow very detailed and definite conclusions about the nature of the interactions and the species formed. However, recent literature favour the view that methanol when adsorbed on acidic substances like protonated zeolites (in particular H-ZSM-5) interact with the acidic OH groups which bridge silicon and aluminium tetrahedral ions [11-14,17]. This interaction causes the marked negative peak at 3601 cm^{-1}, and also the smaller negative peaks at the frequencies 3720 and 3742 cm^{-1}.

There has been some uncertainty as to the fate of the methanol molecule when it is adsorbed. Kubelkova et al. and Mirth and Lercher [11-13] maintain that the methanol will mainly be present in protonated form. The spectra obtained in this work support this view. Forester and Howe, who worked under somewhat different conditions, found no sign of protonated methanol and suggested that it would immediately decompose [14].

It also appears established that when the temperature is increased above 100 °C in vacuum or dry carrier gas the protonated methanol may gradually split off water and the resulting methyl cation CH_3^+ be bonded via an oxide anion to the

zeolite framework. This may explain Forester and Howe's results [14].The resulting carbon containing species is usually termed a methoxide.

The operating conditions were in this work deliberately chosen not to be very idealized, but reasonably close to a realistic operating system, thus hopefully make information available which is not easily obtainable otherwise. It is known that the MeOH/DME interconversion is fast. This was found also here. For this reason adsorption of DME has also been studied. In agreement with the results reported by Forester and Howe CH stretching frequencies were found at 3011, 2971, 2946 and 2842 cm^{-1} [14]. A CH bending band was observed at 1455 cm^{-1}. The OH stretching bands (3600-3700 cm^{-1}) were similar to the methanol case.

The bands appearing simultaneously with the occurrence of C-C activity at 1510 cm^{-1} and 1460 cm^{-1} are evidently not caused by C_1 oxygenates. The 1510 cm^{-1} band has previously been ascribed to partially unsaturated C-C bonds (e.g. aromatic molecules) [17,18].

Based on the above the following description of the processes leading to the transition to C-C activity may be proposed: After methanol has been added to the carrier gas and been partially transformed to DME and water the adsorbate consists of a mixture of $MeOH_2^+$ and $(Me)_2OH^+$ and possibly MeOH/DME hydrogen-bonded to these cations forming clusters [11,12]. The situation is represented by spectrum a in Fig. (3). There is no indication of adsorbed water after flushing with N_2 25 minutes at 177 °C.

The hydrogen bonded cluster molecules are not strongly bound and are the first to desorb, leaving behind the protonated methanol/DME molecules. Simultaneously the reaction forming methoxy groups may go on (presumably faster as the agglomerate molecules disappear). In this way the bands at 2979 and 2955 cm^{-1} decrease less than the bands due to the other species. All species yield a band near 2855, so no clear changes are seen in this band [13].

As the desorption proceeds the adsorbate will be a mixture (unknown proportions) of: Cluster molecules, $(Me)_2OH^+$, $MeOH_2^+$, CH_3O and free OH groups. At a point where some key species are present in the right concentrations the C-C bond formation sets in. The individual mechanistic steps are unknown. It has earlier been shown that the transition from a state where C-C bonds are not formed to one where all C-atoms appear to be bonded to other C-atoms may take place within seconds at temperatures as low as 210 °C [16]. The temperature appears mainly to govern the time needed to obtain the conditions (concentrations) needed for initiation of the process. The water vapour which appeared in gas phase simultaneously with the transition to C-C activity and the disappearance of very broad OH bands between 1500 and 1750 cm^{-1} which also took place at the same time conclusively show that a considerable part of the adsorbate was present as C_1-oxygenate when this transition took place. The pronounced 2979 cm^{-1} band suggests that there was also an important number of framework bound methoxy groups. There are indications, but this is not yet clear, that both are needed. Simultaneously with these processes the appearance of the bands at 1510 and 1460 cm^{-1} suggest that aromatics (or other partially unsaturated species) formation is connected with the initiation reaction. CH-bands around 3000 cm^{-1} are, however, not seen. This suggests the species to be highly deficient in hydrogen. The marked weakening or disappearance of the band at 1455 cm^{-1} also corroborate the notion that the adsorbate is completely reorganized in a short time.

These observations are also in agreement with the strongly decreased interaction of the adsorbate with zeolite OH groups observed simultaneously. The remaining peaks at 2955 and 2854 cm^{-1} indicate formation of $\equiv Si\text{-}O\text{-}CH_3$ groups. This is also in accord with the observed stability of the 3720 and 3740 cm^{-1} bands. They are likely to be associated with Silanol groups [14,20].

The extreme rapidity with which the transition may proceed [16] might suggest that there is a fast chain reaction taking place, which again suggests radical participation. Similar experiments previously carried out in an EPR spectrometer failed, however, to clearly evidence free radical participation [19]. The hydrocarbon adsorbate which is formed contains free radicals, and C-C active systems with no hydrocarbon free radicals were never found, but no convincing correlation between the EPR signal and catalytic activity was obtained, leaving the question unsettled.

It may be noted, in passing, that even under the conditions in the experiment referred to here (and other experiments), where conditions should be favourable for forming trimethyloxonium ions, $(Me)_3O^+$, there was no adsorption to be seen at the expected wavenumbers (3073 and 3052 cm^{-1} [21]). The participation of this ion in the reaction mechanism [2-4] is therefore unlikely. The same conclusion was reached by Howe [17], but his experimental conditions were far less forcing towards $(Me)_3O^+$ formation than those employed here.

The results obtained here concord very well with the author's earlier results where corresponding results were performed in a thermal analysis apparatus, Fig. 2, [16]. The two sets of experiments complement each other. The earlier work permitted estimation of the rate with which the transition may proceed, but water was not analyzed and the adsorbate could n • be characterized.

Activation in the presence of MeOH/DME.

The study of the transition to a C-C active state which may take place when the feed is cut off and a desorption takes place will hopefully illuminate the reactions whereby MeOH/DME is converted into hydrocarbons. It is, however, of equal interest to study the activation process under conditions which are closer to the ones under which the catalyst system is actually working. To this end experiments have been carried out where adsorbate formation, heat effects in the catalyst bed and catalytic activity for forming gas phase hydrocarbons and DME could be followed in a flow system with methanol feed. The apparatus for doing this was described above (Experimental). In this way it is possible to investigate more closely the connection between the adsorbate formation and the catalyst activation.

The following discussion concentrates on one experiment, which serves as an example of the results obtained. It was performed on 30 mg H-ZSM-5 with Si/Al= 30. After having placed the sample inside the apparatus the temperature was raised to 244 °C. This temperature was maintained during the whole experiment. The sample was left in a nitrogen flow (17 mL/min) until well beyond the time needed for a constant weight and a constant (zero) heat (DSC) signal to be reached. At zero time in Fig. 5 an additional nitrogen stream (2.9 mL/min), with methanol (100 mbar), was introduced into the main gas stream, leading to a methanol pressure 14.7 mbar in the atmosphere surrounding the catalyst. The sharp exothermic peak which is observed at this point is caused by the adsorption

which takes place (methanol, DME, water). The sample weight increase is 0.33 mg. The heat signal changes from zero to a new steady state of 0.49 mW due to the exothermic formation of DME + H_2O taking place in the catalyst bed. During the experiment the carrier gas effluent was analyzed at frequent intervals. The figure shows the development of sample weight, heat signal, percentage MeOH converted to DME and hydrocarbons (C_2+C_3 - the dominating hydrocarbons) with time.

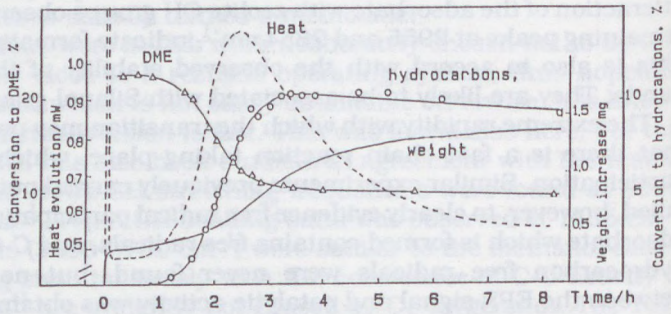

Figure 5. Time dependence of catalyst sample weight (w_o=30 mg), heat evolved in the catalyst - and the catalyst activity for transforming methanol to products; DME and hydrocarbons. Details on the experimental conditions are given in text.

The figure clearly shows that the weight increase, i.e. adsorbate formation, and the hydrocarbon forming activity occur in a parallel manner. The hydrocarbon forming activity is seen to pass through a maximum, but a steady state of lower conversion is eventually reached after about 10 h. The sample weight in the steady state is slightly higher than shown in the figure (Δm=1.42 mg; corresponding to 4.5 % w/w of adsorbate). This parallelism is brought forth by Fig. 6 where the total rate of methanol conversion into hydrocarbons (C_n(ads)+ C_xH_{2x}(g)) is plotted against the amount of adsorbate. At the time of maximum rate of weight increase ($\Delta m/\Delta t$) about 1/3 of the converted methanol ends up as adsorbate, while 2/3 emerge in the gas phase. This ratio is higher in the very early stages of the reaction and falls to zero when the system reaches a steady state.

It is also noteworthy that the activity for forming DME falls sharply with the building up of adsorbate in the sample. Apart from the adsorbate build up, all other conditions were constant during the experiment. The observed decrease in the DME formation must therefore be caused by changes in the catalyst properties - either a fall in intrinsic activity or an increased diffusional resistance due to pore blocking by the adsorbate formation. Since the decrease is pronounced even for very small quantities of adsorbate, and the DME formation becomes essentially constant long before the net adsorbate formation stops, the pore blocking seems unlikely. It is more plausible that the C-C forming sites are less efficient for DME formation than the acidic OH groups originally present. The two reactions do then mostly proceed on two different sets of sites.

The hydrocarbon formation curve, however, may well be influenced by diffusional effects. First there is an increase due to catalytic system activation. The activity then passes a maximum followed by a decrease because the increasing pore filling leads to greater diffusional resistance.

The experiment furnishes a strong indication that presence of adsorbed hydrocarbons (carbenium ions) is necessary for sustained hydrocarbon forming activity in the presence of MeOH or DME. Whether the activation process which takes place in the presence of methanol,although at a much slower rate, proceeds via the same steps as it does in a desorption experiment is not known. That one process, under desorbing conditions, is very fast once it has started, and that the other activation process, where methanol is present, is slow is to be expected if the same fundamental mechanism is involved. It was suggested above that the initial activation would take place when there was simultaneous presence of C_1-oxygenate and methoxy groups, and possibly also free acidic OH groups. Such an occurrence is much less likely when there is a large number of methanol molecules present - but there is still a finite probability.

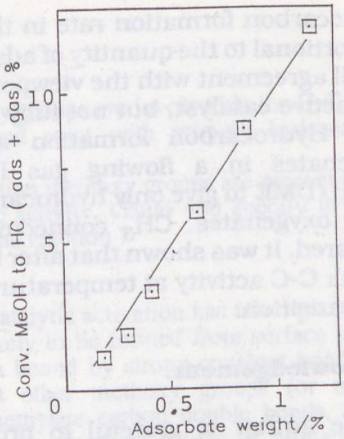

Figure 6. Relationship between catalyst activity for converting MeOH to hydrocarbons and amount of adsorbate in catalyst during the early stages of activation.

When discussing the results obtained in the IR cell it was pointed out that partly unsaturated hydrocarbons had been formed within the zeolite pores during the experiment. The catalyst then ought to exhibit C-C forming activity under conditions where no activity was seen prior to chromatogram A in Fig. 4. This was indeed the case. The catalyst in Fig.s 3 and 4 was left in N_2 flow 14 h at 290 °C after having ended the first part of the experiment. The temperature was then taken down to 245 °C and methanol was again admitted to the cell. A small conversion to hydrocarbons was now observed, showing that C-C activity was now present. The activity was, however, much less than is found in a fully C-C active catalyst. This is to be expected. The amount of adsorbate is estimated to only ≈0.1 % so the number of active sites was very small, see Fig. 6.

It has recently been proposed that the induction period which is observed may be due to a slow diffusion of hydrocarbon molecules out of the zeolite [10]. This is, however, doubtful, because as was apparent from Fig. 5, there is neither weight increase nor exothermicity (above the effect from DME formation) for an appreciable time after methanol admission to the catalyst. Furthermore, also ethylene formation follows the same pattern as propene formation.

Conclusion.

A protonated zeolite like H-ZSM-5 is initially unable to transform MeOH/DME into hydrocarbons at temperatures ≈ 250 °C. There is an induction period. Transition to an active state was obtained in two ways.

A). By leaving the catalyst in the reactor in a methanol flow at ≈ 250 °C.

Hydrocarbon formation rate in the initial stages of the reaction was essentially proportional to the quantity of adsorbate present in the zeolite. The behaviour was in full agreement with the viewpoint that the adsorbate is an essential part of the C-C active catalyst, but not fully reconcilable with an autocatalysis mechanism. B). Hydrocarbon formation was also provoked by TPD of adsorbed C_1-oxygenates in a flowing gas IR cell. The transition from only desorbing MeOH/DME to give only hydrocarbons was abrupt. Simultaneously IR stopped to show oxygenates, CH_3 connected to Al^{3+} diminished strongly and aromatics appeared. It was shown that after this process had occurred the catalyst displayed a weak C-C activity at temperatures where no hydrocarbons were formed prior to the transition.

Acknowledgement.

The author is grateful to professors R. Howe and R. Cooney for fruitful discussions and for having made necessary laboratory facilities available during his sabbatical stay at the University of Auckland. The Royal Norwegian Council for Science and Technology is thanked for financial support.

References.

1. C. D. Chang and A. J. Silvestri, J. Catalysis 47 (1977) 249.
2. C. D. Chang, Catal. Rev. - Sci. Eng. 25 (1983) 1.
3. C. D. Chang, Stud. Surf. Sci. Cat. 36 (1988) 127.
4. G. J. Hutchings and R. Hunter, Catalysis Today 6 (1990) 279.
5. T. Inui, T. Hagiwara, and J. Tarumoto, Sekiyu Gakkaishi 28 (1985) 341.
6. Y. Ono and T. Mori, J. Chem. Soc., Faraday Trans. 1, 77, (1981) 2209.
7. R. Maggiore, S. Galvagno, C. Crisafulli and A. Giannetto, Annali di Chimica 76 (1986) 483.
8. S. Kolboe, Acta Chem. Scand. A40 (1986) 711.
9. S. Kolboe, Stud. Surf. Sci. Cat. 36 (1988) 189.
10. H. Schulz, Zhao Siwei and W. Böhringer, Zeolites for the Nineties. 9 IZC, (1989) 411.
11. G. Mirth and J. Lercher, Stud. Surf. Sci. Cat. 61 (1991) 437.
12. G. Mirth, J. Lercher, M. W. Anderson and J. Klinowski, J. Chem. Soc. Faraday Trans. 86 (1990) 3039.
13. L. Kubelková, J. Novaková and K. Nedomová, J. Catalysis 124 (1990) 441.
14. T. R. Forester and R. F. Howe, J. Am. Chem. Soc. 109 (1987) 5076.
15. R. G. Argauer and G. R. Landolt, US Patent 3,702,886 (1972).
16. S. Kolboe, Acta Chem. Scand. A42 (1988) 185.
17. R. F. Howe, Stud. Surf. Sci. Cat. 36 (1988) 157.
18. M. Sayed and R. P. Cooney, Aust. J. Chem. 35 (1982) 2483.
19. S. Kolboe, Stud. Surf. Sci. Cat. 61 (1991) 413.
20. G. L. Woolery, L. B. Alemany, R. M. Dessau and A. W. Chester, Zeolites 6 (1986) 14.
21. R. F. Howe and M. J. Taylor, Spectrochim. Acta 43A (1987) 73.
22. S. Kolboe, Unpublished.

DISCUSSION

Q: L. Kubelkova (Czechoslovakia)

It is known from the literature that surface methoxy groups are involved in the C-C bond formation via interaction with gaseous methanol and react with primary hydrocarbon products.

According to the IR spectra shown in the contribution methoxy groups are present in the sample even after the drastic increase in the catalytic activity. Could you specify in more details your opinion on the role of methoxy groups in the reaction ?

A: S. Kolboe

The methoxy groups which are present after the catalytic activation has taken place, are, according to their wavenumbers and the literature, likely to be formed from surface silanol groups and thus be fairly inert because they are then bound by strong covalent bonds and have no cationic character. It is quite clear that other methoxy groups (or methyl carbocations) are very reactive, and are likely to methylate carbon double bonds. I can, however, not agree that there is concensus that they are the main source of primary C-C bonds. The methyl carbocation mechanism was originally put forth to account for results obtained in a circulating reactor system (Ono and Mori). It seems difficult to explain that a similar induction period is observed also in a flow reactor. Some of the alkenes which are, or might be formed in the reaction, have a much higher proton affinity than methanol and dimethyl ether making it hard to accept that methyl carbocations would form under ordinary reaction conditions. Other arguments that this mechanism is unlikely may also be found in the literature. My belief is rather that the methoxy groups represent the remains after the methanol or dimethyl ether desorption, and they are not likely to be important for the C-C forming reaction under "normal" operating conditions [1,2].

[1] S. Kolboe, *Acta Chem. Scand.*, **A42**, 185 (1988)
[2] S. Kolboe, *Acta Chem. Scand.*, **A40**, 711 (1986)

Q: W. O. Haag (USA)

Your interesting data give further support to the proposed mechanism for the MTG reaction. It is now clear that there is an induction period (Chen et al., Ono et al. etc.) during which a small amount of olefin is formed. This is a very slow process at low temperatures (<300 ^{0}C). The main methanol conversion occurs by alkylation of this olefin by methanol; this reaction occurs 100-1000 times faster than the induction step. You have nicely shown that the onset of this main reaction is exothermic and rapid confirming the autocatalytic nature of the reaction. The "transformation of the catalyst" found by you, from the "inactive" to the "active" state may then be seen as the slow build-up of a critical olefin concentration.

A: S. Kolboe

I am afraid the sum of my results does not constitute a confirmation that the main methanol conversion occurs by alkylation of olefins in the reaction mixture. Some of the results are already published [1-4].

1) An activated catalyst is active for C-C bond formation also in the absence of gas phase olefins. This has been confirmed by leaving the activated system with a pure carrier gas for 5-50 hours at 250 to 300 ^{0}C i.e. until there was no trace of olefins (or other components) in the exit carrier gas and then carry out activity tests at temperatures below 250 ^{0}C.

2) Ethylene can not be formed by a reaction relying on olefin alkylation and subsequent cracking at 250 ^{0}C or below. The cracking rate to ethylene is insignificant at these temperatures.

3) Ethylene is known to be very unreactive, and thus not a likely source for propene formation although propene could be formed by cracking.

4) The reaction rate (mol s^{-1}) for methanol conversion to olefins is essentially independent of conversion (i.e. olefin concentration) when the reactor is operated as a

quasidifferential reactor, once the C-C active stage has been reached. The conversion being varied by varying the flow rate through the reactor.

5) Isotope work over another zeolite type material has shown very clearly that both ethylene and propene are rather unreactive towards methanol and are converted much slower than methanol itself (unpublished).

[3] S. Kolboe, *Stud. Surf. Sci. Catal.*, **36**, 195 (1988)
[4] S. Kolboe, *Stud. Surf. Sci. Catal.*, **61**, 413 (1991)

Q: J. J. Rooney (Ireland)

A few years ago we showed [5] by spin trapping experiments that free radicals are formed when dimethyl ether is transformed into hydrocarbons on a HZSM-5 zeolite. Therefore one may suppose that free radicals are responsible for the first C-C bond formation just as they are for the following oxidative dimerization of dimethyl ether on SnO_2 catalysts [6] at 200-300 ^{0}C.

$$2CH_3OCH_3 \rightarrow CH_3OCH_2CH_2OCH_3 + H_2O$$

One may therefore speculate that a free radical chain reaction is initiated via alkylation and alkoxylation of the HZSM-5 sites followed by homolytic fission.

E.g.

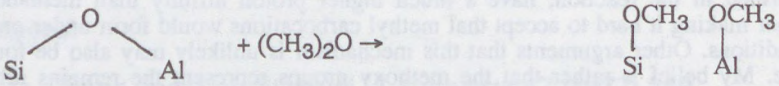

Methoxy, methyl, methylene and H free radicals may be produced which via condensation reactions lead to further flux of free radicals as aromatics are formed.

[5] J. K. A. Clark, R. Darcy, B. F. Hegarty, E. O'Donaghue, V. Amir Ebrahimi and J. J. Rooney, *J. Chem. Soc. Chem. Commun.*, 425, **1986**
[6] H. Yagita, K. Asami, A. Munamatsu, K. Fujimoto, *Appl. Catal.*, **53**, 15 (1989)

A: S. Kolboe

Inspired by your results I have tried to obtain further evidence for the involvement of radicals [4]. The reaction chamber was placed inside the EPR cavity and heated to suitable temperatures. A carrier gas with variable partial pressure of reactant passed through the reaction cell. No particular connection between a carbon radical signal and catalytic activity was, however, observed. On the other hand, it was found that a hydrocarbon adsorbate would always, independent of temperature, yield a radical signal. Unfortunately, the signal appeared too weak to be taken as a strong indication of radical participation in the C-C bond formation. The conclusion was therefore that free radicals are present in the reaction system, but may be not in a sufficient number to account for the reaction.

However, as mentioned in the present contribution the extreme rapidity with which the transformation from adsorbed C_1 oxygenates to hydrocarbons may take place makes the participation of free radicals in that part of the reaction an appealing idea.

Q: A. A. Tsyganenko (Russia)

You have shown very nice IR spectra, where the OH bands diminish, and a new band appears at 1510 cm^{-1} simultaneously with the arising activity. Does it mean that the latter band can be assigned to the carbocations you have shown in the scheme of the reaction?

A: S. Kolboe

I believe they are caused by the carbocations which are formed, and which I believe are a prerequisite for C-C forming activity, but I have not yet had the time for carrying out the necessary experiments for having a well founded opinion on the question. Such experiments are to be carried out as fast as I can find time for it.

Q: W. K. Hall (USA)
I would suggest that the interesting initial heat release is the heat of adsorption of methoxide groups on the surface. Gorte`s data, as I remember it, shows that this is very fast at these temperatures.

A: S. Kolboe
There are several reasons why this is not likely to be a correct explanation. The same immediacy of the initial heat release when methanol is admitted is observed also at much lower temperatures, down to room temperature where it is known that the alcohol does not dissociate, at least not immediately. No water formation is observed. For a given low partial pressure of methanol or dimethyl ether the adsorbed quantity increases with decreasing temperatures as would be expected for a moderately strongly bound species. Gorte has shown that at low temperatures (room) the methanol may be quantitatively pumped off.

Q: A. Bielanski (Poland)
How do you interpret the sudden exothermic effect at the moment of catalyst activation ? It may be supposed that it is a transformation of the solid and not necessarily a surface reaction.

A: S. Kolboe
I have given this question serious thought and concluded that the exothermic effect can not be explained as the result of a phase transformation. It is known that ZSM-5 can switch between the ordinary rhomohedral crystal form and a very slightly distorted monoclinic form. The same exothermic effect has, however, also been observed in experiments with H-Y zeolite (unpublished) where no phase transition is known to take place. It is furthermore quite clear from analysis of the exit carrier gas that essentially all of the hydrocarbon formation takes place within seconds after the onset of the exothermic phenomenon. The IR spectra presented here are also in full agreement with this result. This hydrocarbon formation from methanol (dimethyl ether) is known to be highly exothermic so this transformation is necessarily producing an exothermic signal.

Q: H. Schulz (Germany)
I want to participate in the present discussion of the involvement of radicals in the formation of primary H_2 and also CH_4, which we have observed, and which I understand to proceed via ionic pathways (we have published this in a paper to the 9th International Zeolite Conference in Montreal, July 1992). This reaction relates particularly to the initial stage of conversion of the kinetic regime of incubation, where the selectivity of conversion is mainly the formation of a hydrocarbon deposit on - respectively in - the catalyst and methane as the hydrogen rich coproduct. The crucial step of the CH_4-formation is suggested to be the hydride abstraction from propene to form the rather stable allyl cation and CH_4 as the H-rich coproduct.

$$CH_2{=}CH\text{-}CH_3 + CH_3^+ \rightarrow (CH_2{=}CH\text{-}CH_2)^+ + CH_4$$

So I wonder, if you have as well observed methane as the first volatile hydrocarbon in your experiments (which are generally in high agreement with our above mentioned investigations) ?

A: S. Kolboe
I have also observed methane formation prior to any other gas phase hydrocarbon formation and have the impression that it always is the first gas phase hydrocarbon to be formed. In many cases, however, the quantity formed is minute.

Guczi, L. *et al.* (Editors), *New Frontiers in Catalysis*
Proceedings of the 10th International Congress on Catalysis, 19-24 July, 1992, Budapest, Hungary
© 1993 Elsevier Science Publishers B.V. All rights reserved

H-D EXCHANGE BETWEEN ZEOLITES AND ALKANES. EVIDENCE FOR FORMATION AND REARRANGEMENT OF PENTACOORDINATED CARBONIUM IONS

C. J. A. Mota[a,b], *L. Nogueira*[a], *S. C. Menezes*[a], *V. Alekstich*[a], *R. C. L. Pereira*[a] *and W. B. Kover*[b]

[a]PETROBRAS - CENPES, Ilha do Fundao, Q. 7, Rio de Janeiro 21949, Brazil
[b]Instituto de Quimica, Universidade Federal do Rio de Janeiro, C. Postal 1573, Ilha do Fundao, Rio de Janeiro 21941, Brazil

Abstract

H-D exchange between zeolites and alkanes at 100°C were studied. Only tertiary alkanes were found to undergo the exchange. Reaction with 3-methylpentane afforded mainly monodeuteration. However, the deuterium was incorporated in 1º, 2º and 3º positions. In more constrained zeolites such as BETA and ZSM-5, there is a strong preference for deuterium incorporation in the 1º position. Nevertheless, for Y zeolite, the structural SAR and NFA have almost no influence on the distribution of deuterium incorporation. These results suggest the attack of the zeolite acid site on the 3º C-H bond forming a pentacoordinated carbonium ion which may rearrange with migration of deuterium to the more accessible 1º and 2º positions, where steric effects on the interactions with the zeolite can be minimized. Exchange with methylcyclohexane suggests that there is a need for eclipsed conformation between the migrating groups.

1. INTRODUCTION

The introduction of zeolites as active ingredients of FCC catalysts has lead to considerable improvements either in activity and selectivity (1). Although hydrocarbon transformation over zeolites involves a great variety of reactions (cracking, hydrogen transfer, cyclization, etc.), it is a common opinion that carbenium ions are intermediates in all these reactions. However, a controversy still exist as to the initial step of carbenium ion formation from alkanes. Three mechanisms have been usualy proposed for carbenium ion formation on zeolites:

- initial thermal cracking producing small amounts of olefins which can be protonated by the zeolite acid site.
- Hydride abstraction by a Lewis acid site.
- Protonation of alkane σ bonds to form a pentacoordinated carbonium ion which looses H_2 or an alkane molecule to afford the carbenium ion.

The term carbocation can be used for any cationic specie of carbon (2). The most usual ones are the carbenium ions which possess an eletronic sextet and an empty p orbital and the carbonium ions which have an electronic octet and two electron three center bond (2).

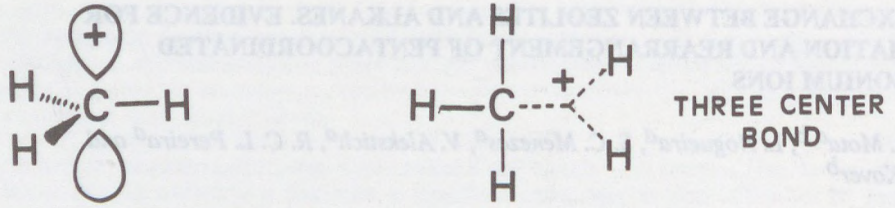

CARBENIUM ION CARBONIUM ION

FIG. 1 - CARBOCATION STRUCTURES

Haag and Dessau proposed the involvement of pentacoordinated carbonium ion to explain changes in constraint index at high temperatures (3). Later on, Corma, Guisnet, Gianetto, Wojciechowski, and Abbot (4-7), all proposed the involvement of pentacoordinated carbonium ion on alkane cracking over zeolites. Recently, Lombardo and Hall (8,9) studying neopentane and isobutane cracking over Y zeolites observed that at low conversions, each mole of neopentane cracked afforded a mole of methane and for isobutane, besides methane formation, large amounts of hydrogen were found in the initial stages of the reaction. These results can be explained by invoking the formation and subsequent cleavage of pentacoordinated carbonium ions formed upon attack at C-C and C-H bonds. Nevertheless, all the previous studies were carried out at high temperatures (ca. 400-500°C) and were based on kinetics and product distribution. At such temperatures, some authors prefer to explain hydrogen and methane formation from cracking of radical species (10,11).

On the other hand, the involvement of pentacoordinated carbonium ion in alkane transformation on superacids at low temperatures is widely recognized (12-14). The H-D exchange between superacids and alkanes can occur under mild conditions and as an event prior to formation of carbenium ions. This reaction has been used to support the involvement of pentacoordinated carbonium ion as intermediates in alkane reactions in superacids (15,16).

Studies on the H-D exchange between solid acids, such as alumina, silica-alumina, zeolites and alkanes or deuterium molecule have been reported in literature (17 - 21). Nevertheless, under the experimental conditions reported it was not possible to exclude the involvement of radical species or carbenium ions. On the other hand, solid superacids like SbF_5 supported on Al_2O_3, can crack and isomerize small alkane molecules near room temperature, but do not undergo H-D exchange (22-23). This has been used to support the carbenium ion formation on these materials by hydride abstraction by a Lewis acid site and to exclude protonation of σ bonds by Bronsted acid sites. Recently, we reported an infrared study on

the H-D exchange between zeolite Y and 3-methylpentane at 100°C (24). Under these conditions, neither cracking products nor olefins were found. This study has provided strong evidence for the involvement of pentacoordinated carbonium ion in the initial step of carbenium ion formation over zeolites. We wish to report now, results of deuterium incorporation in the hydrocarbon which confirms the involvement of pentacoordinated carbonium ions on alkane reactions over zeolites.

2. EXPERIMENTAL PART

2.1. Techniques

The exchange was carried out in a glass unit. The weight of catalyst, in their protonic form (25) (residual Na below 0.5 wt%), was about 550mg for Y zeolites and about 1.5g for BETA and ZSM-5 The catalyst was pre-treated in a flow of 38 ml/min of dry N_2 to 500°C for 30 min. Then, the temperature was set at 200°C and the N_2 flow was driven into a saturator with D_2O kept at room temperature. After 60 minutes the flow of D_2O was stopped and the zeolite was purged with N_2 for 15 minutes. The temperature and N_2 flow were decreased to 100°C and 20 ml/min respectively and the flow directed to a saturator containing the hydrocarbon (3-methylpentane, n-hexane, methylcyclohexane) kept in ice bath, except for methylcyclohexane which was kept at room temperature. The hydrocarbon flow was maintained for 45 minutes with an additional 15 minutes of purge. A trap immersed in acetone-dry ice bath was kept at the reactor outlet to condense the reacted hydrocarbons. These were then subjected to ^2H NMR and capillary gas chromatography with mass analysis (GC/MS).

2.2. Equipments and methods

^2H NMR analysis were done in a VARIAN VXR 300 at 46 MHz with 4 seconds of pulse interval in the unlock mode and with proton decoupling. $CDCl_3$ was taken as internal standard. GC/MS analysis were done in a quadrupole HP 5988 A with electron impact ionization. Corrections were made for natural abundance ^{13}C in standard hydrocarbon samples. A 50 m capillary column of methylsilicone was used.

The chemical shift of ^2H is basically the same for ^1H (26). Due to proton decoupling, the ^2H signals appeared as singlets. ^1H NMR of the standard hydrocarbons were taken in order to make peak assignments.

3. RESULTS AND DISCUSSION

3.1. Experiments with 3-methylpentane and n-hexane

Results of ^2H NMR of recovered 3-methylpentane (3MP) after exchange with several zeolites is shown in table 1.

Table 1
^{2}H NMR of recovered 3-methylpentane

Zeolite	Relative intensities Chemical shift (ppm) 0.9 (1º C-D)	1.2 (2º C-D)	1.4 (3º C-D)
USY (4.5)[a]	1.6	1	1
USY (6)[a]	2.0	1.1	1
DSY (4.5)[b]	1.7	1	1
DSY (7.5)[b]	2.2	1.2	1
USY (4.5)[c]	1.6	1	1
BETA(25)[d]	5.4	1.7	1
ZSM-5(20)[e]	2	---------1[f]--------	

a) Supplied by Akzo Chemie and exchanged with 1M NH_4Cl; () framework Si/Al by IR (27).
b) $(NH_4)_2SiF_6$ (28), and exchanged with 1M NH_4Cl; () framework Si/Al by IR.
c) H-D exchange carried out at 70°C.
d) (29), calcined at 600°C for 6h and exchanged with 1M NH_4Cl; () Si/Al.
e) (30), calcined at 600°C for 6h and exchanged with 1M NH_4Cl; () Si/Al.
f) Sum of 2º and 3º C-D.

For USY, GC/MS analysis revealed about 6% of monodeuteration, with the remained 3MP being undeuterated. A small amount (up to 3 wt%) of 2-methylpentane (2MP) was also found. This 2MP presented a higher index of monodeuteration (ca. 67%) than 3MP. In BETA and ZSM-5 zeolites, isomerization to 2MP was insignificant and the quantification of deuterium incorporation was very difficult, due to the low deuterium content in the zeolite. USY zeolites gave higher isomerization than DSY. No trace of olefins was found neither in the start material nor in the recovered 3MP, suggesting no involvement of carbenium ions.

These results of H-D exchange were very surprising, since in similar experiments in liquid superacids, isobutane showed exchange only at the tertiary hydrogen in contrast to sulfuric acid solutions where the tertiary hydrogen remains unexchanged (15).

Reaction of deuterated USY and ZSM-5 with n-hexane under the same experimental conditions showed neither detectable deuterium incorporation in the hydrocarbon, nor skeletal isomerization to deuterated isomers. This excluded the attack of the zeolite acid site in the 1º and 2º C-H bonds under the experimental conditions used. Thus, the most reasonable explanation for ^{2}H NMR and GC/MS findings of recovered 3MP would be the rearrangement of pentacoordinated carbonium ions over the zeolite surface.

Table 1 also shows that deuterium is preferentially incorporated in primary position, specially in more constrained zeolites. This suggests some steric effects for the exchange reaction in the 3º C-H. Scheme 1 shows a picture of how the exchange with tertiary hydrocarbons takes place. Firstly there is the attack in the 3º C-H bond forming the pentacoordinated 3º carbonium ion. This intermediate is unsymmetric with respect to the acid site, preventing any interaction for exchange of the H atom. Thus, it can undergo an acomodation step, in order to place the 3º hydrogen and the deuterium symmetric to the acid site, possibiliting the exchange to take place. Nevertheless, this may lead to some steric restrictions related to

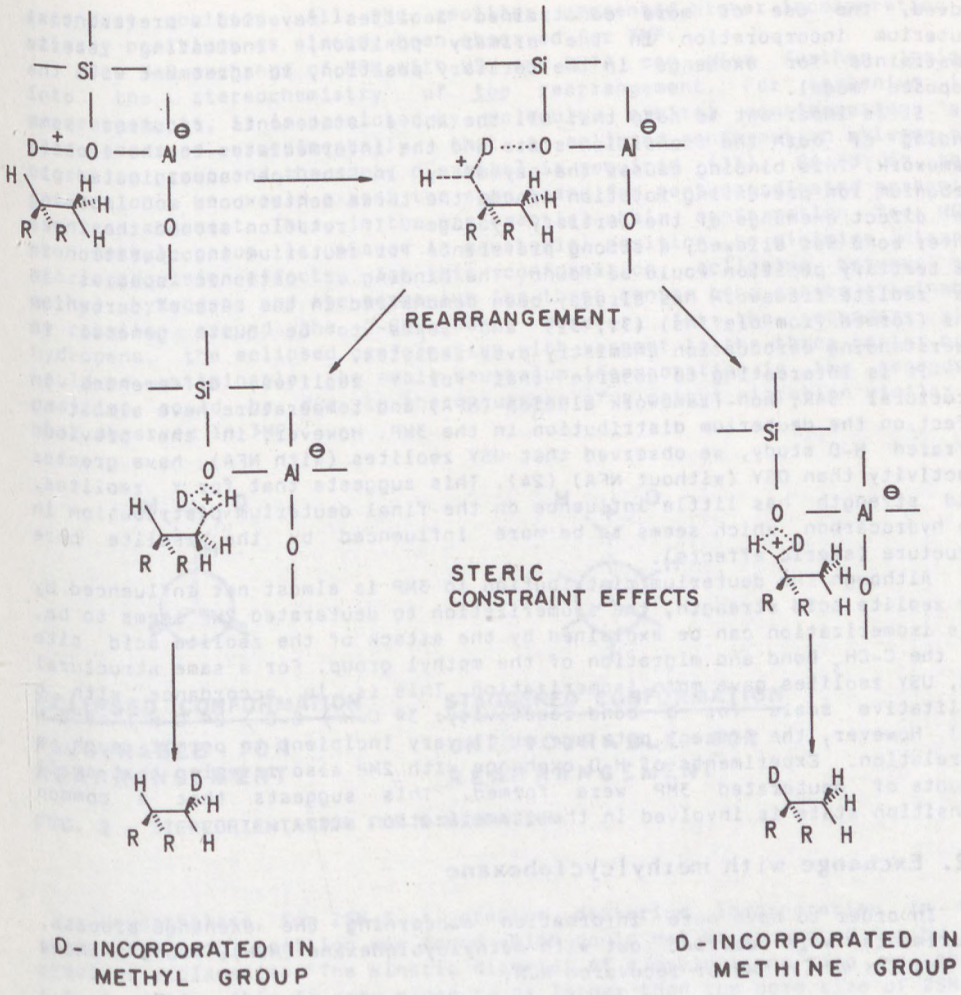

SCHEME 1 - H-D EXCHANGE BETWEEN 3º ALKANES AND ZEOLITES

interactions of hydrocarbon substituent groups with the zeolite framework. On the other hand, the unsymmetric pentacoordinated carbonium ion may undergo a rearrangement to place deuterium in primary or secondary positions and form symmetric intermediates with respect to the acid site. Therefore, the exchange with the acid site is more favourable in primary and secondary positions as large steric interferences are not taking place.

Indeed, the use of more constrained zeolites revealed a preferential deuterium incorporation in the primary position, indicating steric constraints for exchange in the tertiary position, in agreement with the proposed model.

It is important to note that all the above statements requires some binding of both the transition state and the intermediates to the zeolite framework. This binding causes the asymmetry in the pentacoordinated 3º carbonium ion preventing rotation around the three center bond and imparing the direct exchange of the tertiary hydrogen. If rotation around the three center bond was allowed, a strong preference for deuterium incorporation in the tertiary position would be found. The binding of cationic species to the zeolite framework has already been demonstred in the case of carbenium ions (formed from olefins) (31, 32) and seems to be quite general in understanding carbocation chemistry over zeolites.

It is interesting to observe that for Y zeolites, differences in structural SAR, non-framework alumina (NFA) and temperature have almost no effect on the deuterium distribution in the 3MP. However, in the previous infrared H-D study, we observed that USY zeolites (with NFA), have greater reactivity than DSY (without NFA) (24). This suggests that for Y zeolites, acid strength has little influence on the final deuterium distribution in the hydrocarbon, which seems to be more influenced by the zeolite pore structure (steric effects).

Although the deuterium distribution in 3MP is almost not influenced by the zeolite acid strength, the isomerization to deuterated 2MP seems to be. This isomerization can be explained by the attack of the zeolite acid site in the C-CH_3 bond and migration of the methyl group. For a same structural SAR, USY zeolites gave more isomerization. This is in accordance with a qualitative scale for σ bond reactivity: 3º C-H $\rangle$ C-C $\rangle$ 2º C-H $\rangle$ 1º C-H (15). However, the present data are still very incipient to permit such a correlation. Experiments of H-D exchange with 2MP also revealed that small amounts of deuterated 3MP were formed. This suggests that a common transition state is involved in the isomerization step.

3.2. Exchange with methylcyclohexane

In order to have more information concerning the exchange process, experiments were carried out with methylcyclohexane (MCH). Table 2 shows the results of ^2H NMR of recovered MCH.

Table 2
^2H NMR of recovered methylcyclohexane

	Relative intensities Chemical shift (ppm)		
Zeolite	0.7 (1º C-D)	1.1 (2º C-D)	1.5 (3º C-D)
USY (4.5)	2.4	0.1	1
BETA	2	0.2	1
ZSM-5	1.9	0.8	1

These data show that for USY and BETA, incoporation in the secondary position is very small, compared to incorporation in tertiary and primary positions. However, for ZSM-5 there was a significant incorporation in the

secondary position. All the zeolites presented higher incorporation in primary position, as already been observed for 3MP.

The H-D exchange of MCH with USY and BETA can give further insight into the stereochemistry of the rearrangement. For carbenium ion rearrangements, it is precicted by molecular orbital consideration, and also observed experimentally, that an eclipsed conformation between the migrating group and the empty p orbital is required (33). Based on this assumption, we would expect the same trend for pentacoordinated carbonium ion rearrangement. Thus, in the preferential chair conformation for MCH, the methyl group is placed in equatorial position, to minimize internal steric repulsion effects. In this conformation, eclipsing between the methyl hydrogens and the carbonium ion three center bond can be attainable by rotation around the $C-CH_3$ bond. However, for the secondary ring hydrogens, the eclipsed conformation with respect to the three center bond would be unattainable. The small deuterium incorporation in the secondary position could be due to the occurence of a methyl migration similar to that observed in 3MP.

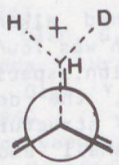

ECLIPSED CONFORMATION

FAVOURABLE FOR REARRANGEMENT

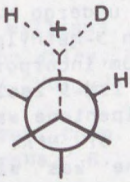

STAGGERED CONFORMATION

UNFAVOURABLE FOR REARRANGEMENT

FIG. 2 - STEREORIENTATION FOR D MIGRATION

Nevertheless, for ZSM-5 a greater deuterium incorporation in the secondary ring position was found which could not be accounted for by the previous explanation. The kinetic diameter of a cyclohexane ring is about 6.0 A (34). This is very close to or larger than the pore size of ZSM-5. Therefore, H-D exchange may be strongly influenced by molecular diffusion of MCH into the pores of ZSM-5. From results of table 2 and assuming that rearrangement of pentacoordinated carbonium ion occurs in eclipsed conformation between the migrating centers, the data for ZSM-5 suggests that MCH diffuses or creep in more flexible twist-boat conformations, which reduces the interactions between the hydrocarbon and the zeolite walls. In twist-boat conformations, due to higher degree of mobility of the ring, eclipsed conformation between secondary ring hydrogens and the carbonium ion center can be easier to achieve than in the chair conformation, allowing a better orbital overlaping for rearrangement. This can explain the higher secondary deuterium incorporation. Thus, the H-D exchange between zeolites and alkanes can be a potential tool in studying molecular conformation of hydrocarbons diffusing in zeolites. A good understanding of the stereochemistry of both the hydrocarbon and the transition state for exchange and pentacoordinated carbonium ion rearrangement is required in order to antecipate the final deuterium distribution in the hydrocarbon.

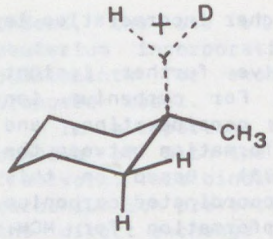

CHAIR CONFORMATION

D-MIGRATION TO
2º RING UNFAVOURABLE

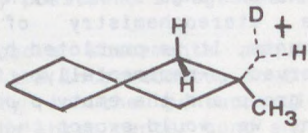

TWIST-BOAT CONFORMATION

D-MIGRATION TO
2º RING FAVOURABLE

FIG. 3 - CYCLOHEXANE RING CONFORMATIONS FOR D MIGRATION

4. CONCLUSIONS

Zeolites can readily undergo H-D exchange with branched alkanes but not with linear ones. With 3-methylpentane, monodeuteration was found, with a preference for deuterium incorporation in primary position, specially in more constrained BETA and ZSM-5 zeolites. For Y zeolites, the deuterium distribution in 3-methylpentane was almost independent of structural SAR, temperature and presence of NFA. In Y zeolites, a small amount of deuterated 2-methylpentane was also formed. These results support the attack of the zeolite Bronsted acid site on the 3º C-H bond forming a pentacoordinated carbonium ion which can undergo a rearrangement with migration of deuterium to primary or secondary positions. This rearrangement can be facilitated, specially in more constrained zeolite, by steric effects imposed on the 3º carbonium ion by the zeolite framework. The model for carbonium ion rearrangement also implies that they remain partially bound to the zeolite framework.

H-D with methylcyclohexane showed that there is a need for eclipising electron pairs between the receiving bond and the three center bond. Therefore, only a small deuterium incorporation in the secondary ring position was found for Y and BETA zeolites. Nevertheless, for ZSM-5 which pore dimensions are of the same order of molecular dimensions, an increased deuterium incorporation in the secondary ring position was found. This result supports that in ZSM-5 MCH diffuses or creeps in more flexible twist-boat conformation which minimizes the interactions with the zeolite walls and eclipsed conformation between the secondary ring hydrogens and the carbonium ion can be achieved.

This study has revealed that zeolites are able to protonate alkane σ bonds to form pentacoordinated carbonium ions. Hence, this mechanism is very reasonable for explaining initial carbenium ion formation in alkane cracking. The binding of the carbonium ion intermediates to the zeolite causes asymmetry in the three center bond with the zeolite, facilitating the rearrangement of the carbonium ion. The H-D exchange can be a potential tool for studying molecular diffusion in zeolites.

ACNOWLEDGEMENTS: The authors thank Chang L. F. and F. Guimarães, for their assistance in carrying out experimental part. We also thank PETROBRÁS for permission to publish this work. W8K thanks the CNPq (Brazil) for support.

5. REFERENCES

1. P. B. Venuto and E. T. Habib Jr (eds.), Fluid Catalytic Cracking with Zeolite Catalysts, Marcel Dekker, New York, 1979.
2. G. A. Olah, J. Am. Chem. Soc., 94 (1972) 808.
3. W. O. Haag and R. M. Dessau, Proc. of the 8th International Congress on Catalysis, Dechema, Berlim, 1984, vol 2 p 305.
4. A. Corma, J. Planelles. J. S. Marin, F. Tomas, J. Catal., 93 (1985) 30.
5. G. Gianetto, S. Sanrase, M. Guisnet, J. Chem. Soc., Chem. Commun., (1986) 1302.
6. J. Abbot and B. W. Wojciechowski, J. Catal., 115 (1989) 1.
7. J. Abbot, Appl. Catal., 47 (1989) 33.
8. E. A. Lombardo, R. Pierantozzi, W. K. Hall, J. Catal., 110 (1988) 171.
9. E. A. Lombardo and W. K. Hall, J. Catal., 112 (1988) 656.
10. G. B. McVicker, G. M. Kramer, J. J. Ziemiak, J. Catal., 83 (1983) 286.
11. G. M. Kramer, G. B. McVicker, J. Catal., 115 (1989) 608.
12. G. A. Olah, R. H. Schlosberg, J. Am. Chem. Soc., 90 (1968) 2726.
13. G. A. Olah, G. Klopman, R. H. Schlosberg, J. Am. Chem. Soc., 91 (1969) 3261.
14. G. A. Olah, G. K. S. Prakash, R. E. Williams, L. D. Field, K. Wade (eds.), Hypercarbon Chemistry, John Wiley, New York, 1987.
15. G. A. Olah, Y. Halpern, J. Shen, Y. K. Mo, J. Am. Chem.Soc., 95 (1973) 4960.
16. H. Hogeveen and A. F. Bickel, Rec. Trav. Chim. Pay-Bas., 88 (1969) 371.
17. R. C. Hansford, P. C. Waldo, L. C. Drake, R. E. Honig, Ind. & Eng. Chem., 44 (1952) 1108.
18. W. K. Hall, H. P. Leftin, F. J. Cheselske, D. E. O'Reilly, J. Catal., 2 (1963) 506.
19. Y. Imanaka, Y. Okamoto, K. Takahata, S. Teranishi, Bull. Chem. Soc. Jpn., 45 (1972) 366.
20. G. C. Lau, W. F. Maier, Langmuir, 3 (1987) 164.
21. J. M. Thomas and C. Williams, Chemical Reactions in Organic and Inorganic Constrained Systems, R. Setton (ed.), D. Reidel, Amsterdam, 1986, p. 65.
22. H. Hattori, O. Takahashi, M. Takagi, K. Tanabe, J. Catal., 68 (1981), 132.
23. O. Takahashi, H. Hattori, J. Catal., 68 (1981), 144.
24. C. J. A. Mota and R. L. Martins, J. Chem. Soc., Chem. Commun., (1991) 171.
25. Calcination: 150°C (30 min), 350°C (30 min), 550°C (120 min).
26. A. C. Faro Jr., C. Kemball, R. Brown, I. H. Sadier, J. Chem. Research (S), (1982) 342.
27. J. R. Sohn, S. J. de Canio, D. J. O'Donnell, J. H. Lunsford, Zeolites, 6 (1986) 225.
28. G. Garralón, V. Fornés, A. Corma, Zeolites, 8 (1988) 268.
29. Y. L. Lam, Br Pat. 8506248 (1985)
30. R. L. Waddinger, G. T. Kerr, E. J. Rosinski, US Pat. 3308069 (1967).
31. J. F. Haw, B. R. Richardson, I. S. Oshiro, N. D. Lazo, J. A. Speed, J. Am. Chem. Soc., 111 (1989) 2052.
32. M. T. Aronson, R. J. Gorte, W. E. Farneth, D. White, J. Am. Chem. Soc., 111 (1989) 840.
33. T. H. Lowry, K. S. Richardson (eds.), Mechanism and Theory in Organic Chemistry, Harper & Row, New York, 1981, p. 376.
34. S. M. Csicsery, Zeolites, 4 (1984) 4202.

DISCUSSION

Q: W. O. Haag (USA)

Your data on the zeolite catalyzed D-exchange with paraffins at relatively low temperature are quite interesting. I would like to suggest, however, to reconsider the mechanism proposed. While D-exchange with zeolites at 400 ^{0}C and above occurs via pentacoordinated intermediates, this is a quickly activated process, which is extremely slow at low temperatures. At this temperature, only superacids can protonate paraffins (Olah); with isobutane, only the tertiary hydrogen is exchanged. Your finding of exchange of secondary and even primary hydrogens, and of skeletal rearranged products, rules out this mechanism, but is in complete agreement with a carbenium ion hydrogen transfer chain process, which involves protonation of olefins that are present as intermediates in equilibrium with the corresponding carbenium ions. Burwell (and others) have studied these exchange reactions with sulfuric acids and silica-alumina with similar findings as yours. The mechanism found to operate in these experiments applies equally well to your data.

A: C. J. A. Mota

Initially we would like to point out that the reason for studying the exchange at low to moderate temperature was to rule out any possibility of involvement of radical species, which presence is always an alternative explanation for hydrogen and methane formation, when working at high temperatures. We believe that our experiments reinforce the mechanism initially proposed by you [1] with pentacoordinated carbonium ions as intermediates or transition states in the cracking process. While in your work the conditions favoured the fragmentation of the carbonium ion to carbenium ion and then to cracked products, under the conditions we used, a high degree of charge transfer to the hydrocarbon is not expected but rather a perturbation in the electron density along the σ-bonds.

The high observed activation energy (above 30-40 kcal/mol) refers to the cracking process and more often to the transformation (β-scission) of the adsorbed carbenium ion, rather than its formation or for carbonium ion formation. Note, we are below cracking thresholds.

Regarding the involvement of carbenium ions in our results, we would like to stress the following facts which carbenium ion chemistry cannot account for.

1) No olefin was detected either in the starting alkanes and in the recovered alkanes after H-D exchange. If carbenium ions were involved, one should expect, at least small amounts of olefins in the recovered alkane. As you remarked, olefins are always in equilibrium with carbenium ions over the zeolite surface.

On ZSM-5 at temperatures ranging between 350-450 ^{0}C, n-hexane is more reactive than 3-methylpentane toward cracking [1]. This fact has been explained by steric effects in the formation of carbenium ions by hydride transfer. If carbenium ions were involved, it would be expected some D-exchange between n-hexane and ZSM-5. However, n-hexane did not exchange with USY and ZSM-5 under the experimental conditions used for 3-methylpentane, indicating no carbenium ions involvement.

2) The exchange at tertiary position, even though no longer specific, can only be reasonably explained by assuming the formation of pentacoordinated carbonium ions, as proposed by Olah.

3) The exchange with methylcylclohexane showed little deuterium incorporation in the secondary position relative to tertiary and especially to primary. If carbenium ions were involved, a much higher deuterium incorporation in the secondary position would be expected since endocyclic olefins are more stable than exocyclic olefins. We do not believe that kinetic control would take place, favouring the formation and exchange in the exocyclic olefin. In the chair conformation, the axial secondary ring hydrogen is in an eclipsed conformation with respect to the empty π-orbital of the carbenium ion. Thus, the elimination to form the endocyclic olefin should be kinetically and thermodynamically more favorable than elimination to form an exocyclic olefin. Indeed, it has been reported that

methylcyclohexene (endocyclic olefin) is a primary product of transformation of methylcyclohexane over USY zeolites. The formation of methylene cyclohexane (exocyclic olefin) was not reported [2].

4) Besides deuterium incorporation in the 3-methylpentane, a small amount of deuterated 2-methylpentane was found. From GC/MS fragmentogram we could assign this compound as essentially the 3-deuterio-2-methylpentane. If carbenium ions were involved, we would not expect the high degree of deuterium incorporation in the 2-methylpentane, as one of the most reasonable paths for its formation from carbenium ion intermediates would be by a 1,2-methyl shift followed by hydride transfer from a gaseous or adsorbed 3-methylpentane molecule. Alternative path for deuterated 2-methylpentane formation from carbenium ions can also be drawn, involving methyl migration and proton elimination-deuterium incorporation, but only one path would lead to the 3-deuterio-2-methylpentane. This cannot account for the specific formation of this isotopomer, since in carbenium ion chemistry, a broad range of isomeric olefin products is commonly observed.

The formation of 3-deuterio-2-methylpentane is better explained by assuming an attack in the C-CH_3 bond forming a pentacoordinated carbonium ion, and methyl migration to an adjacent position as in the following chart.

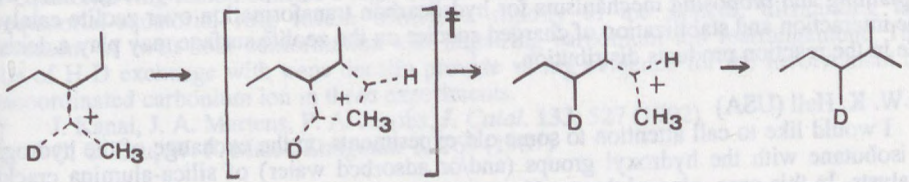

[1] W. O. Haag, R. M. Dessau; *Proc. 8th International Congress on Catalysis*, Dechema, **Vol. 2**, p. 305 (1984)

[2] A. Corma, F. Mocholi, V. Orchilles, G. S. Koermer, R. J. Madon; *"The Hydrocarbon Chemistry of FCC Naphtha Formation"*,(Eds. H. Lovink, L. A. Pine), Technip, Paris, p. 19 (1990)

Q: V. Kazansky (Russia)

1) When speaking about carbonium ions you mean the really existing intermediates or the activated transition states ?

2) Is it possible to distinguish between these possibilities from your experiments based on the kinetics ?

A: C. J. A. Mota

For the first question we would like to point out that the difference between a transition state and an intermediate is basically a question of lifetime. Transition states are usually very short live species formed during bond breaking and bond formation. Intermediates are usually referred as species that although with short lifetime can undergo some molecular movements such as bond rotation and stereochemical orientation. Thus, in order to have rearrangement, which would require bond rotation and reorientation, the species, by definition, would be classified as an intermediate. On the other hand, direct spectroscopic observation of carbonium ion has been reported in literature [3].

Regarding the second question, from a purely kinetic point of view, it is always very difficult to distinguish between intermediates and transition states based only on kinetics. In our experiments, we are not exactly dealing with kinetic measurements, but rather observing the thermodynamics of D incorporation. Nevertheless, some published results on H-D exchange between superacids and alkanes revealed a somewhat greater isotope effect ($k_H/k_D = 7$) when using deuterated acid or deuterated alkane, suggesting a non-concerted reaction, whose rate-limiting step involves breakage of both the alkane C-H and acid O-H

this reaction proceeded by a one step transition state, no different kinetic isotopic effect would be expected, when using deuterated acid or alkane.

[3] L. I. Yeh, .M. Price, Y. T. Lee, *J. Am. Chem. Soc.* **111**, 5597 (1989)
[4] J. E. McMurry, T. H. Lectka, *J. Am. Chem. Soc.* **112**, 869 (1990)

Q: D. Barthomeuf (France)

Molecules in cages of zeolites are submitted to fields and fields gradients which may weaken C-C or C-H bonds. It might not be necessary to have a superacid to form pentacoordinated carbonium ion. A strong acid might be enough to form this ion on a molecule perturbed by the field gradient.

A: C. J. A. Mota

We completely agree with you. Field gradients can help in the polarization step and also in the stabilization of charged species on the zeolite surface. Then, as you pointed out, a strong acid would attack C-C and C-H bonds to form the pentacoordinated carbonium ion.

Indeed, we believe that the zeolites have a special feature, of being the acid and the solvent for this acid. Then, it protonates molecules to form cations and solvates the cations in order to stabilize and to delocalize the charge. However, people usually forget this when explaining and proposing mechanisms for hydrocarbon transformation over zeolite catalysts. The interaction and stabilization of charged species on the zeolite surface may play a decisive role in the reaction products distribution.

Q: W. K. Hall (USA)

I would like to call attention to some old experiments on the exchange of the hydrogens of isobutane with the hydroxyl groups (and/or adsorbed water) of silica-alumina cracking catalysts. In this case, nine of the ten H atoms of isobutane exchange. The tenth and the one that does not is the tertiary hydrogen. This is in contrast with Olah's result with magic acid.

A: C. J. A. Mota

We have cited these experiments with silica-alumina in our paper. It seems that silica-alumina has a behavior closer to sulfuric acid than superacids. However, in experiments with silica-alumina we could not observe any detectable D-exchange under the same experimental conditions used for zeolites.

Q: J. J. Rooney (Ireland)

We have reported [5] that long-lived carbonium ion intermediates on silica-alumina catalysts react with H_2 even at temperatures below 100 ^{0}C. The reaction provides a mechanism for hydrogenation of olefins.

We discussed the mechanism in terms of a simple [2+2] reaction which on reversal, provides a path for paraffin activation by strong Brönsted acids.

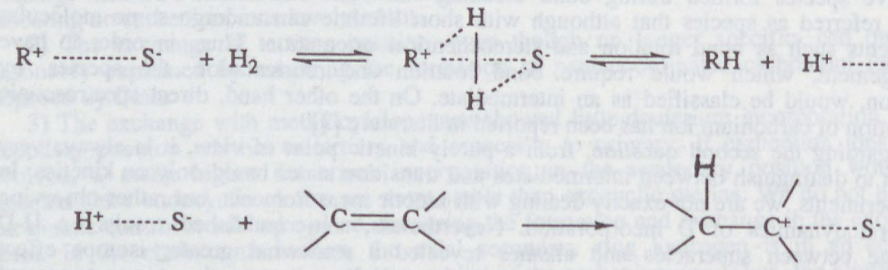

Donation from the HOMO of H_2 to the LUMO of the carbonium ion is postulated, but

simultaneously there is donation from the HOMO of the surface anion S^- to the LUMO of H_2.

Two examples of these ions are 1-adamantyl which cannot form an olefin and norbornyl made from norbornadiene.

[5] J. J. Rooney, *J. Chem. Soc., Chem. Commun.* 1301, **1983**

A: C. J. A. Mota

In fact the reverse of the reaction of carbenium ion with hydrogen can be viewed as the protonation of a C-H bond. Recently, another article concerning hydrogenation of olefins over metal free zeolites also proposed the involvement of pentacoordinated carbonium ion [6].

There is an H-D exchange study between zeolite Y and adamantane at 270 ^{0}C [7]. However, at this temperature it is possible that carbenium ions can be formed and that the zeolite can attack secondary C-H bonds.

On the other hand, some preliminary results of H-D exchange between zeolite USY and cis, trans decalin showed that the trans decalin exchanges only at the tertiary position whereas the cis decalin exchanges at both tertiary and secondary. While in the cis isomer the axial-equatorial ring fusion confers a high degree of flexibility to achieve twist-bost decalin, the equatorial-equatorial ring fusion confers a rigidity to the system, difficulting the achievement of twist-boat conformation and impairing carbonium ion rearrangement. The results of H-D exchange with trans decalin provide strong evidence for the involvement of pentacoordinated carbonium ion in these experiments.

[6] J. Kanai, J. A. Martens, P. A. Jacobs, *J. Catal.* **133**, 527 (1992)

[7] G. C. Lau, W. F. Maier, *Langmuir* **3**, 164 (1987)

Guczi, L. *et al.* (Editors), *New Frontiers in Catalysis*
Proceedings of the 10th International Congress on Catalysis, 19-24 July, 1992, Budapest, Hungary
© 1993 Elsevier Science Publishers B.V. All rights reserved

NEW SURFACE Nb-DIMERS CHEMICALLY INTERACTED WITH SiO_2: REGULATION OF THE CATALYSIS BY MOLECULAR DESIGN OF REACTION SITES

N. Ichikuni and Y. Iwasawa

Department of Chemistry, Faculty of Science, The University of Tokyo, Hongo, Bunkyo-ku, Tokyo 113, Japan

Abstract

New Nb dimers on a SiO2 surface prepared by using [Nb(η^5-C5H5)H-μ-(η^5,η^1-C5H4)]2 were found to have an oxygen-bridged dimeric structure(Nb-O(surface)=0.193 nm; Nb--Si =0.328 nm; Nb--Nb=0.303 nm) by EXAFS. The attached Nb dimers were active for ethanol dehydration in contrast to the dehydrogenation ability of the Nb monomer catalyst. The regulation of the catalysis from dehydrogenation to dehydration, or equivalently from basic property to acidic property, was achieved by the nucleation of one Nb atom to two Nb atoms in active structures. The inverse isotope effect for ethene formation through the late-transition state of reaction was observed. The rate constant for ethene formation reduced by the second ethanol adsorption on the adjacent Nb site. It was also found that the selectivity of ethanol reaction was affected by the separation of Nb-Nb on SiO2.

1. INTRODUCTION

Advances in surface synthesis by surface organometallic technique and characterization by EXAFS spectroscopy are leading to a rapid progress in design of solid catalyst surfaces[1-5]. Observation and control of behaviors of atoms or molecules in active sites are important for molecular-level developments of catalyst preparations as well as for understanding essential factors of the genesis of solid catalysis.

The SiO2-attached Nb monomer(A) has been found to be the first active Nb sample for the catalytic dehydrogenation of ethanol[6,7]. Ethanol adsorbs on Nb=O to form OH and C2H5O groups, but the species(B) was very stable in

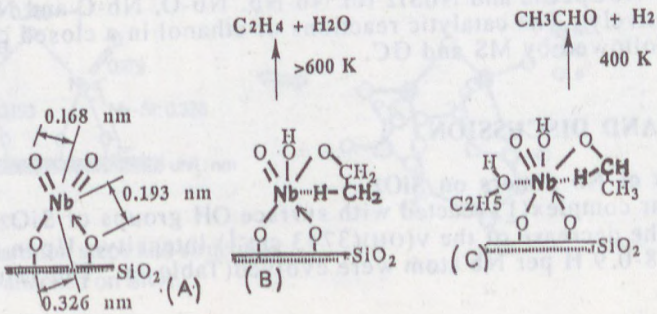

vacuum and decomposed to ethene and water only above 600 K. However, in the presence of the second ethanol the Nb-ethoxide(C) is decomposed even at 400 K, where the switchover of reaction path from dehydration to dehydrogenation is observed(self-assisted dehydrogenation mechanism)[7]. Similar observations about the adsorbate-intermediate interaction leading to catalytic cycles(reactant-promoted mechanism) have been reported for water gas shift reaction[8,9].

The aim of this study is (1)to regulate the catalysis by molecular design of reaction sites, (2)to find the effect of the second Nb atom instead of the second ethanol molecule in species(C), and (3)to understand the cooperative catalysis of two adjacent Nb atoms as a model for general metal oxide catalysts. This article reports the preparation of new Nb-dimers attached on SiO_2 and the first example of the change in acid/base catalytic properties by the nucleation of one Nb atom to two Nb atoms in active structures[10]. The mechanism characteristic of the dimer structure, influencing the rate constants for intra- and intermolecular dehydration of ethanol, is also discussed.

2. EXPERIMENTAL

The dimeric Nb complex$[Nb(\eta^5\text{-}C_5H_5)H\text{-}\mu\text{-}(\eta^5,\eta^1\text{-}C_5H_4)]_2$(1) was synthesized from the reaction of $NbCp_2Cl_2$ with NaH in water-free THF in a similar way to that previously reported[11]. SiO_2(Aerosil 200) pretreated at 673 K was immersed in a toluene solution of (1) to react the complex with the surface OH groups at 313 K under high purity Ar(99.9999%), followed by decantation and washed twice by CaH_2-treated toluene, followed by evacuation to remove the solvent. The attached Nb-dimers(2) obtained were treated with H_2 at 823 K(3) and O_2 at 773 K to make the oxidized catalyst(4) as shown in Figure 1. Conventional supported Nb catalysts were prepared by an impregnation method using a methanol solution of $NbCl_5$, followed by dry and calcination at 773 K.

The surface species(2) and (4) were characterized by EXAFS, XANES, FT-IR, TDS, diffuse reflectance-UV, XPS, MS and chemical analysis. EXAFS measurements for Nb samples were carried out at 80 K at BL10B and 6B of Photon Factory in National Laboratory for High Energy Physics(Proposal No.88-020). The Fourier-filtered data were analyzed by means of the least-square curve-fitting method by using the theoretical EXAFS eqn(1)[12,13].

$$\chi(k)=\Sigma N_j F_j(k)\exp(-2\sigma_j^2 k^2)\sin(2kr_j+\phi_j(k))/kr_j^2 \qquad (1),$$

where N_j, r_j and σ_j represent the coordination number, bond length and Debye-Waller factor, respectively. The curve-fitting analysis for the Nb K-edge EXAFS data was performed by using empirical parameters extracted from Nb foil, $LaNbO_4$, $NbCp_2Cl_2$ and $NbSi_2$ for Nb-Nb, Nb-O, Nb-C and Nb-Si bonds, respectively. The catalytic reactions of ethanol in a closed circulating system were followed by MS and GC.

3. RESULTS AND DISCUSSION

3.1. Structures of Nb dimers on SiO_2

The dinuclear complex(1) reacted with surface OH groups of SiO_2 at 313 K as proved by the decrease of the ν(OH)(3743 cm^{-1}) intensity. Upon the interaction, 0.8-0.9 H per Nb atom were evolved(Table 1). The value is less

than the quantitative amount because the quantitative detection of H_2 evolved during the reaction of (1) with oxides in organic solvents is generally difficult. The IR and MS data reveal that each H ligand of (1) reacted with one(not two) OH group to form (2) as shown in Figure 1. The TD spectra in Figure 2 show twin peaks at 480 and 570 K for cyclopentadiene with a nearly 1:1 ratio(total amount=1.93-2.0 per Nb in Table 1). Similar TD spectra of 0.1 and 1.0 wt% samples in Figure 2 suggest almost uniform distribution of Nb species on SiO_2, where two different cyclopentadienyls(η^5-C_5H_5 and η^5, η^1-C_5H_4) are present also in (2) similarly to (1).

Table 1
Characterization of the Nb species(2)-(4)

Nb content on support/wt%	0.1	0.37	1.0	1.6
Amount of H_2 evolved per Nb	0.4	0.4	0.45	0.45
Number of Cp ligands* per Nb	1.93	2.0	2.0	1.98
Consumption of O_2 per Nb(3→4)	0.75	0.71	0.73	0.75
XPS Nb 3d3/2	—	209.8	209.6	209.6
3d5/2	—	206.8	206.6	206.6
CT bands of (4)/nm	—	227	227	227

*η^5-C_5H_5 and η^5,η^1-C_5H_4 ligands

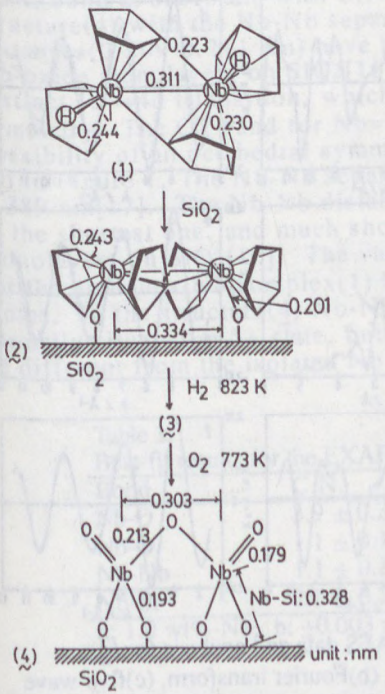

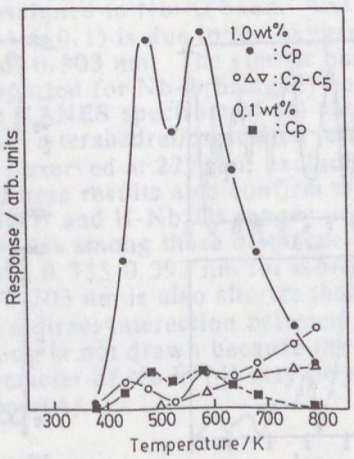

Figure 2. TD spectra of species(2)(1.0wt% and 0.1wt%) in the presence of H_2(13.3kPa).

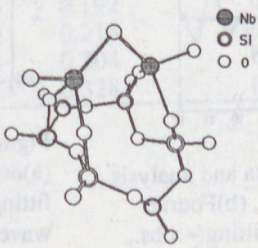

Figure 1. Preparation steps and structures for Nb dimers attached on SiO_2.

Figure 3 shows the k^3-weighted EXAFS oscillation(a) and its associated Fourier transform(b) for (2). The inverse Fourier filtering data were analyzed by a curve fitting technique in Figure 3(c). The best-fit results are listed in Table 2. The observation of Nb-Nb length at 0.334 nm with the coordination number(C.N.) of 0.9(±0.1) demonstrates that the dimeric structure was maintained on SiO_2. The C.N. of 1.3(±0.2) for Nb-O also support the unidentate Nb structure(2).

Table 2
Best-fit results for the EXAFS data of (2) and (4)[a]

Species	Bond	C.N.	r/nm[b]	DW/nm[c]
(2)	Nb-O	1.3 ± 0.2	0.201	0.005
	Nb-C	10.0 ± 1.5	0.243	0.008
	Nb-Nb	0.9 ± 0.1	0.334	0.005
(4)	Nb=O	0.6 ± 0.2	0.179	0.008
	Nb-O	1.9 ± 0.2	0.193	0.005
	Nb-O	1.1 ± 0.1	0.213	0.005
	Nb-Nb	0.9 ± 0.1	0.303	0.006
	Nb-Si	2.3 ± 0.2	0.328	0.004

a: 1.0 WT%-Nb, b: distance(±0.003), c: Debye-Waller factor,
Filtering range: 0.13-0.35 nm(2) and 0.10-0.35 nm(4).

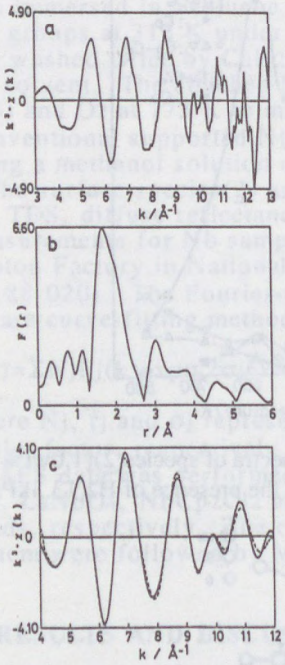

Figure 3. EXAFS data and analysis for (2); (a)oscillation, (b)Fourier transform, (c)curve fitting(–:obs., ···:calc.)

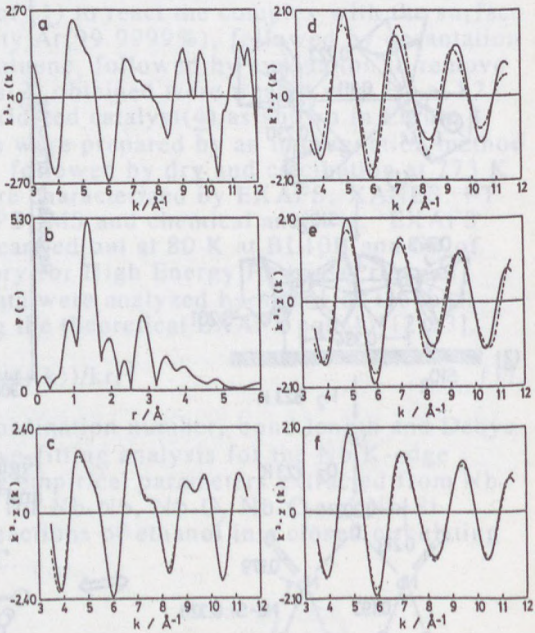

Figure 4. EXAFS data and analysis for (4); (a)oscillation, (b)Fourier transform, (c)five-wave fitting(all bonds), (d)one-wave fitting(Nb-O), (e)two-wave fitting(Nb-O), (f)three-wave fitting(Nb-O); –:obs.,···:calc.

The (2) was reduced with H_2 at 823 K to (3), which was oxidized with O_2 at 773 K to Nb^{5+} level characterized by XPS, uptaking the quantitative amount of O_2 in Table 1. The O_2 uptake was determined by taking account of small amounts of CO_2 formed by oxidation of the residual carbons in (3). Figure 4 shows the EXAFS data of (4). The first peak in the Fourier transform(b) should be due to Nb-O bond, but the analyses based on one-wave fitting(Nb-O) and two-wave fitting(Nb-O and Nb-O) did not give good fits (curves(d) and (e), showing 7.42% and 5.09% of the reliability factor(R), respectively). Then, we performed three-wave fitting(Nb=O, Nb-O and Nb-O) in the curve(f) which showed the best-fit result with R=3.23%. The second peak may be due to Nb-Nb and/or Nb-Si. The shoulder at ca.5.3 $Å^{-1}$ in the oscillation(a) has been attributed to the presence of Nb-Si bond[14,15]. The best-fit result was obtained by two waves of Nb-Nb and Nb-Si. Finally, five-wave fitting analysis(filtering range:0.10-0.35 nm) was performed in the curve(c) of Figure 4. The best-fit results are listed in Table 2. The observation of Nb-Nb bond at 0.303 nm with C.N. of 0.9(±0.1) demonstrates the retention of a dimeric structure on SiO_2. The Nb-Si length was determined as 0.328 nm with C.N. of 2.3(±0.2). The length is similar to 0.326 nm for the Nb monomer(A)[7]. There are two different Nb-O bonds at 0.193 nm and 0.213 nm. The former distance is the same as that for Nb-O (surface) in (A), and the C.N. of 1.9(±0.2) is th onset of Nb-Si. Thus, the 0.193 nm bond is assigned to the bonding of Nb with two surface oxygen atoms as shown in Figure 1. The bond of 0.179 nm is straightforwardly assigned to Nb=O bond. The remaining Nb-O bond at 0.213 nm with C.N. of 1.1 (±0.1) is due to the oxygen-bridged structure(4) with the Nb-Nb separation of 0.303 nm. The similar bond distances(0.209-0.211 nm) have been reported for Nb-O(bridged) bonds for Nb-oxide monolayers on SiO_2[16]. The XANES spectrum of (4) showed a distinct 1s→4d trfansition, which implies a terahedral/disstorted terahedral symmetry. The CT band for Nb=O was observed at 227 nm, excluding the possibility of an octahedral symmetry. These results also confirm the structure (4) in Figure 1. The Nb-Nb separation in T- and H-Nb_2O_5 ranges over 0.299-0.389 nm[17]. The Nb-Nb distance in (4) is among these distances, but close to the shortest one, and much shorter than 0.335-0.392 nm for Nb-oxide monolayers on SiO_2[16]. The value of 0.303 nm is also shorter than 0.311 nm for the dinuclear Nb complex(1) having a direct interaction between two Nb atoms. In the structure(4) Nb-Nb bonding is not drawn because the Nb atom is formally situated in 5+ state, but the character of Nb in (4) may be expected to be different from the isolated Nb monomer(A).

Table 3
Best-fit results for the EXAFS data of (4)[a] after ethanol adsorption

Bond	C.N.	r/nm[b]	DW/nm
Nb-O	3.9 ± 0.3	0.192	0.008
Nb-O	1.1 ± 0.1	0.213	0.004
Nb-Nb	1.1 ± 0.1	0.304	0.006
Nb-Si	2.3 ± 0.2	0.328	0.004

a: 1.0 wt%-Nb, b: ±0.003 nm.

3.2. Regulation of acidity/basicity in catalysis

Ethanol(3.3 kPa) was admitted onto (4) to form Nb(OH)(OC_2H_5) at 373 K followed by evacuation for 30 min($\nu_{(OH)}$:3471 cm^{-1},$\nu_{(CH)}$:2979, 2937, 2900 and 2883 cm^{-1}), and the TD spectrum at a heating rate of 4 K min^{-1} was taken. Ethene and diethyl ether besides ethanol were desorbed. The peak temperature (610 K) for ethene was lower than 690 K for the Nb monomer(B), suggesting the promotion of ethene formation with the dimer(4). The characteristic feature of the EXAFS analysis for the sample saturated with ethanol at 523 K in Table 3 is the disappearance of the Nb=O bond. Instead, the C.N. of the Nb-O bond at 0.192 nm increased to 3.9(±0.3) by 2 from 1.9(±0.2) for the catalyst(4), which agrees with the formation of Nb(OH)(OC_2H_5) by the dissociative adsorption of ethanol. The other bonds remained unchanged, demonstrating no change in the oxygen-bridged dimeric structure.

The catalytic dehydration and dehydrogenation of ethanol were carried out in the temperature range 473-573 K. The Nb monomer catalyst(A) exhibited high activity and selectivity for the dehydrogenation to produce acetaldehyde, indicating a basic charactedr of the Nb monomer[6,7]. On the other hand, the Nb dimer catalyst(4) showed a high selectivity for dehydration to form diethyl ether and ethene in Table 4. The dehydrogenation was remarkably suppressed and the dehydration was promoted on the dimers(4) as compared with the monomers(A). The results imply that the Nb dimers on SiO_2 have an acidic character. The catalytic feature of the Nb dimers was independent of the Nb loadings in the range 0.10-1.6 wt%, suggesting a nearly uniform property of Nb sites on SiO_2(Table 4), which is in agreement with the structural data by EXAFS. The conventional impregnation Nb catalysts were less active and unselective. It is to be noted that the change of the number of Nb atoms in active sites from one to two metal gave rise to the complete reverse of basicity/acidity in catalytic properties.

Table 4
Typical results for activities and selectivities of three different Nb catalysts in the dehydration and dehydrogenation of ethanol

Catalyst*	React. temp./K	Initial rate** (i)	(ii)	Selectivity/% Ethene	Diethyl ether	Acetaldehyde
(A)	523	1.20	0.05	2.8	1.1	96.1
	548	1.55	0.11	6.1	0.7	93.2
	Activation energy/kJ mol^{-1}			–	–	65
(4)						
0.1 wt%	523	0.01	0.19	34.7	61.9	3.4
0.37 wt%	523	0.01	0.17	32.6	63.9	3.5
	573	0.01	1.10	58.1	40.2	1.8
1.0 wt%	523	0.01	0.19	34.2	62.0	3.8
	Activation energy/kJ mol^{-1}			119	79	68
Impreg.Catal.						
0.45 wt%	523	0.05	0.12	26.0	45.3	28.6
0.92 wt%	523	0.01	0.08	27.2	59.8	13.0
	Activation energy/kJ mol^{-1}			129	85	70

* (A): Nb monomer/SiO_2(2.0 wt%), (4): Nb dimer/SiO_2.
** EtOH: 3.3 kPa, mmol min^{-1} $g\text{-}Nb^{-1}$, (i)dehydrogenation, (ii)dehydration.

3.3. Mechanism and change of rate constants

The rate of ethene formation was accelerated 1.7 times by raplacing C_2H_5OH by C_2D_5OD as shown in Figure 5. The subsstitution of the OH hydrogen with deuterium gave almost no effect on the rate. The inverse isotope effect can be explained by a late transition-state theory. By taking into acccout the vibrational partition functions, the ratio of the rate constants(k_D/k_H) is expressed by eqn(2). We adopted ν(OH) of H_2O and ν(CH) of methylene group as the vibra-

$$k_D/k_H=\Pi\exp[\mathbf{h}(\nu_{Hi}^{*} - \nu_{Di}^{*} - \nu_{Hi} +\nu_{Di})/2\mathbf{k}T] \quad (2)$$

tional modes of the transition state(6), while the observed values were used for the vibrational modes of Nb(OH)(OC_2H_5)(5). The calculated inverse isotope effect(k_D/k_H) was 1.6, which is in good agreement with the experimental value.

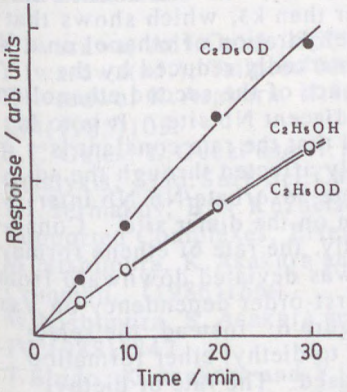

Figure 5. Inverse isotope effect: Ethen formation by the dehydration of C_2H_5OH, C_2H_5OD, and C_2D_5OD(3.3 kPa) at 523 K; 1.0 wt%-Nb.

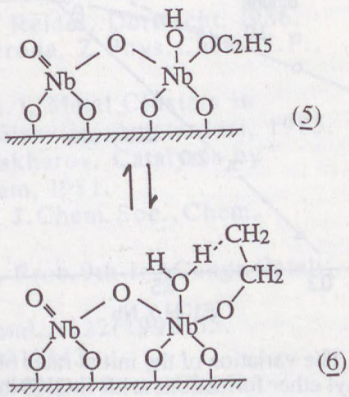

Ethene is formed by the intramolecular dehydration of species(5) and (7). The saturation mass of adsorption for ethanol on the dimer(4) was one ethanol per Nb atom under reaction conditions. Using the equilibrium constants(K_1 and K_2) in eqn(3), the amount of ethanol adsorbed(V_{ad}) is expressed by eqn(5).

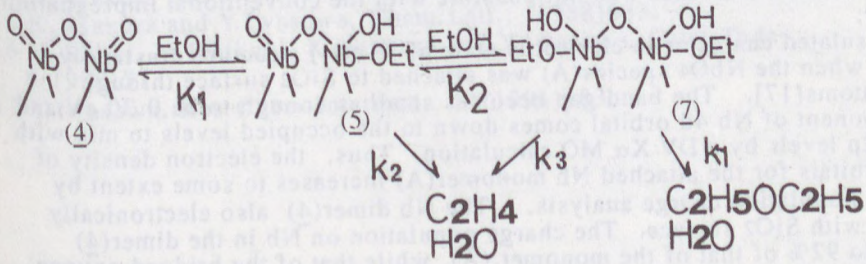

(3)

$$V_{ad}=[S_1Et_1]+2[S_0Et_2] \quad (4)$$

$$=[S]_0(K_1P_E+2K_1K_2P_E^2)/2(1+K_1P_E+K_1K_2P_E^2) \quad (5),$$

where P_E and $[S]_o$ represent the partial pressure of ethanol and the number of adsorption sites, respectively. From eqn(5) and the data of the adsorption isotherm, K_1 and K_2 were determined to be 6.0×10^{-3} Pa^{-1} and 2.1×10^{-3} Pa^{-1} at 523 K, respectively.

As the rate of ethene formation(v) is given by eqn(6),

$$v = k_2[S_1Et_1] + 2k_3[S_0Et_2] \quad (6)$$

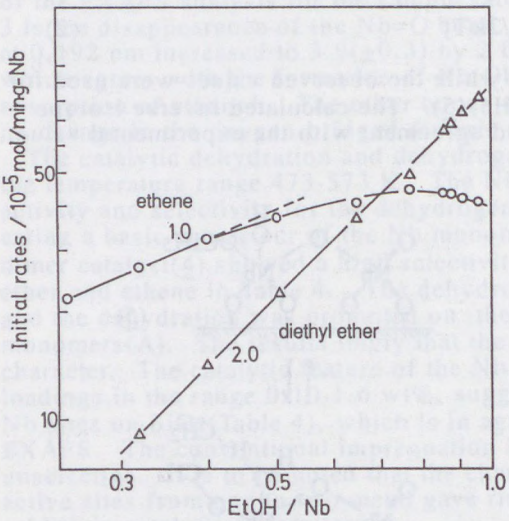

Figure 6. The variation of the initial rates of ethene and diethyl ether formations with EtOH/Nb.

the first-order rate constants, k_2 and k_3, for the dehydration of (5) and (7) obtained to be 4.7×10^{-3} min^{-1} and 1.8×10^{-3} min^{-1} at 523 K, respectvely. k_2 was about 3 times larger than k_3, which shows that the dehydration of ethanol on a Nb site markedly reduced by the presence of the second ethanol on the adjacent Nb site. It is to be noted that the rate constant is largely affected through the adsorbate-adsorbate/Nb-Nb interaction on the dimer site. Consequently, the rate of ethene formation was deviated downward from the first-order dependency on V_{ad} in Figure 6. Instead, the selectivity to diethyl ether formation increased. The rate of diethyl ether formation(v') was proportional to the square of V_{ad} as shown in Figure 6.

The rate constant(k_1) for diethyl ether formation given by eqn(7) was determined to be 8.0×10^{-3} min^{-1}(523 K). The rate constants, k_1-k_3, varied

$$v' = k_1[S_0Et_2] \quad (7)$$

with the Nb-Nb separation. The larger the Nb-Nb separation, the smaller the ratio(k_2/k_3) and the rate ratio(v'/v) became. This kind of control in the ratio of rate constants and rates was not possible with the conventional impregnation catalysts.

The insulated character in electronic state of $[NbO_4]$ structure drastically changed when the NbO_4 species(A) was attached to SiO_2 surface through oxygen atoms[17]. The band gap becomes small as enough to be 0.30 eV and the component of Nb 4d orbital comes down to the occupied levels to mix with oxygen 2p levels by a DV $X\alpha$ MO calculation. Thus, the electron density of Nb 4d orbitals for the attached Nb monomer(A) increases to some extent by Mulliken population charge analysis. The Nb dimer(4) also electronically interacts with SiO_2 surface. The charge population on Nb in the dimer(4) reduced to 92% of that of the monomer (A), while that of the bridged oxygen increased by 9% as compared with that of the oxygen atom without adjacent Nb atom. This trend leads to an increase in acidic character of Nb site. The adjacent Nb atom in the dimer(4) may also change the local conformation of Nb sites. In the dimer structure(4) the access of a second ethanol molecule to the

Nb atom with a first ethanol molecule in a preferable conformation is difficult unlike to the case of the monomer(C). In other words, the assisted-dehydrogenation[7] is not possible with the dimer(4).

On support surfaces unique structures of active sites are possible to create by molecular design using suitable organometallic precursors and by molecular characterization by EXAFS, which may lead to developments of new catalytic systems. The tailored metal catalysts may have great advantages for a deeper understanding of essential factors or origin of solid catalysis and hence can provide molecular-level information on preparations of high-quality catalysts.

4. REFERENCES

1 Y.Iwasawa, Adv.Catal., 35(1987)187.
2 Y.Iwasawa(ed.), Tailored Metal Catalysts, Reidel, Dortrecht, 1986.
3 Y.Iwasawa, K.Asakura, H.Ishii and H.Kuroda, Z.Phys.Chem.N.F., 144(1985)105.
4 B.C.Gates, L.Guczi and H.Knozinger(eds.), Metal Clusters in Catalysis, Stud.Surf.Sci.Catal., Vol.29, Elsevier, Amsterdam, 1983.
5 Y.I.Yermakov, B.N.Kuznetsov and V.A.Zakharov, Catalysis by Supported Complexes, Elsevier, Amsterdam, 1981.
6 M.Nishimura, K.Asakura and Y.Iwasawa, J.Chem.Soc.,Chem. Commun., (1986)1660.
7 M.Nishimura, K.Asakura and Y.Iwasawa, Proc.9th Int.Cangr.Catal., IV(1988)1842.
8 T.Shido, K.Asakura and Y.Iwasawa, J.Catal., 122(1990)55.
9 T.Shido and Y.Iwasawa, J.Catal., 129(1991)343.
10 N.Ichikuni, K.Asakura and Y.Iwasawa, J.Chem.Soc., Chem. Commun., (1991)112.
11 D.A.Lemenovskii, I.F.Urazowski, I.E.Nivant'ev and E.G.Pervalova, J.Organomet.Chem., 292(1985)217.
12 B.K.Teo, EXAFS:Basic Principles and Data Analysis, Inorganic Concepts, Vol.9, Springer, Berlin, 1986.
13 K.Asakura and Y.Iwasawa, J.Chem.Soc., Faraday Trans.1, 84 (1988)2445.
14 K.Asakura and Y.Iwasawa, Chem.Lett., (1986)859.
15 K.Asakura and Y.Iwasawa, Chem.Lett., (1988)633.
16 M.Shirai, N.Ichikuni, K.Asakura and Y.Iwasawa, Catal.Today, 8(1990)57.
17 Y.Iwasawa, Res.Chem.Intermed., 15(1991)183.

DISCUSSION

Q: G. A. Somorjai (USA)

Please comment on the turnover frequency you could achieve and the deactivation behavior if that was observed. Can you prepare a one Nb- and two Nb-containing mixed site catalyst to carry out dehydration simultaneously ?

A: Y. Iwasawa

We achieved repeated runs to take kinetic parameters, to measure isotope effects, and so on for more than two weeks using a catalyst sample, but we did not observe deactivation, suggesting that neither breaking of the dimer to monomers nor aggregation to polymeric species occurred during ethanol reactions and catalyst treatments with O_2. However, the prolonged treatments above 823 K cause some deactivation. The deactivated catalysts have not been characterized. The character of each Nb atom in the dimer was lost and generated a new character as a pair. It is possible and interesting to prepare a Nb- and two Nb-containing mixed sites on SiO_2 by a successive attachment of the monomer and the dimer.

Q: J. W. Hightower (USA)

This question relates to your deuterium tracer experiments. Often, as one increases the acid character of a catalyst, the intermolecular exchange of H atoms increases. This is essentially true of olefinic and allylic H atoms. During the dehydration to form ethene, did you observe an exchange of the C_2H_4 with C_2D_4 product as you increased the acidity in going from the monomer to the dimer?

A: Y. Iwasawa

The dehydration of ethanol on the Nb dimer catalysts were carried out in the temperature range 473-573 K and in changing the pressures of ethanol/deuterated ethanol. Under the present conditions the exchange of H atoms was not observed with ethene product.

Q: D. Wang (China)

Can you make a rough comparison of your catalyst with conventional impregnated catalysts from the following two viewpoints:

1) A tailored shirt fits better but it costs more. Your tailored Nb dimers fit particular reactions better. If you were to commercialize your catalysts with reasonable costs for tailoring, are they economically competitive with impregnated catalysts?

2) What are the analogies with catalysis by a bulk-like niobium oxide that have been gained from the use of tailored Nb moieties?

A: Y. Iwasawa

1) Usual impregnated Nb catalysts exhibit heterogeneous properties of active sites due to easy but hard-controllable aggregation of $NbCl_5$ or $Nb(OC_2H_5)_5$ during the impregnation, resulting in low selectivity. The dimers with 96-98% selectivity should show a good cost performance.

2) A pure bulk niobium oxide can not be an efficient catalyst. Nb-oxide species have band gaps and different electronic structures. The electronic properties drastically changed by bonding of Nb moieties with SiO_2 surface. If a stable defect surface of bulk Nb oxides are created, those Nb sites would behave as active sites similar to the dimer.

Q: R. W. Joyner (United Kingdom)

Your paper is an elegant demonstration that moving from one to two metal atoms can change reactivity dramatically. My question is whether the bridging oxygen between the two niobium ions can be involved in the dehydration reaction? Protonation of this oxygen might be an attractive first step in the reaction.

A: Y. Iwasawa

No Nb-O-Nb bond breaking took place upon the dissociative adsorption of ethanol as proved by EXAFS, while the Nb-OH peak was observed by IR. The Nb=O bond disappeared by ethanol adsorption at saturation. These results suggest that the first protonation took place at the Nb=O sites. If the second deprotonation from ethoxyl ligand occurred at the bridging oxygen and the proton is located on the oxygen without Nb-O-Nb bond breaking, the proton would isomerize 2-butene, but no cis-trans isomerization of butenes coexisted during the dehydration reaction. The comprehensive data suggest the reaction scheme (5) to (6).

Q: H. Kung (USA)

It has been demonstrated that exposure of highly dispersed supported oxide to water vapor results in hydration of the dispersed oxide and possibly migration. Do you have information whether, under reaction conditions where water vapor is produced in ethanol dehydration, the niobia clusters stay as dimers or monomer? Have any of the catalysts been characterized after reaction to see if there are any changes?

A: Y. Iwasawa

Under the reaction conditions the produced water did not have any effect on catalyst change. The dimer is more stable than the monomer to water. Table 3 is the EXAFS data for the sample after ethanol adsorption. We also performed the EXAFS measurements at the steady state of reaction and after the repeated runs. No destroy of the dimer was observed.

Q: K. Jerabek (Czechoslovakia)

You discussed all your results in connection with niobium only. Is not it possible that, especially in respect to the dehydration activity, the results were influenced by SiO_2?

A: Y. Iwasawa

The dehydration behavior of the dimers is not affected by the kind of SiO_2, but the rate constants for intra and intermolecular dehydrations and their ratios are influenced by the kind of SiO_2. Main reason is the change of the Nb structure depending the nature of SiO_2. By choosing SiO_2, we can produce dimers with different Nb-Nb separation, dimers attached to SiO_2 in a tripod form, an so on.

Q: J. C. Volta (France)

Did you compare the eventual presence of impurities at the surface of your Nb monomer and dimer (for example by XPS)?

A: Y. Iwasawa

Besides the determination of Nb 3d binding energies, the high-sensitive wide-scan XPS spectra were taken, which showed no impurity in the Nb samples within the XPS detection limit. The ICP emission analysis for the monomer and dimer catalysts (after decomposition by a strong acid) revealed no particular difference between them. The different catalytic behaviors should be referred to the structures of Nb sites.

Guczi, L. *et al.* (Editors), *New Frontiers in Catalysis*
Proceedings of the 10th International Congress on Catalysis, 19-24 July, 1992, Budapest, Hungary
© 1993 Elsevier Science Publishers B.V. All rights reserved

EXPERT SYSTEMS APPROACH TO CATALYST DESIGN - APPLICATION AND EXPERIMENTAL VERIFICATION

T. Hattori[a], *H. Niwa*[a], *A. Satsuma*[a], *S. Kito*[b] *and Y. Murakami*[a]

[a]Department of Applied Chemistry, School of Engineering, Nagoya University, Chikusa, Nagoya 464-01, Japan
[b]Department of Industrial Engineering, Aichi Institute of Technology, Yagusa, Toyota 470-03, Japan

Abstract

A prototype expert system for catalyst design, INCAP (Integration of Catalyst Activity Pattern), was applied to the estimation of catalytic performances of a series of promoted SnO_2 catalysts in the oxidative dehydrogenation of ethylbenzene, and the estimated performances of eighteen promoted SnO_2 catalysts were compared with those measured experimentally by using a conventional flow reactor. The index to the overall performance adopted in the INCAP agreed fairly well with the experimental one, but the disagreement was significant for some catalysts. Then new indexes to the activity and selectivity were introduced and compared with those measured experimentally. In these cases, good correlations were obtained between them, which strongly demonstrates the feasibility of the expert systems approach to the design of catalysts.

INTRODUCTION

The expert systems approach is said to be a powerful tool to solve the problems by using empirically acquired knowledge, even though a human expert can not tell how to solve the problem. The catalyst design seems to be a typical example of such "ill-defined" problems, and a few attempts have been done to develop the expert system for catalyst development [1,2].

We have also developed a prototype catalyst design expert system: INCAP (Integration of Catalyst Activity Pattern) for the selection of a single catalyst component [3] and INCAP-Muse (INCAP for Multi-Component Catalyst Selection) for the selection of multi-component catalyst [4]. These systems select the catalyst component(s) through the estimation of catalytic performance of individual component, even if the component has never been experimentally examined for the target reaction.

The INCAP was applied to the selection of promoter oxides to be added to a predetermined main component, SnO_2, for oxidative dehydrogenation of ethylbenzene, and the promoting effects of selected oxides were thereafter verified through the experimental catalyst testing [5]. The INCAP-Muse was applied to the selection of binary-oxide catalysts for oxidative dehydrogenation of butene, and the results were in good agreement with the open literatures. These facts suggests the possibility of catalyst design by the aid of expert system [6].

In the present study, the performances of SnO_2 catalysts promoted by

various oxides were experimentally measured through the catalytic test, and their promoting effects were compared with those estimated by the INCAP for the purposes of further demonstration of the feasibility of the expert systems approach to the catalyst design.

OVERVIEW OF INCAP

The INCAP selects a catalyst component through the knowledge based reasonings of reaction mechanism (R1) and catalytic functions (R2) for the target reaction, plausible side reactions (R3), catalytic functions for the side reactions (R4), and integration of catalytic functions (R5). The knowledge required for the reasonings (R1) to (R4) could be encoded in the knowledge base by using the conventional production system and frame system. However, a novel knowledge representation scheme had to be developed for the reasoning (R5) [3,4].

The overall performance of oxide as a catalyst component is estimated by integrating various activity pattern (activity order) data such as "Cu > Co > Mn > Cr ... ". The activity pattern is divided into ten sections, and a numerical value from ten to one named API (Activity Pattern Index) are allocated for each section. The individual API data are multiplied by an evaluation factor (Ef) which expresses the empirical knowledge about the utilization of activity pattern. Negative values are allocated for the Ef's of the catalytic functions causing side reactions. Then, an averaged API (avAPI) is calculated for each function, and is converted into modified API (mAPI) by taking the required strength of catalytic functions into consideration, and mAPI's for all the functions are summed up to give an integrated API expressing the overall performance of the catalyst component. The procedure of integration is schematically shown in Figure 1.

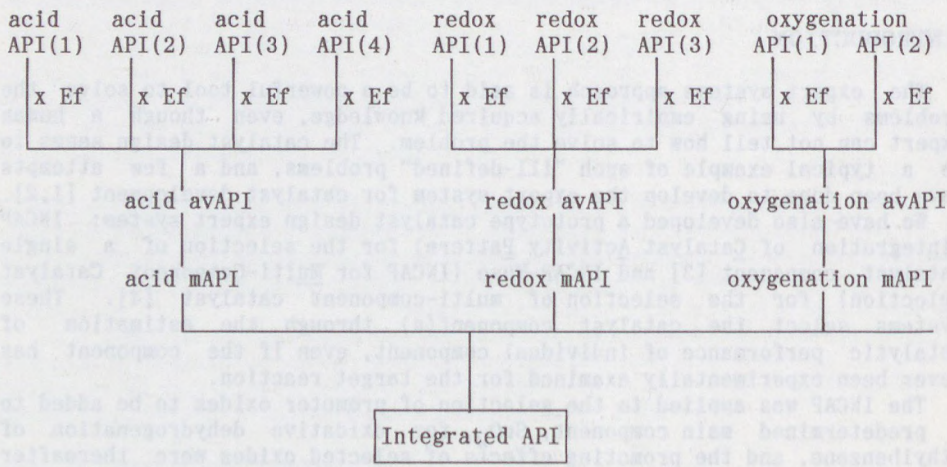

Figure 1. Schematic diagram of integration of catalyst activity pattern. API, activity pattern index; avAPI, averaged API; mAPI, modified API; Ef, evaluation factor.

APPLICATION OF INCAP

The INCAP was applied to the evaluation of promoting effects of various oxides on the catalytic performance of SnO_2 catalyst for the oxidative dehydrogenation of ethylbenzene. As a result of the reasonings (R1) and (R2) based on the acid-base mechanism proposed for Na-loaded silica-alumina catalysts [7], the following catalytic functions were obtained for the target reaction:

(T-1) acidic property of medium strength,
(T-2) basic property, and
(T-3) redox activity.

The reasoning (R3) gave the following side reactions: dealkylation, isomerization, disproportionation, complete oxidation, and partial oxidation of ethylbenzene and polymerization and condensation of styrene. And then the following catalytic functions leading to the side reactions were obtained via reasoning (R4):

(S-1) strong redox activity,
(S-2) strong acidic property, and
(S-3) partial oxidation activity.

Since SnO_2 is expected to have the redox and the basic properties [8,9], the remaining catalytic functions, i.e. (T-1), (S-1), (S-2), and (S-3), were integrated in the reasoning (R5) to estimate the overall catalytic performance. Table 1 indicates the Integrated API's of various oxides as the promoter to be added to SnO_2 catalyst. According to the Integrated API's, the INCAP selected SiO_2, ZrO_2, P_2O_5, Nb_2O_5 and MoO_3 as candidates of promoter. It should be noted that the INCAP did not recommend Re_2O_7 because of its high volatility [3].

Table 1
Integrated API's of various promoters to SnO_2 catalyst for oxidative dehydrogenation of ethylbenzene

1.	Si[a]	740,	11.	Se	240,	21.	Sn[b]	90,	31.	La	-30,	39.	Pd	-200,
2.	Zr[a]	580,	12.	Hf	220,	22.	Pb	80,	32.	Ba	-50,	39.	Rh	-200,
3.	P[a]	530,	12.	Te	220,	23.	Be	70,	33.	Zn	-60,	39.	Ru	-200,
4.	Re[c]	400,	14.	Mg	210,	24.	Cd	50,	34.	Hg	-80,	44.	V	-220,
5.	Nb[a]	320,	15.	B	200,	24.	Sc	50,	35.	Ag	-110,	45.	Cr	-390,
6.	Mo[a]	300,	16.	Th	170,	26.	Y	40,	36.	In	-120,	46.	Mn	-540,
7.	W	285,	17.	Ta	150,	27.	Ga	30,	37.	Fe	-130,	47.	Ni	-580,
8.	As	280,	18.	Ce	110,	28.	Sr	0,	38.	Os	-140,	48.	Co	-790,
9.	Ge	270,	19.	Bi	100,	29.	Ca	0,	39.	Pt	-200,	49.	Cu	-910.
10.	Ti	255,	20.	Al	95,	30.	Sb	-15,	39.	Ir	-200,			

[a] selected as candidates of promoter. [b] "Sn" stands for unpromoted SnO_2.
[c] Re was excluded from the list of candidates of promoter because of high volatility of Re_2O_7.

EXPERIMENTAL

Unpromoted SnO_2 catalyst was prepared by drying tin (II) hydroxide gel at 380K for 24h followed by the calcination at 773K for 2h. For the preparation of tin (II) hydroxide gel, excess ammonium hydroxide was added to an acidic aqueous solution of tin(II) chloride, and thus obtained precipitate was washed with water until no residual chlorine was detected in the filtrate.

Eighteen promoted SnO_2 catalysts, listed in Table 2, were prepared by a gel mixing method or a co-precipitaion method. The promoter oxides were artificially selected so as to include the recommended oxides (Si, Zr, P, Nb and Mo), those estimated to improve the catalytic performance of SnO_2 catalyst (W, Ge, Ti, Mg, B, Ce and Bi) and those estimated to lower the performance (Pb, Sb, V, Ba, Zn and Cu). The promoter content was 10 atom% except SnO_2-SiO_2 which contains 10 atom% of SnO_2. In the gel mixing method, the tin (II) hydroxide gel was mixed with a solution containing promoter ions, followed by drying and calcination in the same way as above. In the co-precipitation method, excess ammonium hydroxide was added to an ethanol solution containing tin (II) chloride and promoter elements. Thus obtained

Table 2
List of promoted SnO_2 catalysts

Promoter		Preparation	S_{BET}
Element	Source	Method	m^2g^{-1}
none[a]	-	-	25
B	H_3BO_3	gel-mixing	4.7
Mg	$Mg(NO_3)_2$	gel-mixing	29
Si[b]	$Si(OC_2H_5)_4$	coprecipitation	163
P[c]	H_3PO_4	gel-mixing	10
Ti	$Ti(OC_2H_5)_4$	coprecipitation	17
V	NH_4VO_3	gel-mixing	24
Cu	$Cu(NO_3)_2$	gel-mixing	55
Zn	$Zn(NO_3)_2$	gel-mixing	12
Ge	$GeCl_4$	coprecipitation	34
Zr	$ZrOCl_2$	coprecipitation	30
Nb	$NbCl_5$	coprecipitation	30
Mo	$(NH_4)_6Mo_7O_{24}$	gel-mixing	58
Sb	$SbCl_3$	coprecipitation	44
Ba	$Ba(NO_3)_2$	gel-mixing	15
Ce	$CeCl_3$	coprecipitation	30
W	WCl_6	coprecipitation	11
Pb	$Pb(NO_3)_2$	gel-mixing	52
Bi	$BiCl_3$	coprecipitation	51

[a] unpromoted SnO_2. [b] contains 10 atom % of SnO_2 and 90% of SiO_2. [c] calcined at 1273K for 24h.

precipitate was washed with water, dried and calcined. The powder catalysts were pressed, and then sieved in the range of 28-48 mesh.

The reaction was carried out by a conventional fixed bed flow reactor at atmospheric pressure in the same way as described previously [8,9]. The standard reaction conditions were as follows: reaction temperature was 698, 723 and 748K; total feed rate was 210 mmol/h; and partial pressures of ethylbenzene, oxygen and water vapor were 19.2, 19.2 and 33.7 kPa, respectively, with nitrogen balance. The amount of catalyst was adjusted so as to obtain a moderate conversion of oxygen.

EXPERIMENTAL RESULTS

The continuous flow reaction of oxidative dehydrogenation of ethylbenzene was conducted to evaluate the catalytic performances of unpromoted and promoted SnO_2 catalysts. Figure 2 shows the results on unpromoted SnO_2. When 3.7g of unpromoted SnO_2 catalyst is used, even at the lowest temperature in the standard condition, the conversion of oxygen is close to 100% and the selectivity of styrene is lower than 45%. Then, the temperature is lowered to 648K, but the selectivity does not increase at all in spite of the decrease in the conversion of oxygen to ca. 20%. Then another run was carried out by using a small amount of catalyst, i.e., 0.5 g. As shown in Figure 2b, the selectivity is still lower than 45%, indicating that the unpromoted SnO_2 catalyst is essentially non-selective.

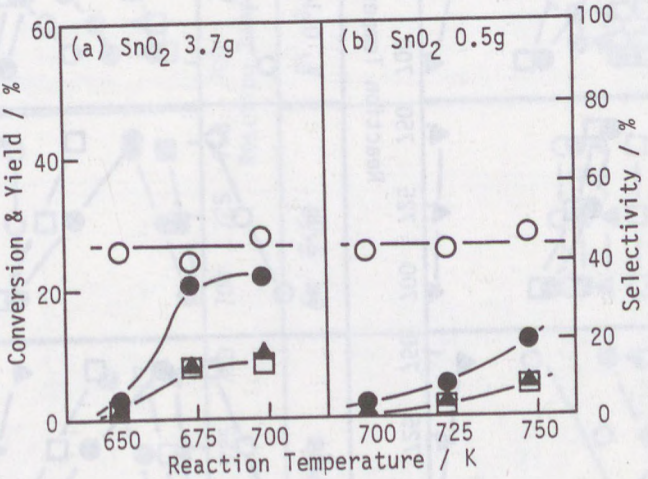

Figure 2. Catalytic performance of unpromoted SnO_2 catalyst.
○, selectivity; ●, conversion; □, yield of styrene; ▲, yield of $CO+CO_2$.

The results on promoted SnO_2 catalysts are summarized in Figure 3. SnO_2-SiO_2 and SnO_2-P_2O_5 catalysts exhibits the highest selectivity among the examined catalysts. We have reported that the SnO_2-P_2O_5 catalyst [8] and the supported SnO_2 catalyst on SiO_2 [9] exhibit very high selectivity

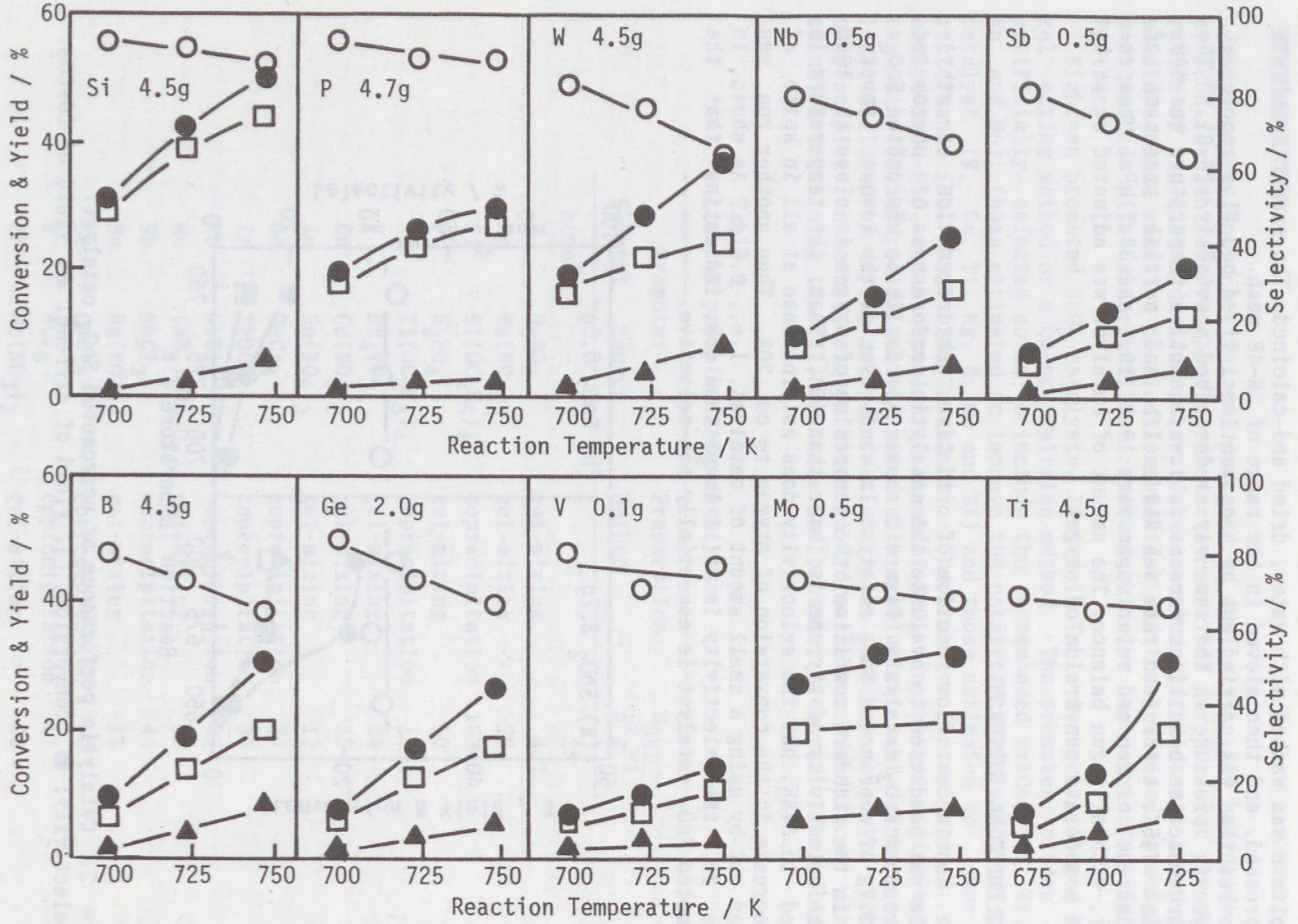
Si 4.5g
P 4.7g
W 4.5g
Nb 0.5g
Sb 0.5g
B 4.5g
Ge 2.0g
V 0.1g
Mo 0.5g
Ti 4.5g
Conversion & Yield / %
Selectivity / %
Reaction Temperature / K
0
20
40
60
80
100
675
700
725
750

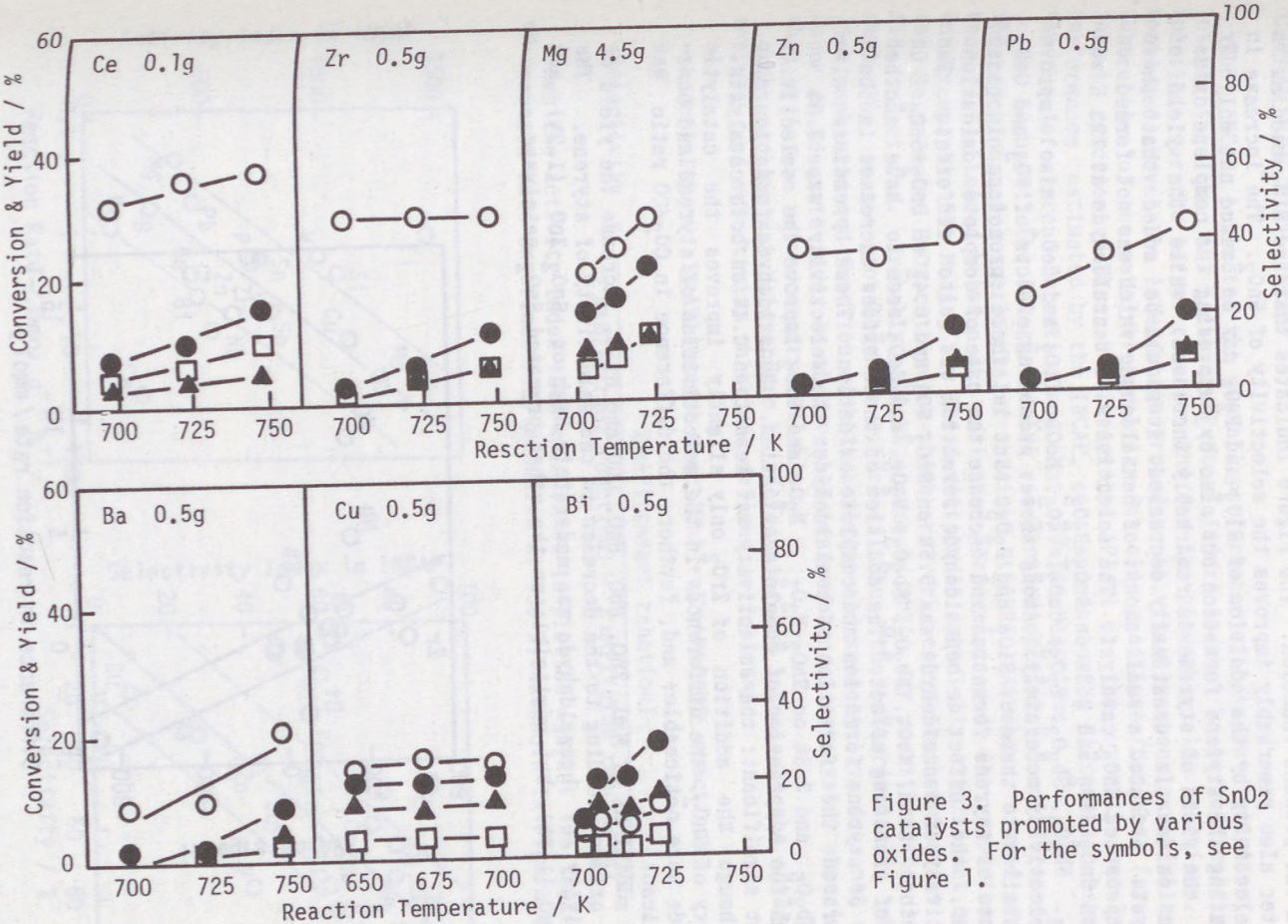

Figure 3. Performances of SnO_2 catalysts promoted by various oxides. For the symbols, see Figure 1.

toward the present reaction. The figure indicates that the SiO_2 used as a promoter also remarkably improves the selectivity of SnO_2. The increase in the selectivity by the addition of SiO_2 and P_2O_5 may be caused not only by activating the styrene formation but also by suppresing the complete oxidation: the yield of styrene is remarkably increased, while the yield of carbon oxides is drastically decreased. It should be added that these catalysts produced a small amount of benzaldehyde which was not formed on the unpromoted SnO_2 catalyst. The selectivity of benzaldehyde at 723 K was 0.9% on SnO_2-SiO_2 and 2.3% on SnO_2-P_2O_5.

WO_3, Nb_2O_5, Sb_2O_3, B_2O_3, GeO_2, V_2O_5, MoO_3, TiO_2 and CeO_2 also improve the selectivity moderately. Among these, promoting effects of WO_3 and GeO_2 are similar to those of SiO_2 and P_2O_5, that is, these promoters increase the rate of styrene formation and decrease the rate of complete oxidation. However, the effect on benzaldehyde formation was quite different. The selectivity of benzaldehyde was 5.5% on SnO_2-WO_3 and 0.4% on SnO_2-GeO_2. On the other hand, MoO_3, Nb_2O_5, Sb_2O_3, V_2O_5, and CeO_2 seem to have another kind of promoting effect. The addition of these oxides increases in both rates of styrene formation and complete oxidation. These promoters also accelerated the formation of benzaldehyde: the selectivity was 7.5% on SnO_2-Nb_2O_5 and 3.5% on SnO_2-V_2O_5. B_2O_3 and TiO_2 improve the selectivity through the suppression of complete oxidation. Benzaldehyde formation also was not significant: the selectivity was less than 0.4% on both catalysts.

Although the addition of ZrO_2 only slightly improves the catalytic property of SnO_2, the differences in the selectivities of styrene and benzaldehyde were noticeable, and, further, the difference in CO_2/CO ratio was significant.

The additions of MgO, ZnO, PbO, BaO, CuO and Bi_2O_3 increase the yield of carbon oxides, leading to the decrease in the selectivity of styrene. The selectivity of benzaldehyde was moderately high on SnO_2-ZnO (1.2%) and SnO_2-CuO (1.8%), but negligible on the other promoted SnO_2 catalysts.

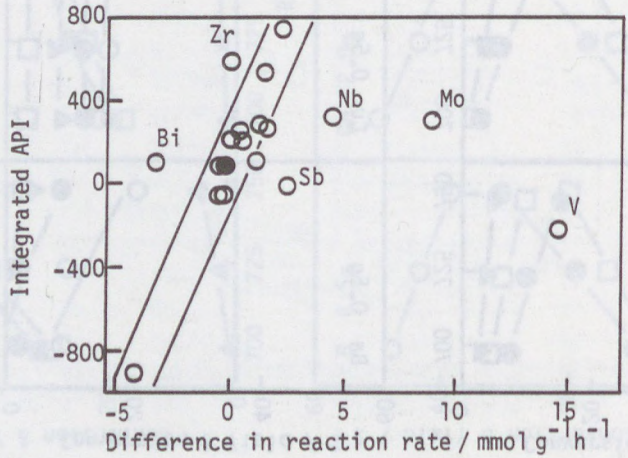

Figure 4. Comparison of overall catalytic performance predicted by INCAP with the difference in reaction rate measured experimentally at 698 K.

COMPARISON WITH INCAP

The INCAP estimates the overall performance of catalyst component by integrating the API (Activity Pattern Index) on the basis of catalytic functions for the target reaction and for the plausible side reactions, as mentioned above. The integration procedure is, roughly speaking, similar to subtraction of the catalytic activity for side reactions from that for the target reaction. Thus, the integrated API, i.e., the overall catalytic performance estimated by the INCAP, corresponds to the difference between the rate of styrene formation and that of side reactions.

In Figure 4, the integrated API was plotted against the difference in the reaction rate experimentally obtained at 698K. As shown, a good agreement was obtained between the estimated performance and the experimental one except Bi, Nb, Mo and V. The deviation is especially significant on V- and Mo-promoted SnO_2 catalysts, which are very active for both target and side reactions. Probably, slight errors in API's may result in the large deviation in the plot shown in Figure 4. Thus, the integrated API, which is a sophisticated function of both activity and selectivity, does not seem to be an adequate index to the overall performance of catalyst, especially when API's are not necessary reliable.

This problem may be overcome by introducing new indexes to the catalytic activity and selectivity which are defined as follows:

$$\text{Activity} = \Sigma\,\text{mAPI(target reaction)} + \Sigma\,\text{mAPI(side reactions)}$$

$$\text{Selectivity} = \frac{\Sigma\,\text{mAPI(target reaction)}}{\Sigma\,\text{mAPI(target reaction)} + \Sigma\,\text{mAPI(side reactions)}}$$

When the activity index thus calculated is plotted against the logarithm of reaction rate experimentally measured at 698 K, as shown in Figure 5,

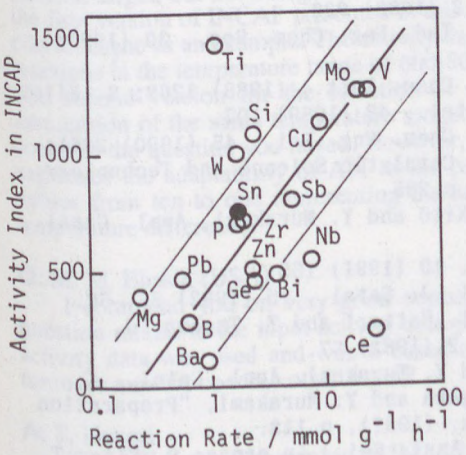

Figure 5. Comparison of activity index estimated by the INCAP with experimentally measured activity.

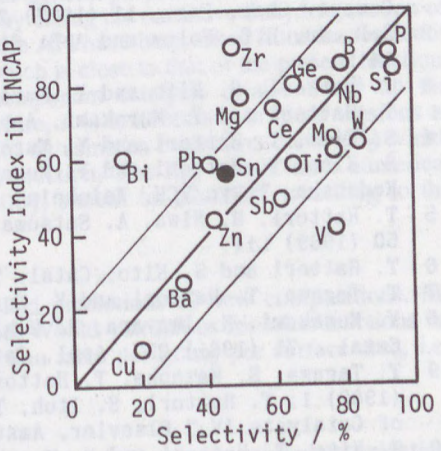

Figure 6. Comparison of selectivity index estimated by the INCAP with experimentally measured selectivity.

a fairly good correlation is obtained with exceptions of Ti- and Ce-promoted SnO_2 catalysts. The selectivity index also agrees fairly well with the experimentally measured selectivity at the conversion of around 20%, as shown in Figure 6. In this case, Zr-, Bi- and V-promoted SnO_2 catalysts form the exceptions. These correlation and agreement strongly demonstrate the feasibility of expert systems approach to the catalyst design.

CONCLUSION AND FUTURE PROSPECT

A good agreement between the catalytic performance estimated by the INCAP with experimentally measured performance demonstrates the feasibility of expert systems approach to the design of catalysts. However, the exceptions such as Ti and Ce in Figure 5 and Zr, Bi, and V in Figure 6 would suggest that still some room for improvement of the INCAP is left. Further experimental verification of the INCAP which is in progress suggests that the disagreement is partly due to the lack of API data for some catalyst components and the poor knowledge about the synergistic effect especially on the generation of acid sites over mixed oxide catalysts. The latter problem is going to be overcome by using a neural network [10]. Another problem of the INCAP is that the reaction mechanism of the target reaction or a similar reaction has to be encoded in the knowledge base in advance. For this problem, an expert system for the creation of reaction mechanism is being developed [11]. These subsystems will be included in an advanced catalyst design system, ARCADE (Artificial Intelligence System for Catalyst Design) [6].

REFERENCES

1 R. Banares-Alcantara, A.W. Westerberg, E.I. Ko and M.D. Rychener, Comput. Chem. Eng., 11 (1987) 265; 12 (1988) 923.
2 X.D. Hu, H.C. Foley and A.B. Stiles, Ind. Eng. Chem. Res., 30 (1991) 1419.
3 T. Hattori, S. Kito and Y. Murakami, Chem. Lett., (1988) 1269; S. Kito, T. Hattori and Y. Murakami, Appl. Catal., 48 (1989) 107.
4 S. Kito, T. Hattori and Y. Murakami, Chem. Eng. Sci., 45 (1990) 2661; S. Kito, T. Hattori and Y. Murakami, Catalytic Science and Technology, Kodansha, Tokyo/VCH, Weinheim, 1991, p.285.
5 T. Hattori, H. Niwa, A. Satsuma, S. Kito and Y. Murakami, Appl. Catal., 50 (1989) L11.
6 T. Hattori and S. Kito, Catal. Today, 10 (1991) 165.
7 T. Tagawa, T. Hattori and Y. Murakami, J. Catal., 75 (1982) 56, 66.
8 Y. Murakami, K. Iwayama, H. Uchida, T. Hattori and T. Tagawa, J. Catal., 71 (1981) 257; Appl. Catal., 2 (1982) 67.
9 T. Tagawa, S. Kataoka, T. Hattori and Y. Murakami, Appl. Catal., 4 (1982) 1; T. Hattori, S. Itoh, T. Tagawa and Y. Murakami, "Preparation of Catalysts IV," Elsevier, Amsterdam, (1987), p.113.
10 S. Kito, T. Hattori and Y. Murakami, Anal. Sci., in press; S. Kito, T. Hattori and Y. Murakami, Ind. Eng. Chem. Res., in press.
11 T. Hattori, S. Kito, Y. Murakami and S. Yoneda, to be presented in 2nd International Symposium on Computer Applications to Materials and Molecular Science and Technology, Sept. 1992, Yokohama, Japan.

DISCUSSION

Q: Y. Sun (China)

1) How do you deal with the conflicts between the intermediate results from the different knowledge bases ?

2) Have you taken into consideration the activity, selectivity and deactivation?

A: T. Hattori

1) In the INCAP, the catalyst design problem is decomposed into five subproblems, and the INCAP consists of five subsystems corresponding to individual subproblems. However, since the subsystems have different tasks and characteristics from each other, it seems impossible that the intermediate conclusions from the different subsystems come into conflict with each other.

In each of subsystems, the following conflict resolution strategies, which are frequently used in the conventional knowledge-based systems, are used: the first-matched rule is preferred and the most recently used rule is preferred.

2) We have adapted the integrated API as a measure of catalytic performance including the activity and the selectivity. But, as shown in the text, it does not seem to be an adequate index, when the API contains some errors. Then, we have introduced new indexes, shown in Figures 5 and 6, representing the activity and the selectivity separately. In an advanced system, overall performance of catalyst will be presented by integrating both indexes, but at present we do not intend to include the deactivation.

Q: A. T. Bell (USA)

A critical input to your algorithm is the API. This index requires knowledge of the relative activities of a series of catalysts for some test reactions. Since the activation energies of different catalysts, for the same reaction, can be different, it is possible that the API for a given catalyst depends on the temperature. How does your program take this into account?

A: T. Hattori

It is highly recommended to develop or to start with a small expert system possessing a realistic target, but not a large system applicable for general purpose. So, we have developed the first version of INCAP presented in this paper by taking the oxidative dehydrogenation of ethylbenzene as an example. The activity data for the API have been taken from the results of reactions in the temperature range of 600-800 K which is close to that of the present reaction. The second version for the selection of multicomponent catalysts is also based on the assumption of the same temperature range. Therefore, it is unnecessary in these versions to consider the question you raised. However, account by using an evaluation factor (E_f) which expresses the adaptability of API to the problem reaction. The E_f , which takes numerical values from ten to one representing the adaptability, should be modified according to the temperature difference.

Q: M. M. Bhasin (USA)

I commend you on very good correlations and predictions of new compositions. My question relates to the input activity data you used. Would you tell us for what reactions the activity data was used and was it based on reaction rates per gram, per surface area, i.e., turnover number or some other basis ?

A: T. Hattori

The API in the first version of INCAP includes the activities for the complete oxidations and partial oxidations of propene, butene and toluene, and thereafter some activity data for the oxidations of ethene, methane, hydrogen, and so on are added. The heat of formation and the electro-conductivity of oxide are also included as a measure of the activity for complete oxidation, though small values are allocated to the evaluation factors (E_f) for these mentally

as well as the partial charge of oxygen in oxide and the electronegativity of cation as a measure of the acid and base properties with small E_f.

The activity data used for the API were, in most cases, based on the rate per surface area, but some activity data per weight are also used, because we prefer to include more API data. It should be noted that the API is not quantitative parameter, but only semi-quantitative one.

Q: V. Ponec (The Netherlands)

Would you specify from which reactions a rather high activity index for SiO_2 has been derived, as well as the high selectivity of this catalyst ?

A: T. Hattori

The API includes the acid and base properties of oxides as well as the activity data for some catalytic reactions. The INCAP reasons that the promoter should possess or synergistically generate the acidic property of medium strength based on acid-base mechanism for the target reaction (7), but not strong redox activity, strong acidic property and partial oxidation activity. The high activity of SnO_2-SiO_2 catalyst is derived from the acidic property of SiO_2, and the high selectivity from the poor redox property and the poor partial oxidation activity of SiO_2.

Q: J. M. Thomas (United Kingdom)

In multicomponent catalysts, it is known that the overall activity is greater than the sum of the activities of the individual components: in other words there is synergy. How does your expert system approach cope with this synergy ? I thought I saw in your final slide reference to neural networks.

A: T. Hattori

In the oxidative dehydrogenation of ethylbenzene on promoted SnO_2 catalysts which is taken in the present study as an example, the most important synergy is considered to be the acid strength of mixed oxide catalysts. The direct approach to this problem has not been taken in the INCAP, but the problem is dealt with indirectly: The electronegativity of promoter cation is used as a measure of the acid strength of synergistically generated acid sites, because the acid strength of mixed oxides is reported to increase with the averaged electronegativity of cations of constituent oxides [1].

We have found that the acid strength of binary oxides can be estimated by using a neural network. Or, in other words, the acid strength can be represented as a complicated function, which is given as a network pattern in a computer, of several physical/chemical properties of constituent oxides. In one of the test-versions of the INCAP, the network pattern thus obtained is used as a subsystem for this problem.

[1] K. Shibata et al., *Bull. Chem. Soc., Japan*, **46**, 2895 (1973)
[2] *IEC. Research*, **31**, 979 (1991)

Q: F. Kapteijn (The Netherlands)

It is a great challenge to design catalysts on the basis of an expert system. What are your expectations in this respect? How far do you think you can come to predict a catalyst composition for a given reaction by this approach.

A: T. Hattori

The catalyst design is a big and complicated problem which requires a lot of experimental works for catalyst preparation, characterization, testing and so on. The present study may suggest that the expert system will be useful to reduce the number of repetitions in the trial-and-error processes of experimental works. We expect that in near future the catalysts can be designed more efficiently by the aid of computer system.

As for the prediction of catalyst composition, it is difficult to say how far it is, because it differs from case to case. The most essential knowledge for the prediction of the composition

is that of the synergistic effect. Then the synergistic effect is less significant or less complicated, the present approach may be useful to some extent. However, another approach will be necessary for the prediction of catalyst composition for general cases. A neural network will be one of the candidates for such purpose.

Q: K. Zheng (United Kingdom)

It seems to me that your expert system only considers the bulk composition of certain elements and compounds. How could you take into account the fact that a small amount of surface segregation could have a drastic effect on the activity and selectivity of catalysts ?

A: T. Hattori

The performance of catalyst depends on many factors such as the catalyst component, the composition, the microscopic and macroscopic structure, and so on. In other words, the total problem of catalyst design consists of many subproblems each of which seems difficult to solve. The first subproblem to be solved is obviously the selection of catalyst components.

The present study aims to solve the first subproblem by the expert systems approach, and this aim has been achieved without taking the other subproblems into account. The scatters in the correlations shown in Figures 5 and 6 may be due to the other factors, possibly including the surface segregation, and these subproblems might be the subjects for future studies.

Guczi, L. *et al.* (Editors), *New Frontiers in Catalysis*
Proceedings of the 10th International Congress on Catalysis, 19-24 July, 1992, Budapest, Hungary
© 1993 Elsevier Science Publishers B.V. All rights reserved

METAL OXIDE VAPOUR SYNTHESIS (MOVS): A NEW PREPARATIVE METHOD FOR HETEROGENEOUS METAL OXIDE CATALYTIC SYSTEMS

E. C. Alyea, K. F. Brown, K. J. Fisher and K. D. L. Smith

Guelph-Waterloo Centre for Graduate Work in Chemistry (GWC)^2, Guelph Campus, Department of Chemistry and Biochemistry, University of Guelph, N1G 2W1 Guelph, Ontario, Canada

Abstract

Metal Oxide Vapour Synthesis (MOVS) has been developed as a new methodology for the preparation of unsupported and supported heterogeneous metal oxide systems. The production of single and mixed metal oxide systems by the cocondensation of volatile metal oxides and a suitable solvent, and if desired, subsequent deposition on a support, is described. Other metal oxides have been incorporated into the preparative procedure by the addition of alkoxides and other soluble metal salts to the condensate, with subsequent conversion to metal oxide forms by calcination. To illustrate the potential of the MOVS methodology for catalyst design, examples are cited of the unique nature and high efficiency in catalytic conversions of molybdenum oxide systems derived from α-MoO_3 by evaporation and cocondensation with methanol.

Introduction

Perusal of the vast literature describing preparative methods for heterogeneous metal oxide catalytic systems indicates the dominance of traditional methods such as impregnation and precipitation [1]. Deposition of soluble metal salts on a support, with subsequent drying and calcination (usually above 500°C), gives the heterogeneous metal oxide catalyst. The ease of incorporating mixed metal oxide and promoter species is a distinct advantage of such classical methods. Modification of the traditional procedures to include organometallic and carbonyl precursors can give highly active catalysts for many organic transformations. An elegant example of such catalyst design for specific activity, as well as spectroscopic characterization of the active sites, is the anchoring of tetra-π-allyl dimolybdenum on silica and alumina by Iwasawa and co-workers [2]. The continuing need for metal oxide catalytic systems of improved dispersion, higher activity and greater selectivity has lead to our development of a new methodology of wide aplicability, Metal Oxide Vapour Synthesis (MOVS).

Our MOVS preparative technique utilizes and extends Metal Vapour Synthesis (MVS) technology, largely developed in the 1970's for the synthesis of novel organometallic compounds [3]. Indeed, MVS itself can be used to obtain zerovalent metal atom slurries which can be dispersed on solid supports and into zeolite frameworks in one step procedures [4, 5, 6]. The enormous potential of MVS for the preparation of new materials and catalytic systems has already been suggested [7]. In initiating studies of heterogeneous catalysts, we reported earlier that molybdenum atoms dispersed on γ-alumina by MVS could be oxidized to a supported oxide form [8]; the generality of the method for converting MVS-deposited metal atoms into heterogeneous metal oxide catalytic systems on any suitable support is outlined in a patent [9]. The present paper describes the general MOVS methodology for the cocondensation of volatile metal oxides with an organic solvent and the subsequent deposition of unsupported and supported metal oxide catalytic systems [9]. A preliminary communication outlining the method highlighted the high efficiency of molybdenum oxide catalysts obtained by MOVS for the partial oxidation of methanol [10].

Experimental

'TORROVAP' Reactor- purchased from Torrovap Industries Inc., Markham, Ontario.

Figure 1 illustrates the 5L rotary reaction vessel of the Torrovap system which encases all the major components involved with a description of the synthetic MOVS method. The reaction vessel encloses a dual resistive evaporation source, heated solvent inlet with shower head, and a tube for product extraction to a Schlenk flask.

A rotary pump is used for initial pumpdown and system roughing to 10^{-3} torr. An oil diffusion pump increases the vacuum to 10^{-7} torr and is protected by a nitrogen trap (also called a cryostatic pump) which prevents the backstreaming of pump oil as well as prevents its contamination by ligand and solvent chemicals used in the synthesis process.

In MVS, the vacuum (10^{-6} torr) is necessary for operation of the electron guns as well as preventing metal atom agglomeration, oxide formation and sometimes even product decomposition. Furthermore, metal atoms can be pyrophoric in the presence of oxygen. Thus, vacuum is a crucial part of the MVS methodology. However, it should be stressed that in the MOVS procedure, the primary role of a vacuum is to reduce the boiling or sublimation point of the metal oxides used. Thus, a vacuum increases the efficiency of the resistive furnace, which has a practical limit of 1500°C, to generate vapours from metal oxides of low volatility, such as Nb_2O_5 (mp 1485°C, bp 2927°C) or WO_3 (mp 1473°C, bp 1850°C)[11]. More volatile metal oxides, such as MoO_3 (mp 795°C, bp 1257°C) or V_2O_5 (mp. 690°C, bp 2052°C)[9], do not require high vacuum. Our evaporation source generally consists of a GTE Products Corp. integral tungsten/alumina crucible, of which several sizes are available.

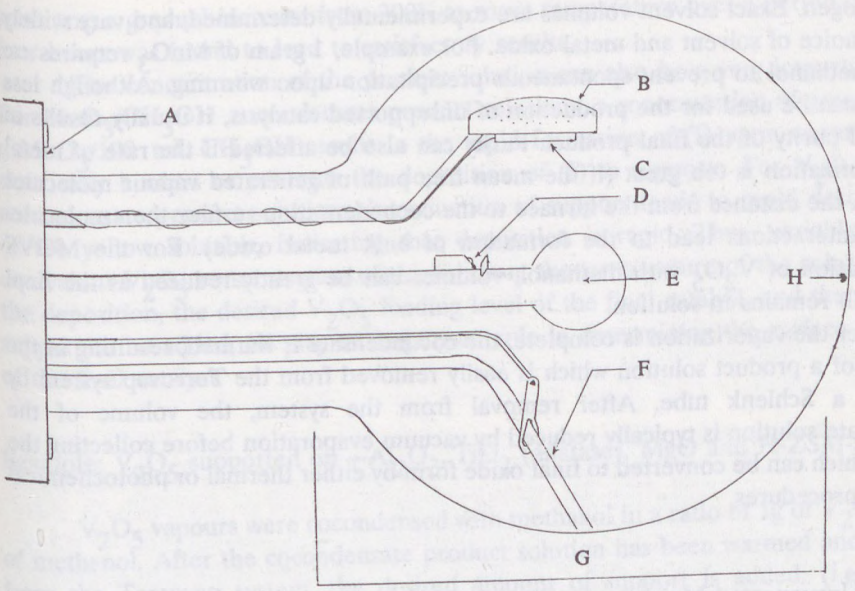

A- Rotary Vacuum Seal
B- Solvent Inlet Head
C- Button Heater
D- Quartz Microbalance
E- Evaporation Source
F- Schlenk Tube
G- Liquid N_2 Bath
H- 5L Rotary Reaction Vessel

Figure 1. The rotary reaction vessel of the Torrovap system.

Catalyst Syntheses

A) Unsupported MOVS Catalysts

Vaporization is usually performed under a vacuum of ca. $3x10^{-6}$ torr. The filament current of the resistive furnace is slowly increased to provide the temperature necessary for vaporization. Under typical operating conditions of the Torrovap, MoO_3 requires 18-20 amps, V_2O_5 requires 20-25 amps, while Nb_2O_5 or WO_3 require full scale of about 30 amps. It should be remembered that filament current is a function of the composition, length and thickness of the resistive filament, thus the maximum current is variable.

Throughout vaporization, a continual flow of solvent is cocondensed with the metal oxide vapours on the sides of the rotating reactor vessel, which is immersed in

liquid nitrogen. Exact solvent volumes are experimentally determined, and vary widely with the choice of solvent and metal oxide. For example, 1 gram of MoO_3 requires ca. 100 mL methanol to prevent spontaneous precipitation upon warming. Although less methanol can be used for the production of unsupported catalysts, it usually results in diminished purity of the final product. Purity can also be affected if the rate of metal oxide vaporization is too great (if the mean free path of generated vapour molecules is less than the distance from the furnace to the cocondensation surface then molecule-molecule interactions lead to the formation of bulk metal oxide). For the MOVS cocondensation of V_2O_5 with methanol, volumes can be greatly reduced as the final product still remains in solution.

After the vaporization is complete, the cocondensate is warmed, resulting in the formation of a product solution which is easily removed from the Torrovap system by means of a Schlenk tube. After removal from the system, the volume of the cocondensate solution is typically reduced by vacuum evaporation before collecting the product, which can be converted to final oxide form by either thermal or photochemical activation procedures.

Example: Unsupported Molybdenum Oxide Catalyst, Photoactivated Form

MoO_3 vapours were cocondensed with methanol in a ratio of 1 gram MoO_3:100 mL of methanol. The cocondensate product solution was allowed to warm to room temperature and precipitation of $Mo_2O_5(OCH_3)_2 \cdot 2CH_3OH$ (I) occurred over 24 hours; the white product was recovered after vacuum evaporation to insure complete formation of (I). BET surface area of (I) was found to be 7.0 m^2/g. The recovered product was lightly ground to produce a uniform powder and then exposed to air and fluorescent light for up to 3 months. During this time (I) turned a light medium blue in colour. This procedure could be accomplished within 24 hours by exposure of (I) to ultraviolet radiation with a Gaussian distribution of less than 350 nm. The photochemically altered molybdenum oxide matrix was converted to its final activated form (a blue amorphous powder) by heating to 280°C in the reactor system under a flow of air.

B) Supported MOVS Catalysts

Supported MOVS catalysts can be readily obtained by introducing a desired support to the MOVS cocondensate product solution extracted from the Torrovap system. In general, once the support has been added to the MOVS cocondensate product solution, the temperature of this solution can be maintained at some fixed value or can be gradually allowed to increase to room temperature at a desired rate. Adjustment of the temperature of the MOVS cocondensate product solution can effect the dispersion properties of the final supported catalysts and therefore, should be experimentally optimized for each case. For MoO_3/CH_3OH cocondensate product

solutions, a gradual increase from 200K to room temperature over a period of three to four hours was found to lead to satisfactory results.

The concentration of the product solution can also be a very important factor. For MoO_3/CH_3OH cocondensate product solutions, a concentration of greater than 1 g MoO_3/100 mL CH_3OH results in the rapid formation of (I) upon warming, which drastically hinders or prevents the deposition of (I) to supports. For V_2O_5/CH_3OH cocondensate product solutions, introduction of support leads to rapid decolorization of the yellow solution, indicating that deposition is rapid. Thus, variables such as equivalent V_2O_5 concentration of the solution, the temperature of the solution during the deposition, the desired V_2O_5 loading level of the final catalyst, and the amount of support to be added, all play an important role in determining the surface properties of the final catalyst.

Example: V_2O_5 supported on γ-Al_2O_3, TiO_2 (anatase), MgO and H-ZSM-5

V_2O_5 vapours were cocondensed with methanol in a ratio of 1g of V_2O_5 :50 mL of methanol. After the cocondensate product solution has been warmed and extracted from the Torrovap system, the desired amount of support is added. (i.e. for 10% loading, 10g of support would be added to the cocondensate product solution in which 1g of V_2O_5 had been cocondensed). This mixture was stirred by a magnetic stirrer. If powders are desirable, a magnetic stirrer works well, however, if the mesh size of the support is to be maintained, then rotation of the flask on a rotary evaporator without vacuum works well. Typically, these solutions are stirred for 24 hours, then the impregnated supports are recovered after concentration by vacuum evaporation, and converted to their final activated oxide form by thermal calcination for four hours at 400°C.

C) Modification of MOVS Catalysts

Incorporation of a second metal oxide component can be readily accomplished by co-evaporation and cocondensation as the Torrovap system is equipped with a dual resistive evaporation source. Thus, mixed metal oxide systems, such as $MoO_3/WO_3/CH_3OH$ or $MoO_3/V_2O_5/CH_3OH$ are readily obtained by placing the appropriate ratio of metal oxides into the two crucibles. These mixed metal oxide cocondensations work well as long as both components have appreciable vapour chemistry. Syntheses of this type of cocondensation follow the methods as outlined in A) and B).

Metal oxides which do not have appreciable vapour chemistry can be incorporated by the addition of soluble metal alkoxides and other soluble metal salts to the MOVS cocondensate product solution. For MoO_3/CH_3OH systems, the addition of these soluble complexes are best performed before the precipitation of (I) occurs.

Example: Addition of $Ti(OC_3H_7)_4$ to MoO_3/CH_3OH cocondensate

MoO_3 was cocondensed with methanol as described in A). After the cocondensate product solution was extracted from the Torrovap system, and placed in an ethanol/dry ice cold bath, titanium isopropoxide was added dropwise to the product solution via a syringe. During this slow dropwise addition, the product solution was stirred resulting in the slow precipitation of a pale yellow solid. After 24 hours, the pale yellow powder was recovered after removal of the solvent by vacuum evaporation. The powder was thermally activated at 400°C for 4 hours.

Results and Discussion

To our knowledge there are no previous reports of the preparation of heterogeneous metal oxide catalytic systems by the cocondensation of a volatile metal oxide with a suitable solvent, followed by deposition on a solid support. Indeed, there are few reports of metal oxide-solvent cocondensations [3]; a pioneering study by Timms and Cook [12] involved MoO_3 and WO_3 and a few common solvents such as acetone and methanol. Following McCarron and co-worker's formulation of a product derived from $MoO_3 \cdot 2H_2O$ and methanol as $Mo_2O_5(OCH_3)_2 \cdot 2CH_3OH$ (I)[13], DeKock and McAfee [14] assigned their MoO_3-methanol cocondensate product as (I). While all of these earlier workers realized, through thermal and photochemical decomposition studies, that (I) was a potential model for the partial oxidation of methanol to formaldehyde, no attempt to support (I) and test its catalytic activity was reported. The theoretical prediction by Allison and Goddard [15] that "dual dioxo dimolybdenum sites", assumed to exist in (I) [15], should greatly enhance catalytic activity for oxidative dehydrogenation, together with the practical demonstration by Iwasawa and co-workers of the high activity of their dimolybdenum catalysts [2] prompted us to begin our MOVS studies by supporting (I) on γ-alumina and testing its catalytic performance for the partial oxidation of methanol. The thermal activation at 550°C of this deposited precursor gave a supported catalyst with an improved performance compared to a commercial $10\%MoO_3/\gamma\text{-}Al_2O_3$ catalyst [8]. Subsequently we found that either unsupported (I) or γ-alumina supported (I), if first photoactivated, yielded excellent catalysts with 100% conversion and 96% selectivity to formaldehyde at temperatures ca. 150°C lower than a traditional standard, $Fe_2(MoO_4)_3/MoO_3$ [10]. This success prompted us to prepare other supported catalysts by the MOVS methodology.

Synthetic details for the unsupported, photoactivated MOVS molybdenum oxide catalyst are provided in the Experimental. The use of a large excess of methanol ensures a slow deposition of (I) over several hours and consequently higher purity. Our recent characterization studies [16], which complement the earlier results of DeKock and McAfee [15] and McCarron and co-workers [14], confirms the presence of dual dioxo dimolybdenum sites and methoxy bridges in (I). After photoactivation and heating

to 280°C, the product is a light blue powder which has been shown by XRD to contain α-MoO_3 and an amorphous component. Particle sizes were estimated from SEM micrographs of 200K magnification to be less than 50 nm [10, 16]. After catalytic testing for methanol conversion the BET surface area was found to be 25 m^2/g and the pore radii range was 16 to 62 angstroms.

Retarding the precipitation of (I) by employing a 200-250 fold excess of methanol in the cocondensation of MoO_3 gives a solution upon warming to room temperature. In addition to the deposition of (I) on alumina as already described [8, 16], we have used a variety of supports for (I), such as H-ZSM-5 and other metal oxides. Preliminary testing results for some of these MOVS molybdenum oxide catalysts on Al_2O_3, TiO_2 (anatase) and SnO_2, activated photochemically and followed by heating to 280°C, indicate high efficiency for the partial oxidation of ethanol to acetaldehyde [17]. The dispersion obtained for a 10% loading (equivalent MoO_3 by AA) on SnO_2 is shown in the micrograph presented in Figure 2a).

In anticipation that other highly dispersed heterogeneous metal oxide catalysts could be obtained by the MOVS methodology, we have cocondensed volatile metal oxides such as WO_3, Nb_2O_5, V_2O_5, FeO, etc. [11] with suitable solvents for subsequent deposition on various supports. The specific example of V_2O_5 is described in the Experimental, and its dispersion on TiO_2 (anatase) is shown in the micrograph presented in Figure 2b). Furthermore, mixed cocondensations involving two metal oxides are readily performed in the Torrovap apparatus. The micrograph of a MoO_3/WO_3 catalyst obtained by deposition from methanol is shown in Figure 2c). Obviously there are a multitude of possibilties to explore utilizing the MOVS methodology, using characterization and testing results as guidelines of which are most worthwhile.

Since many metal oxides are not volatile enough (in practice, if the m.p. is greater than ca. 1500°C) or decompose upon heating [11] their incorporation into a multicomponent catalyst cannot be accomplished by a direct MOVS procedure. However, adding a soluble salt or organometallic compound of the desired metal oxide to the MOVS cocondensate of another metal oxide can give, after deposition and calcination, a mixed metal oxide catalytic system. Alternatively, a promoter or other metal oxide can be added to a catalyst derived by MOVS by the usual wet impregnation method. The specific example outlined in the Experimental section is the preparation of a MoO_3/TiO_2 catalyst by the addition of $Ti(OPr^i)_4$ to the cocondensate of MoO_3 and methanol. The micrograph of the derived catalyst is shown in Figure 2d). The amorphous nature of the product, and/or the small particle sizes produced by the MOVS method, is indicated by XRD. Indeed, XRD generally shows similar results for all the MOVS catalytic systems, with only d-spacings due to the supports being observed. Further details of characterization studies (BET, XRD, FTIR, AA, SEM) will be presented at the conference. Examples of the high efficiency of the MOVS catalytic systems for some selective oxidations will also be described as illustrations of the potential of the MOVS methodology for the preparation of heterogeneous metal oxide systems with excellent catalytic activity.

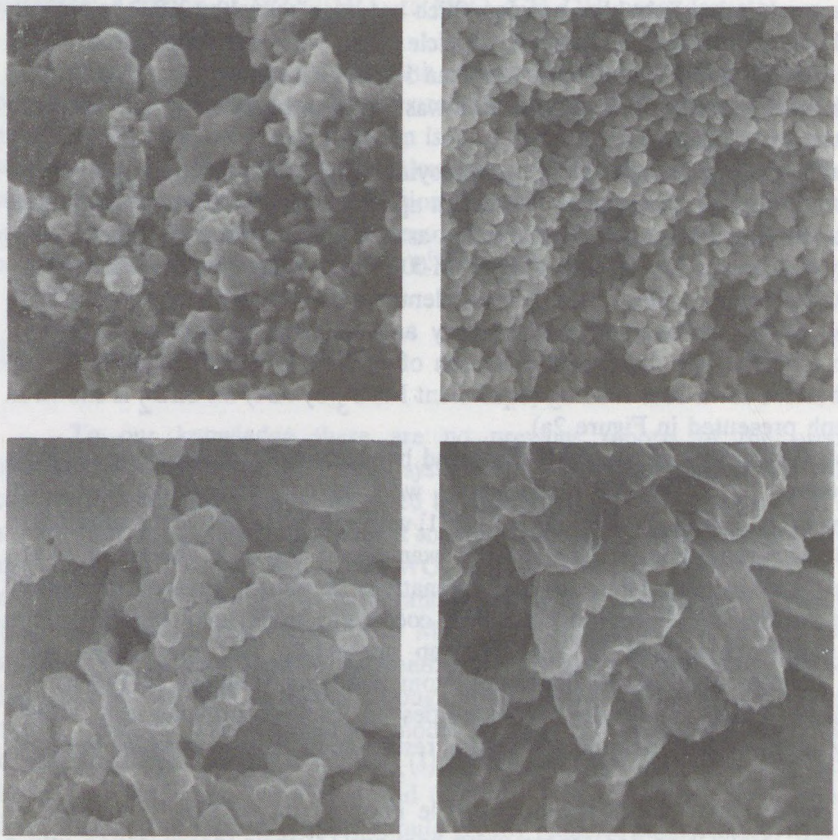

Figure 2. Scanning electron micrographs of MOVS catalysts (clockwise from upper left)
a) 10% equivalent MoO_3 loading on SnO_2; 30K, dotted scale = 1.0 μm
b) V_2O_5 on TiO_2 (anatase); 20K, dotted scale = 1.5 μm
c) unsupported mixed MoO_3/WO_3; 20K, dotted scale = 1.5 μm
d) MoO_3/TiO_2 made by $Ti(OPr^i)_4$ addition; 20K, dotted scale = 1.5 μm

Acknowledgements

Initial studies were funded by an Imperial Oil Ltd. University Research Grant and a NSERC Canada operating grant. Current investigations are funded by a NSERC Canada strategic grant.

References

1. B. Delmon, P. Grange, P.A. Jacobs and G. Poncelot (eds.), Preparation of Catalysts, Vol IV, Studies in Surface Science and Catalysis, 31, Elsevier, Amsterdam, 1987.
2. (a) Y. Iwasawa, H. Kubo, M. Yamagishi, and S. Ogasawara, Chem. Lett., (1980) 1165.
   (b) Y. Iwasawa, S. Ogasawara, Y. Sato and H. Kuroda in Proceedings of the Climax Fourth International Conference on the Chemistry and Uses of Molybdenum, H.F. Barry and P.C.H. Mitchell (eds.), Climax Molybdenum Company, Ann Arbor, Michigan, 1982, p. 283.
3. J.R. Blackborow and D. Young, "Metal Vapour Synthesis in Organometallic Chemistry", Springer-Verlag, New York, 1979.
4. G.A. Ozin, M.P. Andrews, L.F. Nazar, H.X. Huber and C.G. Francis, Coord. Chem. Rev., 48, (1983) 203.
5. M.P. Andrews in "Experimental Organometallic Chemistry", A.L. Wayda and M.Y. Darensbourg, M.Y. (eds), ACS Symposium Series, Chicago, 1985, ACS Press, Washington D.C., 1987.
6. K.J. Klabunde, J. Mol. Catal., 21, (1983) 57.
7. G.A. Ozin, Chem. Tech., 15, (1985) 488.
8. E.C. Alyea, K.F. Brown and K.J. Fisher, Proceedings of the 11th Canadian Symposium on Catalysis, Halifax, July 15-18, 1990, p.364.
9. E.C. Alyea, K.F. Brown and K.J. Fisher, U.S. Patent 5 047 379 (1991).
10. E.C. Alyea, K.F. Brown and K.J. Fisher, J. Mol. Catal., 63, (1990) L11.
11. G.V. Samsonov, (ed),"The Oxide Handbook", 2nd edition, Plenum Press, New York, 1982, p. 51-57.
12. P.L. Timms and N.D. Cook, J. Chem. Soc. Dalton Trans., (1983) 239.
13. E.M. McCarron, R.H. Staley and A.W. Sleight, Inorg. Chem., 23, (1984) 1043.
14. C.W. DeKock and L.V. McAfee, Inorg. Chem., 24, (1985) 4293.
15. J.N. Allison and W.A. Goddard III, J. Catal., 92, (1985) 127.
16. E.C. Alyea and K.F. Brown, "Proceedings of the 12th Canadian Symposium on Catalysis", Banff, May 1992, Elsevier, Amsterdam, 1992.
17. E.C. Alyea, K.F. Brown, L. Durham and I. Svazic, Proceedings of the 12th Canadian Symposium on Catalysis, May 1992, Elsevier, Amsterdam, 1992.

DISCUSSION

Q: J. M. Thomas (United Kingdom)

Molybdenum oxide is very stable in an electron beam, and a great deal is known about the structure of the stoichiometric MoO_3 and the sheer phases (Mo_nO_{3n-1}, Mo_nO_{3n-2},..., n=10-20) of this oxide. Even material that appears X-ray amorphous frequently turns out, not unexpectedly, to possess an ordered structure at the local level. High-resolution electron microscopy ought to be used to characterize your fascinating new catalyst. You would, I imagine, soon find but if, locally, there is α-MoO_3 or any other corner showing (or edge-showing) MoO_6 present.

A: E. C. Alyea

We have initially examined the surface morphology of our MOVS catalysts using scanning electron microscopy, which was more readily available. Now that SEM shows that homogeneous dispersions of fine particles are commonly achieved for the various types of supported catalysts (the original 10 division, 18 mm dotted scales in Figure 2 were omitted during the 50% photoreduction; i.e. the dotted scales are 9 mm long in the published SEM Figure), we certainly plan to use TEM for higher resolution studies.

Q: G. B. Fisher (USA)

What is the range of particle sizes you can make for MoO_3, for other oxides, and for base metals, if possible? How does the particle size typically depend on parameters such as evaporation rates of (i.e. oxygen) pressure or vacuum, solvent choice, time in solvent, etc. ?

A: E. C. Alyea

The particle sizes as estimated by SEM are reproducibly found to be in the 100 nm range for all of the MOVS catalysts. An unsupported photoactivated sample derived from α-MoO_3 had particles in the 15-50 nm range. The optimization of experimental conditions for each catalyst type, as the solvent choice, concentration and deposition rate, is undergoing further development.

Q: J. W. Geus (The Netherlands)

My question is concerned with the application of the oxide from the methanol solution/suspension onto suitable catalyst supports. The question therefore is dealing with the solution/suspension resulting from the vapor deposition usually after concentration by evaporation of part of the liquid. To prevent deposition of the active precursor mostly at the external edge of the bodies of the support, pore-volume impregnation is to be preferred. To achieve a significant loading of the support, a fairly high concentration of the active precursor in the solution/suspension is usually required with the pore volumes of most supports. During concentration by evaporation of methanol formation of colloidal particles of the active precursor generally will result. In view of the low diffusitivies of colloidal particles and of filtration effects a non-uniform distribution of the active precursor throughout the support may result.

Have you data about the penetration of active precursors from concentrated solutions/suspensions into layers of usual support, such as, silica or alumina?

A: E. C. Alyea

As described in the experimental section, many variables are involved and must be controlled in order to achieve a uniform dispersion of the active precursor throughout the support. In the case of α-MoO_3 cocondensation with MeOH, an excess of the solvent allows a solution to be maintained for 24 hours or more; the presence of MoO_3.3MeOH is suggested by the +66 ppm resonance observed by ^{95}Mo NMR spectroscopy. It appears that the insoluble polymeric precursor, $Mo_2O_5(OCH_3)_2.2CH_3OH$ (I), may deposit directly on the supports rather than by prior formation of colloidal particles.

Although our preliminary characterization studies (see ref. 16, now published in Vol. 73 of Studies in Surface Science and Catalysis, p. 279), for further details of the catalysts derived from α-MoO_3 indicate that good distributions of amorphous metal oxide layers with high surface areas may be achieved by MOVS, other surface studies (as TEM and PES) are planned to gain more information on the dispersion and penetration properties of these new catalysts.

Q: Y. Iwasawa (Japan)

You showed a nice crystallographic picture of a molybdenum dimer having methoxy-bridging. Do you suggest that an active intermediate at the steady state of methanol oxidation is also the bridging-methoxy species ?

A: E. C. Alyea

X-ray analysis of the crystalline compound obtained during the epoxidation of cyclohexene by the precursor (I) verified the presence of two methoxy-bridges. This result, coupled with the high efficiency of methanol oxidation (ref. 10), does indeed suggest the presence of "dual dioxo-molybdenum active sites", whose importance was theoretically predicted (ref. 15).

Q: J. S. Yoo (USA)

1) How does the catalytic activity differ between your MOVS catalyst and the classical vapor deposited counter part prepared from volatile precursor such as MoO_2Cl_2 and $MoCl_3$ for the oxidation reactions under normal pressure to produces aldehyde and epoxyde ?

2) Please tell me what was the main chemical cause for your observed remarkable catalytic activity beside the well dispersed particle size effect ?

A: E. C. Alyea

We have not yet made a direct comparison of catalytic activity between our MOVS catalyst derived from α-MoO_3 and catalysts obtained from more volatile molybdenum precursors. Our initial comparison studies (8, 10) showed that either unsupported (I) or γ-alumina supported (I) yielded excellent catalysts with 100% conversion and 96% selectivity for methanol conversion to formaldehyde at temperatures ca 150 ^{0}C lower than the commercial catalyst, $Fe_2(MoO_4)_3/MoO_3$.

The unique dimeric active sites, which are maintained under catalytic conditions (ref. 16), undoubtedly augment the activity due to the high dispersion and surface areas produced by MOVS.

Q: M. M. Bhasin (USA)

Would you clarify if the much higher activity you observed for MOVS synthesized materials is based on measured surface Mo concentration or per gm or surface area bases! Second question is regarding the stability of these materials under reaction conditions or heat alone since they may be metastable or unstable.

A: E. C. Alyea

Our activity calculations for methanol conversion were based on per gram of catalyst. Since typical loadings were in the 5-10% range for the MOVS catalysts derived from α-MoO_3, the latter catalysts displayed activities that were 100-fold or greater than that observed for the standard catalyst. These catalysts are also showing high efficiencies for ethanol oxidation to acetaldehyde (ref. 17), olefin metathesis and oxidation, and syn gas conversions.

The MOVS catalysts we have tested for alcohol oxidation are stable, after activation to 280 ^{0}C, during repeated cycles to 400 ^{0}C over several days.

Q: M. A. Baltanas (Argentina)
Could you please comment on:
1) the long-term stability of your highly dispersed supported oxides, and
2) the feasibility of scaling-up these preparates for later industrial application ?

A: E. C. Alyea
As mentioned above, the supported MOVS catalysts generally have good stability during repeated testing. One exception was (I) deposited on SiO_2, which reverted to α-MoO_3 upon heating to 400 ^{0}C; XRD also showed the presence of α-MoO_3 when unsupported (I) was heated to 280 ^{0}C.
Since α-MoO_3 is both inexpensive and readily volatile (even without a high vacuum), scale-up to an industrial scale is both feasible and anticipated (ref. 9).

Q: J. C. Volta (France)
Can you control the orientation of your MoO_3 on the different support (TiO_2, γ-Al_2O_3, etc,) by your MOVS technique? You do not give any electron diffraction studies on your materials ?

A: E. C. Alyea
The MOVS methodology leads to the deposition of amorphous metal oxide layers on the various supports. Whether any short-range order exists will be determined in future surface studies using TEM.

Q: H. L. Krauss (Germany)
How did you count/characterize the active sites/coordinatively unsaturated sites in your catalysts? How many vacant sites do you claim to exist at the dimeric surface species especially ?

A: E. C. Alyea
This paper, and our work to date on MOVS catalysts, has focused on the novel synthetic procedures for fabricating several varieties of heterogeneous metal oxide catalytic systems. Since initial catalytic testing for selective oxidations have proven to be very promising, further surface characterization studies are therefore warranted. Our first use of TPD/R experiments for surface site identification and characterization has been reported [1] and we plan to answer many "characterization" questions before the next Catalysis Congress.

[1] E. C. Alyea and V. Moravek, in *Studies in Surface Science an Catalysis*, **Vol. 73**, p. 315, (1992)

Guczi, L. *et al.* (Editors), *New Frontiers in Catalysis*
Proceedings of the 10th International Congress on Catalysis, 19-24 July, 1992, Budapest, Hungary
© 1993 Elsevier Science Publishers B.V. All rights reserved

DESIGNING OF NEW CATALYSTS FOR OLEFIN METATHESIS ON THE BASE OF PHOTOREDUCED SILICA-MOLYBDENA

V. B. Kazansky, B. N. Shelimov and K. A. Vikulov

N. D. Zelinsky Institute of Organic Chemistry, Russian Academy of Sciences,
Moscow 117 913, Russia

Abstract

Cyclopropane (CP), methylcyclopropane (MCP) and cycloheptatriene (CHT) chemisorption on Mo/SiO_2 catalysts photoreduced in CO was found to result in a sharp increase of their specific activities in olefin metathesis (propene, 1-hexene, ethyl oleate). IR and UV-VIS spectroscopic studies revealed that promoting effect of CP, MCP and CHT treatment was associated with the formation of thermally stable carbene complexes $Mo{=}CH_2$ and $Mo{=}CH{-}CH_3$, arising from CP, MCP and CHT interaction with low coordinated Mo^{4+} ions in photoreduced Mo/SiO_2. IR data showed fast reversible transformation of $Mo{=}CH_2$ to $Mo{=}CH{-}CH_3$, thus providing the first direct spectroscopic confirmation of a chain carbene mechanism of propene metathesis. Mo=C bond energy in $Mo{=}CH_2$ (-435±25 kJ/mole) was determined from calorimetric measurements.

Introduction

At present it is generally accepted that catalytic olefin metathesis reaction proceeds via a chain mechanism, involving as key intermediates metal-carbenes and metallacyclobutane complexes (mainly, those of Mo, W, and Re) [1]. Most convincingly, participation of these intermediates in the metathesis has been demonstrated for homogeneous catalytic systems. Later this concept was extended on heterogeneous metathesis, and, in particular, on supported molybdena oxide catalysts [2].

Perhaps, the most intriguing step in mechanism of the catalytic metathesis is the initiation, that is generation of carbene species further participating in the chain processes. It is generally believed that in real catalytic systems carbene species are most likely derived from a decomposition or transformations of organo-metallic compounds, formed by alkylation of transition metal salts with co-catalysts or promoters (such as alkyl tin or alkyl aluminum compounds) [1], for example, $L_nM{-}CH_2R$ --->

——> $L_nHM{=}CHR$. However contribution of such a transformation to the overall process of metallocomplex decomposition is very low (1-3 %).

Another possible way to produce metal-carbenes is a direct interaction of olefin molecules with coordinatively unsaturated transition metal ions, for instance, via an intramolecular 1,2-H atom transfer or olefin π-complex conversion to η^3-allyl complex, followed by its transformation to a metallacyclobutane intermediate. However, these reactions should be regarded only as a hypothesis, because corresponding carbene complexes have been never isolated and characterized by any physico-chemical techniques.

In the present work a new approach to designing of metathesis catalysts was employed, based on the combination of low-temperature selective photoreduction of silica-molybdena in carbon monoxide along with subsequent treatment with carbene-generating compounds (cyclopropane, methylcyclopropane, or cycloheptatriene). This way enables to obtain highly active catalysts and produce high concentrations of the surface carbene complexes, sufficient for their spectroscopic identification.

Experimental

Catalyst samples were prepared by routine impregnation of silica with an aqueous solution of ammonium paramolybdate, followed by calcination in air at 773 K and vacuum treatment at 1073 K. Mo-loadings were varied from 0.1 up to 2.5 wt %. Photoreduction was carried out by illumination with unfiltered light of a Hg-lamp in CO atmosphere at room temperature, followed by evacuation at 473 K. The average oxidation state of Mo ions was calculated from the amount of carbon dioxide formed during photoreduction and/or from the amount of oxygen consumed during reoxidation of photoreduced samples at 773 K.

The next step of the activation procedure involved chemisorption of cyclopropane, methylcyclopropane or 1,3,5-cycloheptatriene at 293 K in order to convert photoreduced ions into active surface carbene complexes. To detect them two spectroscopic techniques were used. UV-VIS diffuse reflectance spectra were recorded using a Hitachi M 340 spectrophotometer and diffuse reflectance IR spectra were taken with a Perkin-Elmer 580B spectrophotometer, supplied with a home made diffuse reflectance attachment. The catalytic testing in propene metathesis at 293 K was done in a gas-circulating evacuable system with mass-spectroscopic analysis of the products. Liquid phase metathesis of 1-hexene and ethyl oleate was carried out at 293-343 K with the product analysis by gas chromatography. Calorimetric measurements were performed with a Calvet type DAK-1-1 automatic calorimeter.

Results and discussion

Mechanism of Mo^{4+}/SiO_2 photoreduction.

The first step in catalyst preparation procedure was photoreduction of Mo^{6+}/SiO_2 in CO at 293 K. As discussed earlier [3], photoreduction of Mo^{6+} ions can be described by the following scheme:

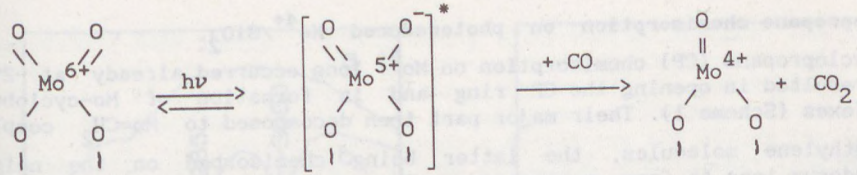

Mo^{4+} yields reached 70-80 % of the total molybdenum content in the sample (for 1 wt % Mo/SiO_2), and selectivity of Mo^{6+} photoreduction to Mo^{4+} was 96-97 % .

UV-VIS diffuse reflectance spectrum of a representative Mo^{4+}/SiO_2 sample is shown in Fig. 1a. Three absorption bands at 350, 630 and 780 nm in the d-d transition region were assigned to Mo^{4+} ions in a distorted tetrahedral or trigonal coordination [3]. Ethylene and propene were strongly chemisorbed on photoreduced Mo^{4+}/SiO_2 at room temperature, apparently forming π-complexes with the Mo^{4+} ions, characterized by a broad intense absorption band at 580-600 nm (Fig. 1b). Olefin desorption from the π-complexes was found to occur only at 573-623 K, Mo^{4+} ions in the original coordination state being regenerated. On the contrary, Mo^{6+}/SiO_2 thermally reduced in H_2 exhibited no distinct absorption bands in the *d-d* transition region and no noticeable changes were found in the spectra after olefin adsorption. Apparently, this can be explained by lower concentrations of coordinatively unsaturated Mo^{4+} ions in the thermally reduced catalysts and/or by their coordinative nonhomogeneity.

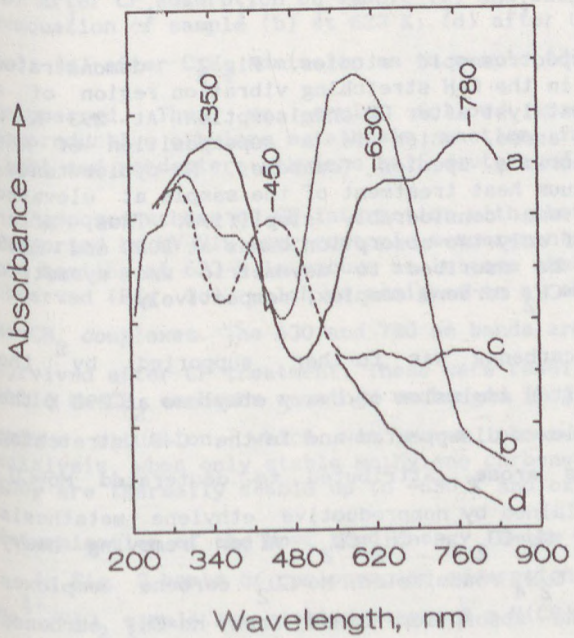

Fig. 1 UV-VIS diffuse reflectance spectra of Mo/SiO_2: (a) photoreduced in CO and outgassed at 423 K; (b) after C_3H_6 adsorption on sample (a); (c) after CP adsorption on sample (a) and evacuation at 623 K; (d) after oxidation of sample (c) by O_2 at 293 K.

Cyclopropane chemisorption on photoreduced Mo^{4+}/SiO_2.

Cyclopropane (CP) chemisorption on Mo^{4+} ions occurred already at 293 K and resulted in opening the CP ring and in formation of Mo-cyclobutane complexes (Scheme 1). Their major part then decomposed to $Mo{=}CH_2$ complexes and ethylene molecules, the latter being chemisorbed on the neighbor molybdenum ions to form π-complexes. Upon heating in vacuum at 623 K ethylene desorbed into the gas phase, while $Mo{=}CH_2$ carbenes remained on the surface, their concentration being almost unchanged. The minor part of Mo-cyclobutane complexes isomerized to propene π-complexes, which at 623 K decomposed to evolve propene. The proposed scheme is supported by analysis of the thermodesorption products, which mainly consisted of ethylene (~95%). The rest were unreacted CP and propene (4-5 %).

Scheme 1.

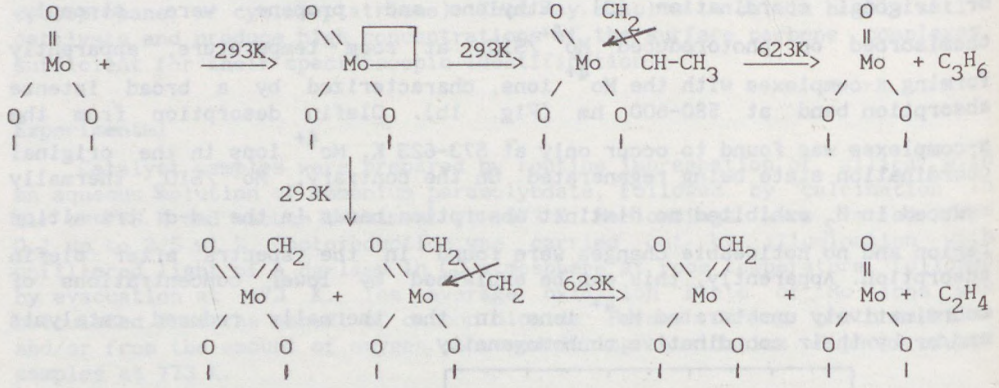

Scheme 1 was confirmed by spectroscopic studies. Fig.2 demonstrates diffuse reflectance IR spectra in the C-H stretching vibration region of a photoreduced silica-molybdena catalyst after CP chemisorption. At 293 K a rather complicated spectrum (b) arose, which is a superposition of the spectra of several kinds of surface species (carbenes, Mo-cyclobutanes, π-complexes). However after vacuum heat treatment of the sample at elevated temperatures its IR spectrum was considerably simplified. Thus, after heating at 623 K it consisted of only two absorption bands at 3080 and 2945 cm^{-1} (Fig. 2c), which could be ascribed to asymmetric and symmetric stretching C-H vibrations in $Mo{=}CH_2$ carbene complex, respectively.

Identification of $Mo{=}CH_2$ carbenes was further supported by the interaction with ethylene-d_4. After admission of heavy ethylene at 293 K the absorption bands of $Mo{=}CH_2$ complexes disappeared and in the C-D stretching region two new absorption bands arose, attributed to deuterated $Mo{=}CD_2$ carbenes (Fig. 2d). This is explained by nonproductive ethylene metathesis reaction: $Mo{=}CH_2 + C_2D_4 \rightleftarrows Mo{=}CD_2 + CH_2{=}CD_2$. After removing heavy ethylene from the gas phase and C_2H_4 readmission, $Mo{=}CD_2$ carbene complexes disappeared (Fig. 2e) and the absorption bands from $Mo{=}CH_2$ carbenes

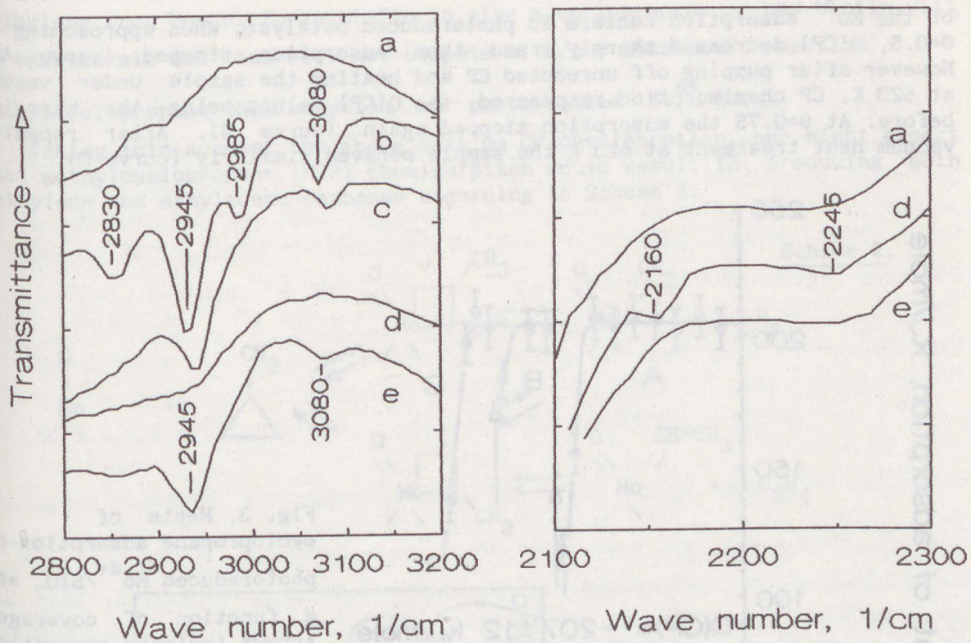

Fig. 2. IR diffuse reflectance spectra of Mo/SiO_2: (a) photoreduced in CO; (b) after CP adsorption on sample (a) and outgassing at 293 K; (c) after evacuation of sample (b) at 623 K; (d) after C_2D_4 admission on to sample (c); (e) after C_2H_4 admission on to sample (d).

reappeared. Thus, we could follow spectroscopically the simplest nonproductive ethylene metathesis reaction, in which from the mixture of light and perdeutero-ethylene half-deuterated ethylene was produced.

Proposed scheme of CP interaction with photoreduced catalysts was also supported by UV-VIS spectroscopic measurements. After CP treatment at 293 K and heating at 623 K in vacuum an intense absorption band at 450 nm was observed (Fig. 1c), which we assigned to a charge transfer transition in $Mo{=}CH_2$ complexes. The 630 and 780 nm bands are due to residual Mo^{4+} ions, survived after CP treatment. These were readily oxidized by oxygen at 293 K, while $Mo{=}CH_2$ carbenes remained unchanged (Fig. 1d). Thus, we have here a unique situation, which was never observed before in heterogeneous catalysis, when only stable methylene carbenes are present on the surface. They are thermally stable up to ~650 K and oxygen resistant at 293 K.

Determination of the Mo=C bond energy in the $Mo{=}CH_2$ complex.

In Fig. 3 heats of cyclopropane adsorption (Q(CP)) on a photoreduced Mo^{4+}/SiO_2 sample are plotted versus $\theta = N(CP)/N(Mo^{4+})$. Below $\theta<0.5$ the Q(CP) values remained constant (-207±12 kJ/mole), thus confirming high homogeneity

of the Mo^{4+} adsorption centers in photoreduced catalyst. When approaching to θ=0.5, Q(CP) decreased sharply, and then adsorption stopped (curve A). However after pumping off unreacted CP and heating the sample under vacuum at 623 K, CP chemisorption reappeared, the Q(CP) values being the same as before. At $\theta \simeq 0.75$ the adsorption stopped again (curve B). After repeated vacuum heat treatment at 623 K the sample behaved similarly (curve C).

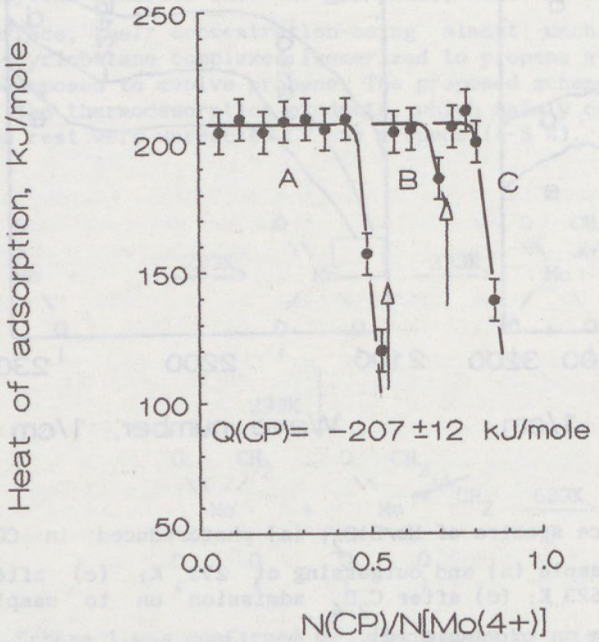

Fig. 3. Heats of cyclopropane adsorption on photoreduced Mo^{4+}/SiO_2 as a function of coverage. Arrows indicate evacuation at 623 K.

Such a peculiar dependence of Q(CP) on θ can be rationalized in terms of Scheme 1, according to which every CP molecule at 293 K reacted with two Mo^{4+} ions, yielding $Mo{=}CH_2$ and ethylene π-complex. Correspondingly, after C_2H_4 desorption at 623 K, the number of Mo^{4+} ions regenerated was equal to one half of its original quantity. After repeated cyclopropane adsorption, $Mo{=}CH_2$ complexes amounted to 75 % of the original Mo^{4+} content, and the rest 25 % formed ethylene π-complexes. After the third cycle was performed (curve C), approximately 90 % of the original Mo^{4+} ions yielded carbenes.

Determination of the Mo=C bond energy in $Mo{=}CH_2$ was done with a thermochemical cycle, using literature value for heat of cyclopropane formation from C_2H_4 and free methylene and measured in this study heats of ethylene ($Q(C_2H_4)$) and CP (Q(CP)) adsorption. Thus, heat of $Mo{=}CH_2$ formation from Mo^{4+} ion and free methylene was found to be 435±25 kJ/mole. This value corresponds well to the predictions of Stevens and Beauchamp [4], who suggested that the metal-carbene bond energy in an active metathesis catalyst should be not less than 419 kJ/mole. In this case transfer of the

methylene from $Mo{=}CH_2$ to an olefin to give a cyclopropane or new olefin will be endothermic and thus will not compete with the metathesis reaction.

Methylcyclopropane chemisorption on photoreduced Mo^{4+}/SiO_2

Taking into account the above data on CP chemisorption, one might expect that methylcyclopropane (MCP) chemisorption would result in producing both methylene and ethyledene carbenes according to Scheme 2.

Scheme 2.

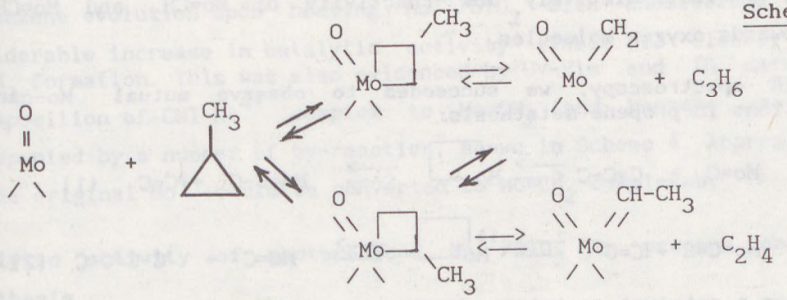

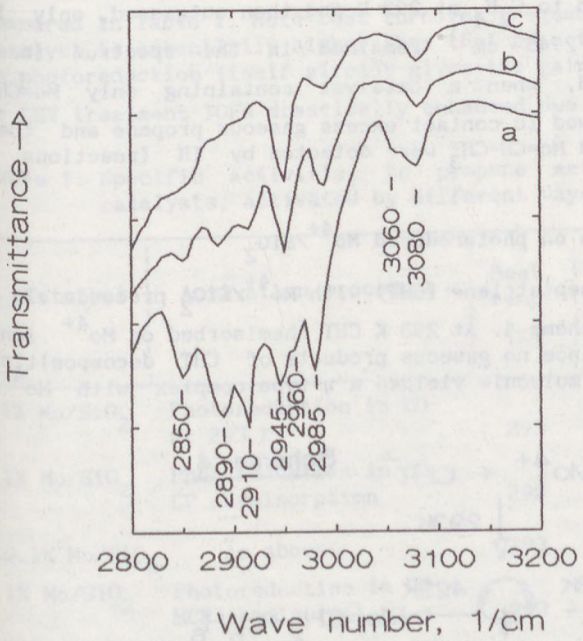

Fig. 4. IR spectra of 2.5% Mo/SiO_2 photoreduced in CO: (a) after MCP adsorption and outgassing at 293 K; (b) after evacuation of sample (a) at 620 K; (c) after evacuation of sample (b) at 640 K.

After MCP chemisorption on a photoreduced 2.5% Mo^{4+}/SiO_2 sample and outgassing at room temperature for an hour IR spectrum exhibited a set of absorption bands (Fig. 4a), among which the bands at 3080 and 2945 cm^{-1} belong to C-H stretches of the $Mo{=}CH_2$ carbene. Upon raising the temperature to 600-620 K and pumping off the sample, the bands at 3060 and 2960 cm^{-1},

which were assigned to ethylene π-complexes with Mo^{4+} ions, disappeared, while the intensities of all other bands somewhat decreased (Fig. 4b). These results allow to assume that four bands at 2985, 2910, 2890 and 2850 cm^{-1} might be attributed to the four normal C-H vibrations in $Mo=CH-CH_3$. Heating the sample at 640 K caused these bands to decrease (Fig. 4c), indicating lower thermal stability of $Mo=CH-CH_3$, as compared to that of $Mo=CH_2$. No change in the IR spectrum after oxygen treatment at 300 K was found to occur. This confirms relatively low reactivity of $Mo=CH_2$ and $Mo=CH-CH_3$ carbenes towards oxygen molecules.

Using IR spectroscopy, we succeeded to observe mutual Mo-carbene transformations in propene metathesis:

$$Mo=C + C=C-C \rightleftharpoons Mo\square \rightleftharpoons Mo=C-C + C=C \quad (1)$$

$$Mo=C=C + C=C-C \rightleftharpoons Mo\square \rightleftharpoons Mo=C + C-C=C-C \quad (2)$$

Thus, when a catalyst containing $Mo=CH_2$ and $Mo=CH-CH_3$ (pretreated with MCP as in Fig. 3b) was exposed to C_2H_4 at 293 K and then outgassed, only IR bands of $Mo=CH_2$ at 3080 and 2945 cm^{-1} remained in the spectrum (back reaction 1). On the other hand, when a catalyst containing only $Mo=CH_2$ (pretreated with CP) was allowed to contact excess gaseous propene and then was evacuated, both $Mo=CH_2$ and $Mo=CH-CH_3$ were detected by IR (reactions 1 and 2).

Cycloheptatriene chemisorption on photoreduced Mo^{4+}/SiO_2

Interaction of 1,3,5-cycloheptatriene (CHT) with Mo^{4+}/SiO_2 proceeds via a rather complicated stepwise scheme 4. At 293 K CHT chemisorbed on Mo^{4+} ions mainly in a molecular form, since no gaseous products of CHT decomposition were found. Most likely, CHT molecule yielded a η-type complex with Mo^{4+},

Scheme 4

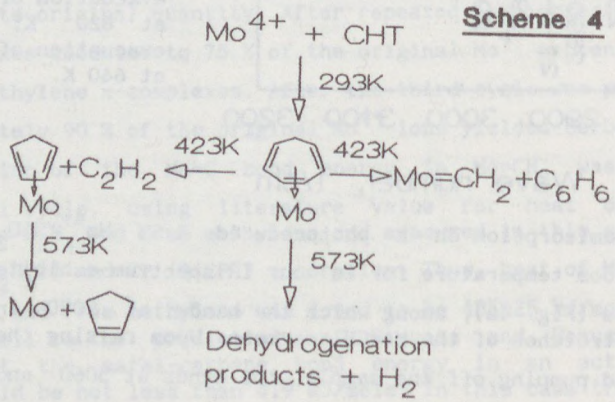

which is characterized by absorption bands at 435 and 690 nm in the UV-Vis spectrum.

Upon heating Mo^{4+}/SiO_2 sample with adsorbed CHT, two thermodesorption maxima (at 400 and 600 K) were observed. The major thermodesorption products at 423 K were CHT, benzene and acetylene, while at 573 K benzene, cyclopentene, acetylene and small amounts of CHT were evolved into the gas phase. Above 473 K hydrogen evolution commenced, evidencing dehydrogenation of the surface hydrocarbon fragments.

Benzene evolution upon heating Mo^{4+}/SiO_2 with chemisorbed CHT and considerable increase in catalytic activity (Table 1) clearly indicate $Mo{=}CH_2$ formation. This was also evidenced by UV-Vis and IR data. However decomposition of CHT-Mo^{4+} complex to $Mo{=}CH_2$ and benzene was obviously accompanied by a number of by-reaction, shown in Scheme 4. Approximately 10% of the original Mo^{4+} could be converted to $Mo{=}CH_2$ complexes.

Catalytic activity of photoreduced Mo^{4+}/SiO_2 in propene and 1-hexene metathesis

Specific activities of Mo/SiO_2 catalysts for propene metathesis are compared in Table 1. Note that turnover frequency (TOF) of a photoreduced catalyst is essentially higher than that of a thermally reduced sample, that is photoreduction itself already gives the gain in activity. After CP, MCP or CHT treatment TOFs drastically enhanced due to formation of $Mo{=}CH_2$ and

Table 1. Specific activities in propene metathesis of silica-molybdena catalysts, activated by different ways.

Catalyst	Activation procedure	Reat. temp. (K)	C_3H_6 pres. (Torr)	Specific activities: molec C_3H_6 / Mo atom .s (TOF)	Specific activities: g C_3H_6 / g cat .s
1% Mo/SiO_2	Photoreduction in CO at 293 K	293	8	0.42	$1.8 \cdot 10^{-3}$
1% Mo/SiO_2	Photoreduction in CO + CP chemisorption	293	157	5.05	$2.1 \cdot 10^{-2}$
0.1% Mo/SiO_2	As above	293	150	12.8	$5.4 \cdot 10^{-3}$
1% Mo/SiO_2	Photoreduction in CO + MCP chemisorption	293	170	2.14	$9.0 \cdot 10^{-3}$
1% Mo/SiO_2	Photoreduction in CO + CHT chemisorption	293	83	1.0	$4.2 \cdot 10^{-3}$
1% Mo/SiO_2	Thermal reduction in CO at 773 K	293	54	0.07	$2.9 \cdot 10^{-4}$
$Mo(\pi\text{-}C_3H_5)_4/SiO_2$	None	363	100	0.17 [5]	

$Mo{=}CH{-}CH_3$ carbenes on the surface. TOF for CP and MCP treated catalysts increased by more than one order of magnitude as compared to those for nontreated catalysts. All photoreduced catalysts exhibited considerably higher activity than SiO_2 with "anchored" π-allyl-Mo complexes, which is usually regarded as one of the most active Mo-containing catalysts.

CP and MCP treatment makes photoreduced catalysts essentially less sensitive to oxygen poisoning. In contrast to nontreated samples, which were completely deactivated by sorption of even small amounts of oxygen at 293 K, exposure of CP treated catalyst to oxygen resulted in a decrease of TOF by a factor of only 1.5. This correlates quite well with the stability of $Mo{=}CH_2$ and $Mo{=}CH{-}CH_3$ complexes in the presence of oxygen.

In another series of experiments the photoreduced catalysts were tested in liquid phase 1-hexene metathesis. After CP treatment they exhibited high catalytic activity, which considerably exceeded that of any known molybdenum oxide catalysts (~20 molecules of hexene-1 per molybdenum atom per second at 293 K). Selectivity for 5-decene is ~95 % and productivity reached ~5300 moles of 1-hexene per molybdenum g-atom.

Metathesis of functionalized olefins over photoreduced Mo^{4+}/SiO_2 catalysts, treated with cyclopropane

Taking into account that the choice of catalysts suitable for metathesis of functionalized olefins with polar groups is very limited, in the present study an attempt was made to apply Mo^{4+}/SiO_2+CP for liquid phase metathesis of ethyl oleate and its co-metathesis with 5-decene:

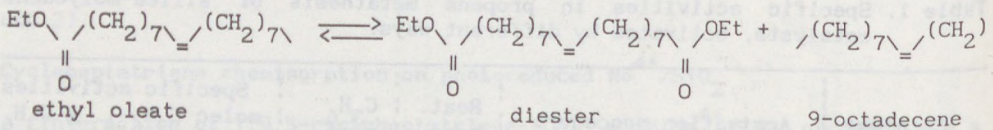

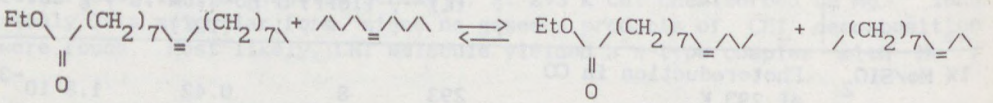

It was found that both reactions readily occurred at 343 K, and conversion of ethyl oleate reached 50-60 % within 10 min. The selectivity of co-metathesis to ethyl myristoleate was 91-93 % [6].

REFERENCES

1. J.C. Mol and J.A. Moulijn, Catal. Sci. Technol., 8 (1988) 69.
2. J. Engelhardt, J. Goldwasser and W.K. Hall, J. Catal., 70 (1985) 364; *ibid.*, 76 (1982) 48.
3. A.N. Pershin, B.N. Shelimov and V.B. Kazansky, J. Catal., 64 (1980) 426.
4. A.E. Stevens and J.L. Beauchamp, J. Am. Chem. Soc., 101 (1979) 6449.
5. Yu. I. Ermakov, B.N. Kuznetsov and V.A. Zakharov (eds), Catalysis by Supported Complexes, Elsevier, Amsterdam, 1981.
6. M.Yu. Berezin, B.N. Shelimov et al., Kinet. Katal, 32 (1991) 379.

DISCUSSION

Q: M. Anpo (Japan)

About 10 years ago we reported that the propene metathesis reaction was induced under UV irradiation of Mo oxides supported on Vycor-glass and SiO_2 and proposed the mechanism involving carbene species which were produced under UV irradiation. You proposed a mechanism which seems to be quite similar to our mechanism.

Do you have any data to compare propene metathesis reaction on the photoreduced system and photo-UV-irradiated (under UV-irradiation of molybdenum oxide in the presence of propene) ?

A: V. B. Kazansky

That was a very interesting publication, one of the first where carbene formation was implied to explain experimental results. Formation of carbene complexes via 4-member rings (either Mo-cyclobutanes or oxygen-containing species) seems to be quite similar in both mechanisms. To answer your question I would like to draw your attention to one of our previous publications [1], where we have compared the activity of both catalysts. We found that even before cyclopropane treatment the photoreduced catalyst was appreciably more active in propene metathesis. After such treatment this difference was much larger.

[1] B. N. Shelimov and V. B. Kazansky, *J. Mol. Catal.*, **38**, 70 (1986)

Q: H. L. Krauss (Germany)

Using a very similar system we found in the MoO_3/SiO_2 case oxidation numbers well below 3 after reduction with CO flow under UV irradiation.

How about your experimental proofs of an O.N. of four as the predominant (or even single) species on the surface? Did you ever try an O_2 titration? How many of Mo(IV) are active centers ?

Do you get typical carbene complexes reactions with your $CH_2{=}Mo^{4+}$ species like formation of cyclopropane with C_2H_4 or exchange of $=CH_2$ for $=O$? Do you find empty coordination sites on these species?

A: V. B. Kazansky

The average oxidation state of molybdenum close to 4+ was confirmed for the photoreduced 1 wt% Mo/SiO_2 by measuring of CO_2 quantity after the reduction was complete as well as by titration of the photoreduced sample at 850 K by O_2. The homogeneity of reduced sites follows from the constancy of heats of adsorption of various gases up to saturation of adsorption centers. This allows us to conclude that we produced mainly Mo(IV) ions. However, I do not mind that in more diluted samples like 0.1% Mo/SiO_2 a deeper reduction up to Mo(III) or Mo(II) may occur, especially during treatment in a flow system. The critical question however is whether such a deep reduction is really necessary for obtaining high catalytic activity. As far as the number of active Mo(IV) sites is concerned, I think that without cyclopropane activation it is rather low, probably a few percent of the total Mo(IV). By chemisorption of cyclopropane it was possible to convert up to 90% of these ions into active $Mo{=}CH_2$ carbene complexes.

We tried several "test" reactions with $Mo{=}CH_2$. Our thermochemical data on the bond energy in these complexes showed that formation of cyclopropane from $Mo{=}CH_2$ and C_2H_4 is energetically unfavorable. In fact we used the opposite reaction to produce carbene complexes. We also failed to observe a Witting-type reaction with acetone at room temperature. These complexes reacted at 400 K with water vapor producing methane. I think that these properties of carbene complexes are due to very strong Mo=C (435 kJ/mole), so that formal oxidation state of the metal is close to 6+. I do not think we can observe any appreciable coordination of CO on these sites, anyhow, this is a good idea to try.

Q: S. Coluccia (Italy)

As a comment to a previous question I may notice that characterization by IR spectra of CO adsorbed On Mo/SiO_2 catalyst reduced by various procedures firmly support the evidence given by Professor Kazansky that photoreduction is very much selective in producing Mo(IV).

The question I would like to ask is: has photoreduction proved to be selective also for other supported transition metal ions which by "standard" reductive treatments (e.g. thermal) would produce several oxidation states ?

A: V. B. Kazansky

We have found in our previous research that not only supported molybdenum ions could be photoreduced with high selectivity. The same phenomenon was characteristic of supported Cr(VI), V(V) and to some extent of Ni(II) on silica. In case of CrO_3/SiO_2 photoreduction in CO at room temperature gave Cr(IV) ions with some admixture of Cr(II), while in case of V_2O_5/SiO_2 V(III) ions were selectively produced. These phenomena were reviewed [2].

[2] Zs. G. Juskovec, N. V. Nekrasov, M. S. Kharson, M. M. Kostjukovskij, M. V. Shimanskaja and S. L. Kiperman, *Kinet. Katal.*, **24**, 1134 (1983)

Q: Y. Iwasawa (Japan)

Photo-excited molybdenum oxide states are rapidly deexcited by CO. What is the probability of the reduction per photon excitation for the formation of Mo(IV) ?

Metal carbenes are usually sensitive to oxygen. Can I have your comments on the oxygen-stable character of the $Mo^{4+}=CH_2$?

A: V. B. Kazansky

We tried to estimate the quantum yield of photoreduction from the rate of Mo(IV) formation under UV-irradiation in CO and found that this value was much less than 1. Unfortunately, it was not possible to measure precisely the probability of the process you are interested in. As far as your second question is concerned, I believe that oxidation state of Mo in the carbene complex is close to 6+ and the $Mo=CH_2$ bond could be formally considered as quite similar to Mo=O one, taking into account very high Mo=C bond energy in $Mo=CH_2$ carbenes. Consequently, one may expect $Mo=CH_2$ would not exhibit strong reducing properties and therefore these species do not readily react with oxygen at room temperature. Of course, at elevated temperatures oxidation was fast.

Q: W. Grünert (Germany)

Your paper is very convincing as far as cyclopropane treatment is involved. i wonder, however, why you do not see any band of the carbene species in the sample activated merely by propene (Figure 1b) ? The activity of this sample is not so low: in Table 1 (lines 1 and 2) you have compared it with the cyclopropane-activated sample at widely different propene pressures. At identical propene pressures the activity could well be of the same order of magnitude. Now, why then is the carbene band not observed in the sample treated with propene ?

A: V. B. Kazansky

I am sorry but there is a mistake in the Table. Instead of 8 Torr of initial propene pressure in line 1 it must be written 85 Torr. Under these conditions the activity of photoreduced catalyst was much lower than that of the sample treated by cyclopropane. I believe that in photoreduced samples a certain amount of carbene complexes are formed as a result of propene transformation from $(\pi\text{-}C_3H_6)Mo^{4+}$ to $Mo=CH\text{-}CH_2\text{-}CH_3$. Thermodynamic data show that this process is almost isoenergetic. However, the concentration of active carbene complexes derived from adsorbed propene seems to be too low to be detected spectroscopically.

Q: J. C. Mol (The Netherlands)

We have developed an alternative photoreduction procedure for MoO_3/SiO_2 catalysts using a laser beam (XeCl, 308 nm) instead of a Hg-lamp, as in your case. After cyclopropane treatment we obtained a catalyst with high activity and stability at room temperature for the metathesis of propene in a flow system. For this laser irradiation only a few minutes are required for the reduction instead of several hours for reduction with a Hg-lamp. Our system also showed good activity in the metathesis of functionalized olefins, e.g. methyl oleate [3].

We have also found that MoO_3/SiO_2-Al_2O_3 even has much higher activity for the metathesis of propene when pretreated in the same way as MoO_3/SiO_2. This silica-alumina catalyst is also more active than the more conventional tetraalkylation-promoted Re_2O_7/Al_2O_3 catalyst.

Did you try to apply your activation method to other catalysts, for instance supported rhenium oxide or tungsten oxide ?

[3] M. Kieboom, M. Sibeijn, J. C. Mol, poster presented at the *9th International Symposium on Olefin Metathesis,* Philadelphia, 1991

A: V. B. Kazansky

Thank you for your comments. As far as the possibility to activate other systems like supported Re_2O_7 and WO_3 by photoreduction is concerned, we have not obtained good results so far. We succeeded in photoreduction of supported Ni(II), Cr(III) and V(V). However, no metathesis activity was found for these systems even treated with cyclopropane.

Q: J. J. Rooney (Ireland)

We showed many years ago [4] that cycloheptatriene is readily converted into benzene and ethylene etc., on a Re_2O_7-SiO_2 metathesis catalyst. Since cycloheptatriene is in equilibrium with norcaradiene, this transformation on such catalyst is easily understood:

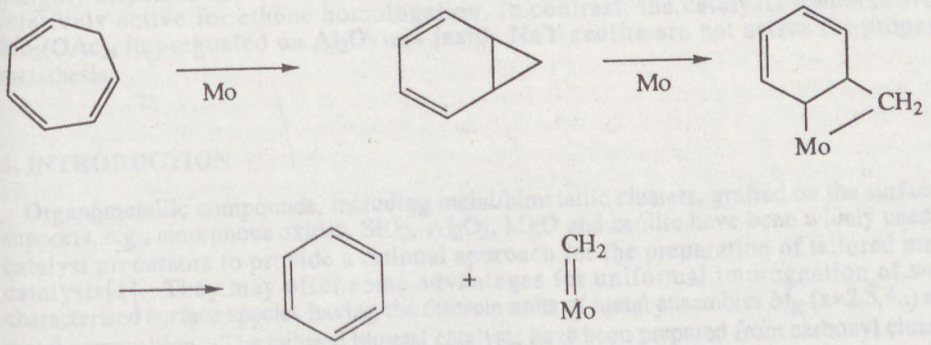

Other surface reactions, of course also occur.

[4] J. J. C. Archibald, J. J. Rooney, A. Stewart, *J. Chem. Soc., Chem. Commun.*, 547 **1975**

A: V. B. Kazansky

Thank you for your comment. Recently we have shown [5] that $Mo{=}CH_2$ carbenes could be produced on photoreduced $Mo(IV)/SiO_2$ by 1,3,5-cycloheptatriene chemisorption, although in this paper a slightly different mechanism of cycloheptatriene interaction with Mo(IV) ions was proposed. However, I believe that your scheme may be valid as well.

[5] K. A. Vikulov, B. N. Shelimov and V. B. Kazansky, *J. Mol. Catal.*, **72**, 117 (1992)

Guczi, L. *et al.* (Editors), *New Frontiers in Catalysis*
Proceedings of the 10th International Congress on Catalysis, 19-24 July, 1992, Budapest, Hungary
© 1993 Elsevier Science Publishers B.V. All rights reserved

SiO_2-GRAFTED DINUCLEAR MOLYBDENUM CATALYST DERIVED FROM $Mo_2(OAc)_4$ HIGHLY ACTIVE FOR OLEFIN METATHESIS REACTION

M. Ichikawa[a], Q. Zhuang[a†], G.-J. Li[a#], K. Tanaka[b], T. Fujimoto[a] and A. Fukuoka[a]

[a]Catalysis Research Center, Hokkaido University, Sapporo 060, Japan
[b]Department of Electronics Engineering, University of Electro-Communication, Chofu, Tokyo 182, Japan

Abstract

SiO_2-grafted dinuclear molybdenum species was prepared from $Mo_2(OAc)_4/SiO_2$. It was demonstrated by ESR, UV-vis, FTIR, XANES and EXAFS spectroscopic studies that $Mo_2(OAc)_4$ reacts with silanol on SiO_2 by thermal activation at 350°C, resulting in uniform formation of a ESR active $[Mo\equiv Mo]^V$ (g=1.928, R_{Mo-Mo}=2.11Å, C.N.=0.6). It was found that the resulting dinuclear Mo species is selective and highly active for propene metathesis at 20°C, whereas inactive for ethene homologation. The excess thermal treatment at above 400°C causes the complete cleavage of Mo-Mo bond of the grafted Mo-dimer species to give a highly dispersed Mo^{5+} oxide , which is negligibly active for propene metathesis, but relatively active for ethene homologation. In contrast, the catalysts prepared from $Mo_2(OAc)_4$ impregnated on Al_2O_3 and inside NaY zeolite are not active for propene metathesis.

1. INTRODUCTION

Organometallic compounds, including metal/bimetallic clusters, grafted on the surface of supports, e.g., amorphous oxides, SiO_2, Al_2O_3, MgO and zeolite have been widely used as catalyst precursors to provide a rational approach for the preparation of tailored metal catalysts[1]. They may offer some advantages for uniformal impregnation of well-characterised surface species having the discrete units of metal ensembles M_x (x=2,3,4..) and metal composition. The tailored bimetal catalysts have been prepared from carbonyl clusters such as $[Rh_4Fe_2(CO)_{15}]^{2-}$, $[Pd_6Fe_6(CO)_{24}H]^{3-}$, and $[FeIr_4Fe(CO)_{15}]^{2-}$, which are remarkably active and selective, compared with those of the conventional metal catalysts for $CO+H_2$ reaction towards oxygenates such as methaol and ethanol[2] and olefin hydroformylation[3]. Dinuclear organometallic compounds, such as $Mo_2(\pi\text{-ally})_4$[4], $Mo_2(NMe_2)_6$ [5], and $Rh(\mu\text{-}CH_2)_2(C_5Me_5)Me]_2$[6] have been used as a precursor to be grafted onto SiO_2 and Al_2O_3.

Catalytic olefin metathesis has received a considerable attention in terms of a foundamental viewpoint of the relationship between homogeneous and heterogeneous catalysis. Different types of organometallic alkylidene complexes have been synthsized as the plausible intermediates for homogeneous catalysis of olefin metathesis and discussed in conjunction of a metallocyclobutane mechanism. Olefin metathesis is also catalystzed by some supported metal catalysts such as MoO_3/SiO_2 and MoO_x/TiO_2, although they have been not well-characterized. Recently, Kazansky et. al.[7] reported that a photo-reduced MoO_x/SiO_2 with

CO exhibited a high activity for propene metathesis possibly in formying the surface carbene species. Tanaka et. al.[8] proposed a metal alkylidene species initially formed in contact to olefin or carbene source, e.g.,$Sn(CH_3)_4$ and CH_2I_2+Mg(Al) attached on metal sites which is responsible for metathesis and homologation of olefin through a metallacycle as a common intermediate. B. Zhang et.al.[9] suggested that Mo^{5+} species is acitive for olefin metathesis. Nevertheless, Mo^{6+} and Mo^{4+} are also proposed as active species for the reaction after the suitable treatments of supported Mo catalysts[10]. So far, it still remains as a controversial to rationalize the active structures, for instance, ensemble size of Mo atoms, their electronic states and metal-support interactions involving the olefin metathesis and homologation.

It was previously reported[5] that the SiO_2-grafted Mo dimer precursor $(Me_2N)_3Mo{=}Mo(NMe_2)_3$ specifically exhibited catalytic activity for ethene dimerization, whereas the monomer $Mo(NMe_2)_6$ derived catalyst showed high activity for ethene homologation, but was inactive for ethene dimerization.

In this work we extend to use $Mo_2(OAc)_4$(Ac=CH_3CO) as a precursor having quadruple Mo-Mo bond grafted on SiO_2, and study on the thermal activation of $Mo_2(OAc)_4/SiO_2$. The surface-bound Mo species derived from $Mo_2(OAc)_4$ has been characterized by FTIR, UV-vis and ESR for reactivity of acetato-ligand and electronic state of Mo_2, and XANES-EXAFS for local structure of Mo-Mo bonding. As the test reactions, propene metathesis and ethene homologation have been conducted to evaluate the catalytic performances of the Mo species from $Mo_2(OAc)_4/SiO_2$ after the thermal activation at different temperatures, compared with those on the catalysts from $Mo_2(OAc)_4$ impreganted on Al_2O_3 and in NaY zeolite.

2. EXPERIMETAL

2.1 Catalyst preparation

The $Mo_2(OAc)_4$ was purchased from Strem Chemicals(99% purity) and used without further purification. Since the compound is air- and moisture sensitive, all the operations were performed under N_2(99.9999%) or in vacuo by means of Schlenck technique. $Mo_2(OAc)_4$ was dry-mixed with the silica (Kiesegel 60, Merck, 487 m^2/g), Al_2O_3 (Nishio Kogyo Co, A-11, 280 m^2/g) and NaY zeolite (LZ-Y52, Si/Al=5.6, 910 m^2/g), which are dehydrated by evacuation at 350°C for 12 h, prior to use by grinding within a glovebox(Shimadzu G-12) in loading of 4.1-6.2 wt%Mo. The negligible XRD peaks associated with a $Mo_2(OAc)_4$ crystal was found after the dry-mixing at 25-150°C, indicative of the complete dispersion of $Mo_2(OAc)_4$ well-spread by sublimation on SiO_2, Al_2O_3 and NaY zeolite. The Mo loading of the impregnated $Mo_2(OAc)_4$ after thermal activation at 25-450°C were analyzed by ICP-MS.

2.2. Activity measurements

Propene metathesis and ethene homologation were carried out in a closed circulating reactor system with a volume of 150 ml The U-type quarz reactor equipped to a ESR tubing and diffuse reflectance UV-vis cell is charged with a given amount of the dry-mixed $Mo_2(OAc)_4$. After the thermal activation in vacuo at 25-450°C, the catalyst was cooled to r.t., and then 10-15 torr of propene or ethene was admitted to the system to perform the reaction at -10°C-20°C. The products were analyzed by GC using the VZ-7 column(4 m, 55°C).

2.3. UV-vis, ESR and FTIR measurements

The difuse reflectance UV-vis spectra were monitored by means of UV-vis spectrometer (Hitachi 330), coupled with an integral converter(Hitachi 210-2101 60f). Varian E-4 ESR spectrometer was used for paramagnetic measurements at 20°C and liquid nitrogen temperature. The microwave power and microwave frequency were 20 mw and 9.5 GHz,

respectively. The g-value and spin concentration were determined by using "Strong Pitch" and $CuSO_4$ as the reference. Shimadzu FTIR 8100 single-beam Fourier transform infrared spectrometer was empolyed to measure the anchoring process of $Mo_2(OAc)_4$ on SiO_2 support by thermal activation. Generally, 100-200 interferograms were coadded to improve the signal-to-noise ratio. The dry-mixed $Mo_2(OAc)_4$ on SiO_2, Al_2O_3 and NaY zeolite(20-40 mg) was pelletized as a self-supporting wafer under N_2 atmosphere and the spectrum was recorded before and after the thermal activation at 25-450°C.

2.4. XANES and EXAFS measurements

Mo K-edge XANES and EXAFS measurements were conducted at 25°C at the SOR, 10B with a Si(311) channel-cut monochrometor in the Photon factory of the National Laboratory for the high Energy Physics(KEK-PF). The dry-mixed $Mo_2(OAc)_4$ samples as a self-supporting wafer after the thermal activation were charged under N_2 in a special designed in-situ EXAFS cell with Kapton^R film windows(500 mm thick) to prevent exposure to air and moisture. The C.N. and atomic distances were evaluated by Fourier Transform curve-fitting analysis using the routin-computor program "PROGRAM 2"[11]. Some reference crystals such as Mo foil, MoO_3, K_2MoO_4 and $Mo_2(OAc)_4$ mixed with BN(boron nitride) were used for analysing the XANES and EXAFS spectra to evaluate Mo-Mo and Mo-O bondings.

3. RESULTS AND DISCUSSINS

3.1. ESR and UV-vis characterization

$Mo_2(OAc)_4$ is a diamagnetic complex, which has a quadruple Mo-Mo bond, as shown in Fig.1. Its electron configuration is characterised by $\sigma^2\pi^4\delta^2$, where each of Mo atoms share 16 electrons, leaving the two axial unoccupied sites for a nucleophilic reagent[12]. The freshly prepared dry-mixed $Mo_2(OAc)_4/SiO_2$ at 25-100°C showed no paramagnetic resonance signal. The diffuse reflectance UV-vis gave a strong absorption peak at 435 nm, which is assigned to d --> d* electron transition characteristic of Mo-Mo bond in $Mo^{II}{\equiv}Mo^{II}X_4$ (X=OAc, EtCO, SO_4) [13]. These results, coupled with the XRD data suggest that by dry-mixing at 25-100°C $Mo_2(OAc)_4$ is highly dispersed and intact to SiO_2 surface in keeping its molecularity of $[Mo{\equiv}Mo]^{IV}$.

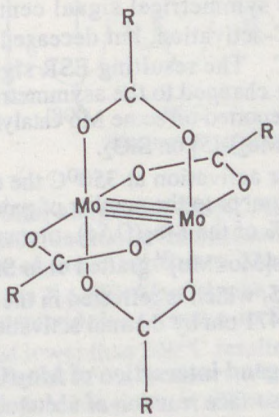

Fig. 1. Molecular Structure of $Mo_2(OAc)_4$ (R=CH_3)

By heating the dry-mixed sample at 250°C in vacuo, it was interesting to find that a intense and sharp ESR signal with a narrow width of 12 gauss appeared by thermal activation, as shown in Fig.2. Owing to the natural abundance of ^{95}Mo and ^{97}Mo, the total nuclear spin of the Mo_2 pair is $J=I^1 + I^2 = 0, 5/2, 5$. Thus, basd on the nuclear-spin coupling, the corresponding eleven ESR signals of hyperfine structure were observed(Fig.2A). The observ- ed ESR spectrum is identical with that of the one-electron oxidized species(g=1.941 with eleven hyperfine structure) of $Mo_2(C_3H_7COO)_4$ in solution reported by Cotton et. al.[14].

$$[Mo{\equiv}Mo]^{IV} \xrightarrow{-e} [Mo{\equiv\!\!\equiv}Mo]^{V}$$

$$\sigma^2\pi^4\delta^2 \qquad\qquad \sigma^2\pi^4\delta^1$$

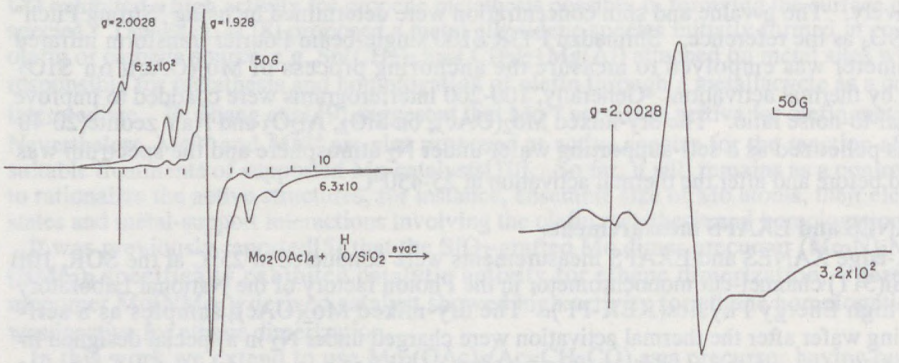

A (350°C) **B** (450°C)

Fig. 2. ESR spectra of $Mo_2(OAc)_4/SiO_2$ by Thermal Activation at 350°C (A) and 450°C (B)

The symmetrical signal centered at g=1.928 reached the maximum intensities by the 350°C-activation, but deceased sharply by heating at the exceeding temperatures above 400°C. The resulting ESR signal (Fig.2(B)) after the thermal activation at 450°C was totally changed to the asymmetric signal similar to that of Mo(V) oxide species which has been reported on some Mo catalysts derived from other Mo precursors such as MoO_3[15] and $Mo(NMe_2)_4$[5] on SiO_2.

After activation at 350°C the catalyst showed the highest spin concentration, the ratio of spin number to the number of paired molybdenum(Mo_2) is 0.83. This result suggests that 83 mole % of the $Mo_2(OAc)_4$ precursor was uniformaly converted to the one-electron oxidised species$[Mo\equiv Mo]^V$ grafted onto SiO_2. The Mo-Mo bond order in $[Mo\equiv Mo]^V$ is chaged from 4 to 3.5, which is reflected in the UV-vis band of d ---> d^* transition being shifted from 435 nm to 471 nm by thermal activation of the $Mo_2(OAc)_4/SiO_2$.

3.2. Ligand interaction of $Mo_2(OAc)_4$ with SiO_2

The surface reaction of acetato ligands in the dry-mixed $Mo_2(OAc)_4$ /SiO_2 was studied by FTIR in varying the activation temperatures in vacuo. As shown in Fig.5, the fresh sample of $Mo_2(OAc)_4/SiO_2$ gave a main pair absorption bands at 1523(asyn) and 1447(syn) with side bands at 1497(asyn) and 1416(syn) cm^{-1} which are assigned to bidentate carboxyls of $Mo_2(OAc)_4$. A small sharp peak at 1353 cm^{-1} is likely to be the deformation of C-H bond in acetate ligand. These carboxyl IR bands are identical with those of $Mo_2(OAc)_4$ in crystal. Additional medium band at 1709 cm^{-1} and a weak band at 1754 cm^{-1} may be due to carbonyl stretching mode of monodentate acetate attached to Mo_2 center and silica surface[13], respectively. During the dry-mixing of $Mo_2(OAc)_4$ with the partialy dehydrated SiO_2 the sharp intense peak at 3710 cm^{-1} assigned to the isolated SiOH was strongly reduced. These results suggest that bidentate acetato-ligands attached to the precursor $Mo_2(OAc)_4$ are partially removed in the reaction with the support SiOH by dry-mixing at 25-100°C, being intact to SiO_2. By raising the activation temepratures above 200°C the main pair bands at 1523 and 1447 cm^{-1} were suppressed in their intensities and broaden and relatively shifted to lower frequencies. The intensities of bands at 1520 and 1440 cm^{-1} after 350°C-activation were decreased to ca 1/4 of those of the original sample. The acetato absorption bands completely disappeared by heating the sample at 450°C.

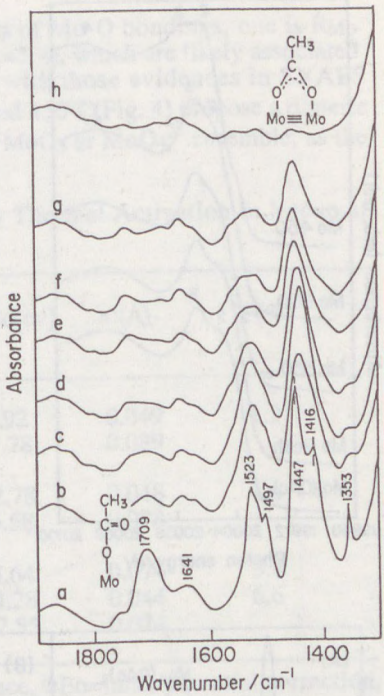

Fig.3. FTIR Spectra of $Mo_2(OAc)_4/SiO_2$ by Thermal Activation at 25°C (a), 100°C (b), 140°C (c), 210°C (d), 270°C (e), 340°C (g), and 450°C (h).

3.3. Mo-K edge XANES and EXAFS characterization of SiO_2-supported $Mo_2(OAc)_4$

The XANES(X-ray near-edge absorption spectrum) can provide crucial information about the site symmetry of Mo atoms and bonding properties of the substrates. The fresh $Mo_2(OAc)_4/SiO_2$ prepared by dry-mixing at 25-100°C gave the XANES idential with that of the reference $Mo_2(OAc)_4$ crystal diluted with BN(boron nitride), as shown in Fig. 4. Further- more, the thermal activation of dry-mixed sample at lower than 350°C resulted in a minor difference of the Mo-K edge XANES, compared with that of the fresh sample. This result reveals that the local structure and symmetry of dinuclear Mo skeleton is still retained even by thermal activation at below 350°C, likely as the original $Mo_2(OAc)_4$, regardless the partial removal of acetato ligands and one-electron oxidation. By contrary, after the exceeding activation at above 400°C, the Mo-K edge XANES showed a substantial change of the spectra (Fig,4 e-d). The resulting XANES at 450°C-activation resembles those of MoO_3(Td symmetry) and K_2MnO_4(Oh symmetry) having a clear shoulder peak due to the pre-edge absorption of 1s-5p transition of Mo(V) or Mo(VI) oxides.

Fig.5 represents a set of the Fourier transforms of the k^3 weighted Mo-K edge EXAFS for the $Mo_2(OAc)_4/SiO_2$ after thermal treatments at 25, 250, 350 and 450°C. The curve-fitting data are summerized in Table 1. The EXAFS data suggested that after activation at 350°C the catalyst has a Mo-Mo distance(R_{Mo-Mo}=2.11Å) and C.N.(coordination number)=0.6 similar to that of the precursor(R_{Mo-Mo}=2.10Å, C.N.=1.0) within the experimental errors, implying the multiple bonding of Mo-Mo is retained after the thermal activation at below 350°C. The C.N. of Mo-O bond(R_{Mo-O}=2.01Å) considerably decreased from 3.7 to 1.8 by heating from 25 to 350°C, reflected in a progressing removal of bidentate acetate ligands.of $Mo_2(OAc)_4$ being grafted on SiO_2. The Mo-Mo distance is slightly enlonged after the 350°C-thermal activation

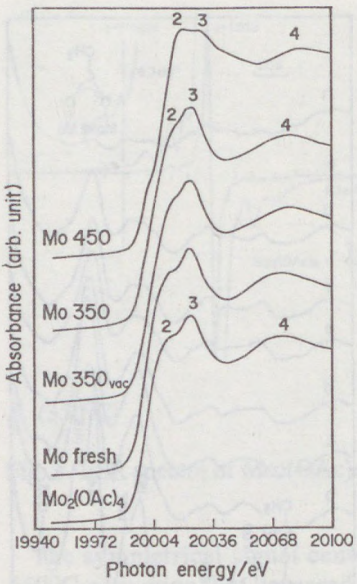

Fig.4. Mo-K edge XANES of $Mo_2(OAc)_4/SiO_2$ by Thermal Activation at Different Temperature in Vacuo

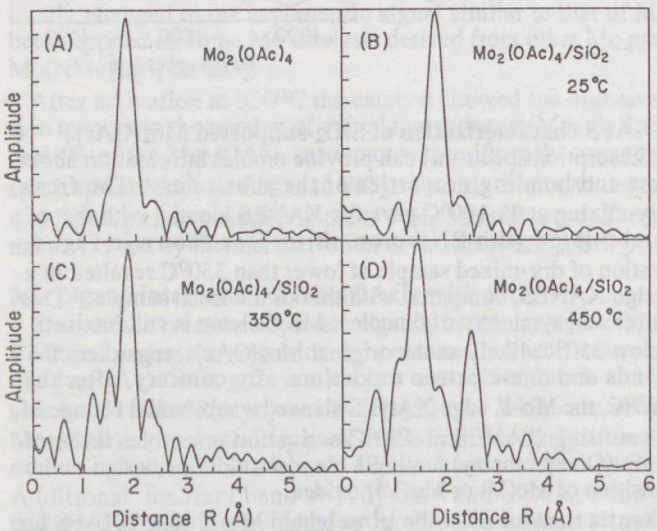

Fig.5. Fourier Transform of EXAFS Data for $Mo_2(OAc)_4$ in crystal(A), $Mo_2(OAc)_4/SiO_2$ after Thermal Activation at 25°C(B), 350°C(C),and 450°C(D)

of $Mo_2(OAc)_4/SiO_2$, possibly due to the one- electron oxidation to give $[Mo\dddot{\equiv}Mo]^V$, where the Mo-Mo bond order is changed from 4 to 3.5. In contrast to these the catalyst activated at 450°C had R_{Mo-Mo}=2.80Å, which is fairly lengthened compared with that of $Mo_2(OAc)_4$(R_{Mo-Mo}=2.10Å), indicative of cleavage of the Mo-Mo bonding. The resulting

sample after 450°C-activation consisted with two kinds of Mo-O bondings, one is R_{Mo-O}=1.73Å (C.N.=0.5) and the other is R_{Mo-O}=2.01Å(C.N.=1.8), which are likely associated with Mo=O and Mo-O bonds, respectively. Along with those evidences in EXAFS evaluation in Table 1, the XANES of the catalyst activated 450°C(Fig. 4) propose a dimeric structure with a bridged oxygen alike a highly dispersed MoO_3 or MoO_4^{2-} ensemble, as the analogy of XANES spectra of the references.

Table 1 EXAFS Parameters for $Mo_2(OAc)_4/SiO_2$ by Thermal Activation in Vacuo at Diferent Temepratures. (4.1wt% Mo loading)

$Mo_2(OAc)_4/SiO_2$ Activation Temp	Bond	C.N.	R(Å)	ΔEo(ev)	σ(Å)	F(%)
25°C	Mo-Mo	1.0	2.10	8.92	0.049	1.2
	Mo-O	3.7	2.11	-7.78	0.089	
350°C	Mo-Mo	0.6	2.11	12.78	0.048	1.6
	Mo-O	1.8	2.06	-6.58	0.078	
450°C	Mo-Mo	0.7	2.80	-4.64	0.074	3.4
	Mo-O(1)	0.5	1.73	44.28	0.044	6.6
	Mo-O(2)	1.8	2.01	-2.55	0.074	

C.N.= coordination number, R(Å)=interatomic distance, ΔEo=inner potential correction, σ(Å)=Debye-Waller factor, F(%): correction factor: Experimental errors: 0.2 for C.N. and 0.02 for R(Å)

Accordingly it is suggested from the data of FTIR, UV-vis, ESR and XANES-EXAFS that a nobel dinuclear Mo species "$[Mo{\equiv}Mo]^{V}$" is homogeneously grafted on SiO_2 by the following successive reactions between $Mo_2(OAc)_4$ precursor and SiO_2 under the thermal activation:

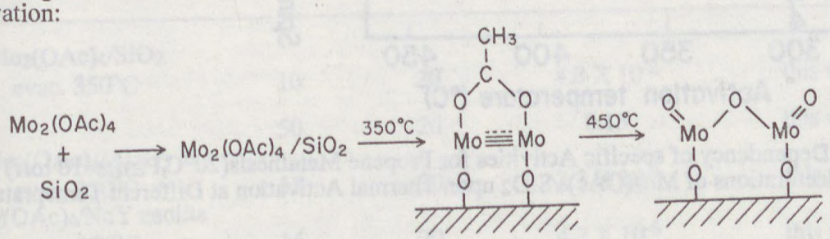

3.4. Actvity of propene metathesis and ethene homologation

The reaction of propene and ethene(10-16 torr) were carried out on the resulting catalyst by using a closed circulating reactor with a 150 ml volume. The amount of catalysts were 0.005-0.3 g. The dry-mixed $Mo_2(OAc)_4/SiO_2$ was completely inactive for propene metathesis(2 $CH_3CH{=}CH_2$ -----> $CH_2{=}CH_2$ + 2-butenes) and ethene homologation($3CH_2{=}CH_2$ -----> 2 $CH_3CH{=}CH_2$) until activated at 200°C, and a quite low activity even after heating at below 300°C. It was of interest that the $Mo_2(OAc)_4/SiO_2$ activated at above 300°C exhibited remarkable actvities for propene metathesis at the reaction temeperature of 0-20°C. Fig.6 shows the specific activities for propene metathesis to give an equal mixture of ethene and but-2-ene(Z:E=ca 0.5) as a function of the activation temeprature

for $Mo(OAc)_4/SiO_2$.The catalyst activated at 350°C provided the highest activity for propene metathesis, whereas it was inactive for the ethene homologation reation even at 110°C. After being activated at 450°C, the specific activity of the catalyst for propene metathesis markedly decreased. In contrast, the 450°C-activated catalyst showed appreciable activity for ethene homologation, as with conventional molybdenum catalysts[8]. The trend of catalyst performance in propene metathesis on the thermally activated $Mo_2(OAc)_4/SiO_2$ parallelled the change in ESR signal intensities(g=1.928) owing the formation of SiO_2-grafted $[Mo{\equiv}Mo]^V$ as depicted in Fig.6. This implys that the SiO_2-grafted $[Mo{\equiv}Mo]^V$ species is specifically resposible for olefin metathesis. The specific activities of propene metathesis on some supported molybdenum catalysts prepared from various Mo precursors, its activation(pretreatment) and supporting materials, as summerized in Table 2. The 350°C-activated $Mo_2(OAc)_4/SiO_2$ gave the highest activity for propene metathesis , which were 10^2-10^5 times more active per unit of Mo sites than those on the catalysts prepared from other Mo precursors and supporting materials under the similar reaction conditions, e.g., reaction temperature and propene pressure.

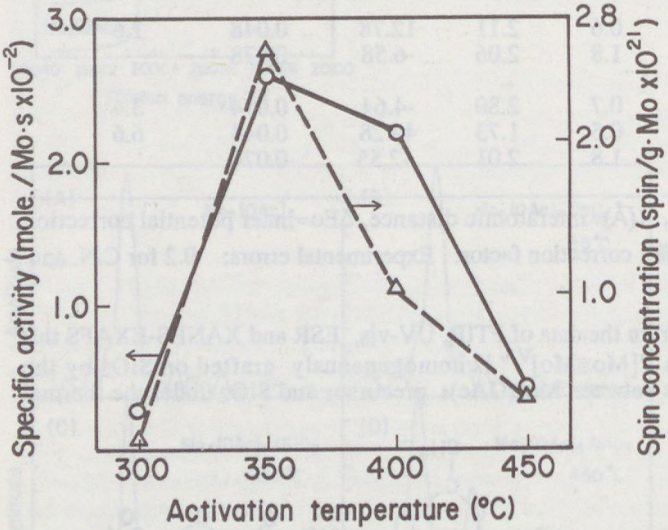

Fig. 6 Dependency of specific Activities for Propene Metathesis(20°C,P_{C3H6}=10 torr) and Spin Concentrations of $Mo_2(OAc)_4/SiO_2$ upon Thermal Activation at Different Temepratures

3.5. Poisoning of NO for propene metathesis on 350°C-activated $Mo_2(OAc)_4/SiO_2$.

It has been reported that NO and O_2 considerably suppress the propene metathesis on the conventional Mo catalysts[16]. NO having an unpaired electron acts as one-electron donating molecule for the paramagnetic species. NO(99.9% Purity) was admitted at 25°C onto the catalyst activated at 350°C, followed with the propene metathesis after evacuation of the gas-phase NO at 25°C. It is of noteworthy that NO efficiently surpress the metathesis activity upon exposure to 350°C-activated $Mo_2(OAc)_4/SiO_2$. The rates of propene metathesis at 20°C decreased in the linear-relatioship with the amount of chemisorbed NO. The number of chemisorbed NO to completely poison the propene metathesis approximately corresponds to the number of a Mo_2 pair as the SiO_2-grafted $[Mo{\equiv}Mo]^V$, which was

equivalent to total spin concentration of ESR signal. It was also found that the ESR signal intensity (g=1.928) greatly decreased upon exposure of NO at 20°C, resulting in the new ESR signal associated with an adduct of $[Mo\equiv Mo]^{V}$ with NO.

3.6. Activity of $Mo_2(OAc)_4$-derived catalysts supported on Al_2O_3 and NaY-zeolite.

In stead of SiO_2 , Al_2O_3 and NaY zelite were used to impregnate with $Mo_2(OAc)_4$. The $Mo_2(OAc)_4/Al_2O_3$ and $Mo_2(OAc)_4$/NaY-zeolite have been prepared by the similar dry-mixing technique with grinding under the N_2 atmosphere at 25°C. The XRD measurements suggest that $Mo_2(OAc)_4$ is highly dispersed on Al_2O_3 and inside NaY-zeolite by heating in vacuo at 50°C and 250°C, respectively, where any $Mo_2(OAc)_4$ crystal does not exist in the dry-mixting samples. The catalysts were prepared by thermal activation of $Mo_2(OAc)_4$/NaY-zeolite in vacuo at 300 and 350°C, which showed a intense but broden ESR signals, relatively different from that of $Mo_2(OAc)_4/SiO_2$ activated at 350°C. The in-situ FTIR study on the surface reaction betwen $Mo_2(OAc)_4$ /NaY zeolite demonstrated that $Mo_2(OAc)_4$ is mainly converted to mono-dentate Mo_2-acetate interacted with the Lewis sites such as Al^{3+} on the internal walls of zeolites, in formying "Mo-O-C(=O --Al^{3+})CH_3" The intense band at 1578 cm^{-1} appeared by thermal activation of $Mo_2(OAc)_4$/NaY at 250-350°C. Nevertheless, the catalysts derived from $Mo_2(OAc)_4/Al_2O_3$ exhibited the catalytic activity for propene metathesis at 25°C with a lower than $Mo_2(OAc)_4/SiO_2$, whereas negligibly on $Mo_2(OAc)_4/SiO_2$ after the similar thermal activation at 300 and 350°C, as shown in Table 4. The results suggest that the surface aciditiy is affected to reduce the stability of $Mo_2(OAc)_4$, resulting in the cleavage of Mo-Mo bond.

Table 2. Relative Activities for Propene Metathesis on supported Molybdenum Catalysts Prepared from Defferent Precursors Impregnated on SiO_2, Al_2O_3 and NaY-zeolite

Precursor/Support (activation)	C_3H_6 (torr)	Temp (°C)	Specific Activity (mole/Mo atom/sec)	reference
$Mo_2(OAc)_4/SiO_2$ evac. 350°C	10	20	4.8×10^{-2}	this work
	50	20	0.15	this work
$Mo_2(OAc)_4/Al_2O_3$ evac, 350°C	15	20	7.2×10^{-4}	this work
$Mo_2(OAc)_4$/NaY zeolite evac, 350°C	15	20	4.2×10^{-6}	this work
$Mo_2(NMe_2)_6/SiO_2$ evac, 280°C	18	25	9.8×10^{-6}	5
$Mo(\pi\text{-ally})_4/Al_2O_3$	21	0	8.2×10^{-5}	18
$Mo_2O_4(C_2O_4)^{2-}/Al_2O_3$ CO red, 500°C	120	25	7.2×10^{-3}	19
$MoOx(x=2.9\text{-}2.3)/TiO_2$ H_2,550°C	25	25	2.7×10^{-7}	17
$SnMe_4$ added	25	25	5.4×10^{-4}	17

4. CONCLUSION

(1) $Mo_2(OAc)_4$ is an effective precursor to homogeneously graft a dinuclear Mo species on SiO_2 by the thermal activation, where bidentate acetato ligands react with OH groups on SiO_2 in keeping the multiple Mo-Mo bonding.

(2) The XANES-EXAFS data suggest that the $Mo_2(OAc)_4$ impregnated on SiO_2 retain its quadruple Mo-Mo bond after thermal activation at below 350°C in vacuo, giving the SiO_2-bound Mo species having a multiple Mo-Mo bond (R_{Mo-Mo}=2,11Å, C.N.=0.6), which is identical with those of the precursor $Mo_2(OAc)_4$ (R_{Mo-Mo}=2.10Å, C.N.=1.0).

(3) The resulting SiO_2-grafted dinuclear species exhibited the remarkable activity for propene metathesis, whereas inactive for ethene homologation.

(4) The surface-bound Mo species prepared from 350°C-activated $Mo_2(OAc)_4/SiO_2$ showed a intense and sharp ESR signals centered with $g//=g_1=1.928$, which is assigned to $[Mo{\equiv}Mo]^V$. By the exceeding thermal activation at above 400°C, the Mo-Mo bond was cleaved to give the highy dispersed Mo^V oxide, which is not active for propene metathesis.

(5) NO specifically poison the propene metathesis on the 350°C-activated catalyst.

(6) The catalysts preparared from $Mo_2(OAc)_4/Al_2O_3$ and $Mo_2(OAc)_4$/NaY-zeolite are not active for propene metathesis.

+On leave form Deartment of Chemical Engineering, Tianjin University, Tianjin, 300072, China; #On leave from Dalian Institute of Chemical Physics, Dalian, 116012, China

Acknowledgement

A part of this work has been financially supported by a Grant-in-Aid for Science Research (02640330) from the Ministry of Education, Science and Culture of Japan.

5. References

1. M. Ichikawa, Tailored Metal Catalysis, ed. Iwasawa, Reidel, Dordrecht, 184, pp184-263: Metal Clusters in Catalysis, ed. B.C. Gates, L. Guczi and H. Knozinger, Elsevier, Amsterdam, 1986
2. M. Ichikawa, Polyhedron, 7, 2351(1988)
3. A. Fukuoka, T. Kimura, N. Kosugi, H. Kuroda, Y. Minai, Y. Sakai, T. Tominaga, and M. Ichikawa, J. Catal. , 126, 434(1990)
4. Y. Sato, Y. Iwasawa, and H. Kuroda, J. C.S., Chem. Commun., 1101(1982
5. Q. Zhuang, K. Tanaka, and M. Ichikawa, J.C.S., Chem. Commun., 1477(1990)
6. K. Asakura, K. Kitamura-Bando, Y. Iwasawa, H. Asakawa, and K. Isobe, J. Am. Chem. Soc.,112, 9096(1990)
7. K.A. Vikulov, I.V. Elev, B.N. Shelimov, and V. A. Kazansky, J. Mol. Catal., 55, 126, (1989)
8. K. Tanaka, K. Tanaka, H. Takeo, and C. Matsumura, J. Am. Chem. Soc., 109, 2422(1987)18: M. Kazuta and K. Tanaka, J. Catal., 123, 164(1990)
9. B. Zhang, Y. Li, Q. Lin, and D. Jin, J. Mol. Catal., 46, 229 (1988)
10. I.V. Elev, B.N. Shelimov, and V.A. Kazansky, J. Catal., 113, 229(1988)
11. N. Kosugi and H. Kuroda, EXAFS2/V03, Research Center for Spectrochemistry, Univ. Tokyo, Japan(1987)
12. F.A. Cotton, J.G. Jr., Norman, J. Coord. Chem., 1, 161(1971)
13. T. Fukushima, H. Arakawa and M. Ichikawa, J. Phys. Chem., 89, 4440(1985)
14. F.A. Cotton and E. Pedersen, Inorg. Chem., 14, 399(1975)
15. R.F. Howe and I.R. Leith, J.C.S., Faraday Trans, I, 69, 1967 (1973)
16. A.A. Olsthoon and J.A. Moulijn, J. Mol. Catal., 8, 147 (1980)
17. K. Tanaka and K-I. Tanaka, J. Chem. Soc.,Faraday Trans.I,71,601(1988)
18. Y. Iwasawa, H. Ichinose, and S. Ogasawara, J. C S., Faraday Trans. I, 77, 1763(1981)
19. A.N. Startsev, O.V. Limov, and S.A. ShKuropat, React. Kinet. Catal. Let.t., 41, 121(1990)

DISCUSSION

Q: A. A. Tsyganenko (Russia)
You have used IR spectroscopy to follow the process of catalyst preparation. Have you not tried to study coordination and oxidation states of molybdenum in the catalyst using CO as a test molecule ?

A: M. Ichikawa
We have performed IR observation on the interaction of CO and NO with the resulting catalysts after the thermal activation of $Mo_2(OAc)_4/SiO_2$. A weak CO band was detected at 2130 cm^{-1} in CO admission on 350 ^{0}C-activated $Mo_2(OAc)_4/SiO_2$, which is reflected in a weak CO interaction with the SiO_2-grafted $[Mo=Mo]^V$ species.

Q: J. C. Mol (The Netherlands)
One of your conclusions is that catalysts prepared from $MoO_2(OAc)_4/Al_2O_3$ and $MoO_2(OAc)_4$/NaY-zeolite are not active for propene metathesis. It can be seen in your Table 2, however, that the alumina-supported $MoO_2(OAc)_4$ catalyst exhibits an activity for propene metathesis which is comparable to that of $SnMe_4$-treated MoO_x/TiO_2. For the latter catalyst this was reported [1] to be a high activity. Why did your say that this system is not active ?
[1] H. Tanaka, K. Tanaka, *J. Chem. Soc. Chem. Commun.*, 748,**1984**

A: M. Ichikawa
Compared with the SiO_2-grafted Mo dimer species, we found that the relative activities of the catalysts prepared from $Mo_2(OAc)_4$ impregnated on Al_2O_3 and NaY zeolite were 102-104 times lower on the basis of $Mo_2(OAc)_4$ as the precursor, although their activities are comparable for those on $SnMe_4$-modified Mo/TiO_2 catalyst. This may be associated with the inhomogeneity of the active Mo sites in the conventional Mo/TiO_2 catalysts, the limited part (less than 1%) of which are catalytically active for the olefin metathesis (ref. 17 in our paper).

Q: W. Grünert (Germany)
You have highly active metathesis catalysts, but they are unusual in many respects. In homogeneous catalysis, there was little success with dimolecular precursors possessing metal-metal-bonds the most active catalysts are monomolecular. The oxidation state of your Mo precursor is different from that usually considered to be active for carbene formation (+4). Now, in addition to your written paper you propose that in your case a pairwise carbene mechanism is operative instead of the widely accepted non-pairwise mechanism. Now, a conclusive decision of the latter problem could be obtained from experiments with labelled olefins. Have you evidence of this kind to support your hypothesis that a pairwise carbene mechanism operates ?

A: M. Ichikawa
We propose the pairwise mechanism for the olefin metathesis to explain the marked activities of $[Mo=Mo]^V$ species grafted on SiO_2, which is by contrary completely inactive for the homologation reaction. This is the crucial evidence to take account in the difference from the carbene mechanism proposed for the conventional Mo catalysts which are active for both reactions. We are performing the ^{13}C-labelling tracer experiment on the SiO_2-grafted Mo dimer catalyst to justify the metathesis mechanism.

Q: W. K. Hall (USA)
We showed over a decade ago that NO can be used as a selective poison to estimate the density of catalytic sites on conventional molybdena-alumina catalysts. You have done likevise and observe that the activity is "killed" by the adsorption of one NO per two molybdenum:

a) does that mean that one NO poisons one dimolecular site, and

b) have you observed $(NO)_2$ species present by IR ? We observed these were the "poison" species in our work.

A: M. Ichikawa

The propene metathesis was completely retarded by NO chemisorbed on SiO_2-grafted $[Mo=Mo]^{V}$ in ca. 1:1 molar ratio, which implies that one NO poisons each site of the paramagnetic $[Mo=Mo]^{V}$ grafted on SiO_2, which is active for the olefin metathesis. We observed the IR bands at 1740 and 1820 cm^{-1} characteristic of dinitrosyl "$(NO)_2$" on the 350 ^{0}C-activated $Mo_2(OAc)_4/SiO_2$ in NO chemisorption at 25-70 ^{0}C, possibly formed in the disproportionation of mono-dentate NO bound with $[Mo_2]^{V}$ species.

Q: J. C. Conesa (Spain)

I should like to ask about the fitting of the EXAFS data in the sample activated at 450 ^{0}C. The fit of the short Mo-O(1) distance needed for the ΔE_0 parameter in a rather large value, 44 eV, quite outside the range normally accepted for this technique. Could you comment on confirmations of the reliability of this result ?

I wish also to have a confirmation of the ESR g value in the work by Cotton quoted by you: is it g = 2.417 as written in the preprint book, or close to 1.9 as mentioned during your oral presentation ?

A: M. Ichikawa

1) We performed the curve-fitting analysis for the Mo K-edge EXAFS data of Mo-O contribution on the sample of 450 ^{0}C-activated $Mo_2(OAc)_4/SiO_2$ using the reference of MoO_3 and K_2MoO_3. The CN and R parameters were obtained with a good fitting in terms of Debye-Waller factor, but they provided larger values of inner potential correction (E_0) and correction factor (F) for shorter Mo=O bond. This is possibly due to the difficulty to extract the smaller contribution of Mo=O bond from the relatively noisy background in the region of R = 0.1-0.2 nm. We have reevaluated the EXAFS data for Mo-O bonding to improve the curve-fitting, giving the final parameters: c.f. CN (Mo=O(1)) = 0.6, R=0.182 nm in E_0 = -10.2.

2) Cotton et al., reported the symmetric sharp ESR band centered at g(parallel) = g(perpendicular) = 1.941 for the one-electron oxidized species of $Mo_2(C_3H_7COO)_4$ with eleven hyperfine structure, which is quite similar to that of $Mo_2(OAc)_4/SiO_2$ after the 350 ^{0}C-activation.

Q: D. C. Koningsberger (The Netherlands)

What is the Mo-Mo coordination distance in your reference compound: $Mo_2(OAc)_4$ ($R=CH_3$) ?

How did you separate in your analysis Mo-O and Mo-Mo at approximately the same coordination distance ?

Did you perform a statistical analysis of your data ?

Is the two shell model: Mo-O(1) and Mo-O(2) of the sample reduced at 450 ^{0}C statistically significant ?

A ΔE_0 value of 44 eV is impossible and much too large: what is your reference for the Mo-O(1) coordinates ?

A: M. Ichikawa

The EXAFS analysis for $Mo_2(OAc)_4$ in crystal provided the Mo-Mo coordination distance of 0.21 nm with CN = 1.0. (R_{Mo-Mo} = 0.21 nm in crystal XRD), which is good agreement with that of the highly dispersed on SiO_2 at room temperature.

We extract first the Mo-Mo contribution in k^{-1} space = 4-12 1/A using the reference values of Mo-Mo distance as reported in the crystal XRD. The Mo-O bond contribution was

separated by subtraction of the Mo-Mo bond in FT data, using the FT parameters for the 450 ^{0}C activated sample having no Mo-Mo bond contribution.

We performed the statistical analysis of our data of 450 ^{0}C activated sample for the two shell model of Mo=O(1) and Mo-O (2) using the references, O_hMoO_3 and $T_dK_2MoO_4$ crystals. The unusually large value of E_0 for Mo=O(1) in the 450 ^{0}C activated sample has been re-examined to improve the curve-fitting analysis, giving the smaller value of E_0 = -10.2, as we discussed in the answer to Dr. Conesa.

Q: J. Vedrine (France)

You have shown that ESR spectrum intensity (Figure 6) follows the activity of propene metathesis as function of activation temperature. However, the ESR signal shown corresponds to a d^1 ion interacting with two Mo ions (II hff lines) as Mo(V)Mo(VI) or Mo(V)Mo(IV). For active dimer you should see (I=1) a spectrum at much lower magnetic field (so called fine structure). The question is: what ESR spectrum did you record between O and 3000 G ?

A: M. Ichikawa

The electronic structure of $[Mo{=}Mo]^v$ species is denoted as $\sigma^2\pi^4\delta^1$ to be consisted of mixed valent Mo(II)-Mo(III). The ESR signals for the $[Mo{=}Mo]^vX_4$ species are reasonably observed at g = 1.02-1.94 varing X=CH_3,C_2H_5,C_3H_7 and SO_4 (ref. 12). No other ESR signals except the sharp band centered at g = 1.928 were observed in the record between 0-3000 G on our samples of $Mo_2(OAc)_4/SiO_2$ after 350 ^{0}C-activation.

Q: J. J. Rooney (Ireland)

M. A. McCann (his results has been published) has recently shown that $Mo_2(OAc)_4$ is a catalyst by itself in solvent at 25 ^{0}C for metathesis polymerization of norbornene the high molecular weight linear polymer. This rules out a pairwise mechanism for the Mo_2 complex.

A metallocyclobutane

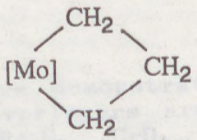

will give metathesis or homologation depending on the oxidation state of Mo.

A: M. Ichikawa

Thank you very much for your suggestive comment (c.f. Mc Cann) to show the catalytic activity of $Mo_2(OAc)_4$ as the precursor in the methathesis polymerization of norbornene, although it is not clear what a Mo species is generated in solution and responsible for the polymerization. We propose a pairwise mechanism for olefin metathesis on our SiO_2-grafted Mo dimer species, but not yet ruled out other possible mechanisms including the metalocyclobutane or carbene intermediate. Recently, we have found in TPD study that $Mo_2(OAc)_4/SiO_2$ gave an equimolar mixture of CO and CH_4 with a small amount of ethene and ethane by the thermal activation at 300-350 ^{0}C. These suggest that acetate ligand of precursor $Mo_2(OAc)_4$ may provide carbene (CH_2:) in the thermal activation to bind with Mo_2 species grafted on silica, which may be incorporated in olefin metathesis. We are studying now by FTIR using ^{13}C- and ^{2}H-labelled olefins and acetate to characterize the in situ intermediate species derived from the SiO_2-grafted $Mo_2(OAc)_4$ active for olefin metathesis.

Guczi, L. *et al.* (Editors), *New Frontiers in Catalysis*
Proceedings of the 10th International Congress on Catalysis, 19-24 July, 1992, Budapest, Hungary
© 1993 Elsevier Science Publishers B.V. All rights reserved

MOLECULAR DESIGN OF SUPPORTED METAL OXIDE CATALYSTS

I. E. Wachs, G. Deo, D. S. Kim, M. A. Vuurman and H. Hu

Zettlemoyer Center for Surface Studies, Departments of Chemistry and Chemical Engineering, Lehigh University, Bethlehem, PA 18015, USA

Abstract

This study demonstrates that molecular design of supported metal oxide catalysts is possible from molecular level information obtained from combined Raman spectroscopy and the methanol oxidation reaction. The important factors that influence the molecular design of the supported metal oxide catalysts are the specific oxide support (factor of $\sim 10^3$) and the specific surface metal oxide (factor of $\sim 10^1$). The synthesis method is not critical since it does not influence the surface metal oxide structure or reactivity. Calcination temperature is not important as long as moderate temperatures (350-500°C) are used.

1. INTRODUCTION

Many recent studies have demonstrated that two-dimensional transition metal oxide overlayers are formed when one metal oxide component (i.e., Re_2O_7, CrO_3, MoO_3, WO_3, V_2O_5, Nb_2O_5, etc.) is deposited on a second metal oxide substrate (i.e., Al_2O_3, TiO_2, SiO_2, etc.) [1]. The molecular structures and reactivity of these surface metal oxide species have been intensively investigated over the past decade because of the importance of these supported metal oxide materials in numerous catalytic applications [1,2]. The major structural information about these surface metal oxide species has been derived from Raman spectroscopy studies because of the molecular nature of this characterization method and its ability to discriminate between different metal oxide species that may simultaneously be present in the catalyst. Corresponding reactivity studies have demonstrated that these surface metal oxide species possess the active sites for many catalytic reactions. The fundamental information currently available about these oxide catalysts is beginning to allow us to molecularly design supported metal oxide catalysts. The molecular design of supported metal oxide catalysts requires that we specify the synthesis method, oxide support, catalyst composition, calcination temperature, location and structure of surface metal oxide species, as well as its reactivity. Consequently, the influence of each of the above parameters

upon the catalytic properties of supported metal oxide catalysts needs to be examined. The present study primarily focuses on the molecular design aspects of supported vanadium oxide catalysts because these catalysts constitute a very important class of heterogeneous oxide catalysts. However, comparison with other supported metal oxide systems (MoO_3, Re_2O_7, and CrO_3) will also be made.

2. EXPERIMENTAL

The oxide supports employed in the present study were: TiO_2 (Degussa, ~55 m^2/g), Al_2O_3 (Harshaw, ~180 m^2/g), SiO_2 (Cabot, ~300 m^2/g), ZrO_2 (Degussa, ~39 m^2/g) and Nb_2O_5 (Niobium Products Co., ~50 m^2/g). Many different synthesis methods have been used to prepare supported metal oxide catalysts. In the case of supported vanadium oxide catalysts, the catalysts were prepared by vapor phase grafting with $VOCl_3$, nonaqueous impregnation (vanadium alkoxides), aqueous impregnation (vanadium oxalate), as well dry impregnation with crystalline V_2O_5 (spontaneous dispersion).

Supported chromium oxide (1% wt.), rhenium oxide (1% wt.) and molybdenum oxide (1% wt.) catalysts were prepared by the incipient-wetness impregnation method using an aqueous solution of chromium nitrate, $HReO_4$, and ammonium heptamolybdate, respectively.

The molecular structures of the supported metal oxide catalysts were characterized by laser Raman spectroscopy under *in situ* as well as ambient conditions. The laser Raman spectroscope consist of a Spectra Physics Ar^+ laser producing 1-100 mW of power measured at the sample. The scattered radiation was focussed into a Spex Triplemate spectrometer coupled to a Princeton Applied Research OMA III optical multichannel analyzer. About 100-200 mg of the pure catalysts were pelletized and used for obtaining the Raman spectra in the *in situ* mode. For ambient spectra 5-20 mg of catalysts was placed on a KBr backing.

The supported metal oxide catalysts were examined for their reactivity in the methanol oxidation reaction. The reactor was operated in the differential mode by keeping conversions below 8%. A methanol/oxygen/helium mixture of ~6/13/81 at 1 atm pressure was used as the reactant gas for all the data presented. The analysis was performed on an online gas chromatograph (GC) (HP 5840A) containing two columns (Poropak R and Carbosieve SII) and two detectors (FID and TCD). Reaction data at 230 °C are presented in the form of turnover number (TON) - defined as the number of moles of methanol converted per mole of vanadium atom per second. The reaction data for some catalysts were also obtained at 200, 240, 260 °C to calculate the activation energy and check for diffusional limitations in the reactor. No mass and heat transfer limitations were observed.

3. RESULTS AND DISCUSSION

It is well known that supported metal oxide catalysts possess surface metal oxide phases (see Figure 1) that are formed by the reaction of the deposited metal oxides with the surface hydroxyls of the high surface area oxide supports. Direct evidence for the titration of the surface hydroxyls (OH) by the deposited metal oxides is obtained from *in situ* infrared studies which reveal the sequential disappearance of the support OH bands during this process [3]. The consumption of surface hydroxyls can also be monitored by CO_2 chemisorption studies since CO_2 titrates the basic surface hydroxyls [3]. Both measurements, infrared spectroscopy of surface hydroxyls and chemisorption of CO_2 on the surface hydroxyls, provide a quantitative measure of the surface coverage of the metal oxide overlayer. Consequently, a necessary condition for the formation of surface metal oxide overlayers is the presence of reactive surface hydroxyls on the oxide support. Oxide supports such as Al_2O_3, TiO_2, ZrO_2, and Nb_2O_5 have a high surface density of reactive surface hydroxyls and tend to form a closed packed monolayer of the surface metal oxide phase, whereas, oxide supports such as SiO_2 which have a lower density of reactive surface hydroxyls do not form a closed packed monolayer of the surface metal oxide phase (see Table 1). Recent studies employing electrochemical methods [4] and non aqueous allyl preparation [5] have demonstrated that somewhat higher surface density on SiO_2 can be achieved with the special preparations, but still resulted in only a small fraction of a close-packed monolayer.

Table 1
Monolayer loading and surface density of some supported metal oxides as a function of oxide support

Oxide support	Surface area (m^2/g)	Monolayer loading (wt.%) V_2O_5	MoO_3	CrO_3	Re_2O_7	Surface density (wt.%/m^2) V_2O_5	MoO_3	CrO_3	Re_2O_7
Al_2O_3	180	20	18	13	17	.11	.10	.07	.09
TiO_2	55	6	6	--	5	.11	.11	--	.09
ZrO_2	39	4	3	--	5	.10	.08	--	.13
Nb_2O_5	55	6	4	4	--	.11	.07	.07	--
SiO_2	300	3	3	2	6.5	.01	.01	.01	.02

Thus, the surface hydroxyl chemistry controls the formation and location of the surface metal oxide species present in supported metal oxide catalysts.

The molecular structures of the surface metal oxide species present in the metal oxide overlayer are not well understood

and the influence of surface coverage (catalyst composition), specific oxide support, preparation method, calcination temperature, and promoters need to be established. The Raman spectra of titania supported vanadia catalysts reveal the presence of three different vanadia species on the TiO_2 support under *in situ* conditions [6]. At low loadings, a single sharp band is present at ~1030 cm^{-1} which is due to an isolated tetrahedral coordinated surface vanadium oxide species containing one terminal V=O bond and three bridging V-O-Ti bonds [7]. At intermediate loadings, a second band is present at ~930 cm^{-1} which has been assigned to a polymerized, tetrahedral coordinated surface vanadium oxide species [7]. At high loadings, a third sharp band is present at 994 cm^{-1} due to crystalline V_2O_5 which indicates that the close-packed surface vanadium oxide monolayer has been formed and all the reactive surface hydroxyls consumed. Thus, the catalyst composition is a critical parameter since it influences the formation of different vanadium oxide structures.

The reactivity of the titania supported vanadium oxide catalysts was probed by the methanol oxidation reaction. The methanol oxidation reaction is very sensitive to the nature of surface sites present in oxide catalysts. Surface redox sites (sites that are capable of being reduced and oxidized) form primarily formaldehyde as well as methyl formate and dimethyl methane as the reaction products. Surface acid sites, Lewis as well as Bronsted, result in the formation of dimethyl ether. Surface basic sites yield CO/CO_2 as the reaction products [8]. The oxidation of methanol over the titania supported vanadia catalysts yielded formaldehyde exclusively, 98%+, as the reaction product. The titania support in the absence of surface vanadia yielded dimethyl ether and trace amounts of CO_2. The almost complete formation of formaldehyde demonstrates that the reactivity of the titania supported vanadia catalysts is due to the surface vanadia redox sites. The reactivity is measured as the turnover number (TON), the number of moles of methanol reacted per surface mole of vanadium atom per second, and is presented in Table 2 as a function of the vanadia loading. The TON increases somewhat with initial surface vanadium oxide coverage, and decreases at surface coverages approaching and exceeding monolayer coverage. Note that the TON of bulk V_2O_5 is two orders of magnitude less than the titania supported vanadia catalysts indicating that crystalline V_2O_5 is significantly less active than surface vanadia species. The slight increase in TON with the increase in surface coverage appears to be related to the presence of the polymerized surface vanadia species. Similar coverage effects were also observed for supported rhenium oxide [9], molybdenum oxide [10] and chromium oxide catalysts [11]. Thus, the reactivity of surface metal oxide species has a slight dependence on surface coverage (less than a factor of 10^1).

Table 2
The TON of V_2O_5/TiO_2 catalysts as a function of loading

wt.% V_2O_5/TiO_2	T.O.N. (sec^{-1})
0.5	1.0
1.0	1.9
1.8	4.4
2.5	8.4
4.5	2.2
5.0	1.7
bulk V_2O_5	0.022

Many research groups claim that the synthesis method is critical for forming metal oxide monolayers that possess specific structures and reactivities. To investigate this issue, a series of V_2O_5/TiO_2 catalysts were synthesized by different methods: equilibrium adsorption, vanadium oxalate, vanadium alkoxides and vanadium oxychloride grafting. The *in situ* Raman spectra of all these catalysts exhibit a sharp band at ~1030 cm^{-1} characteristic of the isolated surface vanadium oxide species. Thus, the synthesis method does not affect the final structure of the surface vanadium oxide species on titania. Similar conclusions were also found for molybdenum oxide supported on titania [12], silica [5], and alumina [5]. Reactivity studies with methanol oxidation exhibited essentially identical turnover numbers. Consequently, the preparation method is not a critical parameter since it does not influence the structure of the surface metal oxide species or its reactivity.

The nature of the supported metal oxide phase is influenced by the calcination temperature. Moderate calcination temperatures, 350-500 °C, are required to decompose the metal oxide precursors (oxalates, alkoxides, oxychlorides, etc.) to form the surface metal oxide species [13]. Insufficient calcination temperatures do not completely decompose the precursors and, consequently, do not react with the surface hydroxyls to form the surface metal oxide species. However, high calcination temperatures, greater than 600 °C, can result in shrinking of the surface area of the oxide support and decreasing the available surface area for the surface metal oxide species. Consequently, high calcination temperatures increase the surface coverage of the metal oxide species and, in severe cases, destroy the surface metal oxide phase and form crystalline V_2O_5 and eventually solid state solutions [13,14]. Thus, calcination temperature is an important parameter that controls the activation and deactivation of supported metal oxide catalysts. However, supported metal oxide catalysts are typically prepared by calcining at 400-500 °C which would eliminate problems with activation and deactivation.

A series of ~1% V_2O_5 catalysts were prepared in order to

investigate the influence of different oxide supports upon the molecular structure and reactivity of the surface vanadium oxide species. The low loading catalysts were selected because at these surface coverages only the isolated surface vanadium oxide species is predominantly present on the different oxide supports and potential complication due to additional surface vanadium oxide species could be eliminated. The *in situ* Raman band due to the V=O bond was found to vary from 1015-1038 cm^{-1} as a function of the different oxide supports (see Table 3). The slight difference in band position is due to slightly different V=O bond lengths of the isolated surface vanadium oxide species on different oxide supports. The important point is that the Raman spectra reveal that the same surface vanadium oxide species are present on all the different oxide supports. The same conclusion is reached from solid state ^{51}V NMR studies of these catalysts [8]. Similar observations have also been made for supported molybdenum oxide [10], rhenium oxide [9,11], and chromium oxide [9,11]. Thus, the *in situ* surface metal oxide molecular structures are independent of the specific oxide support.

Table 3
In situ Raman band position for M=O terminal stretching vibration, as a function of oxide support for 1% supported metal oxide (M_XO_Y) catalysts

Oxide Support	Raman Band for M=O terminal bond			
	V	Mo	Cr	Re
SiO_2	1038	978	985	1015
Nb_2O_5	1031	990	997	1008
TiO_2	1027	993	1009	1005
ZrO_2	1024	986	1010	990
Al_2O_3	1015	992	1002	1000

The reactivity of the surface vanadium oxide species on the different oxide supports was probed by the methanol oxidation reaction. For all the supported vanadium oxide catalysts, with the exception of alumina which possesses a high concentration of acid sites, the surface vanadia redox sites produced formaldehyde almost exclusively. On alumina, only a trace of formaldehyde was formed because the surface acid sites formed dimethyl ether. Thus, for the V_2O_5/Al_2O_3 system the formaldehyde produced was taken as representative of the reactivity of the surface vanadia redox sites. The reactivity of the surface vanadia species on different oxide supports was found to dramatically depend on the specific oxide support (a factor of 10^3). Similar trends were also observed for supported molybdenum oxide [10], rhenium oxide [11], and chromium oxide [11]. The specific oxide support is a critical parameter since it has such a profound effect on the reactivity of the surface metal oxide species.

The origin of this support effect is either due to

differences in the terminal M=O bond or the bridging M-O-Support bond. Many publications have proposed that the terminal bond is responsible for catalysis and its activity is directly related to the M=O bond strength. To investigate this, the reactivity was plotted against the Raman position of the M=O bond (shorter bond corresponds to higher Raman position). The plot of TON versus Raman M=O position for supported vanadium oxide, molybdenum oxide, rhenium oxide, and chromium oxide is presented in Figure 2. There does not appear to be any relationship between the catalyst reactivity and the terminal M=O bond strength as was previously proposed. A more plausible conclusion is that the reactivity is related to the bridging M-O-Support bond since the oxide support has a very significant effect on the reactivity. This suggests that the reactivity should also be a function of the specific metal oxide species. Indeed, supported molybdenum oxide catalysts are about one order of magnitude less reactive than supported vanadia catalysts. The trend in reactivity with specific oxide support appears to be related to the surface reducibility of the oxide supports. The more reducible oxide supports (TiO_2, ZrO_2, and Nb_2O_5) always exhibit very high TON while the irreducible oxide supports (Al_2O_3 and SiO_2) always exhibit very low TON [15].

Additional information about the reactivity was obtained by determining the kinetic parameters during methanol oxidation for vanadia, molybdena, rhenia, and chromia on different oxide supports. For all these systems the activation energy is approximately the same, 18-22 kcal/mol. The activation energy corresponds to that expected for the breaking of the C-H bond of a surface methoxide intermediate, CH_3O_{ads}, and should be independent of the specific catalyst [16]. The pre-exponential factors, however, vary by orders of magnitude as the oxide support is varied. The difference in pre-exponential factors suggest that the number of active sites are responsible for the different TON. In calculating the TON we assume that all the surface vanadia species are participating in the reaction all the time. However, the different pre-exponential factor suggests that on less reducible oxide supports such as Al_2O_3 and SiO_2 only a small fraction of the surface vanadia species participate at a given time in the reaction, and that for reducible oxide supports such as TiO_2, ZrO_2, and Nb_2O_5 a significantly larger fraction of the surface vanadia species participate at a given time in the reaction. The different reactivities may also be due to different activity per active site. Experiments are currently in progress to quantify the number of active sites participating in the reaction at given time and their reactivity. Thus, the oxide supports control the reactivity of the surface metal oxide species.

Table 4
The TON for methanol oxidation reaction for various 1% supported metal oxide catalysts

Oxide Support	TON (sec^{-1})			
	V_2O_5	MoO_3	CrO_3	Re_2O_7
SiO_2	$2.0*10^{-3}$	$3.9*10^{-2}$ †	$1.6*10^{-1}$	$2.0*10^{-2}$ †
Al_2O_3	$2.0*10^{-2}$	--- ‡	$1.6*10^{-3}$	--- ‡
Nb_2O_5	$7.0*10^{-1}$	$3.2*10^{-2}$	$5.8*10^{-2}$	$1.2*10^{-2}$ †
TiO_2	$1.8*10^{0}$	$3.1*10^{-1}$	$3.0*10^{-1}$	$1.2*10^{0}$
ZrO_2	$2.3*10^{0}$	$9.2*10^{-2}$	$1.3*10^{0}$	$1.7*10^{-1}$

† metal oxide was found to be volatile and left deposits on tube
‡ no redox products observed due to activity of alumina support

Many publications have also claimed that the modification or structure of the oxide support is critical for obtaining a good catalyst [17]. To investigate this issue a series of V_2O_5/TiO_2 catalysts were prepared on different TiO_2 support structures (anatase, rutile, anatase+rutile, anatase+brookite, and B). *In situ* Raman characterization revealed that the same surface vanadia species were present on all the different titania supports with a band at 1024-1031 cm^{-1} for 1% V_2O_5/TiO_2. The reactivity of these different titania supported vanadia catalysts was probed with methanol oxidation and found to be identical with a TON of 2.1 ± 0.5 sec^{-1}. Thus, contrary to previous conclusions the structure or modification of the oxide support does not affect the surface metal oxide structure or the catalyst reactivity.

4. CONCLUSIONS

The above discussion demonstrates that it is possible to molecularly design supported metal oxide catalysts with the assistance of molecular characterization methods such as Raman spectroscopy. The formation and location of the surface metal oxide species are controlled by the surface hydroxyl chemistry, and the surface metal oxide species are located in the outermost layer of the catalysts as an overlayer. The catalyst composition is a critical parameter since it affects the presence of different metal oxide species (isolated surface species, polymerized surface species, and crystalline phases), and the reactivity, TON, also varies somewhat with surface metal oxide coverage. The preparation method is not a critical parameter since it does not influence the structure or reactivity of the surface metal oxide species. Calcination temperature is an important parameter that controls activation

and deactivation of supported metal oxide catalysts, but calcination temperature is not critical if moderate temperatures, 350-450 °C, are used. The specific oxide support is a critical parameter since it dramatically affects the reactivity of the surface metal oxide species, but the structure of the oxide support has no effect on the surface metal oxide structure and reactivity. In summary, the critical parameters that affect the catalytic properties are the specific oxide support (factor of 10^3) and catalyst composition or surface metal oxide coverage (factor of 10^1).

5. ACKNOWLEDGEMENT

G. Deo and H. Hu acknowledge the support by NSF grant # CTS-9006258.

6. REFERENCES

1 (a) L. Dixit, D.L. Gerrard, H. Bowley, Appl. Spectrosc. Rev., 22 (1986) 189; (b) J.R. Bartlett, R.P. Cooney, In *Spectroscopy of Inorganic-based Materials*, R.J.H. Clark, R.E. Hester, Eds; Wiley: New York, 1987; p 187; (c) F.D. Hardcastle and I.E. Wachs, In *Proc. 9th Intern. Congr. Catal.*, M.S. Phillips and M. Ternan, Eds., Vol. 4, Chemical Institute of Canada, Ontario, 1988, p 1449.

2. I.E. Wachs, Chem. Eng. Sc. Vol., 45(8) (1990) 2561.

3. K. Segawa and W.K. Hall, J. Catal., 77 (1982) 221; D.S. Kim, Y. Kurusu, I.E. Wachs, In *Proc. 9th Inter. Congr. Catal.*, M.S. Phillips and M. Ternan, Eds., Vol. 4, Chemical Institute Canada, Ontario, 1988, p 1460; A.M. Turek, I.E. Wachs, and E. DeCanio, J. Phys. Chem, submitted.

4. M. de Boer, A.J. van Dillen, D.C. Koningsberger, M.A. Vuurman, I.E. Wachs, and J.W. Geus, submitted to Catal. Lett.

5. C.C. Williams, J.G. Ekerdt, J.M. Jehng, F.D. Hardcastle, A.M. Turek, and I.E. Wachs, J. Phys. Chem., 95 (1991) 8781; C.C. Williams, J.G. Ekerdt, J.M. Jehng, F.D. Hardcastle, and I.E. Wachs, J. Phys. Chem., 95 (1991) 8791.

6. M.A. Vuurman, A.M. Hirt, I.E. Wachs, J. Phys. Chem., 95 (1991) 9928.

7. I.E. Wachs, J. Catal., 124 (1990) 570.

8. H. Eckert, G. Deo , and I.E. Wachs, unpublished results.

9. M.A. Vuurman, I.E. Wachs, D.J. Stufkens, and A. Oskam, J. Mol. Catal., submitted.

10. H. Hu and I.E. Wachs, in preparation.

11. D.S. Kim and I.E. Wachs, J. Catal., submitted

12. T. Machej, J. Haber, A.M. Turek, and I.E. Wachs, Appl. Catal., 70 (1991) 115.

13. R.Y. Saleh, I.E. Wachs, S.S. Chan, and C.C. Chersich, J. Catal., 98 (1986) 102.

14. G. Deo and I.E. Wachs, J. Phys. Chem., 95 (1991) 5889.

15. G. Deo and I.E. Wachs, J. Catal., 129 (1991) 307.
16. T.S. Yang and J.H. Lunsford, J. Catal., 103 (1987) 55; W.E. Fareneth, F. Ohuchi, R.H. Staley, U. Chowdhry and A. W. Sleight, J. Phys. Chem., 89 (1985) 2493.
17. A. Vejux and P.J. Courtine, J. Solid State Chem., 23 (1978) 93.

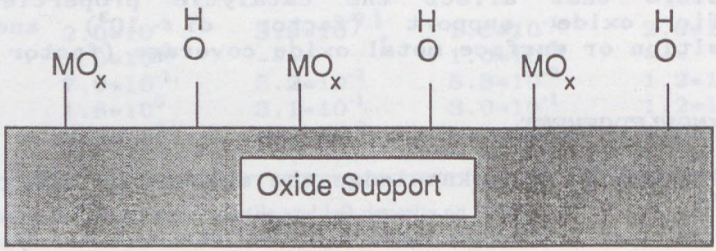

Figure 1 Surface Metal Oxide (MO_x) are formed by Titration of Surface Hydroxyls (OH) on Oxide Supports

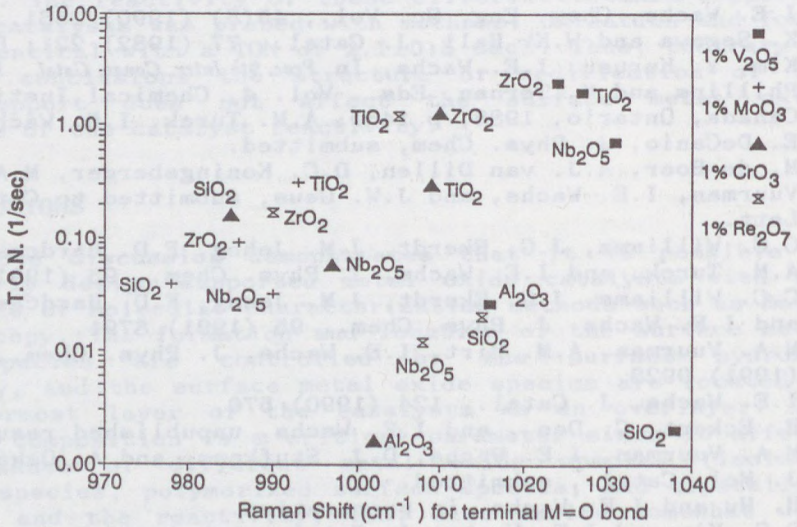

Figure 2 The plot of TON of the various supported metal oxides versus the *in situ* Raman band position of the terminal M=O stretch. The Raman band position is related to the M=O bond strength.

DISCUSSION

Q: U. S. Ozkan (USA)

I have a comment and a question. My comment is that we have compared the two phases of the titania support in selective catalytic reduction of NO over vanadia catalysts. We were able to identify polymeric vanadate species on both phases of the titania support. We did not see more differences between the catalytic activity of the vanadia species found on the two different support materials.

My question is: How did you calculate the turnover frequency (or turnover number, TON) for bulk V_2O_5 ? Could you describe it in detail ?

A: I. E. Wachs

Thank you for your comment regarding the similar properties of anatase and rutile supported vanadia catalysts for the selective catalytic reduction of NO_x.

To calculate the TON for V_2O_5 the surface of crystalline, V_2O_5 was assumed to have the same structure as the bulk, i.e., the area covered by a $VO_{2.5}$ unit was 1.03 nm. In addition, with the two up-two down arrangement of V_2O_5 bulk structure, only half of the area of the bulk of V_2O_5 was considered as active. Based on this assumption the number of active vanadium units could be calculated and, consequently, the TON could be obtained.

Q: F. Solymosi (Hungary)

Your paper contained many interesting data. I have a little problem with your last conclusion, namely that the catalytic behavior of V_2O_5 was completely independent of the structure, preparation, and pretreatment of the TiO_2 support. We know that the properties and reactivity of TiO_2 can be strongly influenced by those factors. Therefore, I would rather prefer to say that in the oxidation of methanol the properties of TiO_2 support do not play an important role. This could be different for other reactions.

A: I. E. Wachs

The reason that many researchers have claimed that the type of TiO_2 support is critical is because they have been using commercial titania pigments that are usually contaminated with K, P, Al, and Si on the surface. We have carefully compared different titania phases that were synthesized in the laboratory and had relatively clean titania surfaces (as determined by XPS). Such clean titania samples show no difference between the type of titania support.

These findings are not limited to methanol oxidation since they have been observed for much more complex reactions (see comments of Professor Trifiro for o-xylene oxidation and Professor Ozkan for selective catalytic reduction of NO_x).

Q: A. K. Datye (USA

Your results show that changing the support can increase the reactivity of the dispersed oxide by 3 orders of magnitude. It is indeed remarkable that the structure of the dispersed oxide as seen by Raman spectroscopy is not affected by the support. For comparison, it would help if you provide data on the reactivity of the corresponding bulk oxides, also as a turnover number.

A: I. E. Wachs

We have also measured the turnover number for bulk crystalline V_2O_5 and found it to be 2.2×10^{-2} s^{-1}, which is two orders of magnitude less than for V_2O_5/ZrO_2 and one order of magnitude more than V_2O_5/SiO_2. It is not possible to measure the TON for Re_2O_7/CrO_3 phases because they are not thermally stable and volatilize/phase transform at the conditions of the oxidation reaction. We have recently measured the TON for bulk MoO_3, and found it to be ~10^{-2} s^{-1}.

Q: F. Trifiro (Italy)

For some years now we have investigated the catalytic behavior of V-TiO_2 (either rutile or anatase) for oxidation of o-xylene to phthalic anhydride and ammoxidation of xylenes and toluenes. We have found very slight differences between the two types of support. I confirm the results of Professor Wachs concerning the TiO_2 as support for V_2O_5.

A: I. E. Wachs

Thank you for your comments regarding the similar catalytic properties of vanadia supported on anatase and rutile for the oxidation/ammoxidation of o-xylene and butenes.

Q: Y. Iwasawa (Japan)

I agree with the question of Professor Solymosi. Different surface structures have been reported from different preparation methods (see pp.503,515,529). My question is concerned with an increase in the TON for methanol oxidation as a function of Mo content on support. Could you make some comment on the meaning of this ?

A: I. E. Wachs

The papers that typically claim different surface metal oxide structures usually do not extensively characterize their samples and do not compare different preparations side by side (especially important in such studies is to maintain the same metal oxide loading). I would be happy to characterize samples from other laboratories by Raman spectroscopy to confirm this conclusion.

Our recent data show that the TON for the MoO_3/TiO_2 catalysts vary from $2x10^{-1}$ to $4x10^{-1}$ s^{-1}, and the apparent increase in the TON is minor.

Q: J. G. van Ommen (The Netherlands)

The fact that you find the same behavior for V_2O_5 on TiO_2 rutile and anatase is very surprising. Why is the type of support so important and not the structure ?

My question is: can you exclude that the anatase you use is not covered with a surface layer of rutile ? If this is the case (or anatase covering rutile, which is not to be expected) you should find the same results for V_2O_5 activity in MeOH oxidation and V_2O_5 reduction.

An other remark: old results also from our group show that careful washing of K and P containing sample gives clean anatase and/or rutile surfaces,which show different behavior in MeOH oxidation, reduction (TPR) and especially in toluene oxidation. This cannot be explained by the presence of surface contaminations ?

A: I. E. Wachs

The reason that different support types (Al_2O_3, TiO_2, SiO_2, etc.) affect the catalytic properties of vanadium oxide monolayers is that the support is a ligand that controls the ease of oxygen removal from the V-O-S (S=support) band. However, this is a local phenomenon that does not depend on long range order (anatase or rutile). Consequently, only the support type (Al_2O_3, TiO_2, SiO_2, etc.) is critical.

This is a very interesting question. Raman spectroscopy is much more sensitive to anatase compared to rutile and, thus, we should be able to detect an anatase overlayer on rutile (which is probable at mild calcination temperatures when rutile is not formed). The reverse situation is more difficult since a rutile overlayer will not be readily detected by Raman spectroscopy. We plan to attempt such a synthesis to address this question, but I feel that the titania overlayers will not adopt the bulk structures because of epitaxial growth.

The surface of the extracted TiO_2 [1] still did contain impurities of P_2O_5 and K_2O as determined by X-ray fluorescence. In addition, the surface concentration is important, not the bulk concentration of these impurities as shown by X-ray fluorescence. For this reason it appears that the surface of these vanadia-titania catalysts still contain the impurities.

[1] B. Claudel, M. Nueilati and J. Andrieu, *Appl. Catal.*, **11**, 317 (1984)

Q: A. Andersson (Sweden)

1) In the case of vanadia on anatase, you have observed two Raman bands at 1030 and 930 cm^{-1} which you assign to isolated and polymerized vanadia species, respectively. Have you considered the possibility that the two bands can be from differing species on different surface planes of titania ?

2) You have found the same vanadia species to be present on the various polymorphs of titania. In our laboratory we have found similar spectral features as you have for vanadia on anatase. However, for vanadia on TiO_2(B) we observed a Raman band at 970 cm^{-1}. Also, we found the monolayer on anatase to give 50% selectivity for benzaldehyde formation in toluene oxidation. The monolayer our TiO_2(B) gave only combustion. Even though vanadia can be in tetrahedral coordination on both supports, the V-O bond lenghts angles most differs. Can you comment on this ?

A: I. E. Wachs

1) I do not think these two Raman bands are due to different surface planes of titania because they are observed on other oxide supports as well. The same surface species are essentially formed on all oxide supports.

2) We have observed the 1030 cm^{-1} Raman band shift to 970 cm^{-1} upon addition of small amounts of K to V_2O_5/TiO_2. Since TiO_2(B) is made from a potassium titanate precursor, it may be possible that some residual K is present which would alter the spectral and catalytic properties of your TiO_2(B) catalysts.

Q: W. K. Jozwiak (Poland)

I like very much your generalizing approach trying to put some order in so complicated matter of the heterogeneous catalysis. Even with the most unfavorable starting materials (such as mechanical mixture of α-Cr_2O_3 and SiO_2 (also Al_2O_3 or MgO) we have been able to obtain the effective ethylene polymerization catalyst. Thus, the process of chromium redispersion (confirmed by XRD and TPR methods) takes place in the oxidative atmosphere above 500 ^0C. Probably the crucial role is played by the support hydroxyl groups, governing the sort of equilibrium sintering $\rightleftharpoons$ redispersion between surface and bulk oxide phases. Do you suppose that such behavior may be common among your oxide/support systems ?

A: I. E. Wachs

The spreading of metal oxides onto supports have been demonstrated in the literature for many oxide systems (MoO_3, V_2O_5, WO_3, etc.). These oxides are all mobile at elevated temperatures and spontaneously diffuse over oxide surfaces of supports (silica is somewhat of an exception because of the low concentration of reactive surface hydroxyls). Thus, oxides with low melting temperature will have sufficient mobility to spontaneously disperse over oxide supports.

Q: D. Wang (China)

Your work demonstrated the importance of surface hydroxyl groups in the preparation of supported metal oxides. Is there any difference in hydroxyl groups (1) of any one support, and (2) of different supports ?

A: I. E. Wachs

The hydroxyl groups of oxide supports depend on the support type (Al_2O_3, TiO_2, SiO_2, etc.) and usually several different hydroxyls are present on the same support. A very detailed article on surface hydroxyls has recently been written [2]

[2] H.-P. Boehm and H. Knözinger in "*Catalysis Science and Technology*", (Eds.: J. R. Anderson and M. Boudart), 1983, **Vol. 4**, Chap. 2

Q: J. M. Thomas (United Kingdom)

In describing the preparation of your surface overlayers you emphasized, not unnaturally, that it is the OH concentration of the exterior surface of the support that is all important. One wonders, therefore, whether you have considered taking several of the minerals that have constitutional OH in their structures as supports. Perhaps kaolinite, with nice flat surfaces such in OH groups, is not stable enough. But what of the oxy-hydroxides (e.g. CrOOH) which would give you the added advantage of being able to graft one functional group in a justaposed manner to another (transition metal) functional group. This would then enable you to produce bifunctional, surface-modified catalysts.

A: I. E. Wachs

I agree with you that it should be possible to react the surface hydroxyls of minerals with metal oxide overlayers. I am currently not aware of any such studies.

Q: H. L. Krauss (Germany)

I wonder how you got good catalytic properties in the Cr/SiO_2 system at such moderate activation temperatures as 350-500 ^0C. Many of our results, in fact all, show that activation temperatures of >600 ^0C, preferentially 800 ^0C, are to be applied to get good catalysts in cases when a reduction of the chromium species is a crucial step in the preparation of the active catalytic species.

A: I. E. Wachs

The methanol oxidation reaction is a unimolecular reaction involving only the active surface site (surface chromate species). However, the types of reactions that you are referring to are bimolecular reactions, which apparently are inhibited by surface hydroxyls adjacent to the active surface site, and elevated calcination temperatures are required to remove these hydroxyls from the silica surface. A detailed discussion of the comparison between methanol oxidation and ethylene polymerization over CrO_3/SiO_2 catalysts can be found recently [3].

[3] D. S. Kim, K. Segawa, T. S. Ya and I. E. Wachs, *J. Catal.*, **136**, 539 (1992).

Q: E. Bordes (France)

You mentioned that by Raman spectroscopy on V-oxides you see a slight difference in V=O band position, corresponding to slight difference in bond length. These differences should be reflected also in catalytic reactivities. I wonder if the reaction with methanol is not too much simple. V-based catalysts have the capability to cyclize molecules. If you used butane, for example, do not you think that the reactivities would be more differentiated, and particularly the selectivities in various products.

A: I. E. Wachs

It has been reported in the literature by many authors that the V=O bond length controls the catalytic activity. However, there was not direct proof of this assumption. We have, for the first time, measured the V=O bond lengths by Raman spectroscopy and find that it does not correlate with catalytic activity. This is not surprising since the V-O-S (S=support) bond is critical in determining the catalytic activity.

The results are not unique to methanol oxidation since we have also found a similar activity trend for butene oxidation. An examination of the literature data for o-xylene oxidation, a significantly more complex molecule, also shows similar activity trend. Thus, the reactivity results for methanol oxidation appear to be quite general.

Q: H. H. Kung (USA)

This was a very nice paper. My question is to ask for you comment as to the possibility that while spectroscopy sees the majority species, the reaction is catalyzed by some minority species. For example, a 1 wt% and a 2 wt% V_2O_5/SiO_2 may be indistinguishable with Raman spectroscopy, yet they are somewhat different catalytically in butane oxidation.

Also what is your view on the possibility that in hydrocarbon oxidation reactions, the water that is produced results in a constant partial pressure of water that causes migration of the surface species ? Thus the catalyst is in a different state than the one characterized structurally.

A: I. E. Wachs

Thank you for your nice comment. It is true that not all the surface species may simultaneously be participating catalytically, but that they may be taking turns performing the catalysis. Furthermore, we find that the same surface metal oxide species are found on all oxide supports because they have a preferred coordination to oxide support surfaces. Thus, it is very unlikely that there is some unusual coordination that is not detected spectroscopically and is responsible for the catalytic behavior. In addition, doping the supported vanadium oxide catalysts with potassium results in change in the Raman spectra and a corresponding change in the methanol oxidation TON suggesting that the active sites are indeed being probed by Raman spectroscopy.

Your results with butane oxidation reflect the complexity of this reactant which may simultaneously be interacting with the surface vanadia species and surface hydroxyls. In such a situation, increasing the vanadia coverage does not affect the vanadia structure (as long as all the vanadia is dispersed), but decreases the surface hydroxyl concentration which is beneficial.

Q: L. Dixit (India)

Your Raman spectral observations on titania supported vanadia catalysts reveal that there exist three different vanadia species on a TiO_2 support. The observation of a single sharp band (at low loading) that is present at 1030 cm^{-1} is due to isolated tetrahedrally coordinated surface vanadium oxide species containing one terminal V=O bond and three bridging V-O-Ti bonds. This is true. However, the assignment of bands at moderate and high loadings of vanadia, which appear at 930 cm^{-1} and 994 cm^{-1}, respectively to polymerised tetrahedrally coordinated surface vanadium oxide species and crystalline V_2O_5 may be mixed.

I would like to know whether structure-dependent position of bands of different vanadium oxide precursors compatible with V=O bond length variations are also compatible in terms of their intensities? Do you have any intensity data of bands in terms of their structures ?

A: I. E. Wachs

The Raman bands at 930 and 994 cm^{-1} are not related since the 930 cm^{-1} band precedes the appearance of the 994 cm^{-1} band due to crystalline V_2O_5. Furthermore, crystalline V_2O_5 does not possess a band in this region.

The different Raman band positions are directly related to the vanadium-oxygen bond lengths [4]. We have no relative intensity data at present, but the bands at higher wavenumbers should be slightly stronger due to the increased electron density of the vanadium-oxygen bonds.

[4] Hardcastle and I. E. Wachs, *J. Phys. Chem.*, **95**, 5031 (1991)

Guczi, L. *et al.* (Editors), *New Frontiers in Catalysis*
Proceedings of the 10th International Congress on Catalysis, 19-24 July, 1992, Budapest, Hungary
© 1993 Elsevier Science Publishers B.V. All rights reserved

STRUCTURAL CHARACTERISTICS OF ALUMINA-SUPPORTED ACTIVATED HYDRODESULFURIZATION CATALYSTS. AN XPS, NO ADSORPTION AND SULPHYDRYL GROUP STUDY

L. Portela[b], *P. Grange*[a] *and B. Delmon*[a]

[a]Unite de Catalyse et Chimie des Materiaux Divises - Universite Catholique de Louvain, 2/17 Pl. Croix du Sud, 1348 Louvain-la-Neuve, Belgium
[b]On leave from: GRECAT - Instituto Superior Tecnico - Depto. Eng. Quimica - Universidade Tecnica de Lisboa, Av. Rovisco Pais, 1096 Lisboa Codex, Portugal

Abstract

In the present work we analysed the surface properties of alumina-supported Co-Mo hydrodesulfurization catalysts, submitted to five different activation procedures. We measured the dispersion of the active elements (by XPS), the coordinative unsaturation state (infrared study of NO adsorption) and the sulfhydryl group (chemical titration with $AgNO_3$) concentration. The results confirmed the deep influence of the activation conditions on the parameters analysed. We also showed that hydrogen sulfide tended to adsorb on the coordinatively unsaturated sites (CUS). The structure of the catalysts was shown to change, from the monometallic samples to the bimetallic, leading to a behaviour different from that of its individual components. Namely, the NO adsorption capability, the SH concentration and, sometimes, the surface sulfur concentration, decreased. The results obtained allowed us to speculate that one of the roles of cobalt, in CoMo catalysts, would be that of improving the efficiency of surface sulfur removal.

1. INTRODUCTION

To be effective, the optimization of catalytic formulations must take into account the structure of the active phase. Since it is known that its structure may change during activation and catalytic work, it is also important to know its final state, after these treatments. This is particularly the case of alumina-supported cobalt-molybdenum catalysts used in hydrodesulfurization (HDS). These catalysts are prepared in their oxide form, although the stable state of the active phase during catalytic work is the sulfided one. Industrially, the activation may be carried-out using the actual feedstock as the sulfiding agent, in the presence of hydrogen. An alternate procedure is to treat first the oxide catalyst with a highly reactive sulfur-containing molecule, to form the sulfided phases, and only then submit it to the reaction mixture. This is the method most frequently used in laboratories. A mixture of hydrogen/hydrogen sulfide is often employed.

In previous investigation works performed in our laboratory, it was found that the type of activation procedure deeply influenced the activity and selectivity of an alumina-supported Co-Mo HDS catalyst (1,2). Other literature results suggest that some of the important features of the active phase structure of these catalysts are CUS, associated with either Mo (3,4,5) or Co (6), and sulfhydryl (SH) groups (7,8). The possible location for this

type of structures in the Mo phase is, according to the literature, the edges of MoS_2 crystallites. Whatever the explanation, the dispersion of the active phase in supported catalysts must be a very important parameter.

In the present work we carried out an IR study of NO adsorption, quantitative SH analysis and X-ray Photoelectron Spectroscopy (XPS), on alumina-supported catalysts (two monometallic, Co and Mo, and two bimetallic, Co-Mo). Then, we analysed the modifications of the active phase of those catalysts, brought by the different activation procedures, in terms of the above mentionned features.

2. EXPERIMENTAL

2.1. Preparation of catalysts

A detailed description of the preparation of the catalysts used in this study was given elsewhere (9). Briefly, the Mo/Al_2O_3 catalyst was prepared by the pore-filling impregnation of a γ-Al_2O_3 (Rhône-Poulenc, $S_{BET} \sim 200\ m^2/g$) with a solution of ammonium heptamolybdate, in two steps, with intermediate drying (373K) and drying and calcination (773K) at the end. The final Mo loading was 15.1 wt% MoO_3, determined by atomic absorption spectroscopy.

The Co/Al_2O_3 catalyst was prepared by wet impregnation of the same support with an aqueous solution of cobalt nitrate. Water was evaporated under vacuum and agitation. The catalyst was dried and calcined as above. The Co loading was 2.9 wt% CoO.

The $CoMo/Al_2O_3$ catalyst (CoMo (lab.)) was prepared by wet impregnation (as above) of the Mo/Al_2O_3 catalyst with a solution of cobalt nitrate in ethanol (77 vol%) and water. The latter was used to avoid the redissolution of MoO_3 during the Co impregnation (10). The catalyst was also dried and calcined as already described. The final composition was 3.1 wt% CoO and 14.9 wt% MoO_3. The second Co-Mo catalyst used was the HR306 from Procatalyse (CoMo (ind.)) with a composition of 2.7 wt% CoO and 13.5 wt% MoO_3.

2.2. Activation of catalysts

All catalysts were activated according to a standard, simultaneous reduction/sulfidation, procedure (RS), under a flow of 15 vol% H_2S in H_2. The catalysts were first dried under Ar at 423K for 30 mn. Then, the activation gases (100cc/mn) were introduced and the temperature raised at 10K/mn up to 673K (60 mn at steady temperature), with an intermediate step at 573K (30 mn.). Four modifications of this procedure were also used, namely pre- or post-sulfidation (resp. S-RS and RS-S) with a mixture of 15 vol% H_2S/Ar, and pre- or post-reduction (resp. R-RS and RS-R) with H_2. In these two-part activations, after the first 60 mn period at the final temperature, the gases were switched to the mixture corresponding to the second part of the activation. Then, the activation continued for another 60 mn period.

2.3. XPS analysis

The experimental conditions of the XPS analyses will be published elsewhere (11). However, it is important to mention that the activated catalysts were never allowed to contact air, from the moment they were activated. This was done by means of an iso-octane meniscus, removed later before the analysis.

2.4. Adsorption of NO

The adsorption of NO was carried out inside the cell where the IR measurements took place. The activated catalysts were ground and wafers of about 5 to 8 mg were made. They were reactivated inside the cell, according to the procedures described above. No argon drying was performed, the activation gases were directly introduced in the cell and the temperature raised as above. In two-part activations, e.g., S-RS, only the second part was performed inside the cell. Afterwards the IR cell was allowed to cool down to room temperature and was evacuated for 1h (final pressure c.a. 10^{-5} torr). At this point reference spectra were taken and the catalyst was evacuated for 30 mn at 473K. After cooling again to room temperature, 40 mbar of NO (purified by the freeze-thaw technique) were admitted in the cell and the adsorption was carried out for 30 mn at ambient temperature. At the end, the excess of NO was removed via condensation in a cold trap (liquid N_2 temperature) and new spectra were taken.

We considered the intensity of the band of NO adsorbed on cobalt, as the height of the peak corresponding to the NO dimer symmetric stretching vibration (around 1850 cm^{-1}) (2). For molybdenum, we took the height of the peak corresponding to the NO dimer asymmetric stretching vibration (around 1700 cm^{-1}) (2). These are the two bands that do not coincide in the bimetallic catalysts. All intensities were normalized to a constant wafer weight of 10 mg.

2.5. Determination of SH groups

The surface SH group concentration was determined according to a method developed by Maternová (12), with the additional feature that, after the activation, the reactor was evacuated at 423K to remove any trace of H_2S that would interfere with the subsequent titrations. A blank run was performed before every measurement. About 750 mg of catalyst were used in each case.

3. RESULTS

3.1. X-ray Photoelectron Spectroscopy

In TABLE 1 we present the results of the XPS analysis of the catalysts. The values represent the ratio of the normalized XPS peak intensities and correspond to atomic ratios.

TABLE 1
XPS peak intensity ratios

	Mo		Co	Co-Mo (lab.)			Co-Mo (ind.)		
ACT.	Mo/Al	S/Mo	Co/Al	Mo/Al	Co/Al	S/Mo	Mo/Al	Co/Al	S/Mo
OXIDE	0.077	-	0.016	0.075	0.032	-	0.074	0.026	-
S-RS	0.031	3.9	0.01	0.067	0.029	2.2	0.058	0.018	2.2
R-RS	0.071	1.6	0.011	0.078	0.02	1.8	0.072	0.023	1.8
RS	0.067	1.9	0.01	0.076	0.026	1.9	0.058	0.018	1.9
RS-S	0.041	3.6	0.009	0.072	0.025	2.6	0.072	0.024	2.2
RS-R	0.055	1.8	0.01	0.075	0.023	2.0	0.065	0.019	1.7

After mathematical decomposition of the Mo3d peak envelope, in the sulfided samples, it was possible to conclude that more than 82% of the original $Mo^{(VI)}$ was converted to lower oxidation states (more than 87% in the Mo catalyst), of which the $Mo^{(IV)}$ is largely majoritary. It was not necessary to assume the presence of oxidation states lower than $Mo^{(IV)}$ to obtain a good fit.

TABLE 1 confirms that the activation procedures always influence the dispersion of Co and Mo on the surface of the catalysts. For a given activation procedure it is observed that the two Co-Mo catalysts present Mo/Al ratios usually higher than those of the Mo catalyst. Nevertheless, the Mo/Al relative variations as a function of the activation procedures, remain similar for all of them. The highest Mo/Al ratio is always achieved with the R-RS treatment.

The influence of the activation procedure is less important for the Co catalyst. For the latter, the Co/Al ratio remains nearly constant. However, when dispersed over Mo, as with the two Co-Mo catalysts, two effects can be observed. First, there is a significant increase in the amount of Co present at the surface; second, the dispersion of Co in the latter case becomes more sensitive to the activation procedures.

The amount of sulfur present at the surface, expressed as the S/Mo ratio, is also sensitive to the activation procedure. It is generally situated around the stoichiometric value (S/Mo=2). This ratio is very high in the cases where H_2S was used in the absence of hydrogen, in a certain stage of the activation (S-RS and RS-S). For the Mo catalyst these two procedures yield S/Mo ratios well above the stoichiometric ratio (S/Mo ~ 4), contrary to what happens with the Co-Mo samples.

3.2. NO adsorption on the catalysts

In fig.1 we present the IR spectra obtained after NO adsorption on the RS (simultaneous reduction/sulfidation) activated catalysts.

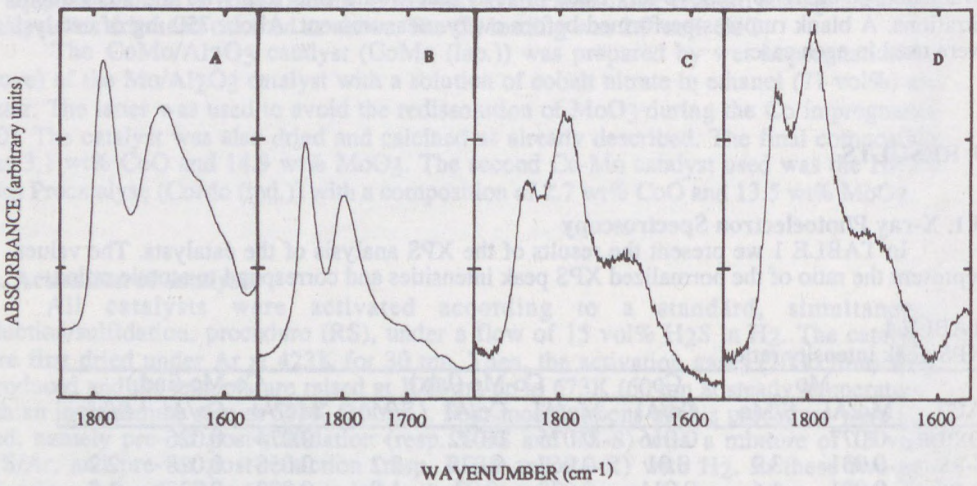

fig.1 NO adsorption on catalysts. A) Mo/γ-Al_2O_3; B) Co/γ-Al_2O_3; C) CoMo/γ-Al_2O_3 (lab.); D) CoMo/γ-Al_2O_3 (ind.)

The position of these bands (1785 cm^{-1} and 1700 cm^{-1} for the Mo; 1857 cm^{-1} and 1796 cm^{-1} for the Co; 1846 cm^{-1}, 1788 cm^{-1} and 1694 cm^{-1} for the two Co-Mo catalysts) agrees with the literature results (2,6). For the rest of the activations the spectra were similar to these ones, within each type of catalysts, except the intensity of the bands. These are reported in TABLE 2.

The results presented in TABLE 2 show that, for monometallic catalysts, the dependence of the intensity of the bands of adsorbed NO on the activation is different from that of the bimetallic ones. Furthermore, the intensities of the bands of NO on the monometallic catalysts are usually higher than the corresponding ones in the bimetallic catalysts. The most evident exception to the previous observation comes from the two Co-Mo catalysts activated by RS-R, where the intensities are higher than those of the corresponding Mo and Co catalysts. Finally, the activation procedure RS-S inhibits almost any NO adsorption on any of the catalysts.

TABLE 2
Normalized intensities of the IR bands of NO adsorbed on Co and Mo

	Mo	Co	Co-Mo (lab)		Co-Mo (ind)	
ACTIV.	I NO(Mo)	I NO(Co)	I NO(Mo)	I NO(Co)	I NO(Mo)	I NO(Co)
S-RS	1.85	3.76	0.84	1.11	0.92	1.69
R-RS	3.28	5.67	0.75	0.86	0.16	0.25
RS	2.96	2.61	1.42	2.28	1.54	3.22
RS-S	0.13	0.4	0.08	0.09	0.04	0.04
RS-R	1.52	1.3	3.17	6.45	3.71	8.85

3.3. SH group determination

In TABLE 3 we present the results concerning the quantitative determination of the surface SH groups of the catalysts. This concentration is also very sensitive to the activation procedures. For the three Mo-containing catalysts the variation of this concentration as a function of the activation procedure is approximately the same. For a given activation, the values presented by the Mo/Al_2O_3 are always higher than those of the two Co-Mo samples.

TABLE 3
Concentration of surface SH groups (mol SH/g)/10^{-4}

ACTIVATION	Mo	Co	Co-Mo (lab)	Co-Mo (ind)
S-RS	5.3	1.0	4.9	4.6
R-RS	8.2	0.6	7.4	7.3
RS	7.7	0.4	6.4	6.2
RS-S	6.4	3.3	6.4	5.8
RS-R	7.5	2.0	5.8	5.8

The Co catalyst presents the lowest SH concentration, and the influence of the activation procedure is not similar to that of the other catalysts.

4. DISCUSSION

From the results presented above, and considering that the metal loading was almost constant, it is evident that the modification of the activation procedure brings about deep changes in the texture and surface structure of the active phase.

4.1. XPS

In alumina-supported Mo-containing catalysts it is known that, upon sulfidation, the structure of the Mo phase changes from a layer (ordered or patch-like) of molybdenum trioxide to small plate-like crystallites of molybdenum disulfide, distributed all over the surface (13,14). The MoS_2 thus formed, can be viewed as a stacking of slabs, each of which consists of a layer of Mo atoms between two layers of sulfur atoms. They form a hexagonal

structure, where each Mo atom is bonded to six sulfur atoms (three in each layer) and each sulfur atom is bonded to three Mo atoms. At the edges of the slabs, the S atoms are bonded to two Mo atoms at the most (18). Due to their lower coordination state, these edge S atoms should logically undergo reactions in an easier way than those present in the basal planes.

The direct consequence of the structural modification due to the sulfidation, is that a larger proportion of Al atoms, that were initially covered by MoO_3, become free from this overlayer. The Al XPS signal increases, in this situation. On the other hand, a loss of Mo signal can also occur due to the "agglomeration" of Mo atoms into MoS_2 crystallites. This explains the general decrease of the Mo/Al ratio we observe upon sulfidation, and it is in close agreement with what was reported by Okamoto et al. (4).

For the three Mo-containing catalysts, the similar response of the Mo/Al ratio to the activation procedures suggests that the same type of transformations is at stake, irrespective of the presence or absence of cobalt. The higher Mo/Al ratio found in the Co-Mo catalysts, despite the possibility that the presence of Co may hinder Mo, could be due to a lower tendency of molybdenum to form larger crystallites, either with larger slabs or with a higher number of slabs per crystallite.

The deposition of cobalt over molybdenum greatly enhances the surface concentration and dispersion of the former. Probably, this occurs via Co-Mo interactions, which may depress the tendency of Co to combine with the support. The higher sensitivity of Co dispersion to the activation procedures, that our results show, would then be explained. In the literature, this Co-Mo interaction is supposed to be the result of the formation of a Co layer between the alumina support and the Mo oxide layer (15, 16). The result we obtained further confirms that cobalt and molybdenum, when present together, have a mutual beneficial influence on the dispersion of each other (21). This is still true, even after the activation.

When H_2S is used in the absence of H_2 (activations S-RS and RS-S), it is possible that a larger amount of sulfur may remain attached to the surface of the catalyst. The higher S/Mo ratio we obtained may be a consequence of it, as was also observed in (17). The much larger values obtained for these activations in the Mo catalyst than in the corresponding Co-Mo ones, strongly suggests that cobalt plays a role in the removal of these sulfur species.

4.2. NO adsorption

The formation of CUS should be favoured at the edges of MoS_2 crystallites, since it is there that the S atoms can be found in a lower coordination state, as developed in the geometrical model proposed by Wambeke et al. (18). The formation of this type of structures could be the result of the full hydrogenation of SH groups or S anions, with the concomitant desorption of H_2S. Another possibility would be the partial hydrogenation of bridging S atoms, with the simultaneous breaking of a Mo-S bond, yielding an SH group and a CUS. The tricoordinated basal plane S atoms would be less prone to undergo similar processes.

The almost complete inhibition of the NO adsorption on all catalysts activated according to RS-S indicates that, most probably, H_2S adsorbs (dissociatively or not) on the same sites as NO, as was suggested by Okamoto and co-workers (4). If we admit that the CUS are the adsorption sites of the reactant molecules, this fact may explain the inhibitive effect of H_2S on the HDS activity of these catalysts, as reported in many references (see, for instance (20)),. Another possibility for explaining this effect is that a higher H_2S partial pressure would render more difficult the desorption, as H_2S, of the S atom left on the CUS after the desulfurization reaction.

In the post-reduction treatment, RS-R, the increased intensity of the band of NO adsorbed on cobalt in the bimetallic catalysts, as compared to what happens with the monometallic samples, could be due to an enhanced reducibility of Co because of its higher dispersion state. On the other hand, since the dispersion state of Mo did not change as much, from the monometallic to the bimetallic catalysts, the increased NO adsorption on this metal should be attributed to other factors. The lower amount of sulfur found in CoMo catalysts,

when compared to the Mo sample, seems to indicate that the enhanced NO adsorption capability of the former could be due to a higher unsaturation state of the Mo phase. The presence of H_2S in the final stages of the other activation procedures, is probably the cause for the fact that such an increased NO adsorption is not verified then. The decrease of the NO adsorption on Mo could also be due to an interference of cobalt with the Mo sites capable of forming CUS, as was observed by Topsøe et al. (6).

Although the total number of sites available for NO adsorption decreases from the monometallic to the bimetallic catalysts, the unsaturation degree of the remaining sites seems to have increased, as the shift towards lower wavenumbers of the bands of adsorbed NO indicate. This fact is true for both Co and Mo atoms. For Co, this effect could be attributed to its enhanced dispersion in the Co-Mo catalysts. However, for Mo it is most probable that a direct effect of the presence of Co, through an enhanced sulfur removal, be the reason for this effect, since its dispersion state did not change as much.

The fact that, logically, the formation of CUS is easier at the edges of the MoS_2 crystallites allows us to give a physical meaning to the variation of the dispersion indicator, the XPS Mo/Al ratio.

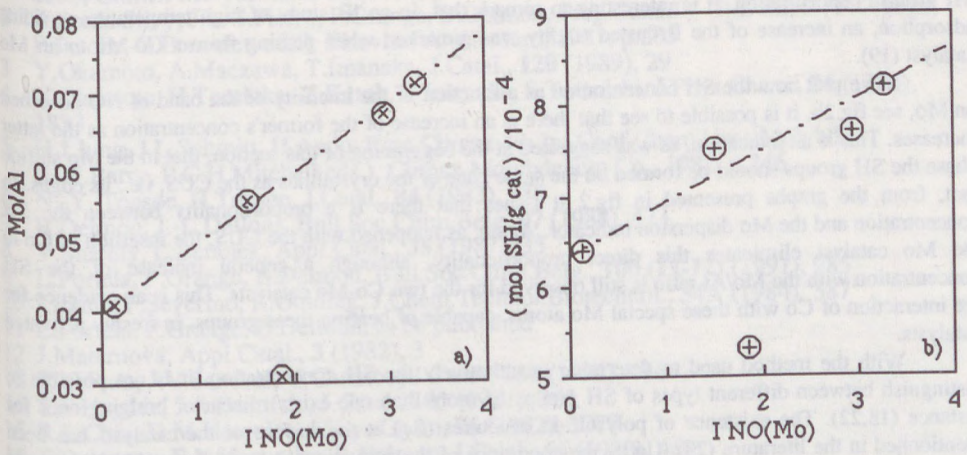

fig.2 a) Variation of the Mo/Al XPS ratio with the intensity of the band of NO adsorbed on Mo in the Mo/γ-Al_2O_3 catalyst; b) Variation of the SH concentration with the intensity of the band of NO adsorbed on Mo (Mo/γ-Al_2O_3 catalyst).

In fig.2a it is possible to see that, with an increase in the intensity of the bands of NO adsorbed on Mo in the Mo/Al_2O_3 catalyst, there is a simultaneous increase of the Mo/Al ratio. This would mean that a high Mo/Al ratio corresponds to a high crystallite edge area. Since the active phase loading is constant, this means that the crystallite size must be changing. More precisely, once a higher edge area is achieved with smaller crystallites, the size should be decreasing with the increase of the Mo/Al ratio. Evidently, no conclusions can be drawn concerning the number of slabs per crystallite, for the total edge area may not be affected by a variation of that parameter. The insertion of Co in the Mo catalyst eliminates the relationship above shown, although there is still a general increase of the ratio, for high intensities of the adsorbed NO band. This is possibly because Co interacts directly with the sites capable of forming CUS.

4.3. Sulfhydryl groups

The above mentionned structural factors, leading to an easier formation of CUS on the edges of MoS_2 crystallites, also favor the formation of SH groups in that place. During activation, SH groups may be formed by the hydrogenation of terminal or bridging sulfur anions. Alternatively, and according to the literature, H_2S may adsorb dissociatively on the CUS forming SH groups (19). These possibilities show that the activation conditions may influence the SH concentration of a catalyst. This is what we observed in the present work. The similarity of behaviour, with regard to the activation, of the three Mo-containing catalysts, strongly suggests that the changes observed are essentially due to the SH groups associated with the Mo phase.

The higher SH concentration presented by the Mo catalyst may seem surprising if one thinks that the corresponding concentration in the Co catalyst is not negligible. As the surface concentration of Co in the Co-Mo catalysts is twice as high as in the Co one, the SH groups associated with Co should be proportionally more important, leading to a much higher overall SH concentration. One may infer, therefore, that the structure of the bimetallic catalyst changed in such a way as to prevent the formation of as many SH groups as if Mo and Co behaved independently. Simultaneously, the cause for the improved sulfur removal on Co-Mo catalysts mentionned above could also lead to the decrease of their SH group's concentration. It is interesting to remark that, in an IR study of high temperature pyridine adsorption, an increase of the Brönsted acidity was remarked when passing from a Co-Mo to an Mo catalyst (19).

If we plot now the SH concentration as a function of the intensity of the band of NO adsorbed on Mo, see fig.2b, it is possible to see that there is an increase of the former's concentration as the latter increases. This is an indication, as was suggested at the begginning of this section, that in the Mo sulfide phase the SH groups should be formed on the same zone of the crystallites as the CUS, i.e., its edges. In fact, from the graphs presented in fig.2 it issues that there is a proportionality between the SH concentration and the Mo dispersion indicator. Again, as happened with the CUS, the insertion of Co in the Mo catalyst eliminates this direct proportionality, although a general increase of the SH concentration with the Mo/Al ratio is still observed for the two Co-Mo catalysts. This is an evidence for the interaction of Co with these special Mo atoms, capable of bearing these groups, in freshly activated catalysts.

With the method used to determine quantitatively the SH concentration, it is not possible to distinguish between different types of SH groups (if more than one exists): linear or bridging ones for instance (18,22). The existence of polysulfide structures (S_x) at the surface of the catalysts has been mentionned in the literature (23). Under the conditions of the activations it could be possible that these species become hydrogenated, and then detected by the SH titration procedure we used. We think, however, that if any polysulfides exist on the surface of the catalysts, it is unlikely that any significant formation of SH groups on them occurs. This is a consequence of the fact that it is precisely in the two situations where the S/Mo ratio largely exceeds the stoichiometric value, that the SH concentration is lower.

5. CONCLUSION

In the present work we confirmed that although the composition of the active phase of HDS catalysts remains constant, it is possible to alter its structure significantly upon submitting them to different activation procedures. Particularly, it was shown that hydrogen sulfide tended to adsorb on the CUS of the catalyst's active phase.

The main changes observed in the analysed parameters when passing from the Mo to any of the CoMo catalysts can be summarized as follows: i) the SH concentration and the intensity of the bands of adsorbed NO decrease, (the latter is always true, except when the

catalysts are post-reduced (RS-R), where a large increase is observed); ii) for the two activations where H_2S is used in the absence of hydrogen, the S/Mo ratio passes from a value that largely exceeds the stoichiometric one, to another close to it; iii) there is a generalized shift of the position of the adsorbed NO bands towards lower wavenumbers. The introduction of cobalt in the Mo catalyst seems to have two main consequences: the first is that Mo atoms that usually bear special type of structures (CUS and SH groups) loose part of their capability for that function; and second, the general reduction state of the active phase elements is increased. The role of cobalt is, then, consistent with the idea of enhancement of the coordinative unsaturation degree of the Mo atoms and more efficient removal of adsorbed sulfur.

6. REFERENCES

1 B.Delmon, Proc.Climax 3rd Int.Conf. Chem.Uses Molybd. (H.F.Barry,P.C.H.Mitchell eds.), Climax Molybdenum Co.,1979, p.73
2 R.Prada Silvy, J.L.G.Fierro, P.Grange, B.Delmon, Prep.Catal.IV (B.Delmon, P.Grange, P.Jacobs, G.Poncelet, eds.), Elsevier, Amsterdam, 1987, p.605
3 Y.Okamoto, A.Maezawa, T.Imanaka, J.Catal., **120** (1989), 29
4 Y.Okamoto, H.Tomioka, Y.Katoh, T.Imanaka, S.Teranishi, J.Phys.Chem., **84** (1980), 1833
5 H.J.Jung, J.L.Schmitt, H.Ando, Proc.Climax 4th Int.Conf.Chem.Uses Molybd., (H.F.Barry, P.C.H.Mitchell eds.), Climax Molybdenum Co., 1982, p.246
6 N.-Y. Topsøe, H.Topsøe, J.Catal., **84** (1983), 386
7 B.Delmon, J.-L.Dallons, Bull.Soc.Chim.Belg.,**97** (1988), 473
8 V.Stuchly, L.Beránek, Appl.Catal., **35** (1987), 35
9 L.Portela, P.Grange, B.Delmon, Bull.Soc.Chim.Belg., **100 (11-12)** (1991), 985
10 J.Laine, F.Severino, R.Golding, J.Chem.Technol.Biotechnol., **34A** (1984), 387
11 L.Portela, P.Grange, B.Delmon, to be published
12 J.Maternová, Appl.Catal., **3** (1982), 3
13 K.C.Pratt, J.V.Sanders, V.Christov, J.Catal., **124** (1990), 416
14 T.F.Hayden, J.A.Dumesic, J.Catal., **103** (1987), 366
15 R.L.Chin, D.M.Hercules, J.Phys.Chem, **86** (1982), 3079
16 F.Delannay, E.N.Haeussler, B.Delmon, J.Catal., **66** (1980), 469
17 J.R.Brown, M.Ternan, Ind.Eng.Chem.Prod.Res.Dev., **23** (1984), 557
18 A.Wambeke, L.Jalowiecki, S.Kasztelan, J.Grimblot, J.P.Bonnelle, J.Catal., **109** (1988), 320
19 N.-Y.Topsøe, H.Topsøe, F.E.Massoth, J.Catal., **119** (1989), 252
20 R.Prada Silvy, P.Grange, B.Delmon, Proc. X Iberoamerican Symp.on Catal., Merida, Venezuela, 1986, p.397
21 P.Gajardo, P.Grange, B.Delmon, J.Catal.,**63** (1980), 201
22 J.L.Gland, E.B.Kollin, F.Zaera, Langmuir, **4** (1988),118
23 B.Scheffer, N.J.J.Dekker, P.J.Mangnus, J.A.Moulijn, J.Catal., **121** (1990), 31

DISCUSSION

Q: H. Topsoe (Denmark)

Let me first congratulate the authors for bringing forward a lot of interesting new information on the effects of changing the sulfiding activation, procedure. The low S/Mo ratios and high Mo/Al XPS intensity found with the prereduced catalysts could together with the increased Mo-O contribution we have reported in EXAFS studies of such catalysts indicate increased spreading and Mo-O-Al bond formation. Why do you feel that these bonds are more difficult to sulfide than those present initially? Your results are also interesting on another account since they show nicely that the Co atoms in the promoted catalysts behave quantitatively very different from those in the Co/Al_2O_3 catalysts. This certainly supports the views expressed in the Co-Mo-S model and differs from those views that Co is "just" behaving as highly dispersed Co. Let me at the end caution you of using the XPS intensity results (I_{Mo}/I_{Al}) to get information about changes in edge dispersion. If the number of MoS_2 slabs is the same, then I_{Mo}/I_{Al} will be the same independent of large changes in edge dispersion. Does this influence some of your conclusions ?

A: B. Delmon

1) Reply to the first question (sulfidation of Mo-O-Al bonds). In the normal reduction-sulfidation process, a beneficial coupling between reduction of Mo(VI) to Mo(IV) and sulfidation takes place, leading to more rapid reaction and a higher degree of sulfidation. An important effect of too-deep a prereduction is to make sulfidation more difficult. The explanation is developed in [1], based on our experiments and those of others [2, 3]

2) Reply to the second point (remarks concerning the comparison of Co/Al_2O_3 and $CoMo/Al_2O_3$). The fact that the Mossbauer signal attributed to a supposed Co-Mo-S species can be found in catalysts containing only cobalt [4] should be a caution against basing too many explanations on the supposed Co-Mo-S phase. It should also be recalled that the corresponding Mössbauer signal has been observed to decrease very rapidly (19 hours) to almost nothing during desulfurization of a vacuum gas oil at 655 K, 100 atm on a catalyst of usual composition (Co/Mo = 0.5) [5]. The evident explanation of our observation is that, with the usual nitrate impregnation, Co alone on Al_2O_3 is much less dispersed than when MoO_3 is present [6] and many papers of other authors reproducing this result.

3) Reply to the last question (use of the I_{Mo}/I_{Al} ratio determined by XPS for evaluating edge dispersion). We agree fully. of course, we used several physicochemical methods when, in a previous work, we attempted to evaluate the edge/base plane ratio [7, 8]. In the present case (end of section 4.2. of our paper) the problem is different. The argument rests on NO adsorption which must reflect edge dispersion. As increasing NO adsorption is observed when the XPS Mo/Al ratio increases, this implies that the overall dispersion (edge + basal planes) increases, hence that the overall crystallite size decreases. We made that point for excluding that the increase of the XPS Mo/Al ratio would reflect a growth of platelets lying on the surface, with only minimal increase of the edge areas. Our findings are in agreement with the general finding that edge and basal plane area change similarly.

[1] B. Delmon, *Chim. Phys.*, **83**, 875 (1986)
[2] A. Steinbrunn et al. (ref. 57, 58 and 59 in this paper)
[3] B. Delmon, in *"Catalysts in Petroleum Refining 1989"* (D. L. Trimm et al., eds.), Elsevier, Amsterdam, 1990, pp. 1-40
[4] M. W. J. Craje, V. H. J. de Beer, A. M. van der Kraan, *Bull. Soc. Chim. Belg.*, **100**, 953 (1991)
[5] H. Topsoe, B. S. Clausen, *Appl. Catal.*, **25**, 273 (1986)
[6] P. Gajardo, P. Grange, B. Delmon, *J. Catal.*, **63**, 201 (1980)
[7] F. Delannay, *Appl. Catal.*, **16**, 135 (1985)
[8] B. Delmon, *Surf. Interf. Anal.*, **9**, 195 (1986)

Q: H. Knözinger (Germany)
H_2-treatment of sulfided Mo catalysts creates SH groups. Literature evidence indicates that additional, still unknown hydrogen species are also created (neutron scattering) and significant H_2-uptake has been reported. Do you have any indication for the formation of any additional ad- or absorbed H-species and their possible effect on the properties of the materials ?

A: B. Delmon
The method we employed to titrate SH groups in activated HDS catalysts developed by Maternova [9] is based on the following reaction

$$-SH + AgNO_3 \rightarrow -SAg + HNO_3$$

Therefore, if any H species exist, other than H bonded to sulfur, they will not be detected by this method. Thus, we do not have information on those species you mention. However, with this chemical method we are not able to differentiate between different types of XH groups (linear, Mo-SH, or bridged, MO-SH-Mo, ones) if they exist. Consequently we cannot assign specific roles to them.

[9] J. Maternova, *Appl. Catal.*, **3**, 3 (1982)

Q: Wm. C. Conner (USA)
You have shown several differences as a result of differences in composition and pretreatment, activation. How (IR) reversible are the pretreatment-activation procedures and how different will the compositions be under HDS conditions ?

A: B. Delmon
I must stress first that the catalyst composition is nearly constant in term of each metal's loading. Therefore, the differences we observed in IR NO bands intensity cannot be ascribed to a changing composition.

We have not performed experiments in order to test whether the changes induced by any activation procedure was reversible if an inverse treatment were applied (e.g. reducing a RS/S activated catalyst, or Ar/H_2S treating a RS/S activated catalyst). We believe that they would be reversible. However, the final state of the catalyst after any treatments will be decisive with regard to the catalyst's performance under reaction. We have shown [10] that the five different treatments we used, induce marked effects on the steady-state activity and selectivity of the catalysts thus activated.

[10] L. Portela, P. Grange, B. Delmon, *Bull. Soc. Chim. Belg.*, **100**, 985 (1991)

Guczi, L. *et al.* (Editors), *New Frontiers in Catalysis*
Proceedings of the 10th International Congress on Catalysis, 19-24 July, 1992, Budapest, Hungary
© 1993 Elsevier Science Publishers B.V. All rights reserved

STRUCTURE-FUNCTION RELATIONS IN LAYERED TRANSITION METAL SULFIDE CATALYSTS

M. Daage, R. R. Chianelli and A. F. Ruppert

Corporate Research Laboratories, Exxon Research and Engineering Company, Route 22 East, Annandale, NJ 08801, USA

Abstract

Chemical and physical studies of MoS_2 single crystals, microcrystals and powders were carried out with the goal of understanding the relation between the edge plane properties and catalytic properties. The bulk electronic structure of MoS_2 is directly related to the catalytically active surface states. The catalytic states, created by edge termination or probably sulfur vacancies, lie just above the dz^2 band near the Fermi level. Optical and electron spectroscopic measurements on geometrically well defined catalysts were used to obtain a "HDS edge site turnover frequency", which does not suffer from an ambiguity in dispersion. Furthermore, the catalytic activity of unsupported molybdenum disulfide is related to the existence of two different sites and their relative concentration is directly dependent upon the morphology of the particle and is controlled by the stacking of the layers.

Introduction

Much progress has been made in understanding the properties of layered Transition Metal Sulfide based catalysts, but some basic problems prevent further advances. The major impediment arises from the highly anisotropic nature of layered materials. In this paper, we report some of our recent progress in understanding how the anisotropic crystal structure of MoS_2 is fundamentally related to its catalytic properties. The structural anisotropy of molybdenum or tungsten disulfide is a consequence of the chemical bonding. Within one layer, the structure can be viewed as a two-dimensional macromolecule with each metal

atom bounded to six sulfurs. With the exception of the sulfur located at the edge of the layer, each sulfur atom is tightly bound to three metal atoms, which results in a weak interaction with the next layer. This generates the Van Der Waals gap which is the main feature of interest in regard to intercalation and lubricity properties (1). Thus, the basal plane (002) has been the general focus of studies in the vast intercalation literature, whereas the "edge" planes become the focus of catalytic studies. The work reported here consists of chemical and physical studies of MoS_2 single crystals, microcrystals and powders with the goal of understanding the relations between the morphology of the particle, the edge plane properties and the catalytic properties.

The catalytic importance of MoS_2 edge planes

The importance of the MoS_2 edge planes has long been recognized and a good example can be found in the linear correlation between the oxygen chemisorption and the HDS of dibenzothiophene (2). In general, HDS activity does not correlate with the BET surface area because the basal plane area contributes to the surface area but not to the catalytic activity. Consequently, widely different edge to basal plane ratios can be obtained by varying the method of preparation. In order to provide a better description of the catalytic sites more detailed physical, theoritical and chemical work is needed. In a recent publication, the effect of molecular oxygen on the electronic structure of MoS_2 was studied by UPS. In this work, the existence of surface states above the dz^2 band near the Fermi level was demonstrated (3). These tail states were reversibly quenched with 900L of oxygen but irreversibly quenched at atmospheric pressure. The irreversible quenching is also associated with the appearance of a bulk oxide phase in the UPS spectrum. This results clearly shows the relation between the bulk electronic states and the active surface. The dz^2 orbitals are the HOMO of MoS_2 and the crucial catalytic electronic states lie just above them arising from the termination of the bulk states. Moreover, in a more recent study, the optical properties of these tail states were examined catalytically and optically (4). The optical properties of powders and platelets were measured in the near infrared using photothermal deflection spectroscopy (PDS). The absorption of small (1.7 μm diameter) and large (36 μm diameter) platelets is compared against the spectrum of a single crystal in figure 1.

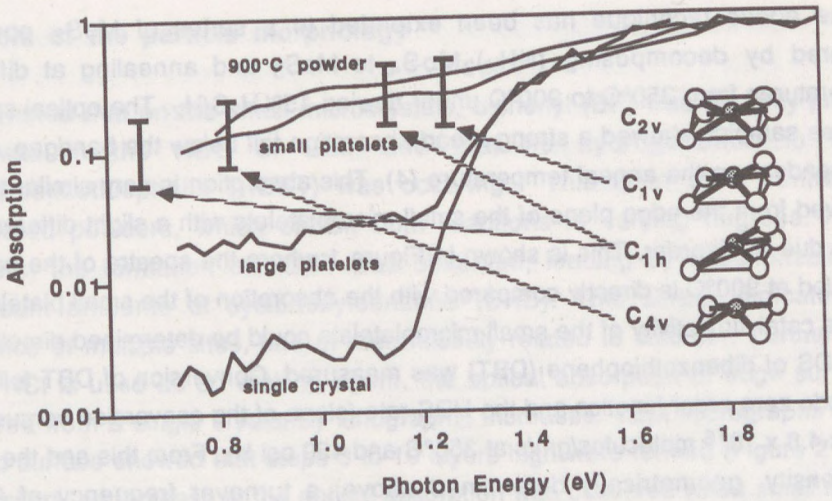

Figure 1: Optical spectra of MoS_2 and theoritical absorption energies of defects

The absorption of the single crystal begins strongly at 1.2 eV and increases toward higher energy due to the indirect bandgap.The flat lower-energy absorption in the single crystal is from defects in the material and varies strongly from sample to sample. The spectrum of large platelets is seen to be very similar to that of the single crystal, except that the defect absorption below 1.2 eV is an order of magnitude higher. The striking similarity of the spectrum of the single crystal and the large platelets between 1.3 and 2.0 eV shows that the large platelets are indeed single crystals. The absorption spectrum of the small platelets is also shown in the upper curve and the low-energy absorption due to the defects is an order of magnitude greater for the small platelets than it is for the large platelets. From these data, it is evident that the optical absorption observed below 1.2 eV is due to the exposed edge defects. In fact, SEM studies of the small and large platelets revealed that the small platelets have a greater edge plane area per gram than that of the large platelets. A statistical study of the micrographs of these samples showed that the edge site density was 6.1×10^{17} sites/gm for the small platelets and 7.2×10^{16} sites/gm for the large platelets (4). From the known density of edge sites (D), the average optical absorption (σ) of a single edge site can be calculated using $A = D.\sigma$, yielding 6.1×10^{17} cm^2 for the small platelets and 8.4×10^{17} cm^2 for the large platelets.

The above technique has been extended to a series of MoS_2 powders prepared by decomposing $(NH_4)_2MoS_4$ to MoS_3 and annealing at different temperatures from 350°C to 900°C under flowing 15%H_2S/H_2. The optical spectra of these samples showed a strong broad absorption tail below the bandgap, which is dependent on the anneal temperature (4). This absorption is very similar to that observed from the edge plane of the small microplatelets with a slight difference in shape due to disorder. This is shown in Figure 1 where the spectra of the powder annealed at 900°C is directly compared with the absorption of the small platelets.

The catalytic activity of the small microplatelets could be determined directly (4). The HDS of dibenzothiophene (DBT) was measured. Conversion of DBT followed a pseudo zero order kinetics and the HDS rate (slope of the conversion versus time plot) is 4.8×10^{16} molecules/gm/s at 350°C and 450 psi H_2. From this and the edge site density, geometrically determined above, a turnover frequency of 0.079 molecule/(edge site)/s was obtained. The catalytic activity of the powders was also measured and a linear correlation between the activities and the absorbance was observed. Assuming that the absorption cross section is the same for the platelets and the powders, the turnover frequency calculated from the slope of the absorption/activity plot was 0.03 molecule/(edge site)/s. This value is approximately two times lower than that obtained from the small platelets, an agreement which is reasonable given the uncertainties in the size and density of the disordered materials. It is also possible that disorder induces sites which, while counted by the PDS method, are not catalytically as effective or as accessible as those on well ordered materials.

The similarity in turnover frequency between the disordered and microcrystalline materials indicates that the active sites for HDS are catalytically similar and located on the edge surface. Such defects would generally be expected to have energy levels lying between the conduction and valence bands and thus absorb photons with below bandgap energies. This is the behavior observed and cross sections ~ 10^{-16} cm^2 are typical of such defects. In fact, $X\alpha$ calculations which model different types of sulfur vacancies which would occur at MoS_2 edges (Figure 1), showed that allowed optical transitions for theses defects fall into the observed energy range below 1.2 eV (5). These results suggest that sulfur vacancies are responsible for both the optical absorption measured for the edge planes and the catalytic activity in the hydrodesulfurization of dibenzothiophene.

The role of the particle morphology

It was noted that on the small microcrystals, biphenyl (BP) was the only product observed in the HDS of DBT and that no hydrogenation to tetrahydrodibenzothiophene (HDBT) was occuring. This is in stark contrast to disordered powders, which exhibit both reactions in varying degrees. In the powders, the formation of HDBT was observed, leading by desulfurization to significant amounts of cyclohexylbenzene (CHB). This clearly indicated the existence of multiple sites, one of them closely related to disorder. Furthermore, when HCl is used as an etching agent, the optical absorption of edge surfaces, prepared from a single crystal by lithography, increases. TEM micrographs of the etched surface showed that steps 3 to 10 layers high were formed (Figure 2 ***a*** and ***b***). Similarly an increase in the optical absorption was observed when small micro-

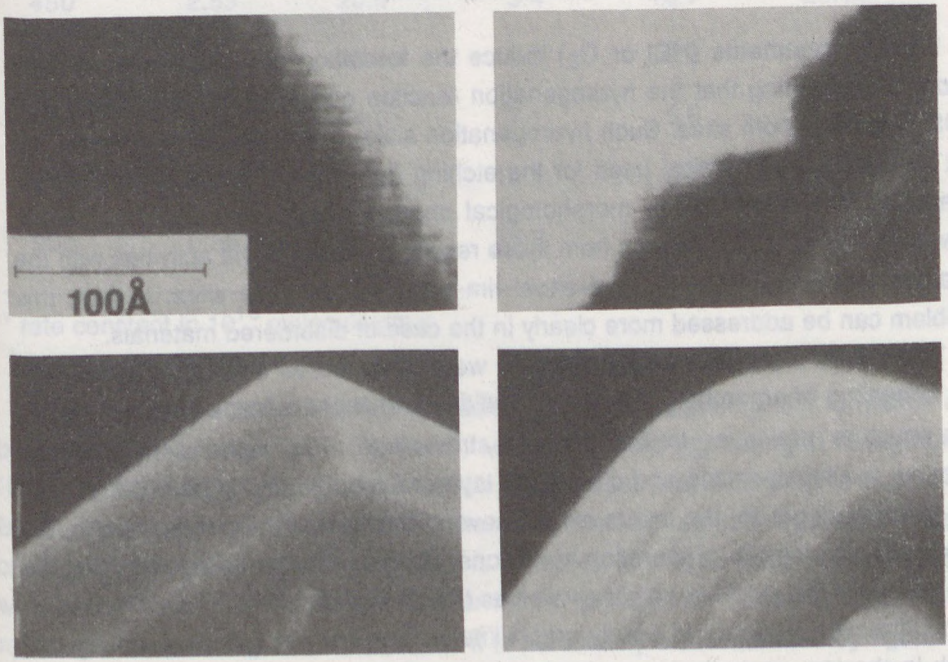

Figure 2. Effect of chemical etching on the structure of the edge surface of MoS_2: ***a***- Synthetic edge surface created by lithography, ***b***- Synthetic edge surface after etching with HCl, ***c***- Edge surface of a microplatelet, ***d***- Edge surface of the platelet after etching with oxygen.

crystals were etched and the smooth surface of the platelet has been roughened (Figure 2 *c* and *d*). Since the optical defect density has been correlated with the HDS activity (4), the change observed reflects a change in the catalytic performance of such microcrystals (Table 1).

Table 1
Effect of chemical etching on the activity and selectivity of MoS_2 catalysts

MoS_2 platelets	rates (10^{16} molecule/g/s)	
	BP	HDBT
Untreated	5.3	0
Oxygen etched	7.8	0.7
HCl etched	6.5	0.4

Etching treatments (HCl or O_2) induce the formation of HDBT as a product, strongly suggesting that the hydrogenation reaction occurs on the steps and that PDS measures both sites. Such hydrogenation sites, which we call "rim" sites are not related to the chemical used for the etching (influence of residual chlorine for example), but rather to the morphological change which introduces the steps. However, it is difficult to extract from these results to correlate the activities with the relative concentration of the two sites: rim sites versus edge sites. In fact, this problem can be addressed more clearly in the case of disordered materials.

The poorly crystalline MoS_2 powders were obtained as described above and the annealing of amorphous MoS_3 in a sulfiding atmosphere leads to the formation of a structure previously termed the "rag" structure (6). The rag consists of several stacked but highly folded and disordered layers. Although only 20 to 100Å thick in the stacking direction, the layers extend several thousand Å perpendicularly to the c axis. By varying the preparation conditions, such as the annealing temperature, one can vary the stacking height as well as the dimension of the layers. Typical X-rays diffraction patterns of poorly crystalline MoS_2 powders exhibit a strong 002 peak in the low angle region and a broad envelope between $2\theta=30°$ to $2\theta=60°$. This envelope contains numerous reflections with well defined maxima for the 100, 103 and 110 reflections. The 103 maximum indicates that the 2H (two layer hexagonal) molybdenite stacking sequence is retained in the crystallites (7). From

the narrowing of the 002 peak, it is clear that the higher temperatures increases the crystalline order along the c-axis. This crystalline order corresponds to an apparent average stacking height (h). After correction of the 002 width from the instrumental broadening, h can be estimated using the Debye-Scherrer equation. The apparent average number of layers for our set of powders are reported in table 2.

Table 2
Average stacking heights and rate constants of MoS_2 as a function of annealing temperature

T (°C)	Δ_{002} (2θ)	h (Å)	n layers	k_{BP} *	k_{H4DBT} *
350	2.64	19.0	3.1	12.0	29.0
450	2.53	20.9	3.4	10.7	23.1
550	2.24	23.4	3.8	6.2	12.1
650	1.20	44.0	7.1	5.6	5.9
750	0.84	62.0	10.1	3.7	2.9
900	0.56	93.5	15.2	1.5	0.8

* rate constant in 10^{16} molecule/gm/s

The rate constants for the hydrogenation reaction (k_{HDBT}) and the formation of biphenyl (k_{BP}), reported in table 2, were obtained by using a Langmuir-Hinshelwood kinetic model to describe the reaction pathway illustrated in Figure 3. Both rate constants decrease as the molybdenum sulfide becomes more crystalline. However, a 36-fold variation is observed for the formation of the HDBT whereas only a 8-fold variation occurs for the BP production. These variations are related to the stacking of the layers, as it is particularly well illustrated by figure 4. The ratio $S = k_{HDBT}/k_{BP}$ is linearly correlated with the linewidth of the 002 reflection peak, i.e. the reciprocal of the stacking height. In figure 4, we also included one

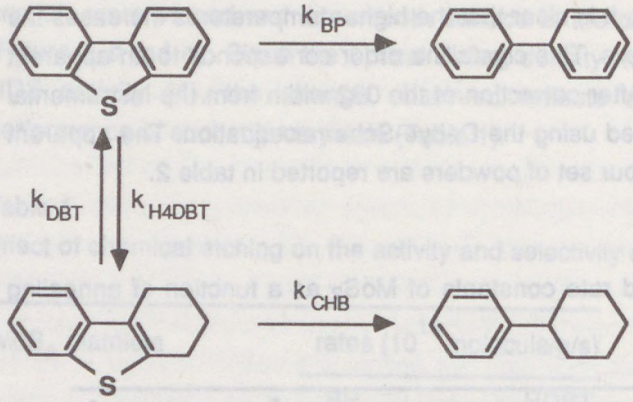

Figure 3. Reaction pathway for the HDS of dibenzothiophene on MoS_2

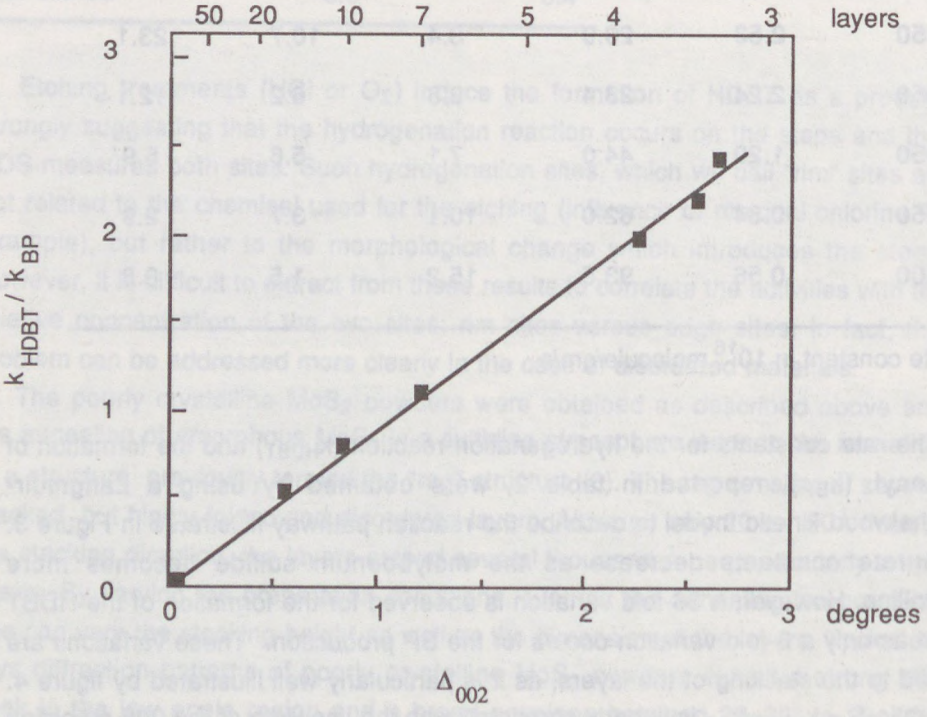

Figure 4. Dependence of the selectivity upon the stacking of the layers

data point to describe the selectivity of the microcrystals which have a negligibly small k_{HDBT} and a 002 linewidth so small that it is instrumentally broadened.

The relative proportion of rim and edge sites can then be calculated by using a simple physical model to describe the morphology of the MoS_2 particle (figure 5).

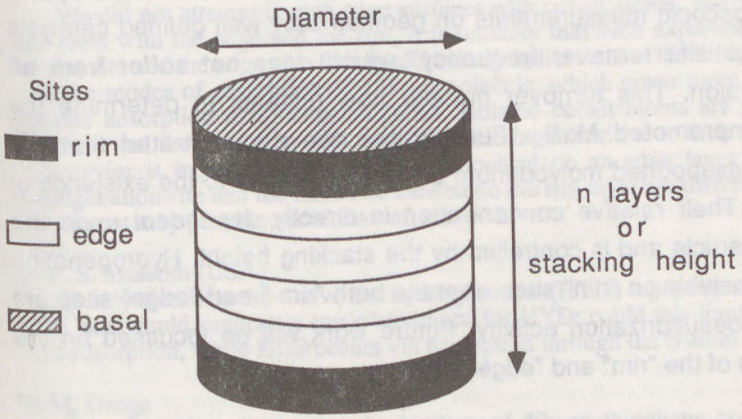

Figure 5. Physical model of a MoS_2 particle

This model assumes that the catalyst particles are made of discs n layer thick and of diameter d. The top and bottom layers have both rim and edge sites while layers in the middle have only edge sites. The top surface of the disc is the basal plane which is assumed to be inert. In this case, the relative density of rim and edge sites can be deduced from the following expression :

$$\frac{r}{r+e} = \frac{2.\pi.d}{\pi.d.n} = \frac{2}{n}$$

where r is the number of rim sites and e the number of edge sites. It is important to note that this relative density does not depend upon the particle diameter or shape but only on the stacking.

Conclusion

Complete understanding of the catalytic properties of MoS_2 requires more knowledge of the edge planes which terminate the anisotropic layers and are the

location of the catalytically active sites. The absence of absolute knowledge of MoS_2 dispersion tends to lead to models which greatly underestimate crystallite sizes. The bulk electronic structure of MoS_2 is directly related to the catalytically active surface states. The catalytic states, created by edge termination or more precisely sulfur vacancies, lie just above the dz^2 band near the Fermi level. Optical and electron spectroscopic measurements on geometrically well defined catalysts yield an "HDS edge site turnover frequency" which does not suffer from an ambiguity in dispersion. This turnover number now unables to determine the dispersion of all unpromoted MoS_2. Furthermore, we demonstrated that the catalytic activity of unsupported molybdenum disulfide is related to the existence of two different sites. Their relative concentration is directly dependent upon the morphology of the particle and is controlled by the stacking height. Hydrogenation reactions occur exclusively on "rim" sites whereas both "rim " and "edge" sites are responsible for the desulfurization activity. Future work will be focussed on the adsorption properties of the "rim" and "edge" sites.

References

(1) M. S. Whittingham, A. J. Jacobson, eds, in: Intercalation Chemistry (Academic Press, New York, 1982).

(2) S. J. Tauster, T. A. Pecoraro and R. R. Chianelli, J. Catal., 63, (1980), 515

(3) K.S. Liang, G.J. Hughes, R.R. Chianelli, J. Vac. Sci. Tech. A2(2), (1984), 991

(4) C.B. Roxlo, M. Daage, A.F. Ruppert,, R.R. Chianelli, J. Catal., 100, (1986), 176

(5) J. Horsley, personal communication

(6) R.R. Chianelli, Int. Rev. Phys. Chem., 2, (1982), 127

(7) K.S. Liang, R.R. Chianelli,F.Z. Chien, S.C. Moss, J. of Non-Crystalline Solids, 79, (1986), 251

DISCUSSION

Q: M. J. Ledoux (France)

If you etch MoS_2 particles with Co atoms, would you observed a selective adsorption or absorption site of the metal atoms? Do they absorb on rim or edge sites?

A: M. Daage

We did not attempt to etch edge surfaces with cobalt atoms. We do agree that the cobalt will react with the edge and the rim, it is unlikely that such experiment would differentiate the rim site and the edge site. Our model clearly indicates that the differentiation is associated with the modes of adsorption of a large molecule, which cover more than one layer for the flatwise adsorption of dibenzothiophene. Isolated cobalt atoms are smaller than the layer thickness and their reaction with the site should be insensitive to their location. No difference in behavior is expected for an HDS site located on an edge layer or a rim layer. If the hydrogenation site and the HDS site located on the rim layer are different in nature, then such experiment may provide additional information.

Q: F. S. Massoth (USA)

If only rim sites are active for hydrogenation (HYD) while all edge sites are active for HDS, this would suggests a steric hindrance for HYD; could this imply HYD occurs via flat-wise adsorption, while HDS occurs via adsorption through the S atom ?

A: M. Daage

Because it is unlikely that the binding of dibenzothiophene occurs simultaneously on two adjacent layers, we agree that steric hindrances are of critical importance for molecules that are larger than the thickness of one MoS_2 layer. Simple geometric models have been used to describe the interaction of dibenzothiophene with the edge of MoS_2 and support such conclusion. In this work, the hydrogenation was modelled by a flat adsorption through an η^6 coordination of one aromatic ring, whereas the HDS was described though the formation of a σ-bond with the sulfur atom. Only Mo sites located on the corners of the MoS_2 layer and on the rim layer can accommodate the η^6 coordination.

Q: M. Breysse (France)

Recently we have studied the activity of molybdenum sulfide catalysts supported and we have concluded that the stacking should have an influence on the HDS properties. As a matter of fact, it is highly unrealistic that two sites on adjacent layers can be simultaneously active due to the size of the reactant molecules. Therefore, we agree to distinguish the top layer from the others, but this is valid for all the reactions and not only for hydrogenation.

1) Have you tried to extend this study to supported materials, which are better defined than unsupported ones ?

2) Did you make direct hydrogenation measurements ?

A: M. Daage

We do not agree that the supported materials are better defined than the unsupported materials because the interaction of MoS_2 with the support is of primary importance and is poorly understood. In addition, the supported materials do not allow to study a wide range of stacking heights and establishing the correlation between the selectivity and the stacking would have been more difficult in that case. However, we think that the rim-edge model can be extended to supported materials, but additional assumptions regarding the interaction with the support should taken in account. Direct hydrogenation measurements have been carried on 2 and 3 ring aromatics and support our conclusions.

Finally, the distinction of the top layer from the other layers should not apply to all reactions. That distinction in our opinion strictly results from the size of the molecule adsorbed and its mode of adsorption. As mentioned in our reply to F.S. Massoth, simple

geometric models clearly demonstrate that effect. The σ-sulfur binding mode results in a quasi vertical mode of adsorption, which does not overlap with the next layer. This is not the case with the η^6 mode of adsorption which results in a flat-wise mode. Note that for small molecules, it is expected that the rim-edge model does not apply.

Q: J. W. Niemantsverdriet (The Netherlands)

First, my compliments for the nice work, but I find it difficult to understand why a "rim" site, which as you suggest is an edge site in the upper layer of MoS_2 differs from the other edge sites. If your suggestion is correct, it would probably imply that supported MoS_2 monolayers are only active for hydrogenation and not for desulfurization. Is it possible that your hydrogenation sites are defects (i.e.-S vacancies) in the outer basal planes ? This might equally well explain the results of Figure 4.

A: M. Daage

Our model suggests that the hydrogenation occurs only a rim sites, but the HDS occurs on both rim and edge sites. Therefore supported MoS_2 monolayers are expected to be active for HDS, which is consistent with the literature. The hypothesis of defects sites associated with the outer basal planes has been considered. The correlation could be explain in those terms. However, the hydrogenation reaction requires an interaction through one aromatic ring (i.e. an η^6 coordination), which results in a flat-wise adsorption. Dibenzothiophene is a large molecule, which would cover an area of 0.78 nm x 1.3 nm when using the Van der Waals radii. Such coverage requires that at least 8 sulfur atoms are removed from the basal plane in order to accommodate the molecule. It is very unlikely that such a reduction of layer would occur at catalytic conditions without leading to a disintegration of the layer. Moreover, the dibenzothiophene would have to be bound simultaneously to 4 molybdenum atoms. Using geometric model led us to conclude that the S bonding mode is the only possible mode of adsorption on basal plane defects. Consequently, such defects would contribute to HDS and not hydrogenation. Such conclusion is inconsistent with our results and the hypothesis has been discarded.

Q: J. A. Moulijn (The Netherlands)

You presented very elegant results which you explain in terms of "rim" and "edge" sites. In our earlier work we (and also many others) have reported that for MoS_2/Al_2O_3, the turnover frequencies (HDS of thiophene) are highly dependent on the Mo loading. We explained that by a varying active-phase/support interaction. Would you advocate another explanation in view of your results ?

A: M. Daage

Our model has been developed on unsupported MoS_2. Additional assumptions regarding the interaction between the support and the active phase have to be done in order to extend our model to supported material. One difficulty in answering your question lies in the fact that both dispersion and stacking are varying. Without a precise knowledge of the dispersion, it would unreasonable to advocate an other explanation. We observed that the turnover frequencies of supported materials was much lower than the turnover frequencies of bulk materials. This would suggest that the stacked layers may have higher turnover frequencies than the first layer which is strongly interacting with the support.

Q: R. Iwamoto (Japan)

If you apply this rim model to supported catalyst, only the upper rim is active for hydrogenation ? I think that the lower rim is in a very different state in the case of supported catalysts.

A: M. Daage

We agree with your comment. The bottom rim of the stack should be strongly interacting with the support and its catalytic properties should be very different. In fact, this is the most important assumption that has to be made if one want to extend our model to supported catalysts.

Q: J. Grimblot (France)

You clearly demonstrated that sites at the rim of the MoS_2 particles behave differently from the classical edge sites. Following your observations, I have two questions:

1) When using supported MoS_2 catalysts, where the particles are well dispersed, i.e. - no stacking, you should have only rim sites. Are then the catalytic results consistent with our data, i.e. - high hydrogenation activity ?

2) What are the fundamental reasons why the rim sites are different from the edge sites ? Do you think that some reactions need two adjacent cooperative layers which then define a particular type of sites ?

A: M. Daage

Many supported catalysts have stacked layers, particularly at high Mo loadings. There are generally difficult to characterize and the presence of the promoter is crucial in that regard. If one assume that well dispersed supported catalysts as you call them have no stacking, then we agree that only rim sites would exist if no stacking is obtained. Our model predicts that these catalysts would have a high selectivity for hydrogenation. The high activity is however controlled by the dispersion of the particles. The results do not contradict your observation, but you should keep in mind that unsupported materials are generally more selective for hydrogenation, probably because of the lack of support/active-phase interaction (see previous replies).

Q: Y. Arnaud (France)

Ten years ago, Mrs J. E. Germain and J. E. Tatibouet have published a work on MoO_3 showing the anisotropy of comportment of this oxide. I am working on this problem for oxides.

The information that I can propose concerns:

1) The fact that a crystallographic face determines a geometry and potentially a selectivity which may change with the face.

2) Activity is associated to the state of these faces depending on ambient conditions.

My question is: Have you observed some changes of activity of your samples ?

A: M. Daage

The layered structure of MoS_2 is fundamentally different from that of MoO_3. The layers are chemically independent and their stacking is due to a Van Der Waals interaction. Their activity is associated with the Mo atoms at the edge of those layers and two crystallographic planes are observed: (1010) and (10$\bar{1}$0). It is not clear that these two planes have different catalytic behaviors. Note however that our model does not address this issue, but rather stresses the fact that when the molecule is large the neighboring layer sterically hinders the adsorption of the molecule, which would be the case for a flat-wise adsorption.

Q: H. Topsoe (Denmark)

In view of the difficulty in studying the MoS_2 edges directly in single crystal studies (demonstrated nicely in the work of Somorjai) your type of model studies should certainly be encouraged, but I believe you have left many other possibilities of explaining your results. The parameter $\underline{n}$ you looked at, represents the order within the Van Der Waals gap and is therefore not expected to give rise to large changes in properties. Your changes in $\underline{n}$ take place when you change the annealing temperature from 350 ^{0}C to 900 ^{0}C. Such large changes would certainly also be expected to change the properties of the MoS_2 edges

(e.g. the fraction of edge to corner sites, the fraction of (1010) and (10$\bar{1}$0) edges, etc.). In view of the large previous literature (Tanaka, Kastelan, Massoth, ourselves and others) I would expect such effects are more likely to influence your results. Anyway, you should be extremely cautious to draw firm conclusions if you do not consider these effects which have been shown to be important.

A: M. Daage

First of all, the parameter n that we measure represents the number of stacked layers. It is not representative in any way of an order along the plane of the layer. In fact, such order is better measured by using the widening of the 110 diffraction peak. For the set of samples we used in our study, this parameter varies from 7.0 to 11.0 nm, which is an effect that is far less important than the effect we measured. However, the question of the relative fraction of corner to edge along the edge of layer is an important question which has not been neglected. Because of the highly anisotropic nature of MoS_2, it is difficult to understand why this fraction would be proportional to the stacking. Anyway, it is possible by considering this hypothesis to model the correlation we presented here. If such explanation is correct, it clearly assigns the hydrogenation function to the corner sites, assignment which has not been clearly demonstrated, but only assumed in the literature. In addition when one considers the ratio of corner to edge needed for the material annealed at 350 ^{0}C, two out of three Mo on the edges ought to be corners. In such cases, most of them would exist within a distance of each other that is shorter than the size of the molecule we used. The dibenzothiophene cannot be aligned with the layer in its flat-wise adsorption mode. The geometric model then clearly indicates that the molecule would rather adsorb in the flatwise adsorption mode but orthogonal the edge of the layer. That is the characteristic of the rim sites. Once again, that is the size of the molecule that we have used which highlights such phenomenon. Consequently, I have to disagree with your statement that we did not consider other possibilities. In fact, most of the literature is based on the desulfurization of thiophene, which is not representative of a large organic molecule. In addition, Kastelan explicitly stated that his model was only valid for small molecules such as thiophene, i.e. - when the size of the molecule does not exceed the thickness of an individual layer of MoS_2. We also considered the possibility of basal plane defects and eliminated that possibility in view of geometric models (see reply to Niemantsverdriet). The explanation presented in our communication represents the most logical and consistent picture. The hydrogenation selectivity for large molecules is mainly controlled by the presence or absence of the neighboring layer. Our model at that time does not exclude the possibility of hydrogenation on all the corner sites. We do think however that their concentration is lower than that of the rim sites. Finally, when considering the fraction of (1010) and (10$\bar{1}$0) edges planes, our model does not differentiate such structures. It is however unlikely that these fractions change in such a dramatic manner. In fact in the 2H structure of MoS_2, they are always present in the same concentration.

Guczi, L. *et al.* (Editors), *New Frontiers in Catalysis*
Proceedings of the 10th International Congress on Catalysis, 19-24 July, 1992, Budapest, Hungary
© 1993 Elsevier Science Publishers B.V. All rights reserved

ELEMENTARY STEPS OF HYDROGENATIVE SULFUR-, NITROGEN- AND OXYGEN-REMOVAL FROM ORGANIC COMPOUNDS ON SULFIDED CATALYSTS

H. Schulz and N.M. Rahman

Engler-Bunte-Institute, University of Karlsruhe, Kaiserstrasse 12, D-W 75 Karlsruhe, Germany

Abstract

Basic reactions of HDSNO conversions are kinetically characterized by means of their dependence on hydrogen availability. Benzofuran and furan are the main model ractants.

INTRODUCTION

The HDS-, HDN- and HDO-conversions are of industrial importance to make pure hydrocarbon products from fossil energy resources. Investigations of these reactions are correspondingly directed to those organic heterocompounds which are commonly found in the fossil fuels and this provides as well the borderline for substances to be taken into account for this study.

In commercial hydrotreating the removal reactions for sulfur, nitrogen or oxygen are generally regarded as one reaction each and their success reported as the degree of heteroatom removal. This is a serious simplification, since even e.g. denitrogenation of a relatively simple compound as quinoline only proceeds in a complicated network of reaction steps [1,2] and such reaction networks are very different for individual organic heterocompounds [1].

On the other hand it can be concluded from current literature that such reaction sequences are composed of a small number of types of elemental reactions. It is the concept of this publication to derive and characterize these elemental reactions from a variety of selectivity data about HDSON-reactions and develop a more general theory of the HDSON conversion on sulfided catalysts. The improved understanding of the basic types of reactions is then thought to be used for the characterization of catalyst active sites with regard to their chemical nature and their geometrical constraints. This is of particular impact for the systems of promoted sulfided catalysts, because their actual surface structure and composition must be regarded as dependent on the temperature and the partial pressures of H_2 and H_2S in a dynamic mode.

ORGANIC HETEROCOMPOUNDS TO BE CONVERTED

Heteroatoms in fossil fuels are generally constituents of stable organic structures and have thus survived degradation and rearrangement processes during ages of transformation of the deposit. The heteroatoms sulfur, nitrogen and oxygen have in particular become part of 5- and 6- membered rings with aromatic character. These heterocyclic aromatic rings are commonly parts of larger ploynuclear substances. Corresponding simple model compounds are given in Table 1. Compounds 1 to 5 (benzothiophene, benzofuran etc.) are generally best suited. Their routes of reaction are of minor complexity, however, contain the intrinsic elemental steps. Conversion of basic monocyclic structures (Nos. 6 to 9) is less closely related to fuel upgrading but highly interesting for the understanding of the catalytic system. The conversion of dibenzoderivatives (Nos. 10 - 13) is already strongly influenced by geometric factors, due to restricted accessibility of individual bonds to the active sites. Phenols 15 and anilines 16 are of great interest as very stable intermediates of HDO- and HDN-reaction sequences.

TABLE 1
MODEL COMPOUNDS FOR HDSNO-CONVERSIONS IN RELATION TO THE UPGRADING OF FOSSIL FUELS

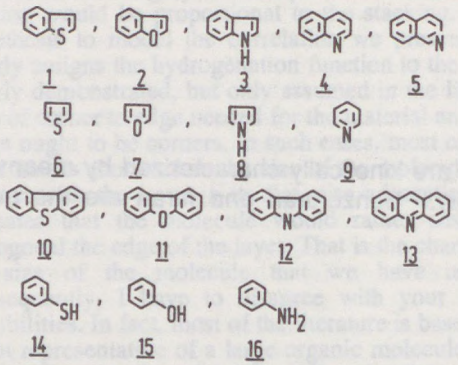

GENERATION OF REACTIVE WEAK BONDS THROUGH HYDROGENATION

An important principle of hydrogenative removal of the heteroatoms sulfur, nitrogen and oxygen from organic constituents in liquid fossil fuels is the labilisation of the heteroatom bonding through hydrogenation. This generation of weak bonds through hydrogenation is essential in the HDSNO-reaction sequences of all the compounds in Table 1 except for thiophenol 14 and dibenzothiophene 10. As a cosequence of technical importance HDN and HDO need more severe hydrogenation conditions (higher hydrogen partial pressure and higher temperature) which corresponds to a higher hydrogen availability, a most governing feature of the system. Generation of reactive weak bonds through hydrogenation (saturation of aromatic structures) is indicated in Table 2 for several main reaction sequences . A more exhaustive comparative discussion has been given in Ref. [8].

The range of reactivity for hydrogenation of rings with aromatic character is very broad. As a measure of reactivity the reaction temperatures for 50 % conversion under representative hydrotreating conditions are given in Table 2. It can be noticed, that reactivity of the heterocyclic ring in the bicyclic compounds is very high: quinoline is converted to 1,2,3,4- tetrahydroquinoline e.g. already below 200 °C.

Table 2
Generation of reactive/weak bonds through hydrogenation in typical HDSON reaction sequences'

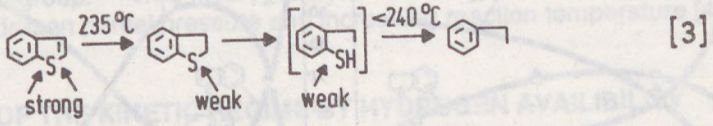

[3]

BENZOTHIOPHENE

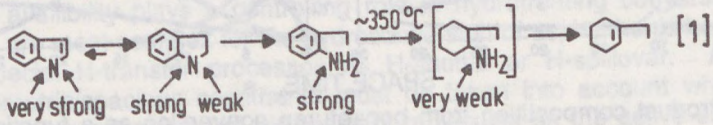

[1]

INDOL

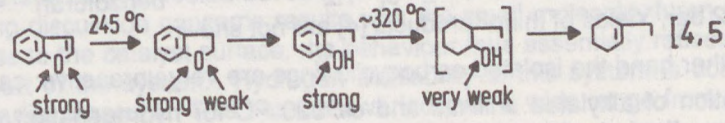

[4,5]

BENZOFURAN

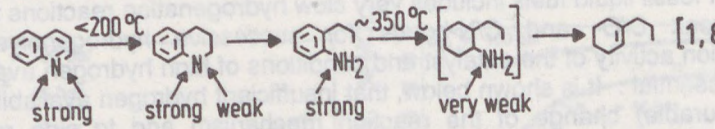

[1,8]

QUINOLINE

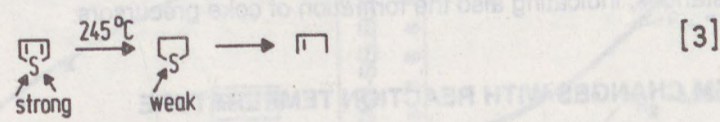

[3]

THIOPHENE

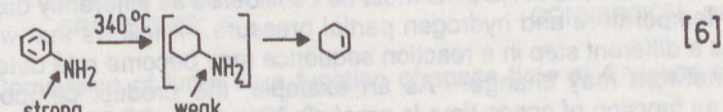

[6]

ANILINE

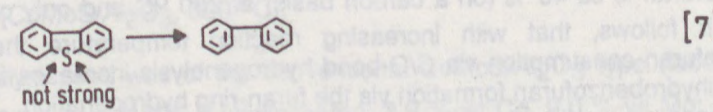

[7]

DIBENZOTHIOPHENE

TEMPERATURES GIVEN ON ARROWS INDICATE REACTIVITY OF THE COMPOUNDS AS MEASURED FOR 50 % CONVERSION UNDER TYPICAL CONDITIONS AS P_{H_2} = 50-100 bar, $CoMoS/Al_2O_3$ ACCORDING TO REF. [8]

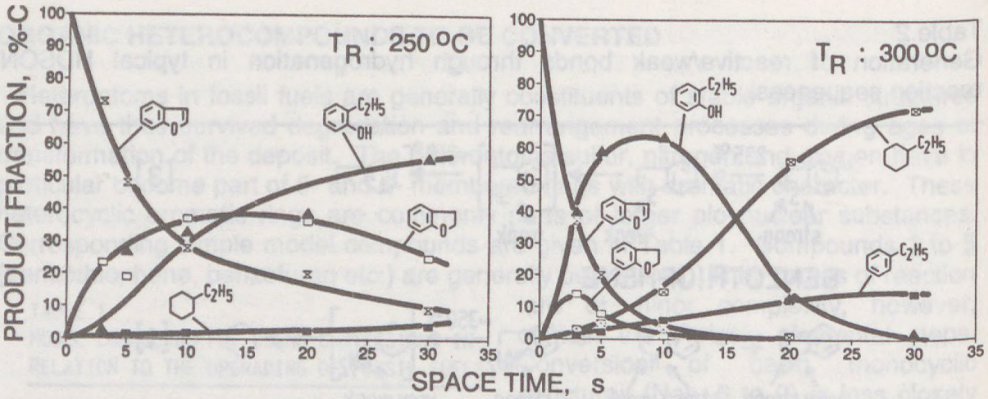

Figure 1. Product compostition from benzofuran conversion as a function of space time at 250 and 300 °C. Co MoS/Al_2O_3, P_{H2} = 100 bar, $P_{benzofuran}$ = 0.6 bar, P_{H2S} = 0.2 bar, Yields of minor products [4] are not shown.

On the other hand the isolated carbocyclic rings are very unreactive: ca 350 °C for hydrogenation of alkylated anilines and ca 320 °C for hydrogenation of alkylated phenols are afforded. As a practical consequence it is stated, that extensive HDN and HDO of fossil liquid fuels includes very slow hydrogenation reactions to generate reactive weak C/O- and C/N-bonds for successive hydrogenolysis. High hydrogenation activity of the catalyst and conditions of high hydrogen availability are therefore essential . It is shown below, that insufficient hydrogen availability leads to an (unfavourable) change of the reaction mechanism and to side reactions of formation of unsaturated compounds, of crackproducts and of higher molecular weight substances, indicating also the formation of coke precursors.

MECHANISM CHANGES WITH REACTION TEMPERATURE

The elemental reactions in HDSNO must be considered as differently dependent on reaction temperature and hydrogen partial pressure. It follows that with change of conditions a different step in a reaction sequence may become rate determining or a reaction network may change. As an example, the product compostion from benzofuran as function of space time is presented for the reaction temperatures 250 and 300 °C in Figure 1. The maximum concentration of the intermediate dihydrobenzofuran is ca 40 % (on a carbon basis) at 250 °C and only ca 17 % at 300 °C. It follows, that with increasing reaction temperature the rate of dihydrobenzofuran consumption via C/O-bond hydrogenolysis increases faster than the rate of dihydrobenzofuran formation via the furan-ring hydrogenation. The same interdependence is valid for benzothiophene hydrodesulfurization. A high intermediate concentration of dihydrobenzothiophene is observed at low temperature and high hydrogen partial pressure [3,6].

At low temperature (250 °C) the HDO-intermediate o-ethylphenol is very stable against hydrogenation and obtained as a major final product. At sufficiently high

temperature (300 °C) the benzene ring of the o-ethyphenol is hydrogenated, leading (together with fast secondery reactions) to ethylcyclohexane as the main HDO product. Ethylbenzene is obtained simultanously via hydrogenolytic removal of the phenolic OH-group. This hydrogenolytic cracking-selectivity is increased with declining hydrogen partial pressure and increasing reaction temperature [4,5].

CHANGES OF THE KINETIC REGIME BY HYDROGEN AVAILIBILITY

Hydrogen availibility plays a controlling role in hydrotreating conversions. The phenomena are most complex for the hydroconversion of asphalthenic heavy oils [9] including special H-transfer processes as H-shuttle or H-spillover. Additionally serious geometric/spacious constraints must be taken into account which do not allow adequate chemisorption of big reactant molecules on the active sites. For a deeper understanding, fundamental studies of the cooperating systems are needed. The following discussion concerns results with the small molecule, furan which has easily access to the catalyst surface. Its behaviour thus essentially reflects the pure chemistry part of the system. Hydrogen availability in this system is controlled by hydrogen partial pressure. This has been varied over a wide range from 0.6 to 100 bar.

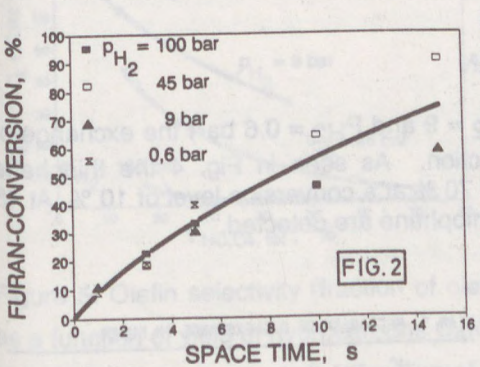

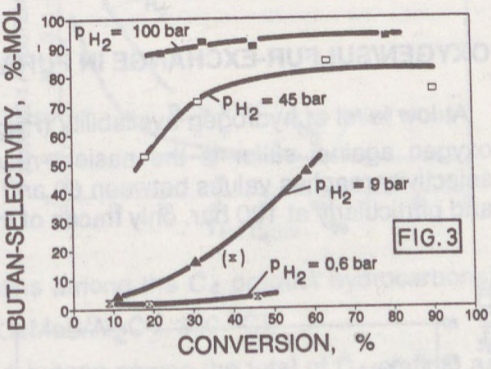

Figure 2. Conversion of furan as a function of space time at 4 values of hydrogen partial pressure (300 °C, $CoMoS/Al_2O_3$)

Figure 3. n-Butane selectivity as a function of furan conversion at 4 hydrogen partial pressures ($CoMoS/Al_2O_3$, 300 °C).

The catalyst used was of the conventional $CoMoS/Al_2O_3$ type (laboratory made sample M8-10 from BASF, Ludwigshafen; 3.9 %-wt Co, 9.0 %-wt Mo; BET: 220m^2/g; Pore volume: 0.5 cm^3/g; particle size 0.4 - 0.5 mm; sulfiding with a 10 % - vol H_2S in H_2 flow at 2 bar and 400 °C for 8 hrs). Conversion of furan as a function of space time at 4 pressures of hydrogen is represented in Figure 2. One sees the expected increase of conversion with space time. The differences in conversion with

change in pressure are generally in the range of scattering. The following representations of selectivity as a function of degree of conversion show a very systematic and elucidating behaviour.

n-Butane is the expected and desired hydrocarbon product compound from furan hydrodeoxygenation.

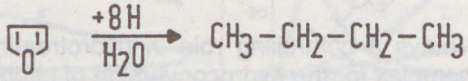

The selectivity of its formation is only high (ca 90 %) at 100 bar of hydrogen partial pressure (Figure 3). At 45 bar the butane selectivity increases from ca 50 % at ca 20 % conversion to a final value of ca 80 % at ca 60 % conversion. At 9 bar the butane selectivity is only ca 5 % at 10 % conversion and attaines ca 45 % at 60 °C conversion. At 0.6 bar the butane selectivity generally reaches only a few per cent. The conclusions are, that pressures up to 100 bar are needed for high HDO-selectivity of saturated hydrocarbons. Experiments at total pressure of only one bar are in no way representative for commercial hydrotreating.

OXYGEN/SULFUR-EXCHANGE IN FURAN

At low level of hydrogen availability (P_{H2} = 9 and P_{H2} = 0.6 bar) the exchange of oxygen against sulfur is the easiest reaction. As seen in Fig. 4 the thiophene selectivity reaches values between 60 and 70 % at a conversion level of 10 %. At 45 and particularly at 100 bar, only traces of thiophene are detected.

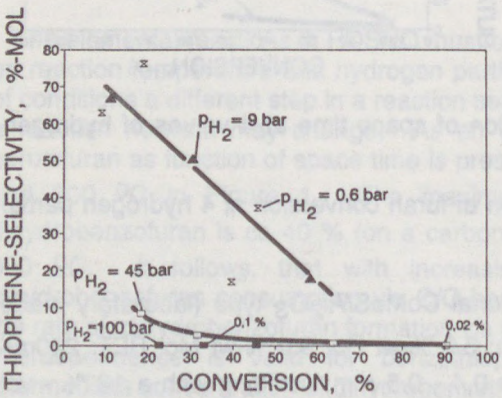

TAB 3 MECHANISM OF O/S-EXCHANGE IN FURAN

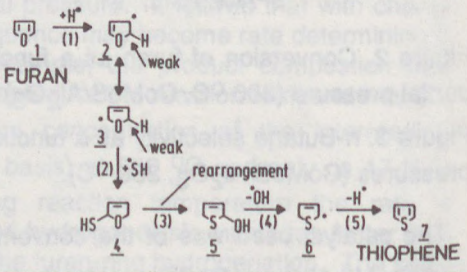

Figure 4. Thiophenselectivity as a function of furan conversion.
at 4 hydrogen partial pressures ($CoMoS/Al_2O_3$).

It is suggested (Table 3) that furan adds one hydrogen atom reversibly. The mesomeric form of this intemediate 3 adds one SH-group to form intermediate 4, which rearranges under exchange of O to S in the 5-membered ring (3). The reactions of this exchange sequence are obviously faster than the addition of further hydrogen. This situation changes at higher hydrogen partial pressure and correspondingly higher hydrogen availability.

C/O- AND C/S HYDROGENOLYSIS AND HYDROCARBON FORMATION

The hydrocarbon, which is preferably primarily formed, through furan-HDO is the 1-butene. This is concluded from Figures 5 and 6. The olefinfraction of the product-hydrocarbons C_4 is shown as a function of the total yield of C_4-hydrocarbons in Figure 5. With decreasing hydrogen partial pressure the olefin selectivity increases strongly. At low conversion the olefin selectivity is as high as 80 - 90 %.

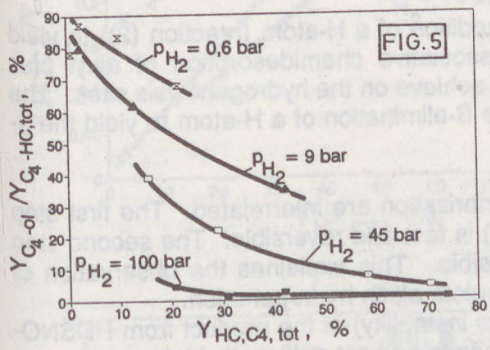

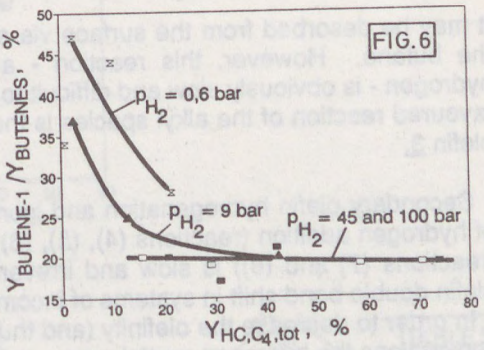

Figure 5. Olefin selectivity (fraction of olefins among the C_4 product hydrocarbons) as a function of yield of hydrocarbons C_4($CoMoS/Al_2O_3$, 300 °C).

Figure 6. 1-Butene-selectivity (Fraction of 1-butene among the total of C_4-olefins) as a function of yield of total C_4-hydrocarbons ($CoMoS/Al_2O_3$, 300 °C).

Figure. 6 indicates that at high hydrogen pressure the concentration of the 1-butene among the C_4-olefins is independent of hydrogen partial pressure and degree of conversion which is explained as an established equilibrium composition. At low hydrogen pressure and low degree of conversion (low HC-yield) the 1-butene selectivity is much higher. It is concluded that 1-olefins are primary hydrocarbon products. They can be secondarily isomerized or hydrogenated. The reaction mechanism is given in Table 4. It is almost identical with the respective partial system in Fischer-Tropsch hydrocarbon formation [10].
The oxygen containing intermediates are all very reactive and only observed as traces in the reaction product. Thus the primary hydrocarbon intermediate to be obtained from butanol hydrogenolysis is the chemisorbed butyl species 1.

Table 4
Kinetic schemes of primary olefin and paraffin formation and of olefin isomerization and secondary olefin hydrogenation

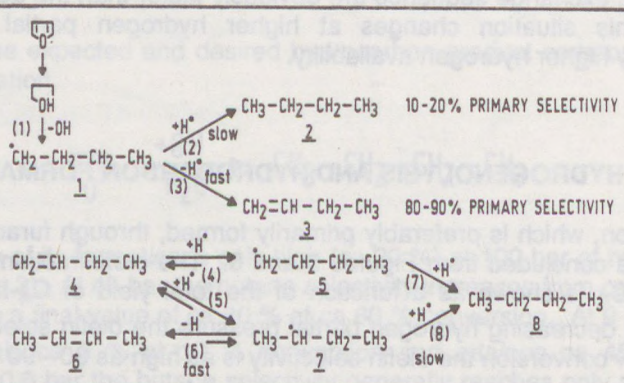

It may be desorbed from the surface via addition of a H-atom (reaction (2)) to yield the butane. However, this reaction - associative chemidesorption of alkyl plus hydrogen - is obviously slow and difficult to achieve on the hydrogenolysis sites. The favoured reaction of the alkyl species is the ß-elimination of a H-atom to yield the 1-olefin 3.

Secondary olefin hydrogenation and isomerization are interrelated. The first step of hydrogen addition (reactions (4), (5), (6)) is fast and reversible. The second step (reactions (7) and (8)) is slow and irreversible. This explaines the observation of olefin double bond shift in systems of incomplete olefin hydrogenation.

In order to decrease the olefinity (and thus instability) of the product from HDSNO-conversions the hydrogen partial pressure has to be kept sufficently high.

CONDENSATION REACTIONS

Small amounts of butyl benzofuran and of C_8-hydrocarbons have been determined. The analytical accuracy is not very high. Several individual compounds have been grouped in the HC-C_8 fraction. The results (Figure 7) indicate secondary formation of these compounds.

DECARBONYLATION

The HDO-conversion of furan is accompanied by an appreciable decomposition into a C_3 and a C_1-species. Fig. 8 indicates the C_3-selectivity to increase strongly with decreasing pressure (5 % at 100 and 45 bar, 10 % at 9 bar, 17 % at 0.6 bar).

C_3-selectivity does not change with conversion (respectively total yield of hydrocarbons.
This reaction must therefore start in parallel with the C_4 hydrocarbon formation at the still oxygen containing aliphatic C_4-intermediate. It is known that C_4 oxygen compounds (similarly to aldehydes) tend to decompose [11,12], into CO and a C_3 fragment. The CO will mainly be hydrogenated to CH_4 under HDO conditions. The corresponding reaction scheme is presented in Tabel 5. Branching of the reaction sequence is assumed to occur at species 3

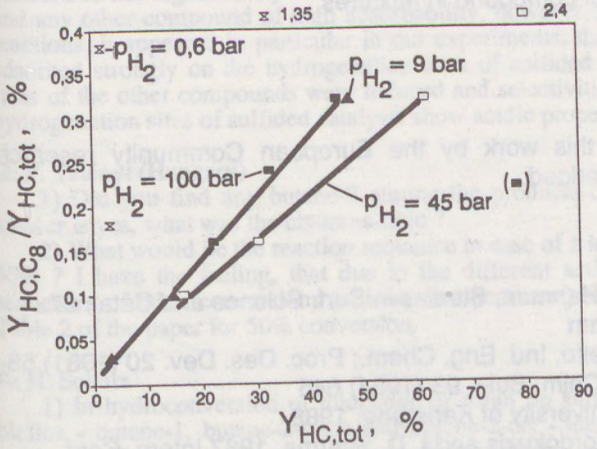

Figure 7. C_8-Hydrocarbon selectivity (fraction of C_8HCs among the total of hydrocarbon products) as a function of yield of total hydrocarbons.

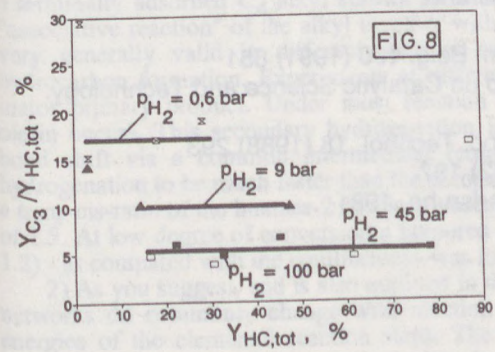

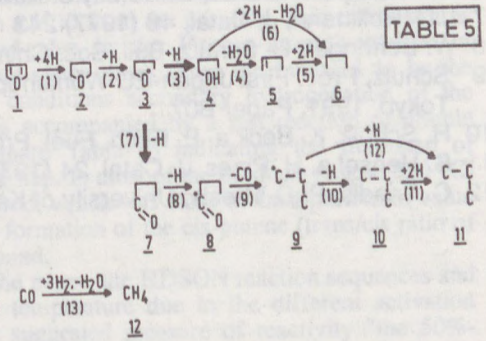

Figure 8. Moles of C_3 hydrocarabons as a fraction of total moles of hydrocarbons in dependence of yield of total hydrocarbons ($CoMoS/Al_2O_3$, 300 °C).

Table 5
Kinetic scheme of (C_3 + C_1)-formation during furan HDO via decarbonylation

CONCLUSION

The results of this investigation demonstrate the controlling function of reactive hydrogen availability for HDSNO reaction networks. Desired selectivity of commercial HDSNO processes increases generally in many respects with increasing hydrogen partial pressure. This concerns catalyst deactivation, hydrogen consumption and yield of valuable products. This paper could only highlight a small segment of the involved problems. Further major areas of research should be the reaction behaviour of big molecules (chemisorption, steric aspects, H-transfer), the specifity of other catalysts than $CoMoS/Al_2O_3$ for individual types of reaction steps and the competitive conversion of compound in mixtures.

ACKNOWLEDGEMENT

Financial support of part of this work by the European Community research programme is gratefully acknowledged.

LITERATURE

1 H. Schulz, M. Schon a. N. M. Rahman, Studies in Surf. Science and Catal. 27 (1986) 204; Elsevier, Amsterdam
2 C.N. Satterfield a. J. F. Cocchetto, Ind. Eng. Chem.; Proc. Des. Dev. 20 (1981) 53
3 H. Schulz a. D.V.Do, Bull.Soc.Chim. Belg. 93 (1984) 645
4 N.M. Rahman, PhD-Thesis, University of Karlsruhe, 1988
5 H. Schulz, N.M. Rahman, G. Kordokuzis and L.D. Sharma, 1987 Intern. Conf. Coal Science, p 269, Ed.K.A. Nater, Elsevier, Amsterdam, 1987
6 D. V. Do, PhD-Thesis, University of Karlsruhe, 1982
7 L.D. Rollmann, J. Catal. 46 (1977) 243
8 W. Böhringer, H. Schulz, Bull. Soc. Chim. Belg. 100 (1991) 851
9 Schulz, Proc. First Japan-EC Workshop on Catalytic Science and Technology. Tokyo, 1991, Paper B07
10 H. Schulz, K. Beck a. E. Erich, Fuel. Proc. Technol. 18 (1988) 293
11 S. Hensel a. H. Pines, J. Catal. 24 (1972) 197
12 C. Triadis, PhD-Thesis, University of Karlsruhe, 1981

DISCUSSION

Q: M. Breysse (France)

In your paper you have shown the controlling function of hydrogen availability on the HDS reaction networks. Have you tried to compare - for the same reaction - results obtained in gas phase with those in liquid phase ?

A: H. Schulz

We have not made this comparison with the compounds which are mentioned in our paper. However, we know from other experiments, that competitive chemisorption can seriously influence specific reaction rates. So, with a paraffin oil as solvent the reaction network is not significantly changed as compared with the gas phase conversion. Solvents and any other compound of high adsorbability, however, do strongly influence the HDSNO reactions. It appeared in particular in our experiments, that basic nitrogen compounds were adsorbed strongly on the hydrogenation sites of sulfided catalysts and thereby the reaction rates of the other compounds were reduced and selectivities changed. It was concluded, that hydrogenation sites of sulfided catalysts show acidic properties (see Ref. 1 in this paper).

Q: P. Tétényi (Hungary)

1) Did you find any butene-2 among the products of conversion of thiophene? If the answer is yes, what was the cis-trans-ratio ?

2) What would be the reaction sequence in case of a lower percentage of conversion, say 30% ? I have the feeling, that due to the different activation energy values the reaction sequences of other conversions (at lower temperatures) can be different of that indicated on Table 2 of the paper for 50% conversion.

A: H. Schulz

1) In hydroconversion of thiophene or furan on sulfided catalysts all the two possible olefins - butene-1, butene-2-trans and butene-2-cis - are commonly observed hydrocarbon products. The two primarily formed hydrocarbons are butene-1 and butane with an olefin/paraffin ratio of more than 10. This indicates that the reaction of β-H-abstraction from a terminally adsorbed C_4 alkyl species to form the olefin, is favoured as compared to the "associative reaction" of the alkyl together with a H to from the paraffin. This conclusion is very generally valid in different systems and also in the Fischer-Tropsch regime of hydrocarbon formation. Experiments at different space times show the butene-1 to be the major primary product. Under most reaction conditions secondary hydrogenation of the olefin occurs. This secondary hydrogenation is accompanied by a fast reaction of double bond shift via a common intermediate (compare Table 4) indicating the first step of hydrogenation to be much faster than the second step. In most of the products (e.g. at 350 ^{0}C) a trans-cis-ratio of the butenes-2 has been observed, which was close to the equilibrium value of 1.5. At low degree of conversion a favoured formation of the cis-butene (trans/cis ratio of 1.2) - as compared with the equilibrium - was found.

2) As you suggest, and is also outlined in the paper, the HDSON reaction sequences and networks do commonly change with reaction temperature due to the different activation energies of the elemental reaction steps. The suggested measure of reactivity "the 50%-conversion temperature" is very valuable for providing a broad overview and a basic understanding about difficult or easy reactions. We have measured for many reactions the degree of conversion and the product composition as a function of reaction temperature and thus as well obtained the "30%-conversion-temperature-values". These are normally ca. 20-25% lower than the 50% - conversion temperatures.

Q: D. Kalló (Hungary)

What is the meaning of "strong" and "weak" bonds in one of the first schemes shown? Does it correspond to real bond strength or express catalytic reactivity ?

Did you observe sulfidation of oxygen or nitrogen containing compounds on sulfided catalysts ? Otherwise O or N were substituted by S ?

A: H. Schulz

This is a very interesting question. The generalization of our results is justified on the basis that for many of the elemental HDSNO-reaction steps, the substrate reactivity is controlled by the bond strength. So the indications "strong" and "weak" in Table 2 actually refer to both, bond strength and reactivity as well.

A very selective oxygen/sulfur exchange has been observed with furan at 300 ^{0}C, $p(H_2S)$ = 0.2 bar, p(furan) = 0.6 bar. At a hydrogen partial pressure of 9 bar and a space time of ca. 1 sec a ca. 10% conversion were obtained. The sulfur/oxygen exchange selectivity was than ca. 65 % (65 % thiophene selectivity). At 30 % furan conversion the thiophene selectivity still amounted to ca. 50%. It may be concluded, that under mild conditions the actual ring opening step is rather inhibited, so that the route of sulfur/oxygen exchange in the ring becomes the main conversion (compare Figure 4 and Table 3).

Q: H. J. Lovink (The Netherlands)

The future diesel oils will have a 50 ppm sulfur specification and recent work has shown that there is one compound which is very difficult to hydrodesulfurize: dimethyl dibenzo thiophene. Can you comment on the reaction steps that should be carried out and promoted ?

We think, that simple compounds with fewer rings and boiling at 100-200 % are not giving a good guidance for industrial workers, that are trying to treat diesel, gasoil and heavier materials. Can you comment on this ?

A: H. Schulz

Model studies for desulfurization of petroleum fractions afford the proper selection of model compounds. For understanding the basic behavior and dynamics of the catalytic system, small molecules as thiophene, benzo thiophene and dibenzothiophene are appropriate.

However, it soon turns out that with heavy feed stocks, the governing factor of compound reactivity is accessibility of the respective bonds for the catalyst active sites and correspondingly the steric factor becomes dominant. A typical example is the 1,8-dimethyl-dibenzo-thiophene, which you are citing, in which the sulfur atom is very effectively shielded against chemisorption. This aspect needs actually intensive investigation and no simple solution appears to me available at the moment.

Q: M. Ramirez de Agudelo (Venezuela)

Regarding competitive adsorption/reaction can you further comment on this effect which can be caused by the partially hydrogenated compounds during furan conversion ?

A: H. Schulz

In furan hydroconversion inhibition through intermediates is not important, however, it can be dominant in HDN conversion.

When co-feeding naphthalene and quinoline we have observed that all the quinoline had to be converted, before the naphthalene had access to the catalyst, because of the much stronger adsorption of the quinoline on the active sites.

When hydrogenating the none basic indole to obtain the dihydroindole which is quite basic, this is very preferentially adsorbed and converted.

Guczi, L. *et al.* (Editors), *New Frontiers in Catalysis*
Proceedings of the 10th International Congress on Catalysis, 19-24 July, 1992, Budapest, Hungary
© 1993 Elsevier Science Publishers B.V. All rights reserved

SITES CHARACTERIZATION ON MODEL RUTHENIUM SULPHIDE

M. Lacroix, C. Mirodatos, M. Breysse, T. Decamp and S. Yuan

Institut de Recherches sur la Catalyse, 2 Avenue Albert Einstein, 69626 Villeurbanne Cedex, France

Abstract

This work reports a systematic study of the changes in the catalytic activities and in adsorptive properties of ruthenium sulphide with sulphur removal. From physicochemical characterization of the reduced samples it is shown that 50% of the initial sulphur content can be eliminated without changing the structure and the morphology of the pyrite phase. The adsorption of CO, NO and H_2S increases with the degree of reduction of the solid. However, the maximum of adsorption capacities for these probe molecules does not correspond to the maximum of catalytic activity observed for the reactions of H_2-D_2 exchange and 1-butene hydrogenation. This suggests that distinct sites are required for adsorption and for catalysis. The use of ammonia as probe molecule seems to be a good tool for determining the Brönsted acidic surface sites. From thermoflash desorption of hydrogen, it has been demonstrated that two different species are retained by the catalyst : one adsorbed on surface sulphur atoms and the other one adsorbed on coordinatively unsaturated ruthenium cation. The concentration of the latter correlates fairly well with the catalytic activities.

1. INTRODUCTION

For complex catalytic systems such as transition metal sulphides the activity has been often related to the presence of coordinatively unsaturated cations formed by removal of superficial anionic species [1, 2]. By analogy with metals, probe molecule adsorption has been also used for numbering the anionic vacancies on sulphide catalysts. Most of the results reported in the literature indicate that a good proportionality exists between the adsorption capacities and the catalytic properties. However, the comparison of the results obtained in different laboratories reveals important variations in the amount of adsorbed molecules. These discrepancies may be ascribed to several parameters such as different sample preparation or catalyst pretreatment. As a matter of fact, for a given chalcogenide, the genesis of the active centre is controlled by the working conditions of the catalyst and their concentration depends mostly on the temperature and also on the nature of the surrounding atmosphere. Consequently, the resulting dynamic process makes the numbering of anionic vacancies much more difficult than over stabilized surfaces such as metallic catalysts.

A reasonable way to tackle this fundamental problem of site quantification on such kind of catalysts would be to relate both the amount of adsorbed molecules and the catalytic properties to the same criterion of surface characterization, i.e. the number of superficial sulphur atom removed from the sample in controlled conditions. Monitoring the number of coordinatively unsaturated sites may be obtained by a progressive desulphurization of the solid by hydrogen treatment at increasing temperature and contact time.

The present work reports a systematic study of the changes in the adsorption capacities and in the catalytic activities of unsupported ruthenium sulphide with sulphur removal. Ruthenium disulphide was selected as model catalyst because of its known high performances in the field of hydrotreating catalysis [3, 4].

2. EXPERIMENTAL

2.1. Catalyst preparation

Ruthenium sulphide was prepared by precipitation at room temperature from an aqueous solution of $RuCl_3$ by pure H_2S and by further sulphurization in an H_2S flow at 673K for 2 h. The catalyst was cooled down to room temperature under the same atmosphere and flushed with an inert gas.

2.2. Catalyst desulphurization.

The desulphurization of the catalyst was carried out in a dynamic microreactor which allowed to measure the amount of H_2S removed under hydrogen by the use of a specific UV-photodetector (HNU Photoionization detector equipped with a 10.2 eV UV light source). The sensitivity of this system allows the detection of about 1 ppm of H_2S. The amount of H_2S evolved from the solid is simply quantified after calibrating the detector with a known concentration of hydrogen sulphide diluted in hydrogen. The sample was first flushed with a nitrogen flow and then contacted with an hydrogen flow of 40 cm^3/min at room temperature. The temperature was then increased either linearly when the set up works in a TPR mode or stepwise. For the latter, the sample was left several hours at each temperature of reduction until less than 10 ppm were still released from the catalyst.

2.3. Catalytic properties

The catalytic properties of the reduced samples have been determined at 273K by using either the H_2-D_2 exchange reaction or the 1-butene hydrogenation. These reactions which basically involve the hydrogen activation have been chosen because they occur at temperatures lower than the temperatures of catalyst pretreatments. Therefore the state of the catalyst is expected to be stable under reaction conditions. Thus, no H_2S, DHS or D_2S has been detected during the H_2-D_2 reaction course.

After each reduction at a given temperature and measurement of the amount of H_2S evolved from the solid, the plug flow microreactor was isolated from the open air and transferred to the catalytic unit. The experimental conditions used for determining the catalytic properties are summarized in table 1.

Table 1
Catalytic test conditions (reaction temperature 273K)

Reaction	Catalyst loading(g)	P_{H2} (torrs)	P_{D2} (torrs)	$P_{1\text{-butene}}$ (torrs)	P_{argon} (torrs)
1-butene	~0.05	710	0	50	0
H_2-D_2	~0.02	50	50	0	660

For the olefin hydrogenation reaction the effluent gases were analysed by gas chromatography equipped with a PLOT Al_2O_3/KCl capillary column which allows the separation of all the C4 hydrocarbons. In this reaction, the activity has been calculated at the pseudo stationary state obtained after few hours on stream. Preliminary experiments were also carried out with the hydrogenation of a diolefin (butadiene), as often used in the literature. For this case, a drastic and continuous deactivation of the ruthenium sulphide catalyst was observed at 323K due to coke formation, by contrast with the present case of monoolefin hydrogenation.

For the H_2-D_2 exchange reaction, the HD concentration was measured by mass spectrometry. For both reactions the total conversion was kept lower than 20% by adjusting the contact time.

2.4. Adsorption measurements.

The adsorption capacities of NO, CO, NH_3 and H_2S were determined by gravimetry in a SARTORIUS 4433 microbalance working in a dynamic mode. The freshly sulphided sample was first transferred into the balance and then submitted to a vacuum pretreatment at 423K for 15h. During this desorption procedure it has been verified by mass spectroscopy that the catalyst did not lose sulphur. The temperature was then decreased down to room temperature and the solid was contacted with hydrogen. The set up was heated up to the desired temperature allowing an in-situ reduction of the catalysts. Adsorption measurements were performed at room temperature by flushing the solid with a mixture containing 75 torrs of a probe molecule (NO, CO, NH_3 and H_2S) diluted in nitrogen until a stabilized weight was achieved. The irreversible adsorption was then obtained by replacing the mixture by a pure nitrogen flow.

Hydrogen adsorption was studied in a separate set up working in the dynamic frontal mode. The amount of adsorbed hydrogen was determined by a flash desorption at 573K of the solid previously contacted with hydrogen at room temperature and under atmospheric pressure.

3. RESULTS

3.1. Reduction of the catalysts.

The low temperature method used for the synthesis of bulk ruthenium sulphide leads to an homogeneous solid, the composition of which corresponds to $RuS_{2.25}$. The surface area of the sample determined by N_2 physisorption was 70 m^2/g and no

porosity was detected from the calculation of pore size distribution. The X-Ray diffraction patterns of such a solid are similar to that of RuS_2 reported in the JCPDS index. From HREM studies, this solid may be considered as formed by a collection of homodispersed spheres having a mean diameter of 45Å in agreement with the particle size determined by X-Ray broadening of the main diffracting lines. As shown in Figure 1 the temperature programmed reduction pattern of this sulphide exhibits three peaks which can be ascribed to different sulphur species. The low temperature peak (domain 1) which corresponds to weakly bonded species is related to the removal of the excess of sulphur since its elimination leads to the stoichiometric RuS_2 phase. If we assume that bulk sulphur species are eliminated at high temperature (domain 3), thus mild reduction (domain 2) should involve mainly the reduction of superficial anions.

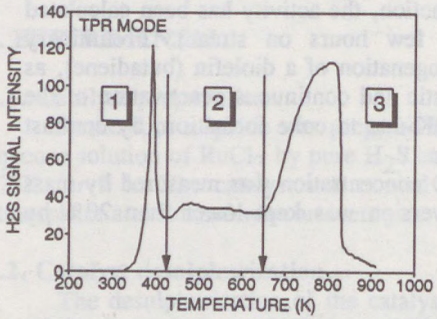

Figure 1. Temperature programmed reduction of unsupported ruthenium sulphide. Evolution of the H_2S formation as a function of the temperature.

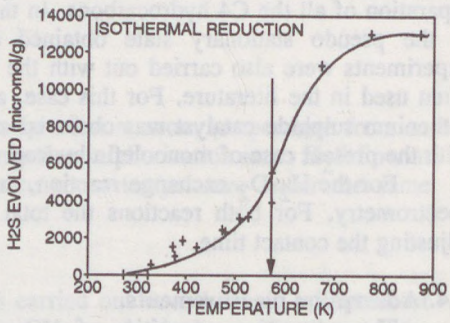

Figure 2. Isothermal reduction of unsupported ruthenium sulphide. Evolution of the H_2S formation as a function of the temperature.

The results obtained during isothermal reduction of the sample are reported in Figure 2. In these experiments, the sample was left several hours in the presence of hydrogen at a given temperature. Below 580K, a fast equilibrium between the solid and the gas phase was reached. As a matter of fact the amount of H_2S released from the solid was only few ppm after 2 or 3 h on stream. At 580K, the amount of H_2S removed from the catalyst was close to 5800 μmol/g and corresponded to the elimination of the anionic species present in the domains 1 and 2. At higher temperatures, the solid continuously lost sulphur whatever the reduction time, and above 600K the reduction of the catalyst tended to be completed.

The kinetic process by which a metal sulphide particle is reduced directly to a metal particle, in a stream of hydrogen under isothermal conditions, may be considered in terms of a nucleation model or a contracting sphere model (Figure 3) [5]. Both models may be discriminated by plotting the degree of reduction α of the solid against time at various temperatures. Results obtained for instance at 673K and illustrated in Figure 4 show that the rate of reduction is already extremely high at the early stages of the reduction process and reaches a constant value with time. This behaviour fits much

better with the contracting sphere model where the rate of reduction is initially high than with the nucleation model where a slow initial process of nucleation should involve a S-shape α-versus-time relationship.

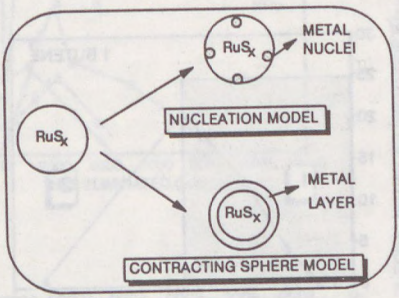

Figure 3. Models of desulphurization of a ruthenium sulphide particle.

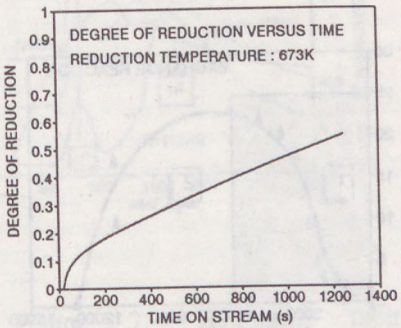

Figure 4. Isothermal (673K) kinetic of desulphurization.

The physico-chemical characterization of the catalyst at different reduction state is reported in table 2.

Table 2
Surface area, particle size and crystalline phase as a function of the reduction temperature (isothermal reduction).

Reduction temperature (K)	Surface area m^2/g	Particle size (nm)	Crystalline phase
273	70	4.4	RuS_2
373	70	4.5	RuS_2
576	70	4.3	RuS_2
673	50	7.8,11*	RuS_2+Ru

* RuS_2 : 78Å, Ru : 110 Å.

Results reported in this table reflects the changes in the texture and in the structure of the catalyst after a hydrogen treatment at various temperatures. No significant changes are observed below 600K i. e. in the temperature domains 1 and 2. At temperatures higher than 600K, the severe reduction of the catalyst leads to a biphasic system containing both the pyrite RuS_2 and the metal phases. The direct transformation of pyrite RuS_2 into Ru metal is in agreement with previous studies which have demonstrated that apart the pyrite phase no other subsulphide exists in the Ru-S system [6].

3.2. Catalytic properties

The changes in the catalytic properties of the catalyst as a function of the amount of H_2S evolved from the solid are represented in Figure 5.

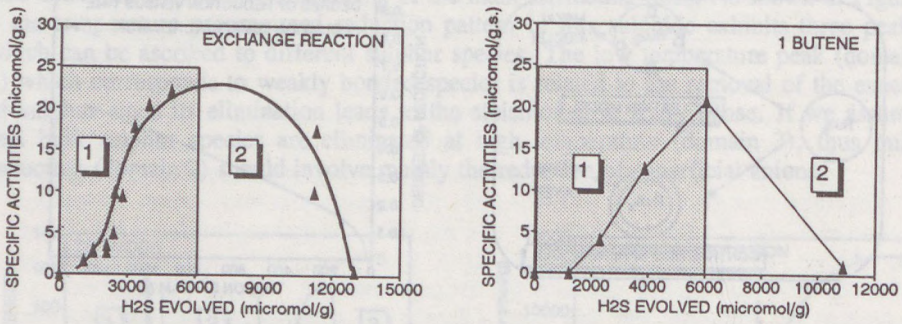

Figure 5. H_2-D_2 exchange and 1-butene activities as a function of the amount of H_2S evolved.

These results clearly show that as long as the stability of the catalyst is preserved (dashed part of the curves), an increase of the degree of desulphurization brings about a large increase of activity for both reactions. The non desulphurized and the totally desulphurized solids do not present any noticeable activity while the intermediate elimination of 6000 μmol/g leads to the most active catalyst. Moreover, both reactions display a very close activity level whatever the sulphur content.

3.3. Adsorption properties.

Figure 6 shows the changes in the amount of irreversibly chemisorbed CO, NO, NH_3 and H_2S as a function of the desulphurization of the catalyst. From these data it appears that i) the amount of chemisorbed CO is very small (20μmol/g) for the non reduced catalyst, ii) the adsorption capacity increases with the amount of H_2S evolved from the solid and reaches a maximum which corresponds to the elimination of ca. 2000 μmol/g, iii) a further reduction leads to a continuous decrease in the amount of adsorbed CO. The changes in the NO or H_2S adsorptions are quite similar to the previous case, excepted that a non negligible amount of these probe molecules is adsorbed on the fully sulphided sample.

In contrast with the adsorption of CO, NO and H_2S, the interaction of ammonia with the solid exhibits an important reversible adsorption which represents ca. 400 μmol/g. However, this reversible uptake is rather independent of the degree of reduction of the catalyst suggesting that it is related to weakly bonded species of physisorbed ammonia. The curve giving the irreversible part of the adsorption presented in Figure 6 shows an initial adsorption of ca. 200 μmol/g. This amount slightly increases at the beginning of the reduction and then linearly falls down and becomes almost undetectable for a reduction state where the adsorption of the other molecules is still significant.

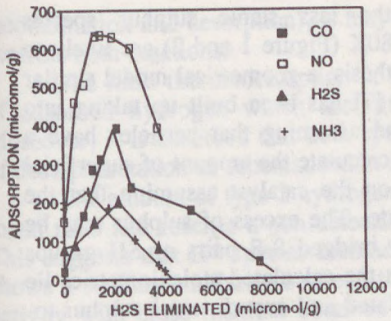

Figure 6. Adsorption of CO, NO, H_2S and NH_3 as a function of the amount of H_2S eliminated.

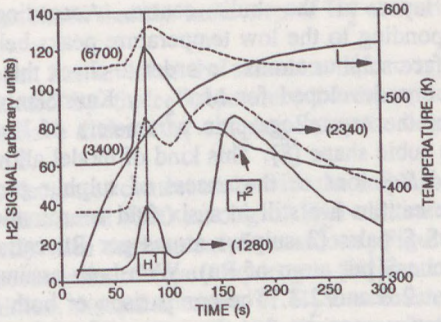

Figure 7. Hydrogen flash desorption patterns as a function of the amount of H_2S eliminated.

The thermoflash desorption (TFD) profiles of hydrogen are reported in Figure 7 and the numbers in brackets represent the amount of H_2S eliminated from the solid expressed in μmol/g. In these experiments, the solid has been reduced at different temperatures and then cooled down to room temperature in the presence of hydrogen. The solid is evacuated at 573K and then contacted with hydrogen under atmospheric pressure at 300K. Under these experimental conditions, the amount of adsorbed hydrogen should be comparable to the one present at the surface of the catalyst during a catalytic run. The total concentration of hydrogen calculated by integrating the H_2 signal against time indicates that the total amount of adsorbed hydrogen decreases with the desulphurization of the catalyst. Moreover the TFD profiles clearly indicate that at least two different hydrogen species are present on the catalyst whatever the degree of reduction of the solid. However, the respective population of each species depends on the sulphur-to-metal ratio. As a matter of fact, the low temperature peak (denoted by H^1 species) increases with desulphurization before decreasing for highly desulphurized sample whereas the second peak (H^2) decreases continuously with desulphurization.

4. DISCUSSION

The study of the reduction process of ruthenium disulphide has shown that about 50% of the total sulphur content can be eliminated from the solid without any noticeable modification of the structural or morphological properties. The temperature programmed reduction clearly indicates that sulphur species presenting different stabilities coexist in this type of compound. Moreover, the kinetic of desulphurization seems to obey to the contracting sphere model where, due to a very rapid nucleation step, the desulphurization concerns the whole surface of the grain, propagating from the

outer layer to the bulk centre. Accordingly, the less stable sulphur species corresponding to the low temperature peaks below 580K (Figure 1 and 2) are likely to be surface sulphur atoms. In order to check this hypothesis, a geometrical model similar to the one developed for MoS_2 by Kazstelan et al. [7] has been built up taking into account the crystallographic parameters of RuS_2 and assuming that particles have a simple cubic shape [8]. This kind of model allows to calculate the amount of superficial Ru and S-S ions or the excess of sulphur present on the catalyst assuming that the surface cations are still in a six fold coordination state. The excess of sulphur may be either S-S pairs (2 sulphur atoms per Ru cation) or bridged S-S pairs or SH groups (only one S per atom of Ru). With both assumptions the calculated stoichiometries lie between 2.6 and 2.3. The comparison of both calculated and experimental sulphur-to-metal ratios suggests that the excess of sulphur comes probably from weakly adsorbed H_2S on some remaining vacancies. Moreover, for the stoichiometric RuS_2 particles, the amount of surface sulphur anions given by this model corresponds to 4500 μmol/g. Therefore, taking into account the excess of sulphur, the calculated amount of surface sulphur atoms presents on the freshly sulphided catalyst is close to ca. 6000 μmol/g which is in agreement with the amount of H_2S eliminated below 580K. Consequently, this simple model reinforces the previous assumption in which domains 1 and 2 (Figure 1) involve mostly surface species whereas the third TPR peak corresponds to a bulk reduction of the solid.

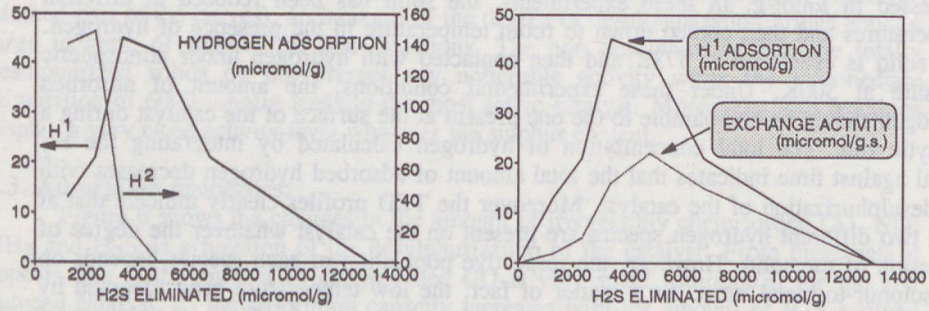

Figure 8. Amount H^1 and H^2 adsorbed as a function of the catalyst desulphurization and correlation with the catalytic activity.

The major increase of the catalytic properties with desulphurization in the temperature range of solid stability rules out that superficial S-S pairs are the main active species involved in the catalytic cycle. This confirms our previous statement [9] emphasizing the catalytic role of anionic vacancies. Interestingly, both reactions studied (H_2-D_2 equilibration and 1-butene hydrogenation) behave quite similarly i.e. the activity maxima are obtained for the same degree of reduction and the activities are in the same order of magnitude. These results strongly suggest that these reactions proceed via the same kinetically limiting step. As the H_2-D_2 equilibration involves only elementary steps dealing with H_2 activation (dissociative adsorption, surface mobility,

recombination and desorption), it may be speculated that the same step of H_2 activation controls both reactions.

The flash thermodesorption of hydrogen has revealed the existence of two types of adsorbed hydrogen which are differentiated by their temperature of desorption. Moreover, it is obserced that both species behave differently with respect to the degree of desulphurization as schematized in Figure 8.

The amount of type 2 hydrogen (H^2) decreases continuously with the sulphur-to-metal ratio and reaches a non detectable level around 4500 μmol/g of H_2S eliminated. This suggests that **H^2 species interact mostly with surface sulphur anions.** Figure 8 shows a striking similarity between the concentration of type 1 hydrogen (H^1) and the activity with close maxima obtained for almost the same extent of H_2S removal. In connection with the previous relationship stated between the rate of hydrogen activation and the density of anionic vacancies, this observation strongly suggests that the **H^1 species are bonded to the anionic vacancies, acting as catalytic sites for hydrogenation reactions.**

Ammonia as a probe molecule may be expected to adsorb either on the Brönsted acid site coming from SH groups or on Lewis sites related to the formation of anionic vacancies. As the change in the amount of adsorbed ammonia versus sulphur removal exhibits a continuous decrease, it seems likely that this molecule reacts preferentially with the protonic acidity. The slight increase of ammonia uptake observed at the beginning of the reduction may reflect the reduction of S-S pairs into SH groups. When the elimination of H_2S reaches ca. 4500μmol/g the remaining surface sulphur atoms are scarce and consequently the adsorption of ammonia on SH groups cannot occur. This behaviour parallels the adsorption of H^2 species which involves also surface sulphur atoms.

From the study of the adsorption of NO, CO and H_2S (Figure 5) it is first obserced that the relative amount of adsorbed molecules is almost constant in the domain of catalyst stability. Thus, for the same degree of reduction, 1, 2 and 4 molecules of H_2S, CO and NO are respectively adsorbed on the catalyst. These stoichiometries may be understood if we assume that i) the H_2S adsorption, dissociative and non mobile at room temperature, will involve two anionic vacancies, ii) the CO adsorption, non dissociative, will involve only one coordinative unsaturation, iii) the NO adsorption, forming dinitrosyl like species, as it was proposed in the literature for molybdenum sulphide based catalyst, will involve only half a site, statistically. Secondly, it is clear that the maximum uptakes are shifted towards lower H_2S removal as compared to the maximum of catalytic activities. This discrepancy between adsorption capacities and catalytic activities is still not completely understood. Although, the catalytic results are not sufficient to determine precisely the number of anionic vacancies surrounding the active site. It may be however stated that the catalytic sites for hydrogenation reactions are highly reduced by comparison with the sites required for NO, CO and H_2S adsorption.

5. CONCLUSIONS

This work has shown that on the very active ruthenium sulphide, the sites involved in hydrogenation reactions are anionic vacancies as already proposed in the

case of molybdenum based catalysts. Moreover, the high lability of $(S\text{-}S)^{2-}$ pairs explains partly the much higher performances of RuS_2 by comparison to the lower lability of S^{2-} anions of the less active MoS_2.

The catalytic and adsorbing properties are drastically influenced by the sulphur-to-metal ratio. It has been shown that for ruthenium sulphide the most active catalytic sites are highly reduced cations. By contrast, the adsorption of probe molecules implies less demanding sites.

Two types of adsorbed hydrogen have been detected, the concentration of which varies differently with the degree of reduction of the catalyst. A very satisfactory relationship has been found between the concentration of hydrogen species adsorbed on the the most reduced sites and the catalytic activity in hydrogenation reactions. This last result demonstrates that the correlation between adsorbing and catalytic properties can be found only when similar sites are implied in both phenomena.

6. REFERENCES

1 K. Tanaka, Adv. in Catal., **33** (1985) 99 .

2 A. Wambeke, L. Jalowiecki, S. Kasztelan, J. Grimblot and J. P. Bonnelle, J. Catal., 109 (1988) 320.

3 T. A. Pecoraro and R. R. Chianelli, J. Catal., **67** (1981) 430.

4 M. Lacroix, N. Boutarfa, C. Guillard, M. Vrinat and M. Breysse, J. Catal., 120 (1989) 473.

5 A. Jones and B. McNicol, "Temperature programmed reduction for solid materials characterization", Chemical Industries/24, M. Dekker Inc., Nex York - Basel, (1986).

6 O. Knop, Can. J. Chem., 41 (1963) 1838.

7 S. Kasztelan, H. Toulhoat, J. Grimblot and J. P. Bonnelle, C. R. Acad. Sc. Paris, Série II, 299 (1984) 289.

8 C. Geantet, A. De Los Reyes, T. Decamp, M. Lacroix and M. Breysse, to be published.

9 M. Lacroix, S. Yuan, T. Decamp, C. Mirodatos and M. Breysse, J. Catal., 132 (1991) 253.

DISCUSSION

Q: J. Grimblot (France)

Your paper is very relevant to the work we have already done in Lille in MoS_2 based catalysts where we have detected site structure evolution upon progressive treatment under H_2.

You observed two hydrogen species (^1H and ^2H) during your desorption experiments. You assign the ^1H species to a hydride-like species (Ru-H). Could you comment a little more about this species? In particular, have you observed Ru-H bond vibration ? What is the number of ^1H species relative to surface exposed Ru atoms ? Is there interconversion between the ^1H and ^2H species ?

A: M. Lacroix

As suggested by the desorption experiments two different hydrogen species exist at the surface of RuS_2 and their relative amount depends on the degree of reduction of the catalyst. In order to get more insight about the chemical nature of ^1H and ^2H, 2 samples were studied by solid ^1H NMR spectroscopy. The NMR spectra of a poorly desulfurized solid (2000 μmol/g of H_2S eliminated) exhibits 2 signals observed at -7.4 and 5.1 ppm with respect to tetramethylsilane. The chemical shift of the later is consistent with an acidic character of the adsorbed species in agreement with the hypothesis of the formation of superficial SH groups whereas the upfield signal (-7.1 ppm) could be most likely ascribed to a hydride type species. For a more reduced catalyst (elimination of ca 4500 μmol/g of H_2S) the spectrum presents only the signal related to the later hydride species.

Taking into account the particle size of RuS_2 and the crystal structure of the pyrite phase, we can estimate the amount of superficial Ru atoms. The calculated value is close to 1500 μmol/g. As the maximum of ^1H concentration corresponds to roughly 50 μmol of H_2/g, the relative number of ^1H species to surface Ru atoms is very small (~6%).

The observed NMR signals have been found extremely narrow excluding chemical exchange between hydrogen atoms belonging to the different sites. Therefore at the present time, we do not believe that an interconversion exists between both adsorbed hydrogen species.

Q: M. Ternan (Canada)

You have indicated that hydrogen was present on the catalyst as hydride ions. Could you review the experimental evidence that supports this finding ?

A: M. Lacroix

The results presented in this work strongly suggest the existence of two types of hydrogen adsorbed at the surface of RuS_2. The characterization of these adsorbed species have been carried out by performing solid NMR (see reply to Professor J. Grimblot) and INS experiments. Both techniques have indicated that hydrogen is adsorbed either as a proton bonded to sulfur ions and as a hydride form linked to a coordinatively unsaturated ruthenium ions.

Q: M. J. Ledoux (France)

In all your measurements (adsorption or catalytic activity) you show that you always go through a maximum.

Can you comment on the decreasing part of these different curves ?

On the increasing part, do you think that this increase is only due to an increase of the number of CUS sites or also due to a change in the electronic structure of the site provided by the higher degree of reduction, or both ?

A: M. Lacroix

Results reported in this paper clearly showed that the hydrogenation and the H_2-D_2

exchange activities increase with the desulfurization of the catalyst, reaches a maximum and then falls down to a non detectable level when the catalyst is almost completely desulfurized. At the maximum and before, we have evidenced that the pyrite phase is stable and the catalyst composition is still homogeneous. Above the maximum, the system becomes heterogeneous and a metallic phase has been detected. Therefore we believe that the decrease in activity could be ascribed to the replacement of the active pyrite phase by a metallic phase poisoned by sulfur which is inactive for hydrogen activation.

Taking into account the catalytic results, we can assume that only the number of CUS is changed in the increasing part of the curves. However as the maxima in activity and in the amount of adsorbed probe molecules are different, it is possible that also the electronic structure of the site is modified by the reduction of the catalyst. Moreover, as the desulfurization state increases, the nature of the CUS (1, 2, 3 or more sulfur vacancies) is obviously changed and consequently the electronic properties of the surface.

Q: K. Klier (USA)

Do you think that under certain conditions the S-S pairs, which are particularly stretched in RuS_2, could be involved in homopolar splitting of hydrogen by activated dissociative chemisorption, formally $S_2^{2-} + H_2 \rightarrow 2SH^-$?

I believe your evidence for involvement of hydridic hydrogen in hydrogenation reactions is strong, but because of suggestions in the literature of homopolar activation of H_2 on sulfides (e.g. Rakowski-DuBois) and because of the lack of reports on Ru-H or Mo-H vibrational spectra, it seems that the general question of dissociative activation of hydrogen is still somewhat open.

A: M. Lacroix

In this work the adsorption of hydrogen has been studied at room temperature. The obtained results showed that the fully sulfided catalyst, which contains mostly $(S_2)^{2-}$ pairs at its surface, does not contain chemisorbed hydrogen. Therefore we think that the reduction of $(S_2)^{2-}$ pairs by an homopolar splitting of hydrogen does not take place in our experimental conditions. However, the hydrogen activation on these pairs as proposed by Rakowski - DuBois could be involved in the very first steps of the reduction of RuS_2 at temperatures around 373 K. Nevertheless, in the following steps of the reduction, this mechanism should not be preponderant.

Q: M. Avalos-Borja (Mexico)

It is not clear to me how a composition like $RuS_{2.25}$ can be determined by STEM.

A: M. Lacroix

STEM studies were performed on a VG HB 501 apparatus equipped with a X-ray spectrometer. This system allows the determination of the S/Ru atomic ratio for various magnifications. Therefore, the composition of different areas of the particle as well as the composition of the whole crystallite could be easily determined.

Q: J. A. Moulijn (The Netherlands)

In your paper you present a nice analysis of the surface of the Ru-particles. You report excess sulphur, SH-groups etc. You correlate the latter with hydrogenation activity. Can you go a step further ? What make a good HDS catalyst ?

A: M. Lacroix

For hydrogenation and hydrodesulfurization reactions it is generally admitted that the active sites are coordinatively unsaturated metal ions. The best catalyst corresponds to a solid containing enough labile anions to form a high number of active sites without destroying the structure of the sulfide phase.

Q: Y. Arnaud (France)

I have found your work very interesting and I am very happy to observe that it corroborates, on sulfides, the observations that can be done on oxides.

In particular it seems that we can define, sulphide surfaces, redox couples associated with surface states. It would explain that the conditions of adsorption of NO, CO and H_2S must be very different of those required for hydrogen activation. If the former species adsorbs on highly reduced sites (high surface coordination) they are strongly adsorbed and they must react in situ.

A: M. Lacroix

The remarks of Professor Arnaud should be considered as a comment and not as a question.

Guczi, L. *et al.* (Editors), *New Frontiers in Catalysis*
Proceedings of the 10th International Congress on Catalysis, 19-24 July, 1992, Budapest, Hungary
© 1993 Elsevier Science Publishers B.V. All rights reserved

HIGH RESOLUTION ELECTRON MICROSCOPY CHARACTERIZATION OF THE POORLY CRYSTALLINE STRUCTURE OF MOLYBDENUM DISULFIDE-BASED CATALYSTS

S. Fuentes[b], *M. Avalos-Borja*[b], *D. Acosta*[b], *F. Pedraza*[a] *and J. Cruz*[b]

[a]Institute Mexicano del Petroleo, Eje Central Lazaro Cardenas 152, 07730 Mexico, D.F., Mexico
[b]Instituto de Fisica, UNAM, A. Postal 2681, Ensenada, B.C. 22800, Mexico

Abstract

Lattice images from molybdenum disulfide-based catalysts have been obtained by high resolution electron microscopy (HREM), in order to determine the influence of the preparation method and promoter concentration on the microstructure of the molybdenum disulfide crystallites.

It was found that the mean number of {002} planes forming the crystallite is only slightly dependent on those parameters while crystal length varies significantly with them. Such results indicate that the edge area (proportional to length times number of stacking layers) is modified when the above mentioned parameters are changed. On the other hand, lattice images from {100} and {h01} showed that their structure is as highly disordered as in the case of {002} planes. The frequency of appearance of such planes was strongly modified by the evaluation test in the thiophene hydrodesulfurization reaction.

1. INTRODUCTION

Better knowledge of the structure of promoted molybdenum disulfides becomes important when considering the industrial applications of these catalysts in the present or the future. Despite enormous dedicated research, the fundamental basis of their catalytic activity is not well understood.

The structure of dichalcogenides is highly anisotropic and many physical and chemical properties are derived from this character. The anisotropy of molybdenum disulfide is increased when low temperatures are used during preparation and the term "poorly crystalline" is, then, better applied (1). Typically, the structure of these samples is highly folded, five to six layers thick and tens to hundreds of nanometers long (2-4). Chien et al. (5) have calculated the x-ray scattered intensities of model structures of "poorly crystalline" molybdenum disulfide and

compared the predictions with experimental results. They concluded that the experimental results can not be explained on the basis of ideal microcrystallite models. Only by introducing defects on the model, like rotation, shift, and folding of the planes, do the predicted patterns agree with the experimental ones. Regarding chemical activity, it is known that the basal plane is relatively inert unless defects are induced on the surface (6). On the other hand, edge planes are known to provide significant chemical reactivity (7-9). Concerning the promoter effect, there is good evidence to conclude that cobalt or nickel atoms are placed on the edge planes of a dichalcogenide structure, creating new, catalytically more efficient sites (10-13). However, more research is needed in order to understand the location of the promoter in this "poorly crystalline" structure of layered dichalcogenides.

In this work, high resolution electron microscopy images from molybdenum disulfide-based catalysts have been obtained in order to gain further insight on their microstructure. In particular, the microstructure changes observed in the molybdenum disulfide crystallites when the preparation method and the promoter concentration were varied.

2. EXPERIMENTAL PROCEDURE

The preparation and pre-treatment of a series of unsupported MoS_2-based catalysts have been described previously (14). High resolution electron micrographs of the following catalysts were taken: molybdenum disulfide (after sulfidation and after reaction), cobalt-promoted molybdenum disulfide (r=Co/(Co+Mo) = 0.3, 0.5, and 0.7), prepared by two methods HSP (11) and ITD (15). Catalyst powders were suspended in n-heptane and dispersed by ultrasound. A drop of this suspension was placed on a holey carbon coated electron microscope copper grid. The observations were carried out in a Jeol 4000 EX electron microscope operated at 400 kV. The spherical aberration coeficient of 1.0 mm guarantees a point to point resolution of 0.18 nm. A throughout focus series was usually taken and the best contrasted image was selected for analysis.

The catalytic measurements were carried out under atmospheric pressure of hydrogen and 2.66 X 10^3 Pa of thiophene in a continuous flow microreactor coupled with a gas chromatograph. Samples were tested in the temperature range of 603 to 623 K. Reaction products were separated using a 20 % carbowax 20 M on chromosorb W column at 343 K.

3. RESULTS

High resolution images of molybdenum disulfide catalysts were taken in areas where the catalysts were thin enough to allow the electron beam to penetrate them. Those areas showed the typical highly disordered structure so called "poorly crystalline", where the small molybdenum crystallites are stacked in all directions. This nanostructure has been observed before (10, 16-19), for unsupported molybdenum disulfide

catalysts. Evidence of {100} planes in well-oriented MoS_2 cobalt-promoted catalyst has been also shown by Lindner et al. (20) Figure 1 shows the MoS_2 catalyst prepared by the ITD method and after sulfidation treatment. Three different zones are identified in this image. The amorphous carbon support film at the upper left, an area with clearly visible {002} planes on the lower left, and an area with mixed orientations at the lower right. The inset at the upper right shows an enlargement of this latter area. By measuring interplanar spacings (in micrographs similar to the above described), the following MoS_2 planes were identified: {002}, {100}, {102}, and {103} among others.

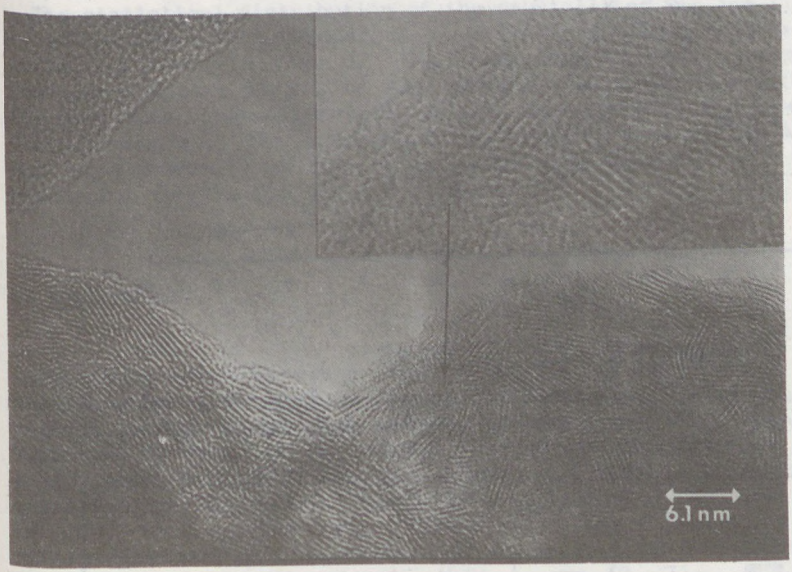

Figure 1. HREM of unsupported MoS_2 (sulfided in 20% H_2S/H_2) at 673K for 4 h.

From enlarged micrographs like these, we counted the number (n) and the length (l) of {002} planes in the MoS_2 crystallites. Histograms of these parameters are shown in Fig. 2, where according to the line histogram the maximum frequency belongs to crystallites with n=3, while the average value of n is 5.5. Figure 2 (inset) indicates that most of the crystallites have lengths in the range 0-5 nm, with an average of around 4 nm (21).

Figure 3 shows the frequency of appearance of the {100} and {h01} planes in the MoS_2 catalyst after sulfidation and after the reaction test (HDS of thiophene). The change in the proportion of these planes from the first sample to the second indicates that a strong reconstruction of the particle microstructure takes place during the reaction. This results are further discussed in a forthcoming paper (21).

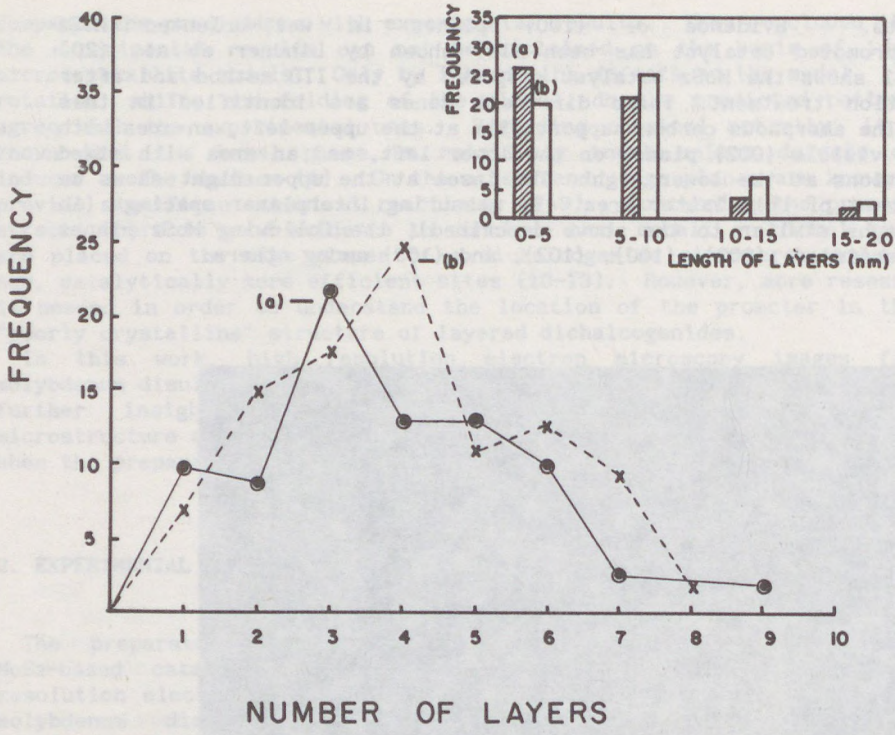

Figure 2. Statistical values of the number of lager (n) (below) and length of layers (l) (inset) for unsupported MoS_2 before (a) and after the catalytic test (b).

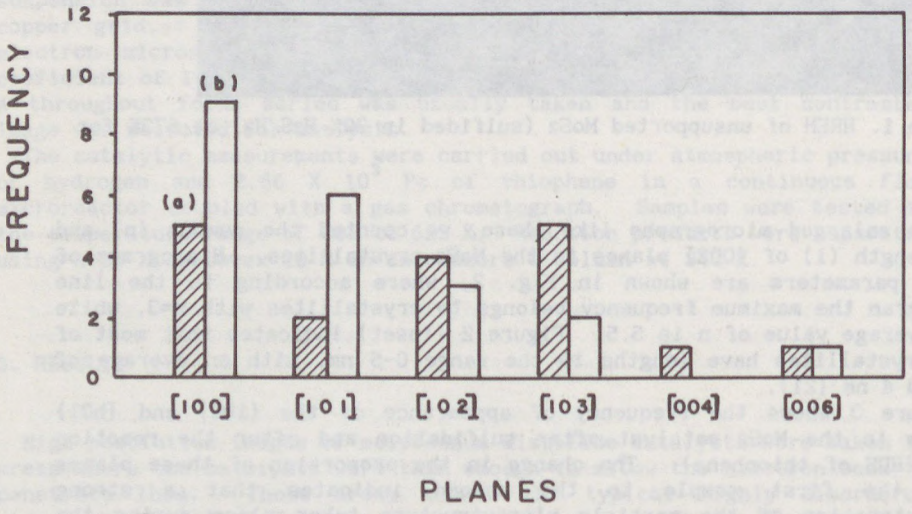

Figure 3. Frequency of appearence of basal-like planes in unsupported MoS_2 before (a) and after the catalytic test (b).

Figures 4a and 4b show typical images of two cobalt promoted (r=0.3) MoS_2 catalysts obtained by HSP and ITD, respectively. A different number density of MoS_2 crystallites has been noted between these samples (higher number density for samples prepared by ITD) (22). This difference is related to a difference in the precursor bulk structure, and does not necesarily mean that the area exposed in the ITD case is larger that in the HSP case. Since we are looking in transmision mode, a number of visible MoS_2 crystals belong to the bulk and do not participate in the reaction.

Figure 5 shows a plot of the crystallite length (l) for the two previously described catalysts. The ITD catalyst shows shorter particles than the HSP, implying a better dispersion (per gram) of molybdenum atoms at the edge surface of the MoS_2 crystallites.

The statistical distribution of the crystallites (in the ITD catalyst) as a function of the number of layers they contain, for each promoter ratio, is shown in Fig. 6. While the differences between plots are considered minor, it can be seen that the distribution maximum at n=5 for pure MoS_2 shifts to n=4 in the 0.3 sample and to n $>\sim$ 5 for the 0.5 and 0.7 samples. The crystallite distribution span varies in a similar way with respect to pure MoS_2, narrowing for the 0.3 sample and broadening for the 0.5 and 0.7 samples.

4. DISCUSSION

In order to correlate the catalytic properties of molybdenum disulfide-based catalysts, the structure has been idealized in terms of perfect hexagonal particles (23). However, in most real catalysts, supported or unsupported, a great deal of disorder exists. In fact, in the layered transition metal sulfides, disorder is very important for catalytic performance. When MoS_2 is prepared by low temperature methods, the compound crystallizes partially in what is termed the "poorly crystalline" structure, which consists of several stacked, but highly folded and disordered MoS_2 layers (2, 7). Our statistical results indicate that most of the crystallites have between 4 and 5 of these layers. This is in agreement with previous work (10, 22) that found a stacking of 3 to 5 layers.

When the promoter concentration is gradually increased, a slight displacement of the most frequent number of stacking layers in the crystallites is observed. This result suggest that the growth mechanism of molybdenum disulfide is affected by the ammount of cobalt atoms. In the low concentration regime (r $\sim$ 0.3) cobalt induces a decrease in the most frequent number of stacking layers, probably because the cobalt atoms are prefer to occupy the edge positions, thus, inhibiting the crystallite sintering mechanism. At higher concentrations, r $\sim$ 0.5-0.7, saturation of the edge areas has taken place and the excess cobalt is seggregated in the form of Co_9S_8 and/or $CoS_{1.035}$ as shown before (14, 24) At this point, MoS_2 crystallites start to grow through the basal plane and therefore, the number of layers increases.

In the next set of experiments, when the Co concentration is maintained, but the preparation method is changed, a different length of crystallites is observed, indicating that the growth mechanism is

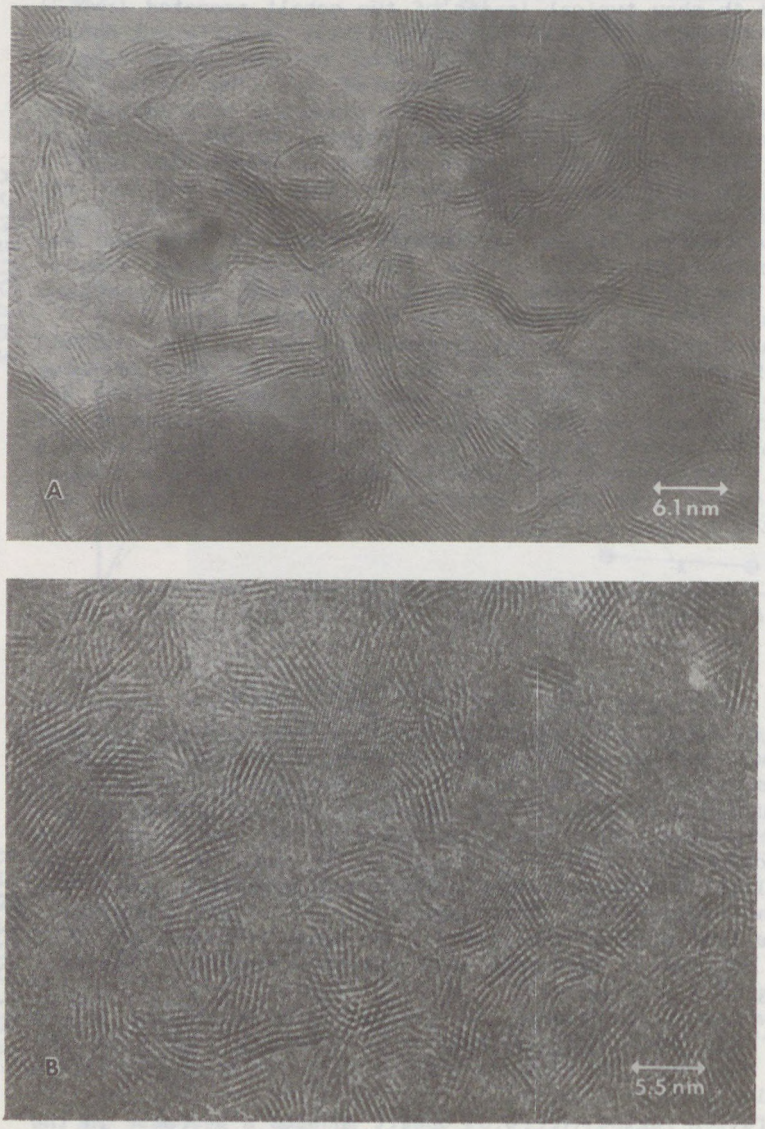

Figure 4. HREM of Co-Mo (r=0.3) unsupported catalysts. a) obtained by HSP. b) obtained by ITD.

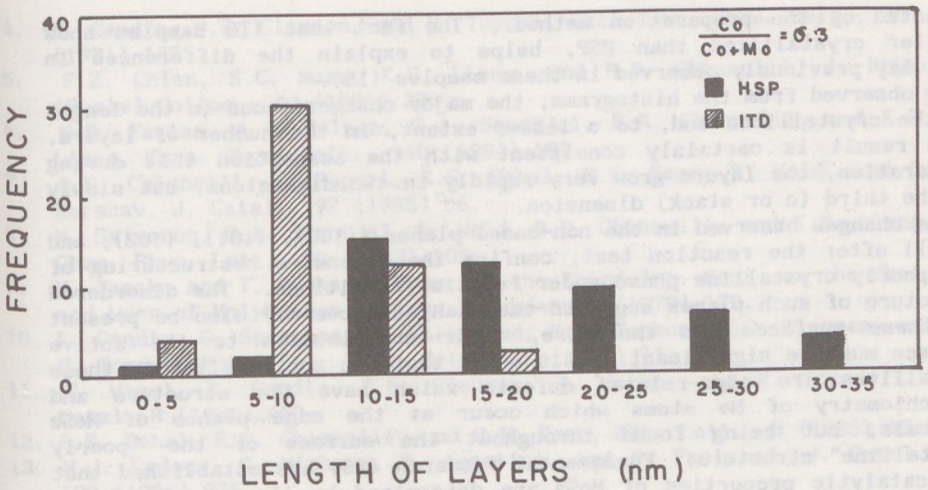

Figure 5. Statistical values of the length of layers as a function of the preparation method, catalysts with r=0.5

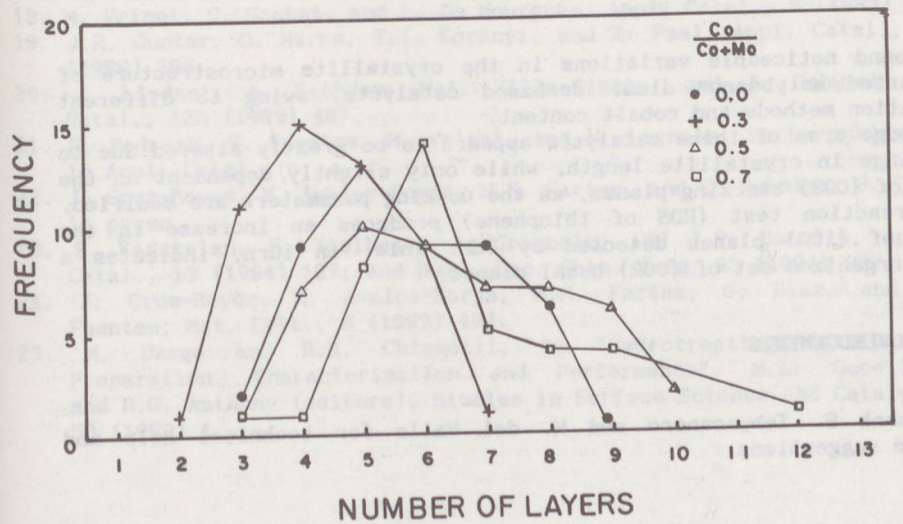

Figure 6. Statistical values of the number of layers as a function of the cobalt atomic concentration.

affected by the preparation method. The fact that ITD samples show smaller crystallites than HSP, helps to explain the differences in activity previously observed in these samples (15).

As observed from the histograms, the major changes occur in the length of the crystallites and, to a lesser extent, in the number of layers. This result is certainly consistent with the assumption that during preparation, the layers grow very rapidly in two dimensions, but slowly in the third (c or stack) dimension.

The changes observed in the non-basal planes ({100}, {101}, {102}, and {103}) after the reaction test, confirm the extensive restructuring of the poorly crystalline phase under reaction conditions. The disordered structure of such planes suggests that many defects may also be present in these surfaces and therefore, their contribution to the active surface must be significant. This means that the active sites in these crytallites are edge-related defects which have the structure and stoichiometry of Mo atoms which occur at the edge planes of MoS_2 crystals, but being found throughout the surface of the "poorly crystalline" structure. Fundamental research (25) has established that the catalytic properties of MoS_2 are determined by its anisotropic or poorly crystalline structure. Our work further shows that this structure is in turn determined by different experimental parameters, namely, the preparation method, the promoter concentration and the reaction conditions.

5. CONCLUSIONS

We found noticeable variations in the crystallite microstructure of unsupported molybdenum disulfide-based catalysts, owing to different preparation methods and cobalt content.

The edge area of these catalysts appears to be greatly altered due to the change in crystallite length, while only slightly dependent on the number of {002} stacking planes, as the working parameters are modified.

The reaction test (HDS of thiophene) produces an increase in the number of {100} planes detected by TEM. This, in turn, indicates a better organized set of {002} basal planes.

6. ACKNOWLEDGEMENTS

We thank S. Tehuacanero and M. del Valle for technical help and valuable suggestions.

7. REFERENCES

1. R.R. Chianelli, Cat. Rev. Sci. Eng., 26 (1984) 361.
2. J.V. Sanders and K.C. Pratt, J. Catal., 67 (1981) 331.
3. K.C. Pratt, J.V. Sanders, and V. Christov, J. Catal., 124 (1990) 416

4. R. Candia, B.S. Clausen, and H. Topsoe, Bull. Soc. Chim. Belg., 90 (1981) 1225.
5. F.Z. Chien, S.C. Moss, K.S. Liang, and R.R. Chianelli, J. Phys. (Paris) Colloq., 40 (1981) 273.
6. M.H. Farias, A.J. Gelman, G.A. Somorjai, R.R. Chianelli, and K.S. Liang, Chem. Phys. Lett., 140 (1984) 181.
7. R.R. Chianelli, F. Rupert, K.S. Behal, B.H. Kear, R. Wold, and R. Kershaw. J. Catal., 92 (1985) 56.
8. M. Salmeron, G.A. Somorjai, R. Wold, R.R. Chianelli, and K.S. Liang, Chem. Phys. Lett., 90 (1983) 105.
9. K. Tanaka and T. Okuhara, Proc. of the Third Int. Conf. on the Chem. and Uses of Molybdenum, Climax Molybdenum, (1979) 170.
10. R. Candia, O. Sorensen, J. Villadsen, N.Y. Topsoe, B.S. Clausen, and H. Topsoe, Bull. Soc. Chem. Belg., 93 (1984) 11.
11. C. Wivel, R. Candia, B.S. Clausen, S. Morup, and H. Topsoe, J. Catal.68 (1981) 453.
12. S.K. Behal, R.R. Chianelli, and B.H. Kear, Mat. Lett., 3 (1985) 381.
13. M.J. Ledoux, O. Michaux, P. Agostini, and P. Panissod, J. Catal., 102 (1986) 275.
14. J. Cruz-Reyes, M. Avalos-Borja, M.H. Farias, and S. Fuentes, Cat. Lett., 9 (1991) 387.
15. S. Fuentes, G. Diaz, F. Pedraza, H. Rojas, and N. Rosas, J. Catal., 113 (1988) 535.
16. J.V. Sanders in "Catalysis, Science and Technology", J.R. Anderson and M. Boudart editors, Springer Verlag, 7 (1985) 51.
17. F. Delaney, Appl. Catal., 16 (1985) 135. And references cited therein.
18. M. Vrinat, C. Gachet, and L. De Mourgues, Appl. Catal., 5 (1983) 43.
19. J.R. Gunter, O. Marks, T.I. Koranyi, and Z. Paal, Appl. Catal., 39 (1988) 285.
20. J. Lindner, A. Sachdev, M.A. Villa-Garcia, and J. Schwank, J. Catal., 120 (1989) 487.
21. F. Pedraza, S. Fuentes, M. Vrinat, and M. Lacroix, to be published in Appl. Catal.
22. J. Cruz-Reyes, M. Avalos-Borja, M.H. Farias, and S. Fuentes, J. Cat. in press.
23. S. Kasztelan, H. Toulhoat, J. Grimbolt, and J.P. Bonelle, Appl. Catal., 13 (1984) 127; and Bull. Soc. Chim. Belg. 93 (1984) 807.
24. J. Cruz-Reyes, M. Avalos-Borja, M.H. Farias, G. Diaz, and S. Fuentes, Mat. Lett., 8 (1989) 492.
25. M. Daage and R.R. Chianelli, in "Hydrotreating Catalysts, Preparation, Characterization and Performance". M.L. Occelli and R.G. Anthony (editors), Studies in Surface Science and Catalysis, 50 (1989) 1.

DISCUSSION

Q: Z. Paál (Hungary)

Let me recall our paper [1] where we observed by EM a few Co_9S_8 particles among the MoS_2 stacks with one sample; this was the sample where due catalytic performance was markedly worse than that of another one where no separate cobalt entities were seen.

[1] J. R. Günter, O. Marks, T. I. Korányi and Z. Paál, *Appl. Catal.*, **39**, 285 (1988)

A: S. Fuentes

I certainly agree with Dr. Paál's remarks.

Q: R. Prada Silvy (Venezuela)

In previous studies investigating the effect of activation temperature on the degree of dispersion of MoS_2 crystallites on $CoMoS/Al_2O_3$ catalysts, we observed homothetic increases in crystal size in the 673 - 923 K temperature range. Basal to edge plane ratio practically remains constant. Did you estimate basal/edge plane ratio as a function of (a) preparation procedure and (b) cobalt loading in the samples ?

A: S. Fuentes

In this work we estimated the change in two series of planes, the (002) basal-like planes and the (101) edge-like planes. For the first series we were able to observe changes in both the cases you mention (more so for the preparation procedure). In the second case, however, we only estimated the change induced by the catalytic reaction itself.

Q: M. Ternan (Canada)

You have reported a 75-80% decrease in HDS. However your changes in geometry, such as number of layers or lengths, are much smaller than 75-80%. Can you comment on whether or not the loss in reaction rate was caused by changes in the geometry of the crystallites.

A: S. Fuentes

The decrease in catalytic activity with time on stream is mainly due to a loss of surface area, which in turn is mostly due to intercrystallite rearrangement. In such a case the activity is not directly related to the number of length of layers. On the other hand, variations in selectivity can be related to a change in crystallite dimensions.

Guczi, L. *et al.* (Editors), *New Frontiers in Catalysis*
Proceedings of the 10th International Congress on Catalysis, 19-24 July, 1992, Budapest, Hungary
© 1993 Elsevier Science Publishers B.V. All rights reserved

DEUTERIUM SOLID STATE NMR STUDY OF MOLECULAR MOBILITY AND CATALYTIC DEHYDRATION OF tert.-BUTYL ALCOHOL ON H-ZSM-5 ZEOLITE

A. G. Stepanov, A. G. Maryasov, V. N. Romannikov and K. I. Zamaraev

Institute of Catalysis, Russian Academy of Sciences, Siberian Division, Prosp. Ak. Lavrentieva 5, 630090 Novosibirsk, Russia

Abstract

Using deuterium solid state NMR, molecular mobility of the initial alcohol and reaction products as well as chemical conversion were studied in the course of dehydration of tert-butyl alcohol, selectively deuterated in methyl groups, in H-ZSM-5 zeolite.

1. INTRODUCTION

Previous studies of the molecules sorbed by zeolites with the aid of deuterium solid state NMR (^{2}H NMR) revealed the possibility to monitor the dynamics of occluded molecules with the help of this method [1-5]. But, so far ^{2}H NMR was used only to study the dynamics under the conditions when these molecules were not involved in chemical reactions. In this work we used ^{2}H NMR to study both molecular mobility and chemical conversions in the course of dehydration of tert-butyl alcohol inside H-ZSM-5 zeolite.

2. EXPERIMENTAL

Two samples of zeolite H-ZSM-5 with Si/Al=29 and 24 have been prepared as described previously [6]. These zeolite samples were tiny, prismatic crystals, which made up secondary spherical aggregates from 7 to 8 μm in diameter. ^{27}Al MAS NMR showed 94% and 93% of tetrahedral Al with respect to the overall amount of Al (tetrahedral+ octahedral) in the samples with Si/Al= 29 and 24, respectively. The absolute concentration of the tetrahedral Al in the samples with Si/Al=29 and 24 was, respectively, 458 and 527 μmole per 1 gram of the zeolite containing 7.7 wt% of atmospheric moisture.

t-BuOH, labelled with deuterium in methyl groups (t-BuOH[2-$^2H_9$]), contained 99% of the main substance with deuterium enrichment 99.5% and water content less than 0.2%.

In order to prepare samples for NMR experiments ca. 0.7 gram of zeolite was loaded in 10 mm glass tube. The sample was then heated at 450°C for 1.5 hour in air to remove atmospheric moisture and for 3-4 hours under vacuum at 10^{-5} torr. Zeolite sample was then exposed to a vapour of the previously degassed alcohol (25 torr) in the calibrated volume (138.5 ml) at 23°C. The amount of adsorbed alcohol was 200-300 μmol/g (2-2.5 wt%). After adsorption was over, the sample was immediately placed into liquid nitrogen to prevent proceeding of the reaction at 296K [7a], and the neck of the tube was sealed off. The sealed tube with the sample was then transferred to a precooled NMR probe just before registration of ^{2}H NMR spectra.

^{2}H NMR experiments were performed at 61.42 MHz with a Bruker MSL-400 spe-

ctrometer. All ^2H NMR spectra were obtained by Fourier transformation of the quadrature detected quadrupole echo, arising in a pulse sequence: $(\theta_1)_{\pm x}-\tau_1-(\theta_1)_y-\tau_2-$ DO, where τ_1= 30 μs, τ_2= 36 μs, DO is a repetition time for the sequence during the accumulation of NMR signal. We used pulse length 4-4.5 μs, which corresponded to θ_1= 70-75°. Spectra were typically obtained with the number of scans, NS=500-5000 and a repetition time DO = 0.4 s. Inversion-recovery experiments were carried out by using the sequence: $(\pi)_x-t_v-(\pi/2)_{\pm x}-\tau_1-(\pi/2)_y-\tau_2-$ DO, where the length of the $\pi/2$ pulse was 5 - 5.4 μs and t_v was a variable delay between 180° inverting and the quadrupole echo sequence.

The temperature of the sample was controlled with a flow of nitrogen gas and stabilized with a variable-temperature unit BVT-1000 with a precision of ca. ±1°C.

3. THEORETICAL BACKGROUND

For slowly reorienting molecules, containing deuterium atom bonded to a carbon atom (with isotropic correlation time τ_c, that is much more then time scale for ^2H NMR ($t_{nmr}=[\frac{3}{4}(e^2qQ/\hbar)]^{-1} = (\frac{3}{4}2\pi Q_o)^{-1}$)) [8,9], ^2H NMR spectrum consists of properly weighted superimposed doublets with the spacing $\Delta\nu(\theta)$ (in frequency units, Hz) given by the formula [9]:

$$\Delta\nu(\theta) = (3/2)(Q_o)(1/2)(3\cos^2\theta - 1), \qquad (1)$$

where $Q_o = e^2qQ/h$ is the quadrupole constant and θ is the angle between the direction of the C-D bond and magnetic field H_o. The spectrum is symmetric with respect to the Larmor frequency ν_o, and the dominant features of this line shape are two strong peaks separated by the splitting $(3/4)Q_o$ and two shoulders separated by $(3/2)Q_o$. For deuterium atom bonded to a tetrahedral carbon atom $(3/4)Q_o$ is usually 120-130 kHz [10].

When CD_3 group rotates rapidly ($\tau_r < 10^{-7}$ s) around the threefold axis, the line shape of the spectrum is not changed, but the quadrupole splitting is reduced and quadrupole constant is defined as [10]:

$$Q_1 = Q_o(1/2)(3\cos^2\beta - 1) \qquad (2)$$

Here β is the angle between the C-D bond and the axis of rotation (β = 109.5° and $Q_1=(1/3)Q_o$ for the CD_3 group). For rapidly rotating CD_3 group the typical value of the reduced quadrupole splitting is 35 -40 kHz [10].

If for the rapidly rotating methyl group, there exists the second rapid rotation around the other axis tilted at the angle β_1 with respect to the first rotation axis, the line shape is not changed again, but further reduction of the quadrupole splitting will be observed [11], so that the reduced (or effective) quadrupole constant becomes equal to

$$Q_2 = Q_1(1/2)(3\cos^2\beta_1 - 1) \qquad (3)$$

For β_1 =109.5° the observed quadrupole splitting is $(3/4)Q_2 \simeq 12 - 14$ kHz.

When the correlation time τ_c becomes equal to inverse value of quadrupole splitting, i.e. $\tau_c \simeq (\frac{3}{4}2\pi Q_o)^{-1}$, a broadening of the spectrum is observed and the sharp features of the spectrum can be washed out [8]. For molecules undergoing rapid isotropic reorientation as in liquids, quadrupole splitting is averaged out and a single line of the Lorentzian shape is observed at ν_o [9].

4. RESULTS AND DISCUSSION

4.1. Molecular mobility of tert-butyl alcohol

Solid t-BuOH[2-$^2H_9$]. We started our ^2H NMR study of adsorption and dehydration of t-BuOH[2-$^2H_9$] on H-ZSM-5 with the preliminary study of the dynamic behaviuor of the alcohol in the polycrystalline solid state. The line shape for t-BuOH[2-$^2H_9$] in the temperature range 170-290K is represented in Fig. 1A. The line shape and effective quadrupole splitting $(3/4)Q_2$= 13.7±0.2 kHz evidence in favour of the existence of two modes of molecular motion in the solid alcohol: fast rotation of the CD_3 groups around C-C bonds with simutaneous rotation of the entire $(CD_3)_3C$ fragment around the C-O bond.

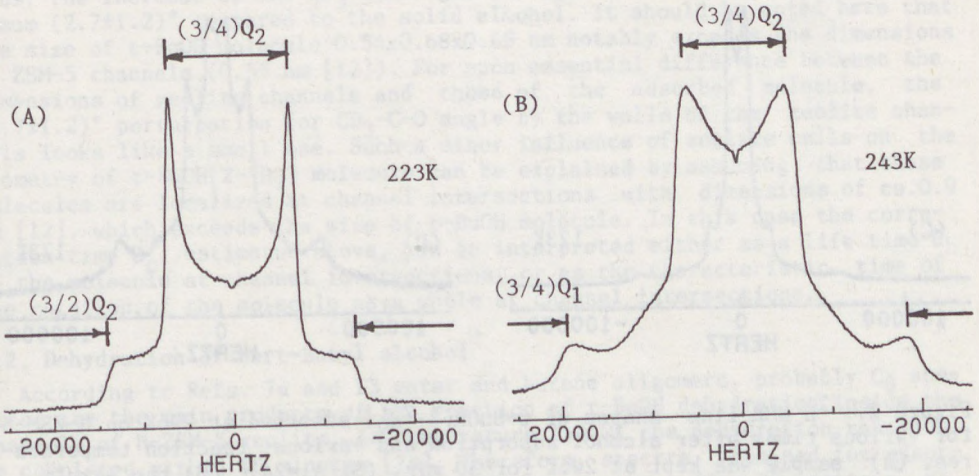

Figure 1. ^2H NMR spectra of t-BuOH[2-$^2H_9$]: (A) polycrystalline alcohol ; (B) alcohol adsorbed on H-ZSM-5 with Si/Al=29 at 296K and kept at this temperature for 2.75 hours. Temperature of the spectra registration is given above each spectrum.

The value Q_2 can be used to characterize the geometry of t-BuOH[2-$^2H_9$] molecule in the solid state. Assuming that the angle D-C-C is an ideal tetrahedral one and using formulae (2) and (3), we find from the quadrupole splitting $(3/4)Q_o$ =130.0±0.5 kHz, obtained for the alcohol at 123K, that the value of the angle CD_3-C-O is β_1 = (110.5±0.6)°.

Adsorbed t-BuOH[2-$^2H_9$]. ^2H NMR spectra of t-BuOH[2-$^2H_9$] adsorbed on zeolite (Figs. 1B and 2) represent a superposition of three signals with the line shape, typical for deuterium solid state NMR and different quadrupole splittings, namely, $(3/4)Q_2$=11.6±0.5 kHz, $(3/4)Q_1$= 37.6±0.5 kHz and $(3/4)Q_o$= 123±2 kHz. The line shape with the splitting 11.6 kHz is seen to be the dominating one in the spectra of samples, that were kept at room temperature up to 2.75 hours (Figs.1B and 2A-C). When keeping the sample at elevated temperature, the relative intensities of the lines with different quadrupole splittings are changed, namely, the intensity of the line with $(3/4)Q_2$ decreases, whereas those for the lines with $(3/4)Q_1$ and $(3/4)Q_o$ grow (fig. 2).

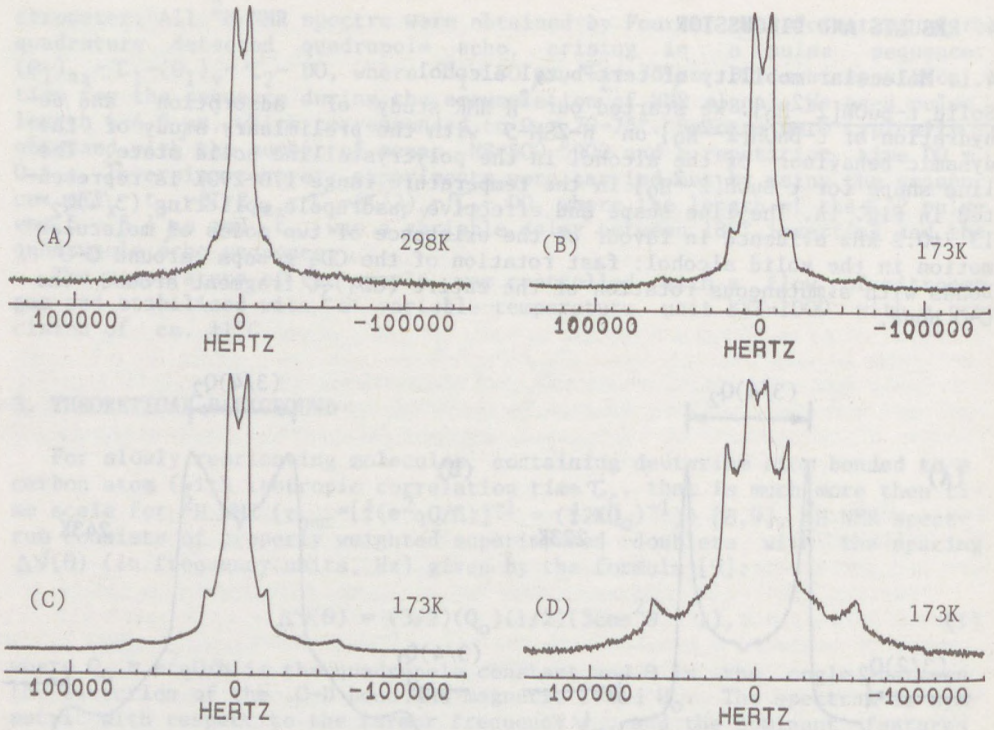

Figure 2. ^{2}H NMR line shapes of t-BuOH[2-$^{2}H_9$] adsorbed at 296K on H-ZSM-5 for various times after alcohol adsorption and various reaction temperatures: (A) sample was kept at 296K for 30 min. (Si/Al=24); (B) the sample was kept at 296K for 20 min. (Si/Al=24); (C) the sample was kept at 296K for 2.75 hours (Si/Al=29); (D) the sample was kept at 313K for 1.3 hours (Si/Al=24). Temperatures of the spectra registration are given above each spectrum.

Investigation of t-BuOH dehydration on H-ZSM-5 by Williams et.al.[7a] and Makarova [7b] showed that about 30% of the alcohol is dehydrated within first 20 minutes after its adsorption at 296K, while the rest amount of alcohol was dehydrated for several hours. Furthermore, they showed that the rates of isomerization and oligomerization of butene, abstracted from the alcohol exceeded the rate of water abstraction. Therefore, it is reasonable to attribute the most intensive line in the spectra (Figs. 2A-C) with $(3/4)Q_2$ = 11.6 kHz, i.e. close to $(3/4)Q_2$=13.7 kHz for CD_3 group in the tert-butyl fragment of solid alcohol, to unreacted t-BuOH[2-$^{2}H_9$].

The line shape of the adsorbed alcohol and the value of quadrupole splitting $(3/4)Q_2$ indicates that two modes of the rapid rotation of CD_3 groups around the C-C and C-O bonds are retained inside the channels of H-ZSM-5 in the temperature range 173-298K (Figs.1B and 2) similar to their rotation in solid alcohol. Furthermore, observation of the splitting $(3/4)Q_2$ points to the fact, that isotropic correlation time τ_c for the reorientation of the

t-BuOH[2-$^2H_9$] molecule as a whole is rather long: $\tau_c >> (\frac{3}{4}2\pi Q_2)^{-1}$, i.e. $\tau_c > 1x10^{-5}$ s. For t-BuOH[2-$^2H_9$] inside the zeolite channels, τ_c refers to dynamic modes, which provide reorientation of the C-O bond with respect to external magnetic field H_o. These modes can be either translational or rotational motion of the molecule as a whole.

An observed difference between $(3/4)Q_2$ for the alcohol in the solid and adsorbed states can be explained by different perturbations of the geometry of t-BuOH[2-$^2H_9$] molecule by the environment in these two states. The scale of this effect can be roughly estimated from the decrease of the observed quadrupole splitting $(3/4)Q_2$ for adsorbed alcohol, compared to that in the solid state. Assuming, that the change of $(3/4)Q_2$ is explained exclusively by the change of CD_3-C-O angle and using equations (2) and (3), one can find, that CD_3-C-O angle is equal to (113.2±0.6)° in the adsorbed alcohol. Thus, the increase of the CD_3-C-O angle for adsorbed t-BuOH[2-$^2H_9$] is at maximum (2.7±1.2)° compared to the solid alcohol. It should be noted here that the size of t-BuOH molecule 0.54x0.68x0.68 nm notably exceeds the dimensions of ZSM-5 channels (0.55 nm [12]). For such essential difference between the dimensions of zeolite channels and those of the adsorbed molecule, the (2.7±1.2)° perturbation for CD_3-C-O angle by the walls of the zeolite channels looks like a small one. Such a minor influence of zeolite walls on the geometry of t-BuOH[2-$^2H_9$] molecule can be explained by assuming that these molecules are localized at channel intersections with dimensions of ca.0.9 nm [12], which exceeds the size of t-BuOH molecule. In this case the correlation time τ_c, estimated above, can be interpreted either as a life time τ_h of the molecule at channel intersections, or as the characteristic time of the rotation of the molecule as a whole at channel intersections.

4.2. Dehydration of tert-Butyl alcohol

According to Refs. 7a and 13 water and butene oligomers, probably C_8 species, are the main products of the reaction of t-BuOH dehydration inside the channels of H-ZSM-5 zeolite. At temperature T>340K the dehydration reaction is completed within 10 minutes [7a]. Therefore, spectra, obtained for adsorbed t-BuOH[2-$^2H_9$] which was heated at 373K for an hour (Fig.3), contain no contribution from the unreacted alcohol and arise only from oligomeric products and water. Fig.3 shows that ^2H NMR spectrum of dehydration products is a superposition of two lines with quadrupole splittings $(3/4)Q_1$, $(3/4)Q_o$ which belong to CD_3 and $CD_2(CD)$ groups of the oligomers formed, plus one more line, located at the center of the spectrum. This line may be tentatively ascribed to the signal of deuterated water, i.e. to D_2O or DHO molecules that can be formed in H-D isotope exchange reaction between CD_3 groups and H_2O molecules, initially formed upon dehydration of $(CD_3)_3COH$[13].

Inversion-recovery ^2H NMR spectra. In order to resolve better various signals that are present in the spectra of Fig.3, we have carried out inversion-recovery experiments. One can expect that various CD_3, CD_2 and CD groups of adsorbed oligomers and adsorbed deuterated water will demonstrate different molecular mobilities and therefore different relaxation times T_1. This means that various components of the observed overall ^2H NMR signal will recover after the inverting 180° pulse with different relaxation rates to the initial equilibrium intensities. It allows one to distinguish more reliably between various lines that contribute to the overall spectrum, and even sometimes to reveal some additional lines that are not observed in the ordinary ^2H NMR spectrum. The following four lines are clearly distinguished in the inversion-recovery spectra, recorded at 243K for the products of the alcohol dehydration (Fig. 4). (1) The line with the quadrupole splitting

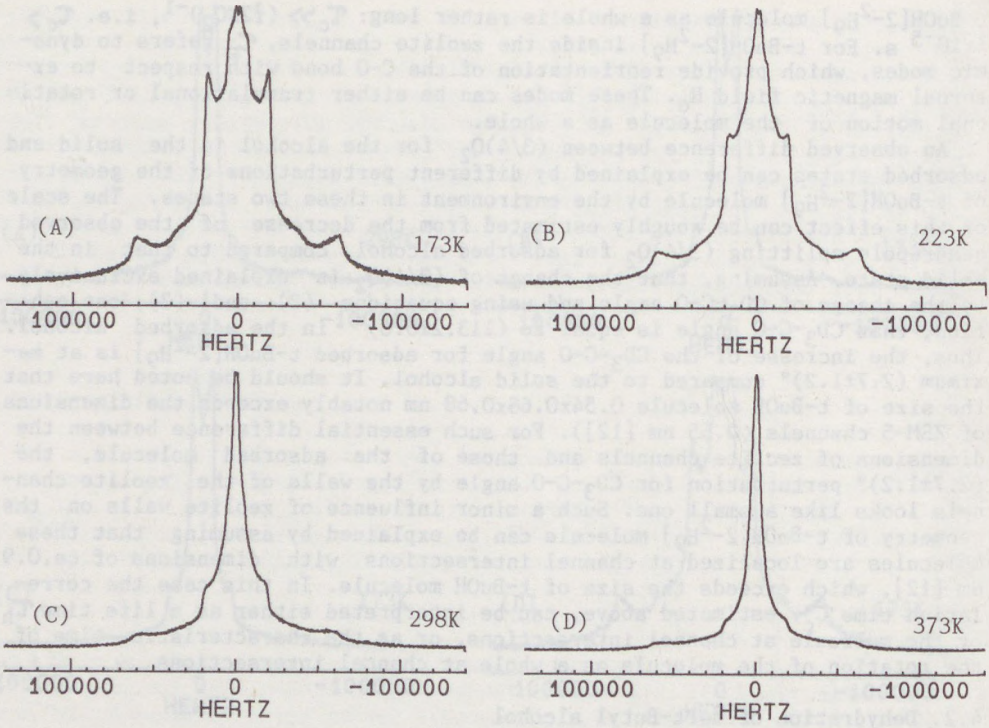

Figure 3. ^{2}H NMR line shapes for the products of t-BuOH[2-$^{2}H_9$] dehydration on H-ZSM-5 (Si/Al=29). Temperatures of the spectra registration are given above each spectrum.

$(3/4)Q_2$=11.6 kHz. The time τ_o, when the intensity of this NMR line turns from the inverted negative position to the normal positive one, i.e. passes through zero, is approximately 10 ms. (2) The line with $(3/4)Q_1$=37.6 kHz and $\tau_o \simeq$15 ms. (3) The line with $(3/4)Q_o$=123 kHz and $\tau_o <$10 ms. (4) The line with $(3/4)Q_3$=1.9±0.1 kHz. For this line $\tau_o \simeq$ 55 ms.

Thus, inversion-recovery experiment allows us to clearly reveal two more lines with quadrupole splittings $(3/4)Q_2$ and $(3/4)Q_3$ in addition to the lines with $(3/4)Q_1$ and $(3/4)Q_o$. The first of the two new lines has the same quadrupole splitting $(3/4)Q_2$ as that for $(CD_3)_3C$ group in t-BuOH[2-$^{2}H_9$], and thus should be attributed to tert-butyl groups in the reaction products. Since water is one of dehydration producta, we assign the signal with $(3/4)Q_3$ to D_2O (or DHO). To prove this assignment we adsorbed D_2O on H-ZSM-5 in the amount equal to the amount of water that should be evolved in the dehydration reaction. D_2O adsorbed on H-ZSM-5 zeolite in this separate experiment exhibits ^{2}H NMR spectrum of the type, given in Fig.5A in the temperature range 290-350K. It is seen that the observed line shape for the signal from adsorbed D_2O (Fig.5A) coincides with that for the signals with the splitting $(3/4)Q_3$, that were observed in both inversion-recovery spectra (Fig.4) and ordinary spectra (Figs.3A-C). Thus, we conclude that the line with $(3/4)Q_3$ indeed belong to D_2O.

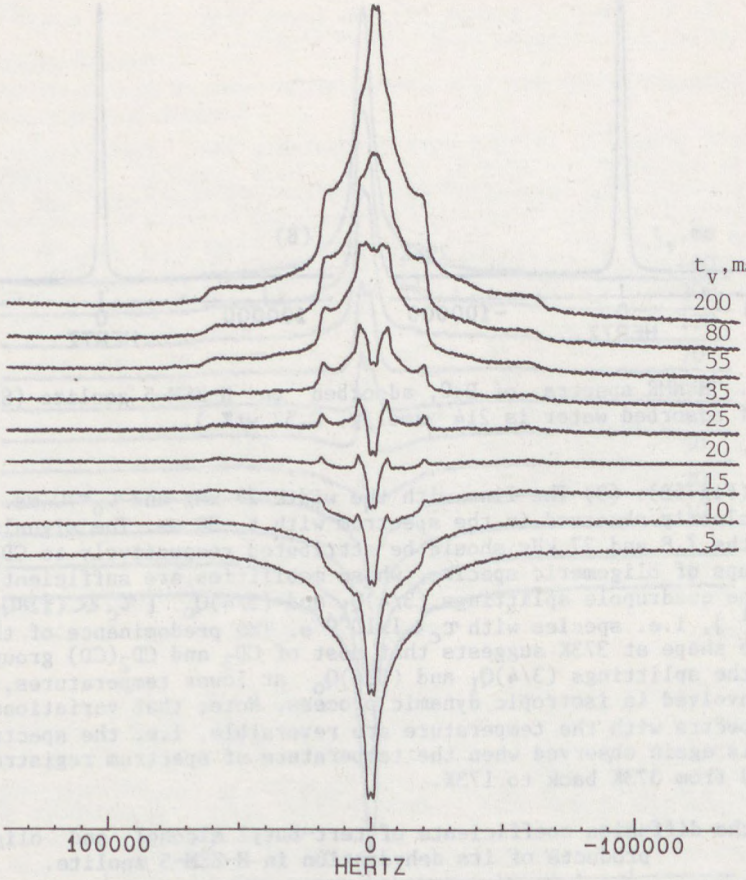

Figure 4. ^2H NMR inversion-recovery spectra recorded at 243K for the products of t-BuOH[2-$^2H_9$] dehydration on H-ZSM-5 (Si/Al=29) at 373K. Delay time t_v is given above each spectrum.

When increasing the temperature of the spectra registration from 173K to 373K, the line intensity at ν_o grows while the relative intensities of the solid-like signals with the splittings $(3/4)Q_1$ and $(3/4)Q_o$ decreases (Fig.3). This redistribution of the line intensities can be explained in terms of existence of the two oligomeric species that differ in their molecular mobilities. In the inversion-recovery spectra (Fig.6), recorded at 373K for the same sample as in fig.4, the following three liquid-like lines, besides two solid-like lines, are clearly distinguished. (1) The line at ν_o with the width 7.8 kHz and $\tau_o \simeq 30$ ms. This line is most clearly observed in the spectrum for t_v=120ms. (2) The narrow line at ν_o with the width of 2.5 kHz and $\tau_o \simeq$120ms., which represents the signal of D_2O (DHO). The shape and the width of this line coincide with those for the line of D_2O on H-ZSM-5

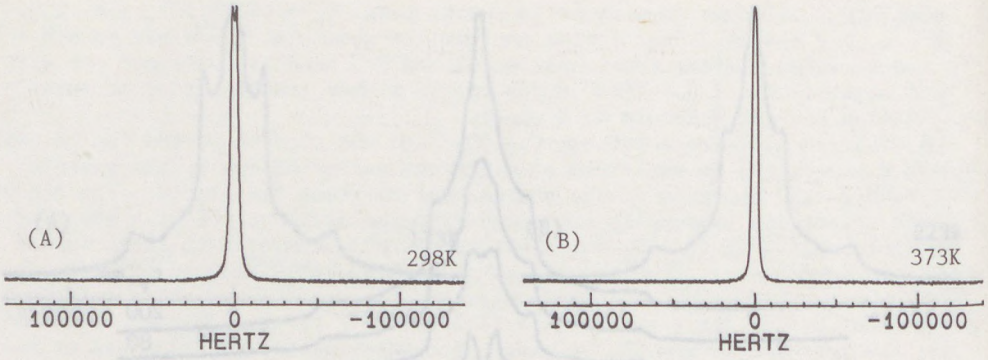

Figure 5. ^2H NMR spectra of D_2O, adsorbed on H-ZSM-5 zeolite (Si/Al =29, amount of adsorbed water is 214 μmol/g, 0.52 wt%).

at 373K (Fig.5B). (3) The line with the width 27 kHz and τ_o=70 ms. This line is most clearly observed in the spectrum with t_v=30 ms. The signals with the line widths 7.8 and 27 kHz should be attributed respectively to CD_3 and CD_2 (CD) groups of oligomeric species, whose mobilities are sufficient to average out the quadrupole splittings $(3/4)Q_1$ and $(3/4)Q_o$ [$\tau_c \ll (\frac{3}{4}2\pi Q_1)^{-1}$, $(\frac{3}{4}2\pi Q_o)^{-1}$], i.e. species with $\tau_c < 1x10^{-6}$ s. The predominance of the liquid-like line shape at 373K suggests that most of CD_3 and CD_2(CD) groups, giving rise to the splittings $(3/4)Q_1$ and $(3/4)Q_o$ at lower temperatures, at 373K become involved in isotropic dynamic process. Note, that variations in the ^2H NMR spectra with the temperature are reversible, i.e. the spectrum of Fig. 3A is again observed when the temperature of spectrum registration is decreased from 373K back to 173K.

4.3. On the diffusion coefficients of tert-Butyl alcohol and oligomeric products of its dehydration in H-ZSM-5 zeolite.

Coefficients of intracrystalline diffusion of the molecules in zeolite at low loadings can be estimated using the Einstein equation [4,5]:

$$D = \frac{\langle l^2 \rangle}{6\tau_h} \qquad (5)$$

where $\langle l^2 \rangle$ is the mean square displacement of the molecule inside the crystalline between successive jumps, τ_h is the mean time of the molecule life on adsorption center. Identifying correlation time τ_c with the life time τ_h of the molecule on the adsorption center (i.e. assuming that $\tau_c = \tau_h$), and $(\langle l^2 \rangle)^{\frac{1}{2}}$ - with the distance between adsorption centers, the diffusion coefficients for benzene, propene, ethene have been calculated in NaX zeolite from the analysis of the width of the Lorentzian type ^2H NMR singlet observed for $\tau_c < (\frac{3}{4}2\pi Q_o)^{-1}$ [4,5]. As it turned out, there was a good agreement between the diffusion coefficients, found from the ^2H NMR line width, and those obtained on the basis of NMR pulse field gradient studies [14-16].

Let us assume that isotropic reorientation of adsorbed molecules (alcohol and oligomeric species), take place when the molecule moves from one channel intersection to another one, where the centers for their adsorption, i.e. Al-OH-Si groups, are also assumed to be localized [17,18]. Furthermore,

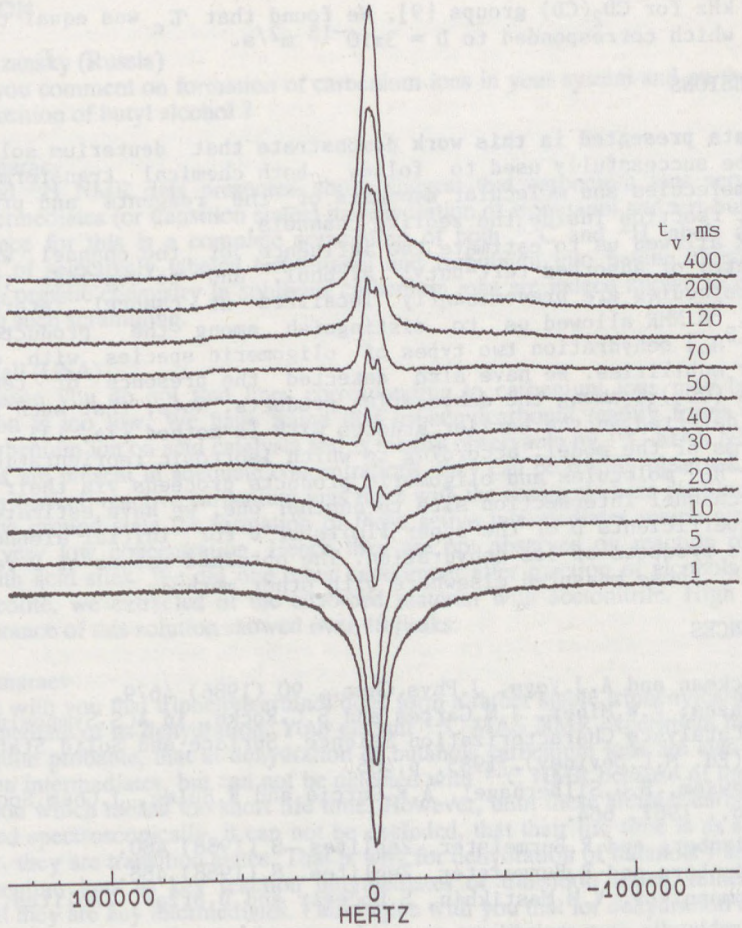

Figure 6. ^2H NMR inversion-recovery spectra recorded at 373K for dehydration products of t-BuOH[2-$^2H_9$] on H-ZSM-5 (Si/Al=29. Delay time t_v is given above each spectrum.

from the known dimension of the unit cell of the ZSM-5 zeolite [12], one can find that the value $(\langle l^2 \rangle)^{\frac{1}{2}}$ is equal to 1.1 nm (the mean length of the channels). Hence, starting from the estimation of $\tau_c > 1 \times 10^{-5}$ s on the basis of quadrupole splitting, the diffusion coefficient for t-BuOH can be estimated, as $D < 2 \times 10^{-14}$ m^2/s. The upper limit obtained for D agrees with the values of the diffusion coefficient measured in Ref.7a (0.5×10^{-14} m^2/s). For oligomers with solid-like line shape and quadrupole splittings $(3/4)Q_1$ and $(3/4)Q_o$, at temperature range 173-373K the lower limit for the correlation time is $\tau_c > 4 \times 10^{-6}$ s and upper limit for the diffusion coefficient is $D < 5 \times 10^{-14}$ m^2/s. For oligomers with liquid-like line shape [$\tau_c < (\frac{3}{4} 2\pi Q_o)^{-1}$, $(\frac{3}{4} 2\pi Q_1)^{-1}$], the correlation time τ_c can be found from the line

width 27 kHz for $CD_2(CD)$ groups [9]. We found that τ_c was equal to 7×10^{-7} s at 373K, which corresponded to $D = 3 \times 10^{-13}$ m^2/s.

5. CONCLUSIONS

The data presented in this work demonstrate that deuterium solid state NMR can be successfully used to follow both chemical transformations of organic molecules and molecular dynamics of the reagents and products of catalytic reaction inside the zeolite channels.

^2H NMR allowed us to estimate the influence of the channel walls on the geometry of adsorbed tert-butyl alcohol, and to conclude that the alcohol molecules are predominantly localized at channel intersections. Moreover, ^2H NMR allowed us to distinguish among the products of t-BuOH[2-$^2H_9$] dehydration two types of oligomeric species with different molecular mobilities. We have also detected the presence of tert-butyl fragments $(CD_3)_3C$ among the dehydration products. Note, that such fragments were not detected in the earlier studies with IR method [7a, 13].

In terms of the model, according to which isotropic reorientation of the t-BuOH[2-$^2H_9$] molecules and oligomeric products proceeds via their movement from one channel intersection site to another one, we have estimated the diffusion coefficients D or the upper limits of D for initial alcohol and oligomeric products of its dehydration. The obtained values of D reasonably agree with those measured elsewhere with other methods.

6. REFERENCES

1 R.R.Eckman and A.J.Vega, J.Phys.Chem., 90 (1986) 4679.
2 D.L.Hasha, V.W.Miner, J.M.Garces and S.C.Rocke, in ACS Symposium.Ser. 288, Catalysts Characterization Science, Surface and Solid State Chemistry, (Ed. M.L.Deviney), 1985, p.485.
3 J.M.Newsam, B.G.Silbernagel, A.R.Garcia and R.Hulme, J.Chem.Soc.,Chem. Commun., 1987, 664.
4 B.Boddenberg and R.Burmeister, Zeolites, 8 (1988) 480.
5 B.Boddenberg and R.Burmeister, Zeolites, 8 (1988) 488.
6 V.N.Romannikov, V.M.Mastikhin, S.Hočevar and B.Držaj, Zeolites, 3 (1983) 311.
7 (a) C.Williams, M.A.Makarova, L.V.Malysheva, E.A.Paukshtis, E.P.Talsi, J.M.Thomas and K.I.Zamaraev, J.Catal., 127 (1991) 377; (b) M.A.Makarova, personal communication.
8 G.W.Stocktone, C.F.Polnaszek, A.P.Tulloch, F.Hasan and I.C.P.Smith, Biochemistry, 15 (1976) 954.
9 A.Abragam, The Principles of Nuclear Magnetism, Oxford University, Oxford, 1961.
10 M.Rinne and J.Depireux, Adv.Nucl.Quadrupole Reson., 1 (1974) 357.
11 L.J.Schwartz, E.Meirovitch, J.A.Ripmeester and J.H.Freed, J.Phys.Chem., 87 (1983) 4453.
12 G.T.Kokotailo, S.L.Lawton, D.H.Olson and W.M.Meier, Nature (London), 272 (1978) 437.
13 M.T.Aronson, R.J.Gorte and W.E.Farneth, J.Catal., 105 (1987) 455.
14 J.Kärger and J.Caro, J.Chem.Soc.,Faraday I, 73 (1977) 1363.
15 J.Kärger and D.M.Ruthven, J.Chem.Soc.,Faraday I, 77 (1981) 1485.
16 A.Germanus, J.Karger and H.Pfeifer, Zeolites, 4 (1984) 188.
17 N.Y.Topsoe, K.Pedersen and E.G.Derouane, J.Catal., 70 (1981) 41.
18 A.Jacobs and R.Von Ballmoos, J.Phys.Chem., 86 (1982) 3050.

DISCUSSION

Q: V. B. Kazansky (Russia)

Could you comment on formation of carbenium ions in your system and on their role in the decomposition of butyl alcohol ?

A: K. I. Zamaraev

^{13}C and ^{2}H NMR data presented above suggest that carbenium ions serve as key reaction intermediates (or transition states) in dehydration of isobutanol and tert-butanol. The main evidence for this is a complete scrambling of both ^{13}C and ^{2}H labels during the dehydration of selectively labeled tert-butanol and isobutanol into butene olygomers and water. From organic chemistry in solutions carbenium ions are indeed known to be capable of providing such scrambling.

Q: W. K. Hall (USA)

The reason you do not find lines corresponding to carbenium ions may be that the concentration is too low. We have found that triphenylcarbonol readily forms the stable triphenylcarbenium ion on acid catalysts and is readily observable by ^{13}C-MAS NMR. Thus, if these ions are present in adequate concentrations, they can be readily observed. I believe Kazansky is correct: reactive carbenium ions react with the conjugate base forming alcohols, these are the ground state for formation of these active intermediates which are therefore present in very low concentration. Hence they are not observed on reaction of ordinary alcohols with acid sites. We did one other experiment after reaction of alcohols or olefins with the zeolite, we extracted of the adsorbed material with acetonitrile. High resolution proton assurance of this solution showed over 40 peaks.

A: K. I. Zamaraev

I agree with you that triphenylcarbinol does form a rather stable triphenylcarbonium ion as an intermediate of its dehydration. Your elegant ^{13}C MAS NMR experiment have proved this. It is quite probable, that in dehydration of butanols carbenium ions are also formed as true reaction intermediates, but can not be detected with ^{13}C NMR because of their too low concentration which means too short life time. However, until these simpler carbenium ions are observed spectroscopically, it can not be excluded, that their life time is as short as ca. 10^{-13} s, i.e. they are transition states. That is why for dehydration of butanols I am speaking about carbenium ions as key reaction intermediates or transition states, rather than say simply, that they are key intermediates. I also agree with you that for dehydration of butanols carbenium ions plus a conjugated base can be in an equilibrium with alkoxides (i.e. butyl silyl ethers), the alkoxide being the state that is more favorable energetically. In fact, Schemes 2 an 3 in our paper include such equilibria for both isobutanol and tert-butanol.

For isobutanol the alkoxide (i.e. isobutyl silyl ether) is seen from our ^{13}C NMR data to be an intermediate that is formed in the main reaction stream. In contrast to this, for tert-butanol the alkoxide (i.e. tert-butyl silyl ether, TBSE) is suggested by our data to be a "side" reaction intermediate, that is formed not in the main reaction stream. Most of the reaction products (i.e. butene oligomers) are formed at 296 K from tert-butanol via carbenium ion states bypassing TBSE, which is insufficiently reactive.

Q: W. M. H. Sachtler (USA)

As oligomerization (via carbenium ions) is supposed to be the first step in coke formation I would like to know how this oligomerization in HZSM-5 differs from that in other acid zeolites which form much more coke than HZSM-5 under identical conditions. In other words: what is the cause of the exceptionally low propensity of HZSM-5 to form coke during hydrocarbon conversion catalysis ?

A: K. I. Zamaraev

At elevated temperature oligomeric species formed upon dehydration of butanols can be desorbed from HZSM-5 zeolite and analyzed with GC-MS. This analysis suggests, that our oligomers are predominantly C_8 species, i.e. dimers of butenes. Perhaps further oligomerization of butenes to form trimers, etc., does not proceed rapidly enough due to steric hindrances created inside the channels of HZSM-5 for the reaction between a rather bulky C_8-dimer molecule and a butene molecule at the Si-OH-Al active site. The slow rate of further oligomerization of hydrocarbon fragments bigger than C_8 can be a reason of the low propensity of HZSM-5 to form coke during hydrocarbon conversion catalysis.

Q: K. P. de Jong (The Netherlands)

You have shown us very nice results of ^{2}H-NMR of oligomeric species inside the channels of HZSM-5. A number of question arises:

1) You did not observe olefinic carbon. Why not ?

2) The data suggested a highly branched structure. Does the framework of the zeolite allow for that ?

3) Did you observe effects of the reaction temperature on the extent of branching of the oligomers ?

A: K. I. Zamaraev

1) Indeed, we have not observed ^{13}C NMR signals from olefinic carbon atoms in butene oligomers. There can be at least two explanations for this:

(i) The lines from olefinic carbon atoms can be broader than those from aliphatic carbon atoms. For instance, the so called "inhomogeneous" broadening can take place due to the scatter of the ^{13}C chemical shifts for olefinic carbon atoms in oligomers with various extent of branching or oligomers adsorbed on various sites inside the zeolite channels.

(ii) Oligomers can be cyclic species. Then there will be no olefinic carbon atoms present. Work is now in progress in our laboratory to clarify this issue.

2) As shown in this study, even rather bulky tert-butyl fragments are accommodated easily inside HZSM-5 zeolite, most probably at channel interceptions. Presumably, branched C_8 oligomers are also located at channel interceptions. But still bigger oligomers are not formed, presumably, due to limitations induced by the framework of the zeolite.

3) At the first glance the data of Figs. 7 and 9-12 suggest, that such effects are observed. However, further studies with ^{13}C ^{2}H/MAS NMR are needed to clarify the effects of temperature on the extent of branching.

Q: R. Burmeister (Germany)

What are the differences in diffusivities determined by chemical or spectroscopic method ?

There are groups working with ^{2}H-NMR on zeolites in Dortmund, Cambridge and Paris. If you wish, I can arrange a contact.

A: K. I. Zamaraev

1) As far as I can understand, you are asking why in our system diffusion rates measured by chemical method and NMR method are the same, while in some other systems they are different. Roughly speaking, the situation is as follows: With NMR method one actually measures the so called "correlation time" τ_c for a molecule or its fragment, rather than directly the rate of translational diffusion. If for a given molecule translational diffusion is the fastest among various processes, that can influence τ_c, then τ_c can be identified with the life time τ_h of the molecule on adsorption site, and can be used to estimate the coefficient D of translational diffusion. If τ_c is determined by some other process, such, e.g., as fast rotation of a molecule in the vicinity of one and the same adsorption site, then τ_c should not be identified with τ_h. Formal use of τ_c as τ_h in the latter case will give an erroneous value for D.

2) I shall be grateful to you, if you arrange such contacts.

Q: J. J. Fripiat (USA)
What was the initial state of your zeolite and in particular what was the ratio of t-butanol/SiOH ?

A: K. I. Zamaraev
The procedure with which our zeolite samples have been prepared is described in the Experimental Section of our paper. The ratio of the number of adsorbed butanol molecules was always smaller or equal to the number of the Si-OH-Al groups in the zeolite.

Q: J. B. Nagy (Belgium)
The ^{13}C-MAS NMR of t-butoxy-groups linked to the surface is rather broad. Does not it suggest that the t-butyl groups are linked to acid sites where the Al atoms are randomly distributed on the 24 (or 12) crystallographycally different sites. The broadness of the line could be due to distribution of chemical shifts.

A: K. I. Zamaraev
I agree that a very probable reason for the substantial broadening of the ^{13}C MAS NMR signal from the carbon atom, that is directly bound to the wall of the zeolite channel, may be the scatter of the chemical shifts due to the scatter of the local environment for the tert-butyl silyl groups attached to various crystallographical sites. However, at this point other reasons for broadening, such, e.g., as a much lower mobility of this carbon atom compared to those atoms, that are not directly bound to the lattice, can not be unambiguously rejected.

Guczi, L. *et al.* (Editors), *New Frontiers in Catalysis*
Proceedings of the 10th International Congress on Catalysis, 19-24 July, 1992, Budapest, Hungary
© 1993 Elsevier Science Publishers B.V. All rights reserved

STATIONARY LIQUID-PHASE HOMOGENEOUS TRANSITION METAL CATALYSIS

I. T. Horváth

Corporate Research Laboratories, Exxon Research and Engineering Company, Annandale, New Jersey 08801, USA

Abstract

Immobilization of homogeneous liquid-phase catalysts on solid carriers could result in novel catalysts, which combine the advantages of homogeneous and heterogeneous catalysis, e.g. high activity, high selectivity, and easy product separation. In order to maintain the catalytic performance of a supported liquid-phase (SLP) homogeneous catalyst, the liquid-phase must remain on the support throughout the reaction. When leaching of the liquid-phase does not occur the SLP catalysts should be called stationary liquid-phase homogeneous catalyst.

We have developed a stationary strong acid phase platinum catalyst which can be used for the hydrogenation of aromatics at 25-75°C and 100-800 psi of H_2. The catalyst is prepared by supporting a solution of $PtCl_2(MeCN)_2$ in $BF_3.H_2O$ on silica or clay, and has been tested in batch and continuous reactors.

1. INTRODUCTION

Although liquid phase homogeneous catalysts generally have higher catalytic activity and selectivity than heterogeneous systems, product separation could be a major obstacle for industrial application [1-2]. The immobilization of the liquid-phase on solid carriers is a possible solution of the separation problem [3-16]. The supported liquid-phase (SLP) can be the catalyst itself, or it may contain a dissolved catalyst. One of the first SLP catalysts was developed in the early 30's for the polymerization of olefins to high quality gasoline [4-6]. The catalyst is prepared in the reactor by soaking fine crushed quartz with 70-85% phosphoric acid, draining the excess acid out, and then charging the hot olefin to the unit.

There are several supported heterogeneous catalysts which become SLP catalysts as the supported solid catalysts melt at reaction temperature [3,7]. The two most important reactions involving molten SLP catalysts are the oxidation of hydrogen chloride to chlorine and water at 450-500°C (Deacon reaction),

and the oxidation of sulfur dioxide to sulfur trioxide above 420°C [3,7]. The Deacon catalyst consists of $CuCl_2$, MCl (M=Na, K), MCl_3 (M=La, Pr), and is supported on pumice or high surface area silica gel. The alkali promoted vanadium catalyst for the oxidation of SO_2 is prepared by immobilizing V_2O_5 and K_2SO_4 on diatomaceous earth.

Several SLP catalysts have been developed by using a high boiling point solvent containing a dissolved transition metal catalyst [8-16], and have been tested for the catalytic isomerization [8], hydrogenation [9-11], and hydroformylation [9-11,15,16] of olefins. SLP catalysts can also use a supported liquid-phase with limited solubility in the reactants, products and solvents. Water or aqueous acids are excellent choice for organic reactions performed in apolar media and several such aqueous systems have been investigated [12-16].

It should be noted, that in order to maintain the catalytic performance of a supported liquid-phase homogeneous catalyst, the liquid-phase must remain on the support throughout the reaction. When leaching of the liquid-phase does not occur the catalysts should be called stationary liquid-phase homogeneous catalyst (Figure 1.).

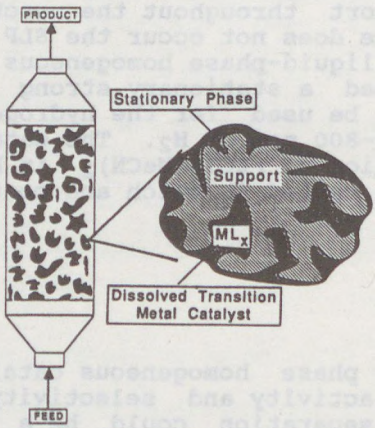

Figure 1. SLP homogeneous transition metal catalyst.

Reduction of aromatic hydrocarbons has recently received much attention as environmental concerns with aromatics have been dramatically increased. Although heterogeneous transition metal catalysts could be used for the hydrogenation of aromatics, they generally require severe reaction conditions under which cracking and other undesirable side reactions could occur. In contrast, there are several homogeneous transition metal catalysts capable of hydrogenating aromatics at mild conditions [17-25]. Their application however, is limited by the difficult separation of the products from the catalysts.

We wish to report the development of a stationary $BF_3.H_2O$ phase platinum catalyst for the catalytic hydrogenation of aromatic hydrocarbons at mild conditions.

2. RESULTS AND DISCUSSION

A typical catalyst is prepared by impregnating a solution of $PtCl_2(CH_3CN)_2$ in $BF_3.H_2O$, an ionic hydrogenation catalyst [24], into silica or clay by the incipient wetness technique under N_2, and is used without further treatment. The fresh solution of $PtCl_2(CH_3CN)_2$ in $BF_3.D_2O$ is light yellow and ^{195}Pt NMR shows two signals at -2048 and -2070 ppm, both in the typical chemical shift region for Pt^{2+} species. The hydrogenation reactions were performed at constant pressures in a 300 mL Hastelloy (H) autoclave equipped with a 7 micron filter attached to the dip-leg for sample removal. In a typical procedure the reactor was charged with the catalyst and the solvent under N_2 at 25°C. The aromatics were charged at reaction pressure and temperature, and the progress of the reactions were followed by GC analysis of the samples taken periodically.

Hydrogenation of aromatic compounds occurs rapidly even at 25°C under 400 psi H_2, and the colorless products can be separated from the catalyst by filtration. The reduction of benzene leads to the quantitative formation of cyclohexane and no GC or NMR evidence was found for the presence of partially reduced, hydrogenolyzed or cracked products (Figure 2). Upon increasing the concentration of $PtCl_2(CH_3CN)_2$, the benzene

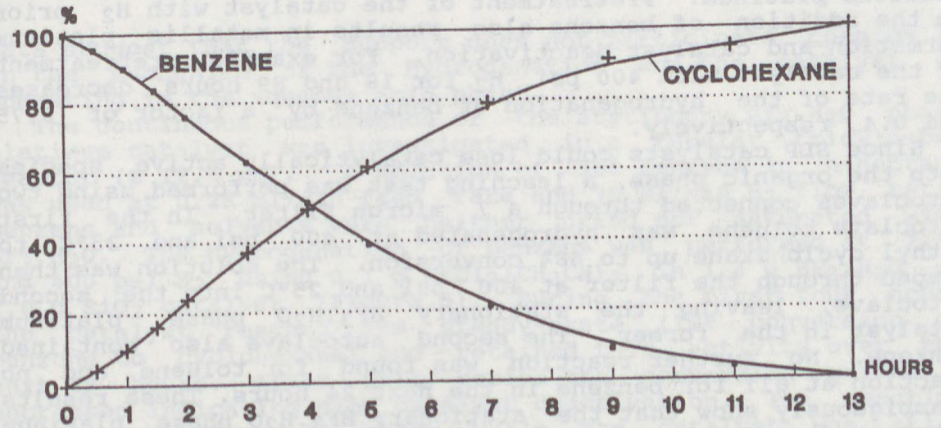

Figure 2. Hydrogenation of benzene (385 mmol) in 70 g heptane and 10 g decane at 25°C under 400 psi H_2 using 0.22 mmol $PtCl_2(CH_3CN)_2$ in 1.4 g $BF_3.H_2O$ on 2.0 g silica (CPG-240: pore volume 0.95 ml/g, pore diameter 237 A, surface area 77.5 m^2/g).

hydrogenation rate increases proportionally. Reduction of naphthalene results in the transient formation of tetralin, as expected, which is then hydrogenated to cis- and trans-decalin in a ratio of 9 to 1 (Figure 3).

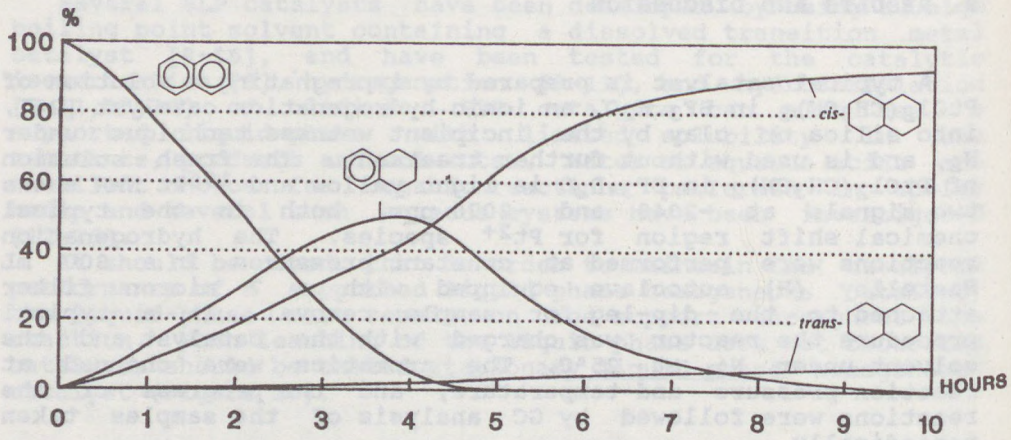

Figure 3. Hydrogenation of naphthalene (78 mmol) in 80 g heptane at 25°C under 400 psi H_2 using 0.20 mmol $PtCl_2(CH_3CN)_2$ in 1.4 g $BF_3.H_2O$ on 2.0 g silica (CPG-240: pore volume 0.95 ml/g, pore diameter 237 A, surface area 77.5 m^2/g).

During the course of the catalytic reactions the catalyst turns black, indicating slow reduction of some Pt^{2+} species to metallic platinum. Pretreatment of the catalyst with H_2 prior to the addition of benzene also results in metallic platinum formation and catalyst deactivation. For example, pretreatment of the catalyst with 400 psi H_2 for 18 and 89 hours decreases the rate of the hydrogenation of benzene by a factor of 0.75 and 0.4, respectively.

Since SLP catalysts could lose catalytically active species into the organic phase, a leaching test was performed using two autoclaves connected through a 7 micron filter. In the first autoclave toluene was hydrogenated at 400 psi and 25°C to methyl cyclohexane up to 68% conversion. The solution was then pumped through the filter at 400 psi and 25°C into the second autoclave, leaving the stationary $BF_3.H_2O$ phase platinum catalyst in the former. The second autoclave also contained benzene. No further reaction was found for toluene and no reaction at all for benzene in the next 24 hours. These results unambiguously show that the stationary $BF_3.H_2O$ phase platinum catalyst doesn't leach catalytically active platinum species under hydrogenation conditions.

In order to monitor the possible role of the chemical composition of the support, the hydrogenation of the mixture of benzene, toluene, o-xylene and 1,2,4-trimethylbenzene was

investigated using different supports. The same catalytic system supported on CPG-240 or on clay, shows almost identical relative aromatics hydrogenation activities (Figure 4). These

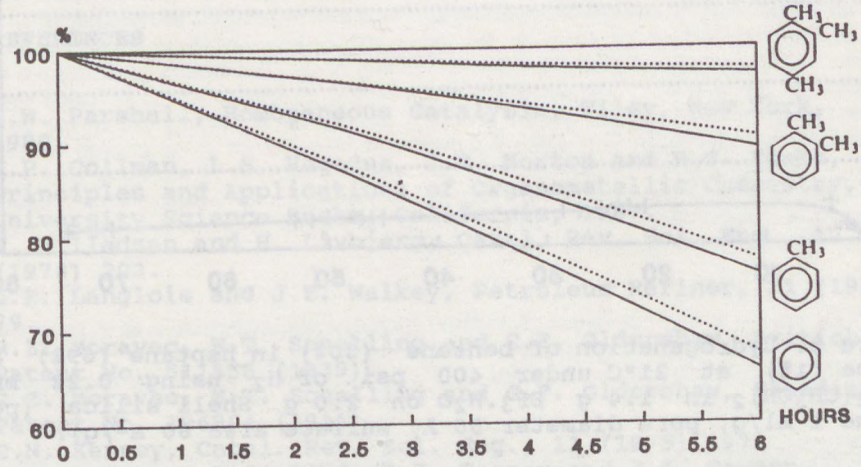

Figure 4. Hydrogenation of 0.1 mol benzene, 0.1 mol toluene, 0.1 mol o-xylene, 0.1 mol 1,2,4-trimethylbenzene in 60g decane at 20°C under 400 psi H_2 using 0.29 mmol $PtCl_2(CH_3CN)_2$ in 1.4 g $BF_3.H_2O$ on 2.0 g support: (——— silica/CPG-240: pore volume 0.95 ml/g, surface area 77.5 m^2/g), (····· clay: pore volume 0.50 ml/g, surface area 110 m^2/g).

data suggest that the support does not participate chemically in the mechanism of the hydrogenation and the catalyst is operating in the aqueous acid phase.

The continuous performance of the stationary $BF_3.H_2O$ phase platinum catalyst was investigated in a tubular trickle-bed reactor (Ø 12.5 mm). A solution of 30% benzene in n-heptane was used at 0.25 ml/min feed rate and 75 ml/min H_2 flow rate. Benzene and solvents were neither dried nor saturated with $BF_3.H_2O$. The hydrogenation of benzene was performed at 21°C and 400 psi H_2 using 0.1 g $PtCl_2(CH_3CN)_2$ in 1.4 g $BF_3.H_2O$ on 2.0 g SiO_2 catalyst (Figure 5). During the first four hours the catalyst reached its steady-state (10% conversion of benzene to cyclohexane) and retained this activity over the next 48 hours. After this period the conversion gradually decreased indicating slow catalyst deactivation. The reaction was stopped after 75 hours, while the catalyst was still active, for catalyst characterization. The used catalyst showed again the presence of some metallic platinum. Elemental and water analyses revealed that the amount of water on the catalyst had increased slightly and that some BF_3 had leached from the $BF_3.H_2O$ phase. Addition of 0.5% $BF_3.OEt_3$ to the feed

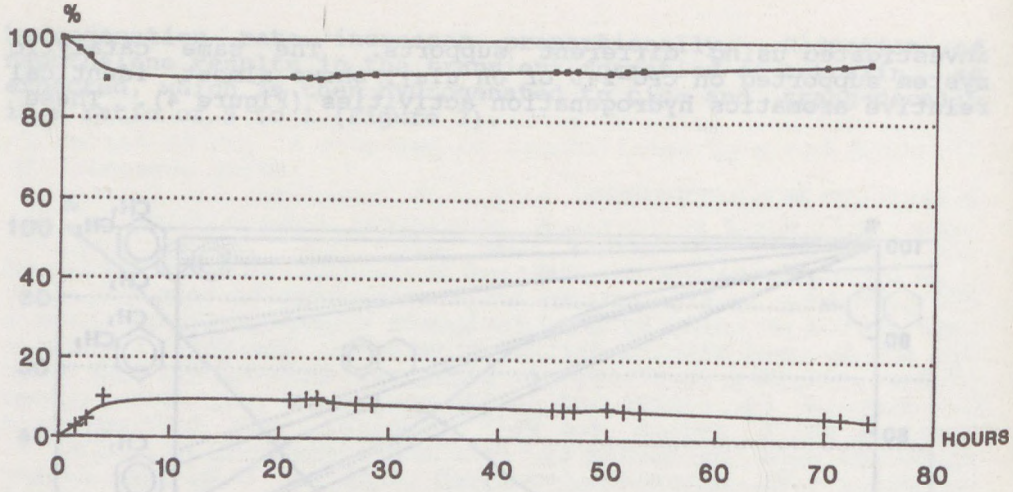

Figure 5. Hydrogenation of benzene (30%) in heptane (69%) and decane (1%) at 21°C under 400 psi of H_2 using 0.22 mmol $PtCl_2(CH_3CN)_2$ in 1.4 g $BF_3.H_2O$ on 2.0 g Shell silica (pore volume 1 ml/g, pore diameter 50 A, surface area 80 m^2/g).

did not stabilize the catalyst, suggesting a complicated deactivation mechanism. These results implied that the BF_3/H_2O ratio decreased during the reaction leading to a weaker and less active acid system. Indeed, when $BF_3 \cdot 1.3H_2O$ was used as a liquid phase for the hydrogenation of benzene, the catalytic activity dropped by 30%.

The observed effect of the lower acidity suggests that the reaction is probably initiated by the protonation of the aromatic ring either by $H^+[BF_3OH]$ or by a cationic platinum species formed by the reaction of $PtCl_2(CH_3CN)_2$ and $BF_3.H_2O$ under hydrogen. In the first case the formed arenonium ion is than hydrogenated by a platinum species able to activate and transfer three moles of molecular hydrogen. In contrast, in the second mechanism the initially formed platinum complex could activate and transfer the H_2 to the already coordinated aromatic ring. To gain further insight how the catalytic system operates, we are currently investigating the hydrogenation of d_6-benzene at 25°C and 400 psi of H_2 pressure. Preliminary GC-MS and NMR analysis of samples taken periodically showed less than 0.5% D/H exchange for d_6-benzene and the formation of 99.5% pure d_6-cyclohexane. ^{13}C-NMR of the CS_2 solution of d_6-cyclohexane revealed the presence of two species in a ratio of 92 to 8. The elucidation of the stereochemistry of $C_6H_6D_6$ is in progress. While the formation of platinum colloids cannot be ruled out at this time, the results are consistent with a homogeneous platinum complex system operating in the liquid phase.

3. ACKNOWLEDGEMENT

The very careful technical work by Raymond A. Cook is gratefully acknowledged.

4. REFERENCES

1 G.W. Parshall, Homogeneous Catalysis, Wiley, New York, 1980.
2 J.P. Collman, L.S. Hegedus, J.R. Norton and R.G. Finke, Principles and Applications of Organometallic Chemistry, University Science Books, California, 1987.
3 J. Villadsen and H. Livbjerg, Catal. Rev. Sci. Eng., 17 (1978) 203.
4 G.E. Langlois and J.E. Walkey, Petroleum Refiner, 31 (1952) 79.
5 R.Z. Moravec, W.T. Schelling and C.F. Oldershaw, British Patent No. 511556 (1939).
6 R.Z. Moravec, W.T. Schelling and C.F. Oldershaw, Canadian Patent No. 396994 (1941).
7 C.N. Kenney, Catal. Rev. Sci. Eng., 11 (1975) 197.
8 G.J.K. Acres, D.C. Bond, B.J. Cooper and J.A. Dawson, J. Catal., 6 (1966) 139.
9 P.R. Rony, Chem. Eng. Sci., 23 (1968) 1021.
10 P.R. Rony, J. Catal., 14 (1969) 142.
11 P.R. Rony and J.M. Roth, J. Mol. Cat., 1 (1975/76) 13.
12 R.E. Robinson, US Patent No. 3 190 912 (1965).
13 K. Fujimoto, Y. Negami, T. Takahashi and T. Kunugi, Ind. Eng. Chem. Prod. Res. Dev., 11 (1972) 303 and 13 (1972) 237.
14 I.S. Shaw, J.S. Dranoff and J.B. Butt, Ind. Eng. Chem. Res., 27 (1988) 935.
15 J.P. Arhancet, M. E. Davis, J. S. Merola and B. E. Hanson, Nature 339 (1989) 454 and J. Catal., 121 (1990) 327.
16 I.T. Horváth, Cat. Lett., 6 (1990) 43.
17 E.L. Muetterties and F.J. Hirsekorn, J. Am. Chem. Soc., 96 (1974) 4063.
18 M.J. Russell, C. White and P.M. Maitlis, J. Chem. Soc., Chem. Commun., (1977) 427.
19 P.M. Maitlis, Acc. Chem. Res., 11 (1978) 301.
20 E.L. Muetterties and J.R. Bleeke, Acc. Chem. Res. 12 (1979) 324.
21 M.A. Bennett, CHEMTECH (1980) 444.
22 R.H. Fish, Ann. N. Y. Acad. Sci. 415 (1983) 292.
23 J. Blum, I. Amer, K.P.C. Vollhardt, H. Schwartz and G. Hohne, J. Org. Chem. 52 (1987) 2804.
24 J.C. Cheng, J. Maioriello and J.W. Larsen, Energy Fuels 3 (1989) 321.
25 R.H. Fish, Aspects of Homogeneous Catalysis, 7 (1990) 65.

DISCUSSION

Q: S. Siegel

A question whether the evidence that the conversion of benzene to $C_6H_6D_6$ in which the deuterium atoms are all cis within the accuracy of your measurements necessarily means that the catalyst is homogeneous. The result only indicates that very little of the adsorbed tetradeuterocyclohexane leaves the reaction site before it is reduced to the $C_6H_6D_6$. Long ago, Hartog and Zwietering came to the same conclusion regarding the deuteration of benzene on platinum metal catalysts from an analysis of the distribution of deuterium in the products. At the first ICC I reported a stereochemical technique which revealed that the hydrogenation of the isomeric xylenes proceeds largely via the desorption of the possible intermediate cyclohexenes; later these intermediates were shown to be present in solution during the hydrogenation, the amount is small and is a function of the metal and reaction conditions. We believe that both the homogeneous and heterogeneous catalyzed hydrogenations referred to here and in your paper proceed via common mechanistic schemes in which the rates of the elementary steps differ.

Q: Wm. C. Conner

1) Do you have any microwave, (or other) spectroscopic information as to the positions of the D atoms on the $C_6H_6D_6$ formed from benzene ?

2) How would you propose to relate TOF's for this system relative to supported metal catalysts ?

Q: K. Zamaraev

The idea you have described in some ways has been put into practice long ago in a well-known commercial process of SO_2 oxidation to SO_3 over vanadia-based metal catalysts. In these catalysts the active component forms a liquid melt under reaction conditions This melt spreads on the surface of the support vs a very thin (about 10 nm) liquid layer, where the reaction actually proceeds.

Q: J. W. Geus

With gaseous reactants, gaseous reaction products and a liquid phase containing the dissolved homogeneous catalyst, the need for a system as described in your paper is less than with liquid reactants and reaction products. When a liquid is passed through a reactor in which a porous fixed bed is contained a non-miscible liquid, leaching of the liquid may be a problem as you pointed out.

However, a reaction system containing a solid catalyst, hydrogen and two non-miscible liquids has been recently proposed for the selective hydrogenation of benzene to cyclohexene. The cyclohexene is selectively removed from the catalyst by the liquid interacting more weakly with the catalyst. For such reaction systems, your design may be also attractive

A: I. T. Horvath

Answers in written form did not arrived.

Guczi, L. *et al.* (Editors), *New Frontiers in Catalysis*
Proceedings of the 10th International Congress on Catalysis, 19-24 July, 1992, Budapest, Hungary
© 1993 Elsevier Science Publishers B.V. All rights reserved

AN IN SITU RADIOACTIVE TRACER TECHNIQUE FOR STUDYING ADSORPTION-DESORPTION DYNAMICS ON A WORKING CATALYST

U. Schröder, L. Cider and N. - H. Schöön

Department of Chemical Reaction Engineering, Chalmers University of Technology, 412 96 Gothenburg, Sweden

Abstract

An *in situ* method for studying adsorption-desorption dynamics using radioactive tracers has been developed. In this technique, the catalyst is mounted as a very thin catalyst wafer in a cell, normally used for transmittance FTIR studies. Gas is allowed to flow through the cell over both sides of the thin wafer. One of the windows of the cell consists of a $CaF_2(Eu)$ scintillator which converts the electrons from the radioactive decay from a soft β^--emitter, for example ^{14}CO, to light. The light is then conducted via a cooled glass rod to a photomultiplier. This arrangement makes it possible to have a higher cell temperature than 50°C, which is the maximum temperature allowed for the photomultiplier at any given time. The photomultiplier allows a direct measurement of the amount of adsorbed species on the catalyst. This technique has been used to examine the isotopic exchange between CO(a) and CO(g) and the cross-desorption of CO(a) in the presence of $C_2H_2(g)$ or NO(g).

1. INTRODUCTION

Different spectroscopic methods have been developed for studying adsorption and desorption on a single crystal surface at high vacuum. These processes have also been studied at atmospheric pressure on thin disces of industrial catalysts by using different IR techniques. Radioactive tracer methods have been a valuable complement to these spectroscopic methods [1,2,3]. The radioactive methods have been used at both vacuum and atmospheric conditions and mainly for the study of processes on surfaces of thin metal films. The limited access to proper radioactive isotopes, as well as the limited access to a measuring technique applicable to elevated temperature and pressure have restricted the use of radioactive methods.

A radioactive technique, based on the use of a gas flow cell, with a solid scintillator window, will be demonstrated in the present work. The scintillator is connected to a photo-counter *via* an external cooled light conductor in order to decrease the risk of overheating the counter. The catalyst is a very thin porous disc formed by pressing disintegrated catalyst. This disc is placed beneath the window but separated by a passage for gas flow.

The equipment has hitherto primarily been used for studying the kinetics of rapid adsorption and desorption processes. By making a step from labelled to unlabelled compounds without changing the chemical composition on the catalyst surface, it is possible to study the true kinetics at stationary conditions. The cell is an open reactor with continuous gas flow, which minimizes the radioactivity from the gas phase in the cell and thus makes it possible to monitor directly the radioactivity emitting from the surface of the catalyst.

A quantitative evaluation of the rate constant of the surface processes must, however, consider:

- o the influence of the mixing characteristics of the gas flow in the cell;
- o the mass transfer between the gas and the external surface of the catalyst disc;
- o the internal transport in the porous catalyst disc;
- o the self-absorption of the emitted soft β^--particles in the catalyst disc.

In the present work the measuring technique was demonstrated for the rapid isotopic exchange of CO in the gas phase for adsorbed CO on a palladium catalyst. A similar rapid desorption of CO is also demonstrated to occur in the presence of C_2H_2 or NO in the gas phase.

2. EXPERIMENTAL

2.1. Reactor and detector

Cross sections of the reactor and the detector are shown in Figure 1. The reactor was, in principle, the same as the one used for *in situ* transmission FTIR studies [4]. It was built from two 2¾″ stainless steel vacuum flanges. The catalyst disc was placed in a sample holder situated in the small volume between two windows. The gas flow was distributed on both sides of the catalyst disc through slits in the sample holder. Channels were bored into one of the flanges for inlet and outlet gas as well as one for a thin thermocouple inserted into the catalyst disc. The reactor was sealed using Kalrez O-rings (Du Pont).

One of the CaF_2 windows (25 mm wide and 7 mm thick), used for transmission FTIR experiments, was replaced with a europium doped CaF_2 window. This acted as a scintillator, which converted the emitted β^--particles from the radioactive decay into light. The light was then transmitted to a photomultiplier (9900B Thorn Emi) *via* a cooled glass rod. This arrangement permitted high temperatures in the reactor without exceeding the maximum allowable temperature of the photomultiplier (50°C). Optical silicone was used to create optical connections between the scintillator, the glass rod, and the photomultiplier.

The photomultiplier and the glass rod were cooled by an air flow in the annulus between them and the housing. The housing was cooled by a water flow in a copper coil around the housing. The reactor could be heated using four heating elements placed in drilled holes. The thermocouple mounted in one of the flanges measured the temperature, controlled by an on/off regulator.

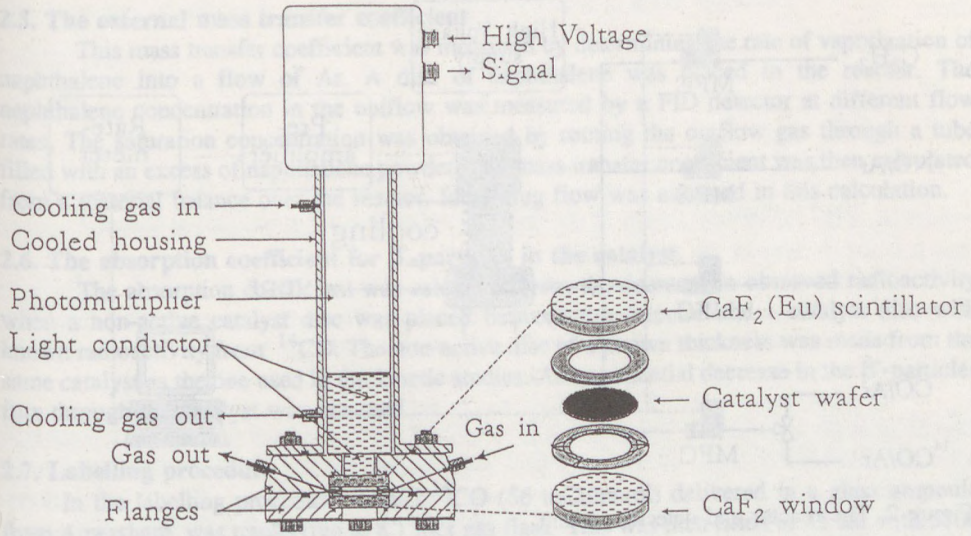

Figure 1. Reactor and detector for *in situ* measurement of adsorbed radioactive species.

2.2. Experimental set up

Figure 2 shows the experimental set up. The photomultiplier was supplied with 680 volts through a voltage divider. The signal from the photomultiplier was amplified 10 times and then analyzed by a rate-meter (Nukab Gamma Spectrometer 9700, window 0-3.4 mV, time constant 3 sec). An A/D converter in the computer read the signal from the rate-meter and the values were stored in a file.

2.3. Catalyst

A commercial (Aldrich) 5% Pd/Al_2O_3 catalyst was used in all the experiments. The properties of the catalyst are given in Table 1. A pressure of 7 tons was used to press the catalyst disc.

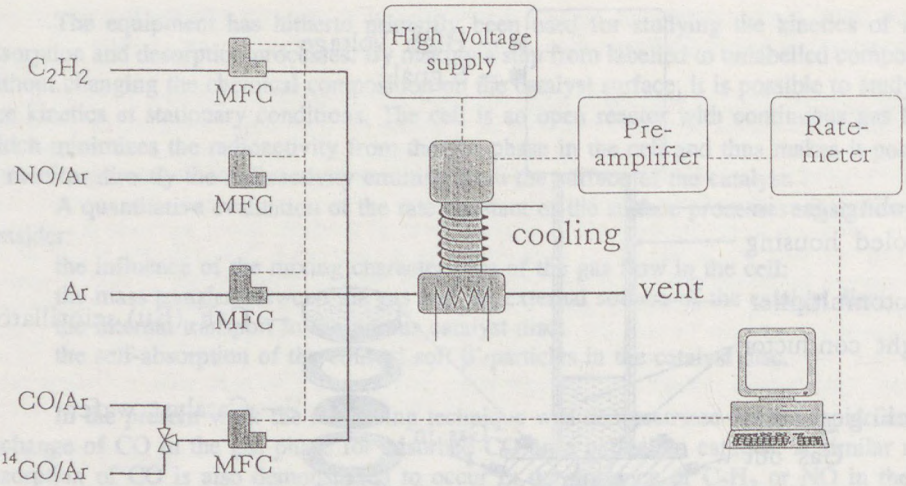

Figure 2. The reactor and detector system.

TABLE 1
Catalyst disc properties

Pd content	5 wt%	Disc thickness	0.23 mm
Pd dispersion*	0.13	Disc diameter	18 mm
BET area** s^{-1}	118 $m^2\ g^{-1}$	External mass transfer coefficient, k_C***	0.0063 $m\ s^{-1}$
Average pore radius**	75 Å	Effective diffusivity in the disc, D_{eff} (25°C)	1.2 10^{-6} m^2
Catalyst porosity, ε	0.59	Absorption coefficient for β^--particles in the catalyst, μ	**12389 m^{-1}**
Catalyst density, ρ	1506 kg m^{-3}		

* Determined by CO adsorption, CO/Pd
** Determined by N_2 absorption (Digisorb 2600)
*** External mass transfer coefficient at 25°C for naphthalene at the flow rate 2 ml/s

2.4. Determination of the effective diffusivity in the catalyst disc

The diffusion rate through the catalyst was obtained by the method of Wicke-Kallenbach [5]. The catalyst disc was mounted in a special cell of Plexiglass, where pure Ar was flowing on one side of the catalyst disc and 112 ppm CO in Ar on the other.

2.5. The external mass transfer coefficient

This mass transfer coefficient was measured by determining the rate of vaporization of naphthalene into a flow of Ar. A disc of naphthalene was placed in the reactor. The naphthalene concentration in the outflow was measured by a FID detector at different flow rates. The saturation concentration was obtained by routing the outflow gas through a tube filled with an excess of naphthalene powder. The mass transfer coefficient was then calculated from a material balance over the reactor. Ideal plug flow was assumed in this calculation.

2.6. The absorption coefficient for β^--particles in the catalyst

The absorption coefficient was calculated from the decrease in observed radioactivity when a non-active catalyst disc was placed between the detector and a catalyst disc with known radioactivity from ^{14}CO. The non-active disc of a known thickness was made from the same catalyst as the one used in the kinetic studies. An exponential decrease in the β^--particles flux through the catalyst was assumed.

2.7. Labelling procedure

In the labelling procedure, 1 mCi ^{14}CO (56 mCi/mmol) delivered in a glass ampoule from Amersham, was transferred to a 1 liter gas flask. This was then filled to 35 bar with 5700 ppm CO/Ar. The carbon monoxide concentration then became 5715 ppm, essentially the same as the unlabelled mixture.

3. THEORY

In the step-response radioactivity method given here, the adsorption and desorption rates are not directly observable. A mathematical model is therefore needed, which gives the relationship between the observed change in the total radioactivity and the rates of these two processes. The amount of the labelled compound inside the porous catalyst disc cannot be neglected despite the fact that the disc is very thin. This amount is several orders of magnitude greater than that adsorbed on the external surface. It will partly serve as a great and rather slow buffer for the externally adsorbed compound, partly contribute to the total radioactivity measured.

The change with time and position of the labelled compound concentration in the gas phase inside the catalyst pores can be calculated from the material balance

$$\varepsilon \frac{\partial C}{\partial t} = D_{eff} \frac{\partial^2 C}{\partial x^2} + (r_d - r_a) \qquad (1)$$

where D_{eff} is the effective diffusivity, ε is the void fraction, C the local concentration of labelled compound, x the length coordinate perpendicular to the external surface of the catalyst disc, and r_d and r_a are the desorption and adsorption rates, respectively.

The change in the local fractional coverage of the labelled compound θ, is calculated

from

$$\frac{\partial \theta}{\partial t} = \frac{1}{N_s \rho} (r_a - r_d) \qquad (2)$$

where N_s is the molar site density of the uniformly distributed active sites per mass of catalyst and ρ is the density of the catalyst disc.

It should be noted that r_a and r_d are functions of C and θ, which must be specified in the solution of the equations in the mathematical model. These functions are also dependent on the nature of reaction and are different for the isotopic exchange between CO(a) and CO(g) and for the cross-desorption of CO(a) in the presence of C_2H_2(g) or NO(g).

To solve eqs (1) and (2), boundary and initial conditions are required. The boundary condition at the external surface of the catalyst disc (x=0) is obtained from a material balance over the reactor. For a sufficiently high flow rate through the reactor, the bulk concentration of the labelled compound can be considered constant. As a consequence of the short residence time in the reactor compared to the time constant of the processes studied, the material balance over the reactor gas volume can, moreover, be formulated as an ideally mixed tank reactor giving

$$q(C_f - C_b) = V\frac{\partial C_b}{\partial t} - D_{eff} A \frac{\partial C(t,0)}{\partial x} \qquad (3)$$

where q is the volumetric flow rate, A the external catalyst disc area, C_f the inlet concentration and C_b the bulk concentration of the labelled compound. The accumulation in the gas phase, $V(\partial C_b/\partial t)$, can be neglected, since the accumulation on the catalyst surface is much greater.

The relationship between the bulk concentration and the concentration at the external surface of the catalyst disc is given by

$$N = k_c(C_b - C_s) \qquad (4)$$

where N is the molar flux, k_c the external mass transfer coefficient and $C_s = C(t,0)$ the concentration at the external surface. The molar flux can also be written

$$N = + D_{eff} \frac{\partial C(t,0)}{\partial x} \qquad (5)$$

Combining eqs (3)-(5) and neglecting the gas phase accumulation give the boundary condition at the external surface of the disc (x=0)

$$C(t,0) = C_f + \left(\frac{1}{k_c} + \frac{A}{q}\right) D_{eff} \frac{\partial C(t,0)}{\partial x} \qquad (6)$$

The boundary condition in the center of the catalyst is due to the symmetry

$$\frac{\partial C(t,\ L/2)}{\partial x} = 0 \tag{7}$$

where L is the thickness of the catalyst disc.

The initial conditions for a step from unlabelled to labelled compound are

$$C(0,\ x) = 0 \tag{8}$$
$$\theta(0,\ x) = 0$$

The eight equations of the mathematical model given above make it possible to calculate the local fractional coverage of the radioactive species as a function of time and position in the catalyst disc.

The next step is to express the observed radioactivity as a function of the total fractional coverage of the labelled compound. The local radioactivity in the catalyst disc is proportional to the local fractional coverage of this compound. However, in order to express the part of the observed radioactivity from this particular local fractional coverage of labelled compound, the decrease in radioactivity due to the absorption of β^--particles in the catalyst must be accounted for. The contribution of the emitted β^--particles from the disc element dx, at the position x, to the observed total radioactivity can be written

$$dI = k\ \theta(x,t)e^{-\mu x}dx \tag{9}$$

where μ is the linear absorption coefficient and k is a constant.

The local fractional coverage is symmetric about the center line x=L/2 of the catalyst disc, since the gas is flowing on both sides of the disc. This means that it is sufficient to integrate from the external surface to the middle of the disc. The total observed radioactivity will thus be

$$I(t) = \int_0^{L/2} k\theta(x,t)(e^{-\mu x} + e^{-\mu(L-x)})dx \tag{10}$$

When the catalyst disc is in isotopic equilibrium with the fresh labelled gas mixture the observed radioactivity is I_{max} and the fractional coverage of labelled CO is θ=1. This makes it possible to calculate k from eq. (10) giving

$$k = \frac{I_{max}}{\int_0^{L/2} (e^{-\mu x} + e^{-\mu(L-x)})dx} \tag{11}$$

and

$$k = \frac{\mu I_{max}}{1 - e^{-\mu L}} \tag{12}$$

The fractional coverage of the labelled compound has to be defined in an appropriate way when determining the constant k in eq. (10). At the partial pressure corresponding to 1000 ppm CO at atmospheric pressure in the present experiment, the palladium part of the catalyst is considered to be completely covered with CO. The fractional coverage of CO is here normalized to unity despite the fact that the fractional coverage according to geometrical constraints may correspond to a value less than unity. Since isotopic effects can be neglected, the fresh mixture with labelled CO is considered as an indivisible unity which during the isotopic exchange process is diluted with unlabelled CO of the same partial pressure. When this fresh labelled mixture is in isotopic equilibrium with the catalyst surface the fractional coverage of labelled CO is given the value $\theta=1$. Whereas, when this labelled mixture is diluted with unlabelled CO the fractional coverage will be $\theta < 1$ and will reach the value $\theta = 0$ when all of the labelled mixture is washed out from the system. Correspondingly the concentration of labelled CO is $C=C_{co,tot}$ in the fresh labelled gas mixture.

4. RESULTS AND DISCUSSION

4.1 Desorption of CO

Fig. 3 shows the rapid decrease of radioactivity from the catalyst disc when the inflow is switched over to unlabelled CO. A similar effect is also demonstrated when the inflow suddenly contains a step of C_2H_2 or NO at low concentration.

It is a well-known fact that CO desorbs very slowly in an inert gas atmosphere or in vacuum at room temperature, but the rate of a desorption is known to increase dramatically in the presence of CO in the gas phase [6-21]. This enhanced desorption is not preceded by any dissociation and recombination of CO on the surface which can proceed on certain catalysts, but occurs *via* the displacement of an adsorbed CO molecule as a whole.

As can be seen from Fig. 3 the isotopic exchange proceeded until the radioactivity completely disappeared.

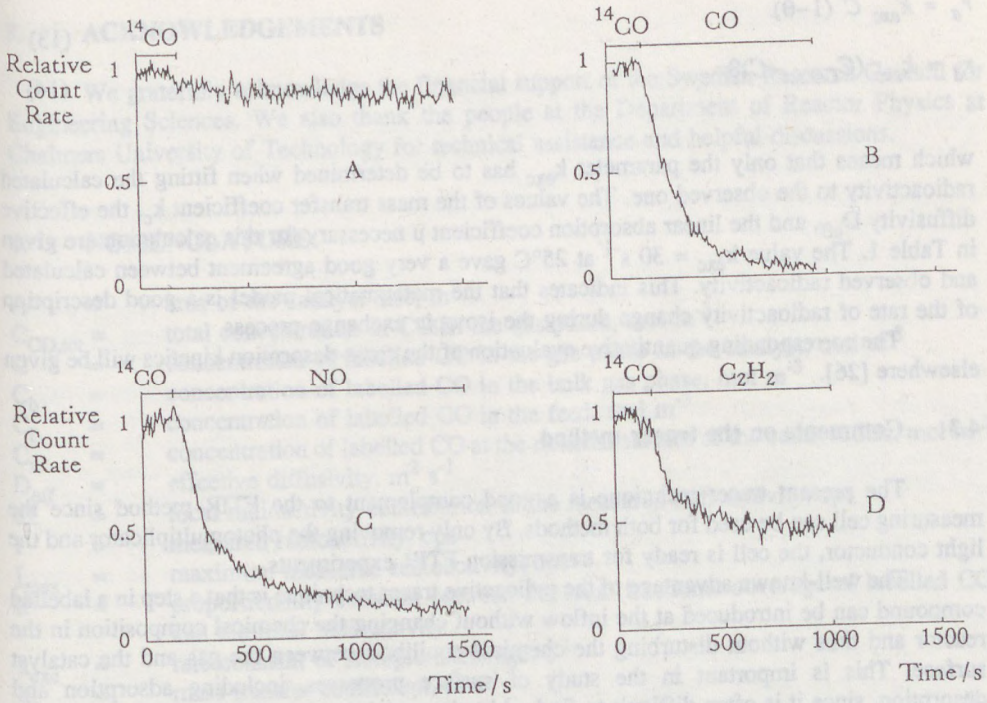

Fig. 3 Count rate from a ^{14}CO covered 5% Pd/Al_2O_3 catalyst. T = 25°C P = 1 atm.
a. Flushed with Ar, 100 ml min^{-1}.
b. Flushed with 1000 ppm CO in Ar, 100 ml min^{-1}
c. Flushed with 1000 ppm NO in Ar, 100 ml min^{-1}
d. Flushed with 1% C_2H_2 in Ar, 100 ml min^{-1}

The desorption of CO in the presence of C_2H_2 is not as rapid as the isotopic exchange of CO. The effect of C_2H_2 is an example of the so-called cross-desorption, which was recently demonstrated by Cider and Schöön [22-25]. As can be seen from Fig. 3 this cross-desorption does not completely remove CO from the catalyst surface. The cross-desorption of CO in the presence of NO, which hitherto has been studied very little, removed on the other hand CO more completely from the catalyst surface.

4.2 Quantitative evaluation of the isotopic exchange

The mathematical model has to be completed by assuming the form of the rate equations for the adsorption and desorption of CO, when the isotopic exchange of CO is to be quantitatively described. In a first attempt these equations were chosen to be

$$r_a = k_{exc}\, C\, (1-\theta) \tag{13}$$

$$r_d = k_{exc}\, (C_{CO,tot}-C)\theta \tag{14}$$

which means that only the parameter k_{exc} has to be determined when fitting the calculated radioactivity to the observed one. The values of the mass transfer coefficient k_c, the effective diffusivity D_{eff}, and the linear absorption coefficient μ necessary for this calculation are given in Table 1. The value $k_{exc} = 30\ s^{-1}$ at 25°C gave a very good agreement between calculated and observed radioactivity. This indicates that the mathematical model is a good description of the rate of radioactivity change during the isotopic exchange process.

The corresponding quantitative evaluation of the cross-desorption kinetics will be given elsewhere [26].

4.3 Comments on the tracer method

The present tracer technique is a good complement to the FTIR method since the measuring cell can be used for both methods. By only removing the photomultiplicator and the light conductor, the cell is ready for transmission FTIR experiments.

The well-known advantage of the radioactive tracer technique is that a step in a labelled compound can be introduced at the inflow without changing the chemical composition in the reactor and thus without disturbing the chemical equilibria between the gas and the catalyst surface. This is important in the study of surface processes, including adsorption and desorption, since it is often difficult to find a kinetic model that is valid over a wide range of chemical compositions.

The maximum allowable temperature with the present set up for radioactivity measurements depends on the cooling of the glass rod and the photomultiplier. Water was used as a coolant medium, but this can be changed to liquid nitrogen to achieve better cooling. The highest temperature used here was 110°C. The upper temperature limit is set by the O-rings, that can withstand 320°C. However, other cells for *in situ* IR studies have been developed that permit even higher temperatures [27]. The O-rings in these cells are replaced by Cu and Graphoil gaskets. It would also be possible to replace a window by a solid scintillator if even higher temperatures are required. The maximum pressure for the cell, in the present work was 20 bar and was determined by the maximum allowable pressure for the windows [28].

Since the average residence time in the reactor cell is very short compared to the time constants of most processes studied, the reactor was considered to behave like a continuous stirred tank reactor from a mixing point of view. However, just after a step change this approximation is not valid for a rapid process. During this short part of the step change, the response data cannot be used for determination of rate constants.

5. ACKNOWLEDGEMENTS

We gratefully acknowledge the financial support of the Swedish Research Council for Engineering Sciences. We also thank the people at the Department of Reactor Physics at Chalmers University of Technology for technical assistance and helpful discussions.

6. NOMENCLATURE

A	=	area of the catalyst disc, m^2
$C_{CO,tot}$	=	total concentration of CO in the gas phase, mol m^{-3}
C	=	concentration of labelled CO in the gas phase in the catalyst, mol m^{-3}
C_b	=	concentration of labelled CO in the bulk gas phase, mol m^{-3}
C_f	=	concentration of labelled CO in the feed, mol m^{-3}
C_s	=	concentration of labelled CO at the external surface of the catalyst disc, mol m^{-3}
D_{eff}	=	effective diffusivity, m^2 s^{-1}
dI	=	local radioactivity contribution to the measured radioactivity, cps
I	=	measured radioactivity, cps
I_{max}	=	maximum measured radioactivity, cps
k	=	proportionality constant between the local fractional coverage of labelled CO and the local radioactivity
k_{exc}	=	rate constant of isotopic exchange, s^{-1}
k_c	=	mass-transfer coefficient, m s^{-1}
L	=	thickness of the catalyst disc, m
N	=	molar flux of labelled CO to the catalyst disc, mol s^{-1} m^{-2}
N_s	=	site density, mol (kg catalyst)$^{-1}$
q	=	volumetric flow rate through the cell, m^3 s^{-1}
r_a	=	adsorption rate of labelled CO, mol $s^{-1}m^{-3}$
r_d	=	desorption rate of labelled CO, mol $s^{-1}m^{-3}$
t	=	time, s
V	=	volume of reactor cell, m^3
x	=	length coordinate perpendicular to the external surface, m

Greek Symbols

ε	=	void fraction
θ	=	fractional coverage of labelled CO
μ	=	linear absorption coefficient
ρ	=	density of the catalyst disc

7. REFERENCES

1 K.C. Campbell and S.J. Thomson, Progr. Surf. Membr. Sci., 9 (1975) 163.
2 G.F. Berndt, Catalysis, 6 (1983) 144, The Royal Society of Chemistry, London 1983.
3 S.J. Thomson in Characterisation of Catalysts, (J.M. Thomas and R.M. Lambert, eds.), John Wiley & Sons, Chichester, 1980.
4 R.F. Hicks, C.S. Kellner, B.J. Savatsky, W.C. Hecker, and A.T. Bell, J. Catal., 71 (1981) 216.
5 E. Wicke and R. Kallenbach, Kolloid Z., 97 (1941) 135.
6 K. Klier, A.C. Zettlemoyer, and H. Leidheiser, Jr., J. Chem. Phys., 52 (1970) 589.
7 J.T. Yates, Jr., T.M. Duncan, S.D. Worley, and R.W. Vaughan, J. Chem. Phys., 70 (1979) 1219.
8 J.T. Yates, Jr., T.M. Duncan, and R.W. Vaughan, J. Chem. Phys., 71 (1979) 3908.
9 J.T. Yates, Jr., D.W. Goodman, J. Chem. Phys., 73 (1980) 5371.
10 T. Matsushima, Surface Sci., 79 (1979) 63.
11 T. Matsushima, Surface Sci., 89 (1979) 665.
12 T. Matsushima, J. Catal., 64 (1980) 38.
13 T. Yamada, T. Onishi, and K. Tamaru, Surface Sci., 133 (1983) 533.
14 T. Yamada and K. Tamaru, Surface Sci., 138 (1984) L155.
15 T. Yamada and K. Tamaru, Surface Sci., 146 (1984) 341.
16 V.P. Zhdanov, Surface Sci., 157 (1985) L384.
17 T. Yamada, T. Onishi, and K. Tamaru, Surface Sci., 157 (1985) L389.
18 K. Tamaru and T. Yamada, Shokubai, 27 (1985) 350.
19 K. Tamaru, T. Yamada, R. Zhai, and Y. Iwasawa, Proc. 9th Int. Congr. Catal., Calgary 1988, The Chemical Institute of Canada, Ottawa, 1988, p. 1006.
20 K. Tamaru, Colloids and Surfaces, 38 (1989) 125.
21 T. Yamada, R. Zhai, Y. Iwasawa, and K. Tamaru, Bull. Chem. Soc. Jpn., 62 (1989) 2387.
22 L. Cider and N.-H. Schöön, Appl. Catal., 68 (1991) 191.
23 L. Cider and N.-H. Schöön, Appl. Catal., 68 (1991) 207.
24 L. Cider and N.-H. Schöön, Ind. Eng. Chem. Res., 30 (1991) 1437.
25 L. Cider, U. Schröder, N.-H. Schöön, and B. Albinsson, J. Mol. Catal., 67 (1991) 323.
26 U. Schröder and N.-H. Schöön, to be published in 1992.>
27 B.J. Savatsky and A.T. Bell in Catalysis Under Transient Conditions, (A.T. Bell and L.L. Hegedus, eds.) ACS Symposium Ser. 178, American Chemical Society, Washington, D.C., 1982.
28 A.T. Bell in Chemistry and Physics of Solid Surfaces, Springer Ser. Chem. Phys., (Chem. Phys. Solid Surf. 5), 35 (1984) 23.

DISCUSSION

Q: M. A. Baltanas (Argentina)

Just a few remarks about your paper, which I enjoyed very much:

1) Concerning the "similar information" you could have obtained via IR, certainly your technique does not require a preformed, transparent pellet. You can as well use a powder sample !

2) Two possible improvements are: (i) the use of a metal holder heated from the exterior with an inductive coil, and (ii) the use of flow-thru set-up to avoid channelling and mixed signals proper of cross flow.

A: U. Schröder

Thank yor for your valuable comments.

Q: D. G. Blackmond (USA)

1) Can you comment on how your technique compares with other steady-state switching techniques which utilize non-radioactive isotopes, detecting the gas-phase exiting the reactor by mass spectroscopy (for example, see p.181and p. 219) ? In particular, your experiment contains information about the changing surface concentration of an isotope together with its changing gas phase concentration. How can these contributions be deconvoluted?

2) The comparison of CO desorption rates in the presence and absence of gas-phase CO appears to be misleading since in the first case the system is under adsorption-desorption equilibrium (CO exchange might be a better term than desorption) and in the second system is far from equilibrium. Can you comment ?

A: U. Schröder

1) The main advantage with our technique is that we measure the adsorption directly on the working catalyst. This means that we, for instance, can follow a slow adsorption process during reaction. This may be difficult with techniques where the adsorption rate is obtained indirectly by measuring the concentration in the effluent from the reactor. Another advantage is that the technique is very cheap and simple.

Since the gas volume of the cell is very small, the gas-phase contribution to the measured radioactivity is also very small. Furthermore, in experiments where we make a step from labeled to unlabeled CO, the radioactivity from the gas-phase is continuously flushed away. The contribution from the radioactivity in the gas-phase can, moreover, be compensated for by making an experiment where you replace the catalyst disc by a disc of only the support material.

2) We completely agree with you that "exchange rate" might be a better term than "desorption rate" since it is possible that the exchange with the gas-phase only occurs from certain sites and that CO on the other sites are displaced because of the mobility of CO on the surface.

Q: A. K. Datye (USA)

The information obtained with this technique can also be obtained, in principle, by IR spectroscopy. Furthermore, IR transparent discs are not necessary since diffuse reflectance can be performed on powders. How wold you compare your technique with other techniques such as IR that provide in situ probes of adsorbed species?

A: U. Schröder

With our technique we actually measure the amount of adsorbed species regardless of the adsorption mode. Using IR measurements for the same purpose, you must correlate the IR absorption with the amount of adsorbed species. This calibration can be very tricky, especially when you have a coadsorption of several species. The IR absorption band is not only dependent on how much of a certain compound that is adsorbed, but also on the

adsorption mode and on the interaction with other adsorbed molecules. IR is a very powerful method to study the adsorption mode but not as a tool for quantitative measurements for complicated mixtures. The evaluations of diffuse reflectance IR is moreover known to be more complicated than for transmission IR. Finally, our technique is cheaper, and in our opinion easier to apply, than IR.

Q: Wm. C. Conner (USA)
Could you envision employing your technique to image the adsorption as contrast with integrating the adsorption over the whole surface. This would complement the studies such as those by R. Schmidts that thermally image the surface.

A: U. Schröder
Yes, one possibility would be to have an aluminium plate with a small hole between the catalyst disc and the scintillator. This plate would screen off all the emitted β-particles except from a small point of the catalyst disc. The only problem one would have to solve, would be how to move the hole over the catalyst disc in situ.

Q: J. W. Hightower (USA)
In the case of ^{14}CO removal by NO, how can you distinguish between ^{14}CO displacement and reactive removal, e.g. $NO + CO \rightarrow 1/2N_2 + CO_2$? Did you measure for CO_2, N_2, N_2O, etc. in the effluent from the reactor system ?

A: U. Schröder
Yes, we measured the concentration of CO, NO and CO_2 in the effluent from the reactor. Under the conditions in the experiments reported here, we did not find any CO_2. At higher temperatures, however, we have found some CO_2.

Q: X. X. Guo (China)
If the thermal desorption is negligibly small, then the only rate process to cause a change in isotopic concentration of the catalyst (Θ), is the exchange process. However, in your paper, eqn. (13) and eqn. (14) are used as two independent rate equations. I can not understand the physical meaning of eqn. (13). It seems to be the diffusion rate equation. But in your experiment, the diffusion process is only to change the intra-particle concentration of isotope molecules in gas (or precursor state) phase. It has no direct relation with Θ, because Θ_x only changes with exchange process.

A: U. Schröder
In eqn. (13) we have assumed that the adsorption rate of labeled CO, r_a, is proportional to the concentration of labeled CO, denoted C, in the gas phase and to the fractional coverage of unlabeled CO on the catalyst, $\Theta_{tot} - \Theta_x$. The reason for this assumption is that some authors have found that the desorption rate of CO is proportional to the concentration of CO in the gas-phase and to the coverage of CO. Under our conditions the coverage is at maximum and therefore the only way that we can get a net adsorption of labeled CO is by displacement of an unlabeled CO. In the same way, the only way we can get a net desorption of labeled CO is to replace the adsorbed labeled CO by an unlabeled CO. The desorption rate of labeled CO must therefore be equal to the adsorption rate of unlabeled CO since we have steady state conditions. In the same way as in eqn. (13) this rate is proportional to the pressure of unlabeled CO in the gas phase and to the fraction of labeled CO, Θ, on the catalyst. The concentration of unlabeled CO can be written as $C_{CO,tot} - C$.

Q: D. Wang (China)
In the work from our laboratory (X. X. Guo et al. Surf. Sci. in press, 1992), we found that desorption from Re(001) under a CO ambience follows a rate law for desorption that is not well-fitted by a 1st order nor a 2nd order rate equation. Instead a (1st + 2nd) order rate

law gives a good fit. Have you tested your data for a desorption (under a gas ambience) rate law and, if you have, how was the test done and what is your deduced rate law?

A: U. Schröder

We have done these experiments at different CO pressures and we have found that the desorption rate is very well fitted by a rate law, which is first order w.r.t. CO pressure. It is always easier to get a better fit if you combine two rate equations instead of only using one of them.

Guczi, L. *et al.* (Editors), *New Frontiers in Catalysis*
Proceedings of the 10th International Congress on Catalysis, 19-24 July, 1992, Budapest, Hungary
© 1993 Elsevier Science Publishers B.V. All rights reserved

APPLICATION OF SCANNING TUNNELING MICROSCOPY/SPECTROSCOPY (STM/STS) TO CATALYST RESEARCH: Pt/SiO_2

M. Komiyama and M. Kirino

Department of Chemistry, Yamanashi University, Takeda, Kofu 400, Japan

Abstract

Scanning tunneling microscopy/spectroscopy (STM/STS) was applied to the system of platinum supported on silica for the first time. This was accomplished by employing a model Pt/SiO_2 catalyst which consists of platinum metal particles vacuum-deposited on thin (ca. 0.7 nm) native silica film present on silicon wafer surface. Choosing optimal tunneling conditions was critical in STM/STS observation of this system. With the optimum tunneling conditions platinum metal particles of few nanometer diameters were routinely observable. Topographic and barrier-height images of the surface were obtained and their interpretations are given. These results open the possibility of applying STM/STS to the samples which have been considered not practical for STM/STS study due to their low conductivities.

1. INTRODUCTION

Scanning tunneling microscopy (STM), with its very high spatial resolution that for some samples reaches atomic level, is a powerful tool for the studies of solid surfaces [1]. STM can observe not only the topographic images of solid surfaces but also surface barrier-height images, electronic density of states near the Fermi edge and other spectroscopic information with similar spatial resolution. Such features make STM a promising tool for the surface study of heterogeneous catalysts, in which local topographic as well as electronic characteristics is of major concern.

Despite such expectations, so far the application of STM/STS to catalyst research has been limited. This may partly due to the fact that STM is considered to be applicable only to conductors and semiconductors, whereas the large body of practical catalysts are non-conductors. The other problem that may arise in studying practical catalysts by STM is that STM by itself is not possible to distinguish elemental species it is observing, and thus unless one know, a priori, surface elemental compositions in relation to surface topograph, it is rather difficult to interpret the STM images obtained.

In our attempt to apply STM/STS to the study of heterogeneous catalysts, we chose supported metal catalysts, in which several interesting topographic and electronic questions to be answered are present. In doing so we tried to circumvent the difficulties stated above by constructing model catalyst systems which simulate the actual supported metal catalysts. Thus the first STM observations of supported metal catalysts concerned platinum ultrafine particles (ca. 2-4 nm in diameter) vacuum-deposited on thin carbon film and on thin titanium oxide film [2,3]. These papers were followed by others,

including palladium [4] and platinum [5] ultrafine particles, both vacuum-deposited on cleaved graphite crystal, platinum ion-exchanged on oxidized graphite surface [6] and platinum vacuum-deposited on gallium oxide film [7].

As may be obvious from these works, STM studies of supported metal catalysts have been limited to the systems with conductor or semiconductor support materials. Few of those who wanted to study the surface topograph of supported metal catalysts on non-conductive materials used atomic force microscope (AFM): AFM images of palladium vacuum-deposited on mica [8] and on silica [9] have been reported. One shortcoming of AFM, however, is that it provides only topograph, and no spectroscopic information is available.

In the present paper we report our challenge to apply STM/STS to metal catalysts supported on non-conductive surfaces. Platinum supported on silica was chosen as a sample system. Very low conductivity of silica was compensated by employing very thin (ca. 0.7 nm) silicon oxide present on a commercial silicon wafer surface as a support. Tunneling conditions were found to be critical in successful STM/STS observation of this system. The optimal tunneling conditions and the topographic and barrier height images of the sample are presented, and their interpretations are given.

2. EXPERIMENTAL

2.1. Equipment

A home-built STM/STS equipment was used in the present study. The STM unit employed here is made of stainless steel and machinable glass. The scanner is a tripod type, and the probe tip was a mechanically formed Pt-Ir wire. This configuration made the scanner operatable under ambient, in situ and ultrahigh-vacuum conditions, although the present work was performed only under ambient conditions. Vibration isolation of the scanner was effected by an air-suspended table and a stack of stainless steel slabs each isolated by pieces of silicone rubber. When operating under ambient conditions the scanner was covered by a lead box in order to isolate it from sound and electronic noises.

The above STM unit is driven by a feedback circuit system. The topographic images were taken either by constant current mode through negative feedback and reading the voltage Vz applied to the z-piezo, or by constant height mode under slow feedback and reading the tunnel current variation. Barrier-height images were obtained by modulating Vz and detecting the tunnel current modulation by a lock-in amplifier. Other spectroscopic information such as It-Vt characteristics and its derivatives were also obtainable using similar modulation-lockin detection procedure.

The topographic, barrier-height and other signals obtained were digitized by 12-bit A/D converter and stored in a microcomputer for data processing. The data handling software constructed include data filtering, base plane subtraction, image rotation, zooming and three- and two-dimensional graphic presentations.

The above STM/STS equipment exhibited atomic resolution for graphite crystal and resolved monoatomic steps of metal surfaces. Barrier-height and other spectroscopic images also showed similar spatial resolutions.

2.2. Sample preparation

As a model silica support a native oxide film present on the surface of a commercial p-type Si(100) wafer was employed. The thickness of the native

oxide was determined by X-ray photoelectron spectroscopy (XPS), and calculated to be close to 0.7 nm from the 2p electron emission intensities originating from 0- and IV-valent Si, taking into account the electron escape depth at each electron energy.

This native oxide-covered Si wafer was ultrasonically cleaned in ethanol, dried and then Pt was vacuum-deposited on its surface. The amount of Pt deposited was determined by XPS. STM/STS observation of this Pt/SiO_2 model catalyst surface was performed under ambient conditions.

3. RESULTS AND DISCUSSION

3.1. Identification of optimal tunneling conditions

STM operates on the principles of electron tunneling. In order for an electron to tunnel from the tip to the sample surface (or vice versa), wave functions of both sides have to meet spatially as well as energetically. The former requirement is satisfied by placing the tip within 1 nm distance from the sample surface. The latter may be satisfied if applied tunneling voltage Vt places the tunneling electron energy at the energy level of non-zero density of states of the material to be tunneled into. For a metal tip and a metal sample this rquirement is satisfied for Vt anywhere around Fermi enegy to few eV above or below it. In the case of a metal tip and a semiconductor sample one may want to place Vt above the energy band gap of the semiconductor surface, unless there exist enough surface density of states in the band gap to accomodate the tunneling current It. Compared to these systems, the system to be examined here, vis., silicon, a semiconductor, covered with thin silicon oxide, a non-conductor, is problematic. In this particular case one has to find the condition for an electron to tunnel into the silica surface, not to the underlying silicon interface. In the latter case electrons would be tunneling through the silica layer, and then we may be losing information on the silica surface, on which we want to place our catalyst metal.

In search of the optimum electron tunneling conditions for this system, we first tried to obtain the energy distribution of its surface density of states (SDOS). With the SDOS of the sample known we may be able to locate the optimum tunneling conditions. In principle SDOS can be obtained by STM as d^2It/dVt^2 versus Vt [1]. Our attempt to obtain this relationship on our SiO_2/Si system, however, was unsuccessful, probably due to the charge buildup at the silica interfaces with the sweeping of Vt, which washed out any details of the SDOS of the sample that may have been present in the above relationship.

Instead of measuring SDOS, therefore, we measured tip-sample distance as a function of Vt at constant It. SDOS is convoluted in the It-Vt relation at constant tip-sample distance, and since the tip-sample distance is exponentially dependent on It, the tip-sample distance as a function of Vt at constant It should also reflect the energy distribution of SDOS. Figure 1 shows this tip-sample distance variation, represented as the variation of the voltage Vz applied to the z-piezo, with Vt at 0.1 nA It. In the figure Vz is found to increase, i.e., tip retracts from the sample surface, stepwise with increasing Vt. Each step increase of Vz reflects the opening of a new tunneling channel for electrons. The long plateau located in between ca. 0.2 V and ca. 2.5 V is interpreted as the region where electrons tunnel into the bulk conduction band of silicon below the surface oxide: below 0.2 V electrons may be tunneling into SDOS in the band gap of silicon.

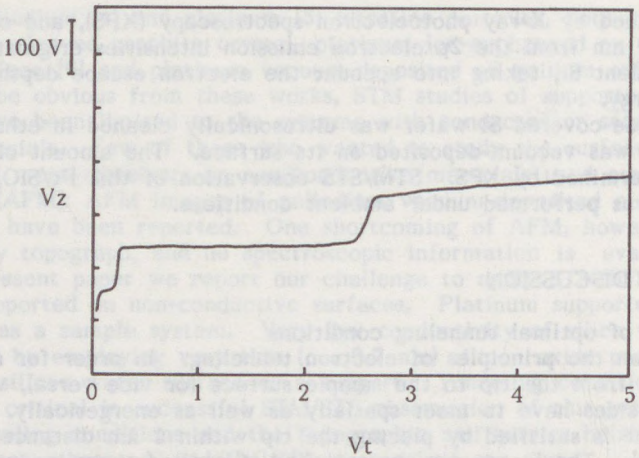

Figure 1. Voltage applied to the z-piezo Vz as a function of tunneling voltage Vt at constant It of 0.1 nA. Increase in Vz means the increase in the tip-sample distance. Sample: native oxide-covered Si. Tunneling current: 0.1 nA, bias: tip negative.

At ca. 2.5 V an opening of another tunneling channel is indicated by the presence of a step increase in the tip-sample distance. We attribute this to the opening of a tunneling channel to the surface silica layer. Above this bias voltage electrons may tunnel into the silica layer and below that they tunnel through the oxide layer into underlying silicon interface directly.

The above discussion suggests the possibility of probing interface between the surface silicon oxide and the silicon substrate if one chooses Vt below the step energy of ca. 2.5 V. This appears to be true, and the detailed study on this point will be published elsewhere [10]. On the other hand if we would like to study the surface of silica layer and anything on it, Figure 1 tells us that we have to keep Vt at the plateau located above 2.5 V. Care must be taken, however, that we also have to keep Vt below the field emission range, which is located above ca. 5 eV for either component of the tip employed here, vis., Pt and Pd.

It is also noted that the relationship exemplified in Figure 1 is also dependent on tunneling current: increasing It tends to shift the steps to higher Vt. In the present study we employed low It value of 0.1 nA, in order to ensure wide Vt range for the tunneling to the oxide surface. Tunneling bias employed here is 4 V, leaving more than 1 V margin on higher and lower sides. These conditions kept us from losing tunneling into the oxide surface due to the small SDOS variation that may be present locally on the surface, and also kept us within the tunneling region and not in the field emission region. The small It employed meant larger tip-sample distance for a given Vt value , and this kept our probe tip from bumping into sharply varying surface structure, although large distance meant losing some of the topographic details.

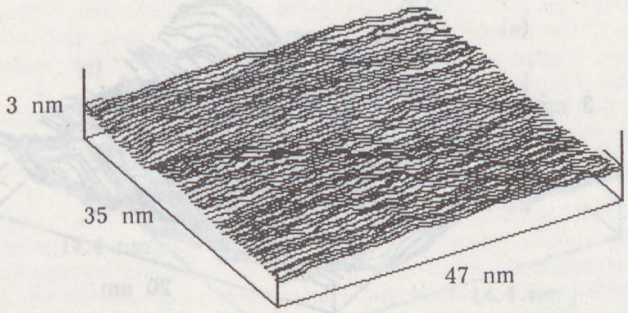

Figure 2. Topographic image of native oxide-covered silicon surface. Image taken under ambient conditions at 4.0 V Vt and 0.1 nA It. Small height variations less than 0.5 nm are observed, and the surface may be considered fairly flat.

3.2. STM image of the native oxide-covered silicon surface

With the optimum tunneling conditions thus identified, the topographic images of the surface of the native oxide on the silicon wafer was obtained. A typical scan, of an area of 47 nm by 35 nm, is shown in Figure 2. Although small height variations of less than 0.5 nm are apparent in the figure, the surface may be considered fairly smooth and flat. This is in accordance with the expectation for this particular surface, which is a single crystal silicon cut and polished to expose (100) surface.

It is noted that the structure at the silica-silicon interface, probed using low Vt, is somewhat different compared to the one shown in Figure 2: one or two clear monoatomic or diatomic step lines are often observed in areas of similar dimensions [10]. The reason that we do not observe such clear structure in Figure 2 may be that the step structure is blurred when the surface is oxidized and/or the large tunneling distance employed here kept us from observing such detailed structures.

It should be emphasized here that Figure 2 is the first relaiable STM image of silicon oxide surface reported. Although its thickness is very thin, the oxide entirely consists of IV-valent Si as found by XPS. This means that the surface of this thin silica film could be used as a model surface to the bulk silica. The low crystallinity expected for this thin silica film would simulate the non-crystalline, high surface area silica. Thus the successful observation of the surface of thin silicon oxide film existing on silicon wafer presents the possibility of applying STM to the studies on silica as well as silica-containing materials, including metal catalysts supported on silica.

3.3. Topographic and barrier-height images of Pt/SiO_2

With the successful STM observation of the surface of thin silica film, we extended our attempts to the examination of platinum ultrafine particles deposited on this silica surface. The platinum was vacuum-deposited on the above native oxide-coverd silicon wafer. The Pt/Si atomic ratio of the prepared sample was 0.4, as determined by XPS.

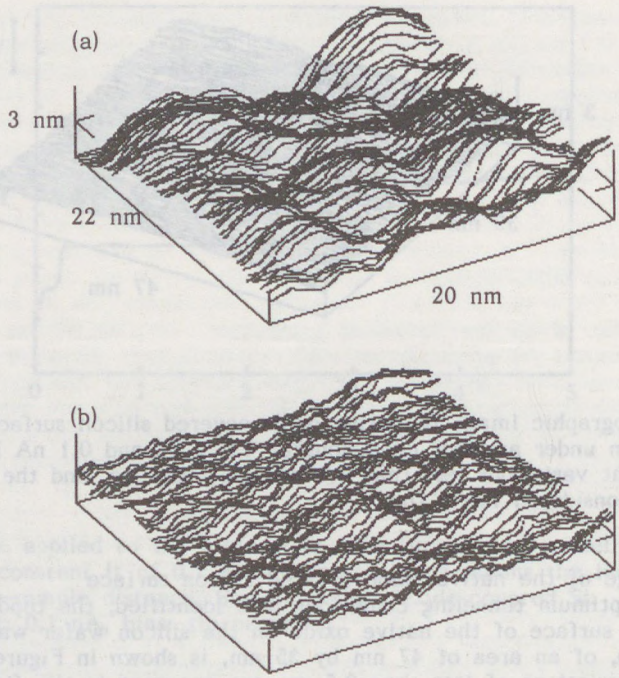

Figure 3. Topographic (a) and barrier-height (b) images of Pt vacuum-deposited on the surface of thin silica film. Scan conditions: Vt 4.0 V, It 0.1 nA, tip negative. The concurrently obtained barrier-height image (b) was taken with Vz modulation amplitude of 160 mV peak-to-peak, which translates to the tip-sample distance modulation of 0.16 nm peak-to-peak. The modulation frequency was 700 Hz. The z-axis of the barrier-height image is arbitrary.

A topographic scan of ca. 20 nm by 20 nm of this sample surface is shown in Figure 3 (a) along with its barrier-height image (b). Figure 3 (c) and (d) on the next page are the two-thirds of the lower left portion of the images (a) and (b), respectively, enlarged and rotated 90 degrees to the left. In the topographic image (a) and its enlargement (c), particles of varying diameters with the height of ca. 1 to 2 nm are apparent. The topographic image (a) is presented as is taken, without any data filtering. The scans were highly stable, as may be apparent in the figure, resulting in the image quality comparable to that of highly conductive Pt/C sample [3].

The scans shown in Figure 3 (a) and (c), and other topographic scans on this sample not shown here, indicate that the size distribution of the Pt particles deposited is very sharp: observed Pt particles were mostly in the size range of 2.5 to 5 nm in diameter. This observation is quite similar to that made on Pt/C samples [2,3], in which vacuum-deposited Pt particles are mostly in the size range of 2-4 nm. As for the absolute value of the Pt particles observed by STM, we always have to take into account the possibility

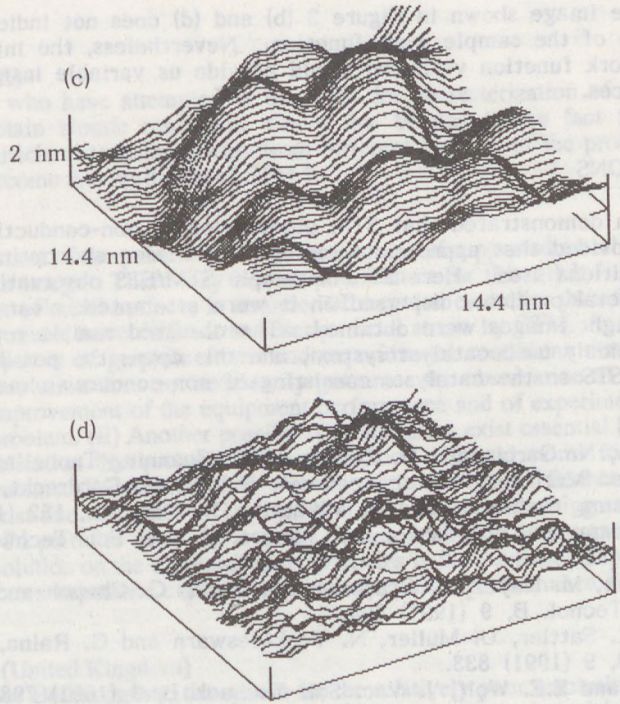

Figure 3 (cont.). Topographic (c) and barrier-height (d) images of two-thirds of the lower left portion of (a) and (b), respectively, enlarged and rotated 90 degrees to the left.

of overestimation [2]. Since no other particle size measurements have been performed on the current sample, unlike the previous Pt/C [2], the extent of size overestimation in the present sample by STM is not accuratly known. However, the main source of overestimation is considered to be in the tip-sample separation distance [2], it is expected not to exceed few tenths of a nanometer.

The barrier-height images shown in Figure 3 (b) and (d), taken concurrently with the topographic images shown in (a) and (c), are slightly noisy, but shows apparent barrier-height variations on the surface. The images show that where Pt particles exist barrier-height is higher compared to the places in between the particles. This barrier-height variation resembles that of the Pt/TiO_2 system [3], in which Pt particles show heigher barrier-height than titania substrate. Compared to these systems it is noted that in Pt/C sample Pt particles exhibited lower barrier-height compared to the substrate carbon [2].

Barrier-height images reflect the surface work function variation [1], and as seen above work function variations with spatial resolution less than a nanometer is obtainable by STM, the resolution of which has not been possible by any other method. It should be noted, however, that because the barrier-height is determined by not only the work function of the sample but also that

of the tip, the image shown in Figure 3 (b) and (d) does not indicate the absolute value of the sample work function. Nevertheless, the information on the surface work function variation would provide us variable insights on the catalyst surfaces.

4. CONCLUSIONS

It has been demonstrated that STM observation of non-conductive materials is possible, provided that appropriate sample was chosen and optimum tunneling conditions used. Here as an example STM/STS observations of silica surface and metal particles dispersed on it were attempted: clear topographic and barrier-height images were obtained. The observed sample represents one of the most widely used catalyst system, and this opens the possibility of applying STM/STS to the catalysts consisting of non-conductive materials.

1 R.J. Behm, N. Garcia and H. Rohrer (eds.), Scanning Tunneling Microscopy and Related Methods, Kluwer Academic Publishers, Dordrecht, 1990.
2 M. Komiyama, S. Morita and N. Mikoshiba, J. Microsc., 152 (1988) 197.
3 M. Komiyama, J. Kobayashi and S. Morita, J. Vac. Sci. Technol. A, 8 (1990) 608.
4 A. Humbert, M. Dayez, S. Granjeaud, P. Ricci, C. Chapon and R. Henry, J. Vac. Sci. Tecnol. B, 9 (1991) 804.
5 J. Xhie, K. Sattler, U. Muller, N. Venkateswarn and G. Raina, J. Vac. Sci. Technol. B, 9 (1991) 833.
6 K. Yeung and E.E. Wolf, J. Vac. Sci. Technol. B, 9 (1991) 798.
7 W. Hanrieder, A. Scholz and H. Meixner, Surf. Sci., 243 (1991) 794.
8 J. Colchero, O. Marti, J. Mlynek, A. Humbert, C.R. Henry and C. Chapon, J. Vac. Sci. Tecnol. B, 9 (1991) 794.
9 R. Eerlandsson, M. Eriksson, L. Olsson, U. Helmersson, I. Lundstrom and L.-G. Petersson, J. Vac. Sci. Tecnol. B, 9 (1991) 825.
10 M. Komiyama, to be published.

DISCUSSION

Q: A. T. Bell (USA)

Many people who have attempted to use STM for characterization of metal particles have failed to obtain atomic resolution. Could this be due to the fact that as the tip approaches the particle channeling occurs from different partions of the probe tip. What is being done to overcome this limitation of STM ?

A: M. Komiyama

It is true that most of the published STM observations of supported metal particles fail to resolve metal atom images. There may be two possibilities for this: (i) It is known that the atomic corrugation of metal surfaces is an order of magnitude smaller than that of graphite, and therefore it is much more difficult to observe metal atoms by STM. An equipment that have a resolving power of graphite atoms and experimental conditions that routinely give graphite atomic resolution does not necessarily guarantee the observation of metal atoms. If this is the case, improvement of the equipment performance and of experimental conditions would solve the problem. (ii) Another possibility is that there exist essential limitations such as electron delocalization that prohibit STM observation of metal atoms for such ultrafine metal particle systems. Whether this is true or not must await further investigations. However, there exist one work on Pd/C system that appears to be reaching atomic resolution for the supported Pd particles of ca. 1.5 nm size (text, ref. 4). This seems to indicate that the lack of atomic resolution on the dispersed metal particles in the published papers is not due to some essential factors but rather dependent on the equipment performance and experimental conditions.

Q: J. M. Thomas (United Kingdom)

If, as Professor Bell suggests, the reason for the relatively poor resolution that STM has so far achieved with supported metal particles stems from the curvature of the small particles - resulting in "delocalized" tunneling - then it might-be useful to employ facetted Pt and Pd surfaces. You may recall the electron micrograph (shown by Professor King in his plenary lecture) published by my two former colleagues Peter Harris and David Jefferson.

When small Pt particles on silica are exposed to H_2S the surfaces become very flat (and develop an ordered "S" overlayer). These sulphided and facetted Pt particles would be worth investigating to test the power of STM. Its spatial resolution may not be any better than that of HREM (high-resolution, electronmicroscopy). But its great attraction is that it may be used (in situ) or in air.

A: M. Komiyama

I thank you for the useful comments.

Q: M. M. Bhasin (USA)

In the STM images of Pt/SiO_2, the silica background appeared a lot rougher than in the silica sample. How do you explain that observation? Could that be due to the Pt deposition procedure used? Also would you comment on the feasibility of obtaining atomic resolution with such supported metal catalysts.

A: M. Komiyama

We believe that the structures found on the Pt-deposited silica surface are all due to the deposited Pt. Platinum was deposited on the surface by vacuum deposition, in which Pt wire was heated on a W rod. The energy of the Pt atoms arriving at the silica surface is expected to be too small to cause any modification on the surface.

As for the feasibility of obtaining atomic resolution on the supported metal, please see the answer to Professor Bell.

Q: Wm. C. Conner (USA)
What do the subsequent imager look like ? Is there any evidence for the STM modifying the surface ?

A: M. Komiyama
Within the experimental conditions employed here, the images are reproducible. Surface modifications are observed when much higher tunneling voltages are employed, or when the tip is intentionally or unintentionally driven to push or scratch the surface.

Q: P. Sermon (United Kingdom)
With regard to the advantages of STM versus AFM in the study of catalysts with an insulator component like silica, I wanted merely to draw your attention to the AFM image of a sol-gel derived silica-based catalyst in this Proceeding (see p.1775). For this delicate assembly of colloidal particles of silica STM was impossible. However, the advantages of STM-STS are clear from your paper. In other words they complement each other well.

A: M. Komiyama
I fully agree with your opinion that AFM possesses advantages over STM/STS for certain samples, and that STM/STS and AFM compliment each other.

Q: A. Datye (USA)
One of the fundamental problems in the application of STM/AFM to small metal particles is that the diameter of the tip is much greater than the diameter of the metal particles. The image obtained represents a convolution of the tip with the sample. What are the prospects of interpreting the image to determine the true morphology of the particles ? Also, do you characterize your tips after obtaining the image?

A: M. Komiyama
What is convoluted in the observed image is not the tip diameter (i.e. apex curvature) but the distance between the surface and the tip apex (text, ref. 2), and the tip diameter would impose the limitations only through the distance it can physically approach to the surface (for instance if the curvature is very large compared to the particle-particle distance then the tip cannot trace the region in between the particles). Therefore it is important (to keep in mind that the STM-observed particle size is always larger by the tip-surface distance, which is commonly a fraction of a nanometer).
Tip characterization after measurements is not normally done, but we routinely check the tip by using a graphite sample, making it certain that the tip can resolve graphite atoms.

Q: J. W. Niemantsverdriet (The Netherlands)
The SiO_2 layer you are using has a thickness of less than a nanometer, and leaves few opportunities to do something with you model catalyst in reaction or adsorption studies with oxidizing species.
1) Is this thin SiO_x layer sufficiently characteristic of a real silica, in the sense that all silicon atoms are in the 4+ oxidation state ?
2) Have you tried taking STM imaging from thicker SiO_2 layers, and if so, have you an idea of the maximum thickness permitted for STM ?

A: M. Komiyama
The system we examined is a "model" system, with the advantages and disadvantages commonly associated with any model systems. We believe that at this moment the present system comes closest to the actual silica-supported catalyst, as far as STM/STS is concerned. Then what we should do is to obtain as much information as possible with this system to the extent the system allows. The limitations of the current system must be complimented by other sample systems and/or other experimental techniques.

For the specific question: (1) As far as XPS is concerned, the oxidic silicon are almost entirely in the 4+ oxidation state. (2) The investigation on the effect of silica thickness on STM/STS observation is in progress.

Q: W. Grünert (Germany)
Is it possible to perform STM at elevated temperatures ? What are the limits of the measurement temperature imposed, for instance, by the piezo ?

A: M. Komiyama
The Curie point of piezo elements do impose a limitation on an upper limit of the operation temperature. This, however, could be able to be circumvented by equipment design that keep temperature rise away from the piezo elements. more severe problem, as it seems, is a temperature drift during STM measurements, which increases with temperature and distorts the tip-sample configuration thus distorting STM images. This should also be able to be circumvented by equipment design, to a certain extent, such as making it highly symmetrical so as to cancel the uneven expansion or contraction of the STM parts caused by the temperature drift.

Q: L. A. Rudnitski (Russia)
You can receive high resolution potential surfaces of barrier-height tunneling for metal ultrafine particles on flat surfaces.
Next one needs interpretation of the investigation results. It is very difficult to do because barrier height is determined not only by the nature of the investigated surface and tip surface, but also by their mutual arrangement in space.
Work function of complicated (rough) surfaces is a mean value formed by contributions of all surface atoms orbital electronegativity but with essential differences in their weight coefficient. The weight coefficient value for a surface atom depends on its size, its coordination, and its distance from the point of electronegativity, meaning that the electronegativity values of surface atoms differing in their coordination can differ by one eV or more. So dependence at small distances from the surface: the value of the work function is stabilized at a distance exceeding 1.5-2 nanometers only. All this applies to tip and surface in investigating work functions. The space variation of the tip work function can be observed when the tip comes down from the metal particle apex to their bases.
So at atomic size order of distance from tip to rough surface of particles one can expect the effect of space changes of contact potential difference value to be displayed. The value of the contact potential difference between the end of the tip and other surface gives on essential contribution to tunneling barrier-height. For rough metal surfaces on which surface atom arrangement is known one can approximately calculate the work function space distribution and then compare results of the calculation with experimental date.

A: M. Komiyama
Thank you for your comments.

Guczi, L. *et al.* (Editors), *New Frontiers in Catalysis*
Proceedings of the 10th International Congress on Catalysis, 19-24 July, 1992, Budapest, Hungary
© 1993 Elsevier Science Publishers B.V. All rights reserved

CHARACTERIZATION AND CATALYTIC PROPERTIES OF Pt-Ir SMALL BIMETALLIC CLUSTER IN NaY

O. B. Yang and S. I. Woo

Department of Chemical Engineering, Korea Advanced Institute of Science and Technology, P.O.Box 150, Chengryang, Seoul, Korea

ABSTRACT

The formation of small Pt-Ir bimetallic clusters (about 1 nm) by the reducton of Pt and Ir co-ion-exchanged NaY with H_2 at 300°C after calcined with oxygen at 300°C was evidenced by temperature programmed oxidation/reduction (TPO/R), ^{129}Xe NMR, hydrogen chemisorption and catalytic probe reaction. These small Pt-Ir bimetallic clusters inside the supercage were more stable than Ir monometallic cluster and remained inside the supercage after re-oxidation treatment below 400°C. Temperature programmed oxidation/reduction (TPO/R) results suggested that the interaction between Pt and Ir takes place in the calcination step prior to hydrogen reduction. The Pt-Ir/NaY bimetallic catalyst showed a higher activity and better activity maintenance than those of Pt/NaY catalyst in n-heptane reforming reaction.

1. INTRODUCTION

Pt-Ir bimetallic catalyst exhibits a higher activity and better activity maintenance than Pt catalyst in the reforming reaction [1]. Sinfelt and co-workers reported that the bimetallic clusters of Pt and Ir were formed in silica [2] and alumina [3]. It has been understood that the special character of Pt-Ir bimetallic catalyst is related to the interaction between Pt and Ir. Interaction between Pt and Ir has been assumed to occur during the reduction of ionic precursors. However, a recent laser Raman study of Pt-Ir/Al_2O_3 catalyst by Chan et al. [4] indicated that interaction between the two metals may in fact take place upon drying the freshly impregnated samples.

The catalyst deactivated in the reforming reaction must be regenerated to be used commercially again. Catalyst regeneration is achieved by burning the coke deposit in an oxygen-containing atmosphere around 500°C. The combustion process of coke, however, causes an increase in the size of the metal crystal size. Therefore, the stability of bimetallic clusters under the oxidation condition is very important in the Pt-Ir reforming catalyst.

Not any works have been known to us for characterization of Pt-Ir bimetallic clusters in NaY. However, our recent result showed that very small (about 1 nm) Pt-Ir bimetallic clusters of uniform size were formed mostly inside the zeolite supercage after calcining and reducing with H_2 at 300°C [5]. The physicochemical characteristics and catalytic properties of small Pt-Ir bimetallic clusters should be different from those of large metallic clusters. The oxidation and reduction properties and catalytic properties of small Pt-Ir bimetallic clusters were studied by temperature programmed oxidation/reduction (TPO/TPR) and n-heptane reaction. ^{129}Xe NMR and hydrogen chemisorption were also used to characterize small Pt-Ir bimetallic clusters in NaY.

2. EXPERIMENTAL

Monometallic Pt and Ir clusters in NaY (abbreviated as Pt(x)/NaY and Ir(x)/NaY and x indicates weight %) were prepared by calcining and reducing $Pt(NH_3)_4^{2+}$-exchanged NaY (PtNaY) and $Ir(NH_3)_5Cl^{2+}$-exchanged NaY (IrNaY) with O_2 and H_2 at 300°C, respectively. Pt-Ir bimetallic clusters in NaY (Pt(x)Ir(x)/NaY) were prepared by calcining and reducing co-ion-exchanged NaY (PtIrNaY) with O_2 and H_2 at 300°C, respectively [5]. The experimental details of ^{129}Xe NMR spectroscopy and hydrogen chemisorption were described in previous work [6].

A conventional apparatus of temperature programmed study was used to determine the TPO/R profiles. TPO spectra were obtained using a high through-put pressure reducing system combined with a computer interfaced mass spectrometer (VG Quadrupoles SX 300). TPO was carried out with 100 mg of ion-exchanged NaY samples by raising temperature from 25°C to 500°C at a rate of 8°C/min. in the 5 % O_2/N_2 flow of 60 ml/min.. The decrease in oxygen partial pressure was recorded every 10 s. The mass numbers monitored during the TPO of the uncalcined ion-exchanged sample were 15 (NH), 17 (NH_3) and 32 (O_2). Hydrogen consumption during the TPR was monitered by a Hewlett-Packard 5890A thermal conductivity detector (TCD). A molecular sieve trap, kept at -80°C, was placed after the TPR cell in order to remove water. After the sample was calcined at 300°C, TPR was performed with 100 mg of sample by raising temperature from 25°C to 500°C at a rate of 8°C/min. in the 5 % H_2/N_2 flow of 40 ml/min..

n-Heptane reforming reaction was carried out in a differential fixed bed reactor with 100 mg of catalyst at atmospheric pressure and 400°C for 4 h. Catalysts calcined at

300°C with O_2 and reduced at 400°C with H_2 for 2 h were used in the reaction. The n-heptane (Aldrich, 99 + %) was fed by a calibrated micro-syringe pump (Sage Instrument Model 3413) into a preheated zone where heptane was mixed with hydrogen and vaporized. The total flow rate (H_2 + n-heptane) was 67 ml/min. with the H_2/n-heptane mole ratio of 8.5. Products were analyzed by an on-line HP 5890A gas chromatograph equipped with a 50 m crosslinked methyl silicon fused silica capillary column and a FID detector.

3. RESULTS AND DISCUSSION

No response was observed for mass number 15 (NH) in all TPO spectra. The loss of ammonia ligand began at 100°C and almost was completed at about 300°C in all samples. The spectra of O_2 consumption during TPO are shown in Figure 1. The TPO spectrum of Pt(4)NaY and Ir(4)NaY showed a sharp peak of O_2 consumption at 308°C and 330°C, respectively. Pt(3)Ir(1)NaY and Pt(2)Ir(2)NaY bimetallic clusters exhibited a TPO peak at 297°C and 298°C, respectively. The TPO peak temperatures of Pt-Ir ion coexchanged NaYs are significantly lower than those of PtNaY and IrNaY indicating that the oxidation of co-ion-exchanged NaYs was facilitated due to the possible interaction between the cationic species of Pt and Ir.

Figure 2 shows the TPR spectra of PtNaY, IrNaY, and PtIrNaY samples calcined at 300°C. The TPR peak temperatures of Pt(4)NaY and Ir(4)NaY were observed at 112°C and 142°C, respectively. The Pt-Ir co-ion-exchanged samples exhibited a TPR peak between 112°C and 142°C. The TPR peak of Pt(3)Ir(1)NaY, Pt(2)Ir(2)NaY and Pt(3)Ir(1)NaY samples appeared at 124°C with shoulders at 112°C and 142°C. The TPR spectra of these Pt-Ir co-ion-exchanged samples can not be obtained by the weight average of corresponding PtNaY and IrNaY. The TPR spectra of these samples calcined at 500°C are also shown in Figure 3. The Pt(4)NaY sample exhibited a pair of peaks at 112°C and 320°C, whereas Ir(4)NaY showed a sharp peak at 210°C. The PtIrNaY samples exhibited a sharp and strong peak at 210°C and weak peaks at 112°C and 320°C. The area of TPR peak of PtIrNaY at 210°C increased with increasing the Ir content, while the area of the peak at 320°C decreased. From the previous works on the TPR of PtNaY [7,8], the peak at 112°C can be assigned to highly dispersed Pt^{2+} inside the supercage of Pt(4)NaY calcined at 300°C. The peak at 320°C is likely due to Pt^{4+} in sodalite cage which requires a reduction temperature higher than Pt^{2+} ions in the supercages of Pt(4)NaY calcined. This peak was not observed when the samples were calcined at 300°C. About 80 % of Pt^{4+} ions are in sodalite cage calculated from TPR peak area. Huang et al. [9] reported that the TPR peak of Ir/Al_2O_3 catalyst at 210°C is due to the reduction of large IrO_2 crystallites. The existence of the agglomerated IrO_2 particles on the exterior surface of NaY can be easily identified by the sharp peak at 210°C in the TPR spectrum of IrNaY precalcined at 500°C (Figure 3), while these agglomerated IrO_2 particles were not present after calcination of IrNaY at 300°C indicated by the absence of TPR peak at 210°C. Our previous ^{129}Xe NMR study

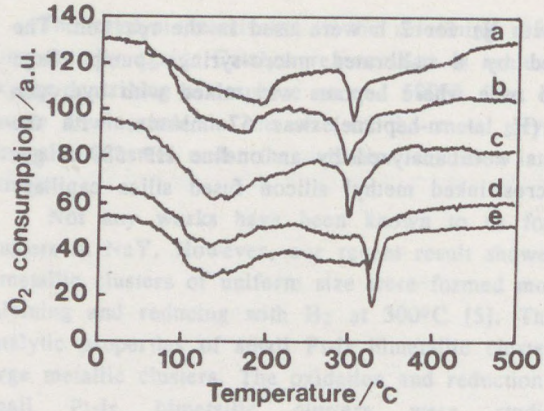

Figure 1. The spectra of O_2 consumption during TPO of ion-exchanged NaYs; Pt(4)NaY (a), Pt(3)Ir(1)NaY (b), Pt(2)Ir(2)NaY (c), Pt(1)Ir(3)NaY (d) and Ir(4)NaY (e).

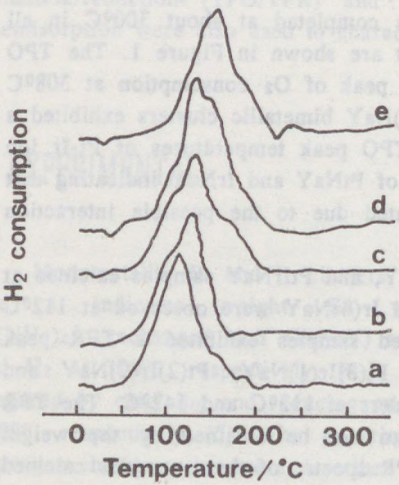

Figure 2. The TPR spectra of PtNaY, IrNaY and PtIrNaY calcined at 300°C; Pt(4)NaY (a), Pt(3)Ir(1)NaY (b), Pt(2)Ir(2)NaY (c), Pt(1)Ir(3)NaY (d) and Ir(4)NaY (e).

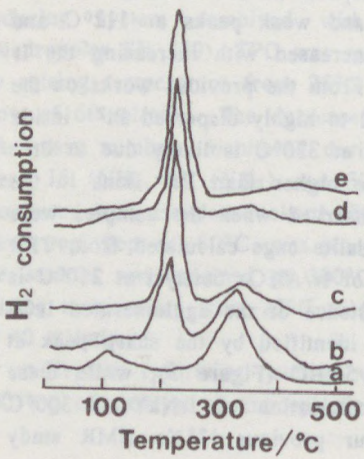

Figure 3. The TPR spectra of PtNaY, IrNaY and PtIrNaY calcined at 500°C; Pt(4)NaY x 1.5 (a), Pt(3)Ir(1)NaY (b), Pt(2)Ir(2)NaY x 0.75 (c), Pt(1)Ir(3)NaY x 0.5 (d), and Ir(4)NaY x 0.5 (e).

indicated that highly dispersed Pt-Ir bimetallic clusters were formed inside the supercage of NaY by calcining and reducing PtIrNaY samples at 300°C [5]. Hence, the peak of TPR spectrum of IrNaY (Figure 2) at 142°C is arising from highly-dispersed Ir clusters inside the supercage of NaY. Therefore, the peak of TPR spectra of PtIrNaYs calcined at 300°C observed at 124°C is ascribed to the reduction of oxygen containg bimetallic Pt-Ir complex located in the zeolite supercage. This bimetallic oxygen containing complex is seemed to be already formed during the calcination step as indicated by the TPO spectra of Figure 1. However, the TPR spectra of PtIrNaYs calcined at 500°C do not have any peaks at 124°C as shown in Figure 3. It can be concluded from these results and further evidences by ^{129}Xe NMR, XRD and H_2 chemisorption results that most of Ir is present on the exterior surface as agglomerated IrO_2 clusters and Pt is present as Pt^{2+} in the supercage and Pt^{4+} in sodalite cage after calcination of PtIrNaY at 500°C.

The chemical shift of ^{129}Xe NMR spectrum is very sensitive to the change in the chemical state and the number of metallic species inside the supercage of Y zeolites. The NMR shifts of Pt/NaY, Ir/NaY and Pt-Ir/NaY after reoxidation at various temperatures were measured to determine the stability of the corresponding metal clusters in NaY. Pt/NaY, Ir/NaY and Pt-Ir/NaY calcined and reduced at 300°C were characterized with ^{129}Xe NMR in our previous work [5] were used as a reference catalyst. The ^{129}Xe NMR chemical shifts of the reference catalyst reoxidized at 300, 400 and 500°C followed by the reduction at 400°C are shown in Figure 4. The dispersions (H/M: adsorbed hydrogen atom / metal atom) of metal clusters after reoxidation and reduction are shown in Figure 5. The chemical shifts of Pt(4)/NaY, Ir(4)/NaY and Pt(1)Ir(3)/NaY decreased as re-oxidation temperature increased, while the chemical shifts of Pt(3)Ir(1)/NaY and Pt(2)Ir(2)/NaY increased below reoxidation temperature of 400°C and

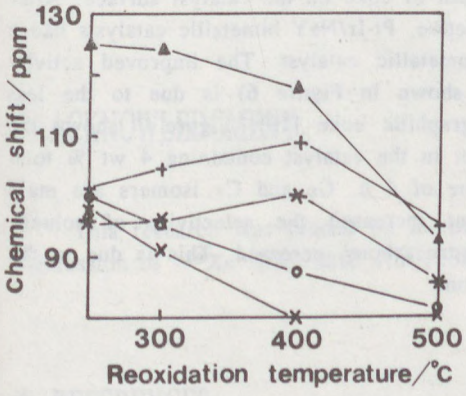

Figure 4. Effect of reoxidation temperature on the ^{129}Xe NMR chemical shift; Pt(4)/NaY (▲), Pt(3)Ir(1)/NaY (+), Pt(2)Ir(2)/NaY (✳), Pt(1)Ir(3)/NaY (○) and Ir(4)/NaY (X).

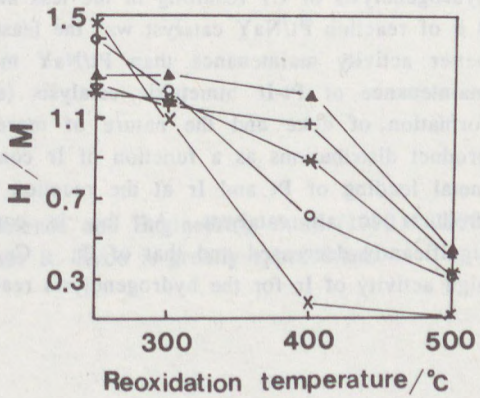

Figure 5. Effect of reoxidation temperature on the metal dispersion; Pt(4)/NaY (▲), Pt(3)Ir(1)/NaY (+), Pt(2)Ir(2)/NaY (✳), Pt(1)Ir(3)/NaY (○) and Ir(4)/NaY (X).

decreased at the reoxidation temperature of 500°C as shown in Figure 4. The chemical shift of Ir(4)/NaY is equal to that of NaY zeolite after reoxidation at 400°C. This indicates that most of Ir clusters are migrated to external zeolite surface to form large IrO_2 particles after reoxidation at 400°C, which was confirmed by the small value of Ir dispersion (see Figure 5) and X-ray diffraction [5]. Migration of Pt clusters to external zeolite surface was insignificant below the reoxidation temperature of 400°C. The chemical shifts of Pt(3)Ir(1)/NaY and Pt(2)Ir(2)/NaY increased with the increase in the reoxidation temperature below 400°C might be due to the surface enrichment of Pt of Pt-Ir bimetallic clusters during the reoxidation below 400°C, because the chemical shift caused by Pt atom is much larger than by Ir atom. Another explanation might be due to the formation of highly dispersed Pt and Ir clusters inside the supercage, which will result in the increase of chemical shift due to the formation of more clusters. This possibility can be ruled out on the basis of metal dispersion as shown in Figure 5. If highly dispersed Ir clusters were formed, the metal dispersion should not decrease. The dispersions of Pt(3)Ir(1)/NaY and Pt(2)Ir(2)/NaY decreased below reoxidation temperature of 400°C. At the reoxidation temperature of 500°C, Ir is totally segregated from the Pt-Ir bimetallic clusters due to the lack of stabilization obtained by forming bimetallic clusters and migrated to the external surface, resulting in the significant decreases in both chemical shift and dispersion. The segregation of Ir clusters from Pt(1)Ir(3)/NaY occured below reoxidation temperature of 400°C due to the higher content of Ir in the Pt-Ir bimetallic cluster.

Figure 6 shows the total conversion of n-C_7 as a function of reaction time. In all catalysts steady state appears to be achieved at 4 h of reaction. Ir/NaY catalyst showed a conversion higher than Pt/NaY and Pt-Ir/NaY bimetallic catalysts. The activity of Ir/NaY catalyst was maintained during the reaction because of high activity of hydrogenolysis of C_7 resulting in the less amount of coke on the catalyst surface. After 4 h of reaction Pt/NaY catalyst was the least active. Pt-Ir/NaY bimetallic catalysts had a better activity maintenance than Pt/NaY monometallic catalyst. The improved activity maintenance of Pt-Ir bimetallic catalysts (as shown in Figure 6) is due to the less formation of coke and the nature of more graphitic coke [10]. Figure 7 shows the product distributions as a function of Ir content in the catalyst containing 4 wt % total metal loading of Pt and Ir at the reaction time of 4 h. C_6 and C_7 isomers are main products in all catalysts. As the Ir content increased the selectivity of toluene significantly decreased and that of C_1 - C_6 hydrocarbons increased. This is due to the high activity of Ir for the hydrogenolysis reaction.

4. CONCLUSIONS

The TPO and TPR results suggested that the interaction between Pt and Ir takes place in the calcination step prior to hydrogen reduction. The small (about 1 nm) Pt-Ir bimetallic clusters formed after calcination and reduction at 300°C, are stable and remain

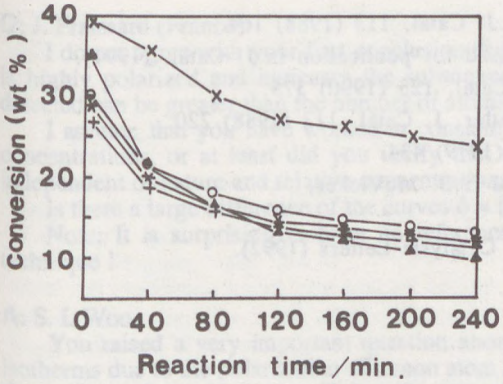

Figure 6. Total conversion of n-heptane as a function of reaction time at 400°C; Pt(4)/NaY (▲), Pt(3)Ir(1)/NaY (+), Pt(2)Ir(2)/NaY (✳), Pt(1)Ir(3)/NaY (○) and Ir(4)/NaY (╳).

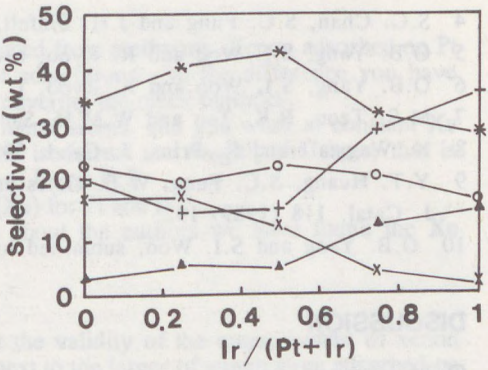

Figure 7. Product distributions of Pt(4)/NaY, Ir(4)/NaY and Pt-Ir/NaY catalysts in n-heptane reaction; C_1 (▲), C_2 - n-C_6 (+), C_6 and C_7 isomers (✳), cyclic compound (○) and toluene (╳).

mostly inside the zeolite supercage after re-oxidation below 400°C. However, these Pt-Ir bimetallic clusters are migrated and agglomerated to large metallic crystallites on the exterior surface of NaY after re-oxidation above 400°C. The Pt-Ir/NaY bimetallic clusters showed a higher activity and better activity maintenance than Pt/NaY monometallic clusters in n-heptane reforming reaction.

5. ACKNOWLEDGMENT

This research was funded by Korea Science and Engineering Fund (1990 - 1993). Discussion of ^{129}Xe NMR data with Professor R. Ryoo is greatly appreciated.

6. REFERENCES

1 J.H. Sinfelt, US Patent No. 3 953 368 (1976).
2 J.H. Sinfelt, G.H. Via and F.W. Lytle, J. Chem. Phys. 76 (1982) 2779.
3 R.L. Garten and J.H. Sinfelt, J. Catal. 62 (1980) 127.

4 S.C. Chan, S.C. Fung and J.H. Sinfelt, J. Catal. 113 (1988) 164.
5 O.B. Yang, S.I. Woo and R. Ryoo, revised for publication in J. Catal. (1991).
6 O.B. Yang, S.I. Woo and R. Ryoo, J. Catal. 123 (1990) 375.
7 M.S. Tzou, B.K. Teo and W.M.H. Sachtler, J. Catal. 113 (1988) 220.
8 N. Wagstaff and R. Prins, J. Catal. 59 (1979) 434.
9 Y.T. Huang, S.C. Fung, W.E. Gates and G.B. McVicker, J. Catal. 118 (1989) 192.
10 O.B. Yang and S.I. Woo, submitted to Catalysis Letters (1992).

DISCUSSION

Q: M. Ichikawa (Japan)

Zeolite frameworks accommodate the alloy particles of Pt-Zr to prevent sintering similar to the Re-Ir cluster in NaY reported by us. You mentioned metal aggregation in a large crystallites after the calcination at 400 ^{0}C.

1) What kind of chemical reaction do you expect for the methyl migration from inside to outside of the zeolite, in particle for Pt and Ir particles ?

Generally, PtO easily sublimes under the oxygen atmosphere even at the lower temperature, which might aid the methyl segregation and aggregation in the PtIr alloy systems.

2) Have you observed any evidence for phase-segregation of PtIr particles in NaY by meas of Xe NMR and TPR before and after the calcinations ?

A: S. I. Woo

Minachev and Isakov reported (ACS Monograph, 171 (1976)) that the stability of Pt clusters entrapped inside NaY supercages. Our result (Figure 4) also indicated that Pt clusters in NaY are stable and not migrated to the exterior surface of NaY below the temperature of calcination and reduction of 300 ^{0}C. However, the calcination above 400 ^{0}C migrated platinum clusters into the exterior surface. hence, it can be explained by your suggestion that volatile or more mobile PtO species easily formed above 400 ^{0}C. The formation of Ir oxide species is more favorable than that of platinum oxide species, resulting in the complete migration of Ir clusters to the exterior surface of NaY [1]. It was reported that sintering the Ir/alumina was occurred via atomic or molecular species of volatile Ir oxide species. Hence, the phase separation of Ir and Pt must be occurred when the Pt-Ir bimetallic clusters are calcined above 400 ^{0}C due to the different rate of formation of volatile oxide phases. Actually, the increase in the chemical shift of Pt(2)Ir(2) and Pt(3)Ir(1) as shown in Figure 4, indicate the phase separation due to the surface enrichment of Pt, arising from the more removal of iridium oxide species during calcination.

[1] Y. F. Chu and E. Ruckenstein, *J. Catal.*, **55**, 281 (1978)

Q: V. Ragaini (Italy)

One of the problems in bimetallic catalysts is to find separately the dispersion of each metal (i.e. the number of surface metal atoms of a type over the total number of metal atoms of the same type). Are your Xe-NMR plus TPR methods able to solve this problem ?

A: S. I. Woo

Yes, it is possible to calculate the surface composition of Pt and Ir metals in the Pt-Ir bimetallic cluster with the assumption that the intrinsic chemical shift caused by one Pt or Ir metal atom is not changed with the formation of Pt-Ir bimetallic clusters. This might be reasonable in the case of Pt-Ir bimetallic clusters, because the electron band structure of these two metals is nearly same. Then the chemical shift of bimetallic clusters can be expressed as $\delta_{Pt\text{-}Ir} = H_{Pt}.\delta_{Pt} + H_{Ir}.\delta_{Ir}$, where H is the surface mole fraction.

Q: J. Fraissard (France)

I do not agree with your first conclusion deduced from isotherms. Xenon adsorbed on Pt is highly polarized and increases the subsequent adsorptions - so the difference you have detected can be greater than the number of atoms covering the metal particles.

I assume that you have worked at constant metal atoms. Did you work at constant Xe concentrations, or at least did you verify that the isotherms are roughly the same, that is independent of nature and relative concentrations of Ir and Pt ?

Is there a large difference of the curves $\delta = f(Xe)$ for Pt and Ir ?

Note: It is surprising to have no reference about the authors we have found the Xe technique !

A: S. I. Woo

You raised a very important question about the validity of the measurement of xenon isotherms due to the polarization of xenon atom next to the larger of xenon atom adsorbed on the surface of metal clusters. This will overestimate the amount of xenon adsorbed on the metal cluster. We performed a variable-temperature xenon adsorption experiment similar to your recent papers [2] with our samples, which will be published after complete analysis. This result indicated that the change in the adsorption temperature resulted in the different amount of xenon adsorbed on metal cluster obtained by the extrapolation of xenon pressure to zero. The higher the adsorption temperature, the higher the amount of xenon adsorbed is. The higher temperature of adsorption is, the mean free path and the dipole moment is the smaller, which indicates that the degree of polarization of xenon gas next to xenon atoms adsorbed on metal clusters decreased. However, the difference is small.

The question about whether the xenon isotherms are independent of the nature and relative concentrations of Ir and Pt is also a good one. Our previous result (to be published in J. Catal. (1992)) indicated that if the number and size of clusters are the same, the xenon isotherms are all identical in the case of Pt-Ir bimetallic clusters. The final question about whether the large difference in the chemical shift of Pt and Ir clusters was observed as a function of xenon pressure, the answer is yes. The chemical shift is strong function of the xenon pressure and increased rapidly as the xenon pressure decreased.

[2] J. Chen and J. Fraissard, *J. Phys. Chem.*, **96**, 1809, 1814 (1992)

Q: Wm. C. Conner (USA)

As Fraissard has shown on numerous occasion, the chemical shift of ^{129}Xe depends on both morphological (Xe-Xe and Xe-wall) interaction as well as prober of the chemical environment. How did you deconvolute the chemical and morphological factors in your ^{129}Xe data, i.e., did you complete δ vs $^{129}Xe_{ads}$ studies ? How would your interpretation compare to those of Fraissard ?

A: S. I. Woo

Yes, you are quite right. The chemical shifts of Pt, Ir and Pt-Ir bimetallic clusters in NaY are composed of the morphological interactions (Xe-Xe and Xe-wall) and the interaction with metal clusters. Our samples have the same number of ion-exchange of cations and the same number of metal clusters. The numbers of H^+ ions after reduction of Pt and Ir cations are almost identical. Hence the difference in the chemical shift is mainly due to the interaction of xenon with metal clusters. We measured δ at the various amounts of xenon adsorbed. This data can be interpreted according to the interpretation of Professor Fraissard's group.

Q: W. M. H. Sachtler (USA)

Reduction of ion-exchanged Pt ions by H_2 creates protons. In n-C_7 reforming therefore two types of coke are usually found, one associated with the metal and one linked to the protons. Why did your TPO data fail to show the coke on acid sites ?

From results of Barbier et al. it is clear that the position of the TPO peak is an indicative of the kinetics of coke combustion not necessary the nature of the coke. If the activation energy of coke combustion catalyzed by Ir is higher than that catalyzed by Pt this would cause a shift in TPO peak even if the nature of the coke were identical.

A: S. I. Woo

The coke formed on the proton site reacted with oxygen to give CO_2 around 450 ^{0}C as reported [3]. The TPO spectra of coke formed on Pt, Ir, and Pt-Ir clusters in NaY shows only one peak which can be assigned to the coke formed on the metal cluster. Pt(4)/NaY, Pt(3)Ir(1)/NaY shows a very weak band around 450 ^{0}C, which might suggest the coke formed on proton site. We speculate that the protons located near metal clusters in the same supercage may not be active to form coke or thermodynamically the formation of coke on the metal cluster might be more feasible. Your comments on the assignment of TPO peak is quite reasonable. We are now trying ESCA study of coke to study its nature.

[3] J. Barbier et al., *Catalyst Deactivation*, (Ed.: D. L. Trimm et al.), p 53, (1987)

Guczi, L. *et al.* (Editors), *New Frontiers in Catalysis*
Proceedings of the 10th International Congress on Catalysis, 19-24 July, 1992, Budapest, Hungary
© 1993 Elsevier Science Publishers B.V. All rights reserved

LASER RAMAN CHARACTERIZATION OF SURFACE PHASE PRECIOUS METAL OXIDES FORMED ON CeO_2 MICRO DOMAINS GENERATED WITHIN AN ALUMINA HOST BY SOL SYNTHESIS

L. L. Murrell, S. J. Tauster and D. R. Anderson

Engelhard Corporation, 101 Wood Avenue, Iselin, NJ 08830-0770, USA

ABSTRACT

Laser Raman Spectroscopy (LRS) has shown in other work that Rh, Ir, Pd, and Pt form a surface phase precious metal oxide structure which interacts strongly with the surface of bulk CeO_2. This interaction leads to a M-O structure interacting with the bulk CeO_2 surface. Recent work from our laboratory has shown that mixed sols of alumina and ceria lead to highly-stable structures of CeO_2 micro domains, or small crystals, within the alumina host structure. By the use of LRS we have been able to observe the formation of the same precious metal surface phase oxides bonded to the surface of the CeO_2 domains, present within the alumina host, as those established to be present on the surface of bulk CeO_2. In addition, we have direct evidence from LRS for the stabilization of very high dispersions of 5% Pt even after calcination at 900°C. This unusual stability is due to the Pt-O surface phase bonded to the CeO_2 micro domain surface.

1. INTRODUCTION

Previous work from our laboratory employing LRS has shown that Rh, Ir, Pd, and Pt form a surface phase precious metal oxide structure, M-O, which interacts strongly with the surface of bulk CeO_2[1]. This Strong Oxide Support Interaction (SOSI) leads to a M-O structure with each group separated by ca. 1 nm from each other for ca. 5 wt% Pt metal-equivalent loading levels on bulk CeO_2 of 130 m^2/g surface area. The M-O surface complex on CeO_2 stabilizes the CeO_2 phase to sintering and surface area collapse, while being stabilized in turn, in a highly-dispersed phase by the CeO_2 support. Reduction of the M-O structure on CeO_2 in flowing hydrogen results in formation of a highly-dispersed metal phase which was characterized by conventional pulsed CO chemisorption techniques[1]. In this work it was also shown that calcination at >900°C results in significant sintering of the CeO_2 phase to ca. 10 m^2/g surface area, with the conversion of the M-O structure to a highly-agglomerated phase which is for the most part detached from the reduced CeO_2 surface area.

In other work from our laboratory[2] mixed sol slurries of alumina and ceria lead to stable thin or thick, rod-shaped CeO_2 micro domains, or crystals, within the alumina host structure, depending on the size of the CeO_2 sol used. By the use of LRS we have been able to observe the formation of the same precious metal surface phase oxides, M-O, as those established to be present on the surface of bulk CeO_2. In addition, we have direct evidence from LRS for the stabilization of high dispersions of 5 wt % Pt even after calcination at 900°C. This unusual stability of a Pt-O surface phase structure is due to bonding to the CeO_2 micro domain surface. Unlike bulk CeO_2 the micro domains of CeO_2 within the alumina host are stable to high temperature conditions. Cyclic redox aging conditions result in very severe sintering of all four of the Group VIII metals investigated for the micro domain Ce-Al system. Despite the observation of precious metal sintering after cyclic aging treatment, probably due to metal sintering under the reducing conditions in the cyclic aging cycle, the CeO_2 domains remain stable within the alumina host structure. The implication of these studies to automotive catalysts suggests that dispersed and stabilized micro domains do not improve performance by improving precious metal dispersion compared to bulk CeO_2 systems.

2. EXPERIMENTAL

The details of the preparation of Rh, Ir, Pd, and Pt samples on the mixed ceria-alumina supports in this paper have been described elsewhere[1], and all samples were prepared by the standard incipient wetness procedure followed by drying and calcination at 500°C. The details of the preparation of mixed Ce-Al systems from mixed slurries of Nyacol sols have also been described elsewhere[2]. The alumina sol employed was a ca. 20 nm size product made by Nyacol Corporation, and the ceria sol was also of 20 nm size obtained from Nyacol. The Raman spectrometer employed in this work has been described in detail elsewhere[3]. All of the normalized Raman intensities for the M-O bands at 600-700 cm^{-1} were obtained by dividing the intensity of these M-O bands by the intensity of the Raman bands at 560 cm^{-1} or 447 cm^{-1} of CeO_2 depending entirely on which was appropriate. The 560 cm^{-1} band, for example, was too close to overlapping with the Raman bands of Rh and Ir at 590 and 614 cm^{-1}, respectively, to be used for the case of the Rh and Ir samples, and the 447 cm^{-1} band was of use only for the case of the 500°C calcined samples where the intensity was similar in size to that of the M-O bands.

3. RESULTS AND DISCUSSION

There are very few references in the literature where mixed sols have been used to prepare novel materials for application in heterogeneous catalysis[4-6]. Nothing has been published to the best of our knowledge where isolated micro domains, or small crystals, of one oxide are stabilized within a porous alumina host by mixed sol synthesis, except for recent work from our laboratory[1]. This is somewhat surprising as transitional aluminas[7], and their surface-stabilized counterparts[8,9]

constitute the most useful supports for high temperature application. The critical role of the alumina sol size in maintaining high pore volume in the gelled alumina has been demonstrated[2], and all of the mixed oxides described in this work used an alumina sol of ca. 20 nm size. The size of the ceria sol has a marked influence on ceria domain size and shape, especially at low ceria contents[2], but the review of these details goes beyond the scope of this paper. In this work, directed at studying high temperature stability of M-O structures on ceria micro domains, the ceria sol size of 20 nm was chosen for all preparations because earlier studies have shown that ceria domain, if smaller than those obtained from a 20 nm ceria sol, convert at high temperatures to a size approximately that obtained from for the 20 nm ceria sol precursor. Two compositions were chosen for study: 20% ceria - 80% alumina and 50% ceria - 50% alumina, hereafter referred to as 20 Ce-80 Al and 50 Ce-50 Al.

The ability of these two mixed oxide compositions to stabilize Pt at high temperature was first investigated using ethane hydrogenolysis as a probe reaction of relative metal dispersions after high temperature calcination treatment. After calcination at 900°C in air for 2 hours, 0.5 wt% Pt on 20 Ce-80 Al and 0.5 wt% Pt on 50 Ce-50 Al had a conversion of ethane to methane at 410°C of 34% and 74%, respectively. If a 0.5 wt% Pt on Al_2O_3 reference sample was calcined at 900°C for 2 hours the ethane conversion was only 3% at 410°C consistent with the formation of >30 nm size Pt particles observed by x-ray diffraction for this calcined sample, see Figure 1. The percent ethane conversion for a 500°C calcined 0.5 wt% Pt on Al_2O_3 catalyst as a reference was 83%. These results show clearly that Pt on micro domain Ce-Al systems maintain very good Pt dispersion when calcined at 900°C in air. These results will be useful to compare to the results obtained from laser Raman spectroscopy for related systems, vida infra.

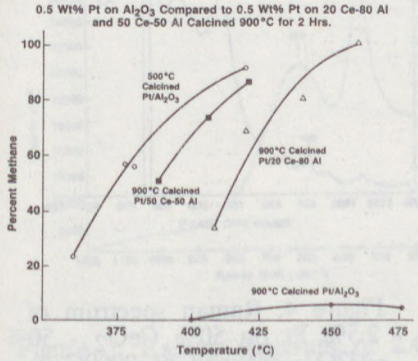

Figure 1. Ethane hydrogenolysis of 0.5 wt % Pt on alumina and on two ceria-alumina compositions.

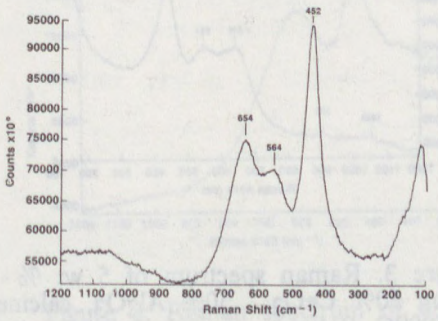

Figure 2. Raman spectrum of 2.5 wt % Pt on 50% CeO_2 - 50% Al_2O_3, calcined at 500°C, 2 hrs.

The ability of Ce-Al micro domain systems to maintain a dispersed Pt phase for low Pt levels of ca. 0.5 wt% when calcined at high temperature is entirely consistent with analogous results for bulk CeO_2 seen in earlier work[1]. The bulk CeO_2 system when calcined at 900°C, however, loses significant surface area as documented elsewhere[1] and, as a consequence, cannot maintain high levels of Pt in a dispersed phase. The key question which can be asked is, do ceria micro domain systems stabilize high Pt contents in a dispersed phase compared to bulk CeO_2 when calcined at high temperature? The answer to this question is one that laser Raman spectroscopy is well suited to address. In previous work[1] it was shown that the intensity of the strong Raman band at ca. 660 cm^{-1} was directly related to the concentration of the Pt-O surface structure interacting with the bulk ceria surface. In an exactly analogous way the Raman spectra for 2.5 and 5 wt% Pt on 50 Ce-50 Al calcined at 500°C shows an intense Raman band at ca. 660 cm^{-1}; see Figures 2 and 3. The Pt-O Raman band at 654 cm^{-1} can be normalized by comparison to the Raman bands at 564 and 452 cm^{-1} assigned to bands of crystalline CeO_2. Note that the Raman band of CeO_2 at ca. 450 cm^{-1} in Figures 2 and 3 are substantially reduced in intensity compared to those reported previously for bulk CeO_2. This remarkable low intensity is possibly due to disorder within the CeO_2 micro domains. The Raman spectra for 2.5 and 5 wt% Pt on 50 Ce-50 Al calcined at 900°C are shown in Figures 4 and 5. Note that intense Raman bands at ca. 660 cm^{-1} are maintained for both of these samples. This is compelling evidence that the micro domain CeO_2 structures within the alumina host have maintained a high capacity to maintain the Pt-O surface structure at high Pt concentrations in marked contrast to bulk CeO_2[1]. The normalized M-O Raman intensities for Rh, Ir, and Pt on 50 Ce-50 Al calcined at 500°C are shown in Figure 6.

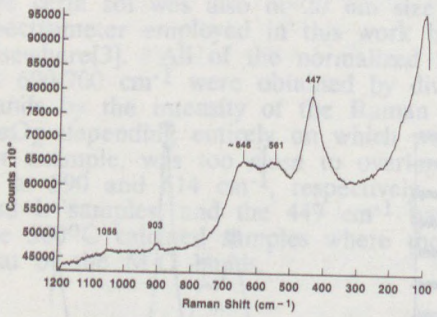

Figure 3. Raman spectrum of 5 wt % Pt on 50% CeO_2 - 50% Al_2O_3, calcined at 500°C, 2 hrs.

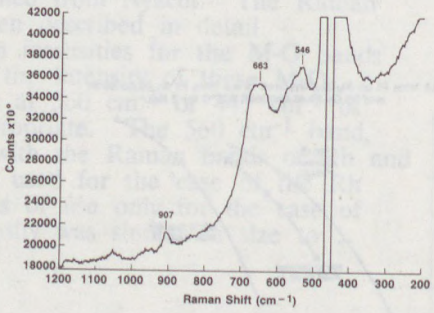

Figure 4. Raman spectrum of 2.5% Pt on 50% CeO_2 - 50% Al2O3, calcined at 900°C, 2 hrs.

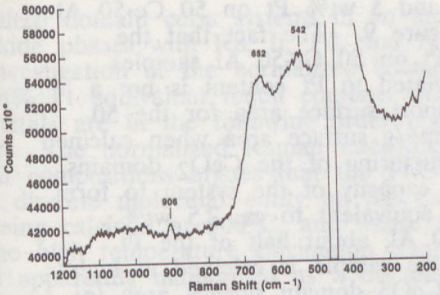

Figure 5. Raman spectrum of 5 wt % Pt on 50% CeO_2 - 50% Al_2O_3, calcined at 900°C, 2 hrs.

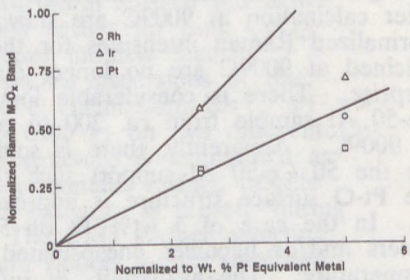

Figure 6. Normalized raman intensities versus normalized metal content for Rh, Ir, and Pt on 50% CeO_2,- 50% Al_2O_3, calcined at 500°C, 2 hrs.

The ability to use the normalized Raman intensity of the Pt-O surface structure as a direct measure of the M-O dispersion on bulk CeO_2 has been discussed previously[1]. It can be noted from Figure 6 that Rh and Pt show a normalized Raman band increasing proportionately to precious metal content, whereas Ir shows significant deviation from a linear relationship. This result for Ir is probably related to a marked tendency for Ir to sinter when calcined at 500°C in air compared to Rh and Pt[10]. In any case, a substantial percent of Ir is interacting with the micro domain CeO_2 surface as judged by the quite intense Raman bands at ca. 620 cm^{-1} for both the 2.4 and the 4.9 wt% Ir on 50 Ce-50 Al samples, see Figures 7 and 8.

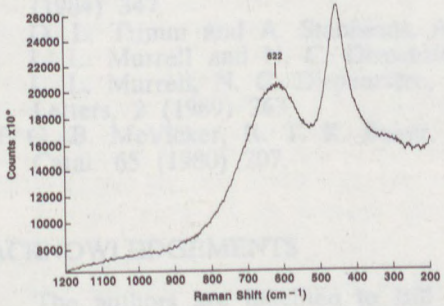

Figure 7. Raman spectrum of 2.4 wt % Ir on 50% CeO_2 - 50% Al_2O_3, calcined 500°C, 2 hrs.

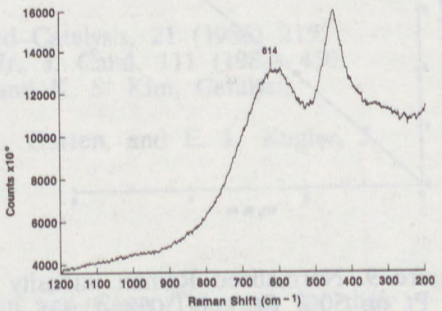

Figure 8. Raman spectrum of 4.9 wt % Ir on 50% CeO_2 - 50% Al_2O_3, calcined at 500°C, 2 hrs.

The relative Raman intensities for 2.5 and 5 wt% Pt on 50 Ce-50 Al after calcination at 900°C are shown in Figure 9. The fact that the normalized Raman intensities for the two Pt on 50 Ce-50 Al samples calcined at 900°C are no longer directly related to Pt content is not a surprise. There is considerable loss of support surface area for the 50 Ce-50 Al sample from ca. 200 to ca. 100 m^2/g surface area when calcined at 900°C. Apparently, there is some re-structuring of the CeO_2 domains for the 50 Ce-50 Al support such that the capacity of the system to form the Pt-O surface structure is approximately equivalent to ca. 2.5 wt% Pt. In the case of 5 wt% Pt on 50 Ce-50 Al, about half of the Pt sinters and/or becomes encapsulated when the sample is calcined at high temperature. The availability of sufficient CeO_2 domain surface area to bond to all of the Pt present in the 5% sample appears to not be a factor, because the normalized Raman intensity for 2.5 wt% Pt on 20 Ce-80 Al calcined at 500 and at 900°C is 2.6, very similar to that for the 2.5 wt% Pt on 50 Ce-50 Al sample, see Figure 6. The main conclusion from these investigations is that despite significant loss in surface area for the Ce-Al systems when calcined at 900°C that ca. 2.5 wt% Pt remains interacting with the ceria micro domain surface as sintering of the support occurs. Apparently, a quite significant amount of ceria surface capable of forming the Pt-O surface structure is maintained after high temperature calcination. Based on comparisons to the studies of bulk CeO_2 systems[1], one can conclude that in the case of 2.5 wt% Pt on either 20 Ce-80 Al or 50 Ce-50 Al that all of the Pt is present as a surface Pt-O phase after calcination at 900°C. In the case of 5 wt% Pt, half of the Pt either sinters or is encapsulated when calcined at 900°C, leaving the remaining half of the Pt highly-dispersed as the Pt-O surface structure.

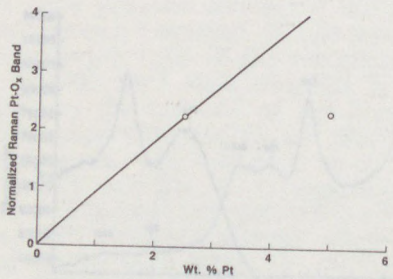

Figure 9. Normalized Raman intensity of Pt on 50% CeO_2 - 50% Al_2O_3, calcined at 900°C, 2 hrs.

4. CONCLUSIONS

Micro domains of CeO_2 formed within an alumina host structure are stable to calcination conditions of 900°C despite a substantial decrease in the composite Ce-Al support surface area. These ceria domains have the structure of "rice-grain" cylinders after calcination treatment, with much higher surface area than would be present for bulk CeO_2. The

micro domain ceria systems in an alumina host form surface interactive oxide phases with Rh, Ir, Pd, and Pt as found earlier for bulk CeO_2. Investigation of the normalized Raman intensities indicate that for 5 wt% Pt equivalent metal contents that the relative dispersions of the metals are in the following order after a 500°C calcination: Rh $\geq$ Pt >> Ir. The normalized Raman intensities of 2.5 wt% Pt on two different Ce-Al compositions argues that the Pt-O surface structure is maintained as a discrete molecular entity on the CeO_2 micro domain surface despite being calcined at 900°C, and where the Pt-O structure is present during the high temperature calcination treatment. The Pt-O surface structure is apparently maintained as a discrete structure bound to the stabilized CeO_2 domains which are, in turn, stabilized by the alumina host structure. At still high Pt contents some of the Pt is lost from the ceria domain surface to form a sintered and/or encapsulated structure during high temperature calcination. The Raman bands for the M-O structure were at 654 and 643 cm^{-1} for Pt and Pd, respectively, and at 618 and 590 cm^{-1} for Ir and Rh respectively, on CeO_2 micro domains.

5. REFERENCES

1 L. L. Murrell, S. J. Tauster, and D. R. Anderson, Proceedings, 2nd Inter. Congress on Catal. and Automotive Pollution Control, CAPoC, Brussels, Belgium (1990) 275.
2 L. L. Murrell, S. J. Tauster, Proceedings, 2nd Inter. Congress on Catal. and Automotive Pollution Control, CAPoC, Brussels, Belgium (1990) 547.
3 I. E. Wachs, F. D. Hardcastle, S. S. Chan, Spectrosc. 1 (1986) 30.
4 A. Baiher, P. Dollenmeier, M. Glinski, A. Reller, and V. K. Sharma, J. Catal. 111 (1988) 273.
5 T. H. Vanderspurt and M. A. Richard, Mater. Res. Soc. Symp. Proc., 111 (1988) 341.
6 R. Roy, S. Komarneni, and D. M. Roy, Mater. Res. Soc. Symp. Proc., 32 (1984) 347.
7 D. L. Trimm and A. Stanislaus, Applied Catalysis, 21 (1986) 215.
8 L. L. Murrell and N. C. Dispenziere, Jr., J. Catal. 111 (1988) 450.
9 L. L. Murrell, N. C. Dispenziere, Jr., and K. S. Kim, Catalysis Letters, 2 (1989) 263.
10 G. B. McVicker, R. T. K. Baker, R. L. Garten, and E. L. Kugler, J. Catal. 65 (1980) 207.

ACKNOWLEDGEMENTS

The authors are indebted to Bill Larsen and Cesar Tolentino for their fine experimental expertise in the preparation of these systems, and to many fruitful discussions with Nyacol personnel during the course of this work, especially Tom Swank and Bob Lurie.

DISCUSSION

Q: F. Bozon-Verduraz (France)

1) Could you comment about the nature of the interaction of the precious metal with the CeO_2 microdomains after the calcination pretreatment and in reducing conditions (ethane hydrogenolysis) ?

2) Ceria is known to chemisorb significant quantities of CO. Did you take it into account on your platinum dispersion measurements ?

A: L. L. Murrell

1) In our work we used both pulsed CO chemisorption and static CO chemisorption to determine the metal dispersion following reduction in flowing H_2 at 500 ^{0}C for CeO_2 of ca. 130 m^2/g surface area. For our high purity ceria support there was not a large uptake of CO by either the pulsed or the static method. Professor J. Kaspar has reported very significant CO uptake on CeO_2 prepared by precipitation from $Ce(NO_3)_3$ solutions. More work will be required to explain the apparent differences seen from different CeO_2 supports used in various laboratories.

2) All of the Group VIII metals, Rh, Ir, Pd and Pt, form the same interactive M-O group with the microdomain ceria surface similar to that obtained for high purity bulk CeO_2. When the samples are investigated for ethane hydrogenolysis activity they are reduced in H_2 at 400 ^{0}C which converts the M-O surface structures to zero valent Group VIII metal atoms/clusters.

Q: S. I. Woo (Korea)

Bulk PtO_2 decomposed above 500 ^{0}C and Pt oxide species supported on alumina also decomposed above 550 ^{0}C as reported in the literature. How can you assign the Pt-O relating band in the Raman spectra of Pt oxide is stable due to the stabilization of CeO_2, what is the stabilization mechanism ? Is there any differences in the stretching vibration of Pt-O between Pt oxides calcined at 500 ^{0}C and Pt oxides calcined at 900 ^{0}C ?

A: L. L. Murrell

The interaction between Pt and the surface of ceria results in the valence stabilization of Pt in a 2+ oxidation state. Since this is also true for Rh, Ir and Pd, there appears to be a specific density of such M-O interactive sites which, in the case of Pt, prevent the transformation of the surface phase Pt-O complex to Pt. The Raman spectra show that PtO on ceria micro domains have exactly the same Pt-O frequency calcined at either 500 or 900 ^{0}C. This frequency invariance is due to separation of the M-O groups on the ceria micro domain surface by ca. 1 nm, similar to that reported previously for bulk CeO_2. The stabilization observed at 900 ^{0}C for PtO on ceria micro domains is simply a reflection that the ceria domains are stabilized within the alumina host structure so that a high ceria surface area is maintained at 900 ^{0}C. This is quite different than bulk ceria which does not have a stable surface area when calcined at 900 ^{0}C.

Q: Wm. C. Conner (USA)

What are the differences in pore structure for CeO_2/Al_2O_3 compared to the pure Al_2O_3 support ? How do you explain the resultant pore morphology based on the physical picture you draw of the CeO_2 in a Al_2O_3 framework ?

A: L. L. Murrell

It is recognized that this is an important and fundamental question related to any oxide prepared by mixed sol synthesis procedures. The mixed ceria-alumina composites made by sol synthesis fall into two extremes of ceria morphology within the alumina acting as the host structure. For both extremes of ceria morphology, stocky cylinders or thin rods, the pore size and the pore volume of the ceria-alumina composites are essentially identical to that of the

alumina itself. This is even true at a 50% ceria-50% alumina composition. The reason for this in the case of high ceria compositions(> 10% ceria) is simply that the crystalline CeO_2 domains within the alumina host are very close to the same size as that of the alumina primary particles, i.e., 20 nm diameter. Therefore, the pore size is produced by primary particles of alumina or ceria of about equal size so that the pore size distribution and pore volume is not altered by substituting ceria for alumina. Thin rod shapes are observed by transmission electron microscopy only for ceria contents below 5wt% when a 1 nm size ceria sol is used as a precursor. At these low ceria contents the thin rods can not alter the pore volume of the alumina host structure in a significant way.

Q: J. C. Conesa (Spain)
I would say that with a such highly dispersed system, showing strong Pt-Ce interaction, EXAFS would be a technique of choice to characterize the system. Have you been able to get data of this kind on your samples ?

A: L. L. Murrell
I would agree that EXAFS of the surface phase oxide structures of the platinum group metals interacting with CeO_2 surface sites would be very informative. Such studies could help us understand the structures responsible for the "redox-center-stabilization" between the M-O functions (seen by Raman spectroscopy) and the specific sites on CeO_2 which form these very high temperature stable surface groups. Such studies were beyond the expertise in our laboratory at the time the work was done.

Q: D. G. Blackmond (USA)
The ethane hydrogenolysis results for the Pt-Ce-Al systems demonstrate that not only does the Ce help to maintain the small particle size of the Pt, but CeO_2 is also prevented from "decorating" these crystallites as has been observed to happen with combinations of noble metals and reducible oxides. Is this a function of the preparation method ?

A: L. L. Murrell
The ethane hydrogenolysis (EH) results are for samples calcined at high temperature followed by reduction in H_2 at 400 ^{0}C. The EH activity of such samples is not greatly different compared to Pt on alumina as a reference reduced at 400 ^{0}C also. At least for a 400 ^{0}C reduction temperature reduced-ceria-species do not seem to be covering the active zero valent metal clusters. A. Datye has observed evidence that for 500 ^{0}C reduction temperatures, some decrease in EH activity occurs compared to a 400 ^{0}C reduced sample. Therefore, it is possible that ceria is capable of typical-SMSI decoration behavior, and/or interaction with surface and sub-surface reduced Ce centers, but at directionally higher reduction temperatures than observed for TiO_2.

Q: M. Ichikawa (Japan)
I would touch on the function of CeO_x to stabilize Pt particles in keeping high dispersion. Seems that some PtO_x is volatile under the strong calcination and high-temperature oxidation reaction. CeO_x would suppress the volatility of PtO_x in forming Pt-O-Ce bonding ? Otherwise, CeO_x is overlayered on Pt particles or Ce(III)/Ce(IV) ion acts as anchor to fix the Pt particle ? Do you have any evidence to discuss the chemistry of CeO_x to promote the stabilization of Pt particle? We have observed the similar promotion of CeO_x on Pd-CeO_x catalysts for CO_2 + toluene conversion, where we discuss on the CeO_x promotion due to its oxygen-reversion and redox-cycle of Ce(III)/Ce(IV).

A: L. L. Murrell
There is no evidence of the PtO surface phase oxide groups on either bulk CeO_2, or on micro domains of CeO_2 within an alumina host being volatile even at 900 ^{0}C. The MO groups (M = Rh, Ir, Pd, Pt) all form the same surface density of oxide groups, probably

interacting to give a M^{d+} - $Ce^{(4-d/2)+}$ interaction. Perhaps the best model is valence stabilization of the platinum group metals similar to Fe(II), interacting with the surface Lewis acid centers of TiO_2. Once the platinum group metal oxides are reduced in flowing H_2, then the CeO_2 support does not have a high stabilization capacity toward the zero valent metal at high temperatures. The stabilization at 900 ^{0}C in oxygen of 2.5 wt% Pt on ceria micro domain is directly related to interaction of PtO with a micro domain ceria phase with an effective CeO_2 surface area of ca. 60 m^2/g for the 50 Ce-50 Al composite described in the paper.

Q: C. H. Bartholomew (USA)

I have two related questions:

1) Did I hear you say that Pt-O structures are only stable one the CeO_2 microdomains? Why is not Pt-O stable on a CeO_2 coating that interacts strongly with Al_2O_3 ? Several patents have claimed that CeO_2 thermally stabilized Pt and Pd on alumina.

2) Pd/Ce/alumina systems are reported to have great thermal stability in oxidizing atmosphere to very high temperatures. Is the some phenomenon operating from the Pd-ceria-alumina system ?

A: L. L. Murrell

All of the platinum group metals, Rh, Ir, Pd, and Pt, form the surface phase M-O groups on both bulk ceria, and on micro domain ceria. Careful studies of CeO_2-coated aluminas where no CeO_2 crystals were present showed no high temperature stabilization capacity towards Pt, and no evidence that a Pt-O structure was present on the surface of the ceria-doped alumina. On some aluminas, for unknown reasons, the surface ceria-doped phase will partially transform to micro crystals upon calcination at > 600 ^{0}C of ca. 7 nm size based on X-ray diffraction. If such CeO_2 crystals are present in the patents mentioned, the stabilization could be provided by either X-ray detectable CeO_2 particles or by X-ray undetectable CeO_2 particles.

In the case of Pd/Ce/alumina systems stable to high temperatures, I would expect that in the absence of CeO_2 microcrystals the stability of Pd/Ce/alumina would be analogous to Pd/La/alumina or Pd/Ba/alumina. The Ce, La, and Ba components act as stabilizers of the alumina phase which is itself a strongly interactive phase towards PdO in high temperature oxidizing environments. Pd does form predominantly a Pd-O surface phase complex with the ceria micro domain surface within an alumina host structure rather than form a PdO phase on the alumina surface.

Guczi, L. *et al.* (Editors), *New Frontiers in Catalysis*
Proceedings of the 10th International Congress on Catalysis, 19-24 July, 1992, Budapest, Hungary
© 1993 Elsevier Science Publishers B.V. All rights reserved

DIRECT PROPANE AMMOXIDATION TO ACRYLONITRILE: KINETICS AND NATURE OF THE ACTIVE PHASE

A. Andersson[a], S. L. T. Andersson[a], G. Centi[c], R. K. Grasselli[b], M. Sanati[a] and F. Trifiro[c]

[a]Dept. of Chem. Techn., Chemical Center, Univ. of Lund, P.O.Box 124, 221 00 Lund, Sweden
[b]Dept. of Chem., Georgetown University, Washington, CD 20057, USA (Presently Central Research Lab., Mobil, Princeton, New Jersey, USA)
[c]Dept. of Ind. Chem. & Materials, V. le Risorgimento 4, 40136 Bologna, Italy

The kinetics of the direct synthesis of acrylonitrile from propane on V-Sb-Al-(W) mixed oxides indicate that acrylonitrile (ACN) forms by two parallel pathways, one directly from propane and the second, which is the prevalent path, through the intermediate formation of propylene (C_3=). The limiting factor in the formation of ACN is the relative slowness of the step of allylic oxidation to ACN of the intermediate C_3=, and the higher rate of C_3= oxidation to carbon oxides as compared to that of ACN to CO_x. The step of C_3= oxidation to ACN is controlled by the surface availability of NH_3 which, in turn, depends considerably on the side reaction of NH_3 oxidation to N_2. The catalytic behavior of different modified V-Sb-(Al)-O systems and their characterization by X-ray diffraction analysis and Raman, Infrared and X-ray Photoelectron spectroscopies indicate that *i)* a reduction of both V and Sb occurs during the catalytic reaction, *ii)* the presence of vanadium not stabilized in the rutile-like phase is responsible for the side reaction of NH_3 oxidation and lowering of the selectivity, *iii)* alumina reacts with antimony forming an $AlSbO_4$ rutile phase which could be epitaxially intergrown or in solid solution with the $VSbO_4/Sb_2O_4$ system, which, in turn, limits the presence of not stabilized (unselective) vanadium species, and *iv)* antimony oxide supported on alumina is also selective in propane ammoxidation, but forming acetonitrile as the main product. The doping with vanadium of this sample increases slightly the activity, but especially gives rise to the formation of acrylonitrile instead of acetonitrile.

Introduction

There is increasing interest in the development of a process for direct acrylonitrile synthesis as an alternative to the conventional method based on the olefinic feedstock [1,2], and recently it was announced that commercialization of the process would be possible in a few years. Multicomponent metal oxide catalysts based on V, Sb, W, Mo and other elements have been patented for this reaction [3-7, and references therein], but an analysis of the patent data indicates that catalysts based on V-antimonate, in particular, seem to be the most promising [4-6].

In this paper we report the results of extensive research on V-antimonate based catalysts directed towards the development of a more rational approach to the design of catalytic systems for direct propane ammoxidation to acrylonitrile. The approach involved *(i)* a kinetic study of the reaction in order to identify the role of the competitive pathways of transformation and *(ii)* combined catalytic and physico-chemical characterization of modified systems in order to establish correlations between catalytic behavior and surface or structural features.

Experimental

The catalysts were prepared, according to patent indications [1,2], using a slurry procedure (over 16 hours under stirring and reflux) with Sb_2O_3, NH_4VO_3, ammonium-tungstate and alumina or $Al(OH)_3$ as the starting compounds. The solid was dried and then calcined up to 600-900°C (as specified in the text) with a heating rate of about 50°C/hours. The surface area of the vanadium-antimonate samples without alumina was in the 10-15 m^2/g range, and about 10 times higher for the samples containing alumina. Further details on the characterization of the samples and on the method of preparation have been reported previously [3-7].

The catalytic tests were made in a fixed-bed quartz tubular flow reactor (with a catalyst charge of about 2-7 grams diluted with quartz spheres) [6] working at atmospheric pressure, with on-line gas chromatographic analyses of reagents and products. HCN and NH_3 conversions were determined by titration after adsorption in 0.1 N NaOH solution, as described elsewhere [6]. Preliminary tests as well as calculations indicate that mass and heat transfer limitations may be considered negligible in our experimental conditions. Homogeneous gas-phase reactions were also checked and found to be negligible in our experimental conditions.

The samples were characterized by X-ray diffraction analysis (XRD), Raman and infrared spectroscopies, and X-ray photoelectron spectroscopy (XPS). In particular, XPS analyses were carried out using a Kratos XSAM 800 instrument with Mg K_α x-ray radiation and using the Au $4f_{7/2}$ peak (84.0 eV) to correct for the charge effect. Quantitative determinations were made by correcting the ratios of the peak areas (Al_{2p}, $V_{2p3/2}$, $Sb_{3d3/2}$ and W_{4d}) of the analyzed elements for the instrumental sensitivities for the various core lines measured for the pure oxides. The $V_{2p3/2}$ intensity was calculated after subtraction of O_{1s} and $Sb_{3d5/2}$ lines generated by the Mg $K_{\alpha 3,4}$ satellites. Raman spectra were recorded on a Bruker IFS66/FRA106 fourier-transformed instrument. Infrared spectra were recorded using a Perkin-Elmer 1700 Fourier-transform instrument.

Results and Discussion

Kinetics and Reaction Network

In order to obtain reliable information on the kinetics and reaction network in propane ammoxidation on V-Sb-Al based mixed oxides, a catalyst formulation and method of preparation analogous to those reported for the best patented catalysts [1,2] was adopted. We shall therefore refer in this section to a V-Sb-Al mixed oxide doped with tungsten; the V:Sb:W atomic ratio is 1:5:1 and the composition is 30% wt of active phase (assumed to be $VSbO_4+2Sb_2O_4+WO_3$) and 70% wt of alumina. The preparation of this sample involves *i)* a two electron redox reaction in aqueous ammonia solution between Sb^{III} and V^V starting from Sb_2O_3 and NH_4VO_3, *ii)* the addition of ammonium tungstate and formation of the mixed hydroxide containing V^{IV} (V^{III} formed in the previous step is oxidized by O_2 dissolved in solution), Sb^{III}, Sb^V and W^{VI} by H_2O/NH_3 removal, and *iii)* drying and calcination up to a final calcination temperature of 650°C [4,6]. The surface areas of the resulting samples are about 110 m^2/g and do not change after catalytic tests.

Reported in Fig. 1 are the results of tubular-flow-reactor tests carried out at 520°C in differential reaction conditions (conversion of the three reagents below about 5%). In these condi-

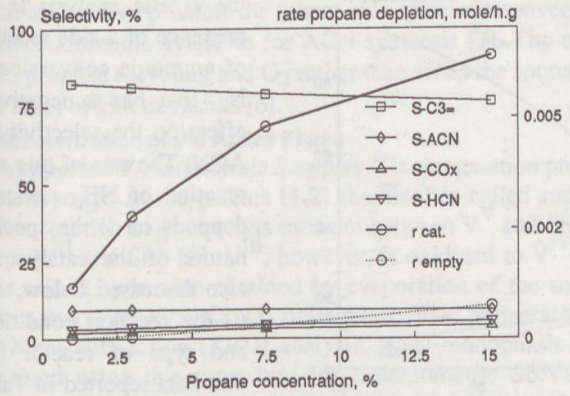

Fig. 1 Rate (r) of propane conversion at 520°C and selectivity to propylene (C_3=), acrylonitrile (ACN) and CO_x as a function of propane concentration for reagent conversions below 5%. *Exp.* : 0.5 g of catalyst (as described in the text), 15.1% O_2, 7.3% NH_3.The dotted line shows the rate of propane depletion in the empty reactor measured to test the contribution of homogeneous reactions.

tions a highly selective transformation of propane to propylene (C_3=) takes place. Acrylonitrile (ACN) forms with a selectivity of about 8-10% and other reaction products (HCN, acetonitrile, carbon oxides and C_1-C_2 hydrocarbons) form with selectivities in the 0-4% range. It should also be noted that the rate of propane transformation increases with increasing alkane concentration following a Langmuir-Hinshelwood model with saturation of the active sites, but the rate of alkane transformation due to homogeneous reactions (empty reactor) is much lower in all ranges investigated.

Reported in Fig. 2 are the results of tests carried out in integral reaction conditions with varying amounts of catalyst at fixed reaction temperature. The composition of the reagent mixture corresponds to that reported in various patents as optimal [1,2]. The selectivity to C_3= decreases continuously with increasing contact time and propane conversion, whereas the ACN selectivity passes through a maximum for a propane conversion of around 40-50%. For higher propane, but also higher ammonia, conversions the selectivity decreases with a parallel increase in the formation of carbon oxides. The maximum in the yield to ACN is obtained for propane conversions around 70-80%. Figures 1 and 2 thus show that propylene is the primary product of propane transformation, whereas ACN forms mainly by consecutive transformation of the C_3= intermediate. The formation of carbon oxides competes with the reaction for the formation of ACN, especially at the higher propane and ammonia conversions.

These data, in combination with a more extensive analysis of the dependence of product formation on reagent concentration, space-velocity and reaction temperature [6] allows the development of a kinetic model of the reaction. The reaction network can be described by six parallel reactions of formation (C_3=, ACN, carbon oxides, acetonitrile, HCN and C_2 hydrocarbons), three reactions of consecutive transformation of the intermediate C_3= to ACN, acetonitrile and HCN, five consecutive reactions of consecutive decomposition to carbon oxides of the other products, and one side reaction of NH_3 oxidation to N_2. Based on a Langmuir-Hinshelwood approach for the reaction rates, it is possible to derive rate and adsorption constants that fit the experimental data over a wide range of reagent compositions (0-20% for propane, oxygen and ammonia) and reaction temperatures (410-530°C) [6]. The lines in Fig. 2 were calculated from the kinetic model and the symbols represent experimental data.

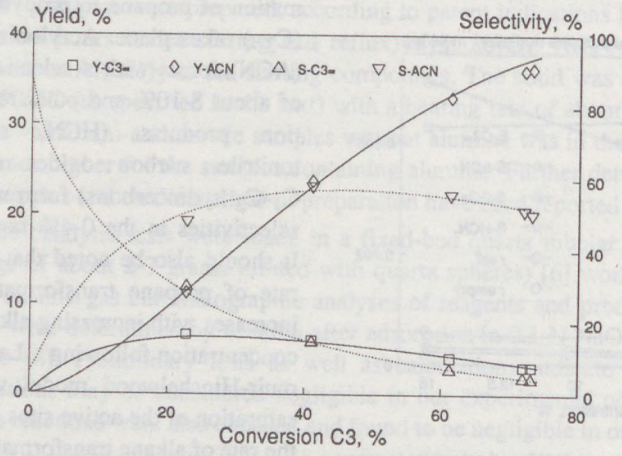

Fig. 2 Yield (Y) and selectivity (S) to propylene (C_3=) and acrylonitrile (ACN) as a function of propane conversion. *Exp.*: temp., 520°C; C_3, 5.62%; O_2, 11.8%; NH_3, 11.8%; catalyst as described in the text, total flow rate 3.6 L/h. ***Symbols***: experimental values. ***Lines***: calculated values from the kinetic model [6].

An especially important aspect that emerges from the kinetic analysis is the presence of a side reaction of ammonia conversion to N_2, that has a negatively effect on the selectivity to ACN. The rate of this side reaction of NH_3 critically depends on *i)* the specific nature of the catalyst, as also discussed below, and *ii)* the reaction conditions and type of reactor [7]. The data reported in Table 1 illustrate how the maximum selectivity to ACN obtained (and relative propane and NH_3 conversions) depends on the NH_3 to propane inlet ratio. NH_3 to C_3 ratios higher than the stoichiometric value of 1.0 are necessary to increase the selectivity and especially the propane conversion corresponding to the maximum in the selectivity. It is also shown that the maximum in ACN selectivity is obtained for relatively low NH_3 conversions.

Table 1 Maximum selectivity to acrylonitrile (ACN) and ammonia and propane conversions corresponding to the maximum in ACN selectivity as a function of the inlet ammonia to propane ratio. *Exp.*: temp., 500°C; propane, 5.9%; O_2 to propane, 2.1.

NH_3/C_3	Max. ACN selectivity, %	conv. for max.ACN selectivity, %	
		NH_3	C_3
0.5	41	43	23
0.9	49	42	30
1.3	53	36	36
1.8	55	29	40
2.2	56	27	42

In conclusion, the kinetics and reaction network analysis show that *i)* ACN forms mainly from the C_3= intermediate, *ii)* the limiting factor in the formation of ACN is the relative slowness of the C_3= to ACN step compared to competitive unselective pathways, and *iii)* the presence of a side reaction of NH_3 oxidation limits the effectively available surface ammonia for ACN synthesis. This also explains why apparently in the V-Sb-W-Al mixed oxide system it is more critical to achieve the C_3= to ACN step as compared to the propane to C_3= step, notwithstanding the different reactivities of olefinic and paraffinic hydrocarbons. It is worth noting also that in all cases (see Fig. 2) not converted C_3= is found together with ACN; this aspect agrees with patented results [1,2].

Kinetics and reaction network analysis also suggest future work in the area of co-catalysts to enhance the C_3= to ACN conversion. Also of critical importance is suitable doping in order to limit as much as possible the rate of side ammonia conversion and to achieve an increase in the surface ammonia available for ACN synthesis [7]. The use of high propane/(O_2+NH_3) ratios with propane recycling and O_2 rather than air as the source of feed oxygen is also suggested on the basis of kinetic results [6].

Characterization of the Active Phase

Unsupported V-Antimonate Samples. The preparation procedure for V-antimonate based catalysts reported in the patents [1,2] (hereinafter called *slurry* method) involves a two electron redox reaction in an aqueous medium between V^V and Sb^{III} (added as NH_4VO_3 and Sb_2O_3) to form V^{III} and Sb^V [8]; V^{III}, however, is oxidized to V^{IV} by the O_2 dissolved in the solution. The mixed hydroxide obtained by evaporation of the solution and drying of the solid transforms to a crystalline $VSbO_4$ rutile phase [9] at temperatures in the 500-700°C range, as shown by X-ray diffraction (XRD) analysis. XRD monophasic samples with rutile structure can be obtained using this procedure for stoichiometric Sb:V=1.0 samples, but infrared (IR) and Raman spectra suggest that these samples are not monophasic. In fact, IR spectra (Fig. 3) show the presence of a band at 1020 cm^{-1} and two strong shoulders at around 920 and 850 cm^{-1} that cannot be attributed to the V-antimonate rutile phase [10,11], characterized from bands at about 740, 660 and 550 cm^{-1}, due to $\nu_{Sb\text{-}O}$ vibrations. The former bands suggest the presence of an XRD amorphous, partially reduced, vanadium-oxide that has not reacted to form the rutile phase. In addition, it is reasonable to assume that unreacted antimony oxide is also present, even though not detected. As shown in Fig. 3 the relative intensities of these bands due to unreacted vanadium-oxide with respect to those of the rutile phase depend on the preparation method. For example, compared in Fig. 3 are the IR spectra of two samples with a Sb:V ratio of 1.0, but prepared by solid state reaction between V_2O_5 and Sb_2O_3 (**a**) and by the slurry method (**b**). Both samples were calcined at 600°C for 6 hours. In agreement, Raman spectra of these samples show the presence of very broad and not well re-

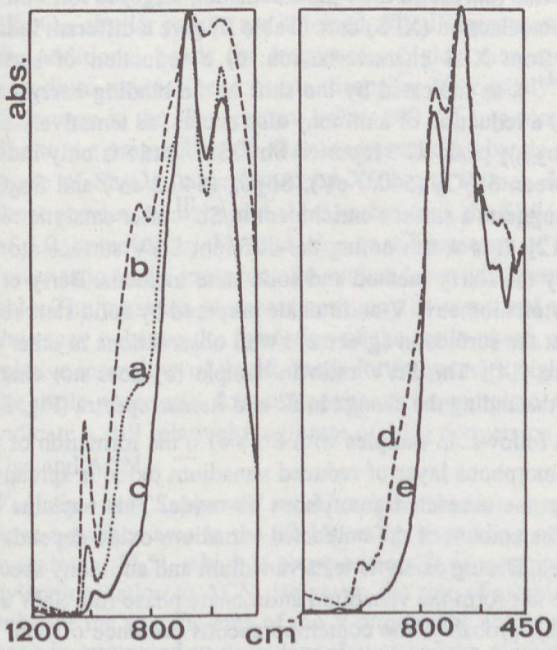

Fig. 3 Infrared spectra (KBr technique) of a fresh Sb:V =1.0 sample prepared by the solid state (**a**) or slurry method (**b**), of used Sb:V=1.0 sample (**c**) (sample b after propane ammoxidation), of fresh and used Sb:V=5.0 sample (preparation by slurry method) (**d** and **e**, respectively).

Table II X-ray photoelectron spectra for unsupported Sb-V-O catalysts. The indicative Sb^{3+}/Sb^{5+} ratio was obtained by fitting components for Sb_2O_3 and Sb_6O_{13} to $Sb_{3d5/2}$ spectra and correcting fora mean valence of 4.33 for Sb_6O_{13}

Sb:V bulk	*Preparation*	Binding energies and *peak width at half height* (in the brackets)		*Surface Sb/V*	*Indicative* Sb^{3+}/Sb^{5+}
		$Sb_{3d3/2}$	$V_{2p3/2}$		
1.0	slurry - *fresh*	540.1 (*1.6*)	517.1 (*1.7*)	0.66	89/11
1.0	slurry - *used*	540.0 (*1.6*)	516.4 (*2.6*)	0.56	100/0
1.0	solid state - *used*	540.4 (*2.1*)	516.6 (*2.1*)	1.2	66/34
5.0	slurry - *fresh*	540.3 (*2.2*)	516.8 (*2.0*)	2.8	68/32
5.0	slurry - *used*	540.1 (*2.1*)	516.2 (*2.1*)	3.8	91/09

solved bands centred at approximately 860 and 400 cm^{-1} in sample (a) and additional weak, but sharper, bands at 995, 700, 284 and 145 cm^{-1} in sample (b)due to V_2O_5. No bands due to antimony oxides were detected in these samples. After catalytic tests in propane ammoxidation, the IR bands at frequencies higher than around 800 cm^{-1} decrease considerably in intensity (Fig. 3) and similar IR spectra are found independently of the preparation. Raman spectra also indicate the disappearence of the band at 860 cm^{-1} as well as V_2O_5 bands, when present.

Thus, apparently, during the catalytic reaction an *in-situ* evolution occurs leading to the further reaction of V-oxide and Sb- oxide (unreacted after the calcination stage) to form the V-antimonate phase. However, X-ray photoelectron (XPS) data (Table II) give a different indication. The following aspects derive from XPS characterization: *a)* a reduction of surface vanadium species occurs (forming V^{4+}), as indicated by the shift in the binding energy and broadening of the $V_{2p3/2}$ peak, and *b)* a reduction of antimony also occurs, as tentatively suggested by the deconvolution of the $Sb_{3d5/2}$ peak. The reported Sb^{3+}/Sb^{5+} ratio is only indicative, because of the small shifts between Sb_2O_3 (540.0 eV), Sb_2O_4 (540.2 eV) and Sb_6O_{13} (540.7 eV); nevertheless the change suggests a surface enrichment in Sb^{III} after catalytic reaction as found also in Sb-Sn oxides [12]. It is worth noting the different Sb/V surface atomic ratio between the samples prepared by the slurry method and solid state methods. Berry et al. [13] in their XPS characterization of stoichiometric V-antimonate prepared by solid state reaction also an enrichment of antimony at the surface in agreement with observations in other antimonate systems with rutile structure [14]. The Sb/V ratio in sample (b) does not change greatly after reaction (Table II), notwithstanding the change in IR and Raman spectra (Fig. 3).

These results can be interpreted as follows. In samples with Sb:V=1.0 the formation of the rutile phase is not complete, but an amorphous layer of reduced vanadium oxide is spread on the $VSbO_4$ particles, and probably on the unreacted amorphous Sb-oxide. This explains the surface enrichment with vanadium. The amount of the unreacted vanadium-oxide depends on the method used to prepare the samples. During catalytic tests vanadium and antimony species are reduced, as shown by XPS, but do not form the vanadium antimonate phase (the Sb/V surface ratio does not change very much); probably, the contemporaneous presence of both reduced vanadium (V^{3+} or V^{4+}) and oxidized antimony (Sb^{5+}) is required [5]. It is reasonable to assume that the latter aspect is inhibited during reaction.

The presence of unreacted surface vanadium-oxide has a considerable influence on the cata-

Table III Catalytic tests in propane ammoxidation of unsupported Sb-V-O catalysts. Exp. cond.: 2 g of catalyst, reaction temp., 510°C, propane, 6.62 ; O_2, 16.9%; NH_3, 9.6%. [AcCN indicates acetonitrile, other symbols as in text].

Sb:V bulk	*Preparation*	*conversion, %*		*selectivity, %*					
		propane	NH_3 to N_2	C_3=	ACN	AcCN	CO	CO_2	HCN
1.0	slurry - *fresh*	34.8	90.3	8.3	1.2	0.9	37.8	38.9	11.7
1.0	slurry - *used*	20.3	43.2	30.8	10.5	3.5	17.4	15.9	18.9
1.0	solid state - *used*	22.4	31.5	36.7	18.9	2.8	16.1	10.4	15.1
5.0	slurry- *fresh*	33.4	79.1	16.9	9.8	3.7	33.4	19.1	16.9
5.0	slurry - *used*	21.9	36.6	33.4	16.9	3.1	16.8	14.3	14.7

lytic behavior in propane ammoxidation, as shown in Table III. The fresh sample is not selective and forms mainly carbon oxides, due to the very high rate of side conversion of NH_3 to N_2. The *in-situ* evolution, as discussed above, leads to an increase in the selectivity to both C_3= and ACN, and a parallel decrease in propane conversion, but especially a decrease in the NH_3 side conversion to N_2. It should also be noted that the sample with a higher surface Sb/V atomic ratio, but equal bulk stoichiometric ratio, shows a lower rate of NH_3 oxidation to N_2 and an enhanced selectivity, even though lower than that shown by alumina supported samples.

In the unsupported V-Sb samples with an Sb:V atomic ratio higher than stoichiometric for $VSbO_4$, similar results are obtained. The IR spectrum (Fig. 3) of the fresh sample also shows the additional bands for frequencies higher than around 800 cm^{-1} attributed to unreacted vanadium-oxide. These bands disappear after catalytic tests in propane ammoxidation. The difference in the IR spectrum below 800 cm^{-1} as compared to that of the V:Sb=1.0 sample is due to the presence of Sb_2O_4 characterized by bands at 765, 750, 660 and 615 cm^{-1}. The presence of Sb_2O_4 is confirmed by XRD and Raman data. The XPS indications are similar to those previously discussed. Also in this case, the Sb/V atomic ratio is lower than the bulk value of 5.0, however, in this case, due to the presence of Sb_2O_4 crystallites, the attribution of the lower ratio to the presence of a surface layer with unreacted vanadium-oxide is more questionable. The presence of excess antimony as compared to the stoichiometric amount for $VSbO_4$ thus may enhance the formation of the rutile phase, as suggested also by the decrease in the relative intensities of the IR bands for frequencies higher than 800 cm^{-1}. Even so, formation of the rutile phase still does not appear to be complete. Catalytic data (Table III), in agreement, indicate a still relatively high rate of NH_3 conversion to N_2 and relatively low selectivities to C_3= and ACN.

V-Antimonate Supported on Alumina. Alumina-supported V-antimonate catalysts generally have a surface area in the 80-150 m^2/g, depending on calcination temperature and method of preparation [4,5], which is about one order of magnitude higher than that of catalysts for propylene oxidation to ACN. However, the role of alumina is not just that of a simple support to enhance the specific area of the V-antimonate active phase due to the lower reactivity of propane as compared to propylene, but rather the alumina interacts directly with both antimony and vanadium modifying the nature of the active component.

In fact, Sb_2O_4 reacts with Al_2O_3 forming the rutile $AlSbO_4$ phase, isostructural with $VSbO_4$. The reaction between Sb_2O_4 and Al_2O_3 occurs in the 800-900°C temperature range of

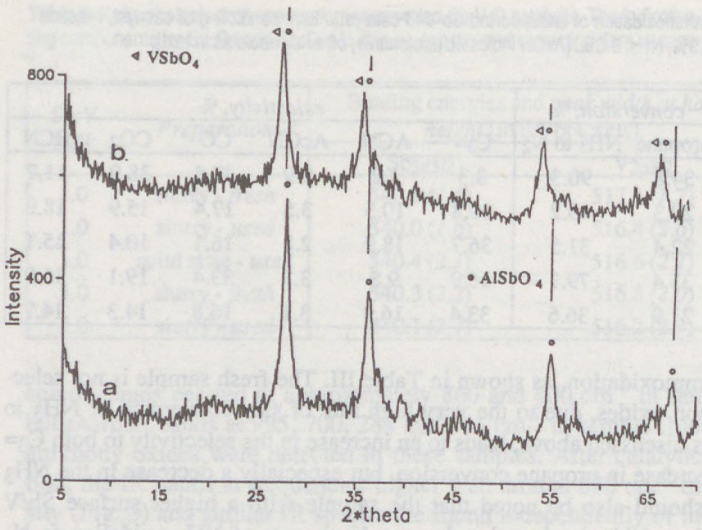

Fig. 4 XRD patterns for Sb-oxide [30% wt] on alumina and calcined at 900°C (a) and subsequently doped with 1% wt (as V_2O_5) of vanadium and calcined again at 900°C (b).

calcination, but in the presence of V the reaction occurs at lower temperatures, in the 700-800°C range. Reported in Figure 4 is the XRD pattern of $AlSbO_4$ formed by solid state reaction between Sb_2O_4 and alumina. Both the method of preparation and the amount of antimony oxide employed are equivalent to that used in the preparation of patented V- antimonate on alumina catalysts [1,2] (see also previous section). The cell parameters of the $AlSbO_4$ phase correspond well to those reported in the literature [10]. When this sample is doped with 1% wt of vanadium-oxide (corresponding to a Sb:V ratio of 10) a shift is observed in the diffraction line (Fig. 4) towards the position found for $VSbO_4$. The cell parameters, accordingly, are intermediate between those of $AlSbO_4$ (a=b=4.51 and c=2.96 Å [10]) and those reported for $VSbO_4$ (a=b=4.61 and c=3.06 Å [9,15]). The extent of modification is proportional to the amount of vanadium introduced. This indicates that V reacts with $AlSbO_4$ to form a solid solution or intergrown phase. No XRD lines due to vanadium- or antimony-oxide are detected. In samples prepared directly with Sb,V and alumina similar observations can be made upon changing the relative amount of alumina with respect to the amount of active phase. Also in this case the cell parameters of the alumina-supported V-antimonate are found to be intermediate between those of Al- and V-antimonate. For these samples, a crystalline rutile phase is detected for calcination temperatures in the 700-800°C range, slightly higher than those used for the catalytic tests (around 650°C), but lower than those required to form the $AlSbO_4$ phase in the absence of vanadium.

Reported in Fig. 5 is the comparison of the catalytic behavior of the sample of antimony oxide on alumina, calcined at 900°C (sample a of Fig. 4) with that of the same sample, but doped with 1% vanadium (sample b of Fig. 4). Tests were carried out at low conversion in order to evidence the initial selectivity of the catalysts more clearly. Doping of the $AlSbO_4/Al_2O_3$ matrix with vanadium leads to a relatively small modification in the activity, but a drastic change in the selectivity. Sb-supported on alumina or $AlSbO_4$ catalysts are capable of selective activation of propane, but mainly towards acetonitrile. On the contrary, when V is introduced in the Al-antimonate rutile matrix, as indicated from XRD data (Fig. 4), ACN forms with relatively high selectivity. It should be noted that 1% wt of vanadium corresponds to a Sb:V = 10 ratio and thus to about half the vanadium present in the samples prepared according to patent indications [1,2]. The NH_3 side conversion is relatively low in both

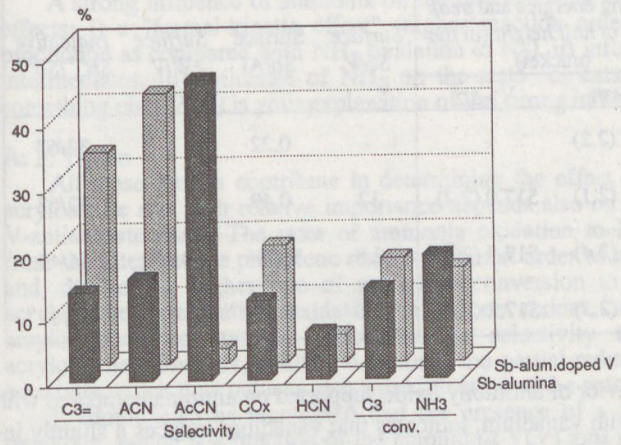

Fig. 5 Comparison of the catalytic behavior of samples (a) and (b) of Fig. 4 (Sb-alumina and Sb-alum. doped V, respectively). *Exp.*: reaction temp., 500°C; propane, 10.8%; ammonia, 15.1; oxygen, 29,4 %.

cases, but decreases after doping.

The XPS characterization of these samples is reported in Table IV. The formation of $AlSbO_4$ induces an enhanced presence of Sb^{5+} as compared to that found on unsupported antimonate samples. Doping with V does not modify the indicative Sb^{3+}/Sb^{5+} ratio, but increases the Sb/Al surface ratio, indicating that reaction with V increases surface spreading. The surface Sb/V ratio is in good agreement with the bulk value.

Also reported in Table IV are XPS data characterizing both fresh and used catalysts prepared according to patent indications. The results indicate that the presence of alumina stabilizes the antimony and vanadium with respect to reduction in comparison to unsupported V- antimonate. After reaction a probable spreading of the phases containing Sb and V occurs, as suggested from the increase in both the surface Sb/V and Sb/Al ratios. The W/V ratio is lower than the bulk value and different preparations gave values between zero and 0.80. Analogous observations of incorporation of W in the antimonate lattice of $GaSbO_4$ based catalysts for propane ammoxidation have been reported [16].

Conclusions

The analysis of the reaction network and the reaction kinetics indicate that propane is transformed to ACN mainly through the intermediate formation of propylene. The limiting factor in ACN selectivity is the rate of this second step of propylene transformation to ACN, which is influenced considerably by the availability of surface ammonia. The latter depends on the rate of the side conversion of NH_3 to N_2. This side conversion of ammonia is tentatively related to the presence of unreacted vanadium oxide, not stabilized by the formation of the rutile antimonate phase, even in the presence of excess antimony.

The use of alumina as the support not only induces a spreading of the active component, but due to the formation of isostructural $AlSbO_4$ *i)* induces site isolation, *ii)* stabilizes Sb and V with respect to reduction and *iii)* probably avoids or limits the presence of not stabilized vanadium oxide, thus reducing the rate of the side reaction of ammonia and increasing the selectivity in propane ammoxidation.

Table IV X-ray photoelectron spectra for Sb-V-O catalysts supported on alumina. The indicative Sb^{3+}/Sb^{5+} ratio was obtained by fitting components for Sb_2O_3 and Sb_6O_{13} to $Sb_{3d5/2}$ spectra and correcting a mean valence of 4.33 for Sb_6O_{13}

Sample	Binding energies and *peak width at half height* (in the bracket)		*Surface Sb/V*	Surface Sb/Al	*Surface W/V*	*Indicative* Sb^{3+}/Sb^{5+}
	$Sb_{3d3/2}$	$V_{2p3/2}$				
fresh Sb-alumina [70% Al_2O_3] calcined 900°C	540.7 (2.2)	-	-	0.22	-	33/67
fresh Sb-alumina doped V calcined 900°C - Sb:V = 10	540.8 (2.1)	517.0 (2.2)	12	0.49	-	37/63
fresh Sb/V/W (5:1:1)-alumina [70% Al_2O_3] - calc. 650°C	540.6 (2.4)	517.5 (2.4)	2.8	0.086	0.48	51/49
used Sb/V/W (5:1:1)-alumina [70% Al_2O_3] - calc. 650°C	540.2 (2.3)	517.2 (2.0)	4.0	0.17	0	83/17

Furthermore, the catalytic behavior of antimony oxide supported on alumina compared with that for the same sample doped with vanadium, indicates that vanadium induces a slightly increase in the activity in propane conversion, but especially creates sites to form selectively acrylonitrile instead of acetonitrile, as occur on Sb-oxide supported on alumina.

Additional studies are necessary for a further clarification of these preliminary indications, but tentatively may be suggested that on a Sb-alumina system operates a different mechanism like an acid-catalyzed mechanism, whereas a metallo-radical mechanism predominates in the presence of vanadium sites. This may explain the change observed in the products of propane ammoxidation when Sb-alumina matrix is doped with vanadium.

References

[1] L.C. Glaeser, J.F. Brazdil, D.D. Suresh, D.A. Orndoff, R.K. Grasselli, *U.S. Patent* 4,788,173 (1988).

[2] A.T. Gutmann, R.K. Grasselli, J.F. Brazdil, *US Patent*, 4,746,641 (1988).

[3] G. Centi, D. Pesheva, F. Trifirò, *Appl. Catal.*, 33 (1987) 343.

[4] G. Centi, R.K. Grasselli, E. Patanè, F. Trifirò, in *New Developments in Selective Oxidation*, G. Centi and F. Trifirò Eds.; Elsevier Science Pub.: Amsterdam 1990; 635.

[5] G. Centi, F. Trifirò, R.K. Grasselli, *Chim. Ind. (Milan)*, 72 (1990) 617.

[6] R. Catani, G. Centi, F. Trifirò, R.K. Grasselli, *Ind. Eng. Chem. Research*, in press (1992).

[7] G. Centi, R.K. Grasselli, F. Trifirò, *Catal. Today*, in press (1992).

[8] B.B. Pal, K.K. Sen Gupta, *Inorg. Chem.*, 14 (1975) 2268.

[9] F.J. Berry, M.E. Brett, W.R. Patterson, *J. Chem Soc. Dalton Trans.*, (1983) 9.

[10] C. Rocchiccioli-Deltcheff, T. Dupuis, R. Frank, M. Harmelin, *J. Chimie Phys. Biol.*, 67 (1970) 2037.

[11] E. Husson, Y. Repelin, H. Brusset, A. Cerez, *Spectrochim. Acta*, 35A (1979) 1177.

[12] P.A. Cox, R.G. Egdell, C. Hardings, W.R. Patterson, P.J. Taverner, *Surf. Sci.*, 123 (1982) 179.

[13] F. Berry, M.E. Brett, R.A. Marbrow, W.R. Patterson, *J. Chem. Soc. Dalton Trans.*, (1984) 985.

[14] G. Centi, F. Trifirò, *Catal.Rev.-Sci.Eng.*, 28 (1986) 165.

[15] J. Birchall, A.W. Sleight, *Inorg. Chem.*, 15 (1976) 868.

[16] S.Yu. Burylin, Z.G. Osipova, V.D. Sokolovskii, I.P. Olen'kova, *Kinet. Catal.*, 30 (1989) 1095.

DISCUSSION

Q: M. Sinev (Russia)

A strong influence of ammonia on the rate and selectivity can be explained by different effects: i) a "formal-kinetic effect" (higher reaction order with respect to NH_3 of ACN production as compared with NH_3 oxidation to N_2), ii) influence of NH_3 on the reactivity of intermediates, iii) influence of NH_3 on the state of catalyst (or its components) and iv) something else. What is your explanation of the strong influence on the reaction ?

A: F. Trifiro

All these factors contribute in determining the effect of ammonia on the formation of acrylonitrile and their relative importance depends also on the specific characteristics of the V-antimonate itself. The rates of ammonia oxidation to N_2 and of acrylonitrile synthesis from the intermediate propylene show a different order as respect to ammonia concentration, and, due to the higher rate of propylene conversion to carbon oxides than the rate of acrylonitrile consecutive oxidation to carbon oxides, a decrease in the propylene to acrylonitrile step strongly influences the selectivity to the sum of propylene plus acrylonitrile. However, additional factor is the partial reduction of the surface induced from ammonia which thus induces also a modification of the reactivity of the catalyst itself.

It should also be mentioned that the presence of a competitive reaction of ammonia oxidation, which is a function of the amount of V(V) ions on the surface, leads to a decrease of the amount of ammonium ions on the surface necessary for the selective transformation of the reaction intermediates to acrylonitrile instead of carbon oxides. On the other hand, the amount of V(V) ions on the surface depends on the characteristics of the sample during the catalytic reaction influenced both from the preparation method and from the reaction conditions. Various factors therefore contribute in determining the effect of ammonia on the selectivity to acrylonitrile, but the key problem is to limit the side reaction of ammonia oxidation in order to increase the selectivity to acrylonitrile.

Q: J. Haber (Poland)

In your catalytic system you have two redox pairs ($V^{3+}/V^{4+}/V^{5+}$ and $Sb^{3+}/Sb^{4+}/Sb^{5+}$). Could you find which of them is responsible for the activation of the hydrocarbon and which for interaction with oxygen ?

A: F. Trifiro

Present knowledges on the mechanism of reaction do not allow an unequivocal answer to this question, because is not clear what is the real role of each of these two components in the reaction mechanism. After reaction we noted by XPS a reduction of both vanadium and antimony which suggests the possible role of both components in the mechanism of reaction. On the other hand, our data indicate that the catalytic behavior of the rutile V-antimonate phase in propane ammoxidation is markedly different from the behavior in the same reaction of various other M-antimonates with rutile structure and the doping of these samples with even small amounts of vanadium can increase considerably the formation of acrylonitrile. This suggests a specific role of vanadium in the mechanism of both activation of propane and selective transformation to acrylonitrile, but vanadium must be stabilized in a valence state lower than five (V(III) and V(IV) from the rutile antimonate structure to be selective. However, these evidences do not allow to clearly assign the catalytic role of each components and our future research programme, in fact, is to study more in detail the mechanism of this reaction and the nature of the active sites for each of the various steps of the reaction.

In conclusion, the V(IV)/V(III) redox couple is tentatively responsible of the oxidative dehydrogenation of propane to propylene, whereas our preliminary indications suggest the V(IV)/V(III) redox couple responsible for the N insertion step. The Sb(III) and Sb(V) ions have mainly a structural role of stabilization of the various valence states of vanadium in the

rutile antimonate structure, but we cannot exclude also a role of Sb(III) ions in the activation step of oxygen and of Sb(V) ions in the N insertion step, even though V-antimonate behaves in a different manner, from the catalytic point of view, from the other Me-antimonates active in propylene ammoxidation.

Q: D. D. Suresh (USA)

You have carried out good investigation in your laboratory. This is a two part question: first, is the surface concentration of V, Sb and Al in the catalyst same as in the bulk ? Second, what is the mechanism of propylene formation from propane, the α-H abstraction and oxygen insertion ?

A: F. Trifiro

The surface concentration is effectively different from the bulk and, in general, we found surface enrichments in antimony as typical of other M-antimonate systems as well as the possibility of surface segregation of antimony oxide particles. However, the correlation between surface characteristics and catalytic behavior is much less clear than, for example, in the case of propylene ammoxidation on other M-antimonate (for example, iron-antimonate). As regards to the second question, tentatively we believe that V(IV) ions in the antimonate matrix are responsible of the activation step of propane to form propylene, whereas some preliminary data indicate that the mechanism of acrylonitrile synthesis differs from that proposed for acrylonitrile synthesis from propylene on other M-antimonates and that vanadium ions are also involved in this step. However, we do not have clear evidences on the mechanism of reaction.

A: R. K. Grasselli

As a general comment, and in partial response also to Dr. Suresh's question, I should like to offer a mechanistic view of propane ammoxidation over Sb-Al-oxide based catalysts and V-Sb-Al-oxide based catalysts, consistent with the experimental data given in our paper.

The propane ammoxidation pathway (attached Scheme 1) over Sb-Al-oxide is predominantly an acid catalyzed reaction which leads via the first formed, chemisorbed propylene intermediate primarily to acetonitrile, HCN and CO_x. It is catalyzed by $[Al\text{-}O\text{-}Sb]^+$ acid sites. However, there are also [Sb-O-Sb] selective oxidation sites in this catalyst from whence a chemisorbed propylene, once formed, can yield an allylic intermediate which results in desorbed acrylonitrile (i.e., the desired product) when there is sufficient NH_3 present to convert the [Sb-O-Sb] site to an [Sb-NH-Sb] site.

Conversely, if there is insufficient NH_3 present, the so formed acrolein at the [Sb-O-Sb] site gets further cracked to acetonitrile, HCN, and CO_x as shown in Scheme 1. The calculated yields agree well with the experimentally observed yields.

On V-Sb-Al-oxide, the propane ammoxidation pathway is metalloradical initiated by [V=O] sites (Scheme 2). The primary intermediate is again propylene which now encounters many more [Sb-O-Sb] and [Sb-NH-Sb] surface sites than acid sites, with the concomitant result of yielding acrylonitrile as the major useful product. It is hypothesized that the presence of vanadium not only provides the [V=O] paraffin activation sites but also helps in the reoxidation mechanism of the [Sb-O-Sb] and [Sb-NH-Sb] sites. The calculated product yields agree well with the experimentally observed yields.

Q: O. V. Krylov (Russia)

The temperature of propane ammoxidation is rather high (500 ^{0}C). It is known that at such temperatures alkanes give alkyl radicals upon interaction with metal oxides. Vanadium oxides are catalysts of such radicals formation. It is possible that the first step of reaction is the radical formation with reduction of V-atoms and initiation of gaseous reaction. The second step is surface redox reaction with Sb participation. What do you think ?

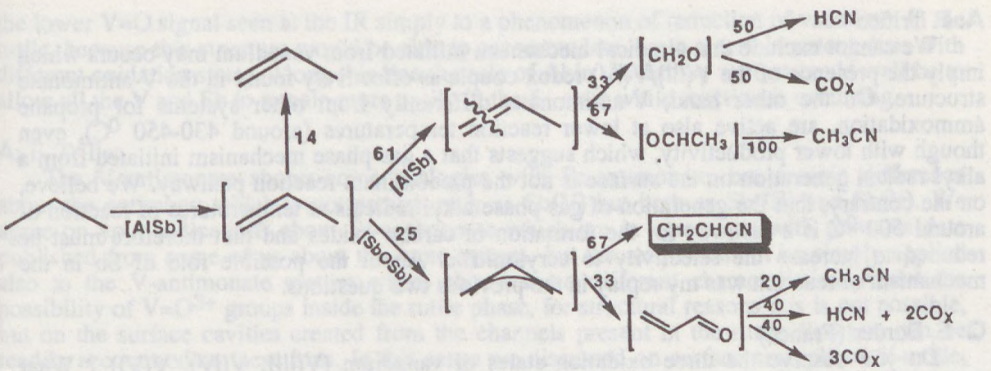

PRODUCTS	$C_3^=$	ACN	AcCN	HCN	CO_x
C-Yield$_{obs.}$	14	17	47	8	12
C-Yield$_{calc.}$	14	17	42	11	16

[ ]= Surface Species

Scheme 1. Propane Ammoxidation Pathways (Acid Catalysed) over Sb-Al-oxide

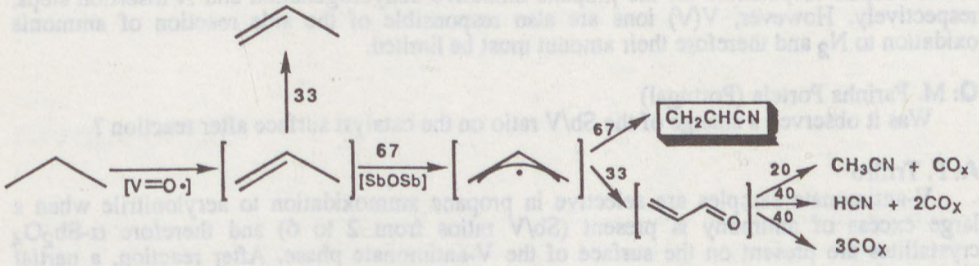

PRODUCTS	$C_3^=$	ACN	AcCN	HCN	CO_x
C-Yield$_{obs.}$	33	44	2	4	17
C-Yield$_{calc.}$	33	45	3	3	16

[ ]= Surface Species

Scheme 2. Propane Ammoxidation Pathways (Metalloradical Catalyzed) over V-Sb-Al-oxide

A: F. Trifiro

We cannot exclude that a radical mechanism initiated from vanadium may occurs which imply the presence of the V(III)/V(IV) redox couple as effectively found in the V-antimonate structure. On the other hand, V-antimonate, differently from other systems for propane ammoxidation, are active also at lower reaction temperatures (around 430-450 ^{0}C), even though with lower productivity, which suggests that a gas-phase mechanism initiated from a alkyl radical generation on the surface is not the predominant reaction pathway. We believe, on the contrary, that the generation of gas-phase alkyl radicals at temperatures of reaction of around 500 ^{0}C is a pathway for the formation of carbon oxides and that therefore must be reduced to increase the selectivity to acrylonitrile. About the possible role of Sb in the mechanism of reaction was my replay in the previous two questions.

Q: E. Bordes (France)

Do you observe the three oxidation states of vanadium (V(III), V(IV), V(V)) ? What could be their role? How vanadyl groups (if exist) would be displayed on the surface ?

A: F. Trifiro

The rutile structure is a quite flexible structure which can accommodate various elements. In particular, along the c axis large channels are present which allow fast ionic diffusion and easily accommodation of foreign elements (such as also V(V)). In addition, our recent data indicate that the V-antimonate is a mixed valence system with vanadium in the (III) and (IV) valence states in the bulk and a consequent presence of also Sb(III)/Sb(V) ions in the structure and this mixed valence situation probably reflects also in some surface modification. In the bulk of the rutile antimonate, vanadyl groups cannot be present due to the ionic radius, but on the surface the situation is different (see above) and by infrared analysis we see, in fact, the presence of V=O double bonds.

About the role of the different valence states of vanadium, we believe that the catalytic behavior of V-antimonate can be associated to the presence of a larger amount of V(IV) ions stabilized in the rutile matrix, but with the presence of both the V(III)/V(IV) and V(IV)/V(V) redox couples responsible for the propane oxidative dehydrogenation and N insertion steps, respectively. However, V(V) ions are also responsible of the side reaction of ammonia oxidation to N_2 and therefore their amount must be limited.

Q: M. Farinha Portela (Portugal)

Was it observed a change of the Sb/V ratio on the catalyst surface after reaction ?

A: F. Trifiro

V-antimonate samples are selective in propane ammoxidation to acrylonitrile when a large excess of antimony is present (Sb/V ratios from 2 to 6) and therefore α-Sb_2O_4 crystallites are present on the surface of the V-antimonate phase. After reaction, a partial change of the dimensions of these crystallites occurs. The XPS analysis, in the presence of a biphasic system with possibility of changes in the relative dimensions of the two components, do not provide enough accurate data to clarify if the Sb/V ratio remains constant or not after reaction, but indicatively suggests an increase.

Q: P. L. Villa (Italy)

In a work to be published on Fe-Sb oxides by Mössbauer, XRD and IR on a sample with Sb/Fe atomic ratio of 2, we found that all Sb was present as Sb(V) in the fresh catalyst and the system was found to be monophasic with a rutile structure. So rutile seems to be a structure able to accommodate unusual amounts of ions in a high valence state, in excess to what produced by stoichiometry ($FeSbO_4$ has Sb/Fe = 1). We also found that the used catalyst contained some Sb in a lower oxidation state. You found only one phase by XRD in your binary V-Sb-O system and V(V) from IR characterization. I would suggest that V(V) is located inside the rutile structure and is not present as an amorphous phase. I would ascribe

the lower V=O signal seen at the IR simply to a phenomenon of reduction of vanadium in the rutile, because this structure would be able to accommodate, up to a certain extent, ions with different oxidation states. Along this line the role of Al in the ternary system could well be to allow all the V and Sb to remain more easily in the 5+ state while reaction is occurring.

A: F. Trifiro

The V-antimonate shows some analogies with Fe-antimonate, but a main difference about the antimony which is not present only as Sb(V) but both as Sb(III) and Sb(V). We agree on your indications about Fe-antimonate which are in agreement with previous data published from some of us about the same system, but the results cannot be simply applied also to the V-antimonate system which shows some different characteristics. About the possibility of $V{=}O^{3+}$ groups inside the rutile phase, for structural reasons this is not possible, but on the surface cavities created from the channels present in the rutile structure can be readily accommodate these ions. In this sense we discussed on surface amorphous V-oxide, not as a real separate phase overlying the V-antimonate. Finally, we perfectly agree about the role of Al which has a structural role of stabilization of the valence states of the V-antimonate elements (especially as regards to the decomposition of the phase when the catalytic reaction is carried out in too strong reducing conditions) and not only of a support for V-antimonate.

Guczi, L. *et al.* (Editors), *New Frontiers in Catalysis*
Proceedings of the 10th International Congress on Catalysis, 19-24 July, 1992, Budapest, Hungary
© 1993 Elsevier Science Publishers B.V. All rights reserved

CATALYTIC OXIDATION OF FLUORENE TO 9-FLUORENONE - DEVELOPMENT AND CHARACTERIZATION OF CATALYSTS

F. Majunke, H. Borchert and M. Baerns

Ruhr-University Bochum, P.O.Box 102148, D-W 4630 Bochum, Germany

Abstract

The title reaction was studied using unsupported V_2O_5-Fe_2O_3 catalysts of different atomic ratios of V to Fe (1 : 0.13 to 1 : 1.4); some of the catalysts were doped with Cs_2SO_4 (atomic ratio of V to Cs = 1 : 0.06). Reaction temperature, fluorene partial pressure and partly calcination temperature were varied within the following limits: $572 \leq T_R/K \leq 673$, $0.2 \leq p_F/kPa \leq 0.7$, T_{calc} = 623 K and 773 K. Optimum catalyst composition for obtaining a maximum in 9-fluorenone selectivity required the presence of cesium sulfate. When adding Cs_2SO_4 selectivity was increased from 70 to 98%. The beneficial effect of cesium sulfate doping on catalytic performance is explained by changes of the acid-base properties of the catalyst surface; this was also manifested by different strengths of adsorption of the reactants as derived from pseudo-adsorption constants of Hougen-Watson-type kinetics.

1. INTRODUCTION

The catalytic gas-phase oxidation of fluorene to 9-fluorenone has received only little attention in the past. Dashevskii et al. investigated the reaction on a pumice-supported V_2O_5-Fe_2O_3-K_2SO_4 catalyst (atom ratios of V : Fe : K = 1 : 0.3 : 0.5); no information on the reaction scheme and the effect of the composition of the catalyst on its performance were given [1, 2]. From anthracene oxidation, however, it is known that the addition of K_2SO_4 to a vanadium-iron-oxide catalyst leads to an increase of the yield of 9,10-anthraquinone up to 90% while without potassium sulfate doping the yield was significant lower [3]. By ir spectroscopy it was found that alkali addition to V_2O_5 weakens the V-O-V-bond strength as derived from a shift of the absorption bands to lower wave numbers [4, 5]. Also, the oxygen-exchange rate between the catalyst and the gas phase increased with alkali compound doping as was found by applying the ^{18}O-tracer technique [6, 7]; this increase was enhanced when an alkali metal of higher molecular mass was used. Recently the effect of different alkali metal sulfate promoters (M = Li, K, Cs) on activity and selectivity in the catalytic gas-phase oxidation of fluorene, anthracene and phenanthrene using V_2O_5-based catalysts was studied [8]; it was observed that alkali addition favors the selectivity of inner-ring

oxidation products. This latter finding was ascribed to a decrease of Lewis-acid sites and to an increase of basic oxygen-anion sites which favor both, selective adsorption of the weakly acidic inner-ring positions of the polycyclic aromatics (i.e., the CH_2-position in the case of fluorene) and probably also insertion of nucleophilic oxygen O^{2-} into the hydrocarbon molecule. Also the increase of the exchange rate of oxygen between the catalytic solid and the gas phase as well as the weakening of the V-O-V-bond may be a further reason for the sharp increase in selectivity; these phenomena may be assumed to contribute to a fast transformation of weakly-bound electrophilic surface oxygen into nucleophilic O^{2-} species suitable for insertion into the molecule.

Against the above background the following objectives were pursued in the present study: (1) investigating the effects of varying the proportions of V_2O_5 and Fe_2O_3 in the catalyst composition, of cesium sulfate doping and of the calcination temperature on the product distribution of the fluorene oxidation (for the reaction scheme see Figure 1); (2) relating the catalytic results to certain properties of the catalyst i.e., acid-base properties and alkali content, which had been reported earlier [8]; (3) elucidating the effect of alkali doping on the basis of adsorption data of fluorene and fluorenone as derived from Langmuir-Hinshelwood-type kinetics.

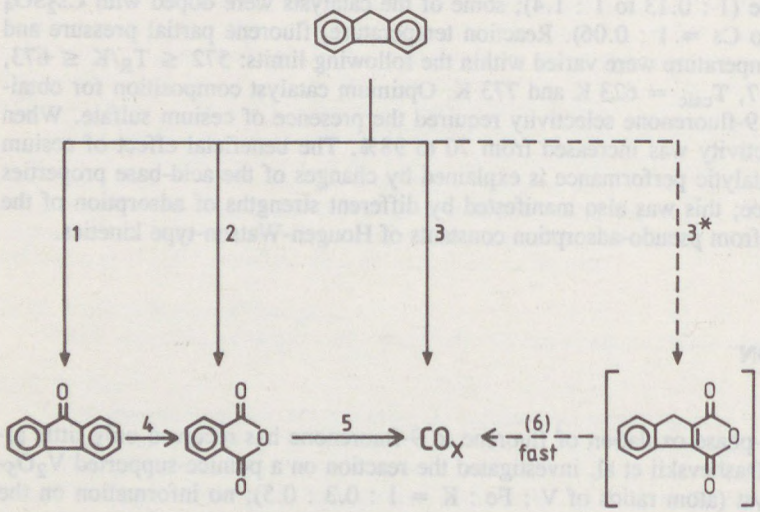

Figure 1. Reaction scheme of the catalytic oxidation of fluorene [9] (since $r_6 \gg r_3^*$ all CO_x formation via step j = 6 was lumped in r_3)

2. EXPERIMENTAL

2.1 Catalyst preparation

Vanadium oxide being the base compound of the catalysts was modified by ferric oxide and cesium sulfate. The catalysts were prepared by coprecipitation of the hydroxides of iron and vanadium by ammonia from an aqueous solution of NH_4VO_3 and $FeCl_3$. Water was then evaporated. The precursor was finally dried at 120°C (for further details see [3, 10, 11]). For doping, Cs_2SO_4 was added to the solution prior to coprecipitation. Catalyst compositions, catalyst pretreatment i.e., temperatures and duration of calcination as well as BET-surface areas of the catalytic solids are listed in Table 1.

2.2 Equipment

Oxidation experiments were performed in an electrically heated fixed-bed quartz reactor (d = 0.8 cm, l_{total} = 30 cm, l_{cat} = ca. 5 cm); the equipment was described in detail previously [12]. For isothermal operation the mass of catalyst of approximately 1 g was diluted by 1 to 2 g of quartz. The products were analyzed by GC and HPLC. Most of the condensable substances (fluorene, 9-fluorenone, phthalic anhydride, 2,3-indenedicarboxylic anhydride and maleic anhydride) were separated on an OV-1 capillary column for GC analysis (Sichromat 2, Siemens, FID); for double check these compounds were also analyzed by HPLC (WATERS 712, UV array detector); for details see [13]. CO and CO_2 were quantitatively determined by GC analysis (Delsi 11, TCD, two columns packed with molecular sieve 5-A and porapack Q).

2.3 Catalyst characterization

The specific surface area was determined by applying the 1-point BET method and using low-temperature (77 K) nitrogen adsorption after the fresh catalyst samples had been calcinated in air for 12 hours at the temperatures given in Table 1. Cesium concentration on the surface as presented in the discussion, was obtained by XPS-analysis using Al cathode (Leybold-Heraeus AG, LHS 10 spectometer). For identification of acid sites by in-situ IR-spectroscopy a DRIFT-equipment was used (for details see [8]).

2.4 Reaction Conditions

The conditions of catalytic testing i.e., reaction temperature and reactant concentration are given in Table 1. Different degrees of conversion at constant reaction temperature were obtained by varying the contact time from 0.07 to 1 g s ml^{-1} to determine the maximum selectivity for 9-fluorenone.

Table 1
Bulk composition (atomic ratio), BET-surface area after calcination of the catalytic material, calcination temperature T_{calc} and reaction temperature T_R (initial concentration of fluorene C_F° = 0.18 mol / m^3_{STP} and oxygen C_{O2}° = 8.8 mol / m^3_{STP})

Catalyst composition V : Fe : Cs	S_{BET} $m^2\ g^{-1}$	T_{calc} K	T_R K
1 : 0.13 : 0	6	723	572; 588; 598 606; 615; 625
1 : 0.77 : 0.06	1	623	623; 653; 673
1 : 1 : 0	4	623	623; 653; 673
1 : 1 : 0.06	2	623	623; 653; 673
1 : 1 : 0.06	1	773	623; 653; 673
1 : 1.4 : 0	4	623	623; 653; 673
1 : 1.4 : 0	3	773	653
1 : 1.4 : 0.06	1	623	623; 653; 673
1 : 1.4 : 0.06	1	773	653; 673

3. RESULTS

3.1 Catalytic performance

As main products of the catalytic oxidation of fluorene, 9-fluorenone, phthalic anhydride and the carbon oxides were observed. Only traces of maleic anhydride and 2,3-indenedicarboxylic anhydride were found for all catalysts. The performance of the various catalysts is described by their activity and product distribution, especially with respect to 9-fluorenone selectivity.

Effect of catalyst composition. Activity was characterized by the initial rates of fluorene consumption r_0 for the various catalysts as derived from kinetics [9]. It decreased by increasing the vanadium-to-iron ratio (see Table 2; run nos. 10/16, 11/17 and 12/18); when the V_2O_5-Fe_2O_3 catalysts were doped with cesium sulfate activity markedly increased as illustrated by comparing run nos. 7/10, 8/11 and 9/12.

Selectivity to 9-fluorenone and phthalic anhydride stayed nearly constant up to fluorene conversions of 95% for all V_2O_5-Fe_2O_3 catalysts; when increasing conversion beyond this value 9-fluorenone selectivity decreased in favor of phthalic anhydride and carbon oxides due to consecutive reaction. When cesium was added, selectivities increased and were nearly constant over the whole range of conversion.

Maximum 9-fluorenone selectivities obtained with the various catalysts at different temperatures are presented in the bar chart shown in Figure 2. Adding Fe_2O_3 to pure V_2O_5 resulted in an increase of 9-fluorenone selectivity when a certain proportion of Fe_2O_3 was exceeded. A vanadium-to-iron ratio of 1 : 0.13 did not show any significant change within experimental accuracy while selectivity increased by about 10 % at ratios of 1 : 1 and 1 : 1.4 respectively.

Table 2
Effect of catalyst-precursor calcination temperature T_{calc} on specific surface area S_{BET} (fresh catalyst) and catalytic performance (initial reaction rate r_0) for different catalysts (C_F° = 0.18 mol/m$^3_{STP}$; C_{O2}° = 8.8 mol/m$^3_{STP}$)

run no.	Catalyst composition V : Fe : Cs atomic ratio	T_{calc} K	S_{BET} m^2 g^{-1}	T_R K	r_0 [1] μmol m^{-2} s^{-1}
1	1 : 0.13 : 0	723	6	572	0.021
2				588	0.037
3				598	0.061
4				606	0.085
5				615	0.121
6				625	0.179
7	1 : 1 : 0	623	4	623	0.053
8				653	0.118
9				673	0.193
10	1 : 1 : 0.06	623	2	623	0.364
11				653	0.450
12				673	0.514
13		773	1	623	0.239
14				653	0.319
15				673	0.382
16	1 : 1.4 : 0.06	623	1	623	0.180
17				653	0.237
18				673	0.288

[1] r_0 was derived from kinetics [9] and is refered to S_{BET}

The addition of cesium sulfate markedly increased the 9-fluorenone selectivity for V_2O_5-Fe_2O_3 catalysts of different vanadium-to-iron ratios applied (1 : 0.77; 1 : 1; 1 : 1.4). The absolute value of the 9-fluorenone selectivity was, however, affected by the vanadium-to-iron ratio in a similar manner as outlined above; the 9-fluorenone selectivity amounted to ca. 95% for V : Fe : Cs = 1 : 0.77 : 0.06, to 97% for V : Fe : Cs = 1 : 1 : 0.06 and to 99% for V : Fe : Cs = 1 : 1.4 : 0.06.

Effect of calcination temperature. By increasing the calcination temperature from 623 K to 773 K there was an decrease of the activity i.e., r_0 for the catalyst with V : Fe : Cs = 1 : 1 : 0.06 given in Table 2 (compare run nos. 10/13, 11/14 and 12/15) decreased.

For the V_2O_5-Fe_2O_3-catalyst having a ratio of vanadium to iron of 1 : 1.4 as well as for the cesium-doped catalyst with V : Fe : Cs = 1 : 1 : 0.06 a slight increase of 9-fluorenone

selectivity was observed from 68% to 72% and 96% to 98% (T_R = 653 K) respectively when the calcination temperature was raised. This relationship could not be validated for the catalysts with V : Fe : Cs = 1 : 1.4 : 0.06 since any changes in selectivity above 99% were beyond experimental accuracy.

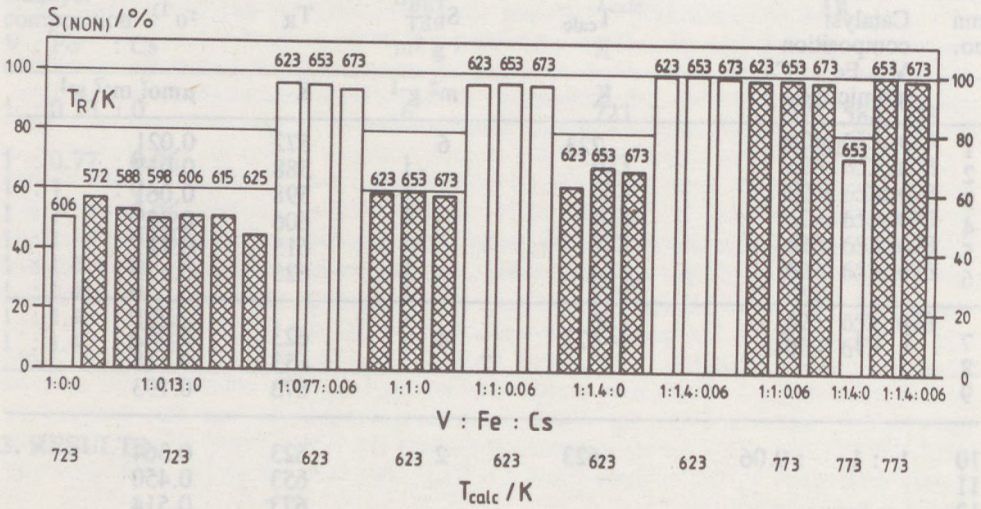

Figure 2. Maximum 9-fluorenone selectivity in air oxidation of fluorene as function of catalyst composition (V : Fe : Cs atomic ratio) and its calcination temperature at various reaction temperature (C_F° = 0.4 Vol.%)

3.2 Adsorption of reactants

For characterizing the adsorption properties of the solids the catalytic surface pseudo-adsorption constants and heats of adsorptions were derived from kinetic data on the fluorene oxidation which have been evaluated according to Hougen-Watson-type rate equation (eq. 1) based on reaction scheme presented in Figure 1 (for details see [9]).

$$r_j = \frac{k_j K_i C_i C_{O2}}{(1 + \Sigma K_i C_i)(1 + K_{O2} C_{O2})} \qquad (1)$$

k_j : reaction rate constant for reaction step j (=1-5)

K_i : pseudo-adsorption constant for the organic compound i

Various V_2O_5-Fe_2O_3 catalysts partly doped with cesium sulfate were included in the kinetic evaluation (see Table 2). For undoped V_2O_5-Fe_2O_3 catalysts the pseudo-adsorption constants for fluorene and 9-fluorenone at a reference temperature of 623 K as well as the respective heats of adsorption are given in Table 3; adsorption of phthalic anhydride was

negligible. From these data it may derived that adsorption capacity for both, fluorene and 9-fluorenone increases with increasing iron content but that the strength of fluorene adsorption is markedly reduced while the strength of 9-fluorenone adsorption is weak for both catalysts.

Equation (1) was, however, only applicable as long as there was no cesium sulfate present. If cesium sulfate was added the adsorption terms ($K_i C_i$) in the denominator of eq. (1) were significantly smaller than 1 and could be therefore neglected. Under these circumstances and when oxygen partial pressure was assumed constant the rate equation (1) could be simplified to

$$r_j = k_i^* C_i \qquad (2)$$

From these results it may be derived that cesium sulfate doping reduces the propensity of the catalytic surface for keeping the reactants and the products adsorbed; whereby their chance to be totally oxidized is markedly decreased which goes along with an increase in selectivity.

Table 3
Adsorption constant K_i for a reference temperature of 623 K and heat of adsorption ΔH_i for V_2O_5-Fe_2O_3-catalysts (F: fluorene, NON: 9-fluorenone; data from [9])

Catalyst composition V : Fe atomic ratio	K_F $m^3\ mol^{-1}$	ΔH_F kJ mol^{-1}	K_{NON} $m^3\ mol^{-1}$	ΔH_{NON} kJ mol^{-1}
1 : 0.13	1398 ±5	-111.8 ±0.3	342 ± 14	-24.3 ±0.4
1 : 1	3149 ±14	-29.8 ±2.6	884 ± 41	-25.6 ±2.5

4. DISCUSSION

Activity and selectivity for the various catalyst compositions are discussed in terms of the V-to-Fe ratio and of cesium sulfate doping.

When increasing the iron content activity related to specific surface area is decreased for undoped as well as for the cesium sulfate doped V_2O_5-Fe_2O_3 catalysts. Selectivty to 9-fluorenone, however, is slightly increased which may be explained on the basis of surface acidity and basicity. Surface acidity of a pumice-supported V_2O_5-Fe_2O_3-catalyst is decreased by an increase of the iron content as was reported earlier [14]. A similar relationship between surface acidity and selectivity derived from in-situ IR-spectroscopy was found for the oxidation of anthracene to 9,10-anthraquinone on supported V-Mo-P-oxide catalysts [8]. These results led to the conclusion that acidic centers favor the formation of strongly adsorbed intermediates and subsequently outer-ring oxidation products are formed which are finally converted to phthalic anhydride and/or to carbon oxides. This reasoning is supported by the conclusion derived from the adsorption of reactants as observed by the kinetics of

fluorene oxidation (see above). Thus, it appears that the increase in 9-fluorenone selectivity has to be related to a change of the acid-base surface properties. The increase in surface basicity and/or the decrease in acidity certainly favors the adsorption of the weak acidic CH_2-position of the inner ring leading to the selective formation of 9-fluorenone. In addition, the adsorption of the electron-rich aromatic rings on the acidic sites assisting total oxidation is suppresed; hereby the non-selective oxidation of fluorene and 9-fluorenone is reduced.

Apart from the effect of the V-to-Fe ratio, selectivity is also markedly enhanced by adding cesium sulfate to the V_2O_5-Fe_2O_3 catalysts. The reasoning for this relationship goes along the same lines as indicated for the positive effect of Fe_2O_3. The cesium sulfate addition leads also to a significant decrease in the adsorption of fluorene and 9-fluorenone as revealed by the kinetic evaluation (see above). This is partly supported by the observation that cesium is enriched on the surface compared to the bulk as observed by XPS [8]. Thus, the promoting effect of the basic alkali compound may be traced back to a decrease of the acidic sites. In addition, a weakening of the V-O-V-bond strength and an increase of the oxygen-exchange rate by alkali doping may also contribute to an increase in selectivity as outlined in the introductory paragraph. Since also activity was increased by cesium doping it may be assumed that the faster transformation of electrophilic surface oxygen into lattice oxygen not only favors the formation of selective nucleophilic oxygen species but also increases the total amount of active sites.

Acknowledgement

This work was supported by Deutsche Forschungsgemeinschaft. Finally, thanks are due to Q. Wei who performed some of the catalytic experiments.

Literature

1 M.M. Dashevskii and G.M. Petrenko, Zhur. Prikland. Khim., 35 (1962) 693.
2 G.M. Oetrenko and G.N. Terent'eva, Zhur. Prikland. Khim., 38 (1965) 1109.
3 FIAT Final Rep. No. 1313 (Vol 1) 332.
4 D.V. Fikis, K.W. Heckley, W.J. Murphy and R.A. Ross, Can. J. Chem., 56 (1978) 3078.
5 T. Tamaka, R. Tsuchitami, M. Ooe, T. Funabiki and S. Yoshida, J. Phys. Chem., 90 (1986) 4905.
6 K. Hirota and Y. Kera, J. Phys. Chem., 72 (1968) 3133.
7 K. Hirota and Y. Kera, J. Phys. Chem., 73 (1969) 3973.
8 M. Baerns, H. Borchert, R. Kalthoff, P. Käßner, F. Majunke, S. Trautmann and A. Zein, in: Stud. Surf. Sci. Cat., to be published
9 M. Baerns and H. Borchert, to be published in 1992
10 N.T. Do, R. Kalthoff, J. Laacks, S. Trautmann and M. Baerns in: "New Develop ments in Selective Oxidation", Stud. Surf. Sci. Cat. (G. Centi and F. Trifiro, eds.), Elsevier Science Publisher B.V., 55 (1990) 247
11 M. Baerns, R. Kalthoff, P. Käßner and A. Zein, Erdöl-Erdgas-Kohle, 106 (1990) 166.
12 M. Baerns, R. Kalthoff, P. Käßner and A. Zein; Dechema Monographie Katalyse (ed.: H. Kral and D. Behrens) Verlag Chemie, Weinheim, 118 (1989) 231.
13 A. Zein and M. Baerns, J. Chromat. Sci., 27 (1989) 249.
14 M. Ai, J. Catal., 52 (1978) 16.

DISCUSSION

Q: R. K. Grasselli (USA)

First let me congratulate you on this excellent piece of work.

1) My question is if the enormous beneficial effect of Cs addition to your catalyst is dependent or independent of the compound of Cs used. Is Cs_2SO_4 preferred over $CsNO_3$, for example ? Is there any evidence of $Cs_2S_2O_7$ in your catalyst ?

2) Since there is no preference of Cs compounds used, you think, then let me comment that in multicomponent molybdenas for the selective oxidation of isobutene to methacrolein, or ammoxidation to methacrylnitrate there too is observed an enormous selectivity advantage to the useful products by Cs addition, it is independent of the Cs compound (Cs_2SO_4 or $CsNO_3$) used. On the contrary, in the old naphthalene to phthalic anhydride catalyst, K_2SO_4 addition appears critical for enhanced useful yields and $K_2S_2O_7$ is observed in the catalyst. I wonder, based on your data and data I quoted above, if the V-oxide based naphthalene to phthalic anhydride catalyst, as well as the V-oxide based catalyst for the all combustion of o-xylene to phthalic anhydride would be improved by using the addition of Cs_2SO_4 instead of K_2SO_4 ?

A: M. Baerns

1) We have not applied any other cesium-compounds than Cs_2SO_4 as promoter. It was our intention to compare the effect of different alkali sulfates on the product distribution. Alkali sulfates were described in literature as useful additives for hydrocarbon oxidation reactions as you yourself frequently mentioned. With respect to the presence of $Cs_2S_2O_7$ we cannot give an answer. The low content of Cs did not allow any identification by XRD.

2) The different strengths of the alkali effect when using different alkali sulfates (Li_2SO_4, K_2SO_4, Cs_2SO_4) has been studied in the oxidation of phenanthrene [1] One may assume that the strength of adsorption of the aromatic ring system on acidic sites is reduced more effectively when a more basic alkali cation is interacting with the catalytic surface. Thus, if one postulates the same kind of mechanism for naphthalene oxidation an improvement in PA selectivity ought to be expected when using Cs_2SO_4 instead of K_2SO_4.

[1] M. Baerns, H. Borchert, R. Kalthoff, K. Kassner, F. Majunke, S. Trautmann and A. Zein, *Stud. Surf. Sci. Cat.*, **72**, 57 (1992)

Q: J. Haber (Poland)

Very often the increase of acidity of the catalyst decreases the selectivity in oxidation of aromatic compounds because the organic molecule becomes more strongly bonded to the surface, its residence time on the surface increases and so does the probability of the attack by electrophilic oxygen. This effect should however show up in the values of the heat of adsorption. Did you observe the change of the heat of adsorption on adding cesium and was this change in line with the variation of selectivity ?

A: M. Baerns

As we have shown by our kinetic study, the addition of Cs_2SO_4 leads to an elimination of the inhibiting term of rate equation which is due to the decrease of the adsorption constant (the term $c_i \times K_i$ becomes negligible compared to 1 resulting in a pseudo-first order rate equation in the hydrocarbon (see equation 2). That is to say no heat of adsorption could be derived. Your assumption on the change of the heat of adsorption appears, however, valid, in another study [1] (see in Table 1) we have, in fact, shown that the initial heat of adsorption is decreased (61 kJ mol^{-1} for V : Fe = 1:1.4 and 13 kJ mol^{-1} for V : Fe : Cs = 1 : 1,4 : 0.06, respectively).

Q: H.-g. Huang (Taiwan)

It is difficult to imagine that the CH_2-group in a hydrocarbon molecule is acidic and needs a basic site to activate it. On the other hand, for most olefinic and aromatic compound

oxidation, as alkali is added, the activity decreases rapidly. How would you compromise your results with the about facts ?

A: M. Baerns

It is well known that CH_2-groups differ with respect to their acidity in aliphatic hydrocarbons. Also in fluorene a weak acidic function may be assumed since a proton can be easily abstracted by a basic site due to the stabilization of the remaining negative charge by mesomeric effects.

In the present study also a decrease of activity could be observed if the reaction rate was related to the catalyst mass. If it is, however, referred to the specific surface area, the reaction rate is enhanced by adding the alkali compound. This is probably due to the weakening of the V-O-V bond.

Q: S. L. Kiperman (Russia)

The equation (1)

$$r_j = \frac{k_j \times K_i \times c_i \times c_{O2}}{(1 + \Sigma K_i \times c_i)(1 + K_{O2} \times c_{O2})}$$

given in this paper, is obviously based on the assumption that there are two kinds of active sites on the catalyst surface. Which evidence does exist for this assumption ? There are two possible cases:

a) this kinetic equation can describe the results obtained;

b) this equation has been selected as the best by discrimination among others.

Both of these cases are not a prove for the hypothesis of two active sites. Indeed, if the terms in brackets of the denominator are multiplied by each other, we obtain:

$$r_j = \frac{k_i \times K_i \times c_i \times c_{O2}}{1 + \Sigma K_i \times c_i + K_{O2}C_{O2} + K_{O2} \times \Sigma K_i \times c_i \times c_{O2}}$$

This equation does not prove the hypothesis, rather it calls about the concentration of intermediate on the surface, this concentration is $c_i \times c_{O2}$.

A: M. Baerns

We have performed two series of experiments; one was designed to study reactant and product inhibition and the other one to elucidate the effect of oxygen partial pressure. In the former case oxygen was in excess and could be considered to be constant while in the latter case oxygen was widely varied. From the experimental evidence, its kinetic evaluation and model discrimination our rate equation (1) was indeed the best. We agree completely with your statement that we cannot prove any mechanistic assumptions by this "kinetic" method; we do believe, however, that a dual-site mechanism in the rate-limiting step of the hydrocarbon oxidation is rather likely.

Q: M. Sinev (Russia)

Do you have an experimental evidence for decreasing of the V-O-V binding energy after the addition of Cs_2SO_4 ?

What is the mechanism of this influence of additive on binding energy ?

A: M. Baerns

It is known from literature that alkali addition to V_2O_5 leads to a shift of the V=O- and V-O-V-stretching bonds to lower wavenumbers, which could be ascribed to a decrease in binding energy [2].

The mechanism of this influence may be explained by an extended distance between the V-atoms because the alkali compound is probably incorporated into the catalyst structure. Furthermore, it is known from literature, that alkali compounds act as electron donors for the neighbored V-atoms; as a consequence the partial positive electronic charge of V is reduced resulting in a less polarized and so less strong V-oxygen bond [3].

[2] D. V. Fikis, W. J. Morphy,. R. A. Ross, *Can. J. Chem.*, **56**, 2530 (1978)
[3] D. B. Dadyburjar, S. S. Jener, E. Ruckenstein, *Catal. Rev. Sci. Eng.*, **19**, 293 (1979)

Q: J. C. Volta (France)

In your introduction, you did connect the study of the variation of the acid base properties of the catalyst with that of the doping by Cs. Why ?

Can you comment on the location and the role of Cs in the catalyst ?

A: M. Baerns

Adding a basic compound like Cs^+ leads to a decrease of the surface acidity of the vanadia-iron catalyst used in this study. This was also shown earlier by ammonia adsorption experiments [1]

The Cs(I) compounds plays a binfunctional role: it can be described as a compound which decreases the acidity of the surface and which also decreases the vanadium-oxygen-binding energy (cp. also our answer to M. Sinev).

From XPS experiments it is known (see the above cited reference, Table 3) that alkali is enriched on the surface; only small amounts are obviously distributed in the bulk of the catalyst.

Ionic radius of the cations contained in the catalysts: Cs(I): 0.167 nm; Fe(II): 0.074 nm; Fe(III): 0.064 nm; V(IV): 0.063 nm; V(V): 0.059 nm.

Guczi, L. *et al.* (Editors), *New Frontiers in Catalysis*
Proceedings of the 10th International Congress on Catalysis, 19-24 July, 1992, Budapest, Hungary
© 1993 Elsevier Science Publishers B.V. All rights reserved

AMMOXIMATION OF CYCLOHEXANONE ON TITANIUM SILICALITE: INVESTIGATION OF THE REACTION MECHANISM

A. Zecchina[a], G. Spoto[a], S. Bordiga[a], F. Geobaldo[a], G. Petrini[b], G. Leofanti[b], M. Padovan[b], M. Mantegazza[b] and P. Roffia[b]

[a]Dipartimento di Chimica Inorganica, Chimica Fisica e Chimica dei Materiali, dell'Universita di Torino, V.P. Giuria 7, 10125 Turin, Italy
[b]ENICHEM ANIC, Centro Ricerche di Bollate, V.S. Pietro 50, 20021 Bollate (MI), Italy

ABSTRACT

In a series of combined adsorption, reactivity and spectroscopic experiments in solution with ketones of different size and shape, the fundamental role of the hydroxylamine pathway in the cyclohexanone ammoximation is established. In presence of H_2O_2 and NH_3, framework Ti(IV) forms octahedrally distorted aquo-hydroperoxo and ammonia-hydroperoxo mixed complexes: the latter one being the precursor of the hydroxylamine formation. This intermediate immediately reacts with cyclohexanone in the channels or diffuses to the external solution where it gives oximation reaction with larger ketones which could not penetrate the channels.

1. INTRODUCTION

Cyclohexanonoxime is the key intermediate in the manufacture of caprolactame, a raw material for the production of synthetic fibers. The main disadvantages of the current technology are: the numerous step involved, the use of hazardous and environmentally undesirable chemicals and the heavy co-production of ammonium sulfate, a low valuable salt. Enichem Anic is developing a new simplified process for the synthesis of cyclohexanonoxime by ammoximation of cyclohexanone with ammonia and hydrogen peroxide on titanium silicalite catalyst TiS [1-3] (a very selective oxidation catalyst with H_2O_2 [4,5]). Two reaction pathways can be hypothesized i.e.:

i) the hydroxylamine path, whereby through the action of Ti centres, NH_3 and H_2O_2 give initially NH_2OH following the scheme:

$$NH_3 \xrightarrow[H_2O_2]{Ti(IV)} NH_2OH \qquad a)$$

which then reacts with cyclohexanone to give cyclohexanonoxime:

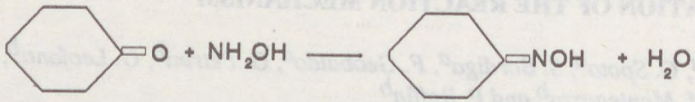

b)

ii) the imine path, whereby in presence of NH_3, cyclohexanone gives primarily the imine:

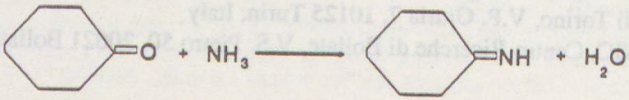

c)

which then reacts with H_2O_2 through the agency of Ti centres to give the oxime:

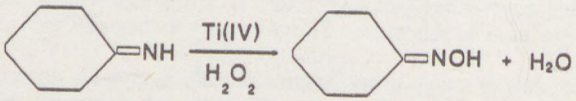

d)

The mechanism via imine intermediate has been proposed in recent contributions [6,7,8] on the basis of spectroscopic experiments. In this paper we report new results on ammoximation which are in favour of a reaction mechanism via hydroxylamine intermediate.

2. EXPERIMENTAL

Samples of TiS were synthesized according to patent literature [9] and characterized by the procedure described in ref. [10]. The adsorption experiments of ketones in liquid phase were carried out at 70° C for 6 hours, by adding 10 ml of the ketone solution (about 1% wt) in t-butanol/water to 1 g of adsorbent. The amount of ketone adsorbed was obtained from the final concentration in the liquid phase, as determined by gas-chromatography. The ammoximation runs were performed under standard conditions as described in detail in ref. [1,2,3]. The oximation runs were performed at 70° C for 40 min. by adding an aqueous solution of hydroxylamine base (50% wt) to a solution of ketone in the same solvent used for the ammoximation reaction. The ammonia oxidation test was carried out as reported in ref [11]. At the end the catalyst was filtered off and hydroxylamine was determined by polarography or by quantitative oximation of cyclohexanone. The IR and UV-Vis spectra have been performed with Bruker IFS 48 and a Varian Cary 5 spectrometer respectively.

3. RESULTS AND DISCUSSION

Catalyst evaluation

The results of cyclohexanone ammoximation tests with TiS and

other Ti containing catalysts are compared in Table 1, and clearly show that TiS is the only catalyst able to give oxime with yields higher than 90% based on hydrogen peroxide (at least in those specific experimental conditions).

Table 1. Ammoximation in water/t-butanol by different catalysts: catalyst concentration 2.0% (wt.); temperature 80°C; NH_3/H_2O_2 2.4; reaction time 1.5 hours.

Catalyst	Ti %	H_2O_2/Cy-Hexanone molar ratio	Cyclohexanone Conv. %	Oxime select. %	Oxime yield based on H_2O_2 %
None	-	1.07	53.7	0.6	0.3
SiO_2 amorphous	0	1.03	55.7	1.3	0.7
Silicalite	0	1.09	59.4	0.5	0.3
H-ZSM 5	0	1.08	53.9	0.9	0.4
TiO_2/SiO_2	1.5	1.04	49.3	9.3	4.4
TiO_2/SiO_2	9.8	1.06	66.8	85.9	54.0
Ti-Silical.	1.5	1.05	99.9	98.2	93.2

According to [2,3] we so conclude that this is the most significant parameter to discriminate properly and unproperly prepared TiS. There is also large evidence that TiS samples giving low ammoximation yields, based on hydrogen peroxide, contain little framework Ti [12]: this allows to hypothesize that the reactive center is a framework isolated Ti.

Catalyst characterization: general considerations

Ti-Silicalite is usually characterized by: I) X-Ray diffraction (expansion of lattice parameters vs Ti content) [9]; II) infrared spectroscopy: characteristic band at 960 cm^{-1}, attributed to a stretching mode of a tetrahedral [SiO_4] unit perturbed by the presence of an adjacent framework titanium or to a stretching mode of a [TiO_4] unit itself [10,14,15]; III) reflectance spectroscopy in the UV-Vis: characteristic band at 48000 cm^{-1} attributed to a C-T transition of tetrahedral (framework) Ti; absence of any relevant absorption in the 40000-30000 cm^{-1} range (extralattice Ti, in form of TiO_2 microparticles) [10,13]; IV) absence of a Raman peak at 140 cm^{-1}, due to extraframework Ti (anatase microparticles) [10]. None of these techniques gives fully quantitative results. However, when all the previous conditions are fulfilled as in the present case (TS1 in ref [10]), it can be stated with confidence that nearly all Ti is in framework.

Ketone reactivity in ammoximation

In order to solve the mechanism dilemma, we have programmed a series of reactivity and adsorption tests in solution, involving ketones with different reactivity, molecular size and shape. Ammoximation is a general reaction for carbonylic compounds like ketones and aldehydes [1] (Table 2).

Table 2. Ammoximation of different ketones in t-butanol/water: TiS concentration 2% (wt.); temperature 80 ° C; NH_3/H_2O_2 molar ratio 2.4; reaction time 5 hours.

Ketone	H_2O_2/Ketone molar ratio	Ketone Conv. %	Ketone Select. %	H_2O_2 yield %
Cyclohexanone	1.08	92.4	99.9	93.8
Cyclopentanone	1.07	99.9	90.4	84.6
4-tbu-Cy-hexanone	1.05	93.6	91.0	82.8
Cyclododecanone	1.02	53.0	99.9	52.0
Acetophenone	1.02	50.8	98.1	48.9
2-tbu-Cy-hexanone	1.06	3.8	14.4	0.5

From these results we conclude that there is a large scale of reactivity ranging from cyclohexanone (the most reactive) to 2-tert-butyl-cyclohexanone (almost non reactive). These results are consistent with both hydroxylamine and imine intermediates hypothesis as they can be explained: i) according to first hypothesis in terms of different reactivity of ketones with hydroxylamine; ii) according to the latter hypothesis in terms of different diffusion properties of ketone or the corresponding imines into the catalyst.

Adsorption of ketones on Ti-Silicalite

To further elucidate the mechanism, we have compared in detail the adsorptive behavior of cyclohexanone and other three ketones: 4-tert-butylcyclohexanone, 2-tert-butylcyclohexanone and cyclododecanone. The adsorption data of these ketones on TiS from an aqueous-alcoholic solution (the same used in the ammoximation test) are shown in Table 3. It can be seen that, near the reaction temperature, cyclohexanone is adsorbed on the catalyst, while the others are not. Because of their shape and size, the three ketones are unable to diffuse to the active sites located in the channels. These results immediately discard the hypothesis of an imine intermediate, because 4-tert-butylcyclohexanone and cyclododecanone, although not present in the channels, give the ammoximation reaction, the first with good yield. In other words, the imine observed by IR appears to

be more a systematic spectator (because of the presence of NH_3), than an active participant in the ammoximation reaction.

Table 3 Adsorption data of ketones in t-butanol/water

Ketone	equilibrium concentration	
	solution (mol/l)	TiS (mmol/100g)
Cyclohexanone	0.12	13
4-tbu-cyclohexanone	0.07	0
2-tbu-cyclohexanone	0.08	0
cyclododecanone	0.08	0

Ketone reactivity in oximation with hydroxylamine

Since hydroxylamine is the reaction intermediate, the different ketone reactivity in ammoximation reported in Table 2 must be explained by a different reactivity of ketones towards hydroxylamine to give oxime. So we made oximation experiments in the same experimental conditions of the ammoximation test but in absence of the catalyst. In Fig. 1 the results are compared with those obtained in ammoximation: there is a strong evidence of a correlation between the ketone reactivity in both reactions. Hence the oximation is the rate determining step of the overall reaction, at least for the ketones but cyclohexanone.

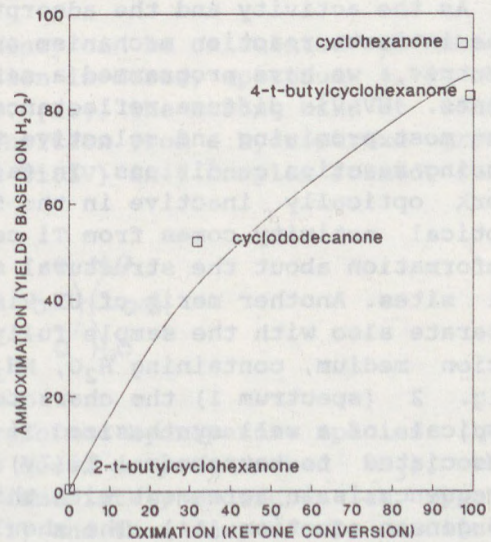

Fig.1. Comparison of ketones reactivity in ammoximation and oximation reactions.

Ammonia oxidation catalyzed by Ti-Silicalite

To complete the investigation we studied the oxidation of ammonia with hydrogen peroxide on TiS. We found that TiS is a very selective catalyst for the oxidation of ammonia to hydroxylamine [11]. From table 4 it can be seen that in the same conditions of ammoximation reaction (but in the absence of cyclohexanone), hydroxylamine can be synthesized with yields, based on hydrogen peroxide, higher than 60%. These results definitely substantiate an ammoximation mechanism via hydroxylamine intermediate.

Table 4. Oxidation of ammonia with H_2O_2 on TiS (temp. 70° C)

Reaction time (h)	Cat. conc (wt %)	NH_3/H_2O_2 molar ratio	H_2O_2 yield (% moles)
0.8	-	30	0.5
0.8	1.7	11	48.0
0.5	1.7	31	63.2

The UV-Vis DRS of the active Ti centres in presence of reactants: reaction mechanism.

As the activity and the adsorption tests could not elucidate the intimate reaction mechanism and the structure of the active centres, we have programmed a series of spectroscopic experiments. UV-Vis diffuse reflectance spectroscopy appears to be the most promising and selective tool for TiS characterization during reaction conditions. In fact, being the siliceous framework optically inactive in the 50000-15000 cm^{-1} range, any optical activity comes from Ti centres and so gives selective information about the structural and chemical situation of the Ti sites. Another merit of UV-Vis spectroscopy is that it can operate also with the sample fully immersed in the liquid reaction medium, containing H_2O, NH_3, H_2O_2 and cyclohexanone. In Fig. 2 (spectrum 1) the characteristic peak at ≈ 48000 cm^{-1} typical of a well synthesized Ti-Silicalite, outgassed at RT, associated to tetrahedral Ti(IV) [14] is shown. The observed frequency is in agreement with that calculated by means of the Jörgensen equation [14]. The shoulder at 34000 cm^{-1} corresponds to a very small amount of extraframework Ti. As it has been shown in previous papers [10,14,15] the ≻Si–O–Ti≺ bonds connecting the $[TiO_4]$ unit to the siliceous framework and emerging in the channel, can be opened by the action of water with formation of ≻TiOH (and more unfrequently ≻$Ti(OH)_2$)

structures. Immersion of TiS in water gives spectrum 2. The abrupt frequency shift of the maximum to lower wavenumbers indicates that a ligand (H_2O) addition reaction has taken place, which can be represented as mainly due to:

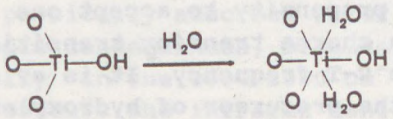

whereby tetrahedrally coordinated Ti(IV) complexes is transformed into distorted octahedrally coordinated aquo-hydroxo complexes. The observed frequency can be derived from the Jörgensen equation [16]. When an ammonia solution is used instead of pure water (spectrum 3), H_2O ligands are substituted by NH_3 and an extra peak at $\approx$ 37000 cm^{-1} due to a C-T transition from coordinated NH_3 to Ti_{oct}(IV) in complexes

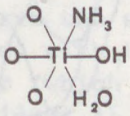

shows up. The observed frequency can be calculated as above [16]. Finally when H_2O_2 solution is dosed, spectrum 4 is obtained: in agreement with ref. [16], the strong band at 25000 cm^{-1} is assigned to a C-T transition from a hydroperoxo group to a octahedrally coordinated Ti(IV) in a complex formed following the reaction:

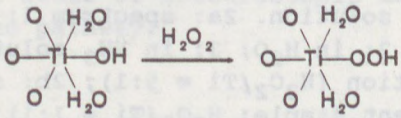

When NH_3 is dosed on the preformed hydroperoxo species (but the same occurs when H_2O_2 is dosed on preadsorbed NH_3), the band initially at 25000 cm^{-1} immediately undergoes an upward shift to 27500 cm^{-1} (spectrum 5) and then very slowly declines (spectrum 6). If the experiment is done at 60° C the second step becomes very fast and the hydroperoxo species is readily consumed. The upward shift can be explained on the basis of the formation of the mixed complex:

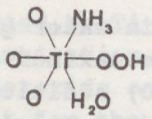

because the insertion of the basic NH_3 ligand in the Ti(IV) sphere, depresses its propensity to accept one electron from the OOH ligand during a charge transfer transition, with subsequent increase of the C-T frequency. It is evident that the mixed complex can be the precursor of hydroxylamine formation in reaction a) (which is very slow at RT but becomes fast at 60° C).

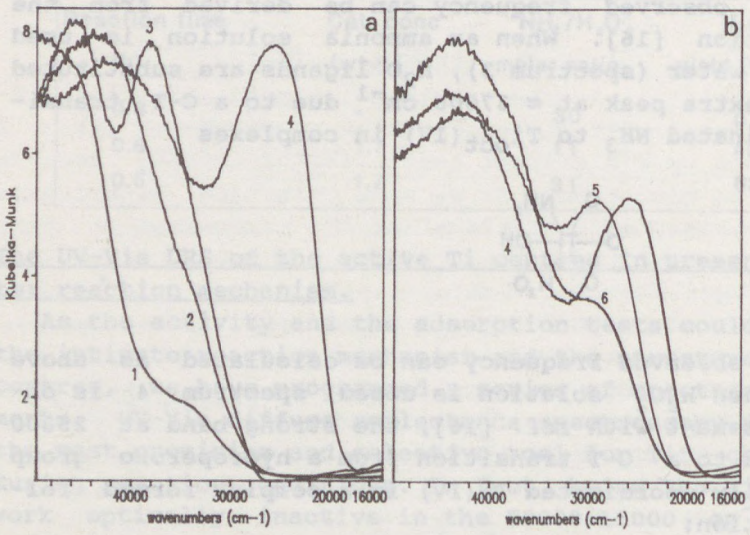

Fig. 2. DRS of TiS in solution. 2a: spectrum 1: TiS in vacuo (reference spectrum); 2: in H_2O; 3: in NH_3 solution (NH_3/Ti = 5:1); 4: in H_2O_2 solution (H_2O_2/Ti = 5:1); 2b: spectrum 4: in H_2O_2 solution (different sample; H_2O_2/Ti = 1:1); 5: the same after NH_3 addition (NH_3/H_2O_2 = 1:1); 6: after 30 min.

Direct dosage of a NH_2OH solution on Ti-Silicalite gives a very similar spectrum. These results, together with the chemical proofs, support the hydroxylamine path. Dosage of cyclohexanone at this stage does not give the usual band at 34000 cm^{-1} of the C=O chromophore (observed when cyclohexanone is dosed first). As oxime does not have any relevant absorption in the 45000-30000 cm^{-1} range, this result is in favour of the reaction b).

The infrared spectra

A similar set of experiments has been performed in an IR cell. In this case the dosage of the reactants was made from both the gas phase and from solution. In order to simulate as much as possible the working conditions, spectra were recorded in presence of physically adsorbed water. This had however severe spectroscopic consequences, because the strong H_2O absorptions (especially in the 3800-3000 cm^{-1} range and at $\approx$ 1600 cm^{-1}) tend to obscure the infrared manifestation of the other reactants (adsorbed NH_3, H_2O_2, etc.). Despite these difficulties, we have found that: 1) dosage of NH_3 on preadsorbed cyclohexanone gives the imine through the reaction c) as demonstrated by the decrement of the carbonyl absorption at 1680-1720 cm^{-1} and formation of a weak imine band at 1655 cm^{-1}; 2) dosage of NH_3 at 60° C on preadsorbed H_2O_2 gives a very weak band at 1590 cm^{-1} indicative of NH_2OH formation (the same band is formed when NH_2OH is directly dosed on TiS); 3) when cyclohexanone is dosed on TiS previously contacted with NH_3 and H_2O_2 at 60° C, we can observe the stretching and bending mode of $-CH_2-$ groups of the ring, with their full intensity, while the carbonyl band is weaker (which is consistent with both of the imine and oxime formation); 4) dosage of cyclohexanone on TiS containing NH_2OH leads to the immediate formation of oxime (essentially the same CH_2 bands of cyclohexanone but no evidence of carbonyl band).

The results shown in poits 1) and 4) indicate that IR spectroscopy alone is not capable to unambiguously discriminate between the two mechanisms (even if evidence of the hydroxylamine formation is obtained). This explains why a few authors, [6,7,8] on the basis of spectroscopic measurements, have suggested the imine pathway.

4. CONCLUSION

Adsorption and reactivity experiments in solution with ketones of different shape and size, demonstrate that the ammoximation reaction procedes *via* hydroxylamine intermediate. The role of the catalyst centres is to form mixed Ti(IV) ammonia-hydroperoxide octahedral complexes which evolve to hydroxylamine. Hydroxylamine can then either immediately react with small ketones diffused in the channels (cyclohexanone) or migrate to the external surface and than react with larger carbonylic compounds which could not penetrate the channels.

REFERENCES

1) P. Roffia, M. Padovan, G. Leofanti, M.A. Mantegazza, G. De Alberti, G.R. Tanszik, U.S. Pat. 4, 794, 198 (1988).
2) P. Roffia, G. Leofanti, A. Cesana, M. Mantegazza, M. Padovan, G. Petrini, S. Tonti, P. Gervasutti, Stud. Surf. Sci. Catal., 55 (1990) 43-51.
3) P. Roffia, G. Leofanti, A. Cesana, M. Mantegazza, M. Padovan, G. Petrini, S. Tonti, V. Gervasutti, R. Varagnolo, Chim. Ind., (Milan) 72 (1990) 598-603.
4) V. Romano, A. Esposito, F. Maspero, C. Neri, M.G. Clerici, Chim. Ind., (Milan) 72 (1990) 610-616.
5) M.G. Clerici, G. Bellussi, V. Romano, J. Catal., 129 (1991) 159-167.
6) A. Thangaraj, S. Silvanasanker, P. Ratnasamy, J. Catal., 131 (1991) 394-400.
7) J. Sudhakar Reddy, S. Silvanasanker, P. Ratnasamy, J. Mol. Catal., 69 (1991) 383-392.
8) Z. Tvaruzkova, K. Haberseberger, N. Zilkova, P. Jiru, Appl. Catal. A: General, 79 (1991) 105-114.
9) M. Taramasso, G. Perego, B. Notari, U.S. Pat. 4.410.501 (1983).
10) A. Zecchina, G. Spoto, S. Bordiga, A. Ferrero, G. Petrini, G. Leofanti, M. Padovan, Stud. Surf. Sci. Catal., 69 (1991) 251-258.
11) M. A. Mantegazza, M. Padovan, G. Petrini, P. Roffia, It. Pat. Appl. MI 91A001915 (1991).
12) G. Petrini, A. Cesana, G. De Alberti, F. Genoni, G. Leofanti, M. Padovan, G. Paparatto, P. Roffia, Stud. Surf. Sci. Catal., 68 (1990) 761-766.
13) G. Bellussi, V. Fattore, Stud. Surf. Sci. Catal., 69 (1991) 79-92.
14) M. Boccuti, K.M. Rao, A. Zecchina, G. Leofanti, G. Petrini, in "Structure and Reactivity of Surfaces" C. Morterra et al. Eds. Elsevier, Amsterdam, (1989) 133.
15) A. Zecchina, G. Spoto, S. Bordiga, M. Padovan, G. Leofanti, G. Petrini, in " Catalysis and Adsorption by Zeolites" Öhlman et al. Eds., Elsevier, Amsterdam, (1991) 671-680.
16) C.K. Jörgensen, Prog. Inorg. Chem., S. J. Lippard Ed. Intersci. Pub., J. Wiley N.Y., 12, (1970) 101.

DISCUSSION

Q: S. Kaliaguine (Canada)

By XPS we have observed that upon adsorption of H_2O_2 the coordination of Ti changes from tetrahedral to octahedral configuration, is in agreement with your UV-visible result.

However, we do not obtain octahedral Ti upon adsorption of water. From your UV-visible spectra would you exclude the possibility of a pentacoordinated Ti formed by the interaction with water. Such a pentacoordinated site has been proposed by the group of Professor Schulz-Ekloff to explain this XANES data and by our own groups in the interpretation of our XANES and EXAFS results.

A: A. Zecchina

Our UV-Vis spectra has been taken with the sample in full immersion in water (in order to approach as much as possible the reaction conditions).

The XANES results you are mentioning are obtained on samples containing some adsorbed water and not fully immersed. The two different conclusions concerning the coordination state can so find a simple explanation on this basis.

Q: H. L. Krauss (Germany)

If the reaction

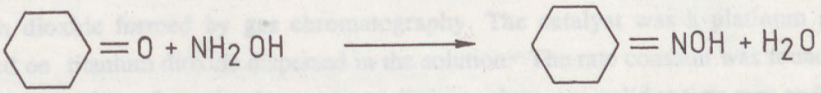

is the rate determining step, then the reaction $NH_3 + H_2O_2 \rightarrow$ should give (in presence of TiS) NH_2OH more than used up in the first reaction. Can you use this procedure (without the cyclohexanone) for a synthesis of hydroxylamine ? It could be better in the sense of avoiding poisons in the waste (environmental danger) compared with old procedures.

A: A. Zecchina

We can assert that the reaction between ketone and hydroxylamine to give oxime is the rate determining step in ammoximation only in the case of ketones which give ammoximation yields lower than cyclohexanone: in fact, as the first step is common, this difference is due to different reaction rates in the second step. About the catalytic oxidation of ammonia to hydroxylamine we agree with you: it is an interesting reaction from the synthetic point of view and we have patented it (ref. 11).

Q: S. Sivasanker (India)

Peroxydicyclohexylamine is an important (major) byproduct of the ammoximation reaction. This compound is formed by the condensation of cyclohexylimine and cyclohexanone with H_2O_2. Your mechanism (hydroxylamine) does not explain the formation of this compound. In fact, the formation of this compound suggests the presence of cyclohexylimine species in the system.

A: A. Zecchina

On the basis of our experimental results, peroxydicyclohexylimine is not a typical byproduct of the ammoximation reaction; it has been found only with catalysts of low activity in ammoximation. The synthesis of peroxydicyclohexylimine is well known: on the subject there are scientific papers [1] and patents: it is a non-catalyzed reaction between cyclohexanone, ammonia and hydrogen peroxide.

[1] E. G. E. Hawkins, *J. Chem. Soc., C*, 2663, **1969**

Guczi, L. *et al.* (Editors), *New Frontiers in Catalysis*
Proceedings of the 10th International Congress on Catalysis, 19-24 July, 1992, Budapest, Hungary
© 1993 Elsevier Science Publishers B.V. All rights reserved

ON THE CATALYTIC OXIDATION OF METHANOL WITH VANADIUM (IV) IN SULPHURIC ACID SOLUTION

R. Larsson and B. Folkesson

Group of Catalysis Research, Chemical Center, University of Lund, P.O.Box 124, 221 00 Lund, Sweden

Abstract

The oxidation of methanol by vanadium(IV) has been studied by measuring in a closed system the carbon dioxide formed by gas chromatography. The catalyst was a platinum sol, precipitated on titanium dioxide dispersed in the solution. The rate constant was found to change during the time of reaction between two distinct values, one valid at time zero and the other one valid for the later part of the reaction period.

1. INTRODUCTION

The direct use of methanol in fuel cells has been severely hindered by the poisoning of the platinum catalysts by oxidation intermediates. Therefore the reduction of suitable redox systems might offer an alternative way to utilize methanol in galvanic devices.

We have studied the oxidation of methanol in sulphuric acid of various concentrations using vanadium(IV) as the oxidant and a Pt/TiO_2 system as the catalyst. The catalyst was prepared in the way prescribed by Mills and Porter [1]. A Pt(IV) solution was reduced with citrate and the collodial sol was precipitated onto TiO_2 (Degussa P25) by adding a solution of concentrated NaCl.

The reaction was performed in a termostated vessel with a reflux condenser. The solution of $VOSO_4$ and H_2SO_4 was brought to the desired temperature and freed from oxygen by bubbling nitrogen through the system. A certain volume of methanol of the same temperature was added . The system was closed and the remaining nitrogen atmosphere was circulated through the system by means of a peristaltic pump. Samples of the gas was

taken for analysis in a gas chromatograph at chosen time intervals. The amount of carbon dioxide found in this way was transformed to a corresponding decrease in the amount of vanadium(IV) assuming the following reaction:

$$CH_3OH + 6VO^{2+} + 6\,H^+ = CO_2 + 6\,V^{3+} + 5\,H_2O. \qquad (1)$$

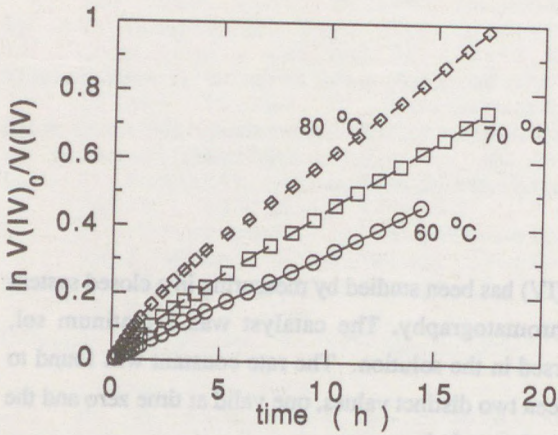

Figure 1. The experimental results for $C_{H_2SO_4}$ = 2 M.

2. RESULTS

2.1. Kinetics experiments

The results were treated in the form ln $V(IV)_0/V(IV)$ versus time. An example of such a plot is given in Figure 1. It is obvious that a simple first order reaction is not the case. The reaction seems to run fast in the starting period and to reach a state of more constant rate later on . In this it follows - almost exactly - the observations made previously [2] from measurements of the concentration of V(III). The conclusions reached at that time, however, must be somewhat modified as it is obviously possible to obtain the same results by measuring both CO_2 and V(III).

We make here the assumption that the catalyst originally has a certain activity but that the catalyst system is changed during the first period of the reaction so that its activity is somewhat decreased. If we designate the rate constant of this process of declination as k", it follows that at the time t the fraction $e^{-k"t}$ remains of the catalyst having the initial activity and the fraction $1 - e^{-k"t}$ has the lower activity. We further designate k_0 as the rate constant of

reaction (1) with the more active catalyst and k_1 as the corresponding rate constant of the same reaction with the less active catalyst.

$$k = k_0 e^{-k'' t} + k_1 (1 - e^{-k'' t}) \quad (2)$$

$$k = (k_0 - k_1) e^{-k'' t} + k_1 \quad (3)$$

$$d [V(IV)]/dt = - k [V(IV)] \quad (4)$$

$$\ln [V(IV)] = (k_0 - k_1)/k'' * e^{-k'' t} - k_1 t + \ln [V(IV)]_0 - (k_0 - k_1)/k'' \quad (5)$$

This is transformed into

$$\ln [V(IV)]_0 / [V(IV)] = (k_0 - k_1)/k'' + k_1 t - (k_0 - k_1)/k'' * e^{-k'' t} \quad (6)$$

For very large values of t this expression is reduced to

$$\ln [V(IV)]_0 / [V(IV)] = (k_0 - k_1)/k'' + k_1 t \quad (7)$$

This is the relation for the straight line defined by the points for very high t values in Fig 1. The intercept of this line makes it possible to determine k'' if k_0 can be determined in other ways.

k_0 can actually be obtained as the limit of eqn (6) for t approaching zero. (For small x it holds that $1-e^{-x} \approx x$.)

$$\lim_{t \to 0} \ln [V(IV)]_0 / [V(IV)] = (k_0 - k_1)/k'' * k'' t + k_1 t = k_0 t \quad (8)$$

k_0 can thus be determined as the limiting slope of curves such as those of Fig 1.

In Table 1 we give the resulting values of k_0, k_1 and k'' for three different values of the sulphuric acid concentration and for three different temperatures.

Figures 2 and 3 give representative examples of the results in the form of Arrhenius graphs. The activation energies that are derived from such graphs are given as a function of the sulphuric acid concentration in Figure 4. . The astonishing result appears that strongly negative activation energies are obtained for the supposed catalyst transformation process, described by k''. This will be discussed in the following.

Table 1

Results of the oxidation of methanol to carbon dioxide.

$C_{H_2SO_4}$ M	Temp °C	k_o $h^{-1}\,g_{Pt}^{-1}$	k_1 $h^{-1}\,g_{Pt}^{-1}$	$(k_o-k_1)/k''$	$k_o - k_1$ $h^{-1}\,g_{Pt}^{-1}$	k'' $h^{-1}\,g_{Pt}^{-1}$
0.5	60	1.92	1.44	0.00141	0.48	340
	70	4.10	1.72	0.01256	2.38	190
	80	6.03	2.03	0.0404	4.00	99
1.0	60	2.03	2.03	0	0	---
	70	3.91	2.49	0.02528	1.42	56
	80	4.23	2.87	0.0351	1.36	39
2.0	60	4.49	4.05	0.00455	0.44	97
	70	7.82	5.15	0.04797	2.67	56
	80	13.5	6.45	0.10212	7.05	69

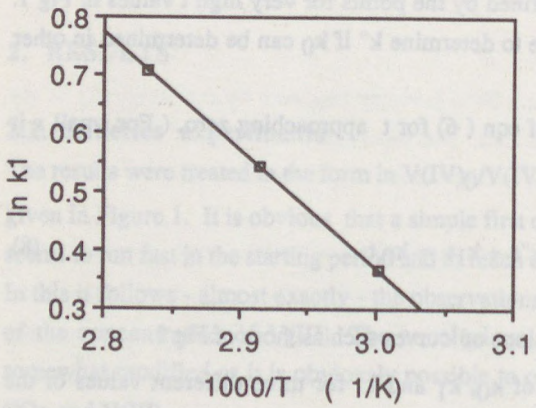

Figure 2. Arrhenius plot for k_1 and $C_{H_2SO_4}$ = 0.5 M.

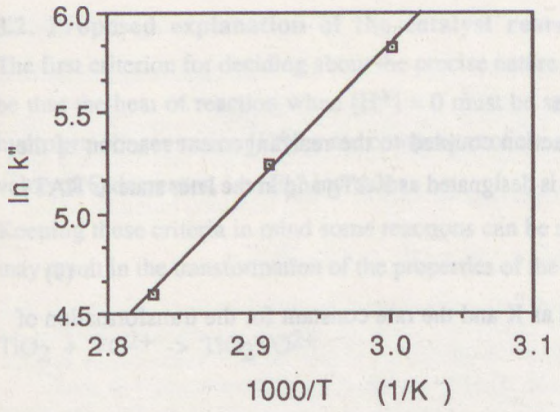

Figure 3. Arrhenius plot for k" and $C_{H_2SO_4} = 0.5$ M

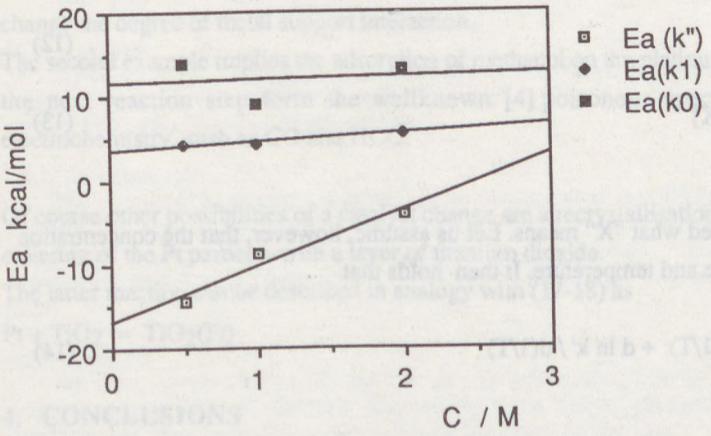

Figure 4. The acid dependence of the activation energies.

2.2 SIMS and XPS results

The catalyst system was investigated by SIMS and XPS before and after each experiment. Some of these investigations have been described before [3]. The most obvious result is that the Pt/Ti ratio as measured by XPS decreases strongly following the reaction.

The SIMS spectrum of an unused catalyst sample showed, besides the Ti and TiO signals also some signals of mass numbers 28, 29 and 41 that can be attributed to decomposition products of the citrate used for preparing the platinum sol. After a short period of reaction, the latter signals were reduced and they dissappeared seemingly after a few hours.

3. DISCUSSION

3.1 Analysis of the kinetics results

Suppose that there is an equilibrium reaction coupled to the rearrangement reaction of the catalyst . The catalyst in the original state is designated as KAT_0 and in the later state as KAT_1

$$KAT_0 + X = KAT_0 X \rightarrow KAT_1 \quad (9)$$

If the equilibrium constant is designated as K and the rate constant for the transformation of $KAT_0 X$ to KAT_1 is called k', we have

$$[KAT_0 X] = K [KAT_0] [X] \quad (10)$$

$$d[KAT_1]/dt = k' K [X] [KAT_0] \quad (11)$$

where

$$k'' = K * k' [X] \quad (12)$$

$$\ln k'' = \ln K + \ln k' + \ln [X] \quad (13)$$

So far we have not indicated what "X" means. Let us assume, however, that the concentration of X is independent of time and temperature. It then holds that

$$d \ln k''/d(1/T) = d \ln K/ d(1/T) + d \ln k' / d(1/T) \quad (14)$$

This means that

$$E_a'' = E_a' - Q \quad (15)$$

where Q is the heat of reaction of the equilibrium (9).

If $Q > E_a'$ equation (15) results in negative activation energies, as observed.

If the trend given in Figure 4 shall be reproduced it follows that the heat of reaction must decrease with increasing acid concentration.

$$Q = A - B [H+] . \quad (16)$$

3.2. Proposed explanation of the catalyst rearrangement

The first criterion for deciding about the precise nature of the species called X in eqn (9) must be that the heat of reaction when $[H^+] = 0$ must be strongly positive. On increasing the the hydrogen concentration $[H^+]$ some component of the equilibrium will be affected so that the value of Q decreases, i.e., E_a" increases.

Keeping these criteria in mind some reactions can be suggested - in a speculative way - that may result in the transformation of the properties of the catalyst.

$$TiO_2 + VO^{2+} \rightarrow TiO_2VO^{2+} \qquad (17)$$

$$Pt + CH_3OH \rightarrow Pt(CH_3OH) \qquad (18)$$

The first example implies the incorporation of vanadyl ions in the lattice of titanium dioxide. The vanadyl ions might in the subsequent step affect the properties of the catalyst, e.g., change the degree of metal support interaction.

The second example implies the adsorption of methanol on the platinum surface where it can in the next reaction step form the wellknown [4] poisonous species found in methanol electrochemistry, such as CO and HCO.

Of course other possibilities of a catalyst change are a recrystallisation of the Pt particles or the covering of the Pt particles with a layer of titanium dioxide.

The latter reaction can be described in analogy with (17-18) as

$$Pt + TiO_2 = TiO_2(Pt) \qquad (19)$$

4. CONCLUSIONS

The present investigation addresses the question, how one might characterize a rearrangement of a catalyst system. In the specific case of methanol oxidation we have measured the precursor activity (k_0), the resultant catalyst activity (k_1) and the rate of transformation (k"). By treating the activation energy of the latter in terms of the true activation constant of the transformation reaction (E_a') and the heat of reaction of a pre-equilibrium one might be able to define criteria for ways in which the rearrangement can take place and rule out others.

It should be remarked that very simple arguments can be used to explain the observed effects. It is not unreasonable that the platinum particles are covered by a TiO_2 layer, through which the reaction takes place. In this way we have a close analogue to the so-called SMSI (strong

metal support interaction) of gas phase catalysis involving Pt / TiO_2 in a reducing atmosphere [5] .One of the explanations [6] of this effect is the one that the reaction takes place at the borderline between Pt and a TiO_x layer creeping up on the catalyst surface.

If this is the case it may be quite reasonable that the Pt/Ti ratio decreases and that there is a well defined rearrangement of the catalyst and a change of its properties.

5. REFERENCES

1 A. Mills and G. Porter, J. Chem. Soc., Faraday Trans. 78 (1982) 3659.

2 B. Folkesson, R. Larsson and J. Zander, J. Electroanal. Chem. 267 (1989) 149.

3 B. Folkesson, R. Larsson and B. Rebenstorf, J. Electroanal. Chem. 272 (1989) 231.

4 B.Beden, A.Bewick and C.Lamy, J. Electroanal. Chem. 148 (1983) 147.

5 S. J. Tauster, S. C. Fung and L. J. Garten, J. Am. Chem. Soc. 100 (1978) 170.

6 R. Burch and A.R. Flambard, J. Catal. 78 (1982) 389.

DISCUSSION

Q: J. C. Conesa (Spain)
Have you considered the possibility of TiO_2 being reduced to give Ti(III) modifying the catalyst properties without having to invoke coverage of Pt particles?

A: R. Larsson
The standard potential (at 25 ^{0}C) for the reaction

$$2TiO_2(h,s) + 2H^+ + 2e^- \rightarrow Ti_2O_3(h,s) + H_2O$$

is E_0 = -0.091 V; there h means hydrated form of the solid oxide system. This Ti(IV) might be reduced by methanol (E_0 = +0.044 V) to Ti(III) to a slight degree. On the other hand, as long as vanadium (IV) is present in excess (E_0 = +0.36 V), it will easily reoxidize Ti(III).

Such a redox sequence may perhaps trigger the recrystallisation of TiO_2 to cover the platinum surface (formula 19), as suggested as one possible explanation for the observed effect.

The suggested coverage is supported by SIMS indicating a decrease in platinum signal intensity after the reaction.

Q: J. Raskó (Hungary)
Once you had methanol, why do you wish to oxidize it into carbon dioxide ?

A: R. Larsson
What we want to achieve is a reduction of V(IV) to V(III) in order to use the couple together with V(V)/V(IV) as a galvanic device. Hence it is advantageous to reach the carbon(IV) oxidation state from methanol.

Q: J. W. Hightower (USA)
The curvature in Figure 1 was explained by assuming two different rate constants k_0 and k_1. Can you absolutely rule out the possibility that the curvature may be caused simply by poisoning? Have you run one experiment to completion, then carried out a second experiment and observed the same curvature without any "regeneration" between the two runs?

A: R. Larsson
We have observed that the catalyst is still active after having filtered it and washed it with water and dried it. As there is probably some loss of platinum in this procedure it is, however, not meaningful to present any absolute data on the rate.

Some - if not all - of the reactions (formulae 17-19) suggested as the cause of change from rate constants k_0 to k_1 can be described as poisoning of the catalyst.

The main idea of the paper was that, given complete thermodynamic data for the various reactions proposed, one should be able to deduce from the acid dependence of the activation energies, which of the poisoning reactions that was at hand.

Guczi, L. *et al.* (Editors), *New Frontiers in Catalysis*
Proceedings of the 10th International Congress on Catalysis, 19-24 July, 1992, Budapest, Hungary
© 1993 Elsevier Science Publishers B.V. All rights reserved

ROLE OF CHROMIUM INTRODUCED INTO 12-MOLYBDOPHOSPHATES AS CATALYSTS FOR OXIDATION OF HYDROCARBONS

K. Brückman and J. Haber

Institute of Catalysis and Surface Chemistry, Polish Academy of Sciences, 30239 Krakow, Poland

Abstract

Chromium 12-molybdophosphate $Cr[PMo_{12}O_{40}]$ was obtained with Cr^{3+} in cationic positions. On heating it transforms reversibly around 650K with the destruction of Keggin anions into an amorphous phase which is stable to about 750K, above which crystalline MoO_3 appears. When after cooling the amorphous phase is exposed to water vapour, reconstructure of the initial phase takes place. XPS shows highly ionic bonding which results in hydroxylation of the surface and generation of strong acidic sites. Presence of chromium in cationic positions increases redox properties of Keggin anions rendering Cr[PMo] a highly active and selective catalyst for oxidation of methanol to formaldehyde, propane to propene and pentane to maleic anhydride. It is suggested that high activity in oxidative dehydrogenation of propane as opposed to high activity in insertion of oxygen in case of pentane may be due to the presence of amorphous phase.

1. INTRODUCTION

Heteropolyoxometalates with Keggin structure are well known as oxidation and acid catalysts, in which the redox and acid-base properties may be modified by choosing different heteroatoms, different atoms of the addenda or substituting the addenda with altervalent atoms [1,2]. One of the most studied as selective oxidation catalyst is the 12-molybdophqsphoric acid and its salts. It has been found that the acid shows highest activity and selectivity in oxidation of hydrocarbons but rather low thermal stability, whereas stable alkali

metal salts are catalytically inactive. Considerable attention has been paid to modification of oxidative properties by substitution of the addenda Mo atoms by altervalent atoms, the mixed vanadomolybdophosphates $H_{3+x}[PMo_{12-x}V_xO_{40}]$ being found to be the most selective in oxidation of alkanes [3].

Very little is known about catalytic properties of chromium containing heteropolyoxometalates. Chromium may enter into the heteropolymetalate structure either as the tetrahedrally coordinated heteroatom of the Keggin unit, or as substituent of the addenda atom or as the cation. One could anticipate that depending on its position it would modify in different way the catalytic properties of the heteropolyoxometalate. It seemed therefore interesting to undertake an attempt to synthesize the 12-molybdophosphates in the presence of various chromium salts in order to introduce chromium in different structural positions of the Keggin salt. In this paper we report the results obtained when chromium is present in form of the cation and we compare catalytic properties of the resulting catalyst with those of the most active vanadomolybdophosphoric and molybdophosphoric acids.

2. EXPERIMENTAL

2.1. Materials

Cr(III) derived preparation was obtained by mixing aqueous solutions of $Cr(NO_3)_3$ and $H_3[PMo_{12}O_{40}]$ (Fluka Garantie puriss. p.a.) in stoichiometric amounts. The precipitated hydrate of chromium molybdophosphate was purified by multiple crystallization. DTG analysis revealed that it contains 25 H_2O per chemical formula of salt. The precipitate was dried and calcined for 24 hr at 623K. Its BET surface area amounted to 1.94 $m^2.g^{-1}$. In order to confirm that chromium is present only in the cationic positions the preparation was dissolved in water and KCl was added to precipitate the Keggin anions in form of insoluble $K_3[PMo_{12}O_{40}]$. XPS analysis showed that the precipitate characterized by X-ray diagram of $K_3[PMo_{12}O_{40}]$ contained no traces of chromium. The IR spectra of the preparation contained bands identical to those of the Keggin anion in $K_3[PMo_{12}O_{40}]$. It may be thus concluded that the catalyst has the composition $Cr[PMo_{12}O_{40}]$. It will be further referred to as CrPMo.

The $H_5[PV_2Mo_{10}O_{40}]$ (HPVMo) preparation was obtained according to the method of Tsigdinos and Hallada [4] and purified by multiple crystallization from aqueous solution. Elemental analysis revealed that the real composition of the preparation was $H_{4.92}[PV_{1.81}Mo_{10.13}O_{40}]$. It was dried at 363K and calcined for 2 hr at 623K. Its BET surface area amounted to 3.84 $m^2.g^{-1}$.

$H_3[PMo_{12}O_{40}]$ (HPMo) was commercial hydrated molybdophosphoric acid (Fluka Chemie A.G.) dried at 363K and calcined for 2 hr at 623K. Its BET surface area was 2.36 $m^2.g^{-1}$.

2.2. Catalytic measurements

Catalytic properties were determined in an isothermal continuous flow microreactor (made of glass for CH_3OH and C_3H_8 oxidation and of metal in the case of pentane oxidation). On-line gas chromatographic analysis was used to determine the composition of the feed before and after the catalytic reactor. In the case of CH_3OH oxidation the mixture of reagents was obtained by passing the flow through methanol saturator maintained at 284.5 K while for C_5H_{12} oxidation by passing it through pentane saturator kept at 273 K. The gas flow rate and the catalyst weight were always adjusted in a way securing the total conversion to be smaller than 10%.

2.3.Differential Thermal Analysis

DTG/DTA experiments were carried out in air with an analyzer F.Paulik L.Erdey. The weight of sample was about 500 mg and the heating rate was 5 $K.min^{-1}$.

2.4.Infrared Spectroscopy

IR spectra were recorded on the FT-IR spectrometer Digilab FTS-14V at room temperature in KBr powder.

2.5.XRD Analysis

Powder X-ray diffraction patterns were obtained with a DRON-2 diffractometer using CuK_α radiation.

2.6.ESCA

XPS spectra were recorded on a VG Scientific ESCA-3 spectrometer using $AlK_{\alpha 1,2}$ radiation (1486.6 eV). Binding energies E_b were referenced to the C1s peak assumed to have E_b value of 285.0 eV.

3. RESULTS AND DISCUSSION

Table 1 presents the E_b values of $Cr2p_{3/2}$, P2p and O1s electrons registered with Cr[PMo] catalyst,strictly stoichiometric $K_3[PMo_{12}O_{40}]$ containing the same Keggin anion as the catalyst, and some reference compounds. The E_b values of P2p and O1s electrons of Cr[PMo] are identical to those of K[PMo] which is consistent with the conclusion

Table 1
Results of XPS analysis

Compound	Binding energy (eV) $Cr2p_{3/2}$	P2p	O1s
Cr $[PMo_{12}O_{40}]$	578.5	134.0	531.0
Cr_2O_3	576.2		
$Cr(OH)_3$	577.3		
CrO_3	580.1		
$K_3[PMo_{12}O_{40}]$		134.0	531.0

that no chromium was incorporated into the Keggin anion. The E_b value of Cr2p electrons corresponds to the range in which values for Cr^{3+} ions are encountered although it is considerably higher than in the oxide and hydroxide. This indicates that bonding between Cr^{3+} cations and Keggin anions is much more ionic than it is in oxide and hydroxide. This is in line with the behaviour of Cr[PMo] in catalytic reactions as discussed below.

In order to determine the thermal stability of the catalyst DTG/DTA experiments were carried out (Fig.1). The broad endothermic peak on the DTA curve with minimum at 418 K is due to the dehydration, water being released in two steps as manifested by corresponding two peaks on the DTG curve. After dehydration further two small endothermic peaks are observed at 663 and 703K, of which the first is accompanied by a small loss of weight, and finally a large exothermic peak appears

with maximum at 768 K, corresponding to the decomposition of Keggin anions. It should be emphasized that in case of H[PM] and H[PVMo] the

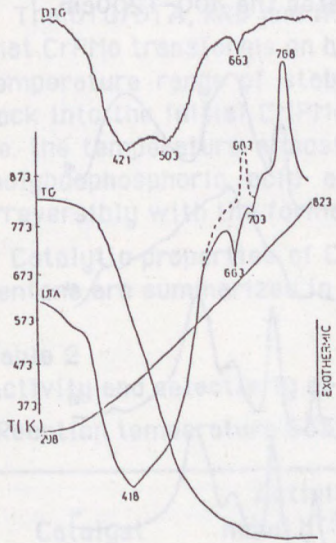

Fig.1. DTG/DTA analysis of $Cr[PMo_{12}O_{40}]$. Sample weight 0.583 g, heating rate $5K.min^{-1}$. Dotted line shows fragment of DTA curve of $H_5[PV_2Mo_{10}O_{40}]$.

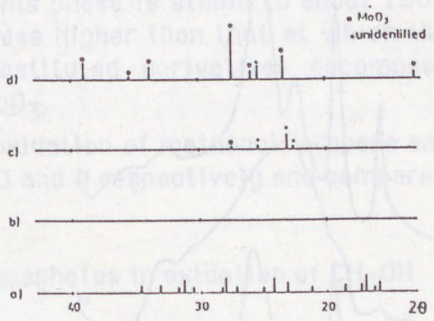

Fig.2. X-ray powder diffraction diagram of $Cr[PMo_{12}O_{40}]$. Fresh sample (a) and samples calcined for 2 hr at 623K (b), 723K (c) 823K (d).

endothermic dehydration peak is immediately followed by strong exothermic peak of Keggin anion decomposition, appearing at 683 K i.e. at the temperature ~100K lower. Comparison with X-ray diffraction patterns registered after calcination at different temperatures (Fig.2) indicates that after heating at 623K at which dehydration is completed, but before the next endothermic peak appears, an amorphous material is formed, which lost its crystal structure but Keggin anions remained unperturbed (cf.IR spectrum a in Fig.3). After heating at 723K i.e. above the two endothermic peaks the material remains amorphous but the Keggin anions were destroyed and few very weak broad lines appear in the X-ray pattern. Only after calcination at 823K above the exothermic peak the X-ray pattern reveals the presence of crystalline MoO_3. Contrary to that in the case of H[PMo] and H[PVMo] peaks of

crystalline MoO_3 appear in the X-ray diagram already after heating at 683 immediately after completion of the dehydration.

Further information on the structure of the catalyst was obtained from IR spectra of these samples.Fig.3A illustrates the 400-1200cm^{-1}

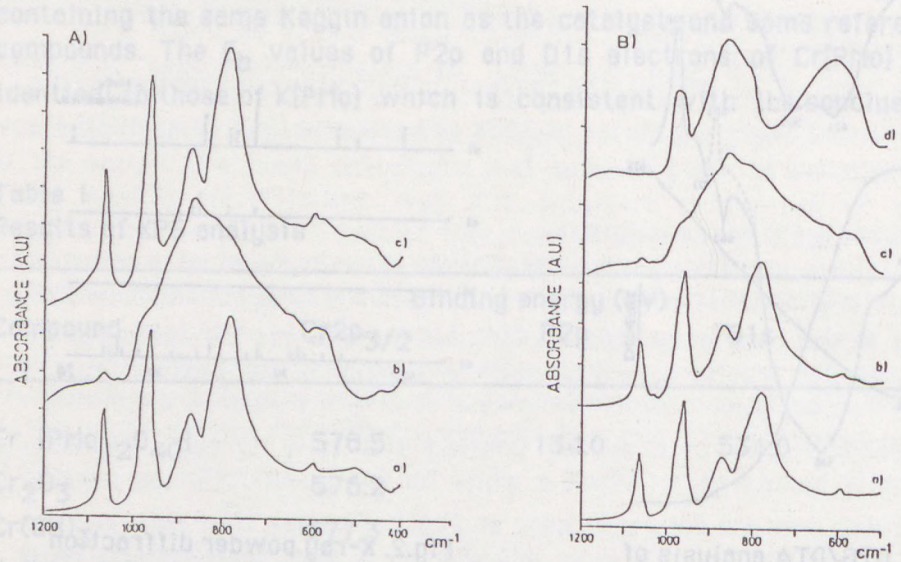

Fig.3. FT-IR spectra of Cr $[PMo_{12}O_{40}]$. A. after different thermal treatment for 2 hr at 623K (a), 723(b), cooled to r.t. and exposed to water vapour (c). B. Fresh sample (a), after calcination for 2 hr at 623K (b), 723K (c) and 823K (d)

range of IR spectra of the Cr[PMo] preparation which has been heated to 723K and then cooled to room temperature and exposed to water vapour and Fig.3B - the same range of IR spectrum for Cr[PMo] which after heating at 723 has been further heated at 823K. It may be seen that after heating at 723K the characteristic spectrum of the Keggin anion with bands at 1062, 965, 871 and 790 cm^{-1} [5] disappears and a broad featureless band builds up instead. When at this point the sample is cooled and exposed to humidity, the spectrum characteristic for the Keggin anion reappears almost unchanged indicating that this anion has been reconstructed. When, however, the sample is further heated to 823K, it shows broad bands at 980, 867 and 618 cm^{-1} indicative of

MoO_3 formation. In the case of H[PMo] and H[PVMo] samples the IR spectrum of MoO_3 becomes visible already after heating to 673K and does not change on cooling and exposure to humid atmosphere.

The DTG/DTA, XRD and IR data discussed above lead to the conclusion that CrPMo transforms on heating into an amorphous phase with a broad temperature range of stability, which can be reversibly transformed back into the initial Cr[PMo] phase. This phase is stable to about 750K i.e. the temperature almost 100 degrees higher than that at which the molybdophosphoric acid and its substituted derivatives decompose irreversibly with the formation of MoO_3.

Catalytic properties of Cr[PMo] in oxidation of methanol, propane and pentane are summarized in Tables 2, 3 and 4 respectively and compared

Table 2
Activity and selectivity of molybdophosphates in oxidation of CH_3OH
(Reaction temperature 533K)

Catalyst	Activity $mmol.h^{-1}g^{-1}$	Selectivity (%) $(CH_3)_2O$	CH_2O	MF*	ML**	CO	CO_2
$Cr[PMo_{12}O_{40}]$	63.1	46.0	38.0	3.4	10.5	1.9	0.2
$Cr[PMo_{12}O_{40}]/SiO_2$	162.7	21.8	56.0	16.8	2.1	2.9	0.3
$H_3[PMo_{12}O_{40}]$	62.0	43.5	18.5	10.5	2.4	28.0	0.1
$H_5[PV_2Mo_{10}O_{40}]$	56.3	49.9	33.0	0.3	9.0	6.0	0.1

*/ MF = $HCOOCH_3$, **/ ML = $(CH_3O)_2CH_3$, $He/O_2/CH_3OH$ = 77/16/7

with the activity of H[PMo] and H[PVMo] known to be the best heteropolyoxometalate catalyst for oxidation of alkanes [3,6,7,8]. At oxide surfaces methanol reacts to form dimethylether on active sites of acid-base properties or transforms into formaldehyde when active sites with redox properties are involved [4]. Analysis of the data summarized in Table 2 shows that in identical experimental conditions the amount of dimethylether formed on CrPMo is comparable to that obtained with molybdophosphoric acid although CrPMo is a neutral salt. Apparently, because bonding in this salt is highly ionic, the surface becomes easily hydroxylated by heterolytic splitting of bonds in H_2O,

with proton being localized on the bulky Keggin anion and the OH group on the Cr^{3+} cation. As the Keggin anion is large, the proton is delocalized over its all oxygen atoms and shows strogly acidic properties. Indeed, IR spectrum of CrPMo even after calcination at 623K shows a broad band centred around 3400 cm^{-1} which may be assigned to hydrogen bonded OH groups or hydrated protons. It is noteworthy that the IR spectrum of amorphous material obtained after calcination at 723K in which Keggin anions have already been destroyed, still reveals the presence of this band, albeit of much smaller intensity (Fig.4). Simultaneously, however, selectivity to formaldehyde on Cr[PMo] is higher than that on H[PVMo] which is the best known oxidation catalyst

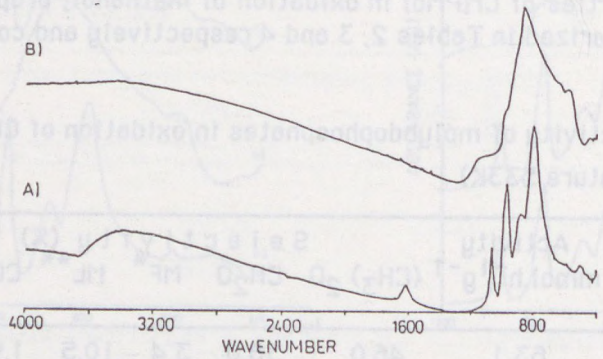

Fig.4. IR spectra of Cr $[PMo_{12}O_{40}]$ calcined at 623K (A) and 723K (B).

Table 3
Activity and selectivity of molybdophosphates in oxidation of propane (Reaction temperature 673K)

Catalyst	Activity $mmol.h^{-1}.g^{-1}$	Selectivity (%) C_1	C_2	C_3H_6	C_3H_4O	HD*	CO	CO_2
Cr $PMo_{12}O_{40}$	0.41	0.02	0.2	55	5.7	1.0	9.2	28.5
$H_5PV_2Mo_{10}O_{40}$	0.48	-	0.02	50	2.0	-	13.6	34.1

Experimental conditions: $He/O_2/C_3H_8$ = 89.5/3.5/7.0

*/ HD = 1,5-hexadiene

among the heteropolyacids and their compounds. Total activity increases dramatically and the relative ratio of the activity along the oxidation route to that along the acid-base route rises when CrPMo is deposited on SiO_2 as support.

Table 4
Conversion and selectivity of molybdophosphate catalysts in pentane oxidation (Reaction temperature 513K)

Catalyst	Conv. %	Selectivity (%) MA*	CO	CO_2
$Cr[PMo_{12}O_{40}]$	19.1	65.7	16.4	17.9
$H_3[PMo_{12}O_{40}]$	10.4	25.8	49.3	24.9
$H_5[PMo_{10}V_2O_{40}]$	15.1	44.0	29.3	26.6

Experimental conditions: $He/O_2/C_5H_{12}$ = 16.2/2.9/0.9

Analysis of the catalytic properties of CrPMo summarized in Tables 2,3 and 4 leads to the conclusion that it is an active and selective catalyst for the oxidation of hydrocarbons. In identical experimental conditions it shows greater activity in oxidation of pentane and considerably higher selectivity to maleic anhydride that H[PVMo] described in literature and patents as catalyst of best performance in the oxidation of pentane. Moreover, its great advantage over the heteropolyacids is a much higher thermal stability and hence prolonged lifetime. It is noteworthy that similarly as in the case of heteropolyacids maleic anhydride is formed from pentane as the single oxygenated product, the only other products being carbon oxides. An interesting general conclusion emerges that the presence of chromium in the cationic sites influences the catalytic activity of the Keggin anions. When propane is oxidized, propene appears as the prevailing product indicating that oxidative dehydrogenation is proceeding fast in comparison with the next step of nucleophilic oxygen addition, in which acrolein is formed. Oxidation of propane was carried out at 673K i.e. in the temperature range, in which the catalyst was reversibly transformed into an amorphous phase and the structure of Keggin anions was destroyed, whereas oxidation of pentane in which addition

of oxygen took place was studied at 513 K when the catalyst could still exist in its crystalline form. One could advance a hypothesis that abstraction of hydrogen from alkanes to form alkenes can proceed on amorphous phase with short range order only. Taking into account the instability of heteropolyacids one could suspect that also in the case of H[PVMo] an undetectable amorphous phase is formed at the surface, which is responsible for the oxidative dehydrogenation of propane.

4. CONCLUSIONS

Chromium 12-molybdophosphate due to highly ionic bonding and large size of the Keggin anion behaves in catalytic reactions as catalyst exhibiting strong acidity, comparable with that of molybdophosphoric acid. Chromium, although it is present as Cr^{3+} in cationic positions, strongly modifies the redox properties of the Keggin anion rendering it a very active and selective oxidation catalyst. On heating it transforms reversibly with the destruction of the Keggin anion into an amorphous phase which shows a broad range of thermal stability between 650 and 750K. In this temperature range it behaves as selective catalyst for oxidative dehydrogenation of propane to propene whereas at lower temperatures it is an efficient catalyst for nucleophilic addition of oxygen in oxidation of pentane to maleic anhydride. A hypothesis may be advanced that the presence of the amorphous phase is responsible for this difference in catalytic properties.

5. REFERENCES

1. M.T.Pope, Heteropoly- and Isopolyoxometalates, Springer Verlag, Berlin 1983.
2. M.Misono, Catal.Rev.-Sci.Eng., 29 (1987) 269.
3. G.Centi, J.Lopez Nieto, C.Iapalucci, K.Bruckman, E.M.Serwicka, Appl. Catal. 46 (1989) 197.
4. G.A.Tsigdinos, C.J.Hallada, Inorg.Chem. 7 (1968) 137.
5. C.Rocchiccioli-Deltcheff, E.Thouvenot, R.Franck, Spectrochim.Acta 32A (1976) 34.
6. K.Bruckman, J.Haber, E.Serwicka, Faraday Disc.Chem.Soc. 89 (1989) 173.
7. M.Ai, J.Catal. 85 (1984) 324.
8. M.Ai, Proc.8th Intern.Congr.Catal.,Berlin 1984,Dechema-Verl.Chemie Frankfurt/Main 1985, vol.5, p.475.

DISCUSSION

Q: F. Trifiro (Italy)

It is interesting to speculate on the strong acidity of the completely solidified heteropolyacid. Is it due perhaps to the fact that free acid is still present or the surface ? We have found the some feature on K-sulfided heteropolyacid. In order to better characterize the calcined amorphous catalysts, it might good to use electronic diffuse reflectance spectroscopy in order to determine the real nature of Cr(III).

A: J. Haber

The system you mentioned, which has been widely studied in our laboratory, consisted of insoluble potassium molybdophosphate, which was impregnated with acid forming thus a supported monolayer. This monolayer could have been washed out leaving the neutral insoluble potassium salt. At variance, the chromium salt is soluble and the catalyst is obtained from chromium nitrate and molybdophosphoric acid. It can be repeatedly dissolved and precipitated, the presence of acid being undetectable. In spite of that the catalyst shows high acidity. Thus, we prefer to speak about surface hydrolysis as the origin of acidity.

Q: J. C. Vedrine (France)

You have nicely shown that neutralizing protons of $H_3PMo_{12}O_{40}$ by Cr(III) clearly enhances oxidation properties. However, the surface area value is small (1 to 3 m^2g^{-1}), i.e. only surfaces of the crystallites are active. Can you comment on this point and discuss in the same sense the effect of calcination temperature since the HPA is transformed into the component oxides ?

A: J. Haber

The chromium molybdophosphate is soluble in water and its behavior is similar to that of the molybdophosphoric acid. Thus, it can be considered as "pseudo-liquid" phase. When the Keggin unit is thermally decomposed and its primary structure collapses, the behavior of the system changes dramatically.

Q: R. K. Grasselli (USA)

1) In your very interesting work on the oxydehydrogenation of propane to propene using your amorphous $CrPMo_{12}O_{40}$ at 673 K, I would like to ask how stable is this catalyst under reaction conditions. Can this catalyst's activity and selectivity be maintained over long periods of time (i.e. days) ?

2) Your data on propane oxydehydrogenation gives 55 % selectivity at low conversion (<10 %), giving a yield of about 6 % propene, what is the maximum sustainable yield you can obtain with your amorphous catalyst (unsupported or supported), i.e. performance at high propane conversion ? As you know, there are quite a few oxydehydrogenation catalysts known which yields 6 to 10 % propane from propane, but very few that give substantially higher yield, - that is, why it would by most interesting to know how far you can push your catalytic system.

A: J. Haber

In our studies we addressed mainly the problem of the influence of the position of transition metal ion on the properties of heteropolycompounds. However, exploratory studies are being carried out to optimize the reaction conditions and determine the stability of the system.

Q: H. Idriss (Saudi Arabia)

MeOH to dimethylether (DME) is not an appropriate experiment to scale the degree of acidity of a catalyst since it can be related to the structure (structure sensitive reaction). How is it possible to be sure that DME formation is not due to the presence of adjacent double

vacancies that can accommodate two methanol ? It is thus not surprising to have a drop in the DME formation when the $Cr[PMo_{12}O_{40}]$ is supported on SiO_2.

A: J. Haber

The well established mechanism of the transformations of methanol on oxide catalysts consists of the formation of a methoxy intermediate on acid sites of the catalyst. This intermediate can either react with another methanol molecule to form dimethylether (acid-base pathway) or undergo a nucleophilic attack of surface oxide ion to form a precursor of formaldehyde (redox pathway). Thus, the ratio of selectivities dimethylether/formaldehyde is a measure of the acidic versus redox catalytic properties [1, 2]. In the case of heteropolyacids an additional factor appears, which is related to the ability of these systems to behave as pseudo-liquid phase, the conversion of methanol becoming a function of its absorption capacity by the secondary structure of the heteropolyacid. On supporting the heteropolyacid on SiO_2 the pseudo-liquid properties are lost, the protons become partly bound by the silanol groups present at the surface and hence the acidic pathway is hindered [3].

[1] J. G. Highfield, J. B. Moffat, *J. Catal.*, **95**, 108 (1985)
[2] K. Brückman, J. Haber, E. M. Serwicka, *Faraday Disc. Chem. Soc.*, **87**, 173 (1989)
[3] J. M. Tatibouët, M. Chem, M. Amirouche, M. Fournier, C. Rocchiccioli-Deltcheff, *J. Chem. Soc. Chem. Commun.*, 1260, **1988**

Q: H. Kung (USA)

Professor Trifiro and co-workers have proposed that the superior ability of a V-P-O catalyst to produce maleic anhydride is because the vanadyl phosphate structure stabilizes the V(IV) ions such that the catalyst undergoes oxidation and reduction much more slowly than in other vanadium compounds. Do you observe any increase in resistance to reduction/oxidation due to incorporation of Cr ?

Also Professor Trifiro reported that pentane oxidation produces a substantial amount of phthalic anhydride over VPO. What do you think is needed for the formation of phthalic anhydride from pentane and why is this not observed on your Cr-molybdophosphate ?

A: J. Haber

It is now a well established fact that in the oxidation of pentane heteropolymolybdate catalysts give only maleic anhydride at variance with V-P-O catalysts, on which always both maleic and phthalic anhydrides are formed. This must be due to the different structure of the adsorbed intermediate on these two catalysts. Professor Trifiro drew attention to the fact that the surface of V-P-O catalysts is composed of vanadyl groups arranged in pairs, and therefore both maleic and phthalic anhydrides are formed. However, in case of molybdophosphates the presence of vanadium is not essential for the transformation of hydrocarbons to anhydrides in which Mo sites are involved, it modifies only the redox potential. One can thus expect that the structure of adsorbed intermediate will be different on the two catalysts. The influence of chromium on the redox properties of the Keggin unit is under study.

Guczi, L. *et al.* (Editors), *New Frontiers in Catalysis*
Proceedings of the 10th International Congress on Catalysis, 19-24 July, 1992, Budapest, Hungary
© 1993 Elsevier Science Publishers B.V. All rights reserved

CORRELATION BETWEEN CATALYTIC AND STRUCTURAL PROPERTIES OF MODIFIED MOLYBDENUM AND VANADIUM OXIDES IN THE OXIDATION OF ETHANE IN ACETIC ACID OR ETHYLENE

M. Merzouki, B. Taouk, L. Tessier, E. Bordes and P. Courtine

Universite de Technologie de Compiegne, Department de Genie Chimique, B.P. 649, 60206 Compiegne Cedex, France

Abstract

The structural and catalytic properties in the oxidation and dehydrogenation of ethane of two catalytic systems, VPO (P/V = 1.15/1) and MoVNb (Mo/V/Nb = 0.73/0.18/0.09) are examined. Methods of preparation are improved and seen to influence strongly the catalytic behavior. A general scheme is the formation of acetic acid at low temperature (200-300°C) and low conversion, and of ethylene at high temperature (350-500°C). The presence of ethylene with acetic acid at low temperature is observed when VPO is doped or when MoVNb is prepared in oxalic acid. Considerations on the nature of active oxygens on the surface of the solids are proposed.

1. INTRODUCTION

Light alkanes C_1-C_2 do not behave similarly, nor in activity nor in selectivity. Owing to their poor activity, no mechanism has yet been experimentally established. They are thought to be activated by means of the attack of a C-H bond by surface oxygens acting as hard base. Contrary to alkenes and aromatics in which case the attack of C-H by surface O^{2-} is followed by an adsorption of a C=C bond over the naked cation, the adsorption of C-C does not seem to be actual. According to the model drawn for the selective oxidation of n-butane in maleic anhydride on vanadyl pyrophosphate (1), the adsorption should rather proceed by means of C-H...O_{surf} bonds between methyl groups and highly unsaturated surface oxygens, which are further incorporated to yield maleic anhydride.

To go further, a comparison between the reactivity of the C_1-C_5 alkanes is fruitful. Basic oxides such as LiO, MgO, La_2O_3, Sm_2O_3,..., are able to activate the most unreactive alkane which is methane (2), by providing hard basic oxygens linked to hard acid cations Li^+, Mg^{2+}, La^{3+},... Aguerro et al., studied oxidation reactions of C_2-C_5 on a same vanadyl pyrophosphate catalyst, in a flow reactor at 400°C and in "oxidizing" conditions (hydroc./O_2/He = 1.2/24.7/74.1) (3). They showed that activity follows quite linearly the number of hydrogen in normal hydrocarbons but selectivities in the corresponding oxidized compounds (acetaldehyde or acetic acid, acrolein, maleic anhydride) are very different. The

reasons are mainly because (i), oxidizing conditions are not optimized, and (ii), vanadyl pyrophosphate is very selective for n-butane and not so for other hydrocarbons, as a result of the "surface crystal field" concept (4).

Selectivity in dehydrogenation, leading to the formation of C=C and H_2O, and selectivity in oxidation, which involves also the incorporation of surface lattice oxygen in the molecule, do not address to the same kind of oxygens. For exemple magnesium vanadates, known to dehydrogenate ethane, propane and butane (5, 6), are unable to oxidize them in aceldehyde, acrolein or maleic anhydride respectively. In the case of ethane, very few people succeeded in obtaining acetaldehyde or acetic acid when molecular oxygen is used instead of N_2O. The earliest paper mentioned the formation of acetic acid using a Mo-V-Nb-O catalyst, but only at a total pressure P = 20.4 atm (7). This system was very recently studied by R. Burch et al., who examined thoroughly the influence of catalytic experimental conditions (partial pressure of C_2H_6 and O_2, temperature, flow or pulse experiments) but, as in (7), found only ethylene at P = 1 atm (8). Erdöhelyi et al., using V_2O_5/SiO_2 (9) at higher temperature (ca. 540-650°C), found mainly ethylene and CO_x and very few acetaldehyde (e.g. selectivity in acetaldehyde 3 %, 30 % of conversion at 540°C). Merzouki et al., examined the performance of several kinds of vanadium and molybdenum-based oxides, selected on the basis of criteria such as the presence of surface $O\text{-}V^{4+}$ or $O\text{-}Mo^{5+}$ able to activate the C-H bond (10). Among the examined formula, Pd doped vanadyl pyrophosphate was found as interesting as $Mo_{0.73}V_{0.18}Nb_{0.09}O_x$ proposed in (7) when prepared in a different way. At P = 1 atm, both lead to the formation of acetic acid at low temperature (250-300°C) and ethylene at higher temperature. We report here more experiments on the catalytic and structural properties of these compounds.

2. EXPERIMENTAL

2.1. Catalyst preparation

Vanadyl pyrophosphate catalysts (P/V=1.15/1) are prepared in three steps according to a procedure mentionned in (10). Pd and Te-doped VPO samples are made by the same way. Promoters are added in the first step, Te as $Te(OH)_6$ and Pd as palladium chloride in 2-butanol (10). In the case of Pd the time of formation of the precursor $VOHPO_4\ 0.5H_2O$ is considerably shortened when Pd/V = 1.0 %. Samples are called, e.g. as $VPO\text{-}Pd_{0,15}$, which means VPO doped with palladium, with Pd/V = 0.15 % (atomic ratio).

The "optimum" composition $Mo_{0.73}V_{0.18}Nb_{0.09}O_x$ (7) has been prepared differently. MoVNb-ox is prepared in oxalic acid by adding a slurry of niobium oxide and ammonium heptamolybdate to a solution of ammonium vanadate (85°C). The grey-violet solid obtained is then calcined in N_2 at 400°C (10). The other sample, MoVNb-Cl, is prepared by the same procedure, except that ammonium vanadate is first reduced in 37 % HCl at 85°C.

2.2. Catalytic experiments

A continuous flow stainless steel microreactor (14 cm length and 1.5 cm diameter) was used to determine the catalytic properties of the samples. The fixed bed reactor containing

pellets was heated by an electric furnace in the range 250-550°C. The various compositions of C_2H_6, O_2 and N_2 were fixed by flow controllers and checked by chromatography. Effluents were analyzed on two gas chromatographs equipped with a catharometer (hydrocarbons and permanent gases) and a FID (oxygenated compounds) (10).

2.3. Characterization of catalysts

X-Ray Diffraction patterns were obtained with a diffractometer using a CuKα anticathode. Surface areas were obtained using the one point BET method with a Quantasorb equipment. Thermal analysis (TGA-DTA) was performed on a Setaram TGA-DTA 92 analyser in flow controlled atmosphere at a heating rate of 10 °C/min. Scanning electron microscopy (SEM) and analysis by X emission were performed on JEOL JSM 840. Transmission electron micrographs and electron diffraction patterns were obtained with a JEOL 1200EX microscope operating at 120 kV. Numerical processing of high resolution images has been previously described (11). XPS spectra were obtained on a KRATOS ES 200 B spectrometer equipped with an Al anticathode.

3. RESULTS

3.1. Vanadyl pyrophosphate catalysts

Catalytic properties of VPO catalysts were examined in the temperature range 280-500°C and O_2/C_2H_6 = 1/1-1/8 (N_2 as diluent). For "pure" VPO (P/V = 1.15/1), at τ = 3.8 sec and O_2/C_2H_6 = 1/2, the conversion of ethane is very low and increases up to 12 % at 450°C (Fig. 1a). The selectivity in acetic acid S_{AcOH} is 100 % at low temperature. When conversion increases S_{AcOH} decreases while ethylene begins to occur, CO_x increases very slightly. This behavior (maximum of acetic acid at low temperature, ethylene at high temperature) is very similar to the one already observed with vanadium dioxide VO_2(B) (10). At T = 293°C and contact time τ = 1.8 sec, increasing the ratio O_2/C_2H_6 leads to an increase in S_{AcOH} and decrease of S_{C2H4} (Fig. 1b), CO_2 being not affected. The conversion reaches a maximum near O_2/C_2H_6 = 4.

Performance of VPO is less good when tellurium is added (Te/V = 10 %). In the same conditions as before (τ = 3.8 sec, O_2/C_2H_6 = 1/2) ethane conversion is 9.6 % at 433°C and S_{eth} = 62, instead of 11.9 and 90 % respectively. Ethylene and CO_x appear at as low as 293°C together with acetic acid : C = 1.6, S_{AcOH} = 69 and S_{eth} = 21 % (Fig. 2). On the contrary Pd has a better influence on VPO. First, the greater the amount of Pd, the more reactive the catalyst in the range of Pd/V = 0.15-1 % studied (Fig. 1b), AcOH occurs at 200°C and acetic anhydride above 300°C. Second, S_{AcOH} and S_{eth} are stabilized throughout the range 250-450°C, particularly with VPO-Pd0.15, which shows the most interesting properties (Fig. 1) in terms of conversion and selectivity in acetic acid. For example at τ = 3.8 sec and 350°C, 11 % of ethane are converted and S_{AcOH} and S_{eth} are 60 and 20 % respectively.

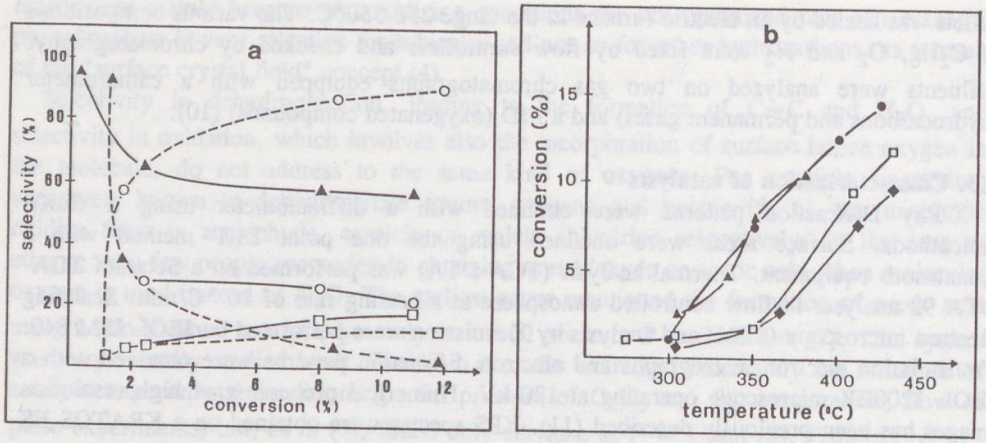

Figure 1. VPO doped and undoped catalysts. a) Selectivity in AcOH (▲), C_2H_4 (○), CO_x (□) *vs* conversion of C_2H_6 for VPO (solid line) and VPO-Pd0.15 (dashed); b) conversion of C_2H_6 vs temperature for VPO (□), VPO-Pd0.15 (▲), VPO-Pd1 (●), and VPO-Te10 (◆).
τ = 3.8 sec, $O_2/C_2H_6/N_2$=2.5/5/92.5.

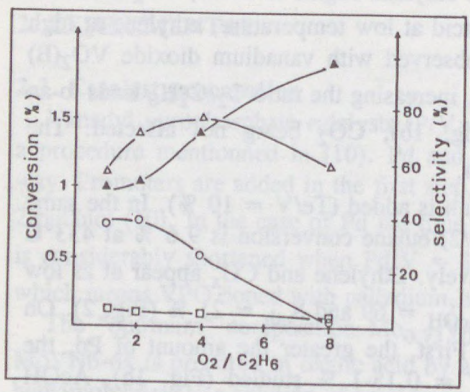

Figure 2. VPO catalyst. Influence of O_2/C_2H_6 on selectivities (same symbols as Fig. 1a) and conversion (△). τ = 1.8 sec, T = 293°C, 2.5% C_2H_6, N_2 diluent

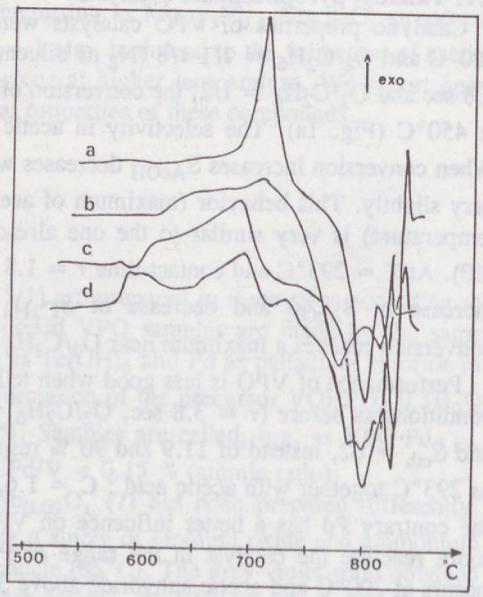

Figure 3. Effect of Pd doping on the oxidation of VPO. DTA in air flow, heating rate 10°C/mn. a) VPO, b) VPO-Pd0.15, VPO-Pd0.2, c) VPO-Pd1.

Analyses of doped and undoped VPO catalysts after calcination show the presence of $(VO)_2P_2O_7$ by XRD and IR spectroscopy. In the case of VPO-Te10, few lines belonging to $Te_2V_2O_9$ (12) are seen, but no compound of Pd nor metallic Pd are detected in VPO-Pd. However X emission and elementary analyses confirm the presence of Pd before and after catalytic test, in the same amount as initially introduced. Surface areas of these catalysts are in the range 19-23 m^2/g.

To examine the reactivity of $(VO)_2P_2O_7$ in presence of some Pd, thermal analysis of its reoxidation in air flow (17 cm^3/mn) was performed. $(VO)_2P_2O_7$ is known to be reoxidized in $VOPO_4$, in its γ form when the morphology of pyrophosphate is plate-like (13). The exothermic signal of oxidation is displayed at 705°C in DTA for VPO, and is replaced by a broader signal for VPO-Pd, the maximum of which is shifted towards lower temperature, at 680°C for VPO-Pd0.2 (Fig.3).

TEM experiments were performed on precursors and catalysts. When Pd is present charge phenomena happen and images are very unstable. However small crystallites looking like metal particles seem are present on pictures of the precursor of VPO-Pd0.15 (Fig. 4). Crystals of catalysts display the usual pattern of (100) plates of $(VO)_2P_2O_7$.



Figure 4. TEM picture of $VOHPO_4,0.5H_2O$ doped with 0.15 % Pd.

3.2. VMoVNb catalysts

Although the optimum composition $Mo_{0.73}V_{0.18}Nb_{0.09}O_x$ is used, the catalytic properties are very dependent on the method of preparation. When we prepared a sample according to the method described in (7), only traces of acetic acid were detected at low temperature. Other methods, such as oxides of Mo, V, Nb mixed and calcined in a tube sealed under vacuum or nitrogen, provided catalysts with poor reactivity (10). On the contrary, the above described methods allow conversions of 8 to 13 % as in the case of

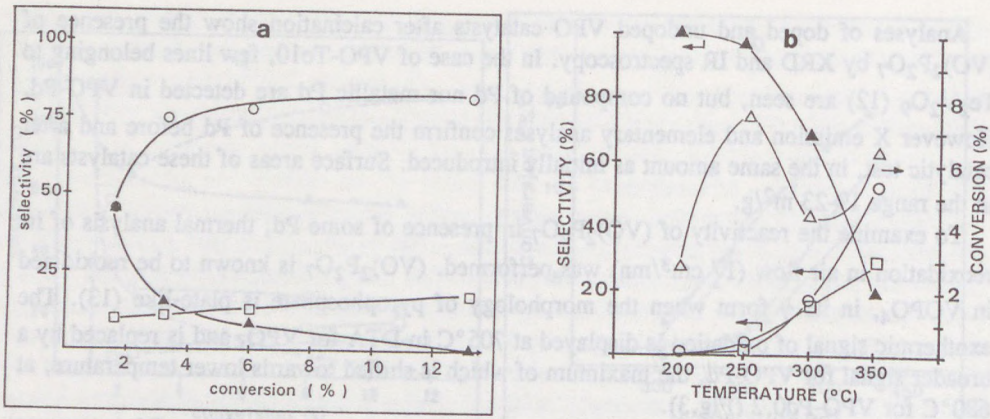

Figure 5. Influence of preparation of MoVNb on performance : a) MoVNb-ox selectivities *vs* conversion (same symbols as Fig. 1a) ; b) MoVNb-Cl selectivities and conversion of ethane *vs* temperature (same symbols as Fig. 2). τ = 6 sec, $C_2/O_2/N_2$ = 9/6/85.

VPO, but the optimal conditions (τ = 6 sec, O_2/C_2H_6 = 2/3) and the behavior of MoVNb are a little different. In the case of MoVNb-Cl, S_{AcOH} is 100 % at 200°C and decreases above, while S_{eth} and S_{CO} increase. However the shape of the conversion curve is reproducible at various contact times, by increasing and decreasing the reaction temperature, and when a new batch of catalysts is used (Fig. 5b). This phenomenon is therefore reversible with temperature. With MoVNb-ox, C_2H_4 is formed, together with AcOH, as low as 200°C (S_{eth} = 44 %) and reaches a high value (82 %) at C = 13 % (Fig. 5a).

By XRD orthorhombic MoO_3 is unambiguously identified in each catalyst, together with $Mo_{18}O_{52}$ (before and after test) in MoVNb-ox, or Mo_5O_{14} (before test), hexagonal MoO_3, Mo_5O_{14} and MoO_2 (after test) in MoVNb-Cl samples. Lines of $Mo_{18}O_{52}$, Mo_5O_{14} or MoO_2 are more or less shifted as compared with pure oxides, accounting for the formation of solid solutions. XPS revealed no significative change of energy levels of Mo or V before and after test. However the Nb/V ratio decreases strongly as compared to the initial value. Surface areas are 13 and 7.4 m^2/g for MoVNb-ox and MoVNb-Cl respectively. Chloride ions are detected in MoVNb-Cl samples before (1700 ppm) and after (800 ppm) test by chemical analysis.

4. DISCUSSION

After the screening of catalysts presented in a former paper (10), our attention was focussed on VPO and MoVNb systems, trying to understand what are the experimental factors allowing us to find acetic acid when other people do not. Supplementary experiments were made with freshly prepared batches of catalysts and found similar to the former ones. In a recent experiment, the relative amount of inert and reactive gas and the

O_2/C_2H_6 ratio were modified in the case of VPO (14). The same trend was observed, that is the formation of AcOH (alone or not) at low, and of C_2H_4 at higher temperatures. When no oxygen is fed, AcOH and/or C_2H_4 (according to the range of temperature) are formed at first and decrease quickly, which confirms that in both cases surface lattice oxygens are involved. According to our results, the (although poor) reactivity of ethane, which is roughly similar for all the examined catalysts, is very sensitive to the operating conditions, namely the oxidant/reducer ratio, and to the own reactivity of the catalyst surface, which depends in turn on the method of preparation.

4.1. Reactivity of solids

These factors, (i), the method of preparation and (ii), the operating oxidant/reducer ratio, influence strongly the kind of species and the reactivity of the catalyst. Taking the example of the selective oxidation of n-butane, in which case activation of butane needs O-V^{4+} and oxygenation O-V^{5+}, the difficulty is that if too much V^{5+} exist poor activation results, and if surface V^{4+} are not able to be reoxidized no oxygenation occurs (15). In oxidation of ethane we have similarly seen that V_2O_5 and MoO_3 are not active at low temperature nor able to induce the formation of AcOH, and that O-V^{4+} or O-Mo^{5+} are necessary for activation. Pure VO_2 (B) or Mo_5O_{14} were active initially for the formation of AcOH, but in the used conditions ($O_2/C_2/N_2$ = 0.06/0.09/0.85) they were partly or totally reoxidized and lost their properties (10). When $(VO)_2P_2O_7$ is used in oxidizing conditions (e.g. 1.5 % C_2 in air) and above 400°C the conversion is higher but carbon oxides are obtained (3). In the case of VPO, samples prepared without post-treatement with hydroxylamine (10) are less active but present a similar catalytic behavior. No macroscopic change is observed after catalytic test, which is in accordance with the fact that only the very first layers of $(VO)_2P_2O_7$ are known to work (16).

On the contrary Te and Pd modify the reactivity of VPO. The high loading of tellurium in VPO was chosen following Ai who found improved properties of VPO in the oxidation of propane in acrylic acid (17). Tellurium promotes the reoxidation of V^{4+} since chemical analysis reveals that after test only 55 % of V^{4+} are seen, which corresponds to the bad performance. Hoever the activity of VPO-Pd is slightly better and ethylene is produced at low temperature with AcOH. Chemical analysis showed that 95 % of V^{4+} are present after test. By DTA the temperature at which oxidation of $(VO)_2P_2O_7$ begins is shown to be lowered (Fig. 3). As in the case of VO_2-Pd (10), one can suppose that Pd is a catalyst for the V^{4+}/V^{5+} redox which results in an increase of conversion. This phenomenon was also observed for Pd-V_2O_5 catalysts experimented in the oxidation of ethylene in acetaldehyde at 250°C (18). According to electron microscopy Pd^0 crystals are present when the precursor $VOHPO_4,0.5H_2O$ is formed, and probably also during calcination which is performed in inert gas. Metallic palladium is well known as a hydrogen reservoir and it could also act as an active site leading for example to the increase in ethylene observed at low temperature.

In the case of MoVNb, the strange shape of conversion *vs* temperature obtained with MoVNb-Cl could account for a reversible solid state change occuring inside the catalyst,

which is still not identified. The same kind of behavior, although irreversible, was observed when the precursor $VO(H_2PO_4)_2$ (P/V = 2/1) was directly put into the reactor (14). Ethylene began to form while conversion increased with increasing temperature, and conversion fell suddenly near 400°C (temperature of decomposition into $VO(PO_3)_2$), to be stabilized again but at a lower value. In the case of MoVNb-Cl, selectivities do not seem to be perturbed and follow the usual trend.

In their extensive study on MoVNb (8), Burch et al., confirmed several points detailed in (7), particularly the same optimum composition and the positive effect of Nb They evidenced also the participation of lattice oxygen but found a new Mo^{4+} phase $(MoO_2)_3$, Nb_2O_5 with MoO_3 and no $V_9Mo_6O_{40}$, although they used the same method of preparation that they qualified as "difficultly reproducible". In fact the criterion proposed by Thorsteinson et al., (7), which is the line at 4.00 Å, is not a good one because this line is present in XRD patterns of nearly all suboxides of MoO_3. The poor reproducibility of preparation and the absence of AcOH, even in the reducing conditions they use, show how sensitive is this catalyst. The reason why we developed our (reproducible) methods of preparation was to promote the interactions between Mo, V, Nb and to increase the number of potentially active sites O-Mo^{5+} and O-V^{4+} (and also the surface area). The result is indeed the formation before and after test of reduced oxides containing these species. Moreover the substitution of Mo by V, and eventually by Nb, is known to be possible and to lead to a stabilization of $(Mo,V)_{18}O_{52}$ and Mo_5O_{14}. TGA of the oxidation of substituted Mo_5O_{14} shows that it is not reoxidized at 450°C and in air flow, contrary to pure Mo_5O_{14}. However the stabilization of MoO_2 by V^{4+} in MoVNb-Cl is not a good thing since very active Mo^{4+} are present. We have already discussed the possible structural schemes consisting in microdomains of these reduced phases inside MoO_3 matrices (10). We also noticed that the relative amount of Nb was sufficient enough to consider that Nb could be in the tetrahedral positions connecting layers of MoO_3 and $Mo_{18}O_{52}$. According to the low amount of Nb on the "surface" seen by XPS, this idea would be still valuable but for "bulk" regions. A base with a definite structural pattern would therefore act as a kind of support, enhancing the properties of the upper layers, in a similar manner to V_2O_5-TiO_2 anatase (19). Several works have also shown that metallic molybdates are more active and selective in oxidation of olefins when a large excess of MoO_3 is present (20, 21).

4.2. Possible mechanism

Since selectivity in ethylene was found independent on temperature, Burch et al. (8) concluded that CO_x are primary products and that ethane could react with specific sites formed on the surface by interaction with O_2. They noticed also that the sensitivity of the reaction to oxygen pressure p_{O2} (at constant p_{C2H6}) changes with temperature : at 370°C the effect of a change in p_{O2} on conversion is low, but becomes higher at 410°C.

These findings and our catalytic results lead us to consider two mechanisms, (I) and (II), involving two kinds of sites at low and high temperature :

t = 200-300°C $\quad C_2H_6 + 3/2\ O_2 \longrightarrow C_2H_4O_2 + H_2O$ (I)

t = 300-500°C $\quad C_2H_6 + 1/2\ O_2 \longrightarrow C_2H_4 + H_2O$ (II)

Let us discuss these possibilities, taking into account that ethane would be activated and oxidized by surface lattice oxygens, the vacancies following desorption of species being replenished by molecular oxygen. VPO catalyst is a good example for this purpose, because after catalysis no macroscopic change is observed.

- (I) is a pure oxygenation reaction, needing site(s) able to activate and to provide two O of different bond energy (becoming one C-OH, one C=O and held by the same carbon). According to the CMAS model already presented for the oxidation of n-butane in maleic anhydride on VPO, (100) plane was shown to display the right selective sites. The same loosely bound O...(O=V) which first anchors butane by means of C-H...O bonds (activation), provides the ketone group of maleic anhydride (1). Other O-(V) or (V)-O-(P) provides sites for abstraction of hydrogens and formation of water, and also O to be inserted as a C-O-C furan ring. In the case of ethane such steric or geometric factors are of less importance. On the same (100) $(VO)_2P_2O_7$, we expect that the same kind of surface lattice oxygen O...(O=V) can act as an activator of ethane, and be further inserted as a C=O. Neighboring oxygens O-(P) and O-(V) catch hydrogens, water being formed and desorbed on O-(V) sites. The same carbon can easily find an acidic OH group in the immediate vicinity, such as a P-OH. Such loosely bound oxygens can exist at low temperature since it has been shown by CMAS that the surface of $(VO)_2P_2O_7$ is equilibrated with oxygens, thermodynamic values being calculated at 25°C. Refilling of surface vacancies would be possible because it is an exothermal process (1), but desorption of water is endothermic and could be, after activation of C_2H_6, a rate-limiting process.

- (II) is an oxidative dehydrogenation involving symmetry if we consider that one H is abstracted from each carbon, leading to C_2H_4, and resulting in water. Two neighboring oxygens should be found easily to act symmetrically. Desorption of water would be more facilitated by temperatures higher than in the former process. Moreover, if ethylene finds naked vanadium sites (e.g. following desorption of water), it can be expected to be readsorbed and oxidized in acetaldehyde and/or acetic acid.

Extending these assumptions to the case of MoVNb is not an easy task, because several phases are found after reaction, with a large amount of MoO_3 itself. However all of them belong to the ReO_3 family and their structure is made with chains of octahedra linked by corners and edges. Several potential sites of oxygen with different energy exist, and among them O...(Mo^{5+}=O) could activate and O...(Mo^{6+}=O) oxidize ethane. The energy of these species and the power of the main redox system, Mo^{5+}/Mo^{6+}, are slightly modified when other cations (V^{5+}, V^{4+}, Nb^{5+}) are present, and better performance results.

5. CONCLUSION

The two catalytic systems, VPO and MoVNb, behave similarly in the oxidation of ethane. When temperature increases, for some catalysts (VPO, MoVNb-Cl), acetic acid decreases while ethylene increases, and for others (VPO-Pd, MoVNb-ox), ethylene is present with acetic acid, even at low temperature. Owing to the own solid state reactivity of each system, the adaptation of operating conditions, namely O_2/C_2, and the methods of preparation are two parameters which condition the formation of acetic acid at low temperature. The validity of the above mechanism in two parts according to the range of

temperature must be verified by a kinetic analysis which is in progress. Schemes (I) and (II) differ probably by the way of attack of one or two C-H bonds by surface lattice oxygens, the energy of which should be different in each case. The reason why (I) and (II) are separated, or concomitant as in the case of VPO-Pd and MoVNb-ox, is still obscure.

Acknowledgment : We are indebted to Dr. F. Oudet for the TEM investigations. We thank also Dr. L. Gengembre for his contribution in XPS experiments.

6. REFERENCES

1 J. Ziolkowski, E. Bordes and P. Courtine, J. Catal, 122, (1990) 126 ; Stud. Surf. Sci. Catal., 55 (1990) 747.
2 J.S.Lee and S.T. Oyama, Catal. Rev. Sci. Eng., 30 (1988) 249.
3 A. Aguero, R.P.A, Sneeden and J.C. Volta, Stud. Surf. Sci. Catal., 41 (1988) 353.
4 E. Bordes, Stud. Surf. Sci. Catal., 67 (1991) 21.
5 D. Patel, M.C. Kung and H.H. Kung, Proc. 9th Int. Cong. Catal., Calgary 1988, Vol. 4, 1554 ; ibid., J. Catal., 105 (1987) 483.
6 D. Siew Hew Sam, V. Soenen and J.C. Volta, J. Catal. 123 (1990) 417.
7 E.M. Thorsteinson, T.P. Wilson, F.G. Young, P.H. Kasai, J. Catal, 52 (1978) 116.
8 R. Burch and R. Swarnakar, Appl. Catal., 70 (1991) 129.
9 A. Erdöhelyi and F. Solymosi, J. Catal., 123 (1990) 31.
10 M. Merzouki, B. Taouk, L. Monceaux, E. Bordes and P. Courtine, 3rd Europ. Workshop Meeting on New Developments in Selective Oxidation, Louvain-la-Neuve (Belgium), 8-10/04/91. Preprints vol. 2.
11 F. Oudet, A. Véjux and H.R. Tietz, J. Microsc. Spectrosc. Electron., 13 (1988) 405.
12 A.S.T.M. File, 18-1330.
13 E. Bordes, P. Courtine and J.J. Johnson, Mater. Sci. Monogr., 28B (1985) 887.
14 L. Tessier, unpublished results.
15 E. Bordes, Catal. Today, 1 (1987) 499 ; ibid, 3 (1988) 163.
16 M. A. Pepera, J.L. Callahan, M.J. Desmond, E.C. Milberger, P.R. Blum and N.J. Bremer, J. Am. Chem. Soc., 107 (1985) 4883.
17 M. Ai, J. Catal., 101 (1986) 389.
18 J.L. Seoane, P. Boutry, R. Montarnal, J. Catal., 63 (1980) 182 and 191.
19 A. Vejux, P. Courtine, J. Sol. State. Chem., 23 (1978) 93 - 103.
20 J.S. Jung, E. Bordes, P. Courtine, Stud. Surf. Sci. Catal., 21 (1985) 345 ; E. Bordes, Stud. Surf. Sci. Catal., 55 (1990) 585.
21 U. Ozkan, R.C. Gill and M.R. Smith, 116 (1989) 171.

DISCUSSION

Q: R. K. Grasselli (USA)

In your presentation you discussed the "optimum" composition $Mo_{0.73}V_{0.18}Nb_{0.09}O_x$ for the oxidation of ethane to acetic acid and ethylene. Could you tell us what is the structure of this compound, what is the arrangement of the respective elements in the structure and the surface, and what is the distribution of vacancies, and which lattice oxygens are involved in the H-abstraction and which in the oxygen insertion steps of the redox process ? Where is the locus of dioxygen dissociation and O^{2-} formation ?

A: E. Bordes

The phases we see by XRD are not the same as those found in Refs. 7 or 8. Using our methods of preparation which differ mainly by the step of reduction of vanadium (by HCl or $H_2C_2O_4$) we observed a great amount of MoO_3 in used catalysts, together with lines corresponding to Mo suboxides but slightly shifted, and no line accounting for Nb. These shifts correspond to solid solutions of V and/or Nb in Mo_5O_{14} or $Mo_{18}O_{52}$, which are known to be more stable than pure suboxides [1]. Pure MoO_3 or V_2O_5 being inactive, we assume that the "structure" can be accounted for by microdomains of Mo suboxides inside a MoO_3 matrix, the atoms of which are activated, at least on the boundaries. The interfaces are coherent because of low crystallographic misfits which allow fast transfer of species across the boundaries. For example, in the case of MoVNb-Cl, substituted $Mo_{18}O_{52}$ is made from slabs of MoO_3 (6 octahedra high) connected by tetrahedral sites in which Nb (or V) could enter. We already proposed such models (see Figs. 6b and 7 in ref. 10 in our paper). Owing to the tendency of MoO_3 to display the (010) cleavage plane, the surface could be constituted by such planes including microdomains of reduced oxides, stabilized by V, Nb (with more Nb atoms in the bulk according to XPS) and laying on a base of excess MoO_3. According to their redox properties, Nb would be a structural stabilizer while V can be considered as an active site. Lattice oxygens involved in H-abstraction should be those linked with Mo(V) and/or V(IV) which are hard acid cations. Oxygens inserted in the hydrocarbon intermediate giving acetic acid are probably linked with V(V) and/or Mo(VI) since a redox system must account for that (or for the formation of ethylene). Dioxygen should be activated on c.u.s. neighboring Mo(V) and/or V(IV) (d^1).

[1] L. Khilborg, *Adv. Chem. Series*, **39**, 37 (1972)

Q: M. Shymanska (Latvia)

In proposed scheme of ethane oxidation mechanism, you assume that acetic acid is unique partial oxidation product formed on interacting of ethane molecule with oxygen at low temperatures (200-300 ^{0}C). It is obvious that such a reaction is starting via the hydrogen atom withdraw from ethane molecule. Do not you assume that at this step the attack of oxygen is possible and formation of acetaldehyde also may occur ?

A: E. Bordes

We do not know how ethane can be activated at low temperature to yield selectively acetic acid. Acetaldehyde is seen in small amounts only at high temperature (at least 400 ^{0}C) when ethylene is formed and seems to be an oxidation product of ethylene itself. At low temperature, after activation by one kind of oxygen (e.g. O-V(IV)), ethane would find on the surface two neighboring labile oxygens and incorporate them. It is not necessary to consider, even temporarily, the formation of ethylene because after such a step hydrogenation should occur. However, on some catalysts ethylene is produced in substantial amounts even at low temperature, together with acetic acid.

Q: F. Trifiro (Italy)

The production of ethylene in the oxidation of ethane is a good confirmation of dehydrogenating properties of $(VO)_2P_2O_7$. The mechanism of formation of CH_3COOH is lesser clear. Do you think that it forms: 1) through ethylene via a reaction type process ethane - ethylene - CH_3CHO-CH_3COOH where the last stage may occur in the gas phase, 2) or by a H-abstraction to form a radical followed by gas-phase oxidation, 3) some other mechanism ?

A: E. Bordes

When using pure $(VO)_2P_2O_7$ at low temperature there is no ethylene, only acetic acid and very few carbon oxides. Ethylene is seen at low temperature only when Pd is added or when using MoVNb catalyst. As said above, it does not seem necessary to consider a gas phase oxidation at 200 ^{0}C. Moreover, radicals are known to be very reactive, and byproducts other than carbon oxides would be formed. So we think to another mechanism involving a kind of peroxidic species, perhaps through the use of surface O^{2-}. Such catalytic species are known to exist on the surface at low temperature.

Q: M. M. Bhasin (USA)

In response to an earlier question you mentioned that ethane oxidation to acetic acid and ethylene is proceeding thru the same mechanism. If that is so, I have difficulty believing that you were able to get 0% acetic acid and rest main product to be ethylene (also in light of the earlier Union Carbide work). Could you also provide the lowest detection limit for acetic acid in your apparatus ?

A: E. Bordes

If I said so, it should only concern the first step of activation of ethane, the H-abstraction. At high temperature when ethylene is produced byproducts are carbon oxides and a few acetaldehyde and formic acid. Let me recall that we modified the preparation Union Carbide used and that we found phases in our MoVNb samples, such as Mo suboxides, which are different from those claimed. To detect acetic acid we used a FID chromatograph with a LAC446 column on which are detected alcohols, aldehydes, ketones, acids and anhydrides.

Q: D. Kalló (Hungary)

What was the stability of your catalysts ? Did you observe any appreciable deactivation. When you did, which amount of acetic acid could be produced on unit amount of catalyst under most suitable conditions ?

A: E. Bordes

Catalysts deactivate in few hours at low temperature when no gaseous oxygen is supplied. With the C_2/O_2 ratios used, a true steady state is observed, and catalysts can last five to six days without a noticeable decrease of performance.

Q: M. Sinev (Russia)

What do you mean when you say that there are two different mechanisms at "low" and "high" temperatures:

- different mechanism of ethane activation, or
- different types of oxygen species taking part in the process ?

A: E. Bordes

I mean only that at low temperature there is no need to consider that acetic acid comes from the oxidation of ethylene, whereas at high temperature acetaldehyde surely does. Now we think that the activation (H-abstraction) step is common, and consequently different types of surface oxygens should be involved. Three and one surface oxygens are needed to form acetic acid (and H_2O) and ethylene ($+H_2O$), respectively. Therefore water can form the same type of O whatever the temperature and the product, whereas special kinds of O would be inserted to give acetic acid. We think that these species could be O^{2-}.

Q: J. C. Vedrine (France)

I can easily understand your thinking when doping $(VO)_2P_2O_7$ catalyst with Pd to simulate partly Wacker process, but I have difficulties to follow your idea when introducing Nb in Mo-V-O system. Is there a structural correlation as suggested in the title or any other reason as changes in oxidation states, change in crystalline structure, etc. Can you comment on it ?

A: E. Bordes

The idea of introducing Nb is not ours and we followed the findings of Thorsteinson et al. (Union Carbide) who found acetic acid from ethane with such a MoVNb system but at high temperature and P = 20.4 atm (see ref. 7 in the paper). Nb was said to stabilize the system. With our methods of preparation we infer that Nb can enter the lattice of Mo suboxides and therefore stabilize species like Mo(V) and oxygens bonded to (or to V(IV)), that we believe involved in the H-abstraction step.

Guczi, L. *et al.* (Editors), *New Frontiers in Catalysis*
Proceedings of the 10th International Congress on Catalysis, 19-24 July, 1992, Budapest, Hungary
© 1993 Elsevier Science Publishers B.V. All rights reserved

THE PROMOTING EFFECT OF La_2O_3 ON THE CO HYDROGENATION OVER Rh/SiO_2

A. L. Borer and R. Prins

Institute of Technical Chemistry, Federal Institute of Technology, 8092 Zürich, Switzerland

ABSTRACT

The impregnation order in the preparation of La_2O_3-promoted Rh/SiO_2 catalysts has a strong influence on the catalytic properties in the high pressure CO hydrogenation as well as on the chemisorption properties. Highly dispersed Rh catalysts are obtained by impregnating $La(NO_3)_3$ prior to $Rh(NO_3)_3$. A La_2O_3-induced decrease of CO chemisorption relative to H chemisorption was not observed. While the turnover frequencies for the formation of hydrocarbons are only influenced by the Rh crystallite size, La_2O_3 promotes the formation of methanol and higher oxygenates. Oxygenate formation is related to the size of the Rh-La_2O_3 interface and therefore decreases at high La_2O_3 content in the catalysts in which Rh was impregnated first.

1. INTRODUCTION

Supported rhodium has found continuous interest as a catalyst for CO hydrogenation because of its ability to form C_1 and C_2 oxygenates. Several groups observed high selectivities to oxygenates using La_2O_3 as a support for Rh [1-6] or Pd [7-9]. High yields to oxygenates have also been observed when La_2O_3 was used as a promotor for Rh/SiO_2 catalysts [5,6,10-12]. The promotor effect has often been attributed to a decoration of the Rh crystallites by the support or promotor and to an intense interaction between the metal and the La_2O_3 overlayer. The interaction between metal and La_2O_3 was evident from negative shifts in the Pd $3d_{5/2}$ [13] and Rh $3d_{5/2}$ [14] XPS binding energies. Underwood and Bell therefore assumed that the La_2O_3 overlayer was partly reduced [4, 15] and, in analogy to the SMSI systems in which metals are supported on reducible supports [16], this may be the reason for the promotor effect. However, lanthanum is very stable in the La^{3+} oxidation state and no La compound is known with a lower oxidation state. It is therefore unlikely that La_2O_3 is involved in a redox cycle during CO hydrogenation, as was proposed for V_2O_3 [17]. Moreover, temperature-programmed reduction experiments indicated that the lanthana promotor on Rh/SiO_2 is not reduced [18].

The decoration of metal crystallites by patches of the support or promotor has been attributed to dissolution of the support during impregnation with the noble metal salt solution and subsequent precipitation of the promotor salt or oxide on the noble metal oxide during

drying [19]. During subsequent calcination and reduction patches of promotor oxide on top of noble metal crystallites will be formed. Studies of vanadia-promoted [20, 21] and niobia-promoted [21] Rh/SiO_2 have shown that upon calcination the promotor and Rh even become intimately mixed in the form of mixed oxides. A similar formation of the perovskite-type $LaRhO_3$ has been proposed for $Rh\text{-}La_2O_3/SiO_2$ catalysts [15]. EXAFS experiments, however, have shown that the formation of $LaRhO_3$ on $Rh\text{-}La_2O_3/SiO_2$ can be excluded, even after high calcination temperatures up to 1023 K [22]. Nevertheless, the EXAFS data, as well as H_2 and CO chemisorption data demonstrated that the Rh dispersion was enhanced by La_2O_3 [22].

To answer these and other questions we have studied the activity and selectivity of $Rh\text{-}La_2O_3/SiO_2$ catalysts in the CO hydrogenation reaction. We have varied the La content of Rh/SiO_2 in order to investigate the evolution of the promotor effect and to follow its impact on dispersion and product selectivities. Since the lanthana support can be dissolved by acidic impregnation solutions [6], we also investigated the order of the impregnation steps with the precursor solutions. This should also enable us to better understand the circumstances under which the migration of LaO_x moieties on the surface of Rh crystallites occurs.

2. EXPERIMENTAL

2.1. Catalyst preparation

The silica support (CF Uetikon, Switzerland, Type C-560) was purified by washing it three times in 2 M HNO_3 (360 K, 1 h) and twice in H_2O (360 K, 1 h), followed by calcination at 773 K. The resulting silica had a surface area of 460 m^2/g and a pore volume of 0.81 ml/g. This support was impregnated to incipient wetness with aqueous solutions of $La(NO_3)_3 \cdot 6H_2O$ (Fluka puriss. p.a.) and $Rh(NO_3)_3$ (Johnson Matthey, 5 % solution in 1.7 M HNO_3). The impregnation was performed in two steps with an intermediate and a final calcination in air at 773 K (3h, 5 K/min), unless otherwise stated. Before calcination, the catalysts were dried at 393 K for 3 h (2 K/min). The rhodium content was kept at 1.5 wt %, while the La:Rh atomic ratio γ was varied between 0 and 11.1. For one series, denoted LaRh, the impregnation sequence was $La(NO_3)_3$ followed by $Rh(NO_3)_3$, while for the other series, RhLa, the reverse sequence was applied. In that case a large batch of Rh/SiO_2 was prepared first and the required amount of La promotor was added to portions of this batch. For high La contents, 2 ($\gamma = 5$) or 4 ($\gamma = 11.1$) $La(NO_3)_3$ impregnation steps were necessary to reach the desired La loading for both series. Between these supplemental impregnations the samples were dried only. The coimpregnated catalysts ($LaRh^{co}$) were prepared in one step with an equimolar solution containing both rhodium and lanthanum. La_2O_3/SiO_2 was also prepared with the incipient wetness method.

2.2. Chemisorption

Volumetric H_2 and CO adsorption measurements were carried out in a stainless steel/glass apparatus using an Edwards 590 Barocel pressure sensor. H_2 was passed over Pd/Al_2O_3 and molecular sieve to remove O_2 and H_2O. Carbonyls in CO (99.997 %, Messer Griesheim) were eliminated with heated 13 X molecular sieve. The samples, usually about 0.1 g, prepared as described above, underwent a reduction at 723 K (1 h, 5 K/min) with subsequent evacuation at 673 K for 30 min at a pressure below 10^{-4} Pa. After cooling under vacuum to 293 K the adsorption isotherm was recorded between 10 and 40 kPa. The

adsorption equilibrium was reached within 10 min for the first adsorption step. For the other points equilibrium was reached immediately. The amount of chemisorbed H or CO was obtained by extrapolating the isotherm to zero pressure. The 2 % La_2O_3/SiO_2 sample did not adsorb a significant amount of H_2.

2.3. CO hydrogenation

A continuous flow stainless steel apparatus with a fixed bed reactor was used. H_2 was purified by Pd/Al_2O_3 and molecular sieve, while CO was passed over heated 13 X molecular sieve (453 K), BTS-Catalyst and A4 molecular sieve in order to minimize carbonyl, O_2 and H_2O impurities. An online gas sampling system was used for product analysis on a Hewlett Packard 5890 A gas chromatograph, equipped with a WCOT fused silica capillary column (Chrompack, Type CP Sil-8 CB) and a FID. The catalysts were first reduced with H_2 at 723 K for 1 h (5 K/min), then cooled to 533 K. The pressure was increased from 0.1 to 4 MPa before CO was introduced into the reactor. Reactions were carried out at 4 MPa total pressure and a H_2/CO ratio of 3. The conversion of CO was always around 2 % with a GHSV of 3800 l/lh. The activities and selectivities quoted in the following were measured after 15 h on stream.

3. RESULTS

3.1. Catalyst characterization

H_2 and CO chemisorption were used to estimate the amount of rhodium exposed and the results are reported in Table 1. In the LaRh series, in which La was impregnated first, a small amount of La caused the H/Rh dispersion to decrease from 0.66 for LaRh0 to 0.54 for LaRh0.12. At higher La loadings, the dispersion increased to values above unity. The RhLa samples showed a different behaviour, the dispersion becoming smaller with increasing La content. As a consequence, RhLa5.0 adsorbed three times less H_2 than LaRh5.0. The trends for the CO chemisorption were similar to those of the H_2 chemisorption (Table 1) and in general, the values for CO and H uptake were equal within the limits of experimental error.

The effect of calcination on the dispersion has been studied with the coimpregnated catalysts. The coimpregnated sample, which was calcined ex situ after preparation, had a higher CO/Rh value than the corresponding sample which was prepared by sequential impregnation (LaRh1.0), although the difference in H/Rh was small. An additional in situ calcination in the reactor at the same temperature as after impregnation (773 K) did not change the adsorption behaviour. But, the dispersion of a catalyst, which was directly reduced and not calcined at all, was much better. The lowest chemisorption values were obtained for a coimpregnated catalyst which had been calcined in situ.

Table 1
H2 and CO chemisorption

	LaRh		RhLa		$LaRh^{co}$ ($\gamma = 1$)		
γ	H/Rh	CO/Rh	H/Rh	CO/Rh	pretreatment	H/Rh	CO/Rh
0 (Rh/SiO_2)	0.66	0.58	0.66	0.58			
0.12	0.54	0.55	0.59	0.58	a)	0.85	0.94
0.5	0.82	0.74	0.53	0.60	b)	0.89	0.94
1.0	0.81	0.81	0.44	0.40	c)	1.02	0.98
2.0	1.00	0.99	0.48	0.45	d)	0.81	0.82
5.0	1.17	1.06	0.38	0.39	e)	0.59	
11.1	1.04	1.18					

a) calcined after preparation (ex situ); b) as a), with additional in situ calcination; c) only dried (393 K) after preparation; d) as c), with in situ calcination; e) calcined at 1023 K after preparation. All calcinations, except e), were performed at 773 K.

Table 2
Activities and selectivities in the CO hydrogenation

Catalyst	γ	Activity [a]	TOF [b]	Selectivities in % [c]						
				CH_4	C_2+	MeOH	C_1 E/E [d]	EtOH	C_2 E/E [d]	MeCHO
Rh/SiO_2	0	2.8	4.3	59	7	2	1	6	6	16
LaRh	0.12	4.1	7.6	37	4	16	3	21	13	5
	0.5	5.3	6.4	20	2	49	4	14	10	0
	1.0	5.9	7.3	24	1	43	4	17	10	0
	2.0	5.6	5.6	18	1	65	2	9	4	0
	5.0	5.9	5.1	16	1	71	2	7	3	0
	11.1	6.4	6.2	15	1	73	1	6	3	0
RhLa	0.12	3.6	6.0	37	5	14	3	21	13	5
	0.5	5.0	9.5	27	4	24	5	20	17	2
	1.0	4.3	9.8	29	4	28	5	18	14	2
	2.0	3.8	7.9	31	5	34	3	16	9	2
	5.0	2.2	5.7	46	4	32	2	9	5	2
$LaRh^{co}$ [e]	1.0	6.8	8.0	21	1	56	3	11	6	0
	1.0	3.9	6.6	25	3	35	4	18	12	2

[a] mmol CO converted / (mol Rh)·s; [b] mmol CO converted / (mol surface Rh)·s; [c] on a CO_2 free basis [d] esters and ethers; [e] calcined at 1023 K after preparation.

In order to determine redissolution effects during the second catalyst impregnation step, 1 g Rh_2O_3/SiO_2 (1.5 %) was stirred in 15 ml 0.46 M $La(NO_3)_3$ (pH≈4) in water for 15 min and the Rh content of the resulting solution was analysed by atomic absorption measurements on a Varian SpectrAA-10 spectrometer. In another experiment 4 g La_2O_3/SiO_2 (2.0 %) were stirred in 20 ml 0.5 M HNO_3 for 15 min and the La content of the solution was determined. The $La(NO_3)_3$ solution corresponded completely to the one used to prepare the RhLa1.0 catalyst, while the HNO_3 solution had the same acid strength as the Rh solution used to prepare the LaRh1.0 catalyst. The AAS results showed that by these treatments 89 % of the La_2O_3 on La_2O_3/SiO_2 dissolved, while only 0.1 % of Rh_2O_3 could be dissolved from Rh_2O_3/SiO_2.

3.2. CO hydrogenation

The results of the CO hydrogenation experiments are presented in Table 2. The turnover frequency (TOF) was based on the number of surface Rh atoms as determined from H chemisorption, assuming an adsorption stoichiometry of one H per Rh. No carboxylic acids could be detected, but esters and ethers were formed in considerable amounts, with esters prevailing. The selectivities were calculated on a CO_2 free basis, taking into account the number of carbon atoms per product molecule, so that methylacetate, for example, contributed for two thirds to the C_2+ oxygenates selectivity and for one third to the C_1 oxygenates selectivity. The selectivities for C_3+ oxygenates were 1 % or less, except for Rh/SiO_2 (2 %).

Rh/SiO_2 had a higher selectivity for hydrocarbons and acetaldehyde than the promoted catalysts and had the lowest turnover frequency of all catalysts. In the LaRh series, the turnover frequency exhibited a sharp increase when some La was present and decreased slightly with higher promotor loadings. The activity, however, reached its maximum only at $\gamma = 11.1$. The oxygenates, CH_4 and C_2+ HC selectivities are presented in Fig. 1a as a function of the La:Rh ratio (γ). Oxygenates selectivities higher than 80 % were obtained at high La loadings, while higher hydrocarbons almost completely disappear. The high yield in oxygenates is mainly due to the formation of CH_3OH. Fig. 2a demonstrates that the CH_3OH selectivity exceeds the C_2+ oxygenates selectivity by a factor of 7 at high La loading. The C_2+ oxygenates selectivity was highest for LaRh0.12.

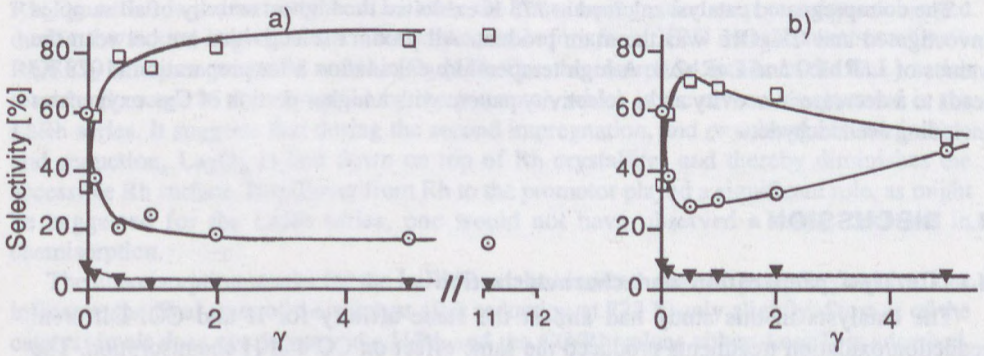

Figure 1. Total oxygenates (□), CH_4 (○) and C_2+ (▼) selectivities for different La/Rh ratios (γ). a) LaRh series, b) RhLa series.

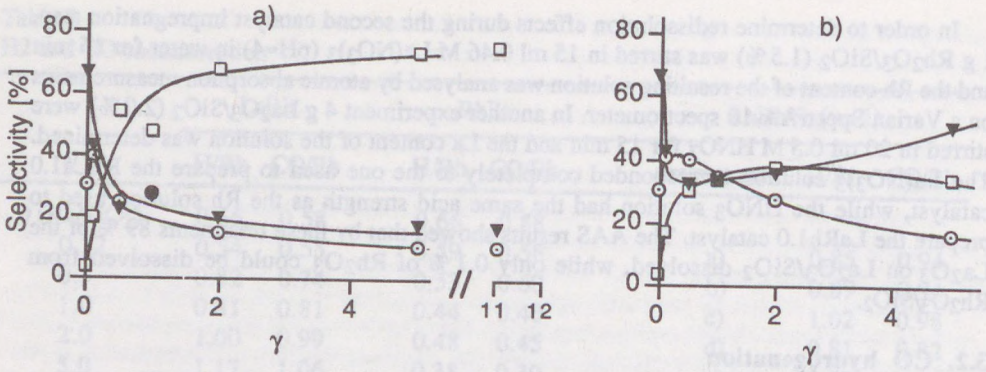

Figure 2. C_1 oxygenates (□), C_2+ oxygenates (○), and total hydrocarbon (▼) selectivities for different La/Rh ratios (γ). a) LaRh series, b) RhLa series.

When Rh was impregnated prior to La, the resulting RhLa catalyst was less active than the corresponding LaRh catalyst impregnated in reverse order. Activity and turnover frequency went through a maximum with increasing La content. RhLa5.0 was even less active than Rh/SiO_2. A maximum was observed for the oxygenates selectivity as well (Fig. 1b). The highest value was obtained with RhLa0.5. The CH_4 selectivity mirrored the oxygenates selectivity, while the C_2+ selectivity stayed on a low level. Yet, the amounts were high compared to those of the corresponding LaRh catalysts, where the C_2+ selectivities were almost negligible. The highest selectivity for C_2+ oxygenates was found for RhLa0.12 (Fig. 2b). The selectivities for C_1 oxygenates were low compared to those of the LaRh catalysts and only above $\gamma = 1$ the C_1 oxygenate selectivity surpassed the selectivity for higher oxygenates. The selectivities for the RhLa series, especially their evolution with increasing γ, are in good agreement with results reported by Underwood and Bell for measurements at a total pressure of 1.2 MPa and a H_2/CO ratio of 2, if one takes the rate parameters into account [10].

The coimpregnated catalyst calcined at 773 K exhibited the highest activity of all samples investigated and CH_3OH was the main product. All product selectivities are between the values of LaRh1.0 and LaRh2.0. A high temperature calcination after preparation (1023 K) leads to a decrease in activity and a selectivity pattern with a higher portion of C_2+ oxygenates including acetaldehyde.

4. DISCUSSION

4.1. Catalyst preparation and characterization

The catalysts in this study had almost the same affinity for H and CO. Different reduction/oxidation treatments produced the same effect on CO and H chemisorption. The reduction temperature of 723 K should be high enough to remove carbonates from La_2O_3 [23]. Underwood and Bell [15] prepared a 4 wt% Rh/SiO_2 catalyst, which was calcined and

reduced at 623 K before passivation. This catalyst was impregnated with different amounts of $La(NO_3)_3$ and subsequently calcined and reduced at 623 K. Their catalysts should therefore be analogous to those of our RhLa series. At high La loadings, their H/Rh values exceeded the CO/Rh values considerably [15]. This is in contradiction with our results, which show a good agreement between H/Rh and CO/Rh. The reason for this is most probably the different reduction temperatures applied. Bernal et al. demonstrated that when $Rh(NO_3)_3/La_2O_3$ catalysts are reduced in H_2 for 1 h at 623 K, catalysts containing Rh on partially carbonated LaO(OH) are obtained. After reduction at 723 K, however, a true Rh/La_2O_3 catalyst is obtained [23]. We therefore believe that the promotor material in our catalysts consists of carbonate-free La_2O_3, while the lanthana on catalysts reduced at 623 K are carbonated to some extent. Carbonated catalysts may be prone to H spillover, thus showing higher H/Rh than CO/Rh values.

For the LaRh series, the H/Rh and CO/Rh values increased with increasing La:Rh ratio, except for LaRh0.12. The increase can be explained by a better dispersion of Rh caused by the precovering of the support by La_2O_3, while we can exclude spillover to the promotor, since not only the H/Rh, but also the CO/Rh values increase with γ, and especially, since the H/Rh and CO/Rh values remain more or less equal. Apparently the La_2O_3 present after the first impregnation and calcination traps part of the $Rh(NO_3)_3$ added during the second impregnation, so that after reduction small Rh particles on top of, or in contact with La_2O_3 are present. Alternatively, one could argue that after the second impregnation most of the Rh is laid down on the SiO_2 support, since even in the LaRh5.0 catalyst, only one La atom per nm^2 SiO_2 surface area is present at the optimum (monolayer) dispersion of La_2O_3. In that case, the La_2O_3 crystallites may prevent the sintering of metallic Rh particles during reduction and the resulting Rh particles will end up in contact with La_2O_3 crystallites.

In agreement with an earlier finding by Kieffer et al. [6], the redissolution experiment showed that about 90 % of the La_2O_3 promotor, in spite of calcination, is dissolved during impregnation. For the LaRh catalysts with $\gamma \leq 1$, the situation is therefore better described as a coimpregnation. The chemisorption data of the coimpregnated catalyst confirm this view. At higher La loadings, however, a significant amount of La_2O_3 will stay on the support without dissolving and the catalyst preparation can rightfully be described by sequential impregnation.

The situation in the RhLa series is different. According to the redissolution experiment, the Rh_2O_3 which is present on the silica after the first impregnation step remains unchanged during the second impregnation. This was noted before from XRD measurements on 4 wt% Rh/SiO_2 catalysts promoted with La_2O_3 [15]. The chemisorption results in the RhLa series reveal a decrease of the adsorption by the promotor, which is the reverse as observed in the LaRh series. It suggests that during the second impregnation, and or subsequent calcination and reduction, La_2O_3 is laid down on top of Rh crystallites and thereby diminishes the accessible Rh surface. If spillover from Rh to the promotor played a significant role, as might be suggested for the LaRh series, one would not have observed a major decrease in chemisorption.

The chemisorption results for the $LaRh^{co}$ catalyst indicate that the preceding calcinations influence the final state of the catalyst after reduction at 723 K only slightly. Storage of the catalyst in air does not decrease the H/Rh and the CO/Rh values either. Less H is adsorbed, however, if the catalyst is calcined at high temparature, due to sintering and or covering, but more Rh surface is present than on RhLa1.0 calcined at lower temperature.

4.2. CO hydrogenation

Rh/SiO_2 exhibits an oxo selectivity of 34 % and acetaldehyde is the main oxygenate. This component is not formed by the LaRh catalysts with $\gamma \geq 0.5$, for which ethanol is an important product. This phenomenon has been observed before and was attributed to the secondary hydrogenation of acetaldehyde to ethanol [3]. The ethers and esters formed can also be regarded as secondary products of alcohols and carboxylic acids, although the latter were never detected in the reactor effluent. Underwood and Bell found by IR, that acetates are hardly removed from the catalysts by hydrogen [10]. La_2O_3, a base, stabilizes the acetates on its surface and the secondary reaction of the acetate to an ester is faster than its hydrogenation to acetic acid.

The activity data for the RhLa series confirm the conclusions deduced from the chemisorption experiments. The Rh surface becomes blocked at higher La loadings, which causes a reversal of the initial promotor effect with increasing La loading. Figs. 1 and 2 show that the order of impregnation for Rh-La catalysts is essential. The C_2+ oxygenates selectivities of the RhLa catalysts are higher than the corresponding ones of the LaRh catalysts for all values of γ. Likewise, the C_2+ selectivity in the RhLa series remains on a 4-5 % level, while the C_2+ formation in the LaRh series is virtually suppressed. Since CO dissociation is a process which requires a relatively large metal ensemble, and since both C_2 oxygenates and C_2+ formation proceed via CO dissociation, we conclude that smaller ensembles are present in the LaRh catalysts than in the RhLa catalysts.

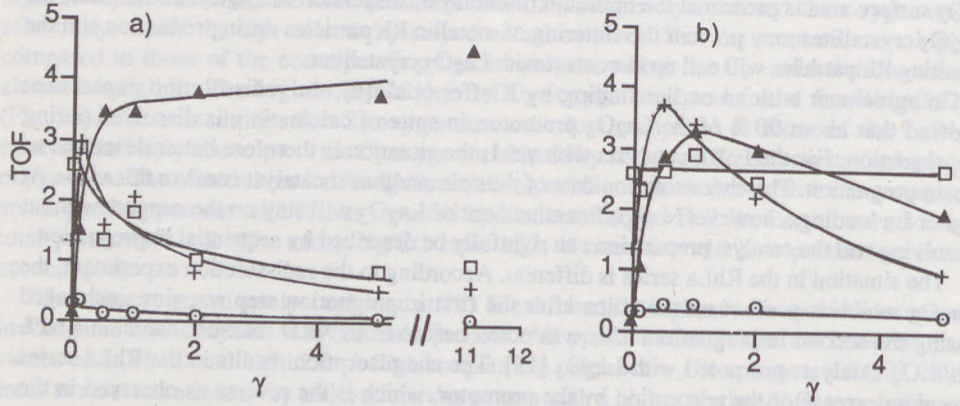

Figure 3. Turnover frequencies (TOF; mmol CO converted to product / mol Rh_s·s) for CH_4 (□), C_2+ hydrocarbons (⊙), C_1 Oxygenates (▲) and C_2+ Oxygenates (+) as a function of the La/Rh ratio (γ). a) LaRh series, b) RhLa series.

The CH_4 and C_2+ turnover frequencies in the RhLa series are independent of the La:Rh ratio (Fig. 3b). This suggests that the activity for hydrocarbon formation on the uncovered part of the Rh crystallites is not influenced by the presence of La_2O_3 on another part of the crystallites. The independence of the CH_4 turnover frequency furthermore suggests that the proposal of Hsiao and Falconer [24], that CH_4 is formed on Pd/Al_2O_3 through the

hydrogenation of CH_3O which is adsorbed on the La_2O_3, may not be true. In the LaRh series, the CH_4 and C_2+ turnover frequencies decrease with γ. This may well be due to structure sensitivity, that is to a less efficient hydrocarbon formation on small Rh crystallites. Indeed, CO hydrogenation studies on Rh/SiO_2 [25] and Rh/Al_2O_3 [26] catalysts as a function of metal dispersion have shown that the hydrocarbon turnover frequency decreases with increasing Rh dispersion.

The C_1 oxo and C_2+ oxo turnover frequencies in the RhLa series first increase and then decrease with increasing γ. This demonstrates that La_2O_3 promotes the formation of oxygenates, but that a too high La_2O_3 loading is harmful because of covering. If the formation of oxygenates is enhanced by the metal-promotor interface [27], then it is clear why the oxygenates formation goes through a maximum, since the size of the interface goes through a maximum with increasing coverage of Rh by La_2O_3. If on the other hand oxygenates formation (especially CH_3OH) takes place via spillover of H atoms formed on the Rh surface to formate groups on the La_2O_3 surface (formed by the reaction of CO with basic OH groups) [2], then oxygenates formation should be proportional to the amount of La_2O_3 being accessible for H atoms through spillover. Oxygenates formation should then roughly be proportional to La_2O_3 amount times Rh surface area. Since in the RhLa series the amount of La_2O_3 increases, but the free Rh surface area decreases with γ, oxygenates formation should also in this explanation go through a maximum.

The CH_3OH turnover frequency in the LaRh series increases sharply from 0.1 to 3.8 mmol CH_3OH/mol Rh_s·s when γ increases from 0 to 0.5 (Fig. 3a). Above $\gamma = 0.5$ the CH_3OH turnover frequency levels off. As in the RhLa series, this can be explained by the size of the Rh-La_2O_3 interface. Initial amounts of La_2O_3 strongly increase this size, while further addition of La_2O_3 has a minor effect as soon as the Rh crystallites are more or less surrounded by La_2O_3. Apparently this is the case around $\gamma = 0.5$. The fact that no decrease of the CH_3OH turnover frequency takes place, even up to $\gamma = 11.1$, indicates that almost no covering of the (small) Rh crystallites by La_2O_3 occurs and that full use of the Rh is made in the LaRh series.

The selectivity as well as the chemisorption results of the $LaRh^{co}$ catalyst calcined at 773 K confirm that the catalyst structure after coimpregnation and after the second impregnation of LaRh1.0 are roughly the same, due to the dissolution of La_2O_3 by the $Rh(NO_3)_3$ impregnation solution. The final state on the catalyst is also influenced by the calcination temperature. The $LaRh^{co}$ catalyst initially calcined at 1023 K exhibits a selectivity pattern similar to those of the RhLa1.0 and RhLa2.0 catalysts. Its H/Rh value is markedly reduced compared to the $LaRh^{co}$ catalyst initially calcined at 773 K, but is still higher than those of the RhLa catalysts. This can be explained by sintering of the Rh_2O_3, which leads to a larger particle size in spite of the contact of Rh_2O_3 with La_2O_3, and by covering of Rh.

5. REFERENCES

1 M. Ichikawa, Bull. Chem Soc. Japan, 51 (1978) 2273.

2 V.L. Kuznetsov, A.V. Romanenko, I.L. Mudrakovskii, V.M. Matikhin, V.A. Shmachkov and Y.I. Yermakov, Proc. 8th Int. Congr. Catal. Berlin (1984), Vol. V, p. 3.

3 R.P. Underwood and A.T. Bell, Appl. Catal., 21 (1986) 157.

4 R.P. Underwood and A.T. Bell, Appl. Catal., 34 (1987) 289.
5 G. van der Lee, B. Schuller, H. Post, T.L.F. Favre and V. Ponec, J. Catal., 98 (1986) 522.
6 R. Kieffer, A. Kiennemann, M. Rodríguez, S. Bernal and J.M. Rodríguez-Izquierdo, Appl. Catal., 42 (1988) 77.
7 R.F. Hicks and A.T.Bell, J. Catal., 90 (1984) 205.
8 E. Ramaroson, R. Kieffer and A. Kiennemann, J. Chem. Soc. Chem. Commun., (1982) 645.
9 C. Sudhakar and M.A. Vannice, J. Catal., 95 (1985) 227.
10 R.P. Underwood and A.T. Bell, J. Catal., 111 (1988) 325.
11 J.M. Driessen, E.K. Poels, J.P. Hindermann and V. Ponec, J. Catal., 82 (1983) 26.
12 B.M. Choudary, K. Matusek, I. Bogyay and L. Guczi, J. Catal., 122 (1990) 320.
13 T.H. Fleisch, R.F. Hicks and A.T. Bell, J. Catal., 87 (1984) 398.
14 G.R. Gallaher, J.G. Goodwin, jr., Chen-shi Huang and M. Houalla, J. Catal., 127 (1991) 719.
15 R.P. Underwood and A.T. Bell, J. Catal., 109 (1988) 61.
16 S.J. Tauster and S.C. Fung, J. Catal., 55 (1978) 29.
17 T. Mori, A. Miyamoto, N. Takahashi, M. Fukagaya, T. Hattori and Y. Murakami, J. Phys. Chem., 90 (1986) 5197.
18 A.L. Borer and R. Prins, to be published.
19 A.G.T.M. Bastein, W.J. van der Boogert, G. van der Lee, H. Luo, B. Schuller and V. Ponec, Appl. Catal., 29 (1987) 243.
20 B.J. Kip, P.A.T. Smeets, J.H.M.C. van Wolput, H.W. Zandbergen, J. van Grondelle and R. Prins, Appl. Catal., 33 (1987) 157.
21 Z. Hu, T. Wakasugi, A. Maeda, K. Kunimori and T. Uchijima, J. Catal., 127 (1991) 276.
22 E. Schultz, A.L. Borer and R. Prins, Catal. Lett., to be published.
23 S. Bernal, F.J. Botana, R. García, F. Ramírez and J.M. Rodríguez-Izquierdo, J. Chem. Soc. Faraday Trans. I, 83 (1987) 2279.
24 E.C. Hsiao and J.L. Falconer, J. Catal., 132 (1991) 145.
25 H. Arakawa, T. Fukushima, M. Ichikawa, K. Takeuchi, T. Matsuzaki and Y. Sugi, Chem. Lett., (1985) 23.
26 H.F.J. van't Blik, J.C. Vis, T. Huizinga and R. Prins, Appl. Catal., 19 (1985) 405.
27 K.J. Williams, A.B. Boffa, M. Salmeron, A.T. Bell and G.A. Somorjai, Catal. Lett., 11 (1991) 77.

DISCUSSION

Q: D. C. Koningsberger (The Netherlands)

Our EXAFS work on Rh_2TiO_2 shows no coverage and a suppressed H_2 chemisorption under SMSI condition, which can be explained by an electronic effect.

Do you believe that the promoter effect of La is only due to coverage and do you think that an electronic effect can be ruled out ?

Did you perform IR experiments with CO on Rh/SiO_2 and on $RhLa/SiO_2$? If so, did you see differences?

A: R. Prins

The promoting effect of La is certainly not only due to covering. The results of the LaRh catalysts, in which La was impregnated first, show that La_2O_3 has a strong promoting effect even though there is (almost) no covering of the Rh by La_2O_3. An electronic effect of the La_2O_3 on the Rh atoms can at the moment not be ruled out, but there are enough possibilities to explain the role of La_2O_3 in a non-electronic way, for instance by the reaction of CO and OH to formate on the La_2O_3, followed by hydrogen spillover from the metal to the La_2O_3 and reduction of the formate to CH_3OH.

We have not performed IR experiments on our catalysts.

Q: F. Pinna (Italy)

The presence of CO_2 could influence significantly the catalytic activity. How much CO_2 formed under the reaction conditions ?

Does La_2O_3 have any influence on the CO_2 formation ?

A: R. Prins

The water gas shift reaction is significantly promoted by the presence of La_2O_3.

Q: P. Johnston (United Kingdom)

Have you determined the Rh particle sizes for the respective catalysts? Have you seen variations of the Rh particle sizes under CO/synthesis gas in a manner analogous to the corrosive CO chemisorption seen on my various supported Rh catalysts either during reduction (pretreatment) or during CO hydrogenation conditions ? If so, may this not influence selectivities/activities observed ?

A: R. Prins

No TEM determination of the Rh particle size have been performed, only H_2 and CO chemisorption as described in the paper. For some catalysts the chemisorption did not change much after reaction.

Q: V. Ponec (The Netherlands)

1) There seem to be three possible active sites for CH_3OH synthesis: i) Rh(IV) embedded in La_2O_3 something like (VO - 3 % of total Rh, I would guess); ii) Rh(0)-CO coactivated by La(III) on the oxygen end, this activation leading to hydrogenation to CH_3OH; and iii) La(III)-CO which is supplied (by spillover) by H-atoms, generated on Rh(0)-particles. As I understand it, you prefer the possibility iii) but are the other two possibilities excluded ?

2) Would you agree that for higher oxygenate formation, the promoter must be on the metal particle and not only under it ?

A: R. Prins

All three models are in principle still possible, but as long as the presence of Rh^{n+} cations in our and similar catalysts systems is a belief rather than a knowledge, we prefer the models ii) and iii) as explained in the paper.

It is difficult to imagine how a promoter under the metal particle can influence the catalysis anyway, but when the promoter is on top of the metal particle, or in close contact, as a neighboring island, it may certainly influence the catalysis via the mechanisms described in the paper.

Q: K. C. Waugh (United Kingdom)

It strikes me that the speculation about the origin of the methanol synthesis activity (whether it is due to hydrogen spillover from the metal, Rh, to formate on the La_2O_3 formed by CO-OH interaction or whether it is simply an interfacial phenomenon) could be solved by simple TPD/TPR experiments on Rh and La_2O_3 alone and on the operating catalyst. Adsorbing HCO_2H on each of these would characterize formate or ether and this could be compared with TPD/TPR of the operating catalyst. Has this been done or is it intended be done ?

A: R. Prins

It sounds like an interesting proposal and, to my knowledge, it has not been performed yet.

Q: J. W. E. Coenen (The Netherlands)

Both questions refer to situations on surfaces:

1) You show TOF after many runs i) is there much activity decline ? ii) Is it one to C-deposition (Boudouard reaction) or change in Rh-dispersions ?

2) Optimum in production of oxygenates at La/Rh-ratio of about 1. This is bulk-ratio. Is there any information surface-compositions ratio ?

A: R. Prins

The initial activity decline is about 50 %, thereafter there is a slow further deactivation of about 1 % per hour.

We have at present no information on the La_2O_3 dispersion, nor on the interface area between La_2O_3 and Rh.

Q: M. Ichikawa (Japan)

Regarding the promotion role of La_2O_x on Pd I would like to address the hydrogen activity modified by La-oxide promoter. We have previously reported that hydrogenation rates in TOF rises for olefin, CO and benzene dramatically on Pd-LaO_x, compared with Pd/SiO_2. This promotion of PdO_x would be associated with the reactivity of chemisorbed hydrogen on modified Pd particles, possibly reflected from stabilization the partial oxidation state in form Pd-O-La overlayer an Pd particles. The in situ FTIR study also shows the appreciate promotion of formate intermediate on Pd-CaO_x surface, compared with Pd. Accordingly, I would like to have your comment on the chemical issue of CaO_x oxide promotion, rather than the morphological methyl-support interaction issue in your system.

A: R. Prins

I refer to the suggestions made in the paper, that the CO hydrogenation to methanol and higher oxygenates takes place either at the metal-promoter interface, or via reduction of formate formed on La_2O_3 by hydrogen atoms spilled over from the metal.

Q: K. Klier (USA)

Do you have data on the water gas shift activity of the La_2O_3-promoted Rh/SiO_2 catalysts ? The product of water gas shift is CO_2 via water produced by hydrogenation of CO to hydrocarbons (e.g. methane), and CO_2 could convert your carbonate-free lanthana to a hydroxycarbonate. Do you have evidence that carbonates are present or absent after the catalysts have been tested ?

A: R. Prins

We have not studied the issue of the water-gas shift reaction over La_2O_3-Rh/SiO_2 in great detail, but the catalyst has indeed a substantial activity for this reaction. According to IR studies published in the literature, carbonate is present during reaction.

Q: M. Schmal (Brasil)

Can you comment on the stability of the catalyst when you increase the La content ? For lower dispersion do you expect higher formation of olefins, because CH_4 declines when Rh is first impregnated ?

A: R. Prins

For your question about catalyst stability, I refer to my answer given to the first question of Dr. J. W. E. Coenen. In the series in which Rh was impregnated first, the C_{2+} and acetaldehyde selectivities were highest in the La_2O_3 free catalyst and decreased to almost zero at $g = 1$.

Q: W. M. H. Sachtler (USA)

Rh is easily oxidized by protons (-OH groups) to Rh^+ and this oxidation is enhanced by CO. How does interactions of Rh with La_2O_3 affect the equilibria:

$$Rh + H^+ \rightarrow Rh^+ + 0.5\ H_2$$

and

$$Rh + H^+ + 2CO \rightarrow Rh^+(CO)_2 + H_2$$

A: R. Prins

I have no idea. All I know is that $Rh(CO)^{2+}$ is not stable under CO + H_2 at reaction conditions and decomposes to Rh metal [1].

[1] H. F. J. van't Blik, J. B. A. D. van Zon, D. C. Koningsberger and R. Prins, *J. Mol. Catal.*, **25**, 379 (1984)

Q: J.G. Goodwin Jr. (USA)

Your comments on La promotion of Rh:

1) Our work and conclusions [2] are in line with yours and those of Bernal and coworkers. There is no reduction of La(III). Rather all changes seen can be explained by the decomposition (partly catalyzed by Rh) of $La(CO_3)_3$

$$La_2(CO_3)_3 \rightarrow La(O)OH \rightarrow La_2O_3$$

2) The negative shift in BE seen for metals promoted by La(III) is similar to that seen for Ru promoted by K or Na (Shya, Goodwin, Hercules, J. Phys. Chem.) which was proved to be due primarily to extra-atomic relaxation.

3) In response to the question raised by Professor Koningsberger about whether the La(III) is present on the metal surface, we showed for a set of catalysts like your series of La-added-after-Rh catalysts [2, 3] that ethane hydrogenolysis is severely poisoned suggesting La decoration of the Rh.

4) It was interesting to note the increase in activity for low loadings of La promoter which we have seen also. Do you have any idea why ?

[2] G. R. Gallaher, J. R. Goodwin Jr, and L. Guczi, *Appl. Catal.* **73**, 1 (1991)
[3] G. R. Gallaher, J. R. Goodwin Jr, *J. Catal.*, **127**, 719 (1991)

A: R. Prins

Thank you for your comments. Indeed, low La_2O_3 loadings already have a strong promotional effect on Rh/SiO_2. Adding La_2O_3 to Rh/SiO_2 at a La/Rh ratio of only 0.12 decreases the hydrocarbon activity slightly, increases the C_2-oxo activity by about a factor

two, and increases the C_1-oxo activity from a very low to a substantial level. A further increase of the La_2O_3 content mainly increases the CH_3OH production. The explanation can only be that even the initial amounts of La_2O_3 are already in contact with the Rh particle. It may well be that after the first calcination the metal oxide, be it La_2O_3 or Rh_2O_3, adsorbs the metal ions present in the second impregnation. In this way there will be an intimate contact between La_2O_3 and Rh_2O_3 and subsequently, after reduction, between La_2O_3 and Rh.

Q: K. P. de Jong (The Netherlands)

From an industrial point of view it would be desirable to combine a high Rh dispersion with a high selectivity to C_2-oxygenates. It is apparent from your study that his combination is difficult to achieve: the LaRh catalysts display higher dispersions but lower selectivities to C_2-oxygenates. Similar observations have been made at the Shell Laboratories for $RhMn/SiO_2$ catalysts: with very small Rh particles MnO is not an effective promoter. Our explanation has been that with very small Rh particles MnO can react easily with the carrier and will not remain on the metal surface. Do you think that this holds for La-promoted Rh/SiO_2 systems ?

A: R. Prins

Indeed, as Figure 3 in our paper demonstrates, the highest TOF for C_2-oxygenates is reached for a catalyst in which Rh is impregnated first. A better Rh dispersion is reached for the catalysts in which La is impregnated first, but in this case the promoter is not as effective for C_2-oxygenates formation. our explanation is that in the LaRh catalysts the Rh particles become too small for an efficient CO dissociation which is a condition for C_2-oxygenates formation, rather than that the contact between promoter and Rh is not good enough.

Q: A. T. Bell (USA)

In the literature it has been proposed that LaO_x and other basic metal oxides promote the formation of methanol over Rh and Pd come be ascribed to one of two mechanisms. The first is that CO interacts with both the metal and the oxide, thereby facilitating the addition of H_2 to the C-O bond. The second hypothesis is that CO on the metal reacts with OH groups and the oxide to form formate groups, the first intermediate on the path to methanol. Do your observations help us pick between these alternatives ?

A: R. Prins

Your first proposal is equal to one of the two proposed in our paper (reaction at the metal-promoter interface). The second is different, because although we both suggest that formate is involved, you propose that the formate is on the metal, whereas we suggest that it is on the promoter. Your suggestion is in line with the proposal described in [4] for the formation of methanol from CO_2 and H_2 over Cu-ZnO catalysts via copper formate. Our present observations can not differentiate between these three proposals.

[4] G. J. Miller, C. H. Rochester and K. C. Waugh, *Catal. Lett.*, **14**, 289 (1992)

Q: F. Solymosi (Hungary)

As CO easily dissociates over Rh under the reaction conditions applied, it may be important to know you this process is influenced by La_2O_3 promoter in your catalyst. We found a long time ago [5] that the dissociation of CO is dramatically affected by the nature of the supports and additives. What is the situation in the present case ? Does the La_2O_3 increase or decrease the rate of this process ?

[5] A. Erdöhelyi, F. Solymosi, *J. Catal.*, **84**, 446 (1983)

A: R. Prins

This is indeed an important question, to which we have no direct answer. All I can say is that in the RhLa catalyst series the CO dissociation capability seems to be constant (judged from the constant CH_4 and C_{2+} turnover frequencies), probably because sufficiently

large Rh ensembles are present. In the LaRh series the CO dissociation capability seems to decrease with La_2O_3 loading, most probably because very small Rh particles can not dissociate CO under steady state reaction conditions.

Q: R. D. Gonzalez (USA)

The sequence of impregnation may result in different levels of contact between the promoter and the Rh metal. What experiments have you performed to insure that there is contact between the two catalyst components ?

A: R. Prins

As I indicated in answer to the question of Dr. J. Goodwin, we believe that there is a good contact between the two catalyst components because of the fact that during the second impregnation the second metal ion (La(III) or Rh(III)) adsorbs on the first metal oxide (Rh_2O_3 or La_2O_3, respectively) formed during the first calcination. This would explain the coverage of Rh by La_2O_3 in the RhLa series, and would suggest that Rh is (partly) on top of La_2O_3 in the LaRh series.

Guczi, L. *et al.* (Editors), *New Frontiers in Catalysis*
Proceedings of the 10th International Congress on Catalysis, 19-24 July, 1992, Budapest, Hungary
© 1993 Elsevier Science Publishers B.V. All rights reserved

EFFECT OF CHLORINE ON THE RHENIUM-ALUMINA INTERACTION IN LOW-LOADED Re/Al_2O_3 AND $PtRe/Al_2O_3$ INDUSTRIAL CATALYSTS

G. Munuera, P. Malet and A. Caballero

Instituto de Ciencia de Materiales de Sevilla, Departamento de Quimica Inorganica, P.O.Box 1115, 41080 Seville, Spain

ABSTRACT

The role of chlorine in promoting the interaction between Rhenium and alumina in $PtRe/Al_2O_3$ industrial reforming catalysts (ca. 0.3 wt% of each metal) has been examined using TPR, XAS (EXAFS/XANES), O_2 adsorption and IR spectroscopy of adsorbed CO. The results indicate that chlorine favor the formation, during the pretreatments at 723K, of a phase containing Re^{4+} strongly interacting with the alumina surface layers that prevents the generation of PtRe-alloyed particles during the reduction of the precursors.

1. INTRODUCTION.

Previous work with Pt/Al_2O_3 and $PtRe/Al_2O_3$ reforming catalysts, using n-butane hydrogenolysis as a test reaction (1) has allowed to assess the formation of PtRe-alloyed particles, showing that the presence of chlorine at the alumina support has a strong influence in the formation of the bimetallic phase, a process that greatly depends on the pretreatment conditions. In particular, we have found that though the formation of the PtRe-alloy in chlorine free PtRe catalysts readily occurs, if chlorine is present at the support, a pretreatment in He or dry air at 723K almost completely prevents the generation of the alloyed phase which is formed when the same catalyst precursor is pretreated under milder conditions (He/523K). In principle, the aim of this work has been to examine in more detail the behavior of the Rhenium in relation with the presence of chlorine in the $PtRe/Al_2O_3$ industrial reforming catalysts.

2. EXPERIMENTAL

2.1. Materials

The two series of catalyst precursors with and without chlorine incorporated to the Al_2O_3, (labeled hereafter as -Cl and -nCl) were the same used in previous works (1,2). The chlorinated Pt-Cl and PtRe-Cl samples (0.95 wt% of Cl) were commercial catalysts provided by Azko Chemie (Ketjen) with references CK303 and CK433 while the Re-Cl sample was prepared from the same chlorinated alumina support (CK300, S_{BET} =187m^2g^{-1}). The set of chlorine-free samples were prepared on a Cyanamid PHF γ-Al_2O_3 support (S_{BET} = 180 m^2g^{-1}), following the procedure described by Kobayashi

et al. (3) by wetness impregnation with aqueous solutions of NH_4ReO_4, $Pt(NH_3)_4$ $(NO_3)_2$ or both. The precursors were dried overnight at 393K and then calcined at 773K for 3 hours and stored in bulbs in a desiccator. Specimens referred to as dechlorinated (-dCl) were prepared from the commercial precursors by flowing wet air (100 ml/min /g.) for ca. 100 h. at 773K. Chlorine contents of all the samples were monitored by XPS. Analyses of the precursors by atomic absorption gives values of ca. 0.30 ∓ 0.01 wt% for each metal as previously reported (1).

2.2. Methods

In the standard thermal treatments of the samples before all type of experiments (TPR, XAS , IR/CO etc), the temperature was raised at a linear heating rate of 5K/min under He or synthetic dry air flows (100 ml/min/g. of sample) maintaining the selected final temperature (usually 523K or 723K) for 1 hour before the reduction step with H_2 under the same flow conditions at 663K (or 873K) for 1 hour. TPR experiments were carried out with a conventional TCD system using a reactive gas stream (5% H_2 in Ar, 10 ml/min) and a constant heating rate of 10K/min. Calibrations using CuO (99.99%) and other details of the procedure have been described elsewhere (1,4).

XAS were recorded at the PWA Frascati Radiation Facility (1.5 GeV, 15-60 mA) using a channel cut Si(111) monochromator. Each sample was pressed to give a self-supported wafer with the amount calculated to yield optimal absorption measurements (total absorbance $\mu x=2.5$) at the Re L_{III}-edge (10534 eV). Standard pretreatments were carried out in pyrex bulbs where the wafers were evacuated ($P < 10^{-5}$ torr) at 523K or 723K and reduced under flowing H_2 and then sealed-off under vacuum. Though transfer of the wafers into air-tight cells (with Mylar windows) used to record the spectra, was made using a glove-bag flushed with He, passivation of the reduced metals (in particular Re) was found that occurs during handling.

IR spectra of adsorbed CO were recorded in a Perkin-Elmer mod.684 with a data station mod.3600 using self-supported thin wafers of the samples in a transmission quartz cell with NaCl windows, where they were pretreated under He flow or vacuum in the standard conditions before introducing CO (ca. 100 torr) at different temperatures (in the range 300-723K). The spectra were recorded at 300K after removal of the excess of CO in the gas phase.

3. RESULTS

3.1. TPR of Rhenium

Fig. 1 shows the effect of the thermal pretreatment in flowing He at 523 or 723K on the TPR profiles of the Pt-Cl and PtRe-Cl samples. Changes from a single peak reduction process to a multiple peak profile occurs in the bimetallic precursor pretreated at 723K. The subtraction of the two TPR profiles indicates that the new peaks at ca. 695K and 710K correspond to Re reduction that becomes more difficult after the pretreatment in He at 723K. Similar results were obtained for the chlorine-free Pt-nCl and PtRe-nCl precursors while the use of dry air, instead of He, only produces minor changes in the TPR profiles of both set of samples

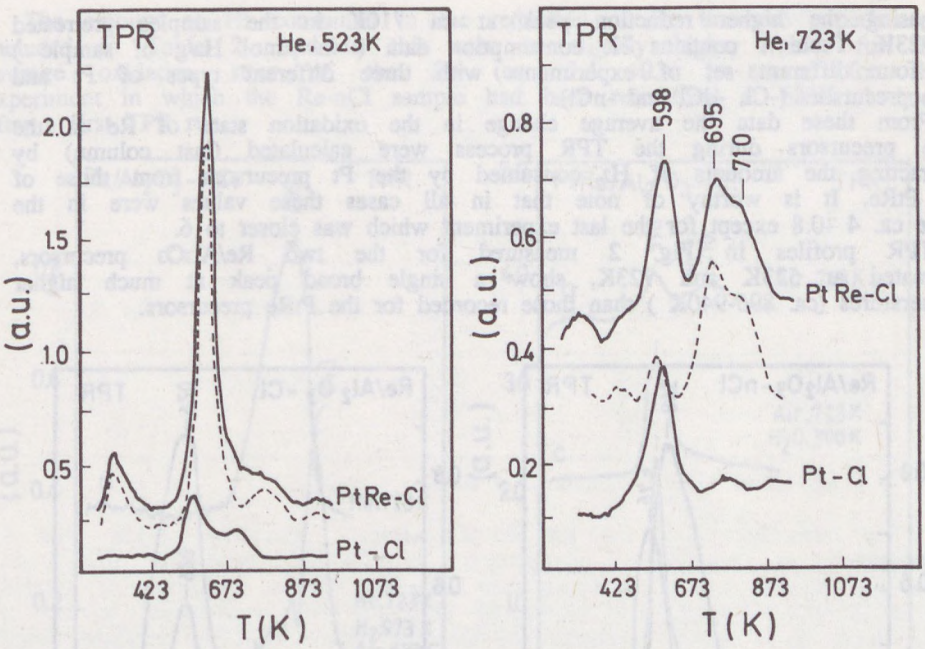

Figure 1. TPR profiles of Pt-Cl and PtRe-Cl precursors pretreated in He. Left: at 523K. Right: at 723K. Dashed lines: difference profiles (PtRe-Pt).

Table 1
H_2 consumptions from TPR experiments in Pt and PtRe Catalysts

Sample	Treatment	Pt	PtRe	PtRe-Pt	$\Delta n(Re^{n+}/Re^0)$
-nCl	He/523K	16	52	36	4.5
-nCl	He/723K	13	52	39	4.8
-nCl*	Reox/623K	25	55	30	3.7
-Cl	He/723K	17	52	35	4.3
-Cl	Air/723K	30	56	26	3.2
-Cl*	Reox/623K	21	54	33	4.1
-dCl	He/523K	24	60	36	4.5
-dCl	He/723K	21	60	39	4.8
-Cl	Air/723K	29	57	27	3.3
-Cl+	H_2O/300K	29	75	46	5.7

* Reoxidized after the previous TPR run;+ Treated with water vapor after air treatment at 723K before the TPR run

increasing the higher reduction peak at ca 710K in the samples pretreated at 723K. Table 1 contains H_2 consumption data (in µmol H_2/g of sample) for four different set of experiments with three different types of Pt and PtRe precursors (-Cl, -dCl and -nCl).

From these data the average change in the oxidation state of Re in the PtRe precursors during the TPR process were calculated (last column) by subtracting the amounts of H_2 consumed by the Pt precursors from those of the PtRe. It is worthy of note that in all cases these values were in the range ca. 4 ±0.8 except for the last experiment which was closer to 6.

TPR profiles in Fig. 2 measured for the two Re/Al_2O_3 precursors, pretreated at 523K and 723K, show a single broad peak at much higher temperatures (ca. 895-940K) than those recorded for the PtRe precursors.

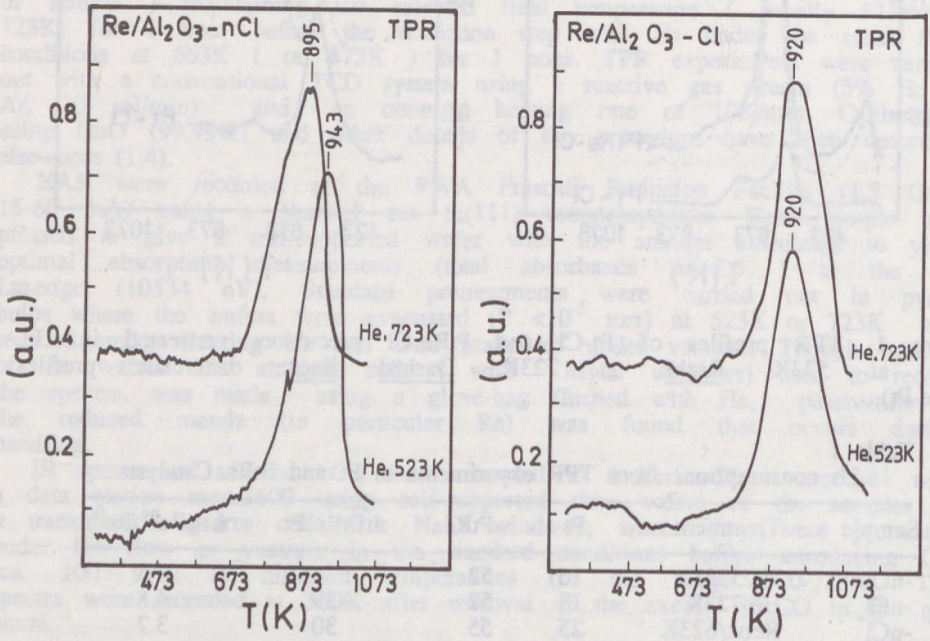

Figure 2. TPR profiles of Re-precursors pretreated in He at 523K and 723K. Left: Re-nCl. Right: Re-Cl.

Table 2
H_2 consumptions by Re/Al_2O_3 Catalysts from TPR experiments (973K)

Pretreatment	Re/Al_2O_3-nCl		Re/Al_2O_3-Cl	
	µmol H_2/g.	$\Delta n(Re^{n+}/Re^0)$	µmol H_2/g.	$\Delta n(Re^{n+}/Re^0)$
He/523K	49	6.0	38	4.7
He/723K	45	5.6	43	5.3
Reox/623K*	31	3.9	--	---

* Reoxidized after a first TPR run up to 973K.

The amount of H_2 consumed in the reduction of Re in these experiments, included in Table 2, lead in this case to slightly higher values for the average oxidation state of the Re (ca. 5.4 ±0.6) except for the experiment in which the Re-nCl sample had been reoxidized at 623K, 1 hour after a first TPR run.

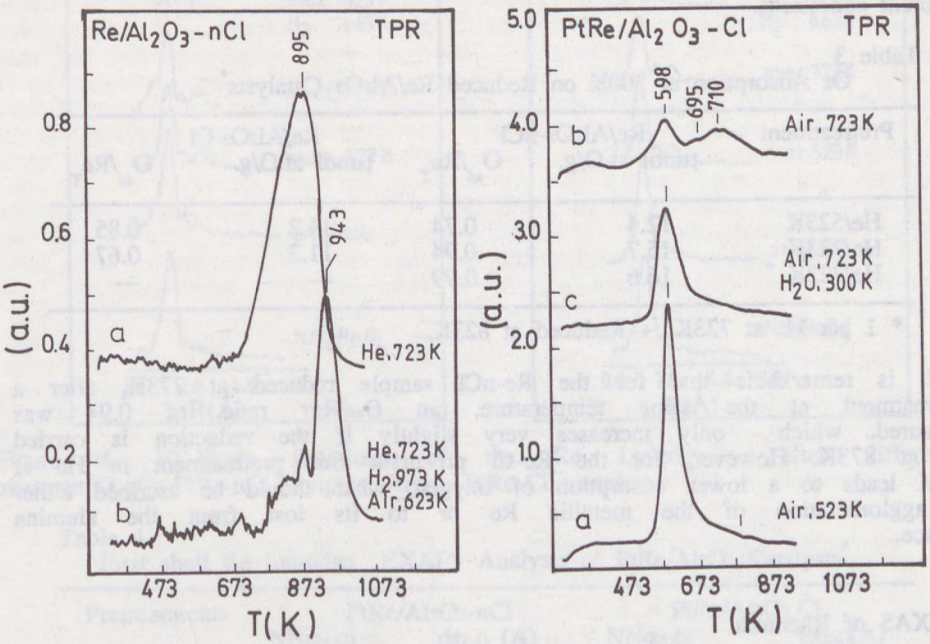

Figure 3. TPR profiles Left: Re-nCl pretreated in He at 723K (a) and reoxidized with dry air at 623K after a first TPR run (b). Right: PtRe-Cl pretreated in air at 523K (a) at 723K (b) and rehydrated with 15 torr of water at 300K after pretreatment at 723K in air (c)

In fact, Fig. 3 shows that in this case the TPR-peak was sharp and more symmetric than in the original sample. The exposure of this reoxidized sample to the air produces a broadening of the TPR profile while the amount of H_2 consumed increases slightly. In principle, this fact, should be ascribed to the presence of water vapor. Meanwhile, as shown also in Fig. 3, the single peak profile, characteristic of the $PtRe/Al_2O_3$ samples pretreated at 523K, could be restored in the samples pretreated at 723K if water vapor (ca. 15 torr) is adsorbed at 300K on the sample before running the TPR. This fact suggests again that adsorbed water and/or hydroxyl groups on the alumina surface, play an important role in the enhanced reducibility of the Re in these $PtRe/Al_2O_3$ samples. Furthermore, TPR experiments using a 1:1 physical mixture of Pt/Al_2O_3 and Re/Al_2O_3,pretreated either at 523K or 723K, lead to profiles which were the sum of those for the two single monometallic precursors thus indicating that the reduction of the Re in the bimetallic $PtRe/Al_2O_3$ precursors at lower temperatures requires the presence of both, Pt and adsorbed water (or hydroxyl groups) on the same alumina support.

3.2. Oxygen Adsorption

Volumetric adsorption of O_2 at 300K on the two Re/Al_2O_3 samples which had been reduced at 723K for 1 hour in flowing H_2 occurs in an irreversible way leading to saturation at very low pressures ($<10^{-3}$ torr). Table 3 shows the saturation coverages (in μmol at.O/g. of sample) for different conditions.

Table 3
O_2 Adsorption at 300K on Reduced Re/Al_2O_3 Catalysts*

Pretreatment	Re/Al2O3-nCl		Re/Al2O3-Cl	
	μmol at.O/g.	O_{ad}/Re_T	μmol at.O/g.	O_{ad}/Re_T
He/523K	12.4	0.74	14.2	0.85
He/723K	15.7	0.94	11.2	0.67
He/723K +	16.6	0.99	---	---

* 1 bar H_2 at 723K; + Reduced at 823K.

It is remarkable that for the Re-nCl sample reduced at 773K, after a pretreatment at the same temperature, an O_{ad}/Re_T ratio of 0.94 was measured, which only increases very slightly if the reduction is carried out at 873K. However, for the Re-Cl precursor this pretreatment in He at 723K leads to a lower adsorption of oxygen, what should be ascribed either to agglomeration of the metallic Re or to its lost from the alumina surface.

3.3 XAS of Rhenium

XAS experiments at the Pt L(III)-edge of the samples have been examined (2) at the XANES and EXAFS regions for all the samples pretreated either at 535K or 723K, before and after reduction in H_2 at 663K. EXAFS and XANES spectra indicate the formation in the reduced samples of very small (<1.0 nm) particles of Pt (or PtRe) which seem to be more stable to passivation in the catalysts containing chlorine and/or Re.

Fig. 4 show the modulus of the Fourier Transforms at the Re L(III)-edge EXAFS function of the two $PtRe/Al_2O_3$ precursors submitted to the different standard treatments. The EXAFS functions obtained by back-Fourier transforming of the first maximum were submitted to fitting analysis assuming O and/or Cl as near neighbors. The best fitting was obtained by assuming only O neighbors, with coordination numbers and Re-O distances summarized in Table 4 for the two PtRe samples.

It is worthy of note that only ca. 4 oxygens seem to exist in the neighborhood of the Re in the unreduced PtRe precursors, either pretreated at 523K or 723K in vacuum, while the Re-O distances were slightly higher in the chlorine-free precursors. The same number of neighbors was also obtained for the two Re/Al_2O_3 samples pretreated under similar conditions. However, reduction at 663K of the PtRe precursors produces a decrease in this number of neighbors, particularly when they had been pretreated at 523K. It is worthy of note that in these two samples a new peak at ca. 2.00 A (without phase correction) could be observed in the FT-exafs function.

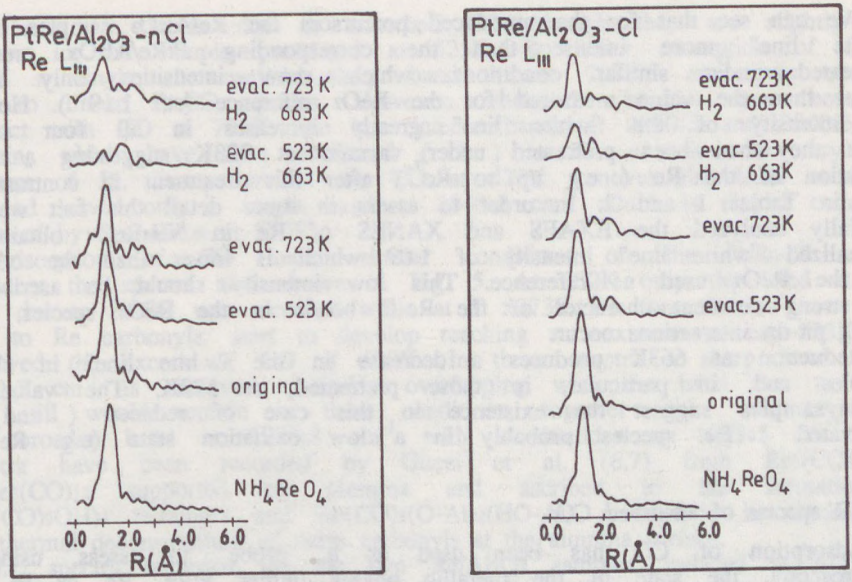

Figure 4. FT-Exafs functions of the Re LIII-edge after different treatments. Left: PtRe-nCl samples; Right: PtRe-Cl samples.

Table 4
First shell Re LIII-edge EXAFS Analysis of PtRe/Al_2O_3 Catalysts*

Pretreatments	PtRe/Al_2O_3-nCl		PtRe/Al_2O_3.Cl	
	$NN_{(Re-O)}$	d_{Re-O} (A)	$NN_{(Re-O)}$	d_{Re-O}(A)
Vac/523K	4.0	1.77	4.0	1.76
Vac/723K	3.3	1.79	4.0	1.75
523K/H_2,663K	0.4	1.80	1.0	1.72
723K/H_2,663K	2.1	1.77	1.7	1.73

* $\Delta\sigma^2$ 5-15 x 10^{-3} A^2 in all samples.

Normalized Re L(III)-edge "white line" intensities for the four precursors containing Re were obtained from the area of the peak in the XANES region and have been summarized in Table 5.

Table 5
Re LIII-edge "white line" intensities in Re/Al_2O_3 and PtRe/Al_2O_3

Pretreatments	PtRe-nCl	Re-nCl	PtRe-Cl	Re-Cl
original	1.21	1.26	1.22	1.27
Vac/523K	1.21	1.26	1.22	1.27
Vac/723K	1.35	1.42	1.30	1.45
523K/H_2,663K	1.14	1.18	1.14	1.15
723K/H_2,663K	1.28	1.27	1.29	1.32

References: Re(metal) = 1.00 and ReO_2 = 1.19

We can see that for the unreduced precursors the Re/Al_2O_3 samples have a "white line" more intense than the corresponding $PtRe/Al_2O_3$ precursors pretreated under similar conditions, which show intensities only slightly higher than the value measured for the ReO_2 reference (ca. 1.19). However, the intensity of the "white line" greatly increases in all four samples when they had been pretreated under vacuum at 723K suggesting a further oxidation of the Re (e.g up to Re^{7+}) after this treatment in contrast with data in Tables 1 and 2. In order to assess in more detail this fact we have carefully analyzed the EXAFS and XANES of Re in NH_4ReO_4 obtaining a normalized "white line" intensity of 1.09 which is lower than the observed for the ReO_2 used as reference. This low intensity should be ascribed to the strong covalent character of the Re-O bonds in the ReO_4 species, where strong $p\pi$-$d\pi$ interactions occur.

Reduction at 663K produces a decrease in the "white line" in all the samples and, in particular, in those pretreated at 523K. The values for these samples suggest the existence in this case of reduced (and then passivated) Re species probably in a low oxidation state (e.g. Re^{2+} or Re^{3+}).

3.4 IR spectra of adsorbed CO

Adsorption of CO has been used as a "probe" to assess, using IR spectroscopy, the state of the metallic phases (either PtRe, Re or Pt) in the two set of samples. As shown in Fig.5 adsorption of CO on the Pt-Cl catalyst reduced at 663K after a pretreatment either at 523K or 723K gives

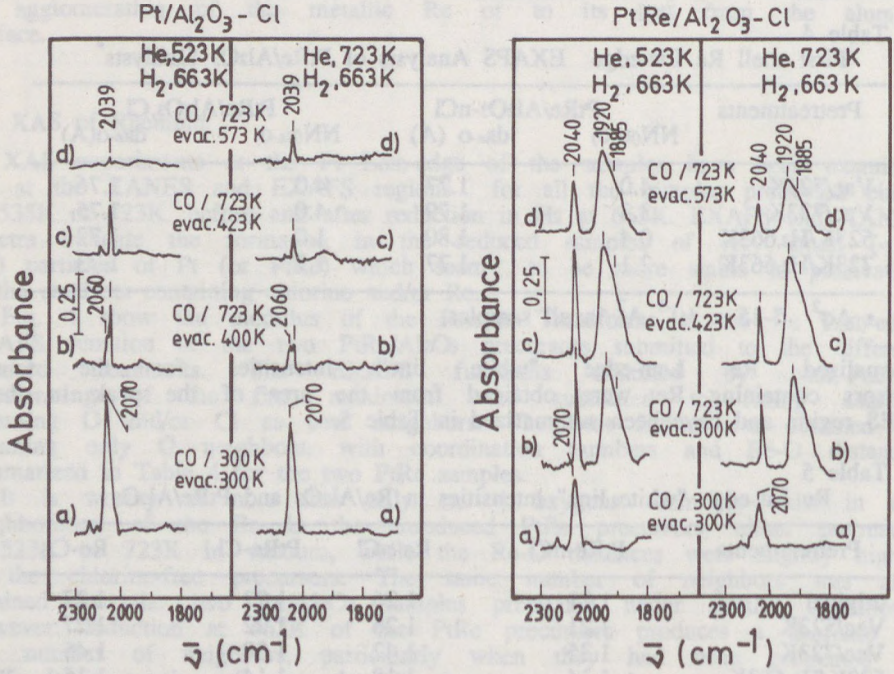

Figure 5. IR spectra of CO adsorbed at 300K and 723K. Left: on Pt-Cl pretreated at 523K and 723K. Right: on PtRe-Cl pretreated at 523K and 723K. Samples reduced at 663K.

the same i.r. bands due to adsorbed CO, though they are slightly more intense in the sample pretreated at 523K. So, after adsorption of CO at 300K a single characteristic sharp band at ca. 2070±3 cm^{-1} was observed, due to linear Pt-CO species. However, when the samples were heated in contact with CO at 723K two less intense bands at 2060±3 and 2040±3 cm^{-1} remain, which have been attributed (5) to the existence of very small clusters of Pt. Evacuation of the CO at 423K removes the band at 2060±3 cm^{-1} and leaves only a single band at 2040±3 cm^{-1} which is almost completely removed by evacuation at 573K

Adsorption of CO under similar conditions on the PtRe-Cl catalyst produces the spectra also shown in Fig. 5. At 300K only the band at 2070 cm^{-1} due to Pt-CO was recorded while at T >573K the formation of new bands, due to Re carbonyls, start to develop reaching a maximum at ca. 723K once removed the excess of CO at 423K. In these spectra a sharp band at ca. 2040±3 cm^{-1} is observed, probably overlapping with the band due to Pt-CO that still would remain in these conditions, together with an asymmetric and broader band at 1920±3 cm^{-1} with a shoulder at 1885±5 cm^{-1}.Similar spectra have been recorded by Guczi et al. (6,7) from $Re_2(CO)_{10}$ or $H_3Re_3(CO)_{12}$ supported on alumina and ascribed to the formation of $(Re(CO)_3OH)_4$ tetramers and $Re(CO)_3(O\text{-}Al)_2(HO\text{-}Al)$ monomeric intermediates in the thermal decomposition of those carbonyls at the alumina surface.

I.r. spectra recorded for the two Re/Al_2O_3 samples, reduced at 873K are shown in Fig. 6 .The reduced Re-nCl catalyst, either pretreated at 523K or 723K, gives bands which are similar to those just described for the PtRe-Cl

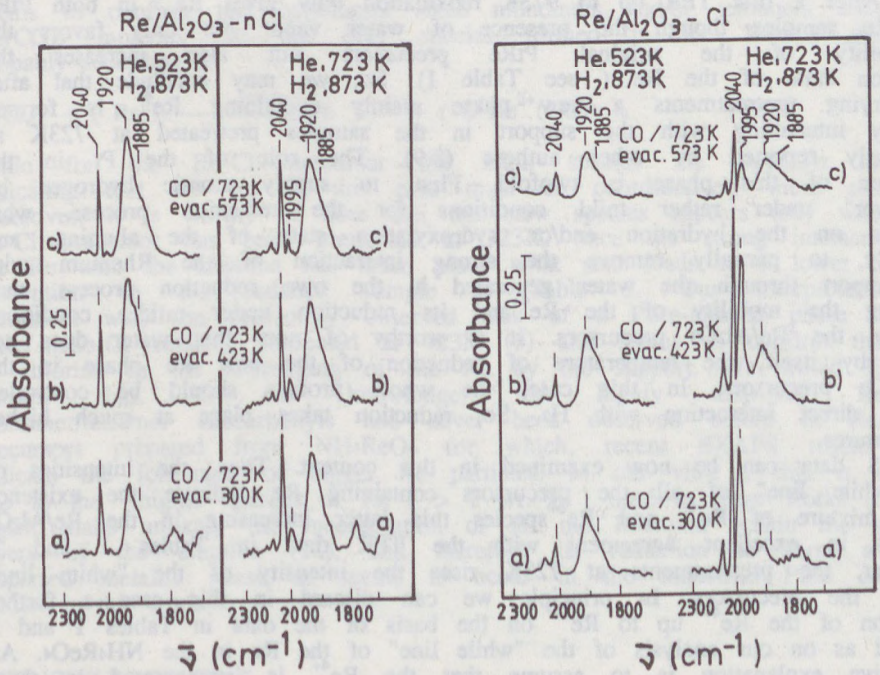

Figure 6. IR spectra of CO adsorbed at 723K. Left: on Re-nCl pretreated at 523K and 723K. Right: on Re-Cl pretreated at 523K and 723K. Samples reduced at 873K.

sample and that are also present in the Re-Cl sample pretreated at 523K though in this case with a slightly lower intensity. However, for the Re-Cl sample pretreated at 723K a much more complex spectrum was recorded in which the same carbonyl species, characterized by the three bands at 2040, 1929 and 1885 cm^{-1} described above, are present together with new species responsible for two, very intense, bands at 2040∓3 and 1995∓3 cm^{-1} which dominate the spectrum, the former overlapping with the one existing in the spectra of the other samples at the same wavenumber, as shown by a deconvolution analysis of the spectra, which suggests the formation of $Re(CO)_2$ species.

4. DISCUSSION

Results from all four type of experiments (TPR, XAS, O_2 adsorption and IR/CO) can be discussed in relation with previous data of n-butane hydrogenolysis on the same Pt and PtRe catalysts which indicate that chlorine plays an important role in the distribution of the Re at the surface layers of the alumina in the thermally pretreated precursors, before the final reduction of the catalysts, and therefore determines the formation of a PtRe-alloyed phase.

As clearly show the TPR profiles, drying at 723K either with He or air makes more difficult the reduction of the Re in the two $PtRe/Al_2O_3$ precursors while the data reported in Table 1 indicate that even after pretreating at 523K the Re is in these samples as Re^{4+} together with some Re^{6+}. After a first TPR up to 973K reoxidation only gives Re^{4+} in both PtRe and Re samples though the presence of water vapor not only favors the reducibility of the original PtRe precursors but also increases the oxidation state of the Re (see Table 1). So, we may conclude that after the drying pretreatments a new phase mainly containing Re^{4+} is formed strongly interacting with the support in the samples pretreated at 723K as previously reported by other authors (8,9). The role of the Pt in the reduction of this phase is twofold. First, to supply atomic hydrogen by "spillover" under rather mild conditions for the reduction process, what depends on the hydration and/or hydroxylation state of the alumina, and secondly, to partially remove the strong interaction of the Rhenium with the support through the water generated in the own reduction process, thus allowing the mobility of the $Re^{4+}$and its reduction under milder conditions than in the Re/Al_2O_3 precursors. It is worthy of note that water does not lower, by itself, the temperature of reduction of the new Re phase in the Re/Al_2O_3 precursors, In this case, the whole process should be controlled by its direct interaction with H_2. So, reduction takes place at much higher temperatures.

XAS data can be now examined in this context. Thus, the intensities of the "white line" of all the precursors containing Re indicate the existence of a mixture of Re^{4+} and Re^{6+}species this latter increasing in the Re/Al_2O_3 samples in excellent agreement with the TPR data in Tables 1 and 2. However, the pretreatments at 723K rises the intensity of the "white line" in all the precursors. In principle we can discard in this case a further oxidation of the Re^{4+} up to Re^{7+} on the basis of the data in Tables 1 and 2 as well as on our analysis of the "while line" of the Re in the NH_4ReO_4. An alternative explanation is to assume that the Re^{4+} is incorporated in these conditions into subsurface layers of the alumina support what provides a more ionic environment to these ions while it makes more difficult their

reduction in the presence of Pt as shown in Fig. 1. In principle, Re^{4+} (with a $5d^3$ configuration) would adopt an octahedral coordination, as in ReO_2, though data in Table 4 indicate a number of neighbors lower than six. This fact could be probably associated to a high static disorder in this new phase formed within a thin layer of the alumina probably due to the big size of the Re^{4+} ions compared with Al^{3+} (0.77 vs 0.67 A) what might introduce a considerable disorder.

Reduction at 773K of the Re/Al_2O_3 precursors under 1 bar of hydrogen seems to reduce almost completely the Re to the metallic state in the the chlorine-free sample. According to the data for oxygen adsorption in Table 3 we can write:

$$n/2\ O_2 + (Re^0)_n \xrightarrow{300K} (Re^{2+}O^{=})_n \qquad (1)$$

thus leading to the formation of low oxidized Re species (e.g.Re^{2+}/Re^{3+}) that under more severe reoxidation conditions lead to Re^{4+}(see Tables 1 and 2). It is well known that Re^{2+} species are able to form dimeric species (10) with very short Re-Re distances (~2.2-2.3 A). So, we can tentatively ascribe the new peak at ca. 2.00 A (without phase correction) in the FT-exafs function (see Fig.4) to this type of species in our reduced (and passivated) PtRe-nCl catalysts pretreated at 523K .

On the other hand, it is remarkable that the O_{ad}/Re_T value in Table 3 for Re-Cl decreases for the sample pretreated at 723K, probably indicating that a fraction of the Re has been deeply incorporated into the alumina support, so reduction can not recover part of this Re. IR data in Fig. 6 seems to confirm this hypothesis since monomers and/or tetramers containing $Re(CO)_3$ moieties are the only species formed in the Re-nCl precursor probably according to:

$$4nCO + (Re^0)_n \xrightarrow{>573K} n\ "C" + (O^{=}Re^{2+}(CO)_3)_n \qquad (2)$$

while for the Re-Cl precursor the main species are $Re(CO)_2$ moieties indicating that the Re in this case must be coordinatively more saturated. Moreover, it is worthy of note that this new species appears only when the Re-Cl precursor has been pretreated at 723K, once the strong interaction of the Re with the alumina has taken place what also leads to a lower oxygen adsorption in the reduced sample in Table 3. Our interpretation is consistent with the previously observed lack of a PtRe-alloyed phase in the $PtRe/Al_2O_3$-Cl catalyst pretreated at 723K (1) and seems to confirm the role of chlorine in the scavenging of the Re by the support. We would like to remark that, to our knowledge, the highly dispersed $Re(CO)_3$ monomer/tetramer subcarbonyls had never been observed before in Re/Al_2O_3 precursors prepared from NH_4ReO_4 for which, recent EXAFS results (11) indicate the formation of bigger Re particles. In our view , this is mainly due to the higher charges of Re (> 1 wt %) used in these works (6,7,11) which make unlikely the incorporation of all the Rhenium within the surface layers of the alumina (12), and therefore its reduction to form a well dispersed metallic phase as seems to occur in the industrial PtRe catalysts studied in this work.

ACKNOWLEDGEMENT

We thanks the financial support from the PGC/MEC Program (Projects PR84/0330 and PB88/263) to this work.

BIBLIOGRAPHY

1. P. Malet, G. Munuera and A. Caballero. J. Catal. 115 (1989) 567
2. A. Caballero, A.R. Gonzalez-Elipe, P. Malet, G. Munuera, J. Garcia, J.C. Conesa and E. Burattini. Physica B 158 (1989) 158.
3. M. Kobayashi, Y. Inoue, N. Tajahashi, R.L. Burwell Jr., J.B. Butt and J.B. Cohen. J. Catal. 50 (1980) 464
4. P. Malet and A. Caballero. JCS Faraday Trans 1,84 (1988) 2369.
5. M.G.V. Moderate and C.H. Rochester. JCS Faraday Trans 1,85 (1989) 3495.
6. L. Guczi A. Beck. Polyhedron 7 (1988) 2387.
7. L. Guczi, S. Dobos, A. Beck , A. Vizi-Orosz. Catal. Today 6 (1989) 97.
8. H.C. Yao, M. Shelef. J. Catal. 44 (1976) 392.
9. D.R. Sort, J.M. Khalid, J.R. Katzer. J. Catal. 72 (1981) 288.
10. F.A. Cotton Acc Chem Res. 11 (1978) 225; ibid 11 (1978) 356.
11. A.S. Fung, P.A. Tooley, M.J.Kelley, D.C. Koningsberger and B.C. Gates, J. Phys Chem. 95 (1991) 225
12. P. Arnoldy, V.M. Van Oers, O.S.L. Bruinsma, V.H.J. DeBeer, J.A. Moujlin, J. Catal. 93 (1985) 231.

DISCUSSION

Q: H. Kluksdahl (USA)

Re(VII) oxide interacts strongly with the alumina support in reforming catalysts and, unlike the high volatibility of the (I) and (VI) oxides, there is no loss of rhenium in an oxidizing atmosphere below ca. 973 K and in reasonably dry atmospheres. We have observed a rather simple procedure for displacing Re(I) from oxidized catalysts by treating with an aqueous solution containing simple, non-oxidizing inorganic anions such as nitrate, chloride, carbonate, etc. (US Patent, H. E. Kluksdahl, J. R. Hopkins, early 1970's). This displacement is virtually quantitative with recoveries of 95% or more. We would not expect lower valent rhenium species to be so displaced.

Some amount of moisture is commonly present in reforming catalyst treatments and usage. Would you expect moisture to hydrolyze your Re(VI)/Cl species ? How dry was your system at the conditions where you claimed Re(IV)/Cl ?

A: G. Munuera

In our samples water vapor is able to produce hydrolysis but not oxidation of the Re(IV)/Re(VI) up to Re(VII). As you can see in Figure 3, water vapor produce changes in the TPR profiles of the samples pretreated at 723 K giving a single-peak profile for Pt + Re reduction due to the hydrolysis of the strong Re(IV)-O-Al^{3+} interactions existing in these dried samples but without change in the oxidation state of the Re that remains as Re(IV)/Re(VI) (see Table 1).

However, using samples with a higher Re loading (ca. 1-3 %) we know by XPS that though dry oxygen is only able to oxidize rhenium up to Re(IV)/Re(VI), in the presence of water vapor a partial oxidation up to Re(VII) occurs the extent of which increases with the temperature and time of reaction (or just by exposure to the air). In the conditions you describe, using aqueous solutions, I can guess that oxygen dissolved in the water or from the air may be involved in the oxidation of all the rhenium up to Re(VII). In our experimental conditions, though water vapor was present in some of the experiments oxygen was always absent what prevent the oxidation up to Re(VII).

Q: R. Prins (Switzerland)

The X-ray absorption white line intensity was influenced by chlorine. This may suggest that Cl is sitting on the Pt, but in that case one should be able to observe a Pt-Cl bond in EXAFS. Did you see such an EXAFS contribution ? One would not expect chlorine to adsorb

on the Pt, because Cl is also strongly adsorbed by the alumina and there is so much more Al_2O_3 surface area. So, how is Cl influencing the Pt white line intensity ?

A: G. Munuera

We have not presented in our paper any EXAFS/XANES data for Pt, as you ask in your written question, but for Re. However, I must say that we have studied both Pt (ref. 2) and Re L_{III}-edges. In our pre-calcined chlorinated precursors, once pretreated either at 423 or 723 K, chlorine is not interacting with the metals as indicated by the fitting analysis of the EXAFS spectra, though XPS shows that it is present at the support. Moreover, the observed increase in the intensity of the L_{III} "white line" in the case of the Re after the pretreatment at 723 K occurs in all four samples used in our work, whatever they contain or not chlorine. Therefore, this fact can not be related to direct interactions of the rhenium with the chlorine.

Q: G. L. Haller (USA)

We have recently investigated $PtRe/Al_2O_3$ TPR using X-ray absorption spectroscopy. Using a variety of Re references compounds, it was observed that there does not exist a linear relation between the Re L_{III} white line and formal oxidation state. However, there is a linear relations between the edge shift and Re formal oxidation state, because these shifts are small, they require a simultaneous observation of a reference material, e.g., Re powder, but with case one can follow the shift in the edge during TPR of catalysts of commercial loading, e.g., 0.3 wt % Pt- 0.3 wt % Re/Al_2O_3. Since the white line intensities (your table 5) an likely affected by ligands, e.g., Cl^- and symmetry, I suggest that you also measure the edge shifts as well as the white line intensity of Re.

A: G. Munuera

I am glad to hear that you also found a non-linear relationship between the Re L_{III} white line intensity and the formal oxidation state, as we have reported in our paper. However, in the context of our work what we like to stress is the observed net increase in the intensity of this line in all the four samples containing Re after the non-oxidizing pretreatments at 723 K which correlates well with the changes observed in the TPR profiles though the oxidation state remains close to Re(IV) and with the same local symmetry (see Table 1 and 4). So, we have ascribed this fact to a deeper interaction of the rhenium with the more "ionic" Al_2O_3 environment what seems confirmed by our CO/FTIR data. In relation with the small "shift" you have observed in the L_{III}-edge for different oxidation states of the rhenium we have not made such a careful study with our samples and reference materials (ReO_2, ReO_3 and ReO_4NH_4) though it seems interesting to obtain the average oxidation state of the rhenium to compare with data from TPR.

Q: B. Notari (Italy)

Chlorine plays important roles both in the preparation of the reforming catalysts and in their utilization.

It is well documented that under typical reforming conditions (753 K, H_2 pressure 10-30 bar) Pt is reduced to Pt metal and it provides the (de)hydrogenation activity while the chlorine is bound to the Al_2O_3 and provides the acid activity. These two functions are necessary to give rise to the "bifunctional mechanism" through which all the different reactions of naphtha reforming take place.

Therefore the role of chlorine during utilization is very clear and is the very reason why industrial catalysts contains chlorine. On top of that, chlorine also has a role during the preparation of the catalyst, but this is a transient role.

A: G. Munuera

As you say, it is well known that the main role of chlorine in the reforming bifunctional catalysts is to provide the acidic function at the support. nevertheless, before their use bimetallics $PtRe/Al_2O_3$ catalysts should be preconditioned, then reduced and finally sulfided

under well specified conditions. The aim of our work was to examine the effect of some of these steps in the final state of the metallic phase and, in particular, in the formation of a PtRe-alloyed phase. What our combined TPR/EXAFS-XANES/FTIR results, together with n-butane hydrogenolysis "tests" (studied in ref. 1), seem to indicate is that chlorine has also a role in the development of such alloyed phase during the conditioning of the industrial catalyst before use what, in our view, is more than a transient effect. In short, what we found is that when the chlorinated industrial catalysts are thermally pretreated at 723 K part of the rhenium is unable to form the PtRe alloy. This may affect the poisoning stability of the metallic phase. it is worth of mention that new formulations of the PtRe reforming catalysts use Pt:Re ratios of 1:2 instead of 1:1.

Q: J. Ryczkowski (Poland)

Usually preparation of bimetallic catalysts in the way of impregnation can create mixed interaction in final catalyst. This preparation procedure should mainly produce metal(1)-support and metal(2)-support interaction. Direct metal(1)-metal(2) interaction can be formed only by chance. How do you think, what is the amount of really alloyed phase in your bimetallic catalysts ? If I am right, in your bimetallic systems you have mainly metal(1) and metal(2)-alumina interaction:

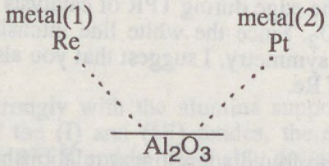

Do not you think, that the observed effects came from separate surface species and the presence of neighboring metal atoms can only influence them ? And finally, how is the alloy phase, if it is present, changing during the experiments and during the course of the reaction ?

A: G. Munuera

Our results in this and in our previous paper (ref. 1) are difficult to explain, in our view, without considering the formation of a PtRe-alloyed phase during the reduction of the catalyst precursors. The way in which alloyed phases are formed in bimetallic catalysts is still unclear, particularly when metal loadings become so small as in our $PtRe/Al_2O_3$ samples.

In principle it seems, as you say, that alloying can only occur by chance unless the two metallic precursors were originally close together at the support. However, we must assume, according to our TPR profiles, that during reduction of the catalyst precursors platinum is reduced first so that small clusters of this metal should be able to diffuse at the surface of the Al_2O_3 support (particularly when it is highly hydroxylated) reaching in their way ReO_x clusters that may be reduced by the hydrogen spelt over from the Pt clusters to form a PtRe-alloyed phase. Of course, some of the Pt particles and some of the reduced Re (in particular when directly reduced at the higher temperatures) can remain as monometallic particles.

During n-butane hydrogenolysis "tests" (ref. 1), using the pulse technique, Re is readily poisoned so, physical mixtures of monometallic catalysts show steady state selectivities (C_3/C_1), after a few pulses, close to that for Pt/Al_2O_3 while in the bimetallic catalysts, where Pt and PtRe particles would remain active, the value depend on their relative amounts. In our mild reaction conditions the PtRe particles should remain unchanged as suggested by the reproducibility of test reaction.

Guczi, L. *et al.* (Editors), *New Frontiers in Catalysis*
Proceedings of the 10th International Congress on Catalysis, 19-24 July, 1992, Budapest, Hungary
© 1993 Elsevier Science Publishers B.V. All rights reserved

A NEW APPROACH TO LOSS OF ALKALI PROMOTER FROM INDUSTRIAL CATALYSTS: IMPORTANCE OF EXCITED STATES OF ALKALI

L. Holmlid[a], *K. Engvall*[a], *C. Aman*[a] *and P. G. Menon*[b]

[a]Department of Physical Chemistry, University of Göteborg and Chalmers University of Technology, 412 96 Göteborg, Sweden
[b]Department of Engineering Chemistry I, Chalmers University of Technology, 412 96 Göteborg, Sweden

Abstract

Using molecular beam and mass spectrometric techniques, the emission of highly excited states (so-called Rydberg states) of potassium from commercial iron-oxide catalysts for the styrene process was studied. The earlier results have been confirmed and extended using surface ionization detection and K molecular beam impact on plane catalyst surfaces. It is shown that clusters of K are very likely to be formed at the catalyst surface at normal operating temperatures in the experiments. The relevance of these results for the observed loss of potassium promoter under process conditions is discussed.

1. INTRODUCTION

The importance and widely prevalent practice of alkali doping to promote various heterogeneous catalysts has been reviewed by Mross [1]. The promoter can influence the activity and selectivity of the catalyst. While the surface physics approach to the promoter effect is concerned mainly with the indirect geometric and/or electronic effects of the alkali promoter like modified bonding of ad-species to the surface, recent progress [2,3] on the other hand stresses the direct chemical interaction between the promoter and adsorbed molecules. In many cases, the promoter effect is still not understood very

well, despite the routine use of promoters in catalytic processes and the intense research in this field.

The migration and loss of potassium from the iron-oxide catalyst for the styrene process continues to be a serious production problem even 60 years after the commercialisation of this process. We have used molecular-beam and mass spectrometric techniques to study emission of K species from commercial styrene catalysts at typical process temperatures of 860-900 K (590-630 °C). Our work [4,5] is complementary to the recent work of Ertl and coworkers [6,7] at Berlin and Geus and coworkers [8,9] at Utrecht, using entirely different techniques.

The techniques we have used [4,5] for detection of highly excited alkali atoms are mainly variations of weak field ionization, at field strengths less than 1000 V/cm. In this way, only highly excited so called Rydberg states are detected. Such states have a very large distance between the core ion and the excited electron or electrons. Another basic technique used in combination with field ionization is direct line-of-sight sampling from the catalyst into the field ionization detector or into a mass spectrometer. In the present study we apply still another technique to detect the alkali lost from the catalyst, namely surface ionization. This method provides absolute measurements of the losses, since it detects all alkali species with a similar efficiency. Clusters of alkali will probably also be dissociated and give ions in the detector, and the signal obtained is thus proportional to the total alkali flux. The present contribution will first describe the results concerning excited state emission from the sample, and after that focus on just one aspect of immediate interest for the loss of promoter, namely the evidence for loss in the form of clusters.

2. EXCITED STATE EMISSION

The loss of alkali promoter from metal oxide catalyst surfaces has been studied with molecular beam methods in a few cases [4,5,10]. The results found for the iron oxide catalysts for the styrene process are summarized in the table, where A and B are the two catalyst types studied in [4,5].

From the results found in [4,5] an energy diagram for the K promoter in the iron oxide material has been obtained, as shown in Fig. 1.

One of the measurement types of interest in the present context is the angular distributions of the emitted K species. In Fig. 2 an example of the results obtained with catalyst A is given. This result is almost cosine shaped, which is the form expected from statistical theory.

Table 1
Summary of results obtained for iron-oxide catalysts

Catalyst	Species detected	Detection technique	Barrier (eV)	Angular dep.	Ref.
A	K	EB	1.0±0.2	T	4
A	K^{2*}	FI	1.7±0.3		4
B	K	EB	3.1±0.2		5
B	K^{2*}	FI	0.84±0.07	NL	5, P
B	all	SI		NL	11, P
B	K^{*}	VFI	1.0;1.5	NP	11

EB: electron impact, FI: field ionization, SI: surface ionization, VFI: ionization in very weak fields, T: thermal, NL: lobe in normal direction, NP: narrow peaks, P: present study

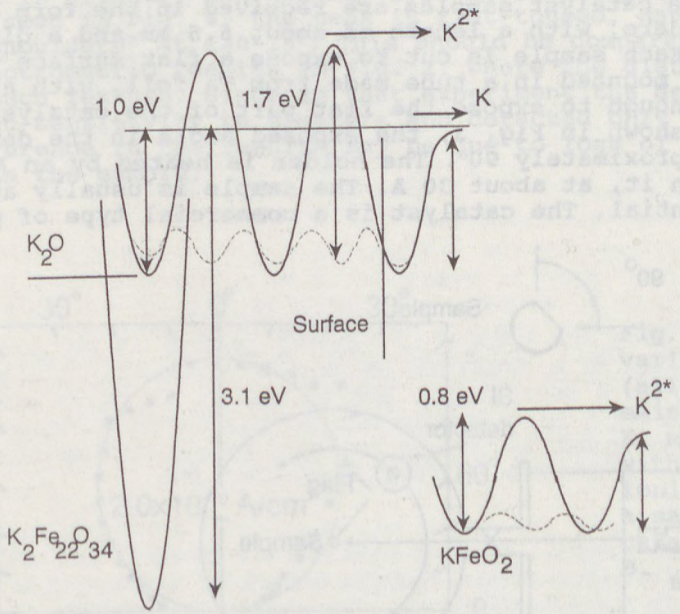

Fig. 1. Energy diagram for the potassium promoter in the iron oxide catalyst material.

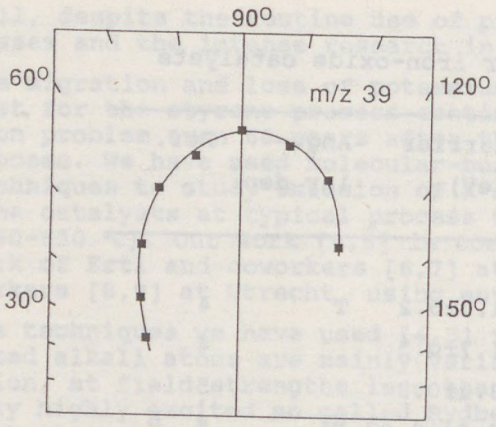

Fig. 2. Angular distribution for K at m/z 39 at 743 K, from a sample of catalyst type A. The mass spectrometer signal was obtained with electron impact ionization.

3. EXPERIMENTAL

The apparatus used is shown schematically in Fig. 3. It is a UHV vacuum chamber with a differentially pumped potassium molecular beam source, with two pump stages. The extruded commercial styrene catalyst samples are received in the form of small cylinders, with a length of about 6.5 mm and a diameter of 3.2 mm. Each sample is cut to expose a flat surface to the beam. It is mounted in a tube made from Ta foil, with an opening large enough to expose the flat part of the catalyst sample. As shown in Fig. 3, the exposed angle in the detector plane is approximately 90°. The holder is heated by an AC current through it, at about 30 A. The sample is usually at ground potential. The catalyst is a commercial type of potas-

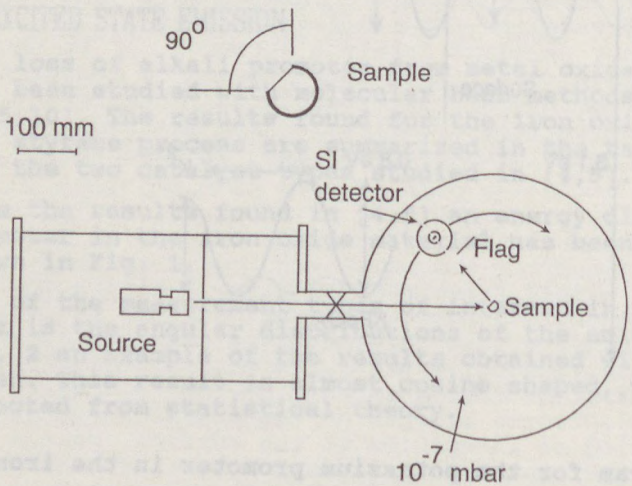

Fig. 3. Schematic drawing of apparatus.

sium promoted iron oxide for the styrene process. Catalyst B is the better one of the two catalysts studied in Ref. [5].

The molecular beam of potassium is a thermal one (effusive) of very low density. It is directed towards the catalyst surface at an angle of -45° towards the surface normal. The beam flux is turned off by closing a slide valve.

The surface ionization detector can be rotated 360° around the sample. In a certain range it blocks the molecular beam. Measurements with the beam on can not thus be obtained in that angular range. The detector consists of a hot Re ribbon with exposed dimensions 0.7x10 mm^2, which ionizes the impinging flux of potassium from the sample. The ribbon temperature is approximately 1450 K, and it is held at a voltage of 150 V. The ions formed on the ribbon surface are accelerated from the ribbon to the concentric collector at ground, where the ion current is measured.

4. RESULTS AND DISCUSSION

The angular variation of the emitted potassium flux is studied as a function of the sample temperature and the electric field strength outside the surface. With no impinging K beam, the emission is slightly non-cosine, i.e. it is not purely thermal. As seen in Fig. 4, the peak is flat-topped, having too large "shoulders" at ±20-25°. This should be compared with the mass spectrometric results in Fig. 2, where the distribution has no such feature. Since in that experiment the detector had almost no sensitivity to clusters and detected only K atoms, the difference in the results may be due to loss of clusters of K from the sample.

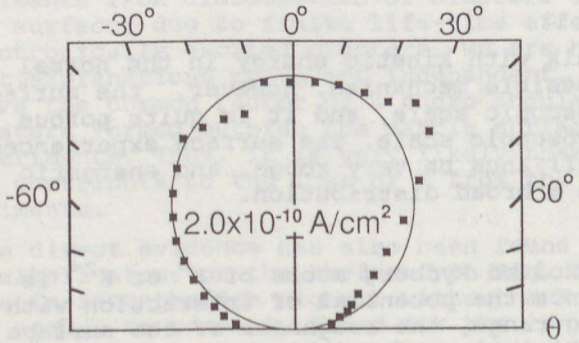

Fig. 4. Angular variation of K (all states) emission at 990 K, measured with surface ionization from a sample of catalyst type B.

In experiments with a K beam impinging on the sample surface, several different types of results are found depending on the

state of the catalyst (e.g. time of use in the experiments), the temperature and voltage of the sample, and the intensity of the beam. Also surface scattering phenomena are observed, but they fall outside the present theme, and will be described elsewhere. Instead, we will focus on the cases where a lobe in the normal direction is obtained. One example is shown in Fig. 5, with quite low sample temperature which gives a low direct emission from the sample. The full angular range is not covered in this figure, since the detector blocks the impinging beam, but the distribution should be symmetrical around the normal direction. Thus, a very strong peak in the normal direction is obtained, which indicates that some special processes act in the desorption. There exist a few possibilities:

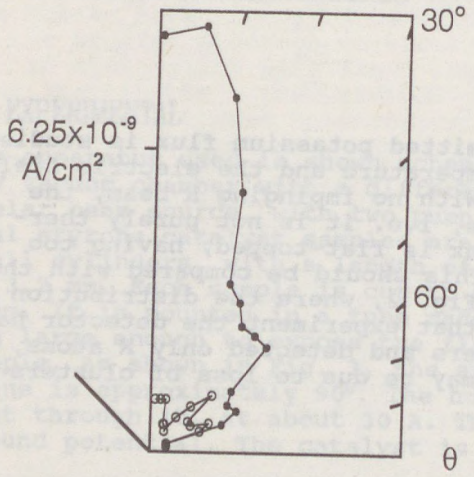

Fig. 5. Angular distribution of emission with a K beam and the sample at 80 V, measured with surface ionization from catalyst type B at 790 K. The inner curve is the signal with the beam off.

1) Emission from the bulk with kinetic energy in the normal direction could be a possible mechanism. However, the surface is only flat on a macroscopic scale, and it is quite porous and irregular on a microscopic scale. The surface experienced by the emitted atoms will thus be very rough, and energetic emission will thus give a broad distribution.

2) Emission of highly excited Rydberg atoms of K^* or K^{2*} is another possibility. Since the potential of interaction with the surface is very long range, the roughness of the surface will not influence the direction of emission very much. Thus, one can expect such a distribution for the excited states. In fact, similar distributions have been obtained in the experiments with field ionization of K^{2*} presented in part in Refs. [5,12]. One example of a sharp distribution in the normal direction is shown in Fig. 6.

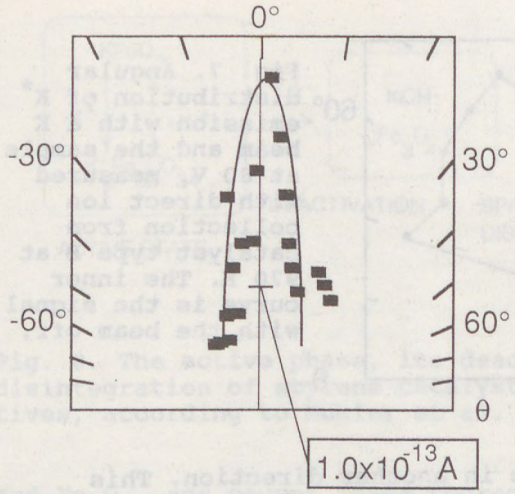

Fig. 6. Angular distribution of K^{2*} from catalyst type A measured by field ionization, at a temperature of 870 K.

3) Emission of clusters K_n. Such clusters are probably formed outside the surface by condensation of excited Rydberg states K^*. The driving force for the condensation is the huge interaction force between pairs of excited atoms K^* [13], and between the excited states and ground state atoms and molecules. The emitted atoms and excited states should have a cosine distribution, as expected from basic theory. The combination of many atoms into clusters will however average out the velocities parallel to the surface, and give the clusters a common direction close to the normal out from the surface. Clusters K_n will thus have the observed sharp angular distribution.

Since we do not know if the states K^{2*} are formed in the experiments from dissociation of clusters at some distance from the surface, due to finite life-time effects of the probably electronically excited clusters, we are not sure that the two last explanations above are independent. In fact, we may observe the common factor of a sharp angular distribution of the clusters formed outside the sample surface in both types of experiments. Thus, it is very likely that clusters are formed and contribute to the loss of K from the catalyst in the experiments.

Some direct evidence has also been found for the interaction of alkali atoms on the surface. In Fig. 7, the signal (in this case in fact the ion signal) without a K beam is a few lobes and peaks, as commonly found for the ion emission [11]. When the thermal K beam is allowed to strike the sample, the angular distribution changes strongly, and the lobe at 14° is removed completely. Instead, the flux from the surface is found in some type of flat-topped lobe at 60°. This means that the atoms from the beam, despite the extremely low density used, combines with the K emitted from the sample, removes it and

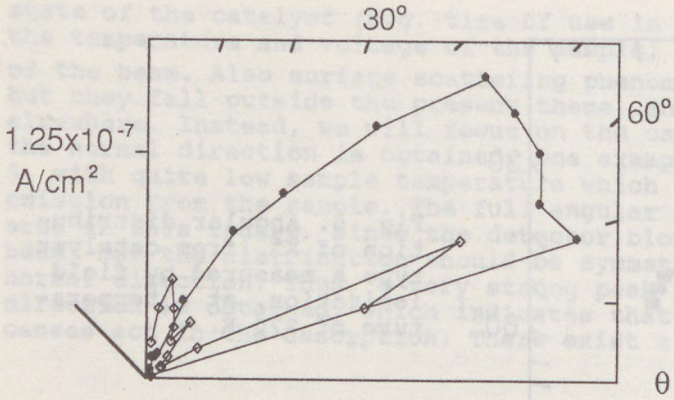

Fig. 7. Angular distribution of K^* emission with a K beam and the sample at 80 V, measured with direct ion collection from catalyst type B at 970 K. The inner curve is the signal with the beam off.

forces it to leave the surface in another direction. This implies strong interaction forces, as can only be expected for excited states K^*, and probably also loss as clusters, in this special case as cluster ions.

5. ALKALI LOSS PROCESSES

One must also inquire into the relevance of the present results for the loss of alkali promoter in real catalytic reactions. First of all, the conditions outside the surface at high surrounding gas pressure are of course very different from the ultra high vacuum experiments which we have performed. However, the mechanisms which give formation of excited states are related only to the actual desorption and emission processes of alkali, which should be quite independent of the coverage on the surface of other molecules. Thus, we expect the formation of excited states to be similar also at high pressure. However, the gas present on the surface and in the gas phase outside the surface will strongly influence the life-time of the excited states. Specifically, the surrounding gas will decrease the rate of cluster formation very much, by quenching and reacting with the excited states before they can combine to form clusters.

The loss of alkali promoter from the styrene catalyst samples in our experiments seems to be much faster than from the catalyst samples used in the real styrene process. This may not be strictly correct since only desorption loss from the catalyst is considered here. The solid-state transformations under real process conditions are determined both by the temperature and also by the presence of superheated steam and the product hydrogen. According to Muhler et al. [7], the active form of the catalyst is a dynamic equilibrium between $KFeO_2$ and $K_2Fe_{22}O_{34}$ phases. The attack of product hydrogen (from dehydrogenation of ethyl benzene) on these active phases reduces them to KOH

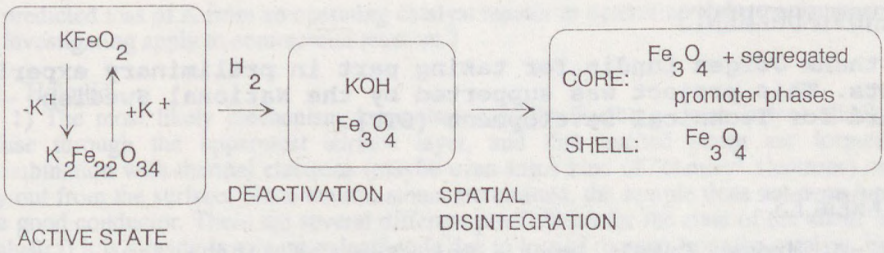

Fig. 8. The active phase, its deactivation, and the spatial disintegration of styrene catalyst without any promoter additives, according to Muhler et al. [7].

and Fe_3O_4, and causes phase segregations in a K-rich core and a K-poor shell within each catalyst extrudate (Fig. 8). These phases are catalytically inactive and nonselective, and also mechanically weak. The ease of thermal desorption of potassium from the catalyst and its mobility under the styrene-process conditions are thus crucial for both the macro-scale migration and loss of K in the direction of process flow in the catalyst bed, and for the micro-scale migration of K from the outside to the core of every catalyst particle or extrudate. Hence we are extending our studies to follow the influence of the ambient pressure and of the nature of the gas (steam, H_2) on the characteristics of potassium emission from the catalyst (subject to the limitations of the UHV system). The alkali loss which takes place could be related to loss as ground state atoms K, but several other possibilities do exist. The detection of loss as excited states K^* and K^{2*} and as clusters K_n shows that the behaviour of alkali loss from the catalyst is much more complicated than hitherto realized. The operational stability of the catalyst under styrene process conditions can perhaps be enhanced by the addition of other oxides (e.g oxides of Ca, La, Ce, V, W) as promoters, which can play a double role:

a) retard the undesired solid state transformations [7], shown in Fig. 8, and

b) raise the temperature threshold for the thermal desorption of K from the catalyst [5].

Our comparative study [5] of two commercial styrene catalyst showed that the better catalyst had indeed a much higher temperature threshold for the desorption of K both as K atoms and as K^{2*} excited species. In this respect, the present molecular beam study is proving to be a valuable fingerprint and possibly even an accelerated life test for the styrene catalyst.

ACKNOWLEDGEMENTS

We thank Jörgen Lundin for taking part in preliminary experiments. This project was supported by the National Swedish Board for Technical Development (STU).

REFERENCES

1 W.-D. Mross, Catal. Rev. - Sci. Eng. 25 (1983) 637.

2 F.M. Hoffmann and M.D. Wiesel, Abstract 85, ECOSS-12 (european Conf. on Surface Science), Stockholm, 1991. To appear in Surface Science.

3 J.B.C. Pettersson, L. Holmlid and K. Möller, Appl. Surface Sci. 40 (1989) 151.

4 J. Lundin, K. Engvall, L. Holmlid and P.G. Menon, Catal. Lett. 6 (1990) 85.

5 K. Engvall, L. Holmlid and P.G. Menon, Appl. Catal. 77 (1991) 235.

6 M. Muhler, R. Schlögl, A. Reller and G. Ertl, Catal. Lett. 2 (1989) 201.

7 M. Muhler, J. Schutze, M. Wesemann, T. Rayment, A. Dent, R. Schlögl and G. Ertl, J. Catal. 126 (1990) 339 and forthcoming publications.

8 D. E. Stobbe, F. R. van Buren, A. V. Stobbe-Kreemers, J. A. Schokker, A. J. van Dillen and J. W. Geus, J. Chem. Soc. Faraday Trans. 87 (1991) 1623, 1631, 1639 and forthcoming publications.

9 D. E. Stobbe, On the Development of Supported Dehydrogenation Catalysts Based on Iron Oxide, Ph.D. Thesis, University of Utrecht, 1990.

10 K. Engvall, L. Holmlid, H. Prinz and H. Hofmann, Catal. Letters 11 (1991) 41.

11 C. Åman and L. Holmlid, to be published.

12 K. Engvall and L. Holmlid, Appl. Surface Sci., accepted.

13 C. Åman, J.B.C. Pettersson and L. Holmlid, Chem. Phys. 147 (1990) 189.

DISCUSSION

Q: G. L. Haller (USA)

1) Since you are detecting neutral and or excited K but potassium exists as K(I) in the catalyst, can you tell us what is being oxidized in the catalyst and how its composition evolves in time ?

2) I realize that practical packed bed reactors would have complications of K readsorption, excited state quenching, etc., but can you make an order of magnitude estimate of

the predicted loss of K from an operating catalyst reactor to determine if the mechanisms you are investigating apply to commercial reactors ?

A: L. Holmlid

1) The most likely mechanism for emission of the Rydberg states is that alkali ions diffuse through the uppermost surface layer, and that excited states are formed by recombination with thermal electrons (maybe even some kind of "convey" electrons) on the way out from the surface. Since neutral atoms are emitted, the sample does not even have to be a good conductor. There are several different possibilities for the state of the alkali in the catalyst: i) it is already in a "zero valent" state due to loss of oxygen from the catalyst, b) it is bound to O(II), and gives a free valence in the iron oxide, which is part of the destruction of the oxide structure, c) it is bound in K_2O leaving KO behind, which may react with H on the surface to form the final inactive form KOH. Since the material is a good conductor, there is always a good supply of electrons.

2) We have discussed and evaluated the efficiency of the loss processes in ref. 4. The rates of loss we observe are much larger than required to explain the loss in the real process, so there is certainly quenching processes etc. taking place. The quenching rates for the excited states are not known yet, so the estimate required is not easy to calculate, but the Rydberg research field is active so there is hope in a few years' time.

Q: K. Kochloefl (Germany)

1) As is well known, K migrates during the catalyst activation and during ethylbenzene dehydrogenation within the catalyst particles (e.g. extrusions).

Did you measure K-losses in the case of activated and spent catalyst as well?

2) According to my experience, K-losses depend first of all on reaction temperature and partial pressure of ethylbenzene in the steam.

A: P. G. Menon

1) During the styrene process, K migrates not only on the microscale of the catalyst extrudate from its exterior to the core, but also on the macroscale of the reactor or catalyst bed in the direction of process flow. This was indeed the motivation for us to undertake this study using the molecular-beam technique. A comparative study of K loss from fresh and used catalysts is of course essential and this is in progress in our laboratory right now.

A: L. Holmlid

2) We agree to this remark. The loss as Rydberg states has activation energies of 0.8-1.7 eV, which means that the rate of loss increases with temperature. The dependence on ethyl benzene partial pressure (decrease of loss rate with increasing partial pressure) may mean that this molecule acts as a very efficient quencher (or even reaction partner) for the Rydberg states, which is expected.

Q: N. Pernicone (Italy)

You know that basically two types of industrial styrene catalysts are currently used, one type is calcined at very high temperatures and contains K ferrites as the main phases. The other type is calcined at lower temperatures, so that no bulk interaction occurs between Fe and K oxides, and contains α-Fe_2O_3 as the main phase. To which type do your A and B catalysts belong ?

Moreover, what is your opinion about possible differences in the alkali loss mechanism between the two types ?

A: P. G. Menon

In reply to Dr. Pernicone, let me point out that the active phase of the styrene catalyst is dynamic equilibrium between $KFeO_2$ and $K_2Fe_{22}O_{34}$, as has been shown by recent work of Hirano in Japan, Ertl and coworkers at Berlin, and Geus and coworkers at Utrecht. This equilibrium is established only under the actual process conditions, and not by the initial

calcination. The catalysts A and B, used in our work, are real commercial samples. In a comparative study of K emission from these two catalysts, we have shown recently that the better catalyst B has indeed a higher temperature threshold for the emission of K species (ref. 5).

Q: A. Baranski (Poland)

The system and the technique that the paper has dealt with are suitable for checking the famous idea concerning "binding the pressure gap between UHV data and industrial practice". Let me remind you that a few years ago in Topsoe Laboratories the industrial yield of ammonia synthesis was successfully calculated [1, 2] from UHV data published by Ertl. In this paper, similarly, UHV data were used to determine the loss of potassium. Once again, pressure is the most essential difference between laboratory and real conditions.

The question is: would it be possible to develop a theory (and an algorithm) enabling one to introduce a pressure correction to laboratory results ?

[1] P. Stolze, I. K. Norskov, *Phys. Rev. Lett.*, **55**, 2502 (1985)
[2] P. Stolze, I. K. Norskov, *J. Catal.*, **110**, 1 (1988)

A: P. G. Menon

The idea of "bridging the pressure gap" is certainly in our minds too. We are already using industrial styrene catalysts directly in an UHV equipment. However, the styrene catalyst undergoes radical solid-state transformations under the actual process conditions with ethyl benzene and steam above 873 K. Simulating such conditions in UHV will not be so easy as was the case with ammonia synthesis. Hence we are concentrating more on comparative studies of K emissions from different commercial styrene catalysts of known process performance as also from fresh and used catalysts of the same type. It is too early to make extrapolations. Still, please see my reply to Dr. Pernicone.

Q: D. G. Blackmond (USA)

What is the initial chemical state of the alkali species on the catalyst surface ? Compounds such as K_2O or KOH tend to be much more stable against loss of potassium component to zero-valent potassium on single metal crystals.

A: L. Holmlid

The various states of the alkali in the catalyst are described by our energy diagram in Figure 1 and the transformations of the catalyst in Figure 8. These figures are consistent with the recent model for the solid state chemistry of the catalyst by Muhler et al.(ref. 7). We imply that the excited states are not formed on the surface, but during emission from the bulk, as shown in that figure. The comparison with a metal surface in any form is not easy to do, since metal surfaces in general do not emit Rydberg states.

Q: C. Cameron (France)

From an inorganic chemistry point of view, it is difficult to believe that potassium metal could be lost from an oxide catalyst composed of potassium and iron oxides. The potential for converting $K^+ \rightarrow K^0$ is very high, and I am sure higher than that required for the reduction of iron oxide to a sub-oxide. (Your energy potential diagram is not convincing).

1) Is it possible that the K^0 that you detect is due to the analytical technique employed ?

2) If you really believe that K^+ is reduced to K^0, where does the electron come from (i.e. $e^- + K^+ \rightarrow K^0$) ?

A: L. Holmlid

The neutral atoms are the result of the dissociation of even strongly ionic species like alkali salts is generally correct and observed experimentally in many cases. This is due to the avoided crossing of the ionic and covalent energy curves (surfaces), which means that an adiabatic (e.g. thermal) dissociation of the ionically bonded molecule gives neutral products. Further, an energy consideration shows that the ion pair K^+ and M^- is at a higher energy (and

thus the less probable state) than K and M: the ionization energy of K is 4.3 eV, while the electron affinity of M is considerably lower (1.5 eV for O). Only in the case of a conductor with a surface work function comparable to or higher than 4.3 eV will a considerable fraction of the desorbing K be emitted through a so called surface ionization process as K^+ ions. We have looked for ions from such a process with the present catalysts and at the temperatures studied, and we can not find any. So, the answer to your questions are as follows:

1) No, the emission of neutral K atoms is not due to the technique we use, but is expected as explained above.

2) The electron mentioned goes with the K atom: during dissociation of an ionic salt the two fragments respectively oxidize and reduce each other, as described above (due to the avoided crossing of the potential energy curves for the two states of the system).

Q: K. Aika (Japan)

Have you measured oxygen element free from the catalyst? During the loss of potassium are you leaving oxygen (counter element of potassium) on the catalyst ?

A: L. Holmlid and P. G. Menon

Oxygen is left on the catalyst sample, but part of it is also lost by desorption from the surface. In ref. 4 we show mass spectra with both m/e 16 and 32 lost from the catalyst. Recent AES studies in our group show considerable oxygen loss from the sample in the industrial process. Please remember here that, in the industrial process, it is the product hydrogen formed in the ethyl benzene dehydrogenation which starts reducing the catalyst, thereby causing the alkali migration and the deactivation and mechanical destruction of the catalyst, as shown in Fig. 8.

Q: G. B. Fisher (USA)

1a) Since this is a commercial catalyst, how is it that for single excited ion emission that loses of emission can be seen from presumably randomly oriented particles ?

1b) If for the emission of clusters of potassium in the normal direction you invoke a long range interaction, how long range does that need to be and does it vary with cluster size or excited K species type ?

2) Does the amount of K you see desorbing depend on temperature ? FS it related K diffusion energies or something else ?

A: L. Holmlid

1a) This point has been specially investigated, and it is treated in detail in two manuscripts submitted recently. In short, the very long-range potential interaction between the surface of the catalyst and the Rydberg states means that the desorption barrier is at such a long distance from the catalyst surface that the surface structure becomes unimportant.

1b) The form of the interaction with the surface is not important for the cluster formation. Any surface will give a cosine distribution for thermally desorbed species. The agglomeration of such species to clusters will give a lobe in the macroscopic normal direction, which is the average direction of the motion of the species from the surface, independent of the form of the interaction.

2) The Rydberg state signal depends on temperature: activation energies of 0.8-1.7 eV are given in Table 1 in the paper and have been published before. The relation to the energetics is shown in Figure 1.

Guczi, L. *et al.* (Editors), *New Frontiers in Catalysis*
Proceedings of the 10th International Congress on Catalysis, 19-24 July, 1992, Budapest, Hungary
© 1993 Elsevier Science Publishers B.V. All rights reserved

THE RELATION BETWEEN CATALYTIC AND ELECTRONIC PROPERTIES OF SUPPORTED PLATINUM CATALYSTS: THE LOCAL DENSITY OF STATES AS DETERMINED BY X-RAY ABSORPTION SPECTROSCOPY

M. Vaarkamp[a], *J. T. Miller*[b], *F. S. Modica*[b], *G. S. Lane*[b] *and D. C. Koningsberger*[c]

[a]Schuit Catalysis Institute, Eindhoven University of Technology, P.O.Box 513, 5600 MB Eindhoven, The Netherlands
[b]Amoco Oil Research Center, P.O.Box 3011, Naperville, IL 60566, USA
[c]Debye Institute, Laboratory of Inorganic Chemistry and Catalysis, University of Utrecht, P.O.Box 80083, 3508 TB Utrecht, The Netherlands

Abstract

The intensity of the white line of the L_{II} and L_{III} X-ray absorption edge spectra of small platinum particles increases with decreasing particle size. The combined white line intensity of the L_{II} and L_{III} X-ray absorption spectra for platinum catalysts with comparable average particle size is higher when dispersed on acidic than on neutral supports. This indicates that platinum particles are more electron deficient on acidic than on neutral supports. The propane hydrogenolysis TOF for platinum supported on γ-Al_2O_3 or H-LTL is found to be more than an order of magnitude higher than for platinum supported on a non-acidic K-LTL zeolite. The differences in catalytic behavior are related to differences in the d-band density of states.

1. INTRODUCTION

Electronic properties of highly dispersed metal particles are thought to be affected by support and/or promoter ions [1]. Charge transfer or polarization at the metal-support or metal-promoter interface may change the d-band density of states leading to different catalytic properties.

Information about the d-band density of states in transition metal clusters can be obtained from the white line intensities of the L_{II} (transition from $2p_{1/2}$ to $5d_{3/2}$) and L_{III} (transition from $2p_{3/2}$ to $5d_{5/2}$ and $5d_{3/2}$) X-ray absorption edges. A basic theory of white lines has been given by Mott [2], Brown et al. [3] and Mattheiss and Dietz [4]. The theoretical calculations of the unoccupied Pt d-states show that the J=5/2 final state is predominant. Brown et al. [3] showed that the J=5/2 states contribute about 14 times more to the final d-states than the J=3/2 states. Mattheiss and Dietz [4] calculated that the ratio of the unoccupied states ($h_{5/2}/h_{3/2}$)

ranges from 3.5 within 0.5 eV of the Fermi level to 2.9 over the entire unoccupied conduction band. These calculations explain why the intensity of the white line of the L_{III} X-ray absorption edge is much higher than the intensity of the L_{II} edge in bulk platinum.

Several authors have used the L_{III} X-ray absorption edge spectra to characterize the chemical state of the absorbing atom in transition metal compounds. Lytle et al. [5,6] have shown for iridium, platinum, and gold that the intensity of the white line of the L_{III} X-ray absorption edge is proportional to the d-electronvacancies. Also, changes in the L_{III} white line intensity of the X-ray absorption spectrum for Pt/SiO_2 have been related to alterations in the d-band density of states resulting from a metal-support interaction at high reduction temperatures [7]. Gallezot et al. [8,9] reported that platinum clusters in Ce-promoted NaY zeolite have a larger number of d-holes than platinum in NaY zeolite.

While the support and promoter ions do affect the white line intensity, the metal particle size is also important. Gallezot et al. [8,9] reported that the white line intensity of the L_{III} edge of 1-nm Pt clusters in Pt/NaY is larger than 3-nm clusters. Mansour et al. [10] carried out a more quantitative study including the white line of the L_{II} absorption edge for Pt/SiO_2 with an average particle size of 15 Å (72 atoms) and determined that there were 14% more d-holes than in bulk platinum metal. For a series of Pt/SiO_2 catalysts with increasing particle size (with first shell EXAFS coordination numbers of N=6.6 and larger), the combined white line intensity of the L_{II} and L_{III} edge increased as the platinum particle size decreased [11].

Here we present the results of a study of the white lines of the L_{II} and L_{III} X-ray absorption edges for a series of platinum catalysts supported on γ-Al_2O_3, H-LTL and K-LTL zeolites. It will be shown that also for very small platinum clusters (N=3.9 to 4.9) in the Pt/K-LTL catalyst, the white lines of both the L_{II} and L_{III} edges are strongly influenced by particle size. After accounting for the particle size, platinum on acidic supports (γ-Al_2O_3 and H-LTL) is more electron deficient than on non-acidic supports (K-LTL). In addition, propane hydrogenolysis has been used as a catalytic reaction to investigate the influence of the changes in the d-band density of states due to support and/or promoter ions on the catalytic properties of the platinum particles.

2. EXPERIMENTAL

2.1. Catalyst Preparation

A 1.0 wt% Pt/γ-Al_2O_3 catalyst (200 m^2/g, 0.6 cm^3/g) was prepared by impregnation with an aqueous solution of H_2PtCl_6. The catalyst was dried in air at 120°C, and reduced (heating rate 5°C/min) at 450°C for 4 hr, followed by passivation in air at RT.

K-LTL was obtained from Linde. Excess alkali was reduced by water wash until the pH of the wash solution was 9.5 to give a K/Al molar ratio of 1.05. H-LTL (K/Al molar ratio of 0.34) was prepared by repeated NH_4NO_3 exchange of K-LTL followed by calcination at 500°C. The Pt was loaded (1.2 wt% Pt/K-LTL and 1.0 wt% Pt/H-LTL) by impregnation using tetraammine platinum (II) nitrate followed by drying at 120°C.

2.2. Propane Hydrogenolysis Reactions

The conversion of propane was conducted at 400°C and atmospheric pressure in a fixed-bed, bench-scale reactor using 3.78 vol% propane in H_2 . The catalysts were prereduced at 450°C or 600°C, and the conversion was adjusted to between 2 to 10% by changing the propane space velocity. Turnover frequency (TOF) was determined using hydrogen chemisorption as a measure of the active platinum surface.

2.3. X-ray Absorption Experiments

X-ray Absorption experiments were carried out at the Synchrotron Radiation Source in Daresbury, U.K., Wiggler Station 9.2, using a Si (220) double crystal monochromator. At the Pt L_{III} edge (11564 eV), the estimated resolution was 3 eV. The monochromator was detuned to 50% intensity to avoid the effects of higher harmonics present in the X-ray beam. The measurements were done in the transmission mode. In order to obtain an absolute energy calibration of the data a third ionchamber was used with a platinum metal foil (thickness 4 μm) placed between the 2nd and the 3rd ionchamber. The data of the foil were used to calibrate the energy axis of the x-ray absorption data of the catalysts. Self-supporting wafers were reduced in a controlled-atmosphere cell [12]. The X-ray absorption data were obtained at liquid nitrogen temperature in the presence of H_2.

The Pt/γ-Al_2O_3 samples were rereduced at 300 and 450°C and are designated as Al(300) and Al(450), respectively. Similarly, Pt/K-LTL samples were reduced at 300 or 450°C and are designated as K-LTL(300) and K-LTL(450). K-LTL(600), which had been prereduced at 600°C, was rereduced in the cell at 450°C (the temperature limit of the EXAFS cell). Pt/H-LTL was reduced at 450°C, and is designated H-LTL(450).

3. RESULTS

3.1. Structural Characterization

Detailed structural characterizations of the catalysts by TPR, H_2 TPD, hydrogen chemisorption, and EXAFS are reported elsewhere for Pt/γ-Al_2O_3 [13], Pt/H-LTL [14] and Pt/K-LTL [15]. The EXAFS first-shell coordination numbers, which are important for an evaluation of the white line results are given in the Table 1.

3.2. Propane Hydrogenolysis

For each of the catalysts, hydrogenolysis of propane yielded methane and ethane in equal molar amounts. The catalytic turnover frequencies are given in the Table. For the Pt/K-LTL and Pt/γ-Al_2O_3 catalysts, there was little deactivation. The Pt/H-LTL catalyst, however, deactivated more rapidly, and conversion is reported at 10 minutes on stream and extrapolated to zero time on stream.

The catalytic activities fall into two groups, predominantly determined by the

Table 1
EXAFS coordination numbers and propane hydrogenolysis activity

Samples	Coordination number	Hydrogenolysis TOF[a]
K-LTL(300)	3.9	-
K-LTL(450)	4.4	0.063
K-LTL(600)	4.9	0.022
H-LTL(450)	5.4	0.53[b]
		0.40[c]
AL(300)	4.7	-
AL(450)	5.6	0.62

[a] 400°C and 1 atm, TOF (molecules/s/surface Pt).
[b] Initial TOF extrapolated to zero time on stream.
[c] TOF at 10 min on stream.

acidity of the support. The TOFs for platinum on acidic supports, e.g. H-LTL(450) and Al(450), were more than an order of magnitude higher than on the non-acidic support, e.g. K-LTL(450) and K-LTL(600). Of the acidic supports, platinum on chlorided alumina was more active.

3.3. White Line Spectra of Pt L_{II} and L_{III} X-ray Absorption Edges

A preedge background was subtracted over the entire range of data for both the L_{II} and L_{III} edges to remove the contribution of all other absorbers to the X-ray absorption spectrum [10]. This isolates the partial cross section being studied. To ensure that the X-ray absorption edge being studied was well separated from the background, the region used for fitting the preedge was extended from 200 to 80 eV below the X-ray absorption edge. The position of the absorption edge (Fermi energy) was defined as the inflection point of the spectrum. The energy scale for the absorption data was defined as the energy above this inflection point ($E-E_{edge}$).

In order to obtain an atomic cross section, the data were normalized by dividing the absorption intensity by the step height of the absorption edge. To do this, the fit of the preedge was extrapolated into the post-edge region. The postedge (EXAFS) region was smoothed by a cubic spline fit of the background and the step height was defined as the intensity difference between this background in the postedge region and the extrapolated preedge, determined at the normalization energy. The L_{II} edge was normalized at 58 eV and the L_{III} edge at 50 eV. This procedure guarantees a systematic approach with a normalization which is independent of the shape of the white line [8].

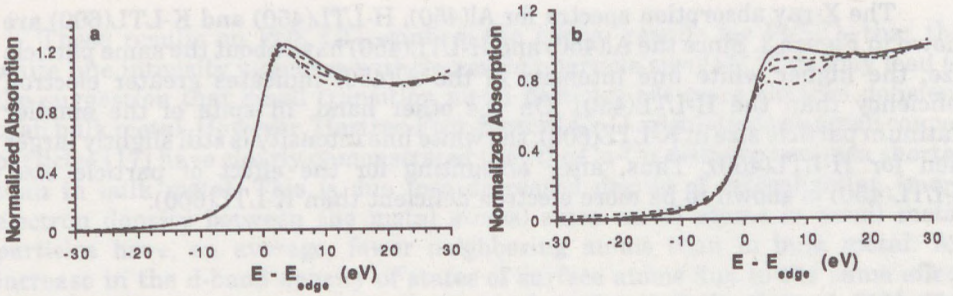

Figure 1. (a) L_{III} en (b) L_{II} x-ray absorption edge of Pt-foil (-·-·-), K-LTL(300) (——)K-LTL(450) (- - -) and K-LTL(600) (— —).

Figure 1 shows the X-ray absorption data of the L_{III} (Figure 1a) and the L_{II} (Figure 1b) edge of platinum foil, K-LTL(300), K-LTL(450), and K-LTL(600). The white line intensities of both the L_{II} and the L_{III} edge decrease with increasing platinum particle size (or increasing reduction temperature).

Since the white line intensity is particle size dependent, the influence of the interaction of the platinum with the support and/or promoter ions on the white line intensity can be properly evaluated only when the particle size is taken into account. For example, despite the larger particle size for Al(300) (N=4.7), the white line intensity of both the L_{II} and the L_{III} edge is higher than for K-LTL(450) (N=4.4) (Figure 2). This indicates that the platinum in Al(300) is more electron deficient than in K-LTL(450).

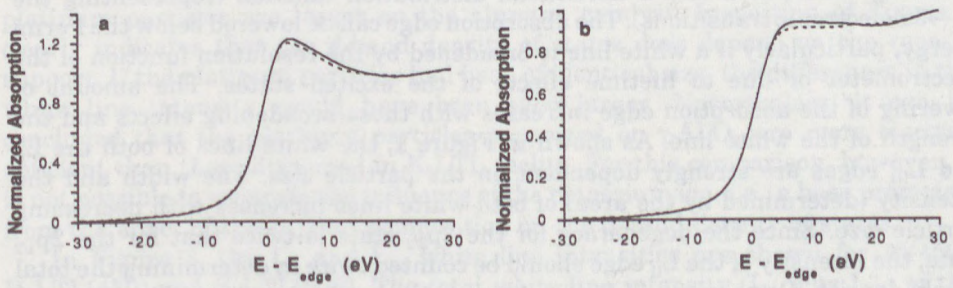

Figure 2. (a) L_{III} en (b) L_{II} x-ray absorption edge of Al(300) (——) en K-LTL(450) (- - -).

The X-ray absorption spectra for Al(450), H-LTL(450) and K-LTL(600) are shown in Figure 3. Since the Al(450) and H-LTL(450) have about the same particle size, the higher white line intensity of the Al(450) indicates greater electron deficiency than the H-LTL(450). On the other hand, in spite of the smaller platinum particle size in K-LTL(600), the white line intensity is still slightly larger then for H-LTL(450). Thus, after accounting for the effect of particle size, H-LTL(450) is shown to be more electron deficient than K-LTL(600).

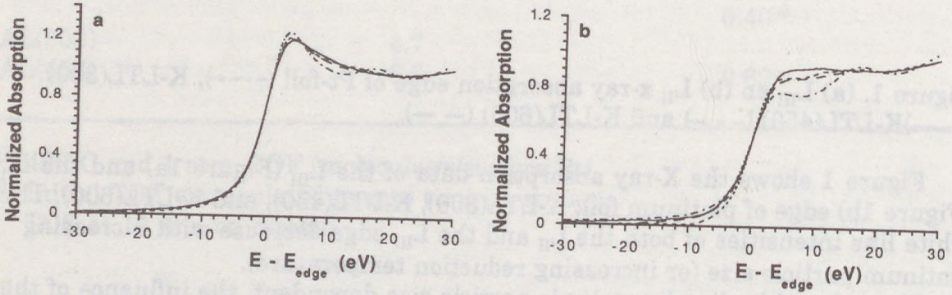

Figure 3. (a) L_{III} en (b) L_{II} x-ray absorption edge of Pt-foil (-•-•-), K-LTL(600) (— —), H-LTL(450) (- - - -) and Al(450) (——).

4. DISCUSSION

As pointed out by Pease [16] and Mansour [10], the white line can be described as a superposition of an arctangent function (representing the atomic cross section for X-ray absorption) and a Lorentzian distribution function (representing the 2p→5d electronic transitions). The absorption edge can be lowered below the Fermi energy, particularly if a white line is broadened by the resolution function of the spectrometer or due to lifetime effects of the excited states. The amount of lowering of the absorption edge increases with these broadening effects and the strength of the white line. As shown in Figure 1, the white lines of both the L_{II} and L_{III} edges are strongly dependent on the particle size. The width and the intensity (determined by the area) of both white lines increases with decreasing particle size. Since the degeneracy for the $2p_{3/2}$ state is twice that for the $2p_{1/2}$ state, the intensity of the L_{II} edge should be counted twice in determining the total d-hole density. Comparison of Figure 1a with 1b clearly shows that the intensity and shape of the L_{II} edge is more strongly influenced by the particle size than the intensity of the L_{III} edge, indicating that the final states with J=3/2 are more sensitive to the particle size than the J=5/2 states. Also apparent in Figure 1a and 1b, is that the onset of the L_{II} and L_{III} absorption edge of both catalysts originates at higher energy than for bulk platinum metal indicating that the small platinum particles are electron deficient compared to bulk platinum metal.

These results on Pt/K-LTL confirm the earlier results for Pt/SiO_2 that the white line intensity increases with decreasing particle size [11]. This may lead to the suggestion that small transition metal particles are more electron deficient than bulk metal. However, Hartree-Fock-Slater LCAO calculations on small copper particles [17] have clearly demonstrated that the Cu-Cu distance becomes shorter than in bulk metal. This is due to a decreased degree of delocalization (more electron density between the metal atoms) since metal atoms in small metal particles have, on average, fewer neighboring atoms than in bulk metal. An increase in the d-band density of states of surface atoms due to the same effect has been discussed by Cyrot-Lackman et al. [18] and Saillard et al. [19]. The decreased d-valence electron bandwidth for surface atoms leads to an increase of the d-valence electron band filling. These studies predict that small transition metal particles have a higher electron density than bulk metal, which is in contradiction with the interpretation above for the results of the white line. The apparent contradiction has been solved by a recent theoretical study of Ravenek et al. on Ir_4 and Ir_{10} clusters [20]. Hartree-Fock-Slater LCAO calculations, indeed, indicate a higher number of d-electrons for the Ir_4 cluster in comparison to Ir_{10}. However, introduction of a core hole, to mimic the X-ray absorption process, into the calculations results in a lower number of d-electrons for the Ir_4^+ compared to the Ir_{10}^+ cluster. The higher electron deficiency for the smaller cluster, as suggested by the larger white line intensity, for example, is actually due to a less efficient screening of the core hole induced by the absorption of the X-ray photon in smaller clusters. The electron density of the neutral metal particle, however, is higher for the smaller particle in contrast to the white line results.

In order to determine the influence of the support and/or promoter ions on the d-band density of states, one must first account for the contribution to the white line resulting from differences in particle size. In Figure 2 the white lines are compared for Al(300) and K-LTL(450), i.e., platinum dispersed on an acidic and non-acidic support. In addition to the differences in the support composition, the platinum particles are larger on the alumina catalyst. Inspection of Figure 2 clearly indicates that the d-band density of states does depend on the type of support. If the platinum particles had been of identical size, the differences in the white line intensity would have been even larger. Nevertheless, it can be concluded that the platinum particles supported on γ-Al_2O_3 are more electron deficient than those dispersed in K-LTL zeolite. For this comparison, however, it is not possible to separate the influence of the potassium ion, i.e., a base promoter, from the effect of the support composition on the d-band density of states.

In Figure 3, the L_{II} and L_{III} white line intensities are shown for Al(450), H-LTL(450) and K-LTL(600). The total white line intensity (L_{II} plus L_{III}) of the acidic Al(450), coordination number 5.6, is higher than for H-LTL(450), coordination number 5.4. Although both supports are acidic, the platinum in the Al(450) is clearly more electron deficient than in H-LTL(450). Without accounting for the particle size, the white line intensity for H-LTL(450) and K-LTL(600) would suggest a slightly larger or similar electron deficiency. However, the platinum particles are smaller in K-LTL(600) than in H-LTL(450), N = 4.9 and 5.4, respectively. Since the white line intensity decreases with increasing particle size,

a H-LTL(450) catalyst with N=5.4 would have a lower white line intensity than K-LTL(600). Therefore, after accounting for particle size effects, the platinum in H-LTL(450) is seen to be more electron deficient than K-LTL(600).

The propane hydrogenolysis TOF was determined for K-LTL(450), K-LTL(600), H-LTL(450) and Al(450) and increased in the order K-LTL < H-LTL < Al. As previously observed for hydrogenolysis of neopentane [21,22] and ethane [23], the propane TOF is higher for platinum on acidic supports, i.e., γ-Al_2O_3 and H-LTL. In each of the previous studies, the increase in activity has been attributed to electron-deficient platinum. The electron deficient nature of the platinum was thought to be an intrinsic property of the small metal particles [23] or the result of donation of platinum electron density to the support [21,22]. In a recent study, Samant and Boudart investigated the electron deficiency of platinum in a series of Pt/Y catalysts of similar platinum particle size by several techniques, including XANES [24]. They concluded that all of the observations ascribed to electron deficiency were the result of the intrinsic properties of the very small platinum particles which form on acidic supports. If the electron deficiency is only the result of the small particle size, then the smallest platinum particles would have the highest hydrogenolysis activity. In this study, the most active catalysts for hydrogenolysis of propane, e.g., the acidic supported catalysts, have the largest particle size. Furthermore, after accounting for the differences in particle size, we determine that the platinum on the acidic supports is more electron deficient as judged by the combined white line intensity. We conclude, therefore, that the support acidity and/or promoter ions do affect the d-band density of states, and that these perturbations in the electronic structure affect the catalytic activity, at least, for hydrogenolysis.

In [13] we show that the nature of the metal-support interface in Pt/K-LTL changes with increasing reduction temperature. Table 1 shows that the propane hydrogenolysis activity decreases by a factor 3 by changing the reduction temperature from 450°C at 600°C. A more systematic study of the white line intensity is needed before the influence of the nature of the metal-support interface can be distinguished from that of promotor ions. The presence of chemisorbed hydrogen also influences the intensity of the white line [7] and this influence should be evaluated as well.

5. CONCLUSIONS

The white line intensity of both the platinum L_{II} and L_{III} X-ray absorption edges increase with decreasing particle size. The changes in the intensity are much larger for the L_{II} edge. This means that the intensity of the L_{II} edge whiteline must be taken into account before any conclusion can be drawn about changes in d-band density of states. After correcting for the differences in particle size, platinum on acidic supports is more electron deficient than on non-acidic supports. The electron deficiency of the platinum increased in the same order as the activity for propane hydrogenolysis. Changes in support acidity and/or promoter ions alters the platinum d-band density of states, affecting the reactivity for hydrogenolysis reactions.

6. REFERENCES

1. M. Boudart and G. Djega-Mariadassou, Kinetics of Heterogenous Catalytic Reactions, Princeton University Press, Princeton N.J., 1984.
2. N.F.Mott, Proc. Phys. Soc. London, 62 (1949) 416.
3. M. Brown, R.E. Peierles and E.A. Stern, Phys. Rev. B, 15 (1977) 738.
4. L.F. Mattheiss and R.E. Dietz, Phys. Rev. B, 22 (1980) 1663.
5. F.W. Lytle, J. Catal., 43 (1976) 376.
6. F.W. Lytle, P.S.P. Wei, R.B. Gregor, G.H. Via and J.H. Sinfelt, J. Chem. Phys., 70 (1979) 4849.
7. F.W. Lytle, R.B. Gregor, E.C. Marques, D.R. Sandstrom, G.H. Via and J.H. Sinfelt, J. Catal., 95 (1985) 546.
8. P. Gallezot, J. Datka, Y. Massardier, M. Primet and B. Imelik, Proc. 6th Int. Congress on Catal., (G.C. Bond, P.B. Wells and F.C. Tomkins Eds.), The Chemical Society, London, 1976, vol 2, p 696.
9. P. Gallezot, R. Weber, R.A. Dalla Betta and M. Boudart, Z. Naturforsch., 34a (1979) 40.
10. A.N. Mansour, J.W. Cook and D.E. Sayers, J. Phys. Chem., 88 (1984) 2330.
11. A.N. Mansour, D.E. Sayers, R.A. van Santen and D.C. Koningsberger, to be published.
12. F.W. Kampers, T.M.J. Maas, J. van Grondelle, P. Brinkgreve and D.C. Koningsberger, Rev. Sci. Instr., 60 (1989) 2635.
13. M. Vaarkamp, J. van Grondelle, R.A. van Santen, J.T. Miller, B.L. Meyers, F.S. Modica, G.S. Lane and D.C. Koningsberger, Proc. 9th Int. Zeolite Conf., Montreal, 1992, accepted.
14. M. Vaarkamp, J.T. Miller, B.L. Meyers, F.S. Modica, G.S. Lane and D.C. Koningsberger, to be published.
15. M. Vaarkamp and D.C. Koningsberger, to be published.
16. D.M. Pease, Appl. Spec., 30 (1976) 405.
17. B. Delley, D.E. Ellis, A.J. Freeman, E.J. Baerends and D. Post, Phys. Rev. B, 27 (1983) 2132.
18. M.C. Desjonquères and F. Cyrot-Lackman, J. Chem. Phys., 64 (1976) 3707.
19. J.Y. Saillard and R. Hoffmann, J. Am. Chem. Soc., 106 (1984) 2006.
20. W. Ravenek, A.P.J. Jansen and R.A. van Santen, J. Phys. Chem., 93 (1989) 6445.
21. R.A. Dalla Betta and M. Boudart, Proc. 5th Int. Cong. on Catal., 2 (1973) 1329.
22. S.T. Homeyer, Z. Karpinski and W.M.H. Sachtler, J. Catal., 123 (1990) 60.
23. C. Naccache, N. Kaufherr, M. Dufaux, J. Pandiera and B. Imelik, Mol. Sieves-II, ACS Symp. Ser. 40 (1977) 538.
24. M.G. Samant and M. Boudart, J. Phys. Chem., 95 (1991) 4070.

DISCUSSION

Q: T. Uematsu (Japan)

Surface activity or reactivity is strongly dependent on the particle size. You have demonstrated the charge transfer and metal-support interaction by EXAFS. The interaction was controlled by the platinum particle size. However, such interaction would be also influenced by the activities of supporting oxides. In this view, the effects of particle sizes of the support must be taken into account, especially for metal clusters (superfine particles) supported on fine particle of supporting metal oxides. What is your opinion ?

A: D. C. Koningsberger

The total white-line intensity of supported small metal particles is in my opinion determined by metal (i) particle size/shape, (ii) type of adsorbate, (iii) type of support and (iv) structure of metal-support interface. The influence of the support is most probably due to a charge transfer from or to the metal particle. However, there is still no conclusive experimental evidence for this. I do not see how the particle size of the oxide support can influence the d-band density of states of the supported metal particles, as you suggest. There is may be an indirect effect, the support particle size may influence the size/shape of the metal particles, which in turn influence the white-line intensity of the supported metal particles.

Q: G. L. Haller (USA)

Because the effects you observed for both Pt L_{II} and L_{III} edges as a function of support acidity and or Pt particle size are changes in line width rather than intensity at the edge, this suggests you may be measuring changes in the 5d bond shape rather than charge transfer. Charge transfer can be measured quantitatively by measuring shifts in the absorption edge (relations to the simultaneously measured edge of a Pt foil references). How did you look at your edge shifts and are they consistent with the charge transfer interpretation ?

A: D. C. Koningsberger

The shape of both the L_{II} and the L_{III} white-line is indeed changing as a function of particle size and type of support. However, we have determined also the total white-line area of both the L_{II} and the L_{III} edge and the total white-line intensity is showing the results which we discussed in the paper. We have not yet measured enough accurate edge position data to relate changes in white-line intensity to changes in edge position.

Q: V. Haensel (USA)

Particle size depends to a large extent on treatment following impregnation. For example, with a γ-alumina support the treatment with air following impregnation (at up to 500 ^{0}C) and subsequent reduction with H_2 produces highly dispersed catalyst particles while H_2 treatment only produces larger catalyst particles and lower catalyst activity.

A: D. C. Koningsberger

I fully agree that particle size depends on the treatment following impregnation. We have found that also direct reduction in hydrogen using a very small temperature ramp (5 K/min) leads to very stable highly active small metal particles.

Q: K. Klier (USA)

Do you have data that could be quantitatively evaluated as to the amount of charge transferred upon chemisorption of "electron accepting" adsorbates, e.g. oxygen, hydrogen and chlorine? Does the L_{II} intensity change correlate with electronegativity of these adsorbates ?

A: D. C. Koningsberger

We do not have yet enough data to correlate the electronegativity of different adsorbates with changes in white-line intensities. We do have found that desorption of chemisorbed hydrogen leads to a decrease in white-line intensity, showing that the chemisorption of hydrogen withdraw electrons from platinum.

Q: A. Renouprez (France)

The normalization, subtraction procedure is known to be a critical step in absorption edge data treatment. Did you try to interpret your results using the L_{III} - k x L_{II} method or L_{III}(foil)-L_{III}(sample)? Do you not think that the larger L_{II} modifications compared to L_{III} (also observed in alloys) could be better interpreted in terms of spd-hybridization or d-rearrangements rather than pure charge transfer ?

A: D. C. Koningsberger

We do have subtracted the white-line data of the samples from the corresponding white-line of the platinum foil to establish the change in white-line intensity. As demonstrated in the paper the spd rehybridization (as we believe to be the origin of the particle size effect on the white-line) is separated from the effect of the support by trying to compare catalysts with the same average metal particle size.

Q: R. W. Joyner (United Kingdom)

In interpreting small changes in X-ray white lines it is important to recall the lessons from XPS studies of small particles. XPS binding energy shifts are observed, but are now considered largely to be caused by find state relaxation effects.

You are careful to limit and define the ways your comparison are mode. However, even if two catalysts have the same average (nearest neighbor coordination number, then size distribution and shape may vary. Thus, even when carefully controlled, white line charges may reflect final state effects rather than electron transfer to or from the support.

A: D. C. Koningsberger

The white-line intensity is most probably determined by final state effects, which means that the white-line is sensitive to the averaged particle size and shape of the metal particles. We have not yet fully established how large this effect is. We have tried in the paper to correct for the particle size effect by trying to compare catalyst with the same averaged particle size. We do not believe that the shape of the platinum particles in H-L and K-L for these small clusters is different. More research is needed before the influence of the shape of the metal particles on the white-line intensity is determined.

Q: R. Prins (Switzerland)

The largest change in white line intensity is observed in the L_{II} edge. However, this line is due to the $2p_{1/2} \rightarrow 5d_{3/2}$ transition, and since the $5d_{3/2}$ bond should be completely filled, actually the intensity of the L_{II} line should be very small. Changes in the L_{II} intensity are then induced by mixing of the $d_{3/2}$ and $d_{5/2}$ bands and this will be very sensitive to the Fermi surface, and thus to metal particle size, shape and metal atom packing. Since most of the change in white line intensity is seen in the L_{II} edge, the total white line intensity change is very sensitive to several factors. If that is true, is there then any hope to use the white line intensity and say something about particle size and charge?

A: D. C. Koningsberger

As already mentioned in my answer to the question made by T. Uematsu I agree that the total white-line intensity is determined by several factors: (i) particle size/shape, (ii) type of adsorbate, (iii) type of support and (iv) structure of metal-support interface. It must be possible to separate support effects from other effects by careful elimination; for

instance by studying metal particles with the same average size reduced at the same temperature (i.e. same metal-support interface) covered with (and without) the same adsorbate.

Q: E. Iglesia (USA)

I concur fully with your experimental observation that the rates of propane reactions increase with increasing acidity of the support. We have observed similar increases in the bifunctional hydrocracking of higher alkanes with increasing support acidity. I disagree, however, with:

1) your description of the process as hydrogenolysis on Pt clusters and

2) your explanation of the phenomenon as one arising from differences in the electronic properties of Pt clusters.

The process is likely to occur by a bifunctional mechanism where the rate-limiting step is the reaction of equilibrium concentrations of propene on acid sites. Therefore, your choice of Pt sites for turnover calculations is the predominant reason for the apparent turnover rate changes. Would you comment on my disagreement? Have you measured the rates of propene cracking on your catalyst supports ?

A: D. C. Koningsberger

While bifunctional hydrocracking of higher alkanes is well known, we do not believe that the enhanced activity for propane conversion we observe for Pt on acidic supports is the result of a bifunctional reaction path. Monomolecular cracking of propene is not possible since neither α-hydrogen elimination from a secondary carbenium ion, nor β-hydrogen elimination can lead to the formation of stable products. Bimolecular reaction of propene (i.e. oligomerization followed by cracking) does not yield methane and, additionally, yields C_3^+ products, which were not observed. Since the reaction products are methane and ethane in a molar ratio of 1:1, the bifunctional reaction pathway can be ruled out.

Guczi, L. *et al.* (Editors), *New Frontiers in Catalysis*
Proceedings of the 10th International Congress on Catalysis, 19-24 July, 1992, Budapest, Hungary
© 1993 Elsevier Science Publishers B.V. All rights reserved

DIRECT MAS/MES EVIDENCE FOR ELECTRONIC METAL-SUPPORT INTERACTIONS IN DILUTE ^{57}Co AND ^{57}Fe CARBON AND ALUMINA-SUPPORTED CATALYSTS

C. H. Bartholomew, L. R. Neubauer and P. A. Smith

BYU Catalysis Laboratory, Department of Chemical Engineering, Brigham Young University, Provo, Utah 84602, USA

Abstract

Mössbauer absorption spectroscopy (MAS) and Mössbauer emissions spectroscopy (MES) studies of 1-3% ^{57}Fe and 1% ^{57}Co on carbon and alumina supports were conducted as a function of reduction temperature. Catalysts were prepared by nonaqueous evaporative deposition to maximize the reduction of cobalt and iron to the metal. Metal surface areas of the catalysts were determined by H_2 adsorption, while extents of reduction to the metal were determined by both Mössbauer spectroscopy and by titration of reduced catalysts with oxygen at 673 K. MAS/MES data for 1 and 3% ^{57}Fe/C and 1% ^{57}Co/C catalysts reduced at 773 K indicate the presence of only one phase--superparamagnetic (SP) clusters of metal having diameters of about 1-2 nm. Room temperature isomer shifts for these carbon supported metal clusters of 0.10-0.15 mm/s indicate a decrease in electron density of the metal nuclei relative to the bulk metals. MES data for ^{57}Co/Al_2O_3 suggest the existence of three phases: Co_{sp} metal, Co(II) oxide, and Co(III) oxide, while MAS generally shows only Fe_{sp} metal clusters and Fe(II) oxides to be present in 1-2% ^{57}Fe/Al_2O_3, except for some ferromagnetic Fe metal in 2% ^{57}Fe/Al_2O_3 reduced at 873 K. Isomer shifts for the metal clusters in the Al_2O_3-supported ^{57}Co and ^{57}Fe catalysts are -0.05 to -0.15 mm/s indicating an increase in the electron density at metal nuclei. The presence of small metals clusters of 1-5 nm in these catalysts is confirmed by H_2 adsorption. Moreover, Debye temperatures measured by Mössbauer are significantly lower than for bulk iron consistent with the lattice dynamics expected for small metal clusters having a large fraction of surface atoms. The very significant isomer shifts observed for SP metal phases by Mössbauer are consistent with electronic modification of small metal clusters in supported Co or Fe. That the isomer shift is positive for metal/C catalysts and negative for metal/Al_2O_3 catalysts indicates this effect must be due to metal-support interactions.

1. INTRODUCTION

Most commercial catalysts incorporate a catalytic phase dispersed on a high surface area carrier or "support" to facilitate the preparation of a well-dispersed, high surface area catalytic phase and stabilize the active phase against loss of surface area; in addition support-active phase interactions can dramatically influence the adsorption and activity/selectivity properties of the catalyst [1-4]. "Metal-support interactions (MSI)" are a collection of phenomena which include (1) decoration/promotion of the metal surface with support moieties, (2) bifunctional/interfacial catalysis, and (3) electronic/geometric modifications of metal clusters by direct interaction with the support. These different MSI are extremely difficult to isolate and investigate; MSI of the third type, electronic effects, are particularly elusive as there are few *in situ* techniques which enable their direct measurement. Nevertheless, Mössbauer absorption spectroscopy (MAS) and Mössbauer emissions spectroscopy (MES) provide this capability for well-dispersed, supported cobalt and iron metal clusters [5-10], since the isomer shift is a measure of the electron density at the ^{57}Fe or ^{57}Co nucleus.

Highly-dispersed, superparamagnetic (SP) clusters of Fe (Fe_{sp}) have been observed by MAS for Fe supported on MgO [5], carbon [6-9,11,12], alumina [7,13,14], and silica [14,15]. Topsoe et al. [5] first reported an isomer shift for supported Fe_{sp}, namely a value for Fe/MgO of -0.2 mm/s; positive isomer shifts of 0.15 and 0.10-0.15 were later reported for Fe_{sp} on carbon by Phillips and Dumesic [6] and Neubauer et al. [7,8] and negative shifts of -0.08 to -0.15 mm/s for Fe_{sp}/Al_2O_3 by Neubauer [7] and Smith and Bartholomew [10]. Only recently was the significance of these isomer shifts addressed [7,8,10].

In this study MAS and MES of carbon- and Al_2O_3-supported ^{57}Fe and ^{57}Co provide evidence that the electronic properties of metal clusters are changed by the support environment.

2. EXPERIMENTAL

2.1. Materials. Catalysts were prepared by evaporative deposition of ^{57}Fe or ^{57}Co metal nitrate or chloride salts in either benzene or acetone; Al_2O_3 supports were previously dehydroxylated at 773-873 K. Catalysts containing ^{57}Co were doped to a 2-3 mCurie level. Catalysts were dried in vacuum at 373 K and reduced *in situ* in H_2 at 673-873 K. Details of the preparation and pretreatment are described elsewhere [7,8,10].

2.2. Apparatus and Procedure. Mössbauer spectra of reduced catalysts were obtained *in situ* at 77 and 298 K using controlled-atmosphere cells and a spectrometer system previously described [7,8]. MAS experiments were conducted in the constant acceleration mode using a moving 50 mCurie ^{57}Fe in a Pd source; MES experiments were conducted with an ^{57}Fe-enriched $Na_4Fe(CN)_6 \cdot H_2O$ absorber driven in the same constant acceleration mode but placed between the ^{57}Co-containing catalyst (serving as gamma ray source) and a proportional counter tube. With the use of an absolute laser velocity calibrator it was possible to measure isomer shifts to within an absolute accuracy of ±0.005 mm/s. Mössbauer spectra were corrected during the collection procedure to remove the curved background of instrumental origin. Mössbauer spectra of reduced catalysts contained in a controlled-atmosphere cell [7,16] were measured at 298 and 77 K in 1 atm of hydrogen to ensure that no oxidation of the samples would occur. Mössbauer spectra were computer-fitted to Lorenzian lines with a least-square optimization procedure [16]. Resonant absorption areas were found from integration of the background curvature-corrected spectra.

H_2 adsorption measurements were carried out in a vacuum adsorption apparatus described previously [17] or in the case of Fe/carbon catalysts in a flow system equipped with a thermal conductivity detector described elsewhere [18] according to a procedure [18] for measuring total chemisorbed hydrogen while minimizing spillover effects. The procedure in all cases involved cooling in H_2 from about 650 K to ensure that a monolayer was adsorbed despite highly activated adsorption.

Metal dispersion and crystallite size calculations were based on the assumptions that Co or Fe metal is present as spherical particles of uniform size and that unreduced iron is present in a separation dispersed oxide layer in intimate contact with the support [19]. Thus, percentage dispersion was calculated for iron catalysts according to the relation

$$\%D = 1.117X / (Wf) \qquad (1)$$

where X is the average H_2 uptake in micromoles per gram of catalyst, W is the weight percentage of iron and f is the fraction of iron reduced to the metal as determined by oxygen titration [20] or Mössbauer spectroscopy. Average crystallite diameters were calculated from %D assuming spherical metal crystallites of uniform diameter d with a site density of 17.3 atoms/nm^2, calculated from a weighted average of the 3 most dense planes of bcc Fe [2]:

$$d(nm) = 122.5 / \%D \qquad (2)$$

Similar equations were used for cobalt catalysts for which the numerical coefficients in Equations 1 and 2 were 1.179 and 96.2 assuming a fcc structure for supported Co [21].

3. RESULTS AND DISCUSSION

3.1. Catalyst properties

H_2 chemisorptive uptakes, metal dispersions, extents of reduction to the metallic state determined from oxygen titration and/or Mössbauer spectroscopy, and average metal crystallite diameters determined from H_2 chemisorption of Fe/carbon, Fe/Al_2O_3, Co/carbon, and Co/Al_2O_3 catalysts are listed in Table 1. The relatively large values of H_2 uptake are indicative of very significant amounts of reduced metal in these catalysts of mostly low metal concentration (1-3 wt.%). Extents of reduction determined by oxygen titration of 38-97% are much higher than reported previously for dilute Fe and Co catalysts prepared by conventional aqueous impregnation or precipitation methods; indeed, in earlier studies of dilute (1-5%) Fe on alumina [2,22-24] it was found that only a small fraction of the Fe could be reduced to the metal even at very high reduction temperatures. While high metal dispersions have been reported previously for Fe/C catalysts [6,8,12], the dispersions of 30-74% observed in this study for Fe/Al_2O_3 and Co/Al_2O_3 catalysts are much higher than those previously reported for similar catalysts prepared by conventional aqueous methods but are comparable with those reported for Fe/Al_2O_3 catalysts

Table 1
H_2 chemisorptive uptakes, dispersions, extents of reduction, and average metal crystallite diameters of Fe/carbon, Fe/Al_2O_3, Co/carbon, and Co/Al_2O_3 catalysts

Catalyst[a]	H_2 Uptake[b] (μmol/g)	% Reduction[c] O_2	% Reduction[c] Möss.	Dispersion[d] (%)	Diam.[e] (nm)
1% Fe/C, Red. @ 623 K	46	-	36	143	<1.2
3% Fe/C, Red. @ 623 K	84	-	41	76	1.6
10% Fe/C, Red. @ 623 K	91	-	72	14	8.8
1% Fe/Al_2O_3 (A), Red. @ 623 K	16	74	24	24	5.1
2% Fe/Al_2O_3 (A), Red. @ 623 K	18	35	23	57	2.2
0.5% Fe/Al_2O_3 (B)					
Reduced @ 773 K	10	66	20	30	4.0
Reduced @ 873 K	24	72	-	74	1.7
2.0% Fe/Al_2O_3 (B)					
Reduced @ 773 K	15	89	25	9	14
Reduced @ 873 K	42	97	54	24	5.1
1% Co/C, Red. @ 623 K	101 (58)[f]	-	91	124	<1.0
1% Co/Al_2O_3, Red. @ 673 K	20 (18)	47	14	50	1.9
2% Co/Al_2O_3, Red. @ 673 K	13 (16)	38	14	40	2.4

a Fe/C, Fe/Al_2O_3 (A) series, and Co catalysts were prepared by evap. dep. from a benzene-/methanol solution of ^{57}Fe nitrate [8] or of ^{57}Co nitrate; Fe/Al_2O_3 (B) series were prepared by evap. dep. from acetone solution of ^{57}Fe chloride.
b Determined by cooling from 650 K in H_2 [2,18]; data are averages of 2-5 measurements on two separate samples; precision estimated to be ±10-15%.
c Determined by O_2 titration at 673 K [2,21] or from Mössbauer areas corrected for recoil free fractions; data are averages of 2-3 measurements ; precision estimated to be ±5-10%.
d Percentage dispersion (percentage exposed) determined from Equation 1.
e Average crystallite diameter from Equation 2.
f Uptakes in parenthesis are for samples reduced at 733 K.

prepared from carbonyl decomposition on dehydroxylated alumina [2]. Accordingly, it is evident that the nonaqueous evaporative deposition techniques used in this study result in highly-reduced, highly-dispersed supported Fe and Co catalysts even at loadings as low as 0.5 wt%. Moreover, it will be shown that these catalysts contain a large fraction of the reduced metal in the form of superparamagnetic clusters.

3.2. MAS and MES results

Figs. 1 and 2 show MES and MAS data for 1% $^{57}Co/C$, 3% $^{57}Fe/C$, 1% $^{57}Co/Al_2O_3$ and 2% $^{57}Fe/Al_2O_3$ catalysts reduced at 673-873 K. Mössbauer parameters for these catalysts are summarized in Tables 2-4. The MES spectrum for 1% $^{57}Co/C$ and the MAS spectrum of 3% $^{57}Fe/C$ (both reduced at 773 K) each consist of a broad singlet that is assignable to the reduced SP metal. The spectrum for 1% $^{57}Co/Al_2O_3$ is most consistent with the existence of three phases: superparamagnetic Co_{sp} metal (indicate by the singlet clearly observable at 77 K), Co(II) oxide, and Co(III) oxide (overlapping doublets) in the approximate molecular percentages of 10-20, 30-40, and 40-50 respectively depending on the reduction temperature. Average metal crystallite diameters are estimated from H_2 adsorption to be about 1.9 and 2.4 nm in the 1 and 2% samples respectively, consistent with the MES implication of tiny superparamagnetic domains. The MAS data (Fig. 1b) combined with oxygen titration data for $^{57}Fe/Al_2O_3$ reduced at 773 K indicate 77% Fe_{sp} metal and 33% Fe(II) oxide to be present; after reduction at 873 K, both SP (singlet) and ferromagnetic (6 lines) Fe metal are present in about equal quantities with 8% Fe(II) oxide remaining. Again, average metal crystallite diameters estimated from H_2 adsorption for 0.5 and 2% Fe/Al_2O_3 samples reduced at 873 K of 1.7 and 4.0 nm are consistent with the implication of SP domains.

While the singlet for SP metal is an undeniable feature of the spectra for 1% $^{57}Co/C$, 3% $^{57}Fe/C$, and 2% $^{57}Fe/Al_2O_3$ reduced at 623, 773 and 873 K respectively (see Figures 1 and 2), the singlet is obscured in spectra for 1% $^{57}Co/Al_2O_3$ and 0.5-1% $^{57}Fe/Al_2O_3$. Nevertheless, the presence of metal clusters in these catalysts is confirmed by measurable hydrogen chemisorption, CO TPD, and CO hydrogenation reaction [7]. Moreover, the facile, complete oxidation of the Fe_{sp} (and Fe^{2+} oxide) to SP α-Fe_2O_3 [25] upon exposure of reduced 3% Fe/C to air at room temperature (Fig. 1b and Table 2) provides further evidence that highly-dispersed metal clusters are present.

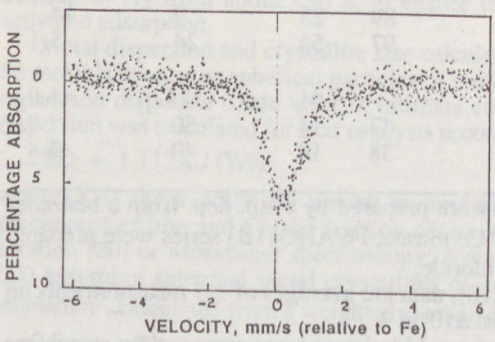

Fig. 1a. MES spectrum of 1% $^{57}Co/C$ (at 298 K; reduced at 773 K).

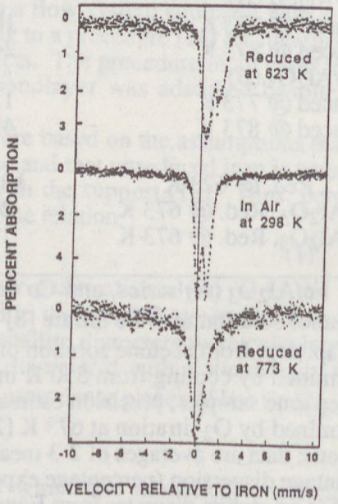

Fig. 1b. MAS spectra of 3% $^{57}Fe/C$ (298 K).

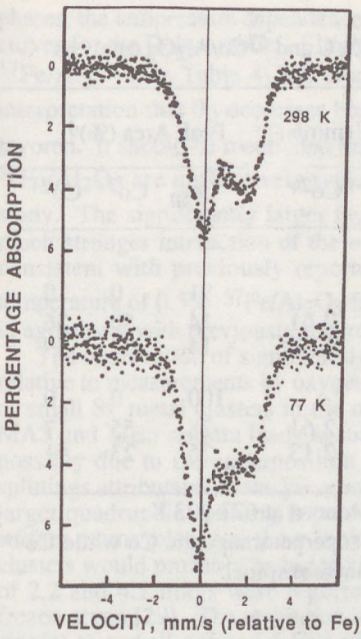

Fig. 2a. MES spectra of 1% $^{57}Co/Al_2O_3$ (at 298 and 77 K; reduced 673 K).

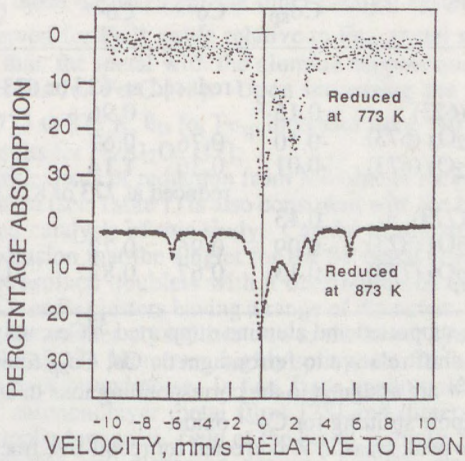

Fig. 2b. MAS spectra of 2% $^{57}Fe/Al_2O_3$ (298 K).

Table 2

Mössbauer spectroscopy parameters determined at 298 K from MAS of $^{57}Fe/C$ and $^{57}Fe/Al_2O_3$ catalysts reduced at 623 or 773 K

Catalyst[a]	Isomer shift (mm/s)[b]			Quad.Splt. (mm/s)[c]	Peak Area (%)[d]		
	Fe_m	Fe_{sp}	Fe^{2+}	Fe^{2+}	Fe_m	Fe_{sp}	Fe^{2+}
1% Fe/C		0.10	1.11	1.42	0	36	64
3% Fe/C		0.14	1.12	1.09	0	41	59
3% Fe/C (exp. air, RT)			0.35[e]	0.94[e]			100[e]
10% Fe/C	0.003	0.18	0.81	-	49	23	28
1% Fe/Al_2O_3 (A)		-0.09	1.11	1.82	0	24	76
2% Fe/Al_2O_3 (A)		-0.05	1.10	1.70	0	23	77
0.5% Fe/Al_2O_3 (B)		-0.15	1.08	1.81	0	20	80
2.0% Fe/Al_2O_3 (B)		-0.08	1.06	1.68	0	25	75

a Carbon-supported and alumina-supported Series A reduced at 623 K, Series B at 773 K.

b Isomer shift relative to ferromagnetic iron; Fe_m and Fe_{sp} refer to ferromagnetic and superparamagnetic iron respectively.

c Quadrupole splitting for Fe^{2+} oxide.

d Relative peak areas in % corrected for recoil-free fractions.

e Fe^{3+} (not Fe^{2+}) parameters corresponding to small crystallites of α-Fe_2O_3.

Table 3
Mössbauer parameters determined at 298 K from MES of $^{57}Co/C$ and $^{57}Co/Al_2O_3$ catalysts

Catalyst[a]	Isomer shift (mm/s)[b]			Quad.Splt. (mm/s)[c]		Peak Area (%)[d]		
	Co_{sp}	Co^{3+}	Co^{2+}	Co^{3+}	Co^{2+}	Co_{sp}	Co^{3+}	Co^{2+}
		reduced at 623 or 673 K						
1% Co/C (623)	0.15	-	0.96	-	-	91	0	9
1% Co/Al_2O_3 (673)	-0.10	0.76	0.67	1.15	2.61	14	50	36
2% Co/Al_2O_3 (673)	-0.01	0.36	1.14	1.41	1.85	14	47	39
		reduced at 773 or 823 K						
1% Co/C (773)	0.13	-	-	-	-	100	0	0
1% Co/Al_2O_3 (823)	-0.09	0.96	0.72	0.79	2.61	28	55	17
2% Co/Al_2O_3 (773)	-0.13	0.67	0.82	0.44	2.13	26	23	51

a Carbon-supported and alumina-supported ^{57}Co catalysts reduced at 623-823 K.
b Isomer shift relative to ferromagnetic Co; Co_{sp} refers to superparamagnetic Co while Co^{3+} and Co^{2+} are assigned to the corresponding ions in an octahedral spinel.
c Quadrupole splitting for Co^{2+} oxide.
d Relative peak areas in % corrected for recoil-free fractions.

Table 4
Isomer shifts, recoil-free fractions and Debye temperatures for 0.5% Fe^{57}/Al_2O_3 reduced at 773 K

Phase	Temp. (K)[a]	I.S.[b] (mm/s)	Recoil-Free Fraction[c]	Debye Temperature (K)
Fe_{sp}	77	-0.20	0.58	140
	298	-0.15	0.13	
Fe^{2+}	77	1.25	0.93	415
	298	1.08	0.79	

a Temperature of Mössbauer data collection.
b Isomer shift relative to ferromagnetic Fe.
c Calculated from changes in spectral area with temperature according to Bartholomew [26].

The substantially lower recoil-free fractions and lower Debye temperature (by a factor of two) for Fe_{sp} relative to those for Fe^{2+} oxide in 0.5% $^{57}Fe/Al_2O_3$ (Table 4) and relative to values of 450-500 K for typical bulk materials [12,25] provide further evidence that metal clusters in this catalyst are small, may have most of their atoms exposed to the surface, and/or may interact strongly with the support. Indeed, a low Debye temperature (θ_D) may be observed for either (i) surface atoms (a factor of two lower relative to bulk atoms) or (ii) clusters loosely bound to the support [12,25]. However, the second effect causes the recoilless fraction of such particles to decrease more rapidly with temperature than is expected on the basis of lattice vibrations alone [12]. In a previous study of Fe/C catalysts by Mössbauer [12] in which a substantially lower recoil-free fraction was also observed for metallic clusters relative to bulk

phases, the temperature dependence of the recoil-free fraction was in accordance with theoretical curves for the Debye model. Similarly, the recoil fractions determined from this study for 0.5% $^{57}Fe/Al_2O_3$ (see Table 4) fall along the predicted curves from the Debye model. Thus, the interpretation that θ_D decreases because of the presence of a large fraction of surface atoms is favored. It should be mentioned that the observed trends in recoil free fraction and θ_D for 0.5% $^{57}Fe/Al_2O_3$ are qualitatively typical of those observed for the other catalyst systems in this study. The significantly larger θ_D observed for Fe^{2+} oxide relative to Fe_{sp} metal suggests a much stronger interaction of the oxide than the metal with the alumina support qualitatively consistent with previously reported results for Fe/C [12]. Upon increasing the reduction temperature of 0.5% $^{57}Fe/Al_2O_3$ from 773 to 873 K, θ_D for Fe_{sp} increases from 140 to 165 K, in agreement with previously reported results for Fe/Al_2O_3 [12].

The observation of significantly lower extents of reduction from Mössbauer measurements relative to measurements by oxygen titration (see Table 1) is also consistent with the hypothesis of small SP metal clusters in the reduced catalysts of this study. Careful examination of the MAS and MES spectra leads to the conclusion that the singlet for the SP metal is very broad possibly due to the superposition of unresolved doublets with a distribution of quadrupole splittings attributable to the presence of Co or Fe clusters having a range of diameters. Indeed, a larger quadrupole splitting is predicted for smaller crystallites due to the lower symmetry of surface atoms relative to those in the bulk [25,27]. Moreover, highly split peaks for the smallest clusters would probably be hidden in the background noise. In fact, large quadrupole splittings of 2.2 and 4.1 mm/s were reported for submonolayer metal films [28] and dimers of Fe in frozen argon [29]. The resolution in an applied magnetic field of the broad, partially hidden SP singlet to a well-defined 6-line spectrum for well-dispersed, reduced Fe/SiO_2 was recently reported by Clausen and Topsoe [15].

The isomer shifts for the SP metal phases in 0.5 to 2% $^{57}Co/Al_2O_3$ and $^{57}Fe/Al_2O_3$ catalysts of -0.05 to -0.15 mm/s (±0.01, relative to ferromagnetic iron) compare with values of 0.10 to 0.15 mm/s for 1-3% $^{57}Co/C$ and $^{57}Fe/C$. The presence of ferromagnetic iron (Fe_m) in the 10% $^{57}Fe/C$ sample provides an internal standard for checking the accuracy of isomer shift measurements. Since the measured isomer shift for Fe_m is within 0.003 mm/s of the predicted zero for bulk iron metal, the *absolute accuracy* of isomer shift measurements in this study is better than ±0.005-0.01 mm/s. Thus, positive or negative shifts of 0.05-0.15 mm/s are clearly experimentally very significant. Assuming the absence of experimental artifacts, the very significant negative shifts for the Al_2O_3-supported catalysts predict a significant increase in the electron density at the nucleus, while the very significant positive shifts for the carbon-supported catalysts indicate just the opposite.

Possible experimental artifacts that must be considered include (i) the so-called second-order Doppler shift [25] and (ii) changes in isomer shifts due to an intrinsic cluster size effect [25], i.e. an intrinsic change in the electronic density of the cluster with particle diameter separate from any interaction with the support.

The second-order Doppler effect is a predicted change in the isomer shift due to temperature differences in the source and absorber. This effect would be nil for most of the data reported in this paper, for which both source and absorber were at the same temperature (295-300 K). In the case of data obtained at 77 K a significant increase in isomer shift (IS) of about 0.15 mm/s relative to that at 300 K is predicted [30] (since the effect is a negative shift with increasing temperature). Nevertheless, the experimentally observed negative shift for bulk Fe_m from 77 to 298 K (0.08 to 0.00 mm/s) is only -0.08 mm/s) [7]. Moreover, the observed change in IS for the Fe/C catalysts of this study was much smaller, i.e. decreases of 0.16 to 0.10 and of 0.16 to 0.14 mm/s for 1 and 3% Fe/C as temperature was increased from 77 to 300 K. Furthermore, the observed changes in IS for 0.5-2% Fe/Al_2O_3 were in the direction opposite to the theoretical prediction and likewise relatively small, e.g. an increase from -0.20 to -0.15 mm/s as temperature was increased from 77 to 298 K (see Table 4). Thus, the second-order Doppler effect cannot explain the IS values of this study.

It is generally agreed that intrinsic changes in the electronic structure of metal crystallites from the bulk metal behavior occur only for clusters of about 2 nm in diameter and containing less than about 150 atoms [31]. It is also generally agreed that narrower bands and fewer orbitals are observed, although there is little consensus on the interpretation of these shifts in terms of the structure of the d-bands and the binding energies of core electrons. Burch [31] notes that while similar changes in electronic properties are observed for many metals and several different supports, they are probably not attributable to support effects.

While significant changes in IS were observed in this study with changes in cluster size, they were smaller than the absolute values of IS and all in the same direction, i.e. a decrease in IS with decreasing average cluster size, e.g. values of 0.18, 0.14, and 0.10 mm/s for 10, 3 and 1% Fe/C with average crystallite diameters of 8.8, 1.6 and 1.2 nm respectively. Accordingly, the observed changes in IS in this study are neither due to a second-order Doppler effect or to intrinsic effects of small cluster size but rather are principally due to changes in s-electron density at the nucleus of ^{57}Co or ^{57}Fe due to electronic interactions with the immediate chemical environment.

The observed increases in electron density for Al_2O_3-supported Fe and Co can be interpreted in terms of a transfer of electrons from the support to the s-orbitals of the metal clusters or alternatively withdrawal of d-electrons from the metal cluster (resulting in less screening by the d orbitals of the metal), while the opposite would be true for carbon. In view of the chemistry of the the particular supports involved, electron transfer from carbon to the metal and from the metal to alumina might be expected; nevertheless, more needs to be learned regarding the electronic structure of metal clusters before this issue can be properly addressed. Irrespective, of the interpretation, *it is clear that very significant changes occur in the electronic structure of Co and Fe metal clusters in the presence of Al_2O_3 and carbon supports and that the effects are opposite for the two supports. Thus, these results are strong evidence that the IS values are due to metal-support interactions which are greatly different for Al_2O_3 and carbon substrates*. The precise nature of the MSI is yet to be defined. However, the fact that SP clusters are observed in catalysts prepared by ionic impregnation/deposition while mainly ferromagnetic clusters are observed in catalysts prepared from decomposition of metal carbonyls [2] suggests that the observed MSI may be due in part to decoration of the metal by support species deposited during the impregnation [2,7,19,31]. The observed changes in the electronic structure of the metal clusters from this study may explain at least in part the abnormally low CO hydrogenation activity of 1% Co/Al_2O_3 catalysts [7,32,33] as well as their inability to dissociate CO, observed in companion studies [32,34].

4. CONCLUSIONS

a. The nonaqueous impregnation methods developed in this study result in the preparation of a well-reduced and highly-dispersed metal phase in dilute, carbon- and alumina-supported Co and Fe systems.

b. A high fraction of the metal in 1% Co/C, 1-3% Fe/C, 1% Co/Al_2O_3, and 0.5-2% Fe/Al_2O_3 catalysts reduced at 623-873 K is present as superparamagnetic (SP) metal clusters of less than about 2-5 nm in diameter.

c. Very significant isomer (chemical) shifts are observed for the Co_{sp} and Fe_{sp} metal phases in these dilute Co and Fe catalysts; the IS is negative (-0.05 to -0.15) for both Co and Fe on alumina and positive (+0.10 to 0.15) for both Co and Fe on carbon. The recoil free-fractions and Debye temperatures for the SP metal phases are substantially lower than for oxide phases, suggesting a weaker interaction with the support of the metal relative to the oxide. Moreover, the Debye temperatures of the SP metal clusters are about half of values typically observed for bulk solids, suggesting that a majority of atoms in these clusters are exposed to the surface.

d. The observed isomer shifts for carbon-supported Co and Fe are consistent with a decrease in electron density at the nucleus while for alumina-supported Co and Fe they indicate an increase.

e. That opposite changes in electron densities are observed for carbon and alumina-supported base-metal clusters provides direct evidence of electronic modifications of these metal clusters by interaction with the support.

5. REFERENCES

1 S. A. Stevenson, J. A. Dumesic, R. T K. Baker, and E. Ruckenstein, Metal-Support Interactions in Catalysis, Sintering, and Redispersion, Van Nostrand Reinhold, New York, 1987.
2 M. Rameswaren and C. H. Bartholomew, J. Catal., 117 (1989) 218.
3 W. H. Lee and C. H. Bartholomew, J. Catal., 120 (1989) 256.
4 B. G. Johnson, C. H. Bartholomew, and D. W. Goodman, J. Catal., 128 (1991) 231.
5 H. Topsoe, J. A. Dumesic, E. G. Derouane, B. S. Clausen, S. Morup, J. Villadsen and N. Topsoe, Preparation of Catalysts II, Elsevier Sci., 1979, 365.
6. J. Phillips and J. A. Dumesic, Appl. Surf. Sci., 7 (1981) 215.
7. L.R. Neubauer, Ph.D. Dissertation, BYU, 1986.
8 V.K, Jones, L.R, Neubauer, and C.H., Bartholomew, J.Phys.Chem., 90 (1986) 4832.
9. E. Hegenberger, N. L. Wu, and J. Phillips, J. Phys. Chem., 91 (1987) 5067.
10 P. A. Smith and C. H. Bartholomew, paper submitted, 1992.
11 J. W. Niemantsverdriet, A. M. van der Kraan, W. L. van der Dijk, and H. S. van der Baan, J. Phys. Chem., 84 (1980 3365).
12 J. W. Niemantsverdriet, A. M. van der Kraan, W. N. Delgass, and M. A. Vannice, J. Phys. Chem., 89 (1985) 67.
13 J. E. Sueiras, N. Homs, P Ramirez de la Piscina, M. Gracia, and J. L. G. Fierro, J. Catal., 98 (1986) 264.
14 M. V. Cagnoli, S. G. Marchetti, N. G. Gallegos, A. M. Alverez, R. C. Mercader, and A. A. Yeramian, J. Catal. 123 (1990) 21.
15 B. S. Clausen and H. Topsoe, Appl. Catal., 48 (1989) 327.
16 C. H. Bartholomew, final report to NSF, No. CPE-8010780, January 31, 1982.
17 C. H. Bartholomew and R. B. Pannell, J. Catal., 65 (1980) 390.
18 R. D. Jones and C. H. Bartholomew, Appl. Catal., 39 (1988) 77.
19 C. H. Bartholomew, Catal. Lett., 7 (1990) 27.
20 C. H. Bartholomew and R. J. Farrauto, J. Catal., 45 (1976) 41.
21 R. C. Reuel and C. H. Bartholomew, J. Catal. 85 (1984) 63.
22 V. G. Bhide and S. K Date, Phys. Rev., 172 (1968) 345.
23 R. L. Garten and D. F. Ollis, J. Catal., 35 (1947) 232.
24 T. Ren-Yuan, Z Su, W. Chengyu, L. Dongbai, and L. Liwu, J. Catal., 106 (1987) 440.
25 J. A. Dumesic and H. Topsoe, Adv. Catal., 26 (1977) 121.
26 C. H. Bartholomew, Ph. D. Dissertation, Stanford Univ., 1972.
27 C. H. Bartholomew and M. Boudart, J. Catal., 29 (1973) 278.
28 M. N. Varma and R. W. Hoffman, J. Vac. Sci. Technol., 9 (1972) 177.
29 P. H. Barrett and T. K. McNab, Phys. Rev. Lett., 25 (1970) 1601.
30 V. I. Goldanskii and R. H. Herber, Chemical Applications of Mössbauer Spectroscopy, Academic Press, 1968, p. 43.
31 R. Burch, in Catalysis, eds. G. C. Bond and G. Webb, Royal Society, 1985, Vol. 7, 149.
32 W.-H. Lee, Ph. D. Dissertation, Brigham Young U., 1988.
33 W.-H. Lee and C. H. Bartholomew, J. Catal., 120 (1989) 256.
34 W.-H. Lee and C. H. Bartholomew, paper submitted, 1992.

DISCUSSION

Q: R. W. Joyner (United Kingdom)

In discussing elution transfer between support and metal particles one fundamental point must be remembered, this is a short-range phenomenon. Many calculations, including our own (Surface Sci., ca. 1984), show that the maximum range is ca. 0.5 nm. At distances greater than this the metal particle simply does not know the support is there. For base metal catalysts you might therefore extend to see 2 sets of Mossbauer signals - are each from the regions affected and unaffected by elution transfer. This conclusion would only change if the particles contained < ca. 20 atoms, were rafts, or were heavily decorated by support particles.

A: C. H. Bartholomew

We find essential agreement with all of your points, including the fundamental concept of short range electronic interactions between support and metal of no greater than about 0.5-0.6 nm. We think our MAS/MES and hydrogen adsorption results together indicate that the predominant phase in our samples consists of very small Co and Fe metal clusters of 0.5-2 nm diameter in which a large fraction of the metal atoms are electronically influenced by the support. The consistent positive isomer shifts for Co/C and Fe/C and negative isomer shifts for singlets in Co/alumina and Fe/alumina coupled with decreases in CO binding energy observed by temperature-programmed desorption studies (unpublished work) on these same samples are consistent with your suggestion that metal clusters are decorated by support material.

Your expectation of two different Mossbauer signals for large and small crystallites is a reasonable one, and is in fact realized in the 2 % Fe/alumina catalyst reduced at 873 K; indeed the MAS evidence indicates that there are two principle phases in this sample: (1) small superparamagnetic clusters having a negative isomer shift of -0.08 mm/s and (2) large ferromagnetic crystallites having no isomer shift with respect to bulk iron. However, in the same catalyst reduced under milder conditions and in all other catalyst samples, only one metallic phase is observed, namely superparamagnetic (SP) iron, having a characteristic isomer (chemical) shift for each support. In the base of SP iron spectral differences due to variations in particle size are manifested over a continuum (rather than in two distinct groups) in two ways: (1) a significant dependence of isomer shift (IS) on cluster size, i. e., a decrease in IS with decreasing crystallite size of -0.08 to 0.10 mm/s in 10 and 1 % Fe/C catalysts (see Table 2) and (2) observation of a broad singlet strongly suggesting the superposition of many singlets having a range of quadrupole splitting or hyperfine fields. As mentioned in our paper, other workers have also observed marked changes in quadrupole splitting (i.e., symmetry of nearest neighbors) with variations in iron cluster diameter.

Q: J. W. Niemantsverdriet (The Netherlands)

Before you assign the changes in isomer shift to a support effect, you need to consider the following points:

1) An increase in isomer shift of the Fe/C particles would also occur if carbon atoms slipped into the iron lattice. Conclusive proof that your particles are pure α-Fe is only obtained at 80 K in an external magnetic field.

2) The isomer shift you are measuring is an average our atoms in the interior and atoms at the surface of the particle, the latter having the larger IS. A particle-size-dependent IS may therefore reflect the fraction of surface atoms.

3) The IS through the 2nd order Doppler effect, depends on the lattice vibrations of the particle. Soft modes (e.g. on the surface) lower the IS. I wonder whether this explains the negative shift of Fe/Al_2O_3.

4) If you have sorted all these effects out, you can start to think about factors which affect the s-electron density in iron. Particle size is one, morphology another, and finally, charge transfer may perhaps play a role.

A: C. H. Bartholomew

We agree that conclusive proof for particles in Fe/C consisting of pure α-Fe can be obtained by one of the two methods you mentioned. Thus, while it is unlikely, our work cannot rule out completely the possibility of dissolved carbon or alumina in our Fe/C and Fe/alumina catalysts until we conduct such experiments. However, as you know, recently published work of which you are conduct such experiments. However, as you know, recently published work [1, 2] provides evidence for metal clusters consisting primarily of pure α-Fe in Fe/C catalysts having preparation and properties very similar to our Fe/C catalysts. Accordingly, we conclude that our Fe/C catalysts probably do not contain dissolved C. Further evidence for pure iron phases in our catalysts is provided by our observation that reduction under more severe conditions of Fe/C and Fe/alumina catalysts containing the subject superparamagnetic phases leads to pure ferromagnetic iron rather than carbide or iron aluminate phases.

On the second point and as mentioned in our response to Professor Joyner, we observe a significant decrease rather than increase in IS with decreasing average crystallite diameter (compare Tables 1 and 2). But we agree that the IS we measure would be an average over surface and bulk atoms and more reflective of surface atoms in the case of smaller clusters. We have not attempted as you did in your paper [3] to fit the superparamagnetic phase to surface and bulk phases having different IS values, but we agree that this is a fruitful approach - in fact one that I used in my dissertation work 20 years ago [4]. Nevertheless in that work I found that surface and bulk phases had the same IS, but the surface phase had a larger quadrupole splitting.

Your third question was addressed in our paper. We mention that the 2nd order Doppler effect would be nil for the room temperature data and that observed decreases in IS with increasing temperature were small relative to the overall magnitude of the IS for both Fe/C and Fe/alumina catalysts and in the opposite direction as expected for a second order Doppler effect in the case of Fe/alumina catalysts. Thus, the second-order Doppler effect cannot explain the IS values of this study and in particular the negative values for Fe/alumina.

We agree that it is hard work to separate out all of the different effects that you mention, but we think it can be done and that it is extremely worthwhile. We perceive that progress is being made towards that end, since your reported IS value of 0.5 mm/s for the surface phase of Fe/C [Bodker et al., 1992] agrees qualitatively with our values of 0.1-0.2 mm/s for the combined surface bulk phases of Fe/C.

[1] P. H. Christensen, S. Morup, J. W. Niemantsverdriet, *J. Phys. Chem.*, **89**, 4898 (1985)

[2] F. Bodker, S. Morup, J. W. Niemantsverdriet, *Catal. Lett.*, **13**, 195 (1992)

[3] F. Bodker, S. Morup, C. A. Oxborrow, M. B. Madsen and J. W. Niemantsverdriet, *J. Magnetism and Mag. Mat.*, **104**, 1695 (1992)

[4] C. H. Bartholomew and M. Boudart, *J. Catal.*, **29**, 278 (1973)

Q: W. N. Delgass (USA)

A number of investigations have found as you have that small Fe particles on carbon can be surprisingly difficult to reduce. Can you comment on the nature of the residual, non-reduced iron and its scheme of stabilization?

A: C. H. Bartholomew

We think that this may be a result of iron interacting strongly with oxygen containing groups, e.g. carboxyl and hydroxyl groups, which are known from IR and NMR studies to be present on the surface of active carbons--especially those that have been activated by heating in air. Fe oxides such as Fe_3O_4 are difficult to reduce and may be further stabilized through interaction with the carbon surface or through formation of

stable oxycarbides. Since most commercial activated carbons contain significant amounts of sulfur, alkali metal oxides, alumina and silica as impurities, the formation of iron sulfides, aluminates, and silicates which contain potassium or sodium oxides is a real possibility, unless precautions are taken to remove or immobilize these impurities. Our group and other research groups have used a treatment in hydrogen at 1173 - 1223 K for 12-16 h to remove reactive sulfur and alkali metals. Whether this treatment is adequate for complete removal of reactive sulfur has not been fully demonstrated. However, the fact that they readily adsorb hydrogen and that the crystallite diameter estimated from hydrogen adsorption agrees with that measured by TEM suggests that our Fe/C catalysts were not poisoned by sulfur or other impurities in the support.

Q: K. P. de Jong (The Netherlands)

In view of the precursors (nitrates, chlorides) and carriers (alumina, carbon) used in your work, I expect in all cases traces of oxygen, chlorine or carbon were present in the lattice of the metallic particles. The questions are:

1) How do you exclude the presence of traces of O/Cl/C in the metal particles ?

2) How would such traces affect the MAS/MES results ?

A: C. H. Bartholomew

In my response to Professor Delgass I have already addressed the issue of potential contaminants from the carbon support. The alumina support from Conoco is of very high purity and would probably not contribute to contamination of the metal. We found that the MAS spectra for Fe/alumina catalysts were not qualitatively different following preparation using either iron nitrate or iron chloride precursors. This suggests that chlorine contaminants, if present, did not affect the iron phases. In addition to reduced metals, unreduced Co and Fe oxides were observed by MAS and MES in both alumina- and carbon-supported materials, although carbon-supported Fe and Co could be completely reduced to the metal at sufficiently high temperature. The presence of significant amounts of carbon in the metal lattice would have been evident by Mössbauer upon reduction at sufficiently high temperatures to obtain the characteristic ferromagnetic carbides--instead, only pure α-iron was observed. As mentioned in my response to Professor Delgass, the presence on the surface of oxygen, chlorine, or carbon would have rendered the catalysts ineffective for adsorption of hydrogen or reaction of CO and hydrogen. Instead, these catalysts were found to adsorb large quantities of hydrogen and to be fairly active for CO hydrogenation.

Q: T. Uematsu (Japan)

Super-paramagnetism is usually dependent on the particle sizes of paramagnetic substances. We have been interested in the preparation properties of superfine particles and of their application as catalysts.

In this view, Professor Bartholomew's talk on the measurement of superparamagnetism on supported metal clusters was suggestive. My three questions are as follows:

1) Are there any thresholds (definite values) on the particle sizes of Co/Al_2O_3 and Fe/Al_2O_3 that you obtained ?

2) Wether or not such super-paramagnetism is influenced by the interaction with supports ?

3) What is your opinion on the experimental results on the relation between catalytic behavior and superparamagnetic properties of metal clusters supported on metal oxides ?

A: C. H. Bartholomew

In answer to your first question, our estimates of crystallite size in Table 1 coupled with our Mössbauer results (Tables 2 and 3) suggest that the critical crystallite size below which super-paramagnetism occurs is probably 3-5 nm. In the two samples for which

ferromagnetism was observed (10% Fe/C reduced at 623 K and 2% Fe/alumina reduced at 873 K) the average crystallite diameters were in the range of 5-8 nm.

In regard to your second question, there is good evidence from work in our laboratory and that of other groups that the observation of super-paramagnetism is greatly influenced by cluster-support interactions. In my response to Professor Joyner mentioned evidence that the metal crystallites in catalysts prepared by the non aqueous impregnation methods of this study are probably decorated with support moieties. In a companion study in our laboratory [5] we reported that highly dispersed Fe/alumina catalysts prepared by reductive decomposition of metal carbonyls on a highly dehydroxylated support contained mainly ferromagnetic iron clusters, even though a large fraction of the crystallites were smaller than 2-3 nm in diameter. Furthermore, the evidence in the latter study suggests that the surfaces of small ferromagnetic iron metal clusters in the carbonyl-derived catalysts were free of contamination by support materials. Accordingly, we think that surfaces decorated with support material are more likely to be superparamagnetic (SP), the support adlayers possibly disrupting the magnetic exchange coupling that would otherwise lead to ferromagnetism.

Finally, regarding the relationship between SP behavior and catalytic activity of clusters on metal oxides, we find that catalysts of this study containing mainly SP Fe on alumina are 1-2 orders of magnitude less active (on a turnover frequency bases) for CO hydrogenation than catalysts prepared by metal carbonyl decomposition and which contain mainly ferromagnetic iron.

[5] M. Rameswarean, C. H. Bartholomew, *J. Catal.*, **117**, 218 (1989)

Q: K. Lázár (Hungary)

Association of a certain number of zerovalent atoms is necessary to form particles of metallic character. The size lower limit mentioned in the talk (~1 nm) might be close to this threshold. On the other hand, iron clusters built up from a few atoms exhibit a quite large negative isomer shift (~-0.4 mm/s; e.g. Pasternak's experiments with noble gas matrix isolation). Is it not possible in the case of alumina support that some of the particles have not attained the threshold limit yet, and that this is the reason that the isomer shift is still negative-originating from not completely metallic particles ? (As it can be assumed particles on alumina can be more separated - and smaller - than on carbon support due to the "surface decoration' taking place during impregnation as was shown e.g. on the extra slide.) As for the particle size the direct comparison of chemisorption data might be misleading for carbon and alumina due also to the mentioned "surface decoration".

A: C. H. Bartholomew

You suggest that the entire negative IS for clusters of less than 1 nm in the case of Fe/alumina might be due to a size effect rather than a support effect. Our results, however, indicate this to be a relatively small effect and not limited to just one catalyst. Indeed, the hydrogen adsorption data indicate that a significant fraction of the iron clusters in Fe/C are also 1 nm or less in diameter and yet the IS is positive not negative. Moreover, we suspect that decoration by support material occurs in both Fe/C and Fe/alumina catalyst systems--otherwise we would not see super-paramagnetism (see response to T. Uematsu). Nevertheless, your proposal could explain the observed decrease in IS with decreasing crystallite diameter (see response to Professor Joyner) which we think is superimposed upon a larger support effect. If, as you suggest, the metal clusters were not metallic in nature, they would probably not adsorb hydrogen; however, they do adsorb large quantities of hydrogen indicating a metallic behavior.

Q: D. Wang (China)

We have worked with a model system for supported Fe where we evaporated Fe atoms onto TiO_2(110). We found that Fe at low coverages are quite different from Fe at

high coverages. At high coverages, Fe behaves like metallic Fe. At low coverages, Fe atoms do not nucleate but remain in atomic dispersion and show adsorption behavior more like Fe carbonyls, with very high stretching frequencies (ca. 2150 cm^{-1}) and a UP spectrum which is more like gas-phase CO than like CO on metallic Fe. If one makes a rough extrapolation from our low coverage case to your low loadings, one might expect atomically dispersed Fe at low loadings. Can your technique detect such Fe, have you seen such Fe, and what kind of support interaction would you expect with such Fe ?

A: C. H. Bartholomew

Our data provide evidence for the presence in our low loading catalysts of very small Co and Fe metal clusters in the range of 1-2 nm. Our data neither support or rule-out the presence of monodispersed atoms of Co and Fe on the support. However, CO TPD data from a companion study (ref. 34 in our paper) indicate that small Co clusters in 1 % Co/alumina have different properties for CO adsorption than those observed for larger metal crystallites in catalysts of higher loading. Indeed, the adsorption behavior on the small crystallites of 1-2 nm is somewhat consistent with your findings in that the adsorption is molecular and nondissociative. The inability of this catalyst to dissociate CO explains to a large degree its low activity for CO hydrogenation (ref. 33 in our paper). Nevertheless, it is interesting that these small crystallites do adsorb hydrogen.

Q: O. A. Kirichenko (Russia)

Have you ever analyzed the dissolution of γ-Al_2O_3 in impregnation solutions or the content of Al in supported phases? We have done that for Fe-O/γ-Al_2O_3 and found the Al-loading in supported Fe-O phases being more than 10 at%. Perhaps, your results for this system are the evidence of the same type loading of supported phase rather than electronic metal-support interaction.

A: C. H. Bartholomew

We have not analyzed the dissolution of alumina in our impregnating solutions, but we are aware that several other research groups including yours have done this. Your observations and those of others could explain how it is possible to decorate metal crystallites with support material during preparation in systems in which the support is not reducible. As mentioned in our paper and in the previous discussion we think our data are consistent with decoration of the exposed metal surfaces with alumina or carbon. If this decoration occurs, the support moieties could act as electronic promoters. This is in our view an electronic support interaction just as much as the electronic interaction at the support/cluster contact.

Q: S. I. Woo (Korea)

We have reported the Ferromagnetic Resonance Spectra of very small cobalt clusters entrapped in NaY and supported on silica and alumina (Applied Catal., 1988; J. Chem. Soc. Faraday Transaction, 1992; Bulletin of Japan Chemical Society, 1991). The FMR technique is the most sensitive technique to characterize small superparamagnetic Co and Fe clusters supported on various oxides. The intensity of ferromagnetic resonance vs. recording temperature clearly indicates the Debye temperature and superparamagnetic behavior. Hence I strongly enhanced by FMR studies.

A: C. H. Bartholomew

We agree that FMR is a useful technique for studying the magnetic and lattice dynamical properties of supported Co and Fe clusters. However, our attempts to obtain FMR data on our Co catalysts through collaboration with other groups were unsuccessful because of difficulties in transferring samples without exposing them to air and in interpreting the very complex data. We are pleased that your recent FMR work provides corroborative evidence that small, superparamagnetic Co and Fe clusters can be prepared on alumina and silica.

Q: F. Solymosi (Hungary)

I am glad to learn that you found an electronic interaction between the metal catalyst and the support, which depends on the nature of the support. For the catalysis, it is now an important question: is this electron transfer large enough to be felt in the catalytic activity of the metals ? Did you study the catalytic behavior of your system; and, if you did, how was the rate of the reaction influenced by the direction of the electron transfer between metal and supports ?

A: C. H. Bartholomew

This is indeed an important question. Yes, we have studied the catalytic behavior of these dilute Co/alumina and Fe/alumina catalysts [5-8] and find that the 1 wt% catalyst and some of the 3 wt% catalysts having low extents of reduction and high dispersions are 1-2 orders of magnitude less active than catalysts of higher loading and lower dispersion. These less active catalysts also appear to dissociate CO at low or negligible rates. This behavior (low activity and low propensity for dissociating CO) can be attributed to a combination of (1) decoration of the metal by the support and (2) changes in the electronic properties of the small metal clusters due to interaction with the support or unreduced metal. The decoration effect can be minimized in preparations involving decomposition of metal carbonyls; in this case we think the low activity/low propensity to dissociate CO is essentially entirely due to the electronic effect.

[6] W. H. Lee, C. H. Bartholomew, *J. Catal.*, **120**, 256 (1989)
[7] B. G. Johnson, M. Rameswaran, M. D. Patil, G. Murahildar, C. H. Bartholomew, *Catalysis Today*, **6**, 81 (1989)
[8] B. G. Johnson, C. H. Bartholomew, D. W. Goodman, *J. Catal.*, **128**, 231 (1991)

Guczi, L. *et al.* (Editors), *New Frontiers in Catalysis*
Proceedings of the 10th International Congress on Catalysis, 19-24 July, 1992, Budapest, Hungary
© 1993 Elsevier Science Publishers B.V. All rights reserved

FORMATION AND PROPERTIES OF DISPERSED Pd PARTICLES OVER GRAPHITE AND DIAMOND

O. S. Alekseev, L. V. Nosova and Yu. A. Ryndin

Institute of Catalysis, Russian Academy of Sciences, Siberian Division, Novosibirsk 630090, Russia

Abstract

According to the TEM and HT data, the size of Pd particles in Pd/C catalysts prepared via interaction of $C_3H_5PdC_5H_5$ complex with the surface of carbon supports and reduced with hydrogen at 573 K ranges from 10 to 20 $\AA$. After increasing reduction temperature up to 873 K, dispersion of Pd/Altunit (ultra dispersed diamond) remains practically the same, while the size of metal particles in Pd/Sibunit (graphite-like carbon) increases up to 100 $\AA$. This difference is due to the peculiarities of the interaction between Pd particles and the surface of graphite and diamond in hydrogen atmosphere. In the reactions of acetylene and vinylacetylene hydrogenation the specific activity of Pd/C is comparable to those of Pd/SiO_2 , but in 1-2 orders lower in reactions of ethane hydrogenolysis and CO hydrogenation.

The introduction of Zr ions to Pd/C results in the following effects: appearance of a new absorption band at 1600 cm^{-1} in the spectrum of adsorbed CO, increase in the specific activity in methanol synthesis by 1-2 orders but drastic decrease in the specific activity in ethane hydrogenolysis, while high temperature oxidation of the samples completely eliminates the inhibitor action of Zr ions. These peculiarities are similar to those previously observed for $(Pd+Zr)/SiO_2$ as well as for Pd/ZrO_2 , and are likely to be due to mixed $Pd\text{-}Zr^{n+}$ active sites formed in the systems.

1. INTRODUCTION

Highly dispersed metal catalysts obtained via the step of anchoring of organometallic compounds on the surface of carriers are convenient model systems for investigation of different problems in catalysis (size effect, promoter action). Porous carbon materials have been widely applied for supporting active metals. However, regularities of formation of active sites of these catalysts still remain unclear, which hampers the development of the scientific basis of their production technology.

The objectives of this paper are: (i) to study the regularities of formation, thermal stability, adsorption and catalytic properties of Pd particles obtained via the step of anchoring of organometallic compounds on the surface of carbon supports with the

graphite-like and diamond-like structures; (ii) to synthesize the active sites, containing Pd atoms and Zr ions, by the method of "surface assembling" on the surface of carbon supports as well as to study the regularities of the modifying action of Zr ions on physico-chemical and catalytic properties of the supported palladium.

2. EXPERIMENTAL

2.1. Catalyst preparation

New types of carbon materials were used as supports: highly pure (ash content less than 0.5 wt.%) mesoporous graphite-like carbon material "Sibunit" (surface area - 600 $m^2 g^{-1}$) [1], and a highly dispersed diamond powder "Altunit" with the surface area of 300 $m^2 g^{-1}$ [2]. Prior to anchoring of Zr and Pd complexes, carbon supports were treated in air at 573 K and then evacuated at 573 K up to 10^{-3} Torr.

Pd/(carbon, silica, alumina) catalysts were prepared by the interaction of $C_3H_5PdC_5H_5$ in pentane solution with oxygen-containing functional groups of the supports.

(Pd+Zr)/C catalysts were prepared without air contact in the following sequence: (a) interaction of $(\pi\text{-}C_3H_5)_4$ Zr pentane solution with carbon support evacuated at 573 K followed by out washing with the solvent of unreacted complex residues and subsequent drying in vacuum at 298 K; (b) removal of organic ligands from Zr/C by hydrogen treatment at 573 K; (c) interaction of $C_3H_5PdC_5H_5$ pentane solution with Zr/C followed by out washing and drying in vacuum at 298 K.

2.2. Catalyst characterization

IR spectra were recorded at 298 K on a Fourier spectrometer IFS-113 V (Bruker) at 1300 - 4000 cm^{-1} with 4 cm^{-1} resolution.

Electron-microscopic study was performed on a JEM-100 CX instrument with point-to-point resolution of 4 $\AA$

XP spectra were taken using a VG ESCA-3 spectrometer with Al $K\alpha$ ($h\nu = 1486.6$ eV) radiation.

Chemisorption measurements were made in a flow pulse system using chromatographic analysis. The samples were out gassed at the reduction temperature to achieve a 10^{-3} Torr pressure, then oxygen chemisorption and hydrogen titration were performed at room temperature.

Ethane hydrogenolysis was carried out in the kinetic region in a static circulation installation at 623 K, $P_{C_2H_6} = 50$ Torr, $P_{H_2} = 150$ Torr with chromatographic analysis of reaction products.

CO hydrogenation was studied in a flow differential reactor at 523 K, 10 atm and space velocity 20000 h^{-1}, with a mixture of composition $CO:H_2 = 1:2$ and conversion of less than 1 %.

Vinylacetylene hydrogenation was carried out in static circulation system at 273 K, $P_{C_4H_4} = 50$ Torr, $P_{H_2} = 150$ Torr, $P_{Ar} = 400$ Torr in the kinetic region [3]. The activity

and selectivity were calculated from the initial part of the composition-time curves at a conversion of less than 10 %.

Acetylene hydrogenation was carried out in the presence of ethylene in a nongradient flow reactor with circulation at 298 K and $P_{C_2H_2} = 8$ Torr, $P_{C_2H_4} = 8$ Torr, $P_{H_2} = 16$ Torr and $P_{Ar} = 720$ Torr [4]. The activity and selectivity were calculated at 50 % conversion.

3. RESULTS AND DISCUSSION

3.1. Genesis of Pd/C and (Pd + Zr)/C catalysts

According to the FTIR data [5], the surface of the oxidized diamond is characterized by the presence of a wide band at 3400 cm^{-1} that can be attributed to O-H stretching vibrations in surface carboxylic or phenolic OH groups of the support, and intensive band at 1750 cm^{-1} attributed to stretching vibrations in carbonyls of a ketone or a carboxyl groups. Note that position of the last band depends from oxidation conditions.

During treatment of the oxidized diamond with a pentane solution of $C_3H_5PdC_5H_5$, a drastic decrease of the surface concentration of C=O groups occurs, and organic ligands of the supported Pd complex (3080-3000, 1400, 1330 cm^{-1}) appear on the support surface [6]. This experimental fact evidences for a chemical reaction between the Pd complex and C=O containing groups of the support. We are not able to differentiate between carbonyls of a ketone or a carboxyl group from IR-spectra, so additional experiments have been carried out for investigation of $C_3H_5PdC_5H_5$ reactivity toward C=O containing groups in liquid solutions.

Upon introducing benzoquinone or acetone into the pentane solution of $C_3H_5PdC_5H_5$ at 298 K, no changes had been seen in IR-spectra of these compounds in C=O region. These experimental data allow to conclude that there is no reaction between Pd complex and carbonyl groups. At the same time, the addition of CH_3COOH to the $C_3H_5PdC_5H_5$ solution is accompanied by drastic decrease in the intensity of band at 1710 cm^{-1} corresponding to C=O stretching vibrations of the carboxyl groups and appearance of bands at 1576 and 1407 cm^{-1} corresponding to asymmetrical and symmetrical stretching vibrations of carboxylate fragments (Fig. 1). These data indicate the occurrence of the chemical reaction between Pd complex and carboxyl groups which proceeds in liquid solution and, apparently in the case of surface carboxyl groups according to the following scheme:

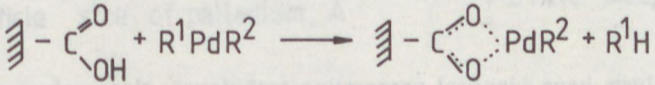

At support treatment with $(p\text{-}C_3H_5)_4Zr$ solution [5], fast irreversible adsorption of the supported complex is visually seen. The IR spectrum reflects a drastic decrease in the intensity of band of C=O groups and appearance of bands typical for allyl ligands (3085,

1535 cm^{-1}). This indicates the occurrence of the chemical reaction between Zr complex and surface carboxyl groups as it was in the case of Pd. The treatment of attached Zr complex with H_2 leads to complete disappearance of allyl ligands absorption bands, which seems to be due to their removal from the surface of modified support. At the same time, concentration of the surface CO groups is not regenerated, which points to the presence of the surface Zr ions chemically bonded with the support's oxygen, in the reduced Zr/diamond catalyst.

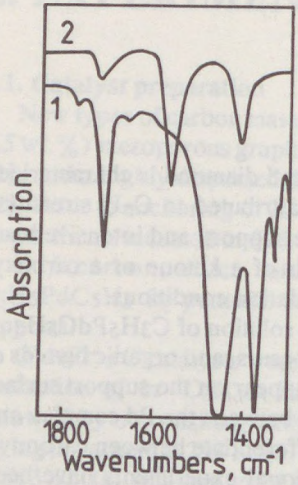

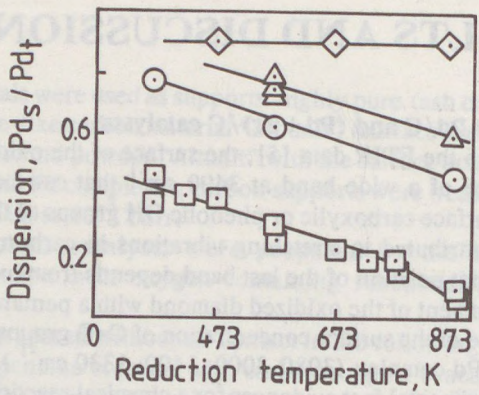

Figure 1. IR spectra of CH_3COOH interaction with Pd complex.
(1) - Spectrum of CH_3COOH in pentane; (2) - after addition of $C_3H_5PdC_5H_5$ complex and evaporation of pentane.
Figure 2. Dependence of palladium dispersion on reduction temperature.
(⊙) Pd/SiO_2, (△) Pd/Al_2O_3, (⊡) Pd/Sibunit, (◇) Pd/Altunit

Upon subsequent interaction of $C_3H_5PdC_5H_5$ with the Zr/diamond the bands typical for organic ligands of the Pd complex appear in the IR spectrum, while the intensity of band of the carboxyl groups remains unchanged [5]. This makes it possible to suppose that the Pd complex interacts with surface anchored Zr ions. The reduction of (Pd+Zr)/diamond obtained in situ is accompanied by complete removal of Pd complex ligands.

3.2. Effects of the support nature and Zr ions on Pd dispersion, electronic and catalytic properties

3.2.1. Dispersion

All studied catalysts have identical preparation techniques, close values of surface concentration and the same initial Pd compound. For this reason, we can accurately compare the sintering of these systems in hydrogen.

The dependence of Pd dispersion on reduction temperature for different supports is shown in Fig. 2. The particles-size distribution (PSD) curves of all the investigated samples are enough narrow and have a single maximum. This fact permits conclusions to be drawn

about the mechanism of Pd sintering that occurs via surface diffusion of particles and their collision and coalescence. Note that the data on Pd dispersion (Pd_s/Pd_t) calculated from TEM data for all catalysts are in good agreement with those obtained by hydrogen titration.

We suggest that the initial distribution of Pd complexes over all support appears to be monomolecular. These surface complexes can be readily reduced with hydrogen with formation of Pd atoms, but the sintering of Pd primary particles in hydrogen differs markedly on the surface of oxides and Sibunit. At 373 K the dispersion of palladium, expressed as the ratio of surface atoms to total atoms, Pd_s/Pd_t , on silica is 0.8 and on Sibunit 0.4 (Fig. 2). On increasing the reduction temperature from 373 to 773 K, Pd_s/Pd_t decreases insignificantly: to 0.5 on silica and to 0.2 on Sibunit, and the particle-size distribution remains monodispersed. The same tendency was observed for Pd/Al_2O_3, but its dispersion and stability to sintering are higher than that of Pd/SiO_2. The authors of the crystallite migration model predict that at temperatures below 773 K the sintering process is limited by the rate of surface diffusion of metal particles, but not by their coalescence. Consequently, the mobility of Pd particles over Sibunit is higher than that over oxides.

According to TEM data (Fig. 3), Pd/Sibunit reduced at 573 K contains metallic particles with a mean surface size ($\overline{d}_s$) of 22 $\mathring{A}$ On increasing temperature of hydrogen treatment of this catalyst up to 873 K, $\overline{d}_s$ increases up to 100 $\mathring{A}$ Electron microscopic data (Fig. 4) indicate that $\overline{d}_s$ in (Pd+Zr)/Sibunit catalyst is 17 $\mathring{A}$ at 573 K, and increases up to 88 $\mathring{A}$ with increasing reduction temperature in interval 573-873 K. These data show that in the presence of Zr ions Pd dispersion and stability towards sintering on Sibunit tends to increase markedly. The high stability of Pd particles in the presence of Zr ions can be explained by a decrease of their mobility due to an increase in energy of binding with the modified support.

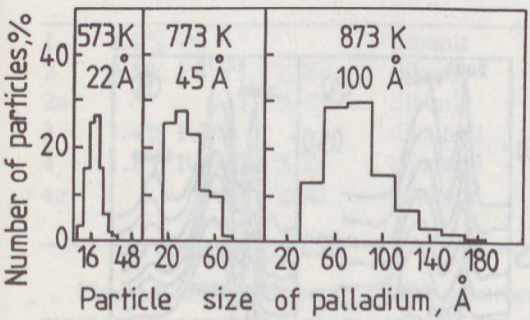

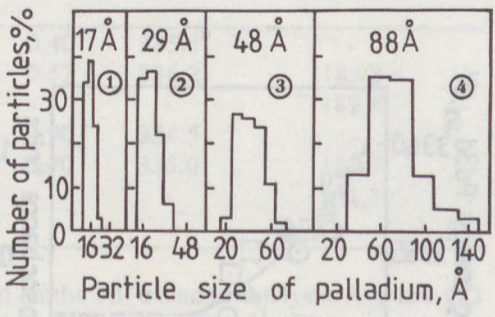

Figure 3. Particle size distribution curves of 2.1% Pd/Sibunit catalyst treated with H_2 at 573 K, 773 K and 873 K.

Figure 4. Particle size distribution curves of (1.9%Pd+3.0%Zr)/Sibunit catalyst treated with H_2 at 573 K (1), 673 K (2), 773 K (3) and 873 K (4).

The micrographs of the Pd/diamond and (Pd + Zr)/diamond catalysts, reduced with H_2 at 573 K and 873 K, are similar to those ones of pure diamond. This fact shows high dispersion ($\bar{d}_s < 10\mathring{A}$) of Pd particles supported on diamond and the absence of its sintering. It follows from comparison of $\bar{d}_s$ for Pd/Sibunit and Pd/diamond that the mobility of Pd particles in H_2 is higher on Sibunit than on diamond. If we propose that the high mobility of Pd particles on graphite might be due to the gasification of the support catalyzed by Pd, as it has been shown in [7], the difference of crystal structure of carbon supports might be the reason for high agglomerating capacity of Pd/Sibunit compared to Pd/diamond. The high thermal stability of Pd/diamond catalyst is very interesting phenomenon which requires additional investigation.

3.2.2. Electronic and chemisorptive properties

XPS data for palladium catalysts are presented in Fig. 5. The binding energy (E_b) of the Pd 3d5/2 level for highly dispersed palladium particles, supported on oxides and Sibunit, is 335,9 eV, which is 0.7 eV higher than that for the bulk Pd, which is equal to 335,2 - 0.2 eV according to different sources. During the sintering of palladium catalysts the E_b value of the Pd 3d5/2 level falls to a value typical of bulk palladium. A comparison of the XPS data with those for palladium dispersion indicates a quantitative correlation between E_b of the Pd 3d5/2 level and average size of Pd particles (Fig. 5). Regardless of the collective properties of the support, the electronic properties of Pd particles larger than 30 $\mathring{A}$ do not depend on the chemical nature of the support and Pd dispersion. When the $\bar{d}_s$ for Pd decreases from 30 to 10$\mathring{A}$, the E_b of the Pd 3d5/2 level tends to increase to 335,9 eV. The existence of such a positive shift for palladium supported on either an insulator (SiO_2, Al_2O_3) or a conductor (graphite) leads us to conclude that this shift is caused by a decreased electron density of Pd atoms in small particles rather than by the relaxation effect.

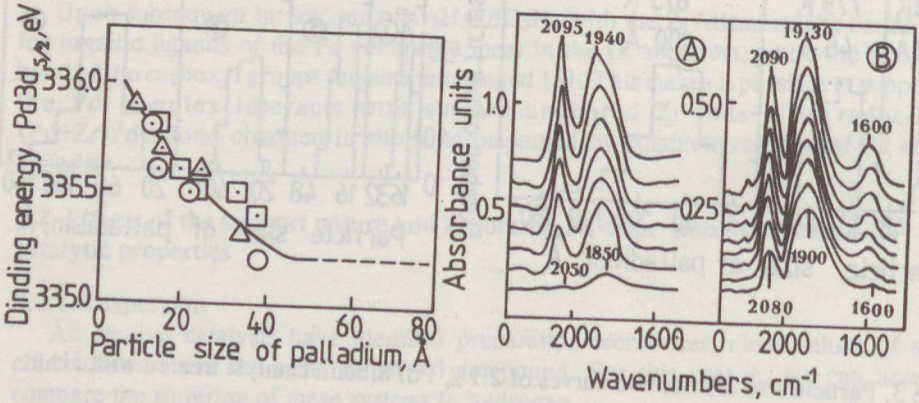

Figure 5. Dependence of E_b of Pd 3d5/2 on palladium particle size.
Figure 6. IR spectra of CO adsorption on Pd/diamond (A) and (Pd + Zr)/diamond (B) reduced with H_2 at 573 K.

Theoretical calculations made using molecular orbital theory show that the electronic structure of atoms forming a small cluster is essentially different from the structure of the bulk metal. For example, the calculation indicates that the d-band of palladium in a cluster containing less than 30 atoms is less occupied than that in large particles [8].

According to the XPS data, in reduced Zr/Sibunit the E_b of Zr 3 $d_{5/2}$ level makes up 182.8 eV, which corresponds to ionic state of anchored Zr. It should be mentioned, that in the case of Zr/diamond and Pd/diamond all the levels are shifted by 1.5 eV compared to Sibunit (Table 1). Taking into account these circumstances our conclusion about the presence of Zr^{n+} ions can be extended to Zr/diamond system as well. Hence, after treatment of the anchored Zr complex with H_2 the bond of Zr ions with support oxygen is retained. The latter conclusion is also valid for (Pd+Zr)/C systems, because after supporting Pd the E_b of Zr 3 $d_{5/2}$ level corresponds to ionic state of Zr (Table 1).

After supporting Pd on Zr/C, a small positive shift of the Zr 3 $d_{5/2}$ line by 0.5-0.6 eV can be observed, despite crystal modification of support (Table 1). Such a shift can indicate the interaction of surface Zr ions with Pd atoms.

A positive shift by 0.5 eV of the Pd 3d level is observed for Pd supported on modified graphite and diamond compared to Pd/C (Table 1). Since Pd dispersion increases insignificantly herein, electron-deficient character of Pd can be attributed to its interaction with Zr^{n+} cations. The same direction of the shift for the Zr 3d and Pd 3d levels in the (Pd+Zr)/C catalysts as compared with those in the Pd/C and Zr/C catalysts is very surprising and the nature of this effect is not clear at the moment, although a specific influence of the carbon support might be suggested.

Table 1
XPS parameters of supported Pd catalysts (T_{red} =573 K)

No	Catalyst composition, wt. %	Support	Pd_s/Pd_t	Pd $3d_{5/2}$ E_b, eV	Zr $3d_{5/2}$ E_b, eV
1	2.1% Pd	Sibunit	0.40	335.8	-
2	0.5% Pd + 1.1% Zr	Sibunit	0.52	336.2	183.3
2a	1.1% Zr	Sibunit	-	-	182.8
3	1.4% Pd	diamond	0.90	334.5	-
4	1.1% Pd + 3.1% Zr	diamond	0.90	335.0	181.7
4a	3.1% Zr	diamond	-	-	181.3

Figure 6 shows IR spectra of CO adsorbed on the Pd/diamond catalysts. At a low CO pressure the spectrum is characterized by bands at 2050 and 1850 cm^{-1} which are assigned to linear and bridge forms of CO adsorbed on metallic Pd. The major difference of the spectrum of CO adsorbed on (Pd+Zr)/diamond from those one on Pd/diamond (Fig. 6) is an additional band at 1600 cm^{-1}, intensity of which increases with increasing P_{CO}. The band in the region 1610 cm^{-1} has been found in [9] at CO adsorption on (Pd+Zr)/SiO_2 catalysts and related to CO adsorbed on mixed Pd-Zr active sites. Thus the experimentally found increase in intensity of the band at 1600 cm^{-1} with increasing P_{CO}, as well as the evidence of [9] makes it possible to suppose its relation to the CO molecule bound with the

Pd atom via the carbon and with the Zr ion via the oxygen atom. It follows from comparison of the spectra of CO adsorbed on (Pd+Zr)/diamond and Pd/diamond that at equal P_{CO} in the presence of Zr^{n+} there occurs a high-frequency shift of the absorption bands of the linear and bridge forms. These data correlate with the XPS data indicating the electron-deficiency of the modified Pd. Thus XPS and FTIR data give evidence for the presence of mixed active sites containing Pd atoms and Zr ions in the (Pd+Zr)/C systems.

3.2.3. Catalytic properties

Fig. 7 and 8 show the dependence of the specific activity (TON) for palladium catalysts in the hydrogenation of acetylene and vinylacetylene (VA) on the particles size of Pd. Regardless of the nature of the support TON of palladium in hydrogenation of VA remains almost constant over a wide range of Pd particles size, from 40 to 180 A°. This is evidence that Boreskov's rule is valid for the reaction under consideration. However, the specific activity falls by one order of magnitude as $\overline{d}_S$ decreases from 40 to 10 A°. Such decrease in the TON in VA hydrogenation was observed for all studied Pd catalysts.

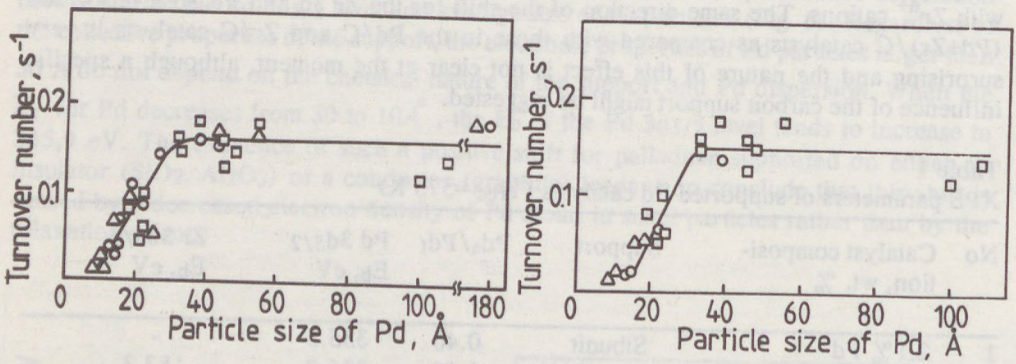

(⊙) Pd/SiO_2, (△) Pd/Al_2O_3, (⊡) Pd/Sibunit

Figure 7. Dependence of TON on Pd size in VA hydrogenation.

Figure 8. Dependence of TON on Pd size in acetylene hydrogenation.

Note that the TON of low-dispersed impregnated Pd catalysts is almost identical with those of samples of organometallic origin. The selectivity of almost all the palladium catalysts studied towards divinyl formation is virtually independent of the Pd dispersion and is equal to ca. 70-80 % mol. Consequently, at the same dispersion of palladium the TON and selectivity are independent of the nature of the support and the method of the preparation of catalysts.

Similar data were obtained for the gas-phase selective hydrogenation of acetylene with ethylene at 298 K (Fig. 8). The TON of Pd catalysts containing particles < 30 A° is 8-10 times lower than that of low-dispersed palladium.

The constancy of the catalytic properties of low-dispersed Pd over different supports agrees well with one of its electronic properties. With a increasing in the E_b of the Pd 3 $d_{5/2}$ level from 335.2 to 335.9 eV, TON decreases monotonically, by an order of magnitude. The decrease in electron density on a small palladium particles will probably contribute to the increase in the bond strength of chemisorbed unsaturated hydrocarbons and thus will lead to a decrease in TON.

In ethane hydrogenolysis introduction of Zr to Pd/C is accompanied by more than one order decrease in the activity of supported Pd, and upon increase in the temperature of sample reduction the inhibiting action of Zr increases as well. These effects seem to be due to the interaction of Pd atoms with Zr^{n+} ions. High temperature oxidation of (Pd+Zr)/C actually completely eliminates the inhibiting action of Zr (Table 2), which is likely due to oxidation and segregation of components.

Table 2
Catalytic properties of Pd catalysts

No	Catalyst	$TON*10^{3*}$	$TON*10^{3**}$	$TON*10^{3***}$	$S^{***}(CH_3OH)$
1	Pd/Sibunit	2.30	-	0.15	73
2	Pd+Zr/Sibunit	0.02	2.60	2.50	98
3	Pd/diamond	2.10	2.00	0.33	94
4	Pd+Zr/diamond	0.29	2.00	7.80	98

* - ethane hydrogenolysis after reduction at 623 K (s^{-1});
** - ethane hydrogenolysis after oxidation at 623 K followed by reduction at 623 K;
*** - CO hydrogenation after reduction at 573 K (s^{-1}).

In CO hydrogenation the specific activity of Pd supported on the carbon modified by Zr ions is by 1-2 orders higher than the Pd/C activity, while the selectivity with respect to methanol markedly increases. The high specific activity of (Pd+Zr)/C catalysts in CO hydrogenation seems to be due to the presence of electropositive Pd in the catalysts as well as due to activation of the CO molecule over mixed Pd-Zr active sites. Note that the adsorptive and catalytic effects of Zr ions on Pd/C properties are similar to those observed earlier for (Pd+Zr)/SiO_2 catalysts [9]. Thus, independently of the support chemical nature (graphite, diamond or SiO_2), the regularities of the modifying action of Zr ions on the properties of the supported metal are quite general.

4. REFERENCES

1 Yu.I. Yermakov, V.F. Surovikin, G.V. Plaksin et. al., React. Kinet. Catal. Lett., 33 (1987) 435.
2 V.L. Kuznetsov, M.N. Aleksandrov, I.V. Zagoruiko et. al., Carbon, 29 (1991) 665.
3 Yu.A. Ryndin, L.V. Nosova, A.I. Boronin and A.L. Chuvilin, Appl. Catal., 42 (1988) 131.

4 Yu.A. Ryndin, M.N. Stenin, A.I. Boronin et. al., Appl. Catal., 54 (1989) 277.
5 Yu.A. Ryndin, O.S. Alekseev, E.A. Paukshtis et. al., J. Mol. Catal., 68 (1991) 355.
6 Yu.A. Ryndin, O.S. Alekseev, P.A. Simonov and V.A. Likholobov, J. Mol. Catal., 55 (1989) 109.
7 P.J. Goethel and R.T. Yang, J. Catal., 108 (1988) 356.
8 R.C. Baetzold, Advan. Catal., 25 (1976) 1.
9 Yu.A. Ryndin, O.S. Alekseev, E.A. Paukshtis et. al., Appl. Catal., 63 (1990) 51.

DISCUSSION

Q: A. T. Bell (USA)

Could you comment on the selectivity effects of Pd/SiO_2 versus Pd/C in CO hydrogenation ?

A: Yu. Ryndin

The selectivity of Pd in respect of methanol is approximately equal 80-90 wt%, and within the experimental error it does not depend on the support nature.

Q: M. A. Vannice (USA)

1) How do your TON's for CO hydrogenation over Pd/sibunit and Pd/diamond compare to typical Pd catalyst such as Pd/SiO_2 or Pd powder ? These will be essentially for CH_3OH synthesis. These should be compared at the same temperature and pressure. If they are lower do you know why ?

2) Do you still see a positive 0.5 eV shift on the modified catalysts after sue in CO hydrogenation ?

A: Yu. Ryndin

1) At the same reaction conditions the TON of Pd/graphite and Pd/diamond catalysts is 3-6 times lower compared to Pd/SiO_2. In C_2H_6 hydrogenolysis the TON of both Pd/C catalysts is about two orders of magnitude lower than that for Pd/SiO_2. But in reactions of benzene, acetylene, and vinylacetylene hydrogenation TON does not depend on support nature. These effects may be due to the dilution of surface Pd atoms by carbon atoms, which should lead to decrease the surface concentration of multiple active sites responsible for CO hydrogenation and C_2H_6 hydrogenolysis.

2) XPS spectra have been taken for Pd catalysts reduced with H_2 in situ, i.e. in the state before catalysis. The used catalysts were not studied.

Q: R. Touroude (France)

You have observed an increase of the Pd 3d B.E. with a decrease of particle size whatever the support, as far as silica, alumina, and graphite are concerned. However when the Pd particles are deposited on diamond, you have observed a very high dispersion (whatever the reduction temperature, even at 873 K) and a very low Pd $3d_{5/2}$ B.E. (334.5 eV), even lower than usually observed in bulk palladium. Can you give any comment on it ? Is this charging effect ? What is the common reference for measuring the binding energy ?

A: Yu. Ryndin

The calculation of binding energies was made with respect to the C 1s line of graphite (284.6 eV) and diamond (285.0 eV) with a 0.2 eV accuracy. No charge effect was observed for Pd/graphite. In comparing B.E. of Pd $3d_{5/2}$ in Pd/graphite with those of Pd/diamond, Pd/SiO_2, and Pd/Al_2O_3, the charge effect of three latter catalysts was taken into account.

Unexpectedly low values of B.E. of the Zr 3d and Pd 3d levels in the case of diamond supported catalysts can be explained by the absence of reliable literature data concerning the value of B.E. of diamond C 1s level, used as an inert standard. This complication reduce the reliability of the obtained absolute values of B.E. for Pd and Zr on diamond, but does not interfere with controlling the changes in the electronic state of Pd in the presence of Zr ions.

Q: V. Ponec (The Netherlands)
Did you consider another explanation of the electropositive character of small Pd particles over SiO_2, Al_2O_3 and graphite ?

A: Yu. Ryndin
The positive shift of Pd core level may be also due to the different relaxation conditions of ionized small and large Pd particles. But the correlation between B.E. and dispersion of Pd on the conductor (graphite) and insulators (SiO_2 and Al_2O_3) indicates, that this shift is rather chemical one, but not relaxation.

Q: X. X. Guo (China)
What is the most probable reason of the low TOF of highly dispersed Pd particles in reactions of acetylene and vinylacetylene hydrogenation ?

A: Yu. Ryndin
It is known from organometallic chemistry that electron density transfer from the hydrocarbon molecule to the metal atom occurs during the interaction of unsaturated hydrocarbons with transition metals. In this instance the increase in electron density on small Pd particles will probably contribute to the increase in the bond strength of chemisorbed acetylene (and vinylacetylene) and thus will lead to a decrease in TOF.

Guczi, L. *et al.* (Editors), *New Frontiers in Catalysis*
Proceedings of the 10th International Congress on Catalysis, 19-24 July, 1992, Budapest, Hungary
© 1993 Elsevier Science Publishers B.V. All rights reserved

KINETICS OF ALKANE HYDROGENOLYSIS ON CLEAN AND COKED PLATINUM AND PLATINUM-RHENIUM CATALYSTS

G. C. Bond, R. H. Cunningham and E. L. Short

Department of Chemistry, Brunel University, Uxbridge UB8 3PH, United Kingdom

Abstract

The dependences of rate upon H_2 and alkane pressures have been determined for the hydrogenolysis of ethane, propane and n-butane on clean and coked Pt/Al_2O_3 and $Pt-Re/Al_2O_3$ catalysts. On clean surfaces, preserved by using only 1 min reaction periods, rates usually exhibited maxima as H_2 pressure was increased, the pressure at the maximum increasing with the size of the alkane; orders in the alkane measured at high H_2 pressure approximated to unity. Coking by reacting n-butane + H_2 at 713 K caused significant differences in the ways in which rates varied with H_2 pressure. Three rate equations have been tested, of which two give satisfactory fits. Constants for one of these, viz.

$$\text{rate} = k_1 P_A P_H / (k_2 P_A + P_H^{k3})$$

are presented, from which it appears that the reactive species may be formed from the reactant alkane by loss of four or five H atoms.

1. INTRODUCTION

While many techniques of physical characterisation are being applied to small metal particles, revealing aspects of their structure in ever greater detail, the ultimate goal of identifying and describing the active centres for catalysed reactions still eludes us; and this is particularly so for reactions showing a high degree of structure-sensitivity. Experience teaches that physical description alone is insufficient to predict catalytic activity, as catalysts having seemingly similar structures can sometimes show very different rates. Progress in structure characterisation therefore needs to be accompanied by more refined and extensive measurements of catalytic properties, and nowhere is this more true than with reactions of hydrocarbons, which frequently lead to the partial coverage of the metal by strongly-held species, usually called 'carbonaceous residues' or 'coke' [1]. Proper measurement of the rate of reaction is impossible if the extent of poisoning is not known. It would of course be best to work with clean surfaces (i.e. under conditions where all adsorbed species were reactive), since the coke might itself have an electronic as well as a site-blocking effect, but this is not easy to do because both the target and the parasitic reactions demand the same temperature range.

Measurement of orders of reaction, or identification of the rate equation, is much more informative than the simple recording of a rate, since it tells us how the reactants appear in the rate-limiting step and suggests, even if

it cannot prove, the mechanism by which the reactions takes place. The purpose of this work was to determine the kinetic equations for the hydrogenolysis of the C_2 to C_4 linear alkanes on Pt/Al_2O_3 and $Pt-Re/Al_2O_3$ catalysts, in conditions under which the surfaces are maintained in an essentially clean state. This has been achieved by using very short pulses of the reaction mixture, interspersed with periods of pure H_2 flow. We felt it important to examine all three of these alkanes, since much of the prior quantitative work [2,3] has employed only ethane. Kinetic equations have also been obtained on partially coked catalysts, in order to see whether the presence of the coke effects changes in the adsorption coefficients of the reactants. We hope that this study will contribute to the continuing debate [4] on the role of carbonaceous deposits as co-catalysts.

2. EXPERIMENTAL

Pt (0.3%) and Pt-Re (0.3% each) supported on Ketjen CK300 Alumina were supplied by AKZO; they are often referred to as EUROPT-3 and -4. They were pretreated in an atmospheric pressure flow system [5] as follows.

(i) Heating in air to 763 K over 7 h, and, after 1 h, cooling to 673 K over 2 h.

(ii) After purging with N_2 for 1 h, reduction in H_2 by heating to 763 K over 2 h, and, after 1 h, cooling to the initial reaction temperature. All flow-rates were 20 ml min^{-1}.

Coking of both catalysts was performed for 2 h at 713 K with the following flow-rates (cm^3 min^{-1}).

With ethane: H_2, 30; ethane, 30.

With propane: H_2, 40; propane, 10.

With n-butane, H_2, 100; n-butane, 10.

With Pt/Al_2O_3, these procedures reduced the activity for ethane and n-butane to <10% of the original value, but for propane by only 40-60%; with $Pt-Re/Al_2O_3$, the residual activities were <2% of the original for n-butane, and about 60% with propane, but these conditions were not severe enough to lower the activity for ethane to the desired extent.

Rate measurements were made with a total flow-rate of 140 ml min^{-1}, the pressure ranges used being: H_2, 0.043-0.818 atm; ethane, 0.029-0.214 atm; propane, 0.057-0.151 atm; and n-butane, 0.030-0.111 atm. N_2 was used as the balance gas. To keep the catalyst in a clean state, a H_2-alkane-N_2 mixture was passed for only 1 min before being analysed; the alkane flow was then stopped, and the H_2 flow kept at its previous value for 15 min. This was then altered to that required in the next reaction period, and after 4 min the next H_2-alkane-N_2 mixture was introduced. Rates were measured at 630 K for ethane and at 611 K for propane and n-butane. With coked catalysts, H_2-alkane mixtures were passed continuously.

3. RESULTS AND DISCUSSION

3.1. Measurement of reaction kinetics

Precise kinetic measurements require the catalyst to be in a reproducible state of activity, a state which must not be significantly altered by changes to reactant composition in order to determine the kinetics. Two types of experiment were therefore performed to anticipate possible problems. On a freshly activated sample of Pt/Al_2O_3, a series of 1 min pulses of H_2/n-butane (10:1) were passed at constant temperature (605 K); there was no significant difference in rate for the eight pulses, so the intervening H_2 periods are sufficient to keep the surface in a reproducibly clean state. Because our general experience leads us to expect that the reactivity of any 'coke' formed in the reaction periods will be even greater with propane and with ethane, and with $Pt\text{-}Re/Al_2O_3$ catalysts, the schedule of reaction and cleansing periods adopted should prove generally satisfactory. Secondly, pulses of H_2/n-butane were passed over a 'coked' Pt/Al_2O_3 sample at 609 K to see whether any coke was removed during the H_2 periods. Very constant rates were observed in eleven pulses showing that 'coke' deposited at high temperature is unreactive under normal reaction conditions.

The effects of H_2 and alkane partial pressures on rates were determined for both the Pt/Al_2O_3 and the $Pt\text{-}Re/Al_2O_3$ catalysts in the clean and the 'coked' conditions; only in the case of ethane and $Pt\text{-}Re/Al_2O_3$ did insufficient deactivation occur at 713 K, so that no results for this system are available. A selection of the results is shown in Figures 1 to 3, the curves being derived as explained below. Although many of the results in the literature are presented as a power rate law in which the H_2 exponent is negative [3], the rate must of course fall to zero at zero H_2 pressure, and the rate maximum has indeed been often observed, particularly by the Budapest group, using higher alkanes [6], since the H_2 pressure at the rate maximum appears to increase with the number of carbon atoms. Our results confirm that, with a fixed alkane pressure of 0.071 atm, the rate maxima occur at H_2 pressures of about 0.1 atm for ethane (Figure 2B), about 0.25 atm for propane (Figure 2A) and >0.3 atm for n-butane (Figure 1). Thus, in the last case, the orders in H_2 are sometimes positive over much or all of the pressure range covered (see Figure 1A, C and D). Orders in alkane are positive and only slightly less than unity in all cases (Figure 3).

Comparison of Figures 1A and B, and of 1C and D, demonstrate very clearly that coking markedly affects the rate dependences on H_2 pressure for both catalysts. For Pt/Al_2O_3, coking induces a distinct rate maximum at a H_2 pressure of $\sim$0.3 atm, while for $Pt\text{-}Re/Al_2O_3$ the curve becomes much flatter.

In general the rate measurements within each data set show a pleasing reproducibility. Occasionally there is some scatter in the first one or two points taken (see e.g. Figure 1A) and with ethane and propane on clean Pt/Al_2O_3 the points taken at H_2 pressures less than about 0.2 atm were notably less consistent than those taken at higher H_2 pressures. In the reaction of propane over 'coked' $Pt\text{-}Re/Al_2O_3$, use of a very low H_2 pressure (0.08 atm) gave a rate lower than expected and this additional deactivation was reflected in the next point at higher H_2 pressure. Only one point was struck out as being inexplicably at variance with the rest of the set.

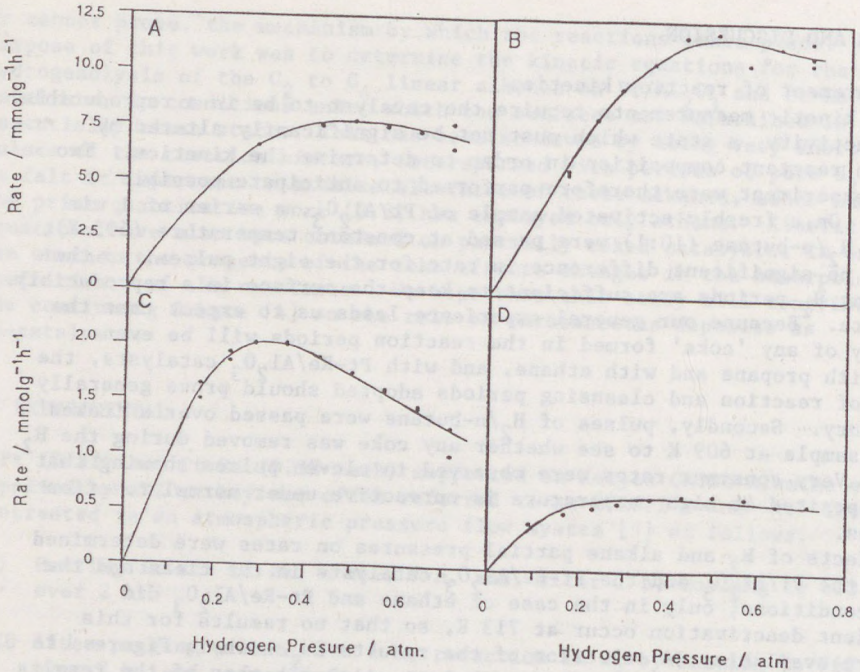

Figure 1. Dependence of rate upon H_2 pressure for n-butane hydrogenolysis: A, on clean Pt/Al_2O_3; B, on coked Pt/Al_2O_3; C, on clean $Pt\text{-}Re/Al_2O_3$; and D, on coked $Pt\text{-}Re/Al_2O_3$. The curves are calculated by equation ES2 using the constants in Table 1.

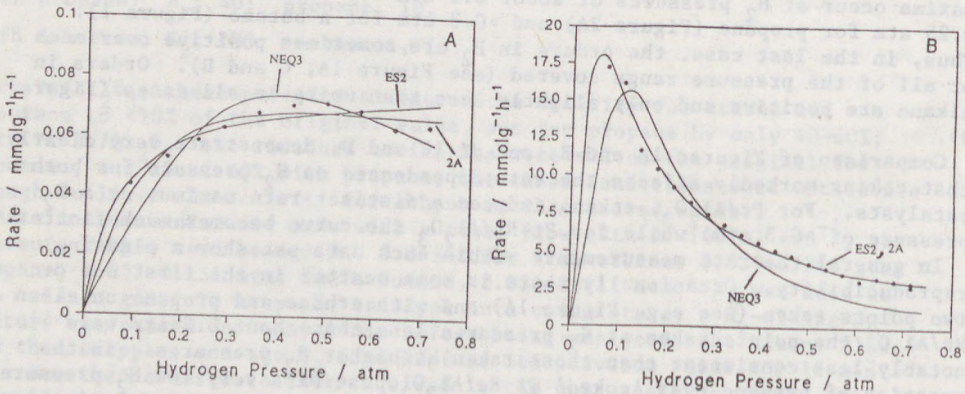

Figure 2. Dependence of rate upon H_2 pressure for: A, propane hydrogenolysis on coked Pt/Al_2O_3; and B, for ethane hydrogenolysis on clean $Pt\text{-}Re/Al_2O_3$. The curves are the optimum calculated for the indicated rate equations (see text).

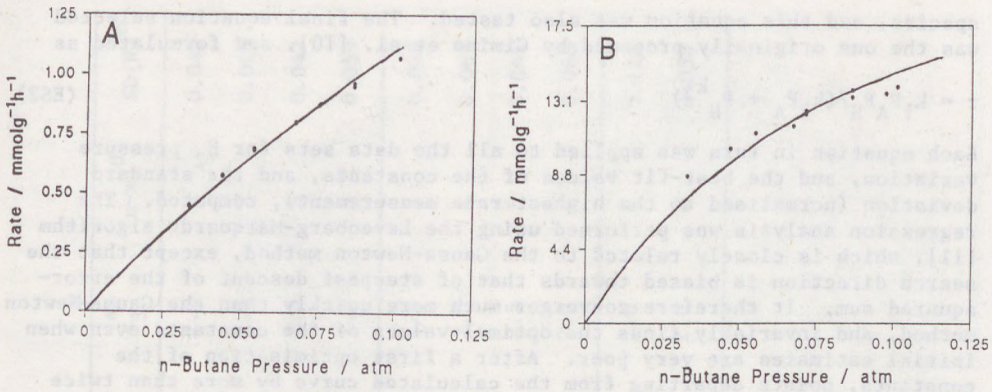

Figure 3. Dependence of rate upon alkane pressure: A, n-butane on coked Pt/Al_2O_3; B, n-butane on clean $Pt\text{-}Re/Al_2O_3$. Curves calculated using the constants in Table 1, save that k_1 is respectively 7.20 and 41.5.

3.2. Selection of rate equation

The kinetics and mechanism of alkane hydrogenolysis have been the subject of numerous studies, which are summarised in two recent reviews [2,3]. The consensus view is that the alkane molecule needs to suffer extensive dehydrogenation before the rate-limiting C-C bond breaking can occur, and that the reactive species cover only a small part of the surface. There is little else that is universally agreed. It is usually accepted [3] that for each system there is one uniquely reactive species, although in one study [7] of ethane hydrogenolysis both C_2H_5 and C_2H_2 were considered as intermediates in different ranges of H_2 pressure. Some groups of workers have taken the rate-limiting step to be either alkane chemisorption [8] or C_1 desorption as methane [9] or one of the dehydrogenation steps of adsorbed alkane [5], and many different rate equations have therefore been proposed [2], but few have been adequately tested for different alkanes and for different catalysts in various states of activity.

We have therefore selected three rate equations to test, making our choice on the basis that (i) the equation should be able to show a rate maximum as H_2 pressure is varied, (ii) that it should suggest an order in alkane of about unity, (iii) that it should contain not more than three variables, and (iv) that it should be of a simple form to facilitate non-linear regression analysis. The first equation chosen was similar to that proposed by Gudkov et al. [7], based on C_2H_2 as the reactive species:

$$r = k_1 P_A P_H^{\,2} / (P_A + k_2 P_H^{\,k_3})^2 \qquad (2A)$$

These authors took k_3 to be 2.5, but we decided to let its value float. Their mechanism was found to generate a family of equations of the form

$$r = k_1 P_A P_H^{\,k_3} / (P_A + k_2 P_H^{\,k_3+\frac{1}{2}})^2 \qquad (NEQ3)$$

where k_3 equals one-half the number of H atoms lost in forming the reactive

species, and this equation was also tested. The final equation selected was the one originally proposed by Cimino et al. [10], and formulated as

$$r = k_1 P_A P_H / (k_2 P_A + P_H^{k_3}) \qquad \text{(ES2)}$$

Each equation in turn was applied to all the data sets for H_2 pressure variation, and the best-fit values of the constants, and the standard deviation (normalised to the highest rate measurement), computed. The regression analysis was performed using the Levenberg-Marquardt algorithm [11], which is closely related to the Gauss-Newton method, except that the search direction is biased towards that of steepest descent of the error-squared sum. It therefore converges much more quickly than the Gauss-Newton method, and invariably finds the optimal values of the constants even when initial estimates are very poor. After a first optimisation of the constants, points departing from the calculated curve by more than twice the standard deviation were rejected, and the best-fit constants re-computed.

Inspection of the standard deviations showed clearly that (i) values obtained with equation NEQ3 were distinctly larger than those given by the others, and (ii) approximately equal values were given by equations 2A and ES2. These conclusions are supported by calculated curves shown in Figure 3. Equation NEQ3 has therefore been discarded, and of the other two the equation ES2 is preferred, because it derives from a definite (if not entirely credible) mechanism. This point will be developed later.

3.3. Significance of the constants in the rate equation

Table 1 lists the data sets under consideration, together with the standard deviations for the best fit curve, obtained with the listed constants. According to the derivation of equation ES2, k_3 is $(n-x)/2$ where n is the number of H atoms in the reactant alkane and x is the number of the reactive intermediate. Some of the k_3 values approximate well to whole or hemi-integers, and so fits were then computed with a fixed value of k_3, chosen as being the nearest whole or half-number to the value first obtained. Somewhat surprisingly, good fits were still obtained using the original k_2 values, although best fit values of k_1 were substantially altered. Normalised standard deviations were $<7 \times 10^{-2}$ in 9 of the 10 cases, values $<10^{-1}$ being taken as generally acceptable. For two of the entries (propane, Pt-Re/Al_2O_3, clean and coked), the rounded k_3 values quoted are not the nearest hemi-integers; the values were chosen to show that the standard deviation is not highly sensitive to the value of k_3 adopted. For the first entry, taking k_3 as 2.0 lowers SD(N) only to 0.036, and in the second case taking k_3 as 2.5 in fact raises SD(N) to 0.082.

Values of the various constants show some interesting regularities (Table 1). In the case of k_3, the number of H atoms lost in forming the reactive species appears to vary between three and five, although most of the values are either four or five. There is no marked variation in this number with alkane, so the kinetic differences (Figures 1 and 2) must find their origin elsewhere. Values of k_2 tend to decrease with increasing size of the alkane: n-butane, 1.2-4.3; propane, 0.3-1.5; and ethane, $\sim 4 \times 10^{-2}$. With n-butane, values for 'coked' catalysts are smaller than for clean; with propane this effect is not noticeable, but values for Pt-Re/Al_2O_3 are consistently smaller than for Pt/Al_2O_3. Values of k_1 follow the opposite trend, which encourages the speculation that the C_2H_x species are in fact more reactive than the corresponding C_3 and C_4 species, the rate for ethane being slower only because of their low concentration.

Table 1
Evaluation of the constants of equation ES2 by variation of H_2 pressure

Alkane	Catalyst	State	r/r_o [a]	N [b]	k_1	k_2	k_3	k_3^* [c]	(n-x) [d]	SD(N) [e]
$n\text{-}C_4H_{10}$	Pt	clean	-	7	30.5	3.52	2.07	2.0	4	0.045
"	"	coked	0.06	17	10.8	1.17	2.60	2.5	5	0.023
"	Pt-Re	clean	-	12	37.0	4.31	2.52	2.5	5	0.047
"	"	coked	0.006	10	0.55	1.57	1.30	1.5	3	0.059
C_3H_8	Pt	clean	-	10	10.5	0.40	2.67	2.5	5	0.049
"	"	coked	0.38	10	4.80	0.32	2.12	2.0	4	0.065
"	Pt-Re	clean	-	10	112	1.03	2.19	2.5	5	0.044
"	"	coked	0.57	10	62.0	1.49	2.37	2.0	4	0.068
C_2H_6	Pt	clean	-	25	410	0.039	1.91	2.0	4	0.120
"	Pt-Re	clean	-	20	582	0.052	1.99	2.0	4	0.058

[a] Rate divided by rate for clean catalyst at $A:H_2 = 1:10$

[b] Number of data points

[c] Rounded value of k_3

[d] Number of H atoms removed to form reactive species

[e] Normalised standard deviation

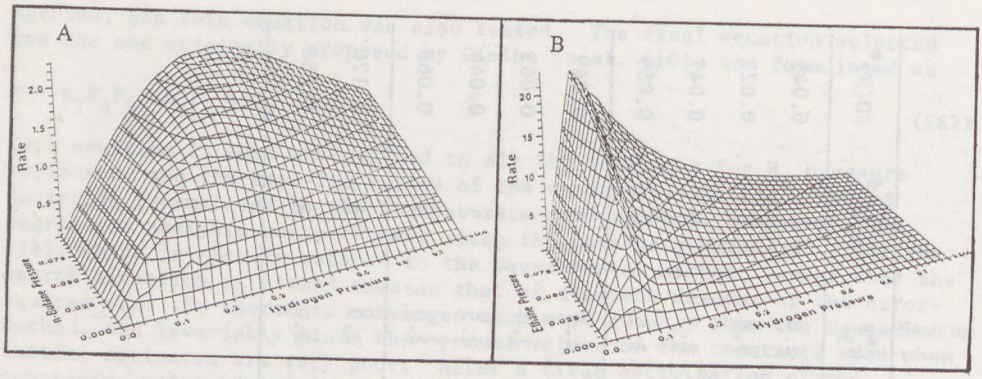

Figure 4. Calculated dependence of rate upon H_2 and alkane pressure: A, n-butane on coked Pt/Al_2O_3; B, ethane on clean $Pt-Re/Al_2O_3$. The curves were derived from equation ES2 using the constants given in Table 1.

However, while non-linear regression analysis of these results has led to best-fit constants, they did not always agree well with those derived from the corresponding H_2 pressure variations, and calculated curves were shown to be somewhat unresponsive to changes in their values. We therefore content ourselves by showing (Figure 3) that the values of 'best fit' values of k_2 and k_3 obtained from the results of H_2 pressure variation (Table 1) provide curves which are an acceptable fit to the experimental points. Values of k_1 have however been adjusted to accommodate slight changes in catalyst activity.

Having defined values for the three constants in equation ES2 for a particular system, it is possible to compute a three-dimensional rate surface to show what the rate should be at any given value of alkane and H_2 pressure. Examples of the results so obtained are shown in Figure 4. These plots are of value in visualizing trends in the predicted rate curves that may provide critical tests of the model, provided such tests can be conducted in an experimentally accessible region. Thus for example Figure 4A shows that for n-butane on clean Pt/Al_2O_3 the order in alkane should be accurately zero if very low H_2 pressures were used, and the locus of the rate maximum moves to higher H_2 pressures as the alkane pressure is raised. With ethane on the other hand the rate maximum is predicted always to occur at a H_2 pressure of 0.06 atm, irrespective of the ethane pressure, and the order in ethane should always be fractionally positive. The occurrence of a maximum in the dependence of rate on ethane pressure [7] would not therefore be consistent with the constants used in this calculation.

3.4. Summary and conclusions

This work demonstrates the difficulty of identifying a rate equation having general utility for alkane hydrogenolysis. While the simple equation ES2 appears to describe our kinetic results with a high accuracy, the mechanism on which it is derived is of the Eley-Rideal type, making no provision for the participation of chemisorbed H atoms. This is an

illogical omission, but the reaction scheme that generates equations 2A (with k_3 = 2.5) [7] and NEQ3 does indeed feature dissociatively adsorbed H_2, and the former at least fits our measurements quite well. Unfortunately this equation yields values of k_3 between one and two, and equation NEQ3 gives k_3 as generally less than 1.5, with moreover considerably worse fits. More complex rate expressions remain to be tested, but these often rest on uncertain specification of site requirements for forming the active species.

Thus although changes due to coking are qualitatively evident (Figure 1; but only for an alkane having the necessary structural complexity), their quantitative interpretation is still under consideration. We are hopeful that work in hand to determine rate responses to reactant pressures at different temperatures will lead us to a fully satisfactory rate expression, from which the effect of coking on the constants of the equation can be reliably deduced.

REFERENCES

1 G.C. Bond, Chem. Soc. Reviews, 20 (1991), to appear.
2 L. Guczi, A. Frennet and V. Ponec, Acta Chim. Hung., 112 (1983) 127.
3 S.A. Goddard, M.D. Amiridis, J.E. Rekoske, N. Cardona-Martinez and J.A. Dumesic, J. Catal., 117 (1989) 155.
4 G. Webb, Catal. Today, 7 (1990) 139.
5 G.C. Bond and M.R. Gelsthorpe, J. Chem. Soc. Faraday Trans. I, 85 (1989) 3767.
6 A. Sarkany, L. Guczi and P. Tetenyi, Acta Chim. Hung., 97 (1978) 221.
7 B.S. Gudkov, L. Guczi and P. Tetenyi, J. Catal., 74 (1982) 207.
8 A. Frennet, G. Lienard, A. Crucq and L. Degols, J. Catal., 53 (1978) 150.
9 J.R. Anderson and B.G. Baker, Proc. Roy. Soc. London, A271 (1963) 402.
10 A. Cimino, M. Boudart and H.S. Taylor, J. Phys. Chem., 58 (1954) 796.
11 E.H. Twizell, Numerical Methods, with Applications in the Biomedical Sciences, Ellis Horwood, Chichester, 1988.

DISCUSSION

Q: S. D. Jackson (United Kingdom)

1) Could the authors state either the weight of catalyst used in the experiments or the gas hourly space velocity (GHSV) ?

2) Even with so-called "clean" catalyst, the activity decreases over the first two-three pulses. Is it not likely that this is due to carbon deposition ? Therefore, are the authors really comparing catalysts with different levels of carbonaceous deposit and, possibly more importantly, with the deposits having different C/H ratios ? The amount of carbon deposited at either temperature could be determined by an oxygen treatment at the end of the experiment.

A: G. C. Bond

1) Catalyst weights were typically 0.2 g and GHSV values therefore about 5400 h^{-1}.

2) Although there was some slight instability in the catalysts during the first few reaction pulses, this was not always associated with a loss of activity: it sometimes increased in this phase, and we are reasonably confident that there is no progressive coke build-up with time, using this technique. Unfortunately (as I have stressed in answer to another question) the coke levels produced by our pretreatments are not the same for each alkane. With hindsight it would have been preferable to spend more time in defining conditions which would produce more equal coke contents. We have tried to estimate coke on used samples by TPO, but amounts are too small for accurate measurement. A rough calculation, assuming 100 % dispersion and a C/Pt ratio of unity, shows that 0.2 g catalyst would contain only about 0.5 mg carbon.

Q: H. Kluksdahl (USA)

Pt-Re-alumina catalysts typically require several days to overcome the excess hydrogenolysis observed in aromatization reactions using hexane or heptane as the feed, both for unsulfided and intentionally sulfided treatment. At the end of this time, the hydrogenolysis activity reaches a minimum and holds at this level for a considerable length of time. This suggests that the catalytic species have then reached a stable, equilibrated state. it is, therefore, surprising to see in your studies that the Pt-Re-alumina catalyst has leveled out in only two hours with no sulfiding treatment.

Did you undertake any additional steps to verify that your Pt-Re catalysts had completely leveled off for excess hydrogenolysis ?

A: G. C. Bond

I think you may have misunderstood the pretreatment which we gave to our catalysts before commencing kinetic experiments. Where we wished to use a "coked" surface, catalysts were treated (after calcination and reduction as described at the start of the Experimental section) with one or other of the alkanes for 2 h at 713 K at the specified H_2/alkane ratio. There is no certainty that this led to catalysts in a "steady state" of coking, but since this temperature was some 100 K higher than that used for the kinetic runs, we were confident there would be no loss of coke at the lower temperature, and so it proved.

Ideally we would have liked to use catalysts coked to about the same extent by each alkane, i.e. having about the same fractional loss of activity; but the very different tendencies of the alkanes used to deposit coke made this difficult, and we did not think it worthwhile to make an extended study of coke formation as a function of time, temperature and H_2/alkane ratio.

Q: D. Duprez (France)

How can you explain the significant differences in coke toxicity towards propane hydrogenolysis versus butane hydrogenolysis ?

A: G. C. Bond

It is not so much a case of the different toxicities of "coke" towards the hydrogenolysis of different alkanes as the various tendencies of the lower alkanes to form toxic deposits. We believe that "coke" formed under our conditions is mainly a highly dehydrogenated form of the parent alkane, rather than any kind of polymer: this is because the tendency to deactivation is roughly proportional to the number of carbon atoms in the alkane. Thus the toxicity depends on the number of single or multiple C-M bonds that can be formed; the greater this number, the greater will be the difficulty of re-hydrogenating the toxic species back to a more reactive form (see ref. 5 of the paper).

Q: S. L. Kiperman (Russia)

It is not clear from this interesting work which reaction mechanism corresponds to the kinetic equations obtained. As a rule the mechanism of the alkane hydrogenolysis is characterized by a fast step involving alkane dissociative adsorption, a slow decomposition of surface intermediates, followed by the quick hydrogenation of the decomposition products. From this point of view the hydrogen concentration is the nominator of the equation, which may be due to the pseudo-equilibrium of the decomposition products on the surface with hydrogen in the gas phase. But in this case, the powers in the nominator and the denominator of the kinetic equations should be quite definite. Therefore, it is of interest to which mechanism thus equations corresponding.

A: G. C. Bond

I believe that the text of the paper makes reasonably clear the connection between the rate equations we have tested and the mechanisms on which they are based. Equation 2A is based on the analysis by Gudkov et al. (Ref. 7 in the paper) where the reactive species is taken to be C_nH_{2n-2}; however rather than constraining k_3 to a value of 2.5 (as they did for ethane) we decided to treat it as an additional variable. However it seemed illogical to assume that only C_nH_{2n-2} and C_nH_{2n+1} species could react, and we therefore tested equation NEQ3, which is based on the same set of reaction steps, but makes no prior assumption about the number of H atoms lost in forming the reactive species. Equation ES2 is that of Cimino, Boudart and Taylor (Ref. 10 in the paper); their mechanism supposes that H_2 formed in dehydrogenation, the alkane is immediately returned to the gas phase, and that the bond-breaking step has Rideal-Eley character. Thus the existence of adsorbed H atom is not accommodated in this mechanism.

Q: J. W. Hightower (USA)

Have you had time to investigate the effect of temperature on the various constants in the kinetic equations ? If so, can you indicate the trends that are observed ?

A presume you took the usual precautions to assure that mass transfer was not limiting your activity. Is this correct ?

A: G. C. Bond

We have determined the response of rate to variation of H_2 pressure for each of the three alkanes at three different temperatures, and the results are still being analyzed. However, of the three rate equations used in our paper it is only ES2 which appears to give a sensible variation of the constants with temperature. One has to remember however that the constants are sometimes complex, i.e. they can be conflations of a number of equilibrium constants for successive desorption steps in the case of R_2. A modification of equation ES2 to allow a role for chemisorbed H atoms appears to represent a further improvement, although we have not yet found an equation which generates the same value for the enthalpy of adsorption of H_2 from the kinetic measurements for all three alkanes. I would regard this as the ultimate criterion for a kinetically "correct" equation.

Q: J. B. Butt (USA)

Was there any study in this work of the dependence of either hydrogenolysis rate or selectivity as a function of the amount of coke on the catalyst ?

A: G. C. Bond

No, we have not yet been able to determine kinetics as a function of amount of carbon deposited, although there is no reason in principle why such experiments should not be carried out. We now have sufficient experience to enable us to vary the carbon content in a systematic manner.

Q: Z. Paál (Hungary)

Do your equations or experiments predict a maximum also on clean Pt surfaces (where only the positive order branch was seen) or only in the presence of coke or Re, which are well-known to disrupt contiguous Pt sites ?

A: G. C. Bond

In principle the rate equations we have tested will all show maxima in the rate vs. H_2 pressure plot; the location of the maximum, and its sharpness, will depend on the values of the constants in the equation. Thus a certain combination of values can give a sharp maximum at low H_2 pressure; others will give a very broad maximum that is scarcely detectable up to H_2 pressure of 1 atm. The latter seems to be the situation with n-butane on clean Pt/Al_2O_3. We really need the facility to make rate measurements at H_2 pressures considerably higher than atmospheric in order to be certain whether a rate maximum exists or not.

Guczi, L. *et al.* (Editors), *New Frontiers in Catalysis*
Proceedings of the 10th International Congress on Catalysis, 19-24 July, 1992, Budapest, Hungary
© 1993 Elsevier Science Publishers B.V. All rights reserved

TOLUENE HYDROGENATION OVER SUPPORTED PLATINUM CATALYSTS

S.-D. Lin and M. A. Vannice

Department of Chemical Engineering, The Pennsylvania Sate University, University Park, PA 16802, USA

Abstract

The specific activity for toluene hydrogenation on supported Pt depended on the support utilized and followed the sequence: Pt/SiO_2-Al_2O_3 > Pt/TiO_2 > Pt/Al_2O_3 ≈ Pt/SiO_2. The activation energy was independent of the support and had an average value of 12 kcal/mol. The apparent reaction order on hydrogen was found to be independent of the support and increased from 0.7 at 333K to over unity at 373K, whereas the reaction order on toluene remained near zero over the same temperature range. These results are qualitatively similar to those found previously with supported Pd catalysts except that the turnover frequencies on Pt catalysts can be more than 30 times higher. A model proposed for Pd is also applicable to Pt catalysts, that is, the enhanced activity can be attributed to a reaction between spilled-over hydrogen and toluene adsorbed on the oxide surface in the metal-support interfacial region.

INTRODUCTION

Metal-support interactions have been found to cause significant changes in the activity for hydrogenation of aromatic compounds over supported palladium catalysts, as reported earlier for benzene, toluene, and xylene hydrogenation[1,2]. It was proposed in these studies that the acidic sites on the support material can act as additional adsorption sites for these aromatic compounds, and in the vicinity of Pd particles these adsorbed species can react with hydrogen spilled over from the metal, thus contributing to the overall activity[1]. To determine if similar behavior occurs with Pt catalysts, the hydrogenation of benzene and toluene over Pt dispersed on these same supports has been studied[3]. This paper reports the results for toluene hydrogenation.

EXPERIMENTAL

All the supported platinum catalysts, except for Pt/SiO_2, were prepared by an incipient wetness method using H_2PtCl_6 (Aldrich, 99.995+%) dissolved in doubly distilled, deionized water and the following support materials : η-Al_2O_3 (prepared by calcination of alumina ß-trihydrate at 873K, Exxon Research & Engineering Co., 245 m^2/g), SiO_2-Al_2O_3 (Davison grade 979, 13%Al_2O_3, 400 m^2/g) and TiO_2 (Degussa P25, 50 m^2/g)[4]. An ion exchange method was used for loading Pt on SiO_2 (Davison grade 57, 220 m^2/g). All the support materials were calcined in dry air at 773K for two hours before impregnation, and the impregnated catalyst powders were dried at 393K overnight and stored in a desiccator for later use. Actual metal loadings were measured by DC plasma emission spectroscopy. Catalyst pretreatments were carried out in situ prior to either adsorption or kinetic measurements. The Pt powder (Johnson Matthey, Puratronic, 99.999%), Pt/SiO_2 and Pt/Al_2O_3 catalysts were reduced at 723K under flowing H_2, then purged with He or evacuated at 698 K; the Pt/SiO_2-Al_2O_3 catalyst was reduced under flowing H_2 at three

different temperatures - 448, 673 and 723K - then either purged with He or evacuated; and Pt/TiO_2 was reduced using either a LTR step, which involved flowing H_2 at 473 K for 2 h followed by either flowing He or evacuation at 473K for another 2 h, or a HTR step, which involved flowing H_2 at 773K for 1 h followed by either flowing He or evacuation at 723 K for another hour. Detailed reduction procedures have been described elsewhere[5]. Irreversible hydrogen uptakes were used to calculate metal dispersions and they were determined by measuring two consecutive isotherms at 300K with a 30 min evacuation in between. The adsorption system has been described previously[6].

Vapor-phase kinetic studies were carried out in a differential, packed-bed microreactor system described earlier.[7] Typically, the reaction mixture of toluene (Aldrich, HPLC grade, 99.9+%) and H_2/He, flowing at atmospheric pressure with a total flowrate 47 sccm, was passed through a glass reactor containing 40-60 mg of the catalyst at reaction temperatures between 333-373K. A bracketing technique in pure H_2 was used to minimize deactivation[7]; however, loss of activity with time on-stream was still observed in some cases. The reactor effluent was analyzed by a Hewlett-Packard gas chromatograph (HP-700 with TCD detector) equipped with a Carbowax 20M column. Conversions were typically below 12% and tests for mass transfer limitation showed this artifact to be absent. The partial pressure dependency on toluene was determined at a constant P_{H2} of 685 torr, while the dependency on H_2 was measured at a constant P_{Tol} of 50 torr.

RESULTS

Results from the H_2 chemisorption experiments with the freshly reduced Pt catalysts are shown in Table 1. All the catalysts have high dispersion, as defined by the H_{ad}/Pt ratio for irreversible hydrogen adsorption. With the Pt/SiO_2-Al_2O_3 samples, increasing the reduction temperature decreased the H_2 uptake, which implies that higher reduction temperatures caused the Pt particles to sinter; however, the much lower uptakes on the (HTR) Pt/TiO_2 samples cannot

Table 1
Irreversible H_2 Uptakes and Kinetics of Toluene Hydrogenation on Supported Pt
(P_{Tol} = 50 torr, P_{H_2} = 680 torr)

Catalyst	H/Pt	r_0[(a)] (μmol/s/g cat)	E_A (kcal/mol)	Activity @333 K	
				μmol/g cat/s	TOF (s^{-1})
0.96%Pt/SiO_2	0.96	6.8×10^6	10.3 ± 1.0	1.27	0.027
0.78%Pt/Al_2O_3-I	1.03	1.6×10^8	12.2 ± 2.1	1.48	0.037
0.78%Pt/Al_2O_3-II	1.03	2.0×10^9	14.2 ± 1.5	0.95	0.024
0.24%Pt/SiO_2-Al_2O_3 (448K)	0.90	9.9×10^6	11.0 ± 1.1	0.58	0.052
0.24%Pt/SiO_2-Al_2O3 (448K)	0.90	1.3×10^7	11.2 ± 2.1	0.56	0.051
0.24%Pt/SiO_2-Al_2O_3 (673K)	0.58	8.1×10^6	10.9 ± 2.1	0.59	0.082
0.24%Pt/SiO_2-Al_2O_3 (723K)	0.44	9.9×10^6	11.0 ± 1.4	0.60	0.112
0.95%Pt/TiO_2 (LTR)	0.73	7.9×10^8	12.9 ± 1.7	2.77	0.078
0.95%Pt/TiO_2 (HTR)	0.02	3.9×10^8	14.4 ± 3.1	1.34	---
0.09%Pt/TiO_2 (LTR)-I	0.80	5.2×10^7	13.9 ± 3.1	0.041	0.011
0.09%Pt/TiO_2 (LTR)-I[(b)]	0.80	2.2×10^7	12.7 ± 1.9	0.099	0.027
0.09%Pt/TiO_2 (LTR)-II	0.80	4.7×10^5	10.6 ± 4.2	0.052	0.014
0.09%Pt/TiO_2 (HTR)	~0	2.4×10^5	10.3 ± 2.8	0.042	---

(a) r_0 is defined as $r=r_0\exp(E_A/RT)$ at standard reaction conditions.
(b) Catalyst rereduced between runs, all other data obtained with a bracketing technique.

be attributed to sintering because numerous studies have shown that the SMSI state induced during the HTR steps decreases H_2 chemisorption by forming a TiO_x overlayer on the Pt rather than by sintering[8].

The activity and activation energies of these Pt catalysts are also listed in Table 1. The activity of the Pt powder could not be accurately recorded because of its rapid deactivation. Generally speaking, the specific activity, i.e., the turnover frequency, follows the sequence: Pt/SiO_2-Al_2O_3 > Pt/TiO_2 > Pt/Al_2O_3 ≈ Pt/SiO_2, thus it shows a trend similar to that found with supported Pd catalysts[2]. The specific activity of Pt/SiO_2 and Pt/Al_2O_3 agrees reasonably well with the limited literature data in Table 2 which could be expressed as TOF values; the exceptionally high TOF's found with the nonsteady-state pulse experiments in Table 2 are very likely a consequence of the difficulties associated with this technique when applied to a zero-order reaction[9,10], and the low activation energies, which are about one half the E_A values found in Table 1, are almost certainly due to pore diffusion effects. A reversible maximum activity at approximately 463K was observed in one run with Pt/Al_2O_3 over a wide temperature range[3]. The reduction temperature had little effect on the activity of the Pt/SiO_2-Al_2O_3 samples on a gram basis, but since the dispersion changed with the reduction temperature, the apparent turnover frequency is somewhat higher after the highest reduction temperature. As for the Pt/TiO_2 catalyst, the HTR sample had a lower activity than the LTR sample; this is consistent with the general understanding that the SMSI state lowers the catalytic activity for most hydrogenation reactions due to coverage of the Pt surface sites by TiO_x[11]. The lower activity of the 0.09% Pt/TiO_2 catalyst, compared to the 0.95% Pt/TiO_2 catalyst, is attributed to deactivation that occurred during reaction since the measured activity of different samples scattered noticeably; however, it could also be due to a more complete coverage of the smaller amount of Pt by TiO_x species. This deactivation problem was also observed in runs with other catalysts, but its influence was minor. The activation energy does not seem to be affected by either the type of support or the reduction temperature, and the average value is approximately 12±2 kcal/mol, which is the same as that found for Pd catalysts[2].

Table 2
Previous Results for Toluene Hydrogenation over Pt Catalysts

Catalyst	Test Conditions			E_A (kcal/mol)	TOF (s^{-1})	TOF @333K (s^{-1})	Ref
	T (K)	P_{H_2} (torr)	P_T (torr)				
6.3%Pt/SiO_2	298	755	5	--	0.010	0.062	20
5%Pt/SiO_2	378	--	--	6.0	6.8[a]	2.31	21
5%Pt/Al_2O_3	378	--	--	6.0	7.5[a]	2.55	21
1%Pt/Al_2O_3	323	744	16	~9.5	0.009	0.015	22
10%Pt/Glass	340	703	57	17.5	0.013	0.007	23
Pt/MgO(100)[b]	475	750	7	11.0	3	0.03	24
Pt/Al_2O_3(1T02)[b]	466	750	7	--	2-12	0.02-0.12	24
1.68%Pt/NaY	373	--	--	12.0	--	--	25
Pt-Cu/NaY	373	--	--	16.0	--	--	25

(a) Pulse reactor.
(b) Pt sputtered on oxide surface.

The results of the partial pressure dependence studies with these Pt catalysts are shown in Figure 1, where the error bars represent 95% confidence limits of the regressed reaction orders. Considering all the Pt catalysts as a group, the reaction order on H_2 increases from 0.7

at 333K to over 1.0 at 373K, whereas the reaction order on toluene is near zero at 333K and increases only slightly up to 373K. Typical data sets from which these dependencies were obtained are shown in Figure 2 for Pt/Al_2O_3. The slight deactivation mentioned previously can also be observed in Figure 2 as it shows that after a sequence of decreasing and increasing the H_2 or toluene partial pressure, the activity was reduced slightly. The partial pressure dependencies associated only with the sites on the SiO_2-Al_2O_3 surface are shown in Figure 3. They were obtained by subtracting the contribution in Figure 2 from similar data for Pt/SiO_2-Al_2O_3.

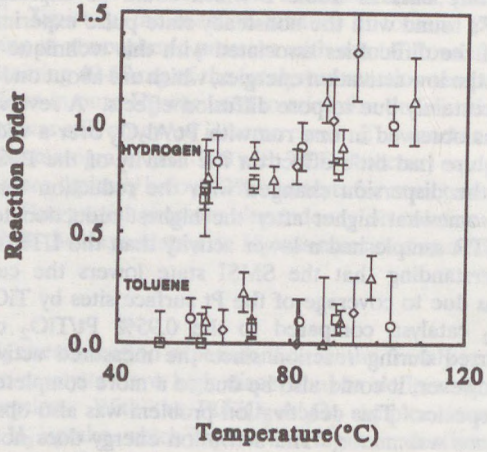

Figure 1. Dependence of Toluene Hydrogenation Reaction Orders on Temperature

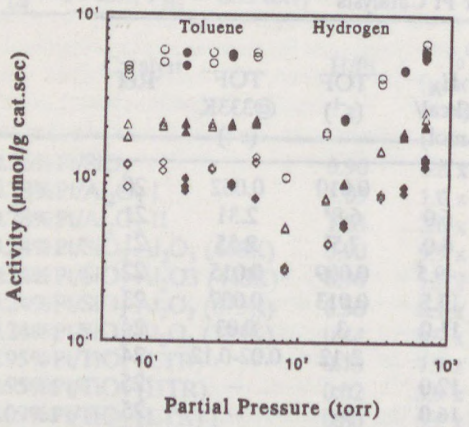

Figure 2. Partial Pressure Dependencies for Toluene Hydrogenation over Pt/Al_2O_3 at 333K (◇, ◆), 344K (△, ▲) and 363K (○, ●); Open symbols — descending P, Closed symbols — ascending P.

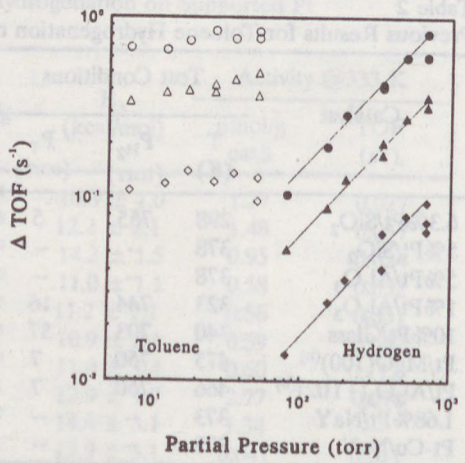

Figure 3. Apparent Partial Pressure Dependencies for Toluene Hydrogenation on Sites on the SiO_2-Al_2O_3 Surface: 333K (◇, ◆), 344K (△, ▲) and 363K (○, ●).

DISCUSSION

Based on LEED studies[12] and the out-of-plane C-H stretching band observed in EELS spectra[13], toluene is assumed to adsorb on Pt surfaces in a π-bonded mode, like benzene. Monolayer coverage on Pt (1-2 molecule/nm^2 or Bz/Pt_s=0.08-0.17) and the work function change at this saturation coverage have been found to be similar for both compounds[12,13], although toluene is considered to adsorb more strongly than benzene[13]. TPD studies have shown that most of the irreversibly adsorbed toluene dehydrogenates during desorption[13-15], thus possibly leaving behind carbonaceous species on the surface. A dissociated adspecies with a structure of $C_6H_5CH_2$ was proposed by Tsai and Muetterties based on their TPD study of deuterated toluene on Pt(111)[14] and Pt(100)[16]. No studies of deuterium-toluene exchange on Pt surface have been found in the literature, but the results for p-xylene on Pt/Al_2O_3, Pt/SiO_2, and a Pt film suggest that the protons on the ring are more capable of exchange with deuterium than the protons in the side group[17,18]; consequently, this indicates that the protons on the ring interact more directly with the metal surface because the bond strength in the methyl side group (88 kcal/mol) is weaker than that for the H atoms attached to the aromatic ring (111 kcal/mol for C_6H_6)[19].

Toluene hydrogenation has been studied less often than benzene hydrogenation and only a few investigations have involved Pt catalysts; Table 2 tabulates the results reported for Pt catalysts[20-25]. Pt catalysts have much higher specific activities than comparable Pd catalysts, as shown in Table 3. Although the influence of the support on the activity of Pt could not be determined from these earlier investigations, it could be observed in this study. Pt catalysts have an average activation energy of 12±2 kcal/mol for toluene hydrogenation, which is similar to that for Pd catalysts[2], and it does not depend on the support. For a given support the apparent TOF on Pt can be almost 40-fold higher, as shown in Table 3, and the average value on Pt, unaffected

Table 3
Rates of Toluene Hydrogenation over Pt and Pd (P_{Tol} = 50 torr, P_{H_2} = 680 torr)

Catalyst	T_{red} (K)	Activity at 373K[a]		Activity Ratio (Pt/Pd)
		TOF (s^{-1})	μmol/s/g cat	
0.96% Pt/SiO_2	723	0.143	6.73	10.7
2.67% Pd/SiO_2	673	0.004	0.63	
0.78% Pt/Al_2O_3	723	0.240	9.45	38.6
0.5% Pd/Al_2O_3	673	0.009	0.24	
0.24% Pt/SiO_2-Al_2O_3	448	0.313	3.46	2.4
1.1% Pd/SiO_2-Al_2O_3	448	0.041	1.44	
0.24% Pt/SiO_2-Al_2O_3	673	0.480	3.45	16.4
1.1% Pd/SiO_2-Al_2O_3	673	0.008	0.21	17.1
0.24% Pt/SiO_2-Al_2O_3	723	0.666	3.59	
0.95% Pt/TiO_2 (LTR)	473	0.631	22.42	9.5
1.1% Pd/TiO_2 (LTR)	448	0.040	2.37	
0.95% Pt/TiO_2 (HTR)	773	0.389[b]	13.80	32.1
1.1% Pd/TiO_2 (HTR)	673	0.020	0.43	

(a) Calculated using the activities and activation energies in this study and references 1-3.
(b) TOF based on the H/Pt value of the Pt/TiO_2 sample reduced at 473K.

by the support, is 27 times that on Pd, as indicated in Table 4. The specific activity of Pt is less dependent on the support than Pd, which can be rationalized by the higher turnover frequencies on Pt because the contribution from the support relative to the overall activity becomes smaller as the metal becomes more active. The SiO_2-Al_2O_3- and TiO_2-supported catalysts have the highest activity, which is as much as four times greater than that on Pt/SiO_2 and Pt/Al_2O_3, and this coincides with the findings for Pd catalysts[2].

The addition of a methyl group to the aromatic ring has been found to decrease the catalytic activity over supported Pt[22,23,26],Pd[2,22], Rh and Co[27]. Compared to the activity of these same Pt catalysts for benzene hydrogenation[28], the activity for toluene is approximately 1/4 to 1/2 that for benzene[3,28]. This activity ratio is somewhat lower than that for Pd catalysts, in which the toluene activity was found to be approximately 40-80% of the benzene activity[1,2], but it is close to the average activity ratio reported for other Pt catalysts[22,23]. On the other hand, the adsorption strength on a metal surface has been found to increase with an increase in the number of methyl groups; this is usually rationalized by a stronger donation from the π-electron cloud to the metal surface since the methyl group increases the ring electron density[12-14]. An analogous explanation has been made for adsorption on an oxide surface as the addition of a methyl group increases the adsorption strength[29]. For a near zero-order reaction like benzene or toluene hydrogenation, the adsorption constant of benzene or toluene (i.e., the adsorption strength) is not a significant parameter in a Langmuir-Hinshelwood rate expression because it cancels out; therefore, if the adsorption strength makes an important contribution, it must be in the intrinsic rate constant. Although this could lead to an implication that an increase

Table 4
Toluene Hydrogenation Activity Associated with the Support Surface (T = 373K)

	Pd Catalysts		Pt Catalysts		Activity Ratio (Pt/Pd)
	TOF (s^{-1} x 10^3)	molec. / $s \cdot cm^2$ x 10^{-10}(b)	TOF (s^{-1} x 10^3) Tol	molec. / $s \cdot cm^2$ x 10^{-10}(b)	
Metal(a)	7		192		27.4
Oxide Support					
SiO_2-Al_2O_3 (448K red)	34	17	122	20	1.2
SiO_2-Al_2O_3 (673K red)	1	0.4	288	28	70.2
SiO_2-Al_2O_3 (723K red)	--	--	475	39	2.2(c)
TiO_2 (448K red)	33	235	--	--	--
TiO_2 (473K red)	--	--	440	1945	8.3
TiO_2 (673K red)	13	34	--	--	--
TiO_2 (773K red)	--	--	197(d)	838	24.7

(a) Metal activity represents the average of SiO_2- and Al_2O_3-supported catalysts.
(b) Oxide activity was calculated by the difference between the overall TOF and this average metal activity. The activity per cm^2 was estimated by first calculating the activity per gram oxide and then dividing by the difference between the total surface area and the metal surface area.
(c) Based on the activity of Pd/SiO_2-Al_2O_3 reduced at 448K.
(d) Based on the H/Pt value of the sample reduced at 473K.

in the adsorption interaction decreases the intrinsic rate constant, it may not be true because a simultaneous surface decomposition reaction can play an important role in the overall mechanism[30,31]. The deactivation observed for some supported Pt catalysts could be a consequence of this surface decomposition reaction to produce hydrogen-deficient surface species.

The similar trend in activity with respect to the type of support suggests that the model previously proposed for Pd catalysts may be applicable to supported Pt catalysts; that is, the metal-support interfacial region can act as an additional region of activity by adsorbing toluene on acid sites on the oxide surface and allowing it to react with hydrogen via a spillover process[1,2,32]. Toluene also adsorbs on oxides via a π-interaction with coordinatively unsaturated cations at the dehydroxylated surface and with acidic surface hydroxyl groups[33-35]. It is also assumed that this adsorption occurs with the ring parallel to the surface[34], and monolayer coverages during physisorption are similar to that on a Pt surface, i.e., 1-2 molecule/nm^2[29,34]. An application of the Kelvin equation indicates that pore condensation probably occurred under the conditions used in these previous adsorption studies, with the exception of one isotherm measured at 423K by Talu et al.[36]. If a surface area of 400 m^2/g is assumed for the silicalite they used, the surface coverage at 423K was approximately 0.4 molecule/nm^2. Toluene adsorption on oxide surfaces is weaker than that on Pt surfaces as a prolonged evacuation at room temperature can remove almost all of the adsorbed toluene[35]. However, the reported heat of adsorption of toluene on a H-ZSM5 zeolite at 300K is about 15-20 kcal/mol[29,37], which is higher than its latent heat of condensation and indicates that toluene chemisorption can occur on acidic oxide surfaces. These recent studies show that toulene can adsorb on oxide surfaces under the reaction conditions used in this study. Spilled-over hydrogen on SiO_2 and Al_2O_3 surfaces has been found to be active for benzene hydrogenation[38,39]; consequently, it is expected that adsorbed toluene can also react with spilled-over hydrogen. As the concentration of hydrogen on the support surface should be highest in the vicinity of the metal particles, the metal-support interfacial region could contribute to the overall activity if the concentration of adsorption sites for toluene is high enough and the hydrogen transport rate is sufficiently rapid.

Following the argument in the model previously proposed[1,2], the overall activity can be separated into that from the metal surface and that from the interfacial region. If it is presumed that the activity of the Pt/SiO_2 and Pt/Al_2O_3 catalysts represents only that on the Pt surface, then the relative contributions from the interfacial region for the Pt/TiO_2 (LTR) and Pt/SiO_2-Al_2O_3 samples can be estimated by subtracting the average TOF value of the former two catalysts from the overall TOF's from the latter catalysts. This calculation indicates that approximately 70% of the overall activity can be attributed to the interfacial region[3]. This relative activity enhancement is significant but it is lower than that found during benzene hydrogenation over these Pt catalysts[3,28] and it is much lower than that obtained for benzene and toluene hydrogenation over Pd catalysts[1,2]. The pure TiO_2 and SiO_2-Al_2O_3 supports were found to be inactive for this reaction[2]; consequently, some type of synergistic metal-support interaction, such as that proposed in these two earlier studies, must be invoked to explain the activity enhancement.

The difference in reactivity among different support materials is expected to be related to the number of adsorption sites on the oxide surface, and it may also reflect the strength of the interaction between the oxide and the toluene. Toluene can interact with acid sites on the oxide through the π-electron cloud, and an acid-catalyzed hydrogenation mechanism for benzene in the liquid phase has been described by Wristers[40]; consequently, a similar heterogeneous pathway on strong acid sites should be possible provided activated hydrogen is available. This can qualitatively explain how a higher overall activity can be induced when Pt or Pd is dispersed on a more acidic support such as SiO_2-Al_2O_3 or TiO_2. If this proposed reaction model is correct, acid strength should be a key factor for high activity catalysts as well as the acid site density.

The consequences of the pretreatment on the more acidic catalysts like Pt/TiO_2 and Pt/SiO_2-Al_2O_3 are not unambiguous in this study. A high-temperature reduction (HTR) of the

Pt/TiO_2 catalyst causes the TiO_2 to migrate over the Pt surface and markedly decrease the chemisorption capacity at 300K; however, the activity (per gram metal) is decreased by only 50%. The migration of TiO_x occurs to a much lesser degree in the LTR sample, as implied by the chemisorption results. One can again infer that some of the activity may not be directly associated with the exposed Pt surface. Similar behavior occurred for benzene hydrogenation over supported Pt catalysts[3,28], and the activity ratios between the HTR and LTR samples are similar in both reactions. It is interesting to note that the HTR sample is still able to provide spilled-over hydrogen to the oxide surface even though the Pt surface is almost completely covered by a TiO_x overlayer, as shown by the measurable hydrogenation activity of 0.09% Pt/TiO_2 (HTR) in Table 2 and its almost zero irreversible H_2 uptake in Table 1. As for the Pt/SiO_2-Al_2O_3 samples, the higher the pretreatment temperature the lower the irreversible (as well as reversible) hydrogen uptake found, as shown in Table 1. This effect was also observed with Pd/SiO_2-Al_2O_3 catalysts but, in contrast to the almost constant per gram activity of the Pt/SiO_2-Al_2O_3 catalysts, the Pd/SiO_2-Al_2O_3 sample reduced at 673K was found to have an order of magnitude lower activity per gram. This was attributed to a decrease in the number of Brönsted acid sites, which were proposed to be the additional adsorption sites[1]. The reason for this difference is not known at this time. One possible explanation might be that a deactivation process occurs similar to that found with benzene hydrogenation over supported Pt catalysts[28].

The apparent reaction order on hydrogen in Figure 1 increases with temperature, while that of toluene remains almost constant. The near zero-order dependence on toluene agrees well with the general understanding that the surface coverage of toluene is high. The type of support does not seem to have a significant effect on the reaction orders, which suggests that the slow step for hydrogen addition to the ring may be similar for all these supported catalysts. This temperature-dependent reaction order on H_2 was not found for benzene hydrogenation over these Pt catalysts in the temperature range from 315 to 355 K[3,28], but it has been reported for both hydrogen and the aromatic compound during benzene and toluene hydrogenation over a NiKY zeolite catalyst between 403 and 523K[41]. A previous study of benzene hydrogenation over Pd catalysts also found an increase in H_2 reaction order from 0.5 to nearly 4 as the temperature increased from 353 to 573K, and it reported an almost constant, near-zero reaction order on benzene between 350 and 450K, but which increased at higher temperature[1]. It was proposed that this temperature-dependent reaction order was due to a surface decomposition reaction occurring concurrently with hydrogenation which put hydrogen-deficient species on the metal surface[30]. We observed serious deactivation during benzene hydrogenation over these Pt catalysts, and we found that the toluene reaction also suffers from some deactivation, especially on Pt powder; thus it is very possible that surface decomposition to give H-deficient aromatic species plays an important role in the overall reaction sequence and induces such a temperature dependency.

An activity comparison between Pt and Pd dispersed on different supports is shown in Table 3; Pt catalysts are obviously more active than the comparable Pd catalysts and the ratio of the relative TOF values ranges from about 2 to nearly 40. Based on the proposed model, the overall activity can be decomposed into two contributions -- that from the metal surface and that from the oxide surface in the interfacial region, as shown by the results in Table 4 which were calculated from the data in Table 3. The TOF on the Pt surface is 27 times that on Pd surface under these conditions. No obvious trend was found for the activity attributed to the oxide surface other than that the activity in the presence of Pt was usually significantly higher. The differences in the activities between Pt/SiO_2-Al_2O_3 and Pt/Al_2O_3 under similar partial pressure conditions were calculated. This difference is attributed to the contribution from the support surface. Although both catalysts showed a temperature-dependent H_2 reaction order, the oxide had a nearly temperature-independent order of 0.9 which is close to the first-order dependence found for the comparable Pd catalysts[2]. Although a mechanism assuming hydrogen adsorption as the rate limiting step would also provide a rate equation with a first-order dependence on

hydrogen, this is not considered likely because the reaction order on toluene would be negative if strong toluene adsorption on the surface is assumed, i.e., $r=kP_{H_2}\theta_V=kP_{H_2}/(K_TP_T)$ where θ_V represents vacant sites. We have found two Langmuir-Hinshelwood type models that can fit these data: the first model invokes dissociative, noncompetitive hydrogen adsorption on the oxide surface, and the second model invokes a mobile surface hydrogen species and adsorption of toluene on an acidic site. These are similar to previous models[30,31].

No individual physical constants could be abstracted from the linearized plotting of the second model, but the chemistry proposed involves a reaction between a mobile surface hydrogen species and a surface carbonium ion formed by the adsorption of toluene on an acidic hydroxyl group. The equilibrium adsorption constants calculated from the linearized plotting of the first model are consistent with physical criteria to evaluate them, that is, they give an exthothermic heat of adsorption and an entropy loss during adsorption[42,43]. The heats of adsorption for toluene and hydrogen on SiO_2-Al_2O_3 calculated from this model turn out to be 13 and 8 kcal/mol, respectively. This value for toluene is close to the range of 15-20 kcal/mol reported on zeolites[29,37], and the low value for hydrogen is not surprising because hydrogen spillover has high mobility on oxide surfaces[44]. This low heat of adsorption for hydrogen is also consistent with the model first proposed by Aben et al. in which only weakly adsorbed hydrogen participates in benzene hydrogenation over Group VIII metals[45,46]. The entropies of adsorption for toluene and H_2 were -13 and -12 entropy units, respectively. The activity of Pt/Al_2O_3 was fitted to the rate equation for the first model, i.e., $r=kK_TK_{H_2}P_TP_{H_2}/\left(1+K_TP_T\right)\left(1+K_{H_2}^{1/2}P_{H_2}^{1/2}\right)$, and ΔH_{ad} values of -7 and -16 kcal/mole were obtained for toluene and H_2, respectively, while ΔS_{ad} values were -3 and -8 e.u., respectively. The ΔH_{ad} value for toluene seems low whereas the value for H_2 is very close to integral ΔH_{ad} values[47]. It is very possible that these values are affected by surface inhibition caused by concurrent surface decomposition reaction to provide H-deficient species[30].

REFERENCES

1. Chou, P. and Vannice, M.A., J. Catal. **107**, 129 (1987).
2. Rahaman, M.V. and Vannice, M.A., J. Catal. **127**, 251 (1991).
3. Lin, S.D., Ph.D Thesis, The Pennsylvania State University, (1992).
4. Palmer, M.B., Jr. and Vannice, M.A., J. Chem. Tech. Biotech. **30**, 205 (1980).
5. Vannice, M.A., Hasselbring, L.C., and Sen, B., J. Catal. **95**, 57 (1985).
6. Vannice, M.A., Wang, S.-Y., and Moon, S.H., J. Catal. **71**, 152 (1981).
7. Sen, B. and Vannice, M.A., J. Catal. **113**, 52 (1988).
8. Baker, R.T.K., Prestridge, E.B., and Garten, R.L., J. Catal. **56**, 390 (1979); **59**, 293 (1979).
9. Vannice, M.A. and Neikam, W.C., J. Catal. **23**, 401 (1971).
10. Moffet, A.J., J. Catal. **27**, 456 (1972).
11. Haller, G.L. and Resasco, D.E., Adv. Catal. **36**, 173 (1989).
12. Gland, J.L. and Somorjai, G.A., Surf. Sci. **41**, 387 (1974).
13. Abon, M., Bertolini, J.C., Billy, J., Massardier, J., and Tardy, B., Surf. Sci. **162**, 395 (1985).
14. Tsai, M.-C. and Muetterties, E.L., J. Am. Chem. Soc. **104**, 2534 (1982).
15. Abon, M., Bertolini, J.C., Billy, J., Tardy, B., Tri, T.M., Massardier, J., and Gallezot, P., Bull. Soc. Chim. Fr. **25**, 321 (1985).
16. Tsai, M.-C. and Muetterties, E.L., J. Phys. Chem. **86**, 5067 (1982).
17. Hightower, J.W. and Kemball, C., J. Catal. **4**, 363 (1965).
18. Harper, R.J. and Kemball, C., 3rd. Int. Cong. Catal. Vol.2, 1145 (1965).
19. CRC Handbook of Chemistry and Physics, 71st Ed., D.R. Lide Editor, 1990-1991.
20. Bond, G.C., Garin, F., and Maire, G., Appl. Catal. **41**, 313 (1988).
21. Orozco, J.M. and Webb, G., Appl. Catal. **6**, 67 (1983).

22. Gomez, R., Del Angel, G., Damian, C., and Corro, G., React. Kinet. Catal. Lett. **11**(2), 137 (1979).
23. Lietz, G. and Völter, J., J. Catal. **45**, 121 (1976).
24. Rabette, P., Deane, A.M., Tench, A.J., and Che, M., Chem. Phys. Lett. **60**(2), 348 (1979).
25. Bandiera, J. and Meriaudeau, P., React. Kinet. Catal. Lett. **37**, 373 (1988).
26. Aramendia, M.A., Borau, V., Jimenez, C., and Marinas, J.M., Rev. Roum. Chim. **33**, 17 (1988).
27. Völter, J., Hermann, M., and Heise, K., J. Catal. **12**, 307 (1968).
28. Lin, S.D. and Vannice, M.A., To be published.
29. Pope, C.G., J. Phys. Chem. **90**, 835 (1986).
30. Chou, P. and Vannice, M.A., J. Catal. **107**, 140 (1987).
31. Rahaman, M.V. and Vannice, M.A., J. Catal. **127**, 267 (1991).
32. Boudart, M., Vannice, M.A., and Benson, J.E., Z. Physik. Chem. N.F. **64**, 171 (1969).
33. Davydov, A.A., Mater. Chem. Phys. **19**, 97 (1988).
34. Nagao, M. and Suda, Y., Langmuir **5**, 42 (1989).
35. Farneth, W.E., Roe, D.C., Gricus Kofke, T.J., Tabak, C.J., and Gorte, R.J., Langmuir **4**, 152 (1988).
36. Talu, O., Guo, C.-J., and Hayhurst, D.T., J. Phys Chem. **93**, 7294 (1989).
37. Pope, C.G., J. Phys. Chem. **88**, 6312 (1984).
38. Lacroix, M., Pajonk, G.M., and Teichner, S.J., Bull. Soc. Chim. Fr. **21**, 265 (1981).
39. Antonucci, P., Truong, N., Giordano, N., and Maggiore, R., J. Catal. **75**, 140 (1982).
40. Wristers, J., J. Am. Chem. Soc. **97**, 4312 (1976); **99**, 5056 (1977).
41. Coughlan, B. and Keane, M.A., Catal. Lett. **5**, 101 (1990).
42. Boudart, M., Mears, D.E., and Vannice, M.A., Ind. Chim. Belg. **32**, 281 (1967).
43. Vannice, M.A., Hyun, S.H., Kalpakci, B., and Liauh, W.C., J. Catal. **56**, 358 (1979).
44. Conner, W.C., Jr., Pajonk, G.M., and Teichner, S.J., Adv. Catal. **34**, 1 (1986).
45. Aben, P.C., van der Eijk, J. and Oelderik, J.M., 5th Int. Cong. Catal., p. 717 (1972).
46. Marécot, P., Paraiso, E., Dumas, J.M. and Barbier, J. Appl. Catal. **74**, 261 (1991).
47. Sen, B., Chou, P. and Vannice, M.A., J. Catal. **101**, 517 (1986).

ACKNOWLEDGMENT

This research was sponsored by the Department of Energy, Office of Basic Energy Sciences (Grant No. DE-FG02-84ER13276).

DISCUSSION

Q: J.-M. Herrmann (France)

You invoke in your work the occurrence of hydrogen spillover to account for toluene hydrogenation around 333 K. We put in evidence hydrogen spillover in hydrogen-involving photocatalytic reactions carried out at 300 K (alcohol dehydrogenation and alkane-deuterium isotopic exchange). In our case the active phase is the support surrounding metal particles. Concerning your system, do you have any idea about the area of the support which is involved in your catalytic scheme ?

Have you carried out the same experiments on the same catalyst, e.g. Pt/TiO_2 but with changing the content and/or the dispersion of the metal in order to change the metal-support interface. Thus, by varying the fraction of support involved in the reaction through hydrogen spillover, one would be able to determine the percentage of efficiency of this phenomenon in the overall process.

A: M. A. Vannice

At this time we do not have any quantitative idea about the support area involved. We have assumed that the active region is restricted to a relatively small area surrounding each metal particle. However, if H spillover is not the slow step, as is implied by the similarity among the activation energies for all the catalysts, then a much larger fraction of the surface could be involved.

We have worked at two Pt loadings on TiO_2 at similar dispersions, as listed in Table 1, and we obtained lower rates at lower loadings. However, the uncertainty about the extent of deactivation with different catalysts complicates these comparisons.

Q: C. Apestequia (Argentina)

According to your model the benzene hydrogenation rate will increase when H_2 spillover rate increases. Hydrogen spillover should be greater for samples of higher metal dispersion. Your results of Pt/SiO_2-Al_2O_3 catalysts show the opposite trend since the most sintered samples give maximum turnover numbers. Could you please comment on this apparent contradiction in your model?

A: M. A. Vannice

The hydrogenation rate will increase as you state only if spillover is the rate determining step; all our evidence argues against this. The results with the Pt/SiO_2-Al_2O_3 samples do run counter to our expectation and the trend is opposite to that observed with Pd/SiO_2-Al_2O_3 samples; however, the overall variation in TOF with the Pt catalysts is only two-fold.

Q: D. Duprez (France)

If you have a contribution of the interfacial region around the metal particle, you should have a certain sensitivity of the reaction to the particle size of metal, particularly in catalysts having the lowest activity (where the contribution of the support could be rate-limiting). Have you observed such an effect in toluene hydrogenation?

A: M. A. Vannice

As mentioned previously, this depends on the relative rate of H spillover compared to the subsequent elementary steps. Furthermore, the particle size effect you mention is dependent upon the number of contact points between each metal particle and the support; this parameter is hard to control and it is particularly variable in the case of oxides like TiO_2, which can wet metal surfaces (see ref. 11, for example).

Q: F. Figueras (France)

From the experimental work of Teichner, the hydrogenation of ethylene by spilled over hydrogen is very slow (many hours for a measurable conversion around 20 %). The reactivity of toluene is lower than that of ethlylene by several orders of magnitude. I therefore doubt that spillover can be the source of higher activity of Pd on silica-alumina.

It is however noticeable that your experiments, as quoted in the paper, were done at relatively high conversion 15 %. You showed before that hydrogenation of benzene cannot be run above 2 % conversion without overheating of the surface. Can you discard that heat transfer limitations perturb the catalytic measurements ?

A: M. A. Vannice

In most, if not all, of the ethylene hydrogenation studies by Teichner and coworkers, the reaction occurred in the absence of the metal after the oxide had been "activated" by H spillover (ref. 44). Consequently, these systems cannot be compared to ours in which the metal was retained. In other spillover experiments by other authors large migration distances were required (see ref. 44). In our model only short distances are assumed to be required.

Our highest conversions were around 12 % but most conversions were below 6-8 %; furthermore, the activities listed in the Tables were routinely compared at low temperature, hence the lowest conversions; i.e. 1-2 %. In the work you cite (ref. 9), TOF values obtained at conversions of 11 and 23 % were about double the TOF's obtained with the remainder of the conversions, which were 4 % or lower, and we mentioned that nondifferential operation could cause temperature gradients.

Q: Wm. C. Conner (USA)

1) As Teichner et al. and we have also shown (and you have noted), spillover can lead to hydrogenation activity on the support. For the cases where the support is activated, the activity depends on prolonged reduction at > 300 ^{0}C, for example. Did you vary the pretreatment conditions and do these influence the kinetics ?

2) Are there any differences (even subtle) in the toluene ad/desorption on these supported systems and how does the amount of hydrogen compare to the toluene adsorption for these systems ?

A: M. A. Vannice

The reduction time at a given temperature was the same for all catalysts - 1 h - except for Pt/TiO_2 (LTR) which was 2 h. Consequently, we do not know if reduction time affects the kinetics. Residual chloride would also have to be checked to clarify any observed influence.

All of our adsorption measurements were conducted volumetrically; hence, toluene adsorption was not determined.

Q: S. L. Kiperman (Russia)

The reasons for the changes of kinetic dependencies with the changes of temperature in this work are not clear. But in connection with it I would like to inform you on our results obtained in the study of kinetics and mechanisms of benzene and toluene hydrogenation over platinum-alumina catalysts. We studied these reactions with a detailed investigation of kinetics in a gradientless system and by a transient response method in isotopic variants. It was found that there are two kinds of hydrogen adsorbed on the platinum surface - weakly and tightly bonded. Surface hydrogenation proceeds via the interaction of the hydrocarbon only with weakly bonded hydrogen but isotopic exchange with tightly bonded hydrogen. A part of weakly bonded hydrogen changes with temperature and therefore changes the kinetics and mechanism of hydrogenation.

A: M. A. Vannice

We agree with your proposed role of weakly adsorbed hydrogen and, in fact, we have stated in our earlier study of benzene hydrogenation over Pd that only the weakly bound hydrogen appeared to be involved (ref. 30). Based on our current studies of benzene hydrogenation on Pt and an assessment of the literature, we agree that your model is possible. However, we think the change in the kinetics with temperature reflects a greater rate inhibition due to an increase in H-deficient surface species at higher temperatures.

Q: W. K. Hall (USA)

Is it not true that the hydrogenation of benzene to cyclohexadiene is thermodynamically uphill (forbidden) under the conditions of your reaction ? In this circumstance a stepwise hydrogenation is not possible. thus, hydrogen spillover may occur, but will not be efficient for benzene hydrogenation because multiple addition is difficult because of the low surface density of H atoms. Do you agree ?

A: M. A. Vannice

Using data from "TRC Thermodynamic Tables", Texas A and M University System, College Station, TX (1985) and calculational procedures used in the DIPPR Data Book,

we have calculated that the free energy change during the reaction $H_2 + C_6H_6(g) \rightarrow C_6H_8(g)$ is about +12.4 kcal/mole, which is close to the activation energies we routinely see on either Pt or Pd and which have been reported for other Group VIII metals. Consequently, the activation barrier for the overall reaction to cyclohexane may well be the formation of a cyclohexadiene intermediate. Over small migration distances away from the metal the spillover hydrogen concentration could easily be high enough to allow two atoms to react with benzene to form cyclohexadiene, which along with cyclohexene is much more reactive than benzene. Furthermore, the simultaneous addition of 4 to 6 H atoms to avoid the formation of cyclohexadiene is statistically very improbable and, if this were the rate determining step, one could expect a 2nd order dependence or higher on hydrogen. Consequently, I do not agree with you.

Q: D. G. Blackmond (USA)

You suggest that two types of sites, one on the metal and one on the support, are responsible for the hydrogenation activity on the acidic catalysts. However, there appears to be no trend in activation energies in comparing acidic and non-acidic supports. The observed activation energy could be a combination of that for the reaction occurring on each type of site. Do you believe that the two types of sites have similar activation energies for toluene hydrogenation ?

A: M. A. Vannice

As mentioned above, activation energies for many metals are frequently reported around 10-14 kcal/mol for benzene and toluene hydrogenation, independent of the support, and this implies that the formation of a cyclohexadiene intermediate may well be the slow step. Our modelling studies show that the proposal of the addition of either the first or second H atom to the benzene ring as the rate determining step can explain the results for metal sites as well as sites on the oxide (to be published); even in the case with Pd where the support contribution is much greater (refs. 2, 30).

Q: W. Grünert (Germany)

My question concerns the use of irreversible hydrogen chemisorption for the assessment of Pt accessible from the gas phase. There was a long story about the origin of the SMSI effect. Certainly, there is migration of TiO_x species onto the metal, but an electronic effect may be also considered. It might weaken the interaction between H_2 and the metal, so that you under-estimate the Pt surface that may still supply weakly bound hydrogen for your reduction. Thus, I suggest that it would be useful to check the amount of Pt accessible to the gas phase by ISS.

A: M. A. Vannice

Our earlier calorimetric measurements of H_2 adsorption on Pt/TiO_2 (HTR) catalysts showed that the average heat of adsorption (13.4 kcal/mole) was close to the average value of 13.5 kcal/mole for all Pt catalysts including Pt powder, and the Q_{ad} values were also similar for irreversible adsorption (ref. 47). For the 0.09 % Pt/TiO_2 catalyst both reversible and irreversible H_2 uptakes were undetectable and for 0.95 % Pt/TiO_2 the reversible uptake was about three times larger than the irreversible uptake. The marked reduction in hydrogen chemisorption is clearly due to physical blockage of the Pt surface. However, the application of ISS could still be a useful characterization technique.

Q: J. B. Butt (USA)

1) Were there significant differences in the amount of chloride contained in the catalysts investigated that might account for some of the differences in apparent acidity ?

2) The values of activation energy for the toluene hydrogenation (~12 kcal/mol) are similar to those reported for benzene hydrogenation over similar catalysts, therefore one might conclude that the methyl group does not significantly affect the energetics of the

hydrogenation reaction. Differences in the magnitude of turnover frequency would thus reside in some appropriate preexponential factor (i.e., changes in TOF are steric effects).

A: M. A. Vannice

We did not analyze our reduced catalysts for residual chloride content but, based on your recent paper [1], we might anticipate little effect, at least for Pt/SiO_2 and Pt/Al_2O_3, because our dispersions were high and our reduction temperature was 450^0 C. However, the effect with SiO_2-Al_2O_3 and TiO_2 is not known, and chloride can alter the acidity of titania surfaces.

The statement about steric effects could well be true, especially if the activation energy is primarily associated with the destruction of the resonance energy of the aromatic ring. However, on Pt TOF values for toluene are only 1/4 to 1/2 the values for benzene hydrogenation, and only a small change in activation energy is required to produce these differences.

[1] A. F. Flores, R. L. Burwell and J. B. Butt, *J. Chem. Soc., Faraday Trans.*, **88**, 1191 (1992)

[2] W. Ranjani, J. Siriwardane and J. P. Wightman, *J. Coll. Interface Sci.*, **94**, 502 (1983)

Q: H. Schulz (Germany)

In your excellent paper you have suggested an inhibiting unsaturated surface species in order to explain the observed kinetics of toluene hydrogenation. Could you perhaps speculate a little about the composition and structure of this species ?

A: M. A. Vannice

During our subsequent studies of benzene and toluene hydrogenation we have found that our kinetic model is best fit by the assumption that a phenyl (or tolyl) species is the predominant H-deficient species. Although no identification of such a species has been reported for Pt yet, three recent papers have reported phenyl groups on Ag(111), Os(0001) and Ni(111), thus we believe this is the most probable species [3-5].

[3] Zhou et al., *Surf. Sci.*, **238**, 215 (1990)

[4] Garen et al., *Chem. Phys Lett.*, **165**, 137 (1990)

[5] H. P. Steinrück, W. Huber, T. Patche, D. Menzel, *Surf. Sci.*, **218**, 293 (1989)

Q: D. Wang (China)

You suggest a correlation that hydrogenation activity is higher with the use of acidic supports. I do not think of TiO_2 as very acidic, nor is Al_2O_3 (although they are more acidic than SiO_2), and that leaves only SiO_2-Al_2O_3 as an acidic support. Has work been done with more (clearly) acidic supports, e.g., Nb oxide and Ta oxide, to supported your correlation?

A: M. A. Vannice

We have not used the oxides you mention. We do not consider this η-Al_2O_3 to be very acidic - it certainly has few Brönsted sites. Titania can have acid sites and the presence of HCl (i.e., chloride) can increase acidity, primarily by forming weak Brönsted sites [2].

Guczi, L. *et al.* (Editors), *New Frontiers in Catalysis*
Proceedings of the 10th International Congress on Catalysis, 19-24 July, 1992, Budapest, Hungary
© 1993 Elsevier Science Publishers B.V. All rights reserved

THE CATALYTIC ACTIVITY OF MoO_x/ZrO_2 IN THE HYDROGENATION AND METATHESIS OF PROPENE

V. Indovina, A. Cimino, D. Cordischi, S. Della Bella, S. De Rossi, G. Ferraris, D. Gazzoli, M. Occhiuzzi and M. Valigi

Centro di Studio del CNR su "Struttura ed Attivita catalitica di Sistemi di ossidi",
Dipartimento di Chimica, Universita La Sapienza, P. le A. Moro 5, 00185 Roma, Italy

Abstract

The catalytic activity of MoO_x/ZrO_2 for propene hydrogenation has been studied in a flow apparatus at 195-298 K. At or above 273 K, propene metathesis is observed in addition to hydrogenation. The catalysts, prepared by equilibrium adsorption at pH=1, 2, 3 or 8, have a Mo surface concentration from 0.5 to 7.7 atoms nm^{-2}. Before ESR, XPS, or catalysis measurements, the samples were heated in O_2 at 773 K and reduced thereafter with H_2 to a controlled extent, expressed by e/Mo (electrons acquired per Mo atom) in the range 448 K to 803 K. Both ESR and XPS analyses show that a large fraction of total Mo (30%) is already reduced to Mo^V at 473 K (e/Mo≃0.3). The Mo^V content remains constant with further reduction up to e/Mo≃3. The ESR spectrum originates from a mononuclear Mo^V species in a square pyramidal configuration (ESR of $^{95}Mo^V$). About 80% of Mo^V is destroyed upon O_2 adsorption at 195 K and restored by evacuation at 773 K. The turnover frequency for the propene hydrogenation (N_h/molecules s^{-1} Mo $atom^{-1}$) is very small up to e/Mo≃1 and increases markedly with e/Mo. The N_h value strongly increases with the Mo content up to about 5.6 atoms nm^{-2}, and decreases at higher Mo loading (aggregation of Mo oxide). The turnover frequency for metathesis, N_m, is nearly constant in the range e/Mo≃1 to 3 and is almost independent of Mo content. The results show that the active sites for hydrogenation and metathesis are different. It is suggested that mononuclear Mo^V are the active sites for metathesis, whereas higher nuclearity species involving molybdenum in lower oxidation state are active for hydrogenation.

1. INTRODUCTION

Supported molybdenum ions, mainly studied on silica, alumina and titania [1-4], show important catalytic properties. It is well known that the dispersion, oxidation state, and structural features of the supported ions may strongly depend on the support. It is therefore of interest to study the activity of molybdenum on other

supports; ZrO_2 was chosen in view of its weak acid-base properties and because of its ability to maintain a high surface area. Within the same framework, we have investigated the activity of chromia/zirconia [5-8], for H_2-D_2 equilibration [5], propene hydrogenation [9-11] and propane dehydrogenation [12]. The activity for propene hydrogenation was substantially higher when zirconia instead of alumina or silica was used to support chromium.

This paper reports the catalytic activity for the hydrogenation of propene on MoO_x/ZrO_2 catalysts, previously reduced by H_2 to a controlled extent. The concomitant metathesis of propene was also studied. The data illustrate the dependence of the activity on (i) the extent of reduction, (ii) concentration of molybdenum and (iii) poisoning with O_2 at 195 K or NH_3 at RT. A preliminary report of catalyst characterization by ESR and XPS spectroscopies, volumetric redox cycles, adsorption of O_2 at 195 K and NH_3 at RT is also given.

2. EXPERIMENTAL

MoO_x/ZrO_2 catalysts were prepared by contacting ZrO_2, prepared as previously described [6], with a solution of ammonium heptamolybdate (AHM) at pH=1, 2, 3 or 8. The ZrO_2 was calcined in air at 383, 823, or 923 K before contact with the AHM solution. The Mo surface concentration was in the range 0.5 to 7.7 atoms nm^{-2}. Some samples were also prepared by adsorption from a solution of enriched ^{95}Mo (96.8%, ESR experiments). The MoO_x/ZrO_2 catalysts are designated as ZMox(T), where x specifies the analytical Mo content (w%) and T the calcination temperature (K) of the ZrO_2 used (Table 1). The catalyst (0.1 to 0.5 g) was placed in a silica reactor which could be connected to the flow section for catalytic experiments or to the gas adsorption section, as described elsewhere [9]. In some experiments, a silica reactor was used equipped with a side ESR and/or XPS tube to which the powder could be transferred without exposure to air. After drying at 383 K, all samples were submitted to redox cycles consisting of (i) heating in oxygen at 773 K, (ii) reduction with hydrogen at 448 to 803 K, and (iii) reoxidation with oxygen at 773 K. The extent of reduction (e/Mo, electrons per Mo atom) was determined by monitoring the decrease of the H_2 (step ii) and O_2 pressure (step iii). After reduction to a controlled extent, O_2 adsorption at 195 K or the catalytic activity for the hydrogenation and metathesis of propene were measured (flow apparatus, GC analysis). The reactant stream (95% H_2, 5% C_3H_6) flowed through the catalyst (20 to 170 cm^3 min^{-1}) at a pressure of about 100 kPa. The reaction was generally followed for 1 h, with a first analysis after 5 min and then after every 15 min. At 195 K, propane was the only product. At or above 273 K, ethene, ethane, butene and butane were detected in addition to propane. The activity for the metathesis was stable (or moderately decreasing) with time on stream, whereas a marked deactivation was observed for hydrogenation, probably due to the formation of carbonaceous species strongly held on the surface of the catalyst. Therefore, the activity for hydrogenation (expressed as average tunover frequency, *vide infra*) was calculated from the initial rate at t=0 [9]. ESR measurements were made at RT or at 77 K on a Varian E-9 spectrometer operated at X-band frequencies. Absolute concentration of Mo species contributing to the ESR spectra were obtained from the integrated area by using a Varian strong pitch standard. The XPS analysis of

samples heated in oxygen at 773 K and reduced *in situ* by flowing H_2 at 473 to 673 K was performed in a Leybold-Heraeus LHS 10 spectrometer. BE values are deduced by a best fitting procedure of the composite peak.

Table 1
Catalysts and their main features

Catalysts	pH	Surface area (a) ($m^2\ g^{-1}$)	Mo surface density (a) (atoms nm^{-2})
Z(383)		118	
ZMo1.67(383)	1	64	1.64
ZMo5.94(383)	1	102	3.65
ZMo3.09(383)	3	64	3.03
ZMo5.49(383)	8	103	3.35
Z(823)		40	
ZMo0.48(823)	2	40	0.74
ZMo2.49(823)	2	37	4.22
ZMo5.64(823)	2	46	7.70
ZMo0.99(823)	8	41	1.52
Z(923)		25	
ZMo0.69(923)	1	21	2.05
ZMo2.09(923)	1	24	5.56
ZMo1.36(923)	2	23	3.71
ZMo0.41(923)	8	25	1.02

(a) Samples heated in O_2 at 773 K

3. RESULTS

3.1. XPS characterization

The analysis of MoO_x/ZrO_2 samples after heating in O_2 at 773 K shows the presence of Mo^{VI} ($Mo3d_{5/2}$ at a BE 232.8 ± 0.2 eV, referred to the $Zr(3d_{5/2})$=182.5 eV peak). A linear correlation is found between the peak area intensity ratios, $I_{(Mo3d)}/I_{(Zr\ 3d)}$, and the surface concentration of Mo, up to about 6 Mo atoms nm^{-2}. The sample ZMo5.64(823), containing 7.7 atoms nm^{-2}, shows evidence of aggregation of molybdenum species (MoO_3 like). Experiments performed on the sample ZMo1.36(923) reduced in situ by flowing H_2 at 473 to 673 K show the presence of Mo^{V} (BE 231.6 ± 0.2 eV) in addition to unreduced Mo^{VI}. The percentage of the Mo^{V} species is 30 ± 10% at all reduction temperatures. After reduction at 623 or 673 K, the presence of Mo^{IV} (BE 228.8 ± 0.2 eV) is also detected.

3.2. ESR characterization

After heating the samples with O_2 at 773 K followed by evacuation at the same temperature, the formation of an extremely weak axial signal with $g_{\perp}$=1.961 and

g_{II}=1.850 was observed at 77 K but not at RT. In view of the ESR parameters and relaxation features of this signal compared with those reported by Che et al. [13] and Shelimov et al. [14] for tetrahedral Mo^V on SiO_2, the signal is assigned to a Mo^V_{4c} species. After reduction with H_2 for 10 min at 523 K, a different signal ($g_{\perp}$=1.955 and g_{II}=1.886), detectable at both RT and 77 K, is observed in all ZMo samples. The ESR analysis of spectra of dilute ZMo samples containing ^{95}Mo allows assigning the signal to a mononuclear Mo^V species on the surface of ZrO_2 (Mo^V_{5c}). On all samples, the Mo^V content increases with increasing extent of reduction, up to $(e/Mo)_{H_2} \simeq 0.3$, and remains almost constant thereafter. The fraction of total Mo detected by ESR as Mo^V is 0.3 in the most dilute samples and decreases markedly with increasing Mo content.

3.3. Redox properties of the system

Samples were reduced with H_2 at 333 K to 803 K to various extents in a random sequence and reoxidized thereafter with O_2 at 773 K. From these experiments a linear correlation between the $(e/Mo)_{H_2}$ values and the corresponding $(e/Mo)_{O_2}$ values is found for all ZMo catalysts. Maximum reduction extents were $(e/Mo)_{H_2}$=3.1, corresponding to an average oxidation number, $\bar{n}$=2.9. In more concentrated samples it was found that $(e/Mo)_{O_2}=(e/Mo)_{H_2}$, whereas in more dilute samples, $(e/Mo)_{O_2}$ values were lower than $(e/Mo)_{H_2}$ by no more than 15%.

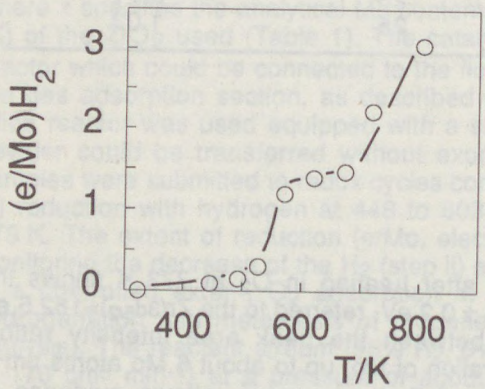

Figure 1. Extent of reduction, $(e/Mo)_{H_2}$, as a function of reduction temperature. Sample ZMo1.36(923).

In some cases, the $(e/Mo)_{H_2}$ values were determined by reduction for 40 min at constant temperature, which was subsequently increased from 323 to 800 K in consecutive experiments. Before passing from a given reduction temperature to a higher one, the sample was heated in O_2 at 773 K and evacuated at the same temperature. The results of a typical experiment on the sample ZMo1.36(923) (Fig. 1) are: (i) upon reduction up to 525 K a value $e/Mo \leq 0.3$ ($n \geq 5.7$) is measured,

(ii) a very steep increase in the e/Mo value from 0.3 to 1.5 (ñ decreases from 5.7 to 4.5) is subsequently observed when the reduction temperature is increased from 525 to 580 K, (iii) above 580 K the e/Mo value tends to level off until 680 K, and (iv) a second marked increase of e/Mo (from 1.5 to 3) is observed when the reduction temperature is increased from 680 to 800 K. In the e/Mo range from 0.3 to 3, the constancy of the surface concentration of Mo^V was checked by ESR.

3.4. Adsorption of oxygen at 195 K and ammonia at RT

The irreversible uptake of oxygen at 195 K (double isotherm method) increases with increasing $(e/Mo)_{H_2}$ up to about 0.5 and remains constant thereafter (O_2/Mo= 0.2 to 0.3). The analogous pattern observed by ESR for the surface concentration of Mo^V as a function of e/Mo suggests that Mo^V is involved in the oxygen adsorption. ESR experiments show in fact that a large fraction of Mo^V (80%) is reversibly destroyed and superoxide species are formed upon adsorption of O_2.

Upon adsorption of NH_3 at RT on ZMo samples reduced to e/Mo≥0.3 and therefore showing the ESR signal of Mo^V_{5c} at its maximum intensity, a different Mo^V species is detected by ESR ($g_\perp$=1.948 and $g_{||}$=1.893). The latter species, identified as Mo^V_{6c} by its similarity to a signal detected on SiO_2 [13], is stable upon evacuation at RT, and is partially transformed in the Mo^V_{5c} species after evacuation at 473 K. After a subsequent evacuation at 673 K the Mo^V_{5c} species is reversibly restored.

3.5. Hydrogenation of propene

The catalytic activity for the hydrogenation of propene at 298 K, expressed as average turnover frequency, N_h (propane molecules per sec per total Mo atoms), is reported in Fig. 2 a for some ZMo catalysts as a function of e/Mo. If unreduced, all ZMo catalysts are inactive, whereas after reduction to e/Mo≥1, a marked increase of activity with increasing extent of reduction is observed.

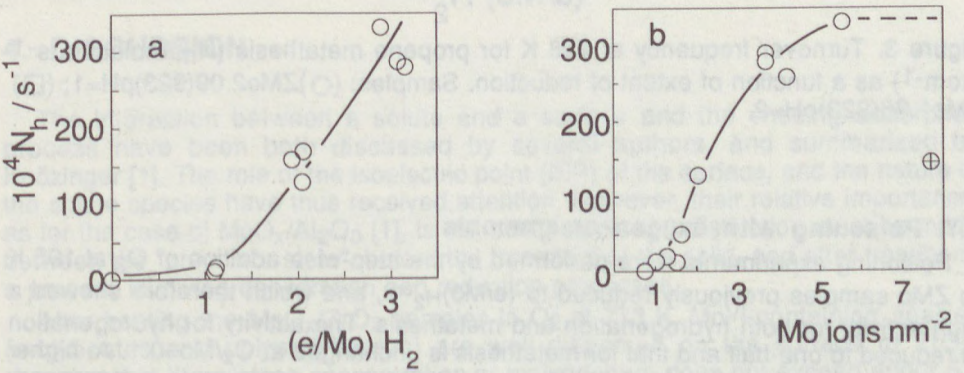

Figure 2. (a): Turnover frequency at 298 K for propene hydrogenation (N_h/molecules s^{-1} $atom^{-1}$) as a function of the extent of reduction; (b): N_h at 298 K as a function of the Mo surface concentration. Crossed circle: MoO_3 present.

When comparing samples of different Mo content reduced to about the same extent (e/Mo≃3), the corresponding N_h values are found to increase strongly (by 2 orders of magnitude) with increasing surface concentration of Mo up to about 5.6 ions nm^{-2}, and are found to decrease thereafter because of segregation of MoO_3 like species (Fig. 2 b).

3.6. Metathesis of propene during hydrogenation

The average turnover frequency for the metathesis of propene, N_m (molecules $atom^{-1}$ s^{-1}) as a function of e/Mo, is reported in Fig. 3. The catalysts show low activity for metathesis when reduced up to $(e/Mo)_{H_2}\simeq 1$. Above this value a marked increase in activity is observed, whereas metathesis is nearly constant for reduction in the region from e/Mo=1 to 3. The N_m values change but little with increasing Mo surface concentration, up to about 7.7 nm^{-2}. All N_m values are within a factor of 3, if samples are reduced to any extent in the range e/Mo=1 to 3.

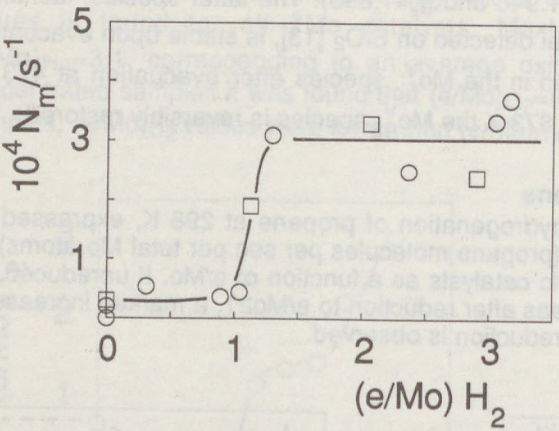

Figure 3. Turnover frequency at 298 K for propene metathesis (N_m/molecule s^{-1} $atom^{-1}$) as a function of extent of reduction. Samples: (○)ZMo2.09(923)pH=1; (□) ZMo1.36(923)pH=2.

3.7. Poisoning with oxygen or ammonia

Poisoning experiments were performed by the step-wise addition of O_2 at 195 K to ZMo samples previously reduced to $(e/Mo)_{H_2}\simeq 3$, and which therefore showed a high activity for both hydrogenation and metathesis. The activity for hydrogenation is reduced to one-half and that for metathesis is unchanged at O_2/Mo=0.1. At higher oxygen coverages (O_2/Mo=0.2), the activity for hydrogenation is suppressed, whereas that for metathesis is still unchanged. When hydrogenation is suppressed, the products of metathesis are ethene and butene only. Upon adsorption of ammonia at RT and evacuation at the same temperature, the activity for metathesis is suppressed, whereas that for hydrogenation is reduced by a factor of two.

3.8. A comparison with MoO_x/Al_2O_3 catalysts

The catalytic activity of MoO_x/γ-Al_2O_3 for the hydrogenation and metathesis of propene has been extensively studied by Hall et al. [2]. In order to have directly comparable activity data, some new experiments were carried out by us on the same MoO_x/Al_2O_3 specimen (Mo 8 wt%) used in ref. 2 [15]. Representative results obtained on the MoO_x/Al_2O_3 system in our or in other laboratories (as specified) are listed below and compared with those obtained on MoO_x/ZrO_2.

The formation of Mo^V in the MoO_x/Al_2O_3 system is considerd first. The Mo^V concentration changes but little (by a factor of two) with increasing reduction with H_2 up to 800 K [4]. The ESR signal of Mo^V is substantially broader on Al_2O_3 compared with ZrO_2, a feature due to superhyperfine interaction with ^{27}Al nuclei [16] rather than to a higher heterogeneity of the Mo^V/Al_2O_3 system [4]. The Mo^V molar fraction is only 0.1 of total Mo in MoO_x/Al_2O_3 compared to 0.3 in MoO_x/ZrO_2.

Adsorption of O_2 at 195 K on reduced MoO_x/Al_2O_3 yields O_2/Mo=0.25 to 0.3, close to the values reported in ref. 17 (O_2/Mo=0.25 to 0.30) and in ref. 4 (O_2/Mo=0.33) for similar catalysts, and close to the values found on ZMo (O_2/Mo=0.2 to 0.3).

Concerning catalysis, the same dependence on e/Mo is observed for either N_h or N_m on MoO_x/Al_2O_3 and MoO_x/ZrO_2. Moreover, the N_h value at 293 K measured on MoO_x/Al_2O_3 is in fair agreement with the value on ZMo2.09(923) at the same temperature (N_h=1.6x10^{-2} s^{-1} and 1.8x10^{-2}, respectively). The corresponding value relative to MoO_x/Al_2O_3, calculated from the data of Fig. 1 of ref. 2, is somewhat lower (0.6x10^{-2}), probably because a circulation technique was adopted. A good agreement is also found when the N_m values on various Mo-containing catalysts are compared: on MoO_x/Al_2O_3, N_m=3.1x10^{-4} s^{-1} [2], N_m=2.5x10^{-4} [18] and N_m=3.0x10^{-4} (our data). These values are close to those measured on MoO_x/ZrO_2 (N_m=2 to 3x10^{-4} s^{-1}, from Fig. 3). Finally, the same poisoning effect is found with O_2 and NH_3 on ZrO_2 and Al_2O_3-supported catalysts. Specifically, NH_3 adsorption poisons the metathesis reaction and partially poisons hydrogenation, whereas O_2 poisons hydrogenation but not metathesis.

4. DISCUSSION

The interaction between a solute and a surface and the ensuing adsorption process have been both discussed by several authors, and summarized by Knözinger [1]. The role of the isoelectric point (IEP) of the surface, and the nature of the solute species have thus received attention. However, their relative importance, as for the case of MoO_x/Al_2O_3 [1], is still being studied. A distinction must be made between the "precursor state", before the treatment of the solid, and after treatment, a process involving dehydration and reduction processes.

After heating the MoO_x/ZrO_2 samples in O_2 at 773 K, Mo^{VI}-containing species (molybdates and polymolybdates) are well dispersed on the surface of ZrO_2, provided that the surface concentration of molybdenum does not exceed about 5.6 atoms nm^{-2}. Some aggregation of molybdenum species (MoO_3 like) is observed by XPS in the most concentrated sample (7.7 atoms nm^{-2} sample). A suggestion concerning the nature of surface molybdenum species formed after reduction can be given on the basis of ESR, XPS and ñ data.

In the early stages of reduction up to 525 K (e/Mo≤0.3, $\bar{n}\geq 5.7$), Mo^{V} is the only species detected by either ESR or XPS, in addition to unreduced Mo^{VI} detected by XPS. The Mo^{V} species is strongly stabilized on the surface of zirconia, as shown by the constancy of its concentration (30%) upon reduction treatments up to 800 K. The apparent decrease of Mo^{V} detected by ESR with increasing Mo concentration is due to magnetic interaction, as has been discussed elsewhere [19]. It should be stressed that almost the same Mo^{V} concentration is found when comparing ZMo samples prepared from AHM solutions at different pH. Therefore, for all ZMo samples, irrespective of the pH of AHM solution, a nearly constant (molybdates)/(polymolybdates) ratio is inferred from the constant concentration of mononuclear Mo^{V} (ESR), which arises from the reduction of mononuclear molybdate species. A buffer effect of the ZrO_2 surface seems to be operating. Specifically, a role of the Brönsted acid-base sites of ZrO_2 can be recognized in the condensation-decondensation of molybdenum anions during heating in O_2 and/or in subsequent reduction with H_2. Thus, whereas the total Mo uptake is mainly controlled by the pH of the AHM solution, the nature of the molybdenum species is to large extent controlled by the nature of the adsorbing oxide; this is in substantial agreement with the case of $MoO_3/\gamma\text{-}Al_2O_3$. Indeed Butz et al. [20] warn against inferring the nature of surface molybdenum species from the study of the supernatant liquid in equilibrium adsorption studies of the $MoO_3/\gamma\text{-}Al_2O_3$ system.

Upon reducing the catalysts at higher temperature (>525 K), two steep increases of the e/Mo parameter are observed when the reduction temperature is increased (Fig. 1). The first increase ($\Delta e/Mo\simeq 1$) occurs when the temperature is brought from 525 to 600 K, and is attributed to the formation of Mo^{IV} by reduction of polymolybdates. The assignment is supported by XPS results, which show the formation of Mo^{IV} in the same temperature region, and by the close agreement between the experimental value of $\bar{n}$ at 650 K ($\bar{n}=6-1.5=4.5$, from Fig. 1) and the corresponding calculated value, $\bar{n}=4.3$. The latter is obtained from

$$\bar{n} = (x_{Mo^{V}} \times 5) + (x_{Mo^{IV}} \times 4)$$

taking $x_{Mo^{V}}=0.3$, as measured by both ESR and XPS, and $x_{Mo^{IV}}=1-x_{Mo^{V}}=0.7$. The second steep increase ($\Delta e/Mo\simeq 1.5$, temperature increasing from 650 to 800 K) is tentatively attributed to the formation of Mo^{II} that arises from the reduction of Mo^{IV}. In this case, the experimental value of $\bar{n}$ after reduction at 800 K, $\bar{n}=6-3=3$ (Fig. 1), is also in reasonable agreement with the calculated value, $\bar{n}=2.9$. The calculation is performed by taking $x_{Mo^{V}}=0.3$, as above, and assuming complete reduction of Mo^{IV} to Mo^{II}.

Coming to catalysis, the nature of the active sites in the hydrogenation and metathesis of the ZMo system can be briefly discussed in light of molybdenum species. The marked differences in the behaviour of ZMo catalysts toward hydrogenation and metathesis, schematically illustrated in Table 2, show that distinct sites are operating for the two reactions.

Metathesis is probably carried out on mononuclear Mo^{V} species. The statement is supported by (i) the fact that Mo^{V} (as detected by ESR) is constant in the same

reduction region where the activity for metathesis is also constant (Fig. 3) and (ii) the facile (structure-insensitive) nature of metathesis on ZMo catalysts. Hydrogenation takes place on more-reduced molybdenum species, possibly Mo^{II}, as suggested by the progressive and marked increase of N_h observed in the region in which the average oxidation number decreases from 5 to 3, namely in the region where Mo^{IV} is progressively reduced to Mo^{II}. The demanding (structure-sensitive) nature of propene hydrogenation on ZMo catalysts and specifically the marked increase of activity with Mo content (Fig. 2 b) suggests the presence of an active site consisting of a polynuclear molybdenum species.

Table 2
Main differences in the behaviour of MoO_x/ZrO_2 catalysts toward hydrogenation and metathesis of propene

Feature observed	Hydrogenation	Metathesis
decay of N with time on stream	marked	moderate
dependence of N on reduction	N_h increases above e/Mo>1	N_m is constant above e/Mo>1
dependence of N on Mo content	N_h increases with Mo content	N_m is constant with Mo content
poisoning with O_2	complete	absent
poisoning with NH_3	partial	complete

5. CONCLUSIONS

Mononuclear Mo^V species in square pyramidal configuration are strongly stabilized on the surface of ZrO_2. The Mo^V species probably arises from molybdate species following reduction with H_2. By increasing the extent of reduction, first Mo^{IV}, and then Mo^{II} are formed, but not from Mo^V whose concentration remains unchanged. It is suggested that the precursors of Mo^{IV} and Mo^{II} are possibly polymolybdate species. Thus, two nearly independent redox couples can be envisaged on the surface of ZrO_2: MoO_4^{2-}/Mo^V and $Mo_7O_{24}^{6-}/Mo^{IV}$, Mo^{II}. The two redox-couples are fully reversible in cycles with H_2 and O_2.

Active sites for the metathesis of propene are different from those for the hydrogenation. The dependence of activity on the extent of reduction and on Mo content, together with the poisoning experiments, suggest that Mo^V ions with special coordinative features are active in metathesis, whereas polynuclear molybdenum species, possibly containing Mo^{II}, are active in hydrogenation. The clear analogies in the catalytic behaviour of MoO_x/Al_2O_3 and MoO_x/ZrO_2 strongly suggest a common nature for the Mo species that are active in the two supports.

Acknowledgements

This work has been financially supported by the Progetto Finalizzato Chimica Fine II of the Consiglio Nazionale delle Ricerche, Rome, Italy

6. REFERENCES

1 H. Knözinger, "*Proceedings 9 Int. Congr. Catal.*" (M. J. Phillips and M. Ternan Eds.), Chem. Inst. Canada, Ottawa, 1988, Vol. 5, p. 20
2 E. A. Lombardo, M. Lo Jacono and W. K. Hall, *J. Catal., 64* (1980) 150
3 K. Segawa, D. S. Kim, Y. Kurusu and I. Wachs, "*Proceedings 9 Int. Congr. Catal.*" (M. J. Phillips and M. Ternan Eds.), Chem. Inst. Canada, Ottawa, 1988, Vol. 4, p. 1960
4 C. V. Caceres, J. L. G. Fierro, J. Lazaro, A. Agudo Lopez and J. Soria, *J. Catal. 122* (1990) 113.
5 A. Cimino, D. Cordischi, S. De Rossi, G. Ferraris, D. Gazzoli, V. Indovina, G. Minelli, M. Occhiuzzi and M. Valigi, "*Proceedings 9 Int. Congr. Catal.*" (M. J. Phillips and M. Ternan Eds.), Chem Inst. Canada, Ottawa, 1988, Vol. 3, p. 1465.
6 A. Cimino, D. Cordischi, S. De Rossi, G. Ferraris, D. Gazzoli, V. Indovina, G. Minelli, M. Occhiuzzi and M. Valigi, *J. Catal., 127* (1991) 744.
7 A. Cimino, D. Cordischi, S. De Rossi, G. Ferraris, D. Gazzoli, V. Indovina, M. Occhiuzzi and M. Valigi, *J. Catal., 127* (1991) 761.
8 A. Cimino, D. Cordischi, S. Febbraro, D. Gazzoli, V. Indovina, M. Occhiuzzi, M. Valigi, F. Boccuzzi, A. Chiorino and G. Ghiotti, *J. Mol. Catal., 55* (1989) 23.
9 A. Cimino, D. Cordischi, S. De Rossi, G. Ferraris, D. Gazzoli, V. Indovina and M. Valigi, *J. Catal., 127* (1991) 777.
10 V. Indovina, D. Cordischi, S. De Rossi, G. Ferraris, G. Ghiotti and A. Chiorino, *J. Mol. Catal., 68* (1991) 53
11 V. Indovina, A. Cimino, S. De Rossi, G. Ferraris, G. Ghiotti and A. Chiorino, *J. Mol. Catal.*, to be published
12 S. De Rossi, G. Ferraris, S. Fremiotti, A. Cimino and V. Indovina, *Appl. Catal.*, in press
13 M. Che, C. Louis and Z. Sojka, *J. Chem. Soc., Faraday Trans., 85* (1989) 3939
14 B. N. Shelimov, V. Pershin and V. B. Kazansky, *J. Catal., 64* (1980) 426
15 The catalyst was kindly supplied by Professor M. Lo Jacono
16 D. Cordischi, V. Indovina and M. Occhiuzzi, 12th European Conference on Surface Science, Stockholm Sept. 9-12, 1991, Europhysics Conference Abstracts (H. Bernhoff, A. Nilsson and L. Wallden, Eds.), Vol. 15 F, Abstract W 432
17 E. Delgado, G. A. Fuentes, C. Hermann, G. Kunzmann and H. Knözinger, *Bull. Soc. Chim. Belg., 93* (1984) 735
18 J. C. Mol and J. A. Moulijn, in "*Catalysis*" (J. R. Anderson and M. Boudart Eds.), Springer-Verlag, Berlin (1987), p. 70
19 D. Cordischi, V. Indovina and M. Occhiuzzi, *J. Chem. Soc., Faraday Trans.,87* (1991) 3443
20 T. Butz, C. Vogdt, A. Lerf and H. Knözinger, *J. Catal., 116* (1989) 31

DISCUSSION

Q: W. Grünert (Germany)

I have some problems with your assignment of the metathesis activity to Mo(V). You reported that you have a constant fraction of Mo(V) between e/Mo = 0.3 to 3. However, in this range, the turnover number increases from 0.5×10^{-4} to 3×10^{-4} s^{-1}, with a pronounced step in between. So, there must be an additional effect with the active site, or even the assignment may be not valid.

A: V. Indovina

The suggestion for Mo(V) as active site for metathesis is mainly based on the fact that Mo(V) is the only Mo species whose concentration remains constant (ESR and XPS evidence) in the same e/Mo region in which also the activity for metathesis is constant (e/Mo = 1 to 3). The pronounced step at e/Mo = 0.3, which you refer to, does in fact suggest that the active Mo(V) must in addition possess special coordinative features and this point is clearly stated in our conclusions. Namely, only a fraction of the total Mo(V) is active, 20 % at most relying on poisoning experiments with O_2. It is plausible that this special Mo(V) species are generated on the surface during the reduction from e/Mo = 0.3 to 1.

Q: M. Ichikawa (Japan)

One common argument to evaluate the promotion of metal oxide addition (ZrO_2 etc.) is how to count the number of the active sites which are incorporated in the particular catalytic reaction. In your paper, oxygen specifically poisons the hydrogenation but not metathesis. Do you have any experimental evidence to evaluate the active sites by using the selective poisoning molecules to differentiate the two catalytic reactivities modified by ZrO_2 on the oxide catalysts ?

A: V. Indovina

Catalytic sites for metathesis have been differentiated from those active for hydrogenation by adsorption of ammonia (which poisons metathesis, nearly selectively) and oxygen (selective for hydrogenation). An assessment of the concentration of the active sites for the two reactions has not been yet performed on MoO_x/ZrO_2. An upper limit for the fraction of total molybdenum which is active in the metathesis (6 % of total Mo) has been evaluated from the fraction of Mo(V) which remains after adsorption of O_2 at RT (ESR measurement).

Q: J. Goldwasser (Venezuela)

Although the similarities between Mo/ZrO_2 and Mo/Al_2O_3 have been underlined, it is worth adding that on Mo/Al_2O_3 the EPR signal is dependent on the Mo loading; the results shown do not indicate very clearly this dependence on Mo/ZrO_2.

A: V. Indovina

The dependence of the Mo(V) ESR signal on the Mo loading and nature of the support has been reported in refs. 16 and 19 of the present paper.

Q: Can Li (China)

Mo(II) and Mo(V) species in molybdenum oxide are very unstable. In your studies, these species may be stabilized by their special coordinative structures, e.g. as you suggested Mo(V) species in a square pyramidal configuration. What is mainly responsible for these species acting as active sites; the oxidation state of molybdenum, the special coordinative structure, or both ? Have you tried to characterize the Mo(II) and Mo(V) species by their structural features ?

A: V. Indovina

Your question draw the attention to the point that the coordinative structure of Mo can play a role in addition to the oxidation state of Mo. We are well aware of this possibility, and in fact when discussing the related CrO_x/ZrO_2 system we have stressed that the electronic structure alone does not guarantee a high catalytic activity. The coordinative unsaturation of the active site is an additional and essential factor (ref. 9 in the present paper). Relying on IR, ESR and catalytic results, we have inferred that active sites for the low temperature hydrogenation of propene on CrO_x/ZrO_2 catalysts are surface mononuclear Cr(III) species with three coordinative vacancies [1]. In an attempt to characterize the structural features of Mo(II) and Mo(V), an analogous investigation on the MoO_x/ZrO_2 system is now in progress.

[1] V. Indovina, A. Cimino, S. De Rossi, G. Ferraris, G. Ghiotti, A. Chiorino, *J. Mol. Catal.*, **75**, 305 (1992)

Q: J. C. Mol (The Netherlands)

You mentioned that in your MoO_x/ZrO_2 catalyst the metathesis reaction takes place on mononuclear Mo(V) species. However, from related systems it is often concluded that in supported molybdenum oxide catalysts Mo(IV) forms the active site for metathesis. In view of the fact that generally the number of active sites is only a small fraction of the molybdenum ions, I would like to ask if you really exclude Mo(IV) as the active site.

With regard to your last conclusion about the analogy in the catalytic behavior of MoO_x/ZrO_2 and MoO_x/Al_2O_3, does this mean that you also think that on alumina Mo(V) is the active site for metathesis ?

A: V. Indovina

I am absolutely convinced by the evidence reported in the literature in favour of Mo(IV) as the active site for metathesis (see for instance p. 515 presented in this Proceedings). However, the Mo(IV) sites active for metathesis are produced by photo reduction of silica-molybdena catalysts in CO at 293 K. The catalysts obtained according to this procedure show a much higher activity compared to those obtained by thermal reduction. This marked difference suggests a different nature for the active sites in the thermally reduced samples. Passing to the last part of your question, the clear analogies in the catalytic behavior of MoO_x/ZrO_2 and MoO_x/Al_2O_3 strongly suggest a common nature for the Mo species that are active in the two supports.

Q: I. E. Wachs (USA)

Can you please comment on the origin of the different effect of the support for MoO_x and CrO_x during hydrogenation and metathesis ?

A: V. Indovina

Your question refers to the oral presentation of the paper in which I have stressed that the catalytic activity of chromium for hydrogenation is substantially affected by the nature of the support (ZrO_2, Al_2O_3, SiO_2), whereas that of molybdenum is not. A tentative explanation of this different effect is the large dimension of the heptamolybdate precursor whose nature is little affected by the support.

Q: W. K. Hall (USA)

In our work (Proc. Conf. on Uses of Molybdenum, 1982), we found that tetrahedral Mo(VI) exists in small amounts on MoO_3/Al_2O_3 catalyst, this can be reduced to Mo(V), but no further. A second Mo(V) signal is developed as the catalyst is reduced, this stems from reduction of the octahedral molybdenum present in the polymolybdate clusters. The latter dominates at intermediate values of e/Mo, but when e/Mo>3, the tetrahedral signal now remains. Have you seen this behavior in your system ? I noted that you said your Mo(V) was monomer.

A: V. Indovina

In the case of MoO_x/ZrO_2, the tetrahedral Mo(V) is formed at very low concentration after heating the samples with O_2 at 773 K followed by evacuation at the same temperature. After reduction with H_2 at 400 to 800 K, a different Mo(V) signal is observed. The ESR analysis of spectra of samples containing ^{95}Mo allows assigning the signal to a mononuclear Mo(V) species on the surface of ZrO_2 ($Mo(V)_{5c}$).

Guczi, L. *et al.* (Editors), *New Frontiers in Catalysis*
Proceedings of the 10th International Congress on Catalysis, 19-24 July, 1992, Budapest, Hungary
© 1993 Elsevier Science Publishers B.V. All rights reserved

Pt-Sn-ALUMINA CATALYSTS: RELATING CHARACTERIZATION AND ALKANE DEHYDROCYCLIZATION DATA

B. H. Davis

Center for Applied Energy Research, University of Kentucky, 3572 Iron Works Pike, Lexington, KY 40511, USA

1. INTRODUCTION

Bimetallic catalysts have been of interest in heterogeneous catalysis for many years. Schwab, in a classic paper (1), called attention to the role of alloy composition in determining catalytic activity. The electronic theory of catalysis (2,3) provided motivation for numerous studies with alloy catalysts during the 1950s. Introduction of the Pt-Re naphtha reforming catalyst by Chevron in the 1960s (4) provided additional motivation for the study of supported bimetallic catalysts.

Many early investigators held the view that d-band electron concentration could be controlled by alloy formation so that catalytic selectivity and/or activity could be influenced through control of the d-band electron concentration (5). Many workers used concepts based upon alloy formation to explain the results from their studies of supported bimetallic catalysts (e.g., refs. 6,7). As more studies were completed with supported bimetallic catalysts, workers began to question the extent of alloy formation in these catalysts. Sinfelt (8) introduced the concept of metal clusters, without specifying a cluster composition, to account for the properties of supported bi- or poly-metallic catalysts.

The Pt-Sn bimetallic catalyst was introduced shortly after the Pt-Re combination. While Pt-Sn received much attention, both for activity and characterization studies, it was not utilized as widely as the Pt-Re catalyst. However, the Pt-Re catalyst requires a complex pretreatment/induction period in order for the catalyst to exhibit its superior selectivity and aging properties. Continuous regeneration naphtha reforming processes have received considerable attention recently. Since it is not practical to use, in this process, catalysts which require elaborate pretreatments, the Pt-Sn bimetallic catalyst is receiving renewed attention.

A considerable number of studies have been devoted to the characterization of supported and unsupported Pt-Sn catalysts. Likewise, a number of studies have been devoted to determining the selectivity and/or activity of these catalysts. Characterization data for supported catalysts can be found to promote the view that incomplete reduction of tin prohibits the formation of an alloy in the supported material; on the other hand, data can be found that supports alloy formation. Most

of the activity studies have been conducted at atmospheric pressures rather than the higher pressures normally encountered in naphtha reforming processes.

We have therefore prepared a series of catalysts, using both acidic and nonacidic supports, with a range of Sn/Pt ratios. These catalysts have been utilized in a number of characterization studies and have been employed in activity measurements both at atmospheric and higher pressure alkane dehydrocyclization studies. A comparison of the characterization and activity data is the subject of this paper.

2. EXPERIMENTAL

2.1. Catalysts.

Acidic porous transitional aluminas were prepared by precipitation from an aluminum salt solution or a nonporous Degussa Aluminum Oxide C was used. Nonacidic alumina was prepared by precipitation from a potassium aluminate solution by bubbling CO_2 into the solution. Surface areas of the supports were in the 110-210 m^2/g range. A number of impregnation techniques were employed. Many of the preparations employed an organic solvent, acetone, to inhibit the hydrolysis of the tin chloride solution. In several instances, a specific bimetallic complex, e.g., $[Pt_3Sn_8Cl_{20}]^{2-}$, was employed. To our knowledge, these early preparations were among the first, if not the first, to employ an organic solvent and a bimetallic complex for the preparation of bimetallic catalysts to ensure an initial uniform distribution of the two metals over the support surface (9). When a specific Pt/Sn complex was not utilized, an acetone solution of chloroplatinic acid and stannous chloride was used to impregnate the support.

2.2. Characterization.

In-situ X-ray diffraction studies (XRD) were carried out wherein the reduction and/or oxidation procedures could be effected without either sample transfer or exposure to air following pretreatment. In other XRD studies the sample was pretreated in hydrogen and then passivated in a helium stream containing 1% oxygen. X-ray photoelectron spectroscopy (XPS) studies involved the pretreatment of the sample in a reaction chamber capable of high pressure (several atmospheres) and temperature (to 500°C) followed by insertion of the sample holder directly into the XPS vacuum chamber without exposure of the sample to the atmosphere. Mössbauer studies were conducted using a reduced sample that had been transferred in a glove box to an argon-filled and sealed holder containing about 450 mg sample. Samples utilized for absorption near edge structure (XANES) and extended X-ray absorption fine structure (EXAFS) spectra were prepared similarly to those employed for the Mössbauer studies.

2.3. Reactions.

For atmospheric conversion studies a glass reactor system, using glass beads as preheater, was utilized; reactant was fed using a syringe pump. For the higher pressure studies a stainless steel plug-flow reactor, utilizing quartz chips as preheater, was employed. Hydrogen feed was controlled using a mass flow regulator and the hydrocarbon was fed using a positive displacement pump. The catalyst was pretreated at 500°C and the reaction was conducted at 482°C. Product analysis was accomplished using gas chromatograph.

3. RESULTS

3.1. Characterization.

In-situ XRD studies of catalysts containing either 5 or 0.6% Pt and varying amounts of Sn on nonporous Degussa Aluminum Oxide C clearly showed the presence of PtSn alloy, and PtSn was the only alloy phase detected (Figure 1). This is surprising since a number of PtSn phases are stable (e.g., Pt_3Sn, PtSn, $PtSn_2$, $PtSn_3$) and alloys containing more Sn would be anticipated for the catalysts with higher Sn/Pt ratios. However, as the Sn/Pt ratio increases the relative area of XRD peaks corresponding to PtSn alloy increases (Figure 2.) Thus, the XRD data indicate

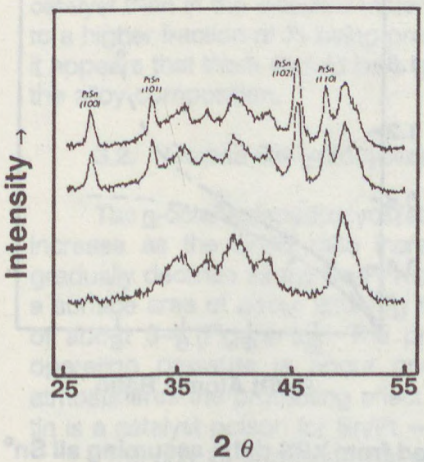

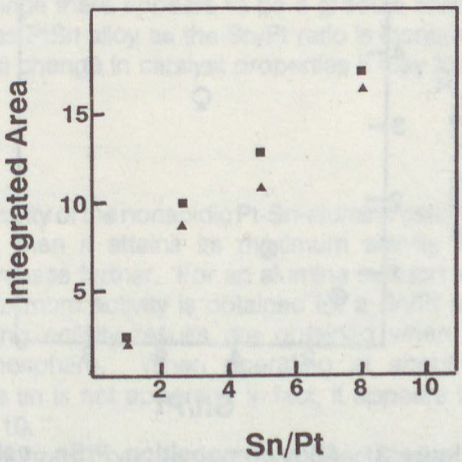

Figure 1. XRD profile for: (bottom) Degussa Aluminum Oxide C alumina support, (middle) 5 wt.% Pt (Pt:Sn = 3:8) on alumina after reduction at 400°C and (top) 5 wt.% Pt (Pt:Sn = 3:8) on alumina after reduction at 500°C.

Figure 2. Integrated intensity of the 100% PtSn (102) alloy profile versus tin content for varying Sn/Pt ratios using United Catalysts, Inc. (■) and Degussa alumina (▲) support.

that for the lower Sn/Pt ratios platinum is present as both Pt° and PtSn alloy; the ratio of the two forms of platinum depends upon the Sn/Pt ratio.

Early XPS studies did not provide evidence for the reduction of tin to the Sn° (10,11). However, later XPS studies using an instrument with a much better vacuum system resulted in the detection of Sn° and showed that as the Sn/Pt ratio increased so did the amount of tin in the PtSn alloy. It must be emphasized that XPS data does not provide direct evidence for PtSn alloy formation. However, it is possible to use the XPS data to obtain a fraction of the tin that is present as Sn° and this, together with the known amount of Pt and Sn present in the catalyst and the assumption, verified using both Rh/Sn catalysts and Pt/Sn on carbon or silica supports, that all platinum is present as Pt°, permits us to calculate the alloy composition for $PtSn_x$. The data, plotted in Figure 3, indicate that the alloy apparently becomes richer in Sn as the Sn/Pt ratio increases (12).

The number of Mössbauer studies of PtSn-alumina catalysts is too large to describe here; however, the general results suggest that tin is present as Sn^{4+}, Sn^{2+} and Sn°. Our results for two PtSn-alumina catalyst series are in agreement with this observation for the valence of tin (13). Moreover, as the ratio of Sn/Pt increases the amount of PtSn increases. In Figure 4 we have plotted the value of $\underline{x}$ for $PtSn_x$ as Sn/Pt increases; in making this plot we have assumed that all of the platinum is present as Pt°.

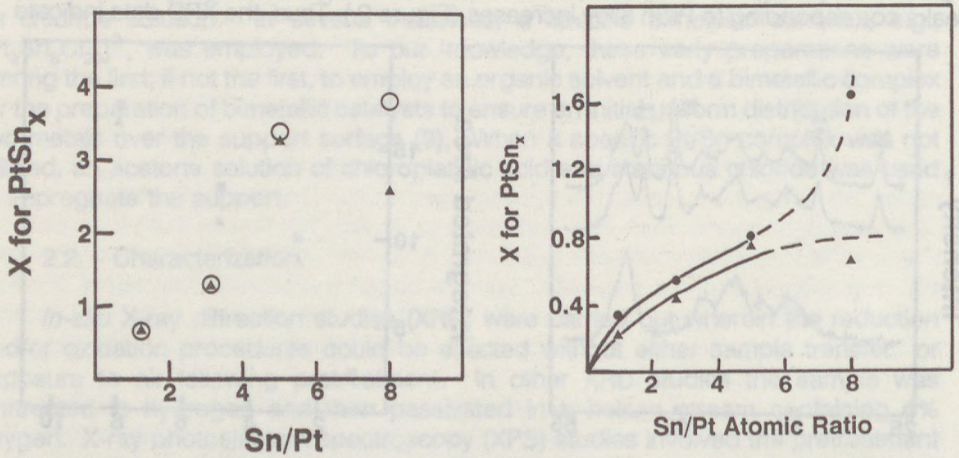

Figure 3. Alloy composition, $PtSn_x$, calculated from XPS data, assuming all Sn° is present as alloy, for varying Sn/Pt ratios using UCI (○) and Degussa (▲) alumina supports.

Figure 4. Composition of PtSn alloy calculated based upon Mössbauer data versus Sn/Pt ratio for Degussa alumina (●) and UCI alumina (▲).

Structures for a series of Pt/Sn-alumina catalysts similar to those described above were obtained from NEXAFS and EXAFS data (14,15). Resolved near-edge

profiles indicate that the higher states of oxidation have larger d band vacancies, presumably due to enhanced ionicity of the platinum centers. Increasing the tin loading decreases the d band vacancy. These results are in general agreement with a report by Lytle et al. (16). EXAFS data indicate three types of Pt bonding in the nearest neighbor bonding: Pt-O, Pt-Cl and Pt-Sn. These data are consistent with PtSn alloy formation but do not require it.

In the preparation of the above catalysts chloride is incorporated since the metals were added as the chloride containing salt. Alumina is particularly effective in retaining the halide added during catalyst preparation (10). The XPS study revealed a surprising fact concerning the surface chloride since the material pretreated in hydrogen at 400°C had a significantly lower Cl/Al peak area ratio than the same material following pretreatment in oxygen at 400°C or higher. Furthermore, it was observed that repeated pretreatments in hydrogen and then oxygen caused the lower and then the higher Cl/Al ratios to also repeat.

In summary, the characterization data indicate that PtSn alloy is formed following reduction of alumina supported catalysts. It appears that the dominant alloy is one with Pt:Sn = 1:1; other alloys, if present, constitute minor components of the bimetallic catalytic material. Furthermore, not all of the Pt is present as an alloy for catalysts with low Sn/Pt ratios and the fraction of alloy increases with increasing Sn/Pt ratios. Chloride is retained by the catalysts when alumina is the support; however, it appears that the fraction of chloride in the surface layers is lower in the reduced catalyst than in the oxidized material. Since there appears to be a gradual change to a higher fraction of Pt being present as PtSn alloy as the Sn/Pt ratio is increased, it appears that there should be a gradual change in catalyst properties if they follow the alloy composition.

3.2. Octane Dehydrocyclization.

The n-octane dehydrocyclization activity of the nonacidic Pt-Sn-alumina catalysts increase as the Sn/Pt ratio increases, then it attains its maximum activity and gradually declines as the Sn/Pt ratio increases further. For an alumina support with a surface area of about 200m^2/g the maximum activity is obtained for a Sn/Pt ratio of about 3-4 (Figure 5). The preceding activity results are obtained when the operating pressure is about one atmosphere. When operating at about 30 atmospheres the promoting effect of the tin is not apparent; in fact, it appears that tin is a catalyst poison for Sn/Pt = 6 to 10.

The only C_8-aromatics that can be formed from n-octane by a direct six-carbon ring closure are ethylbenzene and ortho-xylene. The data in Table 1 show that equal amounts of ethylbenzene and ortho-xylene are formed for a catalyst containing only Pt; the unallowed C_8-aromatics, meta- and para-xylene, are present in minor amounts. There is a change in the distribution of the allowed C_8-aromatics for a catalyst containing Sn/Pt ratio of about 3; for this catalyst ortho-xylene is formed in about twice the amount of the ethylbenzene. Again, for this Sn/Pt catalyst only a minor fraction of the aromatics are those corresponding to those not allowed by a direct C_6 ring closure. Surprisingly, for the higher Sn/Pt ratios, where the total conversion to

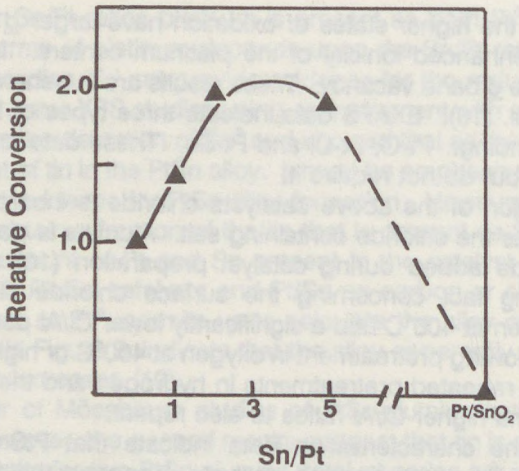

Figure 5. The variation of n-octane conversion at atmospheric pressure with increasing tin loading using a nonacidic alumina support (point at right is for Pt on SnO_2 only).

Table 1
Aromatic Products from n-Octane Dehydrocyclization with Pt-Sn-Nonacidic Alumina Catalysts

		Aromatics			
Catalyst	Pressure	Ethylbenzene	o-Xylene	m-Xylene	p-Xylene
Pt-	1 atm.	48	50	1.2	1.0
Pt-Sn = 3:8	1 atm.	32	59	5.0	2.4
Pt	7.8 atm.	45	48	7.0	trace
Pt-Sn- = 1:3	7.8 atm.	38	62	trace	trace

aromatics is smaller, the fraction of unallowed C_8-aromatics is higher than for Pt only or for low Sn/Pt ratio catalysts. The same aromatic selectivities are obtained at 1 and 7.8 atmospheres.

The C_8-aromatics produced using a Pt-alumina catalyst using an acidic alumina support, are nearly an equilibrium mixture of four possible isomers. Furthermore, the

conversion of n-octane to C_8-aromatics is much slower than the isomerization of n-octane to other isomeric C_8-alkanes (Figure 6). Thus, with the acidic catalyst the isomerization of n-octane to a nearly equilibrium mixture of C_8-alkanes is essentially completed before appreciable C_8-aromatics are formed. In addition, the acidic catalyst produces aromatics more selectively than a corresponding Pt-nonacidic alumina catalyst. This means that there is a bifunctional cyclization pathway that is both more rapid and more selective for C_8-aromatic production than for the monofunctional catalyst based upon a nonacidic support.

The data in Figure 7 is for catalysts based upon an acidic support but with increasing Sn/Pt ratios. It is apparent that the addition of tin has a detrimental effect upon the conversion of n-octane. Thus, for the catalysts prepared by surface impregnated the presence of tin to give Sn/Pt of about 0.5 or higher, the tin acts as a catalyst poison.

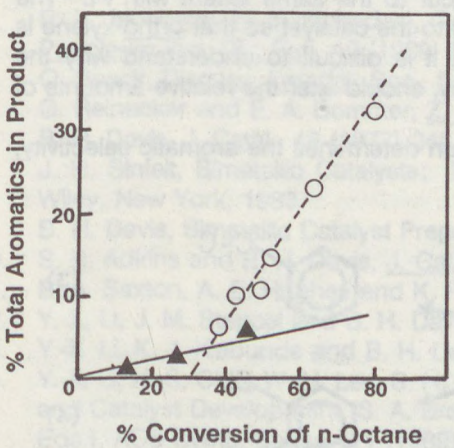

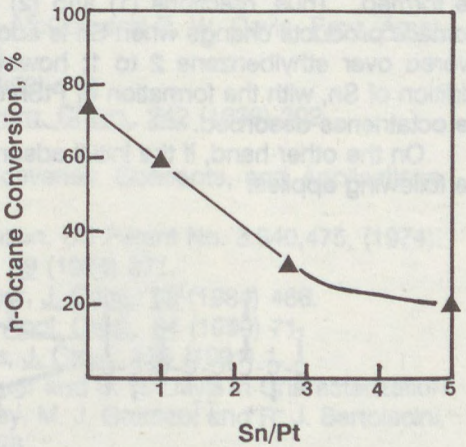

Figure 6. **Aromatics formed from the conversion of n-octane using a nonacidic (▲) and an acidic (○) alumins support (LHSV, varied; 7.8 atm; H_2/n-octane = 3:1; 482°C).**

Figure 7. **n-Octane conversion with increasing Sn/Pt ratio using an acidic alumina support (482°C, 7.8 atm, LHSV = 1.8, and H_2/n-octane = 3/1).**

4. DISCUSSION

One of the proposed pathways for the metal catalyzed dehydrocyclization of alkanes involves the consecutive dehydrogenation to a conjugated triene followed by gas phase thermal cyclization. For dehydrocyclization of n-octane by this pathway with a nonacidic catalyst the following would apply:

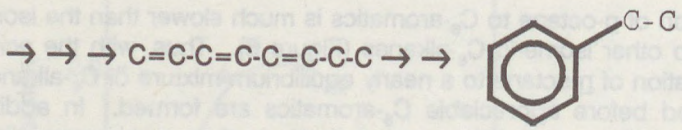

(1)

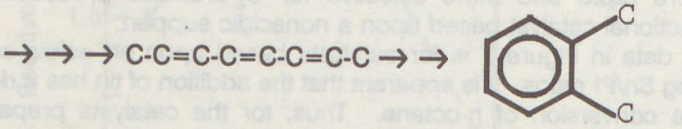

(2)

For the catalyst containing only Pt, equal amounts of ethylbenzene and ortho-xylene are formed. Thus, reactions (1) and (2) occur to the same extent with Pt. The aromatic products change when Sn is added to the catalyst so that ortho-xylene is favored over ethylbenzene 2 to 1; however, it is difficult to understand why the addition of Sn, with the formation of PtSn alloy, should alter the relative amounts of the octatrienes desorbed.

On the other hand, if the initial adsorption determines the aromatic selectivity, the following applies:

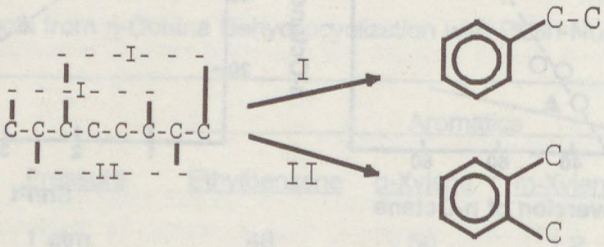

(3)

(4)

Cyclization by I involves a primary C-H and a secondary C-H bond whereas cyclization by II involves two secondary C-H bonds. Primary C-H bonds require more (at least 3 kcal/mole) energy for rupture than do secondary C-H bonds. Thus, reaction pathway 4, with cyclization through II, is favored by the addition of tin provided the adsorption potential of the metal surface is decreased by alloy formation. Since tin presumably donates electrons to decrease the number of d-band holes (e.g., EXAFS data), a product selectivity determined by adsorption appears more reasonable to us than the triene mechanism.

For the bimetallic Pt-Sn on nonacidic alumina, increasing the Sn/Pt ratio increases both the extent of alloy formation and the catalytic activity. Thus, it is concluded that for the single-functional metal catalyzed pathway, the formation of Pt-Sn alloy is beneficial since the alloy is more active than Pt alone.

For the acidic catalyst support, the situation is very different. The bifunctional pathway produces aromatics more rapidly and selectively than the metal catalyzed single-function pathway. Thus, it appears that the loss of acidic sites that is caused by the addition of tin by impregnation more than cancels any gain caused by alloy formation for the metal-only cyclization pathway. For the acidic catalyst it appears that the beneficial role for Sn is to primarily, or only, improve long-term aging by maintaining a better metal dispersion.

REFERENCES

1. G. M. Schwab, Discuss. Faraday Soc., 8 (1950) 166.
2. D. A. Dowden, J. Chem. Soc., (1950) p. 242.
3. D. D. Eley, Catalysis and the Chemical Bond, Univ. of Notre Dame Press, Notre Dame, 1954.
4. R. L. Jacobson, H. E. Kluksdahl, C. S. McCoy and R. W. Davis, Proc. Amer. Petroleum Inst, Div. Ref., 49 (1969) 504.
5. O. Beeck, Discuss. Faraday Soc., 8 (1950) 118.
6. G. Reinacker and E. A. Bommer, Z. Anorg. Chem., 242 (1939) 302.
7. B. H. Davis, J. Catal., 46 (1977) 348.
8. J. H. Sinfelt, Bimetallic Catalysts: Discoveries, Concepts, and Applications, Wiley, New York, 1983.
9. B. H. Davis, Bimetallic Catalyst Preparation, US Patent No. 3,840,475, (1974).
10. S. R. Adkins and B. H. Davis, J. Catal., 89 (1984) 371.
11. B. A. Sexton, A. E. Hughes and K. Foger, J. Catal., 88 (1984) 466.
12. Y.-X. Li, J. M. Stencel and B. H. Davis, Appl. Catal., 64 (1990) 71.
13. Y.-X. Li, K. J. Klabunde and B. H. Davis, J. Catal., 128 (1991) 1.
14. Y.-X. Li, N.-S. Chiu, W.-H. Lee, S. H. Bauer and B. H. Davis in Characterization and Catalyst Development (S. A. Bradley, M. J. Gattuso, and R. J. Bertolacini, Eds.), ACS Symp. Series 411 (1989) 328.
15. N.-S. Chiu, W.-H. Lee, Y.-X. Li, S. H. Bauer and B. H. Davis in Hydrotreating Catalysts. Preparation, Characterization and Performance (M. L. Occelli and R. G. Anthony, Eds.) Elsevier Sci. Pub., Amsterdam, (1989) 147.
16. F. W. Lytle, P. S. P. Wei, R. B. Gregor, G. H. Via and J. H. Sinfelt, J. Chem. Phys., 70 (1979) 4849.

DISCUSSION

Q: A. Duncan (Norway)

It was indicated during the presentation that for a co-precipitated catalyst a constant conversion is obtained with respect to the Sn/Pt ratio, in contact to the co-impregnated system. This, I assume, is due to the absence of PtSn alloying found. I am interested to know if (1) the quoted Sn/Pt ratios for the co-precipitated system relates to the total (bulk) Sn in the alumina support, and (2) if this is the case, is there any knowledge of the alumina surface composition (Sn/Pt) even though alloying in the Pt particles is not observed.

A: B. H. Davis

1) The Sn/Pt ratios for the co-precipitated tin-aluminum oxide refers to the bulk composition, and not to the surface composition.

2) The constant activity for the Sn/Pt ratios = 0, 1, and 3 are taken as an indication that the surface concentration of tin is sufficiently low so that acid sites are not eliminated to a significant extent for a given Sn/Pt ratio compared to a similar catalyst where the tin was added by co-impregnation with the Pt. In other words, for the same bulk Sn/Pt ratio, the co-impregnated sample will have a much higher surface concentration of tin.

Q: S. Csicsery (USA)

1) Did you observe over the nonacidic Pt and Pt/Sn catalyst any meta- or para-xylenes, and, if yes, do you have any hypothesis explaining their formation ? Could 7- or 8-membered ring intermediates be involved ?

2) Did you notice any difference of the CH_4/total hydrogenolysis products ratio between non-acidic Pt and Pt/Sn catalysts ?

A: B. H. Davis

1) For the nonacidic Pt and lower Sn/Pt ratio catalysts at least 90 % or more of the aromatics are ethylbenzene and o-xylene. The minor amounts of m- and p- xylene are believed to be due to isomerization of the n-octane charge rather than the formation of 7- or 8-membered rings. Pines and Chen [1] found only 17 % methyl label from the cyclization of n-[1-^{14}C]-heptane with a nonacidic chromia catalyst, and explained this as being due to the formation of a cycloheptane intermediate. As you are well aware, Pines and coworkers then extended this concept to other catalysts and other reactants [2-4]. Our ^{14}C data for n-heptane dehydrocyclization, using a nonacidic chromia-alumina catalyst prepared according to the recipe provided by Pines and Chen, produced toluene with the ^{14}C in the positions expected for direct six-carbon ring formation (the position meta to the methyl group for n-[4-^{14}C]-heptane and the methyl plus ortho to the methyl group for n-[1-^{14}C]-heptane [5, 6]. We have therefore not obtained data consistent with 7- or 8-membered ring intermediates with nonacidic chromia-alumina catalysts. In our studies [5, 6] we degraded the aromatic ring so that the relative activity of the methyl and each ring position could be calculated. For both [1-^{14}C-] and [4-^{14}C] heptane dehydrocyclization, the ^{14}C ring distribution eliminated cycloheptane as a significant reaction intermediate.

2) The low C_1 - C_4 gas make and the significant molar excess of hydrogen precluded us from making a definite conclusion concerning this point.

[1] H. Pines and C. T. Chen, *J. Org. Chem.*, **26**, 1057 (1961)
[2] H. Pines and C. T. Goetschel, *J. Org. Chem.*, **30**, 3530 (1965)
[3] H. Pines and S. M. Csicsery, *J. Am. Chem. Soc.*, **84**, 292 (1962)
[4] H. Pines, C. T. Goetschel and S. M. Csicsery, *J. Org. Chem*, **28**, 2713 (1963)
[5] J. A. Feighan and B. H. Davis, *J. Catal.*, 4, 594 (1965)
[6] B. H. Davis and P. B. Venuto, *J. Org. Chem.*, **36**, 337 (1971)

Q: G. Maire (France)

For the bimetallic Pt-Sn on non-acidic alumina (see p.) do you exclude formation of both ethylbenzene and ortho-xylene via ring enlargement from the cyclopentanes formed ? It is known from the work of F. Gault (Advances in Catalysis, 1980) that such mechanism takes place on small particles of Pt or even on alloys.

A: B. H. Davis

My view is that the formation of aromatics at both low (1 atm) or high (7-30 atm) occurs over a non-acidic Pt or PtSn catalyst by a direct six carbon ring formation. We are familiar with the work of the late Professor Gault. In fact, Professor Gault compared our earlier work to his data on page 56 in the reference cited [7], "The distribution determined by microwave spectrometry of the toluenes from n-heptane-1-^{13}C is: methyl (^{13}C), 50 %; ortho-^{13}C, 34 %; meta-^{13}C, 16 % [8]. These results can be compared to those obtained by Davis [9] with n-heptane-1-^{14}C. The formation of meta-labeled toluene can be explained neither by direct 1-6 carbon ring closure, nor by cyclic-type isomerization of n-heptane to 3-methyl hexane followed by 1-6 ring closure of the latter. "Alkylcyclopentanes undergo ring-opening hydrogenolysis to produce products that are very similar to the distribution expected for a statistical bond rupture mechanism [10-12]. Thus, for [1-^{14}C]- or [1-^{13}C]-heptane the following applies for cyclization to produce ethylcyclopentane and 1,2-dimethylcyclopentane followed by hydrogenolysis (only pathways leading to methyl hexanes are included; represents the position of the labeled atom):

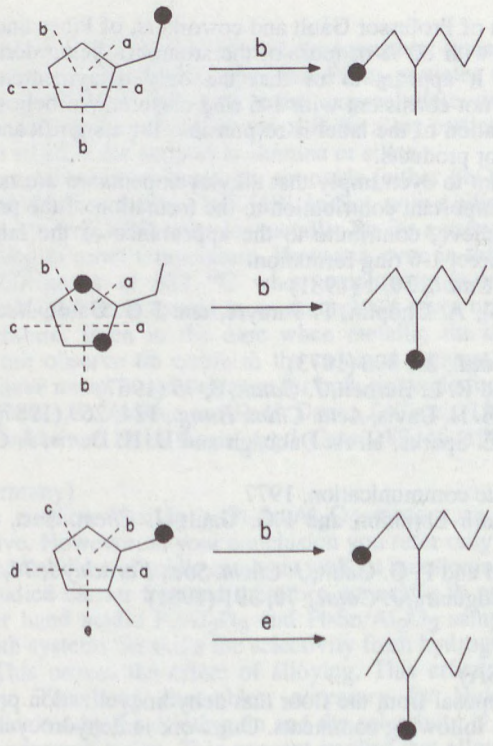

Interchange of the label in the methyl groups of 1,2-dimethylcyclopentane leads to the same products except the bond rupture labels a through e will now be labeled clockwise rather than counter clockwise as above. Direct 1-6 ring closure of the two labeled methylhexanes will produce toluene labeled in the methyl and the meta-ring position, just as was observed by Professor Gault and coworkers with [1-^{13}C]-heptane. Professor Gault and coworkers also converted [1-^{13}C]-heptane with the same catalyst under the same conditions and wrote [13]: "A less accurate analysis of the toluene by microwave spectroscopy shows the presence of meta-labeled toluene only. an accurate mass spectrometric analysis of the methylcyclohexanes obtained by hydrogenation of toluenes shows that only 2.5 + 1 % of the label is located on the methyl group." Thus, the data for [1-^{13}C]-heptane dehydrocyclization, based upon microwave analysis, does not agree with the data Professor Gault and coworkers obtained with [4-^{13}C]-heptane using the same catalyst. Parayre et al. [14] converted 2-methyl [2-^{13}C] hexane with the same catalyst used for the dehydrocyclization of labeled n-heptane and concluded "... that 1-6 and not 1-5 ring closure is the major mechanism of this reaction (dehydrocyclization to toluene).

Amir-Ebrahimi and Gault [15] converted ^{13}C-labeled 3-methylhexane over the same catalyst and reported that "2-methyl hexane is aromatized almost exclusively by 1-6 ring closure..."

Pines and Nogueira [16] found the methyl ^{14}C labeled from the dehydrocyclization of n-[1-^{14}C]-heptane that was in excellent agreement with the data we had reported earlier [9]. Pines and Nogueira chose to explain their data by a combination of mechanisms, including the formation of a cycloheptane intermediate. However, the data of Pines and Nogueira are consistent with more than 80 % of the toluene being formed by 1-6 ring closure.

The experimental data of Professor Gault and coworkers, of Pines and Nogueira, and our data are all consistent with 80 % or more of the aromatics being derived from a 1-6 ring closure mechanism. It appears to us that the only disagreement concerns the formation of the products not consistent with 1-6 ring closure. We believe experimental error in measuring the location of the label is responsible for a significant amount of the "appearance" of these minor products.

Finally, we do not want to even imply that alkylcyclopentanes are not formed, only that they do not make an important contribution to the formation of the primary aromatic products. They do, we believe, contribute to the appearance of the labeled carbon at positions not allowed by direct 1-6 ring formation.

[7] F. G. Gault, *Adv. Catal.*, **30**, 1 (1981)
[8] V. Amir-Ebrahimi, A. Choplin, P. Parayre, and F.G. Gault, *Nouv. J. Chim.*, **4**, 431 (1980)
[9] B. H. Davis, *J. Catal.*, **29**, 398 (1973)
[10] S. M. Csicsery and R. L. Burnett, *J. Catal.*, **8**, 75 (1967)
[11] R. H. Hardy and B. H. Davis, *Acta. Chim. Hung.*, **124**, 269 (1987)
[12] C. S. Huang, D. E. Sparks, H. A. Dabbagh and B. H. Davis, *J. Catal.*, **134**, 269 (1991)
[13] F. G. Gault, private communication, 1977
[14] P. Parayre, V. Amir-Ebrahimi and F.G. Gault, *J. Chem. Soc., Faraday I*, **76**, 1723 (1980)
[15] V. Amir-Ebrahimi and F. G. Gault, *J. Chem. Soc., Faraday I*, **76**, 1735 (1980)
[16] H. Pines and L. Nogueira, *J. Catal.*, **70**, 391 (1981)

Q: W. P. Hettinger, Jr. (USA)

With regard to the proposal from the floor that dehydrocyclization proceeds through a triene species, I have the following comments. Our work in dehydrocyclization in 1952

and reported in Ind. and Eng. Chem., 1955, and the Gordon Research Conference of 1953, clearly showed that dehydrocyclization, although sensitive to pressure, still proceeded quite well at high pressures where dehydrogenation to a triene is highly improbable. Our kinetics as presented, showed no evidence of an intermediate, therefore suggesting one step cyclization followed by high rate dehydrogenation. In later work, reported orally at the 2nd ICC in Paris, 1960, we showed that co-gelation of tetramethyl hexahydroxy platinum, coprecipitated with aluminum acetate produced a white catalyst, which stayed white on H_2 reduction at 500 ^{0}C. This suggested isolation of single platinum atoms, which still showed dehydrocyclization, thereby suggesting cyclization takes place on a single atom, and does not require multiple platinum atoms to achieve cyclization. Therefore, I must support Dr. Davis' conclusion that in his studies direct cyclization to a cyclohexane ring followed by very high rate of dehydrogenation, or cyclopentane isomer formation followed by isomerization to a cyclohexane ring, is the mechanism and is related to the concentration of Pt-Sn content, undoubtedly a surface which highly utilizes the direct cyclization reaction.

A: B. H. Davis
Thank you for your remark

Q: J. Ryczkowski (Poland)
As you have mentioned, not all of the Pt is present as an alloy for catalysts with low Sn/Pt ratios and the fraction of bimetallic phase increases with increasing Sn/Pt ratios. My question is, have you any observation for forming other tin phases except Pt-Sn alloys ? What about tin oxide formation ?

A: B. H. Davis
If one searches long enough in a heterogeneous system, one can find many structures. We have reported, for example, that $PtSn_2$ particles are observed infrequently in a Pt-Sn-alumina catalyst prepared from coprecipitate tin-aluminum oxide [17]. However, in all catalysts the predominance of Pt/Sn alloy particles have the ratio of Pt:Sn = 1:1; this is true whether the support is alumina or silica.

We have never obtained evidence for tin oxide (either SnO or SnO_2) by XRD, even when the material contains Pt:Sn = 1:12 [18]. In fact, with a silica supported catalyst with Pt:Sn = 1:12, we observe XRD lines for metallic Sn for a sample following reduction at 482 ^{0}C and cooling to room temperature. However, even in this case we do not observe metallic Sn XRD peaks at 482 ^{0}C when employing in-situ XRD measurements; presumably the reduced tin is spread in an amorphous layer upon the support surface at this high temperature. Even in the case when metallic tin is formed in the reduced sample, we do not observe tin oxide in the calcined catalyst. In hundreds of catalyst preparation, we have never found evidence for bulk tin oxide formation.

[17] R. Srinivasan, L. A. Rice and B. H. Davis, *J. Catal.*, **129**, 257 (1991)
[18] R. Srinivasan and B. H. Davis, *Appl. Catal.*, **87**, 45 (1992)

Q: J. Völter (Germany)
Our results confirm that in a Pt-Sn/Al_2O_3 system an alloy is formed and is catalytically active. However, in your conclusion you refer only on differences in activity and stability in nonacidic and acidic catalysts without mentioning the selectivities.

We have studied carrier free and therefore nonacidic Pt powder and the PtSn alloy and on the other hand acidic Pt/Al_2O_3 and Pt-Sn/Al_2O_3 samples in the conversion of n-heptane. In both systems Sn shifts the selectivity from hydrogenolytic cracking towards aromatization. This proves the effect of alloying. This effect can be explained by the ensemble theory. The large ensembles, necessary for hydrogenolytic splitting are predominantly blocked by the diluting tin and the selectivity is shifted towards the facile reaction, the dehydrocyclization. This concept implies that alloying is a sufficient but not

a necessary condition because a blockade can be caused by any inactive material. This could be tin as well as tin oxide. We have distinct hints that the bimetal effect on selectivity can be caused by reducible as well as by unreducible oxides of the added second metal. This concept could bridge the gap between the results of Dr. Davis, stressing the role of alloys and the results presented by Dr. Schwank et al., presented in the following paper [19]. They show that under their conditions Pt-Sn alloys are hardly formed.

[19] J. Schwank, K. Balakrishnan and A. Sachdev, *Proc. 10th Int. Congr. on Catal.*, **Vol A**, 905(1992)

A: B. H. Davis

Unfortunately, none of the characterization techniques that permit a direct measure of the crystal phase (TEM, microdiffraction, XRD, etc.) provide a very reliable quantitative measure of the fraction of Pt that is present in an alloy form. Thus, it is not evident that there is a gap between the data we obtained and that of Schwank et al. Our conclusion is that alloy formation increases with an increasing Sn/Pt ratio, and this was observed by Schwank et al. Based upon our XRD intensity data (Figure 2 of our paper) we would not expect more than 10 %, and perhaps less, of the Pt in the Sn:Pt = 1:1 to be present as alloy. Schwank et al. [19] reported electron microscopy results for Sn/Pt = 0.5 and 1.0. We do not view their qualitative observations for these two catalysts to eliminate the formation of alloy. We have prepared a series of catalyst using a Degussa alumina support material that is similar to the one used by Schwank et al. and have obtained both XRD and TEM microdiffraction data to show the presence of Pt:Sn = 1:1 alloy (e.g., Figure 2 of our paper).

Q: Z. Paál (Hungary)

The "gas phase cyclization of hexatrienes" has been mentioned in the paper. I do not believe that a molecules might lose several hydrogen atoms in catalytic steps and when it reaches the ultimate hexatriene stage, (when it may be attached to the surface by its three double bonds) it should desorb from the surface just in order to undergo thermal cyclization, then readsorb to form benzene. My views on the stepwise ("hexatriene") reaction route are illustrated by the scheme. A working Pt surface is likely covered by a partly dehydrogenated hydrocarbon pool even in excess hydrogen [20]; they may undergo further dehydrogenation, rehydrogenation, double bond- or cis-trans-isomerization and they may desorb in either stage. Surface unsaturated species are true intermediates of aromatization; those appearing in the gas phase are the products of surface dehydrogenation and desorption. Desorption should be less likely with increasing unsaturation (as indicated by shorter and shorter arrows). The surface pool "remembers" the original reactant structure, e.g., 1-hexene and 2-hexene have different reactivities [21]. Stepwise dehydrogenation produces either cis- or trans-isomers. The cis-isomer of hexatriene is aromatized likely rapidly and without desorption, the chance of its desorption being practically zero. It is possible that good aromatization catalysts have a special ability to form this precursor structure. The trans-isomer, on the other hand, has to isomerize and, during this process, it has also a minor chance to desorb to the gas phase. Hexatriene detected in the gas phase had always a trans structure [22]. Hydrogen is essential for surface trans-cis isomerization; as well as for the hdyrogenative desorption of unsaturated surface species since they tend to lose more H atoms than corresponding to exact hexene, hexadiene etc., stoichiometries. Trans- species unable to isomerize before their excessive dehydrogenation may be coke precursors [22].

[20] Z. Paál, M. Räth, B. Brose, W. Gombler, *React. Kin. Catal. Lett.*, **47**, 43 (1992)
[21] Z. Paál, B. Brose, M. Räth, W. Gombler, *J. Mol. Catal.*, **75**, L13 (1992)
[22] Z. Paál and P. Tétényi, *J. Catal.*, **30**, 350 (1973)

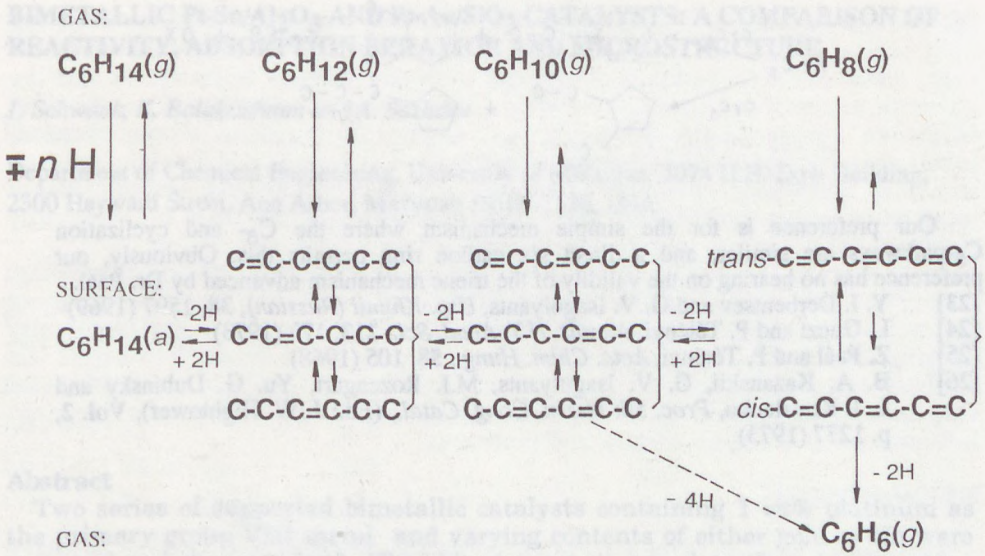

A: B. H. Davis

The results of kinetic tracer studies [23-26] were utilized to support a mechanism based upon gas phase hexatriene intermediates. We argue against the gas phase triene because (1) of the energy scheme the formation of a gas phase hexatriene is very unfavorable relative to the aromatic and (2) it does not account for change we obtain in the C_8 aromatic distribution that is caused by the addition of tin:

ortho-Xylene/Ethylbenzene

Catalysts	Pressure	
	1 atm	13-26 atm
$Pt\text{-}Al_2O_3$	1/1	1/1
$Pt\text{-}Sn\text{-}Al_2O_3$	2/1	2/1
$Pt\text{-}SiO_2$	1/2	-
$Pt\text{-}Sn\text{-}SiO_2$	2/1	-

To obtain convincing evidence to support or refuse the operation of a mechanism involving an adsorbed triene is a demanding task.

Cyclization of n-octane, for example, produces both C_8 aromatics and alkyl substituted cyclopentanes. These substituted alkylcyclopentanes are formed and undergo hydrogenolysis to produce isooctanes more rapidly than the C_8-aromatics are formed [11, 12]. The scheme outlined by Paál does not provide a means of forming these substituted cyclopentanes. For simplicity, we prefer to view the cyclization to be the result of competitive cyclization pathways:

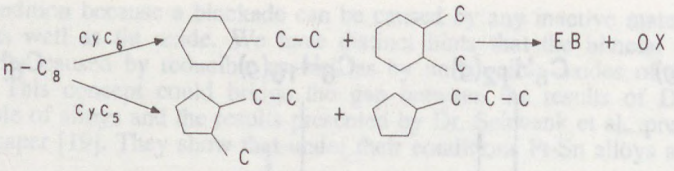

Our preference is for the simple mechanism where the C_6- and cyclization C_5-pathways are similar, and a direct six carbon ring permits this. Obviously, our preference has no bearing on the validity of the triene mechanism advanced by Dr. Paál.

[23] Y. I. Derbentsev and G. V. Isagulyants, *Usp. Khimii (Russian)*, **38**, 1597 (1969)
[24] L. Guczi and P. Tétényi, *Annals. N.Y. Acad. Sci.*, **213**, 173 (1973)
[25] Z. Paál and P. Tétényi, *Acta. Chim. Hung.*, **58**, 105 (1968)
[26] B. A. Kazanskii, G. V. Isagulyants, M.I. Rozengart, Yu. G. Dubinsky and L. I. Kovalenko, *Proc. 5th Intern. Cong. Catal.*, (Ed.: J. W. Hightower), **Vol. 2**, p. 1277 (1973)

Guczi, L. *et al.* (Editors), *New Frontiers in Catalysis*
Proceedings of the 10th International Congress on Catalysis, 19-24 July, 1992, Budapest, Hungary
© 1993 Elsevier Science Publishers B.V. All rights reserved

BIMETALLIC Pt-Sn/Al_2O_3 AND Pt-Au/SiO_2 CATALYSTS: A COMPARISON OF REACTIVITY, ADSORPTION BEHAVIOR AND MICROSTRUCTURE

J. Schwank, K. Balakrishnan and A. Sachdev

Department of Chemical Engineering, University of Michigan, 3074 H.H. Dow Building, 2300 Hayward Street, Ann Arbor, Michigan 48109-2136, USA

Abstract

Two series of supported bimetallic catalysts containing 1 wt% platinum as the primary group VIII metal and varying contents of either gold or tin were prepared and characterized. The objective was to correlate the microstructure with the activity and selectivity trends in reactions of hydrogen with either n-hexane or neopentane. In a multifaceted characterization protocol, special emphasis was placed on temperature programmed reduction, chemisorption of H_2, O_2 and CO, infrared spectroscopy of adsorbed CO, and analytical and high resolution electron microscopy. A major objective was to determine the state of the second metal and to assess the extent of solid solution or alloy formation in individual metal particles. The presence of gold manifested itself predominantly in terms of a geometric effect, breaking up larger ensembles of platinum. The behavior of the Pt-Sn catalysts was more complicated. Most of the tin was in a valence state of either Sn(II) or Sn(IV), according to XPS results, and most likely complexed with the alumina support. Tin was always located within close proximity to platinum particles. In a few instances, a few platinum-tin alloy particles were observed. However, they did not appear to play a significant role in controlling the catalytic behavior. Most of the platinum was present in monometallic form, with some particles in intimate contact with patches of ionic tin.

INTRODUCTION

Supported bimetallic catalysts containing platinum as the primary metal are of great importance both from an industrial as well as a fundamental research point of view. Adding tin to Pt/Al_2O_3 reforming catalysts leads to improved activity maintenance and higher selectivity for cyclization and isomerization, thereby giving a higher octane number product [1]. Adding inert gold to platinum can give fundamental insight into geometric and electronic effects in bimetallic catalysis. Comparing the effect of gold and tin is instructive in view of the differences in miscibility with platinum. The Pt-Au phase diagram shows a miscibility gap between 18 and 98% platinum, and an Au_3Pt solid solution can be formed. In contrast, Sn is completely miscible with platinum in the bulk state and according to the Pt-Sn phase diagram the

following phases exist: Pt_3Sn, PtSn, Pt_2Sn_3, $PtSn_2$, and $PtSn_4$ [2]. However, the bulk phase diagram is not necessarily applicable to the realm of nanometer scale metal particles in intimate contact with the alumina support. Sn and the alumina support can form a so called "Sn-aluminate" complex [3] stabilizing oxidation states of tin different from zero. The extent of metal-metal interactions in supported bimetallic systems is not always predictable based on the bulk miscibility of the two metals. Even if two metals are completely immiscible in the bulk state, they can still interact in the form of "bimetallic clusters" [4].

In this work we have compared the effect gold and tin on the reactivity, adsorption behavior, and surface composition of supported platinum, keeping the nominal loading of platinum constant at 1 wt % while systematically varying the amount of second metal. An effort has been made to correlate the surface characteristics of the catalysts with their bulk composition and structure, with the goal to better understand how the second metal component influences the catalytic behavior of platinum.

EXPERIMENTAL

Two series of supported bimetallic catalysts, containing Pt as the primary group VIII metallic component, were prepared using impregnation techniques. The first series was the Pt-Au/SiO_2 catalyst series where the nominal Pt loading was kept constant at 1 wt % and the Au nominal loading was 0, 0.3, and 0.7 wt %, respectively. In addition, a monometallic Au sample having a nominal Au loading of 2 wt % was prepared. Aerosil 200 silica with a BET surface area of 200 m^2/g was used as support. The Pt-Sn/Al_2O_3 catalyst series had a nominal Pt loading of 1 wt % and the Sn nominal loading was 0, 0.1, 0.5, and 1.0 wt %, respectively. A monometallic Sn sample having a nominal Sn loading of 2 wt % was also prepared. Non-porous Aluminum Oxide C with a BET surface area of 90 m^2/g was used as support. The alumina consisted of mainly the gamma phase and some of it was in the delta phase. There was less than 0.5 % HCl present in the alumina. Hydrogen hexachloroplatinate (IV) hydrate containing 39.7 wt% platinum, hydrogen tetrachloroaurate trihydrate containing 50 wt% gold, and tin (II) chloride having 61.7 wt% tin (all obtained from Aldrich Chemical Company) were used as precursors. The catalyst samples were prepared by impregnation or (for the bimetallics) co-impregnation of the support with a solution of the metallic precursors. The solvent used was distilled water in the case of the Pt-Au/SiO_2 samples and acetone in the case of the Pt-Sn/Al_2O_3 samples. After impregnation the samples were allowed to dry initially at room temperature and then overnight in a stream of flowing high-purity grade air at 393 K. The Pt-Sn/Al_2O_3 samples were calcined in a stream of flowing high-purity grade air at 773 K for 2 hrs. In the case of the silica supported samples the calcination step was avoided. Aliquots of the catalyst samples were then reduced in flowing hydrogen (15 SCCM/min) at 673 K for 5 hrs. Table 1 gives an overview of the catalysts, and lists both the nominal metal content based on the amount of precursor used for catalyst impregnation as well as the actual metal contents as determined by neutron activation after reduction. Temperature programmed reduction experiments were carried out in a flow

reactor on air-dried, unreduced catalyst samples, with a heating rate of 10 K/min in a stream of 3% H_2/N_2.

Table 1
Determination of catalyst composition by neutron activation analysis

Catalyst Code	Pt [wt%]	Au [wt%]	Sn [wt%]
1.0 Pt/SiO_2	1.00	---	---
1.0 Pt-0.3 Au/SiO_2	1.15	0.24	
1.0 Pt-0.7 Au/SiO_2	1.11	0.47	
2.0 Au/SiO_2	---	1.25	
1.0 Pt/Al_2O_3	0.99		---
1.0 Pt-0.1 Sn/Al_2O_3	0.96		0.14
1.0 Pt-0.5 Sn/Al_2O_3	1.00		0.53
1.0 Pt-1.0 Sn/Al_2O_3	0.89		0.99
2.0 Sn/Al_2O_3	---		1.90

Numerical values in the catalyst codes indicate nominal metal loading (wt %).

H_2, O_2, and CO chemisorption experiments were performed in a static-volumetric gas chemisorption system. Characterization by XPS was carried out using a Perkin Elmer PHI 5400 instrument with an Al anode of energy 1486.6 eV. The samples for XPS were reduced in an in-situ reactor directly attached to the analysis chamber so that the samples were not exposed to air at any time between the reduction and spectra collection. Fourier Transform Infrared spectroscopy of adsorbed CO was performed using a Digilab FTS 20/C instrument. The catalysts were pressed into a self-supporting wafer and mounted in a high-vacuum IR cell.

Analytical microscopy was carried out in a JEOL 2000FX operated at 200 kV. The elemental composition of small catalyst regions was determined by using Energy Dispersive Spectroscopy (EDX) with a stationary TEM probe. With this instrument, meaningful EDX results could only be obtained from regions larger than about 6 nm. To get better spatial resolution, a dedicated scanning transmission electron microscope (VG-HB501) was used. This instrument was equipped with a field emission gun which provided a very small electron probe and high current density making it possible to extract EDX signals from regions as small as 1 nm in diameter. A collection period of a maximum of 200 seconds was allowed for each spectrum.

Structural information of metallic regions was obtained from high resolution electron microscopy (HREM) on a JEM- 4000EX microscope operating at 400 kV. To determine the accurate lattice spacings, optical diffractograms of the structure images were obtained. The distances on the diffractograms were calibrated using a Si<111> specimen whose {220} lattice spacings measure 0.192 nm. In some cases it was necessary to compare the

experimental images with image simulations based on the multislice method [5].

Catalytic probe reactions of n-hexane and neopentane with hydrogen were carried out in a flow reactor under differential reaction conditions at pressures close to 1 atm (1 atm = 1.013 x 10^5 Pa). Product analysis was accomplished by means of gas chromatography.

RESULTS AND DISCUSSION

Effect of gold and tin on temperature programmed reduction of platinum

Temperature-programmed reduction experiments were conducted to evaluate the effect of gold and tin on the reducibility of platinum. Figure 1 illustrates the hydrogen consumption of freshly prepared catalysts as a function of reduction temperature, tracking the genesis of reduced metal species in the catalysts. The dashed line in the figures indicates the peak temperature for monometallic Pt reduction.

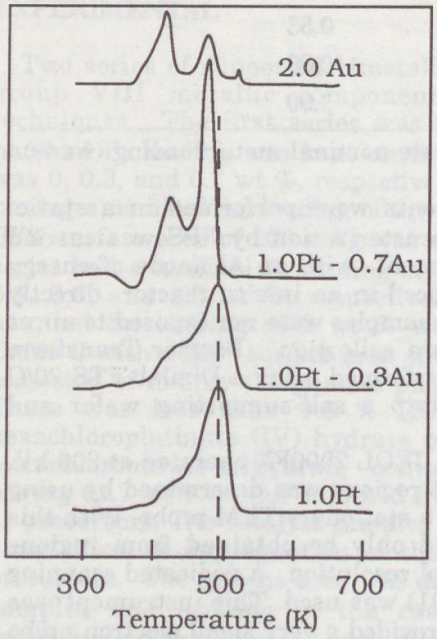

Figure 1 a. Temperature-programmed reduction profiles of Pt-Au/SiO_2 catalyst series.

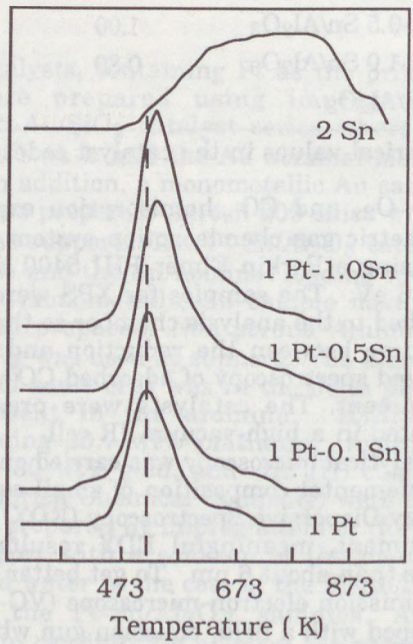

Figure 1 b. Temperature-programmed reduction profiles of Pt-Sn/Al_2O_3 catalyst series.

The monometallic Pt/SiO_2 catalyst had a single reduction peak at 503 K corresponding to the conversion of the precursor, chloroplatinic acid, into zero valent platinum. The 2.0Au/SiO_2 catalyst showed the main reduction peak at 413 K and two minor peaks at 488 K and 528 K. The peak at 488 K can be

attributed to the formation of gold particles with wide size distributions, and the 528 K peak is due to the sublimation of chloroauric acid as $AuCl_3$. The TPR peaks in the bimetallic 1.0Pt-0.3Au/SiO_2 catalyst indicated a lack of significant interactions between Pt and Au. The large peak at 503 K occurred exactly where the Pt peak in 1.0Pt/SiO_2 had appeared. The shoulder at 433 K was probably due to Au reduction. In the 1.0Pt-0.7Au/SiO_2 bimetallic catalyst, on the other hand, the Pt reduction peak maximum was shifted to a lower temperature of 493 K suggesting an interaction with the Au component.

In the Pt/Al_2O_3 catalyst the Pt reduction peak maximum was located at 513 K, 10 K higher than in the corresponding silica supported Pt sample. A shoulder at higher temperatures was most likely due to the reduction of an oxychloridic surface species. The 2.0Sn/Al_2O_3 catalyst exhibited a broad reduction profile, stretching from 493 K to well beyond 800 K. The most striking feature in the TPR profiles of the bimetallic Pt-Sn samples was the almost complete absence of the broad Sn reduction profile stretching into the high temperature region. It seems that Pt facilitated the reduction of Sn, bringing its TPR peak down to a lower temperature where it was masked by the Pt TPR peak. The Pt reduction peak gradually shifted to higher temperatures with increasing tin content. The TPR results convincingly show that Pt and Sn must be in close interaction with each other, so that hydrogen which gets activated on Pt sites can reduce the neighboring Sn(IV) species.

Effect of gold and tin on chemisorption behavior of platinum

Figure 2 compares the results of static volumetric chemisorption experiments of H_2, CO, and O_2, on the Pt-Au/SiO_2 and Pt-Sn/Al_2O_3 catalysts. The data represent the total gas uptake at room temperature. Regardless of catalyst composition, approximately 35-45% of the hydrogen was weakly adsorbed and could be removed by evacuation for 1 hour at room temperature. In the Pt-Au/SiO_2 catalyst series, about 10% of the CO was weakly adsorbed, compared to 16-17 % for the Pt-Sn/Al_2O_3 series. Oxygen, on the other hand, could not be removed by evacuation at room temperature, except for the monometallic Sn/Al_2O_3 sample, where 30% of the oxygen was weakly held. As can be seen from Figure 2, adding Au to Pt drastically lowered the H/Pt, CO/Pt, and O/Pt ratios, suggesting that fewer Pt chemisorption sites were available on the surface of the bimetallic Pt-Au samples. The chemisorption results for the Sn series were quite different. Adding tin increased the gas uptake ratios, with a maximum for the 1Pt-0.1Sn/Al_2O_3 sample having a Sn/Pt atomic ratio of 0.235. There is another important difference between Au and Sn: in the Pt-Au/SiO_2 series, all three adsorbates showed the same trends of decreasing uptake with increasing Au/Sn atomic ratio. In the case of Pt-Sn/Al_2O_3, on the other hand, the oxygen uptake increased even at higher tin loadings, where the H/Pt and CO/Pt ratios levelled off. It is important to note here that the monometallic Sn sample did not chemisorb significant amounts of oxygen at room temperature, most likely due to the fact that Sn by itself is not very effective in activating molecular oxygen at room temperature. However, in presence of Pt, one could envision a scenario where activated oxygen species migrate from Pt sites to Sn sites, oxidizing them to a Sn(IV) state. A more

detailed discussion and interpretation of the chemisorption results has been given elsewhere [6, 7].

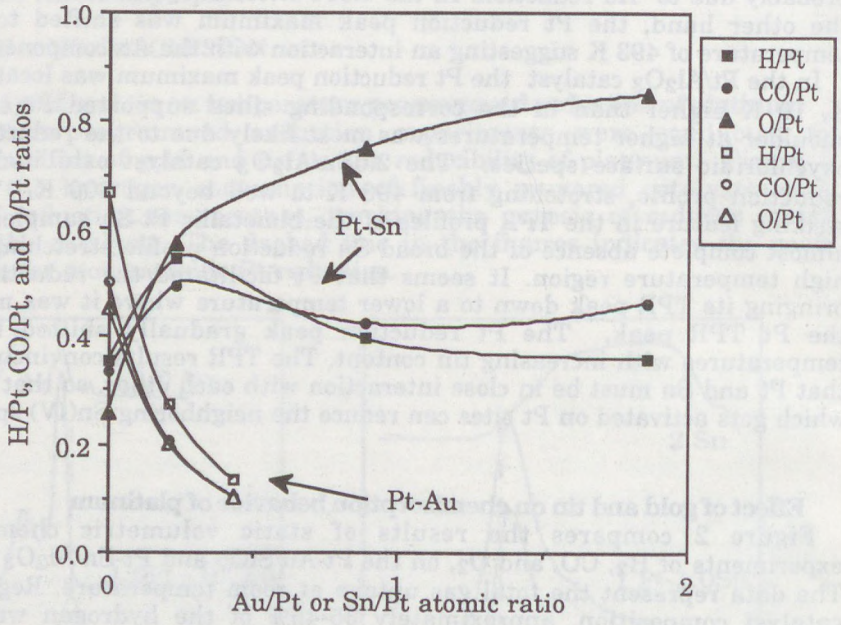

Figure 2. Ratio of H/Pt, CO/Pt, and O/Pt, as a function of overall metal composition. The gas uptake ratios are calculated from total gas uptake values at room temperature and normalized on the basis of total Pt atoms in each catalyst.

FTIR spectra of adsorbed CO indicated that the effects of Au and Sn on CO adsorption were mainly geometric in nature. Figure 3 summarizes the peak position for linearly adsorbed CO after exposure to 1 atm CO for 1 hour, followed by removal of the gas phase CO by evacuation at room temperature for 1 hour. Adding the second metal component led to a shift to lower wavenumbers, most likely due to decreased dipole-dipole coupling of adsorbed CO species. The total integrated intensity of the CO band decreased with increasing Au content, indicating fewer Pt sites exposed on the surface as compared to the monometallic Pt catalyst, in excellent agreement with the chemisorption results for CO. The integrated intensity for the bimetallic Pt-Sn/Al_2O_3 catalysts, on the other hand, was significantly larger compared to monometallic Pt/Al_2O_3, again in agreement with the CO chemisorption data.

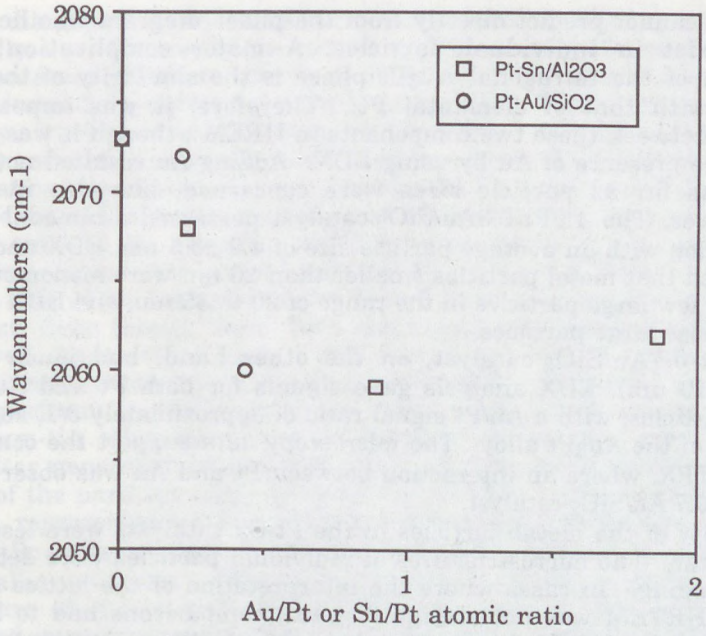

Figure 3. IR peak positions for linearly adsorbed CO on Pt as a function of Au/Pt or Sn/Pt ratio.

In the case of Pt-Sn, CO singleton vibration frequencies were determined by recording the CO vibration frequencies as a function of surface coverage and extrapolating to zero surface coverage. Regardless of Sn content, all catalysts had a singleton wavenumber of 2041 ± 6 cm^{-1}, supporting the notion that electronic effects are not of major importance in this catalyst system, in agreement with the work of Ponec et al. [8].

Characterization by electron microscopy

A detailed electron microscopy study of the Pt-Au/SiO_2 catalyst system has been published previously [9] and, therefore, only a brief summary will be given here. Monometallic Pt/SiO_2 catalysts were highly dispersed and had an average metal particle size of 3.7 ±0.3 nm. Particles larger than 1 nm were found to be monocrystalline and maintained the bulk fcc lattice spacings of 0.227 nm and 0.196 nm for the Pt(111) and Pt(200) planes, respectively. No evidence of lattice expansion or contraction was found in this size range. The average particle size in the monometallic Au/SiO_2 catalyst was 12 nm, and all the Au particles examined had an fcc configuration. A few of the Au particles were multiply twinned.

According to the bulk phase diagram for Pt-Au the formation of the Au_3Pt alloy is feasible for Pt atomic ratios less than 18% and greater than 98%.

However one cannot predict directly from the phase diagram whether or not alloys do exist in individual particles. A major complication in the identification of the tetragonal Au_3Pt phase is the similarity of the lattice parameters with that of elemental Pt. Therefore, it was impossible to differentiate between these two components in HREM , though it was possible to identify the presence of Au by using EDX. Adding Au resulted not only in differences as far as particle sizes were concerned, but also in specific microstructures. The 1.0Pt-0.3Au/SiO_2 catalyst possessed a bimodal particle size distribution with an average particle size of 4.9 ±0.5 nm. EDX and HREM results showed that metal particles smaller than 20 nm were monometallic Pt. There were a few large particles in the range of 20 to 35 nm, and EDX detected only Au in these large particles.

The 1.0Pt-0.7Au/SiO_2 catalyst, on the other hand, had much smaller particles (< 10 nm). EDX analysis gave signals for both Pt and Au within individual particles, with a Au/Pt signal ratio of approximately 3/1, suggesting the presence of the Au_3Pt alloy. The microscopy data support the conclusions drawn from TPR, where an interaction between Pt and Au was observed only for the 1.0Pt-0.7 Au/SiO_2 catalyst.

The majority of the metal particles in the Pt-Sn catalysts were less than 5 nm in diameter. The microstructures of individual particles were determined by lattice imaging. In cases where the interpretation of the lattice spacings observed in HRTEM was not straightforward, comparisons had to be made with computer-simulated images based on the multislice routine of known elements or alloys. However, this type of comparison could only be made for particles larger than 3 nm for which a bulk - type structure could be assumed [10].

In the monometallic 1.0Pt/Al_2O_3 catalyst, the Pt particles were extremely small and from transmission electron micrographs, a number average particle size of 2.5 nm was determined, in good agreement with the surface average particle size of 2.9 nm obtained from hydrogen chemisorption results. The particle size distributions for all the bimetallic Pt-Sn catalysts were very similar, with the majority of the particles, like in the monometallic case, in the <1 nm to 2.5 nm size range.

Major emphasis was placed on characterizing the 1.0Pt-0.5Sn/Al_2O_3 and the 1.0Sn/Al_2O_3 catalyst. The detection of metallic tin species was quite difficult due to the low electron scattering cross-section of Sn which made it nearly indistinguishable from the alumina support. In the monometallic 2.0Sn/Al_2O_3 sample, where tin containing regions were positively identified by microdiffraction and EDX, the Sn atoms appeared to be mobile under electron beam irradiation. This mobility of the tin prevented the formation of well defined particle shapes with sufficient contrast for microscopy.

In the 1.0Pt-0.5Sn/Al_2O_3 catalyst essentially all metal particle regions imaged in high resolution contained only platinum, based on the observed Pt {111} spacings of 2.27Å and Pt{200} spacings of 1.96Å. The distribution and location of the tin species was assessed by x-ray energy dispersive spectroscopy (EDX). Using a dedicated STEM with field emission gun, it was possible to acquire adequate EDX counts from individual catalyst regions as small as 1

nm in diameter. Every metallic region analyzed by EDX contained platinum, regardless of the size of the particles. Tin was only found in regions which also contained platinum. No trace of tin was found in any other region except in the immediate vicinity of a platinum particle. There was no evidence found for any alloy formation or for the presence of zero valent tin both in the unused, freshly reduced, and in the used catalysts. Since EDX indicated that some of the platinum particles were associated with tin, and since XPS indicated that the average oxidation state of Sn, even after reduction, was at least +2 [7], tin might exist in an alumina stabilized ionic state in close proximity to Pt particles, similar to the model proposed by Lieske and Völter [11].

The lack of tin segregation also proved to be true for the 1.0Pt-1.0Sn/Al_2O_3 catalyst. Even though there were again numerous monometallic Pt particles observed, there were now a few exceptions where metal particles were encountered whose lattice spacings could not be attributed to pure platinum. After performing multislice image calculations for all known platinum and platinum-tin alloy structures at various orientations, and comparing the computer generated images with the experimentally obtained micrographs, some of the particles could be identified as PtSn alloy (niggilite phase), while others represented a $PtSn_2$ structure with a [001] orientation. However, PtSn and $PtSn_2$ alloy particles were the exception, rather than the rule, in these bimetallic catalysts. The vast majority of metal particles exhibited the structure of monometallic platinum, with some of these platinum particles situated in regions containing ionic tin species complexed with the alumina support.

Correlation with catalytic performance

In reaction studies of n-hexane over Pt-Au/SiO_2 catalysts [9] the surprising observation was made that the cracking selectivity of the 1.0 Pt-0.3Au/SiO_2 catalyst was much higher than that of the monometallic Pt/SiO_2 catalyst. One would expect Au to disrupt the extended Pt ensembles, thereby leading to lower selectivity for the structure-sensitive cracking reactions. The unexpected behavior of the 1.0 Pt-0.3Au/SiO_2 catalyst could easily be explained once the electron microscopy results became available. It was found that this catalyst had much larger Pt particles as compared to the monometallic Pt/SiO_2 sample. On larger Pt ensembles the isomerization reaction can go through an Anderson-Avery-type bond shift mechanism [12] ultimately favoring cracking products. The 1.0 Pt-0.7Au/SiO_2 catalyst behaved as expected, with Au disrupting the larger Pt ensembles. On very small Pt ensembles the isomerization reaction could proceed via a cyclic intermediate or even a carbonium ion-like mechanism resulting in enhanced n-hexane isomerization selectivity, as was indeed observed [9].

Compared to the monometallic Pt/Al_2O_3 catalyst, the bimetallic Pt-Sn/Al_2O_3 catalysts exhibited a lower rate of deactivation in n-hexane conversions, a result typical for alumina supported Pt-Sn catalysts. The 1.0Pt-0.1Sn/Al_2O_3 gave somewhat higher n-hexane conversions, while the conversion levels for the catalyst loaded with 0.5 and 1 wt% Sn were considerably lower. However, these bimetallic catalysts had excellent excellent activity maintenance, while the monometallic Pt/Al_2O_3 catalyst lost activity with increasing time on stream

[13]. On monometallic Pt, a substantial drop in the benzene selectivity and yield was observed over several hours on stream. The 1.0Pt-0.1Sn/Al_2O_3 catalyst showed a marginal improvement, whereas the 1.0Pt-0.5Sn/Al_2O_3 and the 1.0Pt-1.0Sn/Al_2O_3 catalysts retained most of their original benzene selectivities and yields. This stability in the cyclization and benzene selectivity can be attributed to the lower rate of deactivation of the metallic sites which are responsible for the catalysis of the hydrogenation - dehydrogenation reactions. The patches of alumina stabilized ionic tin may play a major role in modifying the interface between Pt and alumina, thereby leading to improved activity maintenance.

The neopentane reaction brought to light subtle differences in reactivity between the Pt-Au and Pt-Sn catalysts [14]. The turnover frequencies per Pt atom increased slightly with addition of Au, while larger loadings of Sn caused a systematic decrease in the turnover frequencies for neopentane [13]. In contrast to the significant differences in n-hexane isomerization selectivity as a function of gold content, the selectivity for isomerization of neopentane to isopentane and n-pentane was essentially unaffected by adding Au to Pt. Small amounts of tin (1.0 Pt-0.1 Sn/Al_2O_3) lowered the neopentane isomerization selectivity in comparison to the monometallic 1.0 Pt/Al_2O_3 catalyst. However, further addition of tin (1.0 Pt-0.5 Sn/Al_2O_3, and 1.0 Pt-1.0 Sn/Al_2O_3) caused the neopentane isomerization selectivity to increase above that of the monometallic 1.0 Pt/Al_2O_3 sample.

In summary, the effect of gold appeared to be mainly a geometric one, disrupting larger Pt ensembles. In contrast to gold, the role of tin appeared to go beyond a simple geometric effect, with ionic tin in close proximity to platinum playing a major role.

---

1 R. Burch and L. C. Garla, J.Catal. 71 (1981) 360.
2 M. Hansen and K. Anderko, "Constitution of Binary Alloys," McGraw-Hill, New York, 1958.
3 R. Srinivasan, R.J. De Angelis and B.H. Davis, J.Catal. 106 (1987) 449.
4 J. H. Sinfelt, J.Catal. 29 (1973) 308.
5 J. M. Cowley and A. F. Moodie, Acta Crystallogr. 10 (1957) 609.
6 K. Balakrishnan, A. Sachdev and J. Schwank, J. Catal. 121 (1990) 441.
7 K. Balakrishnan and J. Schwank, J. Catal. 127 (1991) 287.
8 A.G.T.M. Bastein, F.J.C.M. Toolenar and V. Ponec, J. Catal. 90 (1984) 88.
9 A. Sachdev and J. Schwank, J. Catal. 120 (1989) 353.
10 G. Fuchs, M. Treilleux, F. Santos Aires, B. Cabaud, A. Hoareau, and P. Melinon, Phil. Mag. A 61 (1990) 45.
11 H. Lieske and J. Völter, J. Catal. 90 (1984) 96.
12 J. R. Anderson and N.R. Avery, J.Catal. 7 (1967) 315.
13 A. Sachdev, Ph.D. Dissertation, University of Michigan, 1989.
14 K. Balakrishnan and J. Schwank, J. Catal. 132 (1991) 451.

DISCUSSION

Q: J. Völter (Germany)

We have studied such bimetallic systems, too. Pt-Sn/Al_2O_3 and Pt-Pb/Al_2O_3 displayed nearly the same catalytic effect in the conversion of n-heptane. IR studies of adsorbed CO in the Pt-Pb/Al_2O_3 system indicated that the bridged form of adsorbed CO is strongly suppressed by the second metal Pb. This indicates a direct interaction of the two metals according to a geometric effect. I expect a similar effect in your IR studies on the Pt-Sn/Al_2O_3 system. Did you observe this ? Concerning the catalytic effect of metallic tin in an alloy or oxidic tin I would refer to my comment on the preceding paper of Dr. Davis.

A: J. Schwank

Yes, we did indeed observe a similar effect in our IR studies of adsorbed CO in Pt-Sn/Al_2O_3 system. On our monometallic Pt/Al_2O_3 catalyst and on the 1.0Pt - 0.1 Sn/Al_2O_3 sample, IR features attributable to bride-bonded CO species were detected. When more tin was added (1.0 Pt-0.5 Sn/Al_2O_3), the amount of bridge-bonded CO decreased significantly. On further addition of tin (1.0 Pt-1.0 Sn/Al_2O_3 and 1.0 Pt - 5.0 Sn/Al_2O_3) the presence of bridge-bonded CO on Pt was no longer detected. Hence, when more and more tin was added the geometric effect of tin became predominant making it less likely to find sites consisting of contiguous ensembles of Pt atoms capable to accommodate bridge-bonded CO. Although IR evidence along with the results of probe reactions indicate that Sn must be on the surface of Pt particles, we cannot state whether Sn is present in form of oxidic or zero-valent species.

Q: J. Ryczkowski (Poland)

Did you observe the effect of Pt dispersion on the TPD as well as H_2 and O_2 chemisorption in the Pt-Sn catalysts ?

A: J. Schwank

Yes, the chemisorption results are in excellent agreement with the results of temperature-programmed desorption of adsorbed CO.

Q: F. Figueras (France)

Previous work by our group has shown that the physical state of the catalyst such as the degree of reduction of Sn and its localization, changes with the atmosphere of reduction: higher Sn reduction can be obtained in presence of water, whereas very low Sn reduction was observed when the sample was reduced in dry conditions. Morevoer, Mossbauer spectroscopy has given evidence of fast reoxidation on Sn^0 to Sn(II) when hydrogen is evacuated from the system. This oxidation can probably explain the fact that Sn(II) is observed (in vacuum) in ESCA measurements.

Recent experiments using model catalysts obtained by controlled surface reaction of $Sn(Bu)_4$ on Pt/Al_2O_3 have shown that Sn can decorate the corners and edges of small particles, if added in small quantities, but is probably distributed on the whole surface at higher contents. My belief is that these model experiments are helpful in order to understand this Pt-Sn system, otherwise endless polemics due to the complexity of real systems will obscure the discussion.

A: J. Schwank

The experimental details of reduction have certainly a great influence on the physical state of the catalyst, and one has to be extra careful to work with clean systems to avoid problems with reoxidation. We spent a considerable amount of time and effort to condition our XPS system so that problems with reoxidation of Sn could be minimized. Two pieces of experimental evidence give us great confidence that the reoxidation

scenario you mention if not of major concern in our case. First, we conducted extensive blank studies on a Sn foil (Aldrich Chemical Co., 99 +% purity), subjected to the same treatment protocol as the supported catalyst samples. The air exposed Sn foil showed only peaks due to tin oxides. Then the foil was sputtered with an argon ion beam for about 0.5 minutes and some of the oxide overlayer was removed. Now, the XPS spectrum showed a mixture of Sn oxides (485.8 eV) and metallic tin (484.3 eV). Placing the sputtered Sn foil into the reactor attached to the XPS system and reducing it in a hydrogen stream followed by transfer into the UHV chamber for XPS analysis resulted in a complete reduction to zero valent Sn, confirming that the sample transfer from the reactor to the UHV chamber of the spectrometer did not expose the foil to even traces of oxygen. The zero-valent state of tin could be preserved in the UHV chamber throughout typical time periods required for XPS data acquisition. This confirms that the surface oxidation states of Sn as detected by XPS are attributable to the extent of reduction of Sn, rather than to an artifact due to accidental oxygen exposure during sample transfer and data acquisition. Secondly, we could maintain within our XPS system zero-valent Sn in SiO_2 supported Pt-Sn catalysts treated exactly like the Al_2O_3 supported Pt-Sn catalyst series.

I agree with you that model systems can give us important insight into key features of catalytic systems and that they can be of tremendous help in understanding the more complex real systems. The decoration of small Pt particles by tin species observed in your model system is in agreement with our chemical probes clearly indicating that the Pt ensembles are disrupted by tin. At this point, we cannot be certain whether these Sn species are ionic or zero-valent, since neither electron microscopy nor XPS were able to detect them, most likely due to their small concentration.

Q: W. Grünert (Germany)

I think the reducibility of the tin compound is very much linked with the mode of preparation. In a small XPS study together with Professor Spiro (Moscow), which has not yet been published, we used catalysts with the tin coprecipitated into the alumina support. We saw no Sn^0 at a reduction temperature of 773 K, but got plenty of it at 923 K. The latter result shows us that our sample transfer was clean and that reoxidation was not relevant. I am aware that other groups found Sn(0) already after reduction at 773 K, and I think the crucial point with all these contradictions is the mode of tin introduction.

A: J. Schwank

You are certainly right that the mode of tin introduction is an important experimental variable influencing the reducibility of tin. It is gratifying to see that your results confirm our observation that it is indeed possible to avoid reoxidation of tin during sample transfer in the XPS chamber.

Q: P. G. Menon (Sweden)

When you want to study the effect of Sn and Au on Pt, why not use the same support? Why do you change the support also at the same time ? Simultaneous change of two variables makes the interpretation of results ambiguous since they could be an effect of the two metals or of the two supports.

A: J. Schwank

The results presented here are part of a much larger study which included also Pt-Sn supported on the same SiO_2 used for the Pt-Au/SiO_2 catalysts. Unlike on alumina supported samples, on silica supported samples almost half of the tin could be reduced to a zero-valent state and, according to high resolution electron microscopy results, the zero-valent tin formed alloys with Pt. In XPS, the tin signal for the 1.0 Pt - 1.0 Sn/SiO_2 catalyst was much weaker than the tin signal for the 1.0 Pt - 1.0 Sn/Al_2O_3 catalyst indicating that there was a lesser amount of tin on the surface of the silica supported

sample as compared to the alumina supported sample for the same nominal Pt and Sn loading.

The two bimetallic Pt-Au/SiO_2 catalysts with their distinctly different particle compositions represent benchmark systems for our chemical probes, making it easier to understand and interpret the chemisorption behavior and catalytic performance of the more complex Pt-Sn system. It would certainly be desirable to extend the study to Pt-Au/Al_2O_3 catalysts to gain additional insight into the effect of the alumina support.

Q: J. K. A. Clarke (Ireland)

You make use in your interpretations, particularly for the Pt-Au catalysts, of the break-up of ensembles. I believe we are presently going through an evolution in thinking which increasingly prefers to view reactions, in almost all cases, as occurring on single metal atoms (see for this debate, the dedicated issue of Catalysis Today, February 1992). Figure 2 shows the sharp decrease in average coordinative unsaturation of Pt surface atoms as Au is incorporated. In line with this, cyclization of alkanes which requires high coordinative unsaturation will be diminished; also hydrocracking of alkane and the related build-up of carburization will be lessened. The bond-shift isomerization is by contrast, relatively unaffected, as you find it's selectivitiy in other words goes up. Burton and Hyman in 1975 showed from surface energy considerations that Au atoms preferentially "block" platinums of highest coordination unsaturation. In line with this Hagen and Somorjai shortly after showed the very rapid effect of small gold additions to a Pt foil surface in depressing dehydrocyclisation and hydrogenolysis of alkanes.

A: J. Schwank

Thank you for your comment. In the light of your remarks, it is interesting to compare the catalytic behavior of the 1.0 Pt - 0.3 Au/SiO_2 with the 1.0 Pt - 0.7 Au/SiO_2 catalyst [1, 2]. While both samples have nearly identical metal particle size distributions, the first sample contains small monometallic Pt particles and separate Au particles of larger diameter, while the latter catalyst consists mainly of Au_3Pt alloy particles.

[1] A. Sachdev, J. Schwank, *J. Catal.*, **120**, 353 (1989)
[2] K. Balakrishnan and J. Schwank, *ibid.* **132**, 451 (1991)

Q: J. Coenen (The Netherlands)

Just a brief comment about reducibility of combinations of Group VIII metal with difficultly reducible metal, like Sn. We observed many years ago that under reduction conditions where tin oxide is not reducible by itself, it can easily be reduced in presence of Ni^0 or Pt^0. Initially the Ni or Pt acts as H-transfer agent (as atomic H on surface). The possibility of alloying of Sn with Ni^0 or Pt^0 may help as additional driving force.

A: J. Schwank

Your observation is in good agreement with ours. Our TPR results confirm that the presence of Pt facilitates the reduction of Sn(IV), most likely involving hydrogen activated on Pt surface atoms.

Q: M. Paffett (USA)

The HRTEM evidence for lack of order on the supported Pt-Sn systems examined is entirely consistent with experiments with annealed Sn/Pt(111) and Sn/Pt(100) systems. Oxygen exposures >1000L ($1x10^{-3}$ Torr x sec) readily oxidize ordered Sn/Pt substitutional surface alloys. The oxidized Sn is pulled out of the surface and covers the metallic substrate. Furthermore, as was reported in 1991 (J. Phys. Chem., Surf. Sci.) it is difficult to force Sn into the bulk of the single crystal templates (e.g. alkaline ion scattering data indicate that for favorable Sn precoverages, Sn will only penetrate 1-2 atomic layers into the substrate lattice upon annealing to 1000 K).

A: J. Schwank

Thank you for your comment. In our case, of course, the HRTEM samples were air exposed, likely causing surface oxidation. While HRTEM showed mainly the structure of monometallic Pt particles, our chemical probes gave indirect evidence that after reduction small amounts of Sn might be present on the Pt surface. However, we cannot tell at this point whether we are dealing with oxidic or zero-valent tin species on the Pt surface.

Guczi, L. *et al.* (Editors), *New Frontiers in Catalysis*
Proceedings of the 10th International Congress on Catalysis, 19-24 July, 1992, Budapest, Hungary
© 1993 Elsevier Science Publishers B.V. All rights reserved

HYDROFORMYLATION OF 1-HEXENE BY SOLUBLE AND ZEOLITE-SUPPORTED IRIDIUM SPECIES

J.-Z. Zhang, Z. Li and C.-Y. Wang

Institute of Chemical Engineering of Coal, Taiyuan University of Technology, Taiyuan 030024, Shanxi, China

Abstract

The hydroformylation of 1–hexene at 150℃ and 40 atm CO : H_2(1 : 1) in toluene using soluble and zeolite–supported iridium species is reported.The presence of excess phosphine during homogeneous and heterogeneous catalysis inhibits its hydrogenation of 1–hexene and slightly lowers activity. The addition of formaldehyde to heterogeneous catalysis system increases the selectivity.

The active species of immobilized catalyst formed in reaction environment is investigated.

1. INTRODUCTION

Hydroformylation is the largest–volume process which employs a homogeneous catalyst[1]. However, homogeneous catalyst system shows many disadvantages (such as difficulties in the separation of catalyst from reaction mixture, instability of catalyst system, etc.) Consequently, a considerable effort has been expanded on the immobilization of homogeneous hydroformylation catalysts. Of interest to this study is the immobilization of transition metals by zeolite for use as heterogeneous olefin hydroformylation catalysts[2–4]. It is based on the theory that the advantage of immobilization transition metals within the pore structure of zeolites is the possible enhancement reaction selectivity due to the molecular sieving effects of the zeolite. The active metal species are located within the narrow channel of zeolite where the formation of intermediate leading to the iso–isomer will be more retarded than that leading to the n–isomer. As a result, the high selectivity to n–aldehyde may be possible. Since rhodium–catalyst shows high activity and selectivity, the rhodium–catalyzed hydroformylation of olefin has been extensively investigated.

Iridium lies in the same column in the Periodic Table as rhodium. Compounds such as $HIr(CO)(PPh_3)_3$, $(Bu_3P)_2Ir(CO)Cl$ and $(Ph_3P)_3Ir(CO)Cl$, which are analogous to the rhodium catalyst with great catalytic activity and selectivity, are

suposed to have similar behavior with rhodium in catalyzing hydroformylation. However, to date there are few reports dealing with iridium–catalyzed hydroformylation homogeneously and no research shows the behavior of iridium–zeolite for use as heterogeneous olefin hydroformylation catalysts.

In our initial report on 1–hexene hydroformylation by iridium–zeolite[5], it was observed that a great hydrogenation of olefin takes place. Mitsuo Yamaguchi[6] hydroformylated 1–hexene using iridium catalyst modified by organic bases. The results showed that the hydrogenation of olefin was strongly inhibited by the addition of phosphine and high selectivity towards linear aldehydes was also obtained. However, Hydrogenation product hexane was still predominant (~80%). The catalyst structure was not exactly clear.

The purpose of this investigation is to compare the behavior of zeolite containing iridium with that of homogeneous iridium species as catalysts for liquid phase hydroformylation. Zeolite–supported iridium carbonyl phosphine complexes is included.

2. EXPERIMENTAL

2.1 Materials

Iridium trichloride trihydrate was purchased from Kunming Noble Metal Research Institute. The zeolite ZSM–5 was obtained in powder on loan from NanKai University. Carbon monoxide and premixed hydrogen and carbon monoxide(1 : 1) were purchased from the Institute of Coal Chemistry Academia Sinica, and was used with further purification by 3093 deoxidant, TG–desulfurizing agent and 5A Zeolite. Toluene and phosphine PPh_3(Ph = phenyl) were purchased from Beijing Chemical Plant and Shanghai First Chemical Plant respectively, and were used without further purification. 1–hexene with purity 99.5% was distilled before using. The other reagents were analytical grade and used without further purification.

2.2 Preparation of catalysts

Homogeneous hydroformylation catalyst, $HIr(CO)(PPh_3)_3$, was synthesized by modified literature methods[7], and characterizd by IR,HMR and elemental analysis.

Cation exchange of Ir^{3+}(from aqueous $IrCl_3$) for Na^+ in NaZSM–5 was performed as follows. The zeolite was slurried in 0.1N NaCl at 95℃ . Then an aqueous solution of $IrCl_3$ was added dropwise over a period of 2h. The pH was maitained at 7.0 throughout the exchange by addition of 0.1N NaOH or 0.1N HCl. The slurry was stirred at 95℃ continuously for 5 h and cooled to room temperature with agitation overnight. The solid was recovered by filtering and washing with water and was dried to a free–flowing powder in air at 120℃ . The powder was pressed and crushed then sieved to 20–40 mesh size.

Iridium content of IrZSM–5 was determined as follows. After filtering and

washing. the liquid was recovered, and was determined spectrophotometrically by a procedure similar to that of Liu [8]. Then the iridium content of the IrZSM–5 was calculated according to the amount added at the begining.

IR spectra were obtained on solid using a Fourier Transform spectrometer (Digilab F.T.S.15).

2.3 Reactor system

hydroformylations were performed in a 100ml stainless steel autoclave. The autoclave was linked with a set of gas purification system (to remove sulfur, oxygen and trace water). After charging with toluene as a solvent, 1–hexene and catalyst, it was flushed with the premixed(1 : 1) H_2–CO and then compressed to the required pressure. The temperature was controlled to ± 1℃ by the heating mantle–temperature controller supplied with the autoclave. After the reaction, the autoclave was rapidly cooled to room temperature and the pressure was released, liquid products were obtained from filtering.

Gas chromatographic analysis was achieved by Shimadzu GC–9A using a column with 10% PEG 20 M packed on chromsorb W.

3. RESULTS AND DISCUSSION

3.1 Homogeneous hydroformylation of 1–hexene

The results obtained from 1–hexene hydroformylation at 40 atm H_2 : CO(1 : 1) in 1.5 molar 1–hexene in toluene at 150℃ by homogeneous iridium Catalyst, $HIr(CO)(PPh_3)_3$, are given in Table 1.

Table 1
Effect of PPh_3 on the homogeneous hydroformylation of 1–hexene

P / Ir (mol)	conversion	selectivity	n / i	product contribution (mol%)		
				hexane	n–heptanal	i–heptanal
1.0	0.993	0.720	2.53	27.8	51.2	20.3
5.0	0.999	0.645	1.83	35.4	41.7	22.8
12	0.994	0.595	1.62	40.2	36.6	22.6
24	0.960	0.650	2.19	33.5	42.9	19.6
98	0.918	0.752	2.49	22.7	49.3	19.8

Reaction conditions: pressure 40 atm, temperature 150℃, CO / H_2 (1 : 1), time 22h

The results indicate that addition of PPh_3 in small amount increases the activity. While the large amount of PPh_3 drastically lower the conversion of the 1–hexene. This is consistent with the results of literature concerning the rhodium

catalyst[1]. In addition, the presence of PPh_3 in reaction solution increaes the seletivity significantly. When the same molar PPh_3 as iridium (P / Ir = 1) was added, the selectivity reaches 72.0%, n / i ratio 2.53, while only 30% 1–hexene was converted to heptanal by using $Ir(CO)_3$as the catalyst with n / i ratio 1.2[6].

The addition of PPh_3 inhibits the hydrogenation of 1–hexene and favors the hydroformylation. First, in the reaction environment, excess PPh_3 inhibits the displacement of PPh_3 (in $HIr(CO)(PPh_3)_3$) by CO, eg.

$$HIr(CO)(PPh_3)_3+CO \rightarrow HIr(CO)_2(PPh_3)_2+PPh_3$$

or further more to form hydrocarbonyl iridium complex, $Ir(CO)_3$, which shows low selectivity to aldehyde (as mentioned above). Next, PPh_3 makes H in the complex more negative which leads to the anti–Markownikoff addition to form normal aldehydle. Also, the steric influence of PPh_3 enhances the selectivity.

3.2 Heterogeneous hydroformylation of 1–hexene

Heterogeneous 1–hexene hydroformylation results at 40 atm H_2 : CO(1 : 1) in 1.5M 1–hexene in toluene are shown in Table 2—4.

Table 2
Heterogeneous hydroformylation of 1–hexene by IrZSM–5 at 40 atm (H_2 : CO 1 : 1) 1.5M hexene in toluene, run time 22h. Ir conc. 0.50mmol / l.

cat.	Ir loss (%)	conv.	select.	n / i	product contribution (mol%)		
					hexane	n–heptanal	i–heptanal
A	1.2	0.993	0.231	0.55	76.7	8.55	15.0
B	3.5	0.971	0.287	2.58	69.2	20.1	7.78
C	3.9	0.926	0.503	1.99	46.0	31.0	15.6
D	5.1	0.920	0.693	2.46	28.2	45.4	18.4
E	11.3	0.925	0.682	2.41	29.5	39.8	16.5

IrZSM–5 was prepared by exchange with $IrCl_3$
Catalyst A: Only IrZSM–5 was used as catalyst
B: Formaldehyde was added in the concentration of 0.40mol / l
C: Excess PPh_3 was added at PPh_3 / Ir mol ratio of 24
D: Both formaldehyde and PPh_3 were added.
E: $HIr(CO)(PPh_3)_3$ was loaded on ZSM–5 by impregnation

Table 2 presents the results that show the behaviors of catalysts prepared from IrZSM–5. Catalyst A was cation–exchanged iridium zeolite ZSM–5 and was used as catalyst without adding any other agents. Compared the data with that of homogeneous catalyst, it shows serious hydrogenation of 1–hexene to hexane. With addition of formaldehyde to the reaction solution (in the situation of B),

slight improvement in selectivity is observed. When the excess PPh_3 is added (in the situation C), the product distribution signficantly changes. More than half 1–hexene is converted to heptanal. While formaldehyde and excess PPh_3 were added simutaniously in the reaction system, the selectivity to heptanal is increased greatly.

Table 3
Effect of P / Ir ratio on the heterogeneous hydroformylation of 1–hexene

P / Ir (mol)	conversion	selectivity	n / i	product contribution (mol%)		
				hexane	n–heptanal	i–heptanal
1.7	0.950	0.315	0.89	65.0	14.1	15.8
5.0	0.931	0.330	0.91	62.4	14.6	16.1
12	0.842	0.442	0.97	47.0	18.3	18.9
24	0.920	0.693	2.46	28.2	45.4	18.4
98	0.916	0.686	2.53	28.2	45.0	17.8

Reaction conditions are the same as table 1.

Table 4
Effect of formaldehyde on the heterogeneous hydroformylation of 1–hexene

Conc.of formaldehyde (mol / l)	conversion	selectivity	n / i	product contribution (mol%)		
				hexane	n–heptanal	i–heptanal
0.04	0.945	0.594	2.00	38.4	37.4	18.7
0.20	0.930	0.727	2.57	25.4	48.7	18.9
0.40	0.920	0.693	2.46	28.2	45.4	18.4
0.80	0.887	0.685	2.50	27.9	43.4	17.4
2.00	0.924	0.625	1.97	34.7	38.3	19.4

Reaction conditions are the same as table 1.

It is also noted from Table 2 that the n / i ratio is no more great than that of homogeneous hydroformylating system. Shape–selective effect of zeolite is not observed.

In order to get an inside view of the system, the heterogeneous catalyst was recovered by filtration and was dried under vacuum. Its IR spectra was recorded. Two bands at 2020$cm^{-1}$and 1880cm^{-1}were observed with small intensities. While the catalyst before reaction gave no absorbtion in this region. Therefore, there must be iridium carbonyl species formed in the reaction environment. The two bands are assigned to stretching vibrations of CO group coordinated with Ir. Since the conditions under which the catalyst D was prepared were the same as

that for the synthesis of $HIr(CO)(PPh_3)_3$[7], it is well known that the homogeneous catalyst $HIr(CO)(PPh_3)_3$ gives two carbonyl stretching frequencies at 2070 $cm^{-1}$and 1930 cm^{-1}[9]. It is likely that the active species for hydroformylation with catalyst D is the complex $HIr(CO)(PPh_3)_3$ on zeolite . The shifts of the frequencies probably is due to the effect of the zeolite.

Table 2 also shows the iridium loss from catalyst. It indicates that the catalyst prepared by cation–exchange losses less iridium than by impregnation.

Table 3 shows the results of hydroformylation of 1–hexene by PPh_3 / IrZSM–5 / Formaldehycle at the same condition as the homogeneous procedure.

It is noted that striking similarity exists between the homogeneous hydroformylation catalyst, $HIr(CO)(PPh_3)_3$, and this type of heterogeneous catalyst. Both of these give high selectivty and high n / i ratios. The addition of PPh_3dramatically inhibits the hydrogenation of 1–hexene although it slightly decreased the overall conversion. When 200 mol PPh_3 / mol Ir was used, the conversion of 1–hexene was still maintaned above 90%.

Table 4 gives the results of hydroformylation of 1–hexene at 150℃ with addition of formaldehyde in reaction solution.

It appears that as the amount of formaldehyde is increased, the conversion of 1–hexene is slightly decreased. However, the selectivity and n / i ratio proceed through a maximum with the increasing concentration of formaldehyde. The proper concentration is 0.20mol / l. Up to now, the reason is not clear.

4. ACKNOWLEDGEMENT

Financial support of this work was provided by National Natural Science Foundation of China.

5. REFERENCES

1 J. Falbe, Carbon Monoxide in Organic Synthesis, Springer, Berlin, 1970
2 Nobuo Takahashi and Masayoshi Kobayashi, J. Catal., 85(1984)89
3 M.Primet, J.C.Vedrine and C.Naccache, J. Mol. Catal., 4(1978)411
4 R.J.Devis, J.A.Rossin and M.E. Daris, J. Catal., 98(1986)477
5 Changyou Wang, Junzhong Zhang, Fifth International Pittsburgh Coal Conference 1197(1987)
6 Mistso Yamaguchi, The Catalyst, 9(1967)161
7 US Patent No. 3,965,192
8 Wangyi Liu, Anal. Chem. 1(1977)12
9 I. Malatesta, G. Caglio and M. Angoletta, J.C.S. A(1965)6979.

DISCUSSION

Q: D. Duprez (France)

It is known that chlorine-metal ligands can affect the interaction of CO and of oxygenated compounds with the metal. In connection to this, did you verify the chlorine content of your Ir-zeolite catalyst and did you try to use a chlorine-free precursor of iridium ?

A: D. Zhang

The paper (presented on the Fifth Annual International Pittsburgh Coal Conference P 1097) discussed the effects of the chlorine (when IrZSM-5 was prepared, different amount of NaCl was added to the ion-exchange solution). It showed that high Cl-concentration reduced the selectivity to aldehyde. We have not verified the chlorine content of the IrZSM-5. $IrCl_3$ was used as the precursor of iridium only.

Q: P. Ratnasamy (India)

Did you check the Ir content of your heterogeneous catalyst before and after the reaction ? How do you explain the lack of these selectivity over IrZSM-5 ?

A: D. Zhang

After measuring spectrophotometrically the Ir content of liquid recovered from ion-exchange slurry and the reaction mixture, the Ir content of IrZSM-5 before and after the reaction was calculated respectively.

Proper pore size and structure of catalyst are the basic condition for shape selectivity. It was assumed that Ir on the IrZSM-5 in the reaction condition is converted to the complex as $HIr(CO)(PPh_3)_3$, which showed high selectivity to aldehyde and it was because the bulky complex was not easily formed in the pore of the ZSM-5 that the catalyst showed little shape selectivity.

Q: J. W. Hightower (USA) and G. Maire (France)

Will you please explain the Table 2 and the effect of A-Z ?

A: D. Zhang

Table 2 shows the results of hydroformylation of 1-hexene by IrZSM-5 with adding other agents. Although adding PPh_3(C) or formaldehyde (B) alone favors the selectivity to heptanal, adding both of them (D) improves the selectivity much greatly. D and E have almost the same behavior, except that the Ir loss in E is greater than D.

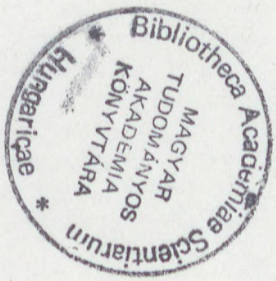

$1-3=12.895$, ——

691788

L. GUCZI
F. SOLYMOSI
P. TÉTÉNYI
Editors

NEW FRONTIERS IN CATALYSIS

A

